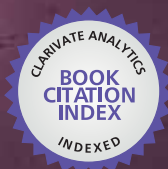




IntechOpen

Ionic Liquids
Current State of the Art

Edited by Scott Handy



WEB OF SCIENCE™

IONIC LIQUIDS - CURRENT STATE OF THE ART

Edited by **Scott Handy**

Ionic Liquids - Current State of the Art

<http://dx.doi.org/10.5772/58515>

Edited by Scott Handy

Contributors

Yanan Gao, Shinya Sasaki, Samir Ibrahim Abu-Eishah, Chuan-Fu Liu, Rafael Martínez Palou, Octavio Olivares-Xometl, Magdalena Maciejewska, Filip Walkiewicz, Elena Sashina, Dmitrii Kashirskii, Titus Alfred Makudali Msagati, Kessy Kilulya, Bhekie B. Mamba, Angeles Dominguez, Noelia Calvar, Elena Gómez, Liang Shiqiang, Kuo-Chuan Ho, Jiang-Jen Lin, Chuan-Pei Lee, Chun-Ting Li, Ling-Yu Chang, Pei-Yu Chen, Miao-Syuan Fan, Wenjun Zheng, Di Li, Wei Guo, Marian Zaborski, Toshiyuki Itoh, Hidetaka Noritomi, Elaheh Kowsari, Farzaneh Shemirani, Negin Fasih Ramandi, Adam McCluskey, Yue Dong, Jana Holm, Ulla Lassi, Clarissa Piccinin Frizzo, Marcos Villetti, Nilo Zanatta, Marcos Antonio Pinto Martins, Caroline Bender, Izabelle Gindri, Aniele Zolin Tier, Helio Bonacorso, Cunying Xu, Yixin Hua, Scott Handy, Jorge Aburto, Luis C. Branco, Gonçalo Carrera, Ana Nunes, Małgorzata Zakrzewska

© The Editor(s) and the Author(s) 2015

The moral rights of the and the author(s) have been asserted.

All rights to the book as a whole are reserved by INTECH. The book as a whole (compilation) cannot be reproduced, distributed or used for commercial or non-commercial purposes without INTECH's written permission.

Enquiries concerning the use of the book should be directed to INTECH rights and permissions department (permissions@intechopen.com).

Violations are liable to prosecution under the governing Copyright Law.



Individual chapters of this publication are distributed under the terms of the Creative Commons Attribution 3.0 Unported License which permits commercial use, distribution and reproduction of the individual chapters, provided the original author(s) and source publication are appropriately acknowledged. If so indicated, certain images may not be included under the Creative Commons license. In such cases users will need to obtain permission from the license holder to reproduce the material. More details and guidelines concerning content reuse and adaptation can be found at <http://www.intechopen.com/copyright-policy.html>.

Notice

Statements and opinions expressed in the chapters are these of the individual contributors and not necessarily those of the editors or publisher. No responsibility is accepted for the accuracy of information contained in the published chapters. The publisher assumes no responsibility for any damage or injury to persons or property arising out of the use of any materials, instructions, methods or ideas contained in the book.

First published in Croatia, 2015 by INTECH d.o.o.

eBook (PDF) Published by IN TECH d.o.o.

Place and year of publication of eBook (PDF): Rijeka, 2019.

IntechOpen is the global imprint of IN TECH d.o.o.

Printed in Croatia

Legal deposit, Croatia: National and University Library in Zagreb

Additional hard and PDF copies can be obtained from orders@intechopen.com

Ionic Liquids - Current State of the Art

Edited by Scott Handy

p. cm.

ISBN 978-953-51-2122-0

eBook (PDF) ISBN 978-953-51-4223-2

We are IntechOpen, the world's leading publisher of Open Access books Built by scientists, for scientists

3,550+

Open access books available

112,000+

International authors and editors

115M+

Downloads

151

Countries delivered to

Our authors are among the
Top 1%

most cited scientists

12.2%

Contributors from top 500 universities



WEB OF SCIENCE™

Selection of our books indexed in the Book Citation Index
in Web of Science™ Core Collection (BKCI)

Interested in publishing with us?
Contact book.department@intechopen.com

Numbers displayed above are based on latest data collected.
For more information visit www.intechopen.com



Meet the editor



Scott Handy is currently the Interim Associate Dean of the College of Graduate Studies at Middle Tennessee State University and Professor of Chemistry. He received his Ph.D. in Chemistry from Indiana University under the direction of Professor Paul Grieco. After an NIH post-doctoral fellowship at Stanford University in the research group of Professor Paul Wender, he began his independent career at Binghamton University, before moving to Middle Tennessee State University. His research interests include the use of non-traditional solvents (ionic liquids and deep eutectic solvents) in Organic Synthesis and the synthesis and study of bioactive natural product derivatives (most recently aurones).

Contents

Preface XIII

Section 1 Synthesis 1

Chapter 1 **“Green” Pericyclic Reactions Assisted by Ionic Liquids 3**
Rafael Martínez-Palou, Octavio Olivares-Xometl, Natalya V. Likhanova and Irina Lijanova

Chapter 2 **Heck Coupling in Ionic Liquids 29**
Ahmed Al Otaibi, Christopher P. Gordon and Adam McCluskey

Chapter 3 **Deep Eutectic Solvents in Organic Synthesis 59**
Scott T. Handy

Chapter 4 **Applications of Ionic Liquids (ILs) in Synthesis of Inorganic Nanomaterials 93**
Wenjun Zheng, Di Li and Wei Guo

Section 2 Enzymatic 119

Chapter 5 **Ionic Liquid-Mediated Activation of Lipase-Catalysed Reaction 121**
Toshiyuki Itoh

Chapter 6 **Solvent Dependence of Enzymatic Enantioselectivity in Ionic Liquids 139**
Hidetaka Noritomi

Section 3 Physical Properties 159

Chapter 7 **Structural and Physical Aspects of Ionic Liquid Aggregates in Solution 161**

Clarissa P. Frizzo, Aniele Z. Tier, Caroline R. Bender, Izabelle M. Gindri, Marcos A. Villetti, Nilo Zanatta, Helio G. Bonacorso and Marcos A.P. Martins

Chapter 8 **Thermal Behaviour of Pure Ionic Liquids 199**

Elena Gómez, Noelia Calvar and Ángeles Domínguez

Chapter 9 **Solubility of Bioactive, Inorganic and Polymeric Solids in Ionic Liquids — Experimental and Prediction Perspectives 229**

Gonçalo V.S.M. Carrera, Małgorzata E. Zakrzewska, Ana V. M. Nunes and Luis C. Branco

Section 4 Extraction 277

Chapter 10 **Various Self-Assembly Behaviors of Amphiphilic Molecules in Ionic Liquids 279**

Bin Dong and Yanan Gao

Chapter 11 **Ionic Liquids as Surfactants – Applications as Demulsifiers of Petroleum Emulsions 305**

Rafael Martínez-Palou and Jorge Aburto

Chapter 12 **Extraction Based on Dispersive Assisted by Ionic Liquids 327**

Negin Fasih Ramandi and Farzaneh Shemirani

Section 5 Biomass 349

Chapter 13 **Imidazolium-Based Ionic Liquids as Solvents for Analysis of Lipophilic Extractives from Biomass 351**

Kessy F. Kilulya, Bhekie B. Mamba and Titus A.M. Msagati

Chapter 14 **Dissolution and Hydrolysis of Lignocellulosic Biomass using Tailored Ionic Liquids 365**

Yue Dong, Jana Holm and Ulla Lassi

Chapter 15 **Pyridinium-Based Ionic Liquids — Application for Cellulose Processing 389**

Elena S. Sashina and Dmitrii A. Kashirskii

- Chapter 16 **Utilization of Ionic Liquids in Wood and Wood-Related Applications — A Review 419**
Samir I. Abu-Eishah
- Chapter 17 **Ionic Liquid as Green Solvent for Ring-Opening Graft Polymerizaion of ϵ -Caprolactone onto Hemicelluloses 461**
X.Q. Zhang, M.J. Chen, H.H. Wang, X.X. Wen, C.F. Liu and R.C. Sun
- Section 6 Electrochemical Applications 479**
- Chapter 18 **Electrochemical Preparation of Titanium and its Alloy in Ionic Liquid 481**
Cunying Xu and Yixin Hua
- Chapter 19 **High-Performance Supercapacitors Based on Ionic Liquids and a Graphene Nanostructure 505**
Elaheh Kowsari
- Section 7 Applications 543**
- Chapter 20 **Vibrational Spectroscopic Study on Lubrication and Corrosive Wear Mechanisms of Imidazolium Based Ionic Liquids 545**
Seiya Watanabe, Miki Nakano, Koji Miyake, Chiharu Tadokoro and Shinya Sasaki
- Chapter 21 **Ionic Liquids Applied to Improve the Dispersion of Solids in Elastomers 557**
Magdalena Maciejewska and Marian Zaborski
- Chapter 22 **Ionic Liquids in the Vulcanization of Elastomers 591**
Magdalena Maciejewska and Filip Walkiewicz
- Chapter 23 **Ionic Liquids Facilitate the Development of Absorption Refrigeration 623**
Shiqiang Liang, Wei Chen, Yongxian Guo and Dawei Tang
- Chapter 24 **New Class of Ionic Liquids for Dye-Sensitized Solar Cells 655**
Chun-Ting Li, Ling-Yu Chang, Miao-Syuan Fan, Pei-Yu Chen, Jiang-Jen Lin, Kuo-Chuan Ho and Chuan-Pei Lee

Preface

The field of Room Temperature Ionic Liquids (RTILs) is an increasingly mature area.¹ At present, the main synthetic approaches and key components are fairly defined, though with some continuing exploration and expansion. Thus, quaternary ammonium, imidazolium, and pyridinium salts with a variety of anions, many of them highly fluorinated dominate the field. The cations are generally accessed via quaternization of the parent amines, imidazoles, and pyridines, which sometimes leads directly to the RTIL (for so-called “halide-free” RTILs). More often, the final RTIL is accessed via anion metathesis of the starting halide-containing salt. The challenges associated with RTIL purity from this approach are well-documented.²

Because of the wide and diverse range of RTILs that can be accessed via this simple approach, they do merit the term “designer solvents” as their physical properties can be widely tuned with respect to viscosity, electrochemical stability, density, solubility/miscibility, and thermal stability, to name just a few. The challenges of synthesizing, characterizing, and demonstrating purity continues to push the development of general and reliable computational methods for the prediction of new RTILs for particular applications.³

Another inescapable issue is the cost and potential toxicity of RTILs. Although toxicity to the user is not as much of an issue, since the negligible volatility of the majority of these materials means that exposure is largely limited to direct contact or ingestion, there is still concern regarding their disposal and recycling.⁴ Further, the cost of the most popular RTILs, such as BMIM BF₄ and BMIM NTf₂, still considerably exceeds that of conventional solvents and effectively precludes their use in all but the most high value of applications. To specifically address this issue, a newer variant on the RTIL theme has emerged – deep eutectic solvents (DES).⁵ Although related, they fundamentally differ in that they are simply combinations of two compounds (often two solids) that result in a mixture with a dramatically lowered melting point. An example is the very common DES comprised of choline chloride and urea in a 1:2 molar ratio. While choline chloride has a melting point in excess of 300 C and urea has a melting point of 12 C, this DES exhibits a melting point of 12 C. Additional advantages include the low toxicity and relative abundance (and thus low cost) of both components. As a result, this DES exhibits a cost that is comparable to that of conventional organic solvents such as DMF and acetonitrile. This new area is discussed specifically in one chapter in this book in the context of applications in Organic Synthesis, although many other applications can and have been explored.

In addition to DES, this book features chapters that cover a wide range of RTIL concepts and applications. One section of chapters focusses on one of the earlier areas of explosive exploration – their use as recyclable solvents in synthesis – including a chapter on Green Pericy-

clic Reactions Assisted by Ionic Liquids and one on Palladium-coupling reactions in Ionic Liquids. A more recent variant on this synthesis theme is found in the chapter on Applications of Ionic Liquids in the Synthesis of Inorganic Nanomaterials.

Related to conventional synthesis, RTILs have found very fruitful applications in the area of enzymatic synthesis as they are often able to stabilize and even enhance the activity of various enzymes in a largely non-aqueous environment. Developments in this area are found in the chapters Engineering of Enzymatic Reactions using Ionic Liquids and Solvent Dependence of Enzymatic Enantioselectivity.

As mentioned above, the ability to predict and rationally design RTILs with specific properties continues to be of great importance, and this topic is addressed in several chapters, including: Structural and Physical Aspects of Ionic Liquid Aggregates in Solution, Thermal Behavior of Pure Ionic Liquids, Solubility of Solids, Liquids and Gases in Ionic Liquids. Extraction issues are more specifically addressed in several additional chapters, including Ionic Liquids as Amphiphile Self-assembly Media, Ionic Liquids as Surfactants: Applications as Demulsifiers, and Extraction Based on Dispersive Assisted by Ionic Liquids.

Many of these extraction and solubilization properties find their greatest application in one specific area – biomass isolation and transformation. It is therefore not surprising to find several chapters that address different aspects of this highly important area: Imidazolium-based Ionic Liquids as Solvents for Analysis of Lipophilic Extractive from Biomass, Dissolution and Hydrolysis of Lignocellulosic Biomass Using Tailored Ionic Liquids, Pyridinium-based Ionic Liquids: Applications for Cellulose Processing, Utilization of Ionic Liquids in Wood and Wood-related Applications: a review, and Ionic Liquids as Green Solvents for Ring-opening Graft Polymerization of Caprolactones onto Hemicelluloses.

A great diversity of other applications continue to arise and are reflected in the chapters of the two remaining sections. First are electrochemical applications (Electrochemical Preparation of Titanium and its Alloys and High-performance Supercapacitors Based on Ionic Liquids), followed by a range of other interesting uses: Spectroscopic Study on Lubrication and Tribo-corrosion Mechanisms of Ionic Liquids Applied to Improve the Dispersion of Solids in Elastomers, Ionic Liquids in Vulcanization of Elastomers, Ionic Liquids Facilitated Development of Absorption Refrigeration, and New Classes of Ionic Liquids for Dye-sensitized Solar Cells.

I hope that you enjoy reading these chapters as much as I have and that they inspire you to explore newer and even more exciting possibilities of involving RTILs in your research. The future remains exciting.

Scott T. Handy
Professor of Chemistry
Middle Tennessee State University
USA

References:

1. Freemantle, M. *An Introduction to Ionic Liquids*. Royal Chemical Society, 2009.
2. For recent papers discussing this issue and the synthesis of halide-free RTILs, see: Vander Hoogerstraete, T.; Jamar, S.; Wellens, S.; Binnemans, K. "Determination of Halide Impurities in Ionic Liquids by Total Reflection X-ray Fluorescence Spectrometry." *Anal. Chem.* 2014, 86, 3931-3938. And Graesvik, J.; Eliasson, B.; Mikkola, J-P. "Halogen-free ionic liquids and their utilization as cellulose solvents." *J. Mol. Struct.* 2012, 156-163.
3. Rooney, D.; Johan, J.; Ramesh, G. "Thermophysical properties of ionic liquids." *Topics in Curr. Chem.* 2010, 290, 185-212. Zhang, S.; Lu, X.; Zhou, Q.; Li, X.; Zhang, X.; Li, S. *Ionic Liquids: Physicochemical Properties*, Elsevier, 2009.
4. Rubio, A.M.; Tomas-Alonso, F.; Fernandez, J.H.; Perez delos Rios, A.; Fernandez, F.J.H. "green aspects of ionic liquids." In *Ionic Liquids in Separation Technology*, 2014, 82-93.
5. Russ, C., Koenig, B. Low melting mixtures in organic synthesis – an alternative to ionic liquids? *Green Chem.* 2012, 14, 2969-2982. Fransisco, M., van den Bruinhorst, A., Kroon, M.C. Low-transition-temperature mixtures (LTTMs): A new generation of designer solvents. *Angew. Chem. Int. Ed.* 2013, 52, 3074-3085. Zhang, Q., Vigier, K.D., Jerome, F. Deep eutectic solvents: syntheses, properties, and applications. *Chem. Soc. Rev.* 2012, 41, 7104-7146.

Synthesis

"Green" Pericyclic Reactions Assisted by Ionic Liquids

Rafael Martínez-Palou, Octavio Olivares-Xometl,
Natalya V. Likhanova and Irina Lijanova

Additional information is available at the end of the chapter

<http://dx.doi.org/10.5772/59179>

1. Introduction

Ionic liquids (ILs) are compounds that consist exclusively of ions. These compounds, which can be considered as salts, feature low melting temperatures (generally below 100°C), at which other salts are solids. The cations in these compounds are of organic type and some of the most common structures are heterocyclic such as imidazolium (1), pyridinium (2), pyrazolium (3) and piperidinium (4), or may also be formed by non-cyclic, heteroatom-containing cations such as ammonium (5) and phosphonium (6) (Figure 1) [1].

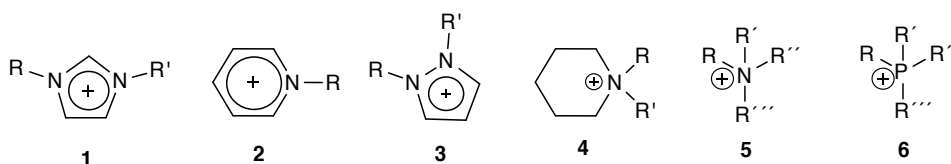


Figure 1. Typical cations in ILs.

Where R, R', R'', R''' are generally alkyl or alkyl functionalized chains.

As for the anions, they can be either inorganic (Cl⁻, Br⁻ and I⁻, which are known to have been part of the first generation ILs, and others such as [BF₄]⁻, [PF₆]⁻, [SbF₆]⁻, [AlCl₄]⁻, [AuCl₄]⁻, [NO₃]⁻, [NO₂]⁻, [SO₄]⁻) or in other cases the anion is organic ([AcO]⁻, Tf⁻, [N(OTf)₂]⁻, [CF₃CO₂]⁻, [CF₃SO₃]⁻, [PhCOO]⁻, [C(CN)₂]⁻, [RSO₄]⁻[OTs]⁻, and [SCN]⁻).

Nowadays, ILs are gaining wide recognition as potential environmental solvents due to their unique properties [2]. Physicochemical properties such as low vapor pressure (evaporation losses are minimized), thermal and chemical stability, catalytic activity, non-flammability and

non-corrosive properties, which decrease the risk of worker exposure and solvent loss to the atmosphere, make ILs powerful candidates to replace the so-called "volatile organic compounds" (VOCs) in the development of more environmentally friendly technologies and specially for the petroleum industry [3, 4].

Pericyclic reactions belong to a very important group of organic reactions, including some of the most powerful synthetically useful reactions like the Diels-Alder reaction, 1,3-dipolar cycloadditions, the Alder-ene reaction, Cope and Claisen rearrangements, the 2,3-Wittig rearrangement, diimide reduction, sulfoxide elimination, Fisher indole synthesis and many others.

In the last years, ILs have been employed as reaction media and/or catalysts and co-catalysts to facilitate the course of many pericyclic reactions. Due to the nature and properties of this kind of compounds, the application of ILs in these reactions has contributed to the development of more efficient and environmentally friendly methodologies. In this chapter, the principles of pericyclic reactions are presented and an overview of the applications of ILs in assisted pericyclic reactions is discussed.

2. Pericyclic reactions

The term Pericyclic reactions refers to a set of reactions that are characterized by concerted processes that proceed via cyclic transition states, which can be interpreted according to the Molecular Orbital Theory. Pericyclic reactions are reactions, where a cyclic, conjugated system of electrons is created in the transition state, having highly predictable stereochemical features [5].

The stereochemistry of the pericyclic reactions can be predicted based on the principle of conservation of orbital symmetry, employing the rules proposed by Robert Burns Woodward and Ronald Hoffmann in 1965 (Woodward-Hoffmann rules) [6]. This principle applies only to the concerted pericyclic reactions, and in this case, it serves as a powerful predictive tool.

The Woodward-Hoffmann rules were established by the authors as:

1. In an open chain system containing a $4n$ electron orbital symmetry of the highest occupied molecular orbital of the ground state is such that a bonding interaction between the ends must engage the overlapping between orbital regions in opposite sides of the system, and this can only be achieved through a conrotatory process.
2. In open systems containing $4n+2$ electrons, the terminal binding interaction between molecules in the ground state requires the overlapping regions of the orbitals of the same side of the system, and this is attainable only by disrotatory displacements.
3. In a photochemical reaction, an electron in the HOMO of the reactant is promoted to an excited state, leading to the reversal of terminal symmetry relations (stereospecificity).

It is said that the organic reactions that obey these rules are allowed by symmetry. Reactions that take the opposite course are forbidden by symmetry and require much more energy if they happen to take place.

The pericyclic reactions are classified according to the number of electrons that are directly involved in the transition state. Processes with 2- and 6-electron (Huckel, $4n+2$) are allowed suprafacially, and 4-electron processes must occur antarafacially (Möbius, $4n$). The main pericyclic reactions are classified as follows:

- Cycloaddition (two new σ and two less π bonds)
- Electrocyclic (one new σ and one less π bonds)
- Sigmatropic (one is changed to another σ -bond)
- Group Transfer (one new σ and one less π bonds)

3. Cycloaddition reactions

Cycloaddition reactions are the most studied pericyclic reactions, where two or more unsaturated systems react to give a cycle with one less unsaturation. This reaction allows simultaneous construction of two new carbon-carbon bonds and the formation of cyclic compounds which gave high versatility and applicability in organic synthesis [7]. A typical cycloaddition reaction is the Diels-Alder reaction.

The Diels-Alder (D-A) reaction was discovered and published for the first time in 1928 by Otto Diels and Kurt Alder [8]. This is a thermal, concerted, suprafacial, $[4+2]$ cycloaddition.

In this reaction 1,3-butadiene (diene) reacts with ethylene (dienophile) to give an adduct cyclic product as described in Figure 2. In this kind of reactions, both σ -bonds are formed at the same time, not by steps.

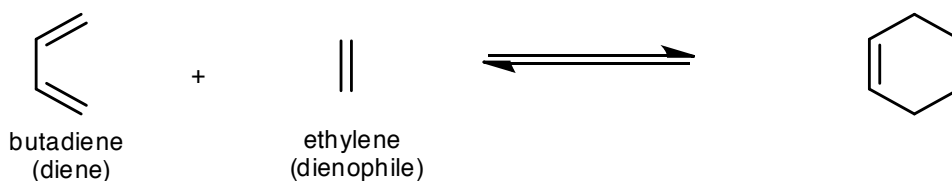


Figure 2. An example of cycloaddition reaction.

These reactions proceed according to the following selection rules:

The suprafacial-suprafacial (S-S) reaction geometry is thermally permitted when $m+n=4k+2$, for example, the Diels-Alder reaction between butadiene and ethylene, where m and n are the number of π electrons (Figure 3).

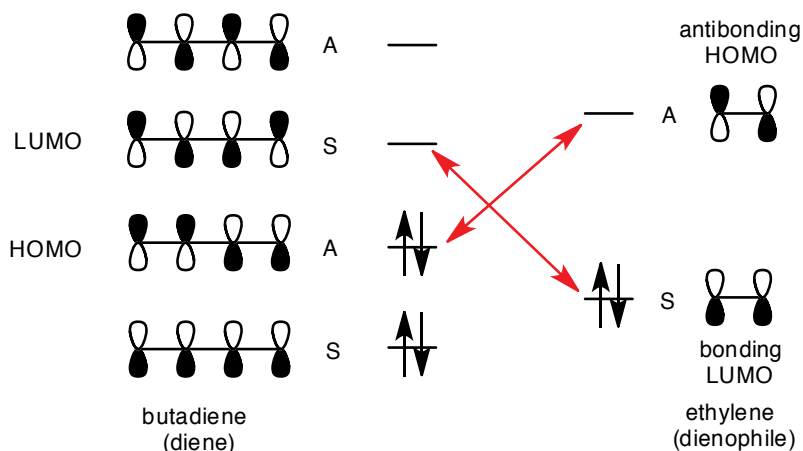


Figure 3. Molecular orbital interaction in a cycloaddition reaction.

Suprafacial (S) means that new bonds are formed on the same face of each reagent, the diene and dienophile. The opposite to suprafacial is antarafacial (A). The term [4+2] refers to a conjugated system of electrons, where a 4- reacts with a 2-electron system.

Figure 3 shows the molecular orbitals (MOs) of 1,3-butadiene and ethylene, and their respective relative energies. As noted earlier, the HOMO-LUMO energy gap is greater in ethylene than in butadiene. For the two compounds to react, the HOMO of one must react with the LUMO of the other one with conservation of orbital symmetry. There are two seemingly isoenergetic possibilities, the SS and AA reactions (red arrows), which conserve symmetry. Both energy gaps are equal and too large for a reaction to occur readily.

1. One way to reduce the HOMO-LUMO energy gap is by lowering the LUMO of one reactant. This is accomplished by using an "ethylene" that has an electron-withdrawing group attached to it.
2. The supra-antara reaction geometry is allowed thermally when $m+n=4k$, for example, cycloaddition [2+2]. The formation of cyclobutane from two ethylenes cannot be concerted by thermal reaction; the HOMO-LUMO gap requires light (photochemical reaction) for the excitation of ethylene (Figure 4).

In the S-S mode, the concerted [4+2] cycloaddition is ground state (thermal) allowed and excited state ($h\nu$) forbidden, while the [2+2] cycloaddition is just the opposite, ground state forbidden and excited state allowed.

The Diels-Alder reactions involving at least one heteroatom in the dienophile (heterodienophile) [9] or in the diene (heterodiene) [10] are known as hetero-Diels-Alder reactions. For example, carbonyl groups can react successfully with dienes to yield pyranoid rings, a reaction known as the oxo-Diels-Alder reaction, or when a nitrogen atom can be part of the diene or the dienophile, the reaction is known as aza-Diels-Alder.

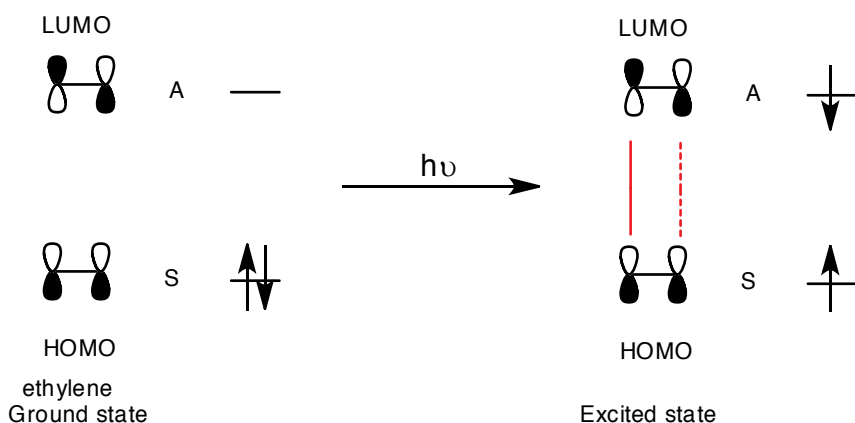


Figure 4. Molecular orbital interaction in [2+2] reaction.

4. Electrocyclic reactions

Electrocyclic reactions are a type of pericyclic reaction which is unimolecular and in which the termini of a conjugated system become σ bonded to each other to form a shortened π system (Figure 5) [11].

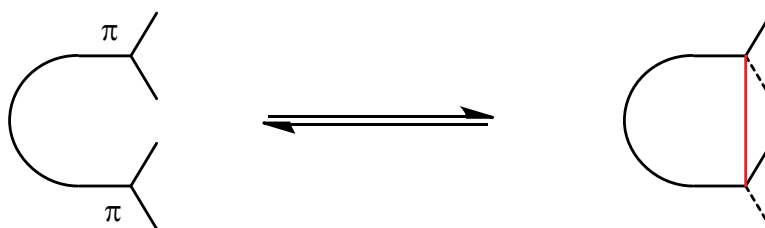


Figure 5. Representation of an electrocyclic reaction.

A typical example of this reaction is the electrocyclization of the 1,3,5-hexatriene to the conjugated cyclic diene (Figure 6).

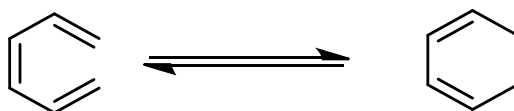


Figure 6. Electrocyclization reaction of the 1,3,5-hexatriene.

When there are substituents at the end of an unsaturated system, these substituents have a definite stereochemistry at the cyclic structure depending on the rotation way of the overlapping molecular orbitals. This relationship might be disrotatory or conrotatory. Fixed geometrical isomerism imposed upon the open chain is related to rigid tetrahedral isomerism in the cyclic array (Figure 7).

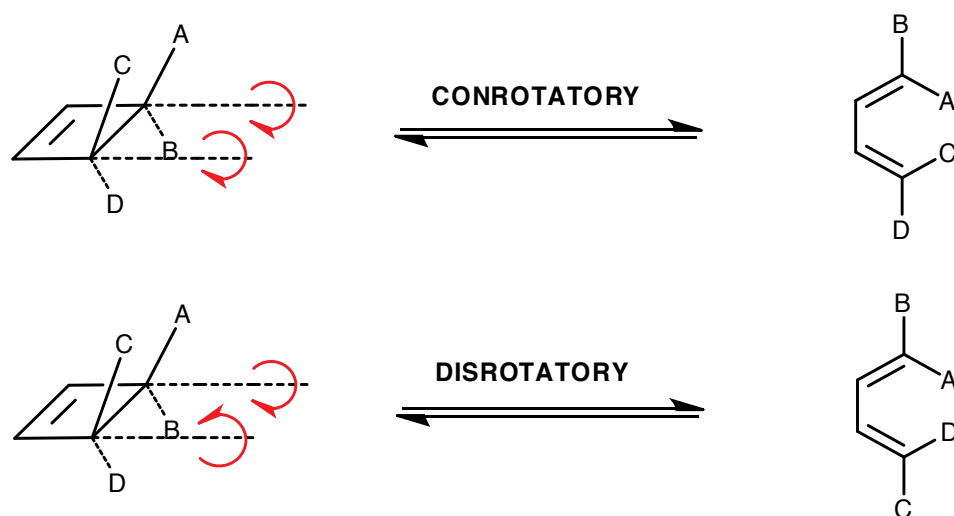


Figure 7. Stereochemistry at the cyclic structure depending on the rotation way of the overlapping molecular orbitals.

For this kind of reaction, the thermal reaction is now disrotatory, while the photochemical reaction is conrotatory. According to the Principle of Conservation of Orbital Symmetry by Woodward & Hoffmann [12], the thermal reaction will be conrotatory for $4n$ systems and disrotatory for $4n+2$ systems, and in the opposite way for photochemical reactions.

5. Sigmatropic rearrangements

In a sigmatropic rearrangement, one bond is broken while another bond is formed across a p system. The numbering system $[m, n]$ gives the number of atoms between the broken bond and the formed bond in both directions [13].

There are two different types of sigmatropic reactions: a) those that involve the migration of a hydrogen atom, and b) those that involve carbon, oxygen or other element atoms. In these reactions, the starting materials are acyclic, but the transition state is cyclic, with pronounced conformational effects. A classical reaction of this type is the Claisen rearrangement (Figure 8). Other typical reactions of this type are the Cope rearrangement and the Fisher indole synthesis.

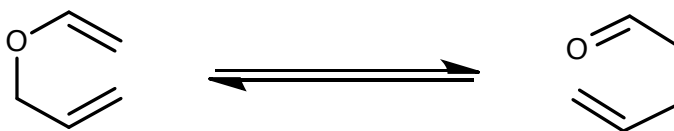


Figure 8. The Claisen rearrangement.

Figure 10. In the hydrogen migration, the hydrogen atom can migrate either suprafacially or antarafacially across the conjugated system, leading to Hückel or Möbius topologies for the transition states. The typical migration for these systems is the [1, 5] hydrogen migration (Figure 9).

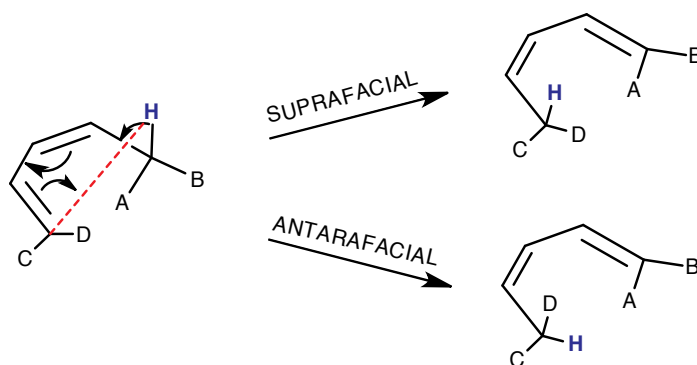


Figure 9. Suprafacial and antarafacial hydrogen migration across the conjugated system.

6. Group transfer reaction

A group transfer reaction is a process, where one or more groups of atoms are transferred from a molecule to another. Unlike other pericyclic reaction classes, group transfer reactions do not have a specific conversion of π -bonds into σ -bonds or vice versa. Typical examples of this process are the ene reaction and the reduction of a double bond by N_2H_2 diimide reaction, which is a supra-supra reaction involving six electrons.

In the ene reaction, an alkene with an allylic hydrogen (the ene component) reacts with a compound containing a multiple bond (the enophile) like olefins, acetylenes, and benzyne or carbon-hetero multiple bonds such as $C=O$, $C=N$, $C=S$, and $C\equiv P$ (carbonyl-ene reactions) in order to form a new σ -bond with migration of the ene double bond and 1, 5 hydrogen shift. The product is a substituted alkene with the double bond shifted to the allylic position (Figure 10) [14].

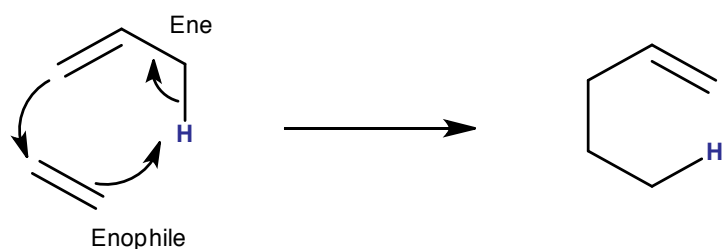


Figure 10. The ene reaction.

Due to the principle of microscopic reversibility, there is a parallel set of pericyclic "retro" reactions which perform the reverse reaction: retro Diels-Alder, retro-ene reaction and the retro-electrocyclic reactions. An example of the last one is the reaction in which the *trans*-3,4-dimethylcyclobutene is cleaved thermally to yield *E,E*-2,4-hexadiene. In this reaction, the cleavage of a σ -bond occurs to generate a longer conjugated system (Figure 11).

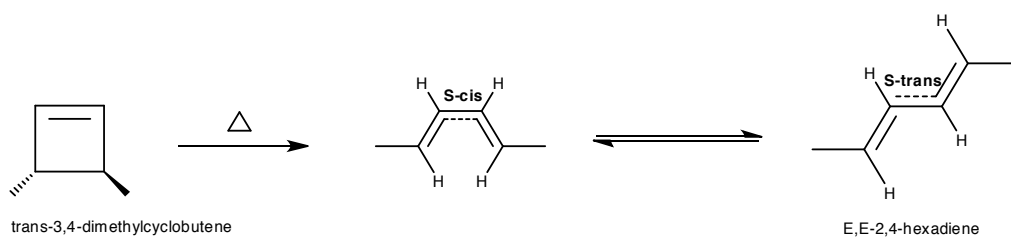


Figure 11. Thermal cleavage of the *trans*-3,4-dimethylcyclobutene.

The cleavage of a σ -bond to generate a longer conjugated system is sometimes called a retro-electrocyclic reaction. As an example of the latter, cyclobutene is cleaved thermally to yield 1,3-butadiene, relieving the extensive strain in the cyclobutene system and gaining the resonance stabilization of the conjugated diene system.

7. IL-assisted cycloaddition reactions

Cycloaddition is a highly versatile protocol to generate new C-C bonds, being a handy tool for the synthesis of natural products [15, 16].

According to E-Village Compendex [17], in the last decade, 120 papers about IL-assisted cycloaddition reactions have been published with an important increment in the last years (Figure 12).

Among cycloaddition reactions, Diels-Alder reactions are by far the most studied, and also the most studied pericyclic reactions employing ILs. The Diels-Alder reaction is an important class of reaction that allows the synthesis of six-membered rings with accurate control on the

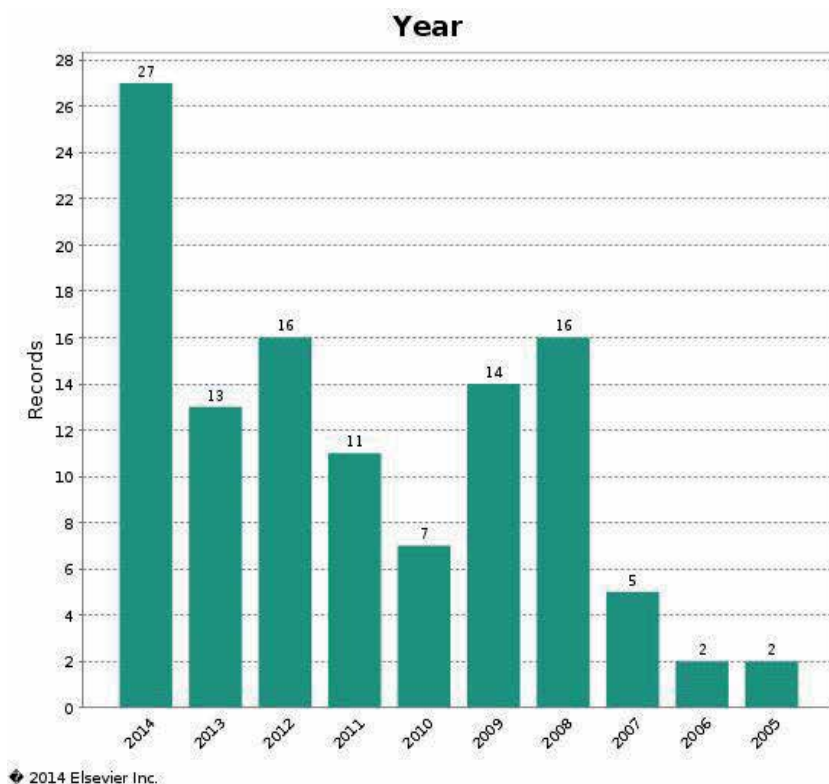


Figure 12. Papers published on IL-assisted cycloaddition reactions in the last decade.

stereoselectivities of the products. It is well known that the Diels-Alder reaction can be accelerated in the presence of a salt and because of their ionic features, ILs have shown good catalytic properties in this kind of reaction. Considering the environmental pollution provoked by using conventional organic solvents and catalysts, ILs have proved to be alternative solvents and catalysts for carrying out this kind of reactions [18].

Erfurt et al. studied the performance of hydrogen-bond-rich ILs obtained from D-Glucose, where chloroalcohols were used as raw materials and sources of hydroxyl groups for the synthesis of IL cations; bis(trifluoromethylsulfonyl)imide was used as an anion to catalyze the reaction between cyclopentadiene and either diethyl maleate or methyl acrylate. The studied ILs showed high activity even when present in catalytic amounts (4 mol% with respect to dienophile). An increase in the number of hydroxyl groups present in the IL structure resulted in higher reaction rates. The IL tends to form a crystal at temperatures in the range of -29 to -16°C , and is thermally stable from ambient temperature to at least 430°C (Figure 13) [19].

Tamariz and coworkers have studied extensively the synthesis of *exo*-heterocyclic dienes and captodative olefines and their applications in Diels-Alder reactions [20-25]. In one of their works, they studied the effect of several ILs in combination with non-conventional energy sources (microwaves and ultrasound) on this reaction. (*Z*)-*N*-substituted-4-methylene-5-

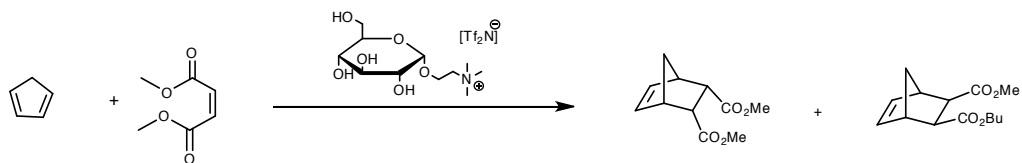


Figure 13. Diels-Alder cycloaddition using hydrogen-bond-rich ILs obtained from D-Glucose and chloroalcohols as catalysts.

propylidene-2-oxazolidinone dienes were prepared by means of a one-step synthesis, starting from 2,3-hexanedione and isocyanates. Diels-Alder cycloadditions of these dienes were carried out in the presence of dienophile methyl vinyl ketone, methyl propiolate, and a captodative olefin, using high polarity solvents, Lewis acid catalysts, and non-conventional energy sources. The reactions carried out with either H₂O/MeOH mixtures or BF₃.Et₂O catalysts yielded the highest regio- and stereo-selectivities. The use of ILs, microwaves, and ultrasound did not significantly increase the selectivity [26].

Vidis et al., also found a low effect of ultrasound and microwave dielectric heating on the selectivity of Diels-Alder reactions in ILs, but a significant effect on the reaction rate [27].

ILs have also proved to be a powerful reaction medium (or additive) for significant rate acceleration in the Diels-Alder cycloaddition (Figure 14). In this sense, ILs were used as a medium in scandium-triflate-catalysed-Diels-Alder reactions, not only for facilitating the catalyst recovery, but also for accelerating the reaction rate and improving the selectivity [28].

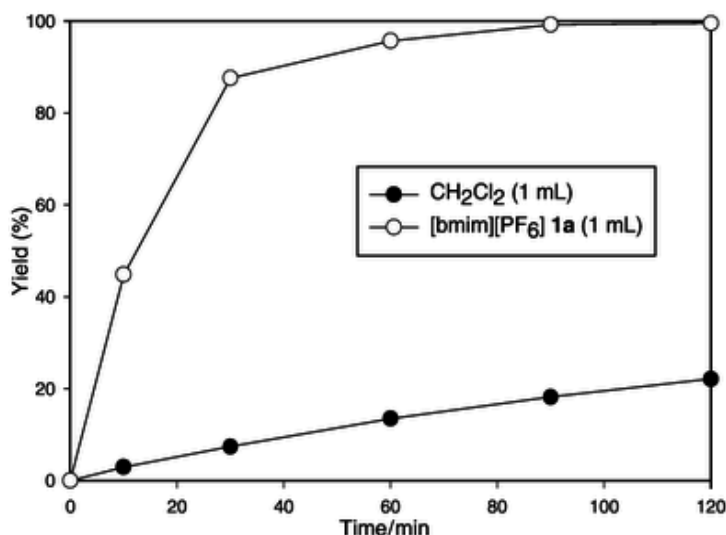


Figure 14. Kinetic studies on the reaction between 1,4-naphthoquinone (1 mmol) and 2,3-dimethylbuta-1,3-diene (3 mmol) in the presence of 0.2 mol% of Sc(OTf)₃ at 20 °C in methylene chloride and IL (Reproduced from ref. 28 with permission from The Royal Society of Chemistry).

A relatively new class of IL-analogues has been widely explored in the last years with extremely wide application prospects. Compared with conventional organic solvents, deep eutectic solvents (DESs) have more advantages: negligible vapor pressure, non-flammability, good chemical and thermal stability, non-toxicity, biodegradability, recyclability and low price among others [29].

The DES concept was first described by Abbott and coworkers [30], which generally refers to a type of solvent composed of a mixture that forms a eutectic through two cheap and reliable components, which are capable of associating via links, by hydrogen bonding, to a melting point much lower than any of the individual components; a DES can be easily formed by mixing two or more simple components under given operating conditions, manifesting poor conductivity properties. In general, DESs are cheaper than classical ILs, and also feature some other properties that make them very attractive: water-chemical inertness, easy storage, easy preparation (eliminating problems of purification and residue formation), biodegradability and environmentally biocompatibility.

In most cases, DESs are obtained by mixing a quaternary ammonium salt with metallic salts or species capable of forming bonds by hydrogen bridges. Figure 15 shows a summary of various widely used salts with hydrogen bond donors for the formation of DESs [31].

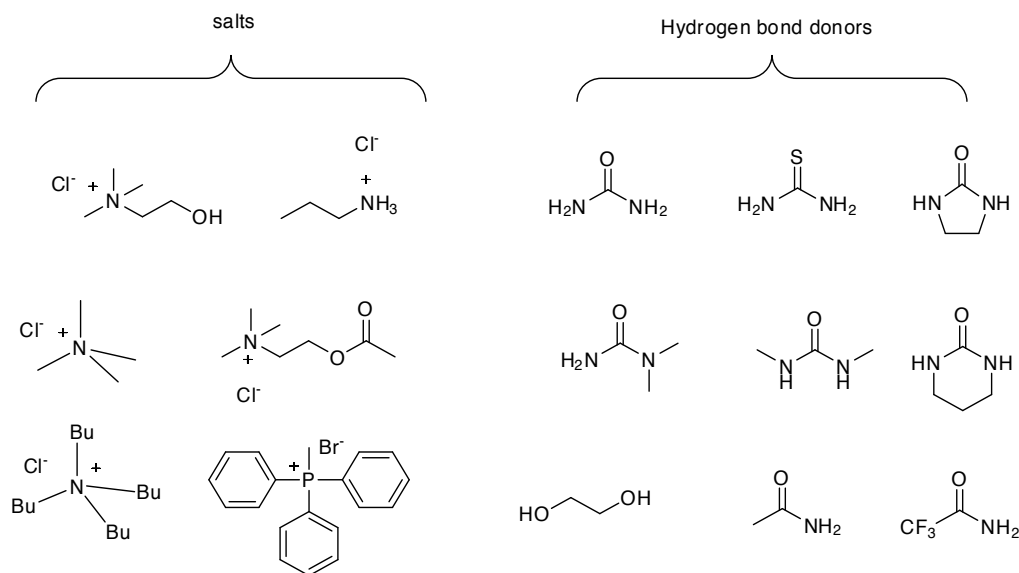


Figure 15. Typical structures of salts and hydrogen bond donors used for the synthesis of DESs.

DESs have shown a very good performance as solvents and catalysts for many organic reactions [32], including Diels-Alder cycloaddition. Particularly, Ilgen and König used DES **1**, obtained from L-carnitine/urea melt, to carry out the D-A reaction between cyclopentadiene and *n*-butylacrylate (Figure 16). The L-carnitine melt shows a very high polarity property to obtain adducts with an excellent yield of 93% with an *endo/exo* selectivity of 3.5/1. High yields

(72-95%) were obtained from D-glucose and lactose melt, respectively [33]. These DESs were also used for Heck and Sonogashira cross-couplings and Cu-catalyzed reactions. The 1, 3-dipolar cycloadditions also proceed cleanly in sugar and L-carnitine based melts, but the applicability of L-carnitine melts for standard organic reactions is limited by their lower thermal stability [34].

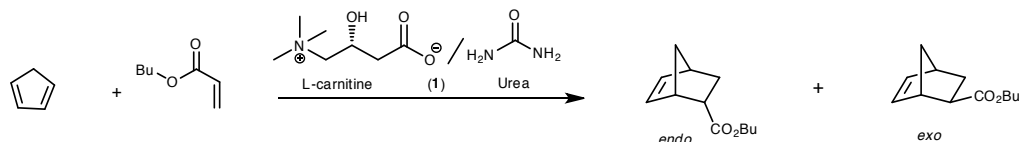


Figure 16. Diels-Alder cycloaddition between cyclopentadiene and *n*-butylacrylate using L-carnitine/urea melt as DES.

Employed IL	Reagents involved in the D-A reaction	Observations	Ref.
Trihexyl-tetradecylphosphonium bis(trifluoromethylsulfonyl)imide.	Cyclopentadiene and α,β -unsaturated esters, aldehydes and ketones.	Several phosphonium-IL-metal chlorides, triflates and bis-triflimides catalyzed very efficiently this reaction. The catalyst can be recycled.	[35]
1-(1-butyl)-3-methylimidazolium tetrafluoroborate ([BMIM][BF ₄])	Cyclopentadiene and naphthoquinone	The second-order rate constants for cycloaddition reaction were determined in various compositions of the IL with water and methanol. Rate reaction constants in pure solvents are in the order of water > [BMIM]BF ₄ > methanol. Reaction rate constant increases with solvophobicity (<i>S_p</i>), hydrogen-bond donor acidity and hydrogen-bond acceptor basicity parameters.	[36]
[BMIM][BF ₄]	N-ethylmaleimide and 2,3-dimethyl-1,3-butadiene	The Diels-Alder reaction was studied in a microemulsion (IL-H ₂ O/AOT/isooctane). The apparent second-order rate constants were determined by spectrophotometry. Those in the IL-microemulsion are five times higher than that in isooctane, and <i>k</i> ₂ in pure IL is at least 10 times higher than that in isooctane. AOT: Sodium bis(2-ethylhexyl)sulfosuccinate.	[37]
[BMIM][PF ₆]	Functionalized 2(1H)-pyrazinones	Significant rate-enhancements for both inter- and intramolecular hetero-Diels-Alder reactions were observed for the reaction in IL- doped CH ₂ Cl ₂ , comparing the standard protocols to the microwave-heated transformations.	[38]
[BuPy]Cl:AlCl ₃ (mole fraction) = 0.6	Cyclopentadiene with methyl acrylate	The acidic chloroaluminate IL can further enhance the catalytic power of an expensive silyl borate catalyst for	[39]

Employed IL	Reagents involved in the D-A reaction	Observations	Ref.
		carrying out Diels–Alder reactions. Less amount of catalyst in the above ionic liquid is required to obtain optimum results.	
Several pyridinium based ILs: 1-butyl pyridinium [BP] ⁺ , 1-hexyl pyridinium [HP] ⁺ , 3-methyl-1-butyl pyridinium [3MBP] ⁺ , 3-methyl-1-hexyl pyridinium [3MHP] ⁺ , 3-methyl-1-octyl pyridinium [3MOP] ⁺ , and 4-methyl-1-butyl pyridinium [4MBP] ⁺ . The anions were tetrafluoroborate [BF ₄] ⁻ and bis(trifluorosulphonimide) [NTf ₂] ⁻	(E)-1-phenyl-4-[2-(3-methyl-2-butenyloxy) benzylidene]-5-pyrazolone	The reaction rates decrease with the increasing viscosity of the ILs. As evident from the anionic effect, the solute-solvent specific interactions play a role in governing the kinetics of the reaction. The lower viscosities of the bistrifluoromethanesulfonimide [NTf ₂] ⁻ based ILs as compared to those based on tetrafluoroborate [BF ₄] ⁻ anion fail to accelerate the reaction rates.	[40]
Pyridinium-based ILs, 1-butyl-pyridinium tetrafluoroborate, 1-butyl-3-pyridinium tetrafluoroborate, and 1-butyl-4-methyl pyridinium tetrafluoroborate	Anthracene 9-carbinol and N-ethyl maleimide	The reaction rates decreased, caused by gradually increasing the volume fraction of ILs in solvents for all three ILs. A temperature-dependent study of kinetics of the D-A reaction was carried out in the binary mixtures of ILs in water and was explained by the entropy-enthalpy compensation effect based upon activation parameters. Kinetics of the D-A reaction in highly aqueous medium was noted to be entropically driven.	[41]
[EMIM]BF ₄ [BMIM]BF ₄ [BDMIM]BF ₄	Ester-tethered 1,3,9-decatriene	The intramolecular D-A reaction of an ester-tethered 1,3,9-decatriene system was significantly accelerated in the studied ILs. Under the present conditions, the D-A reaction proceeded smoothly without the use of Lewis acid catalysts to give cis-fused bicyclic lactones in good yield with high diastereoselectivity	[42]
Several chiral ILs synthesized from camphorsulfonic acid and camphene	Acrylic acid and cyclopentadiene	Chiral ILs were used as solvents in the D-A reaction of acrylic acid and cyclopentadiene and showed good yields and diastereoselectivities.	[43]

Employed IL	Reagents involved in the D-A reaction	Observations	Ref.
1-ethyl-3-methylimidazolium-(S)-2-pyrrolidinecarboxylic acid salt [EMIM][Pro]	A set of cyclic α,β -unsaturated ketones and arylamines with formaldehydes	The chiral IL catalyzed the one-pot direct asymmetric aza D-A reaction in up to 93% yield with up to >99/1 dr and >99% ee. Moreover, the catalytic system can be recycled and reused six times without any significant loss of catalytic activity.	[44]
Triethylammonium acetate (TEAA)	Heteroarylaldehyde, pyrazolone with enol ether	A highly efficient, rapid one-pot procedure has been developed for a three-component domino intermolecular Knoevenagel-intermolecular hetero-Diels-Alder reaction to afford indolyl- and quinolylpyrano[2,3-c] pyrazoles from corresponding TEAA under microwave irradiation. The reaction advantageously precedes in highly regio- and stereoselective ways in combination with the ease of IL recovering.	[45]
Triethylammonium acetate (TEAA)	<i>O</i> -allylated acetophenones/ propiophenone with several 5-pyrazolones	One-pot procedure for the synthesis of some new angular benzopyrano[3,4-c]pyrano-fused pyrazoles, all of which incorporate a tertiary ring junction carbon by means of domino-Knoevenagel-hetero-Diels-Alder reaction TEAA-mediated one-pot method for the synthesis of a new family of angularly fused polyheterocycles providing efficient and improved reaction conditions for unactivated dienophile propargyl, needing no additional catalyst, required for allyl- and prenyl-based substrates is another advantage of this method.	[46]

Table 1. Summary of recent papers studying IL-assisted-D-A reactions.

Another well studied cycloaddition reaction is the one involving the cycloaddition of CO₂ with epoxides [47]. The cycloaddition of CO₂ is a very important reaction because it allows CO₂ fixation, which is a hot topic in current research. The fixation of CO₂ to generate valuable chemicals such as cyclic carbonates is meaningful. Cyclic carbonates are used as polar aprotic solvents, electrolytes in lithium secondary batteries, precursors for the formation of polycarbonates, and intermediates in the production of pharmaceuticals and fine chemicals. According to studies on this reaction mechanism, the cycloaddition between CO₂ and epoxides catalyzed by ILs takes place through a stepwise mechanism and is not properly a pericyclic reaction [48], however, because of the importance of this reaction, it is briefly discussed here.

In a recent paper, a polymer grafted with an asymmetrical dication, IL-based on imidazolium and phosphonium ([P-Im-C₄H₈Ph₃P]Br₂) was synthesized, and for the first time, it was evaluated as a catalyst for the synthesis of cyclic carbonates from epoxides and CO₂ without using any co-catalyst and solvent. The catalyst showed higher activity than the monocation imidazolium and phosphonium ILs. At low catalyst loading (0.38 mol%), high yield (96.8%) and selectivity (99.5%) of propylene carbonate can be obtained at 130°C and 2.5 MPa in 4 h.

The author proposed that both the nucleophilic attack of bromine anions and their activation could explain the good activity of the catalyst. Furthermore, the catalyst showed excellent stability and reusability. It can be reused for up to five runs without any significant loss of catalytic activity after simple filtration [49].

Very recently, a new method for the synthesis of main chain poly-imidazolium salts (**2**) was developed from bisimidazole and silicon tetrachloride. These types of silicon-based poly-imidazolium-salt-poly-ILs were found to be the most efficient metal-free heterogeneous catalysts (TOF=90 h⁻¹) for the fixation of CO₂ with epoxides into cyclic carbonates under metal- and solvent-free conditions (Figure 17) [50].

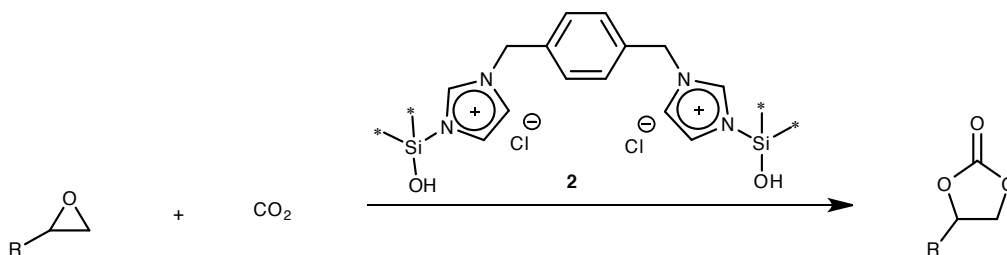


Figure 17. Synthesis of cyclic carbonates under metal- and solvent-free conditions using silicon-based-poly-imidazolium-salt-poly-ILs as catalysts.

8. IL-assisted electrocyclic reactions

ILs are also a very useful option for the development of electrocyclic reactions. Some examples of this reaction using ILs will be discussed below.

The use of microwaves as conventional heating source to carry out chemical reactions is very useful for obtaining high yields of products with short reaction times. In recent years, many reactions have been reported, where the use of microwaves as a heating source and ILs as solvents or catalysts for reactions has been combined. Because of their ionic nature, ILs are heated very quickly when subjected to microwave irradiation. This is an excellent feature to perform very rapid and efficient reactions that match the "green concept" [51-53].

In 2012, Freneda and Blazquez studied the synthesis of β -carbolines (pyrido[3,4-*b*]indole) using the microwave-assisted-tandem-aza-Wittig/electrocyclic-ring-closure methodology in ILs. This efficient procedure using microwave irradiation in combination with the IL [BMIM][BF₄] used as the solvent was useful for the preparation of aryl/aryl-1-substituted-9H-pyrido[3,4-*b*]indoles (Figure 18).

The pyrido-annulation process involved the simultaneous deprotection of an *N*-methoxymethyl group using IL/microwave-assisted irradiation with good yields (65–90%) and short reaction times (15–25 min) as shown in Table 2 [54].

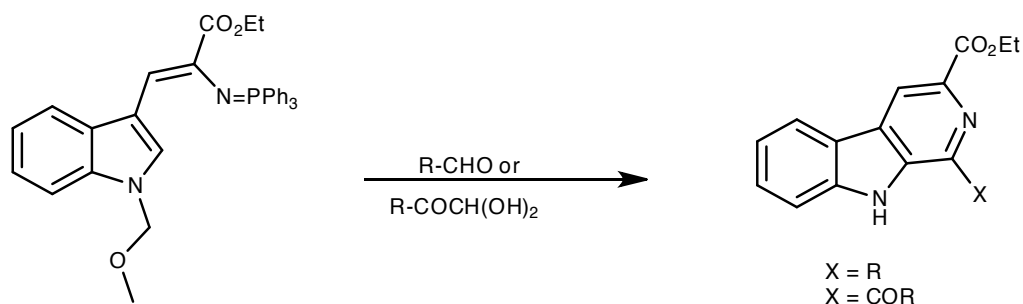


Figure 18. Synthesis of β -carbolines (pyrido[3,4-*b*]indole) using the microwave-assisted tandem-aza-Wittig/electrocyclic-ring-closure methodology in ILs.

R-CHO	R-COCH(OH) ₂	Time (min)	Yield (%)
4-MeOC ₆ H ₄		15	79
4-ClC ₆ H ₄		20	70
C ₆ H ₅		20	73
C ₆ H ₅ -(CH ₂) ₂		20	65
	C ₆ H ₅	15	88
	4-MeOC ₆ H ₄	15	90
	N-MOM-indol-3-yl	25	76

^a (R-CHO/ R-COCH(OH)₂): 1:1, MW, power: 1 W, T: 200°C.

Table 2. Time and yields of β -carboline synthesis using microwave-assisted-tandem-aza-Wittig/electrocyclic-ring-closure methodology in [BMIM][BF₄].^a

9. IL-assisted sigmatropic rearrangements

Another useful application of ILs in organic syntheses is as soluble supports to immobilize certain organic substrates. The high polarity and ionic character of IL supports have proved to exert synergistic effects and reaction rate enhancements.

Dihydropyrimidine and benzimidazole derivatives are key structural elements in many biologically active natural products and pharmaceutical compounds. Some of them constitute key intermediates which have widespread applications in drug research. Recently, an efficient IL-supported synthesis of novel benzimidazole-fused-dihydropyrimidine derivatives catalyzed by Lewis bases was published.

3-Hydroxyethyl-1-methylimidazolium tetrafluoroborate, as an ionic soluble IL support, was employed for immobilizing 2-amino benzo[*d*]imidazole. Twenty primary amines and aldehydes were evaluated in this parallel protocol, furnishing the products with high purity and yields (72-98%) (Figure 19).

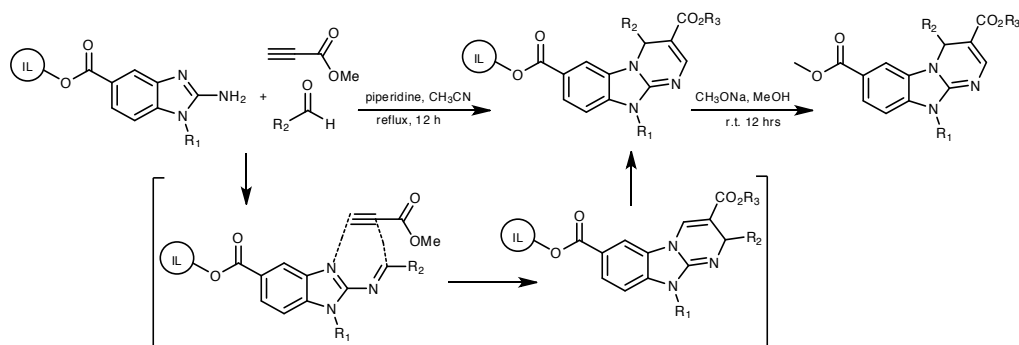


Figure 19. One-pot parallel synthesis of [1,5]-sigmatropic rearrangement involving immobilized 2-amino benzo[d]imidazole.

The novel multicomponent reaction between IL-anchored, 2-aminobenzoimidazoles, aldehydes, and electron-deficient dienophiles, described below, involve a [1,5]-sigmatropic rearrangement, which was compatible with a wide range of substrates to furnish the new scaffolds. The use of the IL as a soluble support facilitates purification by simple precipitation along with advantages such as high loading capacity, homogeneous reaction conditions and monitoring of the reaction progress by conventional NMR spectroscopy [55].

In 2011, an example of [2,3]-sigmatropic rearrangement was published, showing the cyclopropanation of 5-(allyloxymethyl)- and 5-(methallyloxymethyl)-5-ethyl-1,3-dioxanes with methyl diazoacetate catalyzed by Rh_2OAc_4 or $\text{Cu}(\text{OTf})_2$ in the presence of $[\text{BMIM}]\text{Cl}$, $[\text{BMIM}]\text{BF}_4$ and $[\text{BMIM}]\text{PF}_6$, which proceeded regioselectively at the $\text{C}=\text{C}$ bond and led to the formation of the corresponding cyclopropane-containing 1,3-dioxanes in yields up to 62% [56].

In another example of [2,3]-sigmatropic rearrangement, an efficient enantioselective approach towards the construction of quaternary indolizidines from proline building block co-catalyzed by the IL 1-butyl-3-methylimidazolium hexafluorophosphate was shown. In this work, the author explored $\text{N} \rightarrow \text{C}$ chirality transfer under [2,3]-shift of a proline derivative ammonium, yielding stereogenic at nitrogen. The rearrangement was stereospecific because the [2,3]-migrations were restricted to the same face, and the stereoselectivity arose from the previous N-alkylation step. A mechanism was proposed in which the use of an IL showed an improvement in the yields of the Stevens rearrangement due to a possible stabilization and/or activation of zwitterionic species in solution by the IL (Figure 20) [57].

Another type of sigmatropic rearrangement explored with the assistance of an IL is the [3,3]-sigmatropic rearrangement involved in the Fisher indole synthesis.

Widespread occurrence of indoles in natural products and biologically active compounds has led to a continued interest in the practical synthesis of the indole nucleus. Despite the diverse and creative approaches that have been developed so far, the classical Fischer indole synthetic methodology, which involves hydrazone formation and subsequent [3,3]-sigmatropic rearrangement remains the benchmark method.

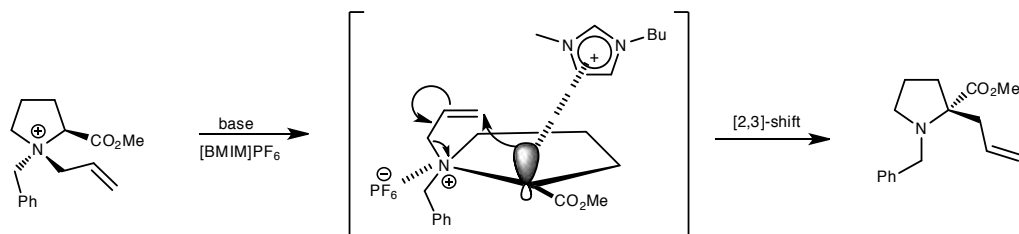


Figure 20. Proposed mechanism for IL stabilization of zwitterionic species in the Stevens [2,3]-sigmatropic rearrangement.

Calderon-Morales et al. carried out the one-pot conversion of phenylhydrazine and ketone to the indole. The Fischer indole synthesis with one equivalent of the IL Choline chloride 2ZnCl_2 ($\text{ChCl}_2 \cdot \text{ZnCl}_2$) with direct product isolation by vacuum sublimation was used. Since an IL has very low vapor pressure, then the vapor pressure of the solution of the indole product in the IL would be expected to be about the same as the vapor pressure of the indole itself. Following this procedure, ten indole derivatives were obtained in high yield with one equivalent of $\text{ChCl}_2 \cdot \text{ZnCl}_2$; exclusive formation of 2,3-disubstituted indoles is observed in the reaction of alkyl methyl ketones, and the products readily sublime directly from the IL. For example, in the case of 2-phenylindole, a 91% yield of product could be obtained by direct vacuum sublimation of the IL reaction mixture, while for 2,3-dimethylindole, a 56% yield was obtained, using this method. In unsymmetrical cases, regiospecific formation of a single product arising from the formation of the most substituted enamine intermediate is observed (Figure 21) [58].

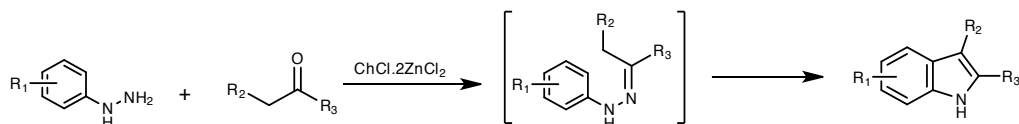


Figure 21. Fischer indole synthesis using $\text{ChCl} \cdot 2\text{ZnCl}_2$.

The Fischer indole synthesis of different ketones using chloroaluminate IL as a solvent as well as a catalyst has been also described [59].

10. IL-assisted group transfer reactions

The ene reaction has been one of the most explored group transfer reactions using ILs. Gore et al., reported, in 2013, a tandem ionic liquid asymmetric catalysis study: carbonyl-ene reactions with trifluoropyruvate with five alkenes catalysed by $[\text{Pd}\{(R)\text{-BINAP}\}](\text{SbF}_6)_2$ were carried out. The synthesized and evaluated ILs showed low antimicrobial toxicity. Excellent yields and enantioselectivities (up to 96% yield and 94% ee) were obtained using IL (**X**) as a solvent. These results were either superior or comparable to those associated with conventional volatile

solvents (e.g. CH_2Cl_2). Substrate scope studies revealed identical enantioselectivity when using methylenecyclopentane in either IL **4** or CH_2Cl_2 . Furthermore, the IL **4** immobilized catalyst $[\text{Pd}\{(\text{R})\text{-BINAP}\}](\text{SbF}_6)_2$ reaction medium was recycled and reused up to 7 times without losing activity (Figure 22) [60].

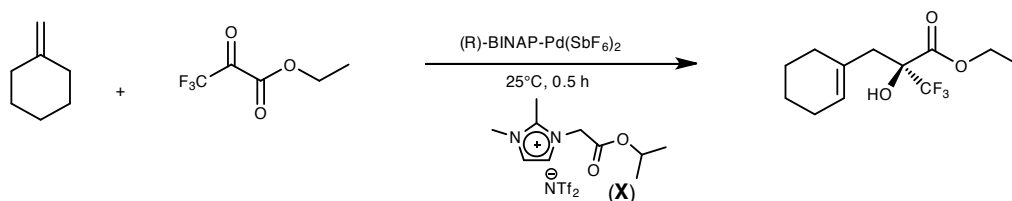


Figure 22. Enantioselective carbonyl-ene reaction using the IL (**X**) as solvent.

In 2012, Kim et al. reported an optimal hydrophobic IL as a solvent for highly enantioselective-glyoxylate-ene reactions catalyzed by a chiral bis(oxazoline)-copper complex. [BMIM] with BF_4 , PF_6 , OTf and SbF_6 were evaluated as solvents. The reactivity and stereoselectivity were highly dependent upon the properties of the IL, being the last one the best IL according to the yield (93%) and selectivity (94% *ee*). Reactions between olefins and ethyl glyoxylate in [BMIM] SbF_6 at ambient temperature provided remarkably enhanced reactivity and stereoselectivity, which greatly exceed those of the corresponding reactions in dichloromethane. Furthermore, the metal-ligand complex was readily recycled up to eight times, while exhibiting no significant decrease in reaction efficiency (Figure 23) [61].

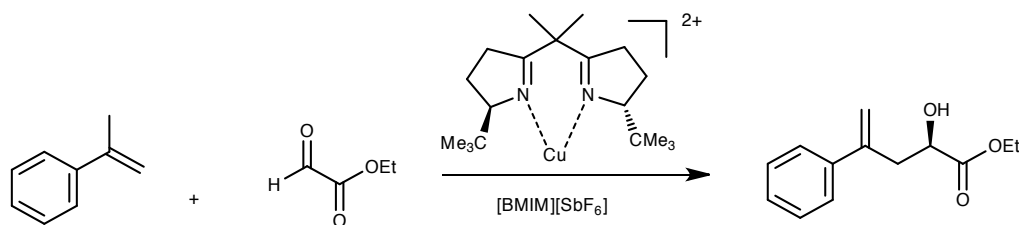


Figure 23. Catalytic enantioselective ene reaction of α -methyl styrene and ethyl glyoxylate with the copper complex as catalyst and IL as solvent.

Very recently, the synthesis of ILs using the ene pericyclic reaction was also described. In this interesting work, a series of new lipid-inspired ILs was synthesized through thiol-ene "click" reaction with a single-step process. This synthesis offers considerable promise as an efficient and orthogonal method to construct structurally diverse imidazolium-type ILs with linear and branched cationic tails, as well as versatility in the placement of the sulfur heteroatom. Profound solvent effect on this ene-reaction regioselectivity has been observed (Figure 24) [62].

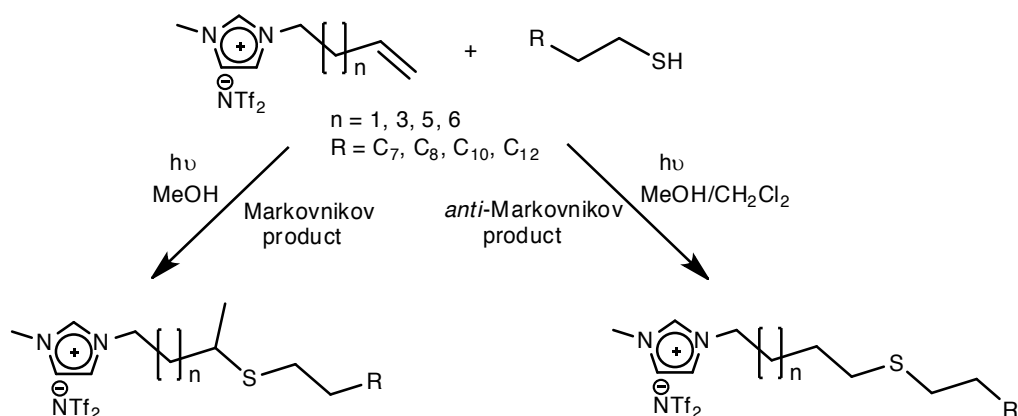


Figure 24. Synthesis of lipid-inspired ILs through thiol-ene "click" reaction as a single-step process.

11. Conclusions

As seen through this chapter, ionic liquids offer a great potential for the development of pericyclic reactions. Ionic liquids have shown to be powerful as catalysts, cocatalysts, solvents and additives in these reactions and in most cases, highly improved results regarding the yields and reaction rates have been observed and in the case of chiral reactions, excellent enantiomeric excesses have also been found. So far, in the case of cycloaddition reactions and particularly for the Diels-Alder reaction the results are very abundant, however, these are still scarce for the rest of pericyclic reactions. Both the results obtained so far and research trends are aimed at developing new methods featuring high efficiency and more environmental suitability with the use of ILs.

Author details

Rafael Martínez-Palou¹, Octavio Olivares-Xometl², Natalya V. Likhanova¹ and Irina Lijanova³

¹ Dirección de Investigación y Posgrado. Instituto Mexicano del Petróleo. México D.F., México

² Benemérita Universidad Autónoma de Puebla, Facultad de Ingeniería Química, Col. San Manuel, Ciudad Universitaria. Puebla Puebla, México

³ Instituto Politécnico Nacional, CIITEC, Cerrada Cecati S/N, Colonia Santa Catarina, Azcapotzalco, México D.F., México

References

- [1] Visser AE, Bridges NJ, Rogers RD. Ionic liquids: Science and Applications. ACS Symposium Serie. 2013.
- [2] Rogers RD, Seddon KR (Eds.). Ionic Liquids: Industrial Applications for Green Chemistry. ACS, Boston, 2002.
- [3] Martínez-Palou R, Luque R. Applications of Ionic liquids for Removing Pollutants from Refinery Feedstocks: A review. *Environm. Energy Sci.* 2014;7(8) 2414-2447.
- [4] Martínez-Palou R, Likhanova NV, Olivares-Xomelt O, Environmental Friendly Corrosion Inhibitors, In: *Developments in Corrosion Protection*, Ch. 19, Rijeka, Intech, Croatia, 2014, 431-446.
- [5] Fleming I. Pericyclic reactions. Oxford: Oxford Chemical Primers 67; 1998.
- [6] Woodward RB, Hoffmann R. Stereochemistry of Electrocyclic Reactions. *J. Am. Chem. Soc.* 1965;87(2) 395-397.
- [7] *Methods and Applications of Cycloaddition Reactions in Organic Syntheses*. Nishiwali N (Ed.). Wiley, New Jersey, US, 2014.
- [8] Diels O, Alder K. Synthesen in der hydroaromatischen Reihe. *Justus Liebig Ann. Chem.* 1928;460 98-122.
- [9] Weinreb SM. Heterodienophile addition to dienes. In: *Comprehensive Organic Synthesis*, Trost BM, Fleming I (Eds.), vol. 4, 1991, 401-449.
- [10] Boger DL. Heterodiene addition. In: *Comprehensive Organic Synthesis*, Trost BM, Fleming I (Eds.), vol. 4, 1991, 451-512.
- [11] Sankararaman S. Pericyclic reactions-A text book. Reactions, applications and theory. Willey-VCH, 2005.
- [12] Woodward RB, Hoffmann R. The Conservation of Orbital Symmetry. Verlag Chemie Academic Press. 2004.
- [13] Miller, Bernard. *Advanced Organic Chemistry*. 2nd Ed. Upper Saddle River: Pearson Prentice Hall. 2004.
- [14] Mikami, K.; Shimizu, M. (1992). Asymmetric ene reactions in organic synthesis. *Chem. Rev.* 1992; 92(5) 1021-1050.
- [15] Corey EJ, Weinshenker NM, Schaaf TK, Huber W. Stereo-controlled synthesis of prostaglandins F-2a and E-2 (dl). *J. Am. Chem. Soc.* 1969;91(20) 5675-5677.
- [16] Nicolaou, K.C. and Sorensen, Erik J. *Classics in Total Synthesis: Targets, Strategies, Methods*, Wiley VCH: New York, 1996.
- [17] Web site: <http://www.engineeringvillage.com>

- [18] Kumar A, Deshpande SS, Pawar SS. Diels-Alder reactions in ionic media: Rate enhancement with green Chemistry. *National Academy Science Letter-India* 2003;26(9-10) 232-250.
- [19] Erfurt K, Wandzik I, Walczak K, Matuszek K, Chrobok A. Hydrogen-bond-rich ionic liquids as effective organocatalysts for Diels-Alder reaction. *Green Chem.* 2014;16(7) 3508-3514.
- [20] Mandal AB, Gómez A, Jiménez-Vázquez HA, Martínez-Palou R, Delgado F, Tamariz J. One Step Synthesis and Highly Regio- and Stereoselective Diels-Alder Cycloadditions of Novel *exo*-2-Oxazolidinone Dienes. *J Org Chem.* 1997;62(12), 4105-4115.
- [21] Martínez-Palou R, Jiménez-Vázquez HA, Tamariz J. Regioselective Synthesis de N-Substituted 4-Methylene-2-oxazolidinones and 4-oxazolin-2-ones. Study of Reactivity in Michael Conjugative Addition. *Tetrahedron* 2000;56 3857-3866.
- [22] Martínez-Palou, R.; Delgado, F.; Jiménez-Vázquez, H. A.; Tamariz, J. Stereoselective Synthesis of 4,5-Diethylidene-2-oxazolidinones as New Dienes in Diels-Alder Reactions. *Helvetica Chim. Acta* 2002;85 464-482.
- [23] Martínez-Palou R, Jiménez-Vázquez HA, Delgado F, Tamariz J. Synthesis and highly selective Diels-Alder cycloadditions of the new dienes N-substituted 2,3,5,6-tetrahydrobenzoxazol-2-ones. *Tetrahedron* 2003;59 481-492.
- [24] Benavides A., Martínez-Palou, R., Jiménez-Vázquez, H. A., Tamariz, J. Synthesis and Cycloaddition Reaction of New Captodative Olefins N-Substituted 5-Alkylidene-1,3-Oxazolidine-2,4-Diones. *Heterocycles* 2001;55 469-485.
- [25] Santoyo BM, González-Romero C, Merino O, Martínez-Palou R, Fuentes-Benites A, Jiménez-Vázquez HA, Delgado F, Tamariz J. A Single-Step Synthesis of 4-Oxazolin-2-ones and Their Use in the Construction of Polycyclic Structures Bearing Quaternary Stereocenters. *Eur. J. Org. Chem.* 2009;15 2505-2518.
- [26] Fuentes A, Martínez-Palou R, Jiménez-Vázquez HA, Delgado F, Reyes A, Tamariz J. Diels-Alder Cycloadditions of New 2-Oxazolidinone Dienes under Polar Solvents, Catalysis, and non-Conventional Energy Sources. *Monatsh Chem.* 2005;46 1119-1122.
- [27] Vidis A, Küsters E, ottfried S, Dyson PJ. Effect of lewis acids on the Diels-Alder reaction in ionic liquids with different activation modes. *J. Phys. Org. Chem.* 2008;21(4) 264-270.
- [28] Song CE, Shim WH, Roh EJ, Lee SG, Choi JH. ILs as powerful media in scandium triflate catalysed Diels-Alder reactions: significant rate acceleration, selectivity improvement and easy recycling of catalyst. *Chem Commun.* 2001; 1122-1123.
- [29] Paiva A, Craveiro R, Aroso I, Martins M, Reis RL, Duarte ARC. Natural deep eutectic solvents-Solvents for 21st century. *ACS Sustain Chem Eng.* 2014;2(5) 1063-1071.

- [30] Abbott AP, Capper G, Davies DL, Rasheed RK, Tambyrajak V. Novel solvent properties of choline chloride/urea mixtures *Chem. Commun.* 2003, 70-71.
- [31] Zhang Q.; Vigier Karine O.; Royer S.; Jerome F. Deep eutectic solvents: syntheses, properties and applications. *Chem. Soc. Rev.* 2012;41 7108-7146.
- [32] Wang AL, Zheng XL, Zhao ZZ, Li CP, Zheng XF. Deep eutectic solvent to organic synthesis. *Prog. Chem.* 2014;26(5) 784-795.
- [33] Ilgen F, König B. Organic reactions in low melting mixtures based on carbohydrates and L-canitine-A comparison. *Green Chem.* 2009;11(6) 848-854.
- [34] Imperato G, Eibler E, Niedermaier G, König B. Low-melting sugar-urea-salt mixtures as solvents for Diels-Alder reactions. *Chem. Commun.* 2005; 1170-1172.
- [35] Janus E, Stefaniak W. The Diels-Alder reaction in phosphonium ionic liquid catalysed by metal chlorides, triflates and triflimides. *Catal. Lett.* 2008;124(1) 105-110.
- [36] Harif-Mood AR, Habibi-Yangjeh A, Gholami MR. Kinetics study of a Diels-Alder reaction in mixtures of an ionic liquid with molecular solvents. *J. Phys. Org. Chem.* 2008;21(9) 783-788.
- [37] Lü H, An X, Yu J, Song X. Diels-Alder reaction in microemulsions with ionic liquid. *Journal of Physical Organic Chemistry* 2012;25(12) 1210-1216.
- [38] Van der Eycken E, Appukkuttan P, De Borggraeve W, Dehaen W, Dallinger D, Kappe CO. High-speed microwave-promoted hetero-Diels-Alder reactions of 2(1H)-pyrazinones in ionic liquid doped solvents. *J. Org. Chem.* 2002;67(22) 7904-7907.
- [39] Kumar A, Pawar SS. IL as powerful solvent media for improving catalytic performance of silyl borate catalyst to promote Diels-Alder reactions. *J. Org. Chem.* 2007;72(21) 8111-8114.
- [40] Tiwari S, Khupse N, Kumar A. Intramolecular Diels-Alder Reaction in Ionic Liquids: Effect of Ion-Specific Solvent Friction. *J. Org. Chem.* 2008;73(22) 9075-9083.
- [41] Khupse, ND, Kumar A. The cosolvent-directed Diels-Alder reaction in ionic liquids. *J. Phys. Chem.* 2011;115(36) 10211-10217.
- [42] Yanai H, Ogura H, Taquchi H. Remarkable rate acceleration of intramolecular Diels-Alder reaction in ionic liquids. *Org. Biomol. Chem.* 2009;7(18) 3657-3659.
- [43] Bica K, Gmeiner G, Reichel C, Lendl B, Gaertner P. Microwave-assisted synthesis of camphor-derived chiral imidazolium ionic liquids and their application in diastereoselective Diels-Alder reaction. *Synthesis* 2007(9) 1333-1338.
- [44] Zheng, Xin Qian Y, Wang Y. Direct asymmetric aza Diels-Alder reaction catalyzed by chiral 2-pyrrolidinecarboxylic acid ionic liquid. *Catal. Commun.* 2010;11(6) 567-570.

- [45] Parmar NJ, Barad HA, Pansuriya BR, Talpada NP. A highly efficient, rapid one-pot synthesis of some new heteroaryl pyrano[2,3-c]pyrazoles in ionic liquid under microwave-irradiation. *RSC Advances*, 2013; 21(3) 8064-8070.
- [46] Parmar NJ, Pansuriya BR, Barad HA, Parmar NJ, Kant R, Gupta VK. Triethylammonium acetate-mediated domino-Knoevenagel-hetero-Diels-Alder reaction: synthesis of some angular polyheterocycles. *Monatsh. Chem.* 2013;144(6) 865-878.
- [47] He Q, O'Brien JW, Kitselman KA, Tompkins LE, Curtis GTC, Kerton FM. Synthesis of cyclic carbonates from CO₂ and epoxides using ionic liquids and related catalysts including choline chloride-metal halide mixtures. *Catal. Sic. Technol.* 2014;4(6) 1513-1528.
- [48] Anthofer MH, Wilhelm ME, Cokoja M, Markovits II, Pöthig, Mink J, Hrrmann WA, Kühn FE. Cycloaddition of CO₂ and epoxides catalyzed by imidazolium bromides under mild conditions: influence of the cation on catalyst activity. *Catal. Sci. Technol.* 2014;4 1749-1758.
- [49] Wei-Li D, Bi J, Shen-Lian L, Xu-Biao, L, Xin-Man T, Chak-Tong A. Polymer grafted with asymmetrical dication ionic liquid as efficient and reusable catalyst for the synthesis of cyclic carbonates from CO₂ and epoxides. *Catal. Today* 2014;233 92-99.
- [50] Wang J, Leong J, Zhang Y. Efficient fixation of CO₂ into cyclic carbonates catalysed by silicon-based main chain poly-imidazolium salts. *Green Chem.* In press.
- [51] Martínez-Palou R. Ionic liquids and Microwave-assisted Organic Synthesis. A "Green" and Synergic Couple. *J. Mex. Chem. Soc.* 2007;51(4) 252-264.
- [52] Martínez-Palou R. Microwave-assisted synthesis using ionic liquids. *Mol. Div.* 2010;14(1) 3-25.
- [53] Martínez-Palou R. Ionic liquids and Microwave: An Efficient Couple for Green Chemistry. In: *An Introduction to Green Chemical Methods*. Luque R, Colmenares JC (Eds.) Future Science Ltd, London, UK, 2013, p. 85-98.
- [54] Fresneda PM, Blazquez JA. Synthesis of beta-carbolines using microwave-assisted aza-Wittig methodology in ionic liquids. *Tetrahedron Lett.* 2012;53(21) 2618-2621.
- [55] Chen CH, Chen CY, Lin PT, Sun CM. Novel ionic liquid supported-multicomponent reaction toward chimeric bis-heterocycles. *Mol. Div.* 2012;16(3) 503-512.
- [56] Ivanova LN, Lobov AN, Fatykhov AA, Sultanova RM, Zlotskii SS, Dokichev VA. Cyclopropanation of 5-(allyloxymethyl)-and 5-(methallyloxymethyl)-5-ethyl-1,3-dioxanes with methyl diazoacetate. *Russian J. Org. Chem.* 2011;47(11) 1755-1760.
- [57] Duran-Lara EF, Shankaraiah N, Geraldo D, Santos LS. Studies towards the Construction of Quaternary Indolizidines. *J. Braz. Chem. Soc.* 2009;20(5) 813-819.

- [58] Calderon-Morales R, Tambyrajah V, Jenkins PR, Davies DL, Abbott AP. The regio-specific Fischer indole reaction in choline chloride 2ZnCl_2 with product isolation by direct sublimation from the ionic liquid. *Chem. Commun.* 2014; 158-159.
- [59] Rebeiro GL, Khadilkar BM. Choloraluminate ionic liquids for Fischer indole synthesis. *Synthesis* 2001;(3) 370-372.
- [60] Gore RG, Truong TKT, Pour M, Myles L, Cannon SJ, Gathergood N. Tandem ionic liquid antimicrobial toxicity and asymmetric catalysis study: carbonyl-ene reactions with trifluoropyruvate. *Green Chem.* 2013;15(10) 2727-2739.
- [61] Kim M, Jeong HS, Yeom CE, Kim BM. Enhanced reactivity and enantioselectivity in catalytic glyoxylate-ene reactions using chiral bis(oxazoline)-copper complex in an ionic liquid. *Tetrah. Assym.* 2012;23(13) 1019-1022.
- [62] Mirjafari A, O'Brien RA, West KN, Davis JH. Synthesis of New Lipid-Inspired ionic Liquids by Thiol-ene Chemistry: Profound Solvent Effect on Reaction Pathway. *Chem. Eur. J.* 2014;20(25) 7576-7580.

Heck Coupling in Ionic Liquids

Ahmed Al Otaibi, Christopher P. Gordon and
Adam McCluskey

Additional information is available at the end of the chapter

<http://dx.doi.org/10.5772/59089>

1. Introduction

Synthetic and medicinal chemistry intersect at the production of compounds. However there are stark contrasts in approach with synthetic chemistry typically producing complex molecules and developing synthetic approaches. In medicinal chemistry, the focus is on compound access to facilitate compound screening and structure activity data acquisition to enable the synthesis of more active compounds. Medicinal chemistry relies on a small range of highly robust and reliable reactions to gain access to a wide array of potentially bio-ficial reactions.[1, 2]

This reliance on robust chemistries has been significantly enhanced through the development of efficient C-C coupling protocols, in particular the coupling of aryl halides with α,β -unsaturated building block. The power of these new coupling technologies has been reflected in the recent Nobel prizes in this area to Heck,[3] Suzuki,[4] Grubb and their co-workers.[5]

While the development of new methodologies is of paramount importance across all areas of synthetic chemistry, simple developments and increased understanding of reaction conditions and reaction media often enhance these new methodologies. In this latter regard the growth of knowledge in and around room temperature ionic liquids and their ability to moderate reaction outcomes through their tuneable nature and ability to act as solvents for a wide range of chemical compounds has proved, arguably, equally important. Importantly, the combination of developments in C-C coupling technology and RTILs has allowed enhancement in the overall process efficiency. That is, these processes are becoming more environmentally sustainable.

Our group's primary focus requires rapid access to focused compound libraries of bioactive molecules spanning multiple potential therapeutic targets: the inhibition of dynamin GTPase, protein phosphatases 1A and 2A and the development of anti-cancer lead compounds.[6-12]

Where possible we are keen to apply green chemistry principles around reagent, solvent and synthetic pathway choice.[13-16] Within our own research efforts we have routinely tolerated low yields and difficult purifications to gain access to the desired compounds.[17, 18] We have thus invested considerable resources in the examination, and application, of RTILs and other emerging technologies to the synthesis of bioactive focused compound libraries.[19-23] A current program focus within our team is the development of robust flow and microwave approaches to Pd-mediated C-C coupling reactions, especially the Heck-Mizoroki (Heck reaction).

1.1. The Heck–Mizoroki reaction (the Heck reaction)

The cross-coupling of organic halides with alkenes in the presence of catalytic quantities of Pd(0) and a base was first reported by Mizoroki and Heck in 1971.[24, 25] Over the next four decades this has become known as “the Heck reaction” and has been the subject of a number of synthetic and mechanistic studies. It is now generally accepted that there are four key requirements / conditions to a successful Heck coupling reaction: 1) *Solvent*: The Heck reaction generally requires a polar solvent such as dimethyl formamide (DMF) and dimethyl sulfoxide (DMSO); 2) *Base*: The Heck reaction bases are usually selected from Et₃N, NaOAc or aqueous Na₂CO₃ or NaHCO₃;^[26] 3) *Catalyst*: The Heck reaction uses 1-5 mol% catalytic palladium (0) or palladium (II) complexes. Most commonly in the form of Pd(0)-phosphine complexes such as tetrakis(triphenylphosphine)palladium(0) [Pd(PPh₃)₄] or dibenzylidene-acetone complexes of Pd(0) such as Pd₂(dba)₃(dba).^[27] Simple palladium salts such as PdCl₂ or Pd(OAc)₂ in the absence of stabilizing phosphine ligands have also been widely used.^{[28]-[30]} 4) *Halide*: The reactivity of the halide precursor effects the time and temperature required to effect the desired coupling reaction (Figure 1).

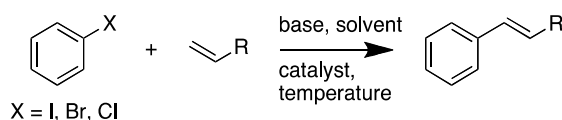


Figure 1. General reaction scheme of a Heck cross coupling between an aryl and an olefin indicating the four key variables: base, solvent, catalyst and temperature.

2. Heck reaction in Room Temperature Ionic Liquids (RTILs)

The emergence of room temperature ionic liquids (RTILs) has allowed the investigation of the Heck reaction in a wide range of novel and tuneable solvents systems.

These novel solvents cover a wide range of structural moieties from the now well established methylimidazolium and pyridinium salts through ammonium and phosphonium based systems. RTILs now comprise a wide array of sub classes including protic (PILs), basic (BILs), chiral (CILs), solid supported (SLIPs) and functionalised (FIL).^[31, 32] Key examples of these

systems are shown in Figure 2. The custom design nature of these RTILs modifies their ability to solubilise materials and affects the outcome of a wide range of chemical transformations. Herein our focus is the Heck reaction. In addition to the variable nature of the RTIL, a number of novel Pd-catalysts have been developed to enhance the Heck coupling outcomes, especially with the use of deactivated aryl halides and olefins. Selected examples of these Pd-catalysts are also shown in Figure 2.

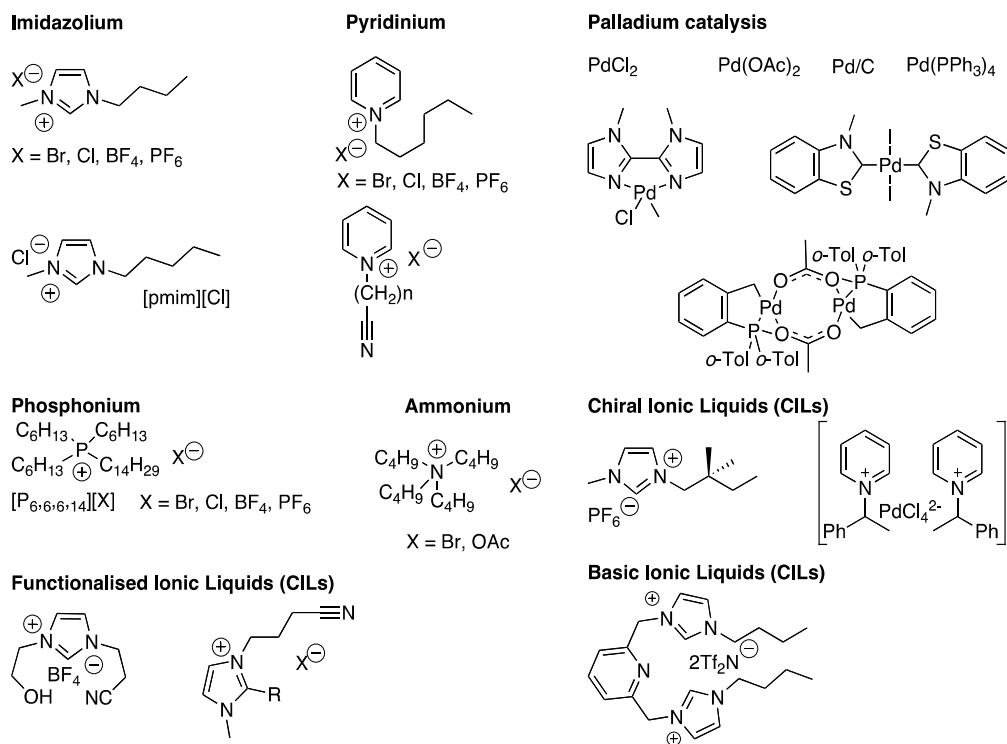
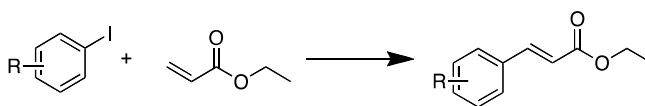


Figure 2. Selected examples of ionic liquids and Pd-catalysts used in the Heck reaction.

2.1. Imidazolium and pyridinium RTILs

The coupling efficiency of ethyl acrylate with iodobenzene mediated by $\text{Pd}(\text{OAc})_2$ was examined in the presence of *N*-hexylpyridinium $[\text{N}-\text{C}_6\text{H}_{13}\text{Py}][\text{X}]$, where $\text{X} = \text{Cl, PF}_6$ and BF_4 , and with $[\text{bmim}][\text{PF}_6]$ and 1-pentyl-3-methylimidazolium chloride ($[\text{pmim}][\text{Cl}]$) RTILs (Scheme 1). The *N*- $\text{C}_6\text{H}_{13}\text{Py}$ systems afforded higher yields of the coupled product, *E*-ethyl cinnamate, than the equivalent $[\text{bmim}][\text{Cl}]$. Similarly, a higher coupling yield was obtained with $[\text{N}-\text{C}_6\text{H}_{13}\text{Py}][\text{BF}_4]$ than $[\text{N}-\text{C}_6\text{H}_{13}\text{Py}][\text{PF}_6]$, but required higher reactions temperatures 80°C and extended reaction durations of 72 h to attain the efficiency of the chloride analogues (Table 1).[33]



Scheme 1. Reagents and conditions: 2 mol % Pd(OAc)₂, a RTIL (see Table 1 for detail), Et₃N or NaHCO₃, 40-100 °C, 24-72 h.

RTIL	Base	Temp. °C	Time (h)	Yield %
[N-C ₆ H ₁₃ Py]Cl	Et ₃ N	40	24	99
[N-C ₆ H ₁₃ Py]Cl	NaHCO ₃	40	24	98
[N-C ₆ H ₁₃ Py][PF ₆]	NaHCO ₃	80	72	42
[N-C ₆ H ₁₃ Py][BF ₄]	NaHCO ₃	80	72	99
[N-C ₆ H ₁₃ Py]Cl	NaHCO ₃	40	24	82
[N-C ₆ H ₁₃ Py]Cl	NaHCO ₃	100	24	99
[pmim]Cl	Et ₃ N	80	72	10
[pmim]Cl	NaHCO ₃	100	24	19
[pmim]Cl	NaHCO ₃	40	24	77

Table 1. Heck coupling of iodobenzene and ethyl acrylate to give *E*-ethyl cinnamate in *N*-hexylpyridinium and methylimidazolium RTILs and 2 mol% Pd(OAc)₂.

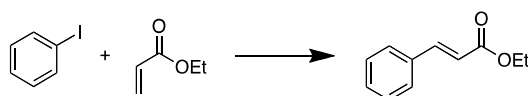
The imidazolium RTILs gave low coupling yield in the absence of phosphine ligands. Addition of Ph₃P to [bmim][PF₆] saw a significant rise in *E*-ethyl cinnamate yield to 99%, and this system could be re-used six times with no observable loss in catalyst activity. Pure product was obtained directly via hexane extraction. This approach was also suitable for coupling of the less reactive 4-bromoanisole where the effect of group 15 ligands was also explored and showed enhanced yields relative to the classical approach. The RTILs [N-C₆H₁₃Py][Cl] and [bmim][BF₄] allowed the facile coupling of benzoic anhydride (as the aryl moiety source) and butyl acrylate giving *trans*-butyl cinnamate in 90-95%. This coupling was conducted at 160 °C with [N-C₆H₁₃Py][Cl] and PdCl₂, and 200 °C with [bmim][BF₄] and Pd(OAc)₂ and P(*o*-tol)₃.^[33] Xiao *et al* noted that [bmim][BF₄] promoted the ionic pathway in the arylation of electron-rich olefins affording high α -regioselectivity (Table 2).^[34]

Yokoyama showed that heating an aryl substrate, olefin and 3 mol% of 10% Pd/C dispersed in [bmim][PF₆] afforded good yields of the Heck coupling product (Scheme 2). Product isolation was by extraction allowing direct reuse of the RTIL and catalyst without loss of coupling efficiency.^[35]

ILs	Aryl halide	Temp. °C	Halide conversion %
[bmim][Br]	iodobenzene ^a	90	94
	4-bromobenzaldehyde ^b	100	71
[bmim][BF ₄]	iodobenzene ^a	90	35
	4-bromobenzaldehyde ^b	100	3

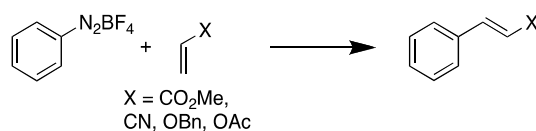
^a reaction with ethyl acrylate, ^b reaction with butyl acrylate.

Table 2. Selected results for Heck reaction between the listed arylhalides and ethyl acrylate or butyl acrylate in [Bmim]Br and [Bmim]BF₄.



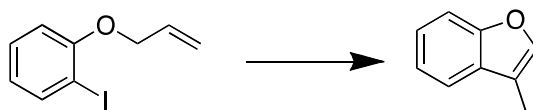
Scheme 2. Reagents and conditions: 3 mol % Pd/C (10%) / [bmim][PF₆], Et₃N, Δ.

Arene diazonium salts in RTILs have proved to be viable alternatives to aryl bromides and iodides in Pd-mediated couplings.[36, 37] In [bmim][PF₆], arene diazonium BF₄ salts were readily coupled with acrylonitrile, but vinyl ethers and esters were less reactive requiring more forcing conditions of higher temperature and longer reaction duration (Scheme 3).[38]



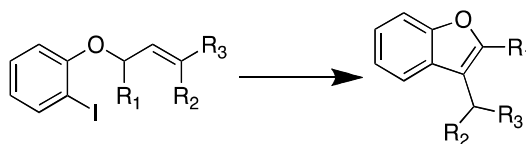
Scheme 3. Reagents and conditions: 2 mol % Pd(OAc)₂, [bmim][PF₆] at 50 °C, 2-4 h.

The Pd(OAc)₂ mediated intramolecular Heck reaction of *o*-iodoarylallyl ethers present an attractive route to benzofurans, but typically requires extended reaction times in traditional solvents (80 °C, 2 days).[39] However, in [bmim][BF₄] treatment of *o*-iodobenzyl allyl ether with 5 mol % PdCl₂, 1.5 eq. (n-Bu)₃N and 1 eq. NH₄OOCH at 60 °C for 24 h gave 3-methyl-benzofuran in a 71% yield (Scheme 4).[40]



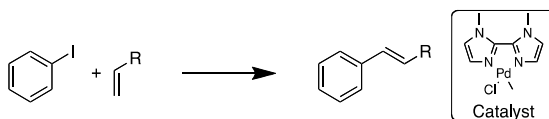
Scheme 4. Reagents and conditions: 5% PdCl₂, (n-Bu)₃N, [bmim][BF₄], 60 °C, 24 h.

The use of more substituted *o*-iodoaryl allyl ethers using the above approach allowed rapid access to 3-substituted benzofurans (Scheme 5). The isolated yields varied from modest to good.[40]



Scheme 5. Reagents and conditions: 5% PdCl₂, (n-Bu)₃N, [bmim][BF₄], 60 °C, 24 h.

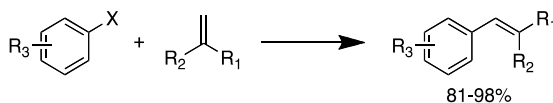
Specialty highly recyclable Pd-complexes, such as Alper's Pd(II)-bisimidazole (Scheme 6), have proved effective recyclable (five cycles with no loss of activity) Heck coupling catalysts. [4][1][4][5]



Scheme 6. Reagents and conditions: 2 mol % Pd-catalyst, [BMIM]BF₄, 60 °C, 24 h.

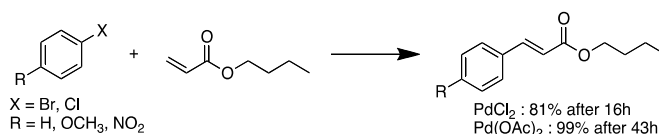
2.2. Phosphonium RTILs

A wide range of phosphonium based RTILs have been explored for use in the Heck reaction. [46] Of particular note was the use of salts such as [P_{6/6/6/14}][Cl] in the Heck coupling of deactivated and sterically demanding aryl halides (Scheme 7).[47-50] Even with deactivated aryl halides these reactions required mild conditions and short reaction duration (50 °C and 2 h). The reaction requires only 50 °C within 2 h. The solvent and catalyst could be reused. Furthermore, the phosphonium RTIL anion influenced reaction outcome chloride and decanoate anions giving superior outcomes than with BF₄ and PF₆. [47]



Scheme 7. Reagents and conditions: [P_{6/6/6/14}][Cl], Pd(OAc)₂, 100 °C, 18-24 h.

The phosphine free Pd(OAc)₂ / or PdCl₂ mediated Heck coupling has been conducted in [P_{6/6/6/14}][Br], which also represented the first report of a Pd-coupling reaction in a RTIL (Scheme 8).[46]

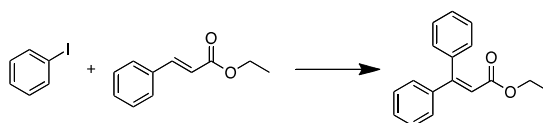


Scheme 8. Reagents and conditions: $[\text{P}_{6/6/6/14}][\text{Br}]$, Pd(OAc)_2 , 100 °C, 124 h.

It was noted with Pd(OAc)_2 , that the addition of 1.5 eq. of NaOAc , improved the coupling rate, but decreased selectivity with 5% of the (*Z*)-isomer detected under these conditions. Also of note with this reaction sequence was the slow precipitation of Pd-clusters on use of PdCl_2 , but not with Pd(OAc)_2 . With Pd(OAc)_2 the catalyst remained soluble and viable, able to catalyze subsequent couplings on removal of the product from the previous catalytic cycle. It was proposed that the RTIL phosphonium salt stabilised the Pd(0) species obtained by *in situ* reduction of the Pd(II) catalyst precursors. This ligand free approach has attracted considerable interest and has purification benefits on reaction scale up.[51]

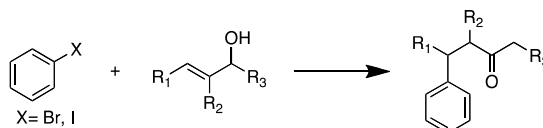
2.3. Ammonium RTILs

Tetraammonium salts are the archetypal ammonium based RTILs used in the Heck coupling, with the simplest being the tetrabutylammonium salts ($[\text{Bu}_4\text{N}][\text{X}]$). Coupling of iodobenzene with arylacrylates gave an expedient synthesis of 3,3-diarylacrylates. This coupling was accomplished in good yield and regioselectivity in molten $n\text{-Bu}_4\text{NOAc}/n\text{-Bu}_4\text{NBr}$ with Pd(OAc)_2 (Scheme 9).[52]

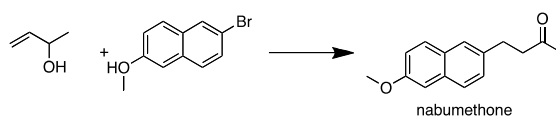


Scheme 9. Reagents and conditions: Pd(OAc)_2 , $n\text{-Bu}_4\text{NOAc}/n\text{-Bu}_4\text{NBr}$, 100 °C.

Others have noted the increased stability of the Pd-catalytic species in RTILs and have exploited this in the PdCl_2 mediated synthesis of β -arylcarbonyl compounds from allylic alcohols in $[\text{Bu}_4\text{N}]\text{Br}$, affording (Scheme 10).[53] Extension of this simple procedure afforded a one-step synthesis of the nonsteroidal antiinflammatory drug (nabumethone), (Scheme 11) and allowed catalyst reuse.[53]

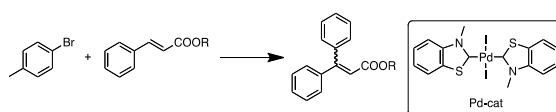


Scheme 10. Reagents and conditions: PdCl_2 , NaHCO_3 , Bu_4NBr , 120 °C, 24 h.



Scheme 11. Reagents and conditions: PdCl₂, NaHCO₃ (1.2 equiv.), Bu₄NBr, 120 °C, 24 h.

The Pd-benzothiazole carbene complex has been successfully used as the Pd-source (1.5 mol %), and easily recycled, in the coupling of both electron rich and electron deficient *trans*-cinnamates in [Bu₄N][Br] at 130 °C with added sodium formate and NaHCO₃ (Scheme 12).[54, 55] The best yields were observed with NaOH and DBU and in these instances the reactions were complete in < 30 min.



Scheme 12. Reagents and conditions: [Bu₄N]Br, NaOAc, NaHCO₃, 130 °C, Pd-cat.

Motevalli's *N*-(diphenylphosphino)triethylammonium chloride (**IL1**) and *N*-(diphenylphosphino)tributylammonium chloride (**IL2**), have been used successfully in Heck couplings of iodobenzene and styrene (Figure 3 and Table 3).[56]

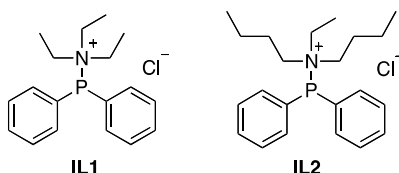
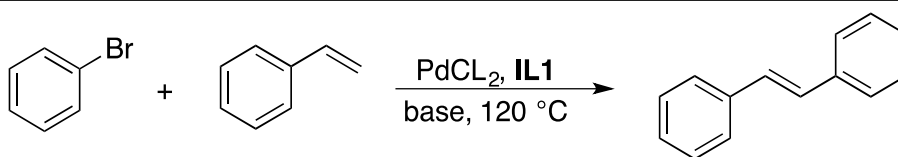


Figure 3. Structures of *N*-(diphenylphosphino)triethylammonium chloride (**IL1**) and *N*-(diphenylphosphino)tributylammonium chloride (**IL2**).

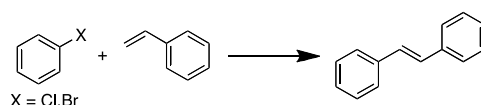
2.4. Studies using imidazolium, pyridinium, phosphonium and ammonium RTILs

The coupling of electron poor chloroarenes with mono and di-substituted olefins across a range of RTILs and Pd-sources has been examined.[57] The model system, resulting in the synthesis of stilbene from chlorobenzene and styrene was best conducted with simple, e.g. PdCl₂, phospho-based Pd-sources (Scheme 13). RTILs examined included: imidazolium, ammonium and phosphonium salts. The tetraalkylammonium salts, in particular [Bu₄N][Br], were superior permitting the coupling of chloroarenes in the presence of less active catalysts such as PdCl₂ and Pd(Ph₃P)₄. Regardless of the conditions used, all imidazolium based RTILs gave poor results, e.g. 22 % for [bmim][BF₄] and 13 % for [bmim][Br] whereas TBAB gave 72 % of the desired stilbene. With [bmim][BF₄] there was clear evidence of the formation of Pd black.[57]



Entry	Base	Time (h)	Yield %
1	Na ₂ CO ₃	24	-
2	CaCO ₃	24	-
3	DBU	25 min	90
4	NaOH	8 min	93
5	Et ₃ N	24	60
6	Bu ₃ N	24	50

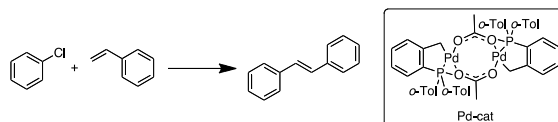
Table 3. Effect of different bases on Heck reaction of bromobenzene and styrene in *N*-(diphenylphosphino)triethylammonium chloride (IL1).



Scheme 13. Reagents and conditions: PdCl₂ or Pd(Ph₃P)₄, 150 °C, [bmim][BF₄] or [bmim]Br or Bu₄NBr reaction of mono and di-substituted olefins in a diversity of RTILs.

Heck couplings have also been conducted in the thermally and chemically stable [P_{6′6′6′14}][X] quaternary phosphonium salts, where X=Br, Cl, I, BF₄⁻ and CH₂(CH₂)₈CO₂⁻ and the resulting FILs used in the coupling of iodobenzene with methylacrylate.[58] The effect of anion on the coupling outcome was determined by screening using Pd₂dba₃.CHCl₃ and each of the phosphonium FILs in turn. High coupling efficiency was observed [P_{6′6′6′14}][CH₂(CH₂)₈CO₂] (75%) and [P_{6′6′6′14}][Cl] (78%), with [P_{6′6′6′14}][Cl] also providing a simpler work up.

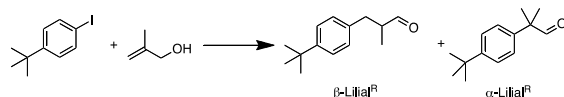
The coupling of bromobenzene and butyl acrylate was examined in a range of what were designated, non-aqueous ionic liquids (NAILs), with *trans*-di(μ-acetato)-bis[*o*-(di-*o*-tolylphosphino)benzyl] dipalladium(II) as catalyst (Scheme 14).[59, 60] These NAILs were drawn from Bu₄NBr, Bu₄NOAc, 1-methyl-3-propylimidazolium bromide ([MPIM]Br), tri-*n*-butyl-*n*-hexadecylphosphonium bromide (TBHDP), triphenylmethylphosphonium chloride (TPMPC) and triphenylmethylphosphonium bromide (TPMPB), all of which gave homogeneous reaction media and permitted facile catalyst recycling.



Scheme 14. Reagents and conditions: 0.5% Pd-cat, NAIL.

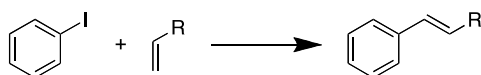
3. Functionalized Ionic Liquids (FILs)

Functionalised (FILs) or, as they are sometimes know, task specific ionic liquids, incorporate additional functional moieties within the cation or anion.[61] FILs can be discrete liquids or be supported reagents and have applications as reagents and catalysts.[62]-[66] FILs have been examined as novel media for the Pd(OAc)₂ mediated Heck reaction of 2-methylprop-2-en-1-ol and 4-*tert*-butyliodobenzene in [*i*Pr₂N(CH₂)₂.mim][NTf₂] and [*i*Pr₂N(CH₂)₂O(CH₂)₂N₁₁₂][NTf₂]. In [Pr₂N(CH₂)₂.mim][NTf₂] only 32 % of 3-(4-*tert*-butylphenyl)-2-methylpropanal (β -Lilial[®]) was present after 10 h; this increased to 84% on using [*i*Pr₂N(CH₂)₂O(CH₂)₂N₁₁₂][NTf₂]. These outcomes correlate well with the relative basicity of these two FILs. The equivalent coupling in neat Hünig's base showed a conversion of 39%, supporting a catalytic role for the PILs.[67] The selectivity between 3-(4-*tert*-butylphenyl)-2-methylpropanal and 2-(4-*tert*-butylphenyl)-3-methylpropanal was found to be >95% respect to β -Lilial[®] and independent of the PIL basicity (Scheme 15).



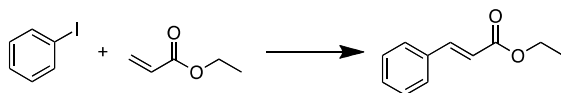
Scheme 15. Reagents and conditions: Pd(OAc)₂, 95 °C, time, base tethered-RTIL.

RTILs based on dialkylimidazolium salts have attracted particular attention, as they are easy to prepare and handle, having good solubility for many substrates and molecular catalyst and are readily synthesised through a variety of green chemistry approaches.[68]-[70] 1-Octyl-3-methylimidazolium nonafluorobutanesulfonate [omim][FNBS] represents a novel dialkylimidazolium based hydrophobic ionic liquid which is effective in ligand-free Heck couplings with electron deficient olefins (Scheme 16).[71]



Scheme 16. Reagents and conditions: Pd(OAc)₂, Et₃N, [omim][FNBS], 100 °C, 3-12 h.

Nitrile modified imidazolium and pyridinium salts have been used in Pd-catalysed cross-coupling reactions (Scheme 17).[72, 73] These FILs are highly effective solvents for the Heck reaction with excellent yields observed (Table 4).[74]

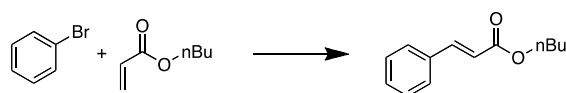


Scheme 17. Reagents and conditions: 5 mol % Pd, [C₃CNmim][Tf₂N], 80 °C, 12 h.

No.	Cat.	Base	Time (h)	Additive	Yield %
1	PdCl ₂	[cholinium][OAc]	12	HCOONH ₄	99
2	(C ₃ CNdmim) ₂ [PdCl ₄]	[cholinium][OAc]	12	HCOONH ₄	96

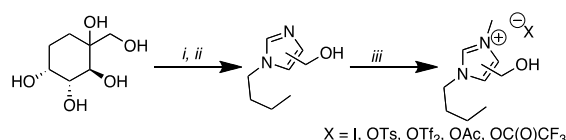
Table 4. Selected examples of the Heck Coupling of Iodobenzene with ethyl acrylate in [C₃CNmim][Tf₂N] at 80 °C.

Numerous studies have highlighted the deprotonation of imidazolium RTILs to yield an imidazol-2-ylidene *N*-heterocyclic carbene (NHC) as a crucial step in subsequent reactions complex generated by deprotonation of the ionic liquid cation.[75-78] Many transition-metal carbene complexes have been prepared and their catalytic applications described.[79, 80] This has led to the evaluation of novel RTILs as catalysts in Pd-coupling reactions.[81, 82] Metal-NHC complexes have been generated and examined in RTILs, with the metal-NHC complex reactivity examined for Heck coupling efficacy in DMF and [bmim][NTf₂] based of an NHC located from an ionic liquid cation and investigate the catalytic activity in both molecular and ionic liquid solvents in the Heck coupling of butyl acrylate and bromobenzene (Scheme 18). [83-86]



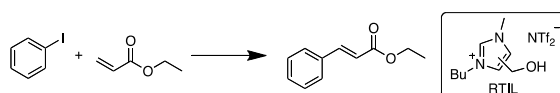
Scheme 18. Reagents and conditions: 5 mol% Pd-cat, Cs₂CO₃, [Bmim][NTf₂], 150 °C, 18 h.

Fructose has been used as a renewable resource in the synthesis of novel hydroxymethylimidazolium based protic ionic liquids (PILs) (Scheme 19).[86-91]



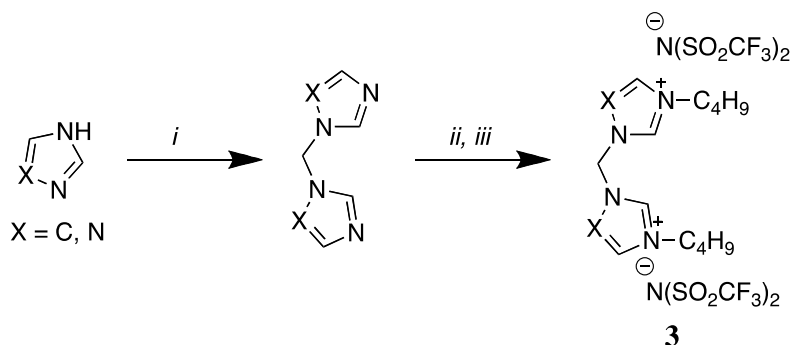
Scheme 19. Reagents and conditions: (i) NH₃, CH₂O, CuCO₃; (ii) BuBr, KOtBu, EtOH; (iii) MeI, CH₂Cl₂; Metal-X.

Use of these fructose derived PILs in the Pd(OAc)₂ mediated Heck coupling of methyl acrylate with iodobenzene afforded rapid conversion (1 h) to methyl cinnamate in > 95% yield at 100 °C (Scheme 20). Both the PIL and catalyst were readily recycled with no loss of activity.



Scheme 20. Reagents and conditions: 2 mol % Pd(OAc)₂, Et₃N, RTIL, 100 °C.

Shreev, *et al*, synthesized the new RTIL, shown in (Scheme 21), which contain the dication 1,1'-methylene-3,3'-dialkylbis(imidazolium) or 1,1'-methylene-4,4'-dialkylbis(1,2,4-triazolium) with NTf₂ as the anion, and evaluated its efficacy in the Heck reaction (Table 5).[92]



Scheme 21. Reagents and conditions: (i) CH₂Cl₂ or CH₂Br₂, KOH, Bu₄NBr; (ii) RI, 110-130 °C, 20; (iii) LiN(SO₂CF₃)₂, CH₃OH/H₂O (10:1), RT, 2 h.

Entry	Pd source	R	X	Time (h)	Yield %
1	PdCl ₂	H	I	6	92
2	PdCl ₂	H	Br	18	71
3	PdCl ₂	H	Cl	24	3
4	PdCl ₂	NO ₂	Br	18	69
5	PdCl ₂	CF ₃	Br	18	57
6	PdCl ₂	CH ₃	Br	12	76

Table 5. Heck cross-coupling reactions in the ionic liquid-3 and different anions (X) with selected aryl halides and butyl acrylate.

In a related study Shreeve *et al*, also examined the use of a range basic RTILs as both the base and solvent for the Heck coupling of iodobenzene and butyl acrylate (see Figure 3 for chemical structures of the BILs). With BILs, **BIL-1**, **BIL-2** and **BIL-3** quantitative conversion and regioselectivity was observed. All other BILs (**BIL-4-BIL-8**) displayed low to no reactivity

under the conditions examined (Table 6). In this study, these results suggest that RTILs with pendant aliphatic tertiary amines are superior to the pyridinium salts.[93]

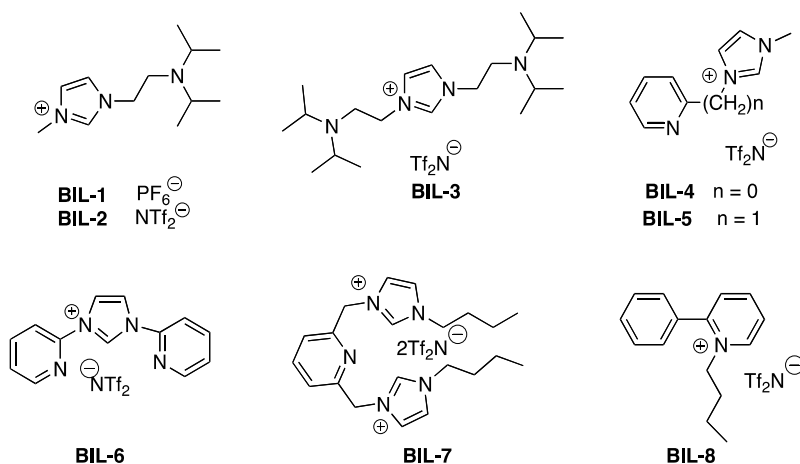


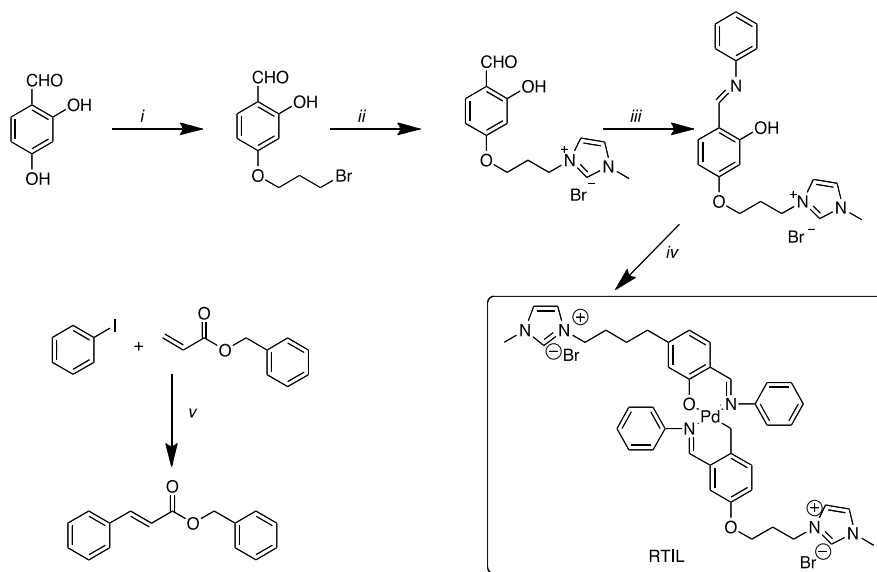
Figure 4. Chemical structures of Basic ionic liquid cations.

ILs	BIL-1	BIL-2	BIL-3	BIL-4	BIL-5	BIL-6	BIL-7	BIL-8
Conv.[%]	100	100	100	0	41	0	5	0

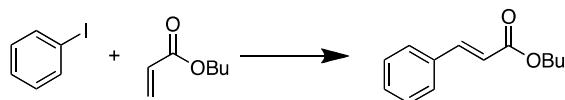
Table 6. Heck reactions between butyl acrylate and iodobenzene in the presence of basic ionic liquid (BIL1-BIL8) (Fig. 3).

The novel imidazolium RTIL tagged Pd-Schiff base complex was active in both Heck and Suzuki couplings in aqueous media. Relative to other Pd-catalyzed reactions in aqueous media, this catalyst was effective in the coupling of water insoluble aryl halides without the aid of a phase transfer catalyst or organic solvents (Scheme 22).[94] Optimised Heck coupling conditions required the use of 1 mol % catalyst, K_2CO_3 and with iodobenzene and cyclohexyl acrylate gave benzyl cinnamate in 96% yield, (Scheme 23).

Chitosan supported $Pd(OAc)_2$ nanoparticles (Pd-NP) in TBAB with added tetrabutyl ammonium acetate (TBAA) gave rise to very rapid Heck couplings of aryl bromides, iodides and activated chlorides (Scheme 23).[95] The supported catalyst was amenable to multiple recycles, whereas the free nano particles rapidly lost activity.

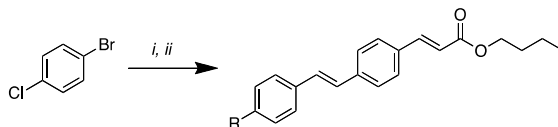


Scheme 22. Reagents and conditions: (i) $\text{BrCH}_2\text{CH}_2\text{CH}_2\text{Br}$, acetone, NaHCO_3 , 60°C , 60 h; *N*-methylimidazole, 80°C , 48 h; (iii) aniline, EtOH, reflux, 4 h; $\text{Pd}(\text{OAc})_2$; (iv) H_2O , imidazolium ILs, 80°C and 4 h; (v) RTIL, 80°C , K_2CO_3 .



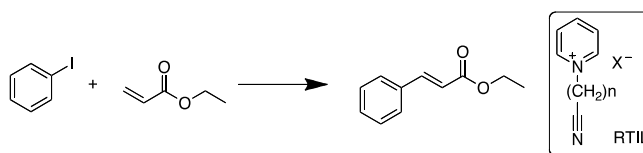
Scheme 23. Reagents and conditions: Pd-NP /chitosan, $[\text{Bu}_4\text{N}][\text{Br}]/[\text{Bu}_4\text{N}][\text{OAc}]$, 15 min to 1.5 h, 130°C .

With Pd-NP in a mixture of $[\text{Bu}_4\text{N}][\text{Br}]/[\text{Bu}_4\text{N}][\text{OAc}]$ it was possible to couple 1-bromo-4-chlorobenzene with two different olefins in a one-pot sequential manner by activating the C-Br and C-Cl bonds on the aromatic ring at two different temperatures of 100 and 120°C (Scheme 24).[96]



Scheme 24. Reagents and conditions: (i) butyl acrylate, Pd-NP, $[\text{Bu}_4\text{N}][\text{Br}]/[\text{Bu}_4\text{N}][\text{OAc}]$, 100°C , 30 min; (ii) styrene, Pd-NP, $[\text{Bu}_4\text{N}][\text{Br}]/[\text{Bu}_4\text{N}][\text{OAc}]$, 120°C , 30 min.

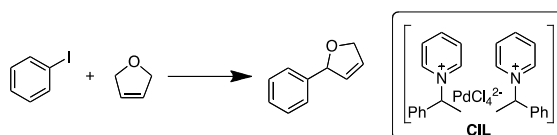
There have been multiple reports on the use of nitrile-functionalized RTILs, such as the imidazolium and pyridinium based systems, in Pd-catalysed reactions, including the Heck reaction. Heck coupling in these FILs typically afforded a 90% isolated yield of the desired product (Scheme 25).[97, 98]



Scheme 25. Reagents and Conditions: 5 mol % Pd-cat; IL, 80 °C, 12 h.

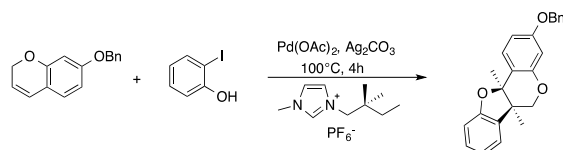
3.1. Chiral Ionic Liquids (CIL)

To date the use of chiral RTILs (CILs) in Heck couplings has met with limited success. The arylation of 2,3-dihydrofuran with iodobenzene catalysed by a chiral pyridinium ILs with $[\text{PdCl}_4]^{2-}$ (Figure 4), (used as a co-solvent with $[\text{bmim}][\text{PF}_6]$), (Scheme 26).[99]



Scheme 26. Reagents and conditions: 2,3-dihydrofuran with iodobenzene catalysed by CILs with $[\text{PdCl}_4]^{2-}$, Et₃N, $[\text{bmim}][\text{PF}_6]$, 100 °C.

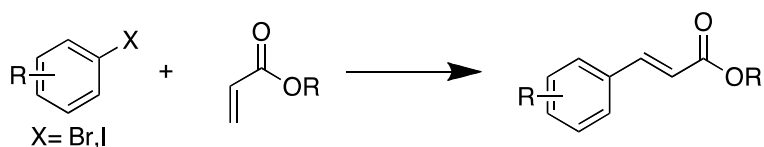
However, the use of the chiral $[\text{bmim}][\text{PF}_6]$, did give rise to the desired 7-benzyloxy-2H-chromene in good yield and modest e.e. (15%) (Scheme 27).[100]



Scheme 27. Reagents and conditions: The oxyarylation of 7-benzyloxy-2H-chromene in CILs, $\text{Pd}(\text{OAc})_2$, Ag_2CO_3 , 100 °C and 4 h.

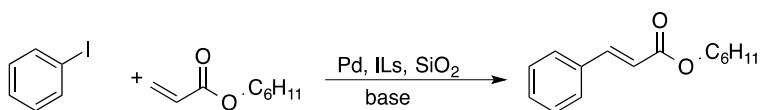
3.2. Supported ionic liquid phase (SILP) catalyst system

Immobilisation of the Pd-catalyst and the RTIL onto high surface area porous solids such as silica yields a supported ionic liquid phase (SILP) catalyst system. SLIPs are considered, while being solids, to contain the active species comprise solubilized in the IL phase behaving as a homogeneous catalyst, and as such offer the potential for novel reactivity. Suzuki has examined this reactivity with a range of $\text{Pd}(\text{OAc})_2$ /silica based SLIP catalyst systems. The SLIPs were air and thermally stable, provided simple storage conditions, easily recyclable and highly effective in the Heck coupling of substituted arylhalides with vinyl esters (Scheme 28).[101, 102]



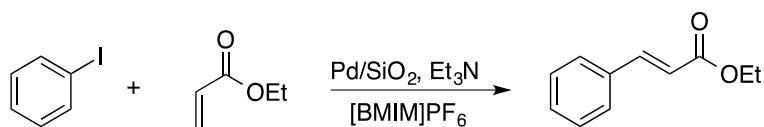
Scheme 28. Reagents and conditions: Pd(OAc)₂, SILP, Na[(Ph)₂P-(*m*-PhSO₃)], 150 °C, 7-17 h.

In a related study, Pd(OAc)₂ and [bmim][PF₆] were immobilized on reversed phase silica gels such as aminopropylated or *N,N*-diethylaminopropylated silica.[103] The Heck reaction between iodobenzene and cyclohexyl acrylate was carried out as shown in (Scheme 29). The catalyst was reused five times with no loss of catalytic activity.



Scheme 29. Reagents and conditions: Pd(OAc)₂, [bmim][PF₆]-SiO₂, 30 °C, 1.5-3 h.

Yokoyama *et al.*, has been reported the use of a SiO₂ supported Pd(II)/[bmim][PF₆] as a highly active and reusable SLIP for the phosphine free Heck reaction of iodobenzene and ethyl acrylate (Scheme 30).[104] The addition of low levels of Et₃N increased the [bmim][PF₆] decomposition temperature in this system from 130 to 160 °C.



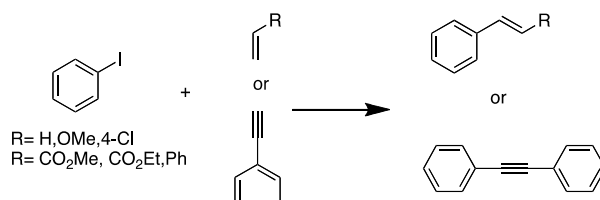
Scheme 30. Reagents and conditions: Pd(II)-SiO/[bmim][PF₆], Pd/SiO₂, Et₃N, [bmim][PF₆], 130-160 °C, 24 h.

3.3. Ultrasonic synthesis approaches

In the RTILs, 1,3-di-*n*-butylimidazolium bromide [bbim][Br] and 1,3-di-*n*-butylimidazolium tetrafluoroborate [bbim][BF₄], under ultrasonic irradiation significant rate enhancements were noted for the NaOAc / PdCl₂ mediated coupling of substituted iodobenzenes with alkenes/alkynes at 120 °C (Scheme 31).[105] Isolated yields were good to excellent (up to 87%) with only the *trans* product obtained. These couplings only required 1.5-3 h.

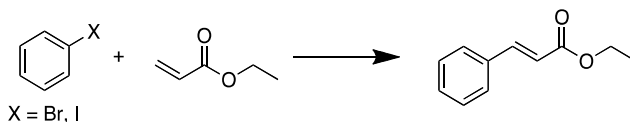
3.4. Microwave synthesis approaches

Microwave heating has been applied to the Heck reaction in RTILs significantly reducing the time required to effect coupling, and influencing product yield and the extent of by-product generation.[106, 110] Generally microwave approaches have focused on the use of aryl iodides



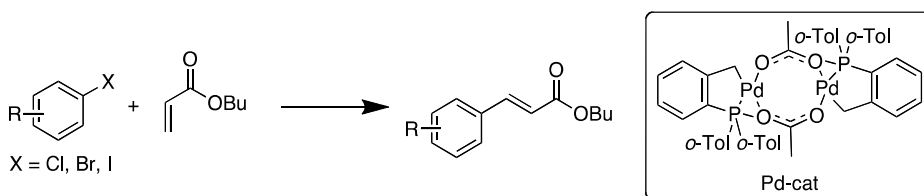
Scheme 31. Reagents and conditions: (i) 2 mol% PdCl₂, [bbim][Br] or [bbim][BF₄], 120 °C, 1.5-3 h.

and active aryl bromide, such as those reported by Larhed *et al* in [bmim][PF₆] (Scheme 32). [111] Using 4 mol % PdCl₂ (4 mol %), P(*o*-tolyl)₃ as the added Pd-ligand, reactions were complete after 5-45 min, at 180 – 220 °C. The catalyst system and RTIL were and the time 20 minutes and 45 minutes for trans formations without the phosphine ligand. This system was recyclable at least five times, and the volatile product was directly isolated in high yield by rapid distillation under reduced pressure.[111]



Scheme 32. Reagents and conditions: PdCl₂, P(*o*-tolyl)₃, Et₃N, [bmim][PF₆], μW, 180-220 °C, 5-45 min.

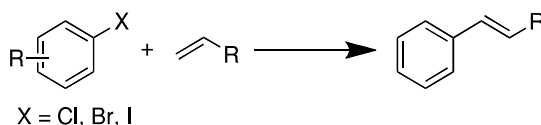
More complex Pd-catalysis such as Herrmann's palladacycle, *trans*-di(μ-acetato)bis(*o*-di-*o*-tolylphosphanyl)-benzyl]dipalladium, have been developed in efforts to enhance Pd-coupling outcomes with unreactive aryl chlorides.[112] Using this Pd-catalyst (1.5 – 10 mol %), Heck coupling in [bmim][PF₆] / dioxane mixtures with aryl chlorides and butyl acrylate gave the desired cinnamic esters.[113] High levels of phosphine ligand (3-20 %) were required dependent on the reactivity of the aryl chloride. Under microwave irradiation the yields were moderate to excellent (Scheme 33).[114]



Scheme 33. Reagents and conditions: Herrmann's palladacycle, [(*t*-Bu)₃PH][BF₄], Cy₂NMe, [bmim][PF₆]/dioxane, μW, 180 °C, 30-60 min.

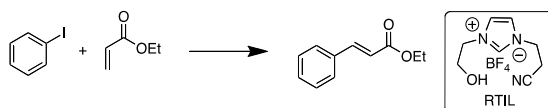
Microwave irradiation of [omim][BF₄] with 3-5 mol % Pd/C proved effective in the phosphine free Heck coupling of aryl iodides and aryl bromides with butyl acrylate. The reactions were typically complete in 1.5 min affording 33-89% yield of the *trans*-butyl cinnamates. This

microwave based Pd-coupling approach was effective across a range of olefinic substrates including styrene, 2-methylbutyl acrylate and methyl cinnamate with iodobenzene. The steric bulk of the olefin affected reaction outcome with yields ranging from 27 – 86 % (Scheme 34). [115]



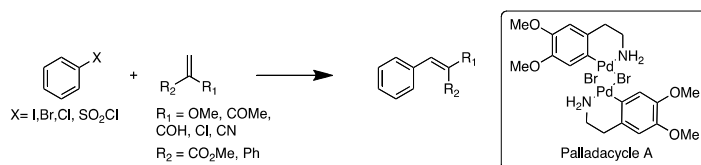
Scheme 34. Reagents and conditions: Pd/C, (n-Bu)₃N, [omim][BF₄], μW, 1.5 min at 375W.

Under conventional heating for 24 h, the Heck coupling of iodobenzene with ethyl acrylate in 1-(2-cyanoethyl)-3-(2-hydroxyethyl)-1*H*-imidazol-3-ium tetrafluoroborate, afforded a modest 25% yield of ethyl cinnamate with PdCl₂. Using microwave irradiation (200 W, 120 °C), the same reaction system gave 88% yields of ethyl cinnamate in 5 min (Scheme 35). The system showed good stability and maintained the efficiency after six consecutive runs without significant loss of activity.[116]



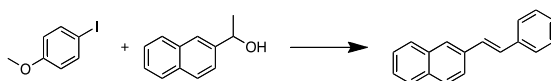
Scheme 35. Reagents and conditions: PdCl₂, RTIL, μW, 120 °C, 5-20 min.

Under microwave irradiation in TBAB, the {Pd[C₆H₂(CH₂CH₂NH₂)-(OMe)₂,3,4](μ-Br)}₂ (palladacycle A) mediated Heck coupling of aryl bromides, aryl iodides, aryl chlorides and arene sulfonyl chlorides increased dramatically with reaction times reducing from hours to minutes (Scheme 36).[117]



Scheme 36. Reagents and conditions: palladacycle A, [Bu₄N][Br], μW, 130 °C, 1-20 min.

The scope of the Heck olefin precursor has been extended through the use of microwave approached to 2° alcohols in a dehydrative Heck coupling approach. The combination of [hmim][Br], [PdCl₂(PPh₃)₂] along with LiCl and the combination of HCO₂Na and piperidine and microwave irradiation reduced reaction times to 15 min (Scheme 37).[118]

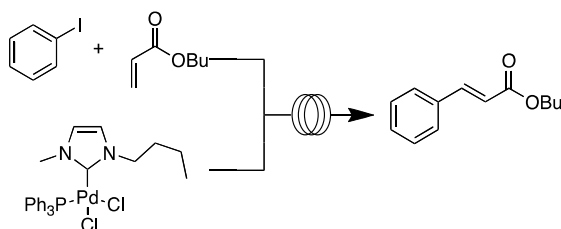


Scheme 37. Reagents and conditions: [hmim][Br], HCO_2Na , $\text{Pd}(\text{OAc})_2$, PPh_3 , μW , $150\text{ }^\circ\text{C}$ at 15-40 min.

3.5. Flow chemistry approaches

Micro reactor technology has had a significant impact on the chemical synthesis and production. This technology has many advantages including: 1) highly efficient material mixing; 2) high volume to area ratio; 3) efficient heat transfers ability; 4) the avoidance of "hot spots" by effective temperature control and mixing; and 5) high operational safety.[119] The transition metal catalysed reactions have been reported by using a micro flow system, such as hydrogenation[120] and oxidation,[121] and the Heck reaction.[122]

RTILs present a challenge for flow chemistry approaches due to their often-high viscosity. Ryu has examined the use of a low viscosity RTIL, [bmim]NTf₂ as well as a high viscosity RTIL, [bmim][PF₆].[122] The Heck coupling of iodobenzene with butyl acrylate was sluggish in [bmim][PF₆], but the use of [bmim][NTf₂] in a CPC CYTOS lab system gave 10 g.h⁻¹ of, and in a single run with catalyst recycling, 115.3g of butyl cinnamate (Scheme 38).[123]



Scheme 38. Reagents and conditions: 0.1-0.5 mL.h⁻¹, [BMIM]NTf₂, $130\text{-}150\text{ }^\circ\text{C}$, 10-50 min residence time.

4. Conclusions

In the last twenty years has shown an increasing interest in applying ionic liquids as green solvents in organic synthesis. This approach has been extended to the palladium-catalysed Heck reactions as a key synthetic protocol for C-C bond formation. Factors affecting this approach including the type of ionic liquid used, the base and the catalyst have been investigated by many research groups. In addition, limited number of microwave-based and flow chemistry based Heck reactions have been reported. Despite these efforts, only simple aryl halides and olefines were used in the reported investigations. Active research in this area is still required to increase the scope of Heck reaction in ILs to involve more complicated substrates and larger scale.

Author details

Ahmed Al Otaibi¹, Christopher P. Gordon² and Adam McCluskey^{1*}

*Address all correspondence to: Adam.McCluskey@newcastle.edu.au

1 Chemistry, School of Environmental & Life Sciences, The University of Newcastle, University Drive, Callaghan NSW, Australia

2 School of Science and Health, University of Western Sydney, Australia

References

- [1] Hill T, Odell LR, Edwards JK, Graham ME, McGeachie AB, Rusak J, Quan A, Abagyan R, Scott JL, Robinson PJ, McCluskey A. Small molecule inhibitors of dynamin I GTPase activity: development of dimeric tyrosophostins. *Journal of Medicinal Chemistry* 2005;48 7781-7788.
- [2] Hill A, Gordon CP, McGeachie AB, Venn-Brown B, Odell LR, Chau N, Quan A, Mariana A, Sakoff JA, Chircop M, Robinson PJ, McCluskey A. Inhibition of dynamin mediated endocytosis by the dynoles-synthesis and functional activity of a family of indoles. *Journal of Medicinal Chemistry* 2009;52 3762-3767.
- [3] Yin L, Liebscher J. Carbon-carbon coupling reactions catalyzed by heterogeneous palladium catalysts. *Chemical Reviews* 2007;107 133-173.
- [4] Han F-S. Transition-metal-catalyzed Suzuki-Miyaura cross-coupling reactions: a remarkable advance from palladium to nickel catalysts, *Chemical Society Reviews* 2013;42, 5270-5298.
- [5] Vougioukalakis GC, Grubbs RH. Ruthenium-based heterocyclic carbene-coordinated olefin metathesis catalysts, *Chemical Reviews* 2010;110, 1746-1787.
- [6] Hill TA, Odell LR, Quan A, Ferguson G, Robinson PJ, McCluskey A. Long chain amines and long chain ammonium salts as novel inhibitors of dynamin GTPase activity. *Bioorganic and Medicinal Chemistry Letters* 2004;14 3275-3278.
- [7] Hill TA, Stewart SG, Gordon CP, Ackland SP, Gilbert J, Sauer B, Sakoff JA, McCluskey A. Norcantharidin Analogues: Synthesis, anticancer activity and protein phosphatase 1 and 2A inhibition. *Chemistry Medicinal Chemistry* 2008;3 1878-1892.
- [8] Hill TA, Stewart SG, Sauer B, Gilbert J, Ackland SP, Sakoff JA, McCluskey A. Heterocyclic substituted cantharidin and norcantharidin analogues synthesis, protein phosphatase (1 and 2A) inhibition, and anti-cancer activity. *Bioorganic and Medicinal Chemistry Letters* 2007;17 3392-3397.

- [9] Odell LR, Howan D, Gordon CP, Robertson MJ, Chau N, Mariana A, Whiting AE, Abagyan R, Daniel JA, Gorgani NN, Robinson PJ, McCluskey A. The Pthaladyns: GTP competitive inhibitors of dynamin I and II GTPase derived from virtual screening. *Journal of Medicinal Chemistry* 2010;53 5267-5280.
- [10] Tarleton M, Robertson MJ, Gilbert J, Sakoff JA, McCluskey A. Library synthesis and cytotoxicity of a family of 2-phenylacrylonitriles and discovery of an estrogen dependent breast cancer lead compound. *Medicinal Chemistry Communications* 2011;2 31-37.
- [11] Bryan MC, Dillon B, Hamann LG, Hughes GJ, Kopach ME, Peterson EA, Pourashraf M, Raheem I, Richardson P, Richter D, Sneddon H.F. Sustainable Practices in Medicinal Chemistry: Current State and Future Directions. *Journal of Medicinal Chemistry* 2013;56 6007-6081.
- [12] Constable DJC, Jimenez-Gonzalez C, Henderson RK. *Organic Process Research and Development* 2007;11 133-137.
- [13] Parczewski KG, Grodowska K Organic solvents in the pharmaceutical industry. *Acta Poloniae Pharmaceutica* 2010; 67 3-12.
- [14] Gordon CP, Hizartzidis L, Tarleton M, Sako JA, Gilbert J, Campbell BE, Gasser RB, McCluskey A. Discovery of acrylonitrile-based small molecules active against *Haemophilus contortus*. *Medicinal Chemistry Communications* 2014;5 159-164.
- [15] McGeachie AB, Odell LR, Quan A, Chau N, Hill TA, Keating DJ, Cousin MA, Dam EMv, Daniel J, Mariana A, Whiting A, Perera S, Novelle A, Gilbert J, Sakoff JA, Chircop M, McCluskey A. Pyrimidyn compounds: dual-action small molecule pyrimidine-based dynamin inhibitors. *ACS Chemical Biology* 2013;8 1507-1518.
- [16] Odell LR, Howan D, Gordon CP, Robertson MJ, Chau N, Mariana A, Whiting AE, Abagyan R, Daniel JA, Gorgani NN, Robinson PJ, McCluskey A. The Pthaladyns: GTP competitive inhibitors of dynamin I and II GTPase derived from virtual screening. *Journal of Medicinal Chemistry* 2010;53 5267-5280.
- [17] Gordon CP, Venn-Brown B, Robertson MJ, Young KA, Chau N, Quan A, Robinson PJ, McCluskey A. Development of second-generation indole-based dynamin GTPase inhibitors. *Journal of Medicinal Chemistry* 2013;56 46-59.
- [18] Tarleton M, McCluskey A. A flow chemistry route to 2-phenyl-3-(1H-pyrrol-2-yl)propan-1-amines. *Tetrahedron Letters* 2011;52 1583-1586.
- [19] Gordon CP, Byrne N, McCluskey A. A facile, protic ionic liquid route to N-substituted 5-hydroxy-4-methyl-3-oxoisindoline-1-carboxamides and N-substituted 3-oxoisindoline-4-carboxylic acids. *Green Chemistry* 2010;12 1000-1006.
- [20] Hizartzidis L, Tarleton M, Gordon CP, McCluskey A. Chemoselective flow hydrogenation approaches to isoindole-7-carboxylic acids and 7-oxa-bicyclo[2.2.1]heptanes. *RSC Advances* 2014;4 9709-9722.

- [21] Otaibi AA, Gordon CP, Gilbert J, Sakoffb JA, McCluskey A. The influence of ionic liquids on the Knoevenagel condensation of 1H-pyrrole-2-carbaldehyde with phenyl acetonitriles – cytotoxic 3-substituted-(1H-pyrrol-2-yl)acrylonitriles. *RSC Advances* 2014;4 19806-19813.
- [22] Mizoroki T, Mori K, Ozaki A. Arylation of olefin with aryl iodide catalyzed by palladium. *Bulletin of the Chemical Society, Japan* 1971;44 581-584.
- [23] Heck R, Nolley J. Palladium-catalyzed vinylic hydrogen substitution reactions with aryl, benzyl, and styryl halides. *Journal of Organic Chemistry* 1972;37 2320-2322
- [24] Beletskaya, I., Cheprakov, A. The Heck reaction as a sharpening stone of palladium catalysis. *Chemical Reviews* 2000;100 3009-3066.
- [25] Beletskaya I, Cheprakov A. The Heck Reaction as a Sharpening Stone of Palladium Catalysis. *Chemical Reviews* 2000;100 3009-3066.
- [26] Trzeciak AMZI, JJ. The role of ionic liquids in palladium-catalyzed C-C bond forming reactions. In *Advances Organometallic Chemistry Research*; Yamamoto K, Ed, Nova Science NewYork, NY, USA, 2007.
- [27] Liu Y, Wang SS, Liu W, Wan QX, Wu HH, Gao GH. Transition metals catalysed carbon-carbon couplings mediated with functionalized ionic liquid, supported ionic liquid phase or ionic liquid media. *Current Organic Chemistry* 2009;13 1322-1346.
- [28] Welton T. Room-temperature ionic liquids, solvents for synthesis and catalysis. *Chemical Reviews* 1999;8, 2071-2084.
- [29] Yan Cao Y, Wu J, Zhang J, Li h, Zhang Y, He J. Room temperature ionic liquids (RTILs): A new and versatile platform for cellulose processing and derivatization. *Chemical Engineering Journal* 2009;147 13-21.
- [30] Carmichael AJ, Earle MJ, Holbrey JD, Mc Cormac PB, Seddon K. R. The Heck reaction in ionic liquids: A multiphasic catalyst system. *Organic Letters* 1999; 1 997-1000.
- [31] J. Mo LX, Xiao J. Ionic liquid-promoted, highly regioselective Heck arylation of electron-rich olefins by aryl halides. *Journal of the American Chemical Society* 2005;127 751-760.
- [32] Hagiwara H, Shimizu Y, Hoshi T, Suzuki T, Ando M, Ohkubo K, Yokoyama C. Heterogeneous Heck reaction catalyzed by Pd/C in ionic liquid. *Tetrahedron Letters*. 2001;42 4349-4351.
- [33] Kabalka GW, Dong G, Venkataiah B. Rhodium-catalyzed cross-coupling of allyl alcohols with aryl-and vinylboronic acids in ionic liquids. *Organic Letters* 2003;5 893-895.
- [34] Kabalka GW, Venkataiah B, Dong G. Preparation of substituted allyl acetates and sulfones from Baylis-Hillman adducts in ionic liquid media. *Tetrahedron Letters* 2003;44 4673-75.

- [35] Kabalka GW, Dong G, Venkataiah B. Investigation of the behavior of arene diazonium salts with olefins in BmimPF₆. *Tetrahedron Letters* 2004;45 2775-2778.
- [36] Yogesh R. J. 1-Butyl-3-methylimidazolium tetrafluoroborate as a green reaction medium. *Synthesis Letters* 2004;(4) 746-747.
- [37] Xie X, Chen B, Lu J, Han J, She X, Pan X. Synthesis of benzofurans in ionic liquid by a PdCl₂-catalyzed intramolecular Heck reaction. *Tetrahedron Letters* 2004;45 6235-6237.
- [38] Bourque SC, Maltais F, Xiao WJ, Tardif O, Alper H, Arya P, Manzer L. E. Hydroformylation reactions with rhodium-complexed dendrimers on silica. *Journal of the American Chemical Society* 1999;121 3035-3038.
- [39] Bourque SC, Alper H, Manzer LE, Arya P. Hydroformylation reactions using recyclable rhodium-complexed dendrimers on silica. *Journal of the American Chemical Society* 2000;122 956-957.
- [40] Arya P, Panda G, V RN, Alper H, Bourque SC, Manzer LE. Solid-phase catalysis: a biomimetic approach towards ligands on dendric arms to explore recyclable hydroformylation reactions. *Journal of the American Chemical Society* 2001;123 2399-2402.
- [41] Park SB, Alper H. Highly efficient, recyclable Pd(II) catalysts with bisimidazole ligands for the Heck reaction in ionic liquids. *Organic Letters* 2003;5 3209-3212.
- [42] Antebi S, Arya P, Manzer LE, Alper H. Carbonylation reactions of iodoarenes with PAMAM dendrimer-palladium catalysts immobilized on silica. *Journal of Organic Chemistry* 2002;67 6623-6625.
- [43] Park SB, Alper H. Highly Efficient, Recyclable Pd(II) catalysts with bisimidazole ligands for the Heck reaction in ionic liquids. *Organic Letters* 2003;5 3209-3212.
- [44] Kaufmann D, Nouroozian M, Henze H. Molten salts as an efficient medium for palladium catalyzed C-C coupling reactions. *Synthesis Letters* 1996; 1091-1092.
- [45] Gerritsma DA, Robertson A, McNulty, J, Capretta A. Heck reactions of aryl halides in phosphonium salt ionic liquids: library screening and applications. *Tetrahedron Letters* 2004;45 7629-7631.
- [46] McNulty J, Cheekoor S, Bender TP, Coggan J. A. A Pronounced anionic effect in the Pd-catalyzed Buchwald-Hartwig amination reaction revealed in phosphonium salt ionic liquids. *European Journal of Organic Chemistry* 2007;1423-1428.
- [47] McNulty J, Jerald JN, Robertson A. Efficient carbonylation reactions in phosphonium salt ionic liquids: anionic effects. *Organic Letters* 2007;9 4575-4578.
- [48] McNulty J, Nair JJ, Cheekoori S, Larichev V, Capretta A, Robertson AJ. Scope and mechanistic insights into the use of tetradecyl(trihexyl)phosphonium bistriflimide: a remarkably selective ionic liquid solvent for substitution reactions. *Chemistry a European Journal* 2006;12 9314-9322.

- [49] Slag, VF, Vries de AHM; Vries de JG, Kellog RM. Practical aspects of carbon-carbon cross-coupling reactions using heteroarenes. *Organic Process Research and Development* 2010;14 30-47.
- [50] Giancarlo B, Sandro C, Giancarlo B. A molten n-Bu₄NOAc/n-Bu₄NBr mixture as an efficient medium for the stereoselective synthesis of (*E*)-and (*Z*)-3,3-diarylacrylates. *Synthesis Letters* 2002;(3) 439-444.
- [51] Bouquillon S, Gauchegui B, Estrine B, Hénin F, Muzart J. Heck arylation of allylic alcohols in molten salts. *Journal of Organometallic Chemistry* 2001;634 153-156.
- [52] Calo V, Del Sole R, Nacci A, Schingaro E, Scordari F. Synthesis and crystal structure of bis(2,3-dihydro-3-methylbenzothiazole-2-ylidene)palladium(II) diiodide: the first palladium complex with benzothiazole carbene ligands suitable for homogeneous catalysis. *European Journal of Organic Chemistry* 2000; 869-871.
- [53] Calo V, Nacci A, Monopoli A, Laera S, Cioffi N. Pd nanoparticles catalyzed Stereospecific synthesis of β-aryl cinnamic esters in ionic liquids. *Journal of Organic Chemistry* 2003;68 2929-2932.
- [54] Iranpoor N, Firouzabadi H, Khalili D, Motevalli S. Easily prepared azopyridines as potent and recyclable reagents for facile esterification reactions. An efficient modified Mitsunobu reaction. *Journal of Organic Chemistry* 2008;73 4882-4887.
- [55] Böhm VPW, Herrmann WA. Nonaqueous ionic liquids: superior reaction media for the catalytic Heck-vinylation of chloroarenes. *Chemistry a European Journal* 2000;6 1017-1025.
- [56] Gerritsma DA, Robertson A, McNult, J, Capretta A. Heck reactions of aryl halides in phosphonium salt ionic liquids: library screening and applications. *Tetrahedron Letters* 2004;45 7629-7631.
- [57] Herrmann WA, Böhm, VPW. Heck reaction catalyzed by phospho-palladacycles in non-aqueous ionic liquids. *Journal of Organometallic Chemistry* 1999;572 141-145.
- [58] Kaufmann DE, Nouroozian M, Henze H. Molten Salts as an Efficient Medium for Palladium Catalyzed C-C Coupling Reactions. *Synthesis Letters* 1996;11 1091-1092.
- [59] Lee S. One-pot noncovalent method to functionalize multi-walled carbon nanotubes using cyclomatrix-type polyphosphazenes. *Chemical Communications* 2006;1049-1051.
- [60] Brochwitz C, Feldhoff A, Kunz U, Vaultier M, Kirschning A. Comparison and Evaluation of Two Immobilisation Techniques for Task Specific Onium Salts (TSOS) in Mizoroki-Heck Cross Coupling Reactions. *Letters in Organic Chemistry* 2006;3 442-446.
- [61] Timofte RS, Woodward S. Preparation of silane-grafted pellets: silica bound reagents in a very convenient form. *Tetrahedron Letters* 2004;45 39-42.

- [62] Yoshizawa M, Hirao M, Ito-Akita K, Ohno H. Ion conduction in zwitterionic-type molten salts and their polymers. *Journal of Materials Chemistry* 2001;11 1057-1062.
- [63] Davis JH, Jr. Task-specific ionic liquids. *Chemistry Letters* 2004;33 1072-1077.
- [64] Visser AE, Swatloski RP, Reichert WM, Mayton R, Sheff SW A; Davis JH, Jr; Rogers RD. Task-specific ionic liquids for the extraction of metal ions from aqueous solutions. *Chemical Communications* 2001;135-136.
- [65] Forsyth SA, Gunaratne HQN, Hardacre C, McKeown A, Rooney DW, Seddon K. R. Utilisation of ionic liquid solvents for the synthesis of Lily-of-the-Valley fragrance (β -Lilial[®]; 3-(4-t-butylphenyl)-2-methylpropanal}. *Journal of Molecular Catalysis Part A: Chemistry* 2005;231 61-66.
- [66] Pore DM, Desai UV, Thopate TS, Wadgaonkar P. P. Anhydrous magnesium sulfate mediated solvent-free synthesis of dihydropyrimidin-2(1*H*)-ones at ambient temperature. *Australian Journal of Chemistry* 2007;60 435-441.
- [67] Pore DM, Shaikh TS, Undale KA, Gaikwad D. S. C. R. A green protocol for catalyst-free synthesis of 1-oxo-hexahydroxanthenes in aqueous medium. *Comptes Rendus Chimie* 2010;13 1429-1432.
- [68] Undale KA, Park YK, Park KM, Dagade DH, Pore D. M. A Revisit to the Hantzsch reaction: unexpected formation of tetrahydrobenzo[*b*]pyrans beyond polyhydroquinolines. *Synthesis Letters* 2011; 791-796.
- [69] Gaikwad DS, Park Y, Pore D. M. A novel hydrophobic fluorinated ionic liquid for ligand-free Mizoroki-Heck reaction. *Tetrahedron Letters*. 2012;53 3077-3081.
- [70] Zhao D, Fei Z, Geldbach TJ, Scopelliti R, Dyson P. J. Nitrile-functionalized pyridinium ionic liquids: synthesis, characterization, and their application in carbon-carbon coupling reactions. *Journal of the American Chemical Society* 2004;126 15876-15882.
- [71] Chiappe C, Pieraccini D, Zhao D, Fei Z, Dyson PJ. Remarkable cation and anion effects on Stille reactions in functionalised ionic liquids. *Advances Synthesis and Catalysis* 2006; 348 68-74.
- [72] Fei Z, Zhao D, Pieraccini D, Ang WH, Geldbach TJ, Scopelliti R, Chiappe C, Dyson PJ. Development of nitrile-functionalized ionic liquids for C-C coupling reactions: implication of carbene and nanoparticle catalysts. *Organometallics*. 2007;26 1588-1598.
- [73] Arduengo A J, Harlow RL, Kline M. A stable crystalline carben. *Journal of the American Chemical Society* 1991;113 361-363.
- [74] L. Xu WC, Xiao J. Heck Reaction in ionic liquids and the in Situ identification of N-heterocyclic carbene complexes of palladium. *Organometallics* 2000;19 1123-1127.

- [75] Mathews C J, Smith PJ, Welton T, White AJP, Williams D. J. In situ formation of mixed phosphine-imidazolylidene palladium complexes in room-temperature ionic liquids. *Organometallics* 2001;20 3848-3850.
- [76] McLachlan F, Mathews CJ, Smith PJ, Welton T. Palladium-catalyzed Suzuki cross-coupling reactions in ambient temperature ionic liquids: evidence for the importance of palladium imidazolylidene complexes. *Organometallics* 2003;22 5350-5357.
- [77] Poyatos M, Sanau M, Peris E. New Rh(I) and Rh(III) bisimidazol-2-ylidene complexes: synthesis, reactivity, and molecular structures. *Inorganic Chemistry* 2003;42 2572-2576.
- [78] Hu X, Castro-Rodriguez I, Meyer K. Copper complexes of nitrogen-anchored tripodal N-heterocyclic carbene ligands. *Journal of the American Chemical Society* 2003;125 12237-12245.
- [79] Poyatos M, Sanau M, Peris E. New Rh(I) and Rh(III) bisimidazol-2-ylidene complexes: synthesis, reactivity, and molecular structures. *Inorganic Chemistry* 2003;42 2572-2576.
- [80] Zhao D, Fei ZG, TJ, Scopelliti R, Dyson PJ. Nitrile-functionalized pyridinium ionic liquids: synthesis, characterization, and their application in carbon-carbon coupling reactions. *Journal of the American Chemical Society* 2004;126 15876-15882.
- [81] Jones SG, Yau HM, Davies E, Hook JM, Youngs TGA, Harper JB, Croft A. K. Ionic liquids through the looking glass: theory mirrors experiment and provides further insight into aromatic substitution processes. *Physical Chemistry Chemical Physics* 2010;12 1873-1878.
- [82] George RD, Edwards GL, Harper J. B. The effects of ionic liquids on azide-alkyne cycloaddition reactions. *Organic and Biomolecular Chemistry* 2010;8 5354-5358.
- [83] Gyton MR, Cole ML, Harper JB. Ionic liquid effects on Mizoroki–Heck reactions: more than just carbene complex formation. *Chemical Communications* 2011;47 9200-9202.
- [84] Handy ST, Okello M, Dickenson G. Solvents from biorenewable sources: ionic liquids based on fructose. *Organic Letters* 2003;5 2513-2515.
- [85] Abbott AP, Capper G, Davies DL, Munro HL, Rasheed RK, Tambyrajah V. Preparation of novel, moisture-stable, Lewis-acidic ionic liquids containing quaternary ammonium salts with functional side chains. *Chemical Communications* 2001; 2010-2011.
- [86] Abbott AP, Capper G, Davies DL, Rasheed RK, Tambyrajah V. Quaternary ammonium zinc- or tin-containing ionic liquids: water insensitive, recyclable catalysts for Diels–Alder reactions. *Green Chemistry* 2002;4 24-27.
- [87] Abbott AP, Capper G, Davies DL, Rasheed RK, Tambyrajah V. Novel solvent properties of choline chloride/urea mixtures. *Chemical Communications* 2003;70-71.

- [88] Trotter, J., Darby, W. In *Organic Syntheses*; Wiley: New York, 1955; Vol. Collect. Vol. III.
- [89] Diez-Barra E, de la Hoz A, Sanchez-Migallon A, Tejada J. *Synthesis Communications* 1993;23 1783-1786.
- [90] Jin CM, Twamley B, Shreeve JNM. Low-melting dialkyl- and bis(polyfluoroalkyl)-substituted 1,1'-methylenebis(imidazolium) and 1,1'-methylenebis(1,2,4-triazolium) bis(trifluoromethanesulfonyl)amides: ionic liquids leading to bis(N-heterocyclic carbene) complexes of palladium. *Organometallics* 2005;24 3020-3023.
- [91] Wang R, Piekarski M, Shreeve J. Pyrazolyl-functionalized 2-methylimidazolium-based ionic liquids and their palladium(II) complexes as recyclable catalysts. *Organic and Biomolecular Chemistry* 2006;4 1878-1886.
- [92] Nehra P, Khungar B, Pericherla K, Sivasubramanian SC, Kuma A. Imidazolium ionic liquid-tagged palladium complex: an efficient catalyst for the Heck and Suzuki reactions in aqueous media. *Green Chemistry*. 2014;16 4266-4271.
- [93] Zhao D, Fei Z, Geldbach TJ, Scopelliti R, Dyson P. J. Nitrile-functionalized pyridinium ionic liquids: synthesis, characterization, and their application in carbon-carbon coupling reactions. *Journal of the American Chemical Society* 2004;126 15876-15882.
- [94] Chiappe C, Pieraccini D, Zhao D, Fei Z, Dyson PJ. Remarkable anion and cation effects on Stille reactions in functionalised ionic liquids. *Advanced Synthesis and Catalysis* 2006;348 68-74.
- [95] Gayet F, Marty JD, Viguerie NLD. Palladate salts from ionic liquids as catalysts in the Heck reaction. *ARKIVOC* 2008;xvii 61-76.
- [96] Kiss L, Kurtan T, Antus S, Brunner H. Further insight in to the mechanism of Heck oxyarylation in the presence of chiral ligands. *ARKIVOC* 2003;v 69-76.
- [97] Hagiwara H, Okabe T, Hoshi T, Suzuki T. Catalytic asymmetric 1,4-conjugate addition of unmodified aldehyde in ionic liquid. *Journal of Molecular Catalysis Part A, Chemistry* 2004;214 167-174.
- [98] Hagiwara H, Shimizu Y, Hoshi T, Suzuki T, Ando M, Ohkubo K, Yokoyama C. Heterogeneous Heck reaction catalyzed by Pd/C in ionic liquid. *Tetrahedron Letters* 2001;42 4349-4351.
- [99] Hagiwara H, Sugawara Y, Hoshi T, Suzuki T. Sustainable Mizoroki-Heck reaction in water: remarkably high activity of Pd(OAc)₂ immobilized on reversed phase silica gel with the aid of an ionic liquid. *Chemical Communications* 2005; 2942-2944.
- [100] Arai M, Guo SL, Shirai M, Nishiyama Y, Torii K. The catalytic activity of platinum-loaded porous smectite-like clay minerals containing different divalent cations for butane hydrogenolysis and ethylene hydrogenation. *Journal of Catalysis* 1996;161 704-712.

- [101] Calo V, Nacci A, Monopoli A, Fornaro A, Sabbatini L, Cioffi N, Ditaranto N. Heck reaction catalyzed by nanosized palladium on chitosan in ionic liquids. *Organometallics* 2004;23 5154-5158.
- [102] Calo V, Nacci A, Monopoli A, Cotugno P. Heck reactions with palladium nanoparticles in ionic liquids: coupling of aryl chlorides with deactivated olefins. *Angewandte Chemie International Edition* 2009;48 6101-6103.
- [103] Deshmukh RR, Rajagopal R, Srinivasan KV. Ultrasound promoted C–C bond formation: Heck reaction at ambient conditions in room temperature ionic liquids. *Chemical Communications* 2001;1544-1545.
- [104] Sawant AD, Raut DG, Darvatkar NB, Salunkhe MM. Recent developments of task-specific ionic liquids in organic synthesis. *Green Chemistry Letters and Reviews* 2011;4 41-54.
- [105] Wang R, Piekarski M, Shreeve J. Pyrazolyl-functionalized 2-methylimidazolium-based ionic liquids and their palladium(II) complexes as recyclable catalysts. *Organic and Biomolecular Chemistry* 2006;4 1878-1886.
- [106] Cai Y, Q Y, Lu YL, Gao, G. H. Imidazolium ionic liquid-supported diol: an efficient and recyclable phosphine-free ligand for palladium catalyzed Heck reaction. *Catalysis Letters* 2007;119 154-158.
- [107] Cai Y, Lu Y, Liu Y, He M, Wan Q. Efficient Heck reactions catalyzed by a palladium/diol-imidazolium salt in aerial atmosphere. *Catalysis Communications* 2008;9 1209-1213.
- [108] Cai Y, Liu Y. Efficient palladium-catalyzed Heck reactions mediated by the diol-functionalized imidazolium ionic liquids. *Catalysis Communications* 2009;10 1390-1393.
- [109] Vallin KSA, Emilsson P, Larhed M, Hallberg A. High-speed Heck reactions in ionic liquid with controlled microwave heating. *Journal of Organic Chemistry* 2002; 67 6243-6246.
- [110] Littke AF, Fu GC. Palladium-catalyzed coupling reactions of aryl chlorides. *Angewandte Chemie International Edition* 2002;41 114-116.
- [111] Herrmann WA, Bohm VPH, Reisinger CP. Application of palladacycles in Heck type reactions. *Journal of Organometallic Chemistry* 1999;576 23-41.
- [112] Datta GK, Vallin KSA, Larhed M. A rapid microwave protocol for Heck vinylation of aryl chlorides under air. *Molecular Diversity* 2003;7 107-114.
- [113] Xie X, Lu J, Chen B, Han J, She X, Pan X. Pd/C-catalyzed Heck reaction in ionic liquid accelerated by microwave heating. *Tetrahedron Letters* 2004;45 809-811.
- [114] Dighe MG, Degani MS. Microwave-assisted ligand-free, base-free Heck reactions in a task-specific imidazolium ionic liquid. *ARKIVOC* 2011, xi, 189-197.

- [115] Hajipoura AR, Rafieea F. Accelerated Heck reaction using ortho-palladated complex in a nonaqueous ionic liquid with controlled microwave heating. *Applied Organometallic Chemistry* 2011;25 542-551.
- [116] Kumar R, Shard A, Bharti R, Thopate Y, Sinha A. K. Palladium-catalyzed dehydrative Heck olefination of secondary aryl alcohols in ionic liquids: towards a waste-free strategy for tandem synthesis of stilbenoids. *Angewandte Chemie International Edition* 2012;51 2636-2639.
- [117] Panke G, Schwalbe T, Stirner W, Taghavi-Moghadam S, Wille G. A practical approach of continuous processing to high energetic nitration reactions in microreactors. *Synthesis* 2003; 2827-2830.
- [118] Wiessmeier G, Hönicke D. Heterogeneously catalyzed gas-phase hydrogenation of cis,trans,trans-1,5,9-cyclododecatriene on palladium catalysts having regular pore systems. *Industrial and Engineering Chemistry Research* 1996;35 4412-4416.
- [119] Kestenbaum H, de Oliveira AL, Schmidt W, Schüth F, Ehrfeld W, Gebauer K, Löwe H, Richter T, Lebiez D, Untiedt I, Züchner H. Silver-catalyzed oxidation of ethylene to ethylene oxide in a microreaction system. *Industrial and Engineering Chemistry Research* 2002;41 710-719.
- [120] Dzyuba SV, Bartsch RA. Recent Advances in Applications of Room-Temperature Ionic Liquid/Supercritical CO₂ Systems. *Angewandte Chemie International Edition* 2003;42 148-150.
- [121] Liu S, Fukuyama T, Sato M, Ryu I. Continuous microflow synthesis of butyl cinnamate by a Mizoroki-Heck reaction using a low-viscosity ionic liquid as the recycling reaction medium. *Organic Process Research and Development* 2004;8 477-481.
- [122] Hagiwara H, Shimizu Y, Hoshi T, Suzuki T, Ando M, Ohkubo K, Yokoyama C. Heterogeneous Heck reaction catalyzed by Pd/C in ionic liquid. *Tetrahedron Letters* 2001;42 4349-4351.
- [123] Wei JF, Jiao J, Feng, Jioa J, Feng J-J, Lv J, Zhang X-R, Shi X-Y, Chen Z-G. PdEDTA Held in an Ionic Liquid Brush as a Highly Efficient and Reusable Catalyst for Suzuki Reactions in Water. *Journal of Organic Chemistry* 2009;74 6283-6286.

Deep Eutectic Solvents in Organic Synthesis

Scott T. Handy

Additional information is available at the end of the chapter

<http://dx.doi.org/10.5772/59254>

1. Introduction

As part of the push towards making Chemistry more environmentally compatible, there has been a major emphasis on the development of greener and more environmentally compatible solvents. Many different options have been explored, including water and supercritical fluids. [1] Each of these families has its own strengths, as well as significant limitations including reactivity to highly basic/nucleophilic reagents and limited solubility of entire families of reagents. These issues have resulted in the great interest displayed in room temperature ionic liquids (RTILs) over the last couple of decades. [2] In particular, the easily ability to tune the properties of these RTILs has attracted much attention. At the same time, essentially all of these RTILs suffer from very high cost compared to conventional solvents, which is a serious deterrent to more wide-spread application. Relatively recently, a potential solution to this problem has been reported – deep eutectic solvents (DES). [3,4,5] Although the specific cost of a DES depends upon its components, the most typical DES, such as choline chloride/urea or choline chloride/glycerol, are comparable in cost to typical organic solvents such as acetonitrile or N,N-dimethylformamide, thus eliminating much of the concern with their use.

Although many DES are theoretically possible, the current examples fall into three main families. The first is exemplified by the prototypical DES – a 1:2 molar ratio of choline chloride and urea – and involves the mixture of a salt and a hydrogen-bond donor. [6] Thousands of variation have been reported and many more can be readily imagined. [7-11] The second family is quite similar and involves the combination of a salt with a metal salt, as exemplified by choline chloride and zinc chloride again in a 1:2 molar ratio. [12-14] Much fewer examples have been studied, although this approach is expected to be quite general. The third family is more complex, involving the combination of a carbohydrate, an urea, and an ammonium salt in varying ratios. [15] The exact choice of components and their ratio does not appear to be readily predictable, but many options have already been reported, making their application relatively straightforward.

All three of these families share similar advantages, including costs comparable to conventional organic solvents, very low volatilities, lower toxicities, recyclability, and, for many components, being based on biorenewable materials. Considering the variety of salts and hydrogen-bond donors or metal salts that can be used, the properties of DES can also be tuned to control a number of fundamental properties, including Lewis or Bronsted acidity, polarity, and solvent miscibility. By exploring further variations of DES, an even greater range of solvent properties should be accessible.

Beyond being theoretically interesting materials, DES have found many significant areas of application. One of the first of these was the area of electroplating and related metal recovery and separations. [16] Tremendous research has been reported in this area and has resulted in some very promising applications. Similarly, DES have been found to be excellent solvents for enzymatic reactions, affording much higher activity and stability than organic solvents or RTILs, or sometimes even water. [17-20] Indeed, their abilities are so significant that they have been termed as potential solvents for the development of prebiotic chemistry. [21]

Despite all of these interesting applications of DES, one rapidly growing facet is their use in Organic Synthesis. Many new reports are appearing on a weekly basis, so this review attempts to cover applications reported through the middle of July of 2014.

2. Choline Chloride/Urea DES

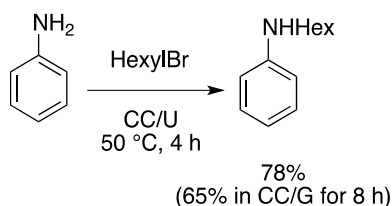
As one of the earlier deep eutectics reported, choline chloride/urea (CC/U) has been one of the most extensively explored in virtually all areas of application, including Organic Synthesis. [6] Part of its attraction is the availability of choline chloride in very large quantities (due to its use as a feed additive for poultry) at very low cost, as well as its low toxicity. The application of CC/U in Organic Synthesis covers a wide range of reaction types, with more continuously appearing.

Another important feature to note regarding CC/U is its ability to be recycled. In general there are two main options that have been reported. In one, the reaction products are separated by extraction with an immiscible organic solvent such as ether or ethyl acetate, resulting in a DES that can be reused following brief drying *in vacuo*. In the second option, this recycling involves dissolving the DES in water to separate it from the reaction product and then removing the water *in vacuo* to recover the DES. This is a fairly energy-intensive process, particularly on larger scale and may not always be worth the expense and effort. Still, the majority of reports use this option for recycling due to its avoidance of organic solvents and easy product isolation.

2.1. Alkylation, substitution, reduction, halogenation, and polymerization in CC/U

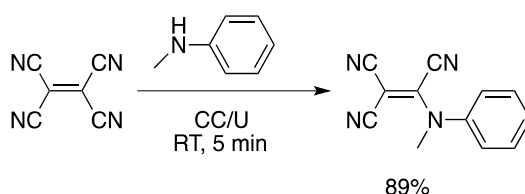
One interesting area of application has been in alkylation and nucleophilic substitution chemistry. Thus, Shankarling and co-workers have reported the simple alkylation of anilines using simple alkyl bromides in the absence of any added base. [22] (Scheme 1) Yields were high under mild conditions and generally short (< 4 hour) reaction times. In addition, the DES

could be readily recycled several times by extraction of the product with ethyl acetate and displayed little loss in activity (the yield for the reaction in Scheme 1 falling from 78% to 65% over 5 recyclings). Interestingly, a related DES, choline chloride/glycerol (CC/G), afforded a similar 65% yield, but required twice as long. The potential for expanding the scope of this chemistry to other nucleophiles (such as phenols and thiols) has not yet been reported, but seems promising.



Scheme 1. Alkylation of Anilines

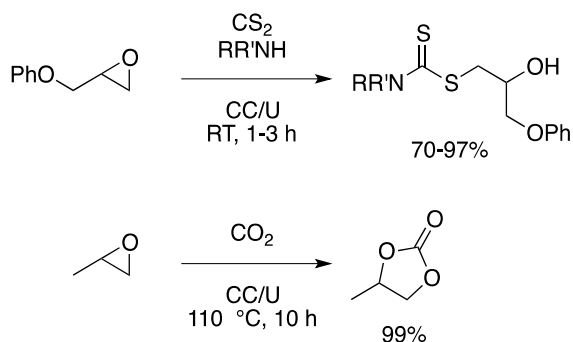
Switching to nucleophilic substitution chemistry, an unusual substitution of tetracyanoethylene with either anilines or indoles was reported by Shankarling and co-workers. [23] In a comparison of lipase and DES mediated reactions, it was shown that the DES conditions generally afforded better yields and better recyclability compared to the enzymatic conditions. A variety of other DES were also examined, and good yields were obtained in most cases. For the reaction seen in Scheme 2, yields fell modestly over 4 recyclings, going from 89% yield to 73% yield. This solvent recycling involved recovery of the DES from the aqueous layer of extraction at the end of the reaction, with care taken to remove the HCN generated in these reactions. The products of these reactions displayed interesting spectral properties, which, when combined with their straightforward synthesis, may raise useful future applications.



Scheme 2. Tetracyanoethylene Substitution

Two related nucleophilic ring openings of epoxides have been reported. Azizi and Gholibeglo have reported the synthesis of dithiocarbamates from the three component coupling of an epoxide, an amine, and carbon disulfide in a combination of CC/U at room temperature. [24] (Scheme 3) The dithiocarbamates could be isolated in good yield from a wide range of amines (mostly secondary, with a few primary examples as well). In addition, alkyl halides or enones could be employed in place of the epoxides to afford an even wider range of dithiocarbamate

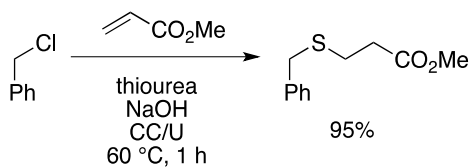
products under the same reaction conditions. The DES could be recycled several times using the water extraction option with only a modest decrease in activity.



Scheme 3. Epoxide reactions

The second epoxide reaction was the fixation of carbon dioxide with propylene oxide in the presence of CC/U. [25] (Scheme 3). In this case, CC/U supported on molecular sieves was found to be superior to simple CC/U, affording very high yields and much reduced reaction times (4-5 hours compared to 10 hours without support). The supported system had the added benefit of being readily recyclable via simple filtration of the catalyst and retained the same levels of activity for 5 recyclings.

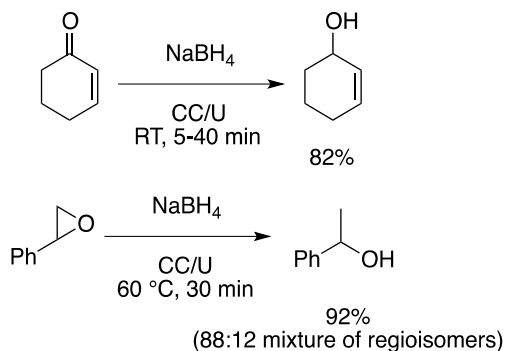
A final nucleophilic reaction in CC/U is a three component thia-Michael reaction. [26] (Scheme 4) In this case, the combination of an alkyl halide, thiourea, a Michael acceptor, and sodium hydroxide afforded very good yields of the thia-Michael products after short (< 2 hours) reaction times at 60 °C. A wide range of alkyl halides, including one example of a secondary one (bromocyclopentane) worked as did a range of Michael acceptors, including acrylates and cyclohexenone.



Scheme 4. Thia-Michael reactions

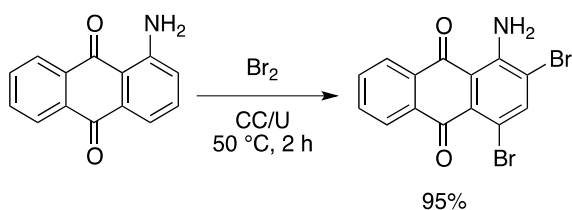
A highly unusual discovery was made by Azizi and co-workers when they studied the reduction of carbonyls and epoxides in CC/U with sodium borohydride. [27] (Scheme 5) Despite the potential for reaction with the urea, they noted clean and rapid reduction of both carbonyls and epoxides. Both aldehydes and ketones reacted well, with enones giving clean 1,2-reduction. Epoxides also reacted well at 60 °C, with even styrene oxide affording primarily the product of reduction at the less hindered end (88:12 ratio of 1-phenylethanol:2-phenyle-

thanol). Interestingly, these reaction conditions demonstrated very good chemoselectivity, with aldehydes and ketones being reduced at room temperature in the presence of imines or epoxides and epoxides being reduced at 60 °C in the presence of imines. The products were isolated via partitioning between water and ether and generally required no further purification.



Scheme 5. Reductions

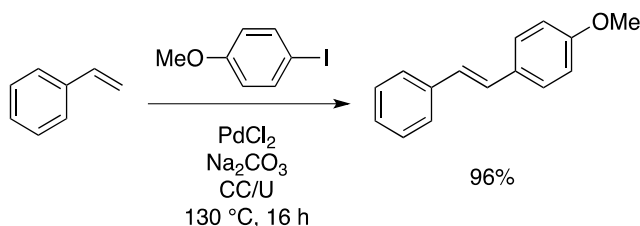
Another usual area of application is in the bromination of 1-aminoanthraquinones. [28] (Scheme 6) A series of these compounds were brominated by treatment with bromine in CC/U at 50-60 °C for 2 hours. In cases where the 4 position was unsubstituted, 2,4-dibromo products were obtained in good yield. Recycling of the DES was also reported via extraction with water followed by evaporation. Although little mechanistic information is discussed, it seems possible that the brominations are being mediated by the transient formation of N-bromo urea. The potential for this system to mediate the bromination of other compounds has yet to be studied, but could be of considerable utility.



Scheme 6. Brominations

Transition-metal-catalyzed couplings, though extensively studied in other DES, have been little explored in CC/U. The only report is found in the original patent on DES and reports some studies of the Heck coupling in CC/U. [29] (Scheme 7) The results were rather unsurprising and afforded results for aryl iodides comparable to those obtained in many conventional solvents. Appropriate selection of base and palladium source were critical for optimal results, with palladium chloride and sodium carbonate giving a 96% yields after 16 hours,

compared to 90% after 1.5 days using sodium acetate as base or 60% after 2 days using sodium acetate and palladium acetate. The patent reports that the catalyst and solvent can be reused, but no details are provided. Still, this does demonstrate that CC/U could be expected to be an inexpensive recyclable solvent/catalyst system for palladium-catalyzed coupling reactions.



Scheme 7. Heck coupling

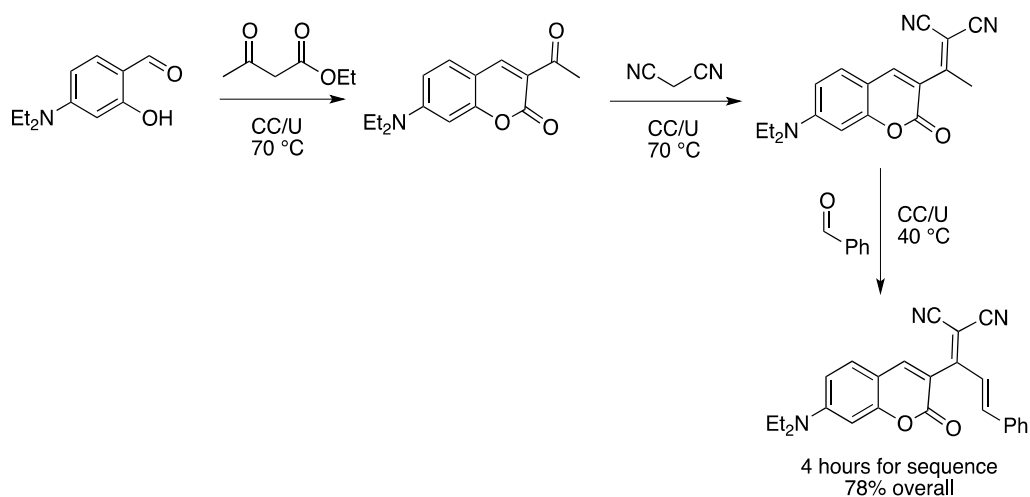
This same patent also reported the application of CC/U to free-radical polymerization. [29] Styrene was polymerized using 1 mol% of AIBN in CC/U at 110 °C for 16 hours to afford a polymer with average molecular weight of 12,000 and a polydispersity of 3.2. There has been little follow-up to this report.

2.2. Condensation reactions in CC/U

A major area of application for CC/U has been in the area of condensation-type chemistry. It appears that the combination of the potential for organocatalytic, H-bonding activation of aldehydes by urea (a known, but weak organocatalyst) and the desiccating properties of CC/U serve to benefit this family of reactions in ways that many other solvents do not. As a result, this section is focused on condensation applications of CC/U.

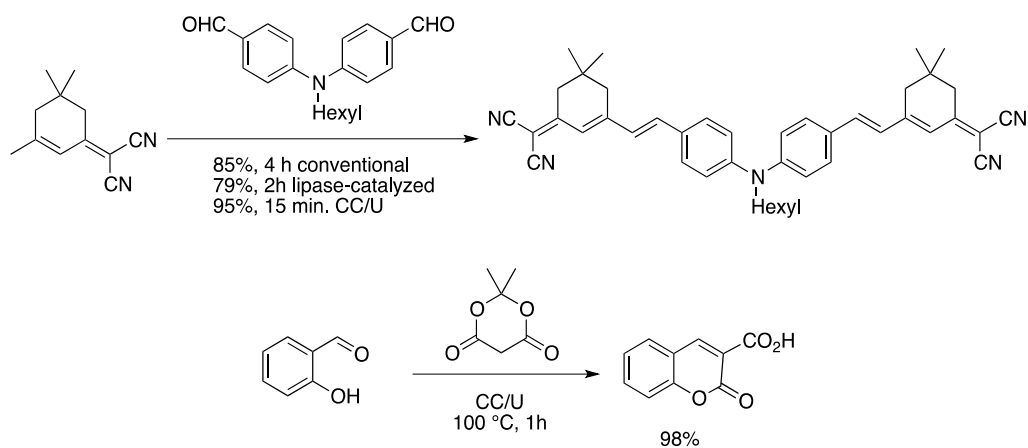
The first sub-set of condensation reactions are simple carbonyl reactions such as Knoevenagel, Perkin, Henry, and related aldol-type reactions. Perhaps the most elegant example of the application of CC/U to condensation reactions comes from a report by Shankarling. [30] (Scheme 8) In this paper, he reported a one-pot synthesis of coumarin styryl dyes via a sequence of two Knoevenagel condensations and one aldol-like condensation. All three condensation reactions were performed in CC/U at temperatures ranging from 30-75 °C and all afforded the desired products in good to excellent yields after reaction times of < 2 hours (< 6 hours for the entire sequence). The CC/U could also be recycled using the procedure commonly employed in the Shankarling group of separation of the DES with water, followed by concentration *in vacuo* to afford the DES ready for reuse. The power and potential demonstrated in this paper have doubtless inspired at least some of the more recent applications of CC/U in this area.

In a related paper focusing just on the Knoevenagel condensation of diphenylamine aldehydes with a variety of active methylene compounds, three sets of reaction conditions were compared: conventional with piperidine as base, lipase-catalyzed, and CC/U mediated. In virtually all cases, the DES conditions afforded the highest yields and the shortest reaction times (< 30 minutes at room temperature). [31] (Scheme 9) As the focus of this paper was on the dyes that



Scheme 8. Condensation sequence

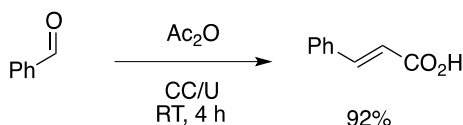
were synthesized and not as much the DES, no comment is made on recycling the DES, but it would seem likely from other papers that such recycling could be readily achieved with good results.



Scheme 9. Knoevenagel condensations

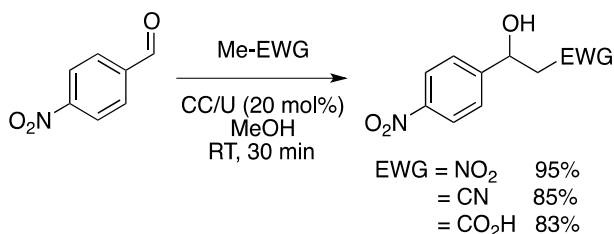
Another study of a different Knoevenagel condensation (salicyl aldehydes with Meldrum's acid and other active methylenes) also reported very good yields of the anticipated coumarins. [32] (Scheme 9) In this case, the reaction temperature was higher (100 °C), but still with short reaction times. Recycling of the DES using the water extraction/concentration method was mentioned, but no data was reported.

Another classic carbonyl condensation reaction that has been reported in CC/U is the Perkin reaction. [33] (Scheme 10) In this case, the reaction of an aromatic aldehyde with an anhydride (acetic anhydride in all but two cases) in CC/U at room temperature for 4-9 hours afforded the cinnamic acid derivatives in generally good yield. A comparison was made with conventional Perkin conditions (excess anhydride in the presence of sodium acetate at 140 °C), with the conventional conditions affording significantly lower product yields after longer reaction times in every case. The DES could be recycled with little loss in activity for 4 reactions using the water extraction/concentration method.



Scheme 10. Perkin reaction

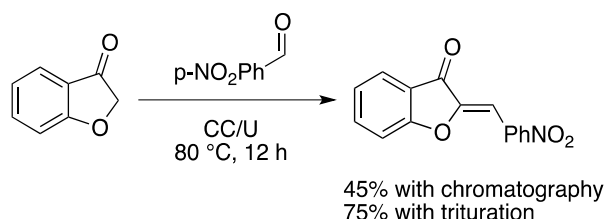
The Henry reaction and a couple of related examples using acetonitrile or acetic acid with aromatic aldehydes were reported by Shankarling. [34] (Scheme 11) Interestingly, the products in these cases were not elimination products, but rather the β -hydroxy products. Part of the reason for this outcome may stem from the fact that the DES was used as a catalyst in methanol for short reaction times at room temperature. It is possible that higher concentrations of DES may lead preferentially to elimination products (see, for example the aurone synthesis by Handy), although this feature has not yet been confirmed.



Scheme 11. Henry reaction

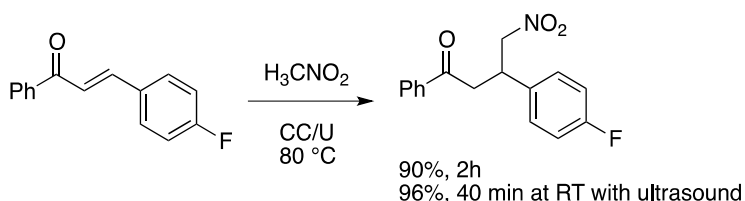
Also within the aldol family of reactions is the synthesis of aurones via condensation of an aromatic aldehyde and a coumarinone reported by Handy and Hawkins. [35] (Scheme 12) A wide range of aldehydes proved compatible with this method, including acid-sensitive ones such as furfural. The yields were quite variable, but subsequent research has demonstrated that much of the problem is associated with purification of the aurone products. By employing a modified purification using trituration with ether in place of the column chromatography, yields could be dramatically improved. For example, the reaction of coumarinone with p-nitrobenzaldehyde in CC/U followed by silica gel chromatography afforded the anticipated

aurone in 45% yield, while the same reaction purified by trituration with ether afforded the same product in 75% yield and analytically pure form.



Scheme 12. Aurone synthesis

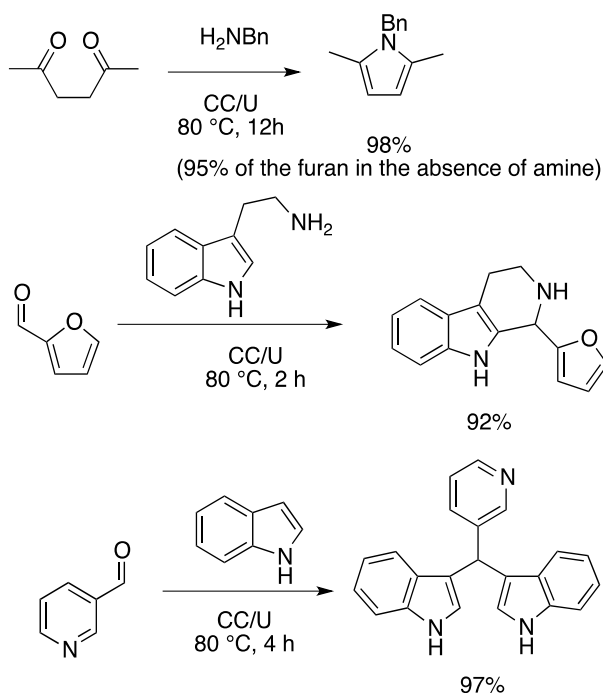
A final reaction from the carbonyl condensation family is the recently reported Michael addition of nitromethane and active methylene compounds (malononitrile, and ethyl cyanoacetate) to chalcones. [36] (Scheme 13) In this case, the use of a combination of CC/U and ultrasound afforded the Michael products in excellent yields after much shorter reaction times and at lower temperatures compared to the same reaction conditions in the absence of sonication. This beneficial combination of the DES and ultrasound is expected to be applicable to many other reactions run in CC/U and possibly other DES as well and certainly merits further exploration.



Scheme 13. Michael reaction

2.3. Heteroaromatic synthesis in CC/U

Another area that has found considerable application of CC/U as a catalytic solvent is in the synthesis of heteroaromatics via carbonyl condensation reactions. In a series of papers, the Handy group has reported several of these types of reactions, beginning with the Paal-Knorr synthesis of pyrroles and furans. [37] (Scheme 14) A variety of amines, including anilines could be condensed with 1,4-diketones in CC/U at 80 °C to afford the anticipated pyrroles in generally good yield. The one exception was the reaction of 2,5-hexanedione with poorly nucleophilic p-nitroaniline which afforded a 56% yield of the pyrrole with the mass balance being the 2,5-dimethylfuran. In the absence of amines, the diketones clearly afforded the anticipated furans after longer reaction times. In addition, the DES could be recycled several times with little loss in activity by extraction of the products with ether and then brief drying *in vacuo*.



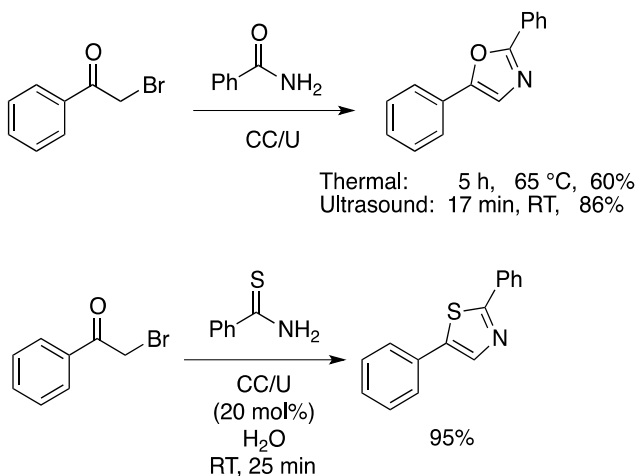
Scheme 14. Heteroaromatic syntheses from the Handy group

A second application was the Pictet-Spengler reaction. [38] (Scheme 14) The acid-free nature of these reaction conditions enabled the synthesis of a wide range of β -carboline derivatives including furyl and pyridyl substituted ones in excellent yield after 2 hours at 80 °C. As with the Paal-Knorr synthesis results, the products could be easily extracted using ether and the remaining DES recycled several times with minimal loss of activity after brief drying *in vacuo*.

A related reaction is the conversion of aldehydes to bis(indolyl)methanes by treatment with 2 equivalents of indole. Reaction in CC/U at 80 °C for 4 hours afforded the bis(indolyl)methanes in excellent yield for a wide range of aromatic aldehydes including the more difficult to access pyridyl systems. [39] (Scheme 14) Interestingly, these reaction conditions proved ineffective with the more demanding aliphatic aldehydes and ketones, affording a complex mixture of aldol products and recovered starting material respectively. As with the previous two reports, the products were isolated via extraction with ether and generally required no further purification. The DES layer could be recovered and recycled following brief drying *in vacuo* with little loss in activity over 5 reactions.

Two related reports from the Shankarling group focus on related approaches to the synthesis of oxazoles and thiazoles. (Scheme 15) For oxazole synthesis, the combination of CC/U and ultrasound again displayed beneficial synergy. [40] Thus, treatment of an α -bromoacetophenone with an amide or urea affords the desired oxazoles. Thermal reactions (65 °C) required 3.5-5 hours to afford modest yields, while the ultrasound reactions could be done at room

temperature and were complete in < 20 minutes to afford high yields of the products. CC/U recycling was also studied and proved to be quite convenient in this case as the products were extracted with methylene chloride (which is immiscible with CC/U) to directly afford the DES ready for recycling. There was no significant decrease in reaction yield over 5 reactions, indicating that the DES is stable to the ultrasound reaction conditions.



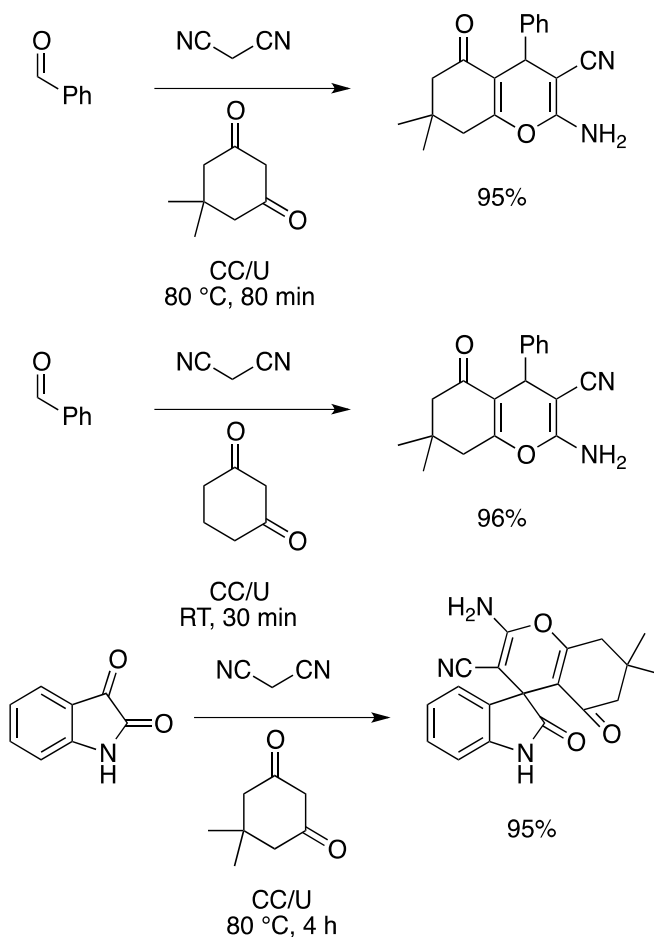
Scheme 15. Thiazole and Oxazole synthesis

The thiazole synthesis is quite similar. [41] (Scheme 15) Again, the combination of an α -bromoacetophenone and an amide or urea was combined in CC/U. There were two differences, though. First, DES and lipase catalyzed reaction conditions were compared, not ultrasound. Second, the DES was used as a true catalyst in aqueous solution at room temperature. Both methods afforded excellent yields of the thiazole products after short (< 20 minute) reaction times. DES recovery (via separation with water and concentration of the aqueous layer) was effective and the DES could be recycled several times with minimal loss in activity.

2.4. Multicomponent reactions in CC/U

A final condensation area that has received significant attention in CC/U is that of multicomponent coupling reactions (MCR). Many different options are imaginable, but virtually all of the reports have centered on reactions initiated by a Knoevenagel condensation, followed by some type of Michael addition. For example, Azizi and co-workers reported the MCR of aromatic aldehydes, malononitrile, and various active methylene compounds (including dimedone, acetylacetone, and acetoacetates). [42] All of these examples afforded good yields after 1-4 hours at 80 °C, thus providing a simple and efficient route to compounds of this type. (Scheme 16) In addition, they explored a few other solvents under identical conditions and found that three acidic DES (CC with malonic acid, citric acid, or tartaric acid) afforded the anticipated products at slightly reduced yields (82%, 60%, and 68% respectively). Finally, the

temperature was important as the same reaction at room temperature in CC/U afforded only a 50% yield of the MCR product.



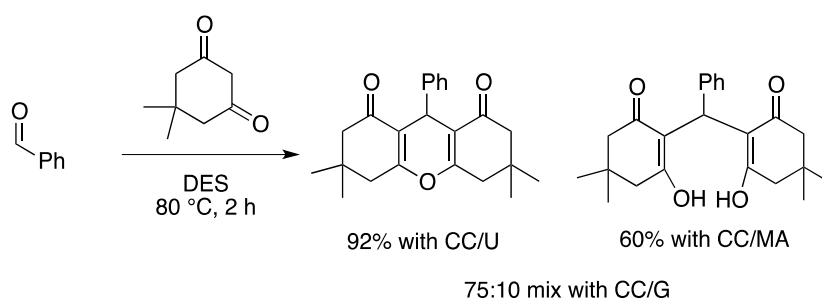
Scheme 16. Malononitrile multicomponent couplings

This temperature observation is quite interesting since another group reported the closely related condensation of aldehydes, malononitrile, and cyclohexane-1,3-dione in CC/U. In this case, they reported clean, high-yielding reactions at room temperature in 30 minutes. [43] (Scheme 16) Considering the very high viscosity of CC/U at room temperature, it is unclear how useful such reaction conditions would be, and the difference in reported results between the two groups is a concern.

A third related MCR is that of 1,2-diketones in place of the aldehyde to afford spirocyclic products. [44] (Scheme 16) A wide range of products were accessible as both malononitrile and methyl cyanoacetate were used in combination with dimedone, cyclohexane-1,3-dione, Meldrum's acid, and 1-naphthol. In general, very good yields were obtained when isatin was

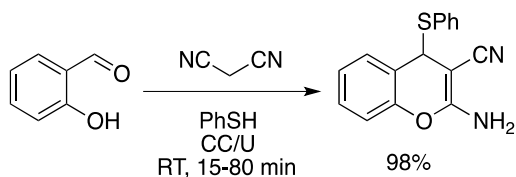
the 1,2-dikeone, although somewhat lower (50-60%) yields were obtained for other diketones. Recycling of the DES was also reported, again using extraction with water, followed by concentration *in vacuo*.

A very interesting report on MCR in CC/U focusing on the condensation of aldehydes with dimedone or cyclohexane-1,3-dione has also appeared. [45] (Scheme 17) In this careful study, the authors noted that the choice of DES controlled the type of product (open or closed) formed. In CC/U, a very high yield of the ring-open product was formed, while use of an acidic DES favored the closed form, with choline chloride/malonic acid (CC/MA) and choline chloride/ ZnCl_2 both affording solely the closed product. Interestingly, choline chloride/glycerol (CC/G) afforded a mixture of the two products, favoring the open form as did the presumably less Lewis acidic choline chloride/ SnCl_2 .



Scheme 17. Other multicomponent couplings

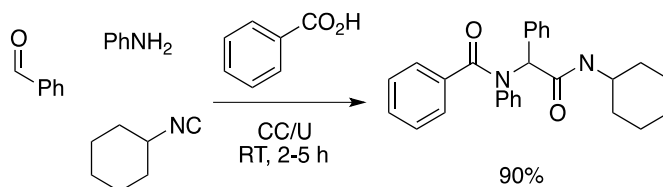
A somewhat different MCR in CC/U was reported based upon the initial condensation of malononitrile with salicylaldehyde, followed by Michael addition of a variety of nucleophiles to afford substituted chromenes. [46] (Scheme 18) The reactions proceeded quickly (all reactions < 4 hours, and most < 1 hour) and in generally excellent yield. Nucleophiles that were studied included many thiols, amines (secondary and one primary), cyanide and indole. The products could generally be isolated in pure form by diluting the reaction with water and then filtering to separate the product. In principle, this separation method should result in the ability to recycle the CC/U, but no recycling data was reported.



Scheme 18. Chromene multicomponent couplings

Finally, the parent MCR, the Ugi reaction, has also been reported in CC/U. [47] (Scheme 19) In this case, the use of a DES afforded much higher yields of the Ugi product than did reaction

under neat conditions or in water or several organic solvents. The mild conditions and short reaction times were complimented by the ease of product isolation (filtration after diluting with water) and recovery and recycling of the DES (via concentration of the water layer *in vacuo*). The recycled DES could be reused three times with only a slight drop in product yield. Finally, a wide range of anilines and aromatic aldehydes, as well as one aliphatic aldehyde and one ketone, all gave good yields of the Ugi products, indicating considerable scope to this method.



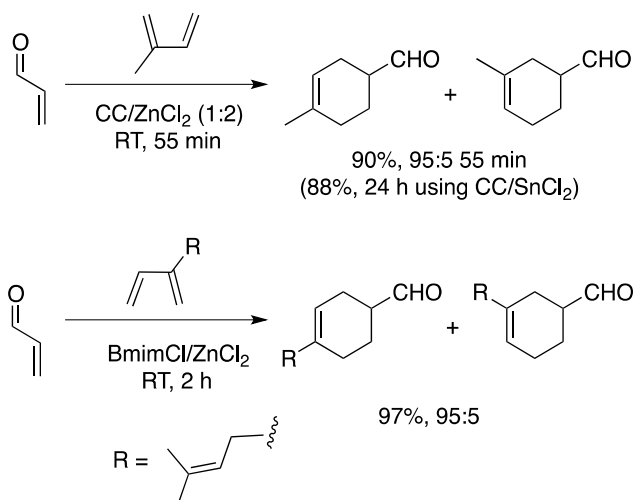
Scheme 19. Ugi multicomponent coupling

3. Lewis acidic DES

One of the early families of DES that was introduced are those composed of choline chloride and a metal salt, most typically zinc or tin chloride in a 1:2 molar ratio. These mixtures form complex metal chloride anions and give liquids that are Lewis acidic. In principle, this same concept should be applicable to combinations with a variety of other metal salts, such as iron, copper, and the lanthanides, although little has been reported along these lines. The obvious Lewis acidity of these DES has resulted in a number of applications in Organic Synthesis and should be applicable to even more than have been presently reported. One potential drawback to these DES is the fact that they would be expected to be moisture sensitive, although different authors have reported these DES as been either moisture sensitive or moisture insensitive. It is likely that there is some sensitivity, but it is likely less than that of the metal salts themselves, which may aid in their handling under normal laboratory conditions.

One reaction that shows considerable promise in these Lewis acidic DES is the Diels-Alder reaction. Considering the great utility that Lewis acids have demonstrated in the catalysis of Diels-Alder reactions, this is not surprising. Nevertheless, the first report by Abbott and co-workers did a fantastic job demonstrating their potential. [48] (Scheme 20) A number of reactions were studied between ester, ketone, and aldehyde substituted dienophiles and a range of simple dienes. Good yields were obtained (85+%) with good regioselectivities after modest (<5 h) reaction times at ambient temperature when CC/ZnCl₂ was employed as the solvent. The use of CC/SnCl₂ resulted in much slower reactions, but still good yields and regioselectivity. Product isolation was simple, involving decantation of the non-polar products from the DES, which could then be recycled at least 5 times with no appreciable loss in activity. A later study similarly noted good results when using zinc-containing DES. [49] A range of

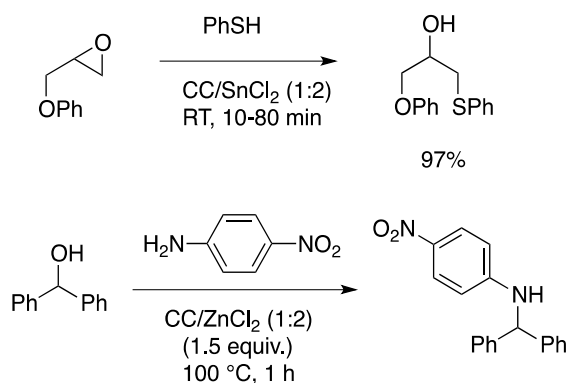
salts, including imidazolium and pyridinium ones were used in combination with varying ratios of zinc chloride. In all cases, 2:1 or higher molar ratios of zinc chloride to the other salt afforded the best yields and regioselectivities. Product isolation again involved decanting the less polar product layer to afford the DES layer which could be recycled.



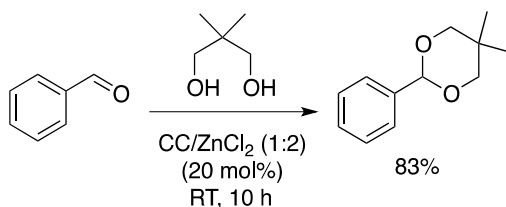
Scheme 20. Diels-Alder Reactions

Beyond Diels-Alder reactions, another obvious application is in the area of nucleophilic substitution chemistry. Azizi and Batebi have reported the ring opening of epoxides with a wide range of nucleophiles, including thiols, anilines, TMSCN, TMSN₃, and methanol. [50] (Scheme 21) These reactions generally afforded very good yields after short (<2 hours) reaction times at room temperature. In addition, the DES layer could be recycled at least 3 times with only a modest loss in activity following extraction of the product by diethyl ether. Another example of nucleophilic substitution chemistry in CC/ZnCl₂ involved the ionization and trapping of stabilized carbocations, such as diphenylcarbinol with a range of nucleophiles including anilines, amines, sulfonamides, and 1,3-dicarbonyl compounds. [51] Yields were good after 1 hour reaction times at 100 °C and the DES could be recycled at least 4 times with no loss in activity. It is worth noting that the DES is used more as a recyclable catalyst, as only 1.5 equivalents were employed. In addition, the DES was recovered by extraction with water and then dried *in vacuo* before reuse, which is operationally more difficult than the extraction option employed by Azizi.

A related reaction is the ketalization of carbonyls using 2,2-dimethyl-1,3-propanediol using the CC/ZnCl₂ DES. [52] (Scheme 22) A wide range of aldehydes as well as two ketones were employed in this chemistry to afford the desired ketals in good yield after modest reaction times (10-20 h). Again, the DES was employed as a catalyst, with only 20 mol% being employed. Further, the DES could be readily recycled following separation of the product via extraction with ether.

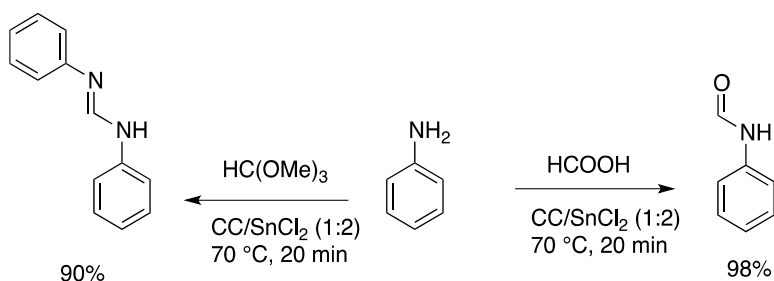


Scheme 21. Nucleophilic Substitutions



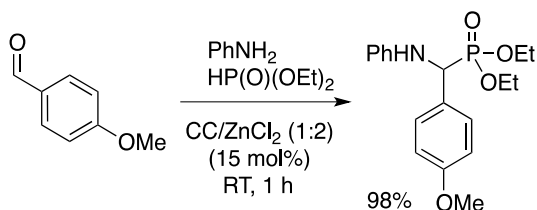
Scheme 22. Ketalizations

A rather unusual application of DES to synthesis is the preparation of either N-formylanilines or N-N'-diarylamidines starting from anilines. [53] (Scheme 2) In this case, CC/SnCl₂ was found to be the best solvent of those studied. Reaction in the presence of formic acid at 70 °C afforded the N-formyl products in good yield, while a slightly higher temperature (90 °C) in the presence of trimethyl ortho formate afforded the amidines instead. In both cases, product isolation involved simple extraction with ethyl acetate, which in principle should enable recycling of the DES, although this was not reported.



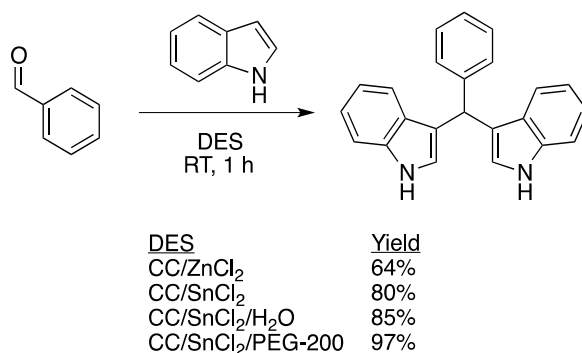
Scheme 23. Formylation and Amidine Formation

Various carbonyl condensation reactions have also been explored in Lewis acidic DES. The Kabachnik-Fields reaction of aldehydes, anilines, and phosphites has been conducted using $CC/ZnCl_2$ at room temperature to afford the desired products in good yield after short reaction times. [54] (Scheme 24) In this case, the DES was employed as a catalyst, with 15 mol% giving optimal results. The products could be readily extracted from the DES using MTBE and the DES recycled after drying *in vacuo*. A slight loss in activity (98% to 86% over five reactions) was observed, which may be due to mechanical loss of the DES over the course of five reactions.



Scheme 24. Kabachnik-Fields Reactions

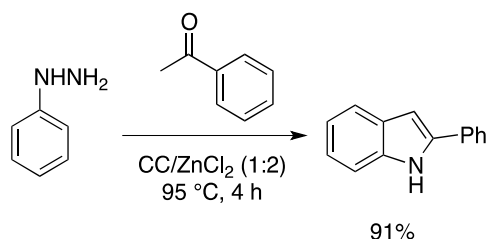
The synthesis of bis(indolyl)methanes (bim) has also been reported in a Lewis acidic DES. [55] (Scheme 25) Interestingly, in this case, $CC/SnCl_2$ proved superior to $CC/ZnCl_2$. Even better results were obtained when using either $CC/SnCl_2$ with water (1:2:3 molar ratio) or with PEG-200 (also a 1:2:3 molar ratio). Reaction times were short (<4 hours) at room temperature and yields high, even for the more problematic alkyl aldehydes. Finally, mention is made of recycling the DES, but no details are provided, although since the products are isolated via extraction with ether or ethyl acetate, this recycling should be straightforward.



Scheme 25. BIM Synthesis

In a final example, Abbott and co-workers have also explored the Fisher indole synthesis in $CC/ZnCl_2$. [56] (Scheme 26) Reaction yields were good and reaction times short (<4 hours), while employing 1-3 equivalents of the DES as the catalyst/solvent for the reaction. An interesting option for product isolation was used in this study, with the desired indoles being

obtained via sublimation from the DES. Recycling of the DES was reported, but activity decreased very rapidly, going from 91% to 72% to 34% over the course of three reactions.



Scheme 26. Fischer Indole Synthesis

4. Bronsted acidic DES

In addition to Lewis acidic DES, there is also the option to form Bronsted acidic DES by simply using a Bronsted acid as the proton donor component of the DES. In this way, a wide range of DES with varying acidity can be formed, with the most common options being various di- and tricarboxylic acids as well as tosic acid. (Figure 1) As with the simple CC/U DES, recycling of these systems has often been reported. In some cases, this simply involves product extraction with an immiscible organic solvent (even just decanting the product in one case), but more frequently is performed by dilution with water and then recovery of the DES from the aqueous layer. This is clearly an area in need of improved options and may benefit from many of the studies performed previously on traditional RTILs.

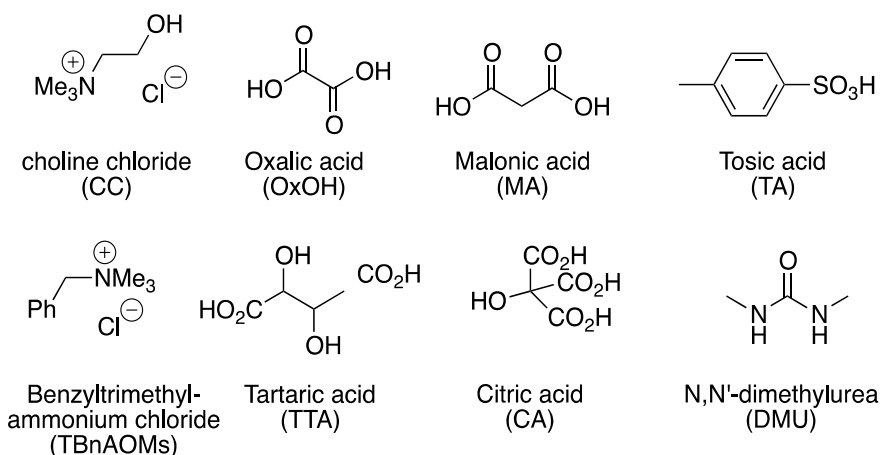
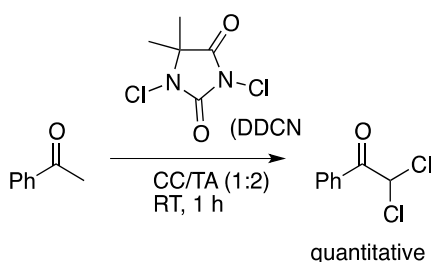


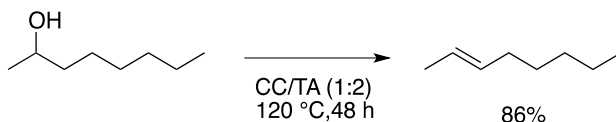
Figure 1. Common Acidic DES Components

One of the more unusual applications of acidic DES in Organic synthesis is the use of the choline chloride/tosic acid (CC/TA) system to effect the dichlorination of methyl ketones using 1,3-dichloro-5,5-dimethylhydantoin (DCDMH). [57] (Scheme 27) Using methanol as the solvent, the chlorinating reagent cleanly affords the expected α -chloroketones in good yield. Upon switching the solvent to CC/TA, though, the dichlorination product is now obtained in nearly quantitative yield after a short 1 hour reaction time at room temperature. The scope of these conditions has not been extensively explored, but it does appear to be an interesting route to these unusual products.



Scheme 27. α -Chlorinations

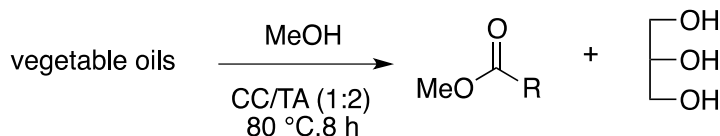
More traditional applications of acid catalysts have also been explored. In some unpublished work, Handy and co-workers have explored the use of CC/TA as a recyclable catalytic solvent for both the elimination of alcohols and the transesterification of esters. For the elimination of alcohols to afford alkenes, this reaction was found to proceed cleanly with simple alcohols such as 2-octanol and cyclohexanol, affording the alkenes in 85+% yields after reaction at 120 °C for 2 days. [58] (Scheme 28) 3° alcohols reacted more readily, with methylcyclohexanol affording the anticipated alkene after 12 hours at 80 °C. In all cases, product isolation involved simple decantation of the alkene, which formed a separate second layer. The remaining CC/TA layer could be reused 4 times with minimal loss of activity (still affording 80% of the alkene product from 2-octanol on the fourth recycling), although the build-up of water would eventually reduce the effectiveness of this acidic DES (usually by the 6th recycling).



Scheme 28. Eliminations

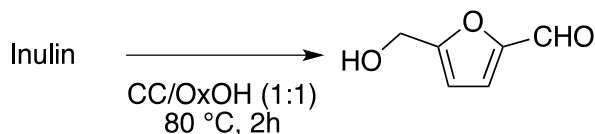
For transesterifications of various vegetable oils (corn, soy, and canola), the same CC/TA DES proved to be effective. [59] (Scheme 29) Yields of the methyl esters were high (>80%) after modest reaction times. Interestingly, the DES could be recycled up to 3 times without the need to remove the glycerol by-product before transesterification was seriously impeded (85, 80, and 76% recovery of the methyl esters for the first three uses of CC/TA, and then a drop to 50%

recovery on the fourth use). To date, attempts to remove the glycerol and regenerate the active DES have not proven to be successful.



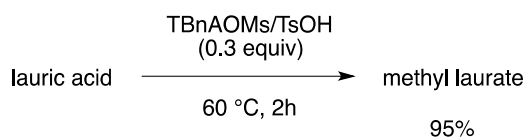
Scheme 29. Transesterifications

In related work, the dehydration of the carbohydrate inulin to form 5-hydroxymethylfurfural (HMF) in CC/Oxalic Acid has also been reported. [60] (Scheme 30) After extensive optimization of the reaction time, temperature and the acidic component of the DES, conditions were determined that allowed HMF to be isolated in 64% yield after only two hours of reaction at 80 °C. As has been reported several times, the inclusion of ethyl acetate aided in preventing decomposition of the HMF as it was formed. This feature also enabled product separate to be achieved by simple phase separation and the remaining DES to be recycled repeatedly with minimal loss of activity. The inexpensive nature of this catalyst system, coupled with the mild conditions and high yield of HMF from more complex carbohydrates (instead of the more easily converted fructose) holds considerable promise for the effective formation of the valuable biorenewable building block HMF.



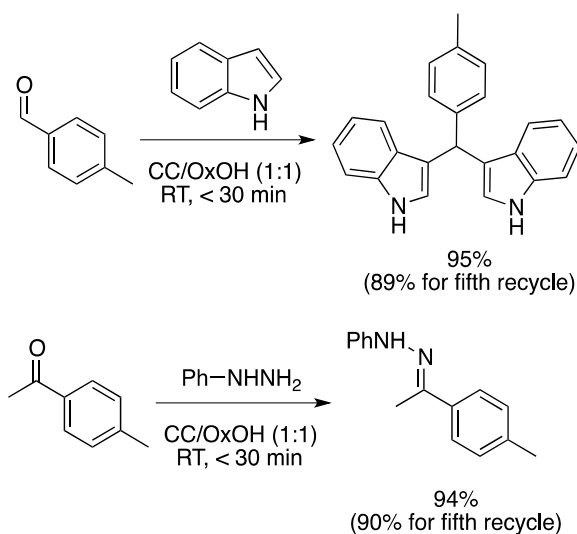
Scheme 30. HMF Formation

In addition to transesterifications, related acidic DES have been used for the Fischer esterification of carboxylic acids. [61] (Scheme 31) A series of new acidic DES were prepared from the combination of various ammonium salts and tosic acid, of which the equimolar combination of TBnAMsO and tosic acid was employed most frequently. It was very effective for the esterification with primary alcohols, affording the esters in near quantitative yields after short 2 hour reaction times at 60 °C. For secondary alcohols (such as isopropanol), the yields did drop to near 50% at the same time and temperature, but the esters could still be easily isolated. Of equal importance was the observation that the acidic DES, which was used as a catalyst (0.3 equivalents), could be recycled several times with only a modest loss in activity. Eventually, the build-up of water reduced this activity over the course of 8 recyclings, but the DES could be readily restored by simple dehydration *in vacuo* and then reused further. In addition, product isolation was very simple, requiring just phase separation of the upper organic layer to isolate the ester product and recovery of the acidic DES.



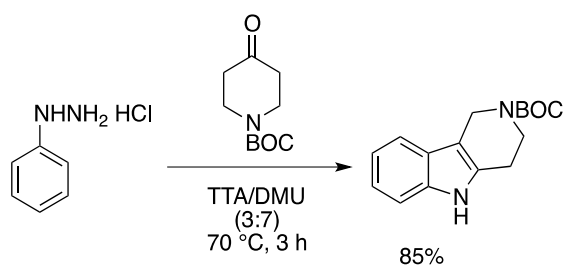
Scheme 31. Fischer Esterifications

Acidic DES have also been used studied in a number of carbonyl condensation type reactions, including the previously mentioned formation of bis(indolyl)methanes (bim) from aldehydes and indoles. [62] (Scheme 32) The DES in this case was again the combination of choline chloride and oxalic acid (CC/OxOH) and was used as a catalyst (10 mol%) for this transformation. The desired bims could be recovered in high yield after very short (5 minutes) reaction times at room temperature by dilution of the reaction with water and filtration. The DES could be recovered by evaporation of the aqueous layer and recycled several times with little loss of activity. The same paper also reported the synthesis of hydrazones from aryl aldehydes and acetophenones under the same reaction conditions. Another paper similarly reported the synthesis of bims by using TTA/DMU at 70 °C for 2-3 hours to afford the anticipated products in good yield. [63]



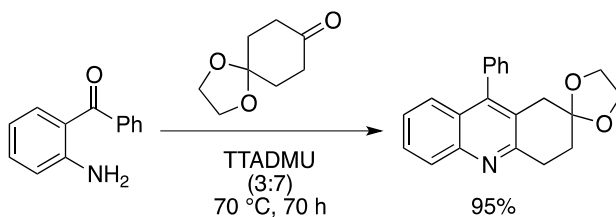
Scheme 32. BIM and Hydrazone Formation

In related work, the Fischer indole synthesis was reported in the tartartic acid/DMU (TTA/DMU) DES. [64] (Scheme 33) This reaction system afforded very good yields for a wide range of ketones, including ones with acid-sensitive functionality such as that seen in Scheme 33. The DES could be recovered from the aqueous layer after the reaction and recycled with minimal loss of activity over 3 uses. It seems likely that other acidic DES may behave similarly for this important reaction.



Scheme 33. Fischer Indole Synthesis

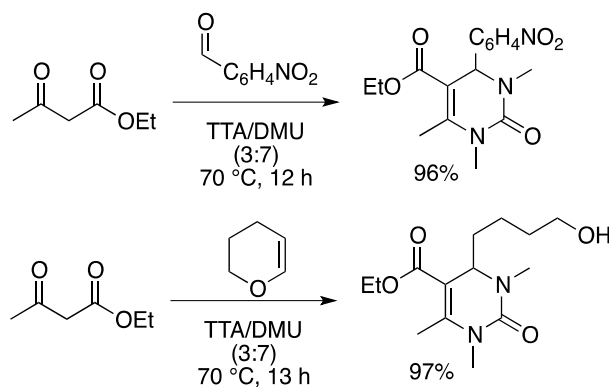
Another Heteroaromatic synthesis that has been reported in the same acidic DES is the Friedlaender synthesis of quinolones. [65] The combination of a ketone and an ortho-aminoacetophenone in TTA/DMU at $70\text{ }^\circ\text{C}$ afforded the target quinolones in good yield. Again, acid-sensitive functionality, such as the ketal in the reaction in Scheme 34, survives these reaction conditions, demonstrating their functional group tolerance. The one drawback to these reaction conditions is the extremely long reaction times (often several days). Nonetheless, there is much promise for this approach.



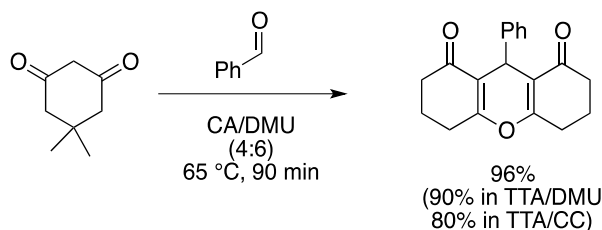
Scheme 34. Friedlaender Quinoline Synthesis

This same TTA/DMU acidic DES has found application in a number of multi-component reactions. In a pair of papers, Koenig and co-workers have reported the formation of dihydropyrimidin-2-ones or pyrimidopyrimidinediones by the combination of DMU and an aldehyde with ethyl acetoacetate and acetophenones respectively. [66, 67] (Scheme 35) In this case, beyond serving as a catalyst and solvent, the DES also serves as the source of the DMU. Non-methylated and thiocarbonyl versions of the products can also be accessed by switching to acidic DES with urea or thiourea respectively. Further, it was noted that vinyl ethers could be used as masked aldehydes, thereby affording access to hydroxyl-terminated alkyl substituents. In all cases, good to excellent yields are obtained after modest reaction times, thereby making this a very general route to these biologically interesting compounds.

A closely related acidic DES – citric acid/DMU – was found to be superior to TTA/DMU for the synthesis of 1,8-dioxo-dodecahydroxanthenes. [68] (Scheme 36) A wide range of aldehydes afforded good results under these reaction conditions and the DES could be recycled up to six times with little loss of activity. Recycling again involved the recovery of the DES from the aqueous layer via concentration *in vacuo*.

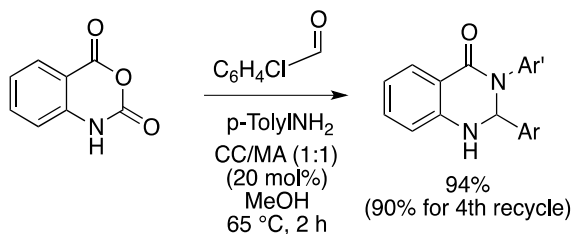


Scheme 35. Dihydropyrimidin-2-one and Derivatives Synthesis



Scheme 36. Xanthene Synthesis

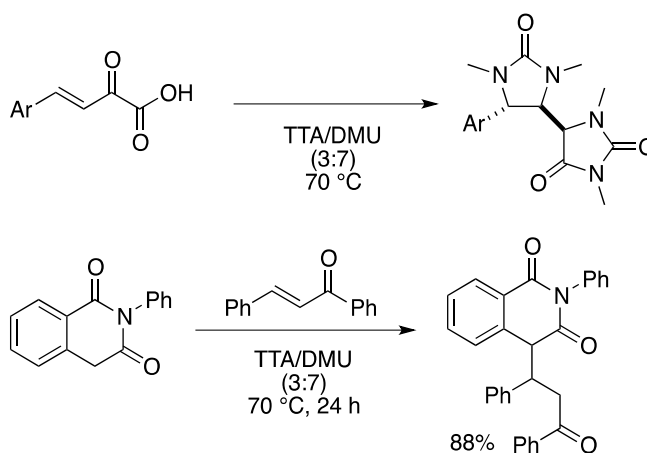
A final example of a multicomponent synthesis in an acidic DES comes from the Shankarling group who used CC/Malonic acid (CC/MA) to prepare 2,3-dihydroquinazoline-4-ones. [69] (Scheme 37) In this case, the DES is really employed as a catalyst (20 mol%) in methanol at 65 °C, instead of as a solvent as well. The DES can be recovered and recycled several times with little loss of activity by recovery from the aqueous layer, following product separation via extraction with ethyl acetate.



Scheme 37. 2,3-Dihydroquinazoline-4-one Synthesis

Finally, two different variations of conjugate addition have been reported in the TTA/DMU acidic DES. (Scheme 38) In the first, Koenig and co-workers have synthesized some complex

hydantoins in this DES, wherein the DES serves as solvent, catalyst, and the source of the urea component. The hydantoins are isolated in good yield as roughly 2:1 mixtures of the syn and anti isomers after several hours at 70 °C. [70] A more traditional Michael addition was reported using the same solvent system at 70 °C for relatively long reaction times (1-2 days). [71] Interestingly, several non-acidic carbohydrate-derived DES also afforded good results, indicating that the acidity may not be crucial for this reaction.



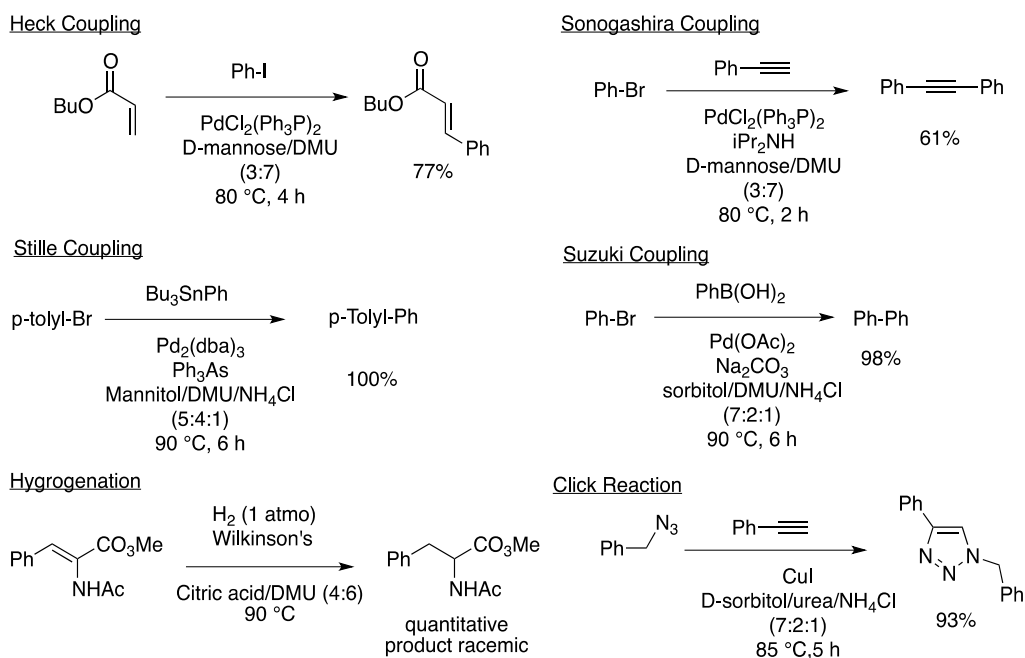
Scheme 38. Conjugate Additions

5. Carbohydrate-derived DES

Another major family of DES that have been extensively explored are those based upon carbohydrates. First popularized by Koenig and co-workers, they generally feature the combination of some carbohydrate (or reduced derivative as is the case with sorbitol and mannitol), a urea (most frequently *N,N'*-dimethylurea), and a chloride salt (most frequently ammonium chloride). [72, 74, 75] These DES frequently exhibit melting points in the 60-90 °C range and are easily prepared from bulk, biorenewable compounds. As a result, they feature an intriguing combination of being inexpensive, non-toxic, and environmentally compatible.

In terms of the chemistry explored in these solvents, much of it has been cross-coupling chemistry. Thus, Koenig and co-workers have employed various carbohydrate DES for Heck, Sonogashira, Stille, Suzuki, hydrogenations, and Click reactions. [74, 75] (Scheme 39) In general, these reactions performed similarly to those conducted in conventional solvents and were applicable, with slight variations in yield, across a considerable range of carbohydrate-derived DES. In a few cases recycling of both the palladium catalyst and the DES were mentioned, but with very little detail on how this recycling was performed. In the case of the Stille coupling between tributylphenyltin and *p*-bromoanisole, the reaction yield fell rapidly during recycling, going from 94% for the first reaction to 70% for the first recycling to 66% for

the second recycling which indicates either limited thermal stability of the catalyst or modest retention of the catalyst in the DES during product isolation.



Scheme 39. Metal-mediated Reactions in Carbohydrate-derived DES

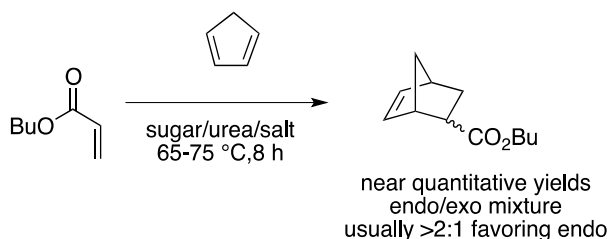
The Heck couplings were only reported using the more reactive aryl iodides, which work well under any of a wide range of reaction conditions. On the other hand, the Sonogashira couplings were reported for the less reactive aryl bromides and were performed in the absence of a copper co-catalyst, which does make these reaction conditions more potentially useful. [72] For the Suzuki coupling, a number of carbohydrate-derived DES were employed, with all affording generally good results for a range of electron-rich and deficient aryl bromides. [74] Across the examples studied, the sorbitol-based DES seen in Scheme 39 did afford modestly better results.

In the case of the hydrogenation reaction, although a chiral acid (citric acid) was used, the product that was obtained was racemic. [72] The use of other carbohydrate-derived DES for this particular reaction resulted in much poorer conversions.

Finally, for the copper-catalyzed Click reaction to form a triazole, the reaction could be either performed using a preformed azide (as shown in Scheme 1), or the azide could be generated in situ from sodium azide and benzyl bromide to afford the same product in 93% yield. [72]

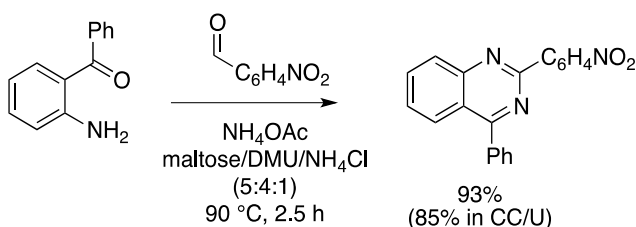
Beyond metal-catalyzed reactions, the Diels-Alder reaction of cyclopentadiene with butyl acrylate was also studied in a wide range of carbohydrate-derived DES. [72, 75] (Scheme 40) The reactions proceed in near quantitative yields in most cases and afforded modest endo selectivity. Unlike the earlier work by Abbott, this study did not report the results of any more

demanding Diels-Alder reactions, leaving the practical utility of these solvent systems in doubt. [48]



Scheme 40. Diels-Alder Reactions in Carbohydrate-derived DES

One example of the application of these carbohydrate-derived DES to the family of condensation reactions has also been reported. [76] Thus, the use of a maltose/DMU/ NH_4Cl DES for a catalyst-free Friedlander-type synthesis of quinazolines was reported. In general, the desired quinazolines were formed in high yield via a multi-component coupling of an aldehyde, an o-aminoacetophenone, and ammonium acetate. (Scheme 41) Interestingly, the omission of ammonium acetate severely decreased the yield of the desired quinazoline product with the reaction seen in Scheme 3 affording a 55% yield compared to a 93% yield in the presence of ammonium acetate. As a result, it appears that the ammonium chloride present in the DES is not able to serve as an effective nitrogen source for this reaction. Finally, these reactions worked well in a wide range of DES, including CC/U (more generally employed in condensation-type reactions). This result may indicate that the carbohydrate-derived DES could have a much broader range of application in condensation chemistry.



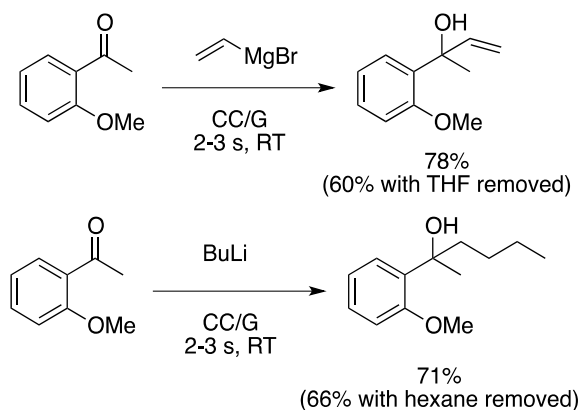
Scheme 41. Multicomponent Quinazoline Synthesis

6. Assorted DES

One of the exciting features of DES is the wide variety of materials that can be prepared. While many examples have been seen in the previous sections, a few additional ones provide excellent examples of this flexibility.

Recently, Del Monte and co-workers reported the use of an acrylic acid/Choline chloride DES as a combined reaction medium/reagent for frontal polymerization to form polyacrylic acids. [77] These polymerizations were initiated thermally using benzoyl peroxide and proceeded very efficiently to form the desired polymers. More interestingly, by dispersing or dissolving carbon nanotubes into this DES, carbon nanotube containing composites could be formed, resulting in materials with high biocompatibility and the potential for future applications as biomaterials. Indeed, this article serves as another reminder that the field of polymer science could benefit considerably from greater application of DES.

A very recent and very surprising result has appeared on the application of DES to main group organometallic chemistry. Although the generally protic nature of virtually all DES would be expected to be incompatible with organometallic reagent such as organolithiums and Grignards, it was noted that very rapid (2-3 seconds) additions to ketones could be achieved under ambient conditions with exposure to air. [78] (Scheme 42) Although several DES were studied, the optimal one was found to be choline chloride/glycerol (CC/G). Most reactions were performed using commercially available solutions of the organometallic reagents in ethereal or hydrocarbon solvents, but it was observed that the reactions still proceeded well when the organic solvent was removed *in vacuo* prior to addition. Unfortunately, attempts to generate the organometallic reagents in the DES failed, but this still constitutes a major advance in making organolithium and Grignard chemistry safer and more environmentally compatible. It will be interesting to note if the heightened reactivity observed in the present cases holds true for other organometallic reagents such as organozincs.



Scheme 42. Organometallic Chemistry in DES

7. Conclusion

In conclusion, in a few short years, DES have made a significant showing in Organic Synthesis. Given the broad range of such materials that can be imagined (neutral, Lewis acidic, and

Bronsted acidic), it is easy to picture continued growth in this area. Recycling has been demonstrated in many cases, although the frequently employed method of recovering the DES from the aqueous layer following extractive work-up of the reaction is undoubtedly energy intensive. It is likely that other superior methods for product separation and solvent recycling can be developed and should certainly be a topic for future focus. Additionally, the ability to tune the solvent properties by developing new DES is a fruitful option for study, although this may require the development of new design parameters beyond those currently in use. In any case, DES are here to stay.

Author details

Scott T. Handy*

Address all correspondence to: shandy@mtsu.edu

Department of Chemistry, Middle Tennessee State University, Murfreesboro, TN, USA

References

- [1] For a good overview of many non-traditional solvents in Organic Synthesis, see: Knochel, P. Ed. *Modern Solvents in Organic Synthesis*, Springer: New York, 1999.
- [2] For an excellent and relatively recent review covering the application of RTILs in Organic synthesis, see: Hallett, J.P., Welton, T. Room-temperature ionic liquids: Solvents for synthesis and catalysis. *Chem. Rev.* 2001, 111, 3508-3576.
- [3] Russ, C., Koenig, B. Low melting mixtures in organic synthesis – an alternative to ionic liquids? *Green Chem.* 2012, 14, 2969-2982.
- [4] Fransisco, M., van den Bruinhorst, A., Kroon, M.C. Low-transition-temperature mixtures (LTTMs): A new generation of designer solvents. *Angew. Chem. Int. Ed.* 2013, 52, 3074-3085.
- [5] Zhang, Q., Vigier, K.D., Jerome, F. Deep eutectic solvents: syntheses, properties, and applications. *Chem. Soc. Rev.* 2012, 41, 7104-7146.
- [6] Abbott, A.P., Capper, G., Davies, D.L., Rasheed, R.K., Tambyrajah, V. Novel solvent properties of choline chloride/urea mixtures. *Chem. Commun.* 2003, 70-71.
- [7] Abbott, A.P., Boothby, D., Capper, G., Davies, D.L., Rasheed, R.K. Deep eutectic solvents formed between choline chloride and carboxylic acids: versatile alternatives to ionic liquids. *J. Am. Chem. Soc.* 2004, 126, 9142-9147.

- [8] Abbott, A.P., Harris, R.C.; Ryder, K.S., D'Agostino, D., Gladden, L.F., Mantle, M.D. Glycerol eutectics as sustainable solvent systems. *Green Chem.* 2011, 13, 82-90.
- [9] Hou, Y., Gu, Y., Zhang, S., Yang, F., Ding, h., Shan, Y. Novel binary eutectic mixtures based on imidazole. *J. Mol. Liq.* 2008, 143, 154-159.
- [10] Parnica, J., Antalík, M. Urea and guanidine salts as novel components for deep eutectic solvents. *J. Mol. Liq.* 2014, 197, 23-26.
- [11] Cherukuvada, S., Nangia, A. Eutectics as improved pharmaceutical materials: design, properties, and characterization. *Chem. Commun.* 2014, 50, 906-923.
- [12] Abbott, A.P., Barron, J.C., Ryder, K.S., Wilson, D. Eutectic-based ionic liquids with metal-containing anions and cations. *Chem. Eur. J.* 2007, 13, 6495-6501.
- [13] Abbott, A.P., Capper, G., Davies, D.L., Munro, H.L., Rasheed, R.K., Tambyrajah, V. Preparation of novel, moisture-stable, Lewis-acidic ionic liquids containing quaternary ammonium salts with functional side chains. *Chem. Commun.* 2001, 2010-2011.
- [14] Abbott, A.P., Capper, G., Davies, D.L., Rasheed, R. Ionic liquids based upon metal halide/substituted quaternary ammonium salt mixtures. *Inorg. Chem.* 2004, 43, 3447-3452.
- [15] Hayyan, A., Mjalli, F.S., AlNashef, I.M, Al-Wahaibi, T., Al-Wahaibi, Y.M., Ali Hashim, M.A. Fruit sugar-based deep eutectic solvents and their physical properties. *Thermochimica Acta* 2012, 541, 70-75.
- [16] Abbott, A.P., Frisch, G., Hartley, J., Ryder, K.S. Processing of metals and metal oxides using ionic liquids. *Green Chem.* 2011, 13, 471-481.
- [17] Gorke, J.T., Sreenc, F., Kazlauskas, R.J. Hydrolase-catalyzed biotransformations in deep eutectic solvents. *Chem. Commun.* 2008, 1235-1237.
- [18] Zhao, H., Baker, G.A., Holmes, S. New eutectic ionic liquids for lipase activation and enzymatic preparation of biodiesel. *Org. & Biomol. Chem.* 2011, 9, 1908-1916.
- [19] Stepankova, V., Vanacek, P., Damborsky, J., Chaloupkova, R. Comparison of catalysis by haloalkane dehalogenases in aqueous solutions of deep eutectic and organic solvents. *Green Chem.* 2014, 16, 2754-2761.
- [20] Yang, Z., Huang, Z-L. Enzymatic synthesis of sugar fatty acid esters in ionic liquids. *Cat. Sci & Tech.* 2012, 2, 1767-1775.
- [21] Choi, Y.H., Spronsen, J., Dai, Y., Verberne, M., Hollmann, F., Arends, I.W.C.E., Witkamp, G-J., Verpoorte, R. Are Natural Deep Eutectic Solvents the Missing Link in Understanding Cellular Metabolism and Physiology? *Plant Physio.* 2011, 156, 1701-1705.

- [22] Singh, B., Lobo, H., Shankarling, G. Selective N-alkylation of aromatic primary amines catalyzed by bio-catalyst or deep eutectic solvent. *Catal. Lett.* 2011, 141, 178-182.
- [23] Sanap, A.K., Shankarling, G.S. Eco-friendly and recyclable media for rapid synthesis of tricyanovinylated aromatics using biocatalyst and deep eutectic solvent. *Catal. Commun.* 2014, 49, 58-62.
- [24] Azizi, N., Gholibegio, E. A highly efficient synthesis of dithiocarbamates in green reaction media. *RSC Advances* 2012, 2, 7413-7416.
- [25] Zho, A., Jiang, T., Han, B., Zhang, J., Xie, Y., Ma, X. Supported choline chloride/urea as a heterogeneous catalyst for chemical fixation of carbon dioxide to cyclic carbonates. *Green Chem.* 2007, 9, 169-172.
- [26] Azizi, N., Yadollahy, Z., Rahimzadeh-Oskooee, A. An atom-economic and odorless thia-Michael addition in a deep eutectic solvent. *Tetrahedron Lett.* 2014, 55, 1722-1725.
- [27] Azizi, N., Batebi, E., Bagherpour, S., Ghafuri, H. Natural deep eutectic salt promoted regioselective reduction of epoxides and carbonyl compounds. *RSC Advances* 2012, 2, 2289-2293.
- [28] Phadtare, S.B., Shankarling, G.S. Halogenation reactions in biodegradable solvent: Efficient bromination of substituted 1-aminoanthra-9,10-quinone in deep eutectic solvent (choline chloride:urea). *Green Chem.* 2010, 12, 458-462.
- [29] Abbott, A.P., Davies, D.L., Capper, G., Rasheed, R.K., Tambyrakah, V. Ionic liquids and their use as solvents. 2007, US patent 7,183,433 B2.
- [30] Phadtare, S.B., Jarag, K.J., Shankarling, G.S. Greener protocol for one pot synthesis of coumarin styryl dyes. *Dyes and Pigments* 2013, 97, 105-112.
- [31] Sonawane, Y.A., Phadtare, S.B., Borse, B.N., Jagtap, A.R., Shankarling, G.S. Synthesis of diphenylamine-based novel fluorescent styryl colorants by Knoevenagel condensation using a conventional method, biocatalyst, and deep eutectic solvent. *Org. Lett.* 12, 1456-1459.
- [32] Harishkumar, H.N., Mahadevan, K.M., Jumar, H.C.K., Satyanarayan, N.D. A facile, choline chloride/urea catalyzed solid phase synthesis of coumarins via Knoevenagel condensation. *Org. Commun.* 2011, 4, 24-32.
- [33] Pawar, P.M., Jarag, K.J., Shankarling, G.S. "Environmentally benign and energy efficient methodology for condensation: and interesting facet to the classic Perkin reaction. *Green Chem.* 2011, 13, 2130-2134.
- [34] Singh, B.S., Lobo, H.R., Shankarling, G.S. Choline chloride based deep eutectic solvents: magical catalytic system for carbon-carbon bond formation in the rapid synthesis of β -hydroxy functionalized derivatives. *Cataly. Commun.* 2012, 24, 70-74.

- [35] Hawkins, I., Handy, S.T. Synthesis of aurones under neutral conditions using a deep eutectic solvent. *Tetrahedron* 2013, 69, 9200-9204.
- [36] Yadav, U.N., Shankarling, G.S. Synergistic effect of ultrasound and deep eutectic solvent choline chloride-urea as versatile catalyst for rapid synthesis of β -functionalized ketonic derivatives. *J. Mol. Liq.* 2014, 195, 188-193.
- [37] Handy, S.T., Lavender, K. Organic synthesis in deep eutectic solvents: Paal-Knorr reactions. *Tetrahedron Lett.* 2013, 54, 4377-4379.
- [38] Handy, S.T., Wright, M. An acid-free Pictet-Spengler reaction using deep eutectic solvents (DES). *Tetrahedron Lett.* 2014, 55, 3440-3442.
- [39] Handy, S.T., Westbrook, N.M. A mild synthesis of bis(indolyl)methanes using a deep eutectic solvent. *Tetrahedron Lett.* 2014, 55, 4969-4971.
- [40] Sing, B.S., Lobo, H.R., Pinjari, D.V., Jarag, K.J., Pandit, A.B., Shankarling, G.S. Ultrasound and deep eutectic solvent (DES): A novel blend of techniques for rapid and energy efficient synthesis of oxazoles. *Ultrasonics Sonochem.* 2013, 20, 287-293.
- [41] Lobo, H.R., Singh, B.S., Shankarling, G.S. Lipase and deep eutectic mixture catalyzed efficient synthesis of thiazoles in water at room temperature. *Catal. Lett.* 2012, 142, 1369-1375.
- [42] Azizi, N., Desfooli, S., Khajeh, M., Hashemi, M.M. Efficient deep eutectic solvents catalyzed synthesis of pyran and benzopyran derivatives. *J. Mol. Liq.* 2013, 186, 76-80.
- [43] Revanna, C.N., Swaroop, T.R., Raghavendra, G.M., Bhadregowda, D.G., Mantelingu, K., Rangappa, K.S. Practical and green protocol for the synthesis of substituted 4H-chromenes using room temperature ionic liquid choline chloride-urea. *J. Heterocyc. Chem.* 2012, 49, 851-855.
- [44] Azizi, N., Dezfolli, S., Hashemi, M.M. Greener synthesis of spirooxindole in deep eutectic solvent. *J. Mo. Liq.* 2014, 194, 62-67.
- [45] Azizi, N., Dezfolli, S., Hashemi, M.M. Chemoselective synthesis of xanthenes and tetraketones in a choline chloride-based deep eutectic solvent. *C.R. Chimie* 2013, 16, 997-1001.
- [46] Azizi, N., Mariami, M., Edrisi, M. Greener construction of 4H-chromenes based dyes in deep eutectic solvent. *Dyes and Pigments* 2014, 100, 215-221.
- [47] Azizi, N., Dezfolli, S., Hashemi, M.M. A sustainable approach to the Ugi reaction in deep eutectic solvent. *C.R. Chimie* 2013, 16, 1098-1102.
- [48] 4Abbott, A.P., Capper, G., Davies, D.L., Rasheed, R.K., Tambyrakah, V. Quaternary ammonium zinc-and tin-containing ionic liquids: water insensitive, recyclable catalysts for Diels-Alder reactions. *Green Chem.* 2002, 4, 24-26.

- [49] Tin, D., Li, C., Li, B., Tao, B., Yin, D. High Regioselective Diels-Alder reaction of Myrcene with acrolein catalyzed by Tin-containing ionic liquids. *Adv. Synth. Catal.* 2005, 347, 137-142.
- [50] Azizi, N., Batebi, E. Highly efficient deep eutectic solvent catalyzed ring opening of epoxides. *Catal. Sci. & Technol.* 2012, 2, 2445-2448.
- [51] Zhu, A., Li, L., Wang, J., Zhuo, K. Direct nucleophilic substitution reaction of alcohols mediated by a zinc-based ionic liquid. *Green Chem.* 2011, 13, 1244-1250.
- [52] Duan, Z., Gu, Y., Deng, Y. Green and moisture-stable Lewis acidic ionic liquids (choline chloride x ZnCl₂) catalyzed protection of carbonyls at room temperature under solvent-free conditions. *Catal. Commun.* 2006, 7, 651-656.
- [53] Azizi, N., Gholibegio, E., Babapour, M., Ghafuri, H., Bolourtchian, S.M. Deep eutectic solvent promoted highly efficient synthesis of N,N'-diarylamidines and formamides. *C. R. Chimie* 2012, 15, 768-773.
- [54] Disale, S.T., Kale, S.R., Kahandal, S.S., Srinivasan, T.G., Jayaram, R.V. Choline Chloride-ZnCl₂ ionic liquid: an efficient and reusable catalyst for the solvent free Kabachnik-Fields reaction. *Tetrahedron Lett.* 2012, 53, 2277-2279.
- [55] Azizi, N., Manocheri, Z. Eutectic salts promote green synthesis of bis(indolyl)methanes. *Res. Chem. Intermed.* 2012, 38, 1495-1500.
- [56] Morales, R.C., Tambyrakah, V., Jenkins, P.R., Davies, D.L., Abbott, A.P. The regiospecific Fischer indole reaction in choline chloride-ZnCl₂ with product isolation by direct sublimation from the ionic liquid. *Chem. Commun.* 2004, 158-159.
- [57] Chen, Z., Zhou, B., Cai, H., Zhu, W., Zou, X. Simple and efficient methods for selective preparation of α -mono or α,α -dichloro ketones and β -ketoesters by using DCDMH. *Green Chem.* 2009, 11, 275-278.
- [58] Handy, S.T., Grant, S. Unpublished Results, Middle Tennessee State University.
- [59] Handy, S.T., Wright, M. Unpublished Results, Middle Tennessee State University.
- [60] Hu, S.; Zhang, Z., Zhou, V., Song, J., Fan, H., Han, R. Direct conversion of inulin to 5-hydroxymethylfurfural in biorenewable ionic liquids. *Green Chem.* 2009, 11, 873-877.
- [61] De Santi, V., Cardellini, F., Brinshi, L., Germani, R. Novel Bronsted acidic deep eutectic solvent as reaction media for esterification of carboxylic acid with alcohols. *Tetrahedron Lett.* 2012, 53, 5151-5155.
- [62] Yadav, U.N., Shankarling, G.S. Room temperature ionic liquid choline chloride-oxalic acid: a versatile catalyst for acid-catalyzed transformation in organic solvents. *J. Mol. Liq.* 2014, 191, 137-141.
- [63] Jella, R.R., Nagarajan, R. Synthesis of indole alkaloids arsindoline A, arsindoline B and their analogues in low melting mixture. *Tetrahedron* 2013, 69, 10249-10253.

- [64] Gore, S., Baskaran, S., Koenig, B. Fischer Indole synthesis in low melting mixtures. *Org. Lett.* 2012, 14, 4568-4571.
- [65] Ma, F-P., Cheng, G-T., He, Z-G., Zhang, Z-H. A new and efficient procedure for Friedlaender synthesis of quinolines in low melting tartaric acid-urea mixtures. *Aust. J. Chem.* 2012, 65, 409-416.
- [66] Gore, S., Baskaran, S., Koenig, B. Efficient synthesis of 3,4-dihydropyrimidine-2-ones in low melting tartaric acid-urea mixtures. *Green Chem.* 2011, 13, 1009-1013.
- [67] Gore, S., Baskaran, S., Koenig, B. Synthesis of pyrimidopyrimidinediones in a deep eutectic reaction mixture. *Adv. Synth. Catal.* 2012, 354, 2368-2372.
- [68] Li, P., Ma, F., Wang, P., Zhang, Z. Highly efficient low melting mixture catalyzed synthesis of 1,8-dioxo-dodecahydroxanthene derivatives. *Chin. J. Chem.* 2013, 31, 757-763.
- [69] Lobo, H.R.; Singh, B.S., Shankarling, G.S. Bio-compatible eutectic mixture for multi-component synthesis: A valuable acidic catalyst for synthesis of novel 2,3-dihydroquinazolin-4(1H)-one derivatives. *Catal. Commun.* 2012, 27, 179-183.
- [70] Gore, S., Chinthapally, K., Baskarran, S., Goenig, B. Synthesis of substituted hydantoin in low melting mixtures. *Chem. Commun.* 2013, 5052-5054.
- [71] Krishnakumar, V., Vindhya, N.G., Mandal, B.K., Khan, F. N. Green chemical approach: low-melting mixture as a green solvent for efficient michael addition of homophthalimides with chalcones. *Ind. Eng. Chem. Res.* 2014, 53, 10814-10819.
- [72] Ilgen, F., Koenig, B. Organic reactions in low melting mixtures based on carbohydrates and L-carnitine – a comparison. *Green Chem.* 2009, 11, 848-854.
- [73] Imperato, G., Vasold, R., Koenig, B. Stille Reactions with tetraalkylstannanes and phenyltrialkylstannanes in low melting sugar-urea-salt mixtures. *Adv. Synth. Catal.* 2006, 348, 2243-2247.
- [74] Imperato, G., Joeger, S., Lenoir, D., Koenig, B. Low melting sugar-urea-salt mixtures as solvents for organic reactions – estimation of polarity and use in catalysis. *Green Chem.* 2006, 8, 1051-1055.
- [75] Imperato, G., Eibler, E., Niedermaier, J., Koenig, B. Low-melting sugar-urea-salt mixtures as solvents for Diels-Alder reactions. *Chem. Commun.* 2005, 1170-1172.
- [76] Zhang, Z-H., Zhang, X-N., MO, L-P., Li, Y-X., Ma, F-P. Catalyst-free synthesis of quinazoline derivatives using low melting sugar-urea-salt mixture as a solvent. *Green Chem.* 2012, 14, 1502-1506.
- [77] Mota-Morales, J.D., Gutierrez, M.C., Ferrer, M.L., Jimenez, R., Santiago, P., Sanchez, I.C., Terrones, M., Del Monte, F., Luna-Barcenas, G. Synthesis of macroporous poly(acrylic acid)-carbon nanotube composites by frontal polymerization in deep-eutectic solvents. *J. Mat. Chem. A* 2013, 1, 3970-3976.

- [78] Vidal, C., Garcia-Alvarez, J., Hernan-Gomez, A., Kennedy, A.R., Hevia, E. Introducing deep eutectic solvents to polar organometallic chemistry: chemoselective addition of organolithium and Grignard reagents to ketones in air. *Angew. Chem. Int. Ed.* 2014, 53, 5969-5973.

Applications of Ionic Liquids (ILs) in Synthesis of Inorganic Nanomaterials

Wenjun Zheng, Di Li and Wei Guo

Additional information is available at the end of the chapter

<http://dx.doi.org/10.5772/59048>

1. Introduction

These years, inorganic nanomaterials, which stands out as an important class of advanced materials, received great attention due to the technological applications in fields as diverse as optoelectronics, energy conversion/production, catalysis, and biomedicine [1-3]. Formation and size or morphology control of nanoparticles are crucial issues in inorganic nanomaterials research. Among the investigated strategies for the synthesis of inorganic nanomaterials, the solution-based chemical process underwent rapid progress over the last two decades and has developed into a promising field in materials chemistry. The most common media for conducting chemical reactions and materials synthesis are aqueous and organic solvents. Nevertheless, a limited number of molecular solvents can be used and some of them may cause environmental problems. Although traditional molten salts have been used as alternative reaction media, their high boiling points (above 100 °C) significantly restricts the scope of applications and make the process impractical [4,5]. In this regard, it remains a great challenge to explore novel and green media that allow particular reactions to occur.

As an organic salts with low melting points (as low as -96°C), ionic liquids (ILs) have received much attention in many areas of chemistry and industry due to their potential as a “green” recyclable alternative to traditional organic solvents. Ionic liquids are not new; the first ionic liquid, [C₂H₅NH][NO₃] (melting point 13-14 °C), was synthesized by Walden via the neutralization of ethylamine with concentrated HNO₃, as reported in 1914 [6]. However, it is only in the past few years that ILs have begun to be used in the inorganic synthesis. The first attempt at using ILs as the reaction medium instead of conventional molecular solvents for the synthesis of inorganic materials was pioneered by Dai and co-workers in 2000 [7]. They introduced ILs for the fabrication of porous silica gels termed as “ionogels”, which are being extensively investigated. After this study, ILs have been actively employed for the synthesis

of a broad range of inorganic materials, and many interesting inorganic materials with various properties have been fabricated [8,9].

ILs offers many distinct advantages (such as negligible vapor pressures, good thermal stability, high ionic conductivity, broad electrochemical potential windows, and high synthetic flexibility) for a wide variety of inorganic and organic materials. This Chapter will focus on the use of ILs in inorganic materials synthesis. We will describe some recent development of synthesizing inorganic nanomaterials (including metal nanoparticles, metal oxides, metal chalcogenides, and zeolites) in ILs. Especially, we focus on the versatile role of ILs that plays in the synthesis of the inorganic nanomaterials.

2. Advantages of ILs in synthesis of inorganic nanomaterials

At the beginning, ILs have been used as functional solvents in the field of organic chemistry. The special physical properties of the ionic liquids that render them interesting as potential solvents for inorganic synthesis, as follows [10]: (1) They are good solvents for a wide range of inorganic materials and unusual combinations of reagents which can be brought into the same phase. (2) They are often composed of poorly coordinating ions, so they have the potential to be highly polar yet noncoordinating solvents. (3) ILs are immiscible with a number of organic solvents and can provide a nonaqueous and polar alternative for the two-phase systems. Hydrophobic ionic liquids can also be used as immiscible polar phases with water. (4) Ionic liquids are nonvolatile, hence they may be used in high-vacuum systems and eliminate many containment problems. Recently, ILs have been employed as reaction media to fabricate inorganic nanomaterials via various routes, such as ionothermal synthesis, ILs-assisted modified hydrothermal/solvothermal methods, and ILs-assisted microwave method [11]. Especially, ionothermal synthesis, which mainly uses ILs as the reaction solvent and, in many cases, structure directing agent (SDA) shows many advantages in the inorganic synthesis [12]. For example, the negligible vapor pressure produced from ILs when heated makes the ionothermal synthesis take place at ambient pressure. This property not only eliminates the safety concerns associated with the high pressure, but also allows for the ionothermal synthesis of materials in glass vessels.

Ionic liquids cannot be regarded as merely a “green” alternative to conventional organic solvents. The most important advantage of using ionic liquids for the preparation of inorganic materials is that ionic liquids form extended hydrogen bond systems in the liquid state and are therefore highly structured, which can be defined as supermolecular fluids [13]. This property of structural organization makes ionic liquids suitable for use as entropic drivers for the generation of well-defined nanostructures with extended order. ILs thus have been widely used as templates for the synthesis of nanomaterials, especially the hollow and porous materials [14,15]. ILs have significant influence on the shapes and structures of the samples based on different mechanisms, including hydrogen bonds and π - π stack interactions, self-assembled mechanism, electrostatic attraction, and so on.

Since ionic liquids can serve as “tailored solvents”, they thus give us an opportunity for designing the ionic liquid according to the crystal structures, compositions, and crystal habits of the target products. ILs containing ions like sulfate, phosphate, carbonate, chloride, and metal cations can be regarded as reactive liquid precursors for the fabrication of inorganic materials. The IL is not only a solvent or template, but it acts as a tailored molecular precursor with a well-defined composition, structure, and reactivity. These parameters can be exploited for the fabrication of uniformly structured inorganic materials with various properties and these ILs can be viewed as “all-in-one” ILs. The hypothesis of ionic liquids as “all-in-one” solvents was first tested on cuprous chloride by Taubert and co-workers [16]. In that study, they introduced a protocol for the synthesis of CuCl nanoplatelets from a Cu-containing IL **1** and 6-O-palmitoyl ascorbic acid **2**. It was found that the mixtures of **1** and **2** could form thermotropic liquid crystals with lamellar self-assembled structures and the plate morphology was therefore caused (Figure 1). After this study, a large range of inorganic nanomaterials with interesting phases and morphologies were fabricated from various all-in-one ILs [13].

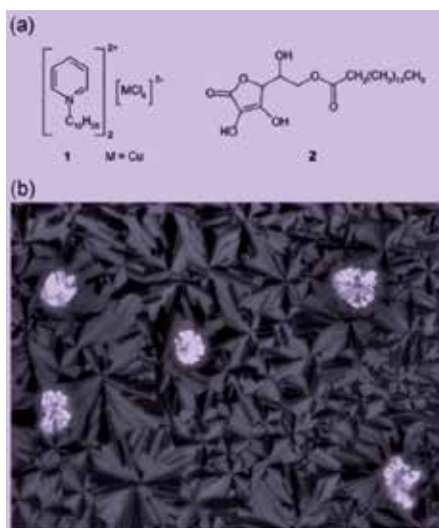


Figure 1. (a) Components of the ionic liquid precursors used for CuCl platelet synthesis: Cu-containing IL **1** and 6-O-palmitoyl ascorbic acid **2**. (b) Optical micrograph (crossed polarizers) of a demixed ionic liquid precursor.

3. Development of ILs in synthesis of inorganic nanomaterials

3.1. Metal nanoparticles

Metal nanoparticles (NPs) have become one of the hottest fields in nanoscience due to their diverse applications in the fields of catalysis, biology, optics, electronics, and nanotechnology [17,18]. Metal NPs can be fabricated by a variety of methods, such as chemical reduction of metal salts, thermal, photochemical or sonochemical decomposition of metal complexes,

hydrogenation of olefinic ligands of metal complexes, vapour phase deposition and electrochemical reduction of metals in high oxidation states. Majority of the metal NPs synthesized in the ILs medium needs the additional reducing reagents such as molecular hydrogen gas, complex hydrides, hydrazine, alcohols, and thiols, leading to a complex synthesis, where the shapes and sizes of the products are strongly affected by the concentration, addition sequence, and rate of addition of the capping and reducing agents. In contrast, ILs have unique and tunable properties useful in the synthesis of metal nanocrystals via chemical or physical routes. The main advantages of using ILs are their dual role of reaction solvent and nanoparticles stabilizer [19] (Figure 2). Thiol-, ether-, carboxylic acid-, amino-, hydroxyl-, or nitrile-functionalized imidazolium cations can stabilize metal NPs even more efficiently through the added functional group[20].

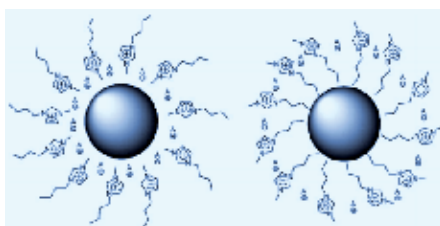


Figure 2. Potential NPs tabilisation in ILs for surface charged/polar NPs (left) and for surface neutral, non-polar NPs (right) [19].

In some cases, ILs acts as reducing agent for the formation of various metal NPs by simple reduction of metal salt compounds. Recently, there are very few reviews on the synthesis of metal NPs [19-22]. For instance, Dupuont and co-workers discussed the structural/surface properties of soluble metal NPs dispersed in ILs, with particular attention paid to the stabilization models proposed to explain the stability and properties of these metal NPs [21]. Luska and Moores reviewed the use of functionalized ILs in the synthesis of metal NPs, with an emphasis on the application of NP:IL catalysts [22]. In this part, we will present the current progress mainly on the chemical reduction synthesis of metal NPs in the presence of ILs.

3.1.1. Monometallic NPs

3.1.1.1. Ir, Ru and Pt

In 2002, Dupont and co-workers for the first time reported the synthesis of Ir NPs with an average size of 2 nm in the IL [BMIM][PF₆] medium with the absence of any surfactant [23]. By using the similar strategies, they later synthesized the stable and isolable nanometric Pt NPs of 2.0-2.5 nm in diameter from the reaction of Pt₂(dba)₃ (dba=bis-dibenzylidene acetone) dispersed in ionic liquid [BMIM][PF₆] with molecular hydrogen (4 atm) at 75 °C [24] (Figure 3). They found that a plethora of imidazolium ILs with different physical-chemical properties can be easily prepared by varying the anion and the alkyl chain on the aromatic ring, and this thereby opens the possibility for the preparation of distinct NPs, for biphasic catalysis. Very

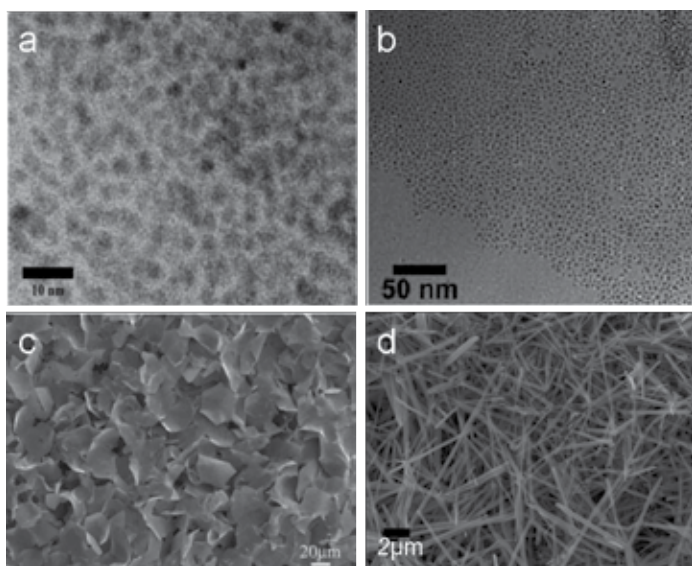


Figure 3. TEM and SEM images exemplifying metal NPs exhibiting different shapes prepared in the presence of ILs: (a) Pt stabilized by ILs [24], (b) Ru stabilized by ILs [26], (c) Au nanosheets [28], (d) Ag nanowires [32].

recently, Zhang et al. [25] reported the electroless deposition of Pt NPs by dissolving $K_2[PtCl_4]$ or $K_2[PtCl_6]$ in 1-ethyl-3-methylimidazolium ILs containing bis-(trifluoromethylsulfonyl)imide (NTf_2) or tetrafluoroborate (BF_4) anion and small cations such as H^+ , K^+ , and Li^+ at various temperatures. The ultrasmall and uniform Pt NPs of ca. 1-4 nm in diameter were produced and the Pt-NPs/[EMIM][Tf_2N] dispersion was kept stably for several months without adding any additional stabilizers or capping molecules.

Dupont and co-workers [26] have presented a simple organometallic approach for the synthesis and catalytic application of Ru NPs in imidazolium ionic liquids using a clean straightforward hydrogenation route with the readily available versatile ruthenium precursor $[Ru(COD)(2\text{-methylallyl})_2]$ (Figure 3). The particles with 2.1-3.5 nm in diameter dispersed in the ionic liquid, no significant agglomeration of the Ru NPs can be observed. Recently, Prechtl and co-workers synthesized the Ru nanoparticles from the reduction and decomposition of $([Ru(COD)(2\text{-methylallyl})_2])$ precursor, which were dissolved in imidazolium ILs undergo reduction and decomposition, respectively [27].

3.1.1.2. Au, Ag and Cu

On the other hand, some ILs itself, such as hydroxylated imidazolium salts, can perform as the reducing agent in the synthesis of metal NPs. For example, Li et al. [28] prepared Au nanosheets with very large size by directly microwave heating of $[BMIM][BF_4]$ or $[BMIM][PF_6]$ solutions (Figure 3). It can be found that the formation of the large-scale Au nanosheets is likely directly related to two-dimensional polymeric structure by hydrogen bonds between the cations and anions in the ILs, which has a template effect for the formation of Au sheets.

In another report, Gao et al. [29] used [BMIM][PF₆] and [BMIM][Tf₂N] as multifunctional molecules and synthesized regular-shaped single-crystal Au nano- and microprisms with controlled sizes (a very broad size range of 3–20 μm in diameter and 10–400 nm in thickness) without the need for additional capping agents and reducing agent. Ren et al. also fabricated Au nano- and microstructures such as polyhedral crystals, large single-crystalline nanoplates, hollow trapeziform crystals, holey polyhedra, and dendrites via microwave heating of H₂AuCl₄·4H₂O in a variety of ionic liquids (ILs) in the absence of capping agents or additional reducing agents [30]. The authors supposed that IL ions act as the capping agent directing Au crystal growth and consequently determining the final shape, owing to the fact that ILs having different absorption abilities and thus leading to the various morphologies observed. Qin et al. [31] reported the synthesis of hierarchical, three-fold symmetrical, single-crystalline Au dendrites were synthesized by the reaction between a zinc plate and a solution of H₂AuCl₄ in the ionic liquid [BMIM][PF₆]. The significantly lowered ion diffusivity and reaction rate in the ionic liquid medium could largely contribute to the formation of the pure single-crystalline Au dendrites.

Suh and co-workers [32] synthesized the Ag nanowires by the simple reduction of a silver precursor in the presence of [BMIM][MeSO₄] (Figure 3). By choosing the different IL, they also synthesized well-defined Ag NPs with cubic and octahedral shape in the presence of [BMIM]Cl and [BMIM]Br, respectively. Importantly, they found that ILs distributed over the nanoparticle surface play an important role in the determination of interparticle interactions, leading different assembly processes with respect to the types of ILs employed. It was speculated that [BMIM][MeSO₄] provides a higher degree of directional polarizability than either [BMIM]Cl or [BMIM]Br, as a result of the bulky and delocalized charge state of the anions. Kim and co-workers [33] reported the water-phase synthesis of Ag nanoparticles with average size of 4.1 and 2.2 nm using 1-(2-hydroxyethyl)-3-methylimidazolium tetrafluoroborate ([HEMIM][BF₄]) and 1-(2'-hydroxyethyl)-2-methyl-3-dodecylimidazoliumchloride ([C₁₂HEMIM]Cl), respectively, in the absence of any other reducing agent. They also found that the size of IL-Ag could be tuned by varying the side chain length of the cation.

IL-mediated nanobelt self-assembly from nanoparticles has been much less well investigated and an intermediate state that transiently appears during the self-assembly process has seldom been observed. Very recently, Zhou and co-workers presented the controlled self-assembly of copper nanoparticles into nanobelts bridged by an IL [34]. They first synthesized Cu nanoparticles via the addition of hydrazine hydrate into the mixture solution of Cu(AcO)₂, ethanol and IL. The formed Cu nanoparticles can assemble into Cu nanobelts in around one week. It was found that the template-like effect of the ionic liquids was the key for the formation of Cu nanobelts.

3.1.2. Bimetallic NPs

The possibility of controlling the electronic and geometric structures of bimetallic NPs by the addition of a second metal is one of the most important approaches to obtain more efficient catalysts [35]. Compared to the monometallic NPs, the synthesis of bimetallic NPs in the ionic liquids was less studied. In 2004, Yang and co-workers [36] for the first time demonstrated the

synthesis of CoPt nanorods, hyperbranched nanorods, and nanoparticles with different CoPt compositions in ionic liquid [BMIM][Tf₂N], from the (Pt(acac)₂) and (Co(acac)₃) precursors in the presence of CTAB. Very recently, Dupont and co-workers [37] prepared unsupported bimetallic Co/Pt NPs with size of 4.4 ± 1.9 nm by a simple reaction of [bis(cyclopentadienyl)cobalt(II)] and [tris(dibenzylideneacetone) bisplatinum(0)] complexes in IL [BMIM][PF₆] at 150 °C under hydrogen for 24 h. The formed bimetallic Co/Pt NPs display core-shell like structures in which mainly Pt composes the external shell (CoPt₃@Pt-like structure). Different from these two works, Vallés and co-workers [38] demonstrated an electrochemical synthesis of alloyed CoPt NPs of different sizes (10-120 nm), using CoPt aqueous solution/[BMIM][PF₆]/Triton X-100 water-in-ionic liquid microemulsions by electrodeposition. The relative amount of aqueous solution to ionic liquid determines the size of the nanoreactors, which serve as nanotemplates for the growth of the nanoparticles and hence determine their size and distribution.

In addition to CoPt, other bimetallic NPs or composites were prepared in the presence of IL. For example, Helgadóttir et al. [39] reported the preparation of core-shell Ru@CuNPs with small diameters and narrow size distributions via the simultaneous decomposition of Ru and Cu organometallic precursors in IL. Ding et al. [40] reported the synthesis of Pd_xNi_y bimetallic NPs (the nominal atomic ratios of Pd to Ni are 2:1, 3:2 and 1:1) supported on multi-walled carbon nanotubes (MWCNTs) by a thermal decomposition process using N-butylpyridinium tetrafluoroborate ([BPy][BF₄]) as the solvent. Fischer and co-workers [41] synthesized Ni/Ga alloy materials by microwave induced copolyolysis of [Ni(COD)₂] (COD=1,5-cyclooctadiene) and GaCp* (Cp*=pentamethylcyclopentadienyl) the ionic liquid [BMIM][BF₄]. They found that, without additional hydrogen, the current method selectively yields the intermetallic phases NiGa and Ni₃Ga from the respective 1:1 and 3:1 molar ratios of the precursors.

3.2. Metal oxides

Metal oxides have been regarded as promising solid-state materials for a wide variety of applications in the fields of nanotechnology and materials science due to their unique chemical, physical and mechanical properties. Till now, many metal oxides have been prepared in ionic liquids or mixed solutions containing ionic liquids by the wet chemical method.

3.2.1. TiO₂

It is widely known that TiO₂ is an important wide band gap semiconducting material and is widely used in the photocatalytic field. Up to now, TiO₂ of different phases (anatase or rutile) and morphologies were synthesized by using ILs as the medium. Zhou et al. [42] used IL [BMIM][BF₄] as medium and synthesized mesoporous spherical anatase aggregates self-assembled from very fine anatase nanocrystals with an average diameter of 2-3 nm under mild conditions. The high crystallinity of the obtained particles underlines the unique advantages of the IL method compared to other synthetic pathways towards TiO₂ nanocrystals. Very interestingly, Nakashima and co-worker [14] synthesized hollow TiO₂ microspheres by subjecting a mixture of [BMiM][PF₆], toluene, and Ti(OBu)₄ to vigorous stirring. The Ti(OBu)₄ molecules dissolved in toluene droplets reacted with trace amount of water at the

interface between the toluene droplets and ionic liquid, leading to the formation of hollow TiO_2 microspheres (Figure 4). It is worth mentioning that no other hard template was needed in the synthesis, indicating the advantages of the ILs as the efficient, simple all-in-one systems for the inorganic synthesis.

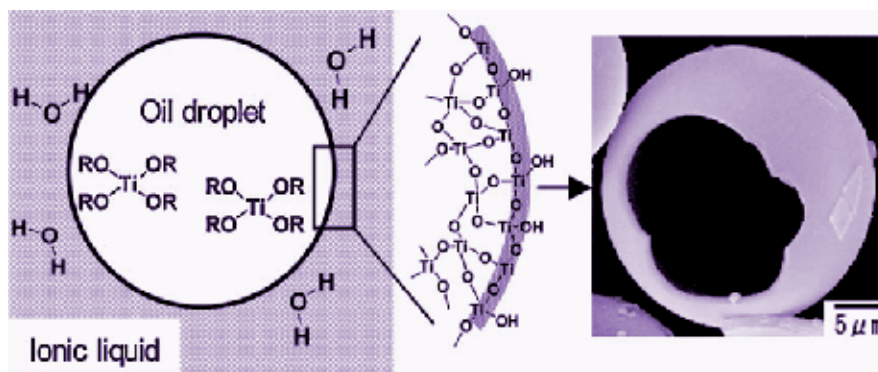


Figure 4. Left: Schematic illustration of the mechanism proposed for the formation of hollow TiO_2 microspheres at the interface between the oil droplet and ionic liquid. Right: SEM image of a hollow TiO_2 microsphere with a broken shell. [14]

In another report, Ding et al. [43] reported a facile method to synthesize cubelike anatase nanocrystals with uniform size and shape via a microwave-assisted route in $[\text{BMIM}][\text{BF}_4]$. Dai and co-workers [44] fabricated hierarchically patterned macroporous TiO_2 architectures via the spontaneous self-assembly of TiO_2 prepared from a mixture of 1-octadecene (ODE) and an ODE-immiscible 1-alkyl-3-methylimidazolium-based ionic liquid as the reaction medium. Wessel et al. [45] reported a fast way to synthesize pure $\text{TiO}_2(\text{B})$ in a mixture of $[\text{C}_{16}\text{MIM}]\text{Cl}/[\text{C}_4\text{MIM}][\text{BF}_4]$. In addition to pure TiO_2 , element-doped TiO_2 nanomaterials were also fabricated. Yu et al. [46] employed, ionic liquid $[\text{BMIM}][\text{BF}_4]$ as both a structure-directing agent and a dopant and prepared fluorinated B/C-codoped anatase TiO_2 nanocrystals through hydrothermal hydrolysis of tetrabutyl titanate. Our group recently reported a facile ionic liquid-assisted synthesis of pure rutile and rutile-anatase composite nanoparticles by hydrolysis of titanium tetrachloride in hydrochloric acid [47]. The ionic liquid, $[\text{EMIM}]\text{Br}$, can serve as a capping agent based on its strong interaction with the (110) facet of rutile. More specifically, we demonstrate that $[\text{EMIM}]\text{Br}$ favors the formation of rutile structure with a rod-like shape due to the mutual π - π stacking of imidazole rings. The ratios of rutile to anatase in the products can be controlled and TiO_2 nanoparticles with arbitrary phase compositions can be obtained in high yields by means of this simple method.

3.2.2. ZnO

Zinc oxide (ZnO), a wide band gap semiconductor, plays an important role in many applications because of its extraordinary electrical and optical properties. Recently, ILs have attracted much attention in the synthesis of ZnO since it can not only acts as functional solvents for

reaction precursors but also morphologic templates for nanostructures. Zhou et al. [48] synthesized ZnO hexagonal micro-pyramids with all their exposed surfaces consisting of polar $\pm(0001)$ and $\{10\bar{1}\}$ planes by using a mixture of oleic acid and ethylenediamine as the solvent, which can be regarded as one kind of ionic liquid ($R\text{-COOH}+R\text{-NH}_2 \rightarrow R\text{COO}^-+R\text{-NH}_3^+$). Zhu et al. [49] prepared hierarchical ZnO structures with diverse morphologies from the metal-containing ILs acting as both solvents and metal-oxide precursors. Our group [50] recently found that low-dimensional ZnO nanostructures from nanoparticles to nanorods to nanowires can be successfully synthesized in ionic liquid at low temperature (Figure 5). We found that the longer alkyl chain at position-1 of the imidazole ring of the ionic liquid will hinder the ZnO nanostructures from growing longer, and the hydrogen bonds may play a crucial role for the directional growth of the 1D nanocrystals. The as-obtained ZnO nanostructures in different ionic liquids show strong size/shape dependence of photocatalysis activity.

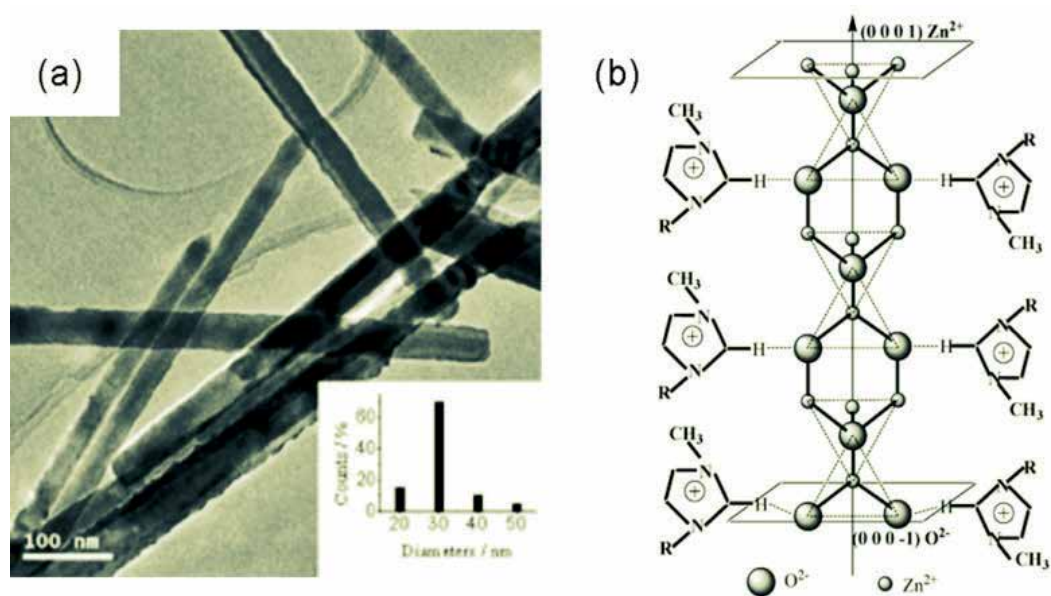


Figure 5. (a) TEM image and size distribution histogram (inset) of the ZnO nanorods prepared in [EMIM][BF₄] at low temperature. (b) Proposed growth schematic diagram of 1D ZnO nanostructures in ionic liquid. [50]

3.2.3. Copper oxide

Copper oxide is a transition-metal oxide with a narrow band gap, and is widely used as a photocatalyst. Li et al. [51] reported the morphology control synthesis of Cu₂O crystals by the electrodeposition method in the presence of ionic liquids. They found that the hydrophilic ionic liquids, 1-methyl-3-ethylimidazolium salts containing ethyl-sulfate anions, have dramatic effects on the morphology changes of electrochemically grown Cu₂O crystals. The shape of Cu₂O crystals evolves from cubic to octahedral and spherical shape only by adding a varied

small amount of ionic liquids in the deposited solutions. Shen and co-workers [52] presented the synthesis of flowerlike Cu_2O architectures in the presence of ionic liquid [BMIM][BF_4] with the assistance of microwave irradiation. It was shown that flowerlike Cu_2O architectures with a band gap of about 2.25 eV and a high surface area of $65.77 \text{ cm}^2\text{g}^{-1}$ consist of many thin nanosheets that could be obtained by adjusting the amount of used [BMIM][BF_4] and exhibited high and stable photochemical activity for the reduction of Cr(VI) to Cr(III) under visible-light irradiation. Recently, stable nanouids comprising of CuO nanoparticles suspended in 1-butyl-3-methylimidazolium acetate and trioctyl(dodecyl) phosphonium acetate have been synthesized and it was found that these ionic liquids provide stabilization to CuO nanoparticles [53]. Gusain et al. [54] prepared CuO nanorods by ultrasound assisted shape regulation in the presence of 1-hexyl-3-methylimidazolium acetate and tetrabutylammonium acetate ionic liquids. The results showed that CuO nanorods, stabilized by ionic liquids, exhibit excellent friction-reduction (15-43%) and improved anti-wear properties (26-43%) compared to the PEG 200 and 10W-40 engine oil.

3.2.4. Iron oxide

Hematite ($\alpha\text{-Fe}_2\text{O}_3$) and magnetite (Fe_3O_4) has attracted a great deal of attention owing to potential applications in fields of catalysis, gas sensors, adsorbent, rechargeable Li-ion batteries, magnetic storage, etc. Recently, our group have successfully prepared $\alpha\text{-Fe}_2\text{O}_3$ with various morphologies, such as nanoparticles, mesoporous hollow microspheres, microcubes, and porous nanorods, via an [BMIM]Cl ionic liquid assisted hydrothermal synthetic method [55]. Importantly, we found that the hydrogen bond-co- π - π stack mechanism is used to be responsible for the present self-assembly of the [BMIM]Cl ionic liquid in the reaction systems for the formation of the $\alpha\text{-Fe}_2\text{O}_3$ with various morphologies. We also successfully synthesized aggregated $\alpha\text{-Fe}_2\text{O}_3$ nanoplates under ionothermal conditions through the self-assembly of nanoplatelets in a side-to-side manner [56]. [PMIM]I ionic liquid was used in the synthesis and is essential for the assembly and coalescence of small nanoplatelets into final nanoplates. Using the similar method, self-assembled Fe_3O_4 nanoflakes with an average diameter of about 15 nm have been synthesized with the assistance of ionic liquid [C_{16}MIM]Cl, which plays a critical role for the self-assembly of nanoparticles into nanoflakes by adsorbing onto the surfaces of the primary Fe_3O_4 nanoparticles [57]. Most recently, Xu et al. [58] prepared $\alpha\text{-Fe}_2\text{O}_3$ hollow microspheres in the presence of metal ion-containing reactable ionic liquid ([OMIM][FeCl_4]) under the solvothermal condition. It was found that [OMIM][FeCl_4] acted not only as Fe source but also as solvent and template for the fabrication of $\alpha\text{-Fe}_2\text{O}_3$ hollow microspheres. In addition, the electrochemical and photocatalytic properties of $\alpha\text{-Fe}_2\text{O}_3$ were investigated. The $\alpha\text{-Fe}_2\text{O}_3$ hollow microspheres exhibited high conductivity, high photocurrent, and high photocatalytic activity. The designed hollow microsphere showed potential applications in photocatalysis.

3.2.5. Other oxides

BiOX (X=Cl, Br and I) has drawn considerable attention because of its optical properties and promising industrial applications, such as catalysts and photocatalysts, ferroelectric

materials, pigments, photoluminescence, and so on. Recently, ionic liquids as “designer liquids” have attracted great interest for the synthesis of BiOX micro/nanostructures. Our group has successfully synthesized ultrathin BiOCl nanoflakes, nanoplate arrays, and curved nanoplates via an ionothermal synthetic route by using an ionic liquid $[C_{16}MIM]Cl$ as “all-in-one” solvent, simply adjusting reaction temperature (Figure 6) [59]. The formation of plate-like BiOCl may be due to fact that the $[C_{16}MIM]Cl$ prefers to selectively adsorbed on the (001) plane of BiOCl, which can effectively inhibit crystalline growth in the (001) direction. Li and co-workers[60] have been successfully synthesized BiOI uniform flowerlike hollow microspheres with a hole in its surface structures through an EG-assisted solvothermal process in the presence of ionic liquid $[BMIM]I$. In this work, ionic liquid $[BMIM]I$ not only acted as solvents and templates but also as an I source for the fabrication of BiOI hollow microspheres and was vital for the structure of hollow microspheres. Yu and co-workers [61] fabricated bismuth BiOBr micropsheres with hierarchical morphologies via an ionothermal synthesis route. Ionic liquid $[BMIM]Br$ acts as a unique soft material capable of promoting nucleation and in situ growth of 3D hierarchical BiOBr mesocrystals without the help of surfactants.

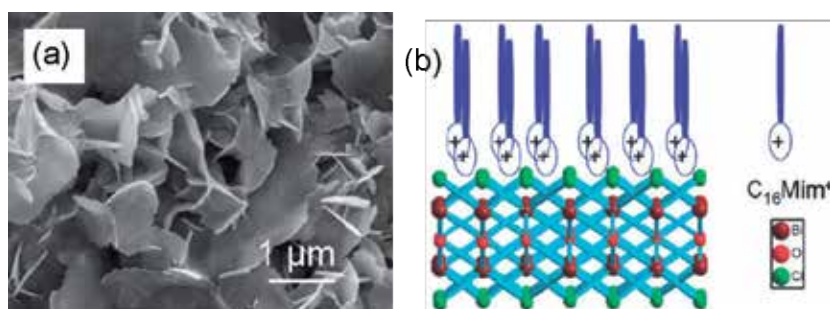


Figure 6. (a) SEM images of BiOCl nanoplates obtained in $[C_{16}Mim]Cl$ at 180 C for 24 h. (b) Schematic illustration of the interaction of BiOCl crystal planes and the head parts of $[C_{16}MIM]Cl$. [59]

Recently, Lian et al. [62] prepared $\gamma-Al_2O_3$ mesoporous nanoflakes via a one-step ionothermal synthetic method under mild conditions using an ionic liquid $[BDMIM]Cl$ as multifunctional material in terms of solvent and template. Duan et al. [63] prepared well-dispersed ammonium aluminum carbonate hydroxide (NH_4-Dw) and $\gamma-AlOOH$ nanostructures with controlled morphologies have been synthesized by employing an ionic liquid ($[BDMIM]Cl$) assisted hydrothermal process. These as-prepared NH_4-Dw and $\gamma-AlOOH$ nanostructures were converted into porous $\gamma-Al_2O_3$ nanostructures by thermal decomposition, whilst preserving the same morphology. Very recently, Li et al. [64] reported a simple and facile hydrothermal method for the synthesis of hierarchical $\alpha-GaOOH$ architectures assembled by nanorods as a precursor, in which ionic liquid ($[BMIM][OH]$), as green and efficient recyclable solvents, play a key role in the formation of the hierarchical structures. After calcining the precursor in air, mesoporous $\alpha-Ga_2O_3$ hierarchical structures were successfully obtained. Furthermore, the as-prepared mesoporous $\alpha-Ga_2O_3$ hierarchical structures display good photocatalytic activity in the degradation of RhB molecules.

3.3. Metal Chalcogenides

3.3.1. M_2X_3 ($M=Bi$ or Sb ; $X=S$ or Se)

Metal chalcogenides have been previously studied and employed in many applications, such as catalysis, light harvesting, energy conversion and storage devices [65,66]. Like metal oxides, a few kinds of metal chalcogenides have been synthesized using methods based on ionic liquids. Jiang et al. [67] synthesized single-crystalline Bi_2S_3 nanorods and Sb_2S_3 nanorods via the microwave-assisted ionic liquid method by using $[BMIM][BF_4]$ as the reaction medium. Later, they synthesized Bi_2Se_3 nanosheets with thicknesses of 50-100 nm by the microwave-assisted ionic liquid method, where selenium powder, $Bi(NO_3)_3 \cdot 5H_2O$, HNO_3 aqueous solution, ethylenediamine or ethylene glycol, and an ionic liquid $[BMIM][BF_4]$ were used [68]. Yu and co-workers [69] prepared uniform Bi_2S_3 flowers composed of uniform nanowires (diameter 60-80 nm) using $BiCl_3$ and CH_3CSNH_2 as the precursors and a mixture of $[BMIM][BF_4]$ and water as the reaction medium (Figure 7).

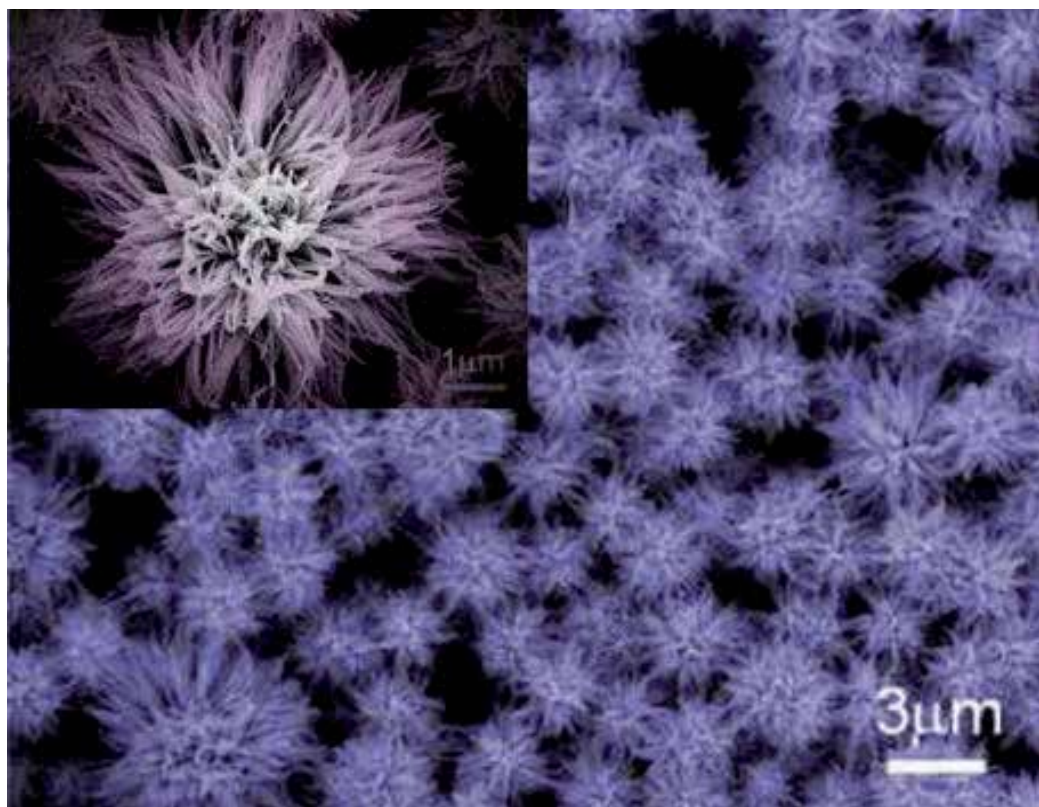


Figure 7. SEM images of Bi_2S_3 nanoflowers synthesized using $BiCl_3$ and CH_3CSNH_2 as the precursors and $[BMIM][BF_4]$ as the solvent and template [69].

Our group recently achieved a morphology control synthesis over the Bi_2S_3 nanostructure by via an ionic liquids-assisted hydrothermal route. One dimensional nanorods, two dimensional nanofabrics, and three dimensional urchin-like microspheres and crossed nanofabrics have been obtained [70]. In another study, we also achieved the morphology-control synthesis of Sb_2S_3 nanostructures [71]. By introducing different organic complex reagents or the amount of ionic liquid [BMIM]Cl in the reaction system, one-dimensional nanorods, two-dimensional nanowire bundles, three dimensional sheaf-like superstructures, dumbbell-shaped superstructures, and urchin-like microspheres can be obtained. It should be noted that, the self-assembly effect of ionic liquid, which could attribute to a combination of the van der Waals forces between the ionic liquid molecules and the hydrogen-bond interactions and electrostatic forces between the citrate cations and ionic liquid, play an important role in the formation of different morphologies.

3.3.2. MX ($M=\text{Cd}$ or Zn ; $X=\text{S}$ or Se)

The Cd-containing metal chalcogenides have motivated much more interest due to their size-dependent optical and electronic properties, and potential applications in the fields of nonlinear optics, light-emitting devices, electronics, and so on. However, there are very few reports on the synthesis of Cd-containing metal chalcogenides using ILs. More recently, Rao and co-workers [72] synthesized CdS nanostructures in the presence of [BMIM][MeSO₄] (where [MeSO₄] is methylsulfate), [BMIM][BF₄], and [BMIM][PF₆]. They also prepared CdSe nanoparticles in [BMIM][BF₄] and ZnSe in [BMIM][MeSO₄]. Arce and co-workers [73] recently successfully synthesized CdS nanoparticles with very small size (3-7 nm) by simply using an ionic liquid and the bulk powder of the material of the target nanoparticle. The method is very simple: First, a mixture of the bulk solid material and the ionic liquid trihexyl(tetradecyl)phosphonium cation ($[\text{P}_{66614}]^+$) is heated, with stirring, then, the mixture is allowed to cool down, and it is centrifuged to remove any excess of the bulk material from the generated nanodispersion. The ionic liquid plays a dual role as nanoparticle former and as a stabilizing agent.

The ability of ionic liquids to act as a reactant, solvent, and surfactant, as a function of other synthesis parameters, also denoted as ionic liquid precursors (or task-special ionic liquids), which offer many advantages over traditional solution-phase methods [13]. Our group recently used a Se-containing ionic liquid 1-n-butyl-3-methylimidazolium methylselenite ([BMIM][SeO₂(OCH₃)]) as a new Se precursor to prepare ZnSe hollow nanospheres with bubble templating through a facile one-pot hydrothermal method [74]. It was found that [BMIM][SeO₂(OCH₃)] not only serves as Se source but also acts as stabilizer for the ZnSe hollow nanospheres. We further reported the synthesis of CdSe dendrites from nanoparticles using ionic liquid precursor [BMIM][SeO₂(OCH₃)] [75]. Our experimental results demonstrate that the CdSe dendrites are obtained by self-assembly through oriented attachment, in which secondary mono-crystalline particles can be obtained through attachments of primary particles in an irreversible and highly oriented fashion.

Differently, we developed a Brønsted acid-base ionic liquid-assisted method for the synthesis of flower-like CdSe dendrites [76]. The CdSe dendrites were synthesized under solvothermal conditions at 150 °C for 24 h, using a mixed solution of water, ethanol, an ionic liquid based

on formic acid and N,N-dimethylformamide, cadmium chloride and selenium dioxide as solvents, cadmium and selenium sources, respectively. Mechanism study reveals that formation of flower-like dendrites depends on the interaction between the polar structure of CdSe crystals and the ionic liquid [DMFH][HCOO].

3.3.3. Other metal chalcogenides

Recently, we prepared ferrimagnetic Fe₃S₄ nanowalls and triple hierarchical microspheres via an ionic liquid-modulated solution-phase process [77]. The nanowalls of Fe₃S₄ were obtained via an ionic liquid modulated hydrothermal process with ascorbic acid and [BMIM]Cl as the reducing reagent and modulating additive, respectively. The Fe₃S₄ hierarchical microspheres assembled from nanoplates were formed under solvothermal process with ethylene glycol as a co-solvent and reducing reagent, and [BMIM]Cl as a modulating additive, respectively. It was found that the organized structure of the [BMIM]Cl possibly has a template effect on the formation of the nanobuilding blocks of Fe₃S₄ superstructures.

Ge and co-workers [78] prepared CuS nestlike hollow spheres assembled by microflakes were successfully synthesized through an oil-water interface route employing copper chloride, carbon disulfide, and sulfur as the starting materials in the presence of the ionic liquid [BMIM][BF₄]. It was found that [BMIM][BF₄] IL played a key role as a surfactant and structure-directing agent in the formation of CuS hollow spheres. By using an ionic liquid precursor 1-n-butyl-3-ethylimidazolium methylselenite ([BMIM][SeO₂(OCH₃)]), we synthesized Cu_{2-x}Se nanocrystals and CuSe nanoflakes through a convenient hydrothermal method [79]. It is found that the [BMIM][SeO₂(OCH₃)] not only serves as Se source but also has influence on the shapes of CuSe nanoflakes. The length of the alkyl unit linking the imidazolium ring can be altered and may have an influence on the morphologies of products.

3.4. Zeolites materials

Microporous and open-framework materials such as zeolites and coordination polymers, have been extensively studied for their potential applications in catalysis, ion-exchange, gas storage, separation, and sensor technology [80,81]. Zeolites are an important class of crystalline porous materials that have been employed for numerous catalytic applications because of their uniform channel size, strong acidity, high thermal/hydrothermal stability, and unique molecular shape selectivity. Generally, most zeolites are synthesized under hydrothermal conditions in an autoclave using an organic template or structure directing agent, commonly a tetraalkylammonium cation, such as tetrapropylammonium cation (TPA⁺) [82]. However, the hydrothermal synthesis of zeolites was not regarded as a green process [83]. Therefore, the development of green or sustainable route for the synthesis of zeolites is important task. As a green medium, ILs-assisted ionothermal synthesis was recently found to be an alternative to the reported hydrothermal method. Because of the vanishingly low vapor pressure of ionic liquids, ionothermal reactions address safety concerns associated with the high pressures of hydrothermal reaction, thus allowing for the synthesis of zeolites at ambient pressure. In addition, separate template was not required in the ionothermal synthesis of molecular sieves.

3.4.1. Aluminophosphate zeolites

In 2004, Cooper et al. [84] for the first time reported the ionothermal synthesis of zeolite and zeotype materials, using the ionic liquid 1-ethyl-3-methylimidazolium bromide ([EMIM]Br) and urea/choline chloride deep eutectic solvents to synthesize aluminophosphate zeolites (designed as SIZ-n, Figure 8). The use of [EMIM]Br resulted in the formation of aluminophosphates SIZ-1, SIZ-3, SIZ-4, SIZ-5, and SIZ-6 [84,85], and the use of choline chloride/urea mixtures resulted in SIZ-2 and AlPO-CJ2 (Figure 3,7). After this study, the ionothermal synthesis has shown to be a highly promising synthetic route for a wide variety of zeolites and zeolites analogues. The ionothermal synthesis method is also employed for the preparation of other metal phosphates. For instance, cobalt aluminophosphate molecular sieves SIZ-7, SIZ-8, and SIZ-9 with zeotype SIV, AEI, and SOD, respectively, were synthesized by the ionothermal synthesis in the presence of [EMIM]Br [86]. SIZ-7 exhibits a novel zeolite framework structure featuring double-crankshaft chains, which run parallel to the crystallographic a-axis, characteristic of a family of zeolites such as the PHI, GIS, and MER structure types. Furthermore, magnesium, gallium, and silicon can be incorporated into the ionothermally prepared aluminophosphate zeolites [87,88]. Very recently, Tian and co-workers [89] successfully achieved the ionothermal synthesis of permeable aluminophosphate molecular sieve membranes on porous alumina disks by substrate-surface conversion. Different types of molecular sieve membranes were synthesized, including CHA, AEL, AFI, and LTA, and the reported method is a simple, and environmentally benign process suitable for large-scale production.

To get more new structures, organic templates such as amines have been introduced into the ionothermal synthesis system. Tian and co-workers [90] have studied the structure-directing role of amines in ionothermal synthesis in the presence of IL [BMIM]Br. It was found that the addition of amines to the IL strongly influenced the dynamics of the crystallization process and improved the phase selectivity of the crystallization, leading to the formation of pure AFI and ATV structures. Therefore, it is possibly an effective way to control the structure of molecular sieves by combining the ionic liquid and organic amine in the synthesis. Later, Xing et al. [91] prepared a novel aluminophosphate (denoted as JIS-1) consisting of an anionic open framework $[Al_6P_7O_{28}H]^{2-}$ with 1-methylimidazole (MIA) and [EMIM]Br as cotemplates. Protonated [MIAH]⁺cations along with [EMIM]⁺ cations act as co-templates and were found to coexist in the intersection of the three-directional channels in the structure. Recently, Tian and co-workers [92] demonstrated the successful ionothermal synthesis of thermally stable aluminophosphate zeolites (denoted as DNL-1) with 20-membered ring pore openings (CLO) by use of 1,6-hexanediamine (HDA) and [EMIM]Br as co-templates for the first time. Both [EMIM]⁺ and protonated HDA remained intact upon occlusion inside the CLO structure, suggesting that the protonated HDA is essential and acts as a co-template together with the ionic liquid cations in the crystallization process of DNL-1.

With the combined advantages of the ionic liquids and microwave heating method, microwave-enhanced ionothermal synthesis is a novel method to prepare molecular sieves. Its advantages are its fast crystallization rate, low synthesis pressure, and high structural selectivity. Xu et al. [93] synthesized a series of aluminophosphate molecular sieves (AlPO4-11 and SAPO-11) in the [EMIM]Br under ionothermal conditions. The microwave heating led to

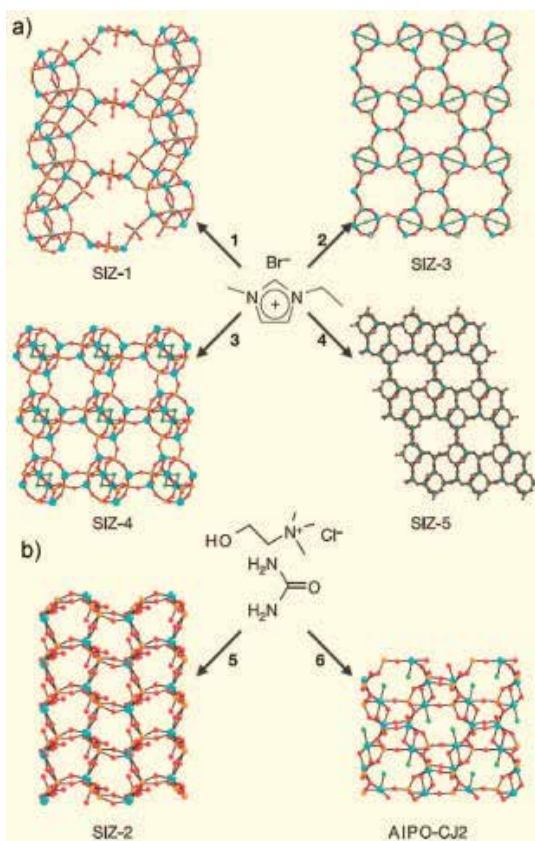


Figure 8. (a) Ball-and-stick diagrams of aluminophosphate materials SIZ-1, SIZ-3, SIZ-4, and SIZ-5 synthesized ionothermally using [EMim]Br. b) SIZ-2 and AIPO-CJ2 synthesized using a choline chloride/urea eutectic mixture [84,85]. The structure-directing agents are omitted for clarity. Orange, cyan, and red spheres correspond to phosphorus, aluminum, and oxygen atoms, respectively.

a more rapid growth of crystalline molecular sieve compared with that by conventional heating during ionothermal synthesis.

3.4.2. Silica-based zeolites

To date, there are only a few literatures on the synthesis of silica-based materials using ionic liquids as templates in the synthesis of silica-based zeolites. The problems associated with the synthesis of siliceous zeolites from ILs can be attributed to the poor solubility of the silica starting materials. In many of the successful attempts at synthesis of silica-based zeolites, the organic additives have been utilized in their hydroxide form in hydrothermal synthesis. Therefore, exchanging the anions of the ILs to those of the hydroxide type is strongly desirable for the ionothermal synthesis of silica-based zeolites [83]. Recently, Wheatley et al. [94] successfully synthesized siliceous zeolites silicalite-1 (MFI) and theta-1 (TON) via an ionothermal method using ionic liquid 1-butyl-3-methylimidazolium hydroxide ([BMIM]

[OH]) as both solvent and structure directing agent. The [BMIM][OH] was obtained from [BMIM]Br via ion-exchange with an anion exchange resin in water, which finally yields a ternary liquid of approximate formula [BMIM]-OH_{0.65}Br_{0.35}. The approximate initial molar composition was 20IL: tetraethyl orthosilicate (TEOS): 4H₂O: 0.38HF, confirming that the IL is indeed the major solvent. The chemical formula of the formed zeolites crystals was determined to be [Si₄₈O₉₆]-F₄(C₈N₂H₁₅)₂(C₂H₇O)₂. This result indicates that it is possible to alter the chemistry of ionic liquids so that they are suitable for the preparation of crystalline silica-based zeolites materials [94].

4. Concluding remarks

In summary, we have briefly highlighted the applications of ionic liquids in the preparation of inorganic nanomaterials, including metal NPs, metal oxides, metal chalcogenides, metal salts, and zeolites. Compared with traditional solvents, ionic liquids have many advantages, such as negligible vapor pressures, good thermal stability, wide electrochemical potential windows, and tunable solubility for inorganic substances. Notably, ionic liquids cannot be only regarded as a “green” alternative, but also provide a powerful medium for the synthesis of inorganic nanomaterials with unique morphologies and controlled phases. As one of the most rapidly growing fields, one can envision that there will certainly be intensified interest in this promising direction. One of the most distinctive features of ionic liquids is that they can be treated as “tailored solvents” due to their unlimited flexibility of combinations of anions and cations. Therefore, one can design the appropriate ionic liquid precursor according to the initial crystal structures, compositions, and crystal habits of target products. These precursors are molecularly defined entities, which can serve as both the reactant and solvent for the reaction, and as the template over the final inorganic material morphology at the same time. This “all-in-one” synthesis route which can make the reaction system simpler, and thus giving more control over the phases and morphologies of the final products.

Although the use of ILs for the synthesis of inorganic nanomaterials has been widely studied, a comprehensive and fundamental understanding on the effect type of ionic liquids and on the rational design of ionic liquids at the molecular level is still lacked. For example, it is also not clear how ionic liquids interact with inorganic or organic species, reactants, and products; how ionic liquids influence the nucleation and growth of materials; how self-assembly processes in ionic liquids differ from those in conventional solvents; and how ionic liquids influence the morphology. We believe that the synthesis of new inorganic materials should go hand-in-hand with the development of understanding of the effect type of ionic liquids. Since the research on well established rules and correlations between molecular structures of the adopted ionic liquids and the morphologies of the resulting inorganic materials is limited, it is highly expected that this understanding will improve with the accumulation of knowledge and the systematic design of experiments.

Author details

Wenjun Zheng^{1,2*}, Di Li^{1,2} and Wei Guo^{1,2}

*Address all correspondence to: zhwj@nankai.edu.cn

1 Department of Materials Chemistry, Key Laboratory of Advanced Energy Materials Chemistry (MOE), TKL of Metal and Molecule-based Materials Chemistry, College of Chemistry, Nankai University, Tianjin, PR China

2 Collaborative Innovation Center of Chemical Science and Engineering (Tianjin), Tianjin, PR China

References

- [1] Rao CNR, Govindaraj A, Vivekchand SRC. Inorganic nanomaterials: Current status and future prospects. *Annual Reports on the Progress of Chemistry, Section A: Inorganic Chemistry* 2006; 102: 20-45.
- [2] Gasparotto A, Barreca D, Maccato C, Tondello E. Manufacturing of inorganic nanomaterials: Concepts and perspectives. *Nanoscale* 2012; 4(9): 2813-2825.
- [3] Cushing BL, Kolesnichenko VL, O'Connor CJ. Recent advances in the liquid-phase syntheses of inorganic nanoparticles. *Chemical Reviews* 2004; 104(9): 3893-3946.
- [4] Volkov SV. Chemical reactions in molten salts and their classification. *Chemical Society Reviews* 1990; 19(1): 21-28.
- [5] Afanasiev P, Geantet C. Synthesis of solid materials in molten nitrates. *Coordination Chemistry Reviews* 1998; 178: 1725-1752.
- [6] Walden P. Molecular weights and electrical conductivity of several fused salts. *Bulletin de l'Académie Impériale des Sciences de St.-Pétersbourg* 1914; 8(6): 405-422.
- [7] Dai S, Ju YH, Gao HJ, Lin JS, Pennycook SJ, Barnes CE. Preparation of silica aerogel using ionic liquids as solvents. *Chemical Communications* 2000; (3): 243-244.
- [8] Wasserscheid P, Welton T. *Ionic liquids in synthesis*, Second Edition. Wiley-VCH, Weinheim; 2008.
- [9] Ma Z, Yu JH, Dai S. Preparation of inorganic materials using ionic liquids. *Advanced Materials* 2010; 22(2): 261-285.
- [10] Welton T. Room-temperature ionic liquids. Solvents for synthesis and catalysis. *Chemical Reviews* 1999; 99(8): 2071-2083.

- [11] Liu XD, Ma JM, Zheng WJ. Applications of ionic liquids (ILs) in the convenient synthesis of nanomaterials. *Reviews on Advanced Materials Science* 2011; 27: 43-51.
- [12] Morris RE. Ionothermal synthesis-Ionic liquids as functional solvents in the preparation of crystalline materials. *Chemical Communications* 2009; (21): 2990-2998.
- [13] Duan XC, Ma JM, Lian JB, Zheng WJ. The art of using ionic liquids in the synthesis of inorganic nanomaterials. *CrystEngComm* 2014; 16(13): 2550-2559.
- [14] Nakashima T, Kimizuka N. Interfacial synthesis of hollow TiO₂ microspheres in ionic liquids. *Journal of the American Chemical Society*. 2003; 125(21): 6386-6387.
- [15] Fechler N, Feller TP, Antonietti M. "Salt templating": A simple and sustainable pathway toward highly porous functional carbons from ionic liquids. *Advanced Materials* 2013; 25(1): 75-79.
- [16] Taubert A. CuCl nanoplatelets from an ionic liquid-crystal precursor. *Angewandte Chemie* 2004; 116(40): 5494-5496.
- [17] Zhang L, Niu WX, Xu GB. Synthesis and applications of noble metal nanocrystals with high-energy facets. *Nano Today* 2012; 7(6): 586-605.
- [18] Guo SJ, Wang EK. Noble metal nanomaterials: Controllable synthesis and application in fuel cells and analytical sensors. *Nano Today* 2011; 6(3): 240-264.
- [19] Richter K, Campbell PS, Baecker T, Schimitzek A, Yaprak D, Mudring AV. Ionic liquids for the synthesis of metal nanoparticles. *Physica Status Solidi (B)* 2013; 250(6): 1152-1164.
- [20] Janiak C. *Metal nanoparticle synthesis in ionic liquids*. Springer-Verlag Berlin Heidelberg; 2013.
- [21] Dupont J, Scholten JD. On the structural and surface properties of transition-metal nanoparticles in ionic liquids. *Chemical Society Reviews* 2010; 39(5): 1780-1804.
- [22] Luska KL, Moores A. Functionalized ionic liquids for the synthesis of metal nanoparticles and their application in catalysis. *ChemCatChem* 2012; 4(10): 1534-1546.
- [23] Dupont J, Fonseca GS, Umpierre AP, Fichtner PFP, Teixeira SR. Transition-metal nanoparticles in imidazolium ionic liquids: Recyclable catalysts for biphasic hydrogenation reactions. *Journal of the American Chemical Society* 2002; 124(16): 4228-4229.
- [24] Scheeren CW, Machado G, Dupont J, Fichtner PFP, Teixeira SR. Nanoscale Pt(0) particles prepared in imidazolium room temperature ionic liquids: Synthesis from an organometallic precursor, characterization, and catalytic properties in hydrogenation reactions. *Inorganic Chemistry* 2003; 42(15): 4738-4742.
- [25] Zhang D, Okajima T, Lu DL, Ohsaka T. Electroless deposition of platinum nanoparticles in room-temperature ionic liquids. *Langmuir* 2013; 29(38): 11931-11940.

- [26] Prechtl MHG, Scariot M, Scholten JD, Machado G, Teixeira SR, Dupont J. Nanoscale Ru(0) particles: Arene hydrogenation catalysts in imidazolium ionic liquids. *Inorganic Chemistry* 2008; 47(19): 8995-9001.
- [27] Prechtl MHG, Campbell PS, Scholten JD, Fraser GB, Machado G, Santini CC, Dupont J, Chauvin Y. Imidazolium ionic liquids as promoters and stabilising agents for the preparation of metal(0) nanoparticles by reduction and decomposition of organometallic complexes. *Nanoscale* 2010; 2(12): 2601-2606.
- [28] Li ZH, Liu ZM, Zhang JL, Han BX, Du JM, Gao YN, Jiang T. Synthesis of single-crystal gold nanosheets of large size in ionic liquids. *The Journal of Physical Chemistry B* 2005; 109(30): 14445-14448.
- [29] Gao YN, Voigt A, Zhou M, Sundmacher K. Synthesis of single-crystal gold nano- and microprisms using a solvent-reductant-template ionic liquid. *European Journal of Inorganic Chemistry* 2008; 2008(24): 3769-3775.
- [30] Ren LZ, Meng LJ, Lu QH, Fei ZF, Dyson PJ. Fabrication of gold nano- and microstructures in ionic liquids-A remarkable anion effect. *Journal of Colloid and Interface Science* 2008; 323(2): 260-266.
- [31] Qin Y, Song Y, Sun NJ, Zhao NN, Li MX, Qi LM. Ionic liquid-assisted growth of single-crystalline dendritic gold nanostructures with a three-fold symmetry. *Chemistry of Materials* 2008; 20(12): 3965-3972.
- [32] Kim TY, Kim WJ, Hong SH, Kim JE, Suh KS. Ionic-liquid-assisted formation of silver nanowires. *Angewandte Chemie* 2009; 121(21): 3864-3867.
- [33] Choi S, Kim KS, Yeon SH, Cha JH, Lee H, Kim CJ, Yoo ID. Fabrication of silver nanoparticles via self-regulate reduction by 1-(2-hydroxyethyl)-3-methylimidazolium tetrafluoroborate. *Korean Journal of Chemical Engineering* 2007; 24(5): 856-859.
- [34] Liu XQ, Li Y, Zheng ZJ, Zhou F. Ionic liquids as two-dimensional templates for the spontaneous assembly of copper nanoparticles into nanobelts and observation of an intermediate state. *RSC Advances* 2013; 3(2): 341-344.
- [35] Wei ZH, Sun JM, Li Y, Datye AK, Wang Y. Bimetallic catalysts for hydrogen generation. *Chemical Society Reviews* 2012; 41(24): 7994-8008.
- [36] Wang Y, Yang H. Synthesis of CoPt nanorods in ionic liquids. *Journal of the American Chemical Society* 2005; 127(15): 5316-5317.
- [37] Silva DO, Luza L, Gual A, Baptista DL, Bernardi F, Zapata MJM, Morais J, Dupont J. Straightforward synthesis of bimetallic Co/Pt nanoparticles in ionic liquid: Atomic rearrangement driven by reduction-sulfidation processes and Fischer-Tropsch catalysis. *Nanoscale* 2014; 6(15): 9085-9092.
- [38] SerràA, Gómez E, López-Barbera JF, Nogués J, Vallés E. Green electrochemical template synthesis of CoPt nanoparticles with tunable size, composition, and magnetism

- from microemulsions using an ionic liquid (bmimPF₆). *ACS Nano* 2014; 8(5): 4630-4639.
- [39] Helgadottir IS, Arquillière PP, Bréa P, Santini CC, Haumesser PH, Richter K, Mudring AV, Aouine M. Synthesis of bimetallic nanoparticles in ionic liquids: Chemical routes vs physical vapor deposition. *Microelectronic Engineering* 2013; 107: 229-232.
- [40] Ding KQ, Liu L, Cao YL, Yan XR, Wei HG, Guo ZH. Formic acid oxidation reaction on a Pd_xNi_y bimetallic nanoparticle catalyst prepared by a thermal decomposition process using ionic liquids as the solvent. *International Journal of Hydrogen Energy* 2014; 39(14): 7326-7337.
- [41] Schütte K, Doddi A, Kroll C, Meyer H, Wiktor C, Gemel C, Tendeloo GV, Fischer RA, Janiak C. Colloidal nickel/gallium nanoalloys obtained from organometallic precursors in conventional organic solvents and in ionic liquids: Noble-metal-free alkyne semihydrogenation catalysts. *Nanoscale* 2014; 6: 5532-5544.
- [42] Zhou Y, Antonietti M. Synthesis of very small TiO₂ nanocrystals in a room-temperature ionic liquid and their self-assembly toward mesoporous spherical aggregates. *Journal of the American Chemical Society* 2003; 125(49): 14960-14961.
- [43] Ding KL, Miao ZJ, Liu ZM, Zhang ZF, Han BX, An GM, Miao SD, Xie Y. Facile synthesis of high quality TiO₂ nanocrystals in ionic liquid via a microwave-assisted process. *Journal of the American Chemical Society* 2007; 129(20): 6362-6363.
- [44] Zhou SH, Ma Z, Baker GA, Rodinone RJ, Zhu Q, Luo HM, Wu ZL, Dai S. Self-assembly of metal oxide nanoparticles into hierarchically patterned porous architectures using ionic liquid/oil emulsions. *Langmuir* 2009; 25(13): 7229-7233.
- [45] Wessel C, Zhao L, Urban S, Ostermann R, Djerdj I, Smarsly BM, Chen LQ, Hu YS, Sallard S. Ionic-liquid synthesis route of TiO₂(B) nanoparticles for functionalized materials. *Chemistry-A European Journal* 2011; 17(3): 775-779.
- [46] Yu JG, Li Q, Liu SW, Jaroniec M. Ionic-liquid-assisted synthesis of uniform fluorinated B/C-codoped TiO₂ nanocrystals and their enhanced visible-light photocatalytic activity. *Chemistry-A European Journal* 2013; 19(7): 2433-2441.
- [47] Zheng WJ, Liu XD, Yan ZY, Zhu LJ. Ionic liquid-assisted synthesis of large scale TiO₂ nanoparticles with controllable phase by hydrolysis of TiCl₄. *ACS Nano* 2009; 3(1): 115-122.
- [48] Zhou X, Xie ZX, Jiang ZY, Kuang Q, Zhang SH, Xu T, Huang RB, Zheng LS. Formation of ZnO hexagonal micro-pyramids: A successful control of the exposed polar surfaces with the assistance of an ionic liquid. *Chemical Communications* 2005; (44): 5572-5574.
- [49] Zhu HG, Huang JF, Pan ZW, Dai S. Ionothermal synthesis of hierarchical ZnO nanostructures from ionic-liquid precursors. *Chemistry of Materials* 2006; 18(18): 4473-4477.

- [50] Wang L, Chang LX, Zhao B, Yuan ZY, Shao GS, Zheng WJ. Systematic investigation on morphologies, forming mechanism, photocatalytic and photoluminescent properties of ZnO nanostructures constructed in ionic liquids. *Inorganic Chemistry* 2008; 47(5): 1443-1452.
- [51] Li H, Liu R, Zhao RX, Zheng YF, Chen WX, Xu ZD. Morphology control of electrodeposited Cu₂O crystals in aqueous solutions using room temperature hydrophilic ionic liquids. *Crystal Growth & Design* 2006; 6(12): 2795-2798.
- [52] Li SK, Guo X, Wang Y, Huang FZ, Shen YH, Wang XM, Xie AJ. Rapid synthesis of flower-like Cu₂O architectures in ionic liquids by the assistance of microwave irradiation with high photochemical activity. *Dalton Transactions* 2011; 40(25): 6745-6750.
- [53] Swadzba-Kwasny M, Chancelier L, Ng S, Manyar HG, Hardacre C, Nockemann P. Facile in situ synthesis of nanofluids based on ionic liquids and copper oxide clusters and nanoparticles. *Dalton Transactions* 2012; 41(1): 219-227.
- [54] Gusain R, Khatri OP. Ultrasound assisted shape regulation of CuO nanorods in ionic liquids and their use as energy efficient lubricant additives. *Journal of Materials Chemistry A* 2013; 1(18): 5612-5619.
- [55] Lian JB, Duan XC, Ma JM, Peng P, Kim T, Zheng WJ. Hematite (α -Fe₂O₃) with various morphologies: Ionic liquid-assisted synthesis, formation mechanism, and properties. *ACS Nano* 2009; 3(11): 3749-3761.
- [56] Ma JM, Wang TH, Duan XC, Lian JB, Liu ZF, Zheng WJ. Ionothermal synthesis of aggregated α -Fe₂O₃ nanoplates and their magnetic properties. *Nanoscale* 2011; 3(10): 4372-4375.
- [57] Liu XD, Duan XC, Qin Q, Wang QL, Zheng WJ. Ionic liquid-assisted solvothermal synthesis of oriented self-assembled Fe₃O₄ nanoparticles into monodisperse nanoflakes. *CrystEngComm* 2013; 15(17): 3284-3287.
- [58] Xu L, Xia JX, Wang K, Wang LG, Li HM, Xu H, Huang LY, He MQ. Ionic liquid assisted synthesis and photocatalytic properties of α -Fe₂O₃ hollow microspheres. *Dalton Transactions* 2013; 42(18): 6468-6477.
- [59] Ma JM, Liu XD, Lian JB, Duan XC, Zheng WJ. Ionothermal synthesis of BiOCl nanostructures via a long-chain ionic liquid precursor route. *Crystal Growth & Design* 2010; 10(6): 2522-2527.
- [60] Xia JX, Yin S, Li HM, Xu H, Yan YS, Zhang Q. Self-assembly and enhanced photocatalytic properties of BiOI hollow microspheres via a reactable ionic liquid. *Langmuir* 2011; 27(3): 1200-1206.
- [61] Zhang DQ, Wen MC, Jiang B, Li GS, Yu JC. Ionothermal synthesis of hierarchical BiOBr microspheres for water treatment. *Journal of Hazardous Materials* 2012; 211-212: 104-111.

- [62] Lian JB, Ma JM, Duan XC, Kim T, Li HB, Zheng WJ. One-step ionothermal synthesis of γ - Al_2O_3 mesoporous nanoflakes at low temperature. *Chemical Communications* 2010; 46(15): 2650-2652.
- [63] Duan XC, Kim T, Li D, Ma JM, Zheng WJ. Understanding the effect models of ionic liquids in the synthesis of NH_4 -Dw and γ - AlOOH nanostructures and their conversion into porous γ - Al_2O_3 . *Chemistry-A European Journal* 2013; 19(19): 5924-5937.
- [64] Li D, Duan XC, Qin Q, Fan HM, Zheng WJ. Ionic liquid-assisted synthesis of mesoporous α - Ga_2O_3 hierarchical structures with enhanced photocatalytic activity. *Journal of Materials Chemistry A* 2013; 1(40): 12417-12421.
- [65] Zhang HT, Hyun BR, Wise FW, Robinson RD. A generic method for rational scalable synthesis of monodisperse metal sulfide nanocrystals. *Nano Letters* 2012; 12(11): 5856-5860.
- [66] Gao MR, Xu YF, Jiang J, Yu SH. Nanostructured metal chalcogenides: Synthesis, modification, and applications in energy conversion and storage devices. *Chemical Society Reviews* 2013; 42(7): 2986-3017.
- [67] Jiang Y, Zhu YJ. Microwave-assisted synthesis of sulfide M_2S_3 (M=Bi, Sb) nanorods using an ionic liquid. *The Journal of Physical Chemistry B* 2005; 109(10): 4361-4364.
- [68] Jiang Y, Zhu YJ, Cheng GF. Synthesis of Bi_2Se_3 nanosheets by microwave heating using an ionic liquid. *Crystal Growth & Design* 2006; 6(9): 2174-2176.
- [69] Jiang J, Yu SH, Yao WT, Ge H, Zhang GZ. Morphogenesis and crystallization of Bi_2S_3 nanostructures by an ionic liquid-assisted templating route: Synthesis, formation mechanism, and properties. *Chemistry of materials* 2005; 17(24): 6094-6100.
- [70] Ma JM, Liu ZF, Lian JB, Duan XC, Kim T, Peng P, Liu XD, Chen Q, Yao G, Zheng WJ. Ionic liquids-assisted synthesis and electrochemical properties of Bi_2S_3 nanostructures. *CrystEngComm* 2011; 13(8): 3072-3079.
- [71] Ma JM, Duan XC, Lian JB, Kim T, Peng P, Liu XD, Liu ZF, Li HB, Zheng WJ. Sb_2S_3 with various nanostructures: Controllable synthesis, formation mechanism, and electrochemical performance toward lithium storage. *Chemistry-A European Journal* 2010; 16(44): 13210-13217.
- [72] Biswas K, Rao CNR. Use of ionic liquids in the synthesis of nanocrystals and nanorods of semiconducting metal chalcogenides. *Chemistry-A European Journal* 2007; 13(21): 6123-6129.
- [73] Rodríguez-Cabo B, Rodil E, Rodríguez H, Soto A, Arce A. Direct preparation of sulfide semiconductor nanoparticles from the corresponding bulk powders in an ionic liquid. *Angewandte Chemie International Edition* 2012; 51(6): 1424-1427.
- [74] Liu XD, Ma JM, Peng P, Zheng WJ. One-pot hydrothermal synthesis of ZnSe hollow nanospheres from an ionic liquid precursor. *Langmuir* 2010; 26(12): 9968-9973.

- [75] Duan XC, Liu XD, Chen Q, Li HB, Li J, Hu X, Li YY, Ma JM, Zheng WJ. Ionic liquid-assisted synthesis of CdSe dendrites from nanospheres through oriented attachment. *Dalton Transactions* 2011; 40(9): 1924-1928.
- [76] Ma JM, Guo W, Duan XC, Wang TH, Zheng WJ, Chang L. Growth of flower-like CdSe dendrites from a Brønsted acid-base ionic liquid precursor. *RSC Advances* 2012; 2(14): 5944-5946.
- [77] Ma JM, Chang L, Lian JB, Huang Z, Duan XC, Liu XD, Peng P, Kim T, Liu ZF, Zheng WJ. Ionic liquid-modulated synthesis of ferrimagnetic Fe₃S₄ hierarchical superstructures. *Chemical Communications* 2010; 46(27): 5006-5008.
- [78] Ge L, Jing XY, Wang J, Jamil S, Liu Q, Song DL, Wang J, Xie Y, Yang PP, Zhang ML. Ionic liquid-assisted synthesis of CuS nestlike hollow spheres assembled by microflakes using an oil-water interface route. *Crystal Growth & Design* 2010; 10(4): 1688-1692.
- [79] Liu XD, Duan XC, Peng P, Zheng WJ. Hydrothermal synthesis of copper selenides with controllable phases and morphologies from an ionic liquid precursor. *Nano-scale* 2011; 3(12): 5090-5095.
- [80] Corma A. From microporous to mesoporous molecular sieve materials and their use in catalysis. *Chemical Reviews* 1997; 97(6): 2373-2420.
- [81] Tao YS, Kanoh H, Abrams L, Kaneko K. Mesopore-modified zeolites: Preparation, characterization, and applications. *Chemical Reviews* 2006; 106(3): 896-910.
- [82] Lehman SE, Larsen SC. Zeolite and mesoporous silica nanomaterials: Greener syntheses, environmental applications and biological toxicity. *Environmental Science: Nano* 2014; 1(3): 200-213.
- [83] Meng XJ, Xiao FS. Green routes for synthesis of zeolites. *Chemical Reviews* 2014; 114(2): 1521-1543.
- [84] Cooper ER, Andrews CD, Wheatley PS, Webb PB, Wormald P, Morris RE. Ionic liquids and eutectic mixtures as solvent and template in synthesis of zeolite analogues. *Nature* 2004; 430: 1012-1016.
- [85] Parnham ER, Wheatley PS, Morris RE. The ionothermal synthesis of SIZ-6-A layered aluminophosphate. *Chemical Communications* 2006; (4): 380-382.
- [86] Parnham ER, Morris RE. Ionothermal synthesis using a hydrophobic ionic liquid as solvent in the preparation of a novel aluminophosphate chain structure. *Journal of Materials Chemistry* 2006; 16(37): 3682-3684.
- [87] Wang L, Xu YP, Wang BC, Wang SJ, Yu JY, Tian ZJ, Lin LW. Ionothermal synthesis of magnesium-Containing aluminophosphate molecular sieves and their catalytic performance. *Chemistry-A European Journal* 2008; 14(34): 10551-10555.
- [88] Ma HJ, Xu RS, You WS, Wen GD, Wang SJ, Xu Y, Wang BC, Wang L, Wei Y, Xu YP, Zhang WP, Tian ZJ, Lin LW. Ionothermal synthesis of gallophosphate molecular

- sieves in 1-alkyl-3-methyl imidazolium bromide ionic liquids. *Microporous and Mesoporous Materials* 2009; 120(3): 278-284.
- [89] Li KD, Tian ZJ, Li XL, Xu RS, Xu YP, Wang L, Ma HJ, Wang BC, Lin LW. Ionothermal synthesis of aluminophosphate molecular sieve membranes through substrate surface conversion. *Angewandte Chemie International Edition* 2012; 51(18): 4397-4400.
- [90] Wang L, Xu YP, Wei Y, Duan JC, Chen AB, Wang BC, Ma HJ, Tian ZJ, Lin LW. Structure-directing role of amines in the ionothermal synthesis. *Journal of the American Chemical Society* 2006; 128(23): 7432-7433.
- [91] Xing HZ, Li JY, Yan WF, Chen P, Jin Z, Yu JH, Dai S, Xu RR. Cotemplating ionothermal synthesis of a new open-framework aluminophosphate with unique Al/P ratio of 6/7. *Chemistry of Materials* 2008; 20(13): 4179-4181.
- [92] Wei Y, Tian ZJ, Gies H, Xu RS, Ma HJ, Pei RY, Zhang WP, Xu YP, Wang L, Li KD, Wang BC, Wen GD, Lin LW. Ionothermal synthesis of an aluminophosphate molecular sieve with 20-ring pore openings. *Angewandte Chemie* 2010; 122(31):5495-5498.
- [93] Xu YP, Tian ZJ, Wang SJ, Hu Y, Wang L, Wang BC, Ma YC, Hou L, Yu JY, Lin LW. Microwave-enhanced ionothermal synthesis of aluminophosphate molecular sieves. *Angewandte Chemie* 2006; 118(24): 4069-4074.
- [94] Wheatley PS, Allan PK, Teat SJ, Ashbrook SE, Morris RE. Task specific ionic liquids for the ionothermal synthesis of siliceous zeolites. *Chemical Science* 2010; 1(4): 483-487.

Enzymatic

Ionic Liquid-Mediated Activation of Lipase-Catalysed Reaction

Toshiyuki Itoh

Additional information is available at the end of the chapter

<http://dx.doi.org/10.5772/59243>

1. Introduction

Ionic liquids (ILs) have very good properties as reaction media in chemical reactions: they are non-volatile, non-flammable, have low toxicity and good solubility for many organic and inorganic materials. [1] It has long been recognized that an enzymatic reaction proceeds in a buffer aqueous solution under appropriate pH conditions, and an enzyme quickly loses its activity in a highly concentrated aqueous salt solution. [2, 3] Therefore, it seems foolish to suggest that enzymatic reaction occurs in a salt medium from the standpoint of biology. However, the use of ILs to replace traditional organic solvents in chemical reactions has recently gained much attention, and it has now been established that ILs could also be used as reaction media for biotransformation: lipase-catalysed reactions in an ionic liquid solvent system have been investigated extensively, and several types of non-lipase enzymatic reactions have even been reported too. [3, 4] This chapter describes recent progress in this area, focusing on “ionic liquid-mediated activation of lipase-catalysed reactions”.

2. Ionic liquids as a reaction medium for biotransformation

The first example of a lipase-catalysed reaction in a pure ionic liquid solvent system was reported by the Sheldon group at the end of 2000. [5, 6] The authors demonstrated two types of *Candida antarctica* lipase (CAL-B)-catalysed reaction in a pure IL: CAL-B catalysed amidation of octanoic acid with ammonia and also catalysed formation of octanoic peracid by the reaction of octanoic acid with hydrogen peroxide (Figure 1).

However, these reactions were not enantioselective ones, and the most important aspect of the biocatalysis reactions should be in the enantioselective reaction. Itoh [7] and Kragl [8] inde-

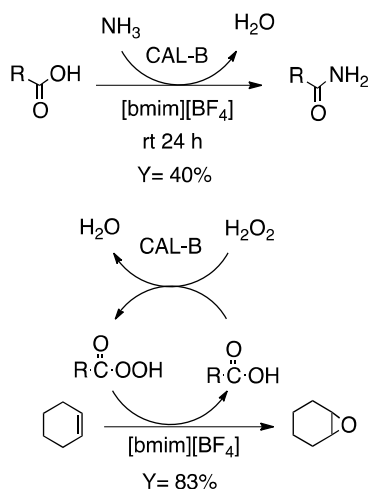


Figure 1. The first enzymatic reaction conducted in a pure ionic liquid solvent system.

pendently reported the first enantioselective enzymatic reactions in early 2001. Itoh demonstrated that lipase was anchored by the ionic liquid solvent, and remained in it after the extraction work-up of the product; they also succeeded in demonstrating that recyclable use of the lipase in the imidazolium type ionic liquid solvent system was possible (Figure 2). [7]

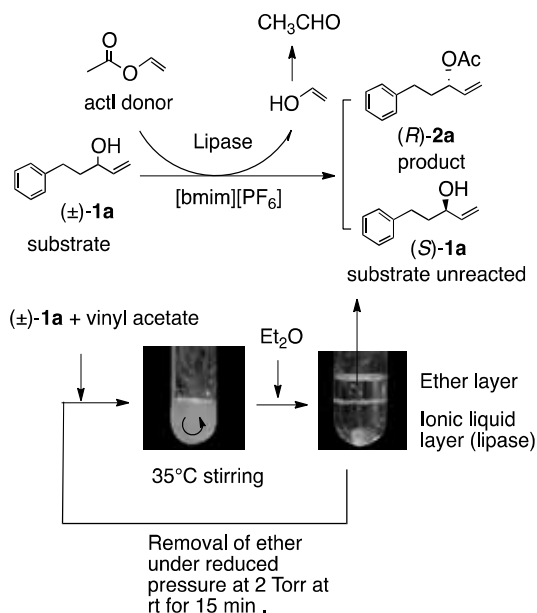


Figure 2. The first example of lipase-catalysed enantioselective transesterification in a pure ionic liquid.

Itoh mentioned an interesting history of the early days of their study in his review. [4a] Scientists encountered a serious problem, in that the results of lipase-catalysed transesterification in ILs as reaction media were significantly dependent on the ionic liquids that they prepared themselves. They found that the quality of ILs influenced the results strongly; it took more than half a year to establish a preparation method for clean ILs and to obtain reproducible results prior to submitting their paper. This highlights that clean ILs should be required for biocatalysis systems compared to chemical reactions. I imagine that all research groups encountered the same problem in the early days of this field. Fortunately, we are free from such trouble, because many types of ILs with high purity are now commercially available. I give the list of ILs that have been applied as reaction media for lipase-catalysed reactions (Figure 3). Hydrophobic ionic liquids generally act as good reaction media for lipase-catalysed reaction; by contrast, hydrophilic ILs give poor or no reaction, though several ILs are exceptions to this.

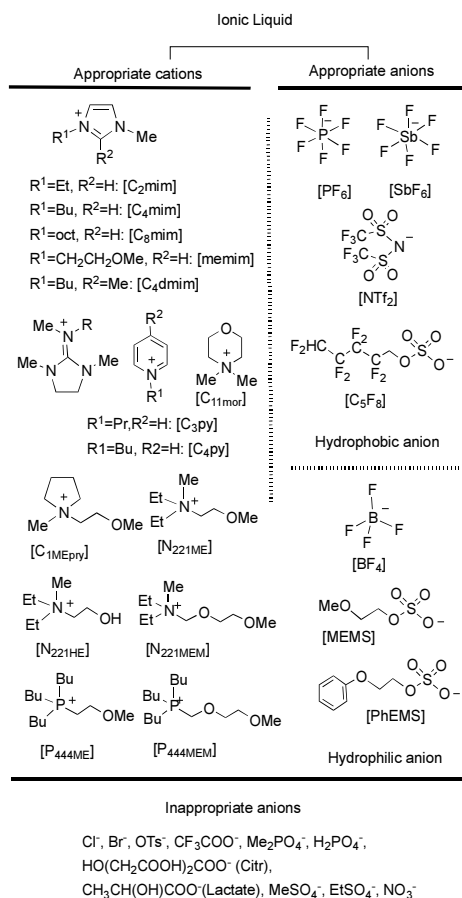


Figure 3. List of ILs for lipase-catalysed reactions.

3. Activation of lipase-catalysed reaction in an ionic liquid solvent system

Vinyl acetate is commonly used as an acyl donor of lipase-catalysed transesterification in organic solvents, because vinyl alcohol produced by the transesterification immediately tautomerizes to acetaldehyde, which easily escapes from the reaction mixture due to its very volatile nature. Thus, no reverse reaction takes place. Then, the reaction equilibrium goes on to produce the desired acetate. Because of this reason, acetaldehyde usually shows no inhibitory action on the lipase, though acetaldehyde acts as an inhibitor of enzymes when it forms a Schiff base with amino residue in the enzyme. [3]

Itoh and colleagues found that the reaction rate of lipase-catalysed transesterification gradually dropped with repetition of the reaction process in 1-butyl-3-methylimidazolium hexafluorophosphate ($[C_4mim][PF_6]$), while enantioselectivity is perfect in all reactions ($E^s > 200$); this drop in reactivity was caused by the inhibitory action of acetaldehyde oligomer which had accumulated in the IL solvent system. [10] Itoh hypothesized that oligomerization of acetaldehyde might be caused by the proton derived from the water molecule trapped by the hydrogen bonding at 2-position of the imidazolium ring, due to the high acidity of the 2-position of imidazolium cation (Figure 4). [11] They solved this problem using two methods.

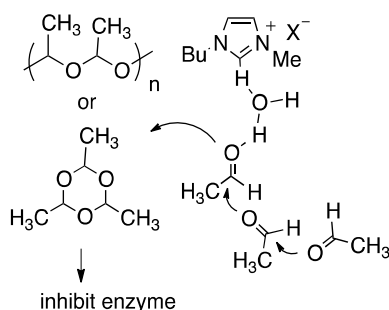


Figure 4. Plausible mechanism for formation of acetaldehyde oligomer in $[C_4mim][PF_6]$.

One solution is the lipase-catalysed transesterification under reduced pressure conditions using methyl ester as an acyl donor. [10] Methyl esters are generally not suitable for lipase-catalysed transesterification as acyl donors, because reverse reaction with produced methanol takes place. [3] However, such a difficulty can be avoided when the reaction is carried out under reduced pressure even if methyl esters are used as the acyl donor, because the methanol produced is removed immediately from the reaction mixture, and thus the reaction equilibrium goes on to produce the ester. [12] The most important characteristics of ionic liquid are its wide temperature range for the liquid phase and its having a very low vapour pressure. [1] The transesterification indeed took place smoothly under reduced pressure at 10 Torr at 40 °C when methyl phenylthioacetate was used as acyl donor in $[C_4mim][PF_6]$ solvent system. Using the system, a completely recyclable use of lipase (Novozym435) was realized (Figure 5): five repetitions of this process showed no drop in the reaction rate while maintaining perfect

enantioselectivity. [10] The same reaction system was applied to esterification and amidation of carboxylic acids by Irimescu and Kato. [13]

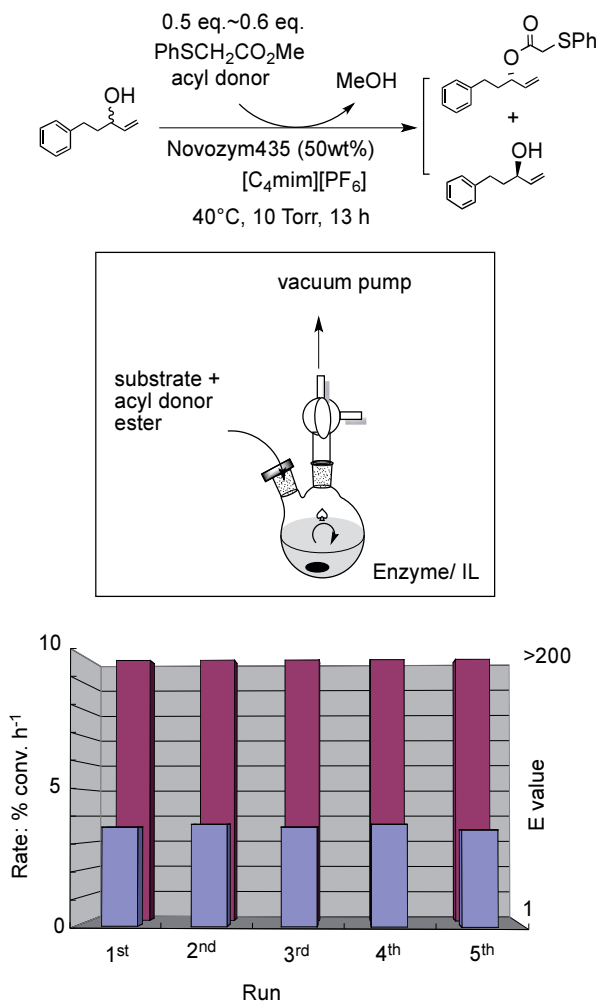


Figure 5. Recyclable use of lipase under reduced pressure conditions in the IL solvent system.

The second method to solve the problem is the use of 1-butyl-2, 3-dimethylimidazolium (C₄dmim) salts, which lacked a hydrogen atom at 2-position on the imidazolium ring:[14] lipase-catalysed transesterification using vinyl acetate was carried out using 1-butyl-2, 3-dimethylimidazolium (C₄dmim) salts as solvent. As expected, no accumulation of an acetaldehyde oligomer was in fact observed in this solvent system since [C₄dmim] cation has no acidic proton. The reaction proceeded very smoothly in [C₄dmim][BF₄] and recyclable use of the enzyme was realized while maintaining perfect enantioselectivity, as shown in Figure 6. [14]

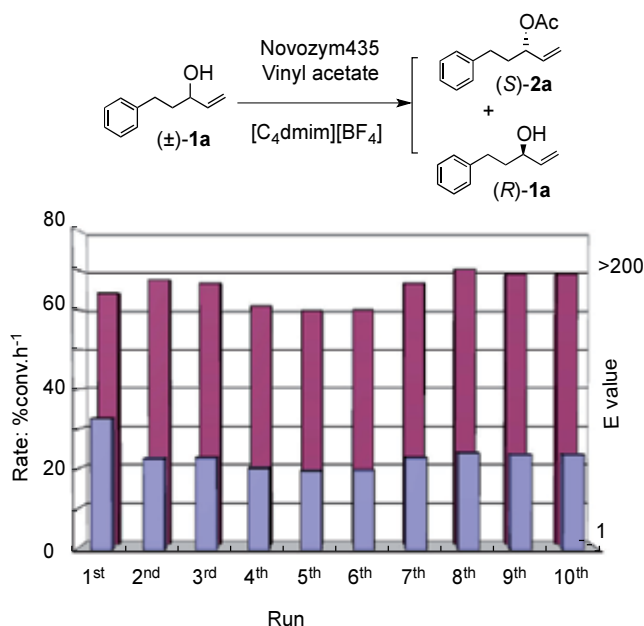


Figure 6. Recyclable use of enzyme in [C₄dmim][BF₄] solvent system.

When performing the reactions, Han found that the lipase was very stable in [C₄dmim][BF₄]. Lipases showed perfect reactivity after two months when lipases were kept in this ionic liquid, although enzymes are generally unstable in organic solvent and even lipases lose its activity quickly in the absence of substrates; both *Burkholderia cepacia* PS (lipase PS) and *Candida antarctica* lipase, Novozym, showed good reactivity after two months in this ionic liquid. [15]

De Diego and colleagues reported a stabilization effect of ionic liquid for lipase-catalysed reaction: the presence of an appropriate substrate was essential for stabilization of enzyme in an ionic liquid solvent. [16] The half-lifetime of native CAL was only 3.2 h in [C₂mim][PF₆] solvent, though it lengthened remarkably to 7, 500 h in the presence of the substrate. Furthermore, Lozano and colleagues demonstrated CAL-B catalysed transesterification of 1-phenylethanol using vinyl butyrate and revealed that ILs solvents gave better reactivity and stability compare to those in hexane: CAL-B maintained activity higher than 75 % after four days of incubation in [C₂mim][NTf₂] solvent. On the contrary, only 25 % of activity was obtained when the lipase was incubated in water or hexane medium. [16] Comparing the ratio of α -helix and β -sheet by CD spectra, the activity was closely related with α -helix content; the content of α -helix reduced to 31 % immediately after lipase was added to hexane and had reached only 2 % after four days in hexane. On the other hand, no significant reduction of α -helix content was obtained in [C₂mim][NTf₂] solvent. Based on these results, the authors concluded that α -helix contents might play an important role in maintaining the enzymatic activity. [16]

Polyethyleneglycol (PEG) treatment is known to cause stabilization of an enzyme. Goto reported that PEG-coated lipase worked well as catalysis for transesterification of vinyl

cinnamate with butanol in $[\text{C}_8\text{mim}][\text{PF}_6]$ as solvent. [17] Russell and colleagues reported that improved activity of lipase by PEG treatment in IL solvent was mainly dependent on the anionic part of the imidazolium salt ionic liquids; high activity was obtained for $[\text{PF}_6]$ salt, while no activity was observed for $[\text{NO}_3]$, $[\text{OAc}]$, $[\text{CH}_3\text{SO}_3]$, $[\text{OTf}]$, or $[\text{NTf}_2]$ salt. [18] The authors proposed that nitric anion or acetate anion might have a strong interaction with some parts of the enzyme protein due to the highly nucleophilic nature of these anions, and caused deactivation of the enzyme activity. [18]

Inspired by these results, Itoh and colleagues prepared two types of alkyl PEG sulphate imidazolium ionic liquids ($[\text{C}_4\text{dmim}][\text{cetyl}-(\text{OCH}_2\text{CH}_2)_{10}\text{-OSO}_3]$ (IL1) and $[\text{C}_4\text{mim}][\text{cetyl}-(\text{OCH}_2\text{CH}_2)_{10}\text{-OSO}_3]$ (IL2)) and used as an additive for lipase-catalysed acylation of 1-phenylethanol. Enhanced enantioselectivity was obtained when IL1 or IL2 was added at 3 mol% vs. substrate in the *Burkholderia cepacia* lipase (lipase PS) catalysed transesterification using vinyl acetate in diisopropyl ether or a hexane solvent system (see Figure 7 and Table 1). [15a]

On the other hand, Lee and Kim reported an IL-mediated activation of a lipase: they prepared "ionic liquid-coated lipase PS" by mixing lipase PS with 1-(3-phenyl)propyl-3-methylimidazolium hexafluorophosphate ($[\text{PhC}_3\text{mim}][\text{PF}_6]$) and found that the resulting lipase showed more enhanced enantioselectivity than that of commercial lipase PS in toluene, though no modification of the reaction rate was obtained (Figure 7 and Table 1). [19] However, as shown in Table 1, enhanced enantioselectivity was not significant and reaction speed dropped when $[\text{PhC}_3\text{mim}][\text{PF}_6]$ -PS was used as catalysis.

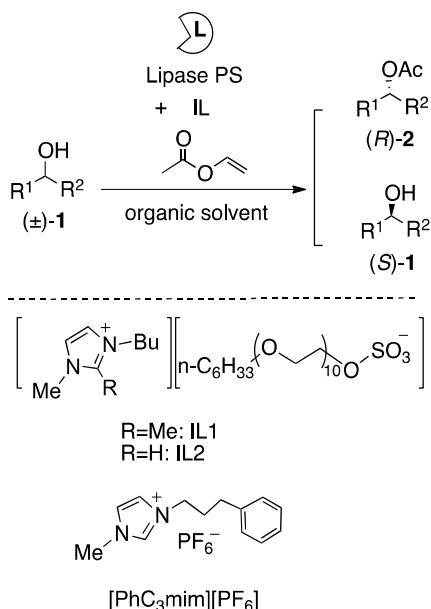
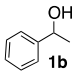
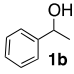
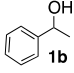
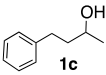
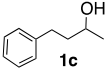


Figure 7. Attempt to activate lipase PS by an ionic liquid.

Substrate	IL	Solvent	E value	% conv. / h	Ref.
	Native PS	i-Pr ₂ O	10	1.4	[15]
	+ IL1 (3 mol%) ^a	i-Pr ₂ O	>200 (1057)	1.8	[15]
	+ IL2 (3 mol%) ^a	i-Pr ₂ O	40	1.6	[15]
	Native PS	toluene	>200 (265)	1.5	[19]
	[PhC ₃ mim][PF ₆]-PS ^b	toluene	>200 (532)	0.4	[19]

^a added as an additive to the reaction mixture. ^b [PhC₃mim][PF₆]-PS was prepared as follows [19]: 1.0 g of [PhC₃mim][PF₆] was heated at 53 °C, then mixed with lipase PS (0.1 g) and the homogeneous solution was stirred for 1 min. then cooled to rt.

Table 1. Attempt to activate lipase-catalysed transesterification by an ionic liquid treatment.

Itoh and colleagues prepared [C₄dmim][cetyl-PEG10-sulphate](IL1) and established that IL1 worked as an excellent activating agent of lipases. The ionic liquid-coated lipase PS (IL1-PS) by the lyophilisation process gave excellent results for enantioselective transesterification of various types of secondary alcohols using vinyl acetate as acyl donor in i-Pr₂O solvent (Figure 8 and Table 2). [15, 20] The results were dependent on the substrates, and more than 500- to 1000-fold acceleration was accomplished for some substrates. [20]

It should be emphasized that IL1-coating made it possible to accelerate the reaction rate and enhanced enantioselectivity, while simple PEG coating of a lipase could accelerate the reaction but caused no significantly enhanced enantioselectivity. [20] MALD-TOF Mass experiments suggested that IL1 binds with the enzyme protein; therefore, it was assumed that the modified activity of lipase might be due to flexibility or conformation change of the lipase protein caused by the IL1-binding. [21] Furthermore, it was established that imidazolium cation affected the enantioselectivity of the lipase; IL1-coated lipase PS gave better enantioselectivity than an IL2-coated one. [20]

Amino acids have been used as a stabilizer of an enzyme during the purification process: commercial lipase PS involves ca. 20 wt% of glycine as an essential stabilizer during prepara-

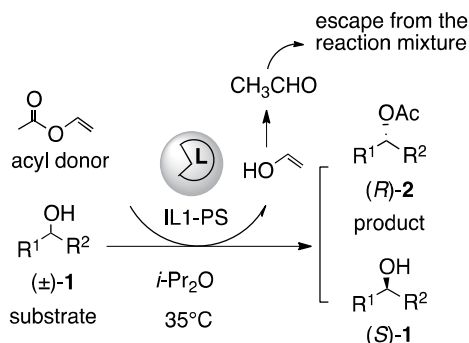


Figure 8. Activation of lipase by coating with alkyl PEG sulphate ionic liquid (IL1).

tion of the lipase protein by the lyophilisation process; Itoh and colleagues found that glycine worked only as a stabilizer of the enzyme and had no influence on the reactivity of lipase PS. [20] Hence, they prepared amino acid-coated lipase PS and investigated its properties in transesterification of (±)-1-phenylethanol (1b) as a model substrate in the presence of vinyl acetate as an acyl donor in the *i*-Pr₂O solvent system. [21] As shown in Figure 9, coating of lipase PS by amino acids neither accelerated nor modified enantioselectivity, though coating of lipase by L-aspartic acid (Asp) and L-cysteine (Cys) caused its significant reduction (see Rate¹ in Figure 9). They finally found very interesting synergetic activation of an enzyme for amino acid with IL1.[21] Great acceleration was obtained by the coating of lipase PS with a combination of amino acid and IL1, which was prepared by treating glycine-free PS with 100 mol eq. of L-amino acid and IL1: 100 to 300-fold acceleration compared to the native or amino acid-coated lipase PS (see Rate² in Figure 9). It was found that the combination of IL1 and L-proline (Pro) was particularly effective for realizing activation of the lipase PS: 330-fold acceleration was accomplished using L-proline and IL1-coated PS (see Rate² in Figure 9). [21]

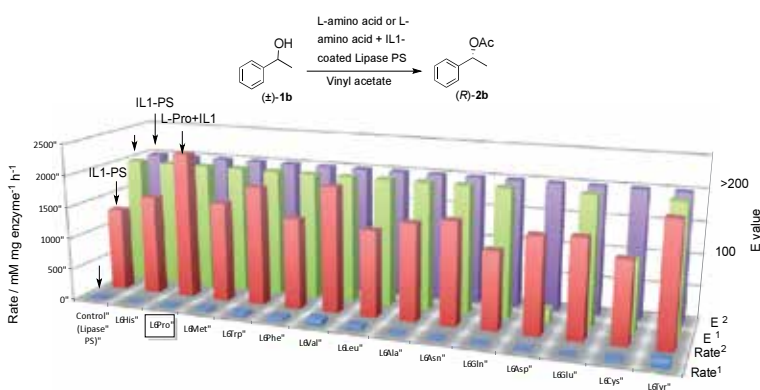


Figure 9. [21] Effect of coating on lipase PS with only an amino acid (Rate¹ and E¹) or with both an amino acid and IL1 (Rate² and E²) on transesterification of (±)-1-phenylethanol (1b) using vinyl acetate as acyl donor.

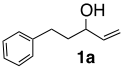
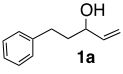
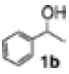
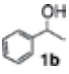
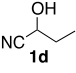
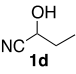
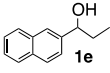
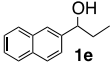
Substrate	IL	E value	% conv. / h
 1a	Native PS	>200	2.6
 1a	IL1-PS	>200	31
 1b	Native PS	>200	65
 1b	IL1-PS	>200	1000
 1d	Native PS	40	100
 1d	IL1-PS	40	9600
 1e	Native PS	199	10x10 ⁻²
 1e	IL1-PS	>200	10.5

Table 2. Typical results of transesterification mediated by lipase PS and IL1-PS.

They compared the coating effect between L-amino acids and D-amino acids for lipase PS using (\pm)-(*E*)-4-phenylbut-3-en-2-ol (1f) as a model substrate, because the reaction rate of lipase PS for this alcohol was not satisfactory, while enantioselectivity was perfect. Some different activation effect levels were found among cysteine, proline, tyrosine, and methionine-coated enzymes. Interestingly, coating with non-natural D-amino acids generally showed a slightly larger acceleration than the natural L-amino acids coating. [21]

Itoh and colleagues attempted to design an ionic liquid-type activating agent for lipase by modification of the cationic part of the IL because it was established that imidazolium cation affected the enantioselectivity of the lipase PS in their previous work. [15, 20] Since it was anticipated that introduction of an appropriate chiral functional group on the imidazolium group may create a more efficient activation of an enzyme, because D-amino acids generally showed a slightly larger acceleration than the natural L-amino acids coating. [21] Cheng and colleagues reported the synthesis of imidazolium ionic liquid derived from L-proline and used it as an efficient asymmetric organocatalyst. [22] Following their method, Itoh's group prepared pyrrolidine-substituted imidazolium bromide and converted it to cetyl-PEG10-sulphate by the metal exchange reaction. [23] Chiral pyrrolidine-substituted imidazolium cetyl-PEG10-sulphate (D-ProMe) derived from D-proline worked as an excellent activating agent of lipase PS; it is particularly interesting that D-isomer of the imidazolium salt worked better than L-isomer. This suggests that the imidazolium cation group directly interacts with the enzyme protein and causes preferable modification of the reactivity. Figure 10 summarizes the results of transesterification of (\pm)-1-phenylethanol (1b) using commercial lipase PS and four types of chiral imidazolium salt-coated lipase PS using vinyl acetate or 2-trifluoroethyl acetate ($\text{CF}_3\text{CH}_2\text{OAc}$) (Figure 10). It was established that chiral pyrrolidine-substituted imidazolium salt worked as an excellent activator of lipase PS. In particular, (*R*)-pyrrolidine-substituted salt (D-ProMe), which was derived from unnatural D-proline, was found to be the best agent: an extraordinary acceleration was accomplished with perfect enantioselectivity for D-ProMe-PS-catalysed reaction and a reaction 58 times faster (vs. lipase PS) was recorded (column 6 in Figure 10). [23]

A kinetic experiment showed that K_{cat} value of the IL1-coated lipase PS-catalysed reactions was increased compared to those of native lipase PS. [24] Modified K_{m} values were also observed between enantiomers of the substrate alcohol when lipase PS was coated by chiral imidazolium salts. [23] On the other hand, the K_{m} value of (*S*)-isomer was reduced from that of PS when D-ProMe-PS was used as catalyst, while the value was increased for (*R*)-isomer (two-fold increase over native PS). [23] These results indicate that the cationic part of the ionic liquid might bind with the lipase protein, causing conformational change of the enzyme and contributing to the difference of K_{m} between enantiomers. Chiral imidazolium cation might strongly affect the enzyme reactivity compared to amino acids when it binds with the protein, mainly on the protein surface, thus contributing to increased flexibility of the enzyme protein. Since these ionic liquids have amphiphilic properties, this also contributes to concentration of the hydrophobic substrate on the enzyme protein, so that an initial acceleration of the rate might be realized.

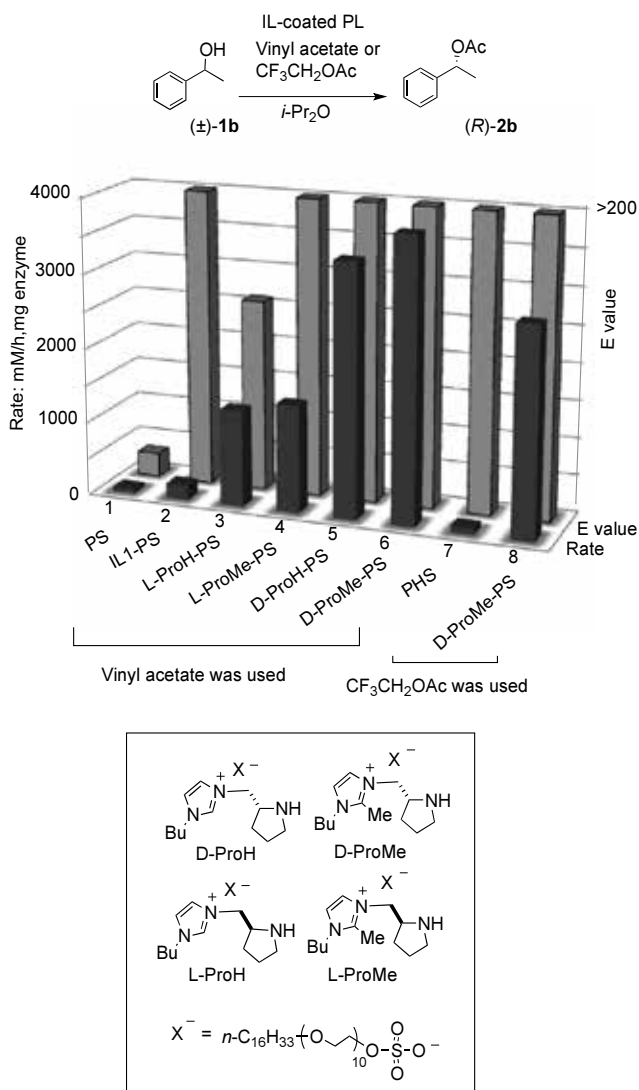


Figure 10. Activation of lipase PS by the chiral imidazolium IL coating

4. Ionic liquid-coated lipase-catalysed reaction in an ionic liquid solvent system

ILs are now established as solvents for use in lipase-catalysed transesterification with excellent enantioselectivity and the IL solvent system makes possible the recyclable use of enzymes. However, there still remains a serious drawback, in that the rate of reaction in an ionic liquid is slower than that in a conventional organic solvent such as $i\text{-Pr}_2\text{O}$. As mentioned before, a

powerful method of activating lipase protein by coating it with imidazolium alkyl PEG sulphate ionic liquid IL1 has now been established: the ionic liquid-coated *Burkholderia cepacia* lipase (IL1-PS) displayed excellent reactivity for many substrates in conventional organic solvents. [15, 20, 23, 25]

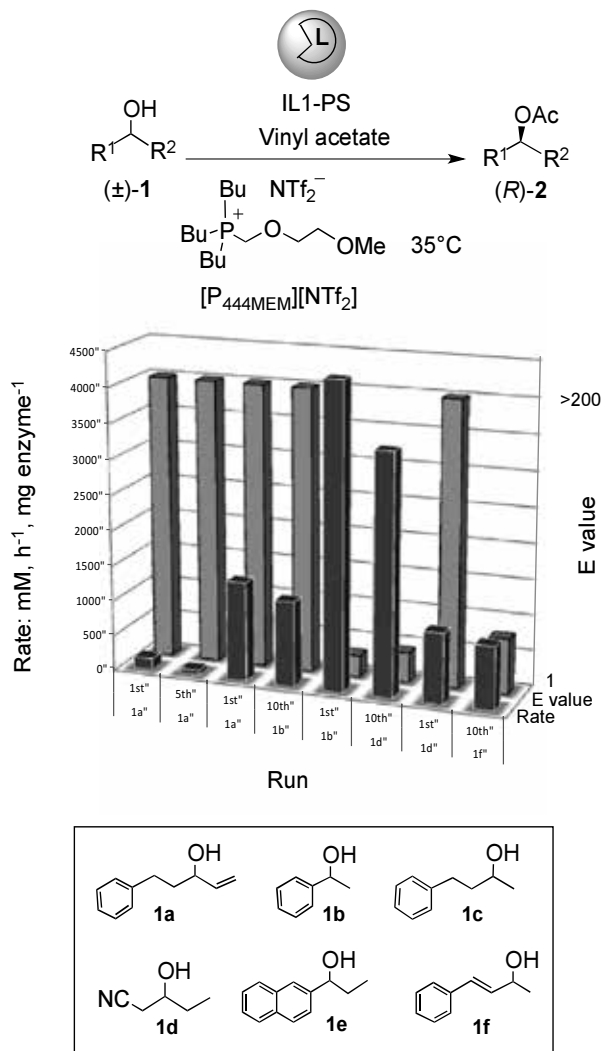


Figure 11. Results of IL1-PS-catalysed transesterification in an IL solvent system.

Itoh and colleagues reported that hydrophilic imidazolium salts ILs, which have alkyl ether functionalized sulphate salts, were appropriate for lipase-catalysed reaction. [26] Dreyer, [27] Guo, [28] Zhao [29] and De Diego [30] have reported that ILs that have an alkyl ether moiety as a cationic part acted as good solvents for these reactions. Zhao and colleagues recently

reported that dissolution and stabilization of a lipase protein took place in ILs that have a long alkyloxyalkyl chain in an ammonium cation, and suggested that this might provide improved catalytic efficiency of the corresponding biochemical reactions. [29] Hence, evaluation of ILs which have alkyl ether moieties was conducted and tributyl((2-methoxyethyl)phosphonium bis(trifluoromethanesulphonyl)amide ($[P_{444ME}][NTf_2]$) [24, 31] and tributyl((2-methoxyethoxy)methyl)phosphonium bis(trifluoromethanesulphonyl)amide ($[P_{444MEM}][NTf_2]$) [32] were developed as useful solvents for IL1-PS-catalysed reactions using 1-phenylethanol (1b) as substrate and realized recyclable use of the enzyme in the IL solvent system. [24, 32]

Phosphonium ionic liquids and ammonium ionic liquids which have alkylether moieties were shown to become excellent reaction media for lipase-catalysed transesterification, especially for ionic liquid-coated lipase PS (IL1-PS). In particular, very rapid acetylation of 1-phenylethanol (1b) has been accomplished using the combination of IL1-PS and $[P_{444MEM}][NTf_2]$ as solvent while maintaining perfect enantioselectivity (Figure 11). This is a record for the most rapid lipase-catalysed transesterification of 1-phenylethanol (1b). [32] It was also established that recyclable use of IL1-PS was possible for various substrates, as shown in Figure 11. Interestingly, $[N_{221MEM}][NTf_2]$ was always superior to $[N_{221ME}][NTf_2]$ in all substrates and that $[P_{444MEM}][NTf_2]$ was especially suitable for the reaction of 1b. [33]

5. Conclusion

In this chapter, I focus on reviewing the activating method of lipase-catalysed transesterification using ionic liquid technology. Ionic liquid has a certain advantage over conventional organic solvents, because the solvent makes it possible to use the enzyme repeatedly and has less volatile and less flammable properties. As shown in this chapter, phosphonium ionic liquid and ammonium ionic liquids which have alkylether moieties become excellent reaction media for lipase-catalysed transesterification, especially for ionic liquid-coated lipase PS (IL1-PS). It has now been disclosed that introduction of alkyl ether moiety in the cationic part of ILs might be a sure way to design ionic liquids suited for enzymatic reaction. After the reaction, we recovered the ionic liquids and used them repeatedly after simple purification. To meet the challenge in chemistry of developing practical processes, the proper choice of a reaction medium is very important. Breakthroughs have sometimes come through innovation of a reaction medium in chemical reactions, and this is true even in enzymatic reactions. I hope this paper may provide some suggestions for the reader's research.

Author details

Toshiyuki Itoh*

Address all correspondence to: titoh@chem.tottori-u.ac.jp

Tottori University, Japan

References

- [1] Reviews see: a) Plechkova, N. V.; Seddon, K. R. *Chem. Soc. Rev.* 2008, 37, 123. b) Hallett, J. P.; Welton, T. *Chem. Rev.* 2011, 111, 3508.
- [2] Reviews see: (a) Wong, C.-H.; Whitesides, G. M. *Enzymes in Synthetic Organic Chemistry*, Pergamon, Oxford, (1994). (b) Bornscheuer, U. T.; Kazlauskas, R. J. *Hydrolases in Organic Synthesis: Regio- and Stereoselective Biotransformations*, John Wiley & Sons Inc., Chichester (1999).
- [3] Faber, K. *Biotransformations in Organic Chemistry, A Textbook*, 6th Edition. Springer, Heidelberg Dordrecht London New York, 2011.
- [4] For reviews of enzymatic reactions in ILs, see: a) Itoh, T. *Future Directions in Biocatalysis*, ed. by Matsuda, T. Elsevier Bioscience, Amsterdam, The Netherlands, 2007, Chap. 1, pp. 3-20. b) Itoh, T. *J. Synth. Org. Chem. Jpn.* 2009, 67, 143. c) Lozano, P. *Green Chem.* 2010, 12, 555. d) Moniruzzaman, K.; Nakashima, M.; Kamiya, N.; Goto, M. *Biochem. Eng. J.* 2010, 48, 295.
- [5] Lau, R. M.; van Rantwijk, F.; Seddon, K. R.; and R. A. Sheldon, *Org. Lett.* 2000, 2, 4189.
- [6] Erbdinger, M.; Mesiano, A. J.; Russell, A. J. *Biotechnol. Prog.* 2000, 16, 1131. Although this paper was sometimes cited as the first example of an enzymatic reaction in the IL solvent, we could not follow their results. We suppose that the IL employed in the paper might contain a fairly large amount of water, hence the resulting liquid might be a two-layer solvent system under their reaction conditions, and that the enzymatic reaction proceeded in the water layer. It is now known that [C₄mim][PF₆] contains water at a maximum near 10 % (v/v), though it looks a pure liquid. Therefore, I believe that the first example of an enzymatic reaction in a pure IL reaction medium might be Ref. 5.
- [7] Itoh, T.; Akasaki, E.; Kudo, K.; Shirakami, S. *Chem. Lett.*, 2001, 262.
- [8] Schöfer, S. H.; Kaftzik, N.; Wasserscheid, P.; Kragl, U. *Chem. Commun.* 2001, 425.
- [9] C.-S. Chen, Y. Fujimoto, G. Girdaukas, C. J. Sih, *J. Am. Chem. Soc.* 1982, 102, 7294.
- [10] (a) Itoh, T.; Akasaki, E.; Nishimura, Y. *Chem. Lett.* 2002, 154. (b) Itoh, T.; Nishimura, Y.; Kashiwagi, M.; Onaka, M. *Ionic Liquids as Green Solvents: Progress and Prospects*, ACS Symposium Series 856, ed. by Rogers, R. D.; Seddon, K. R. American Chemical Society: Washington DC, Chapter 21, pp. 251-261 (2003).
- [11] (a) Amyes, T.L.; Diver, S. T.; Richard, J. P.; Rivas, F. M.; Toth, K. *J. Am. Chem. Soc.*, 2004, 126, 4366. (b) Magill, A. M.; Cavell, K. J.; Yates, B. F. *J. Am. Chem. Soc.*, 2004, 126, 8717. (c) Tsuzuki, S.; Tokuda, H.; Hayamizu, K.; Watanabe, M. *J. Phys. Chem. B*, 2005, 109, 16474.

- [12] a) Haraldsson, G. G.; Gudmundsson, B. Ö.; Almarsson, Ö. *Tetrahedron Lett.*, 1993, 34, 5791. b) Haraldsson, G. G.; Thorarensen, A. *Tetrahedron Lett.* 1994, 35, 7681. c) Sugai, T.; Takizawa, M.; Bakke, M.; Ohtsuka, Y.; Ohta, H. *Biosci. Biotech. Biochem.* 1996, 60, 2059. d) Cordova, A.; Janda, K. D. *J. Org. Chem.*, 2001, 66, 1906.
- [13] Irimescu, I.; Kato, K. *Tetrahedron Lett.* 2004, 45, 523.
- [14] Itoh, T.; Nishimura, Y.; Ouchi, N.; Hayase, S. *J. Mol. Catalysis B: Enzymatic*, 2003, 26, 41.
- [15] a) Itoh, T.; Han, S. -H.; Matsushita, Y.; Hayase, S. *Green Chem.* 2004, 6, 437. b) Details of this study were reported in the PhD thesis by Han Shi-Hui, Development of Lipase-catalyzed Reactions in an Ionic Liquid System, Tottori University, Japan, January 2007.
- [16] De Diego, T.; Lozano, P.; Gmouh, S.; Vaultier, M.; Iborra, J. L. *Biomacromolecules*, 2005, 6, 1457.
- [17] (a) Maruyama, T.; Nagasawa, S.; Goto, M. *Biotechnology Lett.* 2002, 24, 1341. (b) Maruyama, T.; Yamamura, H.; Kotani, T.; Kamiya, N.; Goto, M. *Organic & Biomolecular Chem.* 2004, 2, 1239.
- [18] Kaar, J. L.; Jesionowski, A. M.; Berberich, J. A.; Moulton, R.; Russell, A. J. *J. Am. Chem. Soc.* 2003, 125, 4125.
- [19] Lee, J. K.; Kim, M.-J. *J. Org. Chem.* 2002, 67, 6845.
- [20] Itoh, T.; Matsushita, Y.; Abe, Y.; Han, S.-H.; Wada, S.; Hayase, S.; Kawatsura, M.; Takai, M.; Morimoto, M.; Hirose, Y. *Chem. Eur. J.* 2006, 12, 9228.
- [21] Yoshiyama, K.; Abe, Y.; Hayase, S.; Nokami, T.; Itoh, T. *Chem. Lett.* 2013, 42, 663.
- [22] Luo, S.; Mi, X.; Zhang, L.; Liu, S.; Xu, H.; Cheng, J.-P. *Angew. Chem. Int. Ed.* 2006, 45, 3093.
- [23] Y. Abe, T. Hirakawa, S. Nakajima, N. Okano, S. Hayase, M. Kawatsura, Y. Hirose, T. Itoh, *Adv. Synth. Catal.* 2008, 350, 1954.
- [24] Abe, Y.; Kude, K.; Hayase, S.; Kawatsura, M.; Tsunashima, K.; Itoh, T. Design of phosphonium ionic liquids for lipase-catalyzed transesterification, *J. Mol. Catalysis B: Enzymatic*, 2008, 51, 81.
- [25] IL1-PS is commercially available from Tokyo Chemical Industry Co., LTD. TEL: +81-3-5640-8857, FAX:+81-3-5640-8868.
- [26] Itoh, T.; Ouchi, N.; Hayase, S.; Nishimura, Y. *Chem. Lett.* 2003, 32, 654.
- [27] Dreyer, S.; Kragl, U. *Biotechnol. Bioeng.* 2008, 99, 1416.
- [28] Guo, Z.; Chen, B.; Murillo, R. L.; Tan, T.; Xu, X. *Org. Biomol. Chem.* 2006, 4, 2772.

- [29] (a) Zhao, H.; Baker, G. A.; Song, Z.; Olubajo, O.; Crittle, T.; Peters, D. *Green Chem.* 2008, 10, 696. (b) Zhao, H.; Jones, C. L.; Cowins, J. V. *Green Chem.* 2009, 11, 1128. (c) Zhao, H.; Song, Z.; Olubajo, O. *Biotechnol. Lett.* 2010, 32, 1109.
- [30] De Diego, T.; Lozano, P.; Abad, M. A.; Steffensky, K.; Vaultier, M.; Iborra, J. L. *J. Biotechnology*, 2009, 140, 234.
- [31] Itoh, T.; Kude, K.; Hayase, S.; Kawatsura, M. Design of ionic liquids as a medium for the Grignard reaction, *Tetrahedron Lett.* 2007, 48, 7774: [P₄₄₄ME][NTf₂] is now commercially available from Tokyo Chemical Industry Co., Ltd. (TCI-T2564).
- [32] (a) Abe, Y.; Yoshiyama, K.; Yagi, Y.; Hayase, S.; Kawatsura, M.; Itoh, T. *Green Chem.* 2010, 12, 1976. (b) Itoh, T.; Abe, Y.; Hirakawa, T.; Okano, N. Nakajima, S.; Hayase, S.; Kawatsura, M.; Matsuda, T.; Nakamura, K. Ed. by Molhotra, S. ACS symposium series, Oxford University Press/ American Chemical Society: Washington DC, Vol. 1038, Chap. 13, pp 155-167 (2010).
- [33] Abe, Y.; Yagi, Y.; Hayase, S.; Kawatsura, M.; Itoh, T. *Industrial & Engineering Chemistry Research*, 2012, 51, 9952.

Solvent Dependence of Enzymatic Enantioselectivity in Ionic Liquids

Hidetaka Noritomi

Additional information is available at the end of the chapter

<http://dx.doi.org/10.5772/58998>

1. Introduction

Enantioselective synthesis is a key process in modern chemistry, and is particularly important in the fields of pharmaceuticals, foods, and pesticides, since the different enantiomers or diastereomers of a molecule often have different biological activity. Therefore, the enantioselectivity is the most valuable feature of enzymes from the standpoint of their application as practical catalysts. In nonaqueous reaction system the enantioselectivity of enzymes has been markedly dependent upon organic solvents [1-5]. On the other hand, enzymatic reactions in hydrophilic solvents have the advantage of the solubility of a variety of substrates, including amino acid derivatives, which are poorly soluble in hydrophobic solvents [5]. However, when a hydrophilic solvent is used as a reaction medium, the enzyme molecule directly contacts with the solvent, and thereby its activity and enantioselectivity are strongly influenced by the nature of solvents [1, 2]. Moreover, as the enzyme is insoluble in nonaqueous media, which are 100% organic solvent media or aqueous solutions containing high amount of organic solvents, and is suspended, the reactivity of enzymes tends to be strongly influenced by the dispersion state of enzymes.

Ionic solvent that is liquid at room temperature has attracted increasing attention as innovative nonaqueous media for the chemical processes because of the lack of vapor pressure, the thermal stability, the high polarity, and so on [6]. Chemical and physical properties of ionic liquids can be changed by the appropriate modification of organic cations and anions, which are constituents of ionic liquids. Biotransformation in ionic liquids has extensively been studied [6, 7]. We have so far reported that protease-catalyzed esterification of amino acid and peptide synthesis are highly enhanced in ionic liquids, compared to organic solvents, and the thermal stability of proteins is markedly improved [8, 9].

In the chapter, the solvent effect of ionic liquids on the enantioselectivity of enzymes is mainly discussed on the basis of enzyme kinetics [10].

2. Effect of reaction medium on α -chymotrypsin-catalyzed esterification

As a model enzyme, bovine pancreas α -chymotrypsin has been employed as shown in Fig. 1, since it has been well investigated regarding its structure, properties, and functions [11]. α -Chymotrypsin belongs to the S1 family that is one of the most predominant families of serine protease. Peptide and synthetic ester substrates are hydrolyzed in an aqueous solution by serine protease. The S1 family contains a catalytic triad system consisting of aspartate, histidine, and serine that work together to control the nucleophilicity of the serine residue during catalysis [12]. The serine proteases are widely distributed in nature, where they perform a variety of different functions.

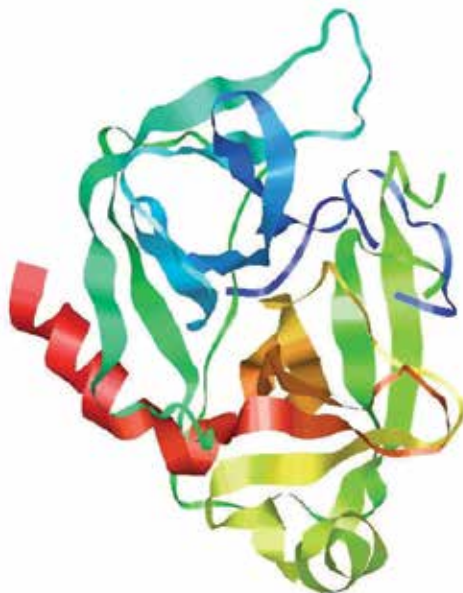


Figure 1. Structure of α -chymotrypsin

The binding site for a polypeptide substrate consists of a series of subsites across the surface of the enzyme, as seen in Fig. 2 [12]. In the figure, P and S are the substrate residues and the subsites, respectively. Except at the primary binding site S_1 for the side chains of the aromatic substrates of α -chymotrypsin, there is no obvious, well-defined cleft or groove for substrate binding. The subsites run along the surface of the protein. The binding pocket for the aromatic side chains of the specific substrates of α -chymotrypsin is a well-defined slit in the enzyme 1 to 1.2 nm deep and 0.35 to 0.4 by 0.55 to 0.65 nm in cross section. This gives a very snug fit,

since an aromatic ring is about 0.6 nm wide and 0.35 nm thick. The binding pocket in α -chymotrypsin may be described as a hydrophobic pocket, since it is lined with the nonpolar side chains of amino acids. It provides a suitable environment for the binding of the nonpolar or hydrophobic side chains of the substrates.

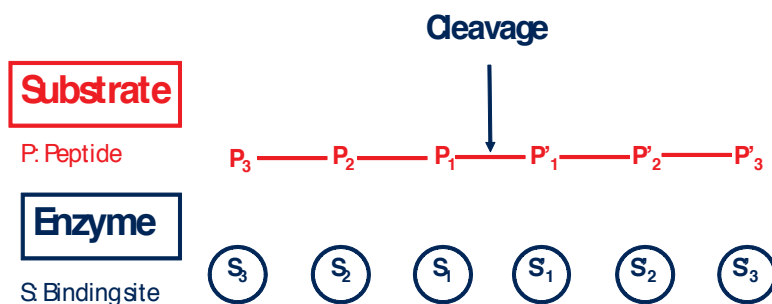


Figure 2. Binding site for polypeptide substrate.

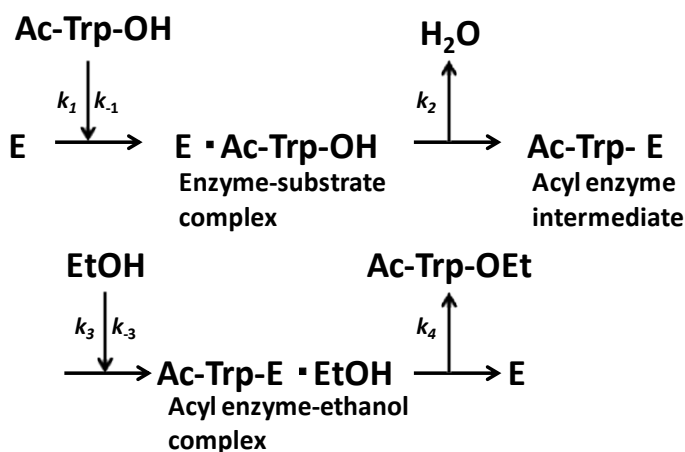


Figure 3. α -Chymotrypsin-catalyzed esterification of *N*-acetyl-tryptophan (Ac-Trp-OH) with ethanol (EtOH) to *N*-acetyl-tryptophan ethylester (Ac-Trp-OEt).

In nonaqueous media, α -chymotrypsin can function as a synthetic catalyst for esterification, transesterification, and peptide synthesis, and α -chymotrypsin-catalyzed esterification of *N*-acetyl-tryptophan (Ac-Trp-OH) with ethanol (EtOH) is proceeded as shown in Fig. 3. The esterification obeys ping-pong kinetics [12, 13]. The enzyme and substrate first associate to form a noncovalent enzyme-substrate complex (E·Ac-Trp-OH) held together by physical forces of attraction. This is followed by the attack of the hydroxyl of serine (Ser-195), which is one of amino acid residues in a catalytic triad system, on the substrate to give acyl enzyme intermediate (Ac-Trp-E) releasing water. The acyl enzyme intermediate and ethanol associate

to form an acyl enzyme-ethanol complex (Ac-Trp-E·EtOH). This is followed by the nucleophilic attack of ethanol on the carbonyl group in Ac-Trp-E to give *N*-acetyl-tryptophan ethyl ester (Ac-Trp-OEt). It is assumed that the esterification proceeds through the steady state approximation. The rate of *N*-acetyl-tryptophan (Ac-Trp-OH) is given as

$$\frac{d[\text{Ac - Trp - OH}]}{dt} = k_{-1}[\text{E} \cdot \text{Ac - Trp - OH}] - k_1[\text{E}][\text{Ac - Trp - OH}] \quad (1)$$

where E and E·Ac-Trp-OH are α -chymotrypsin and enzyme-substrate complex, respectively. Similarly, the rates of E, enzyme-substrate complex (E·Ac-Trp-OH), acyl enzyme intermediate (Ac-Trp-E), acyl enzyme-ethanol complex (Ac-Trp-E·EtOH), H₂O, and *N*-acetyl-tryptophan ethyl ester (Ac-Trp-OEt) are as follows:

$$\frac{d[\text{E}]}{dt} = k_{-1}[\text{E} \cdot \text{Ac - Trp - OH}] + k_4[\text{Ac - Trp - E} \cdot \text{EtOH}] - k_1[\text{E}][\text{Ac - Trp - OH}] \quad (2)$$

$$\frac{d[\text{E} \cdot \text{Ac - Trp - OH}]}{dt} = k_1[\text{E}][\text{Ac - Trp - OH}] - (k_{-1} + k_2)[\text{E} \cdot \text{Ac - Trp - OH}] \quad (3)$$

$$\frac{d[\text{Ac - Trp - E}]}{dt} = k_2[\text{E} \cdot \text{Ac - Trp - OH}] - k_3[\text{Ac - Trp - E}][\text{EtOH}] + k_3[\text{Ac - Trp - E} \cdot \text{EtOH}] \quad (4)$$

$$\frac{d[\text{Ac - Trp - E} \cdot \text{EtOH}]}{dt} = k_3[\text{Ac - Trp - E}][\text{EtOH}] - (k_{-3} + k_4)[\text{Ac - Trp - E} \cdot \text{EtOH}] \quad (5)$$

$$\frac{d[\text{H}_2\text{O}]}{dt} = k_2[\text{E} \cdot \text{Ac - Trp - OH}] \quad (6)$$

$$\frac{d[\text{Ac - Trp - OEt}]}{dt} = k_4[\text{Ac - Trp - E} \cdot \text{EtOH}] \quad (7)$$

Since all enzyme present is either free or complexes,

$$[\text{E}]_0 = [\text{E}] + [\text{E} \cdot \text{Ac - Trp - OH}] + [\text{Ac - Trp - E}] + [\text{Ac - Trp - E} \cdot \text{EtOH}] \quad (8)$$

where [E]₀ is the total concentration of enzyme in the system. Assuming the steady state approximation on the rate of E·Ac-Trp-OH, from Eq. 3

$$\frac{d[\text{E} \cdot \text{Ac - Trp - OH}]}{dt} = k_1[\text{E}][\text{Ac - Trp - OH}] - (k_{-1} + k_2)[\text{E} \cdot \text{Ac - Trp - OH}] = 0 \quad (9)$$

$$K_{S_1} = \frac{[\text{E}][\text{Ac - Trp - OH}]}{[\text{E} \cdot \text{Ac - Trp - OH}]} = \frac{k_{-1} + k_2}{k_1} \quad (10)$$

where K_{S_1} is the dissociation constant of E·Ac-Trp-OH. Assuming $d[\text{H}_2\text{O}]/dt = d[\text{Ac-Trp-OEt}]/dt$, from Eqs. 6 and 7,

$$[\text{Ac - Trp - E} \bullet \text{EtOH}] = \frac{k_2}{k_4} [\text{E} \bullet \text{Ac - Trp - OH}] \quad (11)$$

Assuming the steady state approximation on the rate of Ac-Trp-E·EtOH, from Eq. 5

$$\frac{d[\text{Ac - Trp - E} \bullet \text{EtOH}]}{dt} = k_3 [\text{Ac - Trp - E}] [\text{EtOH}] - (k_{-3} + k_4) [\text{Ac - Trp - E} \bullet \text{EtOH}] = 0 \quad (12)$$

$$K_{S_2} = \frac{[\text{Ac - Trp - E}] [\text{EtOH}]}{[\text{Ac - Trp - E} \bullet \text{EtOH}]} = \frac{k_3 + k_4}{k_3} \quad (13)$$

where K_{S_2} is the dissociation constant of Ac-Trp-E·EtOH. From Eq. 13

$$[\text{Ac - Trp - E}] = \frac{K_{S_2} [\text{Ac - Trp - E} \bullet \text{EtOH}]}{[\text{EtOH}]} \quad (14)$$

From Eq. 8

$$[\text{E}] = [\text{E}]_0 - [\text{E} \bullet \text{Ac - Trp - OH}] - [\text{Ac - Trp - E}] - [\text{Ac - Trp - E} \bullet \text{EtOH}] \quad (15)$$

Concerning the equation obtained from Eqs. 10, 11, 14, and 15, $(k_2+k_4)[\text{EtOH}]$ is much greater than $k_2K_{S_2}$ because of excess $[\text{EtOH}]$. Consequently,

$$[\text{E} \bullet \text{Ac - Trp - OH}] = \frac{\{k_4 + (k_2 + k_4)\} [\text{E}]_0 [\text{Ac - Trp - OH}]}{k_4 K_{S_1} / (k_2 + k_4) + [\text{Ac - Trp - OH}]} \quad (16)$$

The reaction rate v is

$$v = \frac{d[\text{E} \bullet \text{Ac - Trp - OEt}]}{dt} = \frac{d[\text{H}_2\text{O}]}{dt} = k_2 [\text{E} \bullet \text{Ac - Trp - OH}] = \frac{k_{\text{cat}} [\text{E}]_0 [\text{Ac - Trp - OH}]}{K_{\text{M}} + [\text{Ac - Trp - OH}]} \quad (17)$$

where

$$k_{\text{cat}} = \frac{k_2 k_4}{k_2 + k_4} \quad (18)$$

$$K_{\text{M}} = \frac{k_4 K_{S_1}}{k_2 + k_4} = \frac{(k_{-1} + k_2) k_4}{k_1 (k_2 + k_4)} \quad (19)$$

Thus, the reaction rate v corresponds upon Michaelis-Menten type model.

3. Effect of solvent on activity and enantioselectivity of α -chymotrypsin

The performances of enzymes such as activity and specificity in nonaqueous media markedly depend upon the nature of solvents [1, 2]. In order to assess the effect of reaction media on kinetic parameters of α -chymotrypsin, the reaction rates in ionic liquids and organic solvents containing 5% (*v/v*) water were measured at different concentrations of substrates at 25 °C. Figure 4 shows the structures of solvents used in this study. In the figure, 1-ethyl-3-methylimidazolium tetrafluoroborate, 1-ethyl-3-methylimidazolium bis(fluorosulfonyl)imide, 1-butyl-3-methylimidazolium hexafluorophosphate, 1-butyl-3-methylimidazolium bis(trifluoromethylsulfonyl)imide, and tetrahydrofuran are abbreviated as [C2mim][BF₄], [C2mim][FSI], [C4mim][PF₆], [C4mim][TFSI], and THF, respectively. The kinetic parameters, k_{cat} and K_M , were derived by correlating resultant reaction rates with Hanes-Woolf plot, which is the plot of $[\text{Ac-Trp-OH}]/v$ against $[\text{Ac-Trp-OH}]$ giving intercepts at $K_M/k_{cat}[E]_0$ and $-K_M$ [13].

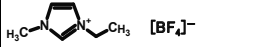
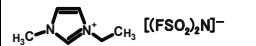
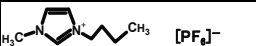
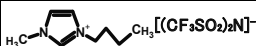

Solvent	Structure	m. p. (°C)	Water miscibility
[C2mim][BF ₄]		15.0	Miscible
[C2mim][FSI]		-12.9	Partially miscible
[C4mim][PF ₆]		6.5	Immiscible
[C4mim][TFSI]		-16.2	Immiscible
THF		-108.5	Miscible

Figure 4. Structures of solvents in this work.

Figure 5 shows the k_{cat} in ionic liquids and THF at 5% (*v/v*) water and 25 °C. The k_{cat} is known as the turnover number or molecular activity as it represents the maximum number of substrate molecules that the enzyme can turn over to product in a set time. The $k_{cat, L}$ for L-enantiomer was much greater than $k_{cat, D}$ for D-enantiomer in ionic liquids and THF. α -Chymotrypsin absolutely favors L-enantiomer in aqueous solutions. Consequently, the structural specificity of native enzyme remained to some extent in ionic liquids and THF. The k_{cat} was strongly dependent upon the kind of solvents. The $k_{cat, L}$ for L-enantiomer in [C₂mim][BF₄] was the greatest, while the $k_{cat, D}$ for D-enantiomer in [C₂mim][FSI] was the greatest. [C₂mim][BF₄] can act as a thermal stabilizer for proteins in aqueous solutions [14]. The k_{cat} is first-order rate constant that refers to the properties and reactions of the enzyme-substrate, enzyme-intermediate, and enzyme-product complexes. It is suggested that the solvent dependence of k_{cat} is due to the conformational changes in the enzyme. As a result, the $k_{cat, L}/k_{cat, D}$ in [C₂mim][BF₄] was the greatest, while that in [C₄mim][PF₆] was the smallest, as shown in Fig. 6.

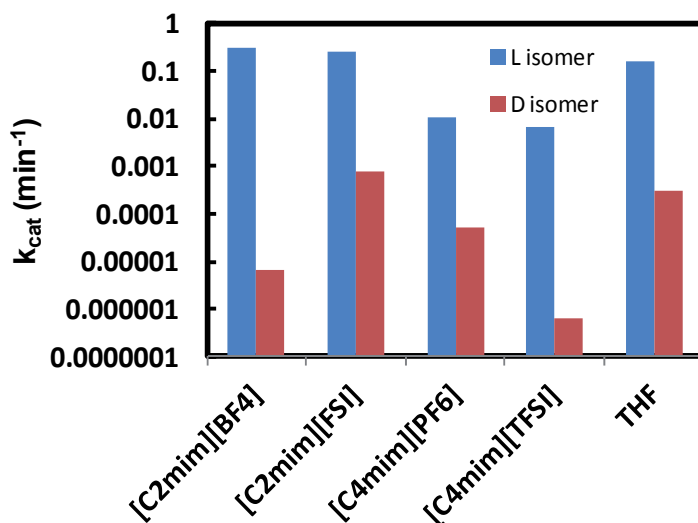


Figure 5. The k_{cat} in ionic liquids and THF at 5% (*v/v*) water and 25 °C.

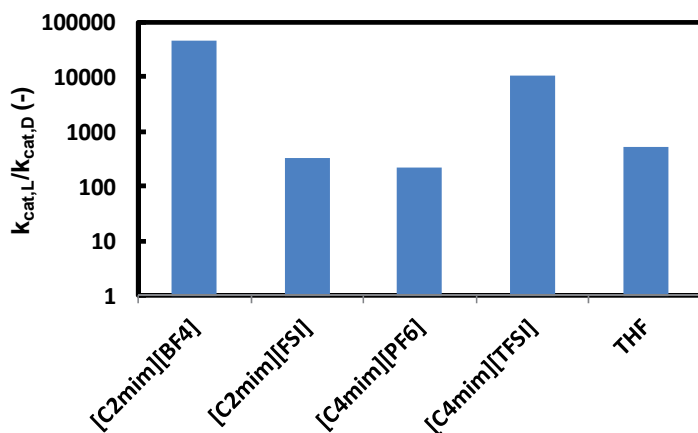


Figure 6. The $k_{cat,L}/k_{cat,D}$ in ionic liquids and THF at 5% (*v/v*) water and 25 °C.

Figure 7 shows the K_M in ionic liquids and THF at 5% (*v/v*) water and 25 °C. The $K_{M,L}$ for L-enantiomer was the smallest in [C₄mim][PF₆], while the $K_{M,D}$ for D-enantiomer was small in [C₂mim][BF₄] or [C₄mim][TFSI], compared with that in other solvents. The K_M is an apparent dissociation constant that may be treated as the overall dissociation constant of all enzyme-bound species. In addition, K_M corresponds upon the substrate concentration when the reaction rate v is half of maximum reaction rate. Consequently, it is easy to form enzyme-bound species for L-enantiomer in [C₄mim][PF₆] and for D-enantiomer in [C₂mim][BF₄] and [C₄mim][TFSI]. As a result, the $K_{M,L}/K_{M,D}$ in [C₄mim][PF₆] was the smallest, while that in [C₂mim][FSI] was the greatest, as seen in Fig. 8.

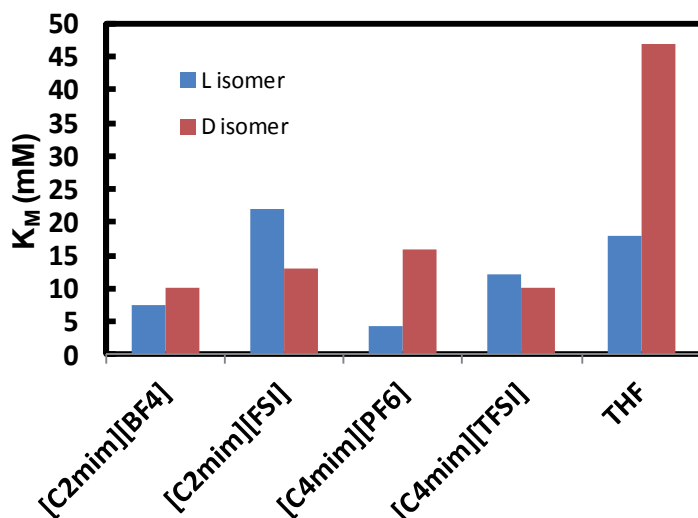


Figure 7. The K_M in ionic liquids and THF at 5% (*v/v*) water and 25 °C.

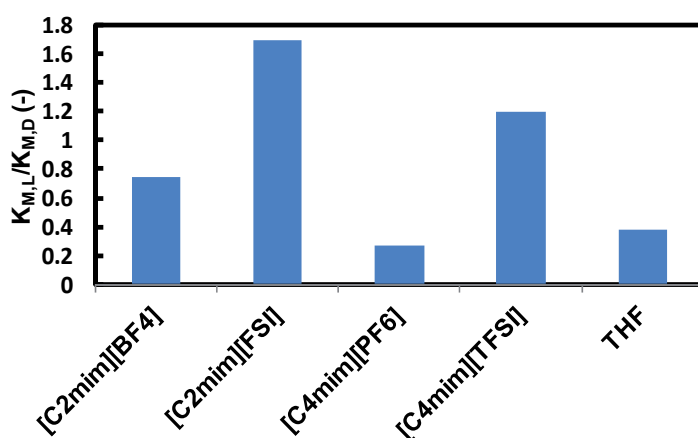


Figure 8. The $K_{M,L}/K_{M,D}$ in ionic liquids and THF at 5% (*v/v*) water and 25 °C.

Figure 9 shows the k_{cat}/K_M in ionic liquids and THF at 5% (*v/v*) water and 25 °C. The $(k_{cat}/K_M)_L$ for L-enantiomer was the greatest in [C₂mim][BF₄], while the $(k_{cat}/K_M)_D$ for D-enantiomer was the greatest in [C₂mim][FSI]. The k_{cat}/K_M is an apparent second-order rate constant that refers to the properties and the reactions of the free enzyme and free substrate. Thus, it sets a lower limit on the rate constant for the association of enzyme and substrate, and corresponds upon the catalytic efficiency of enzymes.

Figure 10 shows the $(k_{\text{cat}}/K_M)_L / (k_{\text{cat}}/K_M)_D$ in ionic liquids and THF at 5% (*v/v*) water and 25 °C. The $(k_{\text{cat}}/K_M)_L / (k_{\text{cat}}/K_M)_D$ in $[\text{C}_2\text{mim}][\text{BF}_4]$ was 65000, while that in $[\text{C}_2\text{mim}][\text{FSI}]$ was 200. The k_{cat}/K_M is referred to as the specificity constant, and determines the specificity for competing substrates [12]. Consequently, the $(k_{\text{cat}}/K_M)_L / (k_{\text{cat}}/K_M)_D$ corresponds upon the enantioselectivity. Figure 10 reveals that the enantioselectivity of α -chymotrypsin in ionic liquids can be forced to span a 325-fold range simply by switching from one solvent to another under otherwise identical conditions. Thus, D-enantiomer can sufficiently be employed as a substrate of α -chymotrypsin in ionic liquids, although α -chymotrypsin catalyzes biotransformation of L-enantiomer in nature.

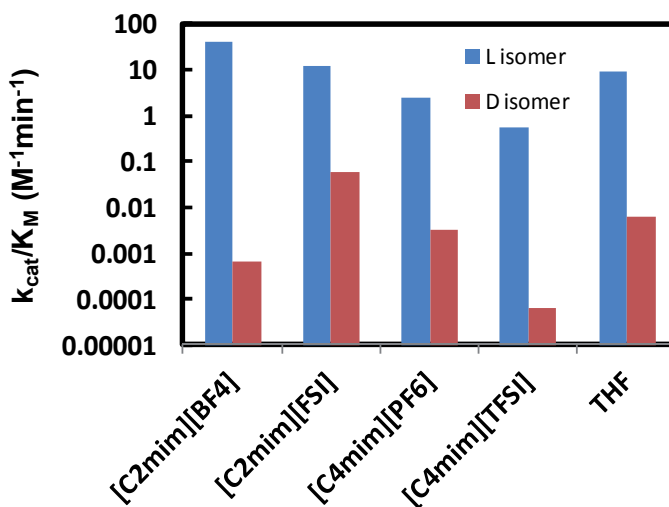


Figure 9. The k_{cat}/K_M in ionic liquids and THF at 5% (*v/v*) water and 25 °C.

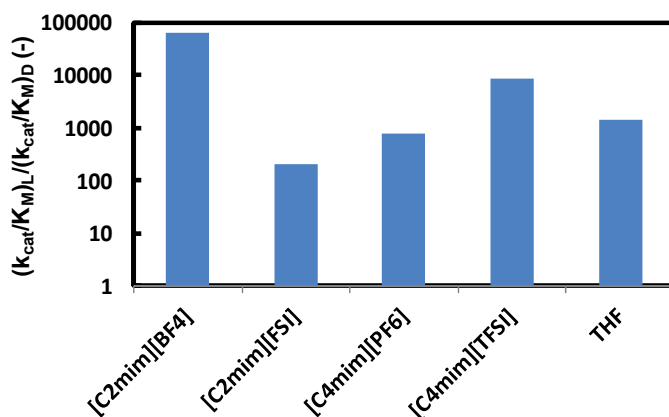


Figure 10. The $(k_{\text{cat}}/K_M)_L / (k_{\text{cat}}/K_M)_D$ in ionic liquids and THF at 5% (*v/v*) water and 25 °C.

4. Effect of water content on activity and enantioselectivity of α -chymotrypsin

A common thread in all studies of enzymes in anhydrous solvents is that the amount of water associated with the enzyme is a key determinant of the properties (e.g. activity, stability, and specificity) that the enzyme exhibits [1]. Moreover, water can act as a substrate in reactions using hydrolytic enzymes. In order to assess the effect of water content on kinetic parameters of α -chymotrypsin, the reaction rate in ionic liquids and organic solvents containing 1% (*v/v*) water was measured at different concentrations of substrates at 25 °C.

Figure 11 shows the k_{cat} in ionic liquids and THF at 1% (*v/v*) water and 25 °C. The k_{cat} depended upon the kind of solvents. The $k_{\text{cat, L}}$ for L-enantiomer was much greater than $k_{\text{cat, D}}$ for D-enantiomer in ionic liquids and THF, similar to the case at 5% (*v/v*) water. The $k_{\text{cat, L}}$ for L-enantiomer in [C₂mim][FSI] was the greatest, while the $k_{\text{cat, D}}$ for D-enantiomer in [C₂mim][BF₄] was the greatest. The $k_{\text{cat, L}}$ for L-enantiomer in [C₂mim][BF₄] at 1% (*v/v*) water was about 81 times smaller than that at 5% (*v/v*) water, while the $k_{\text{cat, L}}$ for L-enantiomer in [C₂mim][FSI] at 1% (*v/v*) water exhibited 18-fold decrease, compared to that at 5% (*v/v*) water. When a certain amount of water is added into the nonaqueous enzymatic reaction system, some water is bound to the enzyme, and thereby has a large influence on the enzyme performance, while the other amount of water is dissolved in the solvent [1]. Water associated with the enzyme activates the enzyme by increasing the internal flexibility of the enzyme molecule, since water acts as a plasticizer to increase the flexibility [15]. On the other hand, the k_{cat} is the kinetic parameter that refers to the properties and reactions of the enzyme-substrate, enzyme-intermediate, and enzyme-product complexes due to the conformational changes in the enzyme. Accordingly, the water content markedly affected the conformation of enzymes in

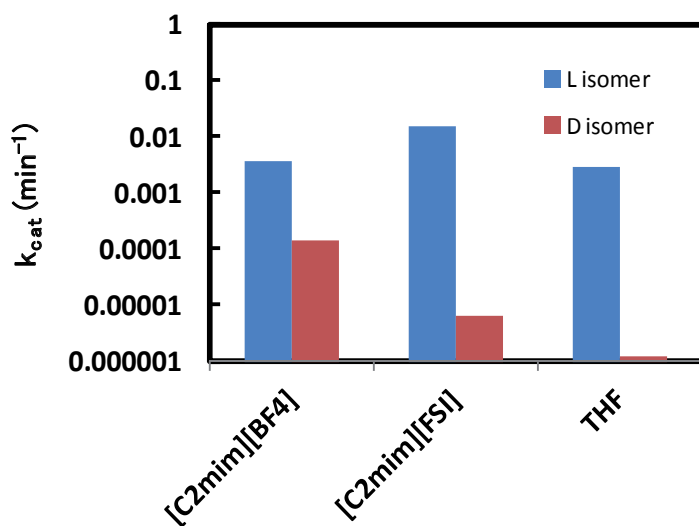


Figure 11. The k_{cat} in ionic liquids and THF at 1% (*v/v*) water and 25 °C.

ionic liquids. As a result, the $k_{cat,L}/k_{cat,D}$ in [C₂mim][FSI] was the greatest, while that in [C₂mim][BF₄] was the smallest, as shown in Fig. 12. Especially, the $k_{cat,L}/k_{cat,D}$ in [C₂mim][FSI] increased with decreasing water content, whereas that in [C₂mim][BF₄] drastically dropped.

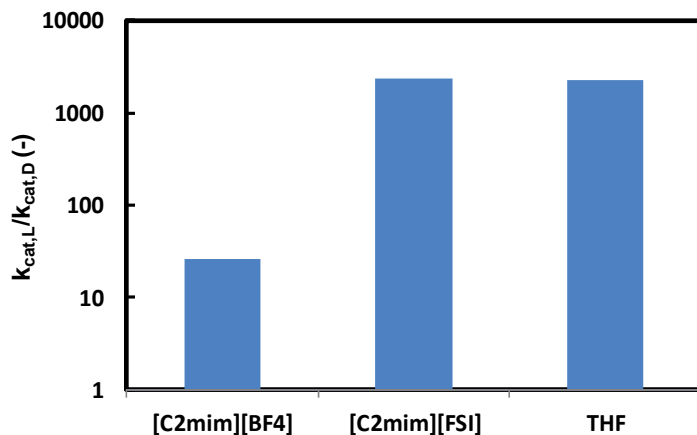


Figure 12. The $k_{cat,L}/k_{cat,D}$ in ionic liquids and THF at 1% (v/v) water and 25 °C.

Figure 13 shows the K_M in ionic liquids and THF at 1% (v/v) water and 25 °C. The $K_{M,L}$ for L-enantiomer was the smallest in [C₂mim][FSI], while the $K_{M,D}$ for D-enantiomer was the smallest in THF. The $K_{M,D}$ in [C₂mim][BF₄] at 1% (v/v) water was eleven times greater than that at 5% (v/v) water, whereas the $K_{M,D}$ in THF at 1% (v/v) water was seven times less than that at 5% (v/v) water. The $K_{M,L}$ in [C₂mim][FSI] at 1% (v/v) water was twenty-nine times less than that at 5% (v/v) water. Therefore, the solvent effect on $K_{M,L}$ and $K_{M,D}$ was dependent upon the kind

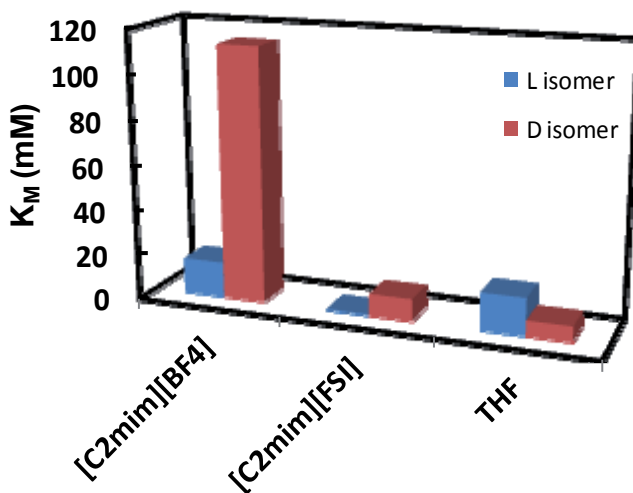


Figure 13. The K_M in ionic liquids and THF at 1% (v/v) water and 25 °C.

of solvents. As a result, the $K_{M,L}/K_{M,D}$ in THF was extremely large, compared with [C₂mim][BF₄] or [C₂mim][FSI], as seen in Fig. 14.

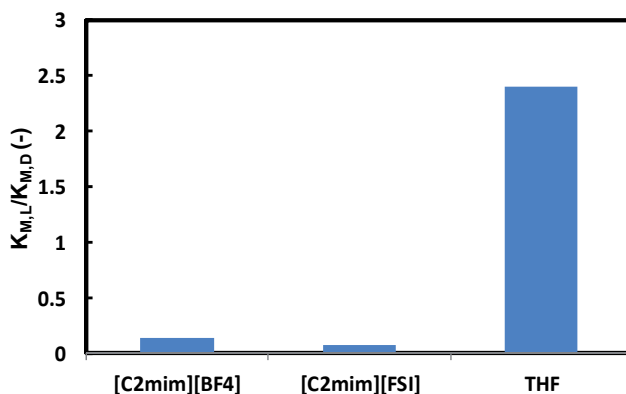


Figure 14. The $K_{M,L}/K_{M,D}$ in ionic liquids and THF at 1% (*v/v*) water and 25 °C.

Figure 15 shows the k_{cat}/K_M in ionic liquids and THF at 1% (*v/v*) water and 25 °C. The $(k_{cat}/K_M)_L$ for L-enantiomer in [C₂mim][FSI] was the greatest, while the $(k_{cat}/K_M)_D$ for D-enantiomer in [C₂mim][BF₄] was the greatest. The $(k_{cat}/K_M)_L$ in [C₂mim][FSI] at 1% (*v/v*) water was 1.7 times greater than that at 5% (*v/v*) water, and the $(k_{cat}/K_M)_D$ in [C₂mim][BF₄] at 1% (*v/v*) water was twice greater than that at 5% (*v/v*) water. In other solvent systems, the $(k_{cat}/K_M)_L$ and $(k_{cat}/K_M)_D$ decreased with a decrease in water content. Especially, the $(k_{cat}/K_M)_L$ in [C₂mim][BF₄] at 1% (*v/v*) water was 175-fold less than that at 5% (*v/v*) water, and the $(k_{cat}/K_M)_D$ in [C₂mim][FSI] at 1% (*v/v*) water was 97-fold less than that at 5% (*v/v*) water.

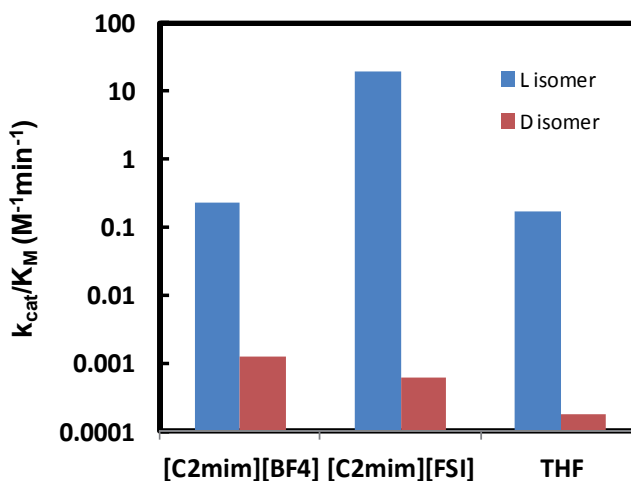


Figure 15. The k_{cat}/K_M in ionic liquids and THF at 1% (*v/v*) water and 25 °C.

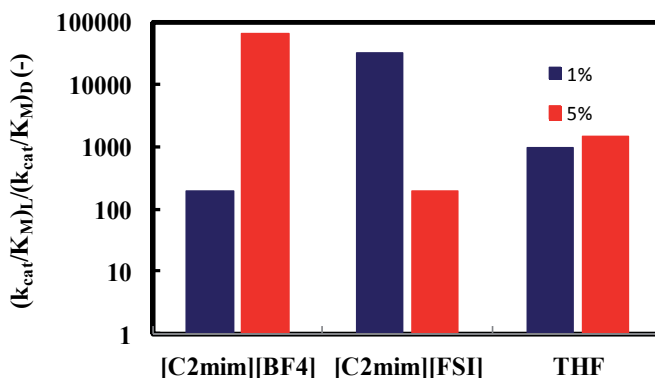


Figure 16. Effect of water content on the enantioselectivity of α -chymotrypsin-catalyzed esterification in ionic liquids and THF at 25 °C.

Figure 16 shows the enantioselectivity in ionic liquids and THF at different water contents. The enantioselectivity of α -chymotrypsin in [C₂mim][BF₄] increased with an increase in water content, while that in [C₂mim][FSI] decreased with increasing water content. The optimum water content for the enzyme performance is due to the balance between kinetic rigidity and thermodynamic stability of enzyme structures, and is called essential water [16]. The kinetic rigidity is relaxed by increasing water content, while native enzyme structure gradually changes through thermodynamic stability. For instance, the activity increases with an increase in the flexibility of rigid enzyme in ionic liquids, and it decreases with an increase in disturbance of enzyme structure [9]. Since the water solubility of [C₂mim][FSI] is much lower than that of [C₂mim][BF₄], the distribution of water to the enzyme molecule in [C₂mim][FSI] is superior to that in [C₂mim][BF₄]. Consequently, the disturbance of enzyme structure at 5% (*v/v*) water might be enhanced to some extent in [C₂mim][FSI] system, since the water solubility of [C₂mim][FSI] is 3.45%. On the other hand, [C₂mim][BF₄] system exhibited the same tendency in the relation between the water content and the enantioselectivity as THF system. [C₂mim][BF₄] and THF systems were probably in the relax of kinetic rigidity at 5% (*v/v*) water, since [C₂mim][BF₄] and THF are water soluble.

5. Effect of reaction temperature on enantioselectivity of α -chymotrypsin in ionic liquids

Enzymatic reactions, as well as chemical reactions, obey the Arrhenius correlation between reaction rate constant and temperature, although the temperature range is quite limited. Accordingly, it is considered that the enantioselectivity is strongly influenced by the reaction temperature. In order to estimate the effect of reaction temperature on α -chymotrypsin-catalyzed esterification in ionic liquids, the kinetic parameters in ionic liquids and THF containing 5% (*v/v*) water were investigated at 40 °C.

Figure 17 shows the k_{cat} in ionic liquids and THF at 5% (*v/v*) water and 40 °C. The k_{cat} was dependent upon the kind of solvents. Comparing the k_{cat} at 40 °C with that at 25 °C, the $k_{\text{cat,L}}$ in THF at 40 °C exhibited about 720-fold decrease, whereas the $k_{\text{cat,D}}$ in THF at 40 °C shows about 480-fold increase. This indicates that thermal perturbation to enzyme structures at THF is large. On the other hand, the $k_{\text{cat,L}}/k_{\text{cat,D}}$ in $[\text{C}_2\text{mim}][\text{BF}_4]$ was the greatest, while that in $[\text{C}_2\text{mim}][\text{FSI}]$ was the smallest, as shown in Fig. 18. Especially, the $k_{\text{cat,L}}/k_{\text{cat,D}}$ in $[\text{C}_2\text{mim}][\text{FSI}]$ and THF decreased with increasing temperature, whereas that in $[\text{C}_2\text{mim}][\text{BF}_4]$ slightly increased.

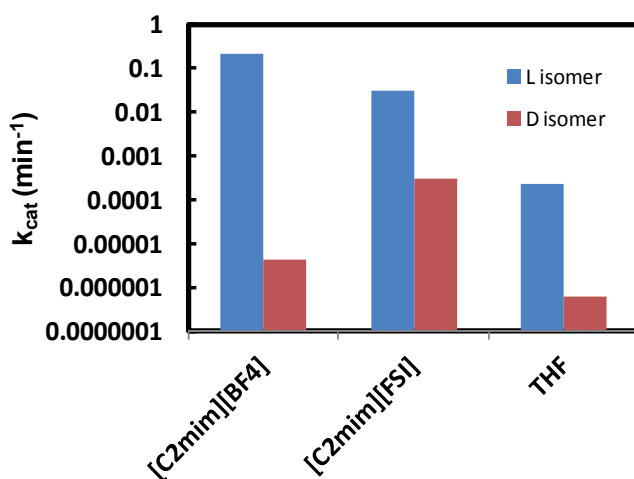


Figure 17. The k_{cat} in ionic liquids and THF at 5% (*v/v*) water and 40 °C.

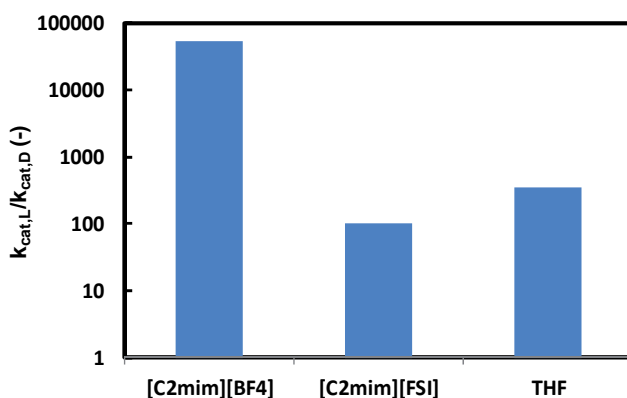


Figure 18. The $k_{\text{cat,L}}/k_{\text{cat,D}}$ in ionic liquids and THF at 5% (*v/v*) water and 40 °C.

Figure 19 shows the K_{M} in ionic liquids and THF at 5% (*v/v*) water and 40 °C. The $K_{\text{M,L}}$ in $[\text{C}_2\text{mim}][\text{FSI}]$ was the smallest, while the $K_{\text{M,D}}$ in $[\text{C}_2\text{mim}][\text{BF}_4]$ and THF was seventy times less than that

in [C₂mim][FSI]. The $K_{M,L}$ in THF at 40 °C was 5.6 times greater than that at 25°C, whereas the $K_{M,D}$ in [C₂mim][FSI] at 40 °C was seven times greater than that at 25 °C. As a result, the $K_{M,L}/K_{M,D}$ in THF was much greater than that in [C₂mim][BF₄] or [C₂mim][FSI], as seen in Fig. 20.

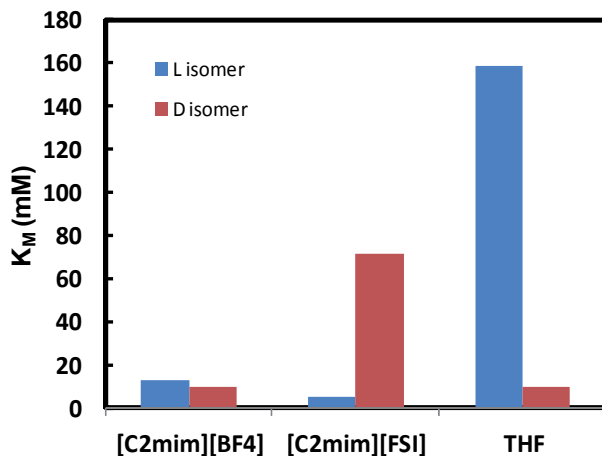


Figure 19. The K_M in ionic liquids and THF at 5% (*v/v*) water and 40 °C.

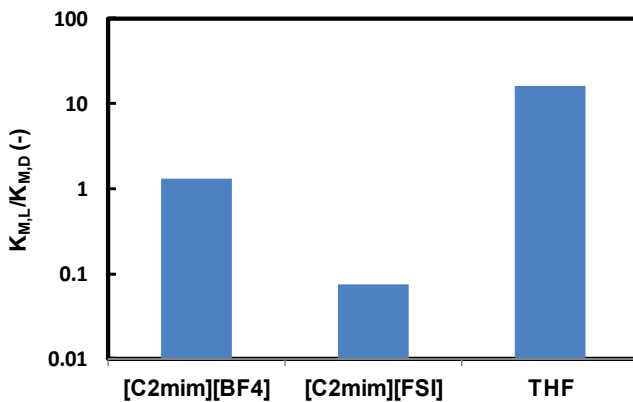


Figure 20. The $K_{M,L}/K_{M,D}$ in ionic liquids and THF at 5% (*v/v*) water and 40 °C.

Figure 21 shows the k_{cat}/K_M in ionic liquids and THF at 5% (*v/v*) water and 40 °C. The $(k_{cat}/K_M)_L$ in [C₂mim][BF₄] was the greatest, while the $(k_{cat}/K_M)_D$ in [C₂mim][FSI] was the greatest. Comparing the k_{cat}/K_M at 40 °C with that at 25 °C, the k_{cat}/K_M in ionic liquids and THF decreased with an increase in temperature. Especially, the $(k_{cat}/K_M)_L$ in THF at 40 °C exhibited about 6000-fold decrease, compared to that at 25 °C. This result indicates that heat extremely damages the catalytic efficiency of enzymes in THF.

As seen in Fig. 22, the enantioselectivity of α -chymotrypsin in $[\text{C}_2\text{mim}][\text{BF}_4]$ at 40 °C was lower than that at 25 °C, while that in $[\text{C}_2\text{mim}][\text{FSI}]$ increased with increasing the reaction temperature. On the other hand, the enantioselectivity of α -chymotrypsin in THF drastically dropped with an increase in the reaction temperature. The temperature dependence of the enantioselectivity of protease and lipase is markedly affected by organic solvents [3]. Thus, the result indicates that the temperature dependence of the enantioselectivity is controlled by changing the reaction medium from one ionic liquid to another, similar to the case of organic solvents.

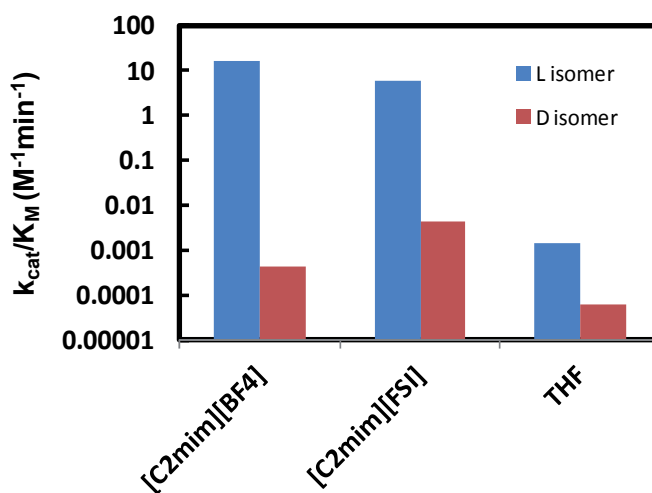


Figure 21. The k_{cat}/K_M in ionic liquids and THF at 5% (v/v) water and 40 °C.

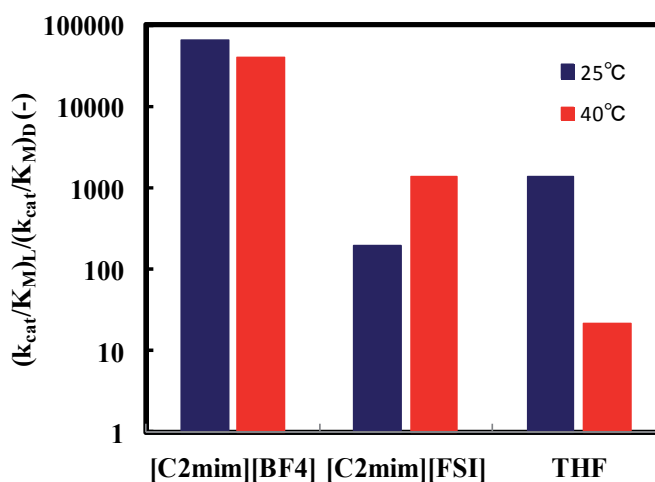


Figure 22. Effect of reaction temperature on the enantioselectivity of α -chymotrypsin-catalyzed esterification in ionic liquids and THF at 5% (v/v) water.

6. Relationship between catalytic efficiency and enantioselectivity of α -chymotrypsin in ionic liquids

As mentioned above, the enantioselectivity is strongly influenced by a kind of ionic liquids, water content, and reaction temperature. In order to assess the correlation between the catalytic efficiency and the enantioselectivity, the $(k_{\text{cat}}/K_{\text{M}})_{\text{L}}/(k_{\text{cat}}/K_{\text{M}})_{\text{D}}$ was plotted against the $(k_{\text{cat}}/K_{\text{M}})_{\text{L}}$, as seen in Fig. 23. One can observe an increase in the $(k_{\text{cat}}/K_{\text{M}})_{\text{L}}/(k_{\text{cat}}/K_{\text{M}})_{\text{D}}$ with increasing the $(k_{\text{cat}}/K_{\text{M}})_{\text{L}}$. The catalytic efficiency $(k_{\text{cat}}/K_{\text{M}})_{\text{L}}$ is attributable to the enzyme structure [11]. Therefore, the higher the native structure of enzymes is kept, the larger the enantioselectivity becomes.

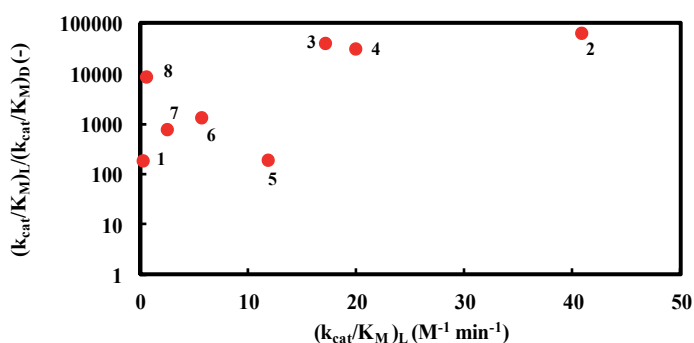


Figure 23. Dependence of the enantioselectivity of α -chymotrypsin in the esterification of *N*-Ac-Trp-OH with EtOH on the catalytic efficiency. Reaction conditions: (1) 1% (*v/v*) water and 25 °C in [C₂mim][BF₄], (2) 5% (*v/v*) water and 25 °C in [C₂mim][BF₄], (3) 5% (*v/v*) water and 40 °C in [C₂mim][BF₄], (4) 1% (*v/v*) water and 25 °C in [C₂mim][FSI], (5) 5% (*v/v*) water and 25 °C in [C₂mim][FSI], (6) 5% (*v/v*) water and 40 °C in [C₂mim][FSI], (7) 5% (*v/v*) water and 25 °C in [C₄mim][PF₆], (8) 5% (*v/v*) water and 25 °C in [C₄mim][TFSI].

7. Conclusion

In this chapter, the solvent effect of ionic liquids on the enantioselectivity of α -chymotrypsin has been described. The k_{cat} and K_{M} in ionic liquids were sensitively influenced by the reaction conditions such as water content and reaction temperature. As a result, the enantioselectivity, $(k_{\text{cat}}/K_{\text{M}})_{\text{L}}/(k_{\text{cat}}/K_{\text{M}})_{\text{D}}$, changed in the wide range. The k_{cat} and K_{M} correspond upon the conformational changes in the enzyme and the overall dissociation constant of all enzyme-bound species, respectively. Consequently, the major change of those parameters indicates that ionic liquids strongly affect the structure of enzyme molecules and the distribution of substrates and products between the reaction medium and the active site of enzymes under a requisite condition. By using the variation of enantioselectivity in ionic liquids, the optical resolution of biological active compounds and the synthesis of nonnative chiral compounds such as D-amino acid derivatives can effectively be carried out. Furthermore, it is expected that the ionic liquid, which exhibits the enantioselectivity suitable for a certain asymmetric synthesis, is

prepared by tailoring the constituents of ionic liquids, since chemical and physical properties of ionic liquids can be changed by the appropriate modification of organic cations and anions, which are constituents of ionic liquids.

Author details

Hidetaka Noritomi*

Address all correspondence to: noritomi@tmu.ac.jp

Department of Applied Chemistry, Tokyo Metropolitan University, Tokyo, Japan

References

- [1] Klibanov, AM. Improving Enzymes by Using Them in Organic Solvents. *Nature* 2001; 409, 241-246.
- [2] Noritomi H., Sasanuma A., Kato S., Nagahama K. Catalytic Properties of Cross-Linked Enzyme Crystals in Organic Media. *Biochemical Engineering Journal* 2007; 33, 228-231.
- [3] Noritomi H., Almarsson Ö., Barletta GL., Klibanov AM. The Influence of the Mode of Enzyme Preparation on Enzymatic Enantioselectivity in Organic Solvents and Its Temperature Dependence. *Biotechnology and Bioengineering* 1996; 51, 95-99.
- [4] Wescott CR., Noritomi H., Klibanov AM. Rational Control of Enzymatic Enantioselectivity through Solvation Thermodynamics. *Journal of the American Chemical Society* 1996; 118, 10365-10370.
- [5] Kise, H., Hayakawa A., Noritomi H. Protease-Catalyzed Synthetic Reactions and Immobilization-Activation of the Enzymes in Hydrophilic Organic Solvents. *Journal of Biotechnology* 1990; 14, 239-254.
- [6] Kokorin A. *Ionic Liquids: Applications and Perspectives*. Rijeka: InTech; 2011.
- [7] Moniruzzaman M., Nakashima K., Kamiya N., Goto, M. Recent Advances of Enzymatic Reactions in Ionic Liquids. *Biochemical Engineering Journal* 2010; 48, 295-314.
- [8] Noritomi H., Nishida S., Kato S. Protease-Catalyzed Esterification of Amino Acid in Water-Miscible Ionic Liquid. *Biotechnology Letters* 2007; 29, 1509-1512.
- [9] Noritomi H., Suzuki K., Kikuta M., Kato S. Catalytic Activity of α -Chymotrypsin in Enzymatic Peptide Synthesis in Ionic Liquids. *Biochemical Engineering Journal* 2009; 47, 27-30.

- [10] Noritomi H., Chiba H., Kikuta M., Kato S. How Can Aprotic Ionic Liquids Affect Enzymatic Enantioselectivity? *Journal of Biomedical Science and Engineering* 2013; 6, 954-959.
- [11] Kumar A., Venkatesu P. Overview of the Stability of α -Chymotrypsin in Different Solvent Media. *Chemical Reviews* 2012; 112, 4283-4307.
- [12] Fersht A. *Structure and Mechanism in Protein Science: A Guide to Enzyme Catalysis and Protein Folding*. New York: W. H. Freeman and Company; 1999.
- [13] Segel IH. *Enzyme Kinetics: Behavior and Analysis of Rapid Equilibrium and Steady-State Enzyme Systems*. New York: John Wiley & Sons, INC.; 1993.
- [14] Noritomi H., Minamisawa K., Kamiya R., Kato S. Thermal Stability of Proteins in the Presence of Aprotic Ionic Liquids. *Journal of Biomedical Science and Engineering* 2011; 4, 94-99.
- [15] Zaks A., Klibanov AM. The Effect of Water on Enzyme Action in Organic Media. *The Journal of Biological Chemistry* 1988; 263, 8017-8021.
- [16] Klibanov AM. Enzymes That Work in Organic Solvents. *CHEMTECH* 1986; 16, 354-359.

Physical Properties

Structural and Physical Aspects of Ionic Liquid Aggregates in Solution

Clarissa P. Frizzo, Aniele Z. Tier, Caroline R. Bender,
Izabelle M. Gindri, Marcos A. Villetti, Nilo Zanatta,
Helio G. Bonacorso and Marcos A.P. Martins

Additional information is available at the end of the chapter

<http://dx.doi.org/10.5772/59287>

1. Introduction

Ionic liquids (ILs) are currently defined as liquid organic salts, composed of organic cations and inorganic or organic anions, at or close to room temperature (melting point $<100^{\circ}\text{C}$) [1], [2]. The liquid state of ILs is thermodynamically favorable due to the large size and conformational flexibility of the ions (headgroup and counterion), leading to small lattice enthalpies and large entropy changes [3], [4]. ILs have negligible vapor pressure, excellent thermal stability, high electrical conductivity, a wide electrochemical window, a strong ability to dissolve many chemicals, and can be easily recycled [5]. The most attractive property of ILs can be effectively “tuned” in the design of the physical, chemical, and biological properties, by simple tailoring the substituent groups which consist of the cation and/or anion. [6]. The most frequently used cations in ILs are alkylammonium, N,N' -dialkylimidazolium, and N -alkylpyridinium cations [7]. Generally, the alkyl chains utilized are methyl, ethyl, butyl, hexyl, octyl, and decyl. A wide range of anions are employed, ranging from simple halides to inorganic anions such as tetrafluoroborate and large organic anions like methane sulfonate, trifluoromethane sulfonate, and bis-(trifluoromethanesulfonyl) amide [8].

Many applications of ILs are closely related to their aggregate formation. It may be expected from the amphiphilicity of ILs that interfacial phenomena play a major role in the behavior of systems which contain ILs. In recent years, most of the investigations in this field have been focused on the formation of IL aggregates in water [9]–[14]. The aggregation behavior of ILs can be modified by changing the alkyl chain length, the type of headgroup, and the nature of the counter-ions [15]–[17]. The structural characteristics of aggregates can be determined by

employing several experimental methods such as conductometry, tensiometry, steady-state fluorescence spectroscopy, isothermal titration calorimetry, small-angle neutron scattering, and nuclear magnetic resonance spectroscopy [18]. Aggregate formations such as micelles, liquid crystals, and microemulsions, depend on the IL structure, solvent, and the conditions of the system being studied like temperature and presence of additives. Whereas that a fine tuning in the aggregation process (e.g., size, morphology and aggregation number) can lead the ILs structures on this systems to different applications.

These characteristics are of great importance from both an academic and technological point of view, since they allow use in synthesis and purification [19], and also as surfactants [20]–[22], lubricants [23], and for nanoparticle coating [24], among other things.

This chapter will illustrate the importance of studying the organization of ILs in solution, and consider the main effects that change this behavior, by reporting the main results obtained and the approaches of these investigations. This chapter includes monocationic and dicationic ILs with different cation, anion, and alkyl chain sizes. The aim of the chapter is to show the influence of: (i) structural effects (length of alkyl chain, polar head, and counter-ion); (ii) temperature effect; and (iii) solvent effect on the aggregation of ILs. We will discuss the influence of these effects on the formation and characterization of IL aggregates through the use of several spectroscopic and non-spectroscopic techniques such as NMR spectroscopy, dynamic light scattering (DLS), fluorescence, conductivity, surface tension, and others.

The data collected for this chapter was selected from a search in the article/reference database *Science Finder*, using “ionic liquid aggregation” as keywords and refining this by requesting “English” language results. The total number of papers found was 597 (between 2002 and 2014). From these papers, studies about IL aggregates in solution that involve water, organic solvents, and water/organic solvent mixtures, including structural effects of the ILs and temperature effect on the aggregation, will be detailed. Due to the wide range of reports, the effect of ionic strength and the addition of surfactants and/or polymers into the system containing IL are not discussed within the scope of this chapter.

2. Effect of the structure of IL aggregation

The idea behind IL aggregation is simple and straightforward. Due to their amphiphilic nature, when IL molecules are dissolved in a solvent the presence of different polarities in their structures causes distortion in the solvent structure, thus increasing the energy in the system. In aqueous solutions, for example, in order to reduce unfavorable interactions, the hydrophobic portion of the IL either directs these interactions to more comfortable interfacial regions (adsorption) or directs them to the inner part of the solution through self-assembly (aggregation) [25], [26].

As a result of aggregation in polar solvents, they can form a structure where all of the nonpolar portion ends are directed toward the core of the aggregates. Aggregation and the aggregate by itself are affected by the complex character of intermolecular interactions between cation/

anion, cation/solvent, and anion/solvent [22], [27], [28]. These interactions consist of hydrogen bonding, as well as coulombic attraction, van der Waals, $n-\pi$, and $\pi-\pi$ interactions [29]–[31]. Furthermore, aggregation and aggregate features are significantly influenced by structural changes in the IL, such as length and composition of the hydrophobic portion, the nature of the head group, and anion characteristics [22], [27], [32]. Therefore, by varying the chemical structure of ions, it is possible to influence intermolecular interactions and self-organization of ILs, which is important for several applications of ILs.

An extensive number of studies have been performed in order to rationalize the influence of IL chemical structure on aggregate formation [1], [33]–[35]. Although there are divergences in the quantitative estimations from different techniques, the general regularities in the dependence of characteristics on IL structure are well correlated. Among the main parameters obtained, the concentration at which aggregates start to be formed, also known as the critical aggregation concentration (cac), is the most documented one and can be accessed by almost all the techniques. The following may be estimated: the Gibbs free energy of aggregation ($\Delta G^\circ_{\text{agg}}$), degree of counter-ion binding (β), the degree of ionization of the aggregate (α) [11], [22], [36], surface activity, (γ_{cac}) and also parameters such as surface tension at the cac, minimum surface area per molecule at the air/aqueous interface (A_{min}), maximum surface excess concentration (Γ_{max}) and standard Gibbs free energy of adsorption ($\Delta G^\circ_{\text{agg}}$) can be estimated. Adsorption in the interfaces can also be evaluated through the effectiveness of the surfactant, in order to decrease the surface tension of the solvent (Π_{cac}) and the adsorption efficiency (pC_{20}) – C_{20} is the concentration at which the surface tension of pure solvent is reduced by 20 mNm $^{-1}$ [27], [31], [37]. The aggregation number (N_{agg}) can also be obtained, usually by fluorescence quenching technique [36], [38].

This overview will discuss the influence of three main features that are related to aggregation in solution: (i) alkyl chain length; (ii) cationic head; and (iii) the nature of the anion. The discussion will take into account not only the cac but also the other parameters mentioned previously, which indicate the stability of aggregates and surface activity of ILs. Each section will cite the main reports in the literature that helped to detail the structural effect on aggregate formation.

2.1. Effect of cationic alkyl chains

The length of alkyl chains has been reported to be one of the main factors influencing the aggregation behavior of ILs [22], [27], [39]. In aqueous solutions, hydrophobic interactions between ILs and polar solvents are the driving force towards aggregation, due to the increase of entropy and consequently decrease of the free energy of the system [27]. In the aggregate, two types of domains can be observed: (i) one is polar, in which cationic heads and anions arrange in a three-dimensional network supported by strong electrostatic interactions; (ii) in the other domain, alkyl groups aggregate to build nonpolar domains where van der Waals interactions are critical [37], [38], [40]. Generally, some observations can be made about homologous series of ILs. A systematic decrease in cac values with an increase in methylene units in the alkyl chain is observed. The $\Delta G^\circ_{\text{agg}}$ tend to become more negative, implying that aggregation comes more easily with the increase of the alkyl chain length, as a direct conse-

quence of the increased hydrophobicity of IL monomers. Significant negative $\Delta G^{\circ}_{\text{agg}}$ values are primarily due to an increase of the entropic contribution, an effect that is common in aggregation processes induced by hydrophobicity of alkyl chains. In aqueous solution, the alkyl chain of the LIs induces a water structure around the chain and this structure breaks down during aggregation, leading to a large entropy increase. The β values increase with an increase in the alkyl chain length, which corresponds to a stronger interaction between anions and aggregates as the alkyl chain's length increases [36], [39]. Furthermore, the surface activity of ILs is improved with an increase in the alkyl chain's length, resulting in smaller γ_{cac} values, and higher Π_{cac} and pC_{20} values.

The organization of an IL as a function of an alkyl chain is similarly affected by the alkyl chain structure. The aggregation behavior of imidazolium-based IL series in aqueous solution has been investigated in independent works [36], [39]. Data related to the conductivities and polarity indexes of pyrene for IL aqueous solutions was determined. The ILs used in both works are [BMIM]Br, [HexMIM]Br, [OctMIM]Br, [DecMIM]Br, [DoDecMIM]Br, [TetDecMIM]Br and [HexaDecMIM]Br and [BMIM][BF₄]. Aggregation was detected for almost all ILs except for [BMIM]Br. These works reported a decrease in cac with an increase in alkyl chain length. The authors related this behavior to a balance between an enhancement of van der Waals interactions by means of alkyl chain-ion inductive force (dielectric polarization) and dispersive interactions. These physicochemical properties depends markedly by the contribution, per (CH₂) group, in the alkyl chain of cations. On the other hand, the aggregation number determined by pyrene fluorescence quenching method did not show a tendency for variation in the IL structures for the work performed by Wang et al. [36]. However, in the study reported by Inoue et al. [39] it was observed from conductivity data an increase of aggregation number with the increase in the alkyl chain.

The surface activity and aggregation behavior of the imidazolium-based ILs [BMIM]Br, [HexMIM]Br, [OctMIM]Br, [DecMIM]Br, [DoDecMIM]Br, [TetDecMIM]Br and [HexaDecMIM]Br and [BMIM]X, [HexMIM]X, and [OctMIM]X (X=Cl, I) were also investigated [32], [41], [42], using surface tension, ¹H NMR spectroscopy, and small-angle neutron scattering (SANS). The cac values decrease with the length of the alkyl chain, following the same trend as the work performed by Wang et al. [36] and Inoue et al. [39]. Tensiometric parameters also showed a strong correlation with the structural changes. The decrease in γ_{cac} as the alkyl chain length increased follows the tendency observed for conventional surfactants and indicates better surfactant activity for ILs with longer alkyl chains. This is also corroborated by the Π_{cac} and pC_{20} values, which increased as the alkyl chain length increased. Finally, upon examining the effect of the chain length on the area per IL molecule at the water/air interface (A_{min}), it was observed that the A_{min} values systematically increased in the following order: [OctMIM]X < HexMIM]X < [BMIM]X (at 30 °C) and [HexaDecMIM]Br < [TetDecMIM]Br < [DoDecMIM]Br < [DecMIM]Br (at 25 °C), in the studies performed by Vaghela et al. [41] and Dong et al. [32]. Vaghela et al. [41] referred to this behavior as the result of a simple monolayer organization with the alkyl chain oriented toward the water side at the interface for the IL [BMIM]X, while the [HexMIM]X and [OctMIM]X may create more complex and closely packed layers. Similar results were observed by Sastry et al. [38] and Vaghela et al. [41] in a study of the aggregation

of the pyridinium-based ILs [N-BPy]Cl, [N-HexPy]Cl, [N-OctPy]Cl, [N-Oct-2-MePy]Cl, [N-Oct-3-MePy]Cl, and [N-Oct-4-MePy]Cl; and also by Zhao et al. [43] for the pyrrolidinium-based ILs [DoDecMPyrr]Br, [TetDecMPyrr]Br, and [HexaDecMPyrr]Br in aqueous solutions. Improvement in both the surface activity and the A_{\min} value was observed with the increase in alkyl chain length, which corroborates with results previously reported. The authors explain this behavior based on the higher hydrophobicity caused by the increased number of methylene units in the alkyl chain. Surface tension data of pyrrolidinium-based ILs showed some peculiarities. No considerable difference was observed in the effectiveness of the surface tension reduction, expressed by the γ_{cac} and Π_{cac} parameters, which is an indication that the structural changes in the alkyl chain did not affect the surface activity of these compounds. On the other hand, the packing at the surface, and the N_{agg} value showed good correlation with the previous works. The increase in the alkyl chain length resulted in better packing at the water/air interface. This result is confirmed by A_{\min} and Γ_{max} values and by high aggregation number.

A cationic head bound to a long alkyl chain and a methyl group characterizes most of the studies reported in the literature that investigate the aggregation of imidazolium-based ILs. The change in the methyl group resulting from a long alkyl chain may also play a dominant role, not only in the aggregation behavior and stability of the aggregate, but also in the surface activity of ILs. For better comprehension, in this discussion the size of different alkyl chains bound to imidazolium cationic heads will be represented by n and m , respectively, as shown in Figure 1.



Figure 1. Representation of cationic head for imidazolium-based dialkyl-substituted IL.

In general, for a homologous series with two long side chains, for a fixed n (longer than the methyl group) and a varying m , lower cac values may be observed than those for analogous ILs in which n is methyl. However, when the length of both alkyl chains varies, it is observed that the longer alkyl chain has the stronger effect, with a smaller cac value [20], [44]. In relation to the thermodynamic properties of aggregates, the $\Delta G_{\text{agg}}^{\circ}$ values are not affected by the insertion of another long alkyl chain, whereas the β values tend to decrease, which indicates a lower charge at the aggregate surface [45]. Surface properties are influenced by insertion of a second alkyl chain in the cationic head. In general, there is an improvement in the surface activity with the increase of alkyl chain length, represented by a decrease in the γ_{cac} , Γ_{max} and N_{agg} while Π_{cac} , pC_{20} and A_{\min} values increase. The packing at the surface does not follow the same trend, and the longer the second alkyl chain is, the worse the IL's packing is at the water/air interface, which results in lower Γ_{max} and higher A_{\min} values [44].

Liu et al. [44] and Baltazar et al. [20] investigated the aqueous aggregation of dialkylimidazolium ILs in two independent works. Liu et al. [44] evaluated the ILs [DoDecMIM]Br, [DoDecEtM]Br, [DoDecPrM]Br, and [DoDecBuM]Br with the dodecyl long chain and the variable

alkyl side chain, while Baltazar et al. [20] varied the length of both alkyl chains. It was found that ILs with one very long and a short chain has a higher cac value than those with two long alkyl chain. This behavior can be confirmed comparing the values of [DoDecBuIM]Br with [HexaDecBuIM]Br. The [HexaDecBuIM]Br has a lower cac value than [DoDecBuIM]Br, which has two long alkyl chains. The lengthening of the alkyl chain resulted in an improvement in tensioactive activity. However, longer alkyl chains result in lower packing efficiency at the water/air interface, as observed in the A_{min} and Γ_{max} values. Tariq et al. [45] also investigated the effect of two long alkyl chains on the aggregation behavior of the pyrrolidinium-based ILs [DoDecMPyrr]Br, [DoDecBuPyrr]Br, and [OctBuPyrr]Br. Results with the same patterns as those of Liu et al. [44] and Baltazar et al. [20] were obtained.

Although most of the studies involving the study of alkyl chain effect on IL aggregation have investigated hydrocarbon chains, some works, which will be discussed in this revision, deal with the introduction of polar groups into the alkyl chain. The introduction of polar groups into the alkyl chain connected to the cationic head was also investigated by Garcia et al. [46]. Two series of long chain imidazolium- and pyridinium-based ILs containing an ester functional group in the alkyl side chain were investigated (Figure 2). The aggregation behavior of the ILs under investigation followed the same pattern as those already discussed. Even in the presence of the ester group, aggregation was favored and surface activity improved with the increase in alkyl chain length for both imidazolium- and pyridinium-based ILs. The enhancement of pC_{20} and Π_{cac} show the increase of the surfactant properties with the lengthening of the IL's alkyl chain, while both γ_{cac} and A_{min} decrease. The decrease of A_{min} corresponds to a better packing at water/air surface.

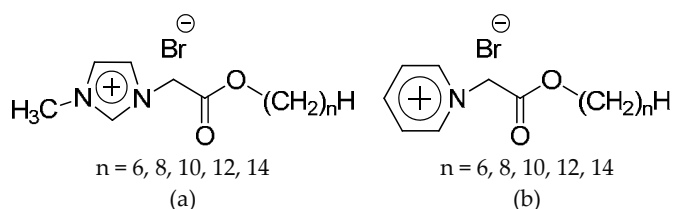


Figure 2. Structure of (a) imidazolium- and (b) pyridinium-based ILs studied by Garcia et al. [46].

The effect of a polar group on one of the alkyl chains connected to the imidazolium head was investigated by Liu et al. [47]. They studied the aggregation and surfactant activity of the hydroxyl-functionalized IL [EtOHDoDecIM]Cl in aqueous solution. The results obtained can be compared with those already published by the same author [44] with an alkyl (ethyl and dodecyl) group connected to each nitrogen in the imidazolium ring. It was possible to observe that the insertion of a polar group did not influence the aggregation behavior and surface properties. Some differences were observed in the parameters related to the packing at the air/water surface; for example, lower Γ_{max} and higher A_{min} values of hydroxyl-functionalized ILs. The authors state that interactions between the hydroxyl group and water molecules are responsible for increasing the area around the molecule on the surface. A second cac (cac_2) was

reported and the N_{agg} for the first (cac_1) and second (cac_2) aggregation was calculated. An increase in monomer units within the aggregate was observed, from cac_1 to cac_2 , and it is suggested that the second cac emerges from an improvement in the aggregate organization in solution.

Li et al. [34] evaluated the aggregation and adsorption behavior of [HexaDecHyPrIM]Br in aqueous solution. The cac obtained for [HexaDecHyPrIM]Br is similar to [HexaDecMIM]Br, showing the predominant effect of the longest alkyl chain on the aggregation. A lower β value was obtained, which might be caused by an increase in electrostatic repulsions between the hydrophilic heads of adjacent IL molecules. Both the factors related to the hydrophilic head-group size and electrostatic repulsion in [HexaDecHyPrIM]Br aggregates lead to looser packing of ILs. Water molecules may more easily penetrate the looser micelles resulting in a higher I_1/I_3 ratios and smaller N_{agg} value. Shi et al. [29] evaluated the aggregation behavior of [DecPhMIM]Br, [DoDecPhMIM]Br, and [TetDecPhMIM]Br in aqueous solutions and showed that the introduction of the 2,4,6-trimethylphenyl group into an imidazolium head favors aggregation, due to the more delocalized charge of the cationic head, which reduces the electrostatic repulsion of the head group. The authors mention a reduction in the steric hindrance of head groups caused by the occurrence of $\pi\pi$ interactions among the adjacent 2,4,6-trimethylphenyl groups, which allows dense arrangement of these IL molecules at the air/water interface.

Besides the substitution at positions 1 and 3 in the imidazolium ring, the insertion of a methyl group at position 2 was also performed and the aggregation behavior of the IL was investigated (Figure 3) [48].

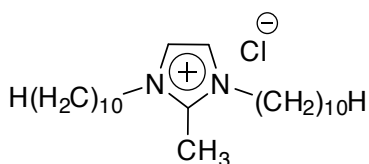


Figure 3. Structure of IL

Figueira-Gonzalez et al. [48] observed two cac values, which were related to a morphological change in the aggregates. The data obtained for β was correlated to a formation of spherical micelles in accordance with cac_1 , and with the transition to cylindrical micelles in accordance with cac_2 . Results obtained from fluorescence spectroscopy, fluorescence anisotropy, and chemical NMR were used to investigate the change in the morphology — the results were consistent with the sphere-to-cylinder transition. Moreover, at higher concentrations, a new conformational change from cylindrical micelles to bilayer aggregates was proposed, based on the analysis of diffusion coefficients obtained by diffusion-ordered NMR spectroscopy (DOSY).

2.2. Effect of cationic head

The influence of cationic head structural characteristics has also been investigated. There are two opposing effects that make the understanding of this effect very complex. Repulsive interactions due to the positive charge, and hydration and steric hindrance among cationic moieties in solution are anti-aggregation effects. Attractive interactions arising from a need to minimize hydrocarbon/water contacts favor aggregation [22]. As seen in the alkyl chain effect, the hydrophobicity of cationic heads also plays an important role, favoring aggregation in aqueous solutions [31], [49]. In the same way, the binding strength between cations and anions has an influence on the aggregate stabilization, by reducing the repulsive interaction among head groups with the increase in β [22], [31], [49].

Galgano et al. [31] investigated the aggregation of ILs with different head groups and with the same alkyl chain and anionic moiety (Cl⁻). The influence of the cationic head was observed and it was determined that the aggregation is favored in the following order: Pyridinium [N-HexaDecPy][Cl] < Imidazolium [HexaDecMIM][Cl] < Ammonium [PentDecAEtBzMe₂][Cl]. The decrease in the ionization degree (α) and N_{agg} for [PentDecAEtBzMe₂][Cl] showed that aggregates formed by this surfactant are stabilized more by counter-ions and they have better packing.

Wang et al. [22] investigated the effect of cationic ring types on the aggregation of ILs in aqueous solutions. It was found that cac and ΔG_{agg}° decrease in the following order: Pyrrolidinium [OctMPyrr]Br > Imidazolium [OctMIM]Br > Pyridinium [N-Oct-4-MePy] Br. This indicates that the pyridinium head has a higher ability to form aggregates. However, there are no substantial differences between the values obtained for different cationic heads. The reason is based on the similar hydrophobic characteristic of the cations under investigation. The authors observed that the van der Waals volumes of cationic rings (167, 150, and 144 Å³ for [BMPyrr], [BMIM], and [N-BPy], respectively), assume an important role in the aggregation process, in which smaller values are related to a more favorable aggregation. The increase in the van der Waals volumes indicates an increase in steric hindrance, which corroborates with the increase in cac . The results for ionization degree of the aggregates (α) demonstrated that anionic counter-ions are less bound to the surface of [OctMPyrr] than [BMIM] and [N-Oct-4-MePy].

2.3. Counter-ion effects

In this discussion, the counter-ion will be considered to be the ion on the surface of the aggregate, which can be both an anion and a cation. The role of the counter-ion can result in significant alterations in the IL aggregation and aggregate stability. As previously mentioned, aggregation is a result of the hydrophobic effect of alkyl chains, which leads to aggregation through attempting to minimize the exposure of the alkyl chain to water, and repulsive interactions among cationic head groups. The counter-ions play a key role in reducing the repulsive headgroup interactions through adsorption on the aggregate surface, thereby lowering the cac values [11], [22]. In the cationic aggregates, the foremost characteristics of the anions are their size, hydrated radius, polarizability, hydrophobicity, and bulkiness [22], [41]. All parameters are related and anions with high polarizability will also have high hydropho-

bicity and a lower hydrated radius. Anions with higher polarizability are more bound at the aggregate surface and decrease the electrostatic repulsion between the head groups of the ILs, thus increasing the tendency toward aggregation [22].

2.3.1. Anionic counter-ion effect

In general, the reports about IL aggregation evaluate cationic head with long alkyl chains and relatively small anions (when compared to the cation size). Strongly hydrated ions such as chloride are partially screened by the surrounding polar water molecules and, therefore, are less effective at reducing the repulsion between the cations when they are absorbed in the surface and do not stabilize the aggregate properly [50]. On the other hand, anions such as BF_4^- and PF_6^- , besides giving a higher overall hydrophobicity to the IL, also tend to promote better stabilization of aggregates [50]. The effect of anions is observed in the cac, $\Delta G_{\text{agg}}^\circ$ and β values. Anions with higher hydrophobicity tend to decrease the cac and $\Delta G_{\text{agg}}^\circ$ values and increase the β values [22], [41], [50].

Wang et al. [22] studied the effect of anions on the aggregate formation of the ILs [OctMIM]X ($X=\text{CH}_3\text{CO}_2^-$, Br⁻, Cl⁻, NO_3^- , CF_3CO_2^-) in aqueous solution. The aggregation of ILs with different anions followed the Hofmeister series [51], [52]. The increase in the hydrophobicity and decrease in hydration radius caused a decrease in the cac and $\Delta G_{\text{agg}}^\circ$ values. It was observed that a more hydrophobic IL leads to lower α values, which indicates a higher concentration of anions on the surface and better stabilization of the aggregate. The aggregates were found to be spherical and the anions had a weak effect on the morphology. On the other hand, the effect of the anion on the size and N_{agg} indicates that the increment in the hydrophobicity of anionic moieties causes an increase in size, with a consequent increase in the number of monomers in the aggregate (N_{agg}).

Vaghela et al. [41] evaluated the surface activity and aggregation behavior in water of the imidazolium-based ILs [BMIM]X, [HexMIM]X, and [OctMIM]X with different anions ($X=\text{Cl}^-$, Br⁻, I⁻). Among the ILs with the same cationic structure but with different anions, a reduction in the cac and $\Delta G_{\text{agg}}^\circ$ values was observed, in the following order: Cl⁻ < Br⁻ < I⁻. This behavior was explained based on the relative hydrophobicity and binding capacity of three different halides to a cation. The more hydrophobic, the more attached the anions are at the surfaces.

The influence of anions on pyridinium-based aggregation in aqueous solution was studied by Bandrés et al. [50]. The results of [N-Bu-3-MePy] cation with BF_4^- and $\text{N}(\text{CN})_2^-$ anions were compared with data obtained by Singh et al. [11] in a previous work with the same cation and the Cl⁻ anion. The authors observed that by changing the anion in the IL, the cac decreases in the following order: [N-Bu-3-MePy][Cl] > [N-Bu-3-MePy][N(CN)₂] ≈ [N-Bu-3-MePy][BF₄]. The most important difference between the chloride and tetrafluoroborate or dicyanamide anions was reported to be related to their size. The bigger the anion structure, the smaller the hydration radius and the greater the hydrophobicity, which implies that tetrafluoroborate or dicyanamide make aggregation easier. Higher β values were observed in the ILs with $\text{N}(\text{CN})_2^-$ and BF_4^- anions, which indicates a decrease in the charge repulsion between the cations when they are absorbed at the aggregate's surface.

2.3.2. Cationic counter-ion effect

Although most reports in the literature consider cationic aggregates with anions as counter-ions, there are also studies in which anions with long alkyl chains are investigated, thus playing a more important role in the aggregation [10], [37], [53]. In this case, the anion acts as a surfactant moiety of the IL and aggregation will mainly be influenced by its structural features of anion, following the trend observed for cationic structure already discussed in the previous sections (see Section 2.1 and 2.2). The cationic moiety is then considered to be the counter-ion and will work in the same way that anions do for cationic aggregates.

Rao et al. [10] investigated the effect of cationic counter-ions on anionic aggregates in aqueous solution with amino acid-based ILs (AAILs). The ILs hydrophobicity was the primary factor influencing aggregation behavior. It was observed that the cac , β , and ΔG°_{agg} values increase in the following order: GluPrELS < ValPrELS < ProPrELS < AlaPrELS < GlyPrELS. The surface activity of the ILs was also influenced by the hydrophobicity of the cationic moiety, showing the same behavior previously described for anionic counter-ions. The increases in the hydrophobicity of amino acid-based cationic moieties lead to higher Π_{cac} , pC_{20} , and A_{min} values and lower γ_{cac} values. The aggregation number and aggregate size of the AAILs were found to depend on the structure of cationic amino acid-based counter-ions. AAILs with bigger cationic moieties formed larger aggregates, but with a lower aggregation number.

Anouti et al. [9] investigated the aggregation behavior of the imidazolium and pyrrolidinium alkylcarboxylate protic ILs, ([IM][AlkylCO₂] and [Pyr][AlkylCO₂]), as a function of alkylcarboxylate chain length (Alkyl=Pent, Hex, Hep, Oct). The effect of the alkyl chain length on the anionic moiety was the same as that observed for cationic aggregates. Decreases in the cac were detected for both groups of ILs, with an increase in the anionic alkyl chain length (n). Furthermore, the surface activity was also improved, with higher hydrophobicity being caused by longer alkyl chains. The sulfate ILs, with pyrrolidinium as cationic counter-ions, showed superior surface activity and favored aggregation more than for imidazolium cations. The cac , ΔG°_{cac} and α values were lower for pyrrolidinium, which means that aggregates are formed easily and are stabler for these IL than for those with imidazolium cations. In general, ILs with a pyrrolidinium cationic moiety presented lower cac and γ_{cac} values and higher Π_{cac} values, and also displayed the best surface activity. Finally, the best packing at the air/water surface was found for imidazolium ILs based, probably due to the lower electrostatic repulsion caused by this cation in relation to pyrrolidinium ones.

In the examples used previously, ILs composed of a cationic and an anionic moiety were investigated in terms of the structural effect on aggregation and surface activity properties. However, Liu et al. [54] investigated the opposite charges on the same molecule through surface tension and fluorescence, and the results obtained were compared with another zwitterionic IL [DoDecIMCH₂COO]. Large A_{min} and cac/C_{20} values were attributed to a carboxymethyl imidazolium group in the [DoDecIMCH₂COO] molecule. The steric effect was shown to be more prominent in aggregation than in adsorption at the air-solution interface for [DoDecIMCH₂COO] triggered by larger head groups.

Finally, Blesic et al. [53] investigated anionic and cationic alkyl-chain effects on self-aggregation in aqueous solutions for ILs denominated as catanionic surfactants (Figure 4). To determine aggregation parameters and surface activity, fluorescence spectroscopy and interfacial tension measurements were used. ILs with relatively small methylsulfonate anions ($n=8, 10,$ and 12 ; and $m=1$) showed similar behavior to conventional single-chain ILs. A decrease in the cac was observed with the increase in the length of the cationic alkyl chain. However, when both the cation and the anion have a long alkyl chain ($n=4$ and 8 ; and $m=4$ and 8), lower cac values and better surface activity were found when compared with those corresponding to the cationic analogues. It was found that the presence of a hydrophobic chain in both the cationic and anionic moiety of the IL works synergistically to favor aggregation and improve the tensoative properties.

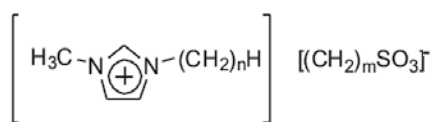


Figure 4. Structure of catanionic surfactant ILs.

2.4. Aggregation of dicationic ILs

Besides the length and introduction of functional groups, a new cationic head can be introduced at the end portion of an alkyl chain in the ILs. This new class of ILs is denominated dicationic or gemini. These ILs consist of a hydrophobic chain connected to each of the polar head groups, which are covalently attached through a spacer group, as schematically represented in Figure 5. Reports investigating the influence of structural changes in the aggregation and surface activity properties of dicationic ILs approach both the structure of the spacer group and the hydrocarbon chain connected to the cationic head [20], [55], [56]. In general, it is observed that dicationic ILs have lower cac values, higher adsorption efficiency and surface activity than analogous monocationic ILs [20], [57]. Among the dicationic ILs, the effect of a spacer group has been evaluated and it was found that for a cationic head connected to an alkyl chain with invariable m , the length increase of spacer groups (higher n values) leads to a decrease in the aggregation trend and surface properties [58]. A cationic head with a fixed spacer group and variable alkyl chain length (increase in m values) favors aggregation, following the same trend as that observed for monocationic ILs [57].

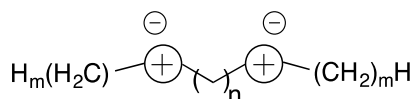


Figure 5. Schematically representation of dicationic IL where n is the spacer group and m are alkyl chain with variable length.

Ao et al. [58] studied the aggregation behavior for the gemini IL [Bis-AlkylDoDecIM]Br₂ with different spacer lengths. Fluorescence measurements showed that there is an increase in the micropolarity of the aggregates and a decrease in N_{agg} as the spacer length increases. The increase in the micropolarity can be explained by considering that the longer the spacer, the more distant the hydrophilic heads will be. According to Ao et al. [58] this would result in a less tightly packing of the palisade layer, and lead more water molecules to exist in the palisade layer of the gemini ILs aggregates. The decrease in N_{agg} is justified based on the conformation of longer spacers which remain in extended conformation, thus allowing them to aggregate relatively loosely and form smaller aggregates. These results also corroborate with the lower β and higher ΔG_{agg}° values for ILs with longer spacer groups, which indicates lower stability for these aggregates. In a second work, Ao et al. [57] investigated the aggregation of the gemini IL [Bis-BuAlkIM]Br₂ with a fixed spacer group and variable alkyl chain (Alk=Dec, DoDec, TetDec) in aqueous solution. A decrease in the cac value was observed with the increase in the alkyl chain length, following the same aggregation characteristic of analogous monocationic ILs. Surface tension results indicated an increase in the tensoative activity with the increase in the alkyl chain length. On the other hand, the packing ability at the air/water surface is lost with an increase in the alkyl chain length, which is demonstrated by a higher A_{min} value for the IL [Bis-BuTetDecIM]Br₂. Zhang et al. [59] investigated the aggregation of gemini pyrrolidine-based ILs in aqueous solution and they showed the same aggregation behavior as that previously described by Ao et al. [57] for gemini imidazolium ILs. These results suggest that changing the alkyl chains and the head groups of the ILs can significantly change the surface activity of the ILs and the aggregation process for dicationic ILs, as it does for analogous monocationic ILs.

2.5. Temperature effect on the IL aggregation

The aggregation behavior of long-chain ILs is generally investigated at room temperature by different techniques, which have been previously mentioned. The main physicochemical properties of ILs determined experimentally are cac , γ_{cac} , pC_{20} , Π_{cac} , Γ_{max} , ΔG_{agg}° and equilibrium constant of aggregation process (K_a) [60]. Studies seeking thermodynamic parameters and the driving force of the IL aggregation process (enthalpic or entropic in nature) within a defined range of temperatures have been reported in the literature [61]. From thermodynamics data – such as enthalpy (ΔH_{agg}°), entropy (ΔS_{agg}°) and ΔG_{agg}° at various temperatures – it is possible to suggest the mechanism of IL aggregate formation. The relationship between thermodynamic parameters determined at several temperatures allows determination of the contribution of the hydrophobic effect (van der Waals interactions) and electrostatic repulsion between ionic portions of the IL structures [62], [63]. Studies are being conducted in order to rationalize how the enthalpy, entropy, and standard Gibbs free energy of IL aggregation changes with temperature. Some works have shown thermodynamic parameters for ILs with several cations and/or sizes of the alkyl chains [10], [31], [64]. The temperature of the system was found to influence the self-assembly of ILs in solutions. An increase in temperature provides more energy to the system and, consequently, intermolecular interactions may be broken. An increase in the cac , α value, and the surface activity of the ILs is observed, and, therefore, less closely packed aggregates are expected [34].

During the aggregation, the hydrocarbon chain of the IL monomer moves from the solvent media to the aggregate core. This process is expected to be exothermic and governed primarily by the entropy gain associated with the hydrophobic ILs being transferred from the solvent environment to the aggregate interior. However, some ILs have demonstrated distinct tendencies in the features associated with thermodynamic analysis [18]. Thus, this section will detail the literature reports that help to understand the temperature effect on aggregate formation.

Inoue et al. [39] studied the aggregate formation of the long-chain imidazolium ILs [DoDecMIM]Br, [TetDecMIM]Br, and [HexaDecMIM]Br in aqueous solution, through electrical conductivity measurements. The data demonstrate that the cac increases with an increase in temperature (20°C–40°C), whereas the β value decreases. The thermodynamic parameters indicate that the entropic term ($-T\Delta S_{\text{agg}}^{\circ}$) plays an important role at low temperatures, whereas the $\Delta H_{\text{agg}}^{\circ}$ contribution becomes dominant at higher temperatures (exothermic process). In other words, the aggregation process for long-chain imidazolium ILs is entropy driven at low temperature, while enthalpy driven at high temperature, and this behavior coincide with micelle formation of conventional long-chained surfactants.

Shi et al. [29] evaluated the aggregation behavior of [DecPhMIM]Br, [DoDecPhMIM]Br, and [TetDecPhMIM]Br in aqueous solutions at temperatures between 25°C and 45°C. In the range of temperatures investigated, the values of $\Delta G_{\text{agg}}^{\circ}$ for the three ILs are negative. The $\Delta G_{\text{agg}}^{\circ}$ values were determined and $\Delta H_{\text{agg}}^{\circ}$ was seen to be the main contributor. This fact suggests that the aggregate formation process for these ILs is enthalpy-driven. This behavior was attributed to the strong electrostatic self-repulsion of the headgroups and the counter-ions, as well as the π - π interactions arising from 2,4,6-trimethylphenyl group introduced into the headgroup, since it is known that the enthalpy change of aggregation is mainly a result of hydrophobic and electrostatic interactions [63], [65]. The β value for these ILs is rather low, thus the contribution of electrostatic interactions should be exothermic.

Shi et al. [62] also studied the aggregation behavior of the ILs [DecPhMIM]Br, [DoDecPhMIM]Br, and [TetDecPhMIM]Br in another IL, [BMIM][BF₄], in the same temperature range. They showed that the cac values of ILs increase with the increase in temperature. For all of the ILs, $\Delta H_{\text{agg}}^{\circ}$ was the main contributor to a large negative $\Delta G_{\text{agg}}^{\circ}$ in the temperature range investigated. Therefore, the aggregates of [DecPhMIM]Br, [DoDecPhMIM]Br, and [TetDecPhMIM]Br in [BMIM][BF₄] are enthalpy-driven, similar to the behavior noted in aqueous systems [29]. In the aggregation process, which is exothermic, the hydrocarbon chain of the IL monomer moves from the IL media to the aggregate core. The [BMIM] cation strongly interacts with the cations of the long chain ILs and this interaction increases the electrostatic repulsion between the polar groups. Meanwhile, the effect of π - π interactions between the adjacent aryl groups may be a reason for the large $\Delta H_{\text{agg}}^{\circ}$ observed in this study. Furthermore, it was found that by increasing the alkyl chain length, the entropic term becomes more pronounced. The cac values of ILs in [BMIM][BF₄] is much higher than that in water suggesting that the aggregation process is more favorable in aqueous system due to the weak solvophobic effect in IL.

Li et al. [34] studied the long-chain IL [HexaDecHyPrIM]Br from the natural amino acid alanine and focused their attention on the adsorption and aggregation behaviors of this IL in aqueous

solution. The temperature dependence of [HexaDecHyPrIM]Br was evaluated by surface tension and conductivity at temperatures between 25°C and 50°C. The cac values increase with the increase in temperature, whereas the surface tension at the cac (γ_{cac}) follows the opposite trend. The cac values plotted as a function of temperature demonstrate a U-shaped curve with a minimum around 25°C. The surface behavior is similar to the ILs without alanine moiety [39]. The adsorption efficiency of the IL at the air-water interface (pC_{20}) improves with the increase in temperature. The higher temperature resulted in a greater minimum area occupied by a single surfactant molecule at the air-water interface (A_{min}) and a lower maximum surface excess concentration (Γ_{max}). According to the authors, this may be due to increased molecular motion at higher temperatures, which enables the adsorption of fewer molecules at the interface. The tendency is in accordance with the decreased effectiveness of the IL to lower the surface tension, observed through the Π_{cac} data, with the increase in temperature. The thermodynamic analysis resulted in negative ΔG_{agg}° values, which suggests that the aggregation process is spontaneous. The ΔH_{agg}° decreases with the increase in temperature and becomes negative at 30°C, indicating that the aggregate formation process is endothermic at lower temperatures and exothermic at higher temperatures. Furthermore, the $-T\Delta S_{agg}^{\circ}$ value increases with the increase in temperature, contributing much to negative ΔG_{agg}° values. Thus, the aggregation of alanine-based ILs was proven to be entropy-driven.

Ao, et al. (2008), studied the thermodynamic properties of the aggregation of two Gemini ILs in aqueous solution at 15°C–35°C: [Bis-AlkylDoDecIM]Br₂ with different spacer lengths [58]; and [Bis-BuAlkIM]Br₂ with different lateral alkyl chain lengths [57]. The negative ΔG_{agg}° values for [Bis-EtDoDecIM]Br₂, [Bis-BuDoDecIM]Br₂, [Bis-BuDecIM]Br₂, and [Bis-BuTetDecIM] are mainly due to the large positive value of ΔS_{agg}° . Therefore, the aggregation process is governed primarily by the entropy gain associated with it (aggregation is entropy-driven). On the other hand, the aggregate formation process of [Bis-HexDoDecIM]Br₂ is enthalpy-driven at lower temperatures, but entropy-driven at higher temperatures. The β values of ILs with different spacer lengths decrease with the increase in temperature. Thus, the authors state that the aggregates of these ILs would be smaller at higher temperatures. The authors confirmed this fact by DLS, which showed that the apparent hydrodynamic radius of [Bis-HexDoDecIM]Br₂ decreases from 4.0 nm at 25°C to 2.5 nm at 35°C. This result is in accordance with the results reported by Pal et al. [64] who used SANS when studying similar IL aggregates in aqueous solution at 30°C–70°C. Furthermore, the increase in the temperature results in a decrease of the aggregation number. Conversely, for the corresponding monomeric IL, the aggregate formation process is entropy-driven at low temperatures and enthalpy-driven at high temperatures [39].

Zhang et al. [59] investigated the aggregation behavior in aqueous solution of gemini pyrrolidine-based ILs [Bis-BuAlkPyr]Br₂, where Alk=Dec, DoDec, TetDec). The temperature dependence in the aggregation process was investigated by electrical conductivity in the temperature range of 25°C–45°C. The cac values increase with the increase in temperature. The negative ΔG_{agg}° value suggests that the aggregation process is a spontaneous process. The values increase with an increase in the hydrophobic chain length, which proves that the increase in alkyl chain length is favorable to the aggregation of the IL in solution. The negative

$\Delta G_{\text{agg}}^{\circ}$ values are mainly contributed to by $\Delta H_{\text{agg}}^{\circ}$ within the range of temperatures investigated, which suggests that the aggregation of [Bis-BuAlkPyrr]Br₂ in aqueous solution is enthalpy-driven. This behavior is different to the corresponding monocationic ILs, [AlkMPyrr]Br, which have entropy-driven aggregate formation at low temperatures and enthalpy-driven formation at high temperatures [43]. On the other hand, the aggregation of dicationic IL with imidazolium head groups [Bis-BuAlkMIM]Br₂ is an entropy-driven process for all the temperatures investigated [57]. These results suggest that changing the structure and the head groups of the ILs can significantly change the surface activity of the ILs and the driving forces of the aggregation process. For the authors, the driving force for the entropy-driven process is the tendency of the hydrophobic group to transfer from the solvent to the interior of the aggregate, while the enthalpy-driven process is probably a result of the increase in the degree of hydration for the hydrophilic head groups.

Tariq et al. [45] studied the self-aggregation properties of three pyrrolidinium-based ILs — [DoDecMPyrr]Br, [DoDecBuPyrr]Br, and [OctBuPyrr]Br — in aqueous solution. The aggregation enthalpies were measured at three different temperatures (15°C, 25°C and 50°C) using isothermal titration calorimetry (ITC) measurements. The focus of this study was to determine the driving force of aggregation. The gradual breakdown of the hydrogen-bonded network of liquid water when the temperature increases (resulting in an increase in entropy) leads to enthalpy-driven aggregation at higher temperatures, whereas entropy-driven processes will usually dominate at lower temperatures. The enthalpy of aggregation of [DoDecMPyrr]Br and [DoDecBuPyrr]Br is positive at lower temperatures and becomes negative at higher temperatures. Higher $\Delta H_{\text{agg}}^{\circ}$ values for [DoDecBuPyrr]Br in comparison with [DoDecMPyrr]Br indicated stronger interactions between the alkyl chains in the first case. On the other hand, the enthalpy of aggregation decreases and approaches zero at around 50°C for [OctBuPyrr]Br, meaning that both contributions to the enthalpy are equally important; that is, the disruption of the structural organization of the water molecules around the hydrophilic and hydrophobic domains of the IL surfactant, and the restoring of the hydrogen-bond structure of water when the aggregate is formed.

Rao et al. [10] investigated the thermodynamic parameters of self-aggregation, in aqueous solution and at different temperatures (25°C, 35°C, and 45°C), for the following AAILs: GlyPrELS, AlaPrELS, ProPrELS, ValPrELS, and GluPrELS. The cac increases with temperature for all the ILs except for GlyPrELS. A significant negative $\Delta G_{\text{agg}}^{\circ}$ value was observed, which indicates a spontaneous aggregation of the AAILs. These values become more negative for ILs that have larger counter-ions. During the aggregation process, the endothermic “breaking” in the network of water molecules ordered around the nonpolar tails of AAILs is greater than the subsequent exothermic association of the molecules, thus leading to the positive entropy. Furthermore, the size and the hydration of the counter-ions are also responsible for the variation in the thermodynamic parameters. The larger and more hydrophobic AAILs, such as GluPrELS, have very high $\Delta S_{\text{agg}}^{\circ}$ values when compared with GlyPrELS which is smaller both in size and degree of hydrophobicity. The aggregation of AAILs are driven by entropic contribution in the temperature range evaluated.

Galgano et al. [31] investigated the micellar properties of [HexaDecMIM]Cl and [N-HexaDecPy]Cl and compared the data with [HDaEtBzDMA] which had been investigated by Shimizu et al. [65]. They showed that cac and values of ILs increase with increase of temperature, while N_{agg} decrease. The enthalpies of aggregation, ΔH°_{agg} were obtained directly by conductivity measurements and ITC. Aggregate formation is entropy-driven at: all studied temperatures (15°C–75°C) for [HexaDecMIM]Cl; up to 65°C for [N-HexaDecPy]Cl; and up to 55°C for [HDaEtBzDMA]. All these data can be rationalized by considering hydrogen-bonding between the head-ions of the monomers in the aggregate. The authors considered that which distinguishes imidazole-based surface active ionic liquids (SAILs) from the other conventional cationic ILs ([N-HexaDecPy]Cl and [HDaEtBzDMA]) to be the strong hydrogen-bonding between the counter-ion and the relatively acidic H2 of the imidazolium ring.

The thermodynamic parameters of the ILs [BMIM]X, [HexMIM]X, and [OctMIM]X ($X=Cl^{-}$, Br^{-} , and I^{-}) in water at temperatures between 25°C and 40°C was investigated by Vaghela et al. [66]. The ΔG°_{agg} value was negative and the values increased from [BMIM]X to [HexMIM]X and again to [OctMIM]X. The enthalpies of aggregation are small but negative. For the [HexMIM]X and [OctMIM]X, the large positive entropy values indicate that the aggregation is an entropy-driven process in which the hydrophobic forces are predominant.

2.6. The solvent effect on IL aggregation

Solvents play a decisive role in controlling the aggregation characteristics of ILs. Organic solvents have high cohesive energies and considerable hydrogen-bonding capability [67]; therefore, aggregation studies of ILs in mixed solvents are of fundamental and practical importance. Mixtures of IL solutions usually form mixed micelles that frequently exhibit characteristic properties which are remarkably different from those of the individual component aggregates [68].

There are three important factors to be examined when considering the effect of the solvent on the aggregation parameters: the dipolarity/polarizability parameter (π^{*}), the solvophobic parameter (S_p), and the Gordon parameter (G). The dipolarity/polarizability parameter measures the non-specific parts of the van der Waals interactions between solvents and solutes; for example, dispersive, inductive, and electrostatic interactions [69]–[72].

Another important characteristic of an organic solvent is the solvophobic parameter, which is equal to the ΔG° of hydrocarbon transfer from a gaseous phase to a given solvent. This parameter can be used for comparative estimation of the intensity of the interaction between the alkyl chains of an IL and a solvent. A high S_p value indicates a weaker solvent–hydrocarbon interaction and, therefore, a stronger tendency of a system to aggregate. Thus, the aggregation behavior of ILs can be regulated by selecting a solvent with an optimal S_p value for a given problem that is of importance for practical applications. Two aspects of view: (i) the changes of driving forces and (ii) the structure of aggregate could be considered to explain the influences of solvent in the aggregate formation. There is a large number of reports about IL aggregation in water (binary systems) compared to reports on organic solvents or organic solvents/aqueous solutions (ternary systems) [73]–[76]. The cac values of the ILs in different organic-solvent systems tend to increase when increasing the content of the organic additive

in solution, with few exceptions. When increasing the organic solvent content in water, the dielectric constant of the mixture is lowered, which results in an increase in the electrostatic forces of the ionic head groups in the IL aggregate [77]. Additionally, the hydrophobic interactions between the hydrophobic groups of the IL aggregate are gradually reduced, hence the aggregation potential decreases. Both effects justify the higher cac values obtained when increasing the organic solvent content. This section will detail the main reports in the literature that help to elucidate the solvent effect on aggregate formation in ILs.

Through conductivity measurements, He et al. [61] studied the effect that the addition of ethylene glycol (EG) had on the aggregation of the mixture of [HexaDecMIM]Br and [N-HexaDecPy]Br. The cac values of the binary mixtures are between the cac values of the individual surfactants and increase with volume percentage of EG and the mole fraction of [TetDecMIM]Br. The $\Delta G^\circ_{\text{agg}}$ values were negative, illustrating that the aggregation process is spontaneous. The $\Delta G^\circ_{\text{agg}}$ increase with the increasing in percentage of EG indicating that the process of micellization becomes less spontaneous. The $\Delta H^\circ_{\text{agg}}$ and $\Delta S^\circ_{\text{agg}}$ values gradually decreased with the concentration of cosolvent. The authors concluded that the aggregation is an entropy-driven process in pure water, whereas the formation of aggregates is enthalpy-driven in the aqueous solution of EG.

Feng et al. [78] investigated the effect of solvents — including acetonitrile, ethylene glycol, N,N-dimethylformamide, formamide, and dimethylsulfoxide solvents — on the aggregation behavior of [DoDecMIM]Br. The study showed that the solvophobic effect and the hydrogen-bonding interaction between the IL anion and the solvents are the main factors affecting the aggregation of ILs in non-aqueous solvents. In aprotic solvent, the cac values increase with the decrease in solvophobic parameters, which indicates that the aggregation of ILs is dominated by the interactions between the alkyl chains of the IL and the solvents. However, in protic solvents, the hydrogen-bonding interactions between the IL anions and the solvents have to be considered. In general, it is found that the aggregation of ILs in non-aqueous solvents can be controlled and regulated by solvent properties. The cac values of [DoDecMIM]Br in non-aqueous solvents are all higher than those for water. The IL cannot form aggregates in ethylene glycol solvent and this result is similar to the previous observation that classical ionic and zwitterionic surfactants exhibited very weak aggregation in EG [79]. They suggest that aggregation can be controlled by selecting appropriate solvent increasing the potential uses of IL in reaction and separation media.

Yan et al. [80] studied the aggregation behavior of [HexaDecTMA]Cl in EG and water mixtures at different temperatures. They observed an increase in cac and a variation tendency for the thermodynamic parameters, upon adding EG. The thermodynamic parameters of the cationic surfactant [HexaDecTMA]Cl in binary EG/H₂O solvent mixtures showed that the cac of [HexaDecTMA]Cl increases from 2 mM to 7 mM, corresponding to the amount of EG added; however, the β value varied little and remained at about 0.5. Moreover, $\Delta G^\circ_{\text{agg}}$ increase with addition of EG highlighting that aggregation process is more difficult to achieve in binary solvent mixtures than in water. Two main factors were considered: firstly, the presence of EG decreases the cohesive energy of the solution, thus increasing the solubility of [HexaDecTMA]Cl in its monomeric form and leading to an increase in the cac value; and secondly, the

dielectric constant of the medium is reduced by the addition of EG, which causes the repulsion effect among the ion head groups to increase.

The aggregation of [EMIM]Cl and [EMIM][TFSA] in water, methanol, acetonitrile, and benzene, was studied by Takamuku et al. [81] using SANS. The SANS results show that the heterogeneity of [EMIM]Cl in acetonitrile mixtures is significant when the acetonitrile content is high; thus, [EMIM]Cl forms clusters in acetonitrile solutions. On the other hand, it has been revealed that [EMIM]Cl is homogeneously dissolved in water and methanol. Remarkably, [EMIM][TFSA] aggregates in methanol solutions, whereas the mixtures of [EMIM][TFSA] with acetonitrile and benzene are homogeneous. They proposed that these homogeneous mixtures are the result of the interactions between benzene molecules and imidazolium rings via π - π interactions; and the hydrogen bonds between the oxygen atoms of TFSA and the hydrogens of benzene.

Furthermore, aggregation of [EMIM]Cl and [EMIM][TFSA] in acetonitrile and methanol, respectively, was examined by using ^1H NMR spectroscopy. The data confirmed the results observed using SANS.

Remsing et al. [82] investigated the solvation and aggregation of [BMIM]Cl in water and dimethylsulfoxide (DMSO) by ^1H and $^{35/37}\text{Cl}$ chemical shift perturbations. Evidence of aggregation of the IL *n*-butyl chains in aqueous environments at IL concentrations of 75–80 wt% was observed in the NMR experiments. A comparison of the data obtained for the imidazolium hydrogens and those in the *n*-butyl group also reflects that the positively charged ring is solvated prior to the alkyl chain. Indeed, the $\Delta\delta$ for the H2 at H_2O concentrations as low as 5 wt%, is larger than 0.3 ppm, but is only 0.03 ppm for H4'. The H2 is the most acidic hydrogen in the imidazolium ring. It forms the strongest hydrogen bonds with the Cl^- ion and its chemical shift is the most affected by variations in the water content of the binary mixture. The authors observed that [BMIM]Cl behaves as a typical electrolyte in water, with both ions completely solvated at low concentrations.

This experimental result can explain how ILs could be employed, for instance, in the dissolution of polysaccharide, which would demonstrate the potential industrial use of ILs.

However, the data reveal that the interactions between the [BMIM] and Cl^- ions strengthen as the DMSO content of the solutions increases. Thus, solvent is unable to effectively disrupt the interactions between ions and IL-rich clusters persist in this solvent even at concentrations below 10 wt%.

Li et al. [76] used the dipolarity/polarizability parameter (π^*) to study the physicochemical and structural properties of the binary or ternary mixtures, [BMIM][PF₆] or [BMIM][BF₄], in organic solvent (acetonitrile, water, ethanol, ethyl acetate, and tetrahydrofuran). The binary systems are miscible at the molecular level; that is, there is no obvious aggregation in the solution. However, for the following systems, non-linear behavior is observed: [BMIM][PF₆] in ethanol/water mixture; [BMIM][PF₆] in ethyl acetate; [BMIM][PF₆] in tetrahydrofuran; [BMIM][BF₄] in ethanol; and [BMIM][BF₄] in an ethanol/water mixture. The reasonable explanation is that aggregation of the systems occurred. From the conductivity study, the

authors deduced that the higher the dielectric constant of the organic solvent, the higher the cac of the IL.

Singh et al. [83] investigated the effect of EG and its derivatives — ethylene glycol monomethyl ether (EGMME) or ethylene glycol dimethyl ether (EGDME) — on the aggregation behavior of [BMIM] in an aqueous medium. The effect of a structural variation in EG by replacing the hydroxyl protons with an ethylene group has been studied and compared. The cac increased least in the case of EG as compared to EGMME or EGDME for the same amount of organic solvent added. They explained this result considering that EG resemble with water in some properties such as high cohesive energy density and capability of hydrogen bonding. For the same amount of EG or EG derivatives added, the aggregation is found to diminish in the order $EG < EGMME < EGDME$. This may be due to the increased solvophobic effect of the solvents as a consequence of replacing the EG's hydroxyl proton with a methylene group. The temperature dependence of conductivity enabled us to explore the thermodynamics of aggregation, and it was concluded that at low organic solvent concentrations, ΔH°_{agg} governs the change in ΔG°_{agg} while $-\Delta S^\circ_{agg}$ dictates the change at higher organic solvent concentrations.

The increase in EG concentration makes it a better solvent for the IL molecules than pure water and it subsequently forms loose aggregates. Dynamic light scattering (DLS) measurements showed that the hydrodynamic radii (R_h) of the aggregates formed in mixed solvents was higher than that in water, which, however, decreased with an increase in content of EG/its derivatives. The N_{agg} results obtained by 1H NMR measurements follow the same pattern. The 1H NMR measurements were used to probe the aggregated structures at a molecular level. It was observed that with an increase in the content of EG/EG derivatives, the magnitude of $\Delta\delta_{obs}$ decreases, except for EGDME, in which it increases. For the same amount of EG/EG derivatives, $\Delta\delta_{obs}$ varies in the order $EG < EGMME < EGDME$, which indicates the increasing solvating ability of the ILs that hinders the aggregation process.

Pino et. al. [84] used surface tensiometry to investigate the influence of organic solvents (methanol, 1-propanol, 1-butanol, 1-pentanol, and acetonitrile) on surface adsorption and aggregation of [HexaDecBuIM]Br and [DiDoDecIM]Br. The cac values of the two ILs in different organic solvent/water systems tend to increase when increasing the content of the organic additive in solution, with few exceptions. For the [HexaDecBuIM]Br IL, the extent of the increase in the cac values (evaluated by comparing slopes) follows the trend: acetonitrile $<$ methanol $<$ 1-propanol \approx 1-butanol $<$ 1-pentanol. In the case of the [DiDoDecIM]Br IL, a fairly similar trend is obtained: acetonitrile \approx methanol $<$ 1-propanol $<$ 1-butanol $<$ 1-pentanol. The authors observed that for the case of the [DiDoDecIM]Br, a fixed amount of organic solvent, the cac value increases with an increase in the length of the alkyl chain of the alcohol additive. In the presence of organic solvents, the interfacial characteristics of the [DiDoDecIM]Br IL are more influenced than those of the [HexaDecBuIM]Br IL. For both ILs, when the organic solvent content in solution was increased, the following resulted: decreases in the maximum surface excess concentration (Γ_{max}), increases in the minimum surface area per surfactant molecule (A_{min}), decreases in the adsorption efficiency (pC_{20}), and decreases in the effectiveness of surface tension reduction (Π_{cac}).

3. Conclusion

In this chapter we examined the literature, considering the main effects involved in the aggregation behavior of ILs. The results demonstrate the potential applications of these designer ILs in the field of colloid and interface science, as well as in several analytical applications. Aggregate features, such as length and composition of the hydrophobic portion, nature of the head group, and anion characteristics, significantly influence the characteristics of ILs. These studies have shown that the self-assembly and surface activity of ILs can be finely modulated by varying the alkyl length chain, introducing specific cation or polar groups in the side chain, or changing the nature of the anion [27], [34], [36], [62]. A systematic decrease in cac values was observed with an increase in methylene units in the alkyl chain of anion or cationic ions. Additionally, ILs with two long alkyl chains had lower cac values than ILs with one long chain. However, when polar groups (like ester) were added to side chains, aggregation behavior was not different to that of apolar alkyl chains.

The surveys of cationic heads revealed that, in general, the aggregation is favorable in the following order: ammonium > imidazolium ~ pyridinium > pyrrolidinium. However, it is important to note that there were no substantial differences among values obtained for different cationic heads. This fact was attributed to the similar hydrophobic characteristics of the cations investigated. The authors observed that the van der Waals volumes of cationic rings can assume an important role in the aggregation process, and smaller values are related to a more favorable aggregation.

In relation to the counter-ion effect, the aggregation of ILs with different anions followed the Hofmeister series. The increase in the hydrophobicity and decrease in hydration radius caused a decrease in the cac and ΔG_{agg}° values. When anion bears the alkyl chain, it has the same effect when alkyl chain is bear for the cation. Thus, it was found that the presence of hydrophobic chains in both cationic and anionic moieties of ILs work synergistically and favor the aggregation and improvement of tensoative properties.

The dicationic IL (gemini) aggregation process was the same for analogous monocationic ILs; however, generally the cac values for dicationic ILs were lower than their monocationic analogues.

The temperature of the system is found by influencing the self-assembly of ILs in solutions. An increase in the temperature strongly affects the cation/anion, cation/solvent, and anion/solvent interactions. In general, cac values increased with an increase in temperature, independent of the IL structure. This occurs because the energy supply to the system can lead to the break in intermolecular interactions and avoid aggregation. The most aggregation process described here for ILs were enthalpy-driven at lower temperature, while entropy-driven at higher temperature. This thermodynamic behavior is similar to conventional surfactants. However, it was found some cases, where aggregation process of ILs on water was only enthalpy-driven or only entropy-driven. The thermodynamic parameters revealed no following of a pattern for cationic or anionic structure.

Finally, the addition of organic solvents was found to have a vital effect on the cac value, the standard Gibbs energy of aggregation, the aggregation number, and aggregate size. Generally, the cac values of the ILs in different organic-solvent systems tend to increase when increasing the content of the organic additive in solution, with few exceptions.

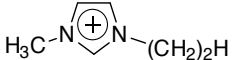
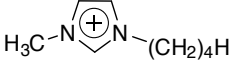
The review addressed in this chapter demonstrates that the interactions present in the IL-solution system are variable, showing that it is essential to have a better understanding of the interactions of ILs with various classes of organic molecules. This particular aspect allows us to actually consider ILs (when dispersed in aqueous and/or organic solutions) to be a new class of surfactants with unique abilities.

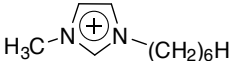
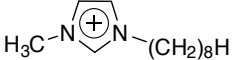
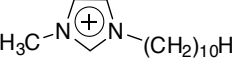
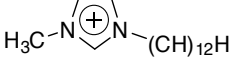
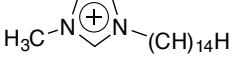
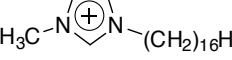





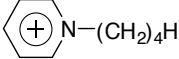
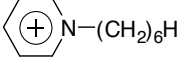
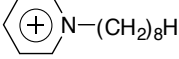
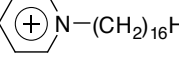
Abbreviations and symbols

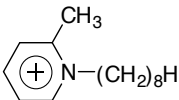
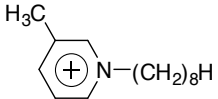
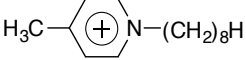
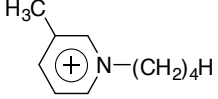
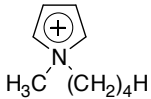
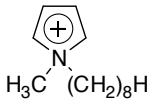
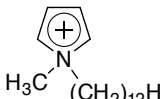
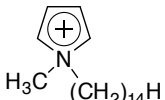
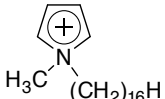
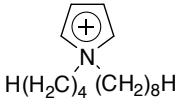
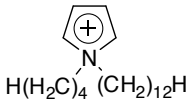
\AA^3	cubic angstroms
AAILs	amino acid ionic liquid
A_{min}	area per molecule at the interface
C_{20}	concentration of IL to reduce the surface tension of pure solvent by 20 mN/m
cac	critical aggregation concentration
cac_1	first critical aggregation concentration
cac_2	second critical aggregation concentration
DLS	dynamic light scattering
DMSO	dimethylsulfoxide
EG	ethylene glycol
EGDME	ethylene glycol dimethyl ether
EGMME	ethylene glycol monomethyl ether
G	gordon parameter
I_I	first emission band of pyrene
I_{III}	third emission band of pyrene
ILs	ionic liquids
ITC	isothermal titration calorimetry
K_a	equilibrium constant of aggregation
mM	millimolar
mN/m	millinewtons per mole
N_{agg}	aggregation number
nm	nanometers

NMR	nuclear magnetic resonance
pC ₂₀	adsorption efficiency
R _h	hydrodynamic radius
SAILs	imidazole-based surface active ionic liquids
SANS	small angle neutron scattering
SAXS	small angle X-ray scattering
Sp	solvophobic parameter
-TΔS ^o _{agg}	entropic term of Gibbs Free Energy equation
wt%	molar fraction
α	degree of counter-ion dissociation
β	degree of counter-ion binding
γ	surface tension
Γ _{cac}	Surface tension at cac
δ _{obs}	chemical shift observed
Δδ	chemical shift variation
π*	polarity/polarizability parameter
Π _{cac}	effectiveness of the IL in decreasing the surface tension of the solvent
Γ _{máx}	excess surface concentration
ΔG ^o	Gibbs free energy
ΔG ^o _{ads}	Gibbs free energy of adsorption
ΔG ^o _{agg}	Gibbs free energy of aggregation
ΔH ^o _{agg}	enthalpy of aggregation
ΔS ^o _{agg}	entropy of aggregation

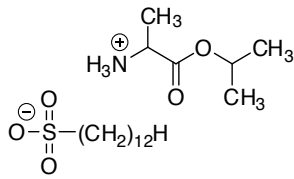
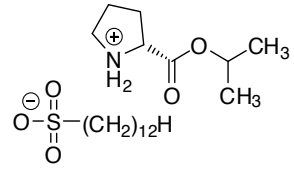
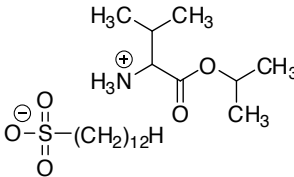
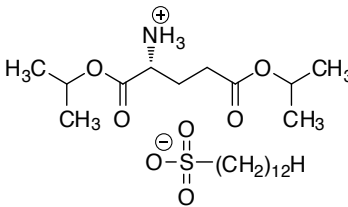

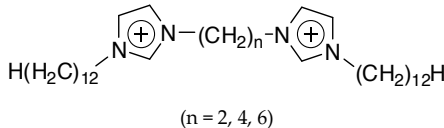
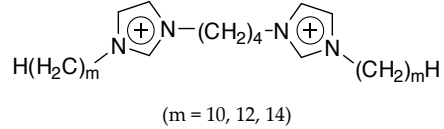
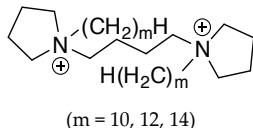
Representation of IL cations in this chapter

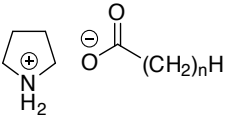
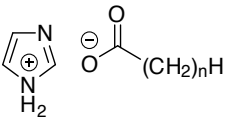
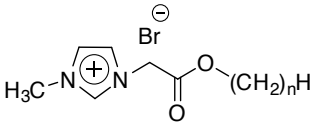
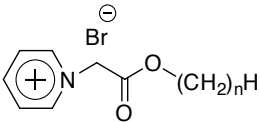
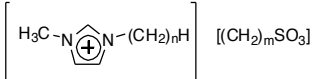
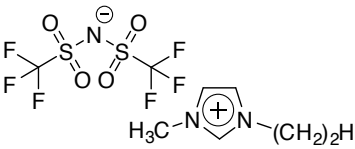
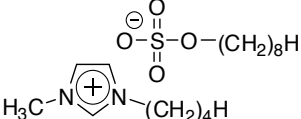
Representation	Structure	Name
[EMIM]		1-Ethyl-3-methylimidazolium
[BMIM]		1-Butyl-3-methylimidazolium

Representation	Structure	Name
[HexMIM]		1-Hexyl-3-methylimidazolium
[OctMIM]		1-Octyl-3-methylimidazolium
[DecMIM]		1-Decyl-3-methylimidazolium
[DoDecMIM]		1-Dodecyl-3-methylimidazolium
[TetDecMIM]		1-Tetradecyl-3-methylimidazolium
[HexaDecMIM]		1-Hexadecyl-3-methylimidazolium
[HexaDecBuIM]		1-Hexadecyl-3-butylimidazolium
[DoDecEtIM]		1-Ethyl-3-dodecylimidazolium
[DoDecPrIM]		1-Propyl-3-dodecylimidazolium
[DoDecBuIM]		1-Dodecyl-3-butylimidazolium
[DiDoDecIM]		1,3-Didodecylimidazolium
[N-BPy]		1-Butylpyridinium
[N-HexPy]		1-Hexylpyridinium
[N-OctPy]		1-Octylpyridinium
[N-HexaDecPy]		1-Hexadecylpyridinium

Representation	Structure	Name
[N-Oct-2-MePy]		1-Octyl-2-methylpyridinium
[N-Oct-3-MePy]		1-Octyl-3-methylpyridinium
[N-Oct-4-MePy]		1-Octyl-4-methylpyridinium
[N-Bu-3-MePy]		1-Butyl-3-methylpyridinium
[BMPyrr]		N-Butyl-N-methylpyrrolidinium
[OctMPyrr]		N-Octyl-N-methylpyrrolidinium
[DoDecMPyrr]		N-Dodecyl-N-methylpyrrolidinium
[TetDecMPyrr]		N-Tetradecyl-N-methylpyrrolidinium
[HexaDecMPyrr]		N-Hexadecyl-N-methylpyrrolidinium
[OctBuPyrr]		N-Butyl-N-octylpyrrolidinium
[DoDecBuPyrr]		N-butyl-N dodecylpyrrolodinium

Representation	Structure	Name
[EtOHDoDecIM]		1-hydroxyethyl-3-dodecylimidazolium
[HexaDecHyPrIM]		S-3-hexadecyl-1-(1-hydroxy-propan-2-yl)imidazolium
[DecPhMIM]		1-(2,4,6-trimethylphenyl)-3-dodecylimidazolium
[DoDecPhMIM]		1-(2,4,6-trimethylphenyl)-3-dodecylimidazolium
[TetDecPhMIM]		1-(2,4,6-trimethylphenyl)-3-tetradecylimidazolium
[1,3-DiDec-2-MIM]		1,3-didecyl-2-methylimidazolium
[HexaDecTMA]		hexadecyltrimethylammonium
[HDaEtBzDMA]		Benzyl(3-hexadecanoylaminoethyl)dimethylammonium
GlyPrELS		Glycine propyl ester lauryl sulfate

Representation	Structure	Name
AlaPrELS		Alanine propyl ester lauryl sulfate
ProPrELS		Proline propyl ester lauryl sulfate
ValPrELS		Valine propyl ester lauryl sulfate
GluPrELS		Glutamine propyl ester lauryl sulfate
[DoDecIMCH ₂ COO]		1-carboxymethyl-3-dodecylimidazolium inner salt
[Bis-AlkylDoDecIM]Br ₂ (Alkyl = Et, Bu, Hex)	 <p style="text-align: center;">(n = 2, 4, 6)</p>	1,2-bis(3-dodecylimidazolium-1-yl) alkane (alkane = ethane, butane, hexane)
[Bis-BuAlkylIM]Br ₂ (Alkyl = Dec, DoDec, TetDec)	 <p style="text-align: center;">(m = 10, 12, 14)</p>	1,2-bis(3-alkylimidazolium-1-yl) butane (alkyl = dec, dodec, tetdec)
[Bis-BuAlkylPyrrr] (Alkyl = Dec, DoDec, TetDec)	 <p style="text-align: center;">(m = 10, 12, 14)</p>	1,1-(butane-1,4-diyl)bis(1- alkylpyrrolidinium) (alkyl = decyl, dodecyl, tetradecyl)

Representation	Structure	Name
[Pyr][AlkylCO ₂]	 (n = 5, 6, 7, 8)	pyrrolidinium alkylcarboxylates (alkyl = pen, hex, hep, oct)
[IM][AlkylCO ₂]	 (n = 5, 6, 7, 8)	imidazolium alkylcarboxylates (alkyl = pen, hex, hep, oct)
[AlkylCMIM]Br (Alkyl = Hex, Oct, Dec, DoDec, TetDec)	 (n = 6, 8, 10, 12, 14)	3-methyl-1-alkyloxycarbonylmethylimidazolium bromide (alkyl = hexyl, octyl, decyl, dodecyl, tetradecyl)
[AlkylCMPy]Br (Alkyl = Hex, Oct, Dec, DoDec, TetDec)	 (n = 6, 8, 10, 12, 14)	1-alkyloxycarbonylmethylpyridinium bromide (alkyl = hexyl, octyl, decyl, dodecyl, tetradecyl)
[C _n H _{2n+1} MIM][C _m H _{2m+1} SO ₃] (n = 8, 10, 12; m=1 and n = 4, 8; m=4, 8)	 (n = 8, 10, 12; m=1 and n = 4, 8; m=4, 8)	1-alkyl-3-methylimidazolium alkylsulfonate (alkyl = metyl, butyl, octyl, decyl, dodecyl)
[EMIM]TfSA		1-ethyl-3-methylimidazolium bis-(trifluoromethanesulfonyl)amide)
[BMIM][C ₈ OSO ₃]		1-Butyl-3-methylimidazolium octyl sulfate

Acknowledgements

The authors are thankful for the Financial support from the Conselho Nacional de Desenvolvimento Científico e Tecnológico (CNPq)—Universal/Proc. 485893/2007-0, Universal/ Proc.

471519/2009-0 and Coordenação de Aperfeiçoamento de Pessoal de Nível Superior-CAPES. The fellowships from CNPq (M.A.P.M., C.R.B., I.M.G., N.Z., H.G.B.) and CAPES (A.Z.T.) are also acknowledged.

Author details

Clarissa P. Frizzo^{1*}, Aniele Z. Tier¹, Caroline R. Bender¹, Izabelle M. Gindri², Marcos A. Villetti³, Nilo Zanatta¹, Helio G. Bonacorso¹ and Marcos A.P. Martins

*Address all correspondence to: clarissa.frizzo@gmail.com

1 Núcleo de Química de Heterociclos (NUQUIMHE), Department of Chemistry, Federal University of Santa Maria, Santa Maria, RS, Brazil

2 Department of Bioengineering, University of Texas at Dallas, Richardson, TX, USA

3 Laboratório de Espectroscopia e Polímeros (LEPOL), Department of Physics, Federal University of Santa Maria, Santa Maria, RS, Brazil

References

- [1] Frizzo CP, Tier AZ, Gindri IM, Buriol L, Villetti MA, Zanatta N and Martins MAP. Nanostructure Evaluation of Ionic Liquid Aggregates by Spectroscopy. In: Kadokawa J-I. (ed.) *Ionic Liquids-New Aspects for the Future*. Rijeka: InTech; 2013.
- [2] Martins MAP, Frizzo CP, Moreira DN, Zanatta N and Bonacorso HG. Ionic liquids in heterocyclic synthesis. *Chemical Reviews* 2008; 108(6) 2015–2050. <http://pubs.acs.org/doi/pdf/10.1021/cr078399y> (accessed 20 june 2014).
- [3] Krossing I, Slattery JM, Dagueuet C, Dyson PJ, Oleinikova A and Weingärtner H. Why are ionic liquids liquid? A simple explanation based on lattice and solvation energies. *Journal of the American Chemical Society* 2006; 128(41) 13427–13434. <http://pubs.acs.org/doi/pdf/10.1021/ja0619612> (accessed 20 june 2014).
- [4] El Seoud OA, Koschella A, Fidale LC and Dorn S. Applications of Ionic Liquids in Carbohydrate Chemistry: A Window of Opportunities. 2007; 8(9) 2629–2647. <http://pubs.acs.org/doi/pdf/10.1021/bm070062i> (accessed 20 june 2014).
- [5] Anderson JL, Armstrong DW and Wei GT. Ionic liquids in analytical chemistry. *Analytical Chemistry* 2006; 78(9) 2892–2902. <http://pubs.acs.org/doi/pdf/10.1021/ac069394o> (accessed 20 june 2014).

- [6] Davis JH Jr. Task-Specific Ionic Liquids. *Chemistry Letters* 2004; 33(9) 1072–1077. https://www.jstage.jst.go.jp/article/cl/33/9/33_9_1072/_article (accessed 20 june 2014).
- [7] Wasserscheid P and Keim W. Ionic Liquids-New ‘Solutions’ for Transition Metal Catalysis. *Angewandte Chemie International Edition* 2000; 39(21) 3772–3789. [http://onlinelibrary.wiley.com/doi/10.1002/1521-3773\(20001103\)39:21%3C3772::AID-ANIE3772%3E3.0.CO;2-5/pdf](http://onlinelibrary.wiley.com/doi/10.1002/1521-3773(20001103)39:21%3C3772::AID-ANIE3772%3E3.0.CO;2-5/pdf) (accessed 20 june 2014).
- [8] Hallett JP and Welton T. Room-temperature ionic liquids: solvents for synthesis and catalysis. 2. *Chemical Reviews* 2011; 111(5) 3508–3576. <http://pubs.acs.org/doi/pdf/10.1021/cr1003248> (accessed 20 june 2014).
- [9] Anouti M, Jones J, Boisset A, Jacquemin J, Caillon-Caravanier M and Lemordant D. Aggregation behavior in water of new imidazolium and pyrrolidinium alkylcarboxylates protic ionic liquids. *Journal of Colloid and Interface Science* 2009; 340(1) 104–111. <http://www.sciencedirect.com/science/article/pii/S0021979709009928#> (accessed 20 june 2014).
- [10] Rao KS, Singh T, Trivedi TJ and Kumar A. Aggregation behavior of amino acid ionic liquid surfactants in aqueous media. *The Journal of Physical Chemistry B* 2011; 115(47) 13847–13853. <http://pubs.acs.org/doi/pdf/10.1021/jp2076275> (accessed 20 june 2014).
- [11] Singh T and Kumar A. Aggregation behavior of ionic liquids in aqueous solutions: effect of alkyl chain length, cations, and anions. *The Journal of Physical Chemistry B* 2007; 111(27) 7843–7851. <http://pubs.acs.org/doi/pdf/10.1021/jp0726889> (accessed 20 june 2014).
- [12] Wang J, Zhang L, Wang H and Wu C. Aggregation behavior modulation of 1-dodecyl-3-methylimidazolium bromide by organic solvents in aqueous solution. *The Journal of Physical Chemistry B* 2011; 115(17) 4955–4962. <http://pubs.acs.org/doi/pdf/10.1021/jp201604u> (accessed 20 june 2014).
- [13] Blesic M, Marques MH, Plechkova NV, Seddon KR, Rebelo LPN and Lopes A. Self-aggregation of ionic liquids: micelle formation in aqueous solution. *Green Chemistry* 2007; 9(5) 481–490. <http://pubs.rsc.org/en/content/articlepdf/2007/gc/b615406a> (accessed 20 june 2014).
- [14] Blesic M, Lopes A, Melo E, Petrovski Z, Plechkova NV, Canongia Lopes JN, Seddon KR and Rebelo LPN. On the self-aggregation and fluorescence quenching aptitude of surfactant ionic liquids. *The Journal of Physical Chemistry B* 2008; 112(29) 8645–8650. <http://pubs.acs.org/doi/pdf/10.1021/jp802179j> (accessed 20 june 2014).
- [15] Zech O, Thomaier S, Bauduin P, Rück T, Touraud D and Kunz W. Microemulsions with an ionic liquid surfactant and room temperature ionic liquids as polar pseudo-phase. *The Journal of Physical Chemistry B* 2009; 113(2) 465–473. <http://pubs.acs.org/doi/pdf/10.1021/jp8061042> (accessed 20 june 2014).

- [16] Zhao Y, Chen X and Wang X. Liquid crystalline phases self-organized from a surfactant-like ionic liquid C(16)mimCl in Ethylammonium nitrate. *The Journal of Physical Chemistry B* 2009; 113(7) 2024–2030. <http://pubs.acs.org/doi/pdf/10.1021/jp810613c> (accessed 20 june 2014).
- [17] Zhao Y, Chen X, Jing B, Wang X and Ma F. Novel gel phase formed by mixing a cationic surfactive ionic liquid C(16)mimCl and an anionic surfactant SDS in aqueous solution. *The Journal of Physical Chemistry B* 2009; 113(4) 983–988. <http://pubs.acs.org/doi/pdf/10.1021/jp809048u> (accessed 20 june 2014).
- [18] Smirnova NA and Safonova EA. Micellization in solutions of ionic liquids. *Colloid Journal* 2012; 74(2) 254–265. http://download.springer.com/static/pdf/747/article%253A10.1134%252FS1061933X12020123.pdf?auth66=1411572167_cb5a445f830931e92fe7a0ee3e334f9f&ext=.pdf (accessed 20 june 2014).
- [19] Sheldrake GN and Schleck D. Dicationic molten salts (ionic liquids) as re-usable media for the controlled pyrolysis of cellulose to anhydrosugars. *Green Chemistry* 2007; 9(10) 1044–1046. <http://pubs.rsc.org/en/content/articlepdf/2007/gc/b705241c> (accessed 20 june 2014).
- [20] Baltazar QQ, Chandawalla J, Sawyer K and Anderson JL. Interfacial and micellar properties of imidazolium-based monocationic and dicationic ionic liquids. *Colloids and Surfaces A: Physicochemical and Engineering Aspects* 2007; 302(1–3) 150–156. <http://www.sciencedirect.com/science/article/pii/S0927775707001318#> (accessed 20 june 2014).
- [21] Ding Z and Hao A. Synthesis and Surface Properties of Novel Cationic Gemini Surfactants. *Journal of Dispersion Science and Technology* 2010; 31(3) 338–342. <http://www.tandfonline.com/doi/pdf/10.1080/01932690903192580#.VCBAQPldWoI> (accessed 20 june 2014).
- [22] Wang H, Wang J, Zhang S and Xuan X. Structural effects of anions and cations on the aggregation behavior of ionic liquids in aqueous solutions. *The Journal of Physical Chemistry B* 2008; 112(51) 16682–16689. <http://pubs.acs.org/doi/pdf/10.1021/jp8069089> (accessed 20 june 2014).
- [23] Stolte S, Steudte S, Areitioaurtena O, Pagano F, Thöming J, Stepnowski P and Igartua A. Ionic liquids as lubricants or lubrication additives: an ecotoxicity and biodegradability assessment. *Chemosphere* 2012; 89(9) 1135–1141. http://ac.els-cdn.com/S0045653512007497/1-s2.0-S0045653512007497-main.pdf?_tid=1a7ea-cec-425f-11e4-9c7d-00000aacb361&acd-nat=1411393876_b434182b3fc02c048ff762f48e02e5f5 (accessed 20 june 2014).
- [24] Gindri IM, Frizzo CP, Bender CR, Tier AZ, Martins MAP, Villetti MA, Machado G, Rodriguez LC and Rodrigues DC. Preparation of TiO₂ Nanoparticles Coated with Ionic Liquids: A Supramolecular Approach. *ACS Applied Materials Interfaces* 2014;

- 6(14) 11536–11543. <http://pubs.acs.org/doi/pdf/10.1021/am5022107> (accessed 20 june 2014).
- [25] Sung J, Jeon Y, Kim D, Iwahashi T, Seki K, Iimori T and Ouchi Y. Gibbs monolayer of ionic liquid+H₂O mixtures studied by surface tension measurement and sum-frequency generation spectroscopy. *Colloids and Surfaces A: Physicochemical and Engineering Aspects* 2006; 284–285, 84–88. http://ac.els-cdn.com/S0927775705008563/1-s2.0-S0927775705008563-main.pdf?_tid=3e9cc65e-425f-11e4-8e37-00000aab0f26&acd-nat=1411393936_c38198703150da55b4348653b7e9c88d (accessed 20 june 2014).
- [26] Mukherjee I, Mukherjee S, Naskar B, Ghosh S and Moulik SP. Amphiphilic behavior of two phosphonium based ionic liquids. *Journal of Colloid and Interface Science* 2013; 395(1) 135–144. http://ac.els-cdn.com/S0021979712013525/1-s2.0-S0021979712013525-main.pdf?_tid=5df9df5a-425f-11e4-b6b4-00000aab0f6c&acd-nat=1411393989_77abffd0ba8bd0fb71918b9f0cd38258 (accessed 20 june 2014).
- [27] Sastry NV, Vaghela NM and Aswal VK. Effect of alkyl chain length and head group on surface active and aggregation behavior of ionic liquids in water. *Fluid Phase Equilibria* 2012; 327, 22–29. http://ac.els-cdn.com/S0378381212001732/1-s2.0-S0378381212001732-main.pdf?_tid=6d0c44ec-425f-11e4-97a9-00000aab0f27&acd-nat=1411394014_74a1d6faeb816d4aee8d0ab4f96ce271 (accessed 20 june 2014).
- [28] Greaves TL and Drummond CJ. Solvent nanostructure, the solvophobic effect and amphiphile self-assembly in ionic liquids. *Chemical Society Reviews* 2013; 42(3) 1096–1120. <http://pubs.rsc.org/en/content/articlepdf/2013/CS/C2CS35339C> (accessed 20 june 2014).
- [29] Shi L, Li N, Yan H, Gao Y and Zheng L. Aggregation behavior of long-chain N-aryl imidazolium bromide in aqueous solution. *Langmuir* 2011; 27(5) 1618–1625. <http://pubs.acs.org/doi/pdf/10.1021/la104719v> (accessed 20 june 2014).
- [30] Fan X and Zhao K. Aggregation behavior and electrical properties of amphiphilic pyrrole-tailed ionic liquids in water, from the viewpoint of dielectric relaxation spectroscopy. *Soft Matter* 2014; 10(18) 3259–3270. <http://pubs.rsc.org/en/content/articlepdf/2014/sm/c3sm53143k> (accessed 20 june 2014).
- [31] Galgano PD and El Seoud OA. Micellar properties of surface active ionic liquids: a comparison of 1-hexadecyl-3-methylimidazolium chloride with structurally related cationic surfactants. *Journal of Colloid and Interface Science* 2010; 345(1) 1–11. http://ac.els-cdn.com/S002197971000127X/1-s2.0-S002197971000127X-main.pdf?_tid=cf187b10-425f-11e4-b729-00000aacb360&acd-nat=1411394179_4eb83af6da97d37d53bfd64a180de72f (accessed 20 june 2014).
- [32] Dong B, Li N, Zheng L, Yu L and Inoue T. Surface adsorption and micelle formation of surface active ionic liquids in aqueous solution. *Langmuir* 2007; 23(8) 4178–4182. <http://pubs.acs.org/doi/pdf/10.1021/la0633029> (accessed 20 june 2014).

- [33] Ao M, Xu G, Pang J and Zhao T. Comparison of aggregation behaviors between ionic liquid-type imidazolium gemini surfactant [C12-4-C12im]Br₂ and its monomer [C12mim]Br on silicon wafer. *Langmuir* 2009; 25(17) 9721–9727. <http://pubs.acs.org/doi/pdf/10.1021/la901005v> (accessed 20 june 2014).
- [34] Li XW, Gao YA, Liu J, Zheng LQ, Chen B, Wu LZ and Tung CH. Aggregation behavior of a chiral long-chain ionic liquid in aqueous solution. *Journal of Colloid and Interface Science* 2010; 343(1) 94–101. http://ac.els-cdn.com/S0021979709014519/1-s2.0-S0021979709014519-main.pdf?_tid=0ba50ab2-4260-11e4-ac53-00000aacb361&acdnat=1411394280_ce70c5439b3b0ed368f7288e57c42594 (accessed 20 june 2014).
- [35] Kusano T, Fujii K, Tabata M and Shibayama M. Small-Angle Neutron Scattering Study on Aggregation of 1-Alkyl-3-methylimidazolium Based Ionic Liquids in Aqueous Solution. *Journal of Solution Chemistry* 2013; 42(10) 1888–1901. http://download.springer.com/static/pdf/727/art%253A10.1007%252Fs10953-013-0080-0.pdf?auth66=1411566945_f81cd1c81e38199b409f97bd14e7079e&ext=.pdf (accessed 20 june 2014).
- [36] Wang J, Wang H, Zhang S, Zhang H and Zhao Y. Conductivities, volumes, fluorescence, and aggregation behavior of ionic liquids [C4mim][BF₄] and [C(n)mim]Br (n=4, 6, 8, 10, 12) in aqueous solutions. *The Journal of Physical Chemistry B* 2007; 111(22) 6181–6188. <http://pubs.acs.org/doi/pdf/10.1021/jp068798h> (accessed 20 june 2014).
- [37] Cheng N, Yu P, Wang T, Sheng X, Bi Y, Gong Y and Yu L. Self-aggregation of new alkylcarboxylate-based anionic surface active ionic liquids: experimental and theoretical investigations. *The Journal of Physical Chemistry B* 2014; 118(10) 2758–2768. <http://pubs.acs.org/doi/pdf/10.1021/jp4124056> (accessed 20 june 2014).
- [38] Sastry NV, Vaghela NM, Macwan PM, Soni SS, Aswal VK and Gibaud A. Aggregation behavior of pyridinium based ionic liquids in water--surface tension, ¹H NMR chemical shifts, SANS and SAXS measurements. *Journal of Colloid and Interface Science* 2012; 371(1) 52–61. http://ac.els-cdn.com/S0021979712000082/1-s2.0-S0021979712000082-main.pdf?_tid=865590b0-4260-11e4-bf40-00000aacb35e&acdnat=1411394486_6def5329fad0cca9988ca5ec98a21e32 (accessed 20 june 2014).
- [39] Inoue T, Ebina H, Dong B and Zheng L. Electrical conductivity study on micelle formation of long-chain imidazolium ionic liquids in aqueous solution. *Journal of Colloid and Interface Science* 2007; 314(1) 236–241. http://ac.els-cdn.com/S0021979707007345/1-s2.0-S0021979707007345-main.pdf?_tid=9b16ff0c-4260-11e4-b43d-00000aacb35f&acdnat=1411394521_6718d194736879a8fd5a676080e18049 (accessed 20 june 2014).
- [40] Takamuku T, Shimomura T, Sadakane K, Koga M and Seto H. Aggregation of 1-dodecyl-3-methylimidazolium nitrate in water and benzene studied by SANS and ¹H

- NMR. *Physical Chemistry Chemical Physics* 2012; 14(31) 11070–11080. <http://pubs.rsc.org/en/content/articlepdf/2012/CP/C2CP40891K> (accessed 20 June 2014).
- [41] Vaghela NM, Sastry NV and Aswal VK. Surface active and aggregation behavior of methylimidazolium-based ionic liquids of type [C_nmim][X], n = 4, 6, 8 and [X] = Cl⁻, Br⁻, and I⁻ in water. *Colloid and Polymer Science* 2010; 289(3) 309–322. http://download.springer.com/static/pdf/966/art%253A10.1007%252Fs00396-010-2332-5.pdf?auth66=1411567211_24c63abe37eeee9649498fd373eea5ce&ext=.pdf (accessed 20 June 2014).
- [42] Dong B, Zhao X, Zheng L, Zhang J, Li N and Inoue T. Aggregation behavior of long-chain imidazolium ionic liquids in aqueous solution: Micellization and characterization of micelle microenvironment. *Colloids and Surfaces A: Physicochemical and Engineering Aspects* 2008; 317(1–3) 666–672. http://ac.els-cdn.com/S0927775707010448/1-s2.0-S0927775707010448-main.pdf?_tid=d4f2a76c-4260-11e4-bb23-00000aab0f01&acdnat=1411394618_5742cff483046f472b9688ea9f39400e (accessed 20 June 2014).
- [43] Zhao M and Zheng L. Micelle formation by N-alkyl-N-methylpyrrolidinium bromide in aqueous solution. *Physical Chemistry Chemical Physics* 2011; 13(4) 1332–1337. <http://pubs.rsc.org/en/content/articlepdf/2011/CP/C0CP00342E> (accessed 20 June 2014).
- [44] Liu X, Hu J, Huang Y and Fang Y. Aggregation Behavior of Surface Active Dialkylimidazolium Ionic Liquids [C₁₂C_nim]Br (n=1–4) in Aqueous Solutions. *Journal of Surfactants and Detergents* 2012; 16(4) 539–546. http://download.springer.com/static/pdf/394/art%253A10.1007%252Fs11743-012-1409-1.pdf?auth66=1411567309_de14a75fa14c7e4cf90cd8b85c1018f2&ext=.pdf (accessed 20 June 2014).
- [45] Tariq M, Podgoršek A, Ferguson JL, Lopes A, Costa Gomes MF, Pádua AA, Rebelo LP and Canongia Lopes JN. Characteristics of aggregation in aqueous solutions of dialkylpyrrolidinium bromides. *Journal of Colloid and Interface Science* 2011; 360(2) 606–616. http://ac.els-cdn.com/S0021979711005315/1-s2.0-S0021979711005315-main.pdf?_tid=131463a0-4261-11e4-9ab0-00000aab0f6c&acdnat=1411394722_e874133dd34130d4f54863b0e38ebfcc (accessed 20 June 2014).
- [46] Garcia MT, Ribosa I, Perez L, Manresa A and Comelles F. Aggregation behavior and antimicrobial activity of ester-functionalized imidazolium- and pyridinium-based ionic liquids in aqueous solution. *Langmuir* 2013; 29(8) 2536–2545. <http://pubs.acs.org/doi/pdf/10.1021/la304752e> (accessed 20 June 2014).
- [47] Liu X, Dong L and Fang Y. Synthesis and Self-Aggregation of a Hydroxyl-Functionalized Imidazolium-Based Ionic Liquid Surfactant in Aqueous Solution. *Journal of Surfactants and Detergents* 2010; 14(2) 203–210. <http://download.springer.com/static/pdf/88/art%253A10.1007%252Fs11743-010-1234-3.pdf?>

- auth66=1411567405_c9aa7042c409b9b6d8ef44e604ef6892&text=.pdf (accessed 20 june 2014).
- [48] Figueira-González M, Francisco V, García-Río L, Marques EF, Parajó, M and Rodríguez-Dafonte P. Self-aggregation properties of ionic liquid 1,3-didodecyl-2-methylimidazolium chloride in aqueous solution: from spheres to cylinders to bilayers. *The Journal of Physical Chemistry B*; 117(10) 2926–2937. <http://pubs.acs.org/doi/pdf/10.1021/jp3117962> (accessed 20 june 2014).
- [49] El Seoud OA, Pires PAR, Abdel-Moghny T and Bastos EL. Synthesis and micellar properties of surface-active ionic liquids: 1-alkyl-3-methylimidazolium chlorides. *Journal of Colloid and Interface Science* 2007; 313(1) 296–304. http://ac.els-cdn.com/S0021979707004663/1-s2.0-S0021979707004663-main.pdf?_tid=5e169378-4261-11e4-b355-00000aab0f26&acdnat=1411394848_e17e9ae61eed052c24053ffbe38f77e8 (accessed 20 june 2014).
- [50] Bandrés I, Meler S, Giner B, Cea P and Lafuente C. Aggregation Behavior of Pyridinium-Based Ionic Liquids in Aqueous Solution. *Journal of Solution Chemistry* 2009; 38(12) 1622–1634. http://download.springer.com/static/pdf/452/art%253A10.1007%252Fs10953-009-9474-4.pdf?auth66=1411567558_b17d415dc75888d39ea783a8e8c0204a&text=.pdf (accessed 20 june 2014).
- [51] Yang Z. Hofmeister effects: an explanation for the impact of ionic liquids on biocatalysis. *Journal of Biotechnology* 2009; 144(1) 12–22. http://ac.els-cdn.com/S0168165609001801/1-s2.0-S0168165609001801-main.pdf?_tid=a0c02c2a-4261-11e4-8e37-00000aab0f26&acdnat=1411394960_6a1f3a58a47b84f37d512945bf611cd7 (accessed 20 june 2014).
- [52] Para G, Jarek E and Warszynski P. The Hofmeister series effect in adsorption of cationic surfactants--theoretical description and experimental results. *Advances in Colloid and Interface Science* 2006; 122(1–3) 39–55. http://ac.els-cdn.com/S0001868606000960/1-s2.0-S0001868606000960-main.pdf?_tid=ae678490-4261-11e4-b7df-00000aab0f02&acdnat=1411394983_813bf4649ce13503fd07c1f1c9abc88b (accessed 20 june 2014).
- [53] Blesic M, Swadźba-Kwaśny M, Holbrey JD, Canongia Lopes JN, Seddon KR and Rebelo LPN. New cationic surfactants based on 1-alkyl-3-methylimidazolium alkylsulfonates, [C(n)H(2n+1)mim][C(m)H(2m+1)SO(3)]: mesomorphism and aggregation. *Physical Chemistry Chemical Physics* 2009; 11(21) 4260–4268. <http://pubs.rsc.org/en/content/articlepdf/2009/cp/b822341f> (accessed 20 june 2014).
- [54] Liu X, Dong L and Fang Y. A Novel Zwitterionic Imidazolium-Based Ionic Liquid Surfactant: 1-Carboxymethyl-3-Dodecylimidazolium Inner Salt. *Journal of Surfactants and Detergents* 2011; 14(4) 497–504. <http://download.springer.com/static/pdf/391/art%253A10.1007%252Fs11743-011-1254-7.pdf?>

- auth66=1411567659_8bcf8cade91e8eef39d3ea2ed52f6499&ext=.pdf (accessed 20 june 2014).
- [55] Shirota H, Mandai T, Fukazawa H and Kato T. Comparison between Dicationic and Monocationic Ionic Liquids: Liquid Density, Thermal Properties, Surface Tension, and Shear Viscosity. *Journal of Chemical & Engineering Data* 2011; 56(5) 2453–2459. <http://pubs.acs.org/doi/pdf/10.1021/jc2000183> (accessed 20 june 2014).
- [56] Bhargava BL and Klein ML. Nanoscale organization in aqueous dicationic ionic liquid solutions. *The Journal of Physical Chemistry B* 2011; 115(35) 10439–10446. <http://pubs.acs.org/doi/pdf/10.1021/jp204413n> (accessed 20 june 2014).
- [57] Ao M, Xu G, Zhu Y and Bai Y. Synthesis and properties of ionic liquid-type Gemini imidazolium surfactants. *Journal of Colloid and Interface Science* 2008; 326(2) 490–495. http://ac.els-cdn.com/S0021979708007881/1-s2.0-S0021979708007881-main.pdf?_tid=f99e2220-4261-11e4-bc0a-00000aacb362&acd-nat=1411395109_c14772825c644e961e08c17c919282e9 (accessed 20 june 2014).
- [58] Ao M, Huang P, Xu G, Yang X and Wang Y. Aggregation and thermodynamic properties of ionic liquid-type gemini imidazolium surfactants with different spacer length. *Colloid and Polymer Science* 2008; 287(4) 395–402. http://download.springer.com/static/pdf/463/art%253A10.1007%252Fs00396-008-1976-x.pdf?auth66=1411567752_d6c85de25a8b836da32e38f7d5bbb097&ext=.pdf (accessed 20 june 2014).
- [59] Zhang S, Yan H, Zhao M and Zheng L. Aggregation behavior of gemini pyrrolidine-based ionic liquids 1,1'-(butane-1,4-diyl)bis(1-alkylpyrrolidinium) bromide ([C(n)py-4-C(n)py][Br₂]) in aqueous solution. *Journal of Colloid and Interface Science* 2012; 372(1) 52–57. http://ac.els-cdn.com/S0021979712000732/1-s2.0-S0021979712000732-main.pdf?_tid=17ff90d2-4262-11e4-97a1-00000aacb360&acd-nat=1411395160_b21b0b96bdd41b34bc9582e2c05b0169 (accessed 20 june 2014).
- [60] Anouti M, Sizaret PY, Ghimbeu C, Galiano H and Lemordant D. Physicochemical characterization of vesicles systems formed in mixtures of protic ionic liquids and water. *Colloids and Surfaces A: Physicochemical and Engineering Aspects* 2012; 395, 190–198. http://ac.els-cdn.com/S092777571100776X/1-s2.0-S092777571100776X-main.pdf?_tid=2801b4b0-4262-11e4-ae0c-00000aab0f6b&acd-nat=1411395187_a1ede5895f18ea100dcb996762c7b0d8 (accessed 20 june 2014).
- [61] He Y, Sun L, Fang D, Han C, Liu C and Luo G. Aggregation behaviour and thermodynamics of mixed micellization of 1-hexadecylpyridinium bromide and ionic liquid in ethylene glycol/water binary mixtures. *Colloid Journal* 2014; 76(1) 96–103. http://download.springer.com/static/pdf/750/art%253A10.1134%252FS1061933X14010062.pdf?auth66=1411567841_684083ddc93f7003bb8a8cbda8fe740d&ext=.pdf (accessed 20 june 2014).

- [62] Shi L, Li N and Zheng L. Aggregation Behavior of Long-Chain N-Aryl Imidazolium Bromide in a Room Temperature Ionic Liquid. *The Journal of Physical Chemistry C* 2011; 115(37) 18295–18301. <http://pubs.acs.org/doi/pdf/10.1021/jp206325d> (accessed 20 june 2014).
- [63] Muller N. Temperature dependence of critical micelle concentrations and heat capacities of micellization for ionic surfactants. *Langmuir* 1993; 9(1) 96–100. <http://pubs.acs.org/doi/pdf/10.1021/la00025a022> (accessed 20 june 2014).
- [64] Pal A, Datta S, Aswal VK and Bhattacharya S. Small-angle neutron-scattering studies of mixed micellar structures made of dimeric surfactants having imidazolium and ammonium headgroups. *The Journal of Physical Chemistry B* 2012; 116(44) 13239–13247. <http://pubs.acs.org/doi/pdf/10.1021/jp304700t> (accessed 20 june 2014).
- [65] Shimizu S, Pires PAR and El Seoud OA. Thermodynamics of micellization of benzyl(2-acylaminoethyl)dimethylammonium chloride surfactants in aqueous solutions: a conductivity and titration calorimetry study. *Langmuir* 2004; 20(22) 9551–9959. <http://pubs.acs.org/doi/pdf/10.1021/la048930%2B> (accessed 20 june 2014).
- [66] Vaghela NM, Sastry NV and Aswal VK. Effect of additives on the surface active and morphological features of 1-octyl-3-methylimidazolium halide aggregates in aqueous media. *Colloids and Surfaces A: Physicochemical and Engineering Aspects* 2011; 373(1–3) 101–109. http://ac.els-cdn.com/S0927775710006023/1-s2.0-S0927775710006023-main.pdf?_tid=c090af56-4262-11e4-a20a-00000aacb35f&acdnat=1411395443_9ea09b6945a1c2a8c4b16f72d6a9f2c0 (accessed 20 june 2014).
- [67] Beesley A. Evidence for the essential role of hydrogen bonding in promoting amphiphilic self-assembly: measurements in 3-methylsyrnone. *The Journal of Physical Chemistry* 1988; 92(3) 791–793. <http://pubs.acs.org/doi/pdf/10.1021/j100314a039> (accessed 20 june 2014).
- [68] Bakshi M. Cetylpyridinium chloride–tetradecyltrimethylammonium bromide mixed micelles in ethylene glycol–water and diethylene glycol–water mixtures. *Journal of the Chemical Society, Faraday Transactions* 1997; 1(22) 4005–4008. <http://pubs.rsc.org/en/content/articlepdf/1997/ft/a703310i> (accessed 20 june 2014).
- [69] Lu J, Liotta CL and Eckert CA. Spectroscopically Probing Microscopic Solvent Properties of Room-Temperature Ionic Liquids with the Addition of Carbon Dioxide. *The Journal of Physical Chemistry A* 2003; 107(19) 3995–4000. <http://pubs.acs.org/doi/pdf/10.1021/jp0224719> (accessed 20 june 2014).
- [70] Katritzky AR, Fara DC, Yang H, Tamm K, Tamm T and Karelson M. Quantitative measures of solvent polarity. *Chemical Reviews* 2004; 104(1) 175–198. <http://pubs.acs.org/doi/pdf/10.1021/cr020750m> (accessed 20 june 2014).
- [71] Laurence C, Nicolet P, Dalati MT, Abboud JLM and Notario R. The Empirical Treatment of Solvent-Solute Interactions: 15 Years of pi.* *The Journal of Physical Chemis-*

- try 1994; 98(23) 5807–5816. <http://pubs.acs.org/doi/abs/10.1021/j100074a003> (accessed 20 june 2014).
- [72] Kamlet M, Abboud J and Taft R. The solvatochromic comparison method. 6. The pi.* scale of solvent polarities. *Journal of the Americal Chemical Society* 1977; 99(18) 6027–6038. <http://pubs.acs.org/doi/pdf/10.1021/ja00460a031> (accessed 20 june 2014).
- [73] Domańska U, Pobudkowska A and Rogalski M. Surface tension of binary mixtures of imidazolium and ammonium based ionic liquids with alcohols, or water: cation, anion effect. *Journal of Colloid and Interface Science* 2008; 322(1) 342–350. http://ac.els-cdn.com/S0021979708001689/1-s2.0-S0021979708001689-main.pdf?_tid=71847c2a-4263-11e4-8162-00000aab0f6b&acd-nat=1411395740_d447ea0b9c9deefd209a1401fce3eea4 (accessed 20 june 2014).
- [74] Zhang G, Chen X, Zhao Y, Xie Y and Qiu H. Effects of alcohols and counterions on the phase behavior of 1-octyl-3-methylimidazolium chloride aqueous solution. *The Journal of Physical Chemistry B* 2007; 111(40) 11708–11713. <http://pubs.acs.org/doi/pdf/10.1021/jp074945f> (accessed 20 june 2014).
- [75] Chen X, Wang J, Shen N, Luo Y and Li L. Gemini surfactant/DNA complex monolayers at the air-water interface: Effect of surfactant structure on the assembly, stability, and topography of monolayers. *Langmuir* 2002; 18(16) 6222–6228. <http://pubs.acs.org/doi/pdf/10.1021/la025600l> (accessed 20 june 2014).
- [76] Li W, Zhang Z, Zhang J, Han B, Wang B, Hou M and Xie Y. Micropolarity and aggregation behavior in ionic liquid+organic solvent solutions. *Fluid Phase Equilibria* 2006; 248(2) 211–216. http://ac.els-cdn.com/S0378381206003657/1-s2.0-S0378381206003657-main.pdf?_tid=9ed383e2-4263-11e4-8957-00000aab0f01&acd-nat=1411395816_96dcdb47eb803d3c373e93dcf181084e (accessed 20 june 2014).
- [77] Huang JB, Mao M and Zhu BY. The surface physico-chemical properties of surfactants in ethanol–water mixtures. *Colloids and Surfaces A: Physicochemical and Engineering Aspects* 1999; 155(2–3) 339–348. http://ac.els-cdn.com/S0927775799000035/1-s2.0-S0927775799000035-main.pdf?_tid=ac6bbfa6-4263-11e4-9881-00000aacb35f&acd-nat=1411395839_dc9750acc22465e92f5d9b452fb9d98e (accessed 20 june 2014).
- [78] Feng Q, Wang H, Zhang S and Wang J. Aggregation behavior of 1-dodecyl-3-methylimidazolium bromide ionic liquid in non-aqueous solvents. *Colloids and Surfaces A: Physicochemical and Engineering Aspects* 2010; 367(1–3) 7–11. http://ac.els-cdn.com/S0927775710003298/1-s2.0-S0927775710003298-main.pdf?_tid=b796a1ca-4263-11e4-8c64-00000aacb361&acd-nat=1411395857_0813d2ebb63401b6744ba1f390c60c32 (accessed 20 june 2014).
- [79] Seguin C, Eastoe J, Heenan RK and Grillo I. SANS studies of the effects of surfactant head group on aggregation properties in water/glycol and pure glycol systems. *Journal of Colloid and Interface Science* 2007; 315(2) 714–720. <http://ac.els-cdn.com/S0021979707009708/1-s2.0-S0021979707009708-main.pdf>

- _tid=c5a01f76-4263-11e4-8182-00000aab0f27&acd-nat=1411395881_3fd4fe417e129db78522b2dc7f42a4c4 (accessed 20 june 2014).
- [80] Yan J, Wang D, Bu F and Yang FF. Investigation of the Thermodynamic Properties of the Cationic Surfactant CTAC in EG+Water Binary Mixtures. *Journal of Solution Chemistry* 2010; 39(10) 1501–1508. http://download.springer.com/static/pdf/954/article%253A10.1007%252Fs10953-010-9551-8.pdf?auth66=1411568526_6be695fca7a6f1fe42931520ef39c87a&ext=.pdf (accessed 20 june 2014).
- [81] Takamuku T, Honda Y, Fujii K and Kittaka S. Aggregation of imidazolium ionic liquids in molecular liquids studied by small-angle neutron scattering and NMR. *Analytical sciences* 2008; 24(10) 1285–1290. https://www.jstage.jst.go.jp/article/analsci/24/10/24_10_1285/_pdf (accessed 20 june 2014).
- [82] Remsing RC, Liu Z, Sergeyev I and Moyna G. Solvation and aggregation of *n,n'*-dialkylimidazolium ionic liquids: a multinuclear NMR spectroscopy and molecular dynamics simulation study. *The Journal of Physical Chemistry B* 2008; 112(25) 7363–7369. <http://pubs.acs.org/doi/pdf/10.1021/jp800769u> (accessed 20 june 2014).
- [83] Singh T, Rao KS and Kumar A. Effect of ethylene glycol and its derivatives on the aggregation behavior of an ionic liquid 1-butyl-3-methyl imidazolium octylsulfate in aqueous medium. *The Journal of Physical Chemistry B* 2012; 116(5) 1612–1622. <http://pubs.acs.org/doi/pdf/10.1021/jp211537m> (accessed 20 june 2014).
- [84] Pino V, Yao C and Anderson JL. Micellization and interfacial behavior of imidazolium-based ionic liquids in organic solvent-water mixtures. *Journal of Colloid and Interface Science* 2009; 333(2) 548–556. http://ac.els-cdn.com/S0021979709002240/1-s2.0-S0021979709002240-main.pdf?_tid=1abc385a-4264-11e4-92cf-00000aacb35e&acd-nat=1411396024_5353fe76f417b1334a274d487b8c9e92 (accessed 20 june 2014).

Thermal Behaviour of Pure Ionic Liquids

Elena Gómez, Noelia Calvar and
Ángeles Domínguez

Additional information is available at the end of the chapter

<http://dx.doi.org/10.5772/59271>

1. Introduction

The interest in ionic liquids (ILs) that has developed during in the past few decades is well-recognized. This interest has developed mainly due to their special properties such as high thermal stability, high electrical conductivity, high heat capacity per unit volume, wide temperature range in a liquid state, good solvent properties and especially their negligible vapour pressure, which render them popular compounds. This popularity is reflected in the great deal of publications that relate the potential applications of ILs in different fields, among which can be highlighted their use as solvents, electrochemical applications and more recently, as heat transfer fluids.

In order to use the ILs at an industrial scale, deep knowledge of their thermophysical properties is vital, since these properties not only determine the equipment size needed, but also directly influence its design parameters; for example, melting and glass transition temperatures are needed to set a feasible temperature operation range and heat capacity is essential for estimating the heat exchange in unit operations, as well as heat storage capacity. Moreover, knowledge of these thermophysical properties, such as freezing, melting, cold crystallization, glass transition temperatures and heat capacities, allows for better understanding the stabilities and structures of these relatively new compounds.

In the extensive literature dealing with thermophysical properties of pure ILs, different authors have applied various methodologies and equipment for the study of the thermal behaviour of ILs and for the determination of their heat capacities. This has led to discovering discrepancies in these literature values. For this reason, special attention must be paid to experimental procedures and to the different factors affecting the determination of these properties. Recently, differential scanning calorimetry (DSC) has been widely used for the determination of these properties due to its simplicity and because only a small sample is required. For all of

the above-mentioned factors, a suitable working protocol for the correct determination of phase transition temperatures and heat capacities using DSC will be described in this chapter.

Nowadays, there are enough experimental data available in the literature concerning the thermal analysis and heat capacities of pure ionic liquids, which allows for drawing general conclusions about the influence of the structure of ionic liquids on these thermophysical properties. As such, the main behaviours of ionic liquids as found in the literature will be described and analysed in this chapter, together with the influence of the structures of the ionic liquids (cation, anion and alkyl-side chains of the cation) on their heat capacities.

In addition, different methods for the estimation of melting and glass transition temperatures, as well as heat capacities can be found in the literature; the basis of these methods, as well as some applications for estimating the thermal properties of IL will be presented. The extension of the selected database for these methods and their average deviation will be compared.

2. Thermal analysis

Thermal analysis allows for establishing the behaviour of a material when it is heated or cooled. The structure of a material undergoes changes such as melting and freezing when it is subjected to changes in temperature. In the case of ionic liquids, this process is necessary not only because most ionic liquids are new substances and therefore have unknown properties, but also because their applicability is conditioned to their liquid state.

Regarding the interpretation of the thermal analyses, in this chapter, melting temperature (T_m) was taken as the onset of an endothermic peak (downward deflection of the curve peak) upon heating, freezing temperature (T_f) as the onset of an exothermic peak (upward deflection of the curve peak) upon cooling, cold crystallization temperature (T_{cc}) as the onset of an exothermic peak upon heating from a subcooled liquid state to a crystalline solid state, solid-solid transition (T_{ss}) as the onset of an exothermic or endothermic peak upon heating from a crystalline solid state and glass transition temperature (T_g) as the midpoint of a small heat capacity change upon heating from the amorphous glass state to a liquid state.

2.1. Methodology

Although thermal analysis is a widely known technique applied for studying the thermal behaviour of substances, there are several factors that affect the determination of transition temperatures. Among these, the most important are sample size, the thermal history of the sample and the cooling and heating rate of the scan. Nowadays, the most used technique for the thermal analysis of pure ionic liquids is differential scanning calorimetry (DSC). Hence, in this section, an adequate work methodology using DSC is described as attending to all of the above-mentioned factors in an attempt to standardize the thermal analysis determination. Standardization of the work methodology is important for comparing data obtained from different authors, since the research studies available in the existing literature do not always state their applied methods in detail. Below, the suggested work methodology is described:

i. Sample preparation.

- a. **Sample amount.** The sample amount recommended for a study on phase transitions is approximately 4-8 mg, since the sample amount is directly related to the peak size (the greater the sample size the greater the signal); however, the resolution will be lower and overlapped effects may appear. For this reason, for the determination of transition temperatures, it is recommended that a small sample size is used.
- b. **Weighing.** Considering that the sample weight is directly related to the accuracy of the measurement, it is vital to use a balance with a precision of at least ± 0.00001 g. Additionally, since the DSC technique uses a reference crucible, it is advisable that the mass of both crucibles (sample and reference) is as similar as possible.
- c. **Crucibles.** Most of the thermal transitions are perfectly determined with a standard aluminium crucible. With this technique, it is possible to work with the crucible open (without lid) or to have it hermetically sealed. It is recommended that hermetically sealed crucibles be used, because in this way, heat flow caused by evaporation is avoided and radiation emitted by the sealed sample and reference crucible, are similar. In addition, when working with sealed crucibles there is the possibility of making a pinhole in the lid to avoid a pressure increase inside the crucible.
- d. **Sample placement.** Besides the usual conditions applied in any experimental measurement, careful attention should be paid to sample placement, which should be done in a manner that facilitates good contact between the sample and the crucible bottom.

ii. Method.

- a. **Dry step.** Due to the known influence of the water amount and impurities present in the properties of ILs, it is necessary to subject the sample to a previous drying step. Therefore, the sample should be heated at a temperature high enough to evaporate water and impurities; for instance, a suggested dry step will be to maintain the sample at $T = 120^{\circ}\text{C}$ for 30 minutes inside the furnace. A good way to know the dryness degree of the sample is to weigh the sample before and after the dry step.
- b. **Thermal history.** Various materials present different thermal effects, depending on their thermal history; this thermal history can be eliminated by subjecting the sample to a previous heating. For this reason, the working protocol must begin with a heating of the sample to eliminate its thermal history which could lead to incorrect results. Note that if the dry step is carried out inside the furnace of the DSC, the thermal history of the ionic liquid will be eliminated.
- c. **Heating and cooling rate.** This is the most important factor in any thermal analysis, as crystallization transitions strongly depend on the cooling and heating rate (low rates can give the ionic liquid time enough to form crystals).

Due to the special nature of ionic liquids, variations upon heating and cooling rates are useful for studying their thermal transitions. Taking into account that at fast rates the phase transition peaks can appear overlapped, while at slow rates these peaks can move apart from each other, a recommended practice is to begin the study of a sample by a scan carried out at a relatively slow heating rate of 2°C/min to gain better information about the thermal behaviour of the sample, including whether the ionic liquid is a crystal or a glass former, the presence of polymorphs, etc.

Taking into account all of the above-mentioned factors, the proposed work methodology for the thermal analysis of pure ionic liquid is explained below.

1. **Dry step.**
2. **First cooling and heating cycle.** The thermal analyses start with a “slow method” consisting of a cooling cycle from 120°C to -140°C, followed by a heating cycle from -140°C to 120°C at 2°C/min. The chosen start and end temperatures are 120°C and -140°C, respectively, because the usual behaviour of ionic liquids shows that in case the IL presents a glass transition, this transition will appear at low temperatures and the ILs will not present transitions above 120°C. It is important for the correct characterization of the thermal behaviour of ILs to reach temperatures low enough to observe the possible apparition of a glass transition. This is why, in the literature, many studies remain incomplete, because in their temperature range the cooling cycle began at room temperature and the heating cycle also ends at room temperature.
3. **Complementary cycles.** Depending on the transitions appearing in the first cooling and heating cycle, for a complete and correct characterization of the sample, other heating and cooling cycles should be carried out. If only a T_g appears in the slow method, the study of the thermal behaviour of this IL is completed and it can be concluded that the studied ionic liquid shows a strong tendency for forming glass. However, if the slow method shows that the ionic liquid presents any other transition but does not present a glass transition, the sample is subjected to a faster cooling or quenching to avoid crystallization. This cooling can be performed in different ways: by cooling the sample from 120°C to -140°C at 40°C/min, followed by a heating cycle, or by introducing the sample into liquid nitrogen to achieve rapid fast cooling. The problem lies in the scans where the association between peaks and phase transition is not clear. At this point, a customized protocol should be proposed.
4. **Study of polymorphic behaviours.** Following on, an approach to the study of an ionic liquid presenting polymorphic behaviour will be discussed with the help of Figure 1. As can be observed, this IL did not form crystals upon cooling at 2°C/min, while upon heating, the IL presented a T_g and T_{cc} at -90°C and -70°C, respectively. These two transitions were easily assigned; the peaks with difficult interpretation were those placed between -35°C and -20°C, which is typical in polymorphic compounds. The peak appearing at -35°C is an endothermic transition; however, it is unclear whether this peak represents a solid-solid or a melting transition. The next peak (which are actually two peaks overlapped)

may have been caused by the melting of different crystals or by a solid-solid transition followed by a melting, or by a melting followed by a recrystallization, which immediately melted. In order to assign with certain reliability these peaks to their corresponding transitions, further experimentation has to be conducted. To answer the first question, a run with a different heating rate that aims to determine whether this peak disappears or moves will be useful; in case it moves, the melting transition is not probable and it can be stated that represents a solid-solid transition (in general, the formation of a metastable crystal). Once confirmed that the first peak corresponds to a solid-solid transition, the second peak can be more easily interpreted. This peak can be associated with the melting of the metastable crystal, which occurs with the recrystallization of a stable crystal that finally melts. In cases like this example, if further cooling and heating rates do not yield better information, it will be necessary to use techniques such as X-ray diffraction. This example shows the importance of subjecting the IL to different heating and cooling rates in order to interpret the thermograms.

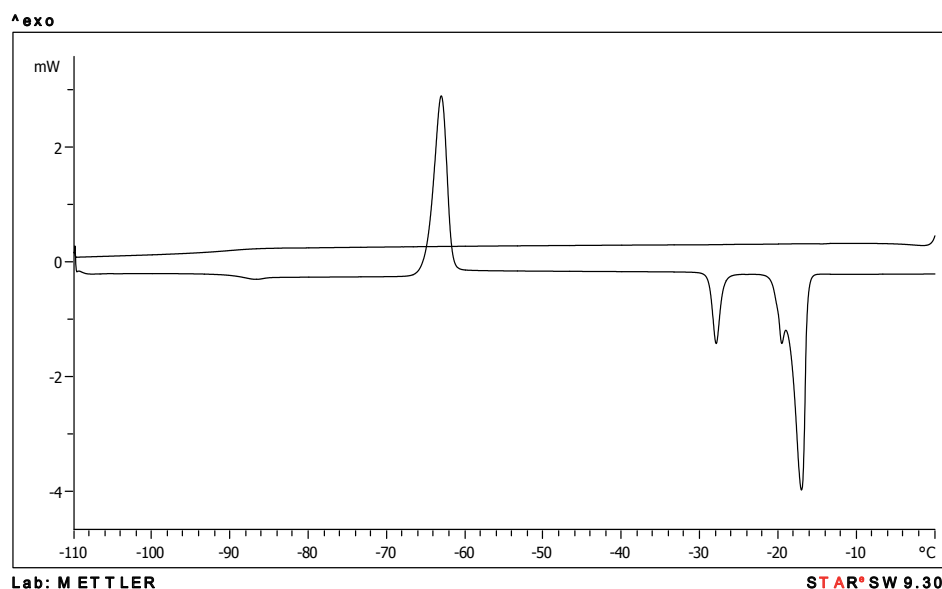


Figure 1. Thermogram of the ionic liquid BMpyrNTf₂ cooling from 120°C to -140°C, followed by heating from -140°C to 120°C at 2°C/min.

It is remarkable that in this example, there was only one solid-solid transition (endothermic), but it is usual in polymorphic ionic liquids that several solid-solid transitions, endothermic and/or exothermic, are present, which increases the difficulty of the interpretation of DSC curves.

In Table 1 below, the transition temperatures observed by several authors for the IL BMpyrNTf₂ are presented. Here, the disparities within the results taken from literature obtained using different methods for the same IL are reflected.

Ref.	T _g / °C	T _{cc} / °C	T _{ss} / °C	T _{ss} / °C	T _m / °C	T _m / °C
1	-87 ^a	-55		-24	-18	
2	-85 ^b	-53		-30	-18	
	-85 ^b	-53				-7
3	-92 ^c	-69	-47			-11
	-87 ^c	-56		-34	-21	
	-87 ^c	-56		-34	-21	-11
4						-6
5	-87 ^d	-53			-18	

^a taken as the onset of the transition upon heating

^b taken as the midpoint of the transition upon heating

^c not stated

^d taken as the midpoint of the transition upon cooling

Table 1. Transition temperatures for the IL BMpyrNTf₂ obtained by several authors.

MacFarlane et al. [1] determined in their study the phase transitions of the IL BMpyrNTf₂ by heating at 10°C/min after quenching from the liquid state; Kunze et al. [2] obtained similar results with a similar method (heating at 10°C/min after quenching at 40°C/min from 40°C to -150°C) and by changing the cooling rate to 2°C/min, determined a T_m = -7°C without detecting a solid-solid transition. The most extensive study on thermal analysis for this ionic liquid was carried out by Stefan et al. [3], who performed three different methods for fully characterizing the IL and found three types of crystals. In the paper published by Kunze et al. [4], the researchers only registered the melting transition by cooling the sample at 20°C/min and heating it at 10°C/min. Finally, Jin et al. [5] reported similar values than those presented in [1] and [2], but did not report the solid-solid transition. The method used by these authors was first a heating cycle to 80°C, followed by a cooling to -150°C at 10°C/min and a final heating cycle to 80°C at 10°C/min. The DSC experimental results shown in Table 1 indicate, as expected, that phase transitions were dependent on the scanning rate and on the cooling method used to obtain the solid phase (quenching or slow cooling).

Finally, it is not always possible to correctly identify the different transitions appearing in a thermogram of a polymorphic ionic liquid using DSC. The techniques that can be used to achieve a clear interpretation are those attached to the DSC, such as crossed polarizing filters or a microscope, as well as techniques that are carried out separately such as X-ray diffraction and infrared spectrometry.

2.2. Types of thermal behaviours of ILs

In this part of the chapter, the main types of thermal behaviours found for ILs are described. In general, in the literature [6-10], these behaviours are divided into three groups:

- i. The first type of behaviour is formed by ionic liquids characterized by presenting only the formation of amorphous glass.

- ii. The second type of behaviour is characterized by presenting a freezing transition, forming crystals upon cooling and a melting transition upon heating.
- iii. The third type of behaviour that appears in ILs does not show a tendency to crystallize upon cooling; however, upon heating, cold crystallization is exhibited.

The thermal behaviour of ILs is not directly related to their structure; for this reason, some examples of ILs presenting each of the three thermal behaviours above will be presented, in a way to explain how ionic liquids with different structures present the same behaviour and ionic liquid with similar structures present different behaviours.

- i. As mentioned above, the first type of behaviour is characterized by no true phase transitions, but only the formation of an amorphous glass. The ILs included in this type do not have melting or freezing points, only glass transition temperatures. These ILs are good glassy-formers, which indicates that they present a weak tendency for crystallization. Several examples of ILs presenting this behaviour can be found in the literature, among them BMimBF₄ [10], BMMimPF₆ [10], C₃CNMimDCA [8], BMpyNTf₂ [6], EMpyESO₄ [6], BMpyBr [6], PMimNTf₂ [11], HMimDCA [11] and PMpyNTf₂ [12]. Taking into account that the glass transitions of ILs usually appear at low temperatures, it is important to work at temperatures as low as -120°C. The glass transition appears both in the cooling and in the heating cycles; when a glass transition temperature for an IL is given, the cycle where it is observed (cooling or heating) must be specified. Figure 2 shows a thermogram for PMpyNTf₂ at a cooling and heating rate of 10°C/min; this IL is characterized by the presence of only a glass transition. In the following section, the influence of the cooling and heating rate on this phase transition temperature will be discussed.

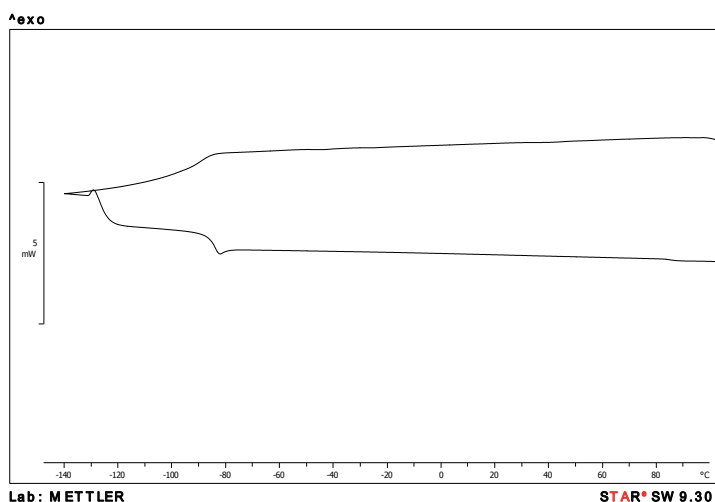


Figure 2. Thermogram of the ionic liquid PMpyNTf₂ [12] cooling from 120°C to -140°C, followed by heating from -140°C to 120°C at 10°C/min.

- ii. The ILs presenting a freezing transition upon cooling and a melting transition upon heating belong to the second type of behaviour. These ILs present a strong tendency for forming crystals. However, there are ILs that in other cooling conditions will undergo a glass transition. To test their tendency to form crystals, these ILs should be subjected to a faster cooling rate to avoid crystallization; this methodology was adopted for the present study, as was indicated in the previous section. Generally, in these ILs freezing temperatures are markedly lower than melting temperatures, an effect known as supercooling. The ILs EMimNTf₂ [11], BmPyTfO [12], BMimTfO [12], EMpyNTf₂ [12], HMimTfO [11], EMMimNTf₂ [10], C3CNTMANTf₂ [8] and BpyBr [6] are examples of ILs presenting this behaviour. In Figure 3, a typical thermogram for this type of behaviour is presented.

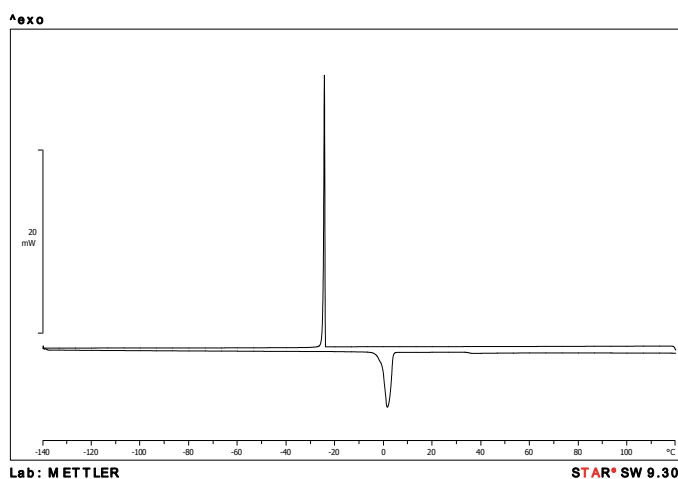


Figure 3. Thermogram of the ionic liquid EMpyNTf₂ [12] cooling from 120°C to -140°C, followed by heating from -140°C to 120°C at 2°C/min.

- iii. The ILs that do not form crystals upon cooling, but present a glass transition at low temperatures and upon heating, and that first suffer a glass transition followed by a cold crystallization to finally melt, are included in the third type of behaviour. The subcooling phenomenon (cold crystallization) is usually associated with polymers and other amorphous materials, and is present in the thermal behaviour of many ionic liquids. Among the ILs belonging to this group are BMimNTf₂ [11], HMimNTf₂ [11], BMimDCA [10,12], EMimNTf₂ [10], BMimPF₆ [10], BMMimBF₄ [10], HpyNTf₂ [6] and C3CNMMimPF₆ [8]. In Figure 4 below, the typical scan for this third behaviour is illustrated.

Note that the three behaviours explained above are the simplest behaviours that can be found in the study of ionic liquids, since the polymorphism phenomenon can be found on ILs included in the second and third groups. This phenomenon deserves careful attention, because the association between peaks and transitions is not always clear. It is noteworthy that an IL

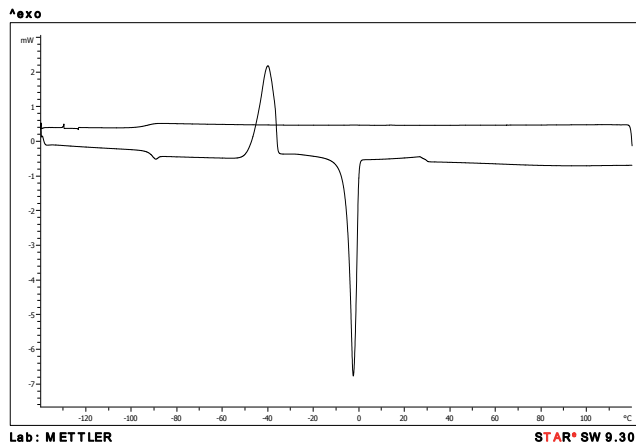


Figure 4. Thermogram of the ionic liquid BMimDCA [12] cooling from 120°C to -140°C, followed by heating from -140°C to 120°C at 2°C/min.

belonging to a certain group and subjected to different conditions can become part of a different group. Figure 5 below illustrates how the ionic liquid BMpyTFO, belonging to the second group, when subjected to a cooling and heating rate of 2°C or 10°C/min becomes an IL belonging to the third group when it is quenched.

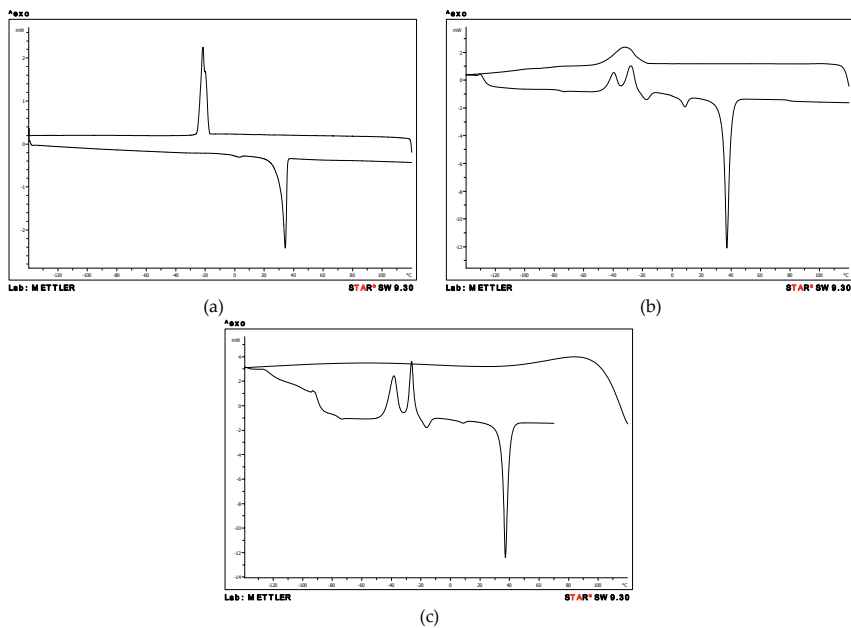


Figure 5. Thermogram of the ionic liquid BMpyTFO [12] cooling from 120°C to -140°C, followed by heating from -140°C to 120°C at (a) 2°C/min; (b) 10°C/min; (c) cooled by quenching at 40°C/min and heated at 10°C/min.

2.3. Influence of the rate on phase transitions

In Figure 6, a thermal scan of the ionic liquid PMpyNTf₂ at cooling and heating rates of 2°C/min and at 10°C/min is presented as an example of the effect of the cooling and heating rate on the glass transition. As can be seen, an increase in the rate leads to higher glass transition temperatures, both upon cooling and heating.

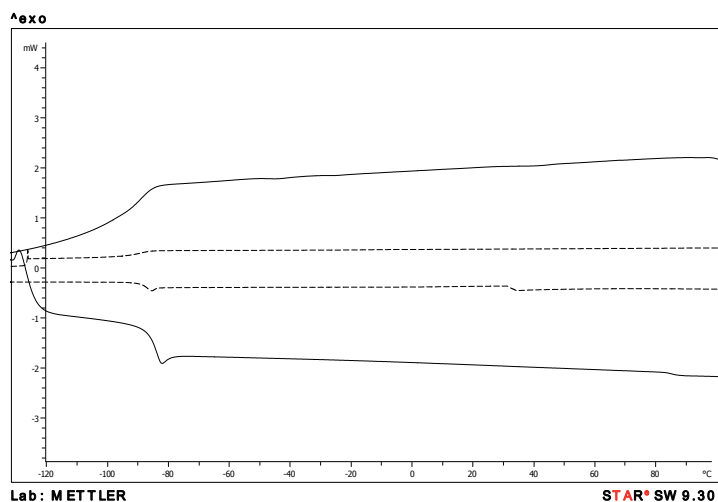


Figure 6. Thermogram of the ionic liquid PMpyNTf₂ [12] cooling from 120°C to -140°C, followed by heating from -140°C to 120°C at 2°C/min (dashed line) and at 10°C/min (solid line).

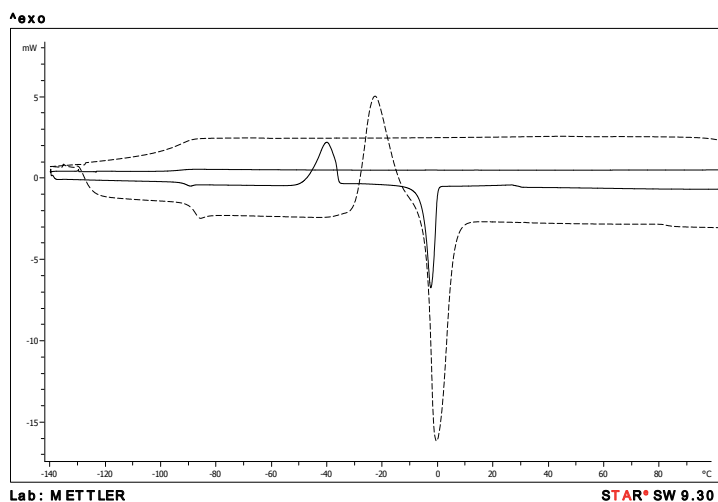


Figure 7. Thermogram of the ionic liquid BMimDCA [12] cooling from 120°C to -140°C, followed by heating from -140°C to 120°C at 2°C/min (solid line) and at 10°C/min (dashed line).

Figure 7 shows the influence of the heating rate on T_g , T_{cc} and T_m . In this example, it can be observed that an increase in the heating rate caused the cold crystallization transition to shift to a higher temperature. Here it can also be seen that, as previously explained in the work methodology section, by increasing the scan rate the cold crystallization and melting peaks overlapped.

As expected, the scan rate did not affect the melting temperature since, as is well-known, the melting temperature of a certain crystal does not change along with the heating rate.

Regarding the influence of cooling rate on the freezing transition, it must be taken into account that nucleation and crystal growth are somehow probabilistic events; thus, the determination of the freezing temperature is not always reproducible. This means that for an IL that suffers freezing upon cooling, when performing the same method for the same IL sample, the freezing peak might not occur at the same temperature.

3. Heat capacities

Heat capacity (c_p) is defined as the amount of energy required to raise the temperature of 1 g (or 1 mole) of a substance by 1 K. From this definition, it can be inferred that heat capacity is an important property for estimating the heating and cooling requirements of a substance and is therefore vital for the application of ILs in industrial applications.

In order to analyse the heat capacity values published in the literature for pure ionic liquids, several factors need to be taken into account. On determining heat capacities, different apparatuses can be used, such as adiabatic calorimeters (AC), differential scanning calorimeters (DSC), modulated DSC (MDSC) or Tian-Calvet DSC (TC). For the determination of the heat capacities of ionic liquids, a desirable characteristic in the technique used is for a small amount of IL to be enough for the determination of its heat capacity. In this context, the DSC and MDSC use much smaller samples than the adiabatic calorimeter or Tian-Calvet DSC. Between these two calorimeters, the MDSC has the advantage that it permits the separation of the signals into their thermodynamic and kinetic components, separating overlapped effects.

In the past few years, due to the simplicity of the technique and the small amount of sample required, DSC has been widely used in the determination of heat capacities. With this technique, different methods can also be followed, i.e., those directly calculating c_p values, the direct and the steady state methods, methods using a reference for calculating the sample c_p , as well as the ADSC and the sapphire methods. The sapphire method is more frequently used due to its higher accuracy [11].

Besides the experimental technique and method used, other variables should be considered for analysing heat capacity values. Among these variables that can affect the experimental values are sample size, the mass of the different crucibles used for the sample and as reference, the interval in which the measurement is carried out and the heating rate; these factors should be considered in addition to the usual considerations concerning the purity and dryness of the ionic liquid sample.

In this section, a proper methodology for the determination of heat capacities of ionic liquids using DSC with the sapphire method is suggested and the influence of the structure of the ionic liquid on this property is discussed.

3.1. Research methodology

As different techniques and methods have been used in the literature for the experimental determination of heat capacities and especially because in many of these studies not all the variables have been stated, the comparison among the values from different studies is particularly difficult. Consequently, taking into account the different aspects that need to be considered, a research methodology for the determination of heat capacities of pure ILs using differential scanning calorimetry and the sapphire method is proposed. A brief description of the sapphire method is provided here to gain a better understanding of the research methodology: in the sapphire method, the DSC signal of the sample was compared with the DSC signal of the calibration sample (sapphire), which had a known specific heat. A total of three measurements were needed for this method: blank measurement (empty crucible), sapphire measurement and the sample measurement.

- i. Sample preparation.
 - a. **Weighing.** The accuracy of the weighing is very important in any measurement of heat capacity; it is vital to carry out all weighing in a precise balance. In the case of the sapphire method, an error in the weighing step will affect the weight of the sample, sapphire and reference crucibles, dramatically increasing uncertainty in the measurement of the heat capacities.
 - b. **Sample size.** It is believed that for the determination of heat capacities, the bigger the sample amount the better, since the signal size is proportional to the sample amount; nevertheless, it should be taken into account that the sapphire method uses a reference compound for the determination of c_p . This means that more reliable results will be obtained when the sample signal is closer to the reference signal (sapphire signal). The differences in the chosen sample size by different authors may be an explanation for the different values obtained for heat capacity for the same ionic liquid. In summary, the quantity of sapphire and sample size should be chosen for yielding signals as close as possible (within the limits recommended for the determination of c_p in the DSC, usually 40-80 mg); therefore, it was desirable that all weighing results involved in the experimental determination of this property were given in the studies.
 - c. **Crucibles.** The crucibles used for the sample, sapphire and as reference must be in perfect condition, without deformations, especially at the bottom. The use of a pinhole in the lid avoids pressurization inside the crucible and allows the evaporation of water and/or impurities in the dry step.

To minimize errors, it is advisable that the weight of the three crucibles used for each measurement (sample, sapphire and reference) be as similar as possible.

- d. **Sample placement.** Good contact between the sample and the crucible bottom must be assured.
- ii. Method. For the determination of heat capacities using the sapphire method, an initial isothermal stage (usually 10-15 minutes), followed by the heating stage to a final temperature, at which point there is another isothermal stage (usually 10-15 minutes), is common practice.
 - a. **Dry step.** Similar to the thermal analysis method, a previous dry step is advised prior to the determination of the heat capacities of a pure ionic liquid.
 - b. **Temperature range.** With regards to taking the c_p values, it must be taken into account that after the initial isothermal segment, some time is needed for the sample to reach a state of dynamic equilibrium; hence, the results obtained at the beginning of the dynamic segment should be discarded. It is also advised that the temperature range does not exceed 90°C. The heat capacity should not be determined during first order transitions in the physical state, for example during a crystallization transition. With the sapphire method, it is recommended that the heat capacities of the liquid and solid states be determined in separate runs, i.e., melting temperature should not be included in the chosen temperature range of the method.
 - c. **Heating rate.** A heating rate of 10°C/min was usually used in the classical c_p measurements; however, nowadays, a heating rate of 20°C/min is generally used as this yields good results and saves time.
 - d. **Repetition of measurements.** It is advisable practice to repeat the heat capacity measurements and to take the mean value as the final result.
 - e. **Sapphire sample.** Although the crucible with the sapphire disks can be used in several runs, its c_p values must be checked regularly.

In general, the more common method for the determination of c_p in the literature consists of an isothermal segment at 0°C for 15 minutes, followed by a dynamic segment from 0°C to 90°C at 20°C/min and a final isothermal segment at 90°C for 15 minutes (considering that the IL is liquid in this range). Since the most required c_p value is a value corresponding to 25°C and taking into account that the first part of the dynamic segment is needed to reach a state of dynamic equilibrium, a method in which the temperature ranges from -15°C to 75°C (again considering that the IL is liquid in this stage) will assure obtaining a reliable value at 25°C.

3.2. Influence of the structure of the IL on heat capacity

Taking all the variables in the determination of heat capacities into account and analysing the c_p literature data for different structures, the influence of the cation, anion and alkyl-side chain of the cation on this property can be analysed. Due to the different techniques and methods used in literature and as mentioned above, the fact that many variables are not usually specified in the corresponding papers, to gain an overview of the influence of the ionic liquid structure

on this property it is more reliable to compare values obtained by the same authors instead of using different sources.

Heat capacity provides information about the amount of energy per molecule that the compound can store before the temperature of the compound increases; this energy is stored in translational, vibrational and rotational modes. As such, it is logical to assume that a molecule containing more atoms will have more energy storage modes and thus, higher heat capacity. Taking this into consideration, the following is an analysis of the influence of the different variables such as the different structures of the ionic liquids and the temperature on the heat capacity values.

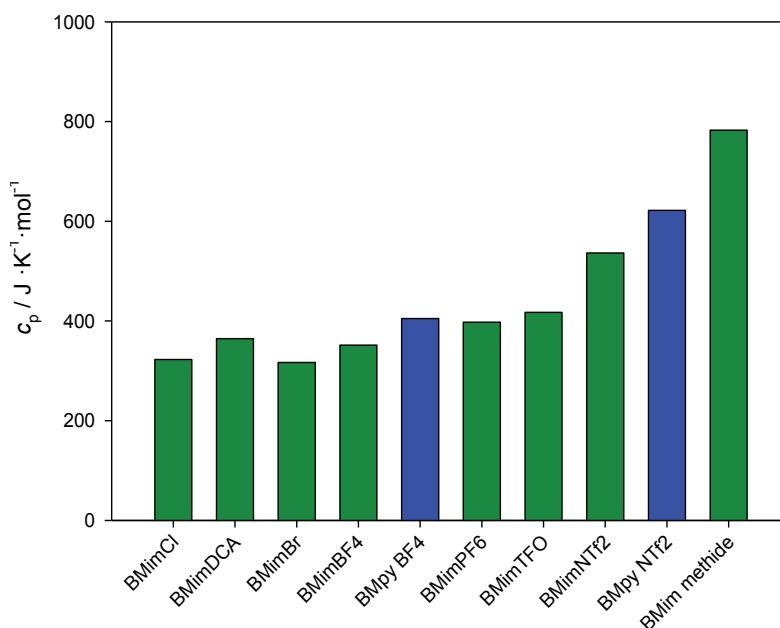


Figure 8. Heat capacities of several ionic liquids.

Considering the influence of the anion in the ionic liquid on heat capacity values, from the literature, it could be inferred that the c_p values were clearly affected by the anion, the general trend being that the higher the molar mass or number of atoms of the anion, the higher the heat capacity [6,10,11,13]. In general, the anions more frequently studied are bromide, chloride, tetrafluoroborate, hexafluorophosphate, trifluoromethanesulfonate, dicyanamide and bis(trifluoromethylsulfonyl)imide, usually attached to imidazolium-based ionic liquids, of which there is the most extensive data in the literature. The limited studies of pyridinium and pyrrolidinium-based ionic liquids usually agree with the results obtained for the wider studies on imidazolium ILs. In summary, for ILs containing similar cations and alkyl-side chains of the cation, the values for heat capacities increase with the molar mass of the anions [6,10], despite the fact that there are studies indicating that this general trend is not always followed [14].

The influence of the structure of the cation has been less studied than the influence of the anion; however, it can nonetheless be concluded that the pyridinium and pyrrolidinium-based ionic liquids present higher heat capacities than analogous imidazolium-based ILs [12, 15]. However, unlike the influence of the anion and alkyl-side chain length of the cation, which many studies have observed, in this case, the need for new experimental data in order to draw better conclusions was clear. In Figure 8, the influence of the anions on the c_p values of the 1-butyl-3-methylimidazolium and 1-butyl-3-methylpyridinium-based ionic liquids is presented, showing that in general, the c_p values increased when the molar mass of the anion increased. Comparisons of the ionic liquids with different cations (BMpyNTf₂/BMimNTf₂ and BMpyBF₄/BMimBF₄) can also be observed.

In the case of the influence of the alkyl-side chain length of the cation, the experimental results from published works indicate that the addition of a $-\text{CH}_2-$ group leads to an incremental increase in the c_p of approximately 30-35 J/K mol [11,13,16], a similar value to that found for liquid alkanes, indicating that the alkyl-side chains of the ILs are similar in structure to those in liquid alkanes [16]. Moreover, it can also be concluded that the addition of a $-\text{CH}_2-$ group has more influence at higher temperatures [11,16]. The influence of the alkyl-side chain length of the cation in the ionic liquid for 1-alkyl-3-methylimidazolium-based ionic liquids with alkyl = ethyl, butyl, hexyl and octyl on the c_p values is plotted in Figure 9, where it can be observed that an increase in the alkyl-side chain length means an increase in c_p values.

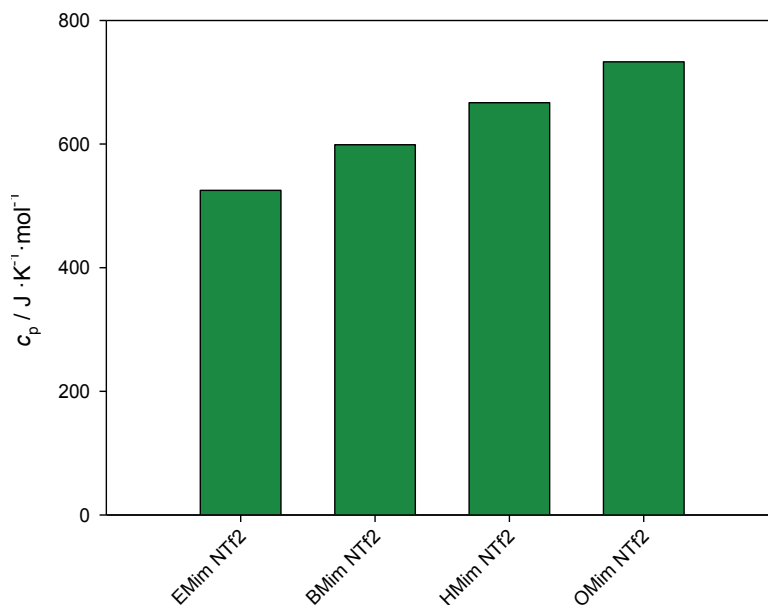


Figure 9. Heat capacities of 1-alkyl-3-methylimidazolium bis(trifluoromethylsulfonyl)imide ionic liquids.

Finally, regarding the fitting of heat capacity values as a function of temperature, these values are generally adjusted to a polynomial expression, usually of a second, third or even fourth

degree, depending on the temperature range taken for their determination. For example, if the temperature range of the method ranges from 0°C to 90°C and the c_p values are taken from 0°C to 90°C, it is probable that a third or fourth degree polynomial expression can be used for the fitting; however, if the c_p values are taken from 20°C to 80°C (neglecting the first minutes to avoid stabilization errors), a first or second degree polynomial expression will provide a proper fitting.

4. Thermal properties estimation

Due to the broad number of ILs, the experimental determination of the thermal properties of all these compounds is not possible; consequently, in order to enhance the selection of task-specific ionic liquids, several methods for estimating the melting temperature, the glass transition temperature or the liquid heat capacity of ILs have been developed, most of them based on the use of quantitative structure-property relationships (QSPR) or on group contribution (GC) methods. The following is a brief description of these methods and their application to T_m , T_g and c_p .

4.1. QSPR and GC methods

4.1.1. QSPR methods

QSPR methods are based on the relationship between the molecular characteristics of a compound and its macroscopic properties. Molecular descriptors, used for characterizing the microscopic properties of compounds, along with experimental data of the property (T_m , T_g , c_p , etc.) for a large number of compounds are needed in order to obtain an expression that will allow for predicting the value of this property for different compounds. A large number of descriptors exist for characterizing molecules; thus, the selection of the more significant among them is one of the main drawbacks of the model. These molecular descriptors, usually calculated using software packages such as DRAGON and CODESSA, can be classified using quantum chemical, electronic and geometrical descriptors that provide information about polar- or hydrogen-bonding interactions, as well as constitutional descriptors that characterize the chemical composition of the molecule and that does not depend on geometric and topological descriptors (TIs) that take into consideration the connectivity of atoms within a molecule [17]. In order to find essential information about molecule structure, a geometric optimization is generally the first stage. The general equation for QSPR methods [17] can be written as:

$$y_0 = b_0 + b_1x_1 + b_2x_2 + \dots + b_px_p \quad (1)$$

where y is the dependent variable (e.g., T_m , T_g or c_p), x_1, x_2, \dots, x_p are the independent variables (the descriptors), b_1, b_2, \dots, b_p are the regression coefficients and b_0 is the intercept.

The quality of the experimental values selected for developing a model is essential for obtaining good results. The main criteria for selecting the experimental values for the data set are the number and the diversity of available data, and these should have been measured under the same conditions, with enough reproducibility and accuracy [17]. The selected data are divided in the training set to develop and train the correlation equation and the test set for determining the predictive ability of the model for compounds that have not been used to develop it.

In order to obtain the relationship between molecular descriptors and the macroscopic property, several models such as neural networks (NN), decision trees, partial least squares (PLS) and multiple linear regressions (MLR) are usually employed. The squared correlation coefficients, R^2 , squared cross-validated correlation coefficients R^2_{CV} and the Fisher criterion value, F , are generally used to assess the quality of the model. Special care must be taken for data points that have been poorly predicted, because this can indicate that the data were incorrectly measured or that the model has failed to include some important characteristics of the compounds [18].

4.1.2. Group contribution methods

Other methods widely used for the estimation of thermal properties are GC methods, which assume that a molecule is formed by several functional groups and the properties of a compound can be estimated as the sum of the contributions of all the functional groups that form the molecule. The contribution of each group to a property (e.g., T_m , T_g or c_p) is obtained from the experimental data of this property and determined for other substances that contain the same functional group. The main problem of this approach is that the way in which it defines groups is not unique; this is the reason why different authors have defined different groups to represent the same compound. Regarding ILs, some GC methods take the imidazolium or pyridinium rings as a group, whereas others divide the ring into many CH and N groups. According to Wu and Sandler [19] the geometry of the functional group should be the same, regardless of the molecule in which the group appears; it should have the same charge in all molecules and it should be the smallest identity into which the molecule can be divided in electroneutral groups. The general form of these methods [20] can be written as:

$$y = \left(\sum_i m_i D_i \right)^a + \left(\sum_j n_j E_j \right)^b + \left(\sum_k p_k F_k \right)^c \quad (2)$$

where y is the dependent variable (e.g., T_m , T_g or c_p), D , E and F are the contribution of the functional groups of order 1, 2 and 3, respectively and m , n and p are the times that groups i , j and k appear in the compound. When $a = b = c = 1$ the model is linear; when any of these numbers are zero, the corresponding contribution is not taken into consideration and if they are other values, the contributions are nonlinear. In the first-order GC methods, the groups behaved as if they were isolated and the effect of neighbour groups was not considered. In the second order GC methods, some information about the molecular structure was included with the purpose of including proximity effects and differentiating among isomers. The third level was

more convenient for the estimation of properties in the case of complex heterocyclic or large poly-functional acyclic compounds [20].

A summary of some of the QSPR and GC models were developed for the estimation of melting points, glass transition temperature and the heat capacity of ILs, and is presented below.

4.2. Melting point estimation

ILs are characterized by their low melting temperatures that depend on the strength of the crystal lattice, which is controlled by several factors such as charge distribution on the anions, H-bonding ability, the symmetry of the ions and the van der Waals interactions. Since it is an important property in the potential applications of ILs, several methods of melting temperature estimation can be found in the literature, most of them based on QSPR methods.

4.2.1. QSPR methods

The first attempt to predict the melting temperature of ILs was made by Katritzky et al. [21]. From a database of 126 pyridinium bromides and optimizing only the cationic part, they developed a six-descriptor equation, obtaining a value of $R^2 = 0.788$. According to the authors, the most significant descriptors were, the indices reflecting the coordination ability of the cation, the average nucleophilic reactivity index for the N atom related to electrostatic intermolecular interactions and the total entropy per atom related to the difference in conformational and rotational degrees of freedom in solid and liquid phases. Many other models [22-29] have been developed for several families of ILs (Table 2), most of them for imidazolium-based ILs with the same anion; consequently, their range of application is quite limited.

A different approach in the selection of the ILs was made by López-Martin et al. [30]. In this case, 22 ILs with the same cation, the 1-ethyl-3-methylimidazolium and 22 different anions were chosen, and the cation and anion geometries were optimized. The main disadvantages of this approach are that the cation-anion interactions are not taken into consideration and that the geometry optimizations correspond to the gas phase. The nine selected descriptors quantify the influence of size, branching, charge distribution and symmetry of the anion, as was previously reported for the cation. In order to test the effectiveness of this approach ($R^2 = 0.955$), a new data set including 62 ILs with 22 different cations and 11 different anions was correlated and a six-descriptor equation ($R^2 = 0.869$) was proposed.

Varnek et al. [31] performed an exhaustive study of QSRP models for melting temperature calculation. A data set with 717 bromides of nitrogen containing organic cations (126 pyridinium bromides, 384 imidazolium and benzimidazolium bromides, as well as 207 quaternary ammonium bromides) with melting temperatures from 5°C to 320°C was selected and results obtained using different machine-learning methods (associative neural networks, support vector machines, k nearest neighbours, modified version of the partial least-squares analysis, backpropagation neural network and multiple linear regression), while different types of descriptors were analysed. The study concluded that the most efficient descriptors/methods combination depends on the data set used. Slightly better results were obtained with neural networks and support vector machine methods, regardless of the chosen parameters. Regard-

ing the descriptors, the study concluded that the performance of the descriptors depends both on the machine learning method and the data set.

Structures	No. of ILs	No. of parameters	R ²	Ref.
Pyridinium bromides	126	6	0.7883	21
Imidazolium bromides	57	5	0.7445	22
Imidazolium bromides	29	5	0.7517	22
Imidazolium bromides	18	3	0.9432	22
Benzimidazolium bromides	45	5	0.6899	22
N-pyridinium bromides	126	5	0.790	23
Tetraalkyl-ammonium bromides	75	6	0.775	23
(n-Hydroxyalkyl)-trialkyl-ammonium bromides	34	5	0.716	23
1-substituted 4-amino-1,2,4-triazolium nitrocyanamides	7	1	0.960	24
1-substituted 4-amino-1,2,4-triazolium bromides	13	3	0.914	25
1-substituted 4-amino-1,2,4-triazolium nitrates	13	3	0.933	25
Imidazolium hexafluoroborates	29	6	0.9207	26
Imidazolium tetrafluoroborates	19	3	0.9047	26
Imidazolium bromides	30	4	0.89	27
Imidazolium chlorides	20	3	0.88	27
Imidazolium bromides and imidazolium chlorides	50	4	0.88	27
Pyridinium bromides, imidazolium bromides, benzimidazolium bromides and 1-substituted 4-amino-1,2,4-triazolium nitrates	288	8	0.810	28
Guanidinium chlorides, guanidinium bromides, guanidinium iodides and guanidinium tetraphenylborate	101	92	0.815	29

Table 2. Some QSPR models for the estimation of melting temperature.

For the purpose of ensuring a reliable prediction for a broad range of ionic liquids, the melting temperature of 705 ILs including sulfonium, ammonium, pyridinium, 1,3-dialkyl imidazolium, tri-alkyl imidazolium, phosphonium, pyrrolidinium, double imidazolium, 1-alkyl imidazolium, piperidinium, pyrrolidine, oxazolidinium, amino acids, guanidinium, morpholinium, isoquinolinium and tetra-alkyl imidazolium was collected by Farahani et al. [32]. The final proposed equation ($R^2 = 0.658$) contained 12 descriptors, eight of them describing the characteristics of the cation and the other four the characteristics of the anion.

Yan et al. [33] proposed an equation using topological indices based on atom characters (atom radius, atom electronegativity, etc.) and atom positions in the hydrogen suppressed molecule

structure. The data set was composed of 394 ILs: 120 imidazolium, 43 benzimidazolium, 109 pyridinium, 19 pyrrolidinium, 65 ammonium, seven sulfonium, 20 triazolium and 11 guanidinium. The resulting equation incorporates 12, 14 and six TIs for the cation, the anion and their interaction, respectively, the obtained value being $R^2 = 0.778$ for the training set and 0.753 for the test set.

4.2.2. Group contribution methods

A group contribution method for the calculation of melting temperatures of ILs was developed by Huo et al. [34] for 155 imidazolium and benzimidazolium ILs. The structural groups, up to a total of 30, were selected in a way that rendered them as small as possible and considering three group types: belonging to a ring, belonging to a no-ring structure and ionic groups. In addition to the structural groups, three characteristic factors were included: (1) σ , which took the values 0 or 1, depending on whether the groups connected to a N atom in an imidazolium ring were the same or different; (2) τ , which was the number of ring groups in the molecule; (3) δ , which could be 0 if there was no group attached to the C2 position in the imidazolium group or 1 if one group was attached. The average relative deviation in this work was 5.86% and deviations of less than 5% were obtained for 106 ILs. The maximum relative deviation was 32.75% for 1,3-dimethylimidazolium chloride.

Using a first-order contribution approach and considering the whole ring as a single group, another group contribution method was proposed by Lazzús [35] using a set of 400 ILs. The group contribution to the melting point was calculated for 31 groups for the cation and 32 groups for the anion, and covered a broad range of ILs. The average relative absolute deviation reported was less than 8% for the 200 ILs used for the group parameters calculation and less than 6% for the other 200 ILs used in the prediction stage.

The most comprehensive melting temperature database was collected by Gharagheizi et al. [36] in order to amplify a GC model with a broad range of applicability. The melting temperature of 799 ILs including 1,3-dialkylimidazolium, 1-alkyl imidazolium, amino acids, ammonium, double imidazolium, guanidinium, isoquinolinium, morpholinium, oxazolidinium, phosphonium, piperazinium, piperidinium, pyridazinium, pyridinium, pyrrolidinium, pyrroline, quinary alkyl imidazolium, sulfonium, tetra-alkyl imidazolium, tetrazolium, thiazolium, tri-alkyl imidazolium, triazolium and uronium was collected and the group contribution for 80 groups (31 anions and 49 cations) were calculated. Some of these groups were not structural groups, because they were defined as the "sum of all the carbons belonging to any aromatic and heteroaromatic structure" (group 6) or the "total number of Ns, Os and Fs in the molecule, excluding N with a formal positive charge, higher oxidation states and pyrrolyl forms of N" (group 13), among others [36, p. 3]. The absolute average relative deviation was 5.82%.

Recently, Valderrama [37] reviewed some of the models proposed for the estimation of melting point [34, 36, 38] and concluded that the experimental determination of melting temperature should be standardized in order to guarantee reproducibility, and further emphasized that even if the data were accurate, none of the present methods serve as a clear solution to the problem of predicting the melting temperatures of ILs.

4.3. Glass transition estimation

Glass transition can be defined as the transition of an amorphous material from a hard and relatively brittle state into a molten or rubber-like state. This transition is accompanied by changes in some properties such as heat capacity and thermal expansibility. Even though many ILs present only glass transition, few models have been developed for their estimation compared to melting temperature. The QSPR and GC methods available in the literature are summarized below.

4.3.1. QSPR methods

Some QSPR-based models for predicting the T_g of ILs have been reported in the literature. Many of them were developed for predicting the glass transition temperature of one family of ILs such as ammonium [39] or 1,3- dialkylimidazolium [40, 41]. In these cases, the T_g is calculated as the sum of the contribution of the anion and the cation, and their corresponding descriptors are included in $T_{g,a}$ and $T_{g,c}$ terms:

$$T_g = \text{intercept} + T_{g,a} + T_{g,c} \quad (3)$$

The model developed for ammonium-based ILs [39] contains 12 descriptors (six for the cation and six for the anion) obtained from the experimental data of 73 ILs (22 different anions and 49 different cations) and the reported R^2 value is 0.9657.

A database of 109 1,3- dialkylimidazolium ILs was selected by Mousavisafavi et al. [40, 41] to develop two models applying both a linear and a nonlinear approach for the selection of the molecular descriptors; similar results were obtained in both cases. The best value of R^2 was 0.91, achieved using the nonlinear approach.

A more general equation was developed by Mirkhani et al. [42] and included 139 ILs (37 different anions and 86 different cations including alkylimidazolium, amino acids guanidinium, isoquinolinium, morpholinium, oxazolidinium, phosphonium, piperidinium, pyrrolidinium and triazolium) in the database. They proposed an equation with 11 descriptors ($R^2 = 0.8897$), three descriptors for the anion and eight descriptors for the cation. The highest and lowest prediction errors, 8.29% and 1.67%, belonged to 1-alkyl imidazolium and oxazolidinium, respectively.

Similar to the estimation of T_m , Yan et al. [43] implemented a QSPR model based on topological indices (TIs) for T_g calculation. A total of 139 ILs including 63 imidazolium, 17 pyridinium, 48 ammonium, seven sulfonium and four triazolium were taken from the literature to develop the model. The resulting expression contained seven TIs for the cation, 16 TIs for the anion and two TIs for their interaction; the overall value for R^2 (0.898) was very close to the value obtained using other descriptors [42].

4.3.2. Group contribution methods

To date, three GC models have been proposed for T_g estimation. One of them is only suitable for 1,3-dialkylimidazolium ionic liquids [44], while the other two [45,46] are appropriated for many types of ILs. In all cases, the IL ring (imidazolium, pyridinium pyrrolidinium, etc.) is considered as a group. The general equation can be written as:

$$T_g = T_{g0} + \sum_{i=1}^{N_a} N_{ai} T_{gai} + \sum_{i=1}^{N_c} N_{ci} T_{gci} \quad (4)$$

where N_{ai} and N_{ci} are the occurrence of the i group in the cation and in the anion, T_{gai} and T_{gci} are the contributions of the group i and T_{g0} is the intercept.

From a data set of 496 ionic liquids (71 anions and 247 cations), Gharagheizi et al. [45] calculated the group contribution parameters for 19 anions and 31 cations. Similar to the method proposed for estimating T_m [36], some of the considered groups were not structural groups. The average absolute relative deviation obtained for the complete data set was 3.65%. Concurrently, Lazzús [46] published another GC model using 150 ILs and proposed the group interaction parameters for 26 cation and 36 anion groups. The average absolute relative deviation reported for the total set was 4.91%. None of these papers provide any indication of the criteria applied to the selection of the groups.

4.4. Heat capacity estimation

Knowledge concerning the heat capacity of ILs is important because of its relationship with other thermodynamic properties i.e., entropy, enthalpy and Gibbs free energy, and also due to the application of ILs in industrial processes or as heat transfer fluids. A brief summary of the c_p estimation methods is presented below.

The relationship between c_p and molar volume has been stated by several authors and some expressions for the calculation of c_p at 25°C have been developed [47, 48]. Including the temperature as a variable, Paulechka et al. [49] proposed another equation that allows to calculate the c_p values at other temperatures.

The only method based on QSPR found in the literature was proposed by Sattari et al. [50]. A database containing the c_p values of 82 ILs including 39 different cations and 24 anions was used to find the most accurate model with an acceptable number of descriptors. In the final 13-parameter equation, a binary combination of two descriptors instead of a single descriptor was included in equation 1. On the basis of the R² values for the training set and the test set (0.990, 0.996), the authors suggest that binary multiplication of the descriptors can be a successful approach.

The first GC method for the estimation of c_p of ILs was developed by Gardas and Coutinho [48] using a second-order group additivity approach. The database was composed of 19 ILs that permitted the calculation of the group contribution parameters for four cations and six anions. According to the authors, these group parameters made it possible to calculate the c_p of at least

200 ILs and in almost all cases, the deviations in predicted heat capacities were inferior to the experimental uncertainties. The group contribution parameters were subsequently extended to amino acid-based ILs by Gardas et al. [51].

Ge et al. [13] adapted the Joback [52, 53] GC method for the prediction of the ideal gas heat capacities of molecular compounds to the estimation of c_p of ILs. From the ideal gas heat capacities and using an estimation method [54] to calculate the critical properties and the acentric factor, the c_p can be calculated. The original parameters [52], along with the parameters calculated for three new groups (B, P, -SO-), were used to predict the c_p of 53 ILs, leading to a relative absolute deviation of 2.9%.

A different approach to the estimation of c_p using a GC method was proposed by Valderrama et al. [55] and combines the group contribution method with mass connectivity indices, which considers the type of connection between groups and the mass of these groups. In order to build a more general method, the database employed for determining the value of the contribution of the groups included 32 ILs of five families (imidazolium, pyridinium, pyrrolidinium, phosphonium and alkyl-ammonium) and 126 organic compounds. The average absolute deviation values were 2.8% in the correlation of the 32 ILs and the 126 organic compounds, and 2.1% in the c_p prediction of nine ILs.

The temperature dependency of c_p for several ions was calculated using a quadratic equation by Müller and Albert [56]:

$$Cp_{ion} = A + BT + CT^2 \quad (5)$$

$$Cp_{IL} = \sum_{i=cations} x_i Cp_i + \sum_{j=anions} x_j Cp_j \quad (6)$$

where A , B and C are the parameters of the anion or cation and x_i and x_j are the molar contributions of the cation or anion on all cations or anions, respectively. The parameters were calculated for 39 cations and 32 anions from a database of 84 ILs. The average absolute deviation was 1.4% and 4.4% for the training set and the test set, respectively.

In addition to the model previously mentioned [50], Sattari et al. [57] presented another model for calculating c_p using a set of parameters such as the number of atoms, of non-h-atoms and of five-membered rings. Four of these 14 parameters were the same as those selected in the QSPR-based model. The average absolute deviation for the 82 ILs included in the database was 1.68%.

For the purpose of deriving an easy-to-use correlation based on very simple molecular parameters, Farahani et al. [58] proposed a correlation equation that only depends on the atom counts in both anion and cation, the number of hydrogen in anions and the number of methyl groups in the cation. In this case, the absolute average relative deviation reported by the authors was 2.48%.

5. Conclusions

Although the use of DSC for the thermal analysis and the experimental determination of the heat capacities of pure ionic liquids is a widely-used technique, there are several factors that have an influence on their correct determination. For this reason, in this chapter, not only was a work methodology proposed for the determination of both phase transition temperatures and heat capacities, but the possible aspects affecting their experimental determination have also been explained.

Attempting to standardize the work methodology is necessary for obtaining high quality and precision-based experimental data, as well as for carrying out comparisons between the results presented by different authors, which will allow for reliable conclusions.

Due to the different results observed in the thermal analysis of the pure ILs characterized thus far, finding a relationship between the structure of the IL and its thermal behaviour is complicated. For this reason, in this chapter, the thermal behaviour of pure ILs was divided into three types, depending on the phase transitions presented by each IL:

- i. The first type of behaviour is formed by ionic liquids characterized by presenting only the formation of amorphous glass.
- ii. The second type of behaviour is characterized by presenting a freezing transition, forming crystals upon cooling and a melting transition upon heating.
- iii. The third type of behaviour in the ILs that does not show a tendency to crystallize upon cooling; however, upon heating, they exhibit cold crystallization.

It is important to state that ionic liquids usually present polymorphic-like behaviour, increasing the difficulty of interpreting the DSC thermograms. Additionally, the phase transitions are strongly dependent on the scanning rate and on the cooling method used to obtain the solid phase (quenching or slow cooling).

The relatively extensive database on the heat capacities of pure ILs allows for drawing some conclusions about the influence of the structure of the ionic liquid on heat capacity values. The c_p values are clearly affected by the nature of the anion, the general trend being that the higher the molar mass or number of atoms of the anion, the higher the heat capacity. In the case of the influence of the structure of the cation, although it has been less studied than the influence of the anion, it can be concluded that pyridinium and pyrrolidinium-based ionic liquids present higher heat capacities than their analogous imidazolium-based ILs. As for the influence of the alkyl-side chain length of the cation, the addition of a $-\text{CH}_2-$ group leads to an incremental increase in the c_p of approximately 30-35 J/K mol and this influence is more remarkable at higher temperatures.

Finally, regarding the estimation of the melting and glass transition temperatures, and liquid heat capacities, although several methods for estimating the thermal properties of ILs can be found in the literature, most of them are based on the use of quantitative structure-property relationship (QSPR) or on group contribution (GC) methods; all of them present several

limitations, which can be attributed to two aspects: all experimental data have not been correctly determined and/or our knowledge of the factors that influence thermal properties is incomplete. A bigger effort should be made from both experimental and academic perspectives to improve the estimation of these properties.

Nomenclature of ionic liquids

EMimNTf ₂	1-ethyl-3-methylimidazolium bis(trifluoromethylsulfonyl)imide
EMMimNTf ₂	1-ethyl-2,3-dimethylimidazolium bis(trifluoromethylsulfonyl)imide
PMimNTf ₂	1-propyl-3-methylimidazolium bis(trifluoromethylsulfonyl)imide
BMimNTf ₂	1-butyl-3-methylimidazolium bis(trifluoromethylsulfonyl)imide
BMimBF ₄	1-butyl-3-methylimidazolium tetrafluoroborate
BMimTFO	1-butyl-3-methylimidazolium triflate
BMimDCA	1-butyl-3-methylimidazolium dicyanamide
BMimPF ₆	1-butyl-3-methylimidazolium hexafluorophosphate
BMimCl	1-butyl-3-methylimidazolium chloride
BMimBr	1-butyl-3-methylimidazolium bromide
BMim methide	1-butyl-3-methylimidazolium methide
BMMimBF ₄	1-butyl-2,3-dimethylimidazolium tetrafluoroborate
BMMimPF ₆	1-butyl-2,3-dimethylimidazolium hexafluorophosphate
C ₃ CNMimDCA	1-butyronitrile-3-methylimidazolium dicyanamide
C ₃ CNMMimPF ₆	1-butyronitrile-2,3-dimethylimidazolium hexafluorophosphate
HMimNTf ₂	1-hexyl-3-methylimidazolium bis(trifluoromethylsulfonyl)imide
HMimDCA	1-hexyl-3-methylimidazolium dicyanamide
HMimTFO	1-hexyl-3-methylimidazolium triflate
EMpyESO ₄	1-ethyl-3-methylpyridinium ethylsulfate
BpyBr	1-butylpyridinium bromide
PMpyNTf ₂	1-propyl-3-methylpyridinium bis(trifluoromethylsulfonyl)imide
BMpyNTf ₂	1-butyl-3-methylpyridinium bis(trifluoromethylsulfonyl)imide
BMpyBr	1-butyl-3-methylpyridinium bromide
BMpyTFO	1-butyl-3-methylpyridinium triflate
BMpyBF ₄	1-butyl-3-methylpyridinium tetrafluoroborate
HMpyNTf ₂	1-hexylpyridinium bis(trifluoromethylsulfonyl)imide
BMpyrNTf ₂	1-butyl-1-methylpyrrolidinium bis(trifluoromethylsulfonyl)imide
C ₃ CNTMANTf ₂	butyronitrile-trimethylammonium bis(trifluoromethylsulfonyl)imide

Acknowledgements

E. Gómez is grateful to the Xunta de Galicia for financial support through the “Axudas de Apoio á etapa inicial de formación posdoutoral”.

Author details

Elena Gómez, Noelia Calvar and Ángeles Domínguez*

*Address all correspondence to: admiguez@uvigo.es

Department of Chemical Engineering, University of Vigo, Campus Lagoas-Marcosende, Vigo, Spain

References

- [1] MacFarlane D.R., Meakin P., Sun J., Amini N., Forsyth M. Pyrrolidinium Imides: A New Family of Molten Salts and Conductive Plastic Crystal Phases. *The Journal of Physical Chemistry B* 1999; 103: 4164-4170.
- [2] Kunze M., Jeong S., Paillard E., Winter M., Passerini S. Melting Behavior of Pyrrolidinium-Based Ionic Liquids and Their Binary Mixtures. *The Journal of Physical Chemistry C* 2010;114: 12364-12369.
- [3] Stefan C.S., Lemordant D., Biensan P., Siret C., Claude-Montigny B. Thermal Stability and Crystallization Of N-Alkyl-N-Alkyl'-Pyrrolidinium Imides. *Journal of Thermal Analysis and Calorimetry* 2010; 102: 685-693.
- [4] Kunze M., Montanino M., Appetecchi G.B., Jeong S., Schönhoff M., Winter M., Passerini S. Melting Behavior and Ionic Conductivity in Hydrophobic Ionic Liquids. *The Journal of Physical Chemistry A* 2010; 114: 1776-1782.
- [5] Jin H., O'Hare B., Dong J., Arzhantsev S., Baker G.A., Wishart J.F., Benesi A.J., Maroncelli M. Physical Properties of Ionic Liquids Consisting of the 1-Butyl-3-Methylimidazolium Cation with Various Anions and the Bis(trifluoromethylsulfonyl)imide Anion with Various Cations. *The Journal of Physical Chemistry B* 2008; 112: 81-92.
- [6] Crosthwaite J.M., Muldoon M.J., Dixon J.K., Anderson J.L., Brennecke J.F. Phase Transition and Decomposition Temperatures, Heat Capacities and Viscosities of Pyrrolidinium Ionic Liquids. *The Journal of Chemical Thermodynamics* 2005; 37: 559-568.
- [7] Yang M., Zhao J.N., Liu Q.S., Sun L.X., Yan P.F., Tan Z.C., Welz-Biermann U. Low-Temperature Heat Capacities of 1-Alkyl-3-Methylimidazolium Bis(Oxalato)Borate Ionic Liquids and the Influence of Anion Structural Characteristics on Thermodynamic Properties. *Physical Chemistry Chemical Physics* 2011; 13: 199-206.
- [8] Zhang Q., Li Z., Zhang J., Zhang S., Zhu L., Yang J., Zhang X., Deng Y. Physicochemical Properties of Nitrile-Functionalized Ionic Liquids. *The Journal of Physical Chemistry B* 2007; 111: 2864-2872.
- [9] Kulkarni P.S., Branco L.C., Crespo J.G., Nunes M.C., Raymundo A., Afonso C.A.M. Comparison of Physicochemical Properties of New Ionic Liquids Based on Imidazoli-

- um, Quaternary Ammonium, and Guanidinium Cations. *Chemistry – A European Journal* 2007; 13: 8478-8488.
- [10] Fredlake C.P., Crosthwaite J.M., Hert D.G., Aki S.N.V.K., Brennecke J.F. Thermophysical Properties of Imidazolium-Based Ionic Liquids. *Journal of Chemical & Engineering Data* 2004;49: 954-964.
- [11] Gómez E., Calvar N., Domínguez A., Macedo E.A. Thermal Analysis and Heat Capacities of 1-Alkyl-3-Methylimidazolium Ionic Liquids with NTf₂⁻, TFO⁻ and DCA⁻ Anions. *Industrial & Engineering Chemistry Research* 2013; 52: 2103-2110.
- [12] Calvar N., Gómez E., Macedo E.A., Domínguez A. Thermal Analysis and Heat Capacities of Pyridinium and Imidazolium Ionic Liquids. *Thermochimica Acta* 2013; 565: 178-182.
- [13] Ge R., Hardacre C., Jacquemin J., Nancarrow P., Rooney D.W. Heat Capacities of Ionic Liquids as a Function of Temperature at 0.1 MPa. Measurement and Prediction. *Journal of Chemical & Engineering Data* 2008; 53: 2148-2153.
- [14] Yu Y.H., Soriano A.N., Li M.H. Heat Capacities and Electrical Conductivities of 1-Ethyl-3-Methylimidazolium-Based Ionic Liquids. *The Journal of Chemical Thermodynamics* 2009; 41: 103-108.
- [15] Shimizu Y., Ohte Y., Yamamura Y., Tsuzuki S., Saito K. Comparative Study of Imidazolium- and Pyrrolidinium-Based Ionic Liquids: Thermodynamic Properties. *The Journal of Physical Chemistry B* 2012; 116: 5406-5413.
- [16] Paulechka Y.A., Blokhin A.V., Kabo G.J., Strechan A.A. Thermodynamic Properties and Polymorphism of 1-Alkyl-3-Methylimidazolium Bis(triflamides). *The Journal of Chemical Thermodynamics* 2007; 39: 866-877.
- [17] Katritzky A.R., Kuanar M., Slavov S. Hall D., Karelson M., Khan I. Dobchev D.A. Quantitative Correlation of Physical and Chemical Properties with Chemical Structure: Utility for Prediction. *Chemical Reviews* 2010; 110: 5714-5789.
- [18] Le T., Epa V.C., Burden F.R., Winkler D.A. Quantitative Structure-Property Relationship Modeling of Diverse Materials Properties. *Chemical Reviews* 2012; 112: 2889-2919.
- [19] Wu H.S., Sandler, S.I. Use of ab Initio Quantum Mechanics Calculations in Group Contribution Methods. 1. Theory and Basis for Group Identifications. *Industrial & Engineering Chemistry Research* 1991; 30: 881-889.
- [20] van Speybroeck V., Gani R., Meier R.J. The Calculation of Thermodynamic Properties of Molecules. *Chemical Society Reviews* 2010; 39: 1764-1779.
- [21] Katritzky A.R., Lomaka A., Petrukhin R., Jain R., Karelson M., Visser A.E., Rogers R.D. QSPR Correlation of the Melting Point for Pyridinium Bromides, Potential Ionic Liquids. *Journal of Chemical Information and Computer Sciences* 2002; 42: 71-74.

- [22] Katrizky A.R., Jain R., Lomaka A., Petrukhin R., Karelson M., Visser A.E., Rogers R.D. QSPR Correlation of the Melting Point of Potential Ionic Liquids (Imidazolium Bromides and Benzimidazolium Bromides) Using the CODESSA Program. *Journal of Chemical Information and Computer Sciences* 2002; 42: 225-231.
- [23] Eike D.M., Brennecke J.F., Maginn E.J. Predicting Melting Points of Quaternary Ammonium Ionic Liquids. *Green Chemistry* 2003; 5: 323-328
- [24] Trohalaki S., Pachter R. Prediction of Melting Points for Ionic Liquids. *QSAR & Combinatorial Science* 2005; 24: 485-490.
- [25] Trohalaki S., Pachter R., Drake G.W., Hawkins T. Quantitative Structure-Property Relationships for Melting Points and Densities of Ionic Liquids. *QSAR & Combinatorial Science* 2005; 24: 485-490.
- [26] Sun N., He X., Dong K. Zhang X., Lu X., He H. Zhang S. Prediction of the Melting Points for Two Kinds of Room Temperature Ionic Liquids. *Fluid Phase Equilibria* 2006; 246: 137-142.
- [27] Yan C., Han M., Wan H., Guan G. QSAR Correlation of the Melting Points for Imidazolium Bromides and Imidazolium Chlorides Ionic Liquids. *Fluid Phase Equilibria* 2010; 292: 104-109.
- [28] Ren Y., Qin J., Liu H., Yao X., Liu M. QSPR Study on the Melting Points of a Diverse Set of Potential Ionic Liquids by Projection Pursuit Regression. *QSAR & Combinatorial Science* 2009; 28: 1237-1244.
- [29] Carrera G.V.S.M., Branco L.C., Aires-de-Sousa J., Afonso C.A.M. Exploration of Quantitative Structure-Property Relationships (QSPR) for the Design of New Guanidinium Ionic Liquids. *Tetrahedron* 2008; 64: 2216-2224.
- [30] López-Martin I., Burello E., Davey P.N., Seddon K.R., Rothenberg G. Anion and Cation Effects on Imidazolium Salt Melting Points: A Descriptor Modelling Study. *ChemPhysChem* 2007; 8: 690-695.
- [31] Varnek A., Kireeva N. Exhaustive QSPR Studies of a Large Diverse Set of Ionic Liquids: How Accurately Can We Predict Melting Points? *Journal of Chemical Information and Modeling* 2007; 47: 1111-1122.
- [32] Farahani N., Gharagheizi F., Mirkhani S.A., Tumba K. Ionic Liquids: Prediction of Melting Point by Molecular-Based Model. *Thermochimica Acta* 2012; 549: 17-34.
- [33] Yan F., Xia S., Wang Q., Yang Z., Ma P. Predicting the Melting Points of Ionic Liquids by the Quantitative Structure Property Relationship Method Using a Topological Index. *Journal of Chemical Thermodynamics* 2013; 62: 196-200.
- [34] Huo Y., Xia S., Zhang Y., Ma P. Group Contribution Method for predicting Melting Points of Imidazolium and Benzimidazolium Ionic Liquids. *Industrial & Engineering Chemical Research* 2009; 48: 2212-2217

- [35] Lazzús J.A. A Group Contribution Method to Predict the Melting Point of Ionic Liquids. *Fluid Phase Equilibria* 2012; 313: 1-6.
- [36] Gharagheizi F., Ilani-KashKouli P., Mohammadi A.H. Computation of Normal Melting Temperature of Ionic Liquids Using a Group Contribution Method. *Fluid Phase Equilibria* 2012; 329: 1-7.
- [37] Valderrama J.O. Myths and Realities about Existing Methods for Calculation the Melting Temperatures of Ionic Liquids. *Industrial & Engineering Chemistry Research* 2014; 53: 1004-1014.
- [38] Aguirre C.L., Cisternas, L.A., Valderrama J.O. Melting-Point Estimation of Ionic Liquids by a Group Contribution Method. *International Journal of Thermophysics* 2012; 33: 34-46.
- [39] Mirkhani S.A., Gharagheizi F., Ilani-Kashkouli P., Farahani N. An Accurate Model for the Prediction of the Glass Transition Temperature of Ammonium Based Ionic Liquid: A QSPR Approach. *Fluid Phase Equilibria* 2012; 324: 50-63.
- [40] Mousavisafavi S.M., Mirkhani S.A., Gharagheizi F., Akbari J. A Predictive Quantitative Structure-Property Relationship for Glass Transition Temperature of 1,3-Dialkyl Imidazolium Ionic Liquids. Part 1. The Linear Approach. *Journal of Thermal Analysis and Calorimetry* 2013; 111: 235-246.
- [41] Mousavisafavi S.M., Gharagheizi F., Mirkhani S.A., Akbari J. A Predictive Quantitative Structure-Property Relationship for Glass Transition Temperature of 1,3-Dialkyl Imidazolium Ionic Liquids. Part 2. The Nonlinear Approach. *Journal of Thermal Analysis and Calorimetry* 2013; 111: 1639-1648.
- [42] Mirkhani S.A., Gharagheizi F., Ilani-Kashkouli P., Farahani N. Determination of the Glass Transition Temperature of Ionic Liquids: A Molecular Approach. *Thermochimica Acta* 2012; 543: 88-95.
- [43] Yan F., Xia S., Wang Q., Shang Q., Ma P. Predicting the Glass Transition Temperature of Ionic Liquids by the Quantitative Structure Property Relationship Method Using a Topological Index. *Fluid Phase Equilibria* 2013; 358: 166-171.
- [44] Gharagheizi F., Keshavarz M.H., Ilani-Kashkouli P., Farahani N., Tumba K. A Group Contribution Method for Estimation of Glass-Transition Temperature of 1,3-Dialkylimidazolium Ionic Liquids. *Journal of Thermal Analysis and Calorimetry* 2013; 114: 1363-1382.
- [45] Gharagheizi F., Ilani-Kashkouli P., Mohammadi A.H., A Group Contribution Method for Estimation of Glass Transition Temperature of Ionic Liquids. *Chemical Engineering Science* 2012; 81: 91-105.
- [46] Lazzús J.A. A Group Contribution Method to Predict the Glass Transition Temperature of Ionic Liquids. *Thermochimica Acta* 2012; 528: 38-44.

- [47] Strechan A.A., Kabo A.G., Paulechka Y.U., Blokhin A.V., Kabo G.J. Thermochemical Properties of 1-butyl-3-methylimidazolium Nitrate. *Thermochimica Acta* 2008; 474: 25-31.
- [48] Gardas, R.L., Coutinho, J.A.P. A Group Contribution Method for Heat Capacity Estimation of Ionic Liquids. *Industrial & Engineering Chemistry Research* 2018; 47: 5751-5757.
- [49] Paulechka Y.U., Kabo A.G., Blokhin A.V., Kabo G.J., Shevelyova M.P. Heat Capacity of Ionic Liquids: Experimental Determination and Correlations with Molar Volume. *Journal of Chemical & Engineering Data* 2010; 55: 2719-2724.
- [50] Sattari M., Gharagheizi F., Ilani-Kashkouli P., Mohammadi A.H., Ramjugernath D. Estimation of the Heat Capacity of Ionic Liquids: A Quantitative Structure-Property Relationship Approach. *Industrial & Engineering Chemistry Research* 2013; 52: 13217-13221.
- [51] Gardas R.L., Ge R., Goodrich P., Hardacre C., Hussain A., Rooney D.W. Thermo-physical Properties of Amino Acid-Based Ionic Liquids. *Journal of Chemical & Engineering Data* 2010; 55: 1505-1515.
- [52] Joback K.G. A Unified Approach to Physical Property Estimation Using Multivariant Statistical Techniques. PhD Thesis, Massachusetts Institute of Technology, Cambridge, 1984.
- [53] Poiling B.E., Prausnitz J.M., O'Connell J.P. *The Properties of Gases and Liquids*. McGraw-Hill: New York; 2001.
- [54] Valderrama J.O., Robles P.A. Critical Properties, Normal Boiling Temperature and Acentric Factors of Fifty Ionic Liquids. *Industrial & Engineering Chemistry Research* 2007; 46:1338-1344.
- [55] Valderrama J.O., Toro A., Robles P.A. Prediction of the Heat Capacity of Ionic Liquids Using the Mass Connectivity Index and a Group Contribution Method. *Journal of Chemical Thermodynamics* 2011; 43: 1068-1073.
- [56] Müller K., Albert J. Contribution of the Individual Ions to the Heat Capacity of Ionic Liquids. *Industrial & Engineering Chemistry Research* 2014; 53: 10343-10346.
- [57] Sattari M., Gharagheizi F., Ilani-Kashkouli P., Mohammadi A.H., Ramjugernath D. Development of a Group Contribution Method for the Estimation of Heat Capacity of Ionic Liquids. *Journal of Thermal Analysis and Calorimetry* 2014; 115: 1863-1882.
- [58] Farahani N., Gharagheizi F., Mirkhani S.A., Tumba K. A Simple Correlation for Prediction of Heat Capacities of Ionic Liquids. *Fluid Phase Equilibria* 2013; 337: 73-82.

Solubility of Bioactive, Inorganic and Polymeric Solids in Ionic Liquids — Experimental and Prediction Perspectives

Gonçalo V.S.M. Carrera, Małgorzata E. Zakrzewska,
Ana V. M. Nunes and Luis C. Branco

Additional information is available at the end of the chapter

<http://dx.doi.org/10.5772/60501>

1. Introduction

Ionic Liquids (ILs) are a well-established class of organic compounds characterized as liquid salts until 100°C as well as higher thermal and chemical stability, negligible volatility, high conductivities and large electrochemical window. Usually the adequate cation and anion combinations from ILs can modulate their thermal, physical and chemical properties. Many experimental and theoretical studies, highlight a regular pattern of variation of the properties of ILs by the introduction of elements, functional groups or specific ions, however due to the complexity associated to such compounds, in many cases, it is not possible to establish a straightforward relation between the variation of a specific property and the introduction of a particular component. Despite very low vapor pressure of ILs, several publications reported significant toxicity behavior associated to several classes of ILs. In this line, the development of biocompatible ILs and derived systems is actually being subject of intense research by the scientific community in order to open new perspectives for the application of this class of compounds. Since the advent of ILs in extractions and chemical reactions, the range of applications, in many areas of knowledge, never stopped to grow. One of the major reasons for such expansion is due to the inherent complexity of this class of compounds, associated with the virtually infinite possibilities of combination between cations and anions. In this context, the search for an ionic liquid with the desirable physical, chemical and biological properties by trial and error is not feasible without aid of background knowledge and predictive tools. Solubility is an essential property, being present in all stages of ILs research activities. The intrinsic complexity of this class of compounds associated to the many different types of possible interactions allows the dissolution of a wide range of different solutes. The

most common interactions observed in ILs classes can be coulombic, hydrogen bonding, permanent dipole - permanent dipole, permanent dipole - induced dipole, induced dipole – Induced dipole, π - π and n- π interactions. According the solubility properties of the system, should be possible to modify, stabilize, capture, control, enhance or mitigate such properties of specific solute molecules.

In this chapter, we are interested to overview the solubility of different classes of solids such as inorganic salts including metals; bioactive compounds including active pharmaceutical drugs; biopolymers and polymers in ionic liquids in particular comparing experimental and predicted research studies. Moreover a rationalization of the inherent structural characteristics behind the observed values of solubility in relevant cases will be also explored.

2. Solubility of inorganic compounds in ionic liquids

This section includes solubility of inorganic salts, elements, metal oxides and organometallic compounds in reference and task-specific ionic liquids. The later class includes ionic liquids with coordinating and common ions which can improve their solubility capacity. Whenever its possible experimental and modeled solubility will be compared and discussed accordingly, otherwise only experimental values will be presented and discussed. In order to contextualize this section a series of applications of such systems will be also described, and the experimental and types of models used in the referenced studies will be presented and discussed.

2.1. Inorganic salts (Halides)

Yang et al [1] reported the solubility of alkali chlorides in [EMIM][EtSO₄] at temperatures from 293.15 to 343.15 K. In this study the experimental solubility was determined by slow addition of metal halide to the ionic liquid until precipitate remain after 8h, afterwards the chloride content was determined by the Mohr method and consequently, the solubility of the metal halide was calculated. The experimental values were fitted with an exponential equation as expressed in the legend of Table 1 with a good agreement between experimental and fitted values. Such systems can be useful in synthesis as well as extraction processes.

MBr (mol.Kg ⁻¹ of solvent) / T (K)	293	298	303	308	313	318	323	328	333	338	343
	NaBr(fit)	0.2643	0.2689	0.2735	0.2779	0.2823	0.2866	0.2909	0.2950	0.2991	0.3032
KBr(fit)	0.2484	0.2522	0.2559	0.2595	0.2631	0.2666	0.2700	0.2734	0.2767	0.2799	0.2831
NaBr(exp)	0.2654	0.2692	0.2733	0.2774	0.2817	0.2859	0.2901	0.2948	0.299	0.3037	0.3083
KBr(exp)	0.25	0.2527	0.2557	0.2589	0.262	0.2654	0.2696	0.2726	0.2765	0.2807	0.2849

Table 1. Fitted vs Experimental solubility (molality) of MCl salts in 1-ethyl-3-methylimidazolium ethylsulfate. *Fitting equation* ($m/m^0 = \exp(A1 + A2(T^0/T) + A3(T/T^0)$).

In the same year, Wang et al. [2] reported the solubility of alkali bromides in the same ionic liquid. Similarly with Yang and co-workers study a broad range of temperatures was tested with the solubility increasing with the increase of the temperature, in good agreement between experimental and fitted values as presented in Table 2. The experimental method to obtain solubility of these salts is identical when compared with Yang's work.

MCl (mol.Kg ⁻¹ of solvent) / T (K)	MCl										
	293	298	303	308	313	318	323	328	333	338	343
LiCl(fit)	0.3679	0.3861	0.4053	0.4256	0.4471	0.4699	0.4939	0.5193	0.5461	0.5745	0.6045
KCl(fit)	0.2283	0.2299	0.2317	0.2338	0.2361	0.2385	0.2412	0.2441	0.247	0.2506	0.2541
NaCl(fit)	0.2325	0.2347	0.2369	0.2392	0.2415	0.2438	0.2461	0.248	0.2508	0.2532	0.2556
LiCl(exp)	0.3687	0.3861	0.404	0.4271	0.4453	0.4685	0.4951	0.522	0.5459	0.5722	0.6056
KCl(exp)	0.2282	0.2304	0.2322	0.2334	0.2358	0.2388	0.2416	0.2444	0.2479	0.2507	0.2535
NaCl(exp)	0.2351	0.2375	0.2399	0.2421	0.2445	0.2469	0.2491	0.2515	0.2539	0.2567	0.2594

Table 2. Fitted vs Experimental solubility (molality) of MCl salts in 1-ethyl-3 methylimidazolium ethylsulfate. *Fitting equation* ($m/m^0 = \exp(A1 + A2(T^0/T))$).

In these two studies, the solubility measurements were performed in a thermostated cell in a glove box under dry atmosphere. In a study of preparation and characterization of alcohol and ether functionalized ionic liquids [3] (Figure 1) was measured the solubility of LiCl, HgCl₂, LaCl₃. The obtained values were expressed in the form of massic solubility constant. The quantification of Hg and La was performed using plasma spectroscopy (ICP), differently the amount of Li was attained by flame photometry. The tested salts are more soluble in these series of alcohol and ether based RTILs than in conventional alkyl based ionic liquids as can be observed in Table 3. These salts represent examples of alkaline, transition metal, lanthanide based halides and the high solubility presented in some cases constitutes potential model systems with application in green chemistry and clean synthesis.

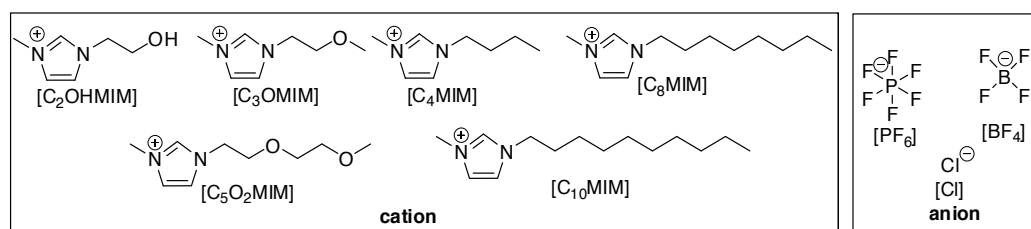


Figure 1. Structures of cations and anions used in solubility studies of Table 3.

IL / $K_s \times 10^6$ g of salt . g ⁻¹ of RTIL	K_s (LiCl)	K_s (HgCl ₂)	K_s (LaCl ₃)
[C ₂ OHMIM][PF ₆]	144.47	44.64	32.47
[C ₂ OHMIM][BF ₄]	18.46	84.73	54.01
[C ₃ OMIM][PF ₆]	12.44	50.13	37.61
[C ₃ OMIM][BF ₄]	14.43	220.86	180.27
[C ₅ O ₂ MIM][Cl]	9.98	295.34	379.23
[C ₅ O ₂ MIM][PF ₆]	35.52	147.48	97.22
[C ₅ O ₂ MIM][BF ₄]	21.36	174.17	292.46
[BMIM][PF ₆]	12.08	4.06	6.58
[BMIM][BF ₄]	15.54	41.41	10.92
[OMIM][PF ₆]	35.32	32.98	8.49
[OMIM][BF ₄]	56.02	35.92	53.25
[C ₁₀ MIM]BF ₄	12.64	2.12	47.12

Table 3. Solubility constants K_s of specific salts in selected ILs at room temperature.

Metal Chloride	[Metal Chloride]/[BMIM.Cl][AlCl ₄] molar
AlCl ₃	1
NbCl ₅	0.1
TaCl ₅	0.2
TiCl ₄	Immiscible
ZrCl ₄	0.8
HfCl ₄	1

Table 4. Solubility of metal chlorides in [BMIM.Cl][AlCl₄] at 298K.

Dotterl et al. [4] reported the solubility of different metal chlorides in [BMIM.Cl][AlCl₄] (Table 4), these mixtures can be used as catalysts in cationic oligomerization, electrochemical oxidation and metal deposition reactions. In this study, it is evident that Al, Zr and Hf based chlorides are highly soluble in this ionic liquid. The values of solubility were obtained by progressive solvent addition to the salt until the complete formation of a saturated solution (all the manipulations were performed under Argon atmosphere).

2.2. Inorganic salts (Miscellaneous)

Rosol et al. [5] reported the solubility of lithium based salts, commonly used as lithium batteries, in alkyl methylimidazolium based RTILs (Table 5). The values of solubility were attained by FTIR-ATR spectroscopic method, with thiocyanate based ionic liquid permitting

much higher values of solubility than other RTILs used in this study. In order to explain such behavior was used COSMO-RS and the higher polarizability of thiocyanate anion is responsible for such optimal observed solubility values.

IL/ solubility mol.dm ⁻³	LiNTf ₂	LiClO ₄	LiPF ₆
[BMIM][Acetate]	0.18	0.10	0.34
[BMIM][SCN]	1.3	4.1	0.60
[BMIM][PF ₆]	0.06	0.09	0.08
[EMIM][NTf ₂]	0.4	0.3	0.1

Table 5. Solubility (M - mol.dm⁻³) of specific salts in selected ILs at 298 K.

Atakilt et al. [6] reported the solubility of NiCl₂ and Cu(NO₃)₂ in [C₄BiPyr] and [C₄C₄BiPyr] based ionic liquids and other reference RTILs based on imidazolium and phenanthroline. Generally, the solubility are low, except for [C₄BiPyr][NTf₂] where the non-substituted nitrogen can coordinate the metal ions that compose the studied salts, increasing dramatically the solubility. The hypothesis of coordination ability of [C₄BiPyr] is confirmed by the poor solubility values in the case of [C₄C₄BiPyr][NTf₂]. The solubility was attained by the addition of the salt to the ionic liquid under nitrogen atmosphere and dissolution under vacuum.

Ionic Liquid/Solubility (mol %)	NiCl ₂	Cu(NO ₃) ₂
[BMIM][BF ₄]	< 0.05	< 0.05
[BMIM][PF ₆]	< 0.05	< 0.05
[BMIM][NTf ₂]	< 0.05	< 0.05
[C ₄ Phen][NTf ₂]	< 0.05	< 0.05
[C ₄ BiPyr][NTf ₂]	> 20	> 20
[C ₄ C ₄ BiPyr][NTf ₂]	< 0.05	< 0.05

Table 6. Solubility of specific inorganic salts in selected ionic liquids at 343 K.

Pereiro et al. [7] reported the solubility of diverse salts in a wide range of ionic liquids at 298.15 K (Table 7), the authors described that dissolving salts in a ionic liquid is a way to boost ionicity but at same time having the possibility of working in a liquid media, these systems can be potentially applied in batteries. The solubility study was obtained by the visual method, with the more promising systems measured by spectroscopic ATR-FTIR method, such compounds were also fitted by a linear equation with a good correlation between experimental and fitted values.

IL/ mass fraction of inorganic salt	[Na]	[NH ₄]	Ca	[NH ₄]	Na	Na ₂	Na	Na	Cs	Li
	[SCN]	[SCN]	Cl ₂	Cl						
	Na[OAc]	Na[SCN]	[NH ₄] [SCN]	Na [Lactate]						
[EMIM][OAc]	0.053	0.187 / 0.234 ^a / 0.232 ^b	0.136	0.152 / 0.161 ^a / 0.159 ^b	0.046	0.0097	0.034	-	-	-
	0.081	-	-	-						
[EMIM][SCN]	0.132 /0.145 ^a /0.135 ^b	0.089	0.042	0.021	0.037	0	0	-	-	-
	-	0.125	0.081	0						
[EMIM][C ₂ SO ₃]	0.053	0.187/ 0.200 ^a / 0.196 ^b	0	0.079 / 0.081 ^a 0.076 ^b	0.037	0	0.0097	-	-	-
	-	-	-	-						
[EMIM][C ₂ SO ₄]	0.095/ 0.104 ^a	0.352 / 0.379 ^a / 0.372 ^b	0.005	0.032	0	0.034	0	-	-	-
	-	-	-	-						
[EMIM][NTf ₂]	0.021		0.0019	0	0	0	0	0.16	0.303 / 0.314 ^a	0.315 / 0.363 ^a / /0.311 ^b 0.359 ^b
	-	-	-	-						
[EMIM][OTf]	0.037	-	0	0	0	0	0	-	-	-
	-	-	-	-						
[EMIM][B(CN) ₄]	0	-	0	0	0	0	-	-	-	-
	-	-	-	-						
[EMIM][PF ₃ (C ₂ F ₅) ₃]	0	-	0	0	0	0	-	-	-	-
	-	-	-	-						
[P _{6,6,14}][NTf ₂]	0	-	0.002	0	0	0	-	-	-	-
	-	-	-	-						
[P _{6,6,14}][L-Lactate]	0	-	0.021	0	0	0	-	-	-	-
	-	-	-	-						
[P _{6,6,14}][OTf]	0	-	0	0	0	0	-	-	-	-
	-	-	-	-						
[P _{4,4,4,1}][C ₁ SO ₄]	0	-	0	0	0	0.01	-	-	-	-

IL/ mass fraction of inorganic salt	[Na]	[NH ₄]	Ca	[NH ₄]	Na	Na ₂	Na	Na	Cs	Li
	[SCN]	[SCN]	Cl ₂	Cl						
	Na[OAc]	Na[SCN]	[NH ₄] [SCN]	Na [Lactate]	Cl	[SO ₄]	[OCN]	[NTf ₂]	[NTf ₂]	[NTf ₂]
[Choline][L-Lactate]	0.132	-	0.016	0.01	0.021	0.02	-	-	-	-
[EtCholine][NTf ₂]	0.042	-	0.002	0	0	0	-	0.176	0.339 ^a / 0.330 ^b	0.433 / 0.484 ^a / 0.479 ^b
[P _{6,6,6,14}][Cl]	-	-	0.044	0	0	-	-	-	-	-

^a Obtained by ATR-FTIR spectroscopic method at 298.15 K, ^b Fitted by linear equation $y = mx + b$.

Table 7. Mass fraction of specific inorganic salts in selected ionic liquids.

2.3. Lanthanides

Lanthanide based systems are very useful in the fields of advanced catalysis and as luminescent materials, one of the major problems that restricts their use is the poor solubility observed for this class of compounds. In order to circumvent this obstacle Li et al [8] developed carboxylate functionalized TSILs (Figure 2) for the dissolution of Europium (III) and Terbium (III) oxides (Table 8). The dissolution of the Lanthanides has been attained by addition to specific ionic liquids which they were mixed with an alcohol, and then the suspension was filtered and the alcohol evaporated under vacuum.

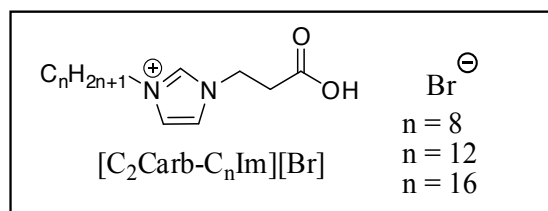


Figure 2. Structures of ILs used in Table 5.

IL/ solubility g·g ⁻¹ of solvent	Eu ₂ O ₃ (363 K)	Tb ₄ O ₇ (393 K)
[C ₂ Carb-C ₈ Im][Br]	soluble but less than 0.176	at least 0.189
[C ₂ Carb-C ₁₂ Im][Br]	soluble but less than 0.151	at least 0.162
[C ₂ Carb-C ₁₆ Im][Br]	not solubilized	at least 0.141

Table 8. Solubility values of lanthanide oxides in TSILs (g salt/ g IL).

2.4. Organometallics

The importance of the solubility studies of organometallic complexes is addressed to their applications in catalysis and photo/electrochemical studies as well as material chemistry field. Testing a phenantroline based TSIL, Villar-Garcia et al. [9] studied the solubility of Nickel(II), Iron(II) and Cobalt(II) complexes containing phenantroline ligands and optimal solubility with $[C_1\text{Phen}][\text{NTf}_2]$ ionic liquid when compared with reference imidazolium ionic liquids was obtained. Flame Atomic absorption Spectroscopy (AAS) analyses were performed after digesting a known amount of each sample in a 1:1 (v/v) $\text{HNO}_3:\text{HClO}_4$ mixture in order to obtain solubility values.

Ionic liquid/ solubility salt mol%	$[\text{Ni}(\text{Phen})_2(\text{OH})_2]\text{Cl}_2$	$[\text{Fe}(\text{Phen})_2(\text{OH})_2]\text{Cl}_2$	$[\text{Co}(\text{Phen})_2(\text{OH})_2]\text{Cl}_2$
$[C_1\text{Phen}][\text{NTf}_2]$	> 10 mol %	> 10 mol %	> 10 mol %
$[\text{BMIM}][\text{NTf}_2]$	< 0.05 mol%	< 0.05 mol%	< 0.05 mol%
$[\text{BMIM}][\text{BF}_4]$	< 0.05 mol%	< 0.05 mol%	< 0.05 mol%
$[\text{BMIM}][\text{PF}_6]$	< 0.05 mol%	< 0.05 mol%	< 0.05 mol%

Table 9. Solubility of metal complexes in selected ionic liquids at 348 K.

In a different study, Yang et al. [10] compared the solubility of ferrocene, ferrocenium, and cobaltocenium based salts in $[\text{BMIM}][\text{BF}_4]$ (Table 10). In this study the solubility of Ferrocenium Tetrafluoroborate was determined by the UV-Visible spectroscopy. This study was complemented by an *ab initio* quantum mechanical study in order to unveil the main interactions between solute-solvent and in the case of ferrocenium based salt, it can only be solvated by solvent anions in the first solvation shell.

Compound	Solubility in $[\text{BMIM}][\text{BF}_4]$
Ferrocene	27.5 mM
Ferrocenium Tetrafluoroborate	134 mM
Cobaltocenium Hexafluorophosphate	327.1 mM

Table 10. Solubility of ferrocene derivatives based compounds in $[\text{BMIM}][\text{BF}_4]$ measured at room temperature

2.5. Elements

Finally, regarding solubility of elements, such studies are important in order to optimize systems in synthesis, electrochemistry and catalysis, among other applications. Boros et al. [11] reported the solubility of sulfur (Table 11) and phosphorous (Table 12) in a diverse range of ionic liquids. The solubility values were obtained by portion-wise addition of sulfur to the ionic liquid and measuring the temperature which the mixture becomes homogeneous

T (K)	[OMIM][NTf ₂]	[P(Bu) ₃ CH ₃][OTs]	[BMIM][OTs]
383	< 1	1	2
398	< 1	1	2
413	2	3	4
428	3	5	6

Table 11. Solubility values of Sulfur in different ionic liquids (wt%).

Ionic Liquid	Weight %	Ionic Liquid	Weight %
[C ₁₀ MIM][CyOCS ₂]	8	[P _{6,6,6,14}][N(CN) ₂]	1
[BMIM][CyOCS ₂]	5	[P _{6,6,6,14}][NTf ₂]	trace
[BMIM][C ₆ H ₁₃ OCS ₂]	4	-	-
[BMIM][C ₄ H ₉ OCS ₂]	3	-	-
[BMIM][C ₂ H ₅ OCS ₂]	2	-	-
[P _{6,6,6,14}][C ₉ H ₁₉ CO ₂]	2	-	-

[CyOCS₂]: O-cyclohexyldithiocarbonate**Table 12.** Solubility of Phosphorus in selected ionic liquids at 373 K.

Finally, the solubility of sulfur was checked in [EMIM][NTf₂] at 393 K by Chen et al [12] that observed a solubility of 80 mM using two independent techniques such as electrochemical and by microwave study of sulfur vapor measurements. The possibility to use ionic liquids as alternative and efficient media to solubilize inorganic compounds could open new horizons to develop novel materials, many of them not be possible using conventional solvents. The complexity associated to ionic liquids and the possibility to establish different interactions with solute molecules are mainly reasons behind optimal dissolution performances. In this context, the introduction of task specific ionic liquids with specific groups/moieties can be able to establish a preferential interaction with the solutes. Different experimental techniques have been used based on visual and spectroscopic techniques. Additionally, in this field the introduction of predictive tools is still in his infancy with a limited number of studies establishing a comparison between experimental and predictive measures. It can be expected that by the increment of the number of experimental measures extended to a wider range of inorganics and ionic liquids as well, more robust models with predictive capability could be defined in a near future. The introduction of non-linear machine learning methods such as neural-networks, support vector machines or random forests could propel this subject of study.

3. Solubility of bioactive compounds in ionic liquids

Bioactive compounds have been subject of great attention regarding their interaction with several ILs. Indeed, various synthetic pharmaceutical ingredients and their precursors, as well

as, proteins and natural bioactive compounds, have been processed using ILs, mainly foreseeing applications in the pharmaceutical, cosmetic and agro-food sectors. Driven by a more demanding and strict regulation on the use of hazardous substances, particularly the pharmaceutical sector, for which 80% of waste generated in APIs synthesis, is related to solvent use, is being forced to look to greener alternatives. [13,14] In an attempt to meet this necessity, several scientific papers reporting successful new strategies for the synthesis of different kinds of APIs using ILs, have been reported. [15,16] Another challenge faced by the pharmaceutical industry, relies on the development of efficient drug carrier systems, which are fundamental to overcome barriers to drug bioavailability. In this context, mixtures of ILs have been used as delivery systems, to increase solubility of poorly water-soluble drugs. Briefly, an hydrophobic IL is used as the drug reservoir, completely dissolving the bioactive substance, while another IL, this time a hydrophilic one, is used as co-solvent, with the purpose of increasing the water solubility of the system.[17,18] Also with interest for the pharmaceutical industry, the utilization of ILs for proteins stabilization and biopreservation, have also been subject of great attention.[19]

A further relevant field on the context of bioactive compounds processing with ILs, is the treatment of wastes contaminated with significant quantities of substances possessing biological activity. For example, in respect to wastewater effluents, numerous studies have alerted for the presence of a wide variety of bioactive substances, which are not eliminated by conventional treatment plants. Under this perspective, many authors have reported successful results on using ILs for the extraction of bioactives from it aqueous solutions. An interesting approach are the well-known Aqueous Biphasic Systems (ABS) that have been the focus of a significant amount of research, extensively reviewed in 2012 by Freire M.G. et al. [20]

More recently, the extraction of natural bioactive ingredients from food industry wastes and other biomass resources has emerged. In this case, the IL is used to recover these high-added value substances from cheap and available raw materials and meant for human consumption. [21] The market for natural ingredients is one of the most attractive markets of the moment and in which the use of clean technologies for extraction, fractionation and purification, is of crucial importance. It is interesting to note that ILs applications involving products for human consumption were triggered with the effort of the scientific community on the development of nontoxic (or less toxic) ILs, by selecting more biocompatible organic cations and inorganic anions.[22] Finally, also in the field of analytical chemistry, the processing of bioactive compounds using ILs, has considerably grown.[23]

Process design and success of all above referred applications, strongly relies on the interactions between bioactive compounds and ILs, which in turn, depends on several distinct and complex factors, such as chemical structure, polarity, hydrophilicity and other physico-chemical properties of both solute and solvent. Therefore, phase equilibrium data of the binary systems (IL+ bioactive compound) is of crucial importance to understand, predict and take control of existing, as well as, to figure new applications. Bogel-Lukasik E. and co-workers are the most active research group working on the experimental determination of solubilities of bioactive compounds in ILs. The authors have focused their attention in classical ILs essentially formed by cations of 1-alkyl-3-methylimidazolium (RMIM, where R= butyl, hexyl and octyl chain) and

counter-ions such as, tetrafluoroborate, [BF₄]; hexafluorophosphate, [PF₆]; trifluoromethanesulfonate, [OTf] and bis(trifluoromethylsulfonyl)amide [NTf₂]. Furthermore, they were the first to address the solubility of natural phenolic compounds, namely, tannic acid, gallic acid and quercetin with the purpose of evaluating the potential of ionic liquids as solvent for their extraction from natural resources, such as biomass.[24] Solubilities were measured using a dynamic method from 273K to 413 K. For the case of tannic acid, the solubility decreased on the following order [BMIM][BF₄] > [BMIM][PF₆] > [BMIM][OTf] > [BMIM][NTf₂]. The authors found out a correlation between the observed differences in solubilities and the E^N_T values for the ionic liquids investigated. This parameter is considered a good scale of polarity for ILs. In addition, ILs hydrophilicity was also an important factor, [BMIM][BF₄] contrary to [BMIM][PF₆] is hydrophilic favoring the formation of hydrogen bonds with weak acids, such as tannic acid. However, for both ILs and for mole fractions higher than 0.2 and temperatures above 323.15 K, a strong acid odour was detected, corresponding the undesired formation of HF. This reveals instability of [BF₄] and [PF₆] at higher temperatures. On the other hand, the solubility of tannic acid in [BMIM][NTf₂] is very low (below 0.001 mole fraction even at high temperatures). The authors highlighted the fact that [BMIM][NTf₂] is a much worse hydrogen bond acceptor than [BMIM][OTf]. This is due to a higher basic character of the [OTf] anion. Comparing the solubilities of tannic acid, gallic acid and quercetin in [BMIM][OTf], at around 380 K, the solubility of phenols particularly gallic acid and quercetin are close to or higher than 0.4 mol fraction of phenolic compound. However, the experimental liquid curve trend is difficult to explain, specially for gallic acid that at lower temperatures is the most soluble phenol, but for higher temperatures stands as the less soluble. In fact, after around 330 K and above 0.2 mol fraction, the solubility of gallic acid increases much more slowly with temperature in comparison with the solubility of tannic acid and quercetin. Curiously, the temperature at which this reversed behavior occurs is around the same temperature at which the thermograph of gallic acid presents a solid-solid phase transition (β₁ crystalline form undergoes to a α₁ plastic form at 351 K). The same phenomena but much less pronounced is observed for tannic acid. This kind of phenomena can be exploited to achieve separation of different compounds by varying temperature conditions. In another work addressing the interaction between natural bioactive compounds and ILs, that was recently published by Alevizou and Voutas [25], the authors measured the solubilities of p-coumaric acid and caffeic acid in six 1-alkyl-3-methyl imidazolium based ionic liquids composed of the same anions, BF₄⁻, PF₆⁻, OTf⁻, NTf₂⁻. Caffeic acid was found to be less soluble in all ILs due to higher melting temperature and heat of fusion comparing to p-coumaric acid. Furthermore hydrophilic ILs based on BF₄⁻ and OTf⁻ were better solvents than hydrophobic ones based on PF₆⁻ and NTf₂⁻. This is due to the fact that hydrophilic ILs interact more strongly with both compounds through hydrogen bonds. Comparing ILs with same imidazolium cation, solubility decreased in the following order BF₄⁻ > OTf⁻ > PF₆⁻ > NTf₂⁻. The authors highlighted that results obtained are in agreement with relative polarity, hydrophilicity and hydrogen bond basicity of studied ILs. For the case of BF₄⁻ and OTf⁻ they were even better solvents than pentanol and ethyl acetate. Comparing ILs with the same anion, as the alkyl chain increases, the solubility of both compounds decreases in the case of hydrophilic BF₄⁻, and increases in the case of PF₆⁻. For biomass-derived compounds, Carneiro et al. [26] proposed the utilization of ionic liquids as future solvents for

biorefining. In this context, the authors investigated the potential of three ionic liquids for the processing of the sugar alcohols sorbitol and xylitol, obtained respectively from glucose/fructose and xilose. The authors [26] measured the solubility of sorbitol and xylitol within the temperature range of 288 K to 328 K in three ionic liquids, specifically, 1-ethyl-3-methylimidazolium ethylsulfate, [EMIM][EtSO₄], [Aliquat]Cl (a mixture of methyltrioctylammonium chloride and methyltridecylammonium chloride), and [Aliquat][NO₃] (the same cation mixture with nitrate as anion). The solubility of both compounds decreased in the following order [EMIM][EtSO₄] > [Aliquat][Cl] > [Aliquat][NO₃]. Since sorbitol and xylitol are very polar and hydrophylic, the hydrophobicity of [Aliquat] cation causes weaker interactions between the ILs and the solutes. As a result lower solubilities were obtained when using the two ammonium based ILs, compared to those obtained using the hydrophilic ionic liquid, [EMIM][EtSO₄]. Furthermore, the study explained the differences on solubility observed between the two Aliquat's, as a result of two factors. The first factor pointed out, was the water content of [Aliquat][Cl], allowing greater quantities of solute to dissolve. The second factor, was the higher Lewis basicity of chloride over nitrate anions, supplying a better capability to establish hydrogen bonds with xylitol and sorbitol hydroxyl groups. For the three ILs, sorbitol was always more soluble than xylitol. For the case of [EMIM][EtSO₄], an additional hydroxyl group in sorbitol resulted in a significant solubility difference due to stronger solute-solvent interactions. In relation to hydrophobic [Aliquat][Cl] and [Aliquat][NO₃], the additional OH group does not play such an important role. The authors also noted that the solubility of the two sugar alcohols could be connected with their melting properties, as lower attraction between solutes and Aliquat based ILs occurs. In this way, because melting enthalpy is lower for sorbitol, its solubility is expected to be higher

Bioactive compound	Ionic liquid	Solubility	T/K	Modelling	Ref.
Caffeic acid	[BMIM][PF ₆]	0.0012-0.0024(x _{mol})	303.1-317.4	NRTL, UNIQUAQ	[26]
	[OMIM][PF ₆]	0.0014-0.0024(x _{mol})	303.1-317.4		
	[BMIM][BF ₄]	0.1536-0.1827(x _{mol})	303.1-317.4		
	[OMIM][BF ₄]	0.0451-0.0626(x _{mol})	303.1-317.4		
	[BMIM][NTf ₂]	0.0003-0.0011(x _{mol})	303.1-317.4		
	[BMIM][OTf]	0.0242-0.0541(x _{mol})	303.1-317.4		
Caffeine	[BMIM][BF ₄]	84(mmol/L)	298.15	NA	[18]
	[OMIM][BF ₄]	83(mmol/L)	298.15		
	[BMIM][PF ₆]	100(mmol/L)	298.15		
	[OMIM][PF ₆]	34(mmol/L)	298.15		
p-Coumaric acid	[BMIM][PF ₆]	0.0062-0.0102(x _{mol})	303.1-317.4	NRTL, UNIQUAQ	[25]
	[OMIM][PF ₆]	0.0063-0.0119(x _{mol})	303.1-317.4		
	[BMIM][BF ₄]	0.1951-0.2513(x _{mol})	303.1-317.4		

Bioactive compound	Ionic liquid	Solubility	T/K	Modelling	Ref.
	[OMIM][BF ₄]	0.0803-0.1100(x _{mol})	303.1-317.4		
	[BMIM][NTf ₂]	0.0028-0.0051(x _{mol})	303.1-317.4		
	[BMIM][OTf]	0.1054-0.1481(x _{mol})	303.1-317.4		
Gallic acid	[BMIM][OTf]	0.0580-0.3596(x _{mol})	273.78-398.42	NA	[24]
	[BMIM][NTf ₂]	0.0052(x _{mol})	400.15		
Quercetin	[BMIM][OTf]	0.0109-0.3954(x _{mol})	294.40-363.97	NA	[24]
	[BMIM][NTf ₂]	0.0022(x _{mol})	411.21		
D-(-)- Sorbitol	[EMIM][EtSO ₄]	0.113-0.310(w _{mass})	289.2-328.3	UNIQUAQ, NRTL, eNRTL	[26]
	[Aliquat]Cl	0.123-0.250(w _{mass})	308.2-343.0		
	[Aliquat][NO ₃]	0.036-0.115(w _{mass})	308.0-344.9		
Tannic acid	[BMIM] [BF ₄]	0.1437-0.2509(x _{mol})	275.91-325.15	NA	[24]
	[BMIM] [PF ₆]	0.0717-0.2544(x _{mol})	289.54-340.04		
	[BMIM] [OTf]	0.0052-0.2601(x _{mol})	276.71-351.13		
	[BMIM] [NTf ₂]	0.008(x _{mol})	410.59		
Xylitol	[EMIM][EtSO ₄]	0.200-0.3377(w _{mass})	298.1-328.3	UNIQUAQ, NRTL, eNRTL	[26]
	[Aliquat]Cl	0.186-0.248(w _{mass})	318.0-343.0		
	[Aliquat][NO ₃]	0.056-0.103(w _{mass})	317.8-344.4		

Table 13. Solubility of natural and natural-derived bioactive compounds in ILs

The first work regarding solubility of pharmaceutical compounds in ILs was published in 2008 by the group of Florence and co-workers.[18] In this study, different drugs were used as models for water-insoluble drugs (albendazole and danazol) and water-soluble drugs (acetaminophen and caffeine). Their solubility in different ionic liquids were measured. ILs formed by the cation 1-alkyl-3-methylimidazolium with butyl, hexyl or octyl as alkyl chains and by the anions, [PF₆]⁻ and [BF₄]⁻ were studied. The authors [18] underlined that drug structures indicate that solute-solvent interactions are likely to involve hydrogen bonds, van der Waal's forces as well as π - π interactions between aromatic ring. For the case of hydrophobic drugs, albendazole presented precisely the expected results, in other words, a higher solubility for ILs with the [PF₆]⁻ anion and an increase in the solubility with an increase in the alkyl chain, was observed. For the case of danazole, an increase in the alkyl chain has also resulted in an increase in the solubility, but curiously, danazole presented a higher solubility in ILs with [BF₄]⁻ anions. As the [PF₆]⁻ salts are more hydrophobic than the [BF₄]⁻ salts it might have been expected that the former would dissolve more a hydrophobic drug molecule as danazole (as indeed was observed for albendazole). For the hydrophilic compound acetaminophen, solubility results were, as expected, higher for ILs with [BF₄]⁻ anions and decreased with the alkyl chain increase of the imidazolium ring. Again, for the case of caffeine, however, none of these expected results

were verified and it was the only case for which solubilities obtained were always lower than it solubility in water. This highlights the difficulty in predicting solubility and the need for systematic studies on drug solubility in a wider range of ILs. After that, Smith K.B. et al.[27] have published solubilities of ibuprofen and acetaminophen on ILs at temperatures of 298.15 K, 308.15 K, 318.15 K, 328.15 K, and 338.15 K. Selected ILs were 1-butyl-3-methylimidazolium hexafluorophosphate [BMIM][PF₆] and 1-hexyl-3-methylimidazoliumhexafluoro phosphate [HMIM][PF₆]. The authors observed that, both ILs were good solvents for ibuprofen and paracetamol, which suggests that drug-solvent interactions are taking place for dissolution to occur. Furthermore and contrary to what was expected, solubilities of both solutes were greater in [HMIM][PF₆] than [BMIM][PF₆] over the conditions studied. Since acetaminophen is water-soluble and ibuprofen is poorly water-soluble, one would expect opposite behaviours. Acetaminophen as observed before, decreased solubility with an increase in the alkyl chain, but not ibuprofen. Ibuprofen is a water poorly soluble drug and its solubility should increase for more hydrophobic ILs. The author referred that [HMIM][PF₆] may have a larger population of cavities within which the drug dissolved leading to the observed higher solubility. Again, these results highlight the difficulty predicting solute solubility in ILs. Furthermore, Bogel-Lukasik E. and co-workers have focused their attention on the solubility of two anti-tuberculosis drugs, namely, isoniazid and pyrazine-2-carboxamide in a series of 1-alkyl-3-methylimidazolium bis(trifluoromethylsulfonyl)amide [RMIM][NTf₂] and 1-hexyl-3-methylimidazolium trifluoromethanesulfonate [HMIM][OTf] ionic liquids. [28,29] Regarding the [NTf₂] ionic liquids and for both drugs studied, the solubility decreases with an increase of the alkyl chain (R). This is a direct result of the decrease of the acidity of the proton in the position 2 of the imidazolium ring for longer alkyl chains. For comparison between [HMIM][NTf₂] and [HMIM][OTf], the solubility of both drugs in [HMIM][OTf] was significantly higher, in agreement with general recognition that [OTf] ILs are better solvents for compounds capable of forming hydrogen bonds. However, isoniazid was slightly less soluble than pyrazicarboxamide which is very likely due to the basic character of hydrazine. The solubility of these anti-tuberculosis drugs were further tested in ammonium-based ILs. [30] Ammonium ionic liquids, namely, didecyl-dimethylammonium nitrate [DDA][NO₃], (benzyl)dimethylalkylammonium nitrate (where alkyl= C₁₂H₂₅ (w=0.4) and C₁₄H₂₉ (w=0.6)) [BDMA][NO₃], ethyl(2-hydroxyethyl)dimethylammonium bis(trifluoromethylsulfonyl)amide [N_{2,2OH,1,1}][NTf₂], were studied. Both drugs presented similar solubility trends, with the highest solubility observed for [DDA][NO₃], followed by [N_{2,2OH,1,1}][NTf₂] and [BDMA][NO₃]. For ammonium ILs, contrary to what was found for imidazolium ILs, isoniazid was slightly more soluble than pyrazicarboxide. Results obtained allowed to conclude that ammonium ILs are better solvents than imidazolium, even imidazolium triflate. Finally Bogel-Lukasik E. and co-workers [31] extended their investigation to other pharmaceutical compounds, namely, N-acetyl-cysteine, coumarin and 4-hydroxycoumarin. In this case ionic liquids investigated were again imidazolium ILs containing the [NTf₂] and [OTf] anions. For hydrophilic compounds (e.g. N-acetyl-cysteine and 4-hydroxycoumarin) and as expected, solubility was higher in the [OTf] ILs than in [NTf₂] ILs, furthermore it decreased with increasing alkyl chain. A longer alkyl chain decreases the acidity of the proton in position 2 of the imidazolium ring, therefore reducing capability of forming hydrogen bonds.

Bioactive compound	Ionic liquid	Solubility	T/K	Modelling Equation/Deviations	Ref.
Acetaminophen	[BMIM][BF ₄]	>132(mmol/L)	298.15	NA	[18,27]
	[OMIM][BF ₄]	126(mmol/L)	298.15		
	[BMIM][PF ₆]	52(mmol/L)	298.15		
	[OMIM][PF ₆]	10(mmol/L)	298.15		
N-acetyl-L-cysteine	[EMIM][OTf]	0.0889-0.9295(x _{mol})	283.34-378.61	Wilson, UNIQUAQ, UNIQUAQ ASM, NRTL, NRTL1, NRTL2	[31]
	[BMIM][OTf]	0.0644-0.9054(x _{mol})	293.11-379.13		
	[BMIM][NTf ₂]	0.0866-0.8775(x _{mol})	306.47-377.79		
	[HMIM][NTf ₂]	0.0635-0.8843(x _{mol})	298.36-378.10		
	[DMIM][NTf ₂]	0.0102-0.8984(x _{mol})	305.35-381.04		
Albendazole	[BMIM][BF ₄]	1.49(mmol/L)	298.15	NA	[18]
	[HMIM][BF ₄]	2.97(mmol/L)	298.15		
	[OMIM][BF ₄]	7.2(mmol/L)	298.15		
	[BMIM][PF ₆]	29(mmol/L)	298.15		
	[HMIM][PF ₆]	53(mmol/L)	298.15		
	[OMIM][PF ₆]	>75(mmol/L)	298.15		
Coumarin	[EMIM][OTf]	0.0714-0.8995(x _{mol})	275.51-338.77	Wilson, UNIQUAQ, UNIQUAQ ASM, NRTL, NRTL1, NRTL2	[31]
	[BMIM][OTf]	0.1463-0.9060(x _{mol})	278.38-337.47		
	[EMIM][NTf ₂]	0.1387-0.8865(x _{mol})	263.58-334.28		
	[BMIM][NTf ₂]	0.2879-0.8844(x _{mol})	274.32-332.38		
	[HMIM][NTf ₂]	0.2651-0.8788(x _{mol})	267.71-330.92		
	[DMIM][NTf ₂]	0.4034-0.8906(x _{mol})	276.24-332.36		
Danazole	[BMIM][BF ₄]	18.9(mmol/L)	298.15	NA	[18]
	[OMIM][BF ₄]	>59(mmol/L)	298.15		
	[BMIM][PF ₆]	11.9(mmol/L)	298.15		
	[OMIM][PF ₆]	35(mmol/L)	298.15		
Erythromycin	[BMIM][NTf ₂]	0.030-0.047(x _{mol})	285.1-348.2	Grant equation	[32]
	[DMIM][NTf ₂]	0.070-0.074(x _{mol})	288.2-356.2		
	[P _{6,6,14}][Cl]	0.085-0.097(x _{mol})	298.0-357.2		
	[N _{4,1,1,1}][NTf ₂]	0.053- 0.056(x _{mol})	296.8-354.5		
	[N _{1,8,8,8}][NTf ₂]	0.097-0.106(x _{mol})	310.2-358.0		
	[Pyr _{4,1}][NTf ₂]	0.016-0.020(x _{mol})	284.4-354.2		

Bioactive compound	Ionic liquid	Solubility	T/K	Modelling Equation/Deviations	Ref.	
4-Hydroxycoumarin	[EMIM][OTf]	0.0711-0.4887(x_{mol})	283.02-408.56	Wilson, UNIQUAQ,	[31]	
	[BMIM][OTf]	0.0566-0.4625(x_{mol})	293.46-415.20	UNIQUAQ, ASM,		
	[BMIM][NTf ₂]	0.0203-0.2667(x_{mol})	321.38-411.60	NRTL, NRTL1, NRTL2		
Isoniazid	[EMIM][NTf ₂]	0.008-0.187(x_{mol})	331.06-409.47	Wilson, UNIQUAQ, UNIQUAQ, ASM, NRTL, NRTL1, NRTL2	[28]	
	[BMIM][NTf ₂]	0.004-0.213(x_{mol})	323.60-415.89			
	[HMIM][NTf ₂]	0.003-0.169(x_{mol})	324.61-413.00			
	[OMIM][NTf ₂]	0.003-0.140(x_{mol})	325.64-409.46	Wilson, UNIQUAQ, UNIQUAQ, ASM, NRTL, NRTL1, NRTL2		
	[DMIM][NTf ₂]	0.003-0.139(x_{mol})	326.69-410.82			
	[DMIM][OTf]	0.006-0.350(x_{mol})	314.17-406.42			
	[DDA][NO ₃]	0.0452-0.4927(x_{mol})	308.36-418.48	Wilson, UNIQUAQ,		[30]
	[BDMA][NO ₃]	0.0429-0.3817(x_{mol})	321.38-415.71	UNIQUAQ, ASM,		
	[N _{2,2OH,1,1}][NTf ₂]	0.0167-0.3236(x_{mol})	292.15-402.51	NRTL, NRTL1, NRTL2		
Pyrazine-2-carboxamide	[EMIM][NTf ₂]	0.0048-0.2122(x_{mol})	294.40-409.43	Wilson, UNIQUAQ, UNIQUAQ, ASM, NRTL, NRTL1, NRTL2	[29]	
	[BMIM][NTf ₂]	0.0036-0.2823(x_{mol})	279.27-423.73			
	[HMIM][NTf ₂]	0.0020-0.2318(x_{mol})	275.27-415.25			
	[OMIM][NTf ₂]	0.0030-0.1940(x_{mol})	275.37-416.66	Wilson, UNIQUAQ, UNIQUAQ, ASM, NRTL, NRTL1, NRTL2		
	[DMIM][NTf ₂]	0.0027-0.1726(x_{mol})	275.32-413.79			
	[DMIM][OTf]	0.0076-0.4867(x_{mol})	290.40-417.42			
	[DDA][NO ₃]	0.0343-0.3912(x_{mol})	320.30-403.83	Wilson, UNIQUAQ,		[30]
	[BDMA][NO ₃]	0.0168-0.2414(x_{mol})	319.63-401.32	UNIQUAQ, ASM,		
	[N _{2,2OH,1,1}][NTf ₂]	0.0068-0.3375(x_{mol})	293.19-409.67	NRTL, NRTL1, NRTL2		

Table 14. Solubility of pharmaceutical compounds in ILs

Manic and Najdanovic-Visak [32] reported on the solubility of erythromycin in imidazolium, ammonium and phosphonium ILs, namely, 1-butyl-3-methylimidazolium bis(trifluoromethylsulfonyl)imide ([BMIM][NTf₂]), 1-decyl-3-methylimidazolium bis(trifluoromethylsulfonyl)imide ([HMIM][NTf₂]), trihexiltetradecylphosphonium chloride ([P_{6,6,6,14}][Cl]), butyltrimethylammonium bis(trifluoromethylsulfonyl)imide ([N_{4,1,1,1}][NTf₂]), methyltrioctylammonium bis(trifluoromethylsulfonyl)imide ([N_{1,8,8,8}][NTf₂]), and 1-butyl-1-methylpyrrolidinium bis(trifluoromethylsulfonyl)imide ([Pyrr_{4,1}][NTf₂]). Results obtained indicate that solubility decreased in the following order, [N_{1,8,8,8}][NTf₂] > [P_{6,6,6,14}][Cl] > [C₁₀mim][NTf₂] > [N_{4,1,1,1}][NTf₂] > [BMIM][NTf₂] > [Pyrr_{4,1}][NTf₂]. Furthermore, longer alkyl chains for both imidazolium and ammonium based ILs led to higher solubility of the studied compound. Azevedo et al. [33] have studied the solubility of a new cardioactive prototype drug, 2-

thienylidene-3,4-methylenedioxybenzoylhydrazine (LASSBio-294) in seven different imidazolium based ILs at room temperature. Selected ILs were the following, 1-ethyl-3-methylimidazolium methyl phosphonate [EMIM][CH₃O(H)PO₂], 1-ethyl-3-methylimidazolium ethyl phosphonate [EMIM][C₂H₅O(H)PO₂], 1-ethyl-3-methylimidazolium acetate [EMIM][CH₃COO], 1,3-dimethylimidazolium methyl phosphonate [DMIM][CH₃O(H)PO₂], 1-butyl-3-methylimidazolium acetate [BMIM][CH₃COO], 1-butyl-3-methylimidazolium tetrafluoroborate [BMIM][BF₄], 1-butyl-3-methylimidazolium bis(trifluoromethylsulfonyl)imide [BMIM][NTf₂]. This time, classical [BMIM][BF₄] and [BMIM][NTf₂] were not able to solubilize LASSBio-294. On the other hand, one of the higher solubility was observed for [BMIM][CH₃COO], probably due to the good capacity of the anion to form hydrogen bond and delocalize charges between the oxygen atoms. Furthermore, the solubility decreased with a decrease in the cation alkyl chain for [EMIM][CH₃COO] due to drug hydrophobicity. At the same level of [BMIM][CH₃COO] is the IL, [EMIM][C₂H₅O(H)PO₂] but decreasing the alkyl chain of the anion for [EMIM][CH₃O(H)PO₂] decreases the drug solubility (also due to a decrease of hydrophobicity). Curiously by comparing LASSBio-294 solubility in [EMIM][CH₃O(H)PO₂] and [DMIM][CH₃O(H)PO₂], the solubility was higher in [DMIM][CH₃O(H)PO₂]. Since in this case an increase in the hydrophobicity was not observed, the authors concluded that the solubility depends not only of each ion separately but also on a combined cation-anion effect. The future of processing bioactive compounds, either synthetic or natural, with ILs, is certainly very promising, which was evidenced by the number of articles published, reporting successful results on several applications. However, with respect to experimental data regarding fundamental studies, to determine interactions between bioactives and ILs (e.g. solubility), until now, very few compounds were explored. Also very few ILs have been tested. Actually most of the authors, have addressed classic imidazolium cations combined with [BF₄], [PF₆], [OTf] and [NTf₂] anions, which are the most studied in terms of thermophysical properties. In this way, some of the authors have actually correlated their results, mainly using local composition models like UNIQUAQ and NRTL, with acceptable deviations and good representations of the experimental data. Nevertheless fundamental data is scarce and it is necessary to further understand and design new successful processes.

4. Solubility of biopolymers in ionic liquids

Biomass is regarded as a permanent source of renewable feedstock on the planet for both material and energy [34]. Various lignocellulosic materials, such as agricultural residues, forestry wastes, waste paper, and energy crops, have been recognized as potential sustainable fonts of sugars for transformation into fuel or value-added products currently derived from petroleum [35]. Biomass primarily consists of polymeric carbohydrates: cellulose and hemicellulose, and the aromatic polymer lignin. These components are firmly cross-linked by numerous inter- and intramolecular hydrogen bonds making processing of biomass an extremely challenging task. In order to access the carbohydrates in the biomass an additional deconstruction step (so called pretreatment) is required. The goal is to disrupt the lignin-

carbohydrate complex, decrease cellulose crystallinity and partially remove lignin and hemicelluloses. Traditional methods currently used either for pretreatment or carbohydrates dissolution typically demand harsh conditions (elevated temperature, and often also elevated pressure, usage of strong acids or bases), and sometimes cause serious environmental, energy, or safety problems [36]. Less energy consuming, more environmentally friendly, and highly efficient approaches are in great need. New solvents systems are crucial for not only deconstruction and separation of biomass components, but also for successful regeneration or derivatisation of sugar polymers under homogeneous conditions.

The capability of ILs to act as media for biomass processing has already been reported [37-42]. After Rogers et al. [43] first reported in 2002 that cellulose could be dissolved in IL, 1-butyl-3-methylimidazolium chloride ([BMIM][C1]), the research on application of ILs to carbohydrate chemistry started to attract a great deal of attention. This subchapter is meant to provide an update on recent advances in the field of solubility of carbohydrates in ILs which has already been reviewed elsewhere [44]. This work covers the solubility data that were published since 2009 till present. Since many comprehensive and excellent reviews on modification of carbohydrates in ILs are already available [45-47], this subject is omitted in the subsequent discussion. Interest in using ILs as media for carbohydrates has so far been centered on the dissolution and processing of cellulose [48-53]. One of the major drawbacks of cellulose concerning its industrial application is the insolubility in water and most of conventional solvents due to its compact structure and chemical complexity. The capacity of certain ILs to dissolve cellulose is primarily related with strong hydrogen bonding between the ILs anion and the hydroxyl groups of cellulose [48,54-57]. This association was confirmed for cellulose or glucose/glucose oligomer models by means of NMR [58-60], neutron scattering [60], molecular dynamic [61-65] and density functional theory computational approaches [66]. It is commonly accepted that the anion of the ILs plays a predominant role in dissolution. A high basicity of the anion is considered as a major criterion to effectively dissolve cellulose [67,68]. The stronger the hydrogen bond basicity of the anion, the stronger the ability of the IL to dissolve cellulose. However, the exact mechanism of cellulose dissolution has not been completely understood so far. In particular, some speculations exist into the role of the cation [48, 69-74]. Most of the researchers attribute the dissolution ability of ILs only to the anion, while the interactions between the cation and the carbohydrate play secondary role [58,60,61,65,75]. However, the idea that both IL ions, anion and cation, participate in the dissolution process by formation of hydrogen bonds has been considered as well [52,71,74,76,77]. Some data have even suggested that since cellulose is amphiphilic the hydrophobic interactions between the IL cation and the cellulose are responsible for the dissolution of cellulose [41,70].

To date, ILs that have been found suitable for cellulose dissolution contain imidazolium- or pyridinium-based cations combined with anions of basic character such as chloride [43,78], carboxylates (formate [79], acetate [56,78]), phosphates [80] or phosphonates [67]. On the other hand, some IL ions have been shown to be unable to dissolve cellulose. Examples include pyrrolidinium and piperidinium cations and tetrafluoroborate, hexafluorophosphate, dicyanamide, bis(trifluoromethanesulfonyl)amide or trifluoromethanesulfonate anions [40,53,56,74]. Bromide and dicyanamide ILs are known to dissolve cellulose only with low

degree of polymerization [81-83]. Dicyanamide-based ILs are not efficient for cellulose dissolution but they are capable of dissolving monosaccharides [84-86]. Table 15 presents solubility data for main lignocellulosic polymers: cellulose, hemicelluloses and lignin [56,74,82,83,87-90]. It is interesting to note, that replacing proton in the acetate anion with electron-withdrawing group, such as hydroxyl (-OH), thiol (-SH), amine (-NH₂) or hydroxymethyl (-CH₂OH) group, results in a decreased solubility of cellulose [56]. Changes in the cation structure are also not insignificant. When the alkyl chain length in the cation is increased, the solvent power of ILs for cellulose seems to decrease [43]. Moreover, for the small alkyl chains (pentyl and shorter) of 1-alkyl-3-methylimidazolium chloride, the strong odd-even effect was observed [58]. Even-numbered alkyl side chains proved to be better suited for cellulose dissolution than odd-numbered chains. Alkyloxy and alkyloxyalkyl groups attached to the imidazolium ring may either enhance or decrease solubility of cellulose [74,91,92]. In some cases IL solvent systems can also be used. Mixtures of ILs and polar organic co-solvent (e.g. dimethylsulfoxide (DMSO), N,N-dimethylformamide (DMF) or N,N-dimethylacetamide (DMA) have been successfully applied [93,94], even at ambient temperature [90]. The great advantage of such mixtures is reduced viscosity of the cellulose solutions that leads to acceleration of the dissolution process from hours down to minutes. Addition of lithium salts (e.g., Li(OAc), LiCl, LiBr, LiNO₃ or LiClO₄) into [BMIM][OAc] significantly increases the solubility of cellulose [56]. This observation was studied by ¹³C NMR spectra, and the results suggest that the enhanced solubility originates from the disruption of the intermolecular hydrogen bond owing to the interaction of lithium cations with the hydroxyl oxygen of cellulose.

The desired high basicity that allows an IL to dissolve cellulose unfortunately makes the IL very hygroscopic. Water is found to perturb the solvation of carbohydrates considerably [43,89,94]. It hydrogen-bonds to the ILs anion or to cellulose removing the primary driving force for the solubility of cellulose, the anion-cellulose hydrogen bonds. Amounts even as low as 0.15 wt% were reported to start precipitation of cellulose in the 1-ethyl-3-methylimidazolium chloride ([EMIM][Cl]) [89]. On the other hand, this is very advantageous for the regeneration of carbohydrates already dissolved in ILs [95]. Cellulose can be easily precipitated from the cellulose-IL solution by addition of solvents, such as water, alcohol, acetone or acetonitrile [38,43,56,68,78]. The regenerated cellulose exhibits typically lower degrees of crystallinity compared to the native cellulose. Various novel cellulose materials can be prepared from cellulose-IL solutions, such as composites [96,97], membranes [98], films [78,99], fibers [100,101] or nanofibrillar cellulose aerogels [102]. The conventional pulping techniques are primarily focused on maximizing the cellulose yield neglecting the potential of lignin and hemicellulose. The first is typically degraded during the delignification step or used as a fuel in subsequent processing, often at really low efficiency [103]. The second can be isolated from cellulose, after the delignification, but this typically involves its partial degradation. The clean fractionation of these polymers is very important for the successful utilization of biomass [39]. Although it is difficult to achieve this goal, the possibility of separation of lignocelluloses components with ILs has already been explored [42]. There exist some reports on selective extraction of hemicellulose [104-107] or lignin [88,108]. Dissolution of wood in ILs has also been studied [38,42,109-111]. However, the data on the solubility of the particular polymers is still scarce [82,88,112-114].

Carbohydrate	Ionic liquid	Solubility	T [K]	Ref.
microcrystalline cellulose	[AMIM][Cl]	~ 2-11 %wt	358.15-383.15	[87]
	[BMIM][Cl]	14 g/100g IL	363.15	[88]
commercial cellulose	[BMIM][Cl]	18.4 mg/g IL	353.15-363.15	[82]
	[BMIM][Cl]	6.2 g/100g IL	363.15	[89]
wood cellulose sulfate (DP=495)	[BMIM][Cl]	5 %wt	363.15	[83]
	[BMIM][Cl]	10 %wt	373.15	[83]
	[BMIM][Br]	4 %wt	373.15	[83]
	[BMIM][SCN]	3.5 %wt	373.15	[83]
	[BMIM][OAc]	10 %wt	363.15	[83]
	[BMIM][OAc]	11.5-19 wt%	313.15-353.15	[56]
microcrystalline cellulose (DP=229)	[BMIM][OAc]/Li[OAc]	12-20 wt%	313.15-353.16	[56]
	[BMIM][OAc]/LiCl	12-20 wt%	313.15-353.17	[56]
	[BMIM][OAc]/LiBr	11.5-19.5 wt%	313.15-353.18	[56]
	[BMIM][OAc]/LiClO ₄	12-21 wt%	313.15-353.19	[56]
	[BMIM][OAc]/LiNO ₃	12-21 wt%	313.15-353.20	[56]
	[BMIM][OAc]	23-58 g/mol IL	313.15-393.15	[74]
	[BMIM][OAc]/DMSO	15%	298.15	[90]
	[BMIM][OAc]/DMF	12.5%	298.15	[90]
	[BMIM][OAc]/DMA	5.5%	298.15	[90]
	[BMIM][(C ₆ H ₅)COO]/DMSO	9%	298.15	[90]
[BMIM][(C ₆ H ₅)COO]	< 1-12 wt%	313.15-343.15	[56]	
[BMIM][CH ₂ CHOHCOO]	8-9.5 wt%	333.15-343.15	[56]	
[BMIM][HCOO]	7.5-12.5 wt%	313.15-343.15	[56]	
[BMIM][HOCH ₂ COO]	7.5-10.5 wt%	323.15-343.15	[56]	
[BMIM][HSC ₂ COO]	< 1-13.5 wt%	313.15-343.15	[56]	
[BMIM][H ₂ NCH ₂ COO]	< 1-12 wt%	313.15-343.15	[56]	
microcrystalline cellulose	[DMIM][Cl]	~ 4-23 %wt	343.15-383.15	[87]
	[EMIM][OAc]	22 g/100g IL	363.15	[88]
commercial cellulose	[(CN)EMIM][Br]	33.8 mg/g IL	353.15-363.15	[82]
	[PrMIM][Br]	16.6 mg/g IL	353.15-363.15	[82]
microcrystalline cellulose (DP=229)	[BDMIM][OAc]	5-37 g/mol IL	323.15-393.15	[76]
	[C ₂ OHMIM][OAc]	1-34 g/mol IL	323.15-393.15	[76]
	[C ₃ OMIM][OAc]	8-56 g/mol IL	313.15-393.15	[76]

Carbohydrate	Ionic liquid	Solubility	T [K]	Ref.
	[BzMIM][OAc]	1-34 g/mol IL	323.15-393.15	[76]
	[BEBIM][OAc]	< 1 g/mol IL	393.15	[76]
	[EEBIM][OAc]	< 1 g/mol IL	393.15	[76]
	[AMMOR][OAc]	1-28 g/mol IL	323.15-393.15	[76]
	[EMMOR][OAc]	1-31 g/mol IL	333.15-393.15	[76]
	[AMPIP][OAc]	10-19 g/mol IL	363.15-393.16	[76]
	[BMPIP][OAc]	1-7 g/mol IL	353.15-393.17	[76]
	[BEBT][OAc]	< 1 g/mol IL	393.15	[76]
	[BMPL][OAc]	1-3 g/mol IL	373.15-393.15	[76]
commercial lignin	[(CN)EMIM][Br]	95.3 mg/g IL	353.15-363.15	[82]
	[PRMIM][Br]	62.4 mg/g IL	353.15-363.15	[82]
	[BMIM][Cl]	87.8 mg/g IL	353.15-363.15	[82]
Kraft lignin Indulin AT	[EMIM][OAc]	2 g/100g IL	363.15	[88]
	[BMIM][Cl]	< 0.1 g/100g IL	363.15	[88]
xylan from birch wood	[MeMe(EtOH)NH][HCOO]	2 g/100g IL	363.15	[88]
	[EMIM][CH ₃ COO]	2 g/100g IL	363.15	[88]
	[BMIM][Cl]	< 0.1 g/100g IL	363.15	[88]
	[MeMe(EtOH)NH][HCOO]	2 g/100g IL	363.15	[88]
DP-degree of polymerisation				

Table 15. Solubility of main lignocellulosic polysaccharides in ILs

Chitin is structurally similar to cellulose with one hydroxyl group on each monomer replaced by an acetylamine group, while chitosan is N-deacetylated product of chitin. In contrast to cellulose, only a few examples of the dissolution of chitin or chitosan in ILs have been reported [87,115,116]. Recently, a series of ILs containing alkylimidazolium chloride, alkylimidazolium dimethylphosphate, and 1-allyl-3-methylimidazolium acetate ([AMIM][OAc]) to dissolve chitin were used. It was noticed that the degree of acetylation, the crystallinity, the molecular weights of chitin, as well as the nature of the anion of the IL all affect the dissolution behavior of chitin in ILs [117]. The acetate anion was strong enough to cleave the hydrogen bond network of chitin, while the chloride anion and dimethylphosphate anion were less efficient. The same was observed for chitosan [118,119]. The dissolving power of acetate ILs for chitosan seems stronger than that of chloride ILs. At a given temperature, the dissolution performance of the ILs for chitosan decreases in the order: [BMIM][OAc] > [BMIM][CH₃CH₂COO] > [BMIM][CH₃CH₂CH₂OO] > [BMIM][C₆H₅COO] > [BMIM][HOCH₂COO] > [BMIM][HCOO] > [BMIM][CH₃CHOHCOO] > [BMIM][N(CN)₂]. The influence of the cation on the solubility of chitosan in chloride-

based ILs was also determined and the solubility decreases as follow: 1,3-dimethylimidazolium chloride ([DMIM][Cl]) > [AMIM][Cl] > [BMIM][Cl] [87]. In the same study, the mixtures of ILs have been tested for the dissolution of chitosan and good results were obtained. Both chitin and chitosan due to their favorable properties such as good biocompatibility, biodegradability, absorptivity and nontoxicity find many applications in the field of tissue engineering, drug delivery, food preservation, waste water purification, packaging or cosmetics [120-123]. Very recently it was reported that chitosan together with agarose [124], or agarose on its own [125,126], were used to prepare ionogels which are shown to be smart polymeric conducting materials [127]. Agarose is an algal polysaccharide comprising alternating D-galactose and 3,6-anhydro-L-galactose repeating units, essentially uncharged. Over the years it was often use for its gelling properties. Similarly to cellulose, due to the large number of hydroxyl groups in its structure, agarose is insoluble in many common organic solvents and cold water. ILs that were found to dissolve agarose are of basic character and are able to disrupt the hydrogen-bonding network of the polymer leading to dissolution [125,126]. Unlike cellulose, where the alkyl chain length of the cation has very limited effect on solubility [58,60,61,65,75], a remarkable decrease of solubility of agarose with increase in alkyl chain length of the cation was observed (compare [bmim][Cl] with 1-octyl-3-methylimidazolium chloride ([OMIM][Cl]) in Table 16 [125]. When compared to neat ILs, an increase in the solubility of agarose is observed in general in the mixed IL-IL system (e.g., compare [MeNH₃][HCOO] with [MeNH₃][HCOO]/[BMPy][Cl] or [MeNH₃][HCOO]/[BMIM][Cl] in Table 16 [126].

Carbohydrate	Ionic liquid	Solubility	T [K]	Ref
Chitin (DA=91.6%)	[AMIM][OAc]	5 %wt	383.15	[117]
	[AMIM][Cl]	0.5 %wt	< 318.15	[117]
	[BMIM][Cl]	ns	453.15	[117]
	[EMIM][(CH ₃ O) ₂ PO ₂]	1.5 %wt	< 333.15	[117]
	[DMIM][(CH ₃ O) ₂ PO ₂]	1.5 %wt	< 333.15	[117]
	[C ₂ OHMIM][Cl]	ns	453.15	[117]
Chitosan (DC=75-85%)	[BMIM][HCOO]	0.6-8.4 %	343.15-423.15	[119]
	[BMIM][OAc]	0.8-14.4 %	343.15-423.15	[119]
	[BMIM][CH ₃ CH ₂ COO]	0.2-12.4 %	343.15-423.15	[119]
	[BMIM][CH ₃ (CH ₂) ₂ COO]	0.2-10.4 %	343.15-423.15	[119]
	[BMIM][HOCH ₂ COO]	0.6-9.6 %	343.15-423.15	[119]
	[BMIM][CH ₃ CHOHCOO]	0.4-6.2 %	343.15-423.15	[119]
Chitosan (DC > 90%)	[BMIM][(C ₆ H ₅)COO]	1.4-7.6 %	343.15-423.15	[119]
	[AMIM][Cl]/[MIM][Cl]	~1-12 %wt	353.15-383.15	[87]
	[DMIM][Cl]/[MIM][Cl]	~ 3-16 %wt	343.15-383.15	[87]

Carbohydrate	Ionic liquid	Solubility	T [K]	Ref
corn starch	[AMIM][Cl]	11.75%	363.15	[128]
wheat starch	[AMIM][Cl]	11.25%	363.15	[128]
rice starch	[AMIM][Cl]	11%	363.15	[128]
mung bean	[AMIM][Cl]	10.50%	363.15	[128]
potato starch	[AMIM][Cl]	9%	363.15	[128]
maiz starch	[BMIM][Cl]	10 wt%	373.15	[131]
	[BMIM][Cl]	16 %wt	343.15	[125]
	[BMIM][CH ₃ OSO ₃]	5 %wt	343.15	[125]
	[OMIM][Cl]	4.5 %wt	343.15	[125]
	[BMPy][Cl]	13 %wt	343.15	[125]
	[HOEtNH ₃][HCOO]	5 %wt	343.15	[126]
	[MeNH ₃][HCOO]	14 %wt	343.15	[126]
	[EtNH ₃][HCOO]	20 %wt	343.15	[126]
	[HOEtNH ₃][HCOO]/[BMIM][Cl]	8 %wt	343.15	[126]
	[MeNH ₃][HCOO]/[BMIM][Cl]	18 %wt	343.15	[126]
	[EtNH ₃][HCOO]/[BMIM][Cl]	7 %wt	343.15	[126]
	[HOEtNH ₃][HCOO]/[BMPy][Cl]	7 %wt	343.15	[126]
	[MeNH ₃][HCOO]/[BMPy][Cl]	21 %wt	343.15	[126]
	[EtNH ₃][HCOO]/[BMPy][Cl]	25 %wt	343.15	[126]
	[HOEtNH ₃][HCOO]/[BMIM][CH ₃ OSO ₃]	14 %wt	343.15	[126]
[MeNH ₃][HCOO]/[BMIM][CH ₃ OSO ₃]	23 %wt	343.15	[126]	
[EtNH ₃][HCOO]/[BMIM][CH ₃ OSO ₃]	26 %wt	343.15	[126]	

DA-degree of acetylation; DC-degree of deacetylation

Table 16. Solubility of polysaccharides in ILs

Starch is another example of one the most abundant natural polymers. Its utilization in its native form is often limited though. This is due to some undesirable characteristics such as poor solubility, low mechanical properties, and instability at high temperature and pH during processing. The derivatisation of starch is typically required in order to overcome these shortcomings and improve its functionality for industrial applications [129]. During the last few years an increasing interest in manufacturing value-added products based on starch utilizing ILs has been observed, whilst much less attention has been paid to the subject of solubility of starch in ILs [130-132]. Very recently, reports comparing the dissolution of starch in IL, [EMIM][OAc], with gelatinization process in water were published [133,134]. Consid-

ering the mechanism of dissolution, it was stated that in case of pure IL, the solvent penetrates starch granule making outer layer slightly swollen and transparent. With time, less and less granules can be seen, up to complete visual disappearance. In water, starch granules first swell with temperature increase and then burst. For mixed [EMIM][OAc]-water systems, the behavior of the solvent depends on the [EMIM][OAc]-water ratio. For 25–75% and 50–50% [EMIM][OAc]-water systems the gelatinisation takes place. The dissolution similar to the one in pure ILs occurs for 75% [EMIM][OAc]-25%water system and the presence of water strongly accelerates it. It seems that water swells the outer layer first facilitating penetration of the IL, and thus starch dissolution. Additionally, the viscosity of the 75% [EMIM][OAc]-25%water system is much lower than that of a pure [EMIM][OAc].

Carbohydrate	Ionic liquid	Solubility	T [K]	Ref.
β-cyclodextrin	[AMIM][Cl]	79.4-112.3 g/100g IL	333.15-353.15	[141]
	[BMIM][Cl]	69.7-106.7 g/100g IL	343.15-363.15	[141]
	[C ₂ OHMIM][Cl]	78.4-110.4 g/100g IL	338.15-358.15	[141]
	[AMIM][N(CN) ₂]	102.3-132.2 g/100g IL	333.15-353.15	[141]
	[BMIM][N(CN) ₂]	73-105.1 g/100g IL	333.15-353.15	[141]
	[C ₂ OHMIM][N(CN) ₂]	90.5-121.5 g/100g IL	333.15-353.15	[141]

Table 17. Solubility of oligosaccharides in ILs

Hydrolysis of starch produces a group of low-molecular-weight carbohydrates named dextrans [135]. Dextrans are mixtures of linear and branched (1,4)-linked α-glucose polymers, while cyclodextrins are a series of cyclic oligosaccharides composed of 6, 7, or 8 D-(+)-glucose units named α-, β-, and γ-cyclodextrin, respectively. The structures of cyclodextrins are identical as each of them contains a molecular cavity. The hydroxyl groups of the oligomer are on the outside of the cavity, while the inner cavity is hydrophobic. Cyclodextrins are able to form inclusion complexes with a number of organic and inorganic guest molecules that are encapsulated in their molecular cavities. Most of the investigations concerning ILs and cyclodextrins are focused on understanding the nature of interactions [136-143]. The solubility data are very limited [44]. Fan and co-workers investigated the solubility of β-cyclodextrin in six kinds of hydrophilic ILs [141]. It is shown that the solubilities were remarkable and followed the order [AMIM][N(CN)₂] > [C₂OHMIM][N(CN)₂] > [AMIM]Cl > [BMIM][N(CN)₂] > [C₂OHMIM]Cl > [BMIM]Cl. Monosaccharides (especially glucose and fructose) and disaccharides (mainly sucrose), after cellulose, are the most studied carbohydrates in ILs.

Table 18 and 19 summarizes the solubility data for disaccharides [85,133,144-146] and monosaccharides [85,86,144-148], respectively. Solubility of sugar in a given IL decreases in the following order: D-(-)-fructose > D-(+)-glucose > sucrose. It can be justified by the chemical structure of sugars and their basic thermal properties (i.e., temperature and enthalpy of fusion), independent of the IL [85,86,147]. The melting temperature and melting enthalpy of carbohydrates are related with their solubility and the larger the properties, the lower the solubility.

Regarding the influence of the cation and anion structure of the ILs on the solubility of carbohydrates, some general conclusions can be drawn from the collected data. Similarly as in the case of cellulose, the role of the cation is not insignificant. It was found that imidazolium-based ILs are capable of dissolving monosaccharides, whereas pyridinium and phosphonium ILs are rather poor solvents for these sugars [145]. Novel ILs containing dimethylguanidinium cation and anions such as saccharine, acesulfame and thiocyanate has also been investigated and some remarkable results were obtained. It was demonstrated that introduction of functionality in the alkyl chain of the dimethylguanidinium-based ILs can improve the dissolution of carbohydrates [146]. Sugars are more soluble in ILs with shorter alkyl chains in their chemical structure. The same as for polycarbohydrates, increasing length of the chain results in a more hydrophobic nature of the cation and IL as a whole, and thus weakens the capacity of dissolving polar solutes like sugars [85,86]. As an example, the lower solubilities of monosaccharides such as D-(+)-glucose, D-(-)-fructose, D-(+)-xylose and D-(+)-galactose in [Aliquat][Cl], in comparison to [EMIM][EtSO₄], can be given. [Aliquat][Cl] is a mixture of methyltriethylammonium chloride and methyltridecylammonium chloride. The hydrophobicity and larger non-polar alkyl chains on the [Aliquat][Cl] which have not much affinity with the hydroxyl groups of the sugars explains its poor solubility power [147]. Among hydrophobic ILs, the more bulky (more hydrophobic) [P_{6,6,6,14}][N(CN)₂] was less capable to dissolve less sugars, when compared with [Aliquat][N(CN)₂] [86]. Regarding the effect of the anion on the solubility of sugars it was observed that all from the investigated carbohydrates (glucose, fructose and sucrose) were more soluble in [BMIM][OTf] compared to [BMIM][N(CN)₂] [85,86]. Glucose and xylose showed the highest solubilities, among the seven various ILs investigated, in either [BMIM][HSO₄] or [BMIM][SCN] [145]. The authors of the study explained that it can be a result of a large affinity of anions towards monosaccharides. In particular, it can be caused by a highly acidic effect of [HSO₄] which acts as strong hydrogen bond donor, and [SCN] responsibility for the strong hydrogen bond accepting interactions due to a high polarizability of the anion and the specific structure stabilised by the resonance. Also, the study of cyano-based ILs revealed that, in general, the monocyano anion is a stronger hydrogen bond acceptor than a more complex multicyno anion. Thus, the solubility of carbohydrates can be higher in [SCN] than in [N(CN)₂] or even in [C(CN)₃]-based ILs.

Carbohyd rate	Ionic liquid	Solubility	T [K]	Modeling	Ref.
sucrose	[BMIM][Cl]	5-40 wt%	343.95-380.3	NRTL, UNIQUAC	[144]
	[BMIM][SCN]	2-35.3 wt%	315.2-411.67	-	[145]
	[BMIM][N(CN) ₂]	18.8-75.3 mol %	325.9-369	PC-SAFT	[85]
	[BMIM][C(CN) ₃]	2-35.3 wt%	381.2-406.64	-	[145]
	[BMIM][OTf]	19.2-86.8 mol %	316.2-365.2	PC-SAFT	[85]
	[BMIM][HSO ₄]	235 wt%	358.74-388.5	-	[145]
	[EMIM]([MeO](EtO)EtOSO ₃)	2.1-25.3 wt%	343.6-410.63	-	[145]

Carbohydrate	Ionic liquid	Solubility	T [K]	Modeling	Ref.
	[EMIM][SCN]	2.5-30 wt%	284.25-383.15	NRTL, UNIQUAC	[144]
	[DMIM][CH ₃ PO ₃]	5-50 wt%	286.15-376.45	NRTL, UNIQUAC	[144]
	[C ₂ OHMIM][Cl]	5-40 wt%	356.15-384.15	NRTL, UNIQUAC	[144]
	[C ₅ O ₂ MIM][Cl]	17.11 wt%	308.15	-	[146]
	[C ₅ O ₂ MIM][N(CN) ₂]	11.06 wt%	308.15	-	[146]
	[P _{4,4,4,1}][CH ₃ C ₆ H ₄ SO ₂]	3.1-10.1 wt%	378.97-402.13	-	[145]
lactose	[BMIM][Cl]	2.5-28 wt%	344.15-381.55	NRTL, UNIQUAC	[133]
	[EMIM][SCN]	2.5-18 wt%	288.05-382.55	NRTL, UNIQUAC	[133]
	[DMIM][CH ₃ PO ₃]	5-39.3 wt%	290.55-356.25	NRTL, UNIQUAC	[133]
	[C ₂ OHMIM][Cl]	2.5-25 wt%	355.75-384.15	NRTL, UNIQUAC	[133]
	[C ₅ O ₂ MIM][Cl]	10.69 wt%	308.15	-	[146]
	[C ₅ O ₂ MIM][N(CN) ₂]	16.55 wt%	308.15	-	[146]

Table 18. Solubility of disaccharides in ILs

As it was mentioned before, cellulose can be easily precipitated from the cellulose-IL solution by means of selective precipitation [38,43,56,68,78]. However, separation of smaller carbohydrates such as glucose from ILs remains a challenging task. Glucose and ILs have extremely low vapor pressure. Therefore, conventional vacuum distillation methods do not serve for their separation. Also, no suitable organic solvent capable of extracting sugar from ILs have been found. In 2011, it was reported for the first time that antisolvent method can be applied to the separation of glucose and IL [149]. An antisolvent method is based on discrepancies in the interactive forces between solute, solvent and antisolvent. An addition of an antisolvent to a binary solution (solute+solvent) causes a reduction in the original solubility of the solute in the binary solution, leading to its crystallization and precipitation. Very recently, the method was adopted for separation of other systems, differing in carbohydrates and ILs [150,144,148].

Carbohydrate	Ionic liquid	Solubility	Temperature [K]	Modeling	Ref.
D-(-)-fructose	[BMIM][Cl]	5-50 wt%	343.15-359.25	NRTL, UNIQUAC	[144]
	[BMIM][N(CN) ₂]	11-74.9 mol %	297.2-367.6	PC-SAFT	[85]
	[BMIM][N(CN) ₂]	28.1-41 wt%	288.15-328.45	NRTL, UNIQUAC	[86]
	[BMIM][OTf]	20.5-88.2 mol %	313.8-365.4	PC-SAFT	[85]
	[EMIM][SCN]	5-45 wt%	281.15-358.15	NRTL, UNIQUAC	[144]
	[EMIM][N(CN) ₂]	33.3-49.5 wt%	288.25-328.25	NRTL, UNIQUAC	[86]

Carbohydrate	Ionic liquid	Solubility	Temperature [K]	Modeling	Ref.
	[EMIM][OTf]	35.5-41.5 wt%	288.05-308.3	NRTL, UNIQUAC	[86]
	[EMIM][EtSO ₄]	25.7-43.5 wt%	288.2-329.3	NRTL, UNIQUAC	[147]
	[DMIM][CH ₃ PO ₃]	5-60 wt%	284.95-344.15	NRTL, UNIQUAC	[144]
	[C ₂ OHMIM][Cl]	10-60 wt%	355.05-369.15	NRTL, UNIQUAC	[144]
	[Aliquat][NO ₃]	13.1-21.8 wt%	307.75-339.75	NRTL, UNIQUAC	[86]
	[Aliquat][N(CN) ₂]	3.2-13 wt%	299.95-339.74	NRTL, UNIQUAC	[86]
	[Aliquat][Cl]	15.4-25.2 wt%	298.2-328.2	NRTL, UNIQUAC	[147]
	[P _{6,6,6,14}][N(CN) ₂]	0.276-5.52 wt%	298.37-328.21	NRTL, UNIQUAC	[86]
	[C ₅ O ₂ MIM][Cl]	14.10 wt%	308.15	-	[146]
	[C ₅ O ₂ MIM][N(CN) ₂]	48.99 wt%	308.15	-	[146]
D-(+)-galactose	[EMIM][EtSO ₄]	4-14 wt%	288.8-328.2	NRTL, UNIQUAC	[147]
	[Aliquat][Cl]	4.2-8.6 wt%	298.3-329.2	NRTL, UNIQUAC	[147]
	[BMIM][Cl]	5.9-50 wt%	343.15-360.45	-	[148]
	[BMIM][SCN]	2-50 wt%	300.77-406.17	-	[145]
	[BMIM][N(CN) ₂]	18.6-76.6 mol %	304.4-366.5	PC-SAFT	[85]
	[BMIM][N(CN) ₂]	13.3-23.6 wt%	288.15-328.45	NRTL, UNIQUAC	[86]
	[BMIM][N(CN) ₂]	18.56 wt%	308.15	-	[146]
	[BMIM][NTf ₂]	0.59 wt%	308.15	-	[146]
	[BMIM][C(CN) ₃]	2-15 wt%	362.18-404.6	-	[145]
	[BMIM][OAc]	39.41 wt%	308.15	-	[146]
D-(+)-glucose	[BMIM][OTf]	16.1-88.9 mol %	298.5-365.3	PC-SAFT	[85]
	[BMIM][HSO ₄]	2-50.2 wt%	350.9-384.8	-	[145]
D-(+)-glucose	[BMIM][C ₄ F ₉ SO ₃]	2-5 wt%	401.13-422.17	-	[145]
	[EMIM][SCN]	6-40 wt%	283.15-345.95	-	[148]
	[EMIM][N(CN) ₂]	17.1-28.1 wt%	288.25-328.25	NRTL, UNIQUAC	[86]
	[EMIM][OAc]	43.89 wt%	308.15	-	[146]
	[EMIM][OTf]	26.1-34.9 wt%	288.47-329.07	NRTL, UNIQUAC	[86]
	[EMIM][EtSO ₄]	10.4-23.7 wt%	288.2-328.3	NRTL, UNIQUAC	[147]
	[EMIM][(MeO)EtOEtOSO ₃]	2.4-33.9 wt%	328.33-393.37	-	[145]
	[DMIM][BF ₄]	0.44 wt%	308.15	-	[146]
	[DMIM][CH ₃ PO ₃]	5-60 wt%	285.15-360.25	-	[148]

Carbohydrate	Ionic liquid	Solubility	Temperature [K]	Modeling	Ref.
	[C2OHMIM][Cl]	12-58 wt%	355.15-370.35	-	[148]
	[C5O2MIM][Cl]	29.28 wt%	308.15	-	[146]
	[C5O2MIM][N(CN) ₂]	19.01 wt%	308.15	-	[146]
	[C5O2MIM][SCN]	18.38 wt%	308.15	-	[146]
	[C5O2MIM][SAC]	18.97 wt%	308.15	-	[146]
	[C5O2MIM][ACES]	14.39 wt%	308.15	-	[146]
	[Aliquat][Cl]	2.26 wt%	308.15	-	[146]
	[Aliquat][NO ₃]	3.93-8.65 wt%	307.75-339.75	NRTL, UNIQUAC	[86]
	[Aliquat][N(CN) ₂]	0.78-3.23 wt%	299.95-339.74	NRTL, UNIQUAC	[86]
	[Aliquat][N(CN) ₂]	1.25 wt%	308.15	-	[146]
	[Aliquat][OAc]	4.05 wt%	308.15	-	[146]
	[Aliquat][Cl]	9-12.5 wt%	297.9-327.9	NRTL, UNIQUAC	[147]
	[P _{6,6,6,14}][Cl]	4.69 wt%	308.15	-	[146]
	[P _{6,6,6,14}][N(CN) ₂]	0.18-0.48 wt%	298.37-329.21	NRTL, UNIQUAC	[86]
	[P _{6,6,6,14}][N(CN) ₂]	0.5 wt%	308.15	-	[146]
	[P _{6,6,6,14}][OAc]	4.9 wt%	308.15	-	[146]
	[P _{4,4,4,1}][CH ₃ C ₆ H ₄ SO ₂]	2-15.4 wt%	365.29-392.89	-	[145]
	[(C ₃ O) ₄ DMG][Cl]	38.58 wt%	308.15	-	[146]
	[(C ₃ O) ₄ DMG][SCN]	11.34 wt%	308.15	-	[146]
	[(C ₃ O) ₄ DMG][N(CN) ₂]	6.19 wt%	308.15	-	[146]
	[(C ₃ O) ₄ DMG][OAc]	31.73 wt%	308.15	-	[146]
	[(C ₃ O) ₄ DMG][SAC]	20.59 wt%	308.15	-	[146]
	[(C ₃ O) ₄ DMG][ACES]	8.44 wt%	308.15	-	[146]
	[(di-h) ₂ DMG][Cl]	6.61 wt%	308.15	-	[146]
	[(di-h) ₂ DMG][SCN]	1.95 wt%	308.15	-	[146]
	[(di-h) ₂ DMG][N(CN) ₂]	2.88 wt%	308.15	-	[146]
	[(di-h) ₂ DMG][OAc]	14.4 wt%	308.15	-	[146]
	[(di-h) ₂ DMG][SAC]	3.66 wt%	308.15	-	[146]
	[(di-h) ₂ DMG][ACES]	2.27 wt%	308.15	-	[146]
D-(+)-xylose	[BMIM][SCN]	2-45.1 wt%	288.93-388.08	-	[145]
	[BMIM][C(CN) ₃]	3.1-20 wt%	351.57-390.04	-	[145]
	[BMIM][C ₄ F ₉ SO ₃]	2-10.5 wt%	382.84-408.5	-	[145]

Carbohydrate	Ionic liquid	Solubility	Temperature [K]	Modeling	Ref.
	[BMIM][HSO ₄]	2-50 wt%	349.58-380.18	-	[145]
	[EMIM][EtSO ₄]	15-27.41 wt%	288.1-328.5	NRTL, UNIQUAC	[147]
	[EMIM][(MeO)(EtO)EtOSO ₃]	2.1-29.9 wt%	325-387.26	-	[145]
	[Aliquat][Cl]	12.6-16.7 wt%	298.5-330	NRTL, UNIQUAC	[147]
	[P _{4,4,4,1}][CH ₃ C ₆ H ₄ SO ₂]	1.8-20 wt%	350.16-395.46	-	[145]

Table 19. Solubility of monosaccharides in ILs

The ability to predict whether a given IL dissolves a particular carbohydrate or not is of outmost interest. There are several empirical and semi-empirical measuring techniques and polarity scales that can predict and explain the solubility of carbohydrates in a solution, e.g. COSMO-RS, Hansen solubility parameters and Kamlet-Taft solvent parameters [41]. The empirical Kamlet-Taft model [67,79] and the quantum mechanical COSMO-RS model [151-153] have been used most frequently to predict or explain the solubility of carbohydrates in ILs, while few literature data exist for Hansen solubility parameters of ionic liquids [154]. The Kamlet-Taft parameters (α , hydrogen bond acidity; β , hydrogen bond basicity; and π^* , polarity) are determined by measuring the UV-VIS spectra of dyes when dissolved in a solvent of interest. It was suggested that solubility of carbohydrates increases with an increase of ILs basicity (ILs that are capable of dissolving carbohydrates are generally characterized by high hydrogen-bond basicity parameter; $\beta > 0.8$), and polarity [41,56,74,119,126,144,148]. The potential of COSMO-RS-based screening of ILs with respect to their dissolving power for cellulose was evaluated in the pioneer research of Kahlen et al. [151]. Cellulose solubility was modeled for more than 2000 ILs using activity coefficients as reference property and the results were in good agreement with the data available in the literature. Later on, the work was extended to the computational COSMO-RS analysis of the affinity of both cellulose and lignin for 320 different ILs [153]. A new reference property, namely the excess enthalpy of the IL + lignin/cellulose mixtures, was used to predict solubilities of lignin and cellulose in ILs. The conclusions achieved were validated in the laboratory for a selected set of ILs. The ability of more than 20 hydrophilic ILs to dissolve *Miscanthus* was also interpreted using Abraham solvation parameters obtained from COSMO-RS [151]. In case of smaller carbohydrates, Carneiro et al. were the first group to correlate the solubility data of monosaccharides in ILs using the NRTL and UNIQUAC thermodynamic models [147]. They investigated solubility of D-(+)-glucose, D-(-)-fructose, D-(+)-xylose and D-(+)-galactose in two ILs: [Aliquat][Cl] and [EMIM][EtSO₄]. Following their success, other works on application of NRTL and UNIQUAC thermodynamic models for correlation of solubilities of glucose [86,148,144], fructose [86,144], sucrose and lactose [144] have been reported. Very recently, perturbed-chain statistical associating fluid theory (PC-SAFT) was applied to model experimental data on solubility of glucose, fructose and sucrose [85,154,155]. This approach occurred to be more promising since it showed better predictive capacity and quite reasonable accuracy. As an equation-of-state model, it enables

the capture of properties of both pure fluids and mixtures. Although some data concerning solubility of carbohydrates in ILs is already available in the literature, it is not sufficient to have a good knowledge of phase equilibria. These investigations cover essentially only the most well-known sugars, glucose, fructose, and sucrose, as well as polysaccharides such as cellulose. In most cases, data are measured by using different experimental procedures and contain single data points at fixed temperature. It makes application of existent or the development of new thermodynamic models a very difficult task. Moreover, solubility of carbohydrates in ILs is sensitive to the presence of impurities, especially water, and even though authors do not report on the water content. ILs have provided a new processing platform for the dissolution, regeneration and functionalization of carbohydrates, thus increasing their chances of exploitation. However, for the purpose of successful process design and optimization, more reliable data on solubility of various carbohydrates in ILs is fundamental.

5. Solubility of specific polymers and macromolecules in ionic liquids

Concerning other classes of polymers and macromolecules, the use of Ionic Liquids represents real challenges in order to solubilize those allowing future modifications and depolymerization in the constitutive monomers.

Wang et al reported the possibility to dissolve and regenerate polybenzimidazole in 1-butyl-3-methylimidazolium chloride, [BMIM][Cl] and other hydrophilic ionic liquids [156]. The authors describe ionic liquids as alternative solvents for dissolution of different organic polymers. Polybenzimidazole (PBI), also known as poly-2,20-(mphenylene)-5,50-benzimidazole, is a polymer composed by linear aromatic polymer chains as well as both donor and acceptor hydrogen-bonding sites. This class of polymers exhibits high thermal stabilities, chemical resistance, and mechanical strength [157]. According with their relevant properties, PBI has been developed as membranes [158], textile fibers [159], and high-temperature matrix resins [160]. One of the problems associated with PBI and similar polymers is their poor solubility and infusibility in common organic solvents. PBI is only soluble after heating highly polar aprotic solvents such as dimethylformamide, dimethylacetamide or dimethyl sulfoxide. The authors described that PBI was insoluble for all tested solvents at room temperature but it was completely soluble in [BMIM][Cl] and [BMIM][OH] yielding brown viscous solutions at 80 to 140°C. It is important to note that PBI was four times more soluble in [BMIM][Cl] or [BMIM][OH] at 140°C than in DMAc (+ 4.5 wt% LiCl) as solvent. The possibility to use a microwave process showed a significant improvement in the dissolution rates as well as an efficient heating of ILs [161,162]. However, ILs having 'non-coordinating' anion like BF₄ was non-effective solvent even with microwave heating. The dissolving mechanism of PBI in ILs is not clear but some publications suggested the use of [BMIM][Cl] due an effective hydrogen-bonding breaking, allowing faster dissolution times as well as higher ability to dissolve PBI. For comparison, [BMIM][Cl] presents almost 3 times higher chloride concentration (around 20 mol%) than in the case of conventional DMAc (+ 10 wt% LiCl; free chloride concentration is around 6.7 mol%) solvent. For complete elucidation of dissolution mechanism of different polymers in ionic liquids is important to perform other dissolution studies and complementary

techniques which can validate the previous proposals. Wang and co-workers reported a similar dissolution mechanism in the case of [BMIM][OH] as well as the use of this IL in order to prepare PBI-based anion-exchange gel electrolyte membranes for alkaline fuel cells. Another attractive point is related with the possibility to precipitate or regenerate PBI from the IL solution by addition of water or other precipitating solutions. The regenerated PBI fibers show no change in chemical structure and thermal stability comparing with fibers formed by conventional systems.

Watanabe and co-workers reported the solubility of poly(methyl methacrylate) (PMMA) in 1-alkyl-3-methylimidazolium ionic liquids (ILs) with different anionic structures [163]. For evaluation of PMMA solubility in ILs were tested monodisperse PMMA-grafted silica nanoparticles (PMMA-g-NPs) as a measurement probe. The solubility was mainly affected by the anionic structures of the ILs rather than by the alkyl chain length of the cationic structure. It is empirically known that PMMA is soluble in hydrophobic ILs such as [BMIM][PF₆] and [BMIM][NTf₂].[164,165] Previously, Watanabe group reported different hydrodynamic radii exhibited by PMMA-grafted silica nanoparticles (PMMA-g-NPs) in these ILs. Additionally, the grafted PMMA chain was more swollen in [BMIM][NTf₂] than in [BMIM][PF₆] [166] suggesting that [BMIM][NTf₂] is a better solvent for PMMA. In conclusion, PMMA solubility in relation to the solvent parameters of the ILs, it is focused in two important factors in order to predict PMMA solubility in ILs. The predominant one is the nonpolar properties of the anion. However, the non-polarity cation IL effect can also contribute for overall PMMA solubility. In general, the PMMA solubility is dependent of two relevant contributions: one from anionic unit (primary) and other from cationic unit (secondary) nonpolarity. The authors considered that the solubility behavior could not be justified by ILs solvent because of complexity in ILs. All published results can contribute for future predictions of PMMA derivatives solubility's such as polyacrylates or polymethacrylates. Wang and Liang groups [167] described a detailed study of the solubility and chain conformation of different types of homopolymers in low viscosity ionic liquids (ILs) in particular 1-allyl-3-methylimidazolium chloride ([AMIM][Cl]) at 50°C and 1-butyl-3-methylimidazolium formate ([BMIM][COOH]) at 25°C using laser light scattering technique (LLS). This technique allows the polymer solubility determination in ILs at low concentrations. The study of polymer and IL systems by LLS is restricted to higher IL viscosities as well as the slow diffusion of polymer chains in IL and water content or other impurities from ILs. Normally, selected ILs are hygroscopic and the water content changes with time. The aggregation effect was observed for all neutral tested polymers (e.g. polyvinyl alcohol and polysulfonamide), except in the case of polyvinyl alcohol in [BMIM][COOH]. Single chain conformations have been observed in the case of DNA and polystyrene sulfonate as negative polyelectrolytes. The authors suggested the condensation of the polymer chains in ILs according with their smaller hydrodynamic polymer radius. In general, the solubility of homopolymers could be qualitatively explained by treating polymer/IL as a ternary system: polymer, cation, and anion. The authors suggested that mutual interactions determined the polymer conformation and solubility in ILs. However, preliminary results indicated us those strong interactions between polymers and bulky cations in ILs are relevant for higher dissolution performance. Several publications proof an effective dissolution of different synthetic polymers in ILs (for example poly(ethylene oxide) (PEO) [168],

poly(methyl methacrylate) [169], polyacrylonitrile [170], poly(m-phenylene isophthal amide) [171], and polyarylsulfone [172]) while many others (e.g. polyethylene, polyester, polyurethane, and nylon) were not soluble in the tested ILs.

In different perspective, efficient polymerization processes as well as preparation of specific polymeric materials using ILs have been also described. In this context, Zhang and co-workers [173] reported the polymerization of acrylonitrile in the presence of [BMIM][Cl] and then for the first time polyacrylonitrile fibers were directly produced from spinning process of the previous polymer solution. According to remarkable acrylic fibers properties (in particular soft and wool-like aesthetics and resistance ultraviolet fading) different fields of application (e.g. home furnishings, outdoor articles, aviation and space fields). From 1980s the wet and dry spinning technologies have been used as most effective processes for PAN fibers production. [174] For wet and dry spinning processes, the use of large amounts of unfriendly solvents to the environment have been required.

It seems that [BMIM][Cl] is a suitable solvent for the polymerization, spinning and dissolution of the acrylic fibers. In this context, different acrylic polymers with tunable properties (higher concentration of acrylonitrile, large molecular weight, and low polydispersity index PDI). The solutions of PAN and [BMIM][Cl] allowed the development of PAN fibers containing good mechanical properties and round profile after efficient spun using dry-jet wet spinning technology.

In 2009, Rodriguez et al [175] reported that 1-alkyl-3-methylimidazolium chloride ionic liquids (ILs) can form immiscible liquid mixtures with some polyethylene glycols (PEGs). PEGs have been largely used in industry because of their reduced toxicity and cost as well as higher biodegradability. [176] Additionally low volatility and melting points of PEGs facilitate their use as alternative solvents or additives in several aqueous biphasic systems. [177] Many publications indicate the possibility to tune PEG properties as relevant characteristic (for example PEGs with shorter chain lengths are liquid at room temperature and water miscible while PEGs with longer chain lengths melt at higher temperatures and with variable water solubility).

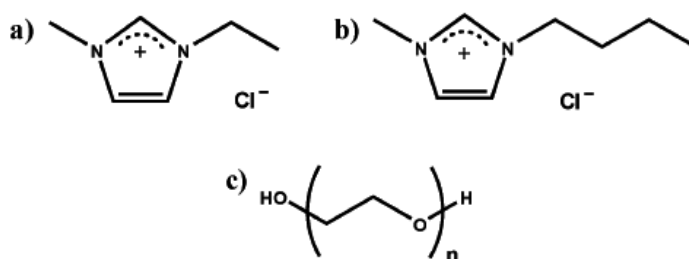


Figure 3. Selected chemical structures: a) [EMIM][Cl]; b) [BMIM][Cl]; c) PEG (PEG-1500)

Recently, PEGs and ILs have been combined for application as polymer electrolytes in batteries, [178] or, homogeneous mixed solvents with distinctive properties. [179] Binary

mixtures between [EMIM][Cl] and PEGs (PEG-1500, 2000, or 3400), or [BMIM][Cl] and PEGs (PEG-2000 or 3400) giving stable biphasic systems over a significant temperature range (from 333.15 K to 413.15 K). [EMIM][Cl]/PEG-1000 and [BMIM][Cl]/PEG-1000 or PEG-1500 are miscible. Negative values for the change of enthalpy and entropy of IL/PEG mixtures have been observed by thermodynamic analysis of the liquid–liquid equilibrium data. The possible tunability according with adequate IL/PEG combinations could be applied for separation of complex solutes by solvent extraction processes at high temperature. The authors tried applied these biphasic, entirely liquid systems, with low volatility and good solvation properties, for the dissolution and separation of cellulose and lignin at elevated temperature, although only modest results have been achieved to date. Samitsu et al [180] reported the dissolution behavior of polyrotaxanes, consisting of α -cyclodextrin and poly(ethylene glycol), with different molecular weights (2000 and 35.000).

Harada et al. and other authors reported some polyrotaxanes, containing α -cyclodextrins (α -CD) as the cyclic molecules and poly(ethylene glycol) (PEG) as a linear polymer. [181, 182] Polyrotaxanes have been largely applied in different fields, in particular drug delivery systems for biological applications [183], insulated molecular wires [184] and photo-induced energy transfer systems for electrical applications. [185] Interlocked polymer networks built from polyrotaxanes have been also tested as gels and rubbery materials for industrial applications.

Several studies reported polyrotaxane solubilities in several ionic liquids mainly based on 1-butyl-3-methylimidazolium cation [BMIM] combined with different anions (e.g. [Cl], [Br], [BF₄], [PF₆], [NTf₂], and [MDEGSO₄]). Transparent homogeneous solutions were obtained in the case of addition of polyrotaxanes to ILs [BMIM][Cl] and [BMIM][Br]. The solubility results indicate that the polyrotaxanes are readily soluble in [BMIM][Cl] and [BMIM][Br] but not in the other tested ionic liquids. Recently, the dissolution performance were studied using ILs containing chloride anions and a variety of organic cations including [EMIM], [BMIM], [HMIM], [OMIM], [C₁₀MIM]. Transparent homogeneous solutions were obtained for the dissolution of polyrotaxanes in all tested ILs.

IL + PEG System	W _{IL} , PEG-rich phase	W _{IL} , IL-rich phase
[EMIM][Cl] + PEG-1500	0.17-0.27	0.88-0.97
[EMIM][Cl] + PEG-2000	0.08-0.14	0.94-0.99
[EMIM][Cl] + PEG-3400	0.02-0.06	0.95-0.98
[BMIM][Cl] + PEG-2000	0.32-0.38	0.86-0.93
[BMIM][Cl] + PEG-3400	0.09-0.16	0.83-0.99

Table 20. Variation of mass fraction of IL (W_{IL}) in the equilibrium phases for the LLE of the binary systems IL +PEG over the temperature range 60- 140 °C.

The solubilities of two polyrotaxanes in ILs as well as the α -CD and PEG solubilities for comparison are summarize in Table 21

Ionic Liquids	PR-A	PR-B	α -CD	PEG 35.000
[BMIM][Cl]	+	+	+	+
[BMIM][Br]	+	+	+	+
[BMIM][BF ₄]	-	-	-	-
[BMIM][PF ₆]	-	-	-	-
[BMIM][NTf ₂]	-	-	-	+
[BMIM][MDEGSO ₄]	-	-	+	-
[EMIM][Cl]	+	+	+	+
[HMIM][Cl]	+	+	+	+
[OMIM][Cl]	+	+	+	+
[C ₁₀ MIM][Cl]	+	+	+	+

Table 21. Solubility of Polyrotaxanes (PR-A and PR-B), α -CD and PEG

As shown in Table 21, ILs are good solvents for both α -CD and PEG, in particular for the cases of ILs with chloride and bromide anions. The same halogenated ILs showed an effective solubilization of polyrotaxanes at room temperature. Both PR-A and PR-B (1 wt %) could be dissolved in ILs [HMIM][Cl], [OMIM][Cl], and [C₁₀MIM][Cl] at room temperature after 2 days of stirring. In general, ILs can dissolve polyrotaxanes at room temperature, but this dissolution process is slower because higher IL viscosity values (the viscosity of DMSO is 1.98 mPa.s at 25°C, while the viscosities of [HMIM][Cl] and [OMIM][Cl] are 10.222 and 33.060 mPa.s at 25°C). Polyrotaxanes dissolved in ILs can be recovered by precipitation after simple addition of organic solvents or water to solution. The authors reported the use of ILs as new solvents for polyrotaxanes in order to develop ionic liquid-containing slide-ring gels (SR gels), that is supramolecular networks of polyrotaxane swollen with ILs, using an integrative non-drying technique followed by optimized solvent exchange method.

Acknowledgements

This work was supported by Fundação para a Ciência e a Tecnologia through projects (PEst-C/LA0006/2013, PTDC/CTM/103664/2008, EXPL/QEQ-ERQ/2243/2013) one contract under Investigador FCT (L.C. Branco); two Postdoctoral fellowships (G.V.S.M. Carrera - SFRH/BPD/72095/2010 and A. V. M. Nunes - SFRH/BPD/74994/2010) and one doctoral fellowship (M. E. Zakrzewska SFRH/BD/74929/2010).

Author details

Gonçalo V.S.M. Carrera, Małgorzata E. Zakrzewska, Ana V. M. Nunes and Luis C. Branco*

*Address all correspondence to: l.branco@fct.unl.pt

REQUIMTE, Departamento de Química, Faculdade de Ciências e Tecnologia, Universidade Nova de Lisboa, Campus da Caparica, Caparica, Portugal

References

- [1] Yang J-Z., Wang B., Zhang Q-G., Tong J. Study on solid-liquid phase equilibria in ionic liquid 1. The solubility of alkali chloride (MCl) in ionic liquid EMISE. *Fluid Phase Equilibria* 2007;251 68-70.
- [2] Wang B., Zhang Q-G., Yang J-Z. Study on solid-liquid phase equilibria in ionic liquid 2. The solubility of alkali bromide in ionic liquid 1-ethyl-3-methylimidazolium ethyl sulfate. *Fluid Phase Equilibria* 2007; 254 163-166.
- [3] Branco L. C., Rosa J. N., Moura Ramos J. J., Afonso C. A. M. Preparation and Characterization of New Room Temperature Ionic Liquids. *Chemistry European Journal* 2002;8 3671-3677.
- [4] Dotterl M., Haas I., Alt H. G. Solubility Behaviour of $TiCl_4$, $ZrCl_4$ and $HfCl_4$ in chloroaluminate ionic liquids. *Zeitschrift für anorganische und allgemeine Chemie* 2011;637 1502-1506.
- [5] Rosol Z. P., German N. J., Gross S. M. Solubility, ionic conductivity and viscosity of lithium salts in room temperature ionic liquids. *Green Chemistry* 2009;11 1453-1457.
- [6] Atakilt A., Admassie S., Villar-Garcia I. J., Chebude Y. 4,4-Bipyridinium ionic liquids exhibiting excellent solubility for metal salts: Potential solvents for electrodeposition. *Inorganic Chemistry Communications*. 2013;29 210-212.
- [7] Pereiro A. B., Araújo, J. M. M., Oliveira F. S., Esperança J. M. S. S., Canongia Lopes J. N., Marrucho I. M. Solubility of inorganic salts in pure ionic liquids. *Journal of Chemical Thermodynamics* 2012;55 29-36.
- [8] Li H., Li D., Wang Y., Ru Q. A series of carboxylic-functionalized ionic liquids and their solubility for lanthanide oxides. *Chemistry Asian Journal*. 2011;6 1443-1449.
- [9] Villar-Garcia I. J., Abebe A., Chebude T. 1,10-Phenanthroline ionic liquids exhibiting excellent solubility for metal complexes: Potential solvents for biphasic and supported ionic liquid phase. *Inorganic Chemistry Communications*. 2012;19 1-3.
- [10] Yang Y., Yu L. Theoretical investigations of ferrocene/ferrocenium solvation in imidazolium-based room-temperature ionic liquids. *Physical Chemistry Chemical Physics*. 2013;15 2669-2683.
- [11] Boros E., Earle M. J., Gilea, M. A., Metlen A., Mudring A-V., Rieger F., Robertson A. J., Seddon K. R., Tomaszowska, A. A. Trusov L., Vyle J. S. On the dissolution of non-metallic solid elements (sulfur, selenium, tellurium and phosphorous) in ionic liquids. *Chemical Communications*. 2010;46 716-718.
- [12] Chen Y., Tarascon J-M., Guery C., Exploring sulfur solubility in ionic liquids for the electrodeposition of sulfide films with their electrochemical reactivity toward lithium. *Electrochimica Acta*. 2013;99 46-53.

- [13] Marrucho, I. M.; Branco, L. C.; Rebelo, L. P. N. Ionic liquids in pharmaceutical applications. *Annual review of chemical and biomolecular engineering* 2014, 5, 527-546.
- [14] Tucker, J. L. Green chemistry, a pharmaceutical perspective. *Organic Process Research & Development* 2006, 10, 315-319.
- [15] Siodmiak, T.; Marszall, M. P.; Proszowska, A. Ionic Liquids: A New Strategy in Pharmaceutical Synthesis. *Mini-Reviews in Organic Chemistry* 2012, 9, 203-208.
- [16] Earle, M. J.; McCormac, P. B.; Seddon, K. R., The first high yield green route to a pharmaceutical in a room temperature ionic liquid. *Green Chemistry* 2000, 2, 261-262.
- [17] Jaitely, V.; Karatas, A.; Florence, A. T. Water-immiscible room temperature ionic liquids (RTILs) as drug reservoirs for controlled release. *International Journal of Pharmaceutics* 2008, 354, 168-173.
- [18] Mizuuchi, H.; Jaitely, V.; Murdan, S.; Florence, A. T. Room temperature ionic liquids and their mixtures: Potential pharmaceutical solvents. *European Journal of Pharmaceutical Sciences* 2008, 33, 326-331.
- [19] Patel, R.; Kumari, M.; Khan, A. B., Recent Advances in the Applications of Ionic Liquids in Protein Stability and Activity: A Review. *Applied Biochemistry and Biotechnology* 2014, 172, 3701-3720.
- [20] Freire, M. G.; Claudio, A. F. M.; Araujo, J. M. M.; Coutinho, J. A. P.; Marrucho, I. M.; Canongia Lopes, J. N.; Rebelo, L. P. N., Aqueous biphasic systems: a boost brought about by using ionic liquids. *Chemical Society Reviews* 2012, 41, 4966-4995
- [21] Tang, B.; Bi, W.; Tian, M.; Row, K. H., Application of ionic liquid for extraction and separation of bioactive compounds from plants. *Journal of Chromatography B-Analytical Technologies in the Biomedical and Life Sciences* 2012, 904, 1-21
- [22] Ventura, S. P. M.; Goncalves, A. M. M.; Sintra, T.; Pereira, J. L.; Goncalves, F.; Coutinho, J. A. P. Designing ionic liquids: the chemical structure role in the toxicity. *Ecotoxicology* 2013, 22, 1-12
- [23] Sun, P.; Armstrong, D. W. Ionic liquids in analytical chemistry. *Analytica Chimica Acta* 2010, 661, 1-16.
- [24] Bogel-Lukasik, R.; Nobre Goncalves, L. M.; Bogel-Lukasik, E., Phase equilibrium phenomena in solutions involving tannins, flavonoids and ionic liquids. *Green Chemistry* 2010, 12, 1947-1953.
- [25] Alevizou, E. I.; Voutsas, E. C., Solubilities of p-coumaric and caffeic acid in ionic liquids and organic solvents. *Journal of Chemical Thermodynamics* 2013, 62, 69-78.
- [26] Carneiro, A. P.; Rodriguez, O.; Macedo, E. A., Solubility of xylitol and sorbitol in ionic liquids - Experimental data and modeling. *Journal of Chemical Thermodynamics* 2012, 55, 184-192

- [27] Smith, K. B.; Bridson, R. H.; Leeke, G. A., Solubilities of Pharmaceutical Compounds in Ionic Liquids. *Journal of Chemical and Engineering Data* 2011, 56, 2039-2043.
- [28] Forte, A.; Melo, C. I.; Bogel-Lukasik, R.; Bogel-Lukasik, E., A favourable solubility of isoniazid, an antitubercular antibiotic drug, in alternative solvents. *Fluid Phase Equilibria* 2012, 318, 89-95.
- [29] Lourenco, C.; Melo, C. I.; Bogel-Lukasik, R.; Bogel-Lukasik, E., Solubility Advantage of Pyrazine-2-carboxamide: Application of Alternative Solvents on the Way to the Future Pharmaceutical Development. *Journal of Chemical and Engineering Data* 2012, 57, 1525-1533.
- [30] Melo, C. I.; Bogel-Lukasik, R.; da Ponte, M. N.; Bogel-Lukasik, E., Ammonium ionic liquids as green solvents for drugs. *Fluid Phase Equilibria* 2013, 338, 209-216.
- [31] dos Santos, A. D.; Morais, A. R. C.; Melo, C.; Bogel-Lukasik, R.; Bogel-Lukasik, E., Solubility of pharmaceutical compounds in ionic liquids. *Fluid Phase Equilibria* 2013, 356, 18-29.
- [32] Manic, M. S.; Najdanovic-Visak, V., Solubility of erythromycin in ionic liquids. *Journal of Chemical Thermodynamics* 2012, 44, 102-106.
- [33] de Azevedo, J. R.; Letourneau, J.-J.; Espitalier, F.; Re, M. I., Solubility of a New Cardioactive Prototype Drug in Ionic Liquids. *Journal of Chemical and Engineering Data* 2014, 59, 1766-1773.
- [34] Clark J. H. Green chemistry for the second generation biorefinery - sustainable chemical manufacturing based on biomass. *Journal of Chemical Technology and Biotechnology* 2007; 82(7) 603-609.
- [35] Corma A., Iborra S., Velty A. Chemical Routes for the Transformation of Biomass into Chemicals. *Chemical Reviews* 2007; 107(6) 2411-2502.
- [36] [36] Kumar P., Barrett D. M., Delwiche M. J., Stroeve P. Methods for Pretreatment of Lignocellulosic Biomass for Efficient Hydrolysis and Biofuel Production. *Industrial and Engineering Chemistry Research* 2009; 48(8) 3713-3729
- [37] Tadesse H., Luque R. Advances on biomass pretreatment using ionic liquids: An overview. *Energy and Environmental Science* 2011; 4(10) 3913-3929
- [38] Mäki-Arvela P., Anugwom I., Virtanen P., Sjöholm R., Mikkola J.P. Dissolution of lignocellulosic materials and its constituents using ionic liquids — A review *Industrial Crops and Products* 2010; 32(3) 175-201
- [39] Sun N., Rodríguez H., Rahman M., Rogers R. D. Where are ionic liquid strategies most suited in the pursuit of chemicals and energy from lignocellulosic biomass? *Chemical Communications* 2011; 47(5) 1405-1421
- [40] Vancov T, Alston A S, Brown T, McIntosh S Use of ionic liquids in converting lignocellulosic material to biofuels *Renewable Energy* 2012; 45 1 - 6

- [41] Brandt A., Gräsvik J., Halletta J. P., Welton T. Deconstruction of lignocellulosic biomass with ionic liquids. *Green Chemistry* 2013; 15(3) 550-583.
- [42] da Costa Lopes A. M., João K. G., Morais A.R.C., Bogel-Lukasik E., Bogel-Lukasik R. Ionic liquids as a tool for lignocellulosic biomass fractionation. *Sustainable Chemical Processes* 2013; 1(3) 1-31.
- [43] Swatloski R.P., Spear S.K.H., Rogers R.D. Dissolution of Cellose with Ionic Liquids. *Journal of the American Chemical Society* 2002; 124(18) 4974-4975.
- [44] Zakrzewska M. E., Bogel-Lukasik E., Bogel-Lukasik R. Solubility of Carbohydrates in Ionic Liquids. *Energy and Fuels* 2010; 24(2) 737-745.
- [45] Murugesan S., Linhardt R. J. Ionic liquids in carbohydrate chemistry – current trends and future directions. *Current Organic Synthesis* 2005; 2(4) 437-451.
- [46] El Seoud O. A., Koschella A., Fidale L. C., Dorn S., Heinze T. Applications of Ionic Liquids in Carbohydrate Chemistry: A Window of Opportunities. *Biomacromolecules* 2007; 8(9) 2629-2647
- [47] Zakrzewska M. E., Bogel-Lukasik E., Bogel-Lukasik R. Ionic Liquid-Mediated Formation of 5-Hydroxymethylfurfurals – Promising Biomass-Derived Building Block. *Chemical Reviews* 2011; 111(2) 397-417
- [48] Wang H., Gurau G., Rogers R.D. Ionic liquid processing of cellulose. *Chemical Society Reviews* 2012; 41(4) 1519-1537
- [49] Ohno H., Fukaya Y. Task specific ionic liquids for cellulose technology. *Chemistry Letters* 2009; 38(1) 1-7
- [50] Liebert T., Heinze T. Interaction of ionic liquids with polysaccharides 5. Solvents and reaction media for the modification of cellulose. *BioResources* 2008; 3(2) 576-601.
- [51] Cao Y., Wu J., Zhang J., Li H. Q., Zhang Y., He J. S. Room temperature ionic liquids (RTILs): A new and versatile platform for cellulose processing and derivatization. *Chemical Engineering Journal* 2009; 147(1), 13-21.
- [52] Feng L., Chen Z. Research progress on dissolution and functional modification of cellulose in ionic liquids. *Journal of Molecular Liquids* 2008; 142(1-3) 1-5.
- [53] Pinkert A., Marsh K. N., Pang S., Staiger M. P. Ionic Liquids and Their Interaction with Cellulose. *Chemical Reviews* 2009; 109(12) 6712-6728.
- [54] Pinkert A., Marsh K.N., Pang S. Reflections on the Solubility of Cellulose. *Industrial and Engineering Chemistry Research* 2010; 49(22) 11121-11130.
- [55] Sellin M., Ondruschka B., Stark A. Hydrogen Bond Acceptor Properties of Ionic Liquids and Their Effect on Cellulose Solubility. *ACS Symposium Series* 2010; 1033(6) 121-135.

- [56] Xu A., Wang J., Wang H. Effects of anionic structure and lithium salts addition on the dissolution of cellulose in 1-butyl-3-methylimidazolium-based ionic liquid solvent systems. *Green Chemistry* 2010; 12(2) 268–275.
- [57] Brandt A., Hallett J. P., Leak D. J., Murphy R. J., Welton T. The effect of the ionic liquid anion in the pretreatment of pine wood chips. *Green Chemistry* 2010;12(4) 672–679.
- [58] Remsing R. C., Swatloski R. P., Rogers R. D., Moyna G. Mechanism of cellulose dissolution in the ionic liquid 1-n-butyl-3-methylimidazolium chloride: a ^{13}C and $^{35/37}\text{Cl}$ NMR relaxation study on model systems. *Chemical Communications* 2006; 28(12) 1271–1273.
- [59] Moulthrop J. S., Swatloski R. P., Moyna G., Rogers R. D. High-resolution ^{13}C NMR studies of cellulose and cellulose oligomers in ionic liquid solutions. *Chemical Communications* 2005; 28(12) 1557–1559.
- [60] Remsing R. C., Hernandez G., Swatloski R. P., Masefski W. W., Rogers R. D., Moyna, G. Solvation of Carbohydrates in $\text{N,N}'$ -Dialkylimidazolium Ionic Liquids: A Multinuclear NMR Spectroscopy Study. *Journal of Physical Chemistry B* 2008; 112(35) 11071–11078.
- [61] Liu H., Sale K.L., Holmes B.M., Simmons B.A., Singh S. Understanding the Interactions of Cellulose with Ionic Liquids: A Molecular Dynamics Study. *Journal of Physical Chemistry B* 2010; 114(12) 4293–4301
- [62] Gross A.S., Bell A.T., Chu J.-W. Thermodynamics of Cellulose Solvation in Water and the Ionic Liquid 1-Butyl-3-Methylimidazolium Chloride. *Journal of Physical Chemistry B* 2011; 115(46) 13433–13440.
- [63] Youngs T. G. A., Holbrey J. D., Deetlefs M., Nieuwenhuyzen M., Costa Gomes M. F., Hardacre C. A Molecular Dynamics Study of Glucose Solvation in the Ionic Liquid 1,3-Dimethylimidazolium Chloride. *ChemPhysChem* 2006; 7(11), 2279–2281
- [64] Youngs T.G.A., Holbrey J.D., Mullan C.L., Norman S.E., Lagunas M.C., D'Agostino C., Mantle M.D., Gladden L.F., Bowron D.T., Hardacre C. Neutron diffraction, NMR and molecular dynamics study of glucose dissolved in the ionic liquid 1-ethyl-3-methylimidazolium acetate. *Chemical Science* 2011; 2(8) 1594–1605.
- [65] Youngs T. G. A., Hardacre C., Holbrey J. D. Glucose Solvation by the Ionic Liquid 1,3-Dimethylimidazolium Chloride: A Simulation Study *Journal of Physical Chemistry B* 2007; 111(49) 13765–13774.
- [66] Guo J., Zhang D., Duan C., Liu C. Probing anion-cellulose interactions in imidazolium-based room temperature ionic liquids: a density functional study. *Carbohydrate Research* 2010; 345(15) 2201–2205.

- [67] Fukaya Y., Hayashi K., Wada M., Ohno H. Cellulose dissolution with polar ionic liquids under mild conditions: required factors for anions. *Green Chemistry* 2008; 10(1) 44–46
- [68] Vitz J., Erdmenger T., Haensch C., Schubert U. S. Extended dissolution studies of cellulose in imidazolium based ionic liquids. *Green Chemistry* 2009; 11(3) 417–424.
- [69] Feng L., Chen Z., Research progress on dissolution and functional modification of cellulose in ionic liquids. *Journal of Molecular Liquids* 2008; 142(1-3) 1.
- [70] Lindman B., Karlström G., Stigsson L. On the mechanism of dissolution of cellulose. *Journal of Molecular Liquids* 2010; 156(1) 76–81.
- [71] Zhang J., Zhang H., Wu J., Zhang J., He J., Xiang J. NMR spectroscopic studies of cellobiose solvation in EmimAc aimed to understand the dissolution mechanism of cellulose in ionic liquids. *Physical Chemistry Chemical Physics* 2010; 12(8) 1941–1947,
- [72] Remsing R. C., Petrik I. D., Liu Z., Moyna G. Comment on “NMR spectroscopic studies of cellobiose solvation in EmimAc aimed to understand the dissolution mechanism of cellulose in ionic liquids” *Physical Chemistry Chemical Physics* 2010; 12(44) 14827–14828.
- [73] Zhang J., Zhang H., Wu J., Zhang J., He J., Xiang J. Reply to “Comment on ‘NMR spectroscopic studies of cellobiose solvation in EmimAc aimed to understand the dissolution mechanism of cellulose in ionic liquids’” *Physical Chemistry Chemical Physics* 2010; 12(44) 14829–14830.
- [74] Lu B., Xu A., Wang J. Cation does matter: how cationic structure affects the dissolution of cellulose in ionic liquids. *Green Chemistry* 2014; 16(3) 1326–1335.
- [75] Novoselov N. P., Sashina E. S., Petrenko V. E., Zaborsky M. Study of Dissolution of Cellulose in Ionic Liquids by Computer Modelling. *Fibre Chemistry* 2007; 39(2) 153–158.
- [76] Heinze T., Dorn S., Schöbitz M., Liebert T., Köhler S. Meister F. Interactions of Ionic Liquids with Polysaccharides – 2: Cellulose. *Macromolecular Symposia* 2008; 262(1) 8–22.
- [77] Ebner G., Schiehser S., Potthast A., Rosenau T. Side reaction of cellulose with common 1-alkyl-3-methylimidazolium-based ionic liquids. *Tetrahedron Letters* 2008; 49(51) 7322–7324.
- [78] Zhang H., Wu J., Zhang J., He J. 1-Allyl-3-methylimidazolium Chloride Room Temperature Ionic Liquid: A New and Powerful Nonderivatizing Solvent for Cellulose. *Macromolecules* 2005; 38(20) 8272–8277.
- [79] Fukaya Y., Sugimoto A., Ohno H. Superior Solubility of Polysaccharides in Low Viscosity, Polar, and Halogen-Free 1,3-Dialkylimidazolium Formates. *Biomacromolecules* 2006; 7(12), 3295–3297.

- [80] Zhao D., Li H., Zhang J., Fu L., Liu M., Fu J., Ren P. Dissolution of cellulose in phosphate-based ionic liquids. *Carbohydrate Polymers* 2012, 87(2) 1490–1494.
- [81] Kosan B., Schwikal K., Meister F. Solution states of cellulose in selected direct dissolution agents. *Cellulose* 2010; 17(3) 495.
- [82] Lateef H., Grimes S., Kewcharoenwong P., Feinberg B. Separation and recovery of cellulose and lignin using ionic liquids: a process for recovery from paper-based waste. *Journal of Chemical Technology and Biotechnology* 2009; 84(12) 1818–1827.
- [83] Sashina E. S., Novoselov N. P. Effect of Structure of Ionic Liquids on Their Dissolving Power Toward Natural Polymers *Russian Journal of General Chemistry* 2009; 79(6) 1057–1062.
- [84] Zhao H., Baker G. A., Song Z., Olubajo O., Crittle T., Peters D. Designing enzyme-compatible ionic liquids that can dissolve carbohydrates. *Green Chemistry* 2008; 10(6) 696–705.
- [85] Padaszynyński K., Okuniewski M., Domańska U., “Sweet-in-Green” Systems Based on Sugars and Ionic Liquids: New Solubility Data and Thermodynamic Analysis” *Industrial and Engineering Chemistry Research* 2013; 52(51) 18482–18491.
- [86] Carneiro A.P., Rodríguez O., Macedo E.A. Fructose and Glucose Dissolution in Ionic Liquids: Solubility and Thermodynamic Modeling *Industrial and Engineering Chemistry Research* 2013; 52(9) 3424–3435.
- [87] Xiao W., Chen Q., Wu Y., Wu T., Dai L. Dissolution and blending of chitosan using 1,3-dimethylimidazolium chloride and 1-H-3-methylimidazolium chloride binary ionic liquid solvent. *Carbohydrate Polymers* 2011; 83(1), 233–238.
- [88] Fu D., Mazza G., Tamaki Y. Lignin Extraction from Straw by Ionic Liquids and Enzymatic Hydrolysis of the Cellulosic Residues. *Journal of Agricultural and Food Chemistry* 2010; 58(5) 2915–2922.
- [89] Mazza M., Catana D.-A., Vaca-Garcia C., Cecutti C. Influence of water on the dissolution of cellulose in selected ionic liquids. *Cellulose* 2009; 16(2) 207–215
- [90] Xu A., Zhang Y., Zhao Y., Wang J. Cellulose dissolution at ambient temperature: Role of preferential solvation of cations of ionic liquids by a cosolvent. *Carbohydrate Polymers* 2013; 92(1) 540–544.
- [91] Kimizuka N., Nakashima T. Spontaneous Self-Assembly of Glycolipid Bilayer Membranes in Sugar-philic Ionic Liquids and Formation of Ionogels. *Langmuir* 2001, 17(22) 6759–6761.
- [92] Liu Q., Janssen M. H. A., van Rantwijk F., Sheldon R. A. Room-temperature ionic liquids that dissolve carbohydrates in high concentrations. *Green. Chem.* 2005, 7(1) 39–42.

- [93] Rinaldi R. Instantaneous dissolution of cellulose in organic electrolyte solutions. *Chemical Communications*, 2011, 47(1) 511–513.
- [94] Gericke M., Liebert T., El Seoud O.A., Heinze T. Tailored Media for Homogeneous Cellulose Chemistry: Ionic Liquid/Co-Solvent Mixtures. *Macromolecular Materials and Engineering* 2011; 296(6) 483–493.
- [95] Hauru L. K. J., Hummel M., King A. W. T., Kilpeläinen I., Sixta H. Role of Solvent Parameters in the Regeneration of Cellulose from Ionic Liquid Solutions. *Biomacromolecules* 2012; 13 (9) 2896–2905.
- [96] Zhao Q., Yam R. C. M., Zhang B., Yang Y., Cheng X., Li R. K. Y. Novel all-cellulose eco-composites prepared in ionic liquids. *Cellulose* 2009, 16(2) 217–226.
- [97] Tsiptsias C., Stefopoulos A., Kokkinomalis I., Papadopoulou L., Panayiotou C. Development of micro- and nano-porous composite materials by processing of cellulose with ionic liquids and supercritical CO₂. *Green Chemistry* 2008; 10(9) 965–971.
- [98] Li X.-L., Zhu L.-P., Zhu B.-K., Xu Y.-Y. High-flux and anti-fouling cellulose nanofiltration membranes prepared via phase inversion with ionic liquid as solvent. *Separation and Purification Technology* 2011; 83 66–73.
- [99] Turner M. B., Spear S. K., Holbrey J. D., Rogers R. D. Production of bioactive cellulose films reconstituted from ionic liquids. *Biomacromolecules* 2004; 5(4) 1379–1384.
- [100] Cai T., Zhang H., Guo Q., Shao H., Hu X. Structure and Properties of Cellulose Fibers from Ionic Liquids. *Journal of Applied Polymer Science* 2010; 115(2) 1047–1053.
- [101] Quan S. L., Kang S. G., Chin I. J. Characterization of cellulose fibers electrospun using ionic liquid. *Cellulose* 2010; 17(2) 223–230.
- [102] Aaltonen O. Jauhiainen O. The preparation of lignocellulosic aerogels from ionic liquid solutions. *Carbohydrate Polymers* 2009; 75(1) 125–129.
- [103] Lee S. Y., Hubbe M. A., Saka H. Prospects for biodiesel as a byproduct of wood pulping - A review. *BioResources* 2006; 1(1) 150-171.
- [104] Ren J.L., Sun R.C., Liu C.F., Cao Z.N., Luo W. Acetylation of wheat straw hemicelluloses in ionic liquid using iodine as a catalyst. *Carbohydrate Polymers* 2007; 70(4) 406–414.
- [105] Froschauer C., Hummel M., Laus G., Schottenberger H., Sixta H., Weber H.K., Zuckerrstatter G. Dialkyl Phosphate-Related Ionic Liquids as Selective Solvents for Xylan. *Biomacromolecules* 2012; 13(6) 1973–1980.
- [106] Anugwom I., Mäki-Arvela P., Virtanen P., Willför S., Sjöholm R., Mikkola J.-P. Selective extraction of hemicelluloses from spruce using switchable ionic liquids. *Carbohydrate Polymers* 2012; 87(3) 2005–2011.
- [107] Hummel M., Froschauer C., Laus G., Röder T., Kopacka H., Hauru L.K.J., Weber H.K., Sixta H., Schottenberger H. Dimethyl phosphorothioate and phosphorosele-

- noate ionic liquids as solvent media for cellulosic materials. *Green Chemistry* 2011; 13(9) 2507-2517.
- [108] Tan S. S. Y., MacFarlane D. R., Upfal J., Edey L. A., Doherty W. O. S., Patti A. F., Pringle J. M., Scott J. L. Extraction of lignin from lignocellulose at atmospheric pressure using alkylbenzenesulfonate ionic liquid. *Green Chemistry* 2009; 11(3) 339-345.
- [109] Abe M., Fukaya Y., Ohno H. Extraction of polysaccharides from bran with phosphonate or phosphinate-derived ionic liquids under short mixing time and low temperature. *Green Chemistry* 2010; 12(7) 1274-1280.
- [110] Sun N., Rahman M., Qin Y., Maxim M. L., Rodríguez H., Rogers R. D. Complete dissolution and partial delignification of wood in the ionic liquid 1-ethyl-3-methylimidazolium acetate. *Green Chemistry*, 2009; 11(5) 646-655.
- [111] Li W., Sun N., Stoner B., Jiang X., Lu X., Rogers R. D. Rapid dissolution of lignocellulosic biomass in ionic liquids using temperatures above the glass transition of lignin. *Green Chemistry* 2011; 13(8) 2038-2047.
- [112] Lee S. H., Doherty T. V., Linhardt R. J., Dordick J. S. Ionic Liquid-Mediated Selective Extraction of Lignin From Wood Leading to Enhanced Enzymatic Cellulose Hydrolysis. *Biotechnology and Bioengineering* 2009; 102(5) 1368-1376.
- [113] Pu Y. Q., Jiang N., Ragauskas A. J. Ionic Liquid as a Green Solvent for Lignin. *Journal of Wood Chemistry and Technology* 2007; 27(1) 23-33.
- [114] Bylin S., Olsson C., Westman G., Theliander H. Solvation Behavior of Cellulose and Xylan in the MIM/EMIMAc Ionic Liquid Solvent System: Parameters for Small-Scale Solvation. *BioResources* 2014; 9(1) 1038-1054.
- [115] Yamazaki S., Takegawa A., Kaneko Y., Kadokawa J., Yamagata M., Ishikawa M. An acidic cellulose-chitin hybrid gel as novel electrolyte for an electric double layer capacitor. *Electrochemistry Communications* 2009; 11(1) 68-70.
- [116] Meng Z., Zheng X., Tang K., Liu J., Qin S. Dissolution of natural polymers in ionic liquids: A review. *e Polymers* 2012; 12(1) 1-20.
- [117] Wang W.-T., Zhu J., Wang X.-L., Huang Y., Wang Y.-Z. Dissolution Behavior of Chitin in Ionic Liquids. *Journal of Macromolecular Science, Part B Physics* 2010; 49(3) 528-541
- [118] Zhu Q. S., Han X. J., Cheng C. Z., Wu C. C. Study on dissolubility of chitosan in four kinds of imidazole-based ionic liquids. *Acta Polymerica Sinica* 2011 11, 1173-1179.
- [119] Chen Q., Xu A., Li Z., Wang J., Zhang S. Influence of anionic structure on the dissolution of chitosan in 1-butyl-3-methylimidazolium-based ionic liquids. *Green Chemistry* 2011; 13(12) 3446-3452.

- [120] Quignard F., Di Renzo F., Guibal E. From natural polysaccharides to materials for catalysis, adsorption, and remediation. *Topics in Current Chemistry* 2010; 294, 165–197.
- [121] Ngah W.S.W., Teong L.C., Hanafiah M.A.K.M. Adsorption of dyes and heavy metal ions by chitosan composites: A review. *Carbohydrate Polymers* 2011; 83(4) 1446–1456.
- [122] Sanchez C., Belleville P., Popall M., Nicole L. Applications of advanced hybrid organic-inorganic nanomaterials: from laboratory to market. *Chemical Society Reviews* 2011; 40(2) 696–753.
- [123] Muzzarelli R.A.A. Biomedical Exploitation of Chitin and Chitosan via Mechano-Chemical Disassembly, Electrospinning, Dissolution in Imidazolium Ionic Liquids, and Supercritical Drying. *Marine Drugs* 2011; 9(9) 1510-1533.
- [124] Trivedi T.J., Rao K. S., Kumar A. Facile preparation of agarose–chitosan hybrid materials and nanocomposite ionogels using an ionic liquid via dissolution, regeneration and sol–gel transition. *Green Chemistry* 2014; 16(1) 320-330.
- [125] Singh T., Trivedi T.J., Kumar A. Dissolution, regeneration and ion-gel formation of agarose in room-temperature ionic liquids. *Green Chemistry* 2010; 12(6) 1029–1035.
- [126] Trivedi T.J., Srivastava D.N., Rogers R.D., Kumar A. Agarose processing in protic and mixed protic–aprotic ionic liquids: dissolution, regeneration and high conductivity, high strength ionogels. *Green Chemistry* 2012; 14(10) 2831-2839.
- [127] Le Bideau J., Viau L., Vioux A. Ionogels, ionic liquid based hybrid materials. *Chemical Society Reviews* 2011; 40(2) 907-925.
- [128] Luo Z., Lu X., Kong X., Fu X., Li F., Luo F. Physicochemical properties of starch dispersed in 1-allyl-3- methylimidazolium chloride. *Industrial Crops and Products* 2013; 46 197– 204.
- [129] Huber K. C., BeMiller J. N. *Modified starch: chemistry and properties*. Boca Raton: CRC Press; 2010.
- [130] Wilpiszewska K., Szychaj T. Ionic liquids: Media for starch dissolution, plasticization and modification. *Carbohydrate Polymers* 2011; 86(2) 424– 428.
- [131] Lu X., Luo Z., Fu X., Xiao Z. Two-Step Method of Enzymatic Synthesis of Starch Laurate in Ionic Liquids. *Journal of Agricultural and Food Chemistry* 2013; 61(41) 9882–9891.
- [132] Jordan T., Schmidt S., Liebert T., Heinze T. Molten imidazole – a starch solvent. *Green Chemistry* 2014; 16(4) 1967-1973.
- [133] Liu W., Budtova T. Dissolution of unmodified waxy starch in ionic liquid and solution rheological properties. *Carbohydrate Polymers* 2013; 93(1) 199– 2064.

- [134] Mateyawa S., D. F. Xie, Truss R.W., Halley P.J., Nicholson T.M., Shamshina J.L., Rogers R.D., Boehm M.W., McNally T. Effect of the ionic liquid 1-ethyl-3-methylimidazolium acetate on the phase transition of starch: Dissolution or gelatinization? *Carbohydrate Polymers* 2013; 94(1) 520–530.
- [135] Wang Y.J., Wang Y., Structures and properties of commercial maltodextrins from corn, potato, and rice starches. *Starch* 2000; 52(8/9) 296–304.
- [136] Gao Y. A., Li Z. H., Du J. M., Han B. X., Li G. Z., Hou W. G., Shen D., Zheng L. Q., Zhang G. Y. Preparation and Characterization of Inclusion Complexes of β -Cyclodextrin with Ionic Liquid. *Chemistry A European Journal* 2005; 11(20) 5875–5880.
- [137] Gao Y., Zhao X., Dong B., Zheng L., Li N., Zhang S. Inclusion Complexes of β -Cyclodextrin with Ionic Liquid Surfactants. *The Journal of Physical Chemistry B* 2006; 110(17) 8576–8581.
- [138] Li N., Liu J., Zhao X. Y., Gao Y. A., Zheng L. Q., Zhang J., Yu L. Complex formation of ionic liquid surfactant and β -cyclodextrin. *Colloids and Surfaces A* 2007; 292(2-2) 196–201.
- [139] Francois Y., Varenne A., Sirieix-Plenet J., Gareil P. J. Determination of aqueous inclusion complexation constants and stoichiometry of alkyl(methyl)-methylimidazolium-based ionic liquid cations and neutral cyclodextrins by affinity capillary electrophoresis. *Journal of Separation Science* 2007; 30(5) 751–760.
- [140] Amajjahe S., Choi S., Munteanu M., Ritter H. Pseudopolyanions Based on Poly(NI-PAAM-co- β -Cyclodextrin Methacrylate) and Ionic Liquids *Angewandte Chemie International Edition* 2008 47(18) 3435–3437.
- [141] Zheng Y., Xuan X., Wang J., Fan M. The Enhanced Dissolution of β -Cyclodextrin in Some Hydrophilic Ionic Liquids. *The Journal of Physical Chemistry A* 2010; 114(11) 3926–3931.
- [142] Ondo D., Tkadlecov M., Dohnal V., Rak J., Kvíčala J., Lehmann J.K., Heintz A., Ignatiev N. Interaction of Ionic Liquids Ions with Natural Cyclodextrins. *The Journal of Physical Chemistry B* 2011; 115(34) 10285–10297.
- [143] Zhang J., Shen X. Multiple Equilibria Interaction Pattern between the Ionic Liquids CnmimPF₆ and β -Cyclodextrin in Aqueous Solutions. *The Journal of Physical Chemistry B* 2011; 115(41) 11852–11861.
- [144] Hassan E.-S.R.E., Mutelet F., Moïse J.-C. From the dissolution to the extraction of carbohydrates using ionic liquids. *RSC Advances* 2013; 3(43) 20219–20226.
- [145] Conceic L.J.A., Bogel-Łukasik E., Bogel-Łukasik R. A new outlook on solubility of carbohydrates and sugar alcohols in ionic liquids. *RSC Advances* 2012, 2(5) 1846–1855.

- [146] Rosatella A. A., Branco L. C., Afonso C. A. M. Studies on dissolution of carbohydrates in ionic liquids and extraction from aqueous phase. *Green Chemistry* 2009; 11(9) 1406–1413.
- [147] Carneiro A.P., Rodríguez O., Macedo E.A. Solubility of monosaccharides in ionic liquids – Experimental data and modeling. *Fluid Phase Equilibria* 2012; 314, 22– 28.
- [148] Hassan E.-S.R.E., Mutelet F., Pontvianne S., Moïse J.-C. Studies on the Dissolution of Glucose in Ionic Liquids and Extraction Using the Antisolvent Method. *Environmental Science and Technology* 2013; 47(6) 2809–2816.
- [149] Liu W., Hou Y., Wu W., Ren S., Jing Y., Zhang B. Solubility of Glucose in Ionic Liquid + Antisolvent Mixtures. *Industrial and Engineering Chemistry Research* 2011; 50(11) 6952–6956.
- [150] Carneiro A.P., Rodríguez O., Macedo E.A. Separation of carbohydrates and sugar alcohols from ionic liquids using antisolvents. *Separation and Purification Technology* 2014; 132 496–504
- [151] Padmanabhan S., Kim M., Blanch H. W., Prausnitz J. M. Solubility and rate of dissolution for Miscanthus in hydrophilic ionic liquids. *Fluid Phase Equilibria* 2011; 309(1) 89-96.
- [152] Kahlen J., Masuch K., Leonhard K. Modelling cellulose solubilities in ionic liquids using COSMO-RS. *Green Chemistry* 2010; 12(12) 2172–2181.
- [153] Casas A., Palomar J., Alonso M.V., Oliet M., Omar S., Rodriguez F. Comparison of lignin and cellulose solubilities in ionic liquids by COSMO-RS analysis and experimental validation. *Industrial Crops and Products* 2012(1); 37(1) 155– 163.
- [154] Mora-Pale M., Meli L., Doherty T. V., Linhardt R. J., Dordick J. S. Room temperature ionic liquids as emerging solvents for the pretreatment of lignocellulosic biomass. *Biotechnology and Bioengineering* 2011; 108(6) 1229-1245.
- [155] Carneiro A.P., Held C., Rodríguez O., Sadowski G., Macedo E.A., Solubility of Sugars and Sugar Alcohols in Ionic Liquids: Measurement and PC-SAFT Modeling. *The Journal of Physical Chemistry B* 2013; 117 (34) 9980–9995.
- [156] Wang B., Tang Y., Wen Z., Wang H. Dissolution and regeneration of polybenzimidazoles using ionic liquids. *European Polymer Journal* 2009, 45, 2962–2965.
- [157] Serad G.A., Polybenzimidazoles, new thermally stable polymers – Comments. *J Polym Sci A Polym Chem* 1996;34(7):1123–4.
- [158] Wainright J.S., Wang J.T., Weng D., Savinell R.F., Litt M. Acid-doped polybenzimidazoles – a new polymer electrolyte. *J Electrochem Soc* 1995;142(7):L121–3.
- [159] Holmes G.A., Rice K., Snyder C.R., Ballistic fibers: a review of the thermal, ultraviolet and hydrolytic stability of the benzoxazole ring structure. *J Mater Sci* 2006;41(13): 4105–16.

- [160] Kim J.S., Reneker D.H. Mechanical properties of composites using ultrafine electrospun fibers. *Polym Compos* 1999;20(1):124–31.
- [161] Varma R.S., Solvent-free accelerated organic syntheses using microwaves. *Pure Appl Chem* 2001;73(1):193–8.
- [162] Varma R.S., Namboodiri VV. An expeditious solvent-free route to ionic liquids using microwaves. *Chem Commun* 2001(7):643–4.
- [163] Ueno K., Fukai T., Nagatsuka T., Yasuda T., Watanabe W. Solubility of Poly(methyl methacrylate) in Ionic Liquids in Relation to Solvent Parameters, *Langmuir* 2014, 30, 3228–3235.
- [164] Susan, M. A.; Kaneko, T.; Noda, A.; Watanabe, M. Ion Gels Prepared by in Situ Radical Polymerization of Vinyl Monomers Ionic Liquid and Their Characterization as Polymer Electrolytes. *J. Am. Chem. Soc.* 2005, 127 (13), 4976–4983.
- [165] Lee, S. Y.; Ogawa, A.; Kanno, M.; Nakamoto, H.; Yasuda, T.; Watanabe, M. Nonhumidified Intermediate Temperature Fuel Cells Using Protic Ionic Liquids. *J. Am. Chem. Soc.* 2010, 132 (28), 9764–9773.
- [166] Ueno, K.; Inaba, A.; Kondoh, M.; Watanabe, M. Colloidal Stability of Bare and Polymer-Grafted Silica Nanoparticles in Ionic Liquids. *Langmuir* 2008, 24 (10), 5253–5259.
- [167] Chen Y., Zhang Y., Ke F., Zhou J., Wang J., Liang D. Solubility of neutral and charged polymers in ionic liquids studied by laser light scattering. *Polymer* 2011, 52, 481–488.
- [168] Triolo A., Russina O., Keiderling U., Kohlbrecher J. *J Phys Chem B* 2006;110:1513–1515.
- [169] Kawauchi T., Kumaki J., Okoshi K., Yashima E. *Macromolecules* 2005; 38:9155–9160.
- [170] Liu W.W., Cheng L.Y., Zhang H.Y., Zhang Y.M., Wang H.P., Yu M.F. *Int J Mol Sci* 2007;8:180–188.
- [171] Zhao T.T., Wang H.P., Wang B., Tu X.P., Zhang Y.M., Jiang J.M. *Polym Bull* 2006;57: 369–375.
- [172] Tu X.P., Zhang Y.M., Zhao T.T., Wang H.P. *J Macromol Sci Phys* 2006;45: 665–669.
- [173] Wan S., Zhang Y., Wang H. Acrylic fibers processing with ionic liquid as solvent. *Polym. Adv. Technol.* 2009, 20 857–862.
- [174] Frushour, B.G. *Polym. Bull.* 1982, 7, 1–8.
- [175] Rodriguez H., Francisco M., Rahman M., Sun N., Rogers R.D. Biphasic liquid mixtures of ionic liquids and polyethylene glycols. *Phys. Chem. Chem. Phys.*, 2009, 11, 10916–10922.
- [176] Herold D., Keil K., Burns D.E., *Biochem. Pharmacol.*, 1989, 38, 73–76.
- [177] Bridges N.J., Gutowski K.E., Rogers R.D., *Green Chem.* 2007, 9, 177–183.

- [178] Shin J.H., Henderson W.A., Passerini P., *Electrochem. Commun.* 2003, 5, 1016–1020.
- [179] Sarkar A., Trivedi S., Pandey S., *J. Phys. Chem. B*, 2008, 112, 9042–9049.
- [180] Samitsu S., Araki J., Kataoka T., Ito K. New Solvent for Polyrotaxane. II. Dissolution Behavior of Polyrotaxane in Ionic Liquids and Preparation of Ionic Liquid-Containing Slide-Ring Gels. *Journal of Polymer Science: Part B: Polymer Physics*, 2006, 44, 1985–1994.
- [181] Harada, A.; Li, J.; Kamachi, M. *Nature* 1992, 356, 325–327.
- [182] Wenz, G. *Angew. Chem. Int. Ed. Engl.*, 1994, 33, 803–822.
- [183] Ooya, T.; Arizono, K.; Yui, N. *Polym Adv Technol* 2000, 11, 642–651.
- [184] Silva, C.; Friend, R. H.; Severin, N.; Samori, P.; Rabe, J. P.; O'Connell, M. J.; Taylor, P. N.; Anderson, H. L. *Nat Mater* 2002, 1, 160–164.
- [185] Tamura, M.; Gao, D.; Ueno, A. *Chem. Eur. J.* 2001, 7, 1390–1397.

Extraction

Various Self-Assembly Behaviors of Amphiphilic Molecules in Ionic Liquids

Bin Dong and Yanan Gao

Additional information is available at the end of the chapter

<http://dx.doi.org/10.5772/59095>

1. Introduction

Surfactants can self-assemble into various ordered structures, involving micelles (spherical, rod-like, worm-like, bilayer, and cylindrical), microemulsions (water-in-oil, bicontinuous, oil-in-water), liquid crystals (lamellar, hexagonal and cubic), vesicles (unilamellar, multilamellar, and oligovesicular), gel and so on. These self-assemblies can be demonstrated as a powerful route towards supramolecular objects with novel architectures, functions and properties. Over the recent years, self-assemblies of amphiphilic molecules in ionic liquids (ILs), a class of novel environmentally benign solvents, have attracted much interest and have been intensively investigated. In this chapter, we summarize the known various self-assembled structures of surfactants in ILs, involving micelles, microemulsions, liquid crystals, vesicles and gel. With a rapid growth in the number of publications on these self-assemblies, it appears that in the near future these neoteric self-assemblies are definitely going to be a versatile media in chemical reaction engineering and material chemistry.

It is known that surfactants are amphiphilic molecules with a hydrophilic headgroup and a hydrophobic chain. The dual character of surfactants makes them self-assemble into various aggregations in order to avoid contact between the water and the hydrophobic tail. The hydrophobic tails of surfactants are inclined to point towards the oil phase or hydrophobic domain. The hydrophilic polar headgroups prefer to contact with water. The self-assembly is highly cooperative and is driven by the hydrophobic effect, because the system is inclined to decrease the amount of unfavorable interactions between the hydrophobic tails and water [1]. The surfactant aggregates have different shapes depending on molecular parameters (such as curvature of aggregate surface and the packing parameter) of the surfactant and system variable such as concentration and temperature. Micelles, microemulsions, liquid crystals, vesicles and gel are most common surfactant aggregates in traditional solvents. The driving

force for the structural aggregation is the minimization of the contact of the hydrophobic groups of the surfactants with water. The curvature of aggregate surface and the packing parameter of the surfactant molecule are two important concepts when discussing aggregate shape. The molecular geometry of the surfactant gives rise to a preferred and spontaneous curvature of the aggregate surface [2,3].

The mean aggregate curvature, H , is described as:

$$H = 0.5 (1/R_1 + 1/R_2) \quad (1)$$

where R_1 and R_2 are the radii of curvature for a surface in two perpendicular directions. The curvature is 1 when aggregates are sphere. When H is less than 1, ($R_1 = \infty$, $R_2 = R$), a cylinder self-assembled structure prefers to form. For a planar bilayer structure, H is 0. Figure 1 shows the mean curvature, H , for three common surfactant self-assembled shapes.

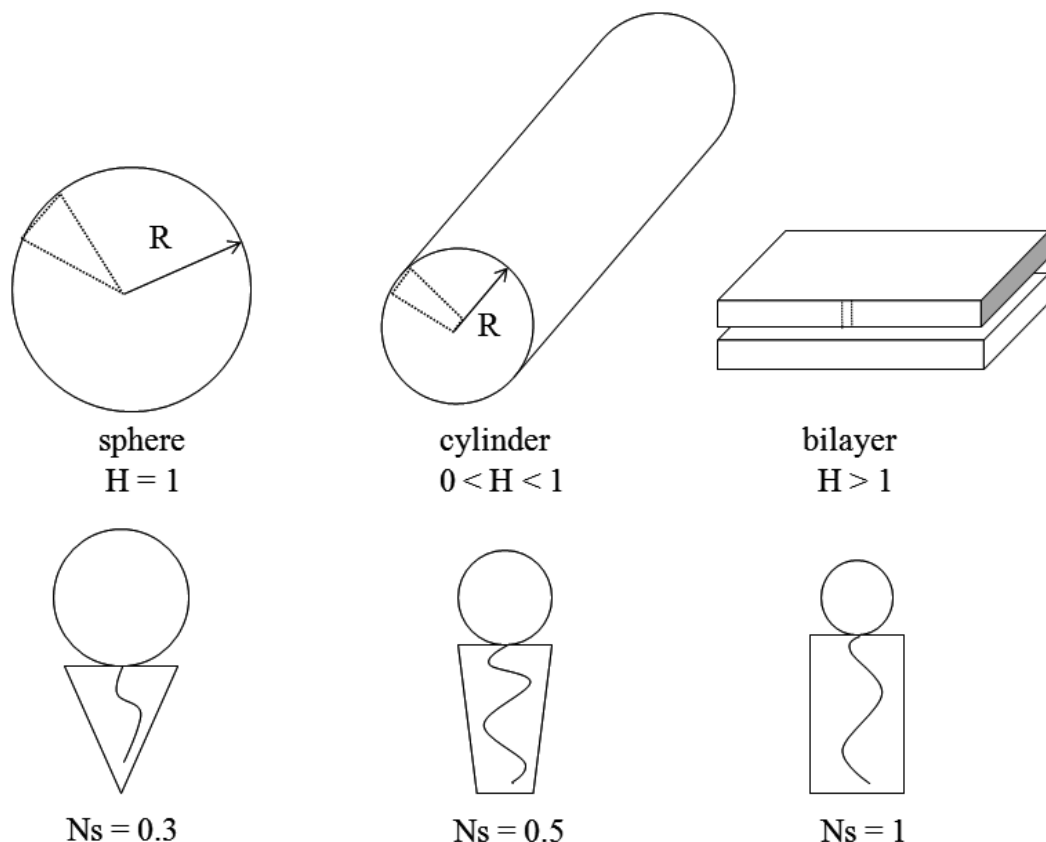


Figure 1. Schematic representation of the mean curvature, H , and the surfactant parameter, N_s , for three common surfactant aggregation shapes: sphere, cylinder and bilayer.

The surfactant parameter, N_s , another important parameter, is relative with the properties of the molecule with the preferred curvature of the aggregates.

$$N_s = v / la_0 \quad (2)$$

where v is the volume of the hydrocarbon chain, l is the length of fully stretched hydrocarbon chain and a_0 is the area per headgroup. The volume of one hydrocarbon chain is evaluated as:

$$v = 0.027 (n_c + n_{Mc}) \quad (3)$$

where n_c is the number of carbon atoms in the hydrocarbon chain, n_{Mc} is the number of methyl groups and l is evaluated as:

$$l = 0.15 + 0.127n_c \quad (4)$$

N_s can reveal the balance between the hydrophobic and hydrophilic parts of the molecules. The relationship between the aggregate shape and surfactant parameter is also shown in Figure 1. If the headgroup of a surfactant is large, this surfactant has a small N_s value and the curvature will be high. In this case, a spherical structure prefers to form. Reversely, a larger N_s value will be obtained if the headgroup of a surfactant is small. Large N_s means a low curvature and cylinders or planar layers are inclined to form.

Ionic liquids (ILs) are a special class of molten salts composed of organic cations and inorganic or organic anions. The melting points of these molten salts are generally below 100°C owing to the large bulk of organic cation that leads to the small lattice energy [4]. ILs have many useful qualities, such as a negligible vapor pressure, nonflammability, high ionic conductivity, wide electrochemical window, and thermal stability [5]. Because of their ultralow vapor pressure, ILs are considered as a possible environmentally acceptable replacements for many volatile organic solvents in chemical reactions [6], separation [7], electrochemical applications [8], and supramolecular self-assembly [9,10]. Of particular recent interest is the combination of self-assembly behaviors of surfactants and ILs. These aggregations can not only overcome the solubility limitations of ILs in immiscible solvents but also provide hydrophobic or hydrophilic nanodomains, thereby expanding potential uses of ILs in microheterogeneous systems as reaction and separation or extraction media [11]. Also, these self-assemblies may have some unknown properties and some potential applications owing to the unique features of ILs and ordered microstructures [12]. ILs as chemical reaction media have been summarized and aggregation behavior has been mentioned [5,13]. In addition, the spatial structure of ILs in itself has been recently reviewed [14]. In this chapter, we present detailed work on various self-assemblies of amphiphilic molecules in ILs for the purpose of informing the readers of the major development in this interesting area. Furthermore, we also have to mention, all self-assembled structures supported by long-chain amphiphilic ILs in non-ILs solvents were not

summarized here, as these amphiphilic ILs only behave in a manner analogous to traditional amphiphilic molecules.

2. Self-assembled micelles in ILs

A micelle is an aggregate of surfactant molecules dispersed in a liquid colloid. A typical micelle in aqueous solution forms an aggregate with the hydrophilic groups in contact with surrounding water, sequestering the hydrophobic tails in the micelle centre. Micelles only appear when the concentration of surfactant reaches a critical micelle concentration (CMC). That is to say, CMC is the minimum concentration of surfactant molecules required for the formation of micelles at a given temperature. In addition, CMC is also an important parameter to characterize the formation of micelles. When the concentration of surfactants is below the CMC, the surfactant molecules exist as free monomers in solution. The formation of micelles is a spontaneous process. Micelles can be classified into normal micelles and inverse micelles. Normal micelles have a continuous polar phase (mostly water phase) with the polar headgroups of the surfactants pointing towards the bulk solvent and the hydrocarbon groups pointing towards the micelle interior, while for inverse micelles the surfactants have the polar headgroup towards the micelle interior with the hydrocarbon groups pointing towards the continuous oil phase.

Evans et al. first reported the aggregation behavior of alkyltrimethylammonium bromides, alkylpyridinium bromides and nonionic Triton X-100 in a low melting fused salt, ethylammonium nitrate (EAN) over 30 years ago [15,16]. Critical micelle concentrations (CMCs) are determined from surface tension measurements and the aggregation behavior was investigated by classical and quasi-elastic light scattering. The solvophobic behavior of EAN shows a number of similarities with that of water. The results of CMCs, micellar aggregation numbers, second virial coefficients, and hydrodynamic radii are consistent with either a small classical spherical micelle containing only surfactant or a spherical mixed micelle containing surfactant and ethylammonium ions as a cosurfactant. The measured second virial coefficients are almost equal to those calculated for hard spheres and reflect highly screened electrostatic interactions in the totally ionized solvent [16].

However, the study of such self-assembly in ILs did not attract much attention until ILs received more and more interest in recent years. Afterwards, the formation of micelles in ILs, 1-butyl-3-methylimidazolium chloride (bmimCl) and hexafluorophosphate (bmimPF₆) were explored by Armstrong et al [17]. The solvation behavior of the micellar-IL solutions was examined using inverse gas chromatography. They found that the dissolution of many different surfactants in ILs also depressed the surface tension in a manner analogous to aqueous solutions, indicating that there are IL solvophobic interactions with the hydrocarbon portion of the surfactants. High hydrogen bond basicity was detected for the micelles of Brij 35 and Brij 700 in bmimPF₆. They ascribed this phenomenon to the existence of hydrophilic polyoxyethylene (POE) groups of surfactants, as oxygen atoms of each individual subunit have lone pair electrons that are capable of accepting a hydrogen bond,

therefore enhancing hydrogen bond basicity [17]. The acidity of imidazolium cations of ILs has been raised, C-2 proton of bmimPF₆ is bonded to a carbon that is located between two positively charged nitrogen atoms, and hence C-2 proton is relatively acidic, as a result C-2 proton can accept electronegative oxygen atoms [18]. Therefore, it is deduced that there exist hydrogen bonds between nonionic surfactants and 1-alkyl-3-methylimidazolium cation of ILs. Merrigan et al. have demonstrated that 1-alkyl-3-methylimidazolium cations with attached long fluorous tails act as surfactants and appear to self-aggregate within 1-alkyl-3-methylimidazolium-based ILs [19].

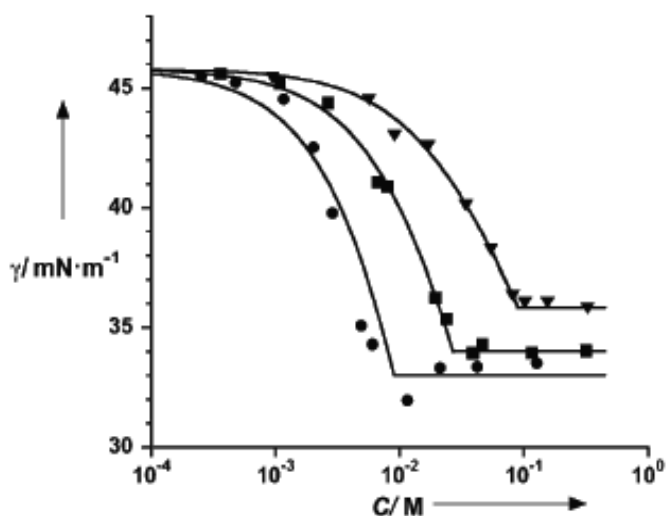


Figure 2. Surface tension (γ) of solutions of C₁₂E₈ (\blacktriangledown), C₁₄E₈ (\blacksquare) and C₁₆E₈ (\bullet) in bmimBF₄ at 25°C. (Reproduced from Ref.[20], with permission).

Aggregation behavior of a series of alkyl poly-(oxyethyleneglycol) ethers, a class of nonionic surfactants, denoted C_nE_m (n=12-16; m=4-8) in 1-butyl-3-methylimidazolium type ILs with various counter ions [BF₄⁻, PF₆⁻, and bis(trifluoromethylsulfonyl)amide (Tf₂N)⁻] has been investigated [20]. The surface tension of the C_nE_m/bmimBF₄ solution decreased as the surfactant concentration increased, indicating their adsorption at the air/solution interface. Figure 2 shows the changes of surface tension of C_nE_m/bmimBF₄ solution with C_nE_m concentration, a similar phenomenon as in water was observed. It was estimated that the molecular area of the surfactant decreased with increasing hydrophobicity of surfactants. The CMCs were two to four orders of magnitude higher than those in aqueous systems. Dynamic light scattering (DLS) measurements have suggested the presence of molecular aggregates. The hydrodynamic radii in bmimBF₄ were smaller than that in water and close to that in formamide. The anions of ILs were found to have a remarkable effect on the nature of micelles, however the formation mechanism was not discussed in this research [20].

Self-assembly processes of nonionic Brij 76 in bmimBF₄ with changing temperature have been detected by Li et al [21]. Under 30°C, Brij 76 self-assembled as nanofibers and a gel formed; as

temperature increased until 85°C, the mixture was clear solution; at about 90°C, Brij 76 self-assembled as vesicles; at even higher temperature of 110°C, a clouding phenomenon was observed. The Dark-field optical micrographs showing the change of aggregations with temperature are shown in Figure 3. The authors proposed that at room temperature, the 1-alkyl-3-methylimidazolium cation and the anion adsorbed to the POE chain of the Brij 76 via the Coulombic force. The cation was adjacent to the oxygen which had a high electron density and the BF_4^- stacked among the cations. The long alkyl chains interacted with each other through the hydrophobic interaction to make the Brij 76 molecule and bmimBF_4 connect like a “rod”.

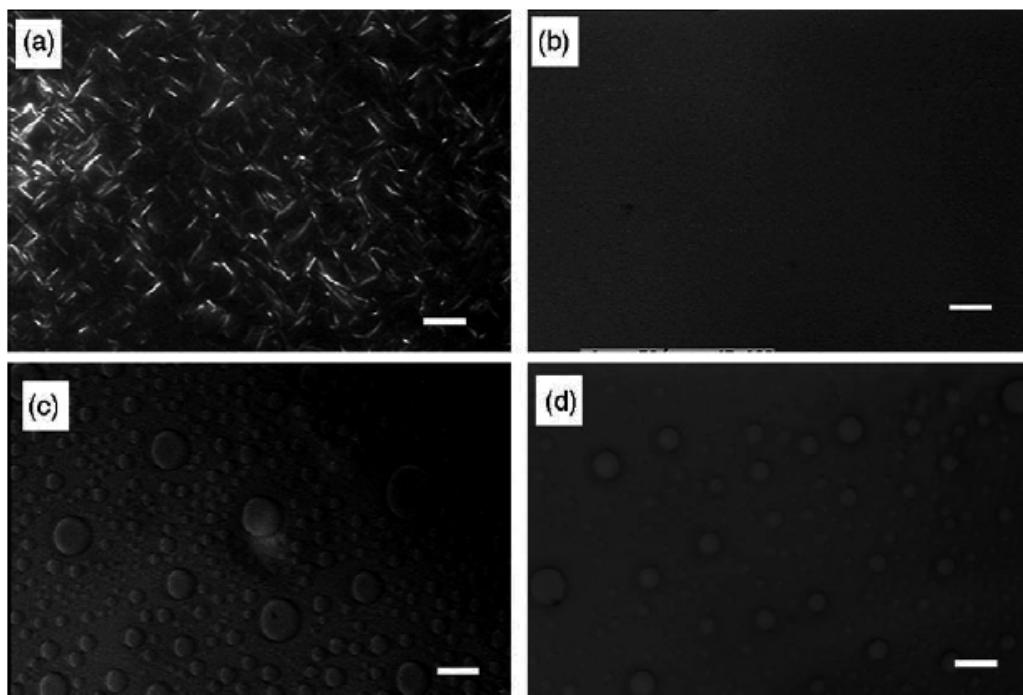


Figure 3. The Dark-field optical micrographs of the surfactant 100 mg Brij 76 dispersed in 1ml bmimBF_4 : (a) 30°C, (b) 60°C, (c) 90°C and (d) 110°C. The scale bar in each image is 10 μm . (Reproduced from Ref.[21], with permission).

Aggregation behaviors of four different alkyl-ammonium nitrates in EAN have been determined by surface tension measurements. The micelles are formed without the increase of molar partial volume meaning that the carbon chain does not perturb the spatial arrangement of the solvent. A theoretical model capable of predicting the CMCs of four alkyl ammonium nitrates in EAN has also been proposed [22]. Moreover, Kunz and coworkers reported that a mixture of two surfactant-like ILs 1-hexadecyl-3-methyl-imidazolium chloride ($\text{C}_{16}\text{mimCl}$) and 1-hexadecyl-3-methyl-imidazolium tetrafluoroborate ($\text{C}_{16}\text{mimBF}_4$) aggregated in EAN. The investigated mixtures are stable up to more than 200°C. The authors attributed this to the electrostatic interactions that do not show a pronounced temperature dependence [23]. This

investigation is much different from the result reported by Li et al [21]. From these results, it can be deduced that in addition to electrostatic interaction, there may be some other interactions between the nonionic surfactants and the 1-alkyl-3-methylimidazolium cation of ILs, such as hydrogen bonds, dipole-induced dipole type of interaction. Among them, one of the forces may dominate in competition under certain condition.

In addition, on the base of the response of solvatochromic probes, the aggregation behavior of few common anionic, cationic, and nonionic surfactants within 1-ethyl-3-methylimidazolium bis(trifluoromethylsulfonyl)imide (emimTf₂N) was also investigated. The possible aggregates were formed by all nonionic surfactants (Brij-35, Brij-700, Tween-20, and Triton X-100), while no aggregation was observed for the cationic surfactant cetyltrimethylammonium bromide (CTAB). The anionic surfactant sodium dodecylsulfate (SDS) does not appear to be solubilized within emimTf₂N at ambient conditions [24]. Moreover, Tran and Yu have reported that nonionic surfactants *N*-dodecylsultaine (SB-12), caprylyl sulfobetaine (SB3-10) formed micelles in bmimPF₆ and emimTf₂N [25]. So far, it seems that nonionic surfactants are more inclined to support the micellar aggregations in ILs.

The interaction between the 1-alkyl-3-methylimidazolium type ILs and nonionic surfactants was further proposed by Pandey group. The addition of bmimPF₆ to aqueous nonionic Triton X-100 solutions can alter/modify physicochemical properties of such systems in favorable manner. BmimPF₆ can partition into the Triton X-100 micellar phase both close to the core as well as in the palisade layer of Triton X-100. They suggested the presence of favorable interactions such as hydrogen bonding between C-2 proton of imidazolium cation and ethoxy/hydroxyl, between PF₆⁻ and H of the Triton X-100 hydroxyl terminal, and dipole-induced dipole type of interaction between Triton X-100 phenyl π -cloud and 1-alkyl-3-methylimidazolium cation between bmimPF₆ and Triton X-100 [26]. In addition to emimTf₂N, Triton X-100 was shown to aggregate and form micellar aggregation in bmimBF₄ and bmimPF₆, respectively [27].

Freeze-fracture transmission electron microscopy (FFTEM) showed that the micelles have an irregular droplet shape and they preferred to assemble into larger clusters. ¹H NMR and two-dimensional rotating frame nuclear Overhauser effect (NOE) experiments (2D ROESY) showed that the addition of Triton X-100 destroyed the ion pairs of pure ILs due to the electrostatic interaction between the positively charged 1-alkyl-3-methylimidazolium cation of ILs and the electronegative oxygen atoms of oxyethylene (OE) units of Triton X-100. The electrostatic interaction behaves similar to hydrogen bond that occurred between the OE units of nonionic surfactants and water molecules in aqueous micelles and cooperates with solvophobicity, leading to the formation of IL micelles [27]. The 2D ROESY analysis revealed that the microstructure of Triton X-100-based micelles in ILs is not regular spherical, which accords with the FFTEM image. Similar to the aqueous micellar systems, the hydrophobic interaction or solvatophobicity was found to drive the formation of micelles [27].

Moreover, Lodge et al. first studied the self-assembly of block copolymers in ILs [28]. It was shown that four amphiphilic poly((1,2-butadiene)-block-ethylene oxide) (PB-PEO) diblock copolymers, another kinds of nonionic surfactants, aggregated strongly and formed micelles in bmimPF₆. The universal micellar structures (spherical micelle, wormlike micelle, and

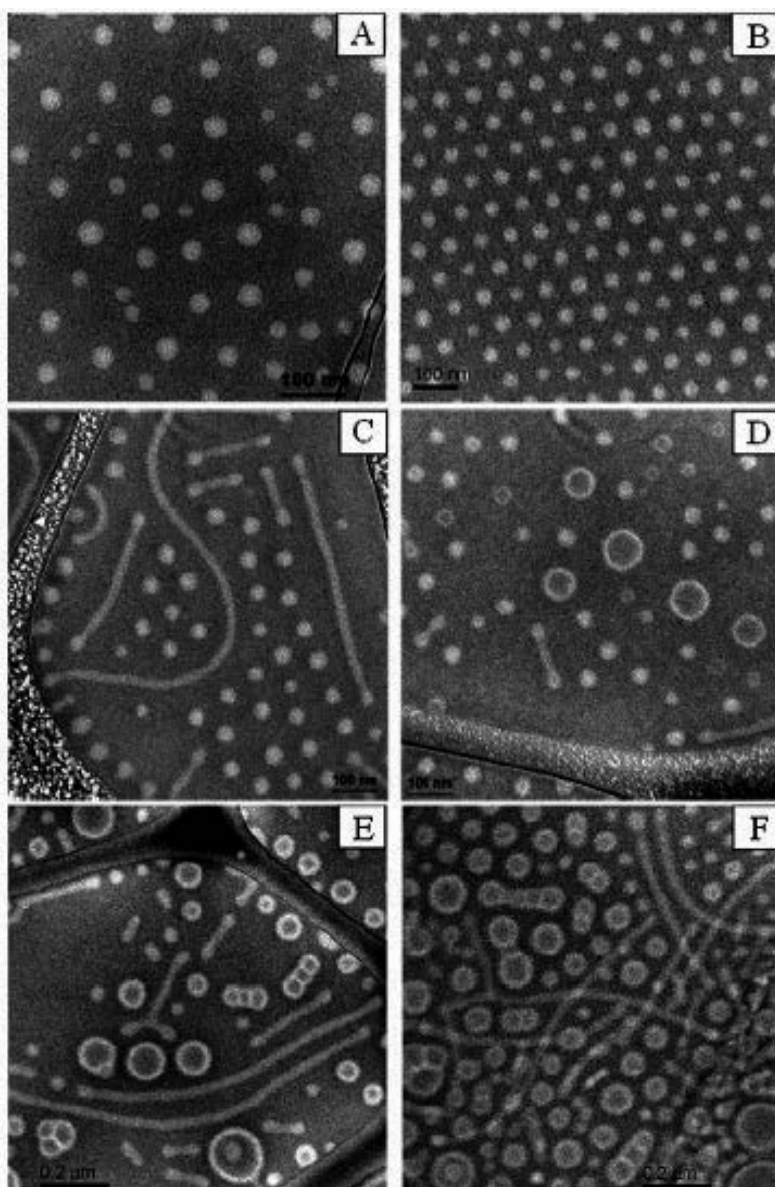


Figure 4. Cryo-TEM images of 1 wt % bmimPF₆ solutions: (A) spherical micelle, BO(9-20) ($f_{\text{PEO}}=0.64$); (B) spherical micelle, BO(9-10) ($f_{\text{PEO}}=0.45$); (C) a coexistence of spherical and wormlike micelles, BO(9-7) ($f_{\text{PEO}}=0.38$); (D) a coexistence of spherical and some vesicles, BO(9-7) ($f_{\text{PEO}}=0.38$); (E) and (F) a coexistence of wormlike micelles and vesicles, BO(9-4) ($f_{\text{PEO}}=0.25$). (Reproduced from Ref.[28], with permission).

vesicle) were all accessed by varying the length of the corona block while holding the core block constant. The nanostructural changes were directly visualized through cryogenic transmission electron microscopy (cryo-TEM) (Figure 4). Compared to aqueous solutions of the same copolymers, bmimPF₆ solutions exhibit some distinct features, such as temperature-

independent micellar morphologies between 25 and 100°C [28]. This is in accordance with the reported aggregation behavior of $C_{16}mimCl$ and $C_{16}mimBF_4$ in EAN by Kunz group [23]. They also found that three polystyrene-block-poly(methyl methacrylate) (PS-PMMA) block copolymers with varying molecular content have been shown to form micelles when dissolved in $bmimPF_6$. A morphological transition from spherical to cylindrical micelles was observed upon reduction of the PMMA volume fraction [29]. The transfer of aggregation structure by changing the surfactant molecular parameters or system variable such as concentration and temperature has been realized in traditional solvents [1].

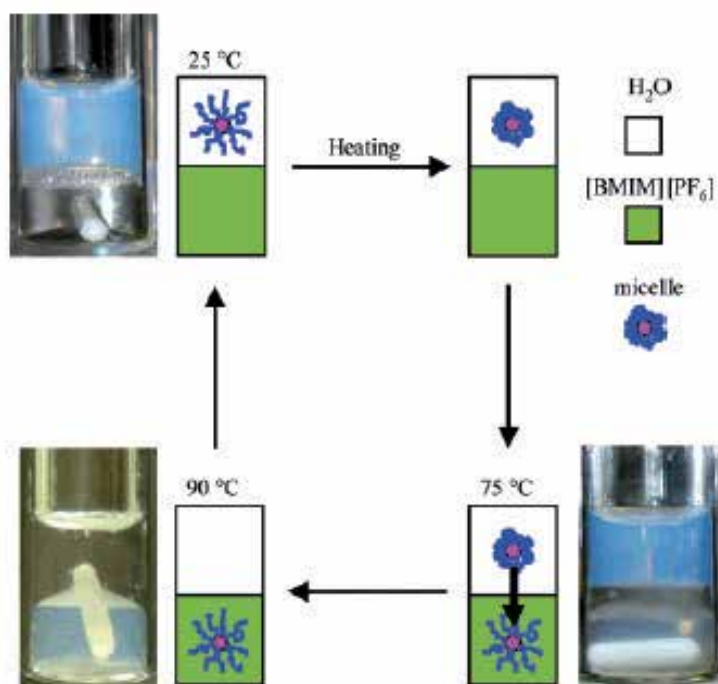


Figure 5. Schematic illustration of the round trip of PB-PEO micelles between $bmimPF_6$ (lower layer) and water (upper layer), accompanied by experimental images at each temperature. (Reproduced from Ref.[30], with permission).

Subsequently, they described an interesting and unusual round trip of the block copolymer micelles between $bmimPF_6$ and water. The reversible micelle transfer between the two media is based on the relative affinity of the two solvents to the corona chains and is triggered by temperature change. This round trip of PB-PEO micelles between $bmimPF_6$ and water with temperature was schematically illustrated in Figure 5. The micelle size and structure are preserved during the reversible transfer process. This phenomenon relies on finding a polymer (PEO in this case) that is nearly equally soluble in two otherwise immiscible solvents. Such a system could find application in transporting hydrophobic reactants/products to/from an IL reaction medium, with only the aqueous phase to handle in the ultimate recovery and purification steps [30]. Subsequently, they reported the reversible micelle transfer between

another hydrophobic ionic liquid, emimTf₂N and water [31]. The transfer was shown to be driven by the deteriorating solvent quality of water for PEO at high temperature, while the ionic liquid remains a good solvent. The transfer temperature could be tuned by adding ionic or nonionic additives to the aqueous phase to change the solvent quality of water for PEO, and by using ILs with different polarities. Moreover, Zheng and his coworkers studied the micellization of three commercially available amphiphilic poly(oxyethylene)-poly(oxypropylene)-poly(oxyethylene) ethers triblock copolymers, denoted Pluronic L61 (PEO₃PPO₃₀PEO₃), Pluronic L64 (PEO₁₃PPO₃₀PEO₁₃), and Pluronic F68 (PEO₇₉PPO₃₀PEO₇₉) [32]. The three copolymers were found to aggregate and form micelles in either bmimBF₄ or bmimPF₆. The surface tension measurements revealed that the dissolution of the copolymers in ILs depressed the surface tension in a manner analogous to aqueous solutions. The CMCs of three triblock copolymers increase following the order of L61, L64, F68, suggesting that micellar formation was driven by solvatophobic effect. CMC and γ_{cmc} decrease with increasing temperature because hydrogen bonds between ILs and hydrophilic group of copolymers decrease and accordingly enhance the solvatophobic interaction. The thermodynamic parameters ΔG_m^0 , ΔH_m^0 , ΔS_m^0 of the micellization of block copolymers in bmimBF₄ and bmimPF₆ were also calculated. The result revealed that the micellization is a process of entropy driving [32]. From these results, it was proposed that micelles formed in ILs follow the traditional self-assembly rules such as the curvature of aggregate surface and the packing parameter of the surfactant molecule.

The properties of self-assembled micelles in ILs have been investigated by Sarkar and his coworkers [33]. The solvent relaxation dynamics is slower in bmimPF₆-Brij micelles as compared to neat bmimPF₆. The steady increase in the solvent relaxation time with addition of the surfactant is ascribed to increase in viscosity of the solution. However, the slowing down in the solvation time on going from neat IL to IL confined micelles is much smaller compared to that on going from water to water confined micellar aggregates. The fast component originates from the translational motion of the anions and does not depend on viscosity. The magnitude of the fast component increases due to the hydrogen bonds between the -OH group of the surfactant and the PF₆⁻ ions. The increase in the rotational relaxation time of the probe after formation of the micelles in bmimPF₆ is significantly smaller than the increase in aqueous micelles. The higher rotational relaxation time in the IL-surfactant mixture is attributed to the increase in the viscosity of the solution [33]. They also studied the solvent and rotational relaxation of coumarin 153 (C-153) in bmimBF₄ and bmimBF₄ confined in C₁₂E₈, and C₁₄E₈ formed micelles, respectively. In the bmimBF₄-C₁₄E₈ micelle, they have observed only a 22% increase in solvation time compared to neat bmimBF₄, whereas in the bmimBF₄-C₁₂E₈ system, about 57% increase was observed in average solvation time due to micelle formation. However, the slowing down in solvation time on going from neat IL to IL-confined micelles is much smaller compared to that on going from water to water confined micellar aggregates. The 22-57% increase in solvation time is attributed to the slowing down of collective motions of cations and anions in micelles. The rotational relaxation times becomes faster in both the micelles compared to neat bmimBF₄ [34].

3. Self-assembled microemulsions in ILs

Microemulsions are the thermodynamic stable colloid mixtures consisting of at least two immiscible solvents stabilized by an adsorbed surfactant film at the liquid-liquid interface and have a tendency to solubilize chemical species in their core and thus have the potential to function as microreactors. Recently, ILs have been used to substitute for traditional organic solvents or water to create a novel IL microemulsion. Han and coworkers first reported that bmimBF_4 can act as polar nanosized droplets dispersed in a continuous cyclohexane with the aid of nonionic surfactant Triton X-100 [12]. The microstructure and morphology of the microemulsion droplets were detected by DLS and freeze-fracture electron microscopy (FFEM). The diameters of the aggregates increase from about 15 nm to 1 μm as $[\text{bmimBF}_4]/[\text{Triton X-100}]$ molar ratio, R , varies from 0.2 to 1.5. The regular swell behavior of the bmimBF_4 -in-cyclohexane IL reverse microemulsion is in accordance with the traditional water-in-oil (W/O) microemulsions, indicating that these unusual systems behave akin to common W/O microemulsions. FFEM revealed that a droplet structure of the bmimBF_4 -in-cyclohexane microemulsion which takes the same shape as "classic" water-in-oil (W/O) microemulsions. Eastoe et al. have also investigated the same microemulsion system by small-angle neutron scattering (SANS) [11]. The result showed a regular increase in droplet volume as micelles were progressively swollen by the added bmimBF_4 , which is in consistent with the measurements of DLS and FFEM reported by Han et al. The SANS data have been treated in accordance with an ellipsoid form factor, and the ellipsoid model gave the best statistical fits, even compared to polydisperse spherical particles. The predicted ellipsoid structure is in accordance with the FFEM images to a large extent.

Recently, the formation mechanism of the bmimBF_4 -in-*p*-xylene reverse IL microemulsion has been also proposed by Zheng's group [35]. The authors discovered that the terminal hydroxyl stretching of Triton X-100 gradually shifts to a high-frequency region of the FTIR spectrum with increasing bmimBF_4 content because the hydrogen bonds between hydroxyl and oxyethylene (OE) units of Triton X-100 were weakened by the formation of electrostatic attraction between the electronegative oxygen atoms of the OE units and the positively charged imidazolium cation of bmimBF_4 . The conclusion was further confirmed by simulating the hydrophilic OE units of Triton X-100 using polyethylene glycols-(PEGs)-600 and polyethylene glycols-(PEGs)-1000 as substitutes. This electrostatic interaction has caused the proton signals of H-2, H-4, and H-5 of bmimBF_4 shift downfield. The downfield shift experienced by these protons is because, with increasing bmimBF_4 content to the microemulsion, the fraction of Triton X-100 in the system is decreased, the number of oxygen atoms attracting imidazolium ring is accordingly decreased. The electropositivity of the imidazolium cation is relatively enhanced, as a consequence the hydrogen atoms on the imidazolium ring are deshielded and resonate in a downfield position [35].

The effect of polyvinylpyrrolidone (PVP) on the microstructure of IL microemulsion has also been investigated [36]. It was found that small amounts of bmimBF_4 solution containing PVP destroyed the initial Triton X-100/cyclohexane micellar structure, while successive addition of the solution again leads to the IL microemulsion formation [36]. The similar result was also

observed for the Triton X-100/benzene/bmimBF₄, Triton X-100/toluene/bmimBF₄ systems [37, 38]. This phenomenon suggests that the IL microemulsion formation cannot be simply regarded as the swelling of initial micelle by bmimBF₄. The major driving force for the IL microemulsion formation may be the weak electrostatic attraction between the electronegative oxygen atoms of OE units of nonionic surfactants and positively charged imidazolium cation. Just due to the weak electrostatic interaction, the required amount of nonionic surfactants to support the microemulsion formation is relatively large compared to traditional microemulsions, as has been mentioned by Eastoe and Atkin [11,39]. This conclusion has been further confirmed by the recent observation that only C-2 proton, C-4 proton, and C-5 proton of bmimBF₄ and protons of all OE units of nonionic surfactant remarkably shift in ¹H NMR spectroscopy [40].

Moreover, it was reported that water has a great effect on the IL-in-benzene microemulsions. The added water molecules mainly behaved as bound water and trapped water in the palisade layers of the bmimBF₄-in-benzene microemulsion. A hydrogen binding network consisting of imidazolium cations and H₂O, BF₄⁻ anion and H₂O, H₂O and H₂O, as well as the electronegative oxygen atoms of the OE units of Triton X-100 and H₂O was bridged in the palisade layers. The hydrogen binding network is much stronger than the weak electrostatic attraction between the positively charged imidazolium cation and the electronegative oxygen atoms of OE units, which was considered as the driving force of IL microemulsion formation. The palisade layers of the IL microemulsion therefore become more firm and thus increase the stability of the microemulsion [37,41]; whereas for the bmimBF₄-in-cyclohexane IL microemulsion system, DLS revealed that the size of microemulsion droplets decreased remarkably with increasing water content although water is often used as a polar component to swell reverse microemulsions [42]. It was deduced that the number of microemulsion droplets was increased which was confirmed by conductivity measurements. ¹H NMR along with two-dimensional rotating frame NOE experiments (2D ROESY) further revealed that water molecules were mainly located in the periphery of the polar core of the microemulsion droplets and behave like a chock to be inserted in the palisade layer of the droplet. This increased the curvature of the surfactant film at the IL/cyclohexane interface and thus led to the decrease of the microemulsion droplet size. A schematic diagram illustrating the microstructural change of the bmimBF₄-in-cyclohexane microemulsion before and after adding water was shown in Figure 6. The order of surfactant molecules arranged in the interface film was increased and thus induced a loss of entropy. Isothermal titration calorimetry (ITC) indicated that an enthalpy increase compensates for the loss of entropy during the process of microstructural transition. Water decreasing the size of IL microemulsion droplets has also been found by DLS measurements when Bhattacharyya and coworkers studied the solvation dynamics of Triton X-100/1-pentyl-3-methylimidazolium tetrafluoroborate (pmimBF₄)/benzene ternary IL microemulsion system [43]. In the IL microemulsion, the surfactant Triton X-100 molecules aggregate in form of a nonpolar peripheral shell around the polar pool of IL. The microenvironment in such an assembly varies drastically over a short distance. They found that the solvation dynamics is slower than that in the IL microemulsion without water, which is ascribed to the smaller size of the water-containing microemulsion [43].

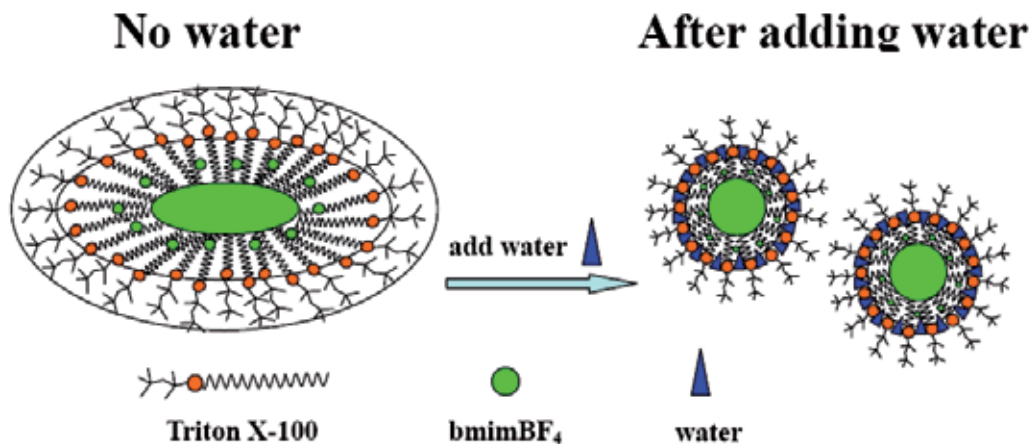


Figure 6. A schematic diagram of the bmimBF_4 -in-cyclohexane microemulsion. A large elliptical droplet structure was presumed in the absence of water and the addition of water may result in the appearance of more small-size spherical microemulsion droplets. (Reproduced from Ref.[42], with permission).

In addition, Zheng and his coworkers found an interesting IL-in-base microemulsion, in which triethylamine acts as either organic solvent or Lewis base. The added water molecules mainly bond the continuous triethylamine to form a surrounding OH^- basis environment [44]. Some of OH^- ions may enter the palisade layers of the IL microemulsions and a continuous basic interface was created. The unique solubilization behavior of water makes it possible to use the IL microemulsion as a template to prepare metal hydroxides and their corresponding oxides materials. Furthermore, the micropolarities of bmimBF_4 /Triton X-100/toluene IL microemulsions were also studied by Zheng's group by UV-Vis spectroscopic analyses [38]. The results showed that the IL pools of the microemulsion possessed a relatively fixed polar microenvironment. In the pools, metal salts $\text{Ni}(\text{NO}_3)_2$, CoCl_2 , CuCl_2 , and biochemical reagent riboflavin could be solubilized, indicating that the IL/O microemulsions have potential application in the production of metallic or semiconductor nanomaterials, and in biological extractions or as solvents for enzymatic reactions. Also, Zheng et al. investigated the phase behavior of the bmimBF_4 /Triton X-100/toluene ternary system [45]. Three different microstructures: the bmimBF_4 -in-toluene, bicontinuous, and toluene-in- bmimBF_4 microemulsion were successfully identified on the basis of the percolation theory by using toluene as the titration phase. The feasibility of the conductivity method was further proved by cyclic voltammetry experiments. In addition, an environmentally friendly IL microemulsion has also been prepared by using a common hydrophobic IL, bmimPF_6 as a replacement of organic solvents [46,47]. Both Triton X-100 and nonionic surfactant Tween-20 support the formation of such IL microemulsion. The hydrodynamic diameter (D_h) of the Triton X-100 based bmimPF_6 -in-water microemulsions is nearly independent of the water content but increases with increasing bmimPF_6 content due to the swelling of the micelles, which accords with the traditional microemulsions. The UV-Vis spectroscopy further confirmed the existence of water domains in the water-in- bmimPF_6 microemulsions [47]. It was revealed that this environmental friendly microemulsion can

solubilized both metal salts and biological molecules, also showing its potential application in nanomaterial, biological extraction or enzymatic reaction fields [46].

Han and coworkers also discovered that bmimPF_6 can also be used as polar nanosized droplets dispersed in toluene [48]. Electrical conductivities of the system with different R ($[\text{bmimPF}_6]/[\text{Triton X-100}]$ molar ratio) values were determined, and the results were used to locate the sub-regions of the single-phase microemulsion. The aggregate size of the reverse microemulsion of bmimPF_6 -in-toluene was determined using small-angle X-ray scattering (SAXS). The results showed that the size depended markedly on the R values. The effect of a compressed CO_2 gas on the properties of reverse micellar solutions with IL polar cores was also studied. It was revealed that compressed CO_2 could enhance solubilization of bmimBF_4 in the reverse micelles considerably at suitable pressures, and formation of the reverse micelles could be controlled easily by pressure. Increase of CO_2 pressure resulted in the decrease of the micellar sizes at fixed R values. Phase behavior study, UV-vis and SAXS techniques were used to investigate the effect of bmimBF_4 on the size and micropolarity of the reverse microemulsions formed by nonionic surfactant Surfynol-2502 (SF) in SC CO_2 [49]. The effect of a compressed CO_2 gas on the properties of reverse microemulsion solutions with bmimBF_4 as polar cores has been investigated. It was found that compressed CO_2 could enhance solubilization of the IL in the reverse microemulsions considerably at suitable pressures, and formation of the reverse microemulsions could be controlled easily by pressure [50].

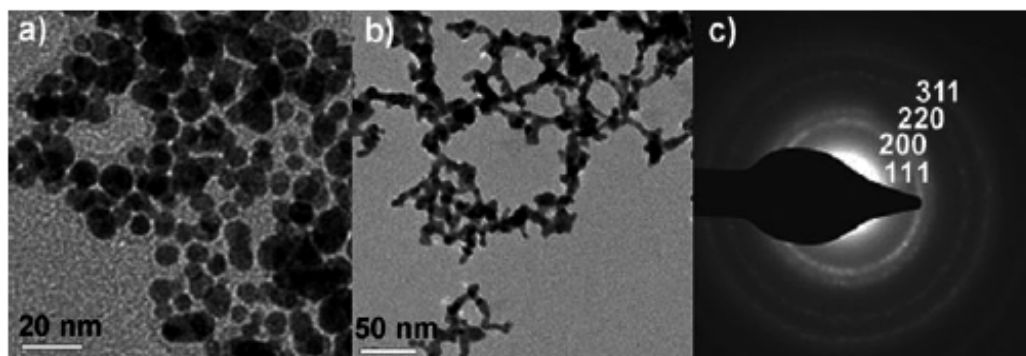


Figure 7. TEM images and electron-diffraction pattern of Au nanoparticles prepared by the RESOLV method at 308.2 K and 20.00 MPa; $[\text{N-EtFOSA}] = 0.060 \text{ gmL}^{-1}$, $[\text{TMGA}]/[\text{N-EtFOSA}]$ molar ratio, $w = 0.41$. a) Weight ratio of HAuCl_4 to TMGT, i.e., $W_{\text{HAuCl}_4}/W_{\text{TMGT}} = 0.01$; b) $W_{\text{HAuCl}_4}/W_{\text{TMGT}} = 0.04$; c) electron-diffraction pattern of the Au particles in (b). (Reproduced from Ref.[53], with permission).

Besides, Han et al. also reported that bmimPF_6 and immiscible ethylene glycol can form droplet and bicontinuous microemulsions in the presence of Triton X-100 [51]. The vapor pressures of ethylene glycol, bmimPF_6 , Triton X-100 are all very low at ambient temperature. Thus, a nonvolatile IL microemulsions was created. Subsequently, they found that bmimPF_6 can be dispersed in another hydrophilic IL propylammonium formate (PAF) with the aid of surfactant AOT. A nonvolatile IL-in-IL (bmimPF_6 -in-PAF) microemulsions is formed [52]. This kind of microemulsions may have potential applications with some advantages due to the water-free

and nonvolatile natures. Very recently, they also discovered that N-ethyl perfluorooctylsulfonamide ($C_2H_5NHSO_2C_8F_{17}$; N-EtFOSA) can form reverse microemulsions in supercritical CO_2 with 1,1,3,3-tetramethylguanidinium ($[(CH_3)_2N]_2C=NH_2^+$) acetate (TMGA), 1,1,3,3-tetramethylguanidinium lactate (TMGL), and 1,1,3,3-tetramethylguanidinium trifluoroacetate (TMGT) domains [53]. The combination of supercritical CO_2 and ILs is interesting from academic, environmental and practical points of view as the systems may combine some advantages of the two fluids. The reverse microemulsion can solubilize salts, such as methyl orange, $CoCl_2$, and $HAuCl_4$. To demonstrate the application of reverse micelles with IL domains, they prepared gold particles by a process known as rapid expansion of a supercritical solution into a liquid solvent (RESOLV). A CO_2 /N-EtFOSA/TMGT reverse micellar solution containing $HAuCl_4$ was expanded into a solution of $NaBH_4$ in ethanol. Spherical Au nanoparticles were formed at a low concentration and an Au network was obtained at a higher concentration of $HAuCl_4$. The electron-diffraction pattern of the Au networks shows that the polycrystalline material corresponds to standard face-centered-cubic Au. TEM images and electron-diffraction pattern of Au nanoparticles prepared by the RESOLV method at 308.2 K and 20.00 MPa are shown in Figure 7.

The properties of the IL microemulsions have been intensively studied by Sarkar and co-workers. For instance, the interaction of water with $bmimPF_6$ in water-in- $bmimPF_6$ microemulsion has been probed by solvent and rotational relaxation of C-153 and coumarin 490 (C-490) as probes [54]. The rotational relaxation and average solvation time of C-153 and C-490 gradually decrease with increasing water content of the microemulsions as the size of the microemulsion increases and consequently the mobility of the water molecules also increases. Moreover, the interaction of $bmimPF_6$ with water in the $bmimPF_6$ -in-water microregions of the microemulsions, has also been studied by the dynamics of solvent and rotational relaxation of C-153 and coumarin 151 (C-151) [55]. In the case of C-153 with an increase in the $bmimPF_6$ content in the microemulsions the change in the solvent relaxation time is small. The rotational relaxation time of C-153 also remains the same with an increase in the $bmimPF_6$ /Triton X-100 ratios. This means that the position of C-153 remains the same, and C-153 may reside at the interface of these microemulsions. However, in the case of C-151, with an increase in $bmimPF_6$ /Triton X-100 ratios, it was shown that the slow component of the solvation time gradually decreases, the fast component gradually increases, and the rotational relaxation time gradually increases. Therefore, the C-151 molecules gradually shifted to the core of the microemulsions.

Microemulsions consisting of nonionic C_nE_m surfactants, alkanes, and EAN have been prepared and characterized [39]. Studies of phase behavior reveal that EAN microemulsions have many features in common with corresponding aqueous systems, the primary difference being that higher surfactant concentrations and longer surfactant chains are required to offset the decreased solvophobicity of the surfactant molecules in EAN compared with water. The response of the EAN microemulsions to variation in the length of the alkane, surfactant headgroup, and surfactant chain has been found to parallel that observed in aqueous systems in most instances. EAN microemulsions exhibit a single broad SAXS peak, like aqueous systems. These are well described by the Teubner-Strey model. A lamellar phase was also

observed for surfactants with longer chains at lower temperatures. The scattering peaks of both microemulsion and lamellar phases move to lower wave vector on increasing temperature. This is ascribed to a decrease in the interfacial area of the surfactant layer. Phase behavior, SAXS, and conductivity experiments have allowed the weakly to strongly structured transition to be identified for EAN systems [39].

4. Self-assembled liquid crystals in ILs

In 1983, Evans et al. investigated that β,γ -distearoylphosphatidylcholine (DSPC) can form liquid crystals in EAN by polarized microscopy and SAXS [56]. The $L_{\beta'} \rightarrow P_{\beta'} \rightarrow L_{\alpha'}$ transitions with increasing temperature are present in analogy with the behavior of DSPC in water. For a 1:1 (by weight) mixture the d spacing for the L_{α} phase is 63 Å, and the surfactant headgroup area is 76 Å². A transition involving a subgel to liquid crystalline transition was observed for L-dipalmitoylphosphatidylcholin (DPPC) bilayers in EAN. This type of transition has not been previously observed for DPPC multilamellar arrays in water [57]. Also, the phase transitions for dipalmitoylphosphatidylethanolamine (DPPE) dispersed in EAN were examined using differential scanning calorimetry (DSC) and time-resolved x-ray diffraction. Lamellar (L_{α}) to hexagonal (H_1) phase transition was observed when using time-resolved x-ray diffraction but not when using calorimetry. The presence of EAN stabilizes the existence of the H_1 phase in DPPE by its influence on the bilayer interfacial properties, primarily on the area per lipid headgroup [58].

The stability of a variety of lyotropic liquid crystals formed by a number of POE nonionic surfactants in EAN was also surveyed and reported. The pattern of self-assembly behavior and mesophase formation is strikingly similar to that observed in water, even including the existence of a lower consolute boundary or cloud point. The only quantitative difference from water is that longer alkyl chains are necessary to drive the formation of liquid crystalline mesophases in EAN, suggesting that a rich pattern of "solvophobic" self-assembly should exist in this solvent [59].

Besides, Chen and coworkers reported that nonaqueous lyotropic liquid crystalline phases of an amphiphilic triblock copolymer P123 ($EO_{20}PO_{70}EO_{20}$) formed in bmimPF₆ [60]. A hexagonal liquid crystal phase (H_1) formed at 38-52% of P123 in bmimPF₆, while at 65-87% of P123, the SAXS peak positions accord with the ratio 1:2:3, indicating a lamellar phase (L_{α}). A schematic diagram of formation mechanism of the liquid crystal was shown in Figure 8. They proposed that the strong solvatophobic interaction between IL and hydrophobic parts of surfactant; hydrogen bonds between the end group of EO block and PF₆⁻ anion; hydrogen bonds between the cation moiety ($-N^+$) of IL and the lone pairs on oxygen atoms of EO groups may favor the appearance of long-range ordered structures. Therefore, the possible structural model of organized P123 assembly in bmimPF₆ should be similar to that of aqueous systems, that is, polar domains are formed with PEO blocks extending into the IL and PPO blocks form apolar or solvatophobic domains [60].

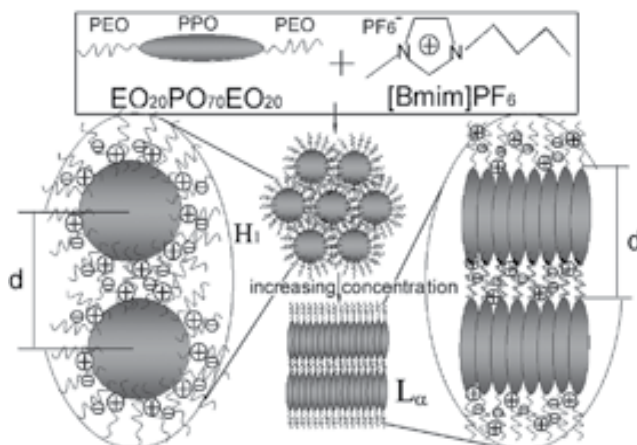


Figure 8. Schematic diagram of formation mechanism of the liquid crystal consisting of P123 (EO₂₀PO₇₀EO₂₀) in bmimPF₆. (Reproduced from Ref.[60], with permission).

Recently, Drummond group investigated forty new surfactant-protic ionic liquids (PIL) systems. On the basis of high throughput surfactant-PIL penetration scans, they found that lamellar, inverse hexagonal, and bicontinuous cubic phases can exist as thermodynamically stable phases in excess PIL in select surfactant-PIL systems. Changes to the cation and anion can be used to modify the liquid crystalline phases [61]. They also discovered that PILs can mediate solvent hydrocarbon interactions and promote amphiphile self-assembly. The main lyotropic liquid crystal phases including hexagonal, cubic, and lamellar phases are observed in the CTAB-PIL systems, Amphiphile self-assembly in PILs has been interpreted in terms of a solvophobic driving force (analogous to the hydrophobic effect in water), with the formed aggregate structures being the result of both local molecular and global aggregate packing constraints [62].

The local sites of two different ILs: hydrophobic bmimPF₆ and relatively hydrophilic bmimBF₄ in nonionic Brij 97 formed hexagonal liquid crystalline were analyzed by SAXS, rheological techniques and polarizing optical microscopy [63]. Hydrophobic bmimPF₆ is dominantly penetrated between the OE chains of surfactant molecules, whereas hydrophilic bmimBF₄ is mainly located in the water layer of hexagonal phases. The strength of the network of hexagonal phase formed in the Brij 97/water/bmimBF₄ system is appreciably stronger than that of the Brij 97/water/bmimPF₆ system, indicated by the smaller area of the surfactant molecule at the interface and the higher moduli (G' , G''). Temperature has a converse effect on the lattice parameters of the two hexagonal phases. Decrease in temperature results in a decrease in lattice spacing for the bmimBF₄ system but an increase in lattice spacing for the bmimPF₆ system [63].

Very recently, the aggregation behaviors of a Gemini surfactant [C₁₂H₂₅(CH₃)₂N⁺(CH₂)₂N⁺(CH₃)₂C₁₂H₂₅]Br₂ (12-2-12) in two protic ionic liquids (PILs), propylammonium nitrate (PAN) and butylammonium nitrate (BAN), were investigated by Chen et al [64]. Compared to those in EAN, the minor structural changes with only one or two methylene units (-CH₂-) increase

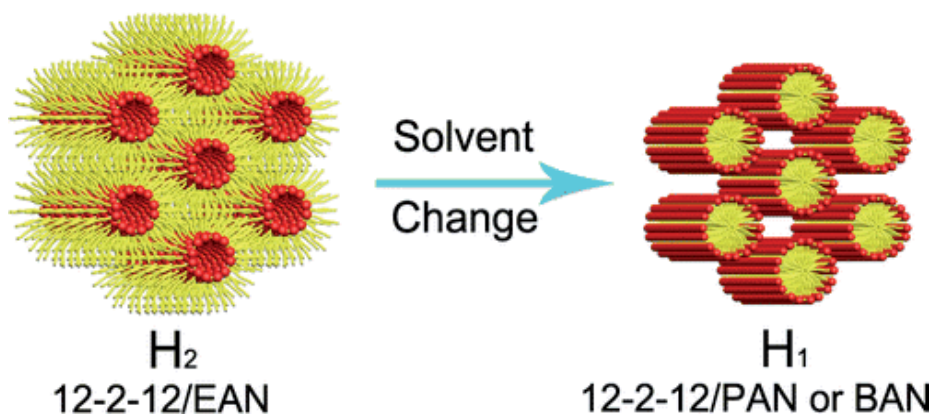


Figure 9. Phase transition of a quaternary ammonium gemini surfactant induced by minor structural changes of protic ionic liquids. (Reproduced from Ref.[64], with permission).

in cationic chain length of PIL, result in a dramatic phase transition of formed aggregates (Figure 9). The critical micellization concentration was increased in PAN, while no micelle formation was detected in BAN. A normal hexagonal phase was observed in the 12-2-12/PAN system, while the normal hexagonal, bicontinuous cubic, and lamellar phases were mapped in the 12-2-12/BAN system. Such aggregation behavior changes can be ascribed to the weaker solvophobic interactions of 12-2-12 in PAN and BAN.

5. Self-assembled vesicles and gels in ILs

Hao and coworkers reported the self-assembled surfactant vesicles formed by $\text{Zn}(\text{OOCCH}_2\text{C}_6\text{F}_{13})_2$ in bmimBF_4 or by mixtures of C_{14}DMAO and $\text{Zn}(\text{OOCCH}_2\text{C}_6\text{F}_{13})_2$ with a $\chi_{\text{C}_6\text{F}_{13}\text{CH}_2\text{COO}^-} = 0.18$ in bmimPF_6 [65]. Well-defined self-assembled surfactant bilayer vesicles of $\text{Zn}(\text{OOCCH}_2\text{C}_6\text{F}_{13})_2$ in bmimBF_4 were identified by negative-staining TEM.

As shown in Figure 10A, the well-defined bilayer vesicles are clearly visible and the diameters of the nanospheres range from about 30 to more than 90 nm. Negative-staining TEM and FFEM (Figure 10B,C) also revealed that the mixed solutions of C_{14}DMAO and $\text{Zn}(\text{OOCCH}_2\text{C}_6\text{F}_{13})_2$ in bmimPF_6 displayed the same self-assembled aggregation behavior as $\text{Zn}(\text{OOCCH}_2\text{C}_6\text{F}_{13})_2$ in bmimBF_4 . The diameters of the aggregation were about 20 to 150 nm, and multilamellar vesicles were visible in the FFEM image. Also, clusters of nanospheres could be seen in the negative-staining TEM image.

Kimizuka developed the ether-containing ILs which are capable of dissolving carbohydrates such as β -D-glucose, α -cyclodextrin, amylose, agarose, and a glycosylated protein, glucose oxidase. Stable bilayer membranes are formed when glycolipids are dispersed in these sugar-philic ILs. Reversible thermal transformation from fibrous assemblies to vesicles was also displayed in Figure 11. Physical gelation of ILs occurs by dissolving amide-group-enriched glycolipids, providing a first example of self-assembling ionogels [66].

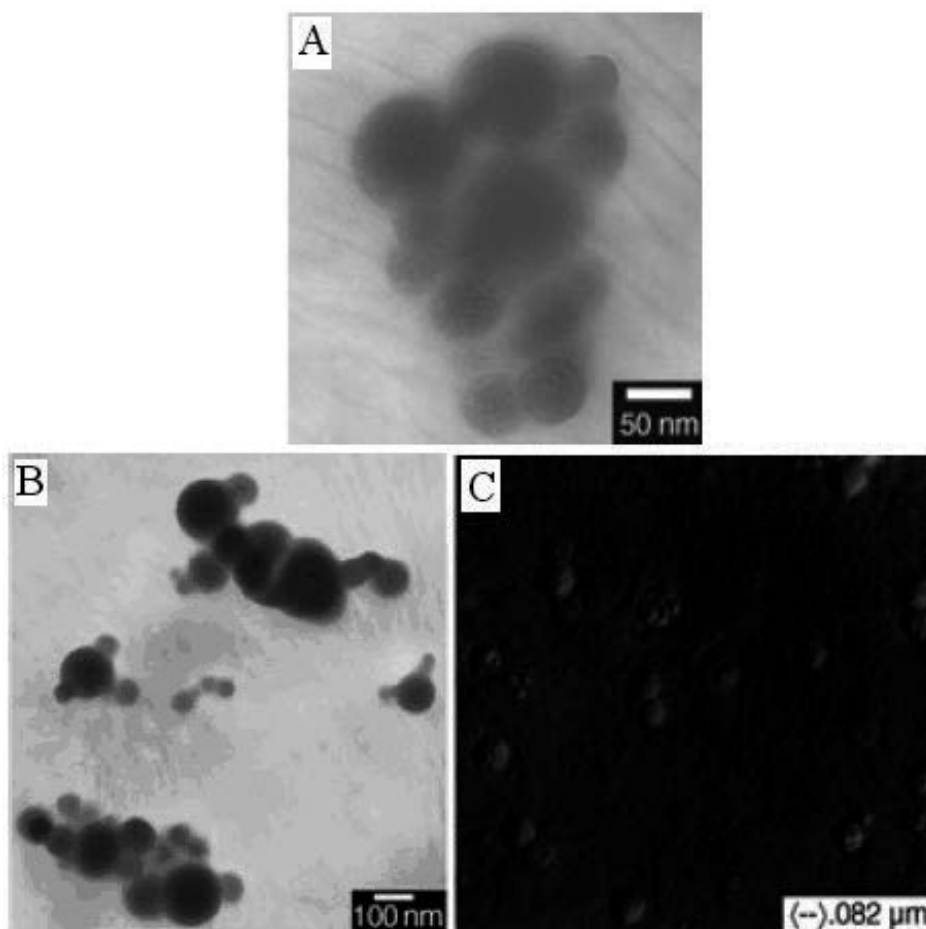


Figure 10. Negative-staining and FFTEM images of self-assembled surfactants in ILs. (A) a typical negative-staining TEM image of the self-assembled $\text{Zn}(\text{OOCCH}_2\text{C}_6\text{F}_{13})_2$ bilayer vesicles in bmimBF_4 ; (B) Negative-staining and (C) FFTEM images of self-assembled surfactant nanospheres of C_{14}DMAO and $\text{Zn}(\text{OOCCH}_2\text{C}_6\text{F}_{13})_2$ in bmimPF_6 . (Reproduced from Ref.[65], with permission).

A thermoreversible ion gel by triblock copolymer, poly(N-isopropyl acrylamide-*b*-ethylene oxide-*b*-N-isopropyl acrylamide) (PNIPAm-PEO-PNIPAm) self-assembly in IL, 1-ethyl-3-methylimidazolium bis(trifluoromethylsulfonyl)-imide (emimTFSI) has been recently reported by Lodge group [67]. The ion gel is highly conductive and possesses sufficient mechanical strength even under large strains. This thermoreversible ion gel offers the advantage of solvent-free processing in practical applications. They also found that ion gel electrolyte can be formed by gelation of poly(styrene-*block*-ethylene oxide-*block*-styrene) (SOS) triblock copolymer in bmimPF_6 . The gelation behavior, ionic conductivity, rheological properties, and microstructure of the ion gels were investigated. The ionic conductivity of the ion gels is only modestly affected by the triblock copolymer network. Its temperature dependence nearly tracks that of the bulk IL viscosity. The ion gels are

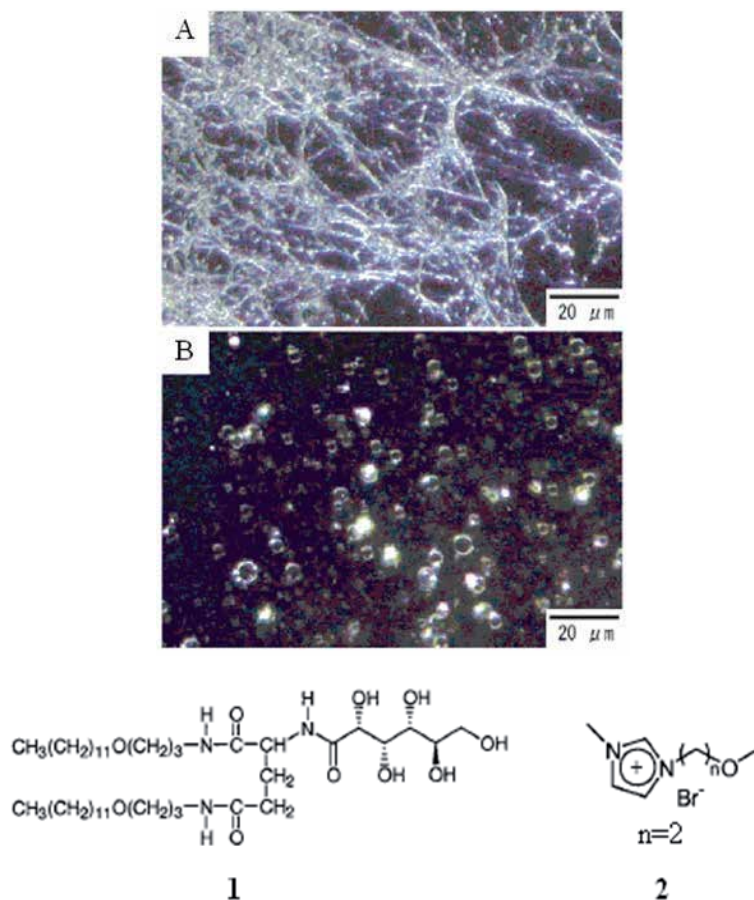


Figure 11. Dark-field optical micrographs of glycolipids dispersed in ILs: (A) fibrous nanostructures composed of **1** in **2** at 20°C; (B) vesicles composed of **1** in **2** at 50°C. (Reproduced from Ref.[66], with permission).

thermally stable up to at least 100°C and possess significant mechanical strength [68]. Moreover, they also fabricated polymer semiconductor thin film transistors using the ion gel as the gate dielectric layer. The gate capacitance of the ion gel can be as large as 40 μF/cm² at 10 Hz and 2 μF/cm² at 1 kHz. The polarization response time of the ion gel is much faster than previously tested solid polymer electrolytes, allowing the ion gel gated transistors to operate at higher frequencies and establishing ion gels as an attractive new class of solution processible gate dielectric materials for organic electronics [69].

6. Conclusion

Due to their unique characteristics and potential environmentally friendly behavior, ILs are finding more and more applications in a variety of research fields, such as extraction, separation, chemical reactions, material preparations, and chromatography, among others. It can be

said that once the physicochemical properties and microstructure of these neoteric self-assembly in ILs are well established and understood, number of their applications of the self-assemblies will increase dramatically as researchers are discovering more and more about these exciting media. There is no doubt that, in the near future, self-assemblies in ILs will establish themselves as important media in many research fields.

Acknowledgements

The authors gratefully acknowledge financial support from the National Natural Science Foundation of China (21273235, 21303076), and the One Hundred Talent Program of CAS for Gao YA.

Author details

Bin Dong and Yanan Gao*

*Address all correspondence to: ygao@dicp.ac.cn

Dalian Institute of Chemical Physics, Chinese Academy of Sciences, Dalian, China

References

- [1] Svensson A. Phase equilibria and structures of oppositely charged polymers and surfactants in water. Doctoral dissertation. Lund University, 2003.
- [2] Jönsson B, Lindman B, Holmberg K, Kronberg B. Surfactants and polymers in aqueous solution; Wiley: Chichester, 1998.
- [3] Dynamics of surfactant self-assemblies: micelles, microemulsions, vesicles, and lyotropic phases, Edited by Raoul Zana, Taylor & Francis Ltd; New 2005.
- [4] Wasserscheid P. Chemistry-Volatile times for ionic liquids. *Nature* 2006;439:797.
- [5] Welton T. Room-temperature ionic liquids. Solvents for synthesis and catalysis. *Chem Rev* 1999;99:2071-84.
- [6] Wasserscheid P, Keim W. Ionic liquids-New "solutions" for transition metal catalysis. *Angew Chem Int Ed* 2000;39:3773-89.
- [7] Huddleston JG, Willauer HD, Swatoski RP, Visser AE, Rogers RD. Room temperature ionic liquids as novel media for 'clean' liquid-liquid extraction. *Chem Commun* 1998;1765-6.

- [8] Dickinson EV, Williams ME, Hendrickson SM, Masui H, Murray RW. Hybrid redox polyether melts based on polyether-tailed counterions. *J Am Chem Soc* 1999;121:613-6.
- [9] Gao YA, Li ZH, Du JM, Han BX, Li GZ, Hou WG, et al. Preparation and characterization of inclusion complexes of beta-cyclodextrin with ionic liquid. *Chem Eur J* 2005;11:5875-80.
- [10] Gao YA, Zhao XY, Dong B, Zheng LQ, Li N, Zhang SH. Inclusion complexes of beta-cyclodextrin with ionic liquid surfactants. *J Phys Chem B* 2006;110:8576-81.
- [11] Eastoe J, Gold S, Rogers SE, Paul A, Welton T, Heenan RK, et al. Ionic liquid-in-oil microemulsions. *J Am Chem Soc* 2005;127:7302-3.
- [12] Gao HX, Li JC, Han BX, Chen WN, Zhang JL, Zhang R, et al. Microemulsions with ionic liquid polar domains. *Phys Chem Chem Phys* 2004;2914-6.
- [13] Hao JC, Zemb T. Self-assembled structures and chemical reactions in room-temperature ionic liquids. *Curr Opin Colloid Interf Sci* 2007;12:129-37.
- [14] Dupont J. On the solid, liquid and solution structural organization of imidazolium ionic liquids. *J Braz Chem Soc* 2004;3:341-50.
- [15] Evans DF, Yamauchi A, Roman R, Casassa EZ. Micelle formation in ethylammonium nitrate, a low-melting fused salt. *J Colloid Interf Sci* 1982;88:89-96.
- [16] Evans DF, Yamauchi A, Wei GJ, Bloomfield VA. Micelle size in ethylammonium nitrate as determined by classical and quasi-elastic light scattering. *J Phys Chem* 1983;87:3537-41.
- [17] Anderson JL, Pino V, Hagberg EC, Sheares VV, Armstrong DW. Surfactant solvation effects and micelle formation in ionic liquids. *Chem Commun* 2003;2444-2445.
- [18] Headley AD, Jackson NM. The effect of the anion on the chemical shifts of the aromatic hydrogen atoms of liquid 1-butyl-3-methylimidazolium salts. *J Phys Org Chem* 2002;15:52-5.
- [19] Merrigan TL, Bates ED, Dorman SC, Davis JH. New fluorinated ionic liquids function as surfactants in conventional room-temperature ionic liquids. *Chem Commun* 2000;2051-2.
- [20] Patrascu C, Gauffre F, Nallet F, Bordes R, Oberdisse J, de Lauth-Viguerie N, et al. Micelles in ionic liquids: Aggregation behavior of alkyl poly(ethyleneglycol)-ethers in 1-butyl-3-methyl-imidazolium type ionic liquids. *ChemPhysChem* 2006;7:99-101.
- [21] Tang J, Li D, Sun CY, Zheng LZ, Li JH. Temperature dependant self-assembly of surfactant Brij 76 in room temperature ionic liquid. *Colloid Surface A* 2006;273:24-8.
- [22] Velasco SB, Turmine M, Di Caprio D, Letellier P. Micelle formation in ethyl-ammonium nitrate (an ionic liquid). *Colloid Surface A* 2006;275:50-4.

- [23] Thomaier S, Kunz W. Aggregates in mixtures of ionic liquids. *J Mol Liq* 2007;130:104-7.
- [24] Fletcher KA, Pandey S. Surfactant aggregation within room-temperature ionic liquid 1-ethyl-3-methylimidazolium bis(trifluoromethylsulfonyl)imide. *Langmuir* 2004;20:33-6.
- [25] Tran CD, Yu SF. Near-infrared spectroscopic method for the sensitive and direct determination of aggregations of surfactants in various media. *J Colloid Interf Sci* 2005;283:613-8.
- [26] Behera K, Dahiya P, Pandey S. Effect of added ionic liquid on aqueous Triton X-100 micelles. *J Colloid Interf Sci* 2007;307:235-45.
- [27] Gao YA, Li N, Li XX, Zhang SH, Zheng LQ, Bai XT, et al. Microstructures of micellar aggregations formed within 1-butyl-3-methylimidazolium type ionic liquids. *J Phys Chem B* 2009;113:123-30.
- [28] He YY, Li ZB, Simone P, Lodge TP. Self-assembly of block copolymer micelles in an ionic liquid. *J Am Chem Soc* 2006;128:2745-50.
- [29] Simone PM, Lodge TP. Micellization of PS-PMMA diblock copolymers in an ionic liquid. *Macromol Chem Phys* 2007;208:339-48.
- [30] He YY, Lodge TP. The micellar shuttle: Thermoreversible, intact transfer of block copolymer micelles between an ionic liquid and water. *J Am Chem Soc* 2006;128:12666-7.
- [31] Bai ZF, Nagy MW, Zhao B, Lodge TP. Thermoreversible partitioning of poly(ethylene oxide)s between water and a hydrophobic ionic liquid. *Langmuir* 2014;30:8201-8.
- [32] Zhang SH, Li N, Zheng LQ, Li XW, Gao YA, Yu L. Aggregation behavior of pluronic triblock copolymer in 1-butyl-3-methylimidazolium type ionic liquids. *J Phys Chem B* 2008;112:10228-33.
- [33] Chakraborty A, Seth D, Chakrabarty D, Setua P, Sarkar N. Dynamics of solvent and rotational relaxation of coumarin 153 in room-temperature ionic liquid 1-butyl-3-methylimidazolium hexafluorophosphate confined in Brij-35 micelles: A picosecond time-resolved fluorescence spectroscopic study. *J Phys Chem A* 2005;109:11110-6.
- [34] Seth D, Chakraborty A, Setua P, Sarkar N. Dynamics of solvent and rotational relaxation of coumarin-153 in room-temperature ionic liquid 1-butyl-3-methyl imidazolium tetrafluoroborate confined in poly(oxyethylene glycol) ethers containing micelles. *J Phys Chem B* 2007;111:4781-7.
- [35] Gao YA, Zhang J, Xu HY, Zhao XY, Zheng LQ, Li XW, et al. Structural studies of 1-butyl-3-methylimidazolium tetrafluoroborate/TX-100/p-xylene ionic liquid microemulsions. *ChemPhysChem* 2006;7:1554-61.

- [36] Gao YA, Voigt A, Hilfert L, Sundmacher K. Effect of polyvinylpyrrolidone on the microstructure of 1-butyl-3-methylimidazolium tetrafluoroborate/Triton X-100/cyclohexane microemulsions. *Colloid Surface A* 2008;329:146-52.
- [37] Gao YA, Li N, Zheng LQ, Bai XT, Yu L, Zhao XY, et al. Role of solubilized water in the reverse ionic liquid microemulsion of 1-butyl-3-methylimidazolium tetrafluoroborate/TX-100/benzene. *J Phys Chem B* 2007;111:2506-13.
- [38] Li N, Gao YA, Zheng LQ, Zhang J, Yu L, Li XW. Studies on the micropolarities of bmimBF₄/TX-100/toluene ionic liquid microemulsions and their behaviors characterized by UV-visible spectroscopy. *Langmuir* 2007;23:1091-7.
- [39] Atkin R, Warr GG. Phase behavior and microstructure of microemulsions with a room-temperature ionic liquid as the polar phase. *J Phys Chem B* 2007;111:9309-16.
- [40] Gao YA, Vogit A, Hilfert L, Sundmacher K. Nanodroplet cluster formation in ionic liquid microemulsion. *ChemPhysChem* 2008;9:1603-9.
- [41] Gao YA, Li N, Zheng LQ, Zhao XY, Zhang J, Cao Q, et al. The effect of water on the microstructure of 1-butyl-3-methylimidazolium tetrafluoroborate/TX-100/benzene ionic liquid microemulsions. *Chem Eur J* 2007;13: 2661-70.
- [42] Gao YA, Liane H, Voigt A, Sundmacher K. Decrease of droplet size of the reverse microemulsion 1-butyl-3-methylimidazolium tetrafluoroborate/Triton X-100/cyclohexane by addition of water. *J Phys Chem B* 2008;112: 3711-9.
- [43] Adhikari A, Sahu K, Dey S, Ghosh S, Mandal U, Bhattacharyya K. Femtosecond solvation dynamics in a neat ionic liquid and ionic liquid microemulsion: Excitation wavelength dependence. *J Phys Chem B* 2007;111:12809-16.
- [44] Li N, Cao Q, Gao YA, Zhang J, Zheng LQ, Bai XT, et al. States of water located in the continuous organic phase of 1-butyl-3-methylimidazolium tetrafluoroborate/Triton X-100/triethylamine reverse microemulsions. *ChemPhysChem* 2007;8:2211-7.
- [45] Gao YA, Wang SQ, Zheng LQ, Han SB, Zhang X, Lu DM, et al. Microregion detection of ionic liquid microemulsions. *J Colloid Interf Sci* 2006;301:612-6.
- [46] Gao YA, Li N, Zheng LQ, Zhao XY, Zhang SH, Han BX, et al. A cyclic voltammetric technique for the detection of micro-regions of bmimPF₆/Tween 20/H₂O microemulsions and their performance characterization by UV-Vis spectroscopy. *Green Chem* 2006;8:43-9.
- [47] Gao YA, Han SB, Han BX, Li GZ, Shen D, Li ZH, et al. TX-100/water/1-butyl-3-methylimidazolium hexafluorophosphate microemulsions. *Langmuir* 2005;21:5681-4.
- [48] Li JC, Zhang JL, Gao HX, Han BX, Gao L. Nonaqueous microemulsion-containing ionic liquid [bmim][PF₆] as polar microenvironment. *Colloid Polym Sci* 2005;283:1371-5.

- [49] Li JC, Zhang JL, Han BX, Gao YN, Shen D, Wu ZH. Effect of ionic liquid on the polarity and size of the reverse micelles in supercritical CO₂. *Colloid Surface A* 2006;279:208-12.
- [50] Li JC, Zhang JL, Han BX, Wang Y, Gao L. Compressed CO₂-enhanced solubilization of 1-butyl-3-methylimidazolium tetrafluoroborate in reverse micelles of Triton X-100. *J Chem Phys* 2004;121:7408-12.
- [51] Cheng SQ, Fu XG, Liu JH, Zhang JL, Zhang ZF, Wei YL, et al. Study of ethylene glycol/TX-100/ionic liquid microemulsions. *Colloid Surface A* 2007;302:211-5.
- [52] Cheng SQ, Zhang JL, Zhang ZF, Han BX. Novel microemulsions: ionic liquid-in-ionic liquid. *Chem Commun* 2007;2497-9.
- [53] Liu JH, Cheng SQ, Zhang JL, Feng XY, Fu XG, Han BX. Reverse micelles in carbon dioxide with ionic-liquid domains. *Angew Chem Int Ed* 2007;46:3313-5.
- [54] Seth D, Chakraborty A, Setua P, Sarkar N. Interaction of ionic liquid with water with variation of water content in 1-butyl-3-methyl-imidazolium hexafluorophosphate ([bmim][PF₆])/TX-100/water ternary microemulsions monitored by solvent and rotational relaxation of coumarin 153 and coumarin 490. *J Chem Phys* 2007;126:224512.
- [55] Seth D, Chakraborty A, Setua P, Sarkar N. Interaction of ionic liquid with water in ternary microemulsions (Triton X-100/water/1-butyl-3-methylimidazolium hexafluorophosphate) probed by solvent and rotational relaxation of coumarin 153 and coumarin 151. *Langmuir* 2006;22:7768-75.
- [56] Evans DF, Kaler EW, Benton WJ. Liquid crystals in a fused salt: beta, γ -distearoylphosphatidylcholine in N-ethylammonium nitrate. *J Phys Chem* 1983;87:533-5.
- [57] Tamura-Lis W, Lis LJ, Quinn PJ. Structures and mechanisms of lipid phase transitions in nonaqueous media: dipalmitoylphosphatidylcholine in fused salt. *J Phys Chem* 1987;91:4625-7.
- [58] Tamura-Lis W, Lis LJ, Quinn PJ. Structures and mechanisms of lipid phase transitions in nonaqueous media. Dipalmitoylphosphatidylethanolamine in fused salt. *Biophys J* 1988;53:489-92.
- [59] Araos MU, Warr GG. Self-assembly of nonionic surfactants into lyotropic liquid crystals in ethylammonium nitrate, a room-temperature ionic liquid. *J Phys Chem B* 2005;109:14275-7.
- [60] Wang LY, Chen X, Chai YC, Hao JC, Sui ZM, Zhuang WC, et al. Lyotropic liquid crystalline phases formed in an ionic liquid. *Chem Commun* 2004;2840-1.
- [61] Greaves TL, Weerawardena A, Fong C, Drummond CJ. Formation of amphiphile self-assembly phases in protic ionic liquids. *J Phys Chem B* 2007;111:4082-8.

- [62] Greaves TL, Weerawardena A, Fong C, Drummond CJ. Many protic ionic liquids mediate hydrocarbon-solvent interactions and promote amphiphile self-Assembly. *Langmuir* 2007;23: 402-4.
- [63] Wang ZN, Liu F, Gao Y, Zhuang WC, Xu LM, Han BX, et al. Hexagonal liquid crystalline phases formed in ternary systems of Brij 97-water-Ionic liquids. *Langmuir* 2005;21:4931-7.
- [64] Li QT, Wang XD, Yue X, Chen X. Phase transition of a quaternary ammonium gemini surfactant induced by minor structural changes of protic ionic liquids. *Langmuir* 2014;30:1522-30.
- [65] Hao JC, Song AX, Wang JZ, Chen X, Zhuang WC, Shi F, et al. Self-assembled structure in room-temperature ionic liquids. *Chem Eur J* 2005;11:3936-40.
- [66] Kimizuka N, Nakashima T. Spontaneous self-assembly of glycolipid bilayer membranes in sugar-philic ionic liquids and formation of ionogels. *Langmuir* 2001;17:6759-61.
- [67] He YY, Lodge TP. A thermoreversible ion gel by triblock copolymer self-assembly in an ionic liquid. *Chem Commun* 2007;2732-4.
- [68] He YY, Boswell PG, Buhlmann P, Lodge TP. Ion gels by self-assembly of a triblock copolymer in an ionic liquid. *J Phys Chem B* 2007;111:4645-52.
- [69] Lee J, Panzer MJ, He Y, Lodge TP, Frisbie CD. Ion gel gated polymer thin-film transistors. *J Am Chem Soc* 2007;129:4532-3.

Ionic Liquids as Surfactants – Applications as Demulsifiers of Petroleum Emulsions

Rafael Martínez-Palou and Jorge Aburto

Additional information is available at the end of the chapter

<http://dx.doi.org/10.5772/59094>

1. Introduction

Emulsions are made by mixing two immiscible phases, preferentially in the presence of an emulsifying agent. Hence, crude oil production is invariably accompanied by water in mature oil reservoirs where the formation of stable water-in-oil (W/O) emulsions are frequently encountered [1]. The dispersion of water droplets in oil is facilitated by the presence of interfacial active agents in the crude oil such as asphaltenes, waxes, resins and naphthenic acids. The content of these natural emulsifiers is more abundant in heavy than in light crude oils, altogether with a specific density closer to water that difficult water separation that favor the formation of more stable emulsions in heavy crude oils [2].

The presence of water causes several operational problems like corrosion in equipments and pipelines, and generally increases the cost of oil production. Therefore, water must be separated from crude oil before refining process [3]. There are several physical methods (thermal, mechanical, electrical and chemical) to break water/oil emulsions. However, chemical demulsification by adding demulsifiers is still one of the most frequently applied industrial method to break crude oil emulsions [4]. The latter are generally combined with physical methods to accelerate the demulsification process [5].

Currently most of the recoverable crude oil around the world is heavy crude, i.e. specific density equal or lower than 20 API. Their composition complexity and high viscosity makes them difficult and expensive to produce and transport through pipeline because of their low mobility and flowability. Different strategies to facilitate the handling and transport of such crude oils are the dilution with condensates or lighter oils, the use of flow improvers and drag reducing additives, and the formation of oil in water emulsion (O/W), known as inverse emulsions, to increase the crude oil fluidity [6].

The formation of O/W emulsions is competitive when compared to conventional technology. However, this approach requires water separation and conditioning prior to crude oil processing and refining [7]. Thus, the demulsification process is important to break direct emulsions, more commonly W/O emulsions in order to avoid operational problems caused by the presence of water in the refining process. Secondly, demulsification is needed to break inverse O/W emulsions, that may also be formed naturally, but most commonly promoted as a method for fluidizing heavy crude before pipelining [8].

In this regard, ionic liquids (ILs) have been widely studied in the last two decades because of their unique properties, as an ecological alternative to solvents, cosolvents and catalysts in organic synthesis [9], and in the chemical industry [10]. Since they have a very low vapor pressure, thermal stability and non-flammability, they have been considered as “green, ecofriendly chemicals” [11]. ILs have found a variety of applications in the oil industry, such as pollutant removal, corrosion inhibitors and viscosity reducers [12-14]. ILs have found also wide applications as surfactants [15-16], and recently the application of ILs as demulsifiers for both W/O and O/W in petroleum industry have been described [17-19].

The purpose of this work is to share the qualitative perspective of ILs applications as surfactants and specially their applications as demulsifiers of petroleum emulsions. The chapter is then divided into two parts. The first part involves a review about generalities about surfactants, theories of emulsion and demulsification, variability of applied chemicals, emulsion's formation, type of emulsion, factors affecting the emulsion's stability, chemical demulsification, and proposed mechanisms for emulsion's breaking. In the second part, we discuss the ILs applications as surfactants with focus as demulsifiers of both O/W and W/O emulsions for oilfield applications. The effect of microwave irradiation on breaking crude oil emulsions in conjugation with ionic liquids is also discussed.

2. Theory about emulsions

2.1. Emulsion formation

An emulsion is generally defined as a system in which a liquid is distributed or dispersed relatively in the form of droplets in another substantially immiscible liquid. An emulsion is a lyophobic colloid, i.e. a sol that cannot be formed by spontaneous dispersion. The emulsions are thermodynamically unstable, but they may be kinetically stabilized by the presence of an emulsifying agent or surfactant. The latter forms a surface film on the existing interface between each droplet and the continuous medium, thereby reducing interfacial tension and preventing coalescence.

When a system containing enough surfactant, water and oil is subjected to mixing, one of the phase is preferentially dispersed as droplets into the other and resulting in an emulsion [20]. The mission of the surfactant is to facilitate the extension of the interface during the formation of the emulsion, and secondly, stabilizing the emulsion by retarding the coalescence of dispersed phase droplets. The surfactant possesses an amphipathic nature, which allows

locating at the interface between each droplet and the continuous medium and thereby reducing interfacial tension and preventing coagulation.

There are three minimal requirements to form an emulsion:

- Two immiscible liquids such as water and oil.
- Enough shear force provided by mixing to disperse one liquid into droplets in the other.
- An emulsifying agent to allow reduction of the free surface energy and stabilize the dispersed phase.

The nature of dispersion and continuous phases may be more complex as is the case of multiple emulsions. By instance, the dispersion of oil droplets into segregated water phases that in turn are dispersed in a continuous oil phase (oil/water/oil, O/W/O emulsion). The petroleum industry uses to classify direct emulsions (Figure 1), i.e. water-in-oil emulsions, as hard and soft. By definition a hard emulsion is very stable and difficult to break, mainly because the dispersed water droplets are very small. Moreover, a smooth emulsion or dispersion is unstable and easy to break. The inverse or oil-in-water emulsions are also present but more like a complex emulsion rather than it self. Emulsions are difficult to treat from the operational point of view and cause several problems, including difficulties to separate gas/oil phases, crude out of specification, generate high pressures in pipes and also because water contains many dissolved salts causing severe corrosion problems in pipelines, storage tanks and equipment.

When water droplets of large diameter are present (> 100 microns), they are often easily removed by gravitational force that favor coalescence and formation of a water continuous phase. The water that is separated in less than five minutes is usually called free water. The amount of water that remains emulsified may vary widely from 1 to 60% by volume. In case of medium and light crude oils (> 20 ° API), emulsions typically contain 5 to 20% by volume of water, while 10 to 35% water may still be present in heavy and extra heavy oil (<20 ° API).

Emulsions can also be classified according to their dispersed phase:

- Between 0 and 5% of dispersed phase, the emulsions present droplets that have no direct interactions with each other..
- Between 5 to 30% of dispersed phase, droplets have some interactions with each other but emulsion properties are mainly ruled by the continuous phase.
- Between 30 and 74% of dispersed phase, emulsions are considered as medium dispersed phase, and their properties show remarkable deviations from Newtonian behavior and rely heavily on their formulation and emulsification protocol.
- More than 74% of dispersed phase results on an emulsion of high dispersed phase, in which contact between the droplets is very large, and the emulsion properties are ruled by the dispersed phase.

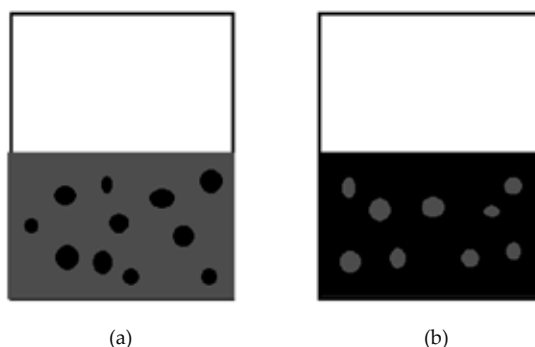


Figure 1. Representative scheme of two type of emulsions, oil-in-water (a) and water-in-oil (b) (oil in black, water in grey).

2.2. Emulsion stability

Some emulsions are easily broken down into water and oil phases after formation, while others can persist for days, months or even years. Stability is a consequence of the small droplet size, the oil/water ratio, the presence of surfactants and factors as temperature, salt content, pH of water, etc. The processes concerning emulsion breaking may be considered as:

- **Creaming:** Creaming is the opposite to the sedimentation phenomenon and is the result of different densities between the two liquid phases which creates a concentration gradient that moves the light dispersed phase to the top, and virtually no coalescence is present because the attractive forces are not strong enough to cause aggregation and coalescence.
- **Sedimentation:** Droplets go to the bottom due to their larger density when compared to the continuous phase but they retain their integrity and no coalescence is present.
- **Coalescence:** it occurs when droplets are near enough to others for a certain time and the attractive forces acting among them cause droplets to merge and form larger drops until a separated phase occurs (Figure 2).

When the interfacial film between droplets has thinned below a critical thickness, it is broken and the difference in capillary pressure causes the emulsion to break. So the properties of the thin film are extremely important for separation. All emulsions except perhaps microemulsions are thermodynamically unstable, but may be relatively stable in the kinetic sense. An emulsion may be kinetically stable against coalescence but unstable with respect to aggregation. The emulsions may be characterized as stable, unstable or mesoestable emulsions.

2.3. Factors affecting the stability of emulsions in petroleum

Some of the most important factors affecting the stability of emulsions are:

- **Heavy fraction of crude:** Emulsions are stabilized by the presence of emulsifiers that locate at the water/oil interface and form an interfacial film. Some organic molecules as asphaltenes

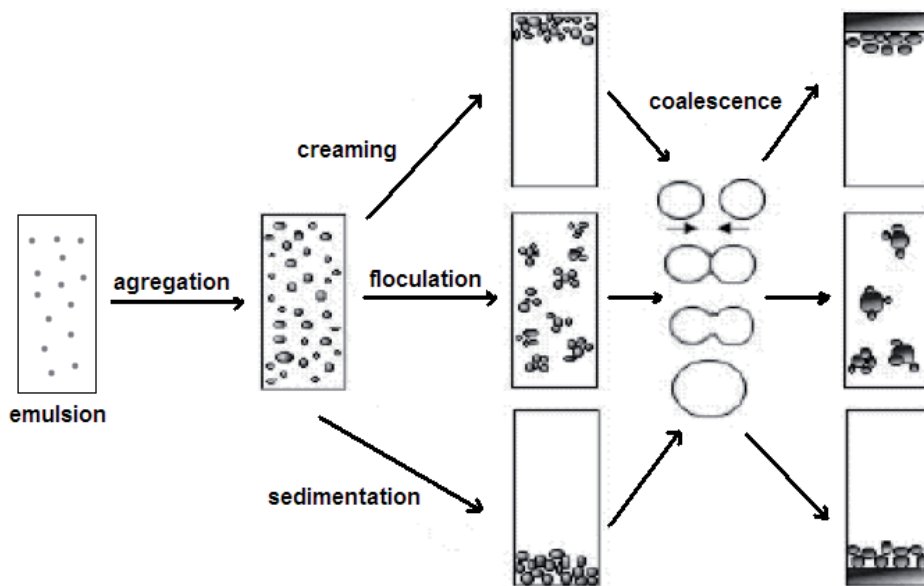


Figure 2. Scheme of emulsion breaking adapted from [4].

and resins present in the crude can act as natural emulsifiers. These polar compounds tend to migrate to the oily surface, reduce the interfacial tension and promote the dispersion and emulsification of water (Figure 3).

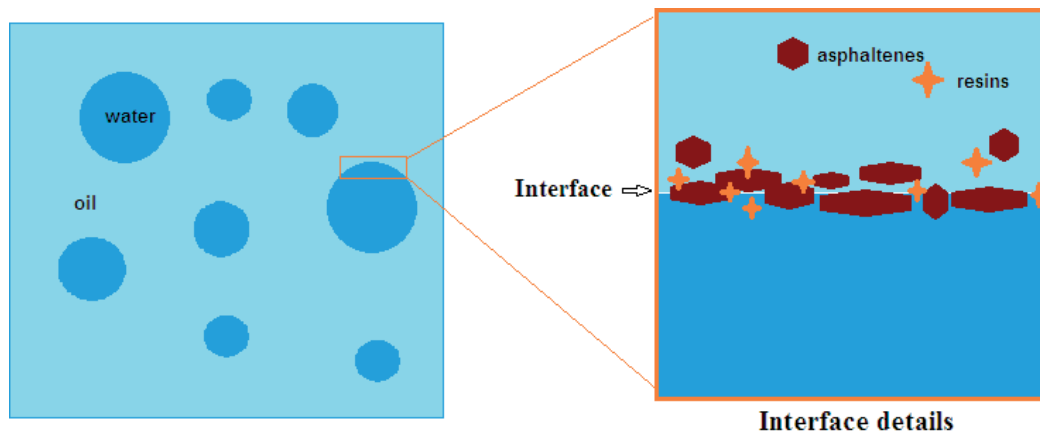


Figure 3. a) W/O emulsion. b) Details of the interface of a drop of water forming a stabilized emulsion.

The asphaltenes are complex structures formed by a variety of polyaromatic and polycyclic compounds. These compounds are attracted by electrostatic forces, mainly π bonds and

hydrogen bonds, that allow an arrangement and packaging that generate clusters with high stability and with paraffins are mainly responsible for the high viscosity and stability of the heavy oil emulsions. In the other side, resins are complex molecules with high molecular weight and soluble in *n*-heptane but very low soluble in ethyl acetate. The role of these compounds is not well defined, but some theories consider that associated with asphaltenes may form micelles that favor emulsion stability. The asphaltene/resin ratio appears to play an important role in the type of film that forms and consequently are associated with the stability of emulsions. Other important macromolecules present in the crude oil and especially in some heavy crude oils are paraffins. Paraffinic compounds with high molecular weight hydrocarbons, known also as waxes, which crystallize when the crude oil is cooled down its cloud point. It has been found that the addition of a specific amount of asphaltene to a waxy oil promotes the formation of stable emulsions. Indeed, paraffins may act synergistically with asphaltenes to produce stable emulsions.

The main factors that can affect the stability of the emulsions are [2]:

- Solids: The presence of finely divided solids in the oily phase favors the stability of emulsions. The effectiveness of the stability of these solids depends on factors such as particle size, interaction between the particles and wettability of the solid particles. Solid particles stabilize the emulsion by spreading across the interface.
- Temperature: The temperature can significantly affect the stability of the emulsion. Temperature affects the physical properties of oil-water interfacial film and the solubility of surfactants, all of which influence the stability of the emulsion. Probably the most important effect is related to the viscosity of the phases in the emulsion since it decreases with increasing temperature. The increase in temperature also causes an increase in the thermal energy of the droplets and therefore the actual number of collisions between them, which in turn reduces the interfacial tension and favor the coalescence of the drops. It has been shown that the increase in temperature causes a gradual destabilization of the oil/water interface. Compressibility of the interface is also affected by changing the surfactants' solubility in the oily or aqueous bulk.
- Drop size: The dispersed droplets into a typical emulsion are found commonly between 1 to 50 microns. Bigger droplets tend to coalesce and resolve into a separated phase. The smaller the droplets are, the emulsion is more stable and its viscosity increases since the free volume between droplets diminished.
- pH: The pH of the aqueous phase strongly influences the stability of the emulsion. The addition of acids or inorganic bases cause ionization of the interfacial film and drastically changes the physical properties of the film. Acid pHs favor the formation of W/O emulsions, while basic pHs favor the formation of O/W emulsions.
- Interfacial tension. A substantial reduction of interfacial tension is not sufficient to increase the stability of the emulsion. It is need also a stabilizing agent that prevent aggregation, sedimentation, creaming and coalescence.

- Viscosity. A high viscosity of the continuous phase decreases the diffusion coefficient and the collision frequency of the droplets, favoring the stability of the emulsion. A high concentration of droplets also increases the apparent viscosity of the continuous phase and stabilizes the emulsion. This effect can be minimized by heating the emulsion.
- Phase volume ratio. Increasing the volume of the dispersed phase, droplet number and/or droplet size favor the probability of collision of droplets and reduce the stability of the emulsion.
- Interface aging. As the emulsion aged, the interface surfactant adsorption is completed and due to the lateral interaction between molecules, the rigidity of the interfacial film reaches a stable value in about 3 to 4 hours. This film or skin around the droplets becomes thicker, stronger and tougher. Furthermore, the amount of emulsifying agents is increased by oxidation, photolysis, evaporation or by the action of bacteria.
- Salinity. The brine concentration is an important factor in forming stable emulsions. Fresh water or brine with low salt promotes emulsion stability. Conversely, high salt concentrations tend to reduce it.
- Nature of oily phase. An oily phase rich in paraffins does not form stable emulsions, whereas the presence of polar compounds as naphthenic acid and favor stable emulsions. The presence of waxes, resins, asphaltenes and solids can influence the stability of the emulsion.
- Density. The net force of gravity acting on a drop is directly proportional to the difference in densities between the droplet and the continuous phase. The increase in density gap by increasing the temperature, accelerates the rate of sedimentation or creaming of the droplets and therefore coalescence.
- The presence of metal ions. Divalent cations such as calcium and magnesium tend to produce a compactation of the adsorbed film, probably as a result of electrostatic screening on both sides, provoking the precipitation of insoluble salts in the interface.
- Interfacial rheological properties. Generally, chemical gradients are generated when an interface with adsorbed surfactant molecules stretches or expands due to external factors and consequently, the interface presents certain elasticity.

2.4. Demulsification

The demulsification is the breaking of an emulsion and resolution of the phases. This process has gained importance in the petroleum industry because many crudes from offshore reservoirs contain emulsified water that must be separated before processing of the crude oil.

The demulsification process can be carried out by four main methods: mechanical, thermal, electrical, chemical and their combinations. The pH adjustment, voltage application, filtration and membrane separation are comprised among the available methods. Thermal demulsification may be reached by the use of microwaves [21]. The radiation favors temperature elevation process by a non-conventional heating mechanism known as dielectric heating. Many works of demulsification have been focused on the effect of microwave irradiation to break emulsions [22-27].

Now, the most common technologies employed in petroleum industry are the combined use of heat and chemicals designed to neutralize and eliminate the effects of the emulsifying agents. The selection of a suitable chemical is crucial to the demulsification process. However, this process is rather an art than a science, because many factors play a role in this very complex phenomenon. A chemical formulation can exhibit excellent performance for demulsification of a crude oil and become completely ineffective when there are changes in the composition of the oil. An emulsifier is usually a formulation of one or more chemicals dissolved in a suitable solvent. The demulsifiers are commonly polymer chains with ethylene oxide alcohols, ethoxylated phenols, ethoxylated alcohols and amines, ethoxylated nonylphenol, polyhydric alcohols and sulfonic acid salts. The more common procedure for selecting a demulsifier is through bottle tests in the laboratory. These tests allow the selection of right chemicals, evaluate a suitable formulation and define the conditions of concentration, residence time and process temperature. Due to the wide variety of components present in the crude oil, it is not surprising that the performance of demulsifiers is largely dependent on the type of oil and composition, whereby the performance of a formulation can vary drastically from one oil to another.

2.5. Possible chemical mechanisms for demulsification

The emulsification with the use of chemicals is a very complex phenomenon. Different theories have been proposed to explain the mechanisms of demulsifier's action. It is known that demulsifiers establish an opposite type emulsion that those formed by the natural emulsifiers (emulsion stabilizers), thereby displacing the emulsifiers of the drop interface, which favors the coalescence of water or oil droplets. Therefore, the efficiency of demulsifier depends on their adsorption capacity at the interface in competition with other surface active species present in the emulsion.

In 1949, Griffin introduced the concept of Hydrophilic-Lipophilic Balance (HLB) as an empirical scale to weight the effect of the structural aspect of surfactant molecule and it is related to the chemical groups that are similar or antagonistic to water [28]. The HLB for polyethoxylated surfactants defined as 20 times the weight of the part consisting of polyoxyethylene. For example, for 5 sets of nonylphenol with ethylene oxide, the HLB is 10 and because this molecule is exactly the same weight of the hydrophilic and lipophilic moiety, a rule has been established that an $HLB \leq 8$ (or $HLB \geq 12$) indicate that this is a lipophilic surfactant (or hydrophilic and this results in a W/O (or O/W emulsion) according to the Bancroft rule. The HBL has the drawback that it does not take into account parameters such as temperature, salinity, or the nature of the hydrophilic group so they cannot be used as a parameter for comparison between different families of surfactants. So it was developed an equivalent taking into account all these effects through a mathematical equation known as hydrophilic-lipophilic deviation (HLD). The HLD can take positive or negative values related to the type of O/W or W/O emulsion. The minimum emulsion stability occurs when the HLD equals zero. The HLD is the dimensionless version of the SAD (surfactant affinity difference) and developed by Salager and coworkers [29-32].

When a surfactant or mixture of surfactants have a high hydrophilic or lipophilic affinity, they generally give non-stable emulsions, as the surfactant is preferably immersed in the medium

bulk by having high affinity and preferably not at the interface stabilizing the emulsion. Moreover, when a surfactant has exactly the same affinity for both phases, also they generate very unstable emulsions. The emulsion stability is high when the surfactant has a moderate lipophilicity (for the case of a W/O emulsion) or moderately hydrophilic (in the case of O/W), which is associated with a HLD of +3 or +4 for the case of a W / O emulsion or -3 to -4 for the case of an O/W. The affinity of the surfactant by either phase can be manipulated through variations in the formulation, i.e. by varying the nature of the components and their interaction with the interface as variation in salinity (salt addition, the electrolyte type and concentration), oil type (number of carbon atoms of the alkane or equivalent), size of the head and tail of the surfactant, alcohol type and concentration, temperature and/or pressure.

The HLD expression for a system containing ethoxylated surfactants can be expressed as following:

$$\text{HLD} = \beta - kEACN + bS - \varphi(A) + c_T \Delta T$$

Where β is a characteristic parameter of the surfactant or surfactant mixture which increases insofar as this is more lipophilic, $EACN$ is the carbon number of the alkane or oil equivalent if this is not an alkane, S is salinity and expressed in % by weight of salt in the aqueous phase, $\varphi(A)$ is a function of alcohol (type and concentration) which is commonly used as a cosurfactant and ΔT is the difference in temperature of the surfactant relative to room temperature (25 °C) and k and c_T are constants. Thus, if the experiment was carried out using distilled water in the absence of alcohol and at room temperature, the last three terms in the equation would be zero and hence the HLD depend only on the characteristics of the surfactant and the concentration of solvent.

When any of these variables change monotonically (i.e. salt concentration or temperature), keeping all other variables constant can be studied very promptly the effect of these on the emulsion stability. Another equation is set to non-ionic surfactants of ethoxylated type, which can be expressed as follows:

$$\text{HLD} = \alpha - EON + b \times S - k \times ACN + t(T - 25) + a \times A$$

Where α , k and t are surfactant parameters, EON is the degree of ethoxylation of surfactant, ACN is the carbon number of the alkane, S and A are the concentration of salt and alcohol, and T the temperature. The above equation may be described as follows:

$$\text{HLD} = k \times \beta + b \times S - k \times ACN + t(T - 25) + a \times A$$

Where the parameter β can be defined as:

$$\beta = (\alpha - EON) / k,$$

W/O emulsions naturally occur to the lipophilic nature of the natural surfactants, which have a HLD value greater than 0, so demulsification essentially involve adding a second surfactant to displace HLD value to 0. Accordingly, the surfactant to be added should be hydrophilic in nature and must be added to such a concentration that the mixture to generate a natural surfactant $HLD=0$, indicating that has the same affinity for the water than oil.

2.6. Chemical products for demulsification

Usually commercial demulsifiers are mixtures of several components having different chemical structures and polymeric materials with a broad molecular weight distribution. Demulsifiers are formed by a 30 to 50% of active material (surfactant) plus the addition of suitable solvents such as alcohols and aromatic naphtha. Many kind of demulsifiers have been employed since 1920 as soaps, naphthenic acids and salts, aromatics and alkylaromatic, sulfonated compounds, sulfonated and castor oils, esters, organic acids, epoxides, block copolymers of ethylene and propylene oxide, alkylphenol-formaldehyde resins, polyamines, fatty alcohols, polyesteramines and oxyalkylated amines and mixtures thereof [33]. Figure 4 shows some structures of commercial chemicals used in the demulsifier formulations in the last decades. Commercial demulsifiers usually contain one or more of these active ingredients in a suitable solvent. For polymers, molecular weight and chain distribution plays also an important role in the demulsifier effects.

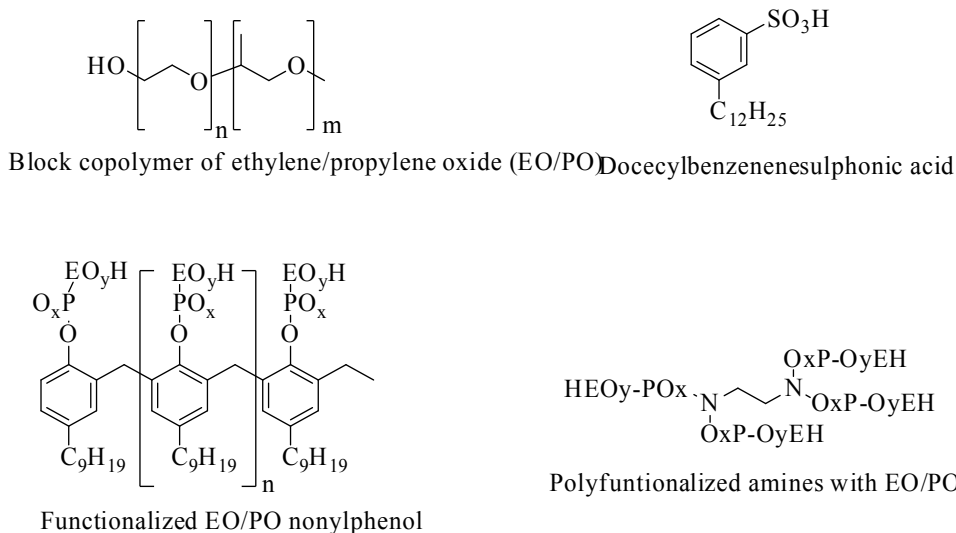


Figure 4. Structures of some commercial chemicals used as demulsifiers in Petroleum Industry.

2.7. Ionic liquids as surfactants

As described throughout this book, ILs present exceptional properties such as high solvent abilities, negligible vapor pressures, extremely high electrical conductivities, chemical and

thermal stability [34-35] that have been exploited in applications as diverse as in organic synthesis [36-37], catalysis [38-39], biocatalysis [40-41], separations [42], extraction [43], dissolution [44], polymerization reactions [45] and electrochemistry [46]. In petroleum industry, ILs have found wide applications as corrosion inhibitors [14, 47], as inhibitors of asphaltene precipitation [48] and for removing pollutants from refineries feedstocks [13].

Moreover, ILs with long-chain hydrocarbon residues exhibit surfactant properties in water [49-53] and in other ILs as solvents [54]. ILs have also been widely explored as potential ionic surfactants with different areas and applications such as extraction of organic compounds, metal ions and radioactive isotopes [55-56], as template to produce micro/mesoporous materials [57-58], in microemulsion [59-61]. The surfactant properties of ILs are easily understood if we consider that these compounds generally have a well-defined structure with hydrophilic character and another with hydrophobic character, i.e. they are amphipatic. Moreover, these compounds may be or anionic or cationic nature depending that in which section of their structure the amphiphilic character is present. Switterion type ILs have also well studied (Figure 5).

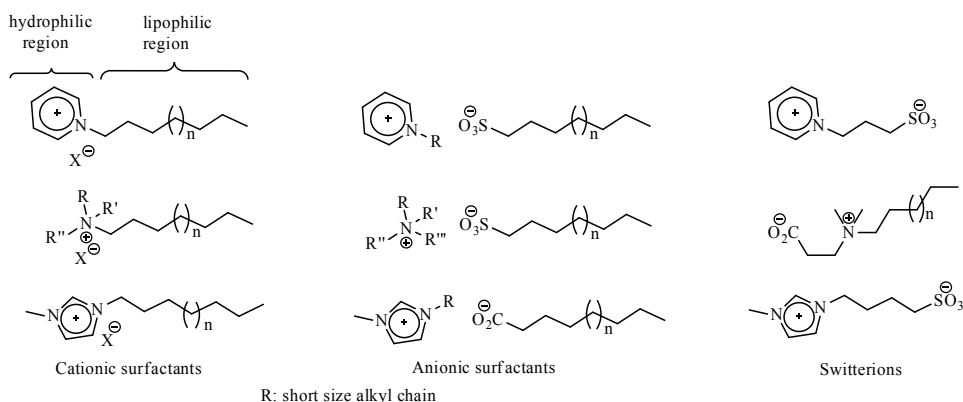


Figure 5. Some examples of surfactants ILs.

There is an interesting study about the influence of ionic and non-ionic amphiphiles, i.e., Cetyltrimethylammonium bromide (CTAB) and 1-(2-aminoethyl)2-heptadecyl-2-imidazoline (1), on the pore hierarchy and morphology of siliceous particles synthesized with. The amphiphile (1) leads to the formation of spherical silica particles of about 250 nm diameter, while the ionic surfactant CTAB led to porous silica spheres of about 750 nm diameter. A single-particle analysis using High Resolution Electron Microscopy and Optical Density Transforms show the inner pore structure of the particles synthesized with CTAB and low molecular weight alcohols co-surfactants (ethanol and propanol) is oriented along the sphere radius, while silica particles synthesized with (1) have a random-like pore structure. Both systems were used as supports for adsorption of a photosensitive spiropyran (i.e., Spiro-6) type compound (1',3',3'-trimethyl-6-nitrospiro-(2H-1-benzopyran-2,2'-indoline)) and their interaction with the silica surface was characterized by IR spectroscopy, showing a weak interaction

with respect to other silicates (lamellar clays). These effects are potentially interesting for applications on biomarkers, stable photosensitive materials, solid-phase organic synthesis and dyes [62].

In petroleum industry, surfactant ILs have been explored as efficient chemicals for Enhanced Oil Recovery (EOR) that is a generic term for techniques that increase the amount of crude oil that can be extracted from a reservoir. It is estimated that two-thirds of crude oil remains in oil reservoirs after primary and secondary (water flooding) recovery stage and with the decrease in world oil reserves and a higher demand for petroleum and its derived products, the effective exploitation of oil reservoirs has become increasingly important.

EOR-assisted by surfactants is an effective method for recovering the oil from reservoirs that have lost their drive after the application of primary and secondary recovery methods. In this sense, ILs have showed good potential as surfactant with this purpose [63-64], thus Lago et al. showed the suitability of several ILs as effective replacements for conventional surfactants in EOR [65-66]. The reservoir fluid has been modelled as a ternary system of water (pure water or aqueous solution of NaCl) plus the IL: trihexyl(tetradecyl)phosphonium chloride plus dodecane. Determination of its liquid-liquid phase equilibrium indicates the formation of a Winsor type III system, with a triphasic region and adjacent biphasic regions. The interfacial tensions in the system corroborate the ability of the IL to act as a surface active agent, as desirable for its use in an EOR process. A relevant transport property such as viscosity, in addition to density, has been experimentally measured for the equilibrium phases [65]. The same research group showed in 2013 that the three-phase system generated when adding trihexamethyl(tetradecyl)phosphonium chloride to the water-oil mixture remain stable in the wide range of temperature and in the presence of salt, in contrast with other system, no co-surfact is required. When the temperature increases, an important decrease of the microemulsion-water/brine interfacial tension was observed [66].

Recently, the application results of ILs was reported, for the first time, at laboratory scale using a sand-pack column model for EOR. A 2 wt% aqueous solution of 1-ethyl-3-methylimidazolium tosylate ($[C_2MIM][OTs]$) was used to recover an aromatic oil. The results show that a flooding processes using only 4 pore volumes (PV) could recover 65.7% (± 1.0) of the oil in place, almost the double of what was recovered with a brine solution (NaCl, 2 wt%). These preliminary results, requiring further optimization of the IL characteristics and concentration, and other process parameters, suggest that water-flooding with aqueous solutions of ILs can contribute to EOR in mature reservoirs [67].

2.8. Ionic liquids as demulsifiers of emulsions in petroleum industry

ILs have also found application as surfactants in demulsification process for oil field application. As discussed above, crude oil is invariably accompanied by water and formations of stable W/O emulsions are frequently encountered in the oil industry. These emulsions contain significant quantities of contaminants, salts and other corrosive compounds and their stability is increased for heavy and ultra-heavy crude oils due to the content of these natural emulsifiers that is more abundant than in light crude oils [33].

Destabilization of emulsions is an important step to obtain water-and salt-free oils, being the chemical demulsification and desalting the most frequently applied industrial methods to break crude oil emulsions. This process can be very difficult and non-efficient to demulsify and desalt water-in-oil emulsions of heavy viscous crude oils, being also time consuming [68]. A study about W/O demulsification for three types of Mexican crude oils was reported using several surface-active ILs analogues. The efficiency of these ILs was studied using emulsions of medium, heavy and ultra-heavy crude oils under conventional heating. Some of these surfactants were able to break water in oil emulsion in heavy and ultra-heavy crude oils. The effect of microwave irradiation as non-conventional energy source to accelerate and increase the efficiency of demulsification for heavy crude oil was also demonstrated [69]. Brazilian researchers have also studied ILs and microwave effect on demulsification of crude oil emulsions [17]. In their more recent work, they investigated the effect of five ILs, [BMIM][NTf₂], [OMIM][NTf₂], [C₁₂MIM][NTf₂], [BPy][NTf₂] and [OMIM][OTf] and a set of operation parameters on the demulsification process, including the heating type (conventional and microwave), IL concentration (0.6 to 6.2 g/dm³), effect of alkyl chain length, and effect of cation and anion type on demulsification efficiency. The results indicated that the demulsification was favored when more hydrophobic ILs and longer cation alkyl chains were employed, such as [C₁₂MIM][NTf₂], reaching values close to 92% of water removal. Also microwaves in conjunction with IL showed the highest demulsification efficiency [70]. Flores et al. studied the anion and cation effect as ammonium type ILs as dehydrating agent of ultra-heavy crude oil from the experimental and theoretical point of view using series of trioctylammonium (TOA) ILs containing the anions: Cl⁻, HSO₄⁻ and H₂PO₄⁻, and other new ammonium salts (OCD) with HSO₄⁻, MeSO₃⁻ and MePhSO₃⁻. According with this study, the ranking of water removal efficiency for the TOA series at 1000 ppm was Cl⁻ > HSO₄⁻ > H₂PO₄⁻, while for ODC series, the rankings for efficiency at 360 min were HSO₄⁻ > MeSO₃⁻. Theoretical studies by means of density functional theory (DFT) suggested that an increase in the softness and electrophilicity of the cations correlated with lesser effectiveness as demulsifiers. Finally, the partition coefficient of the cations showed that if the viscosity of the crude oil is low, it is possible to use ILs with a low partition coefficient (log P), but if the viscosity is high, the log P of IL should be near to the [TOA][Cl] value [71].

Ammonium-type IL anionic surfactants have also shown good efficiency as demulsifiers of W/O emulsions. Four amphiphilic cholinium carboxylates were synthesized by ionic exchange from choline chloride (Vitamin B₄) and fatty acid salts under microwave irradiation (Fig. 6). These environmentally friendly anionic surfactants were evaluated as demulsifiers to break water in crude oil emulsions using short intervals of microwave dielectric heating to follow the kinetics of the demulsification and the results of the evaluations were validated and confirmed by the classical “bottle test” procedure. Choline palmitate showed the best performance as demulsifier of the heavy Mexican crude oil emulsion [72].

Another application of ILs is on the demulsification of O/W emulsions, or inverse emulsions. Unlike the W/O emulsion which tend to increase the viscosity, the inverse emulsion are less common. The continuous phase of such emulsions is water, which substantially reduces the viscosity of high viscous oils like heavy, extra heavy and bituminous oils and represents an

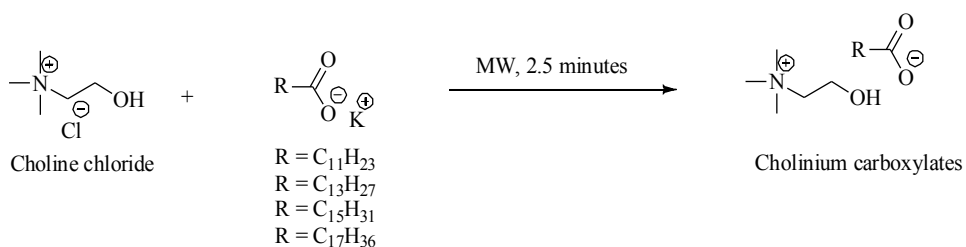


Figure 6. Microwave-assisted anion exchange to obtain choline carboxylates.

interesting alternative for their transportation through pipelines. Nevertheless, crude oils must be conditioned by removal of water and salts before further refining. Hence, the potential of aminoacid based ILs as demulsifiers of O/W emulsions was probed to break an emulsion from heavy crude oil [73]. The aforementioned O/W emulsions were prepared using alkyl-O-glucoside and-cellobioside biosurfactants [74]. The effect of the addition of the ILs surfactant GlyC12 (1000 ppm) on the water separation of an O/W emulsion was evaluated using oil bath or microwave heating at 50 W (Fig. 7). As was observed, microwave heating is more effective than oil bath heating in terms of rate of demulsification. Indeed, MW heating during two minutes allowed water separation of 77% and only 37% under oil bath heating. The emulsion in the presence and in the absence of GlyC12 reaches a water separation of 87% and 89% respectively after 10 minutes of treatment.

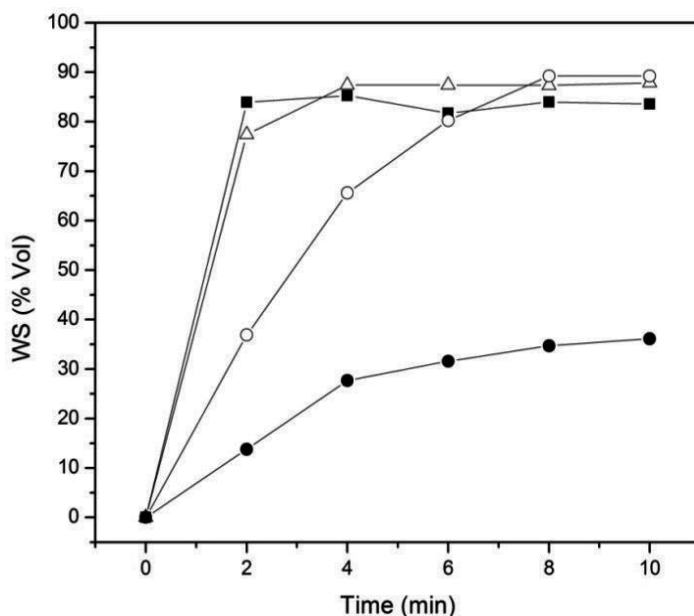


Figure 7. Kinetics of the separated water (WS) from the initial O/W emulsion treated under oil bath (●) and MW heating (■); and in the presence of a demulsifier (GlyC12, 1000 ppm) under oil bath (○) and MW heating (△).

The addition of the demulsifier increased the water separation efficiency for oil bath heating, the separated water increased from 30% to 80% after 6 minutes of contact. It is clear that both demulsifying approaches reached a high percentage of separated water after 10 minutes of heating when the demulsifier was used. MW heating appears to be a good demulsifying process for O/W emulsions since water separation occurs rapidly within the first minutes of heating (Fig. 8) [18].

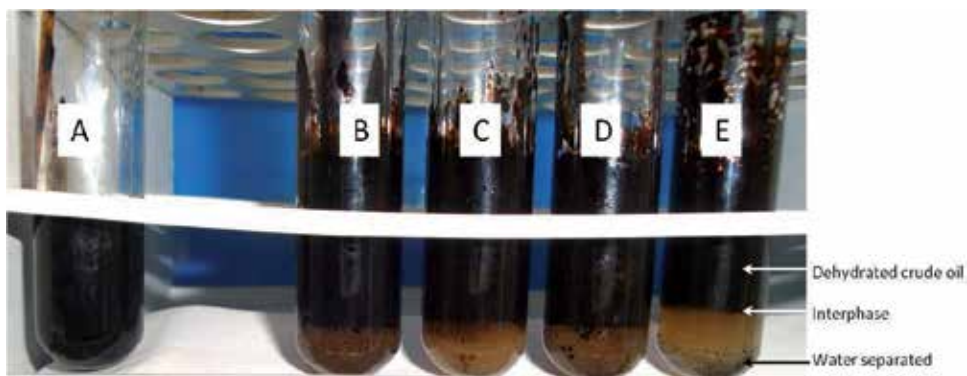


Figure 8. Photographs showing separated water (WS) from the initial O/W emulsion containing GlyC₁₂ (1000 ppm) at 50 W, 60°C. Initial O/W emulsion before MW irradiation (A), emulsion after MW irradiation during 2 (B), 4 (C), 8 (D), 10 minutes (E).

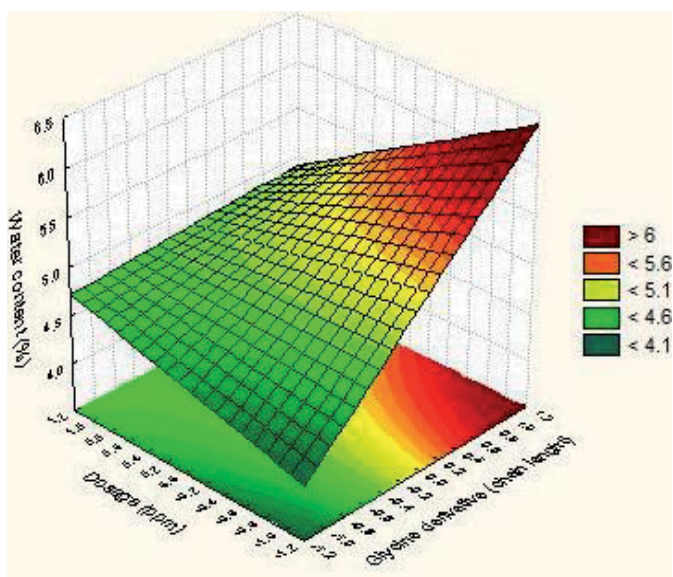


Figure 9. Surface response of the water content respect to the dosage and chain length of Glycine-based demulsifiers at 60°C.

We undertook recently a screening of commercial and synthesized emulsifiers and demulsifiers to develop a comprehensive and environmentally friendly methodology for transporting ultra-heavy crude oil. For the screening of demulsifiers, a factorial 2^k design was employed and demulsification parameters as temperature, demulsifier concentration and pH were studied (Fig. 9). A “green” ionic demulsifiers synthesized from glycine have satisfactory dewatering ability for ultra-heavy crude oil emulsion. When GlyC14 was employed at 900 ppm, the dewatering efficiency reach 89.5% at pH 3. Considering low toxicity surfactants as emulsifier and demulsifier, an environmentally friendly and technically feasible technology was develop for transporting EHCO [75].

3. Conclusions

Complex emulsions are present during production and transporting of crude oil affecting operations in a daily basis and further petroleum refining. It is important to understand the emulsion phenomena: formation, stability and rupture; and all the alternatives that exist to resolve and diminish this problem, including well-known technologies as well as innovatives ones as the use of ionic liquids as demulsifiers of such complex emulsions. Specially for heavy, extra heavy and non conventional crude oils as shale oil, bitumen, etc. Then, ionic liquids present very interesting properties to break out such complex emulsions and resolve in separate aqueous and oily phases. We presented then some current research on the field but strongly believe that ionic liquid research may go further to develop greener chemicals, like amino acid-or sugar-based liquid ionics; instead of conventional pyridinium or imidazolium-based ones.

Acknowledgements

This work was financially supported by IMP project D.60016.

Author details

Rafael Martínez-Palou and Jorge Aburto*

*Address all correspondence to: jaburto@imp.mx

Biomass Conversion Management. Research Directorate of Hydrocarbon Processing. Mexican Petroleum Institute (Instituto Mexicano del Petróleo), San Bartolo Atepehuacan, Gustavo A. Madero, México D.F., México

References

- [1] Scharram LL. *Emulsion Fundamentals and Applications in the Petroleum Industry*, Washington DC: American Chemical Society; 1992.
- [2] Kokal S. *Petroleum Engineering Handbook: General Engineering*, Fanchi JR. (Ed.), Texas: Society of Petroleum Engineering; 2006.
- [3] Goldszal A, Bourrel M. Demulsification of Crude Oil Emulsions: Correlation to Microemulsion Phase Behavior. *Industrial Engineering Chemical Research* 2000; 39: 2746-2751.
- [4] Kokal S. Crude-oil Emulsions: A-State-of-the-Art Review. *SPE Production and Facilities* 2005; February 5-13.
- [5] Feng X, Xu MJ. Biodegradable Polymer for Demulsification of Water-in-Bitumen Emulsions. *Energy & Fuels* 2009; 23:451-456.
- [6] Martínez-Palou R, Mosqueira ML, Zapata-Rendón B, Mar-Juárez E, Bernal-Huicochea C, de la Cruz Clavel-López J, Aburto, J. *Journal of Petroleum Science & Engineering* 2011; 75:274-282.
- [7] Xu XR, Yang JY, Zhang BL, Gao JS. Demulsification of Extra heavy Crude Oil. *Petroleum Science & Technology* 2007; 25:1375-1390.
- [8] Guerrero S, Parra LJ, Abreu E, Montefusco L, Gil L. Orimulsion. *Interciencia* 2004; 29:180-181.
- [9] Martínez-Palou, R. Microwave-assisted synthesis using ionic Liquids. *Journal of Molecular Diversity* 2010; 14:3-25.
- [10] Rogers RD, Seddon KR. (Eds.) *Ionic Liquids: Industrial Applications of Green Chemistry*. Washington DC, American Chemical Society, 2002.
- [11] Rogers RD, Seddon KR, Volkov S. (Eds.). *Green Industrial Applications of Ionic Liquids*. (NATO Science Series), Dordrecht, Kluwer Academic Publishers, 2002.
- [12] Martínez-Palou R, Flores P. Perspectives of Ionic Liquids for Clean Oilfield Technologies. In: Kokorin A (ed.) *Ionic Liquids. Theory, Properties and New Approaches*. Rijeka: Intech; 2011. pp. 567-630.
- [13] Martínez-Palou R, Luque R. Applications of Ionic liquids for Removing Pollutants from Refinery Feedstocks: A review. *Environmental Energy Science* 2014; 7:2414-2447.
- [14] Martínez-Palou R, Olivares-Xomelt O, Likhanova N. Environmental Firendly Corrosion Inhibitors. In: *Progress in Corrosion Inhibitors*. Rijeka: Intech; 2014. pp. 431-465.

- [15] Kunz W, Zemb T, Harrar A. Using Ionic Liquids to Formulate Microemulsions: Current State of Affairs. *Current Opinion in Colloid & Interface Science* 2012; 17:205-2011.
- [16] Qiu Z, Texter J. Ionic Liquids in Microemulsions. *Current Opinion in Colloid & Interface Science* 2008; 13:252-262.
- [17] Lemos RBC, da Silva EB, dos Santos A, Guimaraes RCL, Ferreira BMS, Guarnieri RA, Dariva C, Franceschi E, Santos AF, Fortuny M. Demulsification of water-in-crude oil emulsions using ionic liquids and microwave irradiation. *Energy & Fuels* 2010; 24:4439-4444.
- [18] Martínez-Palou R, Cerón-Camacho R, Chávez B, Vallejo AA, Villanueva-Negrete D, Karamath J, Castellanos J, Reyes J, Aburto, J. Demulsification of heavy crude oil in water emulsion. A comparative study between Microwave and Conventional Heating. *Fuel* 2013; 113:407-414.
- [19] Martínez-Palou R, Cerón-Camacho R, Chávez B, Vallejo AA, Reyes J, Chávez B, Garcia-Caloca G, Bernal-Goicochea C, de la Cruz-Clave J, Aburto, J. Desarrollo de un proceso integral para el transporte de crudos pesados. Estudio para la formación de emulsiones O/W mediante biotensoactivos. *Revista de Ingeniería Petrolera* 2014; 54:233-247 (in Spanish).
- [20] Sjöblom J. editor *Emulsion and emulsion stability. Surfactant Science serie vol 132*, Boca Raton FL: CRC Taylor & Francis; 2006.
- [21] Martínez-Palou R. *Química en Microondas. (E-book)*. Matthew, NC: CEM Publishing; 2006. pp. 131-154.
- [22] Binner ER, Robinson JP, Silvester SA, Kingman SW, Lester EH. Investigation into the mechanisms by which microwave heating enhances separation of water-in-oil emulsions. *Fuel* 2014; 116:516-521.
- [23] da Silva EB, Santos D, Brito MP, Guimaraes RCL, Ferrerira BMS, Freitas LS, Campos MCV, Franceschi E, Dariva C, Santos AF, Fortuny M. Microwave desdemulsification of heavy crude oil emulsions: Analysis of acid species recovered in aqueous phase. *Fuel* 2013; 128:141-147.
- [24] Anisa ANI, Nour AH. Destabilization of heavy and light crude oil emulsions via microwave heating technology: An optimization study. *Journal of Applied Science* 2011; 11:2898-2902.
- [25] Nour AH, Yunus RMA. Continuous Microwave Heating of Water-in-Oil Emulsions: An Experimental Study, *Journal of Applied Science* 2006; 6:1868-1872.
- [26] Nour AH, Yunus RMA. Comparative Study on Emulsion Demulsification by Microwave Radiation and Conventional Heating. *Journal of Applied Science* 2006; 6:2307-2311.

- [27] Fortuny M, Oliveira CB, Melo RL, Nele M, Coutinho RC, Santos AF. Effect of salinity, temperature, water content, and pH on the microwave demulsification of crude oil emulsions. *Energy & Fuels* 2007; 21:1358-1364.
- [28] Griffin WC. Classification of surface active agents by HLB. *Journal of The Society of Cosmetic Chemists* 1949; 1:311-315.
- [29] Alvarez G, Poteau S, Argillier JF, Langevin D, Salager JL. Heavy oil-water interfacial properties and emulsion stability: Influence of dilution. *Energy & Fuels* 2009; 23:294-299.
- [30] Salager JL, Marquez N, Gracia A, Lachaise J. Partitioning of ethoxylated octylphenol surfactants in microemulsion-oil-water systems: Influence of temperature and relation between partitioning coefficient and physicochemical formulation. *Langmuir* 2000; 16:5534-5539.
- [31] Salager JL, Márquez L, Peña AA, Rondón M, Silva F, Tyrode E. Current phenomenological know-how and modeling emulsion inversion. *Industrial Engineering Chemical Research* 2000; 39:2665-2676.
- [32] Salager JL. Microemulsions, In: Broze G. (ed.) *Handbook of Detergents-Part A. Surfactant Science Series 82*. New York: Marcel Dekker; 1999. pp 253-302.
- [33] Kokal S. Crude Oil Emulsion. *Petroleum and Engineering Handbook*. Richardson TX: Society of Petroleum Engineering; 2005.
- [34] Freemantle M. *An Introduction to Ionic Liquids*. Cambridge UK: RSC Press; 2009.
- [35] Martínez-Palou R. Ionic liquids and Microwave-assisted Organic Synthesis. A “Green” and Synergic Couple. *Journal of Mexican Chemical Society* 2007; 51(4): 252-264
- [36] Wasserscheid P, Keim W., editors. *Ionic Liquids in Synthesis*. Weinheim: Wiley-VCH; 2004.
- [37] Rogers RD, Seddon KR., editors. *Ionic Liquids as Green Solvent: Progress and Prospects*. Boston: American Chemical Society; 2003.
- [38] Zhao D, Wu M, Kou Y, Min E. Ionic liquids: Applications in catalysis. *Catalysis Today* 2002; 74:157-189.
- [39] Corma A, García H. Lewis acids: From conventional homogeneous to green homogeneous and heterogeneous catalysis. *Chemical Reviews* 2003; 103:4307-4365.
- [40] Cull SG, Holbrey JD, Vargas-Mora V, Seddon KR, Lye GJ. Room-temperature ionic liquids as replacements for organic solvents in multiphase bioprocess operations. *Biotechnology & Bioengineering* 2000; 69:227-233.
- [41] Sheldon RA, Maderia Lau L, Sorgedragger MJ, van Rantwijk F, Seddon KR. *Green Chemistry* 2002; 4:147.

- [42] Swatloski RP, Visser AE, Reichert WM, Broker GA, Facina LM, Holbrey JD, Rogers RD. On the solubilization of water with ethanol in hydrophobic hexfluorophosphate ionic liquids. *Green Chemistry* 2002; 4:81-87.
- [43] Zhang S, Zhang Q, Zhang ZC. Extractive desulfurization and denitrogenation of fuels using ionic liquids. *Industrial Engineering Chemistry Research* 2004; 23:614-622.
- [44] Swatloski RP, Spear SK, Holbrey JD, Rogers RD. Dissolution of cellulose with ionic liquids. *Journal of the American Chemical Society* 2002; 124:4974-4975.
- [45] Kricheldorf HR, Schwarz G. Cyclic polyimides-A comparison of synthetic methods. *High Performance Polymers* 2004; 16:543-555.
- [46] Yang C, Sun Q, Qiao J, Li Y. Ionic liquid doped polymer light-emitting electrochemical cells. *Journal of Physical Chemistry B* 2007; 107:12981-12988.
- [47] Olivares-Xometl O, López-Aguilar C, Herrasti P, Likhanova N, Lijanová I, Martínez-Palou R, Rivera-Marquez JA. Adsorption and corrosion inhibition performance by three new ionic liquids on API 5L X52 steel surface in acid media. *Industrial Engineering Chemistry Research* 2014; DOI: [dx.doi.org/10.1021/ie4035847](https://doi.org/10.1021/ie4035847)
- [48] Murillo-Hernández J, García-Cruz I, López-Ramírez S, Durán-Valencia C, Domínguez JM, Aburto J. Aggregation Behavior of Heavy Crude Oil-Ionic Liquid Solutions by Fluorescence Spectroscopy. *Energy & Fuels* 2009; 23:4584-4592.
- [49] Bowers J, Butts CP, Martin PJ, Vergara-Gutierrez MC, Heenan RK. Aggregation Behavior of Aqueous Solutions of Ionic Liquids, *Langmuir* 2004; 20:2191-2198.
- [50] Sirieix-Plenet J, Gaillon L, Letellier P. Behaviour of a binary solvent mixture constituted by an amphiphilic ionic liquid, 1-decyl-3-methylimidazolium bromide and water: Potentiometric and conductimetric studies. *Talanta* 2004; 63:979-986.
- [51] Kaper H, Smarsly BZ. Templating and Phase Behaviour of the Long Chain Ionic Liquid C₁₆mimCl. *Journal of Physical Chemistry* 2006; 220:1455-1471.
- [52] Thomaier S, Kunz W. Aggregates in mixtures of ionic liquids, *Journal of Molecular Liquids* 2007; 130:104-107.
- [53] Hezave AZ, Dorostkar S, Ayatollahi S, Nabipour M, Hemmateenejad B. Investigating the effect of ionic liquid (1-dodecyl-3-methylimidazolium chloride ([C12mim][Cl])) on the water/oil interfacial tension as a novel surfactant. *Colloids & Surfaces A* 2013; 421:63-71.
- [54] Smirnova NA, Safonova EA. Miscellization in solutions of ionic liquids. *Colloid Journal* 2012; 74:254-265.
- [55] Sun P, Armstrong DW. Ionic liquids in analytical chemistry. *Analytica Chimica Acta* 2010; 661:1-16.

- [56] Olivier-Bourbigou H, Magna L, Morvan D. Ionic liquids and catalysis: Recent progress from knowledge to applications, *Applied Catalysis* 2010; 373:1-56.
- [57] Zupal A, Thommes M, Cejka J. Synthesis of highly ordered MCM-41 silica with spherical particles, *Microporous & Mesoporous Materials* 2007; 104:52-58.
- [58] Wang T, Kaper H, Antonietti M, Smarsly B. Templating behavior of long-chain ionic liquid in the hydrothermal synthesis of mesoporous silica. *Langmuir* 2007; 23:1489-1495.
- [59] Zech O, Thomaier S, Bauduin P, Rück T, Touraud D, Kunz W. Microemulsions with an ionic liquid surfactant and room temperature ionic liquids as polar pseudo-phase, *Journal of Physical Chemistry B* 2009; 113:465-473.
- [60] Safavi N, Maleki FF. Phase behavior and characterization of ionic liquids based microemulsions. *Colloids & Surface A* 2010; 355:61-66.
- [61] Wang A, Chen L, Jianf D, Yan Z. Vegetable oil-based ionic liquid microemulsions and their potential as alternative renewable biolubricant basestocks. *Industrial Crops & Products* 2013; 51:425-429.
- [62] Domínguez JM, Rosas R, Aburto J, Terrés E, López A, Martínez-Palou R. Synthesis of silica spheres with neutral and ionic amphiphiles and their interaction with photo-sensitive spiropyrans. *Microporous and Mesoporous Materials* 2009; 118:121-133.
- [63] Benzagouta MS, Al Nashef IM, Karnanda WW, A-Khidir K. Ionic liquids as novel surfactants for potential use in enhanced oil recovery. *Korean Journal of Chemical Engineering* 2013; 30:2108-2117.
- [64] Hezave AZ, Dorostkar S, Avatollahi S, Nabipour M, Hemmateeneiad M. Effect of different families (imidazolium and pyridonium) of ionic liquids-base surfactants on interfacial tension water/crude oil system. *Fluid Phase Equilibria* 2013; 360:139-145
- [65] Lago S, Rodríguez H, Khoshkbarchi MK, Soto A, Arce A. Enhanced oil recovery using the ionic liquid trihexyl(tetradecyl) phosphonium chloride: Phase behaviour and properties. *Royal Society of Chemistry Advances* 2012; 2:9392-9397.
- [66] Lago S, Francisco M, Arce A, Soto A. Enhanced oil recovery with the ionic liquid trihexyl(tetradecyl) phosphonium chloride: A phase equilibria study at 75°C. *Energy & Fuels* 2013; 27:5806-5810.
- [67] Pereira JBF, Costa R, Foios N, Coutinho JAP. Ionic liquid enhanced oil recovery in sand-pack columns, *Fuel* 2014; 134:196-200.
- [68] Sjöblom J, Johnsen EE, Westvik A, Ese MH, Djuve J, Auflem IH, Kallevik H. In: Sjöblom J. (ed.) *Encyclopedic Handbook of Emulsion Technology*. New York: Marcel Dekker; 2001 pp. 595-620.

- [69] Guzmán-Lucero D, Flores P, Rojo T, Martínez-Palou, R. Evaluation of ionic liquids as desemulsifier of water-in-crude oil emulsions. Study of microwave effect. *Energy & Fuels* 2010; 24:3610-3615.
- [70] da Silva EB, Santos D, Alves DRM, Guimaraes RCL, Ferrerira BMS, Guarnieri RA, Franceschi E, Dariva C, Santos AF, Fortuny M. Demulsification of heavy crude oil emulsions using ionic liquids, *Energy & Fuels* 2013; 27:6311-6315.
- [71] Flores CA, Flores EA, Hernández E, Castro LV, García A, Alvarez F, Vázquez FS. Anion and cation effects of ionic liquids and ammonium salts evaluated as dehydrating agents for super-heavy crude oil: Experimental and theoretical point of view. *Journal of Molecular Liquids* 2014; 196:249-257.
- [72] Aburto J, Marquez DM, Navarro JC, Martínez-Palou R. Amphiphilic Choline carboxylates Ionic Liquids as Demulsifiers of Water-in-Crude oil Emulsions. *Tenside Surfactants Detergents* 2014; 51: 314-317.
- [73] Cerón-Camacho R, Aburto J, Montiel LE, Flores EA, Cuellar F, Martínez-Palou, R. Efficient Microwave-Assisted Synthesis of Ionic Esterified Amino Acids. *Molecules* 2011; 16:8733-8744.
- [74] Cerón-Camacho R, Martínez-Palou R, Chávez-Gómez B, Cuéllar F, Bernal-Huicochea C, de la Cruz Clavel J, Aburto, J. Synergistic effect of alkyl-O-glucoside and-cellobioside biosurfactants as effective emulsifiers of crude oil in water. A proposal for the transport of heavy crude oil by pipeline. *Fuel* 2013; 110:310-317.
- [75] J. Reyes, R. Cerón-Camacho, R. Martínez-Palou, D. Villanueva, Alba A. Vallejo, J. Aburto. Study on the formation and breaking extraheavy crude oil-in-water emulsions. A proposal strategy for transportation of extra heavy crude oils. Unpublished data.

Extraction Based on Dispersive Assisted by Ionic Liquids

Negin Fasih Ramandi and Farzaneh Shemirani

Additional information is available at the end of the chapter

<http://dx.doi.org/10.5772/60136>

1. Introduction

Determination of heavy metals in environmental, biological and in food samples has become of interesting subject because of their toxic effects on living beings [1, 2]. Despite good developments in the modern analytical instruments, direct determination of trace analytes at low concentrations is often a problem for analytical chemists and as a result, a sample preparation step is required. Therefore, preliminary preconcentration/separation step still remains as a bottleneck of the analytical procedure. Recent efforts on sample treatments techniques have involved following six general trends, namely: simplification, automation, miniaturization, expeditiousness, economical and safety aspects. The continuous quest for novel sample preparation procedures has led to the development of new methods, whose main advantages are their speed and negligible volume of solvents used as well as allowing sample extraction and preconcentration to be done in a single step. In this context, dispersive liquid liquid extraction (D-LLE) [3, 4] and dispersive solid phase extraction (D-SPE) [5] have been emerged as a response to those requirements that in some cases are unattainable with classical techniques. In spite of some strength points, these methods suffer from some drawbacks. For instance in D-LLE a problem still exists and that is continued reliance on using of toxic, hazardous, flammable and environmentally damaging organic solvents. Or typically in D-SPE, dispersion of sorbent in sample solution should assist by ultrasonic waves and phase separation needs to centrifuging step and as a result, extraction will be time consuming. Reducing the amount of organic solvents and using environmentally friendly solvents are the most important aims of analytical chemists. Due to the unique properties of ionic liquids (ILs), by using them in a proper way, these problems can overcome easily [6, 7].

Ionic liquids, emerging in recent years as novel stable and environmentally friendly compounds with amazing properties such as negligible vapor pressure, low flammability, and liquid state in a broad temperature range [8]. They are composed of asymmetrically substituted nitrogen-containing cations (e.g. imidazole, pyrrolidine, pyridine, etc.) with inorganic anions

(e.g. Cl^- , BF_4^- , PF_6^- , $(\text{CF}_3\text{SO}_2)_2\text{N}^-$, etc.). The range of available anion and cation combinations could provide too many different ILs, so at first glance; perhaps it is difficult to select the desired IL. But by considering some aspects, we can select the best IL based on desired application easily. These valuable materials have potential of using in term of D-LLE and D-SPE [6, 7]. D-LLE is a modified solvent extraction method which the appropriate mixture of the extraction and disperser solvents is rapidly injected by syringe into aqueous samples containing analytes. Thereby, a cloudy solution forms. In fact, the cloudy state results from the formation of fine droplets of the extraction solvent, which disperse in the sample solution. Then, this cloudy solution is centrifuged and the fine droplets sediment at the bottom of the conical test tube [9]. Meanwhile, D-LLE based on ionic liquids is being recently considered as replacement for these solvents in sample preparation, due to their unique chemical and physical properties, good extractability for various organic compounds and metal ions as a neutral or charged complex, and miscibility with water and organic solvents. The performance of D-LLE based on ILs for preconcentration/separation of mercury in water samples has shown great improvement in sample treatment techniques which has been done earlier by our research team. This study provided simple, rapid, low cost and low toxicity extraction technique since only very small amounts of an IL as a green extraction solvent used as a replacement of environmentally damaging organic solvents [6].

D-SPE is based on the solid phase extraction (SPE) methodology, but the sorbent is directly added into the extract without conditioning. The clean-up is easily carried out by just shaking and centrifugation. The method was described as QuEChERS, which is the abbreviation of quick, easy, cheap, effective, rugged and safe. Recently our research team has improved D-SPE by using ionic liquid ferrofluids for monitoring lead in food and environmental samples [7].

Ferrofluids (FFs) are stable colloid dispersion of single-domain magnetic nanoparticles in a carrier liquid, which consist of three parts: ferromagnetic nanoparticles, coating of these nanoparticles and a carrier fluid [10]. The stability of the ferrofluid is due to the balance between repulsive (Brownian motions, steric and electrostatic forces) and attractive interactions (Van der Waals and dipolar attractive forces) [11]. The peculiarity of FF is the combination of normal liquid behavior with magnetic properties. As a result, wonderful applications in different fields such as biomedical [12], microelectronics [13], and also analytical chemistry [7, 14] have been reported.

Coating material prevents magnetic nanoparticles from agglomerating; on the other hand it has been proven that some chemical or physical surface modifications of coating material have improved its selectivity and/or affinity towards special target [14]. Therefore, not only the importance of coating material in FF is not deniable but also designs and production of ferrofluid with especial coating material is currently under intensive investigation [15]. For selecting an appropriate coating material, several criteria should be met. For instance, it should be non-toxic, low cost, chemically stable, and also compatible with carrier liquid. On the other hand to provide stable ferrofluid, a proper carrier solvent should have some properties. For instance, it should be immiscible with aqueous solution and have a low vapor pressure to prevent loss during extraction [16].

Due to the presence of electrostatic, hydrogen bonding and Van der Waals interactions, ILs possess unique structure, which provide a protective shell around magnetic nanoparticles and

improve ferrofluids stability greatly [17-19]. Therefore, by choosing ionic liquid as carrier fluid, very stable ferrofluid can be prepared (ionic liquid ferrofluid (IL-FF)), which is suitable for using in sample preparation methods. Due to rapid injection of an appropriate amount of IL-FF in to the aqueous sample by a syringe, extraction can be achieved within a few seconds. In addition, based on attraction of IL-FF to a magnet, there is no need to centrifuge for phase separation. Therefore, ionic liquid ferrofluid based dispersive solid phase extraction (IL-FF-D-SPE) provides very simple, rapid and low cost preconcentration/separation method [7, 14].

The importance of ionic liquids will be appeared more and more by discussing about their applications in dispersive liquid liquid extraction and also in dispersive solid phase extraction. Also in term of selectivity of ionic liquid ferrofluids some recent improvements which have been done by our research team, will be reported. The following key points in regards to application of ionic liquids in dispersive liquid liquid extraction and dispersive solid phase extraction are considerably noteworthy: simplicity, cost efficiency and suitability for batch operations (which could greatly shorten the sample preparation time).

2. Ionic liquid ferrofluid based dispersive solid phase extraction of lead from water, soil and rice samples

2.1. Lead; the occurrence, toxicity and methods of determination

Toxic effect of heavy metals on human life and the environment is one of the most important issues of our century and lead is one of the most hazardous members of the heavy metal family [20]. The increasing industrial use of lead in different fields such as: storage batteries, cable sheath and radiating shielding is contributing to the pollution of nature and using lead in gasoline antiknock products and paint pigments plays substantial role in contaminating the environment [21]. Due to its toxicity, non-biodegradability and tendency to accumulate in living organisms the regular absorption of trace amount of lead may have serious negative effects on humans (especially growing children) including: retardation of mental development, deficiencies in concentration and adverse effects on kidney function, blood chemistry and the cardiovascular system [22, 23]. Therefore, monitoring quantitative trace amount of lead in food, water and other environmental sample is inevitable.

Several analytical techniques have been reported in the literature for determination of lead such as: cloud-point extraction [1, 24], precipitation [25, 26], liquid-liquid extraction (LLE) [27], and solid-phase extraction (SPE) [28-30]. On one hand, SPE is widely used in the preconcentration methodology because of its simplicity, achievement of high recoveries, high sorption capacity, minimal costs due to low consumption of reagents and low extraction time [31]. On the other hand, in dispersive liquid-liquid extraction, as rather newly miniaturizing LLE, because an appropriate mixture of the extraction and disperser solvents are injected into the aqueous sample by a syringe, it is highly dispersed in the aqueous phase and extraction can be achieved within a few seconds [32]. Therefore, by using the advantages of these two techniques at the same time, ionic liquid ferrofluid-based dispersive solid phase extraction (IL-FF-D-SPE) as a new powerful extraction method was used for extraction of trace amount of lead in water, soil and rice samples [7].

2.2. Experimental

2.2.1. Instrumentation

A Varian model AA-400 atomic absorption spectrometer (Santa Clara, USA), equipped with an air-acetylene burner and with lead hollow cathode lamp was used for the determination of Pb(II). The lamp was operated at 5 mA, using the wavelength at 217.0 nm and slit of 1.0 nm, and the flow rates of air and acetylene were set as recommended by the manufacturer. Background correction has been used with a deuterium lamp. All measurements were carried out in peak height mode. A pH-meter Model 692 from Metrohm (Herisau, Switzerland) equipped with a glass combination electrode was used for the pH measurements. In addition, for magnetic separations, a strong neodymium-iron-boron (Nd₂Fe₁₂B) magnet (1.31 T) was used.

2.2.2. Reagents

All chemicals used were of analytical reagent grade unless otherwise stated. 1-Hexyl-3-methylimidazolium tetrafluoroborate [Hmim]BF₄ 98 %, 1-(2-pyridylazo)-2-naphthol (PAN), acetic acid, acetone, tetraethyl orthosilicate (TEOS), NH₃, ethanol, Pb(NO₃)₂ were purchased from Merck (Darmstadt, Germany). Standard stock solutions of Pb(II) were prepared by dissolving spectral pure grade chemical Pb(NO₃)₂ (1000 mg mL⁻¹ in 5 % HNO₃; Merck) in double distilled water with the addition of 5 mL of 12 mol L⁻¹ nitric acid and further diluted daily prior to use. Aqueous working solutions were prepared immediately before use by diluting with water. A solution of 4 × 10⁻⁷ and 8 × 10⁻⁶ and 4.2 × 10⁻⁶ mol L⁻¹ PAN were prepared by dissolving appropriate amount of this reagent in pure ethanol. Nano-Fe₃O₄ was purchased from Sigma-Aldrich (St. Louis, MO, USA) (Fe₃O₄ spheres powder, <40 nm, purity >98 %). Buffer solution (pH = 5.8, 1 mol L⁻¹) was prepared by mixing appropriate amount of potassium hydrogen phthalate and sodium hydroxide. High purity HNO₃ (65 %, ultra-pure, Merck), HClO₄ and HCl were used for the digestion of dust sample throughout this work.

2.2.3. Preparation of Ionic liquid ferrofluid and extraction procedure

In this work Fe₃O₄/SiO₂ NPs were used as a sorbent. It was synthesized as below. Briefly, 2.0 g of Fe₃O₄ nanoparticles were suspended in 200 mL ethanol under sonication for 1 h. Then, 40 mL of concentrated ammonia, 35 mL deionized water and 1 mL TEOS were added to the suspension. Next, for about 1 h the mixture was sonicated and finally approximately for 8 h was mixed vortex. The silica-coated nanoparticles (SCMNPs) were collected simply by magnetic separation and were thoroughly washed with deionized water three times and then dried, yielding nanoparticles a fine powder.

After preparing coated magnetic nanoparticle, one step was needed to prepare ionic liquid ferrofluid. In this context, 10 mg of silica-coated magnetic nanoparticles and 100 mL of acetic acid were mixed in a vial and were heated at 90 °C under stirring for approximately 45 min to allow acetic acid adsorption. Next, acetic acid-coated magnetic nanoparticles were dispersed in 0.1 gr 1-Hexyl-3-methylimidazolium tetrafluoroborate [Hmim]BF₄. To obtain ionic liquid

ferrofluid, the result suspension was sonicated for 30 min. The resulting suspension had a magnetite fraction of 9.1 %. Finally, IL-FF-D-SPE was done simply as below. The sample, or standard solution containing $40 \mu\text{g L}^{-1}$ of Pb(II), PAN ($4 \times 10^{-7} \text{mol L}^{-1}$), NaNO_3 (3.78 w/v%), and 1 mL buffer (pH = 5.8) were poured into a 50 mL tube. Then by using a 1.0 mL syringe, the ionic liquid ferrofluid was injected into the sample solution and a dark cloudy suspension was formed rapidly and the extraction process was quickly completed after approximately 6 seconds. Subsequently, a strong magnet was placed at the bottom of the tube to let the ionic liquid ferrofluid settle. After about 2 min, the solution became clear and limpid and supernatant was simply discarded by decanting. After removing the magnet, 1 mL nitric acid (2mol L^{-1}) was added to the vial to desorb the lead through the sonication. By using the magnet at the bottom of the vial, the clear solution containing of eluted metal ions was obtained. By transferring this limpid solution to the glass tube, the analyte in the eluent was determined by flame atomic absorption spectrometry (FAAS). A schematic view of IL-FF- D-SPE experimental set up is shown in Figure 1.

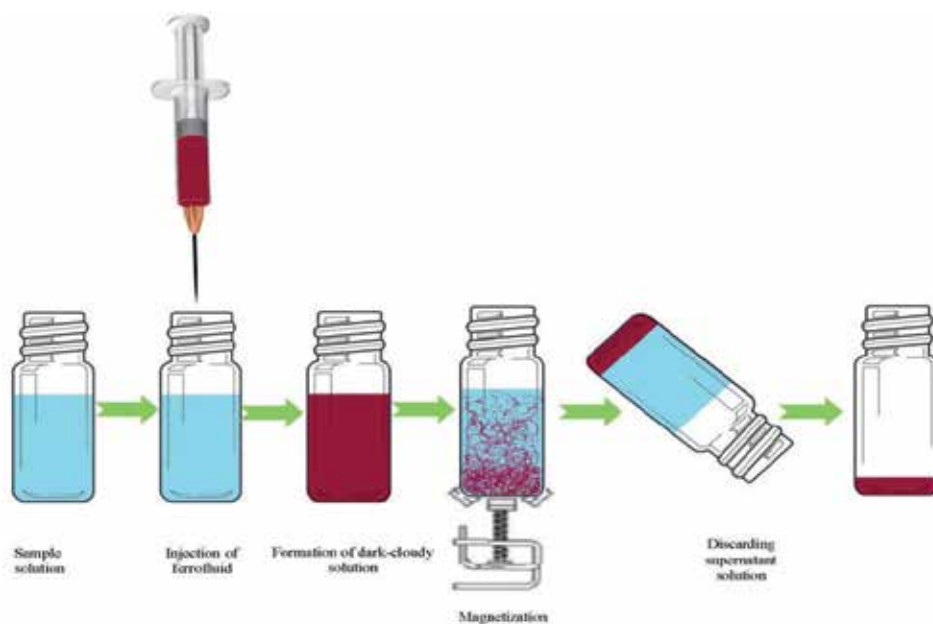


Figure 1. A schematic view of IL-FF-D-SPE experimental set up [7].

2.3. Result and discussion

2.3.1. Selection of ionic liquid for preparation of the ferrofluid: type and volume

When selecting an appropriate carrier (solvent), several criteria should be met. For instance, the solvent should be immiscible with aqueous solution and have a low vapor pressure to prevent loss during extraction. According to these criteria, some ionic liquids such as 1-

Hexyl-3-methylimidazolium tetrafluoroborate [Hmim]BF₄, 1-Hexyl-3-methylimidazolium hexafluorophosphate [Hmim]PF₆, 1-Hexyl-3-methylimidazolium bis(trifluoromethylsulfonyl)imide [Hmim]Tf₂N, were selected and by the qualitative observation of sedimentation of each ferrofluid, the stability of the suspensions was checked.

For this purpose, in three vials, the same amount of coated magnetic nanoparticles added to the same amount of these three ionic liquids separately. After 30 min sonication, the stability of these three ferrofluids against sedimentation was investigated. As the result, only in the case of using [Hmim]BF₄ as the carrier, the ferrofluid maintained stable even after about 8 h. Therefore, [Hmim]BF₄ was selected as an environmentally friendly carrier to achieve stable ferrofluid.

When choosing the minimum volume of [Hmim]BF₄ for a quantitative extraction of Pb(II), the range of 0.1-0.3 g was determined. Finally, 0.1 g [Hmim]BF₄ was enough to preconcentration the metal ions, at the studied concentrations and using 50 mL of sample. For higher amount of [Hmim]BF₄, the extraction efficiency was almost constant.

2.3.2. Selection of eluent

Various types of solvents such as: acetone, ethanol, ethanol (1% HNO₃) and HNO₃ were examined in order to find the best eluent. Based on the desorption of Pb(II) from modified nanoparticles in the acidic medium, nitric acid was chosen as the best eluent.

2.3.3. Screening and optimization strategy

The effect of the following six factors namely pH, concentration of 1-(2-pyridylazo)-2-naphtol (PAN) as ligand to form complex with lead, sorbent amount, eluent volume, extraction time, ionic strength which effected the extraction recovery of Pb(II) was investigated with the help of chemometrics method. Therefore, in screening step by a half-factorial design these six factors were evaluated in two levels. The low and high values were selected from the results of previous experiments (Table 1).

Parameters	unit	Level	
		Low	High
pH (A)	-	4	8
Concentration of PAN (B)	(mol L ⁻¹)	4×10^{-7}	8×10^{-6}
Sorbent amount (C)	(gr)	0.01	0.06
Eluent volume (D)	(mL)	0.5	1
Extraction time (E)	(s)	2	6
Ionic strength (F)	(w/v %)	0	10

Table 1. The experimental factors and levels of them in ferrofluid- based D-SPE of Pb(II) [7].

By referencing the results of the ANOVA and Pareto charts, the main effects were selected. Evaluation of the normalized results of the experimental design was based on $P=95\%$ and the standard effect is estimated for computing a t-statistic for each effect. When its value is higher than $\pm t$, a parameter is considered as significant; otherwise the parameter is not significant in the studied range. The analysis of the results is visualized using standardized main effect Pareto charts ($P=95\%$) was shown in Figure 2. As it can be concluded from Figure 2, ionic strength and pH are effective parameters which have negative and positive effects on the extraction recovery respectively.

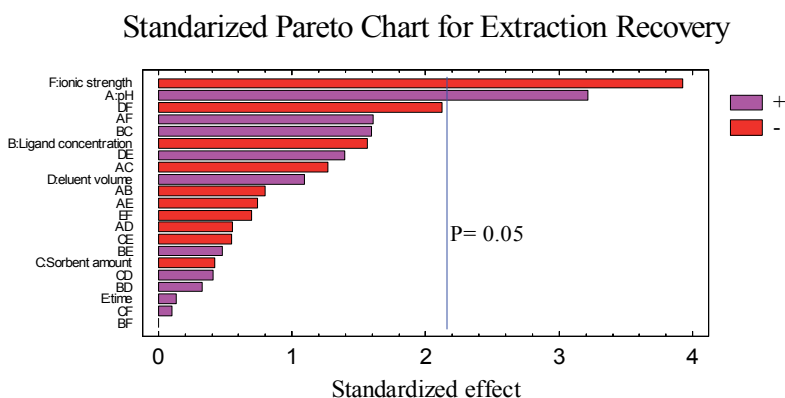


Figure 2. Standardized ($P=0.05$) Pareto chart, representing the estimated effects of parameters obtained from the half-fraction factorial design [7].

The results illustrated in Figure 2 also confirm that pH has significant effect on extraction recovery because it not only influences the surface active centers and charge of sorbent, but also affects the degree of ionization and solubilization of sorbate in aqueous solutions. According to Figure 2, extraction time has no significant effect on extraction recovery. This can be explained by the fact that based on the rapid injection of ferrofluid into the aqueous solution; the extraction was completed in only a few seconds. Due to the relatively large surface area, the highly active surface sites lead to a very fast mass transfer process and generally offer a fast extraction process. Therefore, time has no significant effect on extraction recovery. Based on these results, to continue the optimization; four insignificant parameters were fixed at appropriate amount (concentration of PAN: 4×10^{-7} mol L⁻¹, sorbent amount: 0.01 gr, eluent amount: 1 mL, time: 6 s).

The central composite design (CCD) was performed to evaluate the optimum condition of performance of ionic liquid Ferrofluid-based dispersive solid phase extraction of Pb(II) for the two significant parameters: pH and ionic strength. The number of experimental points (N) is defined by the expression: $N = 2^f + 2f + C_p$, where f is the number of variables and C_p is the number of center points. In this study, f and C_p were set at 2 and 3, respectively, which meant 11 experiments had to be done.

The 3D response surface plot and its related counter for the extraction recovery (%) were shown in Figure 3. As seen in Figure 3, the extraction recovery had an upward trend by increasing the pH and ionic strength and reached a peak value at pH 5.8 and ionic strength 3.78 (w/v %). Following that, the extraction recovery had a decline by increasing the pH and ionic strength. It is not surprisingly that pH 5.8 was chosen as the optimum pH value, because at lower pH values, ligand was protonated and at higher pH, Pb(II) could easily be precipitated with OH⁻, as a result in both cases the extraction recovery plummeted to minimum value.

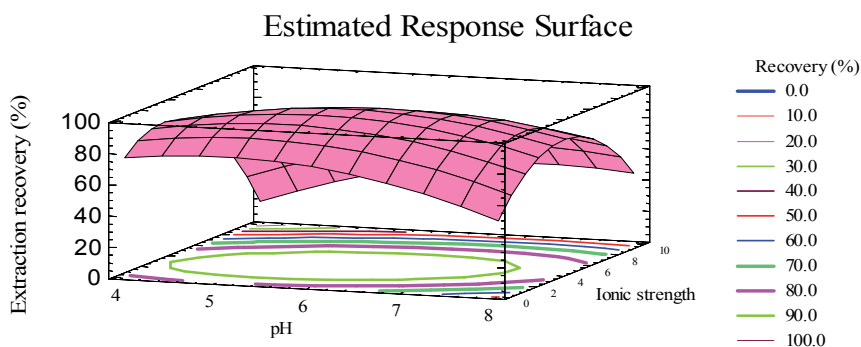


Figure 3. Estimated response surface by plotting extraction recovery (%) versus ionic strength and pH, with related contours [7].

2.3.4. Effect of potentially interfering ions

In order to assess the applications of the recommended procedure, the influences of possible matrix ions in the environmental samples and some transition metals on the recoveries of Pb(II) were also examined. By spiking appropriate amounts of potentially interfering ions in range of 50-10000 $\mu\text{g mL}^{-1}$ to 50.0 mL of solution containing 40 $\mu\text{g L}^{-1}$ of Pb(II) and excess amount of PAN at optimum condition, the effect of them in the natural water samples on the extraction recovery percent of Pb(II) were studied. A given species was considered to interfere if it resulted in a $\pm 5\%$ variation of the absorbance. Based on obtained results, no interference was observed for Na⁺, K⁺ and NO₃⁻ up to 10000 $\mu\text{g mL}^{-1}$, for Ni²⁺, Ag²⁺, Zn²⁺ and Ca²⁺ up to 1000 $\mu\text{g mL}^{-1}$, for Mg²⁺, Cu²⁺, Hg²⁺ and CO₃⁻ up to 100 $\mu\text{g mL}^{-1}$ and for some species such as: Pd²⁺, Fe²⁺ and Fe³⁺ up to 50 $\mu\text{g mL}^{-1}$. This results show that this preconcentration/separation method could be applied to the highly saline samples and the samples that contains some transition metals at $\mu\text{g mL}^{-1}$ levels.

2.3.5. Figures of merit and comparison of IL-FF-D-SPE with other methods

At the optimum condition the limit of detection (LOD) of 1.66 $\mu\text{g L}^{-1}$, linear range of 5-372 ng mL⁻¹, and also relative standard deviation of 1.34 % were achieved. The obtained results were compared with other literatures in Table 2. As it can be concluded from Table 2, in addition to

simplicity of this method (in comparison to a solid phase extraction), the presented IL-FF-D-SPE method has good limit of detection ($1.66 \mu\text{g L}^{-1}$), good repeatability (RSD %). The proposed method is much faster due to dispersion of sorbent in the aqueous phase also there is no need to shake the sample solution. Moreover, for phase separation, there was no need to centrifuge or conical the bottom glass tube, which can be easily damaged and are difficult to clean.

Sorbent	PF/EF ^a	LOD ^b ($\mu\text{g L}^{-1}$)	RSD ^c (%)	Linear range (ng mL^{-1})	Sorption capacity (mg g^{-1}) ^f	Extraction time (min)	Ref
Chromosorb101 (FAAS)	31	2.85	2.7	0.5- 10 ^d	7.50	10	[33]
MnO ₂ /CNTs (ETAAS)	100	4.4	3.2	-	6.7	2	[34]
Solid sulfur (FAAS)	250	3.2	4.7	10-300	15.6 ^e	33	[35]
Graphene (FAAS)	125	0.61	3.25	10-600	16.6	50	[36]
Ambersorb-572 (FAAS)	75	3.65	2	-	0.17 ^f	4.5 ^h	[37]
SCMNPs (FAAS)	200	1.66	1.34	5-372	10.66	6 ^s	This study

^a Preconcentration factor or enrichment factor.

^b Limit of detection.

^c Relative standard deviation.

^d mg L^{-1} .

^e $\mu\text{g g}^{-1}$.

^f mmol gr^{-1} .

^h Hour.

^s Second.

Table 2. Comparison of the published preconcentration methods for Pb(II) with the proposed method [7].

2.3.6. Analysis of real samples

After digestion of dust and rice sample according to previous report [38, 39] the standard addition method was applied for determination of trace amounts of Pb(II) in water, soil, and rice samples. Generally, the recoveries of Pd(II) ions were obtained in the range between 99.6-110.2 % (Table 3).

Sample	Spiked (ng mL ⁻¹)	Found (ng mL ⁻¹)	Recovery (%)
Mineral water ^a	0	ND ^e	-
	10	9.6 ± 0.2	96.0
	20	20.9 ± 0.5	104.5
Tap water ^b	0	ND	-
	10	10.3 ± 0.3	103.0
	20	21.3 ± 0.6	106.5
Road dust ^c	0	8.6 ± 0.4	-
	50	59.1 ± 0.9	118.2
Rice ^d	0	ND	-
	20	20.7 ± 0.5	103.5

^a Zam zam mineral water, Iran.

^b From drinking water system of Tehran, Iran.

^c From Niyayesh highway, Tehran, Iran.

^d From Mazandaran, Iran.

^e Not detected.

Table 3. Analytical result for determination of Pb(II) in different samples [7].

3. Selective ionic liquid ferrofluid based dispersive-solid phase extraction for simultaneous preconcentration/separation of lead and cadmium in milk and biological samples

3.1. Lead and Cadmium; the occurrence, toxicity and methods of determination

Determination of heavy metals in biological and in food samples has become a key interest because of their toxic effects on living beings [1]. Heavy metals such as Cd(II) and Pb(II) cause irreparable effects on the urinary tract, liver, blood chemistry and the cardiovascular system [40]. Several studies have been reported for separation/ preconcentration of Cd(II) and Pb(II) such as solid phase extraction [41, 42] liquid liquid extraction [43] and dispersive liquid liquid extraction [3, 4]. In spite of some benefits, these methods suffer from many drawbacks. Therefore, improvements are necessary. So for the first time our research team wanted to report a very simple, fast, efficient, and selective separation/ preconcentration method which is assisted by ionic liquid ferrofluid for cadmium and lead [14]. For this purpose, TiO₂ as an excellent coating material for magnetic nanoparticles was chosen and also improve its selectivity by loading 1-(2-pyridylazo)-2-naphthol on its surface. Additionally, to provide a stable ferrofluid, 1-Hexyl-3-methylimidazolium tetrafluoroborate was chosen as the carrier liquid. Therefore, selective ionic liquid ferrofluid based dispersive solid phase extraction (IL-FF-D-SPE) was used for separation/ preconcentration of cadmium and lead in milk, human urine, and blood plasma samples combined with FAAS which is a very fast, easy, cheap, and

selective determination technique in comparison with other methods such as ICP-MS. Additionally, different parameters which effected the extraction recovery of Pb(II) and Cd(II) were investigated with the help of chemometrics method [14]

3.2. Experimental

3.2.1. Instrumentation

The determination of Pb(II) and Cd(II) was carried out using a Varian Spectra AA-400 atomic absorption spectrometer (Santa Clara, USA), equipped with a deuterium background correction and an air-acetylene burner. The lamp currents were set at 5 and 4 mA for Pb(II) and Cd(II), respectively. All measurements were carried out in the peak height mode at 217.0 and 228.8 nm, using a spectral band width of 1.0 nm and 0.5 nm for Pb(II) and Cd(II), respectively. A pH-meter Model 692 from Metrohm (Herisau, Switzerland) equipped with a glass combination electrode was used for the pH measurements. Additionally, for magnetic separations, a strong neodymium-iron-boron ($\text{Nd}_2\text{Fe}_{12}\text{B}$) magnet (1.31 T) was used. For separation of human blood plasma from a blood sample, a refrigerated centrifuge (Hettich, Universal 320R, Buckinghamshire, England) equipped with an angle rotor (6 place, 9000 rpm, cat no 1620A) was used.

3.2.2. Reagent

All chemicals used were of analytical reagent grade unless otherwise stated. The stock standard solutions of Cd(II) and Pb(II) (1000 mgL^{-1}) were prepared from appropriate amounts of their nitrate salts (Merck, Darmstadt, Germany) in ultra-pure water and working standard solutions were prepared by appropriate stepwise dilution of the stock standard solutions. 1-Hexyl-3-methylimidazolium tetrafluoroborate [Hmim] BF_4 98 %, 1-Hexyl-3-methylimidazolium hexafluorophosphate [Hmim] PF_6 , 1-Hexyl-3-methylimidazolium bis(trifluoromethylsulfonyl)imide [Hmim] Tf_2N , 1-(2-pyridylazo)-2-naphthol, tetra-n-butyl orthotitanate (TBOT), NH_3 , ethanol, sodium dodecyl sulfate were purchased from Merck (Darmstadt, Germany). Nano- Fe_3O_4 was purchased from Sigma-Aldrich (St. Louis, MO, USA, Fe_3O_4 spheres powder, <40 nm, purity >98 %). Buffer solution ($\text{pH} = 6.7$, 1 molL^{-1}) was prepared by dissolving appropriate amounts of potassium dihydrogen phosphate (1 molL^{-1}) and sodium hydroxide (1 molL^{-1}). High purity HNO_3 , H_2O_2 , HClO_4 and HCl were purchased from Merck (Darmstadt, Germany), which were used for the digestion of milk, urine, and blood plasma samples throughout this project. The pipettes and vessels were cleaned before use by soaking in 10 % nitric acid solution for at least 24 hours and then rinsed thoroughly with distilled water.

3.2.3. Preparation of Ionic liquid ferrofluid and extraction procedure

To prepare TiO_2 coated Fe_3O_4 nanoparticles, first 10 mL of tetra-n-butyl orthotitanate was dissolved in 70 mL ethanol to form a clear solution. Then, 0.2 g Fe_3O_4 nanoparticles were dispersed in this solution under sonication for approximately 5 min. While the suspension stirred vigorously over a period of 15 min, a 1:5 (v/v) mixture of water and ethanol was added slowly with a dropper into this mixture. Then, the mixture was stirred further for 1 hour. Finally, after separating and washing the residue with ethanol, the obtained powder was oven-dried and calcinated at 200°C for 6 h. In the next step to immobilize 1-(2-pyridylazo)-2-naphthol

on sodium dodecyl sulfate -coated $\text{Fe}_3\text{O}_4/\text{TiO}_2$ the following procedure was done. In a 250 mL beaker, 1.0 g of $\text{Fe}_3\text{O}_4/\text{TiO}_2$ nanoparticles were dispersed in 20 mL of 0.001 molL^{-1} HCl, under sonication. During sonication of this mixture, to avoid any changes in ionic strength, 0.3 mL of 1 molL^{-1} NaNO_3 was added using a dropper. The pH of the solution was adjusted to 5. Then, 3 mL of 1 molL^{-1} sodium dodecyl sulfate was added and solution was stirred for 1 h. After that 0.2 g 1-(2-pyridylazo)-2-naphtol was added and the solution was stirred for further 1 h at 60°C in a water-bath. Finally, the suspension result was filtered and dried under a vacuum.

To form a selective ionic liquid ferrofluid, 30 mg of modified titana-coated magnetic nanoparticles with 1-(2-pyridylazo)-2-naphtol and 100 mL acetic acid, as a stabilizing agent, were mixed in a vial. The mixture was stirred and heated at 90°C for approximately 45 min. Next, the resulted powder was dispersed in 0.3 g $[\text{Hmim}]\text{BF}_4$. After 30 min of sonication of this mixture, stable suspension of magnetic nanoparticles (ionic liquid- ferrofluid) was obtained.

Finally, the selective IL-FF-D-SPE was done simply as below. The sample, or standard solution contains $40 \mu\text{g L}^{-1}$ $\text{Pb}(\text{II})$ and $30 \mu\text{g L}^{-1}$ $\text{Cd}(\text{II})$, NaNO_3 (0% w/v), at pH 6.7 which were poured into a 50 mL tube. Then, by using a 1.0 mL syringe, the ionic liquid-ferrofluid, containing 0.03 g sorbent and 0.3 g ionic liquid was injected into the sample solution to form a dark cloudy suspension. Due to the rapid injection of the ferrofluid into the aqueous sample, extraction was achieved within a few seconds. By using a strong magnet at the bottom of tube, the ferrofluid was settled and the solution became clear. After removing the supernatant by decanting, 1 mL nitric acid (1.59 molL^{-1}) was added to the vial to desorb the $\text{Pb}(\text{II})$ and $\text{Cd}(\text{II})$ through 8 min sonication. Subsequently, a strong magnet was placed at the bottom of tube and immediately the solution became limpid. By using a syringe this clear solution was transferred to a vial for analyzing with FAAS.

A schematic view of selective ionic liquid ferrofluid based dispersive solid phase extraction is shown in Figure 4.

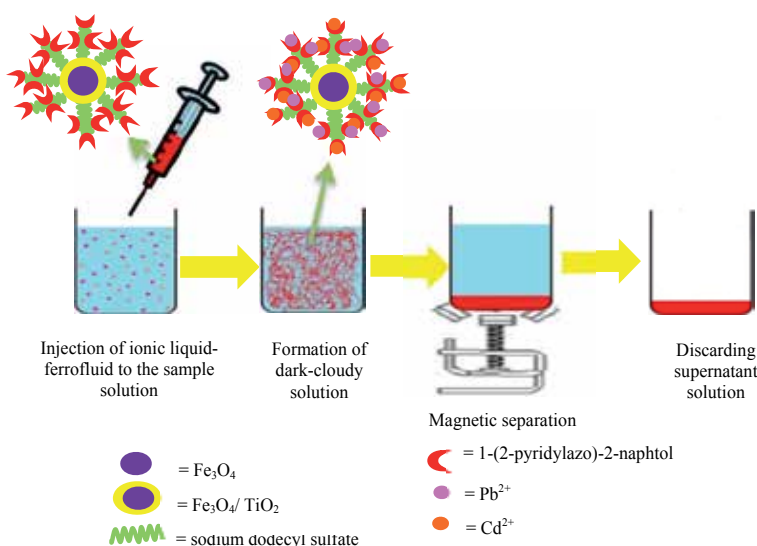


Figure 4. A schematic view of selective IL-FF-D-SPE experimental set up [14].

3.3. Result and discussion

3.3.1. Selection of ionic liquid for preparation of the ferrofluid

For selecting the best carrier fluid, apart from providing a stable ferrofluid, several criteria such as: immiscibility with an aqueous solution, non-toxicity, having low vapor pressure to avoid any loss during extraction, and compatibility with coating material should be met. For this purpose, some ionic liquids such as 1-Hexyl-3-methylimidazolium tetrafluoroborate [Hmim]BF₄, 1-Hexyl-3-methylimidazolium hexafluorophosphate [Hmim]PF₆, 1-Hexyl-3-methylimidazolium bis(trifluoromethylsulfonyl)imide [Hmim]Tf₂N, were selected and by the qualitative observation of sedimentation of each ferrofluid, the stability of the suspensions was checked. Finally 1-Hexyl-3-methylimidazolium tetrafluoroborate [Hmim]BF₄ was chosen.

3.3.2. Selection of eluent

Based on the desorption of Pb(II) and Cd(II) from modified nanoparticles in the acidic medium, this medium would be preferred in desorption step. To avoid any losses of sorbent, chloric acid was not chosen because this acid can dissolve Fe₃O₄ nanoparticles. Also based on the possibility of formation of precipitate of lead in presence of sulfate ions, sulfuric acid was not chosen too. Therefore, the possibility of desorption of lead and cadmium ions in acidic medium was examined by using nitric acid. Also some organic solvent such as ethanol, ethanol (1% HNO₃) and acetone were selected to examine the possibility of desorption of these ions in organic medium. Based on the obtained result, nitric acid was chosen as the best eluent.

3.3.3. Screening and optimization strategy

In this study, Plackett-Burman screening design was used to select the variables that mainly effect the extraction recovery of Pb(II) and Cd(II). Based on the preliminary experiments, the effects of seven factors, at two levels were investigated. pH (4 and 8), sorbent amount (0.01 and 0.03 g), ionic liquid amount (0.3 and 0.5 g), ionic strength (0 and 10% NaNO₃) eluent volume (1 and 2 mL), eluent concentration (0.5 and 2 molL⁻¹), and desorption time (5 and 10 min) were the variables of interest in this experiment. The total design matrix showed 15 runs (12 + 3 center points) to be carried out randomly in order to eliminate the effects of extraneous or nuisance variables. The evaluation of the main effects was done based on ANOVA results and Pareto charts.

As it can be concluded from Figures 5 and 6, pH has significant positive effect on extraction recovery of Pb(II) and Cd(II). Also the results illustrated in Figures 5 and 6 confirm that eluent concentration and desorption time have significant positive effects on extraction recovery of Pb(II) and Cd(II), respectively. And other parameters show no significant effect on the extraction recovery of both elements.

Therefore, the Box-Behnken design (BBD) was performed to evaluate the optimum condition of performance of selective IL-FF-D-SPE of Pb(II) and Cd(II) for the three significant parameters: pH, eluent concentration, and desorption time. The 3D response surface plots for the extraction recovery (%) of both elements were shown in Figures 7 and 8. As seen in Figures

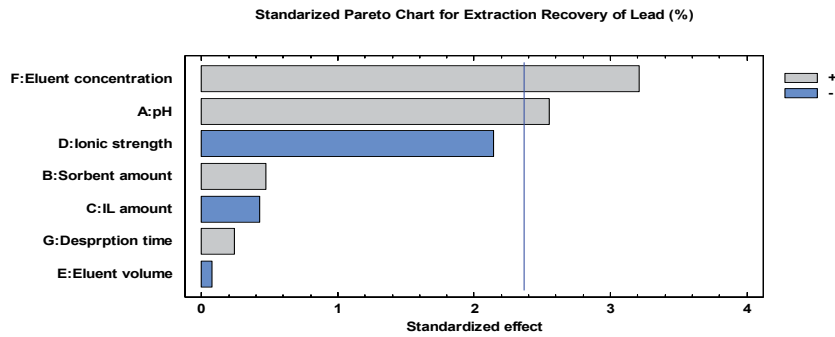


Figure 5. Standardized ($P = 0.05$) Pareto chart, representing the estimated effects of parameters obtained from the Plackett-Burman screening design for lead [14].

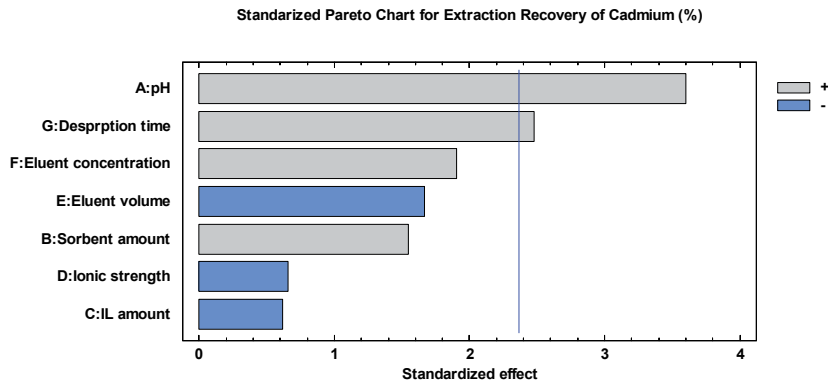


Figure 6. Standardized ($P = 0.05$) Pareto chart, representing the estimated effects of parameters obtained from the Plackett-Burman screening design for cadmium [14].

7 and 8, an optimization showed that the best pH is 6.7, eluent concentration of 1.59 molL^{-1} , and desorption time of 8 min.

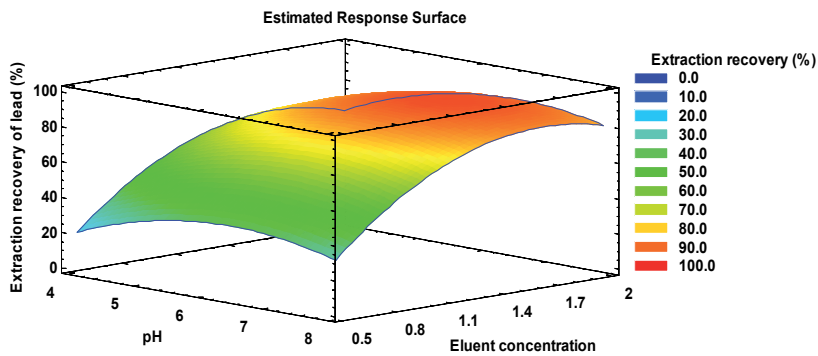


Figure 7. Estimated response surface by plotting extraction recovery (%) versus pH and eluent concentration [14].

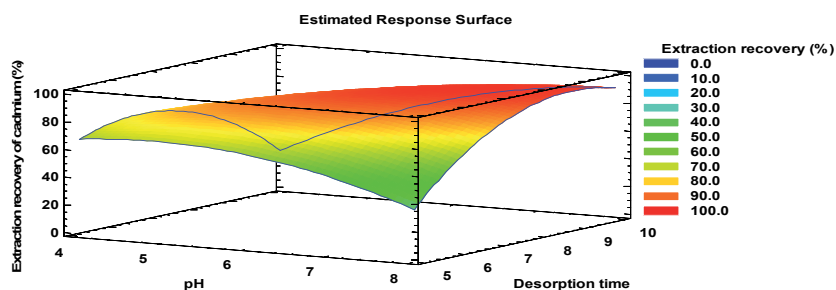


Figure 8. Estimated response surface by plotting extraction recovery (%) versus pH and desorption time [14].

3.3.4. Effect of potentially interfering ions

In order to assess the applications of the recommended procedure, the effect of potentially interfering ion on the extraction recoveries of Pb(II) and Cd(II) were also examined. For this purpose, by spiking appropriate amounts of potentially interfering ions in the range of 50-15000 $\mu\text{g mL}^{-1}$ to 50.0 mL of solution containing 40 $\mu\text{g L}^{-1}$ of Pb(II) and 30 $\mu\text{g L}^{-1}$ of Cd(II) evaluation was done. The obtained results were summarized in Table4.

Ions	Concentration ($\mu\text{g mL}^{-1}$)	Extraction recovery (%)	
		Pb(II)	Cd(II)
Na ⁺	15000	101.2 ± 2.4	98.8 ± 2.5
K ⁺	10000	97.8 ± 2.2	99.1 ± 2.5
Pd ²⁺	1000	96.9 ± 2.5	100.5 ± 2.6
Cu ²⁺	50	101.6 ± 2.4	101.3 ± 2.7
Ni ²⁺	100	98.4 ± 2.6	97.6 ± 2.4
Ag ⁺	50	98.9 ± 2.5	100.7 ± 2.6
Zn ²⁺	50	97.4 ± 2.3	96.9 ± 2.5
Mg ²⁺	500	99.2 ± 2.2	96.5 ± 2.4
Cl ⁻	10000	96.5 ± 2.3	97.2 ± 2.6
NO ₃ ⁻	15000	100.7 ± 2.4	98.4 ± 2.6

Table 4. Effect of coexisting ions on recovery of 40 $\mu\text{g L}^{-1}$ of Pb(II) and 30 $\mu\text{g L}^{-1}$ of Cd(II) (n = 3) [14].

3.3.5. Figures of merit and comparison of selective IL-FF-D-SPE with other methods

Under the optimum conditions, the relative standard deviations of 2.2 and 2.4 % were obtained for lead and cadmium, respectively (n = 7). The limit of detections were 1.21 $\mu\text{g L}^{-1}$ for Pb(II) and 0.21 $\mu\text{g L}^{-1}$ for Cd(II). The preconcentration factors were 250 for lead and 200 for cadmium and the maximum adsorption capacities of the sorbent were obtained 11.18 and 9.34 mg g^{-1} for lead and cadmium respectively.

The obtained results were compared with other literatures in Table 5. As it can be concluded from Table 5, in addition to selectivity of ionic liquid ferrofluid, the presented IL-FF-D-SPE method has lower limit of detection ($1.21 \mu\text{g L}^{-1}$ for lead and $0.21 \mu\text{g L}^{-1}$ for cadmium), higher preconcentration factor (250 and 200 for lead and cadmium respectively), good repeatability (RSD%) and sorption capacity.

Sorbent	PF/EF ^a		LOD ^b		RSD ^c (%)		Linear range ^d		Sorption capacity ^e		Ref.
	Cd ²⁺	Pb ²⁺	Cd ²⁺	Pb ²⁺	Cd ²⁺	Pb ²⁺	Cd ²⁺	Pb ²⁺	Cd ²⁺	Pb ²⁺	
Amberlite XAD-2 /PAN	50	50	23.2	0.8	4.1	2.9	0-3000	0-1000	1.35	2.56	[41]
Surfactant mediated Fe ₃ O ₄	25	25	0.74	0.15	3.82	3.15	1000-10000	100-1000	-	-	[42]
Chromosorb 101 / <i>Bacillus thuringiensis var. israelensis</i>	31	31	2.85	0.37	2.7	2.5	500-10000	20-2000	7.50	8.90	[44]
MWCN/tartrazine	40	40	6.6	0.8	-	-	500-8000	20-3000	-	-	[45]
Fe ₃ O ₄ /TiO ₂ /PAN	250	200	1.21	0.21	2.2	2.4	4-470	1-110	11.18	9.34	This work

^a Preconcentration factor or enrichment factor.

^b Limit of detection ($\mu\text{g L}^{-1}$).

^c Relative standard deviation.

^d ($\mu\text{g L}^{-1}$).

^e (mg g^{-1})

Table 5. Comparison of the proposed method with other SPE method used for preconcentration and FAAS determination of lead and cadmium ions [14].

3.3.6. Analysis of real samples

After digestion of milk, urine and blood plasma samples according to previous report [14], the standard addition method was applied for determination of trace amounts of Pb(II) and Cd(II) in these samples. The results are summarized in Table 6.

Sample	Pb(II)			Cd(II)		
	Spiked ($\mu\text{g L}^{-1}$)	Found ($\mu\text{g L}^{-1}$)	Recovery (%)	Spiked ($\mu\text{g L}^{-1}$)	Found ($\mu\text{g L}^{-1}$)	Recovery (%)
Milk ^a	0	ND ^b	-	0	ND	-
	10	10.2 ± 0.3	102.0	5	5.2 ± 0.2	104.0
	20	19.8 ± 0.5	99.0	15	14.6 ± 0.4	97.3
Urine	0	ND	-	0	ND	-
	10	10.4 ± 0.3	104.0	5	4.8 ± 0.2	96.0
	20	21.1 ± 0.6	105.5	15	15.3 ± 0.4	102.0
Blood Plasma plasma	0	ND	-	0	ND	-
	10	9.8 ± 0.3	98.0	5	5.2 ± 0.2	104.0

Sample	Pb(II)			Cd(II)		
	Spiked ($\mu\text{g L}^{-1}$)	Found ($\mu\text{g L}^{-1}$)	Recovery (%)	Spiked ($\mu\text{g L}^{-1}$)	Found ($\mu\text{g L}^{-1}$)	Recovery (%)
	20	20.9 \pm 0.6	104.5	15	15.1 \pm 0.5	100.6

^a Pegah milk, Tehran, Iran.

^b Not detected

Table 6. Determination of Cd (II) and Pb(II) in real samples [14].

4. Conclusion and future work

Ionic liquids as environmentally friendly solvents with amazing properties such as negligible vapor pressure, low flammability, and liquid state in a broad temperature range can be used in sample preparation step such as D-LLE and also D-SPE, as mentioned in above studies. In term of D-LLE by choosing IL as extraction solvent, great improvement was achieved since only very small amount of the ionic liquid as a green extraction solvent was used as a replacement of environmentally damaging organic solvents in extraction procedure.

In addition, by introducing ionic liquid ferrofluids and also selective ionic liquid ferrofluid in to the field of sample preparation, great improvements were achieved. In order to simplicity and cost efficiency, in these environmentally friendly methods due to dispersion of sorbent in the aqueous phase, extraction is much faster in comparison with SPE which is time consuming column passing. Moreover, the magnetic separation greatly improved the separation rate. Therefore, no centrifugation is need for phase separation.

We believe that by combinations of ferrofluidic materials with appropriate chelators may lead to extraction schemes for various other ions. Typical combination may include ammonium pyrrolidine dithiocarbamate (APDC), 1-(2-thiazolylazo)-2-naphthol (TAN) and 1-Phenylthiosemicarbazide (1-PTSC) as chelate agents for complexation for Pb(II), Cd(II), Co(II) and Cu(II) or this method can be used in preconcentration of dyes without any need to chelate agents and determination by spectrophotometry methods. Finally, we hope in near future we all use the benefits of ionic liquids combined with these fast extraction methods.

Author details

Negin Fasih Ramandi and Farzaneh Shemirani*

*Address all correspondence to: shemiran@khayam.ut.ac.ir

Department of Analytical Chemistry, University College of Science, University of Tehran, Tehran, Iran

References

- [1] Shah F, Kazi TG, Afridi HI, Naeemullah, Arain MB, Baig JA. Cloud point extraction for determination of lead in blood samples of children, using different ligands prior to analysis by flame atomic absorption spectrometry: A multivariate study. *Journal of Hazardous Materials*. 2011;192(3):1132-9.
- [2] Xiang G, Wen S, Wu X, Jiang X, He L, Liu Y. Selective cloud point extraction for the determination of cadmium in food samples by flame atomic absorption spectrometry. *Food Chemistry*. 2012;132(1):532-6.
- [3] dos Silva ES, Correia LO, dos Santos LO, dos Vieira EVS, Lemos VA. Dispersive liquid-liquid microextraction for simultaneous determination of cadmium, cobalt, lead and nickel in water samples by inductively coupled plasma optical emission spectrometry. *Microchimica Acta*. 2012;178(3-4):269-75.
- [4] Anthemidis AN, Ioannou KIG. Development of a sequential injection dispersive liquid-liquid microextraction system for electrothermal atomic absorption spectrometry by using a hydrophobic sorbent material: Determination of lead and cadmium in natural waters. *Analytica Chimica Acta*. 2010;668(1):35-40.
- [5] Han L, Sapozhnikova Y, Lehotay SJ. Streamlined sample cleanup using combined dispersive solid-phase extraction and in-vial filtration for analysis of pesticides and environmental pollutants in shrimp. *Analytica Chimica Acta*. 2014 5/27;827(0):40-6.
- [6] Gharehbaghi M, Shemirani F, Baghdadi M. Dispersive liquid-liquid microextraction based on ionic liquid and spectrophotometric determination of mercury in water samples. *International Journal of Environmental Analytical Chemistry*. 2009;89: 21-33.
- [7] Fasih Ramandi N, Shemirani F, Davudabadi Farahani M. Dispersive solid phase extraction of lead(II) using a silica nanoparticle-based ionic liquid ferrofluid. *Microchimica Acta*. 2014; 181: 1833-1841.
- [8] Soylak M, Yilmaz E. Ionic liquid-based method for microextraction/ enrichment of gold from real samples and determination by flame atomic absorption spectrometry. *Atomic Spectroscopy*. 2013;34(1):15-9.
- [9] Gharehbaghi M, Shemirani F, Baghdadi M. Dispersive liquid-liquid microextraction and spectrophotometric determination of cobalt in water samples. *International Journal of Environmental Analytical Chemistry*. 2008; 88: 513-23.
- [10] Raj K, Boulton RJ. Ferrofluids - Properties and applications. *Materials and Design*. 1987;8(4):233-6.
- [11] Vollmer C, Janiak C. Naked metal nanoparticles from metal carbonyls in ionic liquids: Easy synthesis and stabilization. *Coordination Chemistry Reviews*. 2011;255(17-18):2039-57.

- [12] Shi D, Sun L, Mi G, Sheikh L, Bhattacharya S, Nayar S, et al. Controlling ferrofluid permeability across the blood-brain barrier model. *Nanotechnology*. 2014;25(7).
- [13] Jain VK, Pant RP, Kumar V. Applications of ferrofluids in micro electro mechanical systems (mems) and micropumps. *Magneto hydrodynamics*. 2008 (4):417-24.
- [14] Fasih Ramandi N, Shemirani F. Selective ionic liquid ferrofluid based dispersive-solid phase extraction for simultaneous preconcentration/separation of lead and cadmium in milk and biological samples. *Talanta*. 2015 (131) 404-411.
- [15] Brullot W, Reddy NK, Wouters J, Valev VK, Goderis B, Vermant J, et al. Versatile ferrofluids based on polyethylene glycol coated iron oxide nanoparticles. *Journal of Magnetism and Magnetic Materials*. 2012 6//;324(11):1919-25.
- [16] Farahani MD, Shemirani F, Gharehbaghi M. Ferrofluid-based dispersive solid phase extraction of palladium. *Talanta*. 2013;109:121-7.
- [17] Rodríguez-Arco L, López-López MT, Durán JDG, Zubarev A, Chirikov D. Stability and magnetorheological behaviour of magnetic fluids based on ionic liquids. *Journal of Physics Condensed Matter*. 2011;23(45).
- [18] Oliveira FCC, Rossi LM, Jardim RF, Rubim JC. Magnetic fluids based on γ -Fe₂O₃ and CoFe₂O₄ nanoparticles dispersed in ionic liquids. *Journal of Physical Chemistry C*. 2009;113(20):8566-72.
- [19] Jain N, Zhang X, Hawke BS, Warr GG. Stable and water-tolerant ionic liquid ferrofluids. *ACS Applied Materials and Interfaces*. 2011;3(3):662-7.
- [20] Di Nezio MaS, Palomeque ME, Fernández Band BS. A sensitive spectrophotometric method for lead determination by flow injection analysis with on-line preconcentration. *Talanta*. 2004 5/28//;63(2):405-9.
- [21] C. Adams F, Heisterkamp M, Candelone J-P, LTURNUS F, van de Velde K, F. Boutron C. Speciation of organometal and organohalogen compounds in relation to global environmental pollution [dagger]. *Analyst*. 1998;123(5):767-72.
- [22] Citak D, Tuzen M, Soylak M. Simultaneous coprecipitation of lead, cobalt, copper, cadmium, iron and nickel in food samples with zirconium(IV) hydroxide prior to their flame atomic absorption spectrometric determination. *Food and Chemical Toxicology*. 2009 9//;47(9):2302-7.
- [23] Es'haghi Z, Khalili M, Khazaeifar A, Rounaghi GH. Simultaneous extraction and determination of lead, cadmium and copper in rice samples by a new pre-concentration technique: Hollow fiber solid phase microextraction combined with differential pulse anodic stripping voltammetry. *Electrochimica Acta*. 2011;56(9):3139-46.
- [24] Silva EL, Roldan PdS. Simultaneous flow injection preconcentration of lead and cadmium using cloud point extraction and determination by atomic absorption spectrometry. *Journal of Hazardous Materials*. 2009;161(1):142-7.

- [25] Doner G, Ege A. Determination of copper, cadmium and lead in seawater and mineral water by flame atomic absorption spectrometry after coprecipitation with aluminum hydroxide. *Analytica Chimica Acta*. 2005 8/15/;547(1):14-7.
- [26] Tufekci M, Bulut V, Elvan H, Ozdes D, Soylak M, Duran C. Determination of Pb(II), Zn(II), Cd(II), and Co(II) ions by flame atomic absorption spectrometry in food and water samples after preconcentration by coprecipitation with Mo(VI)-diethyldithiocarbamate. *Environ Monit Assess*. 2013 2013/02/01;185(2):1107-15. English.
- [27] Amorim FAC, Ferreira SLC. Determination of cadmium and lead in table salt by sequential multi-element flame atomic absorption spectrometry. *Talanta*. 2005 2/28/;65(4):960-4.
- [28] Er C, Filiz Senkal B, Yaman M. Determination of lead in milk and yoghurt samples by solid phase extraction using a novel aminothioazole-polymeric resin. *Food Chemistry*. 2013 4/15/;137(1-4):55-61.
- [29] Jiao F, Gao H-W. On-site solid-phase extraction and application to in situ preconcentration of heavy metals in surface water. *Environ Monit Assess*. 2013 2013/01/01;185(1):39-44. English.
- [30] Ensafi AA, Shiraz AZ. On-line separation and preconcentration of lead(II) by solid-phase extraction using activated carbon loaded with xylenol orange and its determination by flame atomic absorption spectrometry. *Journal of Hazardous Materials*. 2008 2/11/;150(3):554-9.
- [31] Zhao X, Shi Y, Cai Y, Mou S. Cetyltrimethylammonium Bromide-Coated Magnetic Nanoparticles for the Preconcentration of Phenolic Compounds from Environmental Water Samples. *Environmental Science & Technology*. 2008 2008/02/01;42(4):1201-6.
- [32] Rezaee M, Assadi Y, Milani Hosseini M-R, Aghaee E, Ahmadi F, Berijani S. Determination of organic compounds in water using dispersive liquid-liquid microextraction. *Journal of Chromatography A*. 2006 5/26/;1116(1-2):1-9.
- [33] Citak D, Tuzen M. A novel preconcentration procedure using cloud point extraction for determination of lead, cobalt and copper in water and food samples using flame atomic absorption spectrometry. *Food and Chemical Toxicology*. 2010 5//;48(5):1399-404.
- [34] Yang B, Gong Q, Zhao L, Sun H, Ren N, Qin J, et al. Preconcentration and determination of lead and cadmium in water samples with a MnO₂ coated carbon nanotubes by using ETAAS. *Desalination*. 2011 9/1/;278(1-3):65-9.
- [35] Parham H, Pourreza N, Rahbar N. Solid phase extraction of lead and cadmium using solid sulfur as a new metal extractor prior to determination by flame atomic absorption spectrometry. *Journal of Hazardous Materials*. 2009 4/30/;163(2-3):588-92.
- [36] Wang Y, Gao S, Zang X, Li J, Ma J. Graphene-based solid-phase extraction combined with flame atomic absorption spectrometry for a sensitive determination of trace

- amounts of lead in environmental water and vegetable samples. *Analytica Chimica Acta*. 2012 2/24;/716(0):112-8.
- [37] Baytak S, Türker AR. Determination of lead and nickel in environmental samples by flame atomic absorption spectrometry after column solid-phase extraction on Ambersorb-572 with EDTA. *Journal of Hazardous Materials*. 2006 2/28;/129(1-3):130-6.
- [38] Ye QY, Li Y, Jiang Y, Yan XP. Determination of trace cadmium in rice by flow injection on-line filterless precipitation-dissolution preconcentration coupled with flame atomic absorption spectrometry. *Journal of Agricultural and Food Chemistry*. 2003;51(8):2111-4.
- [39] Mirzajani R, Pourreza N, Najjar SSA. β -Cyclodextrin-based polyurethane (β -CDPU) polymers as solid media for adsorption and determination of Pb(II) ions in dust and water samples. *Research on Chemical Intermediates*. 2013:1-13.
- [40] Ataro A, McCrindle RI, Botha BM, McCrindle CME, Ndibewu PP. Quantification of trace elements in raw cow's milk by inductively coupled plasma mass spectrometry (ICP-MS). *Food Chemistry*. 2008;111(1):243-8.
- [41] Bermejo-Barrera P, Martínez Alfonso N, Díaz López C, Bermejo Barrera A. Use of Amberlite XAD-2 loaded with 1-(2-pyridylazo)-2-naphthol as a preconcentration system for river water prior to determination of Cu 2+, Cd2+ and Pb2+ by flame atomic absorption spectroscopy. *Mikrochimica Acta*. 2003;142(1-2):101-8.
- [42] Jalbani N, Soylak M. Ligandless surfactant mediated solid phase extraction combined with Fe₃O₄ nano-particle for the preconcentration and determination of cadmium and lead in water and soil samples followed by flame atomic absorption spectrometry: Multivariate strategy. *Ecotoxicology and Environmental Safety*. 2014 4//;102(0): 174-8.
- [43] Kinaree S, Chanthai S. Ultra-trace determination of Pb(II) and Cd(II) in drinking water and alcoholic beverages using homogeneous liquid-liquid extraction followed by flame atomic absorption spectrometry. *Chemical Papers*. 2014;68(3):342-51.
- [44] Mendil D, Tuzen M, Usta C, Soylak M. *Bacillus thuringiensis* var. *israelensis* immobilized on Chromosorb 101: A new solid phase extractant for preconcentration of heavy metal ions in environmental samples. *Journal of Hazardous Materials*. 2008 1/31;/150(2):357-63.
- [45] Soylak M, Topalak Z. Multiwalled carbon nanotube impregnated with tartrazine: Solid phase extractant for Cd(II) and Pb(II). *Journal of Industrial and Engineering Chemistry*. 2014;20(2):581-5.

Biomass

Imidazolium-Based Ionic Liquids as Solvents for Analysis of Lipophilic Extractives from Biomass

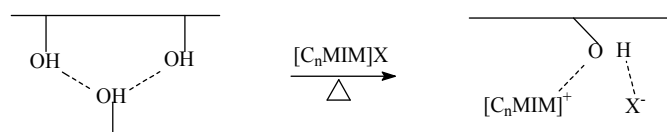
Kessy F. Kilulya, Bhekie B. Mamba and
Titus A.M. Msagati

Additional information is available at the end of the chapter

<http://dx.doi.org/10.5772/59075>

1. Introduction

Ionic liquids are organic salts made of cations and anions of which most of them are liquids at room temperature [1-3]. This is generally a newly emerging class of compounds which so far has been discovered to have numerous applications in chemistry [2] due to their attractive features such as negligible vapour pressure, high thermal stability, biodegradability, ability to solvate compounds of different polarity and miscibility with aqueous and organic solvents [4], [5]. Different classes of ionic liquids have been synthesised so far, such as, imidazolium, ammonium, pyridinium, isoquinolinium, sulfonium, phosphonium, pyrrolidinium and others [6]. Since their discovery ionic liquids have raised a considerable excitement among researchers due to their ability to combine with different reagents in number of applications. The other aspect of ionic liquids is their ability to be recycled which minimizes the cost of usage as well as making them environmentally friendly. Ionic liquids so far have been used as solvents in different areas including for catalysis, synthesis and purification [6]. They have high ability of dissolving biopolymers such as cellulose and other biomass due to their ability to interact with biopolymer matrix forming hydrogen bonding [7] (Scheme 1).



Scheme 1. Schematic diagram showing dissolution of biopolymer in ionic liquid $[C_nMIM]X$ [3] [5]

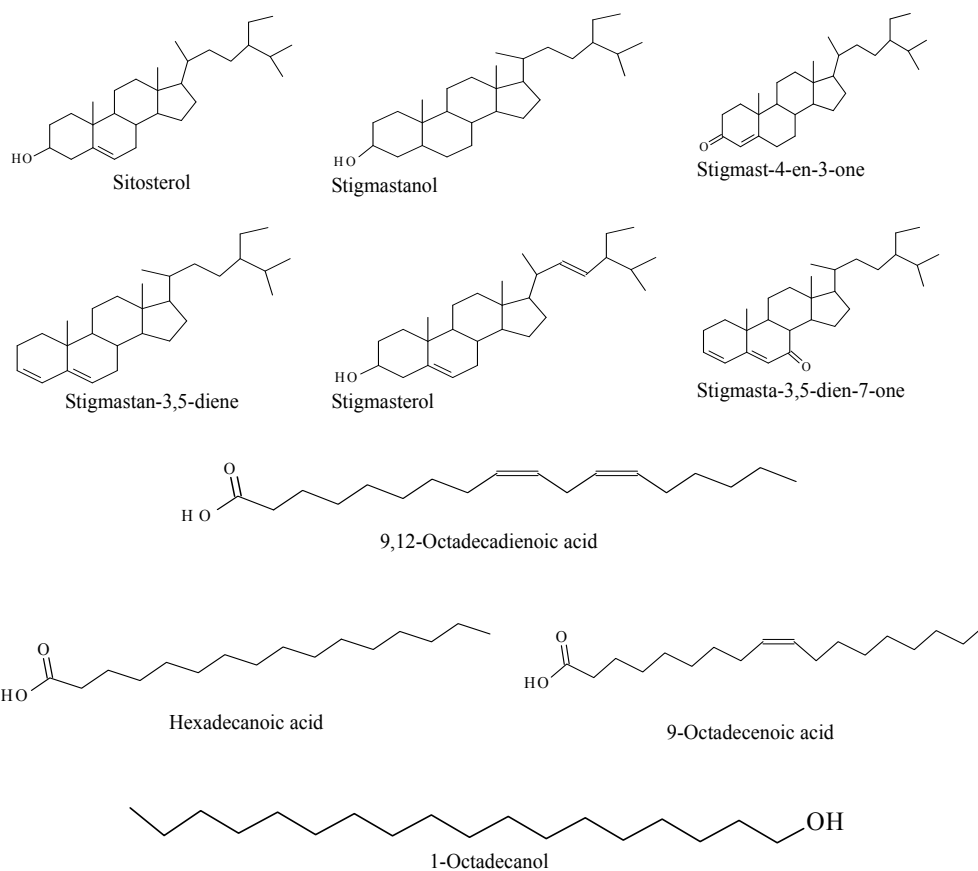


Figure 1. Chemical structures of some lipophilic extractive components reported from different biomass

Ionic liquids are known to have low toxicity due to their low volatility, a property which makes them to be considered as green and therefore recommended to replace volatile organic solvents in different chemical processes [6, 8].

Lipophilic extractives are a class of non-structural component of the biomass composed of low-molecular weight compounds such as fatty acids, fatty acid esters, sterols, sterol esters, fatty alcohols, triglycerides, hydrocarbons, steroid hydrocarbons and steroid ketones [9-12].

Figure 1 shows some of the common lipophilic extractives obtained from different biomass.

Lipophilic extractives have received attention from researchers partly due to their negative effect in paper and pulp industries as well as their importance in biofuel production and other applications [13, 14]. Lipophilic extractives from wood materials used for the production of pulp and paper affect negatively the pulping process as well as the final product. Whereas lipophilic extractives from other biomass such as blue-green algae are common used for other application such as biofuel production. Thus, effective and quick lipophilic extractives analytical methods are required to characterize and study their qualitative and quantitative

composition in the biomass. Thus, the application of ionic liquids in the analysis of lipophilic extractives is attributed to their ability to dissolve biopolymers and biomass [14] whereby upon adding precipitating solvents (polar solvents), they regenerate pure biopolymers and release non-polymeric materials into the solution. Thus, lipophilic extractives can be easily extracted from the ionic liquid aqueous solution using a small volume of non-polar solvents. The approach is advantageous due to its use of small volume of organic solvent and shorter extraction time. This chapter therefore, reports on the use of imidazolium-based ionic liquids as an effective approach of extracting lipophilic extractives from chemical cellulose and blue-green algae biomass prior to chromatographic analysis.

2. Chemical reagents and instrumentation

The following chemicals purchased from Sigma Aldrich (Steinheim, Germany) were used; 1-butyl-3-methylimidazolium chloride [BMIM]Cl (98.0%), 1-ethyl-3-methylimidazolium chloride [EMIM]Cl (98.0%), 1-butyl-3-imidazolium acetate [BMIM]Ac, (97.0%), 1-ethyl-3-imidazolium acetate [EMIM]Ac (97.0%), 1-butyl-3-imidazolium methylsulphate [BMIM]MESO₄, 1-butyl-3-imidazolium hexafluorophosphate [BMIM]PF₆ (97.0%). Methanol (HPLC grade), acetone (HPLC grade), hexane (HPLC grade), ethyl acetate (99.7%), hydrochloric acid (37.0%), and sodium sulphate anhydrous (99 – 100.5%). Chromatographic instruments used were an Agilent GC-MS, 7890A GC System with a triple-axis detector (5975C MSD), Shimadzu (GC-MS, QP2010, Kyoto, Japan), and GCxGC-TOFMS (Pegasus 4D, LECO Corporation). FT-IR; PerkinElmer Spectrum 100 FT-IR spectrometer with attached diamond attenuated total reflectance (ATR) accessory, TGA measurement was performed on a Perkin Elmer TGA 4000 Thermogravimetric Analyser.

3. Experimental

3.1. dissolution of chemical cellulose in imidazolium-based ionic liquids

A variety of imidazolium-based ionic liquids were initially screened for their ability to dissolve chemical cellulose at different temperatures. Chemical cellulose samples were accurately weighed and dissolved in molten ionic liquid at 90°C forming a 5 % solution. 25 mL of distilled water at 90°C was added to regenerate cellulose. Then samples were filtered and filtrates extracted using hexane followed by hexane: ethyl acetate by first sonicating for 5 minutes then auto shaking for 20 minutes. The extracts were dried, weighed and dissolved in 0.5 mL of acetone for derivatization before GC-MS analysis.

3.2. Dissolution of blue-green algae biomass

A freeze dried algae biomass sample was accurately weighed in duplicate and dissolved in a molten ionic liquid at 90°C forming a non viscous uniform solution of 5% algae biomass. About 5 mL of methanol was added to form slurry followed by addition of derivatization reagent.

The mixture was heated for 1 h at 60°C in a thermostated water bath then cooled at room temperature followed by extraction of fatty acids methyl esters (FAMES) with 4 mL of hexane under vigorous vortexing. The dried extracts were then dissolved in 1 mL of HPLC grade hexane, filtered using PTFE disc filters for GCxGC-TOFMS analysis.

4. Ultrasonic solid liquid extraction using organic solvent

For comparison purpose the results of the qualitative and quantitative composition of lipophilic extractives obtained from biomass by ionic liquid based extraction was compared with the results obtained using volatile organic solvent under ultrasonic solid liquid extraction technique (USLE) utilizing the mixture of acetone and methanol for chemical cellulose and chloroform and methanol for blue-green algae biomass. The extraction was carried out at an optimized temperature for 1 h. Extracts were then derivatized and analysed by GC-MS and GCxGC-TOFMS analysis.

5. FT-IR and TGA analysis of extracted and un-extracted biopolymers (cellulose)

For the investigation of the effect of ionic liquids on the analysed biopolymers the FT-IR and TGA analyses were performed. The extracted and un-extracted biopolymers (cellulose) were thoroughly washed with acetone followed by deionised water then dried in an oven at 90°C prior to FT-IR and TGA analyses.

The FT-IR analysis was achieved using a PerkinElmer Spectrum 100 FT-IR spectrometer with attached diamond attenuated total reflectance (ATR) accessory. Spectra were recorded from 4000 cm^{-1} to 650 cm^{-1} in transmittance mode with 4 scans per spectrum at a resolution of 4 cm^{-1} .

Thermogravimetric analysis (TGA) measurements were performed on a Perkin Elmer TGA 4000 Thermogravimetric Analyser. About 10 mg of sample aliquots were placed in a platinum sample holder pan. The TGA curves were recorded at temperatures ranging between 80°C and 700°C at a ramp-up rate of 10°C/min under nitrogen flow rate of 20 mL/min.

6. Results and discussion

6.1. Dissolution of biomass in ionic liquids

During the screening of ionic liquids on their abilities to dissolve chemical cellulose and blue-green algae biomass it was observed that the dissolution capacity depends on the anions in the ionic liquids and temperature. The dissolution trend was observed to be in the following order: 1-butyl-3-imidazolium acetate > 1-ethyl-3-imidazolium acetate > 1-butyl-3-methylimi-

dazolium chloride > 1-ethyl-3-methylimidazolium chloride whereas those with methyl sulphate and hexafluorophosphate anions were found to be non-solvent, Figure 2. It has to be noted that the chloride (Cl) and acetate (CH₃COO⁻) anions are all strong hydrogen bonding acceptor and thus have ability to disrupt the hydrogen bonding network in biomass biopolymers leading to their dissolution [7, 15, 16].

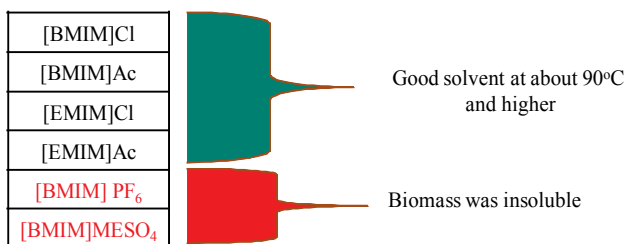


Figure 2. Solubility of biomass in different imidazolium based ionic liquids

The effect of ionic liquids on the biomass was investigated by checking their effect on the extracted and un-extracted chemical cellulose. This was examined using FT-IR and TGA and the result showed no significant difference between the original and the regenerated cellulose with an exception of the percentage of mass residues in the TGA profile, which was higher for regenerated cellulose, compared to that of the original cellulose at 600°C, Figures 3 and 4. This confirms that ionic liquids are just solvents because they have no reaction with biopolymers and therefore can be used for analytical processes of biopolymers.

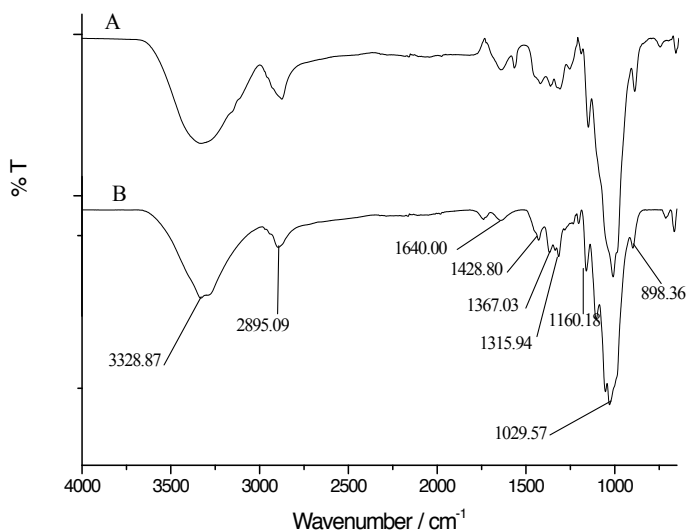


Figure 3. FT-IR spectra of regenerated cellulose from ionic liquid (A) and original cellulose (B)

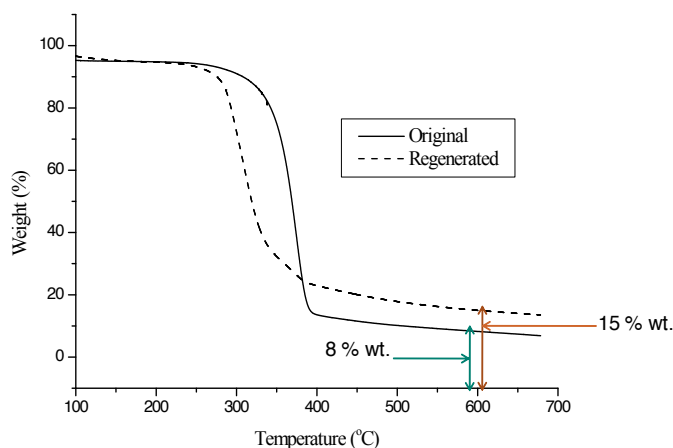


Figure 4. TGA analysis of original and regenerated chemical cellulose at a temperature ranging from 80°C to 700°C

Thus, 1-butyl-3-methylimidazolium acetate and 1-butyl-3-methylimidazolium chloride were selected for further investigation through which it was found that ionic liquids with chloride anion was able to recover higher amount of lipophilic extractives.

Since [BMIM]Cl and [BMIM]Ac were identified to be suitable solvent for biopolymers, an investigation and comparisons on their capacity to extract lipophilic extractives was performed. It was found that [BMIM]Cl extracted higher amount of lipophilic extractives than [BMIM]Ac, Figure 5. This difference could be explained by the nature of the anions of the two ionic liquids in which acetate has basic properties whereas chloride ionic liquid is acidic.

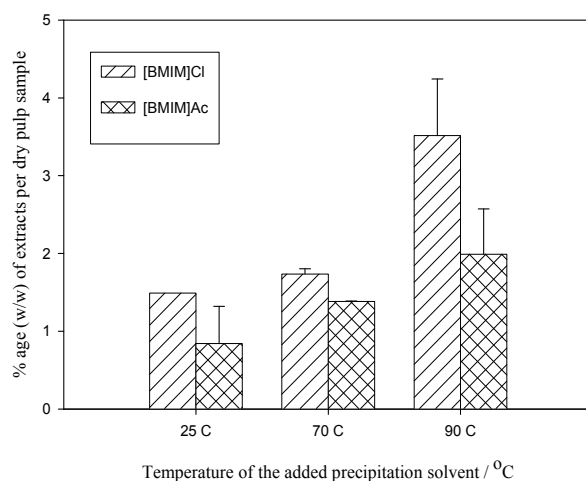


Figure 5. Comparison of [BMIM]Cl and [BMIM]Ac in the extraction of lipophilic extractives at 25°C, 75°C and 90°C of the added water for biopolymers precipitation

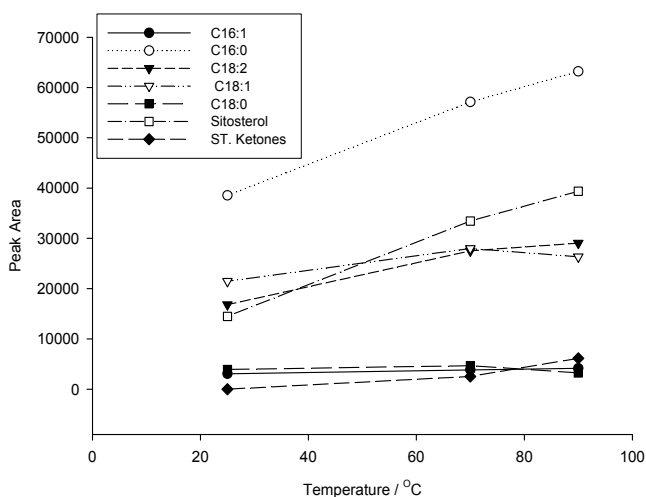


Figure 6. Amount of lipophilic extractives per precipitating solvent temperature

The effect of temperature on the extraction ability of these two types of imidazolium ionic liquids was also considered and found that the amount of lipophilic extractives obtained from biopolymers (cellulose) increased with temperature as presented in Figure 5. Further investigation for effect of precipitating solvent temperature on the amount of lipophilic extractives obtained was performed on the individual compounds as indicated in Figure 6. Thus, the percentage recovery of the individual compounds was also verified to increase with temperature of the added precipitation solvent.

This can be explained by the fact that, at low temperature of the precipitation solvent, lipophilic extractives precipitate on the surface of the cellulose due to their hydrophobicity. In this study water was found to be the best polar solvent for precipitation of dissolved cellulose. When trying to avoid the problem of lipophilic extractives depositing on cellulose surface during regeneration of cellulose, the possibility of using any other polar volatile organic solvents as cellulose precipitating solvents, was considered. However, most of these volatile organic solvents boil at low temperatures while the dissolution temperature in this study was fixed at the optimal temperature of 90°C which was too high for volatile organic solvent to exist as liquids and therefore would result into serious environmental pollution.

In comparing with the conventional volatile organic solvent extraction, it was observed that ionic liquids could quickly extract lipophilic extractives from biomass in which the qualitative and quantitative compositions were found to be similar to that obtained using conventional volatile organic solvents. In blue-green algae biomass the ionic liquid was used to extract fatty acids in which it was confirmed that both ionic liquid extraction and volatile organic solvent extraction obtained similar compositions. Therefore, the result warranted the use of ionic liquids as extraction medium for lipophilic extractives analyses and the process is quick and environmentally friendly.

6.2. Identification and quantification of lipophilic extractives

Lipophilic extractives determined by GC-MS analysis on the extracts from chemical cellulose were fatty acids, sterols, fatty alcohols, steroid hydrocarbons and steroid ketones. On the other hand the GCxGC-TOFMS analysis of fatty acids composition of the extracts from blue-green algae biomass was dominated by 7-hexadecenoic acid (C16:1), hexadecanoic acid (C16:0), γ -linolenic acid (γ -C18:3); linoleic acid (C18:2); linolenic acid (C18:3); 6,9,12,15-octadecatetraenoic acid (C18:4); oleic acid (C18:1) and octadecanoic acid (C18:0). The peaks of identified fatty acids in blue-green algae biomass by GCxGC-TOFMS are shown in the one dimension (1D) chromatogram with its corresponding two dimension (2D) contour chromatogram of the C18s fatty acids which were somehow eluting at relatively very close retention times, Figure 7. Thus, the determination of the fatty acids which were analysed as their methyl esters involved the consideration of 1D and 2D chromatography with application of Windows-based ChromaTOF software of the GCxGC-TOFMS.

Generally it can be observed that for the fatty acids with a chain of 18 carbon atoms (C18s) were coeluting in 1D chromatography, however, through the application of deconvolution power of the Pegasus 4D GCxGC-TOFMS they were properly determined, Figure 8. The tendency of C18s fatty acids isomers to coelute and bear the identical mass spectra is actually due to the fact that they all have similar chemical structures which only differs in the number and positions of double bonds. Hence it can be observed in the given chromatograms that C18s fatty acids methyl esters of Linolenic acid (C18:3), Oleic acid (C18:2) and 9-Octadecanoic acid (C18:1) were somehow coeluting in this analysis. But their actual determination was achieved by the employment of the deconvolution algorithm of ChromaTOF software which made the separation of their mass spectra, identification and quantification accurately done. It is this aspect of the GCxGC-TOFMS technique which makes this study to recommend it as a more suitable and advanced technique for analysis of lipophilic extractives if one is to obtain reliable data. Figure 8 shows the 1D GCxGC-TOFMS mass spectra of C18s fatty acids.

The obtained fatty acids composition from blue-green algae biomass using ionic liquids (IL) [BMIM]Cl and that of volatile organic solvent (VOS) was found to be similar, Figure 9. It can be easily observed that the quantitative composition of different fatty acids components obtained by the two extraction techniques were similar with some few exceptions, i.e., the amount of 7-hexadecenoic acid (C16:1), γ -6,9,12-octadecatrienoic acid (γ -C18:3) and 9,12-octadecadienoic acid (C18:2) were relatively higher in ionic liquid extraction. While on the other hand, hexadecanoic acid (C16:0), 6,9,12,15-octadecatetraenoic acid (C18:4), 9,12,15-octadecatrienoic acid (C18:3) and octadecanoic acid (C18:0) were relatively higher in volatile organic solvent extraction technique. To justify the similarity of the quantitative composition of fatty acids one-way analysis of variance (ANOVA) was performed and confirmed that at the 0.05 level there was no significant difference ($P \gg 0.05$) between the means of the data sets obtained by the two extraction techniques. This information indicates that there is no reaction (such as oxidative reaction) between fatty acids and ionic liquid [BMIM]Cl and therefore, ionic liquids are just solvents of fatty acids and lipophilic extractives in general.

The similarity in qualitative and quantitative composition of fatty acids from blue-green algae biomass obtained using ionic liquid based extraction (IL) and conventional volatile organic

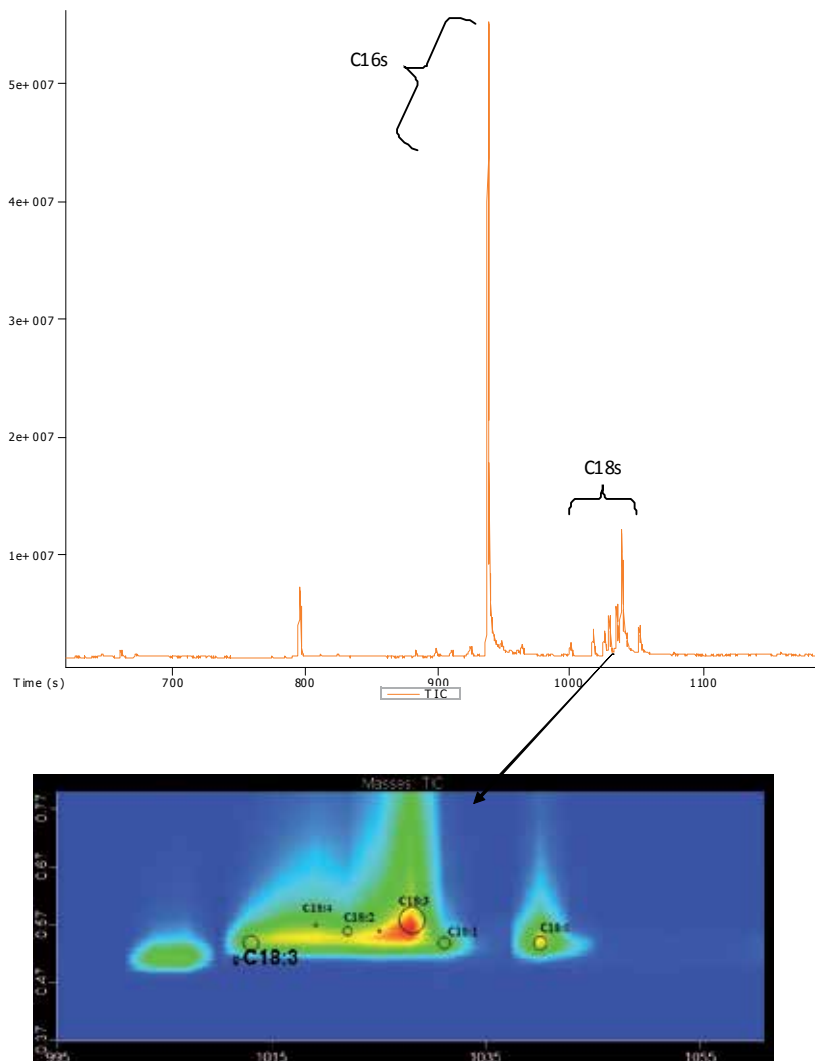


Figure 7. 1D and 2D GCxGC-TOFMS chromatogram indicating the main fatty acids from blue-green algae biomass (C16s=C16:1 and C16:0, whereas C18s= γ -C18:3, C18:4, C18:2; C18:3, C18:1 and C18:0). The 2D chromatogram shows the corresponding C18s fatty acids methyl esters elution region in which the X-axis is retention time (second) on the primary column and the Y-axis is retention time (second) on the secondary column

solvent extraction (VOS) method justified that ionic liquid is a suitable solvent to replace volatile organic solvent for reduced environmental pollution.

This study also investigated the difference between the amounts of fatty acids extracted from blue-green algae biomass using ionic liquid extraction followed by derivatization stage against the one with direct derivatization. The data showed that the extraction under direct derivatization enhanced the amount of fatty acids obtained. It was observed that the total amount of fatty acids increased from 6.07 mg/g (of dry biomass sample) in ionic liquid extraction with

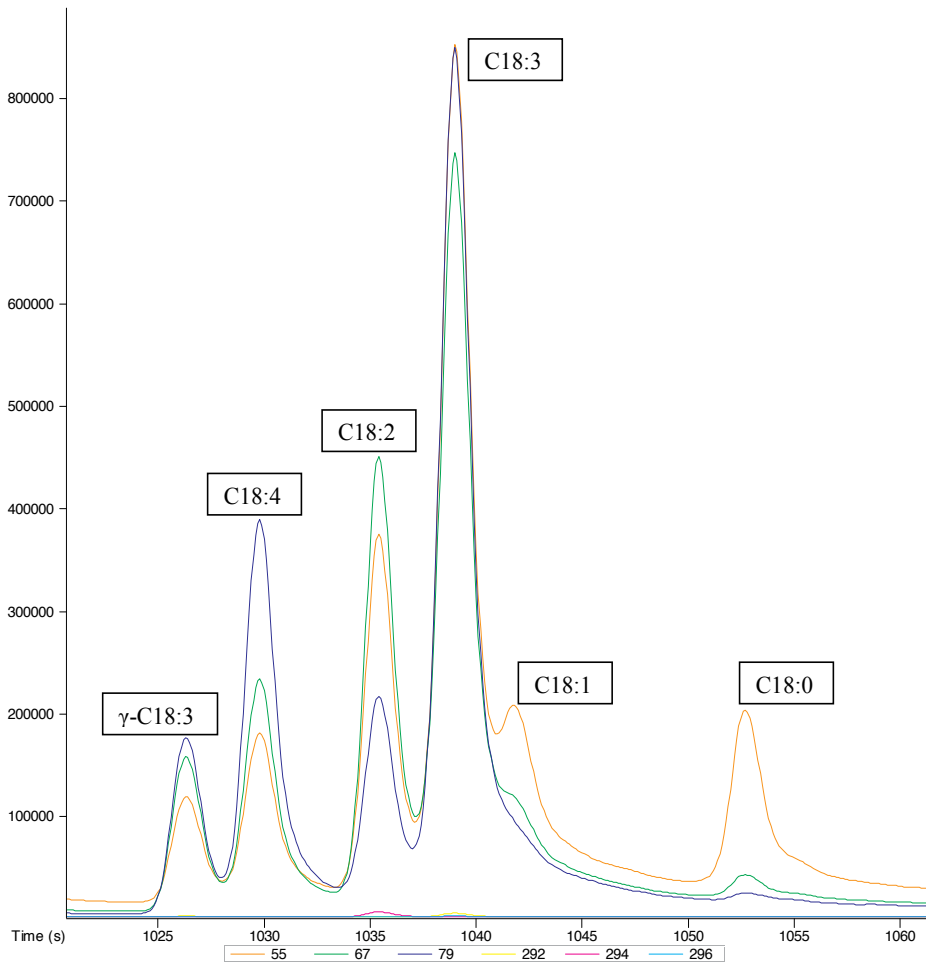


Figure 8. 1D GCxGC-TOFMS mass spectral deconvolution of C18s fatty acids used for identification

separate derivatization step to 21.96 mg/g (of dry biomass sample) in ionic liquid extraction with direct derivatization. It was further observed that for the saturated fatty acids the increase was from 3.64 mg/g (of dry biomass sample) in ionic liquid extraction with separate derivatization step to 12.80 mg/g (of dry biomass sample) in ionic liquid extraction with direct derivatization. For the unsaturated fatty acids the increase was from 2.43 mg/g (of dry biomass sample) in ionic liquid extraction with separate derivatization step to 9.16 mg/g (of dry biomass sample) in ionic liquid extraction with direct derivatization. Therefore in order to exhaust the amount of fatty acids in blue-green algae biomass using ionic liquid extraction approach, direct derivatization method is vital.

The use of ionic liquid can significantly reduce the pollution of the environment not only due to its properties [4, 17-19] but also its miscibility with water, a property which makes it reduce

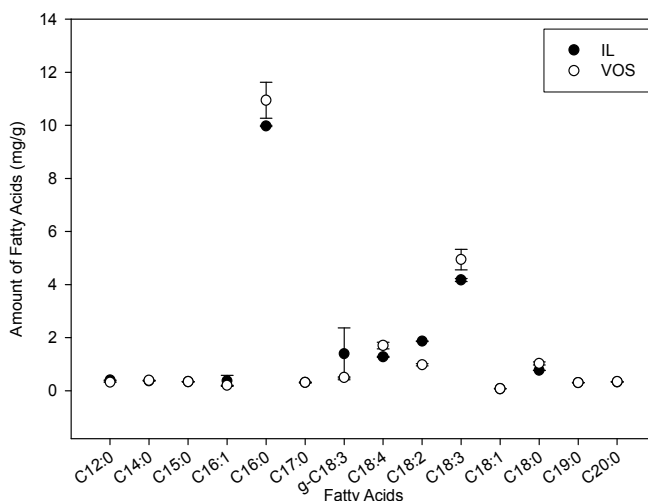


Figure 9. Comparison of fatty acids composition of ionic liquid (IL) extraction and volatile organic solvent extraction methods (VOS) (mg/g of dry algae biomass).

the use of volatile organic solvent in analytical procedures [19]. Due to the ability of ionic liquids in dissolving biomass, the extraction of lipophilic extractives becomes more efficient due to the fact that lipophilic extractives are released into the solution in which cellulose is regenerated by the addition of precipitation solvent such as water. Thus, the extraction of analytes is easily achieved using small amount of volatile organic solvents in the ionic liquid-aqueous filtrate [5].

7. Conclusion

This study has demonstrated the application of imidazolium based ionic liquids in the extraction of lipophilic extractives from biomass. Ionic liquids were screened for their dissolution capacity of biomass and their ability to extract lipophilic extractives from the analysed biomass (i.e. blue-green algae and chemical cellulose). It was observed that ionic liquids particularly the ones with anions which are strong hydrogen bonding acceptor such as chloride (Cl⁻) and acetate (CH₃COO⁻) can easily dissolve biopolymers and other biomass. [BMIM]Ac and [BMIM]Cl were identified to be the most suitable ionic liquids solvents for the extraction of lipophilic extractives, in which [BMIM]Cl was found to extract more lipophilic extractives than [BMIM]Ac. The study investigated the suitability of imidazolium ionic liquids in extracting lipophilic extractives from biomass in which the composition obtained by using volatile organic solvents and that of ionic liquids were similar. Therefore, imidazolium based ionic liquids is just a solvent and suitable to replace volatile organic solvents for minimized environmental pollution. The ionic liquid based extraction procedure was found to be quick, effective and efficient as compared to volatile organic solvents based extraction procedure. Based on the observed results direct derivatization for the ionic liquid based extraction is

recommended when using ionic liquids for the extraction and analysis of lipophilic extractives from biomass.

Acknowledgements

The authors are grateful to the Research Unite of Nanotechnology for Water Sustainability, UNISA, South Africa for financial support and instrumentation facilities.

Authors also thank the Chemistry Department, University of Dar es Salaam, Tanzania.

Author details

Kessy F. Kilulya^{1*}, Bhekie B. Mamba² and Titus A.M. Msagati²

*Address all correspondence to: msagataam@unisa.ac.za

1 University of Dar es Salaam: Department of Chemistry, Dar es Salaam, Tanzania

2 University of South Africa: Research Unit of Nanotechnology for Water sustainability, UNISA Science Campus, Florida, Johannesburg, South Africa

References

- [1] Kiefer, J., Obert, K., Bösmann, A., Seeger, T., Wasserscheid, P., and Leipertz, A. (2008). Quantitative Analysis of Alpha-D-glucose in an Ionic Liquid by Using Infra-red Spectroscopy. *ChemPhysChem* 9, 1317-1322.
- [2] Kubisa, P. (2004). Application of ionic liquids as solvents for polymerization processes. *Progress in Polymer Science* 29, 3-12.
- [3] Kosan, B., Michels, C., and Meister, F. (2008). Dissolution and forming of cellulose with ionic liquids. *Cellulose* 15, 59-66.
- [4] Doherty, T.V., Mora-Pale, M., Foley, S.E., Linhardt, R.J., and Dordick, J.S. (2010). Ionic liquid solvent properties as predictors of lignocellulose pretreatment efficacy. *Green chemistry* 12, 1967-1975.
- [5] Kilulya, K.F., Msagati, T.A.M., Mamba, B.B., Ngila, J.C., and Bush, T. (2012). Determination of Lipophilic Extractives in Ionic Liquid Extracts of Eucalyptus Pulp by Gas Chromatography-Mass Spectrometry. *Tanzania Journal of Science* 38, 14-26.

- [6] Zhang, S., Sun, N., He, X., Lu, X., and Zhang, X. (2006). Physical properties of ionic liquids: database and evaluation. *Journal of physical and chemical reference data* 35, 1475-1517.
- [7] Swatloski, R.P., Spear, S.K., Holbrey, J.D., and Rogers, R.D. (2002). Dissolution of Cellulose with Ionic Liquids. *J. Am. Chem. Soc.* 124, 4974-4975.
- [8] Jeon, Y., Sung, J., Seo, C., Lim, H., Cheong, H., Kang, M., Moon, B., Ouchi, Y., and Kim, D. (2008). Structures of Ionic Liquids with Different Anions Studied by Infrared Vibration Spectroscopy. *J. Phys. Chem. B* 112, 4735-4740.
- [9] Sun, R.C., Salisbury, D., and Tomkinson, J. (2003). Chemical composition of lipophilic extractives released during the hot water treatment of wheat straw. *Bioresource Technology* 88, 95-101.
- [10] Marques, G., Río, J.C.d., and Gutiérrez, A. (2010). Lipophilic extractives from several nonwoody lignocellulosic crops (flax, hemp, sisal, abaca) and their fate during alkaline pulping and TCF/ECF bleaching. *Bioresource Technology* 101, 260-267.
- [11] Qin, M.H., Xu, Q.H., Shao, Z.Y., Gao, Y., Fu, Y.J., Lu, X.M., Gao, P.J., and Holmbom, B. (2009). Effect of bio-treatment on the lipophilic and hydrophilic extractives of wheat straw. *Bioresource Technology* 100, 3082-3087.
- [12] Marques, G., Rencoret, J., Gutiérrez, A., and Río, J.C.d. (2010). Evaluation of the chemical composition of different non-woody plant fibers used for pulp and paper manufacturing. *The Open Agriculture J.* 4, 93-101.
- [13] Ryckebosch, E., Muylaert, K., and Foubert, I. (2012). Optimization of an analytical procedure for extraction of lipids from microalgae. *Journal of the American Oil Chemists' Society* 89, 189-198.
- [14] Kim, Y.-H., Choi, Y.-K., Park, J., Lee, S., Yang, Y.-H., Kim, H.J., Park, T.-J., Hwan Kim, Y., and Lee, S.H. (2012). Ionic liquid-mediated extraction of lipids from algal biomass. *Bioresource Technology* 109, 312-315.
- [15] Spiridon, I., Teacă, C.-A., and Bodîrlău, R. (2010). Structural changes evidenced by FTIR spectroscopy in cellulosic materials after pre-treatment with ionic liquid and enzymatic hydrolysis. *BioResources* 6, 400-413.
- [16] Feng, L., and Chen, Z. (2008). Research progress on dissolution and functional modification of cellulose in ionic liquids. *J. Mol. Liq.* 142, 1-5.
- [17] Pragya, N., Pandey, K.K., and Sahoo, P. (2013). A review on harvesting, oil extraction and biofuels production technologies from microalgae. *Renewable and Sustainable Energy Reviews* 24, 159-171.
- [18] Kline, L.M., Hayes, D.G., Womac, A.R., and Labbe, N. (2010). Simplified determination of lignin content in hard and soft woods via UV-spectrophotometric analysis of biomass dissolved in ionic liquids. *BioResources* 5, 1366-1383.

- [19] Kilulya, K., Msagati, T.M., Mamba, B., Ngila, J.C., and Bush, T. (2012). Ionic Liquid–Liquid Extraction and Supported Liquid Membrane Analysis of Lipophilic Wood Extractives from Dissolving-Grade Pulp. *Chromatographia* 75, 513-520.

Dissolution and Hydrolysis of Lignocellulosic Biomass using Tailored Ionic Liquids

Yue Dong, Jana Holm and Ulla Lassi

Additional information is available at the end of the chapter

<http://dx.doi.org/10.5772/59049>

1. Introduction

Over the course of the last few decades, the growing demand for energy globally has a wide range of problems associated with it. Anthropogenic emission of greenhouse gases is the severest among these. An increase of carbon dioxide (CO₂) released by burning fossil carbon contributes significantly to the greenhouse effect. Much discussion of limiting CO₂ emission, using renewable energy, generating energy from alternative renewable sources and waste is the primary subject at present [1].

The international Energy Agency (IEA) has reported, approximately 10% of the world's total primary energy supply was biomass-based energy in 2009 [2]. The European Commission aim is to receive 20% of the total energy in the EU from renewable sources (wind, solar and hydropower as well as geothermal energy and biomass) by 2020 [3]. The European Network of Transmission System Operators (ENTSO) expects through The ENTSO-E Ten-Year Network Development Plan (TYNDP) 2014, the total electricity consumption in 34 European countries will integrate up to 60% of renewable energy [4].

The term "biomass" refers to the abiotic organic matter and the living plants that store energy through photosynthesis. Biomass is one of the most plentiful and common utilized sources that is used to generate renewable energy in the world. Biomass-based energy is considered as CO₂ neutral based on the life cycle assessment (LCA) and carbon dynamics in the biosphere. Therefore, biomass-based energy plays an important role in carbon mitigation, especially in the replacement of fossil fuels [5] [6].

Significant research has been made on the conversion of lignocellulosic biomass to biofuel as an alternative replacement of transportation fuel, due to its abundance and low cost. There are three major stages in conventional production of biofuel from lignocellulosic biomass: i)

delignification (pretreatment), ii) hydrolytic depolymerisation (hydrolysis) and iii) fermentation. The amount of sugar that is produced in the former two steps affects the amount of produced biofuel in the latter fermentation process. The pretreatment of lignocellulose is, therefore, an essential step in improving the production of biofuel [7] [8].

Cellulose is an abundant renewable polymer that exists readily in nature, typically combined with lignin and hemicellulose in the cell walls of lignocellulosic biomass. The conception of pretreatment of lignocellulosic biomass is to reduce the crystallinity of cellulose and increase the porosity of biomass so that expanding the accessible surface area of cellulose for hydrolysis. The challenging pretreatment of using available cellulose involves its dissolution [9] [10].

Numerous studies have argued that the dissolution of lignocellulosic biomass with imidazolium-or pyridinium-cation and anions like Cl⁻, Br⁻, [OAc]⁻ and [CH₃CH₂PO₂]⁻-based ionic liquids (ILs), such as 1-Butyl-3-methylimidazolium Chloride ([BMIM]Cl) and 1-Allyl-3-methylimidazolium chloride ([AMIM]Cl) would significantly improve sugar conversion in the depolymerisation step [8] [11]. Recently, novel ILs that are especially tailored to combine dissolution and hydrolysis of lignocellulosic biomass simultaneously brings the utilization of lignocellulose to a new scenario.

2. Lignocellulosic biomass

Lignocellulosic biomass accounts for 50% of the world's biomass, such as residues of forest and agriculture, grass and municipal solid waste. It represents an abundant carbon source that stores sunlight energy through photosynthesis. Currently, biomass is the biggest source provider of renewable energy, in all 28 EU countries (See Figure 1) [12] [13].

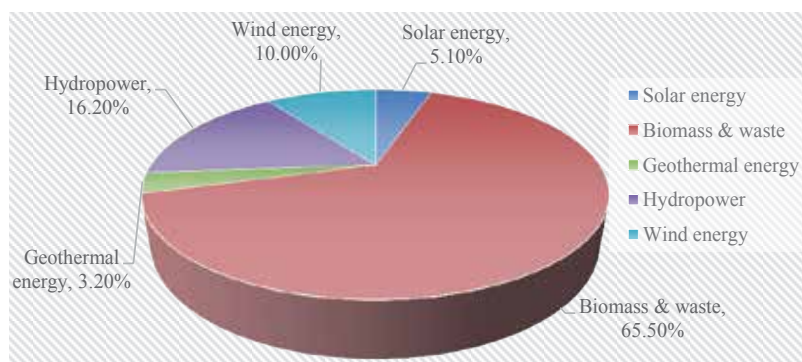


Figure 1. Primary production of renewable energy in the European Union, 2012 [12].

Figure 2 shows the growth of final renewable energy consumption and the renewable energy generated from biomass, wind and solar in all 28 EU countries in the last 12 years. Biomass currently plays a dominant role in renewable energy production and the growth of biomass demand is expected to increase as much as 50% of current demand within the next decade [12].

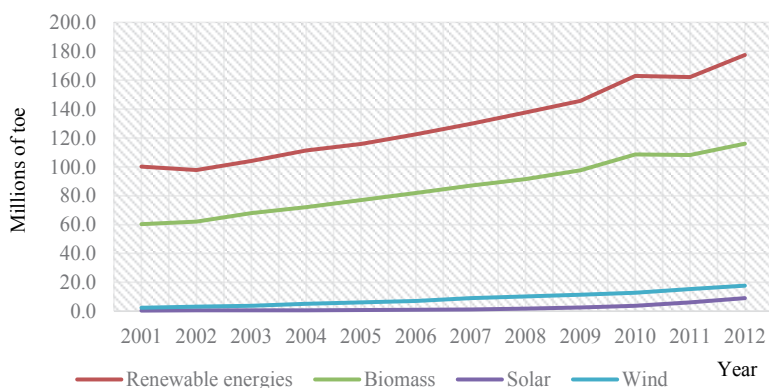


Figure 2. Final renewable energy consumption and renewable energy generated from biomass, solar and wind in all 28 EU countries 2001-2012 [12].

Cellulose (the most abundant organic polymer in terrene), hemicellulose and lignin are the three major organic components that constitute the general rigid structure of lignocellulosic biomass. In general, lignocellulosic biomass contains 30-50% of cellulose by mass, 15-35% of hemicellulose, 10-30% of lignin and small amounts of pectins, starches, extractives, sugars and proteins [8] [14].

Cellulose is a natural linear homopolysaccharide of β -1,4-linked anhydro-D-glucose which accounts for a large proportion of plant biomass. Pure cellulose has crystalline and amorphous regions and is composed of 7000 to 15000 linked glucose ($C_6H_{10}O_5$) monomers. Due to hydrogen bonding between hydroxyl groups and oxygen atoms, cellulose chains form microfibril which further forms cellulosic fiber (See Figure 3 and Figure 4). Approximately 95% of wood derived cellulose is used in papermaking while cellulose derivatives, mainly ethers and esters are also modified in a large-scale [10] [14] [15].

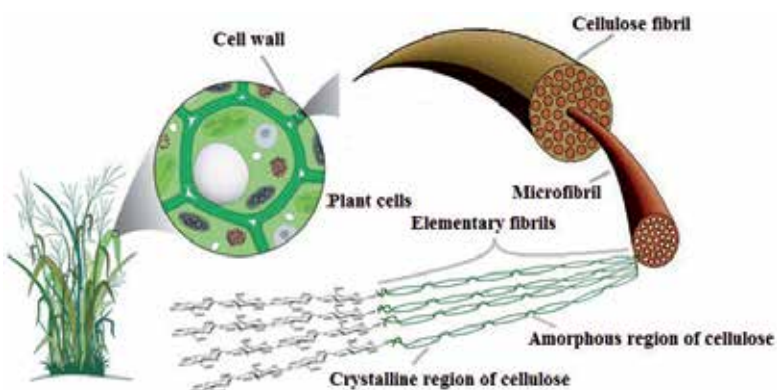


Figure 3. Cellulosic fiber structure with emphasis on the cellulose microfibril adopted and redrawn from Quiroz-Castañeda and Folch-Mallol and Lavoine, et al [16] [17]

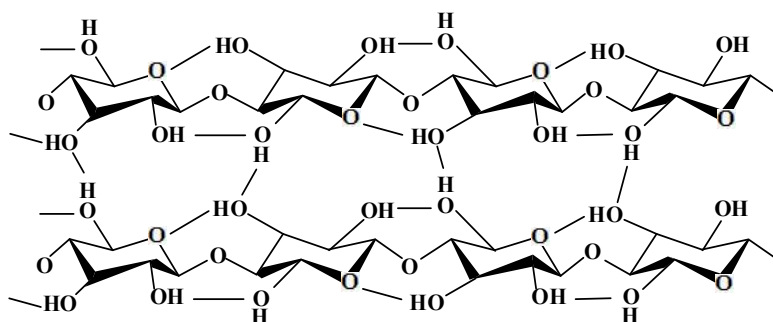


Figure 4. Intra- and intermolecular hydrogen bonds in cellulose redrawn from Pinkert et al. [18].

Cellulose has an amphiphilic property, which has become a more recent perspective highlight in the dissolution of lignocellulosic biomass. Three hydroxyl groups are located on the equatorial positions of the glucopyranose ring which causes the hydrophilic character of cellulose. Whereas, a hydrophobic character is observed on the axial direction since the hydrogen atoms of C-H bonds are located axially (See Figure 5). Cellulose molecules therefore have an intrinsically structural anisotropy [10] [19] [20] [21].

Bergensträhle et al. have estimated the contributions of both hydrophobic stacking and hydrogen bonding to the insolubility of crystalline cellulose by calculating the potentials of mean force for separating the short cellulose oligomer in an aqueous solution through molecular dynamic simulations [22]. A significant hydrophobic pairing energy was found to favor a crystal-like association of cellulose oligomers over solution. Furthermore, the magnitude of hydrophobic pairing energy was estimated to be much higher than that of the hydrogen bond contribution [19] [21] [22].

As discussed above, hydrogen bonding and hydrophobic interactions are the major forces to have influence on both the interactions and solubility of cellulose. However, most of the time hydrophobic interactions are neglected [19] [21] [22].

In contrast to cellulose, the hemicellulose fraction of lignocellulosic biomass is an amorphous heterogeneous polymer which comprises of five and six carbon sugars, abundant D-xylose, L-arabinose, D-galactose, D-glucose and D-mannose monomers. Hemicellulose is characterized as a non-bonding steric repulsion and consequently it is more reactive than hydrogen bonded cellulose. In the cell wall, hemicellulose interlaces with cellulose fibers and keeps microfibrils separate (See Figure 6) [14] [23] [24].

The main non-carbohydrate component of lignocellulosic biomass, lignin, is usually a highly branched aromatic polymer, which has a random complex and cross-linked network structure. The basic building blocks of lignin are *o*-coumaryl alcohol, coniferyl alcohol and sinapyl alcohol. The unmodified structure of lignin is therefore not well defined. Lignin fraction of lignocellulosic biomass is usually found in plant cells and is always associated with hemicellulose by covalent bonds. In a rigid three-dimensional structure of the cell wall, lignin works as cement in cross-linking cellulose and hemicellulose. Hemicellulose and cellulose are

shielded by lignin from, such as enzymatic and chemical degradation. Thus, the major barrier of utilizing lignocellulosic biomass more widely in energy is its strong structure. To achieve this, its structure can be broken through dissolution to further dissolve cellulose and hemicelluloses [14] [26] [27].

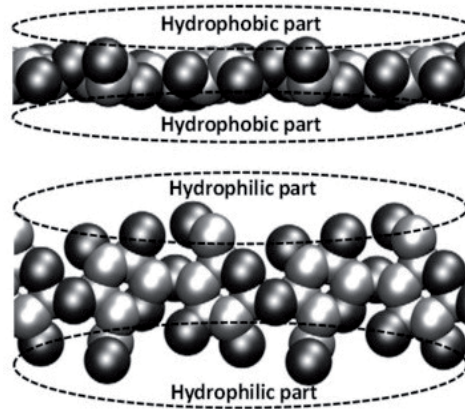


Figure 5. Hydrophilic and hydrophobic parts in cellulose molecules adopted from Medronho et al. [21].

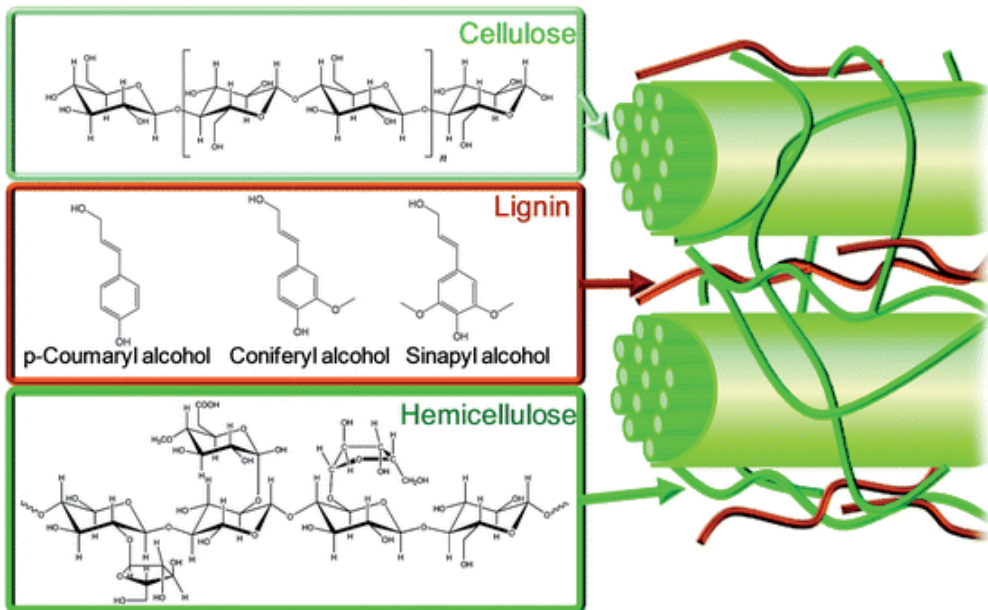


Figure 6. Lignocellulosic biomass structure adopted from Alonso, et al. [25]

3. Ionic liquid

Ionic liquids (ILs) are traditionally defined as liquids that consist exclusively or almost exclusively of ions as well as molten salts or fused salts. In contrast to molten salts, ILs have lower melting points. Hence, ILs are more or less defined as salts that have melting points below the boiling point of water (100°C). Aqueous solutions of salts are not classified as ILs due to the purity of ions. [28].

ILs are usually comprised of organic cations and organic or inorganic anions. Due to the existence of a bulky and asymmetrical cation structure in ILs, there is a low tendency for ILs to crystallize. Since the properties of ILs can be tailored for a particular need, ILs are also known as “designer solvents” or “task-specific ionic liquid” (TSIL) [29] [30].

In general, it is possible to tailor the properties of ILs with almost infinite combinations of suitable cations and anions. For instance, anions are responsible for such qualities such as air and water stability while cations are responsible for organic solubility and melting temperature. Figure 7 and Figure 8 represent the structures of commonly used cations and suitable anions. In comparison to volatile organic compounds (VOCs), ILs are considered as remarkable “greener” solvents in chemical processes, due to, for instance, their high thermal stability, negligible vapour pressure and their ability to remain in a liquid form over a wide temperature range. However with an increase of research on the utilization and toxicity of ILs, these “greener solvents” have been questioned. [29] [30].

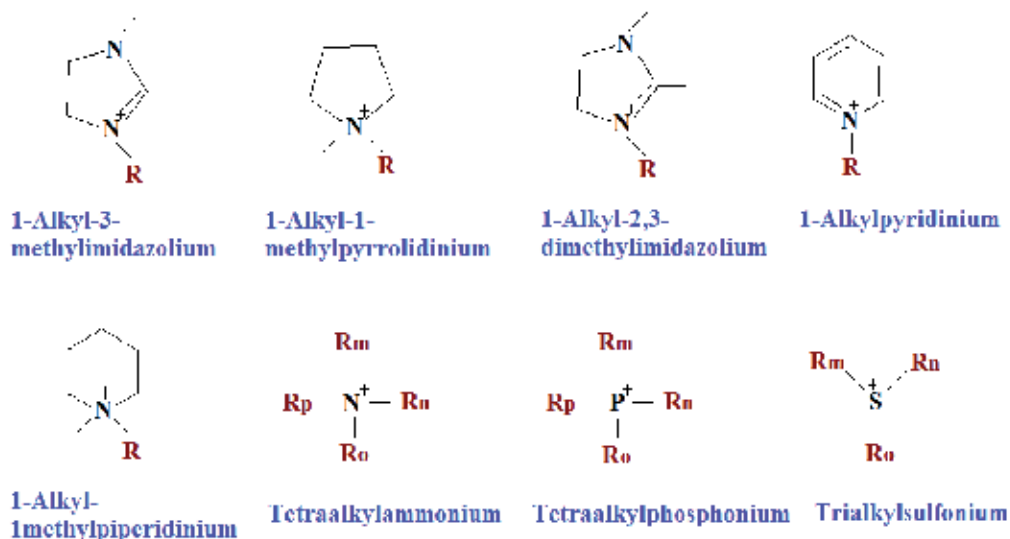
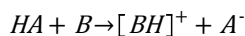


Figure 7. Commonly used cations in modern ionic liquids redrawn from Brandt, et al. [31].

For the commonly used ILs, it is possible for them to be classified as two groups based on their cation structures: aprotic (AILs) and protic (PILs) ionic liquids. PILs can be easily synthesized by the transfer of a proton from an acid which can donate a proton (Brønsted acid HA) to a base which can accept a proton (Brønsted base B):



The reaction shows the basic formation of PIL through proton transfer from a Brønsted Acid (A) to a Brønsted Base (B). PILs do not necessary contain entirely of ions, for instance, a small amount of molecular species c can be found in PILs, due to the incomplete proton transfer [28] [32].

AILs have been used as “classic” or “conventional” ILs for more than a decade. The main difference between AILs and PILs is that AILs are not protonated but based on substitution [29] [33] [34].

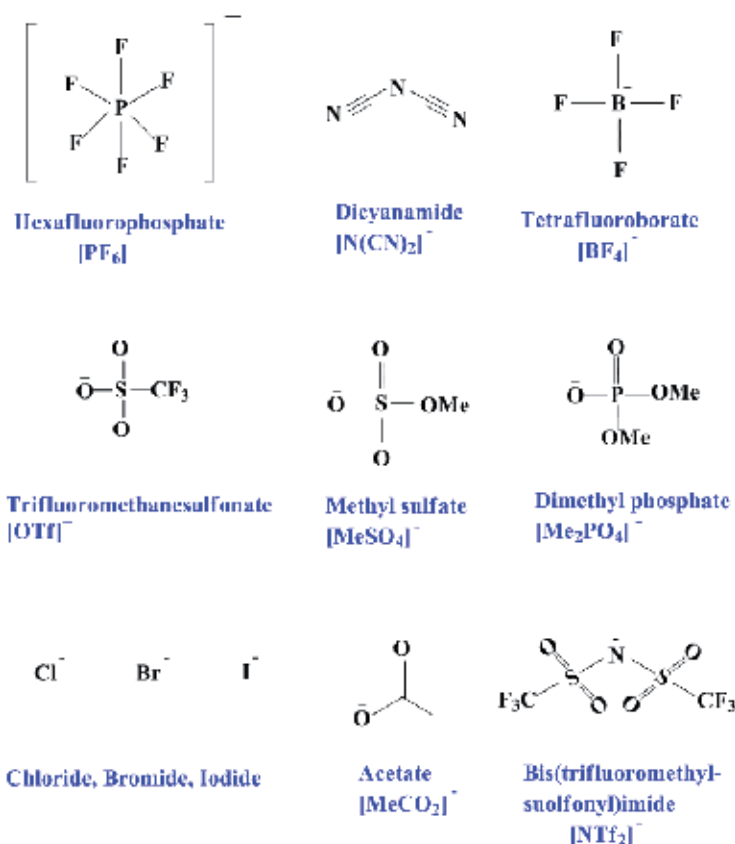
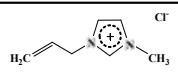
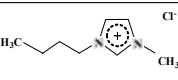
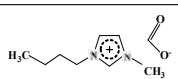
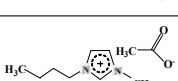
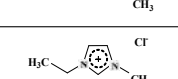
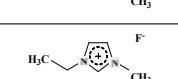
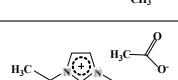
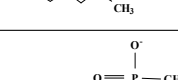
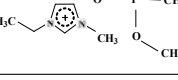
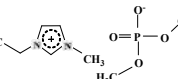
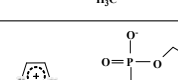
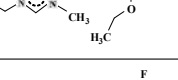


Figure 8. Commonly used anions in modern ionic liquids redrawn from Brandt, et al. [31].

In dissolving lignocellulosic biomass, the dissolution of the major component, cellulose, is mostly discussed, due to its structure and abroad applications. Imidazolium-or pyridinium-cation and anions like Cl⁻, Br⁻, [OAc]⁻ and [CH₃CH₂PO₂]⁻-based ILs have been identified as a good combination in dissolving cellulose. Table 1 lists some of the tested ILs used in cellulose dissolution and their dissolving abilities [8] [11].

Regarding dissolution of hemicellulose and lignin, no great differences from dissolution of cellulose are expected. However, the efficiency of lignin dissolution is not as good compared to cellulose dissolution [8] [11] [35].

	Ionic Liquid	Substrate	Solubility wt/wt	T (°C)	Structure of ionic liquid	Ref.
1	[AMIM]Cl	Cellulose (Avicel)	9%	120		[36]
		Cellulose (Pulp)	14%	80		[37]
2	[BMIM]Cl	Cellulose (Avicel)	13%	110		[38]
		Cellulose (Pulp)	18%	83		[39]
3	[BMIM][HCOO]	Cellulose (Avicel)	8%	110		[40]
4	[BMIM][OAc]	Cellulose (Avicel)	12%	100		[41]
6	[EMIM]Cl	Cellulose (Avicel)	12%	80		[42]
7	[EMIM][F]	Cellulose (Avicel)	2%	100		[41]
8	[EMIM][OAc]	Cellulose (Avicel)	15%	110		[40]
		Cellulose (Avicel)	5%	90		[43]
9	[EMIM][MePO ₃ Me]	Microcrystalline cellulose	10%	45		[44]
10	[EMIM][(MeO) ₂ PO ₂]	Microcrystalline cellulose	10%	65		[44]
11	[EMIM][(EtO) ₂ PO ₂]	Cellulose (Avicel)	12-14%	100		[41]
12	[EMIM][BF ₄]	Cellulose (Avicel)	Insoluble	90		[43]
13	[HexMIM][Cl]	Cellulose (Avicel)	5%	50		[43]
		Cellulose (Avicel)	7%	100		[45]

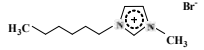
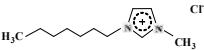
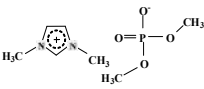
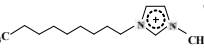
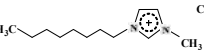
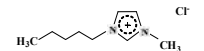
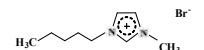
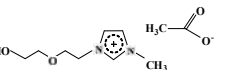
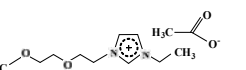
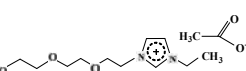
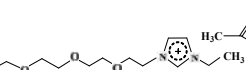
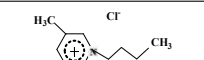
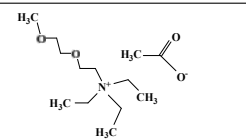
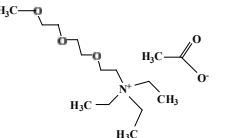
Ionic Liquid	Substrate	Solubility wt/wt	T (°C)	Structure of ionic liquid	Ref.
14 [HexMIM][Br]	Cellulose (Avicel) 1-2%		100		[41]
15 [HepMIM][Cl]	Cellulose (Avicel) 5%		100		[45]
16 [MMIM][(MeO)2PO2]	Cellulose (Avicel) 10%		100		[41]
17 [NMIM][Cl]	Cellulose (Avicel) 2%		100		[45]
18 [OMIM][Cl]	Cellulose (Avicel) 4%		100		[45]
19 [PeMIM][Cl]	Cellulose (Avicel) 1%		100		[41]
20 [PeMIM][Br]	Cellulose (Avicel) 1-2%		100		[41]
21 1-(3,6-dioxahexyl)-3-methylimidazolium acetate	Cellulose (Avicel) 5%		110		[40]
22 1-ethyl-3-(3,6-dioxaheptyl)imidazolium acetate	Cellulose (Avicel) 12%		110		[40]
23 1-ethyl-3-(3,6,9-trioxadecyl)imidazolium acetate	Cellulose (Avicel) 12%		110		[40]
24 1-ethyl-3-(3,6,9,12-tetraoxatridecyl)imidazolium acetate	Cellulose (Avicel) 10%		110		[40]
25 [3MBPy][Cl]	Cellulose (Pulp) 39%		105		[46]
26 N,N,N-triethyl-3,6-dioxaheptylammonium acetate	Cellulose (Avicel) 10%		110		[40]
27 N,N,N-triethyl-3,6,9-trioxadecylammonium acetate	Cellulose (Avicel) 10%		110		[40]

Table 1. Commonly tested ionic liquids in cellulose dissolution and their dissolving capacities.

4. Dissolution of lignocellulosic biomass in an ionic liquid

4.1. Aim of dissolution

Different types of lignocellulosic biomass contains different components of cellulose, hemicellulose, lignin and other extractives. However, the three major components are cellulose, hemicellulose and lignin. In any lignocellulosic biomass, cellulose is present in the form of amorphous and crystalline structures. The form of crystalline cellulose in a cell wall is tightly packed and highly resistant to chemical and biological hydrolysis, due to a complex biopolymeric network [9] [10].

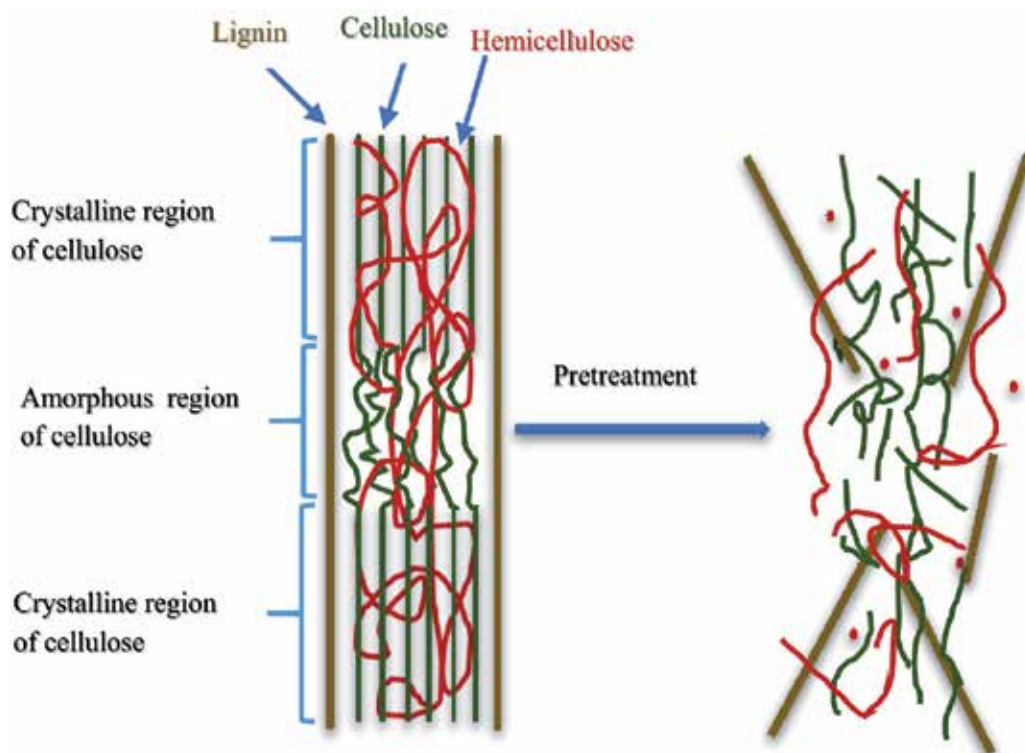


Figure 9. Pretreatment of lignocellulosic biomass redrawn from Holm and Lassi [8].

Cellulose has a clear amphiphilic nature and it is insoluble in common aqueous or organic solvents, though polysaccharide is soluble. The hydrophobicity of crystalline cellulose forms, together with acid, a dense layer of water on the hydrated cellulose surface, which resists to further acidic hydrolysis. The strong intra- and intermolecular hydrogen bonding network in crystalline cellulose obstructs enzymatic hydrolysis, whereas amorphous hemicellulose and cellulose are possibly hydrolyzed. Thus, many applications of cellulose can be applied through its dissolution to break the intra- and intermolecular hydrogen bond network, in order to

increase the active accessible surface area of cellulose (See Figure 9). Other minor factors of interactions among cellulose molecules have been mostly ignored [9] [10].

5. Anion and cation of ionic liquids and effects on dissolution of cellulose

The design of ILs for a specific application is critical to determine the properties of an IL. One of the extraordinary features of ILs is their wide adjustable properties, such as the variations of acid-base character, hydrophilicity and melting temperature. Designing properties and trends of ILs can be achieved by modifying cation and anion independently. However, the impurities, like water, halide anions and organic bases that are mainly from preparations of ILs, may have an effect on the properties as well, which might lead to an unexpected side reaction [18] [47] [48].

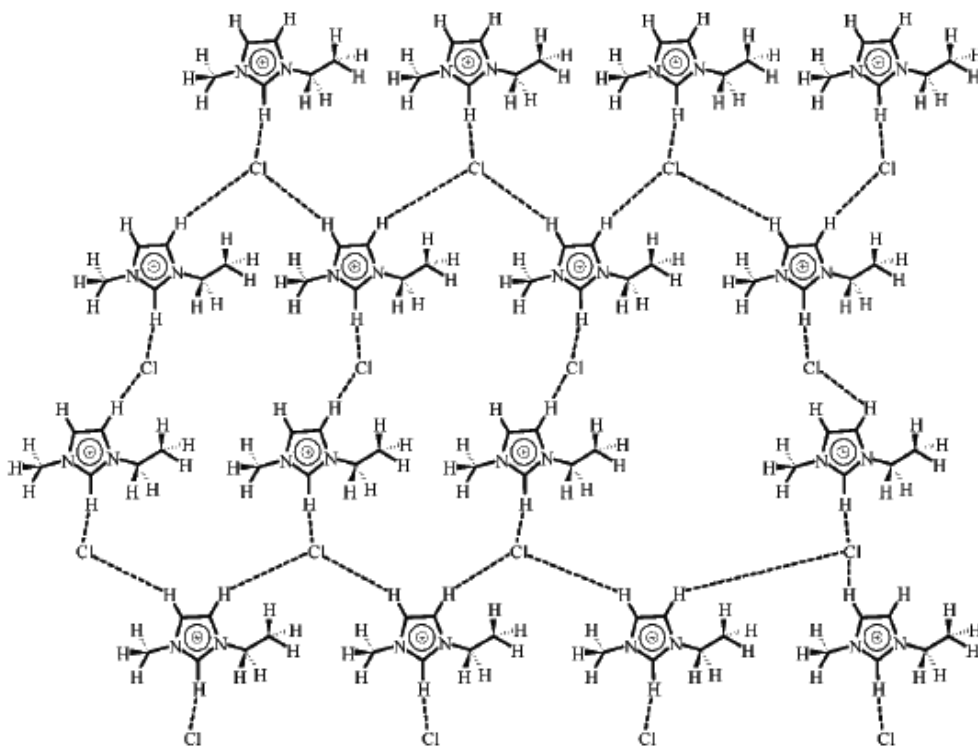


Figure 10. Schematic representation of hydrogen bonding in [EMIM]Cl adapted from Heinze, et al. [46]

The structure of IL is the critical factor that influences the outcome of the dissolution. As known, ILs consist of anion and cation, and both can be varied, in order to provide different functions of ILs. The size, symmetry, hydrogen bond interactions and charge delocalization

of ILs judge van der Waals force and electrostatic interaction which govern the thermal properties of ILs. Anion type shows greater significant effects on the melting temperature and viscosity of ILs than cation. Recently, many researches have pointed out that dissolution in ILs is driven mainly by the formation of hydrogen bonds between cellulose and anions and hydrophobic interactions with cations. The reduction of anion size leads to the increase of the melting point of IL, due to the increase of the Coulombic attraction contributions to the lattice energy of the crystal and of the covalency of the ions. Hydrogen bonds that are present or absent in ILs influence the melting temperature as well. In addition, greater charge delocalizations can be caused by larger anions. The symmetry of the ions also have a direct relationship to the melting points. Reducing symmetry in the ions reduces the melting points and therefore, lowers the freezing point of ILs [18] [49] [50].

Similarly to many solvents, the viscosities of many ILs strongly depend on temperature. Nevertheless, anion and cation properties, such as the anion's ability of forming weak hydrogen bonds with a cation, and the impurities in the ILs also vary the viscosity. Mantz et al. have described that a series of non-haloaluminate ILs have the same cation, but with changes in the anion, the viscosity can be clearly effected, however, not according to the size of the anions. Conversely, for ILs with the same anion, but different cations, the larger the cation size, the greater the viscosity. Another contributing factor on the effect of viscosity is the asymmetric substitution of a cation. It has been identified as a highly asymmetric substitution obtaining a low viscosity IL [51]. The low viscosity of an IL identifies high mobility of ions which promote the dissolution process [10] [52] [53].

The solubility of water in ILs can be varied by changing cation substitution and anion types present in ILs. Generally, coordinating anions relate to the miscibility of ILs with water and conversely, large, non-coordinating, charge-diffuse anions produce hydrophobic ILs. As organic solvents, ILs usually appear with high polarity, due to their ionic nature and respect to organic solutes. Lignocellulosic biomass can be dissolved in ILs while the solubility of cellulose increases in more polar ILs. The interactions between solvent and solute are greater when the ILs have a better hydrogen bond acceptor capability, such as chloride. ILs become more lipophilic with increasing alkyl substitution to reduce further the Coulombic ion-ion interactions, resulting in an increasing solubility of hydrocarbons and non-polar organics [54].

Up to now, it has been reported that the ILs' ability of dissolving cellulose is governed by the interactions between anion and oligomers, although cations are of minor influence. Therefore, theoretically, good hydrogen bond accepting anions bring better influence in the dissolution of cellulose. Figure 10 demonstrates the strong hydrogen bonded network of [EMIM]Cl that are formed by three imidazolium ring protons in three dimensions. Whereas pairing with certain cations can also create negative effects [10] [52] [53].

6. Effect of water in an ionic liquid

Water always exists in ILs, even in a neat IL. The role of water in an IL is rather complex. It is considered as an impurity, which influences the properties of ILs. Stark, et al. reported that a

hydrogen bonding network exists in a 'neat' IL due to the interactions between cations and anions [55] [56] [57].

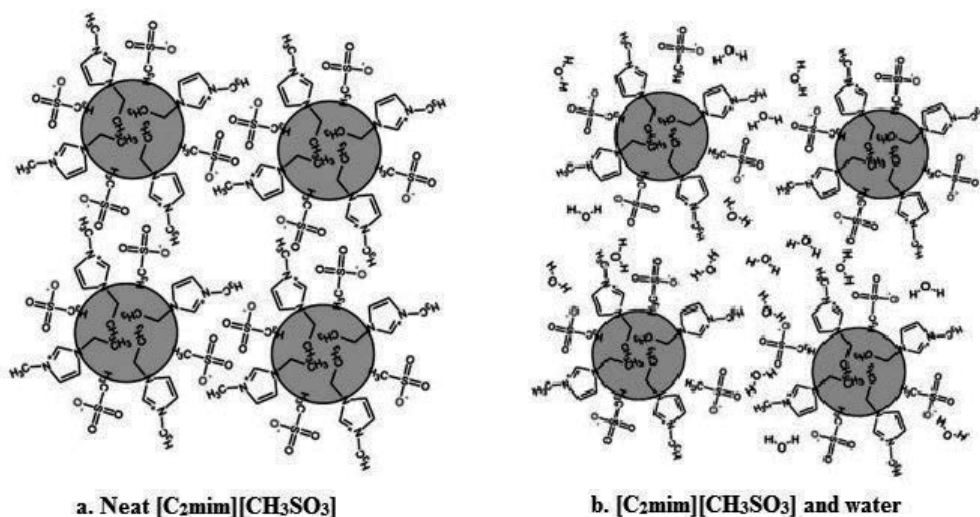


Figure 11. Graphical representation of the structural domains of [C₂mim][CH₃SO₃] and its mixtures with water (tail-tail aggregates, water–anion hydrogen-bonding) adopted from Stark [56].

Depending on the properties of anions and cations in an IL, water can have either positive or negative effects in the utilization of ILs. Figure 11a illustrates that in [C₂mim][OAc] cations' ring plane a cation interacts with several anions to form a hydrogen bonding network [55] [56] [57].

When water is added into the IL, the order of the cation–anion hydrogen bonding network is disturbed. A strong hydrogen bond acceptor [OAc] is disrupted which interacts with water and becomes tightly incorporated into the hydrogen bond network of water. Hence, the amount of water in [C₂mim][OAc] reduces the ability of interactions between ions and cellulose (See Figure 11b) [55] [56] [57].

7. Methods and considerations of cellulose dissolution using a tailored ionic liquid

The conversion of lignocellulosic biomass to biofuel as an alternative replacement of transportation fuel can be proceeded through dissolution, hydrolysis and fermentation processes. Dissolution plays a major role among these steps and such methods have been previously discussed. The dissolution of lignocellulosic biomass breaks down intra-and intermolecular hydrogen bonds, which mainly increases the accessible surface area of cellulose for further hydrolysis [9] [10].

Tailored ILs refer to the ILs that are designed for specific needs. In our early research, three ILs (See Figure 12) were tailored to combine dissolution and hydrolysis of cellulose in a single step (See Figure 13). As can be seen in Figure 12, besides common properties of ILs, these tailored ILs also provide an acidic nature, which can simultaneously dissolve and acid hydrolyze lignocellulosic biomass. Similar to the ILs that are used in lignocellulosic dissolution, it is possible for tailored ILs to be recycled and reused again, based on our previous study, but more research is required.

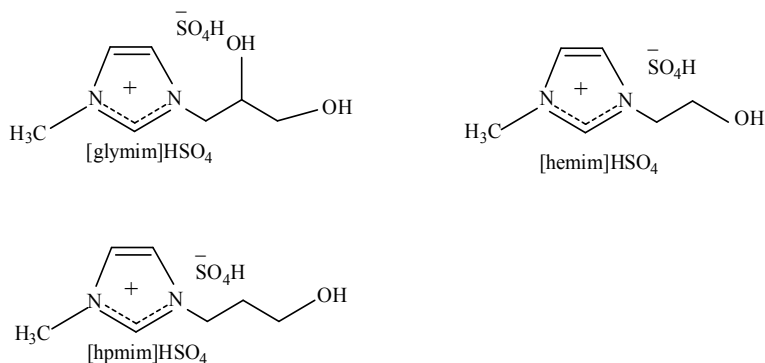


Figure 12. Structures of tailored ionic liquids, [glymim]HSO₄, [hemim]HSO₄ and [hpmim]HSO₄.

Fiber sludge is a by-product from chemical pulping, which was used as the cellulose sample. According to chemical analysis, fiber sludge contained a mass fraction of approximately 93-94% cellulose and 6-7% hemicelluloses of total carbon materials. In addition, water content in fiber sludge is around 53% of the total mass.

The method is rather similar to conventional dissolution of lignocellulosic biomass. Besides dissolution of cellulose, cellulose is hydrolyzed simultaneously (See Figure 14). Thus, the regenerated cellulose solution (Figure 14, right) consists of reducing sugars, tailored IL, anti-solvent and regenerated cellulose. Based on the DNS method, the total reducing sugar yield was measured which indicated that approximately up to 30% of the dry mass sample was converted to sugars.

A couple of factors influence the outcome of lignocellulosic biomass pretreatment with ILs. Certainly, the type of lignocellulosic biomass and IL are key considerations. The temperature and reaction time should be controlled accordingly. The temperatures of typically used ILs in lignocellulosic biomass pretreatment are between 70 and 150°C, with reaction times from 20 mins up to 15 hours. It is suggested that the temperature of dissolution should be controlled approximately 10°C above the melting point of the IL. Too long a dissolution time and high temperature runs the risk of degradation [18].

The production of derivatives are also possible as a by-product due to the unexpected side reactions caused by impurities in ILs or feedstock [18]. In our early research, a gel formed during the reaction and it is thought that the gelation is possibly caused by methylcellulose

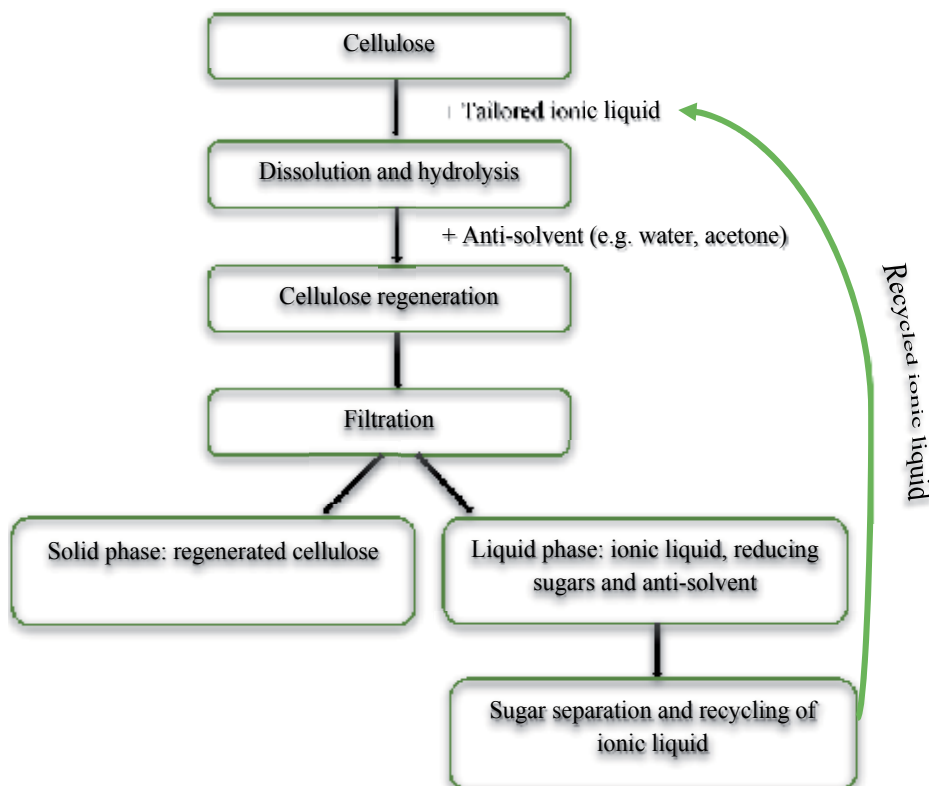


Figure 13. Fractionation scheme in one-step dissolution and hydrolysis of cellulose in a tailored ionic liquid.

that is a derivative of cellulose. In the pulp mill industry, pulp is soaked and cooked in a solution of sodium hydroxide (NaOH) for softening before the resulting pulp is subjected to further processes. Fiber sludge, the residual from a pulp mill, consists of hydroxyl groups and was rapidly dissolved in the ILs. This resulted in methylcellulose as the by-product in the substitution reaction by replacing hydrophilic hydroxyl groups (-OH) with hydrophobic methoxide groups (-OCH₃) [58] [59] [60]. Based on the experimental data, it is reasonable to believe that the impurities in the ILs had a side reaction with the fiber sludge and produced methylcellulose. Methylcellulose has thermo-sensitive properties that allow it to be dissolved in water at low temperature (approximately under 40°C) and it displays reversible gelation at a particular temperature [61] [62] which may block further reactions.

According to the experimental results, cellulose dissolution using tailored ILs with a certain amount of water gave higher yields of reducing sugars. Interestingly, the amount of water in ILs also improved the efficiency of cellulose dissolution. Figure 15 presents images of filtrated regenerated cellulose after dissolution (filter paper) with (right) and without (left) water in a tailored IL. Almost no cellulose dissolution could be found in cellulose without water (Figure 15 left), but significant dissolution occurred when additional water was added (Figure 15 right).



Figure 14. One-step dissolution and hydrolysis of fiber sludge (left) using tailored ionic liquid (middle, tailored IL and fiber sludge) and regeneration of cellulose (right).

Presumably, the hydrophilic and hydrophobic parts of cellulose adjusted their conformation in water while the contacts between hydrophobic parts and water was reduced [48]. It is possible the IL in water disassociated and weakened the hydrophobic interactions in cellulose. The anion of HSO_4^- can also be further disassociated in water and provide H^+ in hydrolysis.



Figure 15. Filtrated regenerated cellulose (dry filter paper) after dissolution of cellulose with (right) and without (left) water in a tailored ionic liquids.

8. Cellulose regeneration

The shape of regenerated cellulose depends on the method and conditions of regeneration. Typically, the dissolved cellulose is precipitated in a polar anti-solvent, such as water, ethanol and acetone however distilled water is often preferred for clear economic reasoning. When the crystalline cellulose is broken down, the regenerated cellulose is usually in the form of amorphous and cellulose II. [11] [18].

There have been a significant number of studies published on the dissolution of cellulose in an IL, however, only a few of these discussed the mechanism of cellulose regeneration. The mechanistic understanding of the interactions between an IL, water and cellulose still remains

elusive. For example, Liu, et al. used molecular dynamics simulations to study the structural and dynamic properties of water, IL and cellulose in cellulose regeneration [11].

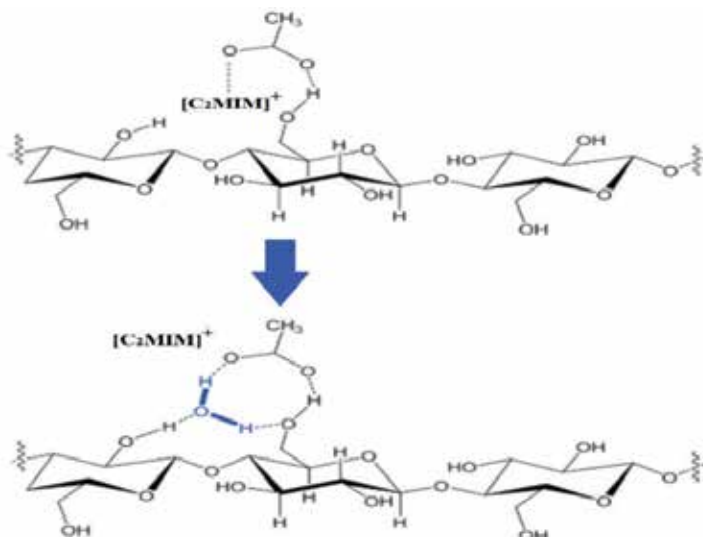


Figure 16. Intermediate structure of cellulose regeneration from [C₂MIM][OAc] in water adopted from Liu, et al. [11]

It has been proposed that the regeneration of cellulose should go through a key intermediate process due to the strong ion-ion interaction between cation and anion in the IL. The number of hydrogen bonds among water molecules and polymer increases and form an anion-water-cellulose hydrogen bonding network, when water diffuses inside the first solvation shell of cellulose. Presumably, water forms hydrogen bonds with cellulose and acts as both a hydrogen bond donor and a hydrogen bond acceptor, which displaces cation out of the first solvation shell to the second solvation shell. However, existing anions in the second solvation shell bond displaces cations in the second solvation shell through strong electrostatic interactions. The hydrogen bonds' bonded anions are liberated from dissolved cellulose into the water solution, because the hydrogen bonds are pushed out to the first solvation shell. The formation of this new hydrogen bonding network finally leads to cellulose precipitation [11].

9. Conclusion

The major barrier in many applications of lignocellulosic biomass is the crystal-like structure and solubility of cellulose for water, acid or enzymes. With a good understanding of the lignocellulose's structure, the solubility of cellulose is mainly affected by intra- and intermolecular hydrogen bonds in cellulose and hydrophobic interactions. Hydrophobic interactions have shown a significant contribution on the solubility of cellulose, as well as on its crystal-

like structure, that is even stronger than hydrogen bonding. Hydrophobic interaction is, therefore, a perspective highlight in lignocellulosic biomass dissolution.

Cellulose has an intrinsic structural anisotropy which shows an amphiphilic nature, due to the intra-and intermolecular hydrogen bonding. It is reasonable to think that an amphiphilic IL would facilitate the dissolution of cellulose.

The properties of ILs can be designed for specific lignocellulosic biomass by carefully choosing suitable cations and anions. Based on the ILs' properties, water may promote or obstruct the dissolution. In our research, we have tailored three types of acidic ILs to perform dissolution and hydrolysis in a single step, and the total reducing sugar yield in the regenerated cellulose solution was calculated, up to 30% of the dry mass, based on the DNS method. The water content in tailored ILs is not as critical as in usual ILs in dissolution, due to the simultaneous hydrolysis reaction.

The mechanistic understanding of interactions between IL, water and cellulose has been barely discussed, however, water as an anti-solvent, is also expected to play an important role in cellulose regeneration. According to molecular dynamics simulations, a key intermediate process between cation and anion in the IL is performed.

Clearly, tailored ILs can be used in an one-step dissolution and hydrolysis of lignocellulosic biomass. This is especially the case for wet lignocellulosic biomass which can be directly used in tailored ILs that also differ from general ILs. The existing impurities in ILs or substrates can cause side reaction in dissolution, which may obstruct or promote further reaction. A longer reaction time could cause sugar degradation in tailored ILs.

Acknowledgements

This work has been carried out within the Forest Refine project (EU Interreg funding 00162639) which is gratefully acknowledged.

Author details

Yue Dong^{1,2*}, Jana Holm³ and Ulla Lassi^{1,2}

*Address all correspondence to: yue.dong@chydenius.fi

1 University of Oulu, Department of Chemistry, University of Oulu, Finland

2 University of Jyväskylä/Kokkola University Consortium Chydenius, Kokkola, Finland

3 Centria University of Applied Sciences, Kokkola, Finland

References

- [1] Fricke J, Borst WL. Essentials of energy technology sources, transport, storage, conservation. 1st ed. Weinheim: Wiley-VCH Verlag & Co. KGaA; 2013. p. 1-9.
- [2] International energy agency's renewable energy division, (RED). Technology road-map bioenergy for heat and power. 2012. p. 10-16.
- [3] Directive 2009/28/EC. Directive 2009/28/EC of the European parliament and of the council on the promotion of the use of energy from renewable sources and amending and subsequently repealing Directives 2001/77/EC and 2003/30/EC. OJ 2006 Jun: L140/16-62.
- [4] Regulation (EU) No 347/2013. Regulation (EU) No 347/2013 of the European parliament and of the council on guidelines for trans-European energy infrastructure and repealing decision No 1364/2006/EC and amending regulations (EC) No 713/2009, (EC) No 714/2009 and (EC) No 715/2009. OJ 2013 Apr: L115 39-75.
- [5] Nomiya T, Aihara N, Chitose A, Yamada M, Tojo S. Biomass as local resource. In: Tojo S, Hirasawa T, editors. Research approaches to sustainable biomass systems, Waltham, USA: Academic Press; 2014. p. 7-16.
- [6] Cherubini F, Guest G, Strømman AH. Bioenergy from forestry and changes in atmospheric CO₂: Reconciling single stand and landscape level approaches. J Environ Manag 2013 Nov; 129: 292-301.
- [7] Singh R, Shukla A, Tiwari S, Srivastava M. A review on delignification of lignocellulosic biomass for enhancement of ethanol production potential. Renew Sustain Energy Rev 2014 Apr; 32: 713-728.
- [8] Holm J, Lassi U. Ionic liquids in the pretreatment of lignocellulosic biomass. In: Koronin A, editor. Ionic liquids application and perspectives Rijeka: InTech; 2011. p. 545-560.
- [9] Behera S, Arora R, Nandhagopal N, Kumar S. Importance of chemical pretreatment for bioconversion of lignocellulosic biomass. Renew Sustain Energy Rev 2014 Aug; 36: 91-106.
- [10] Medronho B, Lindman B. Brief overview on cellulose dissolution/regeneration interactions and mechanisms. Adv Colloid Interface Sci 2014 May (Available online).
- [11] Liu H, Sale KL, Simmons BA, Singh S. Molecular dynamics study of polysaccharides in binary solvent mixtures of an ionic liquid and water. J Phys Chem B 2011 Aug; 115: 10251-10258.
- [12] Eurostat. Renewable energy statistics. 2014 Mar; Available at: http://epp.eurostat.ec.europa.eu/statistics_explained/index.php/Renewable_energy_statistics#Further_Eurostat_information. Accessed July 22nd, 2014.

- [13] Ibraheem O, Ndimba BK. Molecular adaptation mechanisms employed by ethanologenic bacteria in response to lignocellulose-derived inhibitory compounds. *Int J Biol Sci* 2013; 9(6): 598-612.
- [14] Lestander TA. Chemical composition of biomass. In: Bundschuh J, editor. *Biomass as energy source resources, systems and applications* Leiden, the Netherlands: CRC Press/Balkema; 2013. p. 35-56.
- [15] Turley DB. The Chemmical value of biomass. In: Clark JH, Deswarte FEI, editors. *Introduction to chemicals from biomass* New York City, USA: John Wiley & Sons, Ltd; 2008. p. 21-46.
- [16] Lavoine N, Desloges I, Dufresne A, Bras J. Microfibrillated cellulose – Its barrier properties and applications in cellulosic materials: A review. *Carbohydr Polymer* 2012 Oct; 90(2): 735-764.
- [17] Quiroz-Castañeda RE, Folch-Mallol JL. Hydrolysis of biomass mediated by cellulases for the production of sugars. In: Chandel AK, da Silva SS, editors. *Sustainable degradation of lignocellulosic biomass-techniques, applications and commercialization* Croatia: InTech; 2013. p. 119-142.
- [18] Pinkert A, Marsh KN, Pang S, Staiger MP. Ionic liquids and their interaction with cellulose. *Chem Rev* 2009; 102: 6712–6728.
- [19] Medronho B, Romano A, Miguel MG, Stigsson L, Lindman B. Rationalizing cellulose (in)solubility: reviewing basic physicochemical aspects and role of hydrophobic interactions. *Cellulose* 2012; 19: 581–587.
- [20] Lindman B, Karlström G, Stigsson L. On the mechanism of dissolution of cellulose. *J Mol Liq* 2010; 115: 76–81.
- [21] Medronho B, Lindman B. Competing forces during cellulose dissolution: From solvents to mechanisms. *Curr Opin Colloid Interface Sci* 2014; 9(1): 32–40.
- [22] Bergensträhle M, Wohlert J, Himmel M, Brady J. Simulation studies of the insolubility of cellulose. *Carbohydr Res* 2010 Sep; 345(14):2060-2066.
- [23] Gírio FM, Fonseca C, Carvalheiro F, Duarte LC, Marques S, Bogel-Lukasik R. Hemicelluloses for fuel ethanol: a review. *Bioresource Technology* 2010 Jul; 101(13): 4775-4800.
- [24] Alonso DM, Bond JQ, Dumesic JA. Catalytic conversion of biomass to biofuels. *Green Chem* 2010 Dec; 12(9): 1493-1513.
- [25] Alonso DM, Wettstein SG, Dumesic JA. Bimetallic catalysts for upgrading of biomass to fuels and chemicals. *Chem Soc Rev* 2012 Aug; 41(24): 8075-8098.
- [26] Thakur VK, Thakur MK. Processing and characterization of natural cellulose fibers/thermoset polymer composites. *Carbohydr Polymer* 2014 Aug; 109: 102-117.

- [27] Zheng Y, Zhao J, Xu F, Li Y. Pretreatment of lignocellulosic biomass for enhanced biogas production. *Progr Energ Combust Sci* 2014 Jun; 42: 35-53.
- [28] Freemantle M. *An Introduction to ionic liquids*. Cambridge, UK: The Royal Society of Chemistry; 2010. p. 1-10.
- [29] Peric B, Sierra J, Martí E, Cruañas R, Garau MA, Arning J, et al. (Eco)toxicity and biodegradability of selected protic and aprotic ionic liquids. *J Hazard Mater* 2013 Oct; 261: 99-105.
- [30] Mallakpour S, Dinari M. Ionic liquids as green solvents: progress and prospects. In: Mohammad A, Inamuddin, editors. *Green solvent II properties and applications of ionic liquids* Heidelberg: Springer; 2012. p. 1-30.
- [31] Brandt A, Gräsvik J, Hallett JP, Welton T. Deconstruction of lignocellulosic biomass with ionic liquids. *Green Chem* 2013; 15: 550-583.
- [32] Greaves TL, Drummond CJ. Protic ionic liquids: properties and applications. *Chem Rev* 2008; 108: 206-237.
- [33] Peric B, Sierra J, Martí E, Cruañas R, Garau MA. A comparative study of the terrestrial ecotoxicity of selected protic and aprotic ionic liquids. *Chemosphere* 2014 Aug; 108: 418-425.
- [34] Pakiari AH, Siahrostami S, Ziegler T. An insight into microscopic properties of aprotic ionic liquids: A DFT study. *J Mol Struct* 2010 Sep; 955(1-3): 47-52.
- [35] Achinivu EC, Howard RM, Li G, Gracz H, Henderson WA. Lignin extraction from biomass with protic ionic. *Green Chem* 2014; 16(3): 1114-1119.
- [36] Dadi AP, Schall CA, Varanasi S. Mitigation of cellulose recalcitrance to enzymatic hydrolysis by ionic liquid pretreatment. *Biotechnol Appl Biochem* 2007; 137:407-421.
- [37] Zhang H, Wu J, Zhang J, He J. 1-Allyl-3-methylimidazolium chloride room temperature ionic liquid: a new and powerful nonderivatizing solvent for cellulose. *Macromolecules* 2005 Oct; 38(20): 8272-8277.
- [38] Zhao H, Jones CL, Baker GA, Xia S, Olubajo O, Person VN. Regenerating cellulose from ionic liquids for an accelerated enzymatic hydrolysis. *J Biotechnol* 2009; 139: 47-54.
- [39] Heinze T, Schwikal K, Barthel S. Ionic liquids as reaction medium in cellulose functionalization. *Macromol Biosci* 2005; 5(6): 520-525.
- [40] Zhao H, Baker GA, Song Z, Olubajo O, Crittle T, Peters D. Designing enzyme-compatible ionic liquids that can dissolve carbohydrates. *Green Chem* 2008; 10(6): 696-705.
- [41] Vitz J, Erdmenger T, Haensch C, Schubert US. Extended dissolution studies of cellulose in imidazolium based ionic liquids. *Green Chem* 2009; 11(3): 417-424.

- [42] Barthel S, Heinze T. Acylation and carbanilation of cellulose in ionic liquids. *Green Chem* 2006; 8(3): 301-306.
- [43] Zavrel M, Bross D, Funke M, Büchs J, Spiess AC. High-throughput screening for ionic liquids dissolving (ligno-)cellulose. *Bioresource Technology* 2009 May; 100(9): 2580-2587.
- [44] Fukaya Y, Hayashi K, Wada M, Ohno H. Cellulose dissolution with polar ionic liquids under mild conditions: required factors for anions. *Green Chem* 2008; 10(1): 44-46.
- [45] Erdmenger T, Haensch C, Hoogenboom R, Schubert US. Homogeneous tritylation of cellulose in 1-butyl-3-methylimidazolium chloride. *Macromol Biosci* 2007; 7(4): 440-445.
- [46] Heinze T, Dorn S, Schöbitz M, Liebert T, Köhler S, Meister F. Interactions of ionic liquids with polysaccharides – 2: cellulose. *Macromol Symp* 2008; 262: 8-22.
- [47] Freemantle M. An introduction to ionic liquids. Cambridge, UK: The Royal Society of Chemistry; 2010. p. 31-39.
- [48] Olivier-Bourbigou H, Magna L, Morvan D. Ionic liquids and catalysis: Recent progress from knowledge to applications. *Appl Catal Gen* 2010; 373: 1-56.
- [49] Holbrey JD, Rogers RD. Physicochemical properties of ionic liquids: melting points and phase diagrams. In: Wasserscheid P, Welton T, editors. *Ionic liquids in synthesis* Weinheim: Wiley-VCH; 2008. p. 57-72.
- [50] Gupta KM, Jiang J. Cellulose dissolution and regeneration in ionic liquids: A computational perspective. *Chem Eng Sci* 2014 July (Available online).
- [51] Mantz RA, Trulove PC. Viscosity and density of ionic liquids. In: Wasserscheid P, Welton T, editors. *Ionic liquids in synthesis* Weinheim: Wiley-VCH; 2008. p. 72-87.
- [52] Stark A, Sellin M, Ondruschka B, Massonne K. The effect of hydrogen bond acceptor properties of ionic liquids on their cellulose solubility. *Sci China Chem* 2012 Aug; 55: 1663-1670.
- [53] Weerachanchai, Piyarat, Chen, Zhengjian, Leong SSJ, Chang, Matthew Wook, Lee o. Hildebrand solubility parameters of ionic liquids: Effects of ionic liquid type, temperature and DMA fraction in ionic liquid. *Chem Eng J* 2012 Dec; 213: 356-362.
- [54] Cocalia VA, Visser AE, Rogers RD, Holbrey JD. Solubility and solvation in ionic liquids. In: Wasserscheid P, Welton T, editors. *Ionic liquid in synthesis* Weinheim: Wiley-VCH; 2008. p. 89-102.
- [55] Stark A, Zidell AW, Hoffmann MM. Is the ionic liquid 1-ethyl-3-methylimidazolium methanesulfonate [emim][MeSO₃] capable of rigidly binding water? *J Mol Liq* 2011; 160: 166-179.

- [56] Stark A. Shaping micro-and macroscopic properties of ionic liquid–solute systems: Multi-functional task-specific agents. *J Mol Liq* 2014 Apr; 194: 144–152.
- [57] Brehm M, Weber H, Pensado AS, Stark A, Kirchner B. Proton transfer and polarity changes in ionic liquid–water mixtures: a perspective on hydrogen bonds from ab initio molecular dynamics at the example of 1-ethyl-3-methylimidazolium acetate–water mixtures—Part 1. *Phys Chem Chem Phys* 2012; 14: 5030-5044.
- [58] Chang C, Zhang L. Cellulose-based hydrogels: present status and application prospects. *Carbohydr Polym* 2011 Feb; 84(1):40-53.
- [59] Kadokawa J, Murakami M, Kaneko Y Y. A Facile preparation of gel materials from a solution of cellulose in ionic liquid. *Carbohydr Res* 2008 Mar; 343(4): 769-772.
- [60] Ye D, Farriol X. Improving accessibility and reactivity of celluloses of annual plants for the synthesis of methylcellulose. *Cellulose* 2005 Oct; 16(5): 507-515.
- [61] Bain MK, Bhowmick B, Maity D, Mondal D, Mollick MMR, Rana D, et al. Synergistic effect of salt mixture on the gelation temperature and morphology of methylcellulose hydrogel. *Int J Biol Macromol* 2012; 51(5): 831-836.
- [62] Thormann E, Bodvik R, Karlson L, Claesson PM. Surface forces and friction between non-polar surfaces coated by temperature-responsive methylcellulose. *Colloid Surface Physicochem Eng Aspect* 2013; 441: 701-708.

Pyridinium-Based Ionic Liquids — Application for Cellulose Processing

Elena S. Sashina and Dmitrii A. Kashirskii

Additional information is available at the end of the chapter

<http://dx.doi.org/10.5772/59286>

1. Introduction

Over the last two decades new direct solvents for cellulose and other natural polymers have been actively explored; these are ionic liquids (ILs). The unique properties of this new class of compounds allow the use of ILs in various fields of science and technology, among which the use of ILs as the reaction medium for biomass processes occupies an important place [1-3], especially for cellulose dissolution [4-13], and the dissolution of other natural polymers [14], and produces from their solutions new biodegradable materials, including films, fibres and membranes [15].

On the whole, imidazolium-, ammonium- and pyridinium-based ILs can be used for cellulose dissolution (Figure 1). Imidazolium ILs are studied here in great detail, but the comparisons between the cost of synthesis, toxicity [16-18] and dissolving power [4, 6] of the three classes of ILs shows pyridinium-containing salts to be of most benefit. The most effective salts have a pyridinium ring with position 1,3 of alkyl substituents [6, 7].

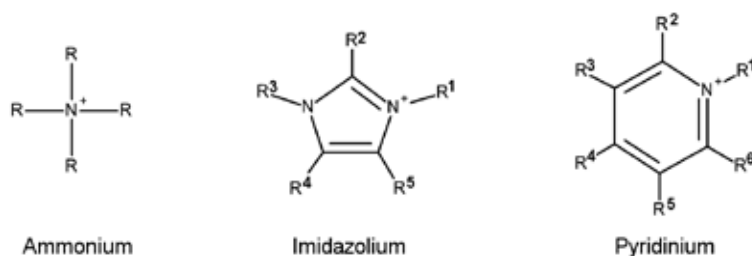


Figure 1. IL cations suitable for cellulose dissolution

The important feature of ILs is the possibility of selecting the cation-anion pairs for the purposeful synthesis of solvents with desirable properties in technology. In view of the large numbers of ILs available, the selection of ionic solvents out of all the possible cation-anion pairs is a big problem. To make a reasonable selection it is important to understand the relationship between the structure, physicochemical properties, and dissolving power of ILs.

2. Experimental

2.1. Quantum-chemical calculations

Quantum-chemical calculations were performed using the Gaussian 03 program by HF/3-21G(d) and HF/6-31G(d) methods [7]. As the IL models were used the ionic pairs which they contained associated cation and anion. For the cellulose model, we took the cellotetraose (i.e., saccharide consisting of four glycoside units). The interaction energy of the IL's cation-anion pairs, E_p , was calculated as a difference: the energy of the cation-anion complex, E_{ca} , minus the sum of the energies of the cation, E_c , and the anion, E_a :

$$E_p = 2625.5 \cdot \{E_{ca} - (E_c + E_a)\},$$

where 2625.5 is the conversion factor of the Hartree energy (atomic units) in kJ mol^{-1} .

2.2. $^1\text{H-NMR}$ spectroscopy

An analysis of the chemical shifts was carried out by the $^1\text{H-NMR}$ spectra obtained with the Bruker Avance II Plus 700 MHz spectrometer (at an operating frequency of 700 MHz) at a temperature of 27 °C. For the preparation of the samples, a sample of the IL (19 – 27 mg) was dissolved in CDCl_3 (0.65 mL, $\delta=7.240$ ppm). Solutions of cellulose with ILs were investigated using the CDCl_3 ($\delta=7.240$ ppm). TMS ($\delta=0$) was used as the internal standard [19].

2.3. Thermal analysis

Differential scanning calorimetry (NETZSCH-Gerätebau GmbH Thermal Analysis DSC 204), thermogravimetry methods (F. Paulik J. Paulik L. Erdey system) and Boëtius heated stage (VEB Wagetchnik Rapido) were used for the thermal analysis [20]. The conditions of the experiment are shown in Table 1. For the Boëtius heated stage: the samples were placed on a microscope slide and the cover glass, and these were added to the heated stage, and the melting process was observed with the aid of a microscope PHMK 05 (with an increasing of 16 times). For the melting point, the state of the total loss of the sharp edges of the salts' crystals is taken.

2.4. Gas chromatography–mass spectrometry

The IL samples were identified on the Shimadzu GCMS-QP2010 Plus. For this equipment the FNNC 1.2 and NIST08 libraries were used. The main analysis conditions involved a capillary

Method	Temperature range, °C	Heating rate, deg/min	Sample mass, mg	Atmosphere
DSC	-80 ÷ 350	10	7.80 – 8.50	Nitrogen
DTG	20 ÷ 200	7.9	~ 90.00	Air
Boëtius heated stage	20 ÷ m.p.	10	7.00 – 10.00	Air

Table 1. Conditions of the thermal analysis of ionic liquids [20].

chromatographic column (30 m), a stationary phase SLB-5ms, the carrier gas was helium, and the evaporator temperature was 200 °C. The thermostat columns had a temperature range of 40 °C (for five minutes) to 280 °C, a heating rate of 10 deg/min and exposure for 15 minutes. The detector of the mass spectrometer with the quadrupole mass analyser had a detection range of M/Z 40 – 450 Da. The delay of the start of the registration (for the cut-off of the solvent) was 2.2 min. For the sample preparation, IL crystals (5 mg) were dissolved in ethanol (1:200), 1 µL of solution was injected into the evaporator chromatograph with a microsyringe.

2.5. Fourier transform infrared spectroscopy

The FTIR spectra of the samples were recorded on a Nicolet 6700 FT-IR from Thermo Scientific. The resolution was 0.5 cm⁻¹. The spectra were recorded at room temperature using an NXR FT-Raman module.

2.6. Dissolution of cellulose with ILs

Cellulose was added to the solvent after the complete dissolution of the previous sample (in this case the solution was transparent to light and did not contain any undissolved cellulose fibres visible under the microscope). To determine the maximum dissolving power of the ILs, the dissolution was carried out for not less than 12 hours with a constant stirring and temperature control using the magnetic stirrer. The calculation of the dissolved cellulose concentration was given by the formula:

$$D = \frac{m_1}{m_1 + m_2} \cdot (100 - W),$$

where D is the concentration of the cellulose solution with ILs, wt%; m_1 and m_2 are the mass of the cellulose and ILs, respectively, g; W is the water content of the cellulose, wt% [7].

2.7. Optical microscopy

A microscopic examination of the samples was carried out using a laboratory microscope Euler Science 670TD. A digital camera was used DCM 510 (5-MPix, 1/2" CMOS) with a maximum resolution of 2592×1944, and a sensitivity of 0.90 V/lux-sec at 550 nm.

2.8. Degree of polymerization of cellulose

To determine the degree of polymerization (DP) of the initial cellulose and the regenerated polymer (i. e. the film obtained from solution of cellulose with ILs) from an aqueous solution of cadmium-ethylenediamine complex (cadoxene), containing 29 wt% ethylenediamine. The cellulose was used at the following concentrations (D): 0.1, 0.2, 0.3, and 0.4 wt%. We used an Ostwald viscometer (the capillary of which had an internal diameter of $d=0.99$ mm), analytical balance (with a precision of four decimal places) and a thermostat at U15^c MLW (bath temperature: 20 °C). Using the time of the expiration (in sec.) of pure cadoxene (τ_0) and the solution (τ_i) the relative viscosity was calculated:

$$\eta_r = \frac{\tau_i}{\tau_0}.$$

The specific viscosity was determined from the relationship: $\eta_s = \eta_r - 1$, and the reduced viscosity: $\eta_{i,r} = \eta_r / D$. The intrinsic viscosity $[\eta]$ found by graphical extrapolation to the value of $D=0$ using the software package Origin 9.0 was:

$$\lim_{D \rightarrow 0} \frac{\eta_s}{D} = \lim_{D \rightarrow 0} \frac{\ln \eta_r}{D}.$$

The intrinsic viscosity is related to the DP value for a given diameter of the viscometer capillary as $[\eta] = 7 \cdot 10^{-3} DP^{0.9}$, therefore

$$DP = \left(\frac{[\eta]}{0.007} \right)^{\frac{1}{0.9}}.$$

3. Physical and chemical properties of pyridinium-based ionic liquids

3.1. Theoretical studies of the 1-alkylpyridinium- and 1-alkyl-3-methylpyridinium-based salts, and their structural features

Quantum chemical calculations can give an insight into geometry and the charge distribution of organic compounds. We studied pyridinium derivatives with different alkylic lengths and the numbers of the substituents of the ring have different anions.

3.1.1. Features of the structures of the 1-substituted pyridinium-based ILs

Theoretically, the optimal geometry of the studied pyridinium derivatives can be determined based on the results of quantum chemical calculations (method HF/3-21G(d)) as coordinates of the minimum (minima) on the potential energy surface, PES. As an example, Figure 2 shows the function of a cation-anion pair's interaction energy, E_p , the distances between the cation and anion $r_{(H2 \cdots Cl)}$, the torsion angle Θ between the atoms N, C², H² of 1-methylpyridinium rings, and the chloride-anion Cl for [C₁Py]Cl [11].

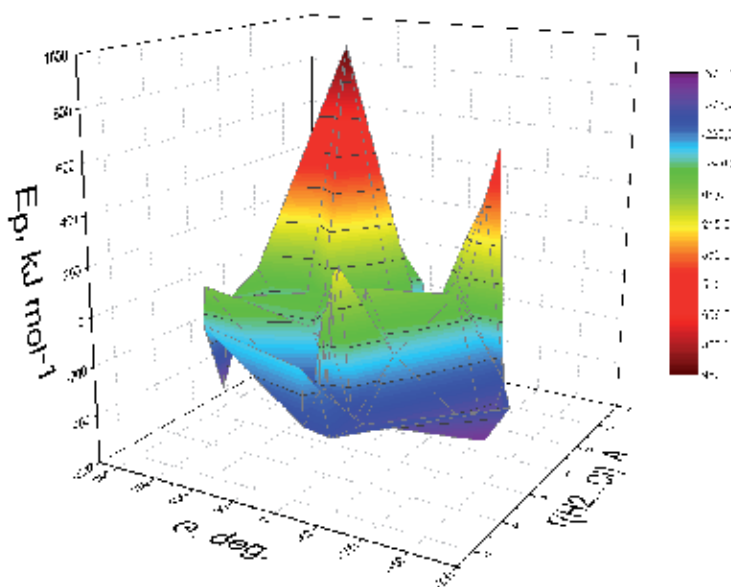


Figure 2. PES for [C₁Py]Cl

The minimum of the E_p value corresponds to the location of the anion near the atom H² (the most electron-deficient atom) of the ring and H⁶ of the aliphatic chain (Fig. 3A). At the point of the global minimum, the torsion angle between atoms N, C², H², and Cl becomes 0°, since the ring of pyridine and its derivatives have a rigid and almost planar structure, and the anion is located on the same plane. The energy of the complex is -519 kJ mol⁻¹, $r_{(\text{H}2\cdots\text{Cl})}$ 2.17 Å. There are local minima with energy $E_p = -367.06$ kJ mol⁻¹ at $r_{(\text{H}2\cdots\text{Cl})} = 5.87$ Å, and $\Theta = 23.38^\circ$ (Fig. 3B) and -363.45 kJ mol⁻¹ at $r_{(\text{H}2\cdots\text{Cl})} = 2.73$ Å and $\Theta = 10.87^\circ$ (Fig. 3C). The least probable relative positions of anion and cation correspond to the maximum positive value of $E_p = +948.00$ at $r_{(\text{H}2\cdots\text{Cl})} = 3.08$ Å, $\Theta = 90.61^\circ$, (Fig. 3D). In this case the anion is located above the plane of the ring. A positive value of E_p is due to the repulsion of the anion by the π -bonds of the pyridinium ring saturated with electron density.

The 1-substituted formation from pyridine molecule (Py) leads to minimal changes in the bond lengths and angles on the pyridinium ring (Table 2). It indicates that these structures have rigid and high symmetry geometry [21]. Appreciable differences were noted only in the angle values of α and β for the 1-substituted pyridinium compared with Py.

Calculations show that the distance between the anion and the cation increases slightly with the increasing length of the cationic substituent, but the distance between the anions and cationic substituents (atom H¹) is reduced. So, in a series of C₁–C₆ the distance between the chloride anion and the nearest H² atom of the ring increases (2.190 → 2.225 Å). Starting from C₃ the anion approaches the substituents, and the distance between the anion and the nearest atom H² of the cationic substituent is shortened (2.624 ← 2.525 Å). In the C₀–C₄ series, as in the case of the imidazolium-based ILs [22], there is a tendency for a gradual decrease in the

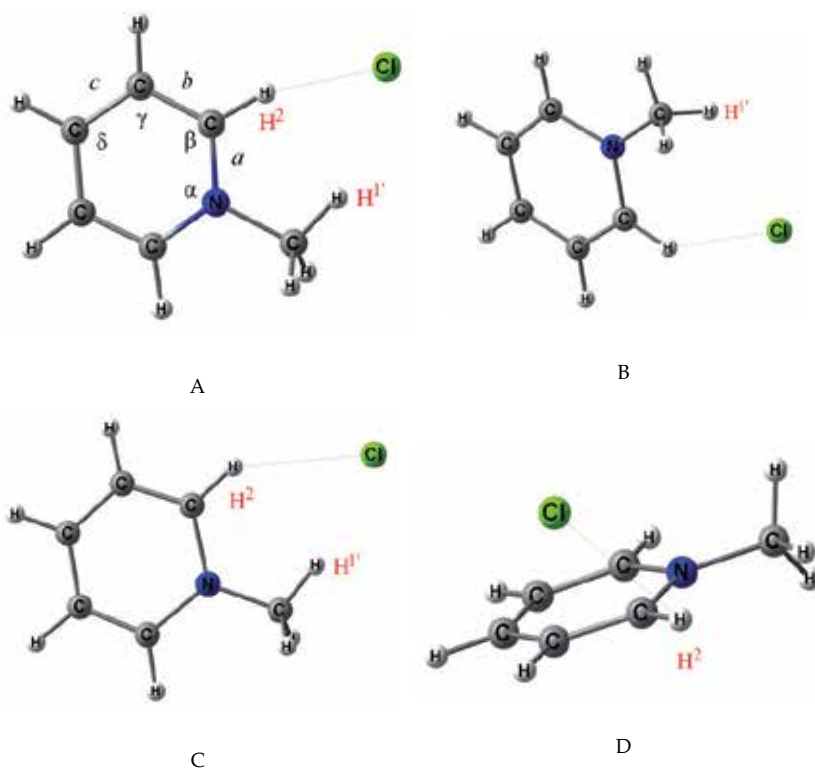


Figure 3. Models of $[C_1Py]Cl$ with different arrangements of the anion around the cation, calculated by HF/3-21G(d)

interaction energy between the cation and the anion; this trend correlates with the experimentally observed decrease in the dissolving power toward cellulose and other higher plants (Table 3). It can be assumed that this leads to changes in the degree of the ordering of the ionic liquid (density fluctuation) manifested as the appearance of polar and nonpolar domains [23]. In any case, increases in the length of the substituent leads to a decrease in the density of the polar component.

Paramet ers:	Py		[HPy]Cl	[C ₁ Py]Cl	[C ₂ Py]Cl	[C ₃ Py]Cl	[C ₄ Py]Cl	[C ₅ Py]Cl	[C ₆ Py]Cl	[APy]Cl	[BzPy]Cl
	Calc.	Ref. [21]									
<i>a</i>	1.321	1.335	1.325	1.331	1.333	1.334	1.334	1.331	1.333	1.331	1.331
<i>b</i>	1.385	1.381	1.377	1.388	1.386	1.384	1.384	1.387	1.385	1.386	1.386
<i>c</i>	1.384	1.379	1.387	1.374	1.376	1.377	1.377	1.375	1.377	1.375	1.375
α	117.704	117.670	122.744	121.34	121.21	121.19	121.06	121.06	121.21	121.28	121.14
β	123.607	122.990	120.268	119.96	120.08	120.17	120.20	120.21	120.11	120.07	120.19
γ	118.229	118.840	118.285	119.48	119.44	119.42	119.41	119.41	119.41	119.39	119.39

Paramet ers:	Py		[HPy]Cl	[C ₁ Py]Cl	[C ₂ Py]Cl	[C ₃ Py]Cl	[C ₄ Py]Cl	[C ₅ Py]Cl	[C ₆ Py]Cl	[APy]Cl	[BzPy]Cl
	Calc.	Ref. [21]									
δ	118.624	118.650	120.149	119.46	119.44	119.41	119.40	119.39	119.45	119.48	119.39
$r_{(H2-Cl)}$				2.190	2.201	2.203	2.205	2.221	2.225	2.221	2.208
$r_{(Cl...H1)}$			1.821	2.464	2.575	2.624	2.623	2.525	2.592	2.537	2.564
q_{Cl}			-0.746	-0.852	-0.862	-0.864	-0.864	-0.852	-0.866	-0.866	-0.852
q_N	-0.515		-0.685	-0.603	-0.604	-0.605	-0.605	-0.603	-0.611	-0.607	-0.602
q_H^2	0.202		0.293	0.363	0.364	0.363	0.363	0.357	0.365	0.359	0.361
$q_H^{1'}$			0.431	0.325	0.305	0.304	0.305	0.317	0.299	0.314	0.314
E_p			-436.965	-369.919	-367.434	-364.033	-362.158	-363.133	-365.211	-365.149	-866.474
$\vec{\mu}, D$	2.31	2.20 [24]									

Table 2. The main geometrical parameters, the effective charge values on the atoms, q , the cation-anion interaction energy, E_p (kJ mol⁻¹), and the dipole moment, (D), of the models Py, 1-substituted pyridinium-based chlorides, calculated by HF/6-31G(d) [11]

Solvents	Dissolving power
[HPy]Cl	biomass poplar 80 mg g ^{-1*} , pine 60 mg g ^{-1*} at 60°C [25]
[C ₂ Py]Cl	cellulose ~ 5 %, at 90 – 100 °C [26]
[C ₄ Py]Cl	biomass poplar 30 mg g ^{-1*} at 60 °C [25]
[APy]Cl	biomass poplar mg g ^{-1*} at 60 °C [25]; cellulose ~ 5 % at 105 – 110 °C [26]
[APy]Br	biomass poplar 5 mg g ^{-1*} at 60 °C [25]
[BzPy]Cl	cellulose ~ 5 % at 110 – 115 °C [26]

* by dilution in DMSO (1:2).

Table 3. The solubility biomasses with 1-alkylpyridinium-based salts, according to the works [25,26]

Regardless of the kind of anion (we examined 1-methylpyridinium cation-based models of salts with chloride-anion, bromide-anion and acetate-anion, Figure 4), these have been placed near the pyridinium ring H² atom, which is characterized by low electron density (Table 4). The bond lengths of the pyridinium rings with chloride-, and bromide-based anions have identical values. Effective negative charges on the nitrogen atoms are virtually identical to chloride-, bromide-, and acetate-based salts which have a 1-methylpyridinium cation. Acetate anion has the greatest negative charge on the O¹ and O² atoms. The main calculated parameters of the optimized complexes are presented in Tables 4 and 5 [11].

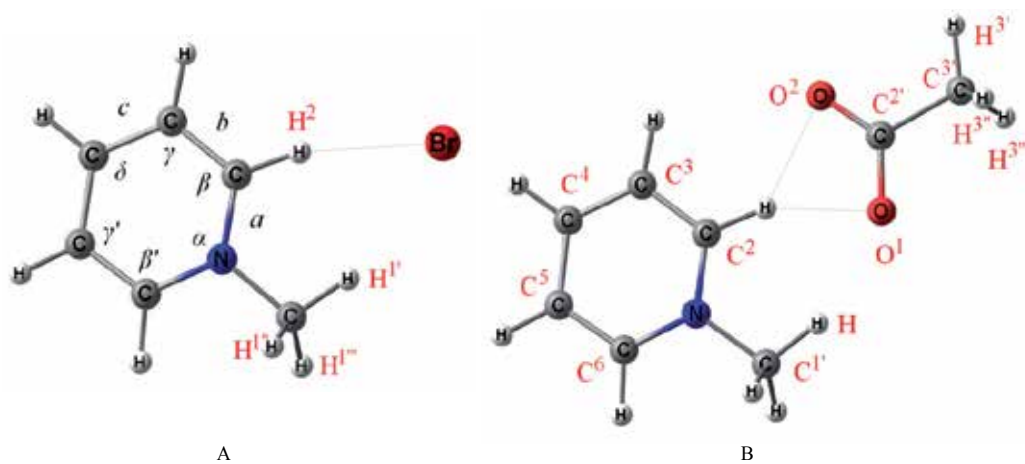


Figure 4. Optimized models of 1-methylpyridinium bromide (A), and 1-methylpyridinium acetate (B)

	Parameters	[C ₁ Py] ⁺	[C ₁ Py]Cl	[C ₁ Py]Br
Geometry	<i>a</i>	1.339	1.331	1.331
	<i>b</i>	1.372	1.387	1.387
	<i>c</i>	1.388	1.374	1.374
	α	120.68	121.36	121.24
	β	121.13	119.95	120.02
	β'	121.13	121.27	121.32
	γ	118.80	119.49	119.48
	γ'	118.80	118.49	118.50
	δ	119.46	119.46	119.43
		$r_{(x...H2)}$		2.191
	$r_{(x...H1)}$		2.463	2.580
Charges	q_x		-0.852	-0.839
	q_N	-0.655	-0.603	-0.604
	q_{C^2}	0.163	0.185	0.174
	q_{C^3}	-0.271	-0.301	-0.301
	q_{C^4}	-0.087	-0.097	-0.097
	q_{C^5}	-0.271	-0.284	-0.283
	q_{C^6}	0.163	0.156	0.165
	$q_{C^{1'}}$	-0.332	-0.353	-0.356

Parameters	[C ₁ Py] ⁺	[C ₁ Py]Cl	[C ₁ Py]Br
q _H ²	0.311	0.363	0.367
q _H ³	0.293	0.275	0.275
q _H ⁴	0.296	0.248	0.258
q _H ⁵	0.293	0.257	0.255
q _H ⁶	0.311	0.255	0.266
q _H ^{1'}	0.236	0.325	0.316
q _H ^{1''}	0.235	0.206	0.207
q _H ^{1'''}	0.244	0.206	0.206
E _p		-369.918	-372.344

Table 4. The bond lengths (Å), angles (deg.), interaction energies E_p (kJ mol⁻¹) and atomic charges of 1-methylpyridinium chloride and bromide, calculated by HF/6-31G (d). X=anion [11]

	Parameters	Values
Geometry	<i>a</i>	1.328
	<i>b</i>	1.389
	<i>c</i>	1.371
	α	121.37
	β	120.36
	β'	120.91
	γ	119.11
	γ'	118.73
	δ	119.52
	r _(O1...H2)	1.981
	r _(O2...H2)	2.045
	angle (O ¹ C ² O ²)	125.59 (110.57)
	r _(C2'...C3)	1.527
Charges	q _N	-0.603
	q _C ²	0.138
	q _C ³	-0.301
	q _C ⁴	-0.104
	q _C ⁵	-0.283
	q _C ⁶	0.148
	q _C ^{1'}	-0.362

Parameters	Values
$q_C^{2'}$	0.760 (0.723)
$q_C^{3'}$	-0.554 (-0.554)
$q_H^{2'}$	0.442
$q_H^{3'}$	0.298
$q_H^{4'}$	0.252
$q_H^{5'}$	0.248
$q_H^{6'}$	0.258
$q_H^{1'}$	0.342
$q_H^{1''}$	0.200
$q_H^{1'''}$	0.200
$q_H^{3''}$	0.155 (0.116)
$q_H^{3'''}$	0.160 (0.114)
$q_H^{3''''}$	0.155 (0.116)
$q_O^{1'}$	-0.789 (-0.758)
$q_O^{2'}$	-0.759 (-0.758)
Σ (CH ₃ COO)	-0.872 (-1.000)
E_p	-418.464

Table 5. Bond lengths (Å), angles (deg.), interaction energies E_p (kJ mol⁻¹) and atomic charges of 1-methylpyridinium acetate, calculated by HF/6-31G (d). (The values of the parameters for isolated acetate-anions are shown in parentheses) [11].

It is important to note that in the series of acetate > chloride > bromide the negative charges of the anion have been decreasing (for acetate-anion is the total value of the charges on the O¹ and O² atoms), and it decreases the positive charges on the cations which interact due to the H² and H¹ atoms with the anions. This is due to a decrease in the electron density transfer during interionic interactions. As a result, in the same series, the interaction energy between the cation and anion decreases, and the distance between the anion and cation increases. In practice, this could be the reason for the decrease in the solubility of the cellulose in these salts. For example, [APy]Cl dissolves in seven times more biomass poplar than [APy]Br (Table 3). It is also important that the imidazolium-based ILs produce similar theoretical and experimental results [22, 27].

3.1.2. Features of the structures of 1,3-disubstituted-pyridinium-based ILs

Figure 5 shows the potential energy surface for the 1,3-disubstituted pyridinium IL from the example of [C₄MPy]Cl. For [C₄MPy]Cl we observed two structures of ion pairs in mutual arrangement. These structures correspond to the minima of E_p : chloride-anion is located near

the protons H² (Figure 5, point I) and H⁶ (Figure 5, point II). The E_p values of both the cation-anion pairs with variable positions (Figure 6) for these ions are not significantly different.

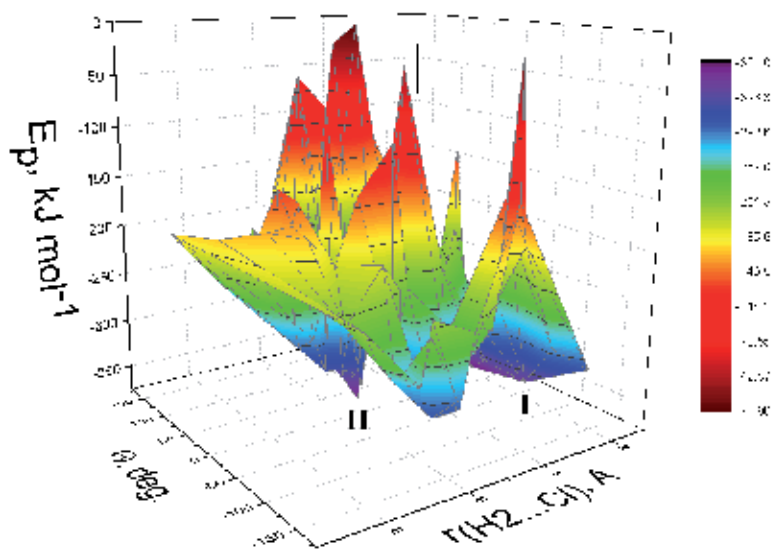


Figure 5. PES for [C₄MPy]Cl. The Roman numerals indicate the points of the energy minima on the PES

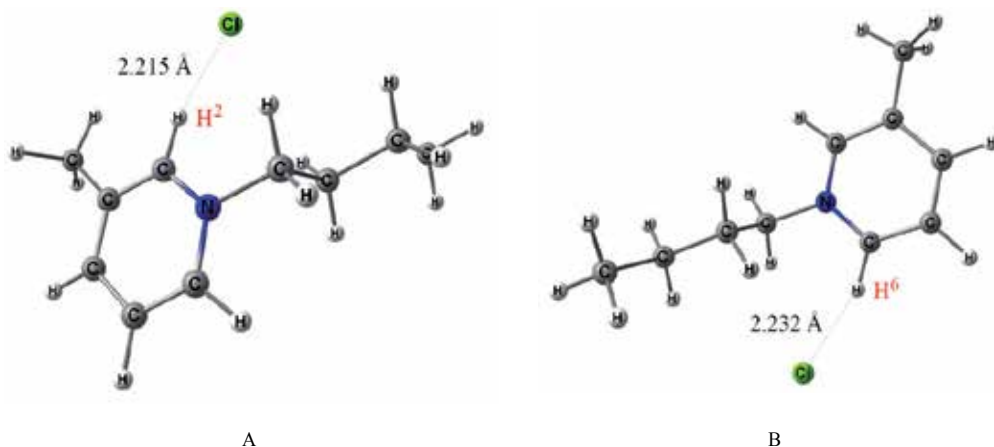


Figure 6. Two optimized models of [C₄MPy]Cl: on a PES to point I corresponds to structure A, and for point II – structure B

The results of the quantum chemical calculations for the other IL models give similar geometries with the mutual arrangement of the anion around the cation. The optimized models of $[\text{C}_4\text{MPy}]\text{CH}_3\text{COO}$ and $[\text{C}_4\text{MPy}]\text{Br}$ are shown in Figure 7.

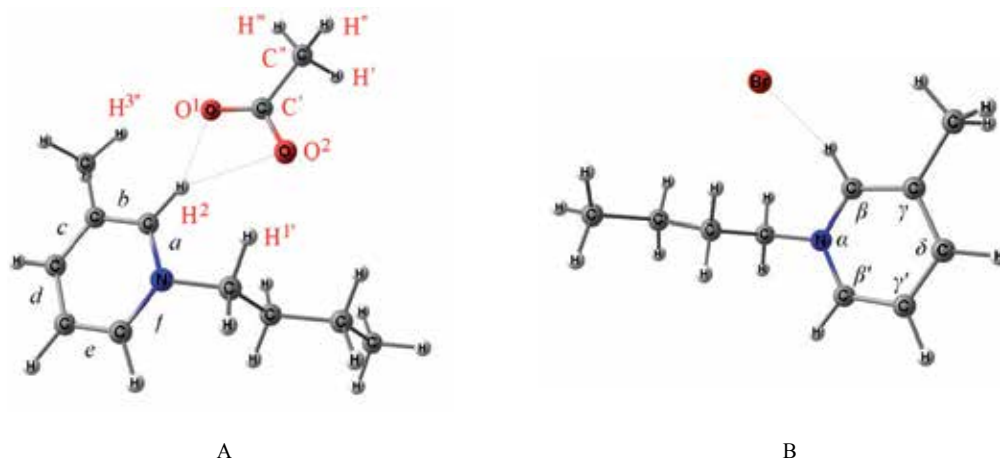


Figure 7. Optimized models of $[\text{C}_4\text{MPy}]\text{CH}_3\text{COO}$ (A), and $[\text{C}_4\text{MPy}]\text{Br}$ (B)

Since we observed the global minimum of the potential energy on the PES for the model with the anion located near to the H^2 ring proton, this model was adopted for all subsequent calculations of geometry. The main results of the quantum chemical calculations are shown in Tables 6 and 7. The mutual arrangement of the anion around the cation is characterized by the torsion angle Θ between the anion X, and the pyridinium ring atoms H^2 , C^2 , and N, and the distance $r_{(\text{H}^2 \dots \text{X})}$ between the anion X and the H^2 atom. Thus, for 1,3-disubstituted chloride-containing pyridinium models, the torsion angle Θ has a range from 0.2° (for $[\text{C}_1\text{MPy}]\text{Cl}$) to 11.1° and 14.2° (for the substituted pyridinium-based chlorides with chain lengths of C_2 to C_{10}). We can compare, for monosubstituted 1-methylpyridinium chloride the $\Theta \approx 0^\circ$. The Θ angle for bromide-containing models is $7 - 15^\circ$ more than the same chloride-based models. Having the anion located further away from the plane of the pyridinium ring, and the increase in the Θ between the cation and anion in the homologous series, and finally the changing of the anion Cl^- to Br^- makes the cation-anion pair still less associated. The reason for this is the reducing of the ion's packing density in the IL crystal, and thus their melting point was changed. A decrease in the degree of the association is also confirmed by a characteristic change in the E_p values. The length of the C—C bonds, and angles with the pyridinium ring for the calculated models in general are not very different from each other. Monosubstituted and disubstituted salts have different geometric parameters: the long distances of b and c , and the relatively large angles of α and β have a 1-alkyl-3-methylpyridinium ring relative to the 1-alkylpyridinium ring. These differences are caused by relatively strong interactions with the anions.

ILs	$r_{(H2...X)}$	$r_{(C2...H2)}$	a	b	c	d	e	f	α	β	β'	γ	γ'	δ	Θ	Φ
[C ₁ MPy]Cl	2.182	1.085	1.331	1.391	1.380	1.396	1.363	1.342	121.48	121.20	120.56	117.47	118.76	120.53	0.193	
[C ₂ MPy]Cl	2.192	1.085	1.332	1.389	1.382	1.393	1.366	1.340	121.36	121.30	120.65	117.45	118.74	120.50	11.148	
[C ₃ MPy]Cl	2.213	1.084	1.333	1.388	1.382	1.393	1.366	1.339	121.36	121.31	120.65	117.43	118.73	120.51	10.827	177.687
[C ₄ MPy]Cl	2.215	1.084	1.333	1.388	1.383	1.392	1.366	1.339	121.36	121.32	120.65	117.43	118.74	120.51	13.791	177.768
[C ₅ MPy]Cl	2.216	1.084	1.333	1.388	1.383	1.393	1.366	1.338	121.36	121.32	120.65	117.43	118.74	120.51	13.547	177.479
[C ₆ MPy]Cl	2.216	1.084	1.333	1.388	1.383	1.392	1.367	1.338	121.36	121.32	120.65	117.43	118.73	120.51	14.083	177.477
[C ₇ MPy]Cl	2.216	1.084	1.333	1.388	1.383	1.392	1.366	1.338	121.36	121.32	120.65	117.43	118.74	120.51	14.185	177.482
[C ₈ MPy]Cl	2.216	1.084	1.333	1.388	1.383	1.392	1.367	1.338	121.36	121.32	120.65	117.43	118.74	120.51	14.190	177.479
[C ₉ MPy]Cl	2.216	1.084	1.333	1.388	1.383	1.392	1.367	1.338	121.36	121.32	120.65	117.43	118.73	120.51	14.191	177.496
[C ₁₀ MPy]Cl	2.216	1.084	1.333	1.388	1.383	1.392	1.366	1.338	121.36	121.32	120.65	117.43	118.73	120.51	14.192	177.500
[AMPy]Cl	2.223	1.081	1.329	1.393	1.379	1.396	1.363	1.343	121.40	121.38	120.56	117.39	118.79	120.52	54.890	114.289
[C ₂ MPy]Br	2.335	1.083	1.332	1.388	1.382	1.393	1.366	1.339	121.20	121.52	120.66	117.39	118.81	120.42	26.664	177.256
[C ₄ MPy]Br	2.377	1.082	1.333	1.387	1.383	1.392	1.367	1.338	121.23	121.49	120.66	117.38	118.78	120.45	20.810	175.746
[C ₄ MPy]CH ₃ COO	1.841*	1.088	1.333	1.389	1.382	1.393	1.366	1.339	121.45	121.12	120.70	117.58	118.72	120.45		177.256

* The distance from the O¹ oxygen atom of acetate-anion to H² of pyridinium ring; distance from O² to H² is 2.526 Å.

Table 6. The main geometrical parameters: bond lengths (Å), and angles (degrees) for 1,3-disubstituted pyridinium salts, calculated by HF/6-31G (d) (An explanation of the symbols is given in the text and in figure 7)

ILs	q_x	q_H^2	q_H^6	$q_H^{1'}$	$q_H^{3''}$	q_N	q_R	q_M	μ, D	E_p
[C ₁ MPy]Cl	-0.854	0.356	0.262	0.321	0.253	-0.604	0.381	0.117	15.268	-366.799
[C ₂ MPy]Cl	-0.863	0.357	0.261	0.300	0.251	-0.604	0.401	0.114	14.903	-364.635
[C ₃ MPy]Cl	-0.865	0.359	0.262	0.297	0.249	-0.610	0.409	0.113	14.683	-364.851
[C ₄ MPy]Cl	-0.866	0.360	0.262	0.295	0.249	-0.611	0.411	0.113	14.547	-363.813
[C ₅ MPy]Cl	-0.867	0.360	0.262	0.295	0.249	-0.611	0.412	0.113	14.501	-363.096
[C ₆ MPy]Cl	-0.867	0.360	0.262	0.295	0.249	-0.611	0.412	0.113	14.447	-362.593
[C ₇ MPy]Cl	-0.867	0.360	0.262	0.295	0.249	-0.611	0.412	0.113	14.447	-362.245
[C ₈ MPy]Cl	-0.867	0.360	0.262	0.295	0.249	-0.611	0.412	0.113	14.414	-362.009
[C ₉ MPy]Cl	-0.867	0.360	0.262	0.295	0.249	-0.611	0.412	0.113	14.430	-361.838
[C ₁₀ MPy]Cl	-0.867	0.360	0.262	0.295	0.249	-0.611	0.412	0.113	14.403	-361.719
[AMPy]Cl	-0.871	0.350	0.264	0.307	0.248	-0.607	0.395	0.115	14.622	-362.775
[C ₂ MPy]Br	-0.849	0.363	0.262	0.286	0.249	-0.606	0.390	0.113	15.094	-370.408
[C ₄ MPy]Br	-0.848	0.363	0.263	0.283	0.245	-0.611	0.397	0.112	14.778	-371.665
[C ₄ MPy]CH ₃ COO	-0.774*	0.443	0.257	0.328	0.267	-0.612	0.398	0.104	11.269	-412.003

* A partial charge of the O¹ oxygen atom; partial charges to other atoms of the acetate-anion: -0.749 for O², 0.753 for C', -0.556 for C'', 0.160 for H', 0.156 for H'', 0.156 for H''', the total charge of the acetate-anion $q_{(CH_3COO^-)}$ is -0.854e.

Table 7. The partial charges q for atoms and the substituents by the Mulliken value, energy E_p (kJ mol⁻¹) and dipole moments (μ) for the models of 1,3-disubstituted pyridinium salts, are calculated by HF/6-31G(d).

For the IL which has an allylic substituent we observed a relatively more larger in the Θ angle relative to $[\text{C}_3\text{MPy}]\text{Cl}$. This may be the result of the interaction of the anion with the π -electrons of the allylic substituent. Because the anion for all of the salts slightly shifted toward the substituent on the nitrogen atom (including $[\text{C}_1\text{MPy}]\text{Cl}$), then in the comparison of these two compounds the closest anion is located in the more polar allylic substituent than the propylic substituent (the distance between the chloride-anion and H^1 atom are 2.617 Å and 2.675 Å, respectively). This may indicate a more dense atomic packing for $[\text{AMPy}]\text{Cl}$. The Φ angle value for $[\text{AMPy}]\text{Cl}$ on average is less than the other models.

With respect to the values of the electron density distribution in the ion pair, an increase in the alkyl chain length of the cation clearly affects only the length of C_4 . A further increase in the length of the substituent does not lead to significant changes in the charge of the atom H^2 . This leads to a decrease in the solvent polarity as a result of increasing the volume portion of the non-polar components. The electric dipole moment $\bar{\mu}$ values, which are characteristic of the electron density asymmetry, are gradually reduced in chloride-containing ILs, where the length of the substituents are increased. The displacement dipole of the moment vector along the alkyl chain length takes place gradually, as shown in Figure 8. The calculated values of μ for bromide-containing ILs are also subject to a similar downward trend of the alkyl chain elongation.

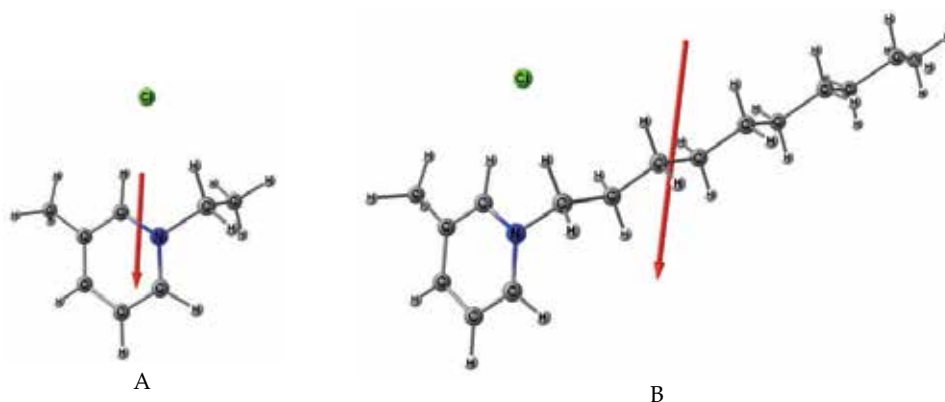


Figure 8. The displacement vector of the dipole moments for $[\text{C}_2\text{MPy}]\text{Cl}$ (A) and $[\text{C}_{10}\text{MPy}]\text{Cl}$ (B)

3.2. Physical and chemical properties of 1-alkyl-3-methylpyridinium-based ILs

A series of 1-alkyl-3-methylpyridinium-based ILs (Table 8) was examined experimentally. The synthesis of these solvents was performed as described in paper [7].

A feature common to most hydrophilic IL crystals (shown in the micrographs on Figure 9) is the gradual saturation of water from the atmosphere. Two of the synthesized ILs, $[\text{C}_4\text{MPy}]\text{Br}$ and $[\text{C}_4\text{MPy}]\text{CH}_3\text{COO}$, are liquid at room temperature, i.e. they belong to a subclass RTIL.

No.	ILs	Symbol	M, g mol ⁻¹
1	1-Ethyl-3-methylpyridinium chloride	[C ₂ MPy]Cl	157.6415
2	1-Propyl-3-methylpyridinium chloride	[C ₃ MPy]Cl	171.6682
3	1-Butyl-3-methylpyridinium chloride	[C ₄ MPy]Cl	185.6949
4	1-Pentyl-3-methylpyridinium chloride	[C ₅ MPy]Cl	199.7215
5	1-Hexyl-3-methylpyridinium chloride	[C ₆ MPy]Cl	213.7482
6	1-Heptyl-3-methylpyridinium chloride	[C ₇ MPy]Cl	227.7759
7	1-Octyl-3-methylpyridinium chloride	[C ₈ MPy]Cl	241.8016
8	1-Nonyl-3-methylpyridinium chloride	[C ₉ MPy]Cl	255.8282
9	1-Decyl-3-methylpyridinium chloride	[C ₁₀ MPy]Cl	269.8549
10	1-Allyl-3-methylpyridinium chloride	[AMPy]Cl	169.6523
11	1-Ethyl-3-methylpyridinium bromide	[C ₂ MPy]Br	202.0924
12	1-Butyl-3-methylpyridinium bromide	[C ₄ MPy]Br	230.1458
13	1-Butyl-3-methylpyridinium acetate	[C ₄ MPy]CH ₃ COO	209.2859

Table 8. List of investigated solvents: 1-alkyl-3-methylpyridinium-based ILs, and their molecular weight

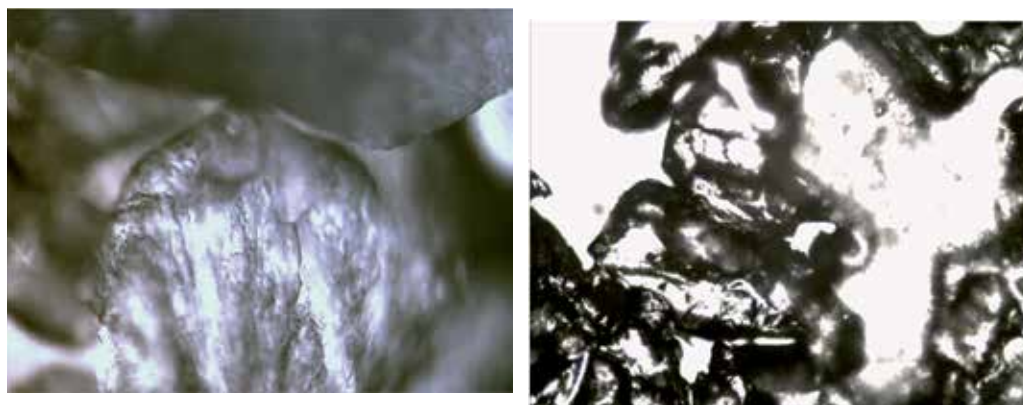


Figure 9. Crystals of [C₂MPy]Cl (A) and [C₄MPy]Cl (B) when magnified 10 times

3.2.1. Study of 1-alkyl-3-methylpyridinium-based ILs by ¹H-NMR spectroscopy

The experimental data of the chemical shifts and spin-spin coupling (*J*-coupling) are presented in Table 9 [19]. Figure 10 shows the general scheme of the 1-alkyl-3-methylpyridinium ring and acetate-anion numbered to correlate with corresponding the chemical shifts (δ) of protons and proton groups.

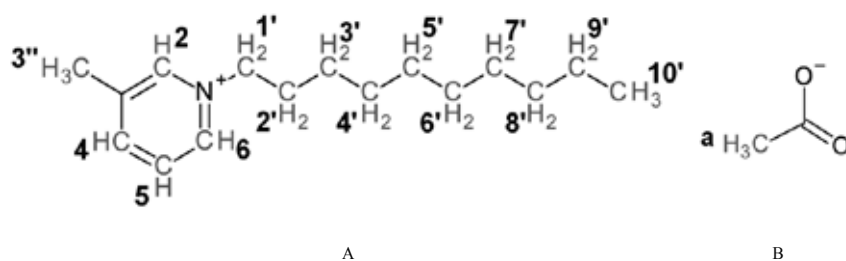


Figure 10. The numbering of the protons and the proton groups for the 1-alkyl-3-methylpyridinium cation $[C_n\text{MPy}]^+$ (A) and the acetate-anion CH_3COO^- (B)

For the peaks of the resonance signals of the ring protons, we observed singlet (H^2), duplet (H^4 and H^6) and triplet (H^5). Here, the J for H^4 peak are 7.7 or 8.4 Hz, for H^5 $J=14$, 11.9 or 14.7 Hz (for $[\text{C}_4\text{MPy}]\text{CH}_3\text{COO}$), and for H^6 $J=5.6$, 6.3 or 4.2 Hz (for $[\text{C}_4\text{MPy}]\text{CH}_3\text{COO}$).

We observed the greatest changes in the values of the chemical shifts during the alkyl chain lengthening for H^2 and H^6 atoms (labelled peaks 2 and 6, respectively) of the 1-alkyl-3-methylpyridinium ring (to $\Delta\delta=0.30$ and 0.24 ppm, respectively) [19]. According to the quantum-chemical calculations, these provisions in the ion pairs are the most optimal. The changing of the δ value confirms the calculations made on the basis of the findings of the interaction of these atoms with an anion Cl^- , as well as to change the distance between the ion pair in the homologous series of ILs.

With an increase of the alkylic chain length, the δ signals for the H^2 and H^6 atoms begin to move upfield (shielding), while the resonance frequency of the H^4 and H^5 protons are practically unchanged. The upfield δ gives an increase in the distance between the chloride-anion and the corresponding hydrogen atoms of the aromatic ring. For example, according to calculations (see Table 6), the distance $r_{(\text{H}^2\cdots\text{Cl})}$ for $[\text{C}_2\text{MPy}]\text{Cl}$ is 2.192 Å, and Θ angle=11.148°, whereas $[\text{C}_{10}\text{MPy}]\text{Cl}$ is 2.216 Å, and 14.192°, this corresponds to a change δ^2 of 9.617 ppm to 9.323 ppm.

The replacement of the Cl^- -anion with the Br^- -anion leads to a significant move upfield for the IL hydrogen atoms. This can be attributed to differences in the effective charges on the atoms and the distances between the cations and the Cl^-/Br^- -anions. According to quantum chemical calculations, the $r_{(\text{H}^2\cdots\text{Cl})}$ distances for some of the chloride-based models are less than the corresponding bromides.

For almost all the pyridinium-based salts, we did not observe any significant changes in $\Delta\delta$ for the hydrogen atoms of the methyl (labelled 3'' and extreme in the ring from 2' to 10') and methylene (except for the extreme groups: from 2' to 9') groups following changes of the alkyl chain length and/or anion species. This indicates the relatively minimal interaction of the anion with the hydrocarbon atoms of the alkyl chain. It may be noted that for $[\text{AMPy}]\text{Cl}$, the H^3 atom is more upfield shifted in comparison with the same atom for $[\text{C}_3\text{MPy}]\text{Cl}$. These effects can be explained by the greater sensitivity due to the π -electron contribution to the allylic substituent, and the presence of two doublets splitting for the group 3' from two magnetically inequivalent protons in the *cis*- and *trans*-positions (Figure 11).

ILs	2	3''	4	5	6	1'	2'	3'	4'	5'	6'	7'	8'	9'	10'	a
[C ₂ MP y]Cl	9.617	2.597	8.182	7.949	9.475	4.974	1.650									
	s	s	d, J=7.7	t, J=14	d, J=6.3	t, J=21.7	t, J=14.7									
[C ₃ MP y]Cl	9.441	2.601	8.207	7.984	9.353	4.888	2.053	0.959								
	s	s	d, J=7.7	t, J=14	d, J=6.3	t, J=14.7	J=36.4	t, J=14.7								
[C ₄ MP y]Cl	9.633	2.584	8.192	7.968	9.450	4.928	1.974	1.348	0.880							
	s	s	d, J=7.7	t, J=14	d, J=5.6	t, J=14.7	J=30.1	J=37.8	t, J=14.7							
[C ₅ MP y]Cl	9.307	2.585	8.211	7.995	9.237	4.869	1.976	1.294		0.817						
	s	s	d, J=7.7	t, J=14	d, J=5.6	t, J=14.7	J=29.4	J=11.2		t, J=14.7						
[C ₆ MP y]Cl	9.338	2.576	8.205	7.993	9.241	4.855	1.961	1.270	1.197		0.780					
	s	s	d, J=7.7	t, J=14	d, J=5.6	t, J=14.7	J=30.1	J=58.8	J=49.7		t, J=14.7					
[C ₇ MP y]Cl	9.592	2.579	8.191	7.979	9.394	4.909	1.974	1.292	1.240	1.157		0.760				
	s	s	d, J=7.7	t, J=14	d, J=5.6	t, J=15.4	J=30.1	J=29.4	J=28.7	J=42		t, J=14				
[C ₈ MP y]Cl	9.566	2.573	8.188	7.979	9.370	4.890	1.966	1.286	1.227	1.142		0.758				
	s	s	d, J=7.7	t, J=14	d, J=5.6	t, J=14.7	J=30.8	J=29.4	J=28.7	J=53.2		t, J=14				
[C ₉ MP y]Cl	9.488	2.591	8.198	7.987	9.341	4.906	1.978	1.304	1.257	1.186	0.793					
	s	s	d, J=7.7	t, J=14	d, J=6.3	t, J=15.4	J=30.1	J=30.1	J=20.3	J=67.2	t, J=14				0.793	
[C ₁₀ MP y]Cl	9.323	2.586	8.207	7.992	9.235	4.871	1.966	1.278	1.215	1.178	1.805					1.805
	s	s	d, J=8.4	t, J=13.3	d, J=5.6	t, J=14.7	J=29.4	J=45.5	J=27.3	J=13.3	t, J=14					
[AMPy]Cl	9.473	2.598	8.221	7.962	9.557	5.682	6.123	5.565								
	s	s	d, J=8.4	t, J=14	d, J=6.3	t, J=6.3	J=39.9	d, d								
[C ₂ MP y]Br	9.510	2.626	8.224	7.972	9.357	5.007	1.697									
	s	s	d, J=8.4	t, J=14	d, J=6.3	t, J=21.7	t, J=14									
[C ₄ MP y]Br	9.490	2.614	8.236	7.987	9.312	4.924	1.998	1.385	0.917							
	s	s	d, J=7.7	t, J=11.9	d, J=4.2	t, J=14.7	J=28.7	J=37.1	t, J=14.7							
[C ₄ MP y]CH ₃ COO	9.198	2.573	8.119	7.928	9.198	4.818	1.934	1.344	0.900							3.540
	s	s	d, J=8.4	t, J=14.7	d, J=4.2	t, J=15.4	J=23.1	J=37.8	t, J=14.7							

Table 9. Chemical shifts δ (ppm), and spin-spin coupling J (Hz) from the ¹H-NMR spectra for ILs with CDCl₃ [19]

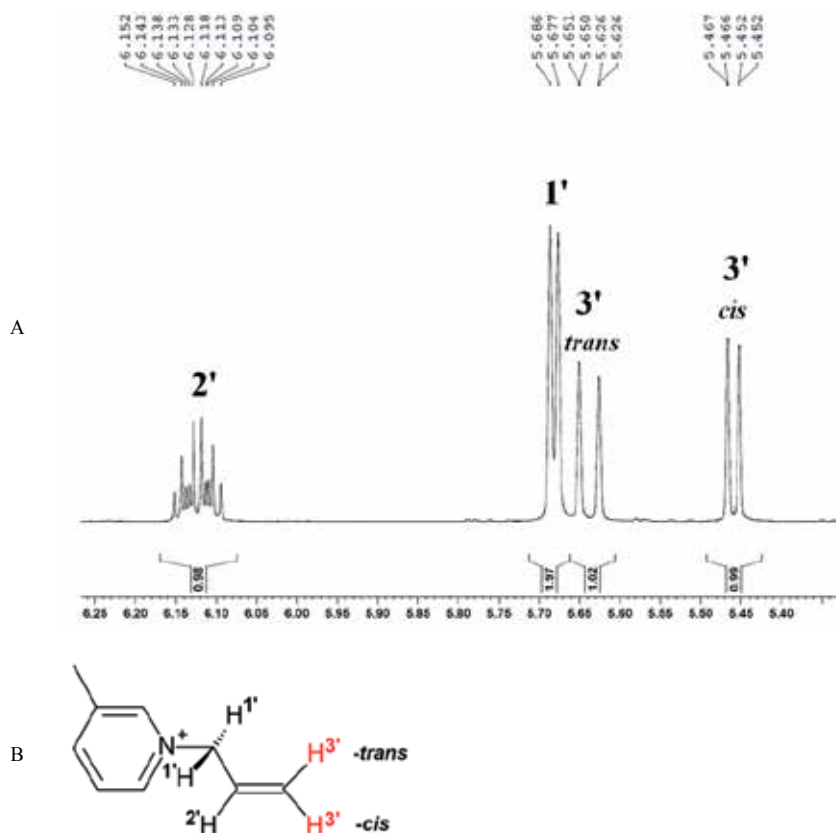


Figure 11. Fragment of the $^1\text{H-NMR}$ spectrum, indicating the peaks of the allylic substituent in $[\text{AMPy}]\text{Cl}$ (A), and the structure of the $[\text{AMPy}]^+$ cation (B). Here $\delta=5.459$ ($d, J=10.5$ Hz, 1H) – 3',-cis; $\delta=5.639$ ($d, J=17.5$ Hz, 1H) – 3',-trans; $\delta=5.682$ ($d, J=6.3$ Hz, 2H) – 1'; $\delta=6.123$ ($ddt, J=39.9$ Hz, 1H) – 2'

In this way, the $^1\text{H-NMR}$ signals of the spectra for ILs depend strongly on the structure, and this firstly depends on the distances between the cation and anion.

3.2.2. Thermal analysis of 1-alkyl-3-methylpyridinium-based ILs

The phase transition for ILs was investigated using DSC calorimetry and the heated stage [20]. Table 10 shows the melting points and glass transition values for IL.

It should be noted that the glass transition was not revealed for all the ILs. It appeared that the DSC-method was not useful for finding the melting points of some of the ILs, mainly with an odd number of carbon atoms in the alkylic chain. Most of the melting peaks obtained by DSC were not clearly defined. It was impossible to determine the melting point of $[\text{C}_4\text{MPy}]\text{Br}$ by means of DSC, but that IL was a greenish-brown viscous liquid at room temperature, and therefore it could be related to the room temperature ionic liquid (RTIL) species. In contrast, the salt $[\text{C}_2\text{MPy}]\text{Br}$, due to the high value of its melting point, was not considered as an ionic liquid.

ILs	Glass trans. (DSC)			Melting (DSC)			Melting (Bo.)
	Onset	T _g	Endpt	T _m	Endpt	Ref.	
[C ₂ MPy]Cl	25	29	33				130
[C ₃ MPy]Cl	9	18.5	28				92
[C ₄ MPy]Cl	17	35	53	93	113	95 [4], 111.35 [9]	97
[C ₅ MPy]Cl	16	21.5	27				92
[C ₆ MPy]Cl				62	84	81.95 [9]	77
[C ₇ MPy]Cl	8	16.5	25				72
[C ₈ MPy]Cl				69	83	67.1 [10], 80.05 [9]	74
[C ₉ MPy]Cl							64
[C ₁₀ MPy]Cl				55	82	79.35 [9]	64
[AMPy]Cl	18	27.5	37				108
[C ₂ MPy]Br				146	165		163
[C ₄ MPy]Br							RTIL
[C ₄ MPy]CH ₃ COO							RTIL

Table 10. ILs glass transition temperature and melting obtained by differential scanning calorimetry (DSC) and use of the Boetius heated stage (Bo.), °C [20]

In general, it was noticed that there is a tendency that the melting point values of 1-alkyl-3-methylpyridinium chloride-based ILs are reduced with a lengthening of the alkylic chain. This trend could be explained by a decrease in the packing density of the ion pairs of IL following an increase in the number of the alkylic chain carbon atoms.

A complete decomposition of the IL sets is seen at a temperature of about 250 °C [20]. The decomposition temperature values slightly decreased with the growth of the alkylic chain length. Furthermore, again the quaternary pyridinium salts, [C₂MPy]Cl and [C₃MPy]Cl, appeared to be the exceptions, as well as with respect to the melting point tendency. A change of the anion ambiguously affected the decomposition temperature, thus [C₂MPy]Br decomposed at a higher temperature than [C₂MPy]Cl but the decomposition temperature of bromides and chlorides with the [C₄MPy]⁺cation was comparable.

With the use of a gas chromatography-mass spectroscopy, we can identify the fragments resulting from the decomposition [C₄MPy]Cl (at temperatures up to 280 °C). In the chromatogram shown in Figure 12A, there are two significant peaks. Peak 1 (*M/Z* 93, 94, Figure 12B) corresponds to 3-methylpyridine, CAS №108-99-6 (with a similarity of 94%). This result is expected, since the 3-methylpyridine is a natural result of the fragmentation of these salts. Peak 2 (*M/Z* 150, 151) when compared with the libraries FFNSC 1.2 and NIST08 does not give a satisfactory result. The said peak value may correspond to an isolated cation (C₁₀H₁₆N) with a molecular weight of 150.2417 g mol⁻¹. A peak with different *M/Z* values is less intense, but the molecular weight can suggest some probable fragments (Figure 13). From the analysis of

Figures 12B and 13, it becomes obvious that the peaks with an M/Z of less than 79 – 77 may represent fragments of the ILs, formed in the destruction of the pyridinium ring.

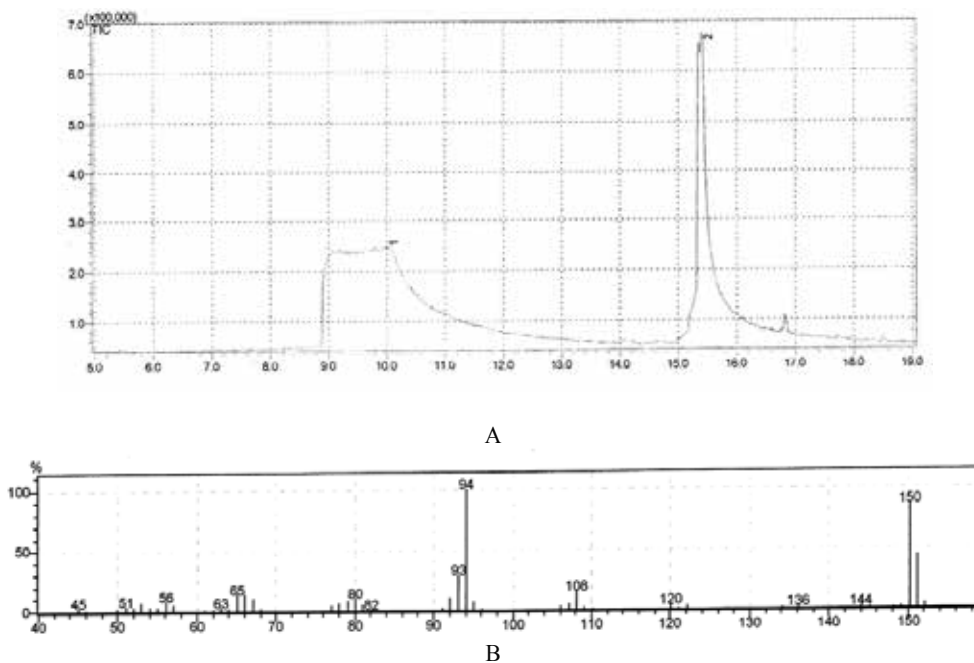


Figure 12. Chromatogram: the function of the time input sample $[C_4MPy]Cl$, and the values of the detector signal (A); mass spectrum: the M/Z function and the peaks' intensity (B)

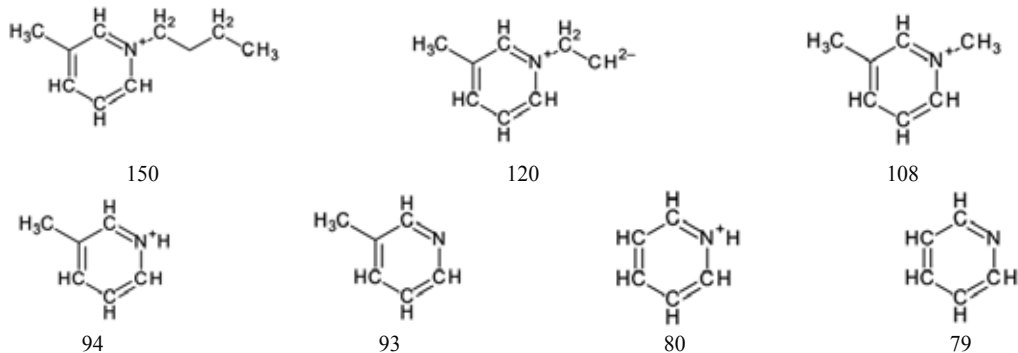


Figure 13. Series of hypothetical fragments formed during the decomposition of $[C_4MPy]Cl$. Numerals showing the molecular weight of these fragments

Thus, the decomposition fragments of $[C_4MPy]Cl$ are 1-alkyl-3-methylpyridinium cations, 3-methylpyridine, *etc.*

3.2.3. Solvatochromism of 1-alkyl-3-methylpyridinium-based ILs solutions

To determine the Kamlet-Taft hydrogen bond acceptor (basicity, β parameter) for the series of ILs we used indicator [Cu(tmen)(acac)](ClO₄). The obtained data of the β parameter for ILs (from 0.70 to 0.99) indicate a relatively high basicity of the 1-alkyl-3-methylpyridinium-based ILs. More detailed information will be published in other works.

4. Dissolution mechanism of cellulose in pyridinium-based ionic liquids

4.1. Dissolution of cellulose with 1-alkyl-3-methylpyridinium-based ILs

Our study of the solubility of cellulose in the synthesized ILs showed that for the same cation the 1-alkyl-3-methylpyridinium bromides show a lower dissolving ability than chlorides, the latter providing more concentrated solutions of cellulose (Table 11). This is consistent with the results of studies on 1-alkyl-3-methylimidazolium halides [7]. An increase in the temperature from 110 to 165 °C leads to a twofold increase in the maximum concentration of cellulose in the solutions of the bromide-containing ILs. With the increasing length of the substituent in the pyridinium chloride ionic liquids, their dissolving power toward cellulose decreases. A similar trend was found for 1-alkylpyridinium [25-29] and 1-alkyl-3-methylimidazolium [27] halides.

ILs	Temperature, °C	D, wt%
[C ₂ MPy]Cl	140	26
[C ₃ MPy]Cl	110	22
	120	22.5
[C ₄ MPy]Cl	120	23
[C ₅ MPy]Cl	110	21
	120	21
[C ₆ MPy]Cl	110	19
	120	19
[C ₇ MPy]Cl	110	14.5
	120	15
[C ₈ MPy]Cl	110	6.5
	120	8
[C ₉ MPy]Cl	110	4
	120	5.5
[C ₁₀ MPy]Cl	110	6

ILs	Temperature, °C	D, wt%
	120	7.5
[AMPy]Cl	130	24
[C ₂ MPy]Br	165	6.5
	110	3.5
[C ₄ MPy]Br	165	7
[C ₄ MIm]Cl	120	17

Table 11. The maximum achieved concentration (D) of cellulose Alicell Super (DP 599) in chloride- and bromide-based ILs [7]

Thus, the results obtained suggest that 1,3-disubstituted pyridinium cation-based ILs are the most effective solvents for cellulose. Pyridinium salt can dissolve 1.5 times more cellulose than the imidazolium salt with the same substituents and anion. This is confirmed by the data of [4, 6]. We can obtain the 5–6 wt% cellulose solutions in [C₂MPy]Cl, [C₃MPy]Cl, [C₄MPy]Cl, [C₅MPy]Cl, [C₆MPy]Cl during 7–15 min (Figure 14).

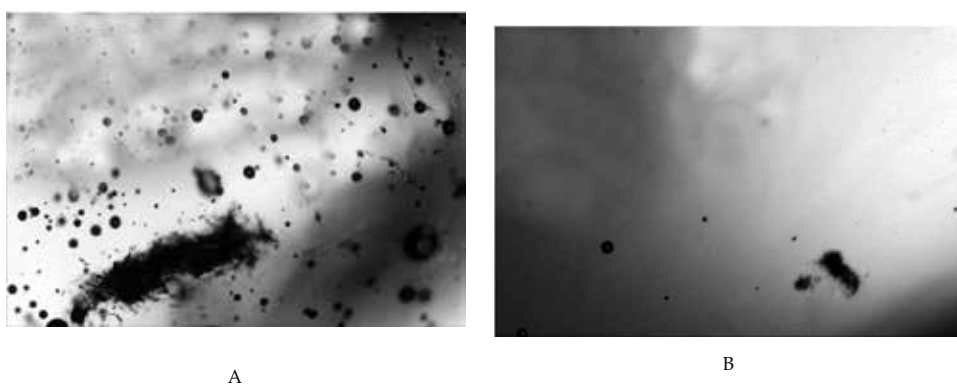


Figure 14. Dissolution of 5 wt% of cellulose with [C₄MPy]Cl for 1 min (A), and 10 min (B) at 120 °C. Increased by four times

The influence of the temperature during the dissolution is accompanied by the degradation of the natural polymer, as exemplified by the reduction in the degree of polymerization (DP) (Table 12).

Dissolution time, min	0	20	120	180
DP	734	419	137	<100

Table 12. DP changing for regenerated cellulose films from their solution in [C₄MPy]Cl at 120 °C, and its influence on dissolution time:

In the FTIR spectra of regenerated cellulose samples of IL, we observed the appearance of characteristic peaks at $\sim 1000\text{ cm}^{-1}$ corresponding predominantly to the $\text{C}^6\text{H}_2\text{-O}^6\text{H}^6$ group. Their presence indicates the modification of cellulose II [30]. For the modification of cellulose I (Alicell Super) stretching vibrations of $\nu_{\text{C}^6\text{-O}^6}$ were observed at 1031 cm^{-1} . The appearance of two bands at 3440 cm^{-1} and 3484 cm^{-1} (the weak hydrogen bond group of $\text{C}^2\text{-O}^2\text{H}^2$) also indicate the modification of cellulose II (Figure 15).

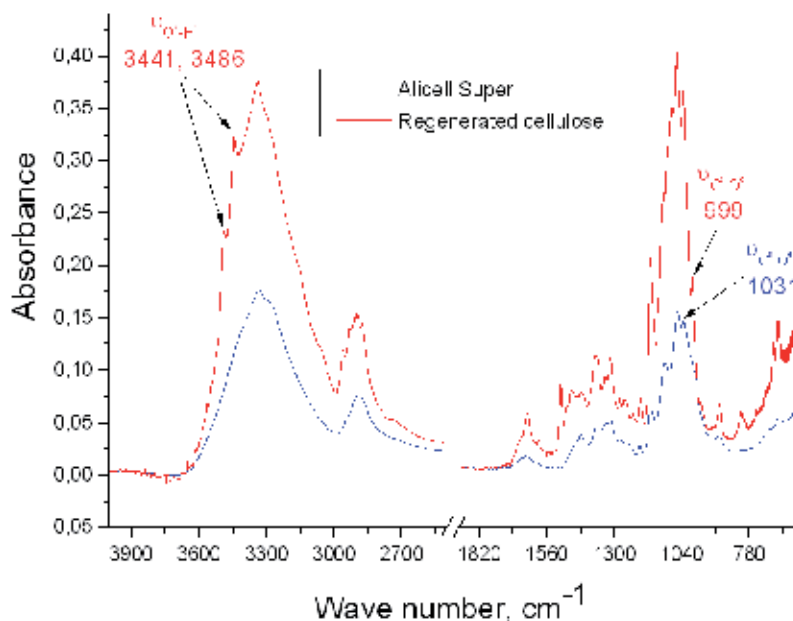


Figure 15. FTIR spectra of Alicell Super and regenerated cellulose from a 23 wt% solution in $[\text{C}_4\text{MPy}]\text{Cl}$

4.2. Study of cellulose solutions with 1-alkyl-3-methylpyridinium-based ILs by $^1\text{H-NMR}$ spectroscopy

Table 12 presents $^1\text{H-NMR}$ chemical shifts values for cellulose solutions in $[\text{C}_4\text{MPy}]\text{Cl}$ and $[\text{C}_4\text{MPy}]\text{CH}_3\text{COO}$. The $\Delta\delta$ values for cellulose varied insignificantly for each of the peaks. We observed the greatest change of $\Delta\delta$ ($\Delta\delta = \delta_{\text{solution}} - \delta_{\text{IL}}$) for cellulose in $[\text{C}_4\text{MPy}]\text{Cl}$ for H^2 and H^6 protons of the pyridine ring, which shifted upfield. This could be related to the distancing of the anion interacting with the cellulose at the formation of the hydrogen bond. The chemical shifts of H^2 and H^6 changed insignificantly for $[\text{C}_4\text{MPy}]\text{CH}_3\text{COO}$ after adding cellulose to the solution. It could be assumed that this was related to the ability of the acetate anion to interact simultaneously with two electron-acceptor centres (cellulose hydroxyls and the IL cation). The δ^a downfield shift of the acetate hydrogen's atoms of the $-\text{CH}_3$ group confirmed that the anion of the IL interacted with the cellulose.

ILs	2	4	5	6		
[C ₄ MPy]Cl	9.573 (-0.060)	8.199 (0.007)	7.977 (0.009)	9.425 (-0.025)		
[C ₄ MPy]CH ₃ COO	9.202 (0.004)	8.117 (-0.002)	7.926 (-0.002)	9.202 (0.004)		
A. IL ring protons						
ILs	3''	1'	2'	3'	4'	a
[C ₄ MPy]Cl	2.601 (0.017)	4.943 (0.015)	1.986 (0.012)	1.367 (0.019)	0.903 (0.023)	
[C ₄ MPy]CH ₃ COO	2.569 (-0.004)	4.814 (-0.004)	1.931 (-0.003)	1.340 (-0.004)	0.917 (0.017)	3.780 (0.240)
B. IL protons of -CH ₃ and -CH ₂ groups						

Table 13. Chemical shifts (δ), taken from the ¹H-NMR spectra of cellulose solutions in [C₄MPy]Cl, [C₄MPy]CH₃COO, and their changing $\Delta\delta$ (shown in parentheses) of relative solvents (see Table 9). The solutions were obtained in CDCl₃ [19]

Therefore, the interaction of cellulose with pyridinium-based ILs is caused by the ability of the IL anion to exist as the hydrogen bond acceptor.

4.3. Study of the mechanism of cellulose solvation by 1-alkyl-3-methylpyridinium-based ILs using a quantum-chemical calculation

A study of the formation of 'cellulose – ionic liquids' complexes were performed by HF/6-31G(d) quantum-chemical calculation method for the 'cellotetraose – 1-butyl-3-methylpyridinium X' model, wherein X are acetate-, chloride-, and bromide-anions. The geometry of the complexes with optimum energy characteristics are shown in Figure 16.

The formation of the solvate complex is accompanied by the appearance of two hydrogen bonds between the anion and the primary O⁶H⁶, and the secondary O²H² hydroxyl from the neighbouring glycosidic link of the cellotetraose. The distance between the anion and the hydrogen atoms of the cellotetraose hydroxyls, $r_{(H6-X)}$, $r_{(H2-X)}$, ranges from 1.8 to 2.7 Å, and increases in the series of [[C₄MPy]CH₃COO < [C₄MPy]Cl < [C₄MPy]Br.

The geometric characteristics obtained meet the criteria for the formation of the hydrogen bonds [31]: for example, the formation of a hydrogen bond with the chloride-anion has a distance C_{sp³}-OH...Cl⁻ in ranges from ~2 Å to ~2.4 Å, and a bond angle (between O, H and Cl) > 140°. The anion of the solvent model is positioned closer to the hydrogen atom of the primary hydroxyl group C⁶H₂-O⁶H⁶.

The interaction of [C₄MPy]Br with the model of the cellulose (Figure 16B), as shown by quantum-chemical calculations, is similar: anion forms hydrogen bonds with both the primary

and secondary hydroxyl groups. The distance between the bromide-anion and the cellotetraose hydroxyl is larger than it is for the chloride-anion (2.445 Å for $O^6H^6 \dots Br$, 2.710 Å for $O^2H^2 \dots Br$ and 2.295 Å for $O^6H^6 \dots Cl$, 2.514 Å for $O^2H^2 \dots Cl$), because the length of the hydrogen bond between the halide and H-donor increases with the radii of the halide-ions [31].

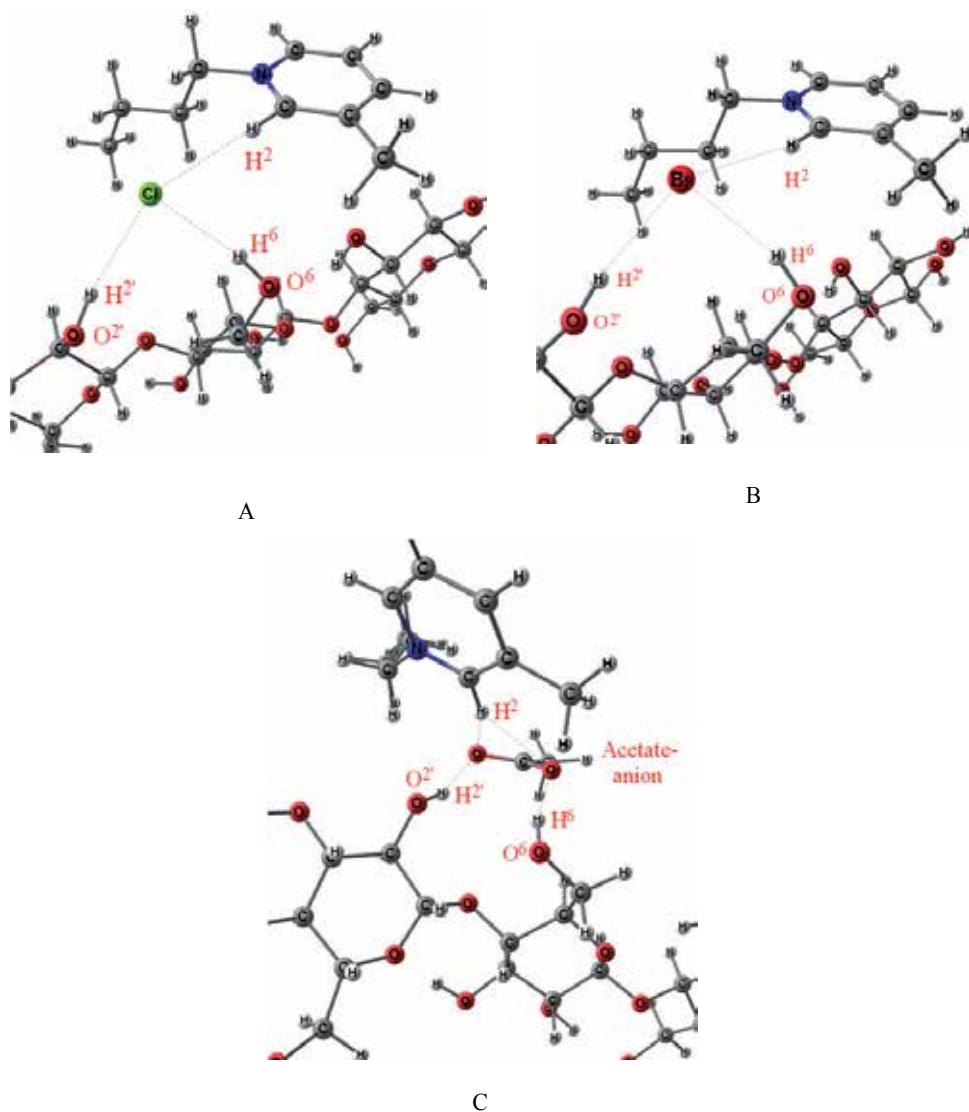


Figure 16. Fragments of optimized complexes of cellotetraose with 1-butyl-3-methylpyridinium chloride (A), bromide (B), and acetate (C)

	Parameters	$[C_4MPy]CH_3COO$	$[C_4MPy]Cl$	$[C_4MPy]Br$
Distances	$r_{(H2...X)}$, Å		2.531 (0.316)	2.640 (0.263)
	$r_{(H2...O1)}$, Å	2.403 (0.562)		
	$r_{(H2...O2)}$, Å	2.252 (-0.274)		
	$r_{(H2'-X)}$, Å	1.853	2.514	2.710
	$r_{(H6-X)}$, Å	1.806	2.295	2.445
Angles	X-O ² -H ² , deg.	160.17	166.52	167.46
	X-O ⁶ -H ⁶ , deg.	165.33	163.94	158.09

Table 14. The main calculated parameters for the solvation complexes of cellotetraose with $[C_4MPy]CH_3COO$, $[C_4MPy]Cl$, and $[C_4MPy]Br$. (In parentheses are the values of the changing parameters relative to the IL pairs, see. Tables 6 and 7)

5. Conclusion

Thus, using quantum-chemical calculations, the features of the interaction of cellulose with 1-alkyl-3-methylpyridinium-based ILs were identified. This shows a decrease in the intensity of the binding of the hydroxyl anions in the series CH_3COO^- , Cl^- , Br^- , which explains the difference in the solvent power of ILs.

According to the theoretical studies (quantum-chemical calculations) and experimental studies (analysis of the chemical shifts), we propose a probable mechanism of the solvation of pyridinium ILs with cellulose, shown in Figure 17.

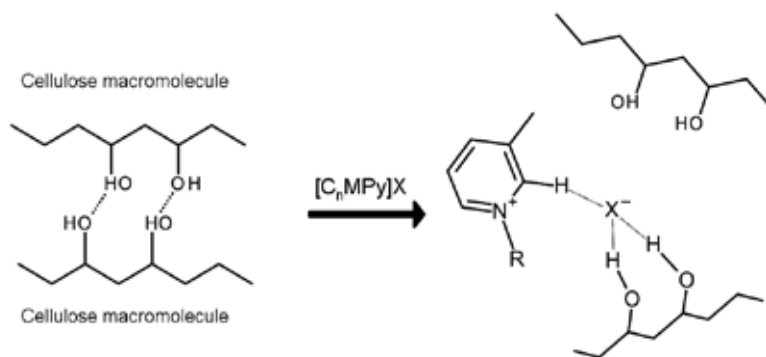


Figure 17. Schematic representation of the interaction mechanism of cellulose with pyridinium-based ILs

In the first stage, the interaction of the polymer with the solvent's anion forms hydrogen bonds with primary and secondary cellulose hydroxyls. The anion maintains ionic bonding with the cation, which at solvation was weakened (the distance between the ions increases).

Acknowledgements

This work was supported by the Ministry of Education and Science of the Russian Federation (State Task No. 2014/186).

Author details

Elena S. Sashina* and Dmitrii A. Kashirskii

*Address all correspondence to: organika@sutd.ru

Institute of Applied Chemistry and Ecology, St. Petersburg State University of Technology and Design, St. Petersburg, Russia

References

- [1] Tan S.S.Y., MacFarlane D.R. Ionic Liquids in Biomass Processing, *Topics in Current Chemistry* 2010; 290 311-339.
- [2] da Costa Lopes A.M., Joãoa K.G., Rubik D.F., Bogel-Lukasik E., Duarte L.C., Andraeus J., Bogel-Lukasik R. Pre-treatment of lignocellulosic biomass using ionic liquids: Wheat straw fractionation. *Bioresource Technology* 2013; 142 198-208.
- [3] da Costa Lopes A.M., João K.G., Morais A.R.C., Bogel-Lukasik E., Bogel-Lukasik R. Ionic liquids as a tool for lignocellulosic biomass fractionation. *Sustainable Chemical Processes* 2013; 1 3.
- [4] Heinze T., Schwikal K., Barthel S. Ionic liquids as reaction medium in cellulose functionalization. *Macromolecular Bioscience* 2005; 5 520-525.
- [5] Swatloski R.P., Spear S.K., Holbrey J.D., Rogers R.D. Dissolution of Cellulose with Ionic Liquids. *Journal of the American Chemical Society* 2002; 124(18) 4974–4975.
- [6] Basa M.L.T.N. Ionic Liquids: Solvation Characteristics and Cellulose Dissolution. PhD thesis. University of Toledo; 2010.
- [7] Sashina E.S., Kashirskii D.A., Zaborski M., Jankowski S. Synthesis and dissolving power of 1-alkyl-3-methylpyridinium-based ionic liquids. *Russian Journal of General Chemistry*. 2012; 12(82) 1994-1998.
- [8] Harjani J.R., Singer R.D., Garcia M., Scammells P.J. Biodegradable pyridinium ionic liquids: design, synthesis and evaluation. *Green Chemistry*. 2009; 11 83-90.

- [9] Pereiro A.B., Rodriguez A., Blesic M., Shimizu K., Lopes J.N.C., Rebelo L.P.N. Mixtures of Pyridine and Nicotine with Pyridinium-Based Ionic Liquids. *Journal of Chemical & Engineering Data*. 2011; 56 4356-4363.
- [10] Sastry N.V., Vaghela N.M., Macwan P.M., Soni S.S., Aswal V.K., Gibaud A. Aggregation behavior of pyridinium based ionic liquids in water – Surface tension, ¹H NMR chemical shifts, SANS and SAXS measurements. *Journal of Colloid and Interface Science*. 2012; 371 52–61.
- [11] Sashina E.S., Kashirskii D.A., Martynova E.V. Features of the molecular structure of pyridinium salts and their dissolving power with respect to cellulose. *Russian Journal of General Chemistry*. 2012; 4(82) 729-735.
- [12] Conceição L.J.A., Bogel-Łukasik E., Bogel-Łukasik R. A new outlook on solubility of carbohydrates and sugar alcohols in ionic liquids. *RSC Advances* 2012; 2 1846-1855.
- [13] Zakrzewska M.E., Bogel-Łukasik E., Bogel-Łukasik R. Solubility of Carbohydrates in Ionic Liquids, *Energy & Fuels*. 2010; 24 737-745.
- [14] Sashina E.S., Novoselov N.P., Kuz'mina O.G., Troshenkova S.V. Ionic liquids as new solvents of natural polymers, *Fibre Chemistry*. 2008; 3(40) 270-277.
- [15] Kuzmina O.G., Sashina E.S., Novoselov N.P., Zaborski M. Blends of cellulose and silk fibroin in 1-butyl-3-methylimidazolium chloride based solutions. *Fibres & Textiles in Eastern Europe*. 2009; 6(77) 36-39.
- [16] Cho C., Jeon Y., Pham T.P.T., Vijayaraghavan K., Yun Y. The ecotoxicity of ionic liquids and traditional organic solvents on microalga *Selenastrum capricornutum*. *Ecotoxicology and Environmental Safety*. 2008; 71 166–171.
- [17] Couling D.J., Bernot R.J., Docherty K.M., Dixona J.N.K., Maginn E.J. Assessing the factors responsible for ionic liquid toxicity to aquatic organisms via quantitative structure–property relationship modeling. *Green Chemistry*. 2006; 8 82-90.
- [18] Docherty K.M., Kulpa C.F. Toxicity and antimicrobial activity of imidazolium and pyridinium ionic liquids. *Green Chemistry*. 2005; 7 185-189.
- [19] Sashina E.S., Kashirskii D.A., Jankowski S. PMR study of structural features of ionic liquids based on 1-alkyl-3-methylpyridinium and mechanism of their interaction with cellulose. *Fibre Chemistry*. 2014; 5(45) 268-273.
- [20] Sashina E.S., Kashirskii D.A., Janowska G., Zaborski M. Thermal properties of 1-alkyl-3-methylpyridinium halide-based ionic liquids. *Thermochimica Acta*. 2013; 568 185-188.
- [21] Krygowski T.M., Szatyłowicz H., Zachara J.E. How H-bonding Modifies Molecular Structure and π -Electron Delocalization in the Ring of Pyridine/Pyridinium Derivatives Involved in H-Bond Complexation. *The Journal of Organic Chemistry*. 2005; 70 8859-8865.

- [22] Sashina E.S., Novoselov N.P. Effect of structure of ionic liquids on their dissolving power toward natural polymers. *Russian Journal of General Chemistry*. 2009; 6(79) 1057-1062.
- [23] Zherenkova L.V., Komarov P.V., Pavlov A.S. A polymer in an ionic liquid: Structural properties of a system during attraction between the polymer and cations of the ionic liquid. *Polymer Science Series A*. 2010; 8(52) 864-871.
- [24] Klots T.D., Emilsson T., Ruoff R.S., Gutowsky H.S. *The Journal of Physical Chemistry*. 1989; 93(4) 1255–1261.
- [25] Holm J., Lassi U. Ionic Liquids in the Pretreatment of Lignocellulosic Biomass. In: Kokorin A. (ed.) *Ionic Liquids: Applications and Perspectives*. Rijeka: InTech; 2011. p529-544. Available from <http://www.intechopen.com/books/ionic-liquids-applications-and-perspectives/ionic-liquids-in-the-pretreatment-of-lignocellulosic-biomass> (accessed 21 February 2011).
- [26] Cellulose solution – United States Patent 1943176/ Charles, Graenacher Publication Date: 01.09.1934.
- [27] Aerov A.A., Khokhlov A.R., Potemkin I.I. Why Ionic Liquids Can Possess Extra Solvent Power. *The Journal of Physical Chemistry B*. 2006; 33(110) 16205-16207.
- [28] Park T.-J., Murugesan S., Linhardt R.J. Cellulose composites prepared using ionic liquids (ILs)-Blood Compatibility to Batteries. In: Edgar K.J., Heinze T., Buchanan C.M. (ed.). *ACS Symposium Series: Polysaccharide Materials: Performance by Design*. Washington: American Chemical Society; 2009. p.133-152.
- [29] Bentivoglio G., Röder T., Fasching M., Buchberger M., Schottenberger H., Sixta H. Cellulose processing with chloride-based ionic liquids. *Lenzinger Berichte*. 2006; 86 154-161.
- [30] Maréchal Y., Chanzy H. The hydrogen bond network in I β cellulose as observed by infrared spectrometry. *Journal of Molecular Structure*. 2000; 523 183-196.
- [31] Bernet B., Vasella A. Intra-and Intermolecular H-Bonds of Alcohols in DMSO, ¹H-NMR Analysis of Inter-Residue H-Bonds in Selected Oligosaccharides: Cellobiose, Lactose, N,N'-Diacetylchitobiose, Maltose, Sucrose, Agarose, and Hyaluronates. *Helvetica Chimica Acta*. 2000; 9(83) 2055-2071.

Utilization of Ionic Liquids in Wood and Wood-Related Applications — A Review

Samir I. Abu-Eishah

Additional information is available at the end of the chapter

<http://dx.doi.org/10.5772/59079>

1. Introduction

The development of potentially “green” technologies based on renewable feedstock’s is one of the main challenges for mankind in the next decades and centuries underlining the social and economic importance of research conducted in this area [1]. Wood is one of the most versatile biological raw materials that is available today in large, renewable reserves around the world. Wood products have countless important industrial applications, such as in design, furniture and construction. These applications have a bright future ahead. At the same time, chemical and mechanical wood processing provides the basis for a growing range of globally significant fiber-based tissue, paper and packaging applications and solutions. At the sharp end, advances in the use of the individual chemicals and polymers that make up wood are creating the foundation for future biorefineries and helping change the shape of society for the better. The human use of wood reaches back thousands of years. The nowadays escalating global population and limited natural resources, however, call for new ways of improving the efficiency of our use of this vital natural resource. This opens up significant opportunities for products based on renewable, non-food materials (‘non-food bio-products’) [2].

In addition, the fading fossil resources with the simultaneously increasing demand for global energy and arising environmental concerns generate a strong need for new technologies based on renewable and inexhaustible resources. Thus in the face of the current oil prices and the sustainability challenges, the bio-economy concept is the fast winning ground. The question arises, can we increase the share of “consumer products” using renewable raw materials, like wood, instead of the non-renewable resources, like oil? The forest-based industry sees this opportunity and believes that the industry will play a decisive role in the development towards a bio-economy. With this goal in sight, diversifying the product output of the primary wood

refining process – pulping – is a rational strategic starting point. The pulp mills of today are being redefined as the biorefineries of tomorrow [2].

Fossil fuel resources are limited so alternative renewable resources are needed to fill the gap that inevitably will be created once the fossil resource supplies start to dwindle. Biomass has the potential to fill this gap. To utilize this renewable resource in the production of fuel and chemicals, the so called “biorefineries” specialized in fractionation and making use of all components of the biomass are needed [3].

The development of potentially “green” technologies based on renewable feedstocks is one of the main challenges for mankind in the coming years underlining the social and economic importance of research conducted in this area. On this regard, biomass is expected to have the potential to fill the gap of the dwindling fossil fuel resources. Replacement of fossil fuels with new sustainable resources is becoming crucial due to the depleting petroleum reserves, increasing global energy demand, and arising environmental concerns. In particular, ligno-cellulosic biomass can be an alternative to fossil resources as a sustainable and environmentally-friendly feedstock for producing chemicals and fuels. However, today, only a small portion of the world’s annual production of biomass is utilized by mankind, while the rest is allowed to decay naturally.

With the inevitable depletion of petroleum-based resources, there has been an increasing worldwide interest in renewable resources such as biomass. One reason for the current approaches being taken to utilize biomass is the difficulty in processing lignocellulosic materials and the energy needed for separation of their components. The three major components of biomass (cellulose, lignin, and hemicellulose) are covalently bonded together, which makes dissolution and further separation of these components difficult. This has been recognized as the grand challenge for biomass utilization [4]. Ionic liquids (ILs) are relatively new family of solvents for dissolution of cellulose and could aid in this task.

The use of ILs for cellulose dissolution stems from the unique properties of these solvents to interact with the strong hydrogen bonds of polysaccharides. The scientific discovery of the dissolution of cellulose in ILs is being translated into new processing technologies, cellulose functionalization methods and new cellulose materials including blends, composites, fibers and ion gels. These materials can replace current analogs to overcome the environmental issues associated with petroleum-based products. Although there are many ILs available that can dissolve cellulose, the processing difficulties such as fractionation need to be overcome to support large-scale use. The dissolution and functional modification of cellulose in ionic liquids based on previous researches have been reviewed and summarized by reference [5]. However, due to the chemical versatility of both cellulose and ILs new developments leading to the next generation of cellulosic materials are expected in the near future [6].

Dissolution of cellulose in ILs allows the comprehensive utilization of cellulose by combining two major “green” chemistry principles; using environmentally-preferable solvents and bio-renewable feed-stocks. However, the utilization of cellulose or cellulosic materials has not been developed entirely because of its poor solubility in common organic solvents. But the cellulose dissolved in ILs can be regenerated with anti-solvents such as water, ethanol and acetone.

Ionic liquids are organic compounds that contain at least one ionic bond. ILs consist of organic cations and organic or inorganic anions. ILs are salts with melting points below 100 °C, which possess many advantageous properties. Moreover, ILs are non-volatile, non-toxic, nonflammable and thermally and chemically stable. Due to their larger molecular radii, ILs exhibit only weak cohesion compared with common salt.

In 2002, it was discovered that cellulose is soluble in ILs. Later ILs have been investigated as powerful solvents and reaction media for cellulose in its pure form and in its naturally surrounding matrix including hemicelluloses and lignin. ILs can dissolve cellulose as well as remove or reduce the lignin content in lignocellulosic materials. But it was shown that these solvents are not entirely inert and thus have to be selected carefully.

Hundreds of papers have been published in the literature in the past few years alone. Some ionic liquids such as [Amim]Cl and [Emim][OAc] have been proven highly effective in the dissolution of cellulose, lignin, and hemicellulose in different types of lignocellulosic biomass including corn stover, switchgrass, rice straw, and various hard and softwoods [7].

Investigation of the dissolution mechanism of lignocellulose in ILs revealed an ongoing degradation of the solute in dependence of temperature and solvent purity. Finally, ILs were shown capable to significantly reduce the energy demand of mechanical crushing steps in wood-based technologies as a consequence of their lubricating nature [1].

The bulk of the cellulose currently employed by industry is isolated from wood through Kraft pulping; a process which traditionally involves a barrage of environmentally detrimental chemicals and is undeniably “non-green”. Lignocellulosic materials are potentially a relatively inexpensive and abundant feedstock for biofuel production. The key to unlocking lignocelluloses recalcitrance is in part, the development of an effective pretreatment process [8].

A promising new pretreatment method for lignocellulosic materials relies on their solubility in solvent systems based on ILs and the interaction of natural polymers (present in wood) with ILs. The precipitated cellulose and lignin act as a natural binder for the wood particles thus avoiding the use of toxic organic resins as adhesives. The obtained composites present good water stability and compressive mechanical strength. Additionally, carbohydrates are important natural products that play important biological and commercial roles as food, drug and chemical feedstock. However, the use of natural carbohydrates has two main drawbacks: low solubility in most solvents and their complex highly chiral structures [9].

Lignin, a readily available form of biomass, is a potential source of renewable aromatic chemicals through catalytic conversion. Recent work has demonstrated that ILs are excellent solvents for processing woody biomass and lignin. Seeking to exploit ILs as media for depolymerization of lignin, the reactions of lignin model compounds in or with ILs has been investigated [10].

Looking at the solubility of lignocellulosics in ionic liquids, a thorough literature review was performed by reference [11]. The survey combined with additional screening of a range of in-house ionic liquid structures allows identifying potential opportunities with regard to efficiency of cellulose and lignin dissolution as well as wood fibrillation.

Ionic liquids have shown great potential in the field of biomass processing in general and in the pretreatment of lignocellulose in particular. However, a few things need to be addressed before any large-scale processing can be considered: Finding new routes for IL synthesis that make “on-site” production possible; investigation into the challenges facing IL pretreatment of lignocellulose such as possible depolymerization of cellulosic material during the pretreatment and investigating what influence different ILs have on the pretreatment of cellulosic material by methods like enzymatic hydrolysis [3].

Lignocellulose dissolution in ILs is a relatively new biomass pretreatment technology that is receiving growing interest from the biofuels community as a route to provide readily-hydrolyzable holocellulose. Despite its proven advantages over other pretreatment technologies – including feedstock invariance, high monomeric sugar yields over short saccharification times and extensive delignification– there are several core issues that stand in the way of commercialization. These include the relative high cost of the ILs themselves, a lack of knowledge in terms of process considerations for a biorefinery based on these solvents, and scant information on the coproducts this pretreatment technology could provide to the marketplace. An initial techno-economic model of a biorefinery that is based on the IL pretreatment technology has been presented and identified by reference [12], through a comprehensive sensitivity analysis, the most significant areas in terms of cost savings/revenue generation that must be addressed before IL pretreatment can compete with other, more established, pretreatment technologies. This new pretreatment technology has been evaluated through the perspective of a virtual operating biorefinery, and although there are significant challenges that must be addressed, there is a clear path that can enable commercialization of this novel approach.

Although some basic studies of ILs, such as their economical syntheses and toxicology are eagerly needed and some engineering problems still exist, research for application of ILs in wood-related industries has made great progress in recent years. The use of ILs has provided a new platform for efficient utilization of wood. A comprehensive database on toxicity of ILs has been established by reference [13]. The database includes over 4000 pieces of data. Based on the database, the relationship between IL's structure and its toxicity has been analyzed qualitatively. Furthermore, quantitative structure-activity relationships (QSAR) model has been conducted to predict the toxicities (EC_{50} values) of various ILs toward the Leukemia rat cell line IPC-81.

In this chapter, applications of ILs in wood and wood-related industries are reviewed. First, the use of ILs in wood preservation and the improvement of wood anti-electrostatic and fire-proof properties are illustrated. The dissolution of wood main constituents (cellulose, lignin, and hemicellulose) in ILs and its application are described along with “green” wood processing with ILs. Finally, application of ILs in dissolution of wood biomass and product retrieval media are briefly reviewed. A summary table of the abbreviations of the ionic liquids used in this chapter is presented in the Appendix.

2. Ionic liquids as wood preservatives

Wood is a widely-used, economical, and renewable building resource. However, untreated wood is subject to attack by insects and microorganisms, for example, decay, stain, mould fungi, and bacteria. To ensure long-term structural performance, wood must be protected from biotic wood degradation factors. Preserved wood can be defined as lumber or plywood that has been treated with wood preservatives to protect it from termites and fungal decay. Many preservatives have been used in wood industry, and still many efforts are made to develop new preservatives. The reason is that most of the wood preservatives in current use are chemicals that might be harmful to human health or are not eco-friendly [14].

Natural fibers are made up from different components; cellulose, hemicellulose and lignin are the main elements, but many natural fibers also contain pectin, small amounts of ash and may exhibit a thin wax layer on the surface [15]. Lignin is a 3-D, heavily cross-linked copolymer with aliphatic and aromatic structures. The aromatic structures are formed by the removal of water from a sugar unit. Several monomers can form lignin and the types and properties depend on the source material. In contrast to cellulose and hemicellulose, lignin is hydrophobic in nature. Together with the hemicellulose, it provides matrix for the strong cellulose fibrils [16]. Lignin also resists most microorganisms and its aerobic breakdown is slow, and therefore it protects the load bearing cellulose from a premature degradation [17,18].

Different types of lignin can be found in different plants and even within different plant structures. This can have a strong effect on not only biodegradation but also susceptibility to microbial activity and therefore fiber-retting during fiber processing [19].

Like cellulose, lignin is considered one of the most abundant bio-polymers of the world. However, to date, most of the industrially processed lignin is mainly used as an energy source for the paper industry and finds only few industrial applications [20]. Lignin is hydrophobic in spite of being completely amorphous. Lignin is found in close proximity to the cellulose micro-fibrils in natural fibers [21]. The varying interaction of cellulose, hemicellulose and lignin with moisture is responsible for the complex swelling behaviour of natural fibers [16].

ILs have shown great potential in becoming the eco-friendly, as well as free of both arsenic and pentachlorophenol, and yet they also show effectiveness as wood preservatives. An extensive research has been done on this subject in [22-24]; ILs in wood preservation has been addressed in [22] and protic ILs with organic anion as wood preservative has been discussed in [23]. Some ILs with a nitrate counter ion, such as 3-alkoxymethyl-1-methyl-imidazolium tetrafluoroborates and hexafluoro-phosphates, didecylmethyl-ammonium and benzalkonium nitrates, exhibited good fungicidal activity and could be potential candidates as wood preservatives [24]. In addition, the use of ILs in strategies for saving and preserving cultural artifacts has been discussed in [25].

On the other hand, four pyridinium-based ILs have been successfully tested in [26] as components of potential wood preservatives: 1-alkoxymethyl-3-dimethylamino-pyridinium chlorides, 1-alkoxymethyl-4-dimethylamino-pyridinium chlorides, 1-alkoxy methyl-3-dimethylamino-pyridinium acesulfamates and 1-alkoxymethyl-4-dimethylamino-pyridinium

acesulfamates. These ILs are new biocides that penetrate well into wood. The tested pyridinium ILs with an alkoxymethyl substituent, consisting of 8, 9 or 10 carbon atoms, exhibited fungicidal activity against the basidiomycetes *Coniophora puteana* and *Trametes versicolor* and the blue-stain fungus *Sclerophoma pityophila*.

However, the doses and toxic values of tested 1-decyloxymethyl-4-dimethylamino-pyridinium chloride and acesulfamate were found comparable with benzalkonium chloride and didecyl dimethyl ammonium chloride but the ILs tested were found largely unextractable from wood by water [26]. The mechanical properties of the wood treated with the former two ILs were lower than natural wood. Wood treated with the chloride and acesulfamate was, however, characterized by lower absorption of free water than the control wood. Only in the case of treatment with acesulfamate was the hygroscopicity of the treated wood distinctly lower than that of control wood. The durability of the wood was increased by 1-decyloxymethyl-4-dimethylamino-pyridinium chloride and acesulfamate.

Due to the high interest in the applications of ILs, new, cheaper, multifunctional ILs which are easy to prepare are highly desired. A new group of air- and moisture-stable, hydrophobic ammonium-based ILs and their properties, including the single-crystal X-ray structure of benzethonium nitrate has been presented in [24]. These salts have utility as anti-bacterial, anti-fungal agents. Additionally, the potential application of these ILs for wood preservation was tested with positive results. The toxicity of benzalkonium and didecyl dimethyl ammonium nitrates were studied and are presented therein.

Ranke [27] presented tabulated and referenced data to show that the use of conventional molecular solvents as a reference for IL toxicity to microorganisms and cell cultures has become common practice. On the other side of the activity spectrum, both cationic surfactants with antimicrobial or germicidal activity and reactive biocides have been chosen for convenient comparison of biological effects. The numerical results given in these studies suggest that IL toxicities toward microorganisms and cell cultures cover the whole range of biocidal potencies from rather inactive molecular solvents, such as ethanol or dimethyl sulfoxide that are biocompatible up to very high aqueous concentrations, up to highly active biocides, leading even to the proposal of some ILs as wood preservatives [23].

The use of ILs has provided a new platform for efficient utilization of wood. The applications of ILs in wood-related industries have been reviewed by [14]: dissolution of wood in ILs and its application, ILs used for wood preservation and improvement of wood anti-electrostatic and fire-proof properties, and finally, 'green' wood processing with ILs.

ILs with low hydrogen-bond basicity are not able to break the hydrogen bonds in the matrix and therefore do not expand it at all or only minimally, as observed for [Bmim][OTf] IL at 120°C. Since these ILs cannot dissolve the cellulose fibers, the wooden ultrastructure is preserved and no extraction is observed [28].

The wettability of wood surface protected with three ILs differing in terms of cation and anion structure as well as fungicidal properties has been tested and measured by [29]. [Ciech][1] IL with didecyl dimethyl ammonium cation and herbicidal anion; [DDA][ABS] didecyl dimethyl ammonium dodecyl benzene sulfonate, and [ArqC35][NO₃] nitrate(V) with cation derived

from natural coconut oil. The tests were carried out on *Pinus sylvestris* L. wood. The results indicated that the ILs containing 12-carbon hydrophobic alkyl chain in their structure, i.e. [DDA][ABS] and [ArqC35][NO₃], worsened wood wettability, thus improved the protection of wood against water.

The results of tests on the effectiveness of the action of a new group of synthesized biocidal ILs are presented in [30]. These ILs are derivatives of the leading structure, i.e. didecyl dimethyl ammonium nitrate, and demonstrated strong action against mould fungi. Natural quaternary ammonium salts, mainly extracts from coconut and soybean, and from vegetable fats, were the basis for syntheses. Mycological tests were carried out on the *Pinus sylvestris* L. sapwood in accordance with the method assumed binding for the assessment of biocide efficacy.

The impregnation of wood with wood preservatives may have an influence on its physical and mechanical properties. The knowledge about the character of that influence is of great importance for characterisation of functional properties of wood and, as a consequence, determination of its use classes. The ILs of imidazolium tetrafluoroborates series, which penetrate very well into Scots pine wood, are active against wood-destroying fungi and generally have a positive, although insignificant, influence on physical and mechanical properties of wood, especially on its resistance to colour change during exposure to light. However, various ILs may differ widely in that respect. A research has been carried out in [31] to clarify the influence of dodecyl dimethyl ammonium nitrite, [DDA][NO₂], and IL with dodecyl dimethyl ammonium cation and anion of herbicide character, [DDA][herbicide], on selected physical and mechanical properties of Scots *Pinus sylvestris* L. wood. The miniature sapwood samples were subjected to sorption with the ILs by vacuum method.

Strongly hydrophobic ammonium ILs penetrating the wood structure and protecting solid wood from water absorption have been developed by [32] and found that by covering the surface of the wood with ammonium IL, the wood became hydrophobically and antiseptically protected for a long time. The swelling and water absorption of the protected wood was several times less compared to unprotected wood and its dimensional stability was also improved.

The application of didecyl dimethyl ammonium nitrate, [DDA][NO₃], and benzalkonium nitrate, [BA][NO₃], ILs in preservation of panels resistant to biotic factors has been investigated by [33]. The method for application of ILs to particleboards, the type and amount of chosen ILs, as well as their influence on standard parameters of the panels were also investigated. The amine resin available on the domestic market and particles obtained from debarked Scots pine chips were used in the tests. The results demonstrated that ILs worsened parameters of the panels, but improved their resistance to decay fungi.

The subject of wood finishes that are often used to improve the durability of wood by protecting it from scratching and wearing, minimizing swelling when in contact with water or acting as UV stabilizers for lignin and cellulose has been addressed by [34]. Traditional wood finishes include tung oil or polymerized linseed oil-based products, wax, shellac, rosin, paraffin, synthetic polyurethane, acrylic resin and epoxy-based products. One disadvantage of traditional wood finishes include the use of volatile organic solvents, such as toluene, acetone, or ethanol-acetone mixtures, which are expensive and possess an environmental risk,

also by their capacity to transform their selves in the atmosphere, under the influence of UV radiation and the catalytic action of the nitrogen oxides, in more aggressive species with carcinogenic potential. As consequence, the replacement of the traditional volatile solvents from wood industry with less toxic and volatile solvents became an important aim for the scientists working both in material science and in environmental protection.

The solubility of four frequently used wood finishing products, namely Paraloid B72 thermoplastic resin, paraffin, rosin and bees wax in three types of alkyimidazolium-based ILs: [Bmim]Cl, [Hmim][BF₄] and [Hmim][PF₆], at 23 °C and 90 °C, by using the turbidimetric method also determined by [34] and found that the selected ILs were able to dissolve the respective wood finishes, in amounts higher than those achieved by using traditional volatile organic solvents. It was also found that the solubilities of Paraloid B72 in these ILs are higher than those reported for the traditional organic solvents. For paraffin, rosin and bees wax the obtained solubilities are similar to those reported by using volatile organic solvents. Taking into account that the studied ILs are non-volatile, electrically conductive, that they possess anti-fungal character and they are able to plastify wood, their use as solvents for finishes could impart some useful properties to the treated wood, such as higher workability and durability.

The influence of the two ILs [Bmim][BF₄] and [Bmim][PF₆] on the properties of sycamore maple (*Acer pseudoplatanus*) veneers at different temperatures by using contact angle measurements and Fourier transform infrared spectroscopy analysis has been studied in [35]. The measurements showed that the wood wettability is increased by IL treatment. It has been determined that the ILs decrease the crystallinity and improve the flexibility of the cellulose matrix. Also, it has been determined that at 60 °C and 80 °C delignification of wood occurred, thus making the studied ILs useful alternatives to traditional toxic and expensive reagents used in wood industry.

The Wood Technology Institute in Poznan (Poland) conducts innovative research on the use of ILs (derivatives of quaternary ammonium salts) in wood preservation technology and wood materials in order to increase the sustainability of wood. The research resulted in the development of "multi-tasking" fungicides, which are alternative to commercial wood preservatives that are environmentally toxic and contain heavy metals. One of the goals of such research is the development of innovative technologies of increasing durability of wood and composite wood materials using ILs. This goal has been established through the development of bioactive derivatives of azoles in the form of ILs in order to intensify biocidal activity, increase penetration, and minimize the necessary amount of these biocides introduced to protect lignocellulosic materials [36]. The activity of azole-derivative ILs against decaying *Coniophora puteana* fungus (pine *Pinus sylvestris* L.) have been determined. Thanks to innovative solutions, a new type of biodegradable biocides with low threshold values against fungi and bacteria (pathogens of wood) was developed. The threshold values for [Azole][Cytr] are ED₅₀: 1 ppm; ED₁₀₀: 10 ppm; LD: 50 ppm, and for [[Azole][HCl] are ED₅₀: <0.1 ppm; ED₁₀₀: 5 ppm; LD: 5 ppm. These biocides have significant economic and environmental effects and at the same time no adverse effects on humans. The result is an original in the world. The ILs used in the tests were prepared in the Poznan University of Technology laboratory, according to the method described by [30]. The main substances used in the tests were didecyldimethyl ammonium

nitrite ([DDA][NO₂]) and IL with didecyldimethyl ammonium cation and anion of herbicide character ([DDA][herbicide]). The concentration of each of the tested ILs was 91–97% and they were easily dissolved in propanol-2 and water-propan-2-ol mixture. The FTIR spectra of the treated wood confirmed the bond of ammonium ILs to wood. Formation of ammonium carboxylate in the chemical structure of wood and wood modification by long alkyl chain was observed [36].

The use of ILs in protecting technologies for wood-based panels and plywood allowed development of novel protic ILs that can be used as hardeners of adhesive amine resins [36]. The designed structure of these compounds, their parallel multi-activity, plays a role in curing resins and biocides, which is extremely desirable in the process of protection of wood materials. It was concluded that (1) the innovative nature of proposed solutions lies in creating stable and sustainable, deeply wood-penetrating new ILs as wood preservatives of specific properties with respect to microorganisms responsible for wood degradation, and at the moment of (insignificant) wood leaching easily degradable by the micro-flora in soil and water environment; (2) the results of physico-chemical research on the effect of ILs on material allowed identification of bonds of new biocides and wood, which is indispensable for identifying application of ILs in wood preservation; and (3) the ability of combining ILs with other biocides, e.g. boron or copper compounds, is an offer of new generation of antifungal preparations for the chemical and wood industries as well as building construction [36].

The biotic properties of novel structure of tebuconazole IL derivatives: tebuconazole hydrochloride, allyl tebuconazole chloride, methyl tebuconazole iodide, tebuconazole dihydrocitrate have been examined in [37]. Their investigation against wood-degrading fungi contained also the dodecyl dimethyl ammonium 3-aminotriazolate as well as didecyl dimethyl ammonium nitrate(V), [DDA][NO₃], with tebuconazole or with (tebuconazole+propiconazole). It was found that the most active compound against brown and white rot fungi were precursor of ILs tebuconazole hydrochloride. The fungistatic dose (ED₅₀) for *Coniophora puteana* reached 0.1 ppm, the fungitoxic dose (ED₁₀₀) 5 ppm and the lethal dose (LD) 5 ppm. The fungicidal value of didecyl dimethyl ammonium nitrate(V) with tebuconazole for *Coniophora puteana* were < 0.73 kg/m³, for *T. versicolor* ranged from 0.81 kg/m³ to 1.76 kg/m³. The investigation of protic triazole-based ILs demonstrated the strongest action against blue stain and mold fungi. The growth of mycelium on the surface of wood samples was inhibited in the amount of application 15 g/m². The penetration depth into Scots *Pinus sylvestris* L. wood of didecyl dimethyl ammonium nitrate(V) including the tebuconazole reached 6.2 mm [37].

It was also found that the most active compound against brown and white rot fungi were precursor of ILs tebuconazole hydrochloride [37]; the fungicidal values for *C. puteana* and *T. versicolor* reached was < 0.2 kg/m³. In the case of tebuconazole dihydrocitrate the biocidal activity for *T. versicolor* was at the level of 0.86–1.38 kg/m³. Ammonium-based ILs with a cation containing a substituent derived from coconut oil exhibited fungicidal values against *C. puteana* at levels ranging from 2.7 to 4.6 kg/m³. Dissolution of 15% tebuconazole or its mixture with propiconazole in didecyldimethyl ammonium nitrate or nitrite reinforced the biocidal action of this compound (<0.73 kg/m³ for *C. puteana*) and increased the penetration depth into wood up to 6.2 mm. This allowed effective protection of processed wood against blue stain

fungi comparable with the reference preparation of Sadolin base (150 g/m²). Quaternary tebuconazole derivatives with methyl and allyl substituents demonstrated a slightly weaker fungicidal action than tebuconazole. The majority of the examined salts were characterized by a strong anti-mould action when only 15 g/m² were applied onto the surface of pine wood. Hydrophobic ILs did not undergo leaching from treated wood. Water-soluble triazole-based ILs with 3-aminotriazolate anion got fixed in treated wood. The ATR spectra analysis of treated Scots pine wood indicated the presence of the cation [DDA]⁺ and the 3-aminotriazolate anion in the structure of wood. The positive results of the investigations of the novel functional ILs presented in this study make their potential application in wood protection possible [37].

A very interesting group of ILs is that with a long chain quaternary ammonium cation. They are formed by direct synthesis or by an anion-exchange reaction in quaternary ammonium halides. Popular and cheap precursors for the preparation of ILs are dodecyl dimethyl ammonium chloride and benzalkonium chloride. These compounds have biological activity and are widely used in industry [38]. Use of cations with long alkyl chains suggests that the resulting ILs will have biocidal and wood preservative properties [39,40]. It has been found that didecyldimethyl ammonium and benzalkonium bisulfates (IV), propionates, sorbates and undecyles are hydrophobic compounds and thus have the ability to preserve wood and refresh its surface [38].

A study aimed at improving the functionality of linen fabric by antimicrobial finishing with the use of IL, i.e., quaternary ammonium salt has been carried out in [41]. Antimicrobial activity of ILs strongly depends on their structure. The study included testing the susceptibility of linen fabric protected with didecyl dimethyl ammonium nitrate, [DDA][NO₃], IL to the biodegradation process with special attention paid to fungi resistance. Finished linen fabric was tested in relation to the action of five mildew mixtures. The degree of microorganism growth and its effect on physico-mechanical properties of the fabrics were evaluated. The antimicrobial effectiveness of the IL applied to linen fabric was determined by the use of SEM. Applying this biocide in the finishing processes of natural textile materials allows the attainment of antimicrobial barrier properties.

The influence of three types of imidazolium chlorides ILs, namely, [Bmim]Cl, [Hmim]Cl, and [Dmim]Cl, on the surface properties of wood (*Populus sp.*) veneers has been studied in [42] by using contact angle and electrical conductivity analysis. The measurements showed that wood wettability has increased by IL treatment, thus enabling a higher compatibility of wood with polar additives or adhesives. The electrical conductivities of treated wood by the method presented in [42] are in the 0.8-1.65 mS/cm range, higher than the ones reported in the reference literature, which confers the treated wood anti-electrostatic properties. The treatment of wood veneers with ILs could be useful in improving the workability of wood by decreasing its rigidity, and in preventing the build-up of static electric charges on the surface of the wood during finishing, as well as improving its wettability, thus increasing its compatibility with polar adhesives or additives. Still further studies need to be conducted in order to assess also the influence of weathering conditions (humidity, temperature, UV irradiation) and duration on the surface properties of the wood treated with ILs. Another direction of study should focus on evaluating the antibacterial properties of the wood treated with the selected ILs, in order

to have a complete overview of the plethora of useful properties that IL treatment may impart to wood materials [42].

3. Dissolution of wood biomass in Ionic liquids

Dissolution of wood biomass in common solvents is practically difficult due to the 3-D network structure of lignin which binds the plant cells together, providing mechanical strength to it. Therefore, to break this network and for further wood biomass processing, various types of methods have been used to manipulate its properties for various applications. But each of these methods has some drawbacks. Biological methods require long time of treatment [43]. Physical methods (mechanical milling) are energy demanding, expansive and ineffective in complete removal of lignin. Chemical methods (acid or base treatment) are costly and not environmentally benign [44]. Physiochemical methods (steam explosion), even though considered as very promising methods require high pressures/ temperatures and the use of catalysts [45].

Cellulose is one of the most abundant biological and bio-renewable materials in the world, with a long and well-established technological base. Derivatized products have many important applications in the fiber, paper, membrane, polymer, and paints industries. The application of cellulose is widely distributed among various industries such as fiber, paper, pharmaceutical, membrane, polymer and paint. However, the utilization of cellulose or cellulosic materials has not been developed entirely because of its poor solubility in common organic solvents. Cellulose dissolved in ILs can be regenerated with anti-solvents such as water, ethanol and acetone. It was pointed out that dissolved pulp cellulose (subjected to certain heating methods) is soluble in [Bmim]Cl, [Bmim]Br, [Bmim][SCN], and [Hmim]Cl; insoluble in [Bmim][BF₄] and [Bmim][PF₆]; and slightly soluble in [Omim]Cl [46].

The efficient dissolution of cellulose is a long-standing goal in cellulose research and is still of great importance. Cellulose can be dissolved in several ILs and can easily be regenerated by contacting with water. A short survey of the relevant literature with respect to historical developments and potential industrial uses of ILs is given in [47], which then proceeded to the latest results in cellulose/IL chemistry. The dissolution and reconstitution experiments, fiber characteristics and molecular mass distribution data have been also described in [47].

Dissolution of cellulose with ILs allows the comprehensive utilization of cellulose by combining two major green chemistry principles: using environmentally preferable solvents and bio-renewable feed-stocks. The dissolution of cellulose with ILs and its application is reviewed in [48] and found that (1) cellulose can be dissolved, without derivation, in some hydrophilic ILs, such as [Amim]Cl and [Bmim]Cl; (2) microwave heating significantly accelerates the dissolution process; (3) cellulose can be easily regenerated from its IL solutions by addition of water, ethanol or acetone; and (4) the ILs can be recovered and reused after its regeneration. Typical applications include fractionation of lignocellulosic materials and preparation of cellulose derivatives and composites. It was concluded that although economical syntheses and toxicology of IL studies are still much needed, commercialization of these processes has made great progress in recent years [48].

It was demonstrated that both hardwoods and softwoods are readily soluble in various imidazolium-based ILs under gentle conditions [49]. More specifically, a variety of ILs can only partially dissolve wood chips, while ILs such as [Amim]Cl and [Bmim]Cl have good solvating power for Norway spruce sawdust and Norway spruce and Southern pine thermo-mechanical pulp (TMP) fibers. Despite the fact that the obtained solutions were not fully clear, these ILs provided solutions which permitted the complete acetylation of the wood.

Alternatively, transparent amber solutions of wood could be obtained when the dissolution of the same lignocellulosic samples was attempted in 1-benzyl-3-methylimidazolium chloride, [Bzmim]Cl. This realization was based on a designed augmented interaction of the aromatic character of the cation of the IL with the lignin in the wood. After dissolution, wood can be regenerated as an amorphous mixture of its original components. The cellulose of the regenerated wood can be efficiently digested to glucose by a cellulase enzymatic hydrolysis treatment [49]. It was thus demonstrated that the dissolution of wood in ILs now offers a variety of new possibilities for its structural and macromolecular characterization, without the prior isolation of its individual components. Furthermore, considering the relatively wide solubility and compatibility of ILs with many organic or inorganic functional chemicals or polymers, it is envisaged that this research could create a variety of new strategies for converting abundant woody biomass to valuable biofuels, chemicals, and novel functional composite biomaterials [49].

A simple and a novel alternative approach for processing of lignocellulosic materials that relies on their solubility in solvent systems based on the IL [Bmim]Cl has been presented in [8]. Dissolution profiles for woods of different hardness are presented, making emphasis on the direct analysis of the cellulosic material and lignin content in the resulting liquors. The cellulose obtained can be readily reconstituted from the IL-based wood liquors in fair yields by the addition of a variety of precipitating solvents. Spectroscopic and thermogravimetric studies indicated that the polysaccharide obtained in this manner is virtually free of lignin and hemicellulose and has characteristics that are comparable to those of pure cellulose samples subjected to similar processing conditions.

The effect of the anion of ILs on air-dried pine (*Pinus radiata*) dissolution has been investigated in [28]. All ILs used in that study contained the 1-butyl-3-methylimidazolium cation; the anions were trifluoromethane sulfonate, methyl sulfate, dimethyl phosphate, dicyanamide, chloride and acetate. Using a protocol for assessing the ability to swell small wood blocks (10 x 10 x 5) mm, it was shown that the anion has a profound impact on the ability to promote both swelling and dissolution of biomass. Time course studies showed that viscosity, temperature and water content were also important parameters influencing the swelling process. The Kamlet-Taft parameters were used to quantify the solvent polarity of the ILs and found that the anion basicity described by the parameter β correlated with the ability to expand and dissolve pine lignocellulose. It was shown that 1-butyl-3-methylimidazolium dicyanamide, [Bmim][DCA], dissolves neither cellulose nor lignocellulosic material. It was also shown that the lignocellulosic components, particularly the carbohydrate polymers, are rich in hydroxyl groups and the IL anions that can strongly coordinate these hydroxyl groups (high β), are able to weaken the hydrogen-bonding interactions in the wood matrix and allow the chips to expand [28].

A challenge in producing wood-plastic composites (WPCs) with a high wood content using extrusion processes is the poor processability, which gives rise to inadequate properties of the resulting WPC. Plasticizing the stiff wood cell walls can be a strategic response to this challenge. Two thoughts to improve the plasticity of wood particle cell walls: use of ILs or use of low molecular weight organic thermal conductors is addressed in [50]. An IL can dissolve the cell wall surface and therefore reduce the stiffness of the cell wall during the extrusion process. Incorporation of ILs can also impart anti-microbial and antistatic properties to the resulting composites, as well as improving the fire retardancy and resistance against fungal decay. However, high cost and leachability of ILs are the main issues that impede their application in wood-plastic composites (WPCs) processes. In addition, ILs exhibit extremely high polarity and can absorb moisture from surrounding environment, which may cause dimensional instability of the resulting WPC. The presence of ILs may also cause the formation of a weak interfacial layer between wood particles and plastic matrices [50].

One other achievement of the Wood Technology Institute in Poznan (Poland) project was the development of a method for cellulose isolation from lignocellulosic raw materials using developed new morpholine ILs. The project focused on development of a novel method of dissolving papermaking raw materials and semi-finished products in ILs in order to extract the carbohydrate from the lignin fraction and ultimately obtain cellulose from a chemical-morphological conglomerate that wood is. The results of the investigation of application of ILs blends as cellulose solvents is expected to be an innovative R&D trend in the forest-based sector [36].

An ideal IL for cellulose transformation should possess the following properties: (1) high dissolution capacity for cellulose; (2) low melting point; (3) good thermal stability; (4) non-volatile; (5) non-toxic; (6) chemically stable; (7) no cellulose decomposition; (8) easy cellulose regeneration, and (9) low cost and simple process [51]. Imidazolium is one of the most commonly used cations of ILs, while anions include quite a number such as chloride, hexa-fluorophosphate, tetrafluoroborate and others. To improve the solubility of cellulose and lignocellulose in ILs, it is important to optimize the suitable anions and cations in ILs, sometimes necessitating structural modifications [52].

The dissolution of cellulose and lignocellulose in various ILs including key properties such as high hydrogen-bonding basicity, which increases the ability of the IL to dissolve cellulose has been described in the review by [9]. As a pretreatment in biofuel production, the review in [9] details aspects such as the regeneration of cellulose from ILs, structural changes that arise in the regenerated cellulose and its effect on enzymatic hydrolysis, the potential for IL recycling, and finally, exploiting ILs in an integrated bioprocess. The review in [9] also presented the solubility of assorted lignocellulosic material and constituent polymers using different ILs. The outcomes clearly show that some ILs such as [Bmim]Cl are beneficial in dissolving biomass samples (cellulose solubility of up to 25 wt.%), whilst other ILs containing large non-coordinating anions [PF₆]⁻ and [BF₄]⁻ are unsuitable as a solvent for either cellulose [46] or lignin liquefaction [53]. Longer chained substituted ILs such as [Hmim]Cl and [Omim]Cl also appear to be less efficient in dissolving cellulose [46,53]. At 100 °C, [Hmim]Cl was found to dissolve only 5 wt.% of cellulose, whereas [Bmim]Cl dispersed up to 10 wt.% of cellulose.

The discovery of [Bmim]Cl, which is reported to completely dissolve cellulose without the formation of derivatives, has created a basis for studying the use of ILs in wood processing. This finding paved the way for a many studies on interactions between cellulose and ILs [54]. The superiority of [Bmim]Cl in breaking the extensive hydrogen-bond network present in cellulose can be attributed to its high chloride anion concentration. Owing to its strong hydrogen-bonding basicity, ILs with elevated chloride anions possess the capacity to rapidly dissolve greater amounts of cellulose [9]. The poor performance of ILs containing [PF₆]⁻ and [BF₄]⁻ anions was attributed to the weak hydrogen-bonding basicity of these anions [55]. However, weak activity associated with longer-chained substituted ILs such as [Hmim]Cl and [Omim]Cl may be ascribed to a reduction in the effective chloride concentration of these ILs [9].

ILs based on polar organic solvents such as dimethyl formamide (DMF), dimethyl acetamide (DMAc), dimethyl imidazolidinone (DMI) or dimethyl sulfoxide (DMSO) and usually coupled with charged species such as LiCl, are frequently used for dissolving cellulose. Methylsulfate imidazolium-based ILs showed excellent results when dissolving softwood Kraft lignins [52].

The research efforts in processing of lignocellulosic biomass using ILs as solvents is described [4]. Cellulose composite fibers were prepared based on IL solution with dispersion of the additives. Wood and bagasse were completely dissolved in ILs. Partial separation of the components was obtained using selected reconstitution solvents. High temperature and fast dissolution was found to be an efficient method for both dissolution and separation of biomass components. Biomass composite fibers can be prepared directly from such biomass solutions. With selected catalysts in solution, improved dissolution and separation was achieved, making the delignification and pulp yield comparable to the Kraft pulping process [4].

The interaction of natural polymers (Avicel, wood, "beech" cellulose) with the [Emim]Cl IL and their structural features before and after the regeneration process have been investigated in [56]. The observed dissolution mechanisms were found to be fully controlled by the physical and chemical organizations of the macromolecular chains. The XRD results indicated that the crystalline structure of the substrates regenerated from the IL is mostly disrupted.

One of the major challenges of biomass-based technologies is to extract sugars that are covalently trapped inside the lignocellulosic biomass efficiently. ILs have been recognized as promising solvents for mild and rapid hydrolysis of biomass feedstocks with higher sugar yields. An IL-based biomass hydrolysis strategy for large-scale production of fermentable sugars from corn stover has been developed and evaluated in [57]. Toward this aim, a process simulation model based on literature experimental studies and a simulated-moving-bed (SMB) system has been developed. The IL cost has been identified as the major cost driver. Analysis suggested that process alternatives with lower IL consumption and/or separation strategies that would allow higher recycle of ILs should be studied [57].

Pine and eucalyptus woods were dissolved in ILs [Emim][OAc], [Amim]Cl, [Bmim]Cl and [Emim]Cl, and successfully regenerated lignin from the solutions of these woods in the chloride-based ILs after 24 h at 150 °C in a thermostatic bath using methanol or ethanol as anti-solvents or after 1 h at 170 °C in a microwave oven [58]. Similarly, cellulose was recovered from

the wood solutions in [Amim]Cl after 20 min at 120 °C in the microwave oven. The regenerated products were found to be similar to the reference samples [58].

The [Bmim]Cl IL was used to dissolve two lignocellulosic materials including bagasse soda lignin and *Populus deltoides* wood flour at 70 °C for 72 h while stirring in [59]. The lignin and wood flour samples were acetylated with addition of acetic anhydride to each container with a 1:1 ratio and heated for 3 days at 110 °C. The functional groups and the number and type of carbon as well as their structure were examined and identified.

The dissolution and regeneration of both hardwood and softwood dissolving pulps with and from the two ILs ([Bmim][OAc] and [Bmim]Cl) were investigated in [60]. The impact of treating cellulose with ILs was also evaluated by using different analytical techniques (size exclusion chromatography, thermal gravimetric analysis and scanning electron microscopy).

Regarding IL recyclability, the new classes of 'switchable' and 'distillable' ILs can effectively lignocellulose. Whereas previous structures have low recyclabilities, the new structures can be converted from their 'ionic' form into "neutral" species, which allows for distillation of the materials in high yields and recovery. This increases the overall sustainability of the prospective processes, beyond what was capable before and offers significant energy savings [11].

A route for IL synthesis making use of alcohols and carboxylic acids both commonly found in a biorefinery is presented in [3]. Some of these ILs have also been tested for their ability to dissolve cellulose. He addressed the possibilities but also challenges upon IL-mediated lignocellulose processing. This includes investigating several ILs and their efficiency as a pretreatment solvent for enzymatic hydrolysis; these studies involve a large variety of different cellulosic materials. It has been demonstrated that depolymerization during the IL pretreatment is a possibility and that this can complicate the recovery processes and gives guidance into what type of ILs might be suited as pretreatment solvents for different cellulosic materials, including amorphous and crystalline cellulose, processed and native lignocellulose, different types of wood samples and hemicellulose [3].

Pretreatment of lignocellulosic biomass materials from poplar, acacia, oak, and fir with different ILs containing 1-alkyl-3-methylimidazolium cations and various anions was carried out [61]. The dissolved cellulose from the biomass was precipitated by adding anti-solvents into the solution with vigorous stirring. Commercial cellulases were used for the hydrolysis of untreated and pretreated lignocellulosic biomass. The hydrolysis of the cellulose was facilitated by the pretreatment with [Emim][OAc] and [Emim][CF₃COO]. Among the tested ILs, [Emim][OAc] showed the best efficiency and resulted in highest amount of liberated reducing sugars. It was also found that enzymatic hydrolysis using combined pretreatment techniques could result in significant improvements of enzymatic hydrolysis efficiency. Combined pretreatment of the lignocellulosic biomass using glycerol-ILs and dilute acid-ILs were evaluated and compared with single pretreatment using glycerol, ILs or dilute acid [61].

Lignin was isolated from rubber wood using 1,3-dimethylimidazolium methyl sulfate IL in [62], and the optimum parameters to isolate lignin, namely, concentration of IL (0.5 mol), isolation duration (120 min) and isolation temperature (100 °C) investigated. Lignin could be isolated from rubber wood up to 13.03 wt.% by IL which is less than that obtained using acid

(22.15 wt.%) and alkaline (18.56 wt.%) isolation methods. The lignin preliminary structures isolated by IL have been confirmed based on Fourier transform infrared (FTIR) results. However, the isolated lignin by IL provides a lignin without other related isolatives. In addition, the IL can be recycled up to three times compared to acid and alkaline isolation methods [62].

A new composite material was obtained by using a waste resulted from wood industry, namely spruce wood flour and an ecologic green solvent for lignocellulose, namely 1-butyl-3-methylimidazolium chloride, [Bmim]Cl [63]. The method consists of dissolving wood in ILs followed by precipitation by water addition. The precipitated cellulose and lignin act as natural binders for the wood particles thus avoiding the use of toxic organic resins as adhesives. The obtained composites showed good water stability and compressive mechanical strength. Taking into account that the studied IL is non-volatile, the proposed method is more ecological than other traditional fiberboard-obtaining processes, which are energetically inefficient and contribute to the pollution of the atmosphere [63].

Lots of reports are available on dissolution of cellulose in ILs and its applications [48,64]. Dissolution of cellulose samples in some imidazolium-based ILs, collected from references [46, 65-69] is available in [70]. Selected results for cellulose dissolution in ILs are presented in [4]. Recently, the extent of cellulose solubility in the most commonly used ILs is summarized in [6]. On the other hand, a summary table on the dissolution behavior of various types of wood-based lignocellulose in different ILs, based on data from [49] and [71], are provided in [72].

However, dissolution of wood in ILs is far more complicated than cellulose dissolution due to the wood complex structure from the 3-D lignin network [49]. Up to now, wood dissolution in ILs is limited to the imidazole-based ones [14]. A summary of the ILs used for wood dissolution according to various published sources [8,49,73,74] is presented in [14].

Wood fractionation through IL-mediated pretreatment for obtaining simple fermentable sugars, namely oligo- and mono-saccharides, and in particular hexoses (and pentoses) has been investigated in [75] focusing on softwood, Scots pine (*Pinus sylvestris*) and Norway Spruce (*Picea abies*), exposed to 1-ethyl-3-methylimidazolium chloride, [Emim]Cl, IL. Since both [Emim]Cl and the mono-saccharides are water-soluble and dissolve readily in similar solvents, the separation of this hydrophilic IL from sugars is difficult. Moreover, the analysis of mono-saccharides released from lignocellulosics with the help of [Emim]Cl is challenging [75].

It was found that both softwood (southern yellow pine) and hardwood (red oak) can be completely dissolved in the IL 1-ethyl-3-methylimidazolium acetate, [Emim][OAc], after mild grinding [76]. Complete dissolution was achieved by heating the sample in an oil bath, although wood dissolution can be accelerated by microwave pulses or ultrasound irradiation. It was shown that [Emim][OAc] is a better solvent for wood than 1-butyl-3-methylimidazolium chloride, [Bmim]Cl, and that variables such as type of wood, initial wood load, particle size, etc. affect the dissolution and the dissolution rates; for example, red oak dissolves better and faster than southern yellow pine [76].

Lipophilic wood extractives composition is currently a big concern of pulp and paper industries due to their negative impacts on the quality of the pulp and on the environment. Because of the shortcomings of different extraction procedures using volatile organic solvents in capturing residual lipophilic extractives in pulp, the use of ILs as an effective approach for such extraction is reported in [77]. The capacity of [Bmim][OAc] and [Bmim]Cl ILs to recover wood extractives was compared and observed that [Bmim]Cl recovered a higher amount of extractives than [Bmim][OAc]. Thus, the effectiveness of the IL in this process was due to the anion and not the cation of the solvent [77]. Based on the fact that ILs are biodegradable, non-volatile and non-flammable, this approach of analysis is definitely a highly green process for the determination of lipophilic extractives in dissolving pulp.

Lignin is an aromatic, amorphous, heterogeneous polymer that represents the second most abundant natural polymeric material on Earth [78]. It is known that the bulk of lignin in wood consists of non-phenolic aryl-glycerol- β -O-aryl ether units. Other units, such as phenylcoumaran (β -5), resinol (β - β), and dibenzodioxocins(5-5/ β -O-4, α -O-4) are also present within the lignin macromolecule [79]. Furthermore, lignin is usually covalently linked to carbohydrates forming a refractory lignin-carbohydrate network [80].

Ionic liquids, especially those based on imidazolium cations, are capable of dissolving cellulose in a wide range of values of the polymerization degree (even bacterial cellulose) without covalent interactions [81,82]. Scientists are currently investigating the application of ILs as the solvent for the chemical modification of cellulose [See for example, 81,83-86].

The dissolution mechanism of cellulose in ILs involves the oxygen and hydrogen atoms of the cellulose-OH groups in the formation of electron donor-electron acceptor (EDA) complexes which interact with the IL. On the basis of the analysis of experimental and theoretical data, it was found that hydrogen-bond interactions are created between H-atom of OH-groups in cellulose and electron-donor center of the anion of the IL [87]. The cation of the IL doesn't interact with the cellulose directly. The cations role is considered as a steric obstacle for the prevention of interactions between polymeric chains, shielding them from each other after dissolution [87].

Lignin contributes to the recalcitrance of lignocellulosic biomass and affects enzymatic activity during biorefinery operations, therefore, it must be removed before further processing [88]. Organic solvents and ILs are two important pretreatments for delignifying lignocellulosic biomass; both have been proven beneficial for fractionating and recovering cellulose and hemicellulose, as well as lignin with useful physicochemical properties. Volatility and harsh conditions of the acidic systems that result in toxicity, corrosion, and pollution are the main problems of organic solvents. Ionic liquids, generally recognized as green solvents, have also been proposed as a possible solution to the challenge of using lignocellulosic biomass. Ionic liquids can either dissolve the lignocellulosic biomass completely or dissolve it into individual fractions. The advantages and disadvantages of organic solvents and ILs were considered, since both are important methods to fractionate lignocellulosic biomass in their main components which can be converted into value added products [88].

The application of selected ILs as aprotic green solvents for dissolution of lignin (isolated from pine Kraft pulp) were examined in [53]. Up to 20 wt.% lignin could be dissolved in [Hmim][CF₃SO₃], [Mmim][C₁SO₄] and [Bmim][C₁SO₄]. For the [Bmim]⁺-containing ILs, the order of lignin solubility for varying anions was: [MeSO₄]⁻ > Cl⁻ ~ Br⁻ ≫ [PF₆]⁻, indicating that the solubility of lignin was principally influenced by the nature of the anions. ILs containing large, non-coordinating anions [PF₄]⁻ and [PF₆]⁻ were unsuitable as solvents for lignin [53].

The enzymatic pretreatment of wood biomass for degrading lignin, which is a complex aromatic polymer, has received much attention as an environmentally safe or “green” process. However, this process for lignin degradation has been found to be very slow, even needed several months. To overcome this limitation, a new approach for enhanced enzymatic delignification of wood biomass using ILs—a potentially attractive “green” and “designer” solvent-as co-solvents and/or pretreated agents has been reported in [89]. This approach comprised pretreatment of wood biomass prior to enzymatic delignification in ILs-aqueous systems with the aim of overcoming low delignification efficiency associated with the difficulties in enzyme accessibility to the solid substrate and the poor substrate and products solubility in aqueous system. The results showed that IL [Emim][OAc] was a better solvent for wood delignification than IL [Bmim]Cl. The recovered cellulose rich materials obtained from combination effects of IL and biological pretreatment contained significantly lower amounts of lignin as compared to the amounts found when each method applied alone. It is believed that this newly developed process will play a great role in converting cellulosic biomass to biomaterials, biopolymers, biofuels, bioplastics and hydrocarbons [89].

The [Bmim]Cl and [Bmim][MeSO₄] ILs have been examined to dissolve wood flour, cellulose and chemical-mechanical pulp (CMP) in [90]. The overall evaluation indicated the inability of [Bmim][MeSO₄] in full dissolution of lignocellulosic materials and sample treatment with this solvent led to water-soluble degradation products, whereas, [Bmim]Cl was able to dissolve lignocelluloses. Density, clarity, water absorption and thickness swelling of regenerated cellulose films were significantly higher than those of CMP and wood flour, and CMP higher than wood flour. Also, cellulose film has the lowest water vapor permeability compared to wood flour and CMP. Tensile strength, Young's modulus and strain at breaking point of cellulose film were significantly higher than the CMP and wood flour samples [90].

The state of art on the dissolution of cellulose, lignin and wood using ionic liquids is presented in [91] with emphasis on the relationship between the properties of ionic liquids and the dissolution capacity. The impact of the solvation parameters, namely, Hildebrand solubility parameter and hydrogen-bond basicity were related to the dissolution of lignocellulosic material. Good solvents for cellulose are [Bmim]Cl, [Amim]Cl and [Emim][OAc], whereas for lignocellulosic material the best solvents are [Emim][OAc] and [Amim]Cl [91]. In the allyl group, the ethylene functionality facilitates B-interactions with the aromatic lignin structure. Furthermore, small polarizable anions are also powerful when aiming at dissolution of cellulose. The properties of the regenerated cellulose and the reconstituted lignin were compared with those of the native materials and the results from the regeneration and reuse of ionic liquids were presented [91].

The dissolution of ball-milled poplar wood (PW), chemical-mechanical pulp (CMP), and cotton linter (CEL) in two imidazolium ILs, namely, 1-butyl-3-methyl-1-imidazolium chloride, [Bmim]Cl, and 1,3-methylimidazolium dimethyl sulfate, [Dimim][MeSO₄] have been tested in [92]. The overall evaluation indicated the inability of [Dimim][MeSO₄] in complete dissolution of lignocellulosic materials, and sample treatment with this solvent did not lead to water soluble degradation products. However, [Bmim]Cl was able to dissolve all used lignocellulosic materials by destroying inter- and intra-molecular H^{*}bonds between lignocelluloses. The physical and mechanical properties of the regenerated CEL films were much higher than those of CMP and PW composites. In addition, CEL film showed the lowest water vapor permeability compared to the WF and CMP composite films [92].

4. Lignin extraction in ionic liquids

Biodegradable plastics and biocompatible composites, generated from renewable biomass feedstock, are regarded as promising materials that could replace synthetic polymers and reduce global dependence on fossil fuel sources [93]. Wood cellulose, the most abundant biopolymer on earth, holds great potential as a renewable biomass feedstock for the future. The lignocellulosic biomass composes a diversity of feedstock raw materials representing an abundant and renewable carbon source and a key sustainable source of biomass for transformation into biofuels (e.g. bioethanol) and bio-based products (feedstock molecules for the chemical industry such as phenols and other aromatics). Because of the worldwide energy shortage and environmental pollution, the world has to make full use of lignocellulose in order to develop clean energy and bio-products in the future. However, the great diversity of lignocellulosic biomass opens a great opportunity for the production of various commodities using the wise valorization processes [94].

In majority lignocellulose is constituted by carbohydrate macromolecules, namely, cellulose (30-50 wt.%) and hemicellulose (15-30 wt.%), and by lignin (10-30 wt.%); a poly-phenylpropanoid macromolecule. Between these bio-macromolecules, there are several covalent and non-covalent interactions defining an intricate, complex and rigid structure of lignocellulose. The deconstruction of the lignocellulosic biomass makes these fractions susceptible for easier transformation to large number of commodities including energy, chemicals and material within the concept of biorefinery [94].

Cellulose is a major component in plant cell walls, which is made up of 6 carbon sugar (glucose) in the form of long chains. Hemicellulose is composed of 5 carbon sugars (xylose) which is the second most abundant source in the plant cell walls, and it is interconnected with cellulose molecules. Lignin provides the structural strength for the plant. Due to the complex structure of lignocellulose, it is resistant to traditional solvents, which inhibits hydrolysis and commercial utilization. Since different lignocellulosic materials have different physico-chemical characteristics, it is necessary to adopt suitable pretreatment methods for the lignocellulosic biomass [95]. However, the separation of lignin from cellulose and hemicellulose is a vital step. Also lignocellulosic biomass is highly recalcitrant (unmanageable) to biotransformation, both

microbial and enzymatic, which limits its use and prevents economically viable conversion into value-added products. As a result, effective pretreatment strategies are necessary, which invariably involve high energy processing or results in the degradation of key components of the lignocellulose [96]. To unlock the entire scope of potential benefits of this feedstock, the wood components, namely cellulose, hemicellulose and lignin, need to be separated and processed individually [93].

Lignin is a renewable bio-resource with a variety of applications. It is an important component of the biomass from which several useful chemicals can be derived as indicated by the work initiated in the second half of the last century and the renewed interest today. Lignin valorization constitutes an important component of the modern biorefinery scheme, and the structure and composition of lignin offer unique routes to produce several fine and bulk chemicals. The different approaches and strategies currently available for catalytic lignin valorization are presented in [97]. Generally, lignin reduction catalytic systems produce bulk chemicals with reduced functionality, whereas lignin oxidation catalytic systems produce fine chemicals with increased functionality [97].

The development of green processes for wood dissolution and lignin regeneration would be really useful in the context of biorefinery and biomass efficient employment. One of the most traditional methods to lignin extraction used in the industry is by the Kraft process. Even though most of the lignin is extracted, the Kraft process has several major disadvantages: (1) high temperature and pressure; (2) pollution; (3) odor problem (due to the use of sulphite); (4) high water usage; and (5) large plant size [98]. Several other methods to extract lignin from lignocellulose have been designed and developed in the past. These include physical (limited pyrolysis and mechanical disruption/comminution), physiochemical (steam explosion, ammonia fiber explosion), and chemical (acid hydrolysis, alkaline hydrolysis, high temperature organic solvent pretreatment, oxidative delignification) methods [52]. The above extraction methods have one main disadvantage; the lignin starts to degrade after a certain amount of lignin is extracted.

Generally, the biomass pretreatment depends on the final goal in the biomass processing. The recalcitrance of lignocellulose materials is the main limitation of its processing once the inherent costs are excessively high for the conventional pretreatments. Furthermore, none of the currently known processes is highly selective and efficient for the satisfactory and versatile use, thus, new methodologies are still broadly under study [94].

The IL technology on biomass processing is relatively recent and first studies were focused on the lignocellulosic biomass dissolution in different ILs. The dissolution in IL drives to the structural changes in the regenerated biomass by reduction of cellulose crystallinity and lignin content contrasting to the original biomass. These findings provided ILs as tools to perform biomass pretreatment and the advantageous use of their specific properties over the conventional pretreatment processes [94].

ILs have played an important role in the production of clean energy owing to their excellent physico-chemical properties and outstanding performance in the dissolution and separation

of lignocellulose. However, the research in this area is still at its infant stage and some problems have to be solved. In the future work, the following main issues are suggested [70].

1. To study the interaction mechanism between ILs and cellulose, hemicellulose or lignin further through macroscopic and microcosmic methods, and to know how cations and anions of the ILs disrupt the cross-linked structure, and the intra-and inter-molecular hydrogen bonding of lignocellulose.
2. To develop the knowledge of the relationship between the structure of ILs and their dissolution performance for cellulose, hemicellulose and lignin, and then to design and prepare more new task-specific ILs which are ought to have low viscosity, low melting points and high dissolution and separation capability for lignocellulose.
3. To develop inexpensive methods for the recovery and recycle of ILs, and to promote the application of microwave heating and other intensification technologies in the dissolution and separation of lignocellulose components with ILs.
4. To investigate the effect of precipitation solvents on the crystalline state and thermo-physical properties of regenerated cellulose, hemicellulose and lignin, and then to regulate the structure and properties of the regenerated components for different applications.

ILs have proven the inordinate potential in reactions and separation including biomass processing. The pretreatment of lignocellulosic biomass can affect its physical properties, such as alter the structure of cellulosic biomass to make cellulose more accessible to the enzymes that convert carbohydrate polymers. Subsequently, when lignocellulose is separated into its components, it can be hydrolyzed to fermentable sugars (monosaccharides) using mineral acids or enzymes. Mono-saccharides can then be further converted to other valuable bio-based chemicals [95].

ILs can dissolve extensive quantities of biomass, and even be designed to be multifunctional solvents [99]. In the past decade, ILs have been used as solvents for natural polymers, including cellulose and starch [e.g., 8,46,48]. Current methods to separate wood components, such as Kraft pulping for example, suffer considerable drawbacks and cannot be considered environmentally benign [85]. These drawbacks lead researchers to trying to design and develop ILs that are able to dissolve lignin and thus, extracting them from the lignocellulosic biomass with the aim of minimizing lignin degradation. In order to separate lignin from plant constituents using ILs, the ideal IL should possess properties such as: high dissolution capacity for lignin; low melting point; good thermal stability; non-volatile; non-toxic; chemically stable; no lignin decomposition; easy lignin regeneration; low cost and simple process [51,52].

The tremendous chemical and physical breadth of ILs can be exploited in the design of new ILs with improved lignin extraction capability while providing a ready source of highly degradable cellulose and hemicellulose. Further studies, such as precipitation or extraction of lignin and removal or reuse of ILs by ion exchange, are needed to evaluate the efficient removal of the pristine lignin from the IL, thereby providing a new source for highly functionalized natural product [96].

The unique solvating properties of ILs foster the disruption of the 3-D network structure of lignin, cellulose, and hemicellulose, which allows high yields of fermentable sugars to be produced in subsequent enzymatic hydrolysis. Lignocellulosic biomass pretreatment in ILs is a promising alternative, with comparable or superior yields of fermentable sugars, than conventional pretreatments. The broad number of ILs that can be synthesized allows the design of solvents with specific physicochemical properties that play a critical role interacting with lignocellulosic biomass subcomponents [72]. Today, these interaction mechanisms are better understood. However, future challenges rely on the ability to make this process economically attractive. This might be achieved by optimizing large-scale pretreatment conditions, performing post-pretreatment steps in ILs, reusing ILs, recycling the ILs with reduced energy consumption and enhancing process efficiency, and producing high-value products in addition to ethanol (e.g., products traditionally derived from petroleum, fine chemicals or fuels with higher energy value). Moreover, the potential high-value of lignin suggests that it might instead be used in the large-scale diversified manufacture of high value chemicals, traditionally obtained from petroleum [72].

The physico-chemical properties of ILs that make them effective solvents for lignocellulose pretreatment, including mechanisms of interaction between lignocellulosic biomass subcomponents and ILs, along with the several recent strategies that exploit ILs and generate high yields of fermentable sugars suitable for downstream biofuel production, and new opportunities for use of lignocellulosic components, including lignin, have been summarized and highlighted in [72].

A variety of ILs have been used to dissolve lignocellulosic biomass. The mostly reported efficient ILs used to dissolve lignocellulose are those containing Cl⁻ anion, e.g. [Amim]Cl and [Bmim]Cl. The ions in these ILs dissociate to individual cations and Cl⁻ ions. The free Cl⁻ ions associate with the cellulose hydroxyl proton, which are the hydrogen-bond accepters and the free cations are moderate hydrogen-bond donators that complex with the cellulose hydroxyl oxygen. This leads to the disruption of hydrogen bonds in cellulose and to the dissolution of cellulose [95]. However, chlorine has been proved as an ecologically destructive element in the industrial utilization and its by-products are also harmful for human. Therefore, finding new chlorine-free ILs that also provide good dissolution ability on lignocellulosic biomass (cellulose, hemicellulose and lignin) is underway [95].

Recently, a number of publications introduced a variety of technical developments and solvent systems based on several types of ILs to fractionate lignocellulose into individual polymeric components, after full or partial dissolution [100]. Many new technical advances are apparent, including more refined ILs, electrolytes, pretreatments and processing techniques. However, the application of fundamental knowledge related to the connectivity of wood biopolymers, morphology, ultrastructure, and even the wood solubility in ILs seems to have been largely neglected. Increasing awareness related to IL reactivity has brought both challenges and possibilities to wood fractionation. Depolymerization during fractionation can result in undesired products. This is most relevant when molecular weight distributions should be maintained, e.g. for the production of cellulosic pulps. However, in some cases degradation

may be beneficial, e.g. for dissolving the lignin-carbohydrate complexes (LCC) network or reducing the recalcitrance of wood for biofuel production [100].

On the other hand, the polar nature of ILs has the ability for dissolution and fractionation of wood biomass for various applications. Dissolved wood biomass fractions are regenerated by the addition of non-solvents, i.e., water, acetonitrile, etc. [46,101]. Using ILs for the preparation of cellulose and wood biomass composites and derivatives will contribute towards reducing the dependency on petroleum as raw material whilst enhancing the use of wood biomass. Though ILs are considered as green solvents, there are some drawbacks associated with them such as non-biodegradable, expensive and the toxicity is still not known. This calls for further research in order to understand their toxicity and also to develop new economically viable methods for producing ILs at industrial scale [102].

The application of ILs in cellulose dissolution has promising futures due to three factors: (i) ILs properties such as like extremely low vapor pressure, high polarity, and high chemical and thermal stabilities, and the most important properties of ILs is the possibility of reaction at high temperature without hazard; (ii) cellulose abundance, biodegradability and biocompatibility; and (iii) the dissolution of cellulose in ILs takes place in wide temperature range (60–130°C) which may help in applying different types of modifiers in the blending process of grafting copolymerization [103].

Modification of cellulose in ILs media provides possibilities for preparation of various advanced materials, including cellulose derivatives and composites, which may replace synthetic polymers, which biodegrade slowly or to a less extent. The important target for this technology is how to increase the solubility efficiency, which may be achieved by careful design of what is called “Task-Specific IL (TSIL)” [104]. TSIL is a design specific type of ILs produced by introducing functional groups at the imidazolium cation to make the IL more effective in the cellulose dissolution process [55]. A reactive extrusion process to modify the cellulose has been successfully applied where a specific IL has been used with cellulose and cyclic anhydride to modify the cellulose by using twin screws. This process may open a new horizon for cellulose modification through melting process or may lead to regeneration of cellulose through melting process [103].

In a typical process of lignocellulose biomass pretreatment, lignocellulose and IL are heated up to 100°C for a certain time. The dissolution time depends on the structure of the cellulose and the type of the IL. The dissolved cellulose in the IL can be precipitated by adding a non-solvent (anti-solvent), such as water, methanol, ethanol, or acetone and separated by filtration. The filtrated IL can be recovered and reused through the distillation of the anti-solvent [95].

The dissolution of three wood species in the IL [Amim]Cl, followed by pretreatment with small amounts of hydrochloric acid, has been studied as a function of time in [105]. The materials regenerated from the IL solutions were determined to contain significantly higher amounts of lignin than the original wood. Detailed analyses of the recovered IL revealed the presence of typical wood degradation compounds. Thus an IL-based acid pretreatment of wood may offer a potential platform for the efficient conversion of woody biomass to readily digestible carbohydrates and other valuable chemicals.

The effect of temperature on enhancing the enzymatic hydrolysis of cellulose wheat straw in the IL [Amim]Cl has been studied and the morphology, enzymatic hydrolysis rate, the recovery and the composition of the recovered solid have been investigated in [106]. It was concluded that treatment with [Amim]Cl is an efficient pretreatment method to enhance the enzymatic hydrolysis of wheat straw; too intense treatment condition would induce degradation of wheat straw and the most easily degradable component is hemicellulose. Heating at 150°C for 2 h is a suitable condition for the pretreatment [106].

The chemical interaction of dissolving pulp with ILs, where softwood and hardwood industrial dissolving pulps were pretreated with ILs [Bmim][OAc] and [Bmim]Cl have been investigated in [107]. Time (28-330 h) and temperature (80 °C and 105 °C) dependence of the dissolution process as well as the impact of the pretreatment on the molecular weight properties, thermal stability, morphology, and crystallinity of the cellulose were evaluated. It was shown that the dissolution of cellulosic material in ILs is a temperature-dependent process; however, the viscosity of the IL affected the efficiency of dissolution at a given temperature. Molecular weight properties were affected negatively by increased dissolution temperature, while the type of anti-solvent for the regeneration of cellulose had no major impact on the degree of polymerization of the cellulose. Water was found to be more efficient than ethanol for the regeneration of cellulose when performed at an elevated temperature. The pretreatment decreased the crystallinity of the cellulosic material. This might lead to the increased accessibility and reactivity of the cellulose [107].

Various wood samples (subjected to some mechanical pretreatment) were dissolved in some Cl-containing ILs, namely, [Amim]Cl, [Bmim]Cl, and [Bzmim]Cl for 8 h at temperatures between 80 and 130 °C and results showed that wood can be dissolved in some ILs, including [Amim]Cl and [Bmim]Cl, with high wood regeneration yield [49].

Cellulolytic enzymatic hydrolyses of wood regenerated from IL solutions was determined to produce higher saccharification yields than those of untreated wood. When these ILs were used for additional wood pretreatment cycles, it was observed that the hydrolysis rate of the cellulose increased, accompanied by lignin degradation. As such, it became of interest to investigate the effect of small amounts of acid in ILs on wood degradation and its hydrolytic conversion during such a pretreatment stage. In this effort, three wood species pretreated with dilute hydrochloric acid in water and in [Amim]Cl have been compared. The lignin contents of the regenerated wood were determined, and the components that remained within the recycled IL were examined [49]. However, studies on the recycled ILs from the pretreatment of wood revealed that the ILs contain carboxylic acids from the dissolved hemicelluloses [108].

The IL [Emim][ABS] has been used for extraction of lignin from sugarcane bagasse. The results showed that the lignin extraction increases with elevating temperature (170-190 °C), and when the extraction time increases from 30 min to 120 min. Also, a lignin extraction with more than 93% yield was successfully attained at atmospheric pressure [109].

The pretreatment of oil palm frond (OPF) lignocellulosic feedstock with the IL [Bmim]Cl, followed by regeneration of cellulose using an anti-solvent, to facilitate the conversion of the OPF into fermentable sugar (glucose) has been investigated [110]. SEM analysis showed a

significant destruction of the biomass structure after pretreatment with the IL, which in turn reduced the crystallinity and improved the enzymatic digestibility of the biomass. An optimum 100% glucose recovery was found with pretreatment conditions of 80 °C, a 15-min retention time and 10% solid loading [110].

Some difficulties in dissolving and extracting lignin from maple wood flour were faced by [96] using the same ILs used earlier in [53], namely, [Hmim][CF₃SO₃], [Mmim][MeSO₄] and [Bmim][MeSO₄]. However, Cl⁻-containing ILs, [Amim][Cl] and [Bmim][Cl], have shown better capabilities. This might be due to the high solubility of the wood flour as a whole. However, Cl⁻ ions are good H⁺ acceptors and are able to interact with the OH groups of the sugars, causing dissolution of cellulose too. It was also found that [Emim][OAc] IL provides a balance between good lignin extraction and low wood flour solubility [96]. Hence, lignin extraction can be done using [Emim][OAc] without much disruption of the cellulose and hemicellulose structures [98]. On the other hand, an extensive summary on lignin dissolution in ILs is presented in [96] while solubilities and extraction efficiency of lignin in various ILs are presented in [97].

The imidazolium-based ILs were used for the study of the dissolution of residual softwood lignin isolated from a southern pine Kraft pulp (at 25-100 °C). It was found that the lignin solubility can be influenced by the nature of the anion when different [Bmim]⁺-containing ILs are used. It was also concluded that ILs containing large, non-coordinating anions like [BF₄]⁻ and [PF₆]⁻ are not suitable for dissolving lignin; and that imidazolium methyl sulfate-based ILs are effective for dissolution of such lignins. The solubilities of lignin in some imidazolium-based ILs (at 50-120 °C) are presented; and almost similar conclusions are still valid [53].

The IL 1-ethyl-3-methylimidazolium glycine [Emim][Gly], which has a high hydrogen-bond basicity, has been used to dissolve bamboo biomass and found to be effective at 120 °C in 8 h. While, 1-ethyl-3-methylimidazolium trifluoroacetate, [Emim][TFA], which contains an acetate-based anion, and choline propionate, which has high hydrogen-bond basicity, none of them could dissolve the bamboo biomass after 24 h [102].

Food additive-derived imidazolium acesulfamate ILs have been used for extraction of lignin from wood flour and showed promising results without disrupting the cellulose crystallinity [93]. Among all, 1-ethyl-3-methylimidazolium acesulfamate [Emim][Ace] IL is desirable for industrial processing due to its physical properties. The extracted lignins have a larger average molar mass as well as a more uniform molar mass distribution compared to that obtained from the Kraft process. This adds to another advantage of using imidazolium acesulfamate ILs. The various extraction conditions: extraction temperature and time; water content; wood load, particle size and species; types of IL cation; effect of IL recycling; multi-step treatment and use of co-solvents were also examined in [93]. Interestingly, the use of dimethyl sulfoxide (DMSO) as a co-solvent in weight ratios of ($w_{IL}: w_{DMSO}=9:1$) increased the extraction efficiency by almost 50%. It is believed that the penetration and interaction of the lignocellulosic biomass with IL are enhanced due to loosening of the tight hydrogen bond network of the cellulose and the decrease in the overall viscosity of the mixture caused by the use of DMSO [93]. The lignin extract and the wood residues were characterized *via* infrared spectroscopy, elemental analysis, thermogravimetric analysis, differential scanning calorimetry, X-ray diffraction, and gel permeation chromatography. An extraction efficiency of 0.43 of wood lignin was achieved

in one gentle extraction step (100°C, 2 h), and it was found that the presence of a co-solvent increased the extraction efficiency to 0.60. Gentle conditions during IL treatment did not decrease the crystallinity of the wood sample, and the extracted lignin had both a larger molar mass and a more uniform molar mass distribution, compared to commercially available Kraft lignin [93].

On the other hand, lignin extraction can also be done after complete dissolution of the whole cellulosic biomass. A cellulose-lignin mixture system has been separated and recovered from ILs [Bmim]Br and [Bmim]Cl. The cellulose precipitates when water is added to the solution (cellulose-lignin mixture in IL). Lignin is then recovered from the precipitate formed when the filtrate is treated with ethanol. The IL can be regenerated by evaporating the ethanol from the second filtrate with more than 95% yield. On the other hand, lignin yields of 69% and 49% were isolated from [Bmim]Br and [Bmim]Cl, respectively [111]. However, the influence of water on dissolution of cellulose in selected ionic liquids is discussed in [112].

Both softwood and hardwood were dissolved in [Emim][OAc] and lignin was extracted using acetone/water (1:1 v/v) and the effects of IL, particle size, wood species, and initial wood concentration and pretreatment were evaluated [76]. The same method in [102], lignin has been extracted from the solution using acetone/water anti-solvent. The ideal process flow of the dissolution and regeneration of wood in IL is shown in Figure 1.

It was reported also that IL [Emim][OAc] is an effective solvent for lignin extraction from triticale straw, flax shives and wheat straw and the extraction yields were much higher than those of [Bmim]Cl. The extraction capability was found to increase with higher temperatures (up to 150°C) and longer extraction times (up to 24 h) [113].

The structural features of poplar wood lignin extracted using IL [Emim][OAc] has been compared with that using dioxane-water (classical method). A higher yield of extraction was obtained using the IL [114]. Even though the lignins obtained from both extractions have relatively similar methoxy and phenolic hydroxyl contents, the molecular weight of that obtained from classical method is higher. However, the poly-dispersity index (PDI) of IL extraction is lower and thus, indicating that lignin from IL extraction is of rather uniform size. This suggests that some form of depolymerization had occurred. On top of that, thermal behaviour of the lignins were also analyzed. Lignin obtained from classical method has a higher maximum decomposition rate and temperature, indicating that it is thermally more stable [114].

A large number of ILs, sorted by cations and anions, have been screened for their solubility characteristics towards infinite concentrations of cellulose. The calculations show a very well-defined dependency on the anion for the dissolution kinetics. Further calculations concern the influence of water in ILs, because in experiments a very rapid decrease in the solubility of cellulose in ILs has been observed. At this point, a link to experimental results must be established in order to validate the calculations and to develop the routines and databases of a COSMO-RS software. These calculations can then be used as reliable screening method to identify new candidates of eligible ILs for the dissolution of wood [115].

Fractions of pulverized Norway spruce (*Picea abies*) and *Eucalyptus grandis* wood were solvated and precipitated by agitating and heating the lignocellulosic materials in IL [Amim]Cl followed by precipitation using non-solvents, such as acetonitrile (MeCN) and water [116]. The efficiency of precipitation was found to be dependent upon molecular weight, with the dissolved higher molecular weight and partially soluble wood components precipitating first. Moreover, when coarse sawdust samples were fractionated, the selective dissolution of cellulose from the fiber was observed; this allowed for the regeneration of a fraction of delignified and bleachable cellulose. Additionally, finely milled softwood samples, with demonstrated narrowly distributed low molecular weights, did not efficiently fractionate most likely due to the presence of an extensive lignin-carbohydrate complexes (LCC) network [116].

A comparison of the fractionation of coarse and finely pulverized wood from [Amim]Cl identified that fractionation mainly is dependent on molecular weight and not chemical composition. This was observed for softwood (Norway spruce) and hardwood (*Eucalyptus*) species. When finely milled wood is completely dissolved in [Amim]Cl, most of its components can be precipitated in the order of decreasing molecular weight using MeCN and MeOH as non-solvents [116]. Contrary to reports of highly efficient fractionation of cellulose doped with high purity lignin [111], it was only possible to fractionate the finely pulverized and dissolved spruce wood with marginal selectivity. It is likely that the presence of extensive LCCs, especially within the softwood material, is preventing the separation of lignin and polysaccharides. This suggests the need for a pretreatment of wood so as to break the LCCs in order to increase the selectivity of fractionation [116].

In the fractionation of sawdust, it was determined that cellulose preferentially dissolves in the initial dissolution step and that lignin is relatively resistant to being removed from the fiber. After precipitation of the residual insoluble material it was possible to precipitate the dissolved cellulose in bleachable grade and relatively high purity [116]. This result, using [Amim]Cl, is contrary to previous publications [76] using [Emim][OAc] and suggests either a different mode of dissolution of wood between the two classes of ILs or between different species. Additionally, extraction of the residual fibrous and the precipitated materials after the fractionation of sawdust afforded acetylated galactoglucomannan (a water-soluble hemicellulose, consisting of galactose, glucose and mannose) with relatively high molecular weight [116].

On the other hand, the IL [Emim][OAc] was used as a pretreatment solvent to decrease both lignin content and cellulose crystallinity of maple wood flour [96]. The cellulose in the pretreated wood flour becomes far less crystalline without undergoing solubilization. In addition, [Emim][OAc] was easily reused, thereby resulting in a highly concentrated solution of chemically unmodified lignin, which may serve as a valuable source of a poly-aromatic material as a value-added product. The [Emim][OAc] did not dissolve the wood flour; however, facile extraction of the lignin was achieved. A strong inverse relationship was found between the effectiveness of cellulase-catalyzed hydrolysis of wood flour cellulose and both lignin content and cellulose crystallinity. Complete lignin removal was not needed and maximal cellulose degradability (> 90%) was achieved even at 40% total lignin extraction. Finally, [Emim][OAc] was reusable without significant loss in the yield of lignin extracted and subsequent cellulose hydrolyzed after four cycles. Furthermore, chemically unmodified lignin

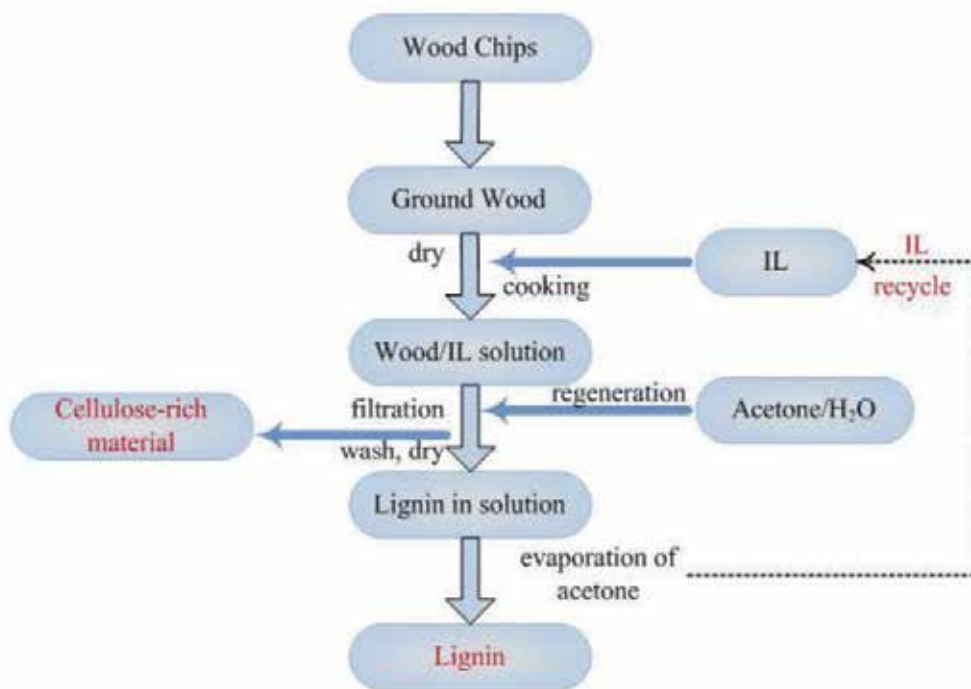


Figure 1. Flowchart for the process of dissolution and regeneration of wood in IL [4].

with high hydrophobicity could be easily precipitated from concentrated lignin solution in [Emim][OAc] by adding excess water [96].

It was also demonstrated in [117] that the IL [Emim][OAc] can be used as a potential solvent for the pretreatment of lignocellulosic biomass such as energy cane bagasse (ECB). Furthermore, the sugar yields obtained post pretreatment have great potential as building blocks in the production of renewable fuels and chemicals. The energy cane bagasse pretreated with recycled [Emim][OAc] resulted in a decrease of lignin removal as compared to bagasse pretreated with the original IL. However, further research is still needed to improve the efficiency of this pretreatment on energy crops. Among the future research work that still to be investigated are the optimal pretreatment conditions with extended design space, assess the efficiency of recycled IL pretreatment at optimal processing conditions, and calculate the cost for the entire conversion process and energy returned on energy invested.

The regeneration of lignin from some woods dissolved in imidazolium-based ILs: [Bmim][OAc], [Emim][OAc], [Emim]Cl, [Bmim]Cl and [Amim]Cl have been studied in [118]. The lignin was successfully regenerated by precipitation with an anti-solvent from solutions of wood in [Amim]Cl, [Bmim]Cl or [Emim]Cl. The regenerated lignin, characterized by Fourier transform infrared spectroscopy, ^{13}C nuclear magnetic resonance, elemental analysis, thermogravimetric analysis, and differential scanning calorimetry, was compared to Indulin AT lignin, and showed different properties depending on the IL employed and the wood species.

On the other hand, the latest developments and knowledge in the field of fractionation of lignocellulosic materials with ILs have been briefly reviewed and an alternative fractionation method based on the controlled regeneration of components from [Amim]Cl has been introduced in [100]. Norway spruce (*Picea abies*) and *Eucalyptus grandis* woods were dissolved in their fibrous state or by utilizing ball milling to improve solubility. The resulting wood solutions were precipitated gradually resulting into fractions by addition of non-solvents, such as acetonitrile and water. Further water extraction of the crude fractions resulted in better separations. Fractionation efficiency was found to be highly dependent on the modification of the wood cell wall ultrastructure and the degree of reduction of the molecular weights of the main components, arising from mechanical degradation. Isolation of cellulose enriched fractions was achieved with Spruce sawdust and ball milled *Eucalyptus*, evidently following from distinct dissolution mechanisms [100]. It was also demonstrated that wood (sawdust and highly pulverized spruce) is *not* completely soluble in [Amim]Cl in its native state. One possible reason for this is the presence of a lignin-carbohydrate complexes (LCC) matrix in wood that is simply of too high molecular weight and interconnected to dissolve. This property can be utilized to extract cellulose, as it is not covalently bound to the insoluble LCC matrix. Cellulose is extracted and by careful control of non-solvent addition, the insoluble lignin-hemicellulose rich fraction can be first isolated, followed by regeneration of relatively pure cellulose. *This cellulose extraction procedure is not yet at a stage that would yield a technically useful pulp, due to apparent depolymerization, in comparison to technical pulps and holocellulose.* However, the more we learn about the stability of wood and lignocellulose, in technical and pure ILs, the better are our chances of yielding close-to native polymers [100].

Samples of corn stover, Norway spruce, and *Eucalyptus grandis* were pulverized to different degrees, subjected to quantitative analyses, upon the basis of pre-dissolution into imidazolium chloride-based ILs [Amim]Cl and [Bmim]Cl, followed by labeling of hydroxyl groups as phosphite esters and quantitative “wood solubility” using ^{31}P NMR analysis. Analysis of different pulverization degrees provided semi-empirical data to chart the solubility of Norway spruce in these ILs [119].

The solubility of the Norway spruce wood samples (subjected to varying degrees of mechanical pulverization) in a range of common ionic and molecular solvents, was quantified using a novel ^{31}P NMR technique [120]. The results showed that intact wood is not soluble under mild treatment conditions, in cellulose-dissolving or swelling solvents. Further refinement afforded an optimized method of analysis of the lignin phenolic functionalities, without prior isolation of the lignin from the fiber. The lignin in the samples was further enriched using cellulase and acidolysis treatments, allowing for comparison with the fibrous samples. Analysis of all samples charts the polymerized-monomer availability for each stage of the treatment. Conditions required for adequate signal-to-noise ratios in the ^{31}P NMR analysis were established with a notable improvement observed upon the lignin enrichment steps [120].

The critical outlook on the study of biomass dissolution and changes occurred in the biomass during this process as well as on the influence of several crucial parameters that govern the dissolution and further pretreatment process are reviewed in [94]. The currently known methods of biomass fractionation in IL and aqueous-IL mixtures are also discussed and

perspectives regarding these topics are given as well. The review in [94] also shows that ILs have potential to be used in the biomass pretreatment and demonstrated that ILs can be successfully used to obtain cellulose, hemicellulose and lignin fractions with purity and efficiency equal or superior to the classical pretreatment methods. The exploitation of ILs in the lignocellulosic biomass processing demonstrates the enormous potential in this research area, especially in the context of a biorefinery; however, an extensive research is still required to better understand and predict the outcomes of these processes.

The multi-functional use of ILs with respect to lignin processing has been reviewed in [99] and the use of ILs in selectively or non-selectively dissolving lignin, the attempted depolymerization reactions on lignin in ILs, and the observed effect of ILs on such processes have been highlighted. Some of the challenges and issues that must be addressed before the informed and large-scale application of ILs can be realized for lignin processing has been presented and finally it was concluded that, there is both great scope for innovation and huge potential in the sophisticated application of ILs, in order to produce high yields of chosen, monomeric aromatics from a wide variety of lignin sources [99].

The up-to-date progress in selective breakdown of lignocellulose in ILs, especially molecular level understanding of the dissolution of biomass in ILs, strategies for the conversion of lignocellulose into fermentable sugars and furans, and related chemicals have been highlighted [121]. Further research in the area of selective breakdown of lignocellulose, or utilization of biomass incorporating ILs technology, is expected for example in, exploitation of novel chemistry of lignocellulose in ILs or IL-containing media; integration of the ILs processes with other chemical or biological processes; design and preparation of cheaper, greener and process-compatible ILs; developing new strategies for ILs recycling and product recovery.

The complex structure and the 3-D lignin network that binds lignocellulosic components together makes it practically impossible to dissolve lignocellulosic materials in their native form in conventional solvents. The aromatic electron-rich cationic moiety creates strong interactions for polymers which undergo π - π stacking (lignin). The chloride anion in an IL is the most efficient in disrupting the extensive inter- and intra-molecular H-bonding interactions present in wood (cellulose) allowing the IL [Amim]Cl, for example, to diffuse into the interior of the material [122].

The conversion of lignocellulosic biomasses has been considered to be economically unfeasible due to the crystalline structure of cellulose. Molecular dynamic simulation (MDS) tools have been applied to (1) determine driving force(s) for the crystalline structure of cellulose, (2) illuminate the interactions between cellulose molecules and candidates of decrystallization chemicals, and (3) search for a novel chemical to allow the decrystallization of cellulose followed by the saccharification without an intervening process [123].

5. Future prospects

Use of ionic liquids provided a new platform for comprehensive utilization of wood, although many problems need to be further addressed: First, dissolution of wood in ILs has opened a

new avenue for wood chemistry research and to improve the efficient utilization of wood. Second, the ILs can be used as wood preservatives or to improve wood's anti-electrostatic and fire-proof properties. This will extend the range of wood applications and reduce the use of some dangerous chemicals. Finally, use of ILs is also a competitive alternative exhaust treatment technology in the wood processing, which can reduce the energy consumption and waste of resources [14]. However, application of ILs in wood-related industry at industrial scale still faces some challenges.

1. The cost of ILs hampers the use of ILs at a commercial scale. Therefore, economical synthesis of ILs and efficient recovery and recycling technologies play vital roles in their industrial applications. Depending on the IL used and the application performed on it, a variety of recycling methods were possible. By picking the right purification steps, an individually optimized work-up procedure can be obtained [124]. Several procedures on how to recover ionic liquids from their solution have been reviewed in [125]: distillation/stripping at some suitable temperature (< 300 °C) and under vacuum, liquid-liquid extraction (using objectionable VOCs!), supercritical fluids (using CO₂ at room temperature and several MPa), and membrane separation (to separate nano size particles from ILs).
2. The biodegradability, toxicology, and thermodynamic data of ILs are still scarce. There are also lots of engineering problems that need to be solved. ILs have the reputation of being "green" chemicals, but not all of them can pass favourably the tests evaluating their environmental effects. For example, reference [126] focused on ionic liquids' environmental impact, ecotoxicity and potential biodegradability, while compiling results of different ecotoxicological studies. A comprehensive database on toxicity of ILs has been established in [13] in a database that includes over 4000 pieces of data. Based on this database, the relationship between IL's structure and its toxicity has been analyzed qualitatively. Furthermore, quantitative structure-activity relationships (QSAR) model has been conducted to predict the toxicities (EC₅₀ values) of various ILs toward the Leukemia rat cell line IPC-81.
3. The most challenging engineering problem is the high viscosity of ILs, which is expected to cause severe mass and heat transfer problems during their industrial use. Some measures have been taken to reduce ILs viscosity, such as development of low viscous ILs [66] and use of mixtures of ILs [49], but these measures can only partially resolve this problem.

Although these challenges still exist, great progress has been made in research for application of ILs in wood-related industries in recent years. Although many problems associated with application of ILs in wood-related industries need to be solved, it is quite clear that in the near future these applications will be implemented at a full industrial scale and society can be expected to benefit greatly from these applications [14].

Thus understanding of ILs volatility, purity, stability, biodegradability and toxicity is necessary for their recovery, since this determines whether an IL can be sustainably developed. In other words, a long way is still to go before large-scale implementation of ILs becomes feasible

and practical. However, issues over the cost of ionic liquids for industrial applications still exist.

Appendix: Abbreviations of some of the ionic liquids used in this chapter

Ionic liquid	Abbreviation
1-allyl-3-methylimidazoium chloride	[Amim]Cl
1-butyl-3-methylimidazolium chloride	[Bmim]Cl
1-butyl-3-methylimidazolium chloride	[Bmim]Br
1-butyl-3-methylimidazolium acetate	[Bmim][OAc]
1-butyl-3-methylimidazolium methyl sulfate	[Bmim][C ₁ SO ₄]
1-butyl-3-methylimidazolium trifluoromethane sulfonate	[Bmim][OTf]
1-butyl-3-methylimidazolium tetrafluoroborate	[Bmim][BF ₄]
1-butyl-3-methylimidazolium hexafluorophosphate	[Bmim][PF ₆]
1-butyl-3-methylimidazolium sulfocyanate	[Bmim][SCN]
1-benzyl-3-methylimidazolium chloride	[Bzmim]Cl
1-ethyl-3-methylimidazolium chloride	[Emim]Cl
1-ethyl-3-methylimidazolim glycine	[Emim][Gly]
1-ethyl-3-methylimidazolim trifluoroacetate	[Emim][TFA]
1-ethyl-3-methylimidazoium acetate	[Emim][OAc]
1-ethyl-3-methyl-imidazolium trifluoroacetate	[Emim][CF ₃ COO]
1-ethyl-methylimidazolium alkyl benzene sulfonate	[Emim][ABS]
1-ethyl-3-methylimidazolium acesulfamate	[Emim][Ace]
1-hexyl-3-methylimidazolium chloride	[Hmim]Cl
1-hexyl-3-methylimidazolium tetrafluoromethane sulfonate	[Hmim][CF ₃ SO ₃]
1-hexyl-3-methylimidazolium tetrafluoroborate	[Hmim][BF ₄]
1-hexyl-3-methylimidazolium hexafluorophosphate	[Hmim][PF ₆]
1,3-dimethylimidazolium methyl sulfate	[Mmim][C ₁ SO ₄]
1-methyl-3-octylimidazolium chloride	[Omim]Cl

Author details

Samir I. Abu-Eishah

United Arab Emirates University, United Arab Emirates

References

- [1] Schrems, M. (2011). Green Refinery-Ionic Liquids as Novel Media for Biomass Processing, PhD Thesis, University of Natural Resources and Life Sciences, Vienna, Austria.
- [2] Hannus, M. (2011). Forward: Future Biorefinery, Programme Report 2009–2011, Forestcluster Ltd., ISBN 978-952-92-9719-1.
- [3] Gräsvik, J. (2013). Ionic Liquids in Bio-Refining: Synthesis and Applications, PhD Thesis, Umeå University, Umeå, Sweden.
- [4] Sun, N. (2010). Dissolution and Processing of Cellulosic Materials with Ionic Liquids: Fundamentals and Applications, PhD Thesis, The University of Alabama, Tuscaloosa, Alabama, USA.
- [5] Feng, L.; Chen, Z. (2008). Research progress on dissolution and functional modification of cellulose in ionic liquids, *J. Molecular Liquids*, 142: 1–5.
- [6] Isik, M.; Sardon, H.; and Mecerreyes, D. (2014). Ionic liquids and cellulose: dissolution, chemical modification and preparation of new cellulosic materials: Review. *Int. J. Mol. Sci.*, 15: 11922–11940.
- [7] Luo, J.; Cai, M.; Gu, T.; (2013). Pretreatment of Lignocellulosic Biomass Using Green Ionic Liquids, Chap. 6, pp. 127–153, In: *Green Biomass Pretreatment for Biofuels Production*, T. Gu (ed.), Springer Briefs in Green Chemistry for Sustainability.
- [8] Fort, D.A.; Remsing, R.C.; Swatloski, R.P.; Moyna, P.; Moyna, G.; Rogers, R.D. (2007). Can ionic liquids dissolve wood? Processing and analysis of lignocellulosic materials with 1-n-butyl-3-methyl imidazolium chloride, *Green Chem.* 9: 63–69.
- [9] Vancov, T.; Alston, A.-S.; Brown, T.; McIntosh, S. (2012). Use of ionic liquids in converting lignocellulosic material to biofuels, *Renewable Energy* 45: 1–6.
- [10] Binder, J.B.; Gray, M.J.; White, J.F.; Zhang, Z.C.; Holladay, J.E. (2009). Reactions of lignin model compounds in ionic liquids, *Biomass and Bioenergy* 33: 1122–1130.
- [11] King, A.W.T. (ed.) (2011). Novel Ionic Liquids for Wood Processing, pp. 12–23, In: *Future Biorefinery*, Programme Report 2009–2011, Forestcluster Ltd, ISBN 978-952-92-9719-1.
- [12] Klein-Marcuschamer, D.; Simmons, B.A.; Blanch, H.W. (2011). Modeling and analysis: techno-economic analysis of a lignocellulosic ethanol biorefinery with ionic liquids pretreatment, *Biofuels, Bioprod. Bioref.* 5(5): 562–569.
- [13] Zhao, Y.; Zhao, J.; Huang, Y.; Zhou, Q.; Zhang, X.; Zhang, S. (2014). Toxicity of ionic liquids: Database and prediction via quantitative structure-activity relationship method, *J. Hazardous Materials*, 278: 320–329

- [14] Han, S.; Li, J.; Zhu, S.; Chen, R.; Wu, Y.; Zhang, X.; Yu, Z. (2009). Potential applications of ionic liquids in wood related industries, *BioResources* 4(2): 825–834.
- [15] Mohanty, A.K.; Misra, M.; Hinrichsen, G. (2000). Biofibers, biodegradable polymers and biocomposites: An overview. *Macromolecular Materials & Engineering*, 276/277(1): 1–24.
- [16] Huber, T. (2012). Processing of all Cellulose Composites via an Ionic Liquid Route, PhD Thesis, University of Canterbury, Christchurch, New Zealand.
- [17] Biagotti, J.; Puglia, D.; Kenny, J.M. (2004). A review on natural fiber-based composites – Part I: structure, processing and properties of vegetable fibers. *J. Natural Fibers*, 1: 37–68.
- [18] Bismarck, A.; Jimenez, A.B. (2005). Truly Green Composites: Fiber, Polymer & Interface Characterisation. in Bio-based/Green Materials and Processing Technology-The Annual Meeting, Cincinnati, USA.
- [19] Akin, D.E. (2010). Chemistry of plant fibers. in industrial applications of natural fibers structure, properties and technical applications, M. Eder and I. Burgert (eds.), John Wiley & Sons Ltd., Chichester, UK.
- [20] Thielemans, W.; Wool, R.P. (2005). Kraft lignin as fiber treatment for natural fiber-reinforced composites. *Polymer Composites*, 26 (5): 695–705.
- [21] John, M.J.; Thomas, S. (2008). Review: Biofibers and Biocomposites. *Carbohydrate Polymers*, 71: 343–364.
- [22] Pernak, J.; Zabielska-Matejuk, J.; Kropacz, A.; Foksowicz-Flaczyk, J. (2004). Ionic liquids in wood preservation. *Holzforschung* 58: 286–291.
- [23] Pernak, J.; Goc, I.; Fojutowski, A. (2005). Protic ionic liquids with organic anion as wood preservative, *Holzforschung* 59: 473–475.
- [24] Pernak, J.; Śmiglak, M.; Griffin, S. T.; Hough, W. L.; Wilson, T. B.; Pernak, A.; Zabielska-Matejuk, J.; Fojutowski, A.; Kita, K.; Rogers, R. D. (2006). Long alkyl chain quaternary ammonium-based ionic liquids and potential applications, *Green Chemistry* 8: 798–806.
- [25] Pernak, J.; Jankowska, N.; Walkiewicz, F.; Jankowska, A. (2008). The use of ionic liquids in strategies for saving and preserving cultural artifacts, *Polish J. Chem.* 82: 2227–2230.
- [26] Stasiewicz, M.; Fojutowski, A.; Kropacz, A.; Pernak, J. (2008). 1-Alkoxymethyl-X-dimethylaminopyridinium-base ionic liquids in wood preservation, *Holzforschung*, 62: 309–317.
- [27] Ranke, J.; Stolte, S.; Störmann, R.; Arning, J.; Jastorff, B. (2007). Design of sustainable chemical products– the example of ionic liquids, Appendix 1, *Chem. Rev.*, 107, 2183–2206.

- [28] Brandt, A.; Hallett, J.P.; Leak, D.J.; Murphy, R.J.; Welton, T. (2010). The effect of the ionic liquid anion in the pretreatment of pine wood chips, *Green Chem.*, 12: 672–679.
- [29] Fuczek, D., Zabielska-Matejuk, J., Pernak, J., Przybylska, W. (2010). Wettability of wood surfaces treated with ionic liquids, *Drewno: Prace Naukowe, Doniesienia, Komunikaty* 53 (184): 45–53.
- [30] Zabielska-Matejuk, J.; Pernak, J., Kropacz, A., Kot, M., Stangierska, A. (2010). Activity of new ammonium ionic liquids against fungi causing wood moulding, *Drewno: Prace Naukowe, Doniesienia, Komunikaty*, 53(184): 11–19.
- [31] Fojutowski, A.; Noskowiak, A.; Kot, M.; Kropacz, A.; Stangierska, A. (2010). The assessment of mechanical properties of wood treated with ionic liquids, *Drewno: Prace Naukowe. Doniesienia. Komunikaty*, 53(184): 21–37.
- [32] Kot, M., Kowaluk, G. (2010). Wood hydrophobization by ammonium ionic liquids, *Drewno: Prace Naukowe. Doniesienia. Komunikaty*, 53(184): 39–44.
- [33] Frąckowiak, I.; Zabielska-Matejuk, J.; Fuczek, D.; Kot, M. (2010). Application of ammonium ionic liquids in particleboard technology, *Drewno: Prace Naukowe, Doniesienia, Komunikaty*, 53(184): 55–63.
- [34] Croitoru, C.; PaŃachia, S.; Porzsołt, A. (2011-a). Alkyl imidazolium ionic liquids as ecologic solvents for wood finishing materials, *Bulletin of the Transilvania University of Braşov, Series I: Engineering Sciences*, 4(53): 37–42.
- [35] Croitoru, C.; Patachia, S.; Porzsołt, A.; Friedrich, C. (2011-b). Ecologic modification of wood using alkyl imidazolium-based ionic liquids, *Environmental Eng. and Management J.* 10(8): 1149–1154.
- [36] Zabielska-Matejuk, J. (2011). Ionic liquids in new technologies in the forest-based sector: research status. In: *Pacing Innovation for the Bioeconomy, 7th Conference of the European Forest-Based Sector Technology Platform*, Warsaw, Sept. 26–27.
- [37] Zabielska-Matejuk, J.; Pernak, J.; Frąckowiak, I.; Stangierska, A.; Przybylska, W.; Kot, M. (2012). Triazole-based ionic liquids to protect of lignocellulosic materials against fungi, *The Int. Research Group on Wood Protection, IRG – IUFRO Conference*, Estoril, Portugal, July 8–13.
- [38] Rogala, A.; Ksiezniak, K. (2013). Bioactive quaternary ammonium ionic liquids, *PhD Interdisciplinary J.* 2: 83–88.
- [39] Obłak, E.; Gamian, A. (2010). The biological activity of quaternary ammonium salts (QASs), *Postepy Hig Med Dosw* 64: 201–211 (in Polish).
- [40] Rogers, R.D.; Daly, D.T.; MacFarlane, D.; Scott, J.L.; Seddon, K.R.; Gurau, G.; Bica, K.; Turanjanin, J.; Dean, P.M. (2012). Dual Functioning Ionic Liquids and Salts Thereof, US20120046244 A1.

- [41] Foksowicz-Flaczyk, J.; Walentowska, J. (2013). Antifungal activity of ionic liquid applied to linen fabric, *Int. Biodeterioration & Biodegradation*, 84: 412–415.
- [42] Patachia, S.; Croitoru, C. (2013). Potential applications of ionic liquids in ecologic wood processing, *Pro Ligno*, 9(4): 211–216. Online ISSN 2069-7430.
- [43] Sun, Y.; Cheng, J. (2002). Hydrolysis of lignocellulosic materials for ethanol production: a review. *Bioresour. Technol.*, 83: 1–11.
- [44] Chandra, R.P.; Bura, R.; Mabee, W.E.; Berlin, A.; Pan, X.; Saddler, J.N. (2007). Substrate pretreatment: The key to effective enzymatic hydrolysis of lignocellulosics. *Adv. Biochem. Eng. Biotechnol.*, 108: 67–93.
- [45] Galbe, M.; Zacchi, G. (2007). Pretreatment of lignocellulosic materials for efficient bioethanol production. *Adv. Biochem. Eng. Biotechnol.*, 108: 41–65.
- [46] Swatloski, R.P.; Spear, S.K.; Holbrey, J.D.; Rogers, R.D. (2002). Dissolution of cellulose with ionic liquids, *J. Am. Chem. Soc.* 124: 4974–4975.
- [47] Laus, G.; Bentivoglio, G.; Schottenberger, H.; Kahlenberg, V.; Kopacka, H.; Röder, T.; Sixta, H. (2005). Ionic liquids: current developments, potential and drawbacks for industrial applications, *Lenzinger Berichte* 84: 71–85.
- [48] Zhu, S.; Wu, Y.; Chen, Q.; Yu, Z.; Wang, C.; Jin, S.; Ding, Y.; Wu, G. (2006). Dissolution of cellulose with ionic liquids and its application: A mini-review, *Green Chem.* 8: 325–327.
- [49] Kilpeläinen, I.; Xie, H.; King, A.; Granstrom, M.; Heikkinen, S.; Argyropoulos, D.S. (2007). Dissolution of wood in ionic liquids. *J. Agric. Food Chem.* 55: 9142–9148.
- [50] Wang, Q.; Ou, R.; Shen, X.; Xie, Y. (2011). Plasticizing cell walls as a strategy to produce wood-plastic composites with high wood content by extrusion processes, *BioResources*, 6(4): 3621–3622.
- [51] Olivier-Bourbigou, H.; Magna, L.; Morvan, D. (2010). Ionic liquids and catalysis: Recent progress from knowledge to applications. *Appl. Catal. A: General*, 373(1-2): 1–56.
- [52] Yinghuai, Z.; Biying, A.O.; Siwei, X.; Hosmane, N.S.; Maguire, J.A. (2011). Ionic liquids in catalytic biomass transformation, Chap. 1, pp. 3-26, In: Applications of ionic liquids in Science and Technology, S.T. Handy (ed.), 2011. InTech, Rijeka, Croatia.
- [53] Pu, Y.; Jiang, N.; Ragauskas, A.J. (2007). Ionic liquid as a green solvent for lignin, *J. Wood Chemistry & Technology*, 27: 23–33.
- [54] Shcherbakov, I.; Toikka, A.; Kraslawski, A. (2013). Application of ionic liquid for modification of cellulose and preparation of cellulose/magnetite composite, Poster [B.3.5.29], Symp. B-Energy, Environmental & Structural Hybrids, March 3-5. Available from http://www.hybridmaterialsconference.com/resources/downloads/poster_programme-2013.pdf

- [55] Ohno, H.; Fukaya, Y. (2009). Task specific ionic liquids for cellulose technology. *Chem. Lett.*, 38: 2–7.
- [56] Teacă, C.-A.; Bodîrlău, R.; Spiridon, I. (2011). Dissolution of natural polymers in ionic liquids, *Rev. Roum. Chim.*, 56(1): 33–38.
- [57] Sen, S.M.; Binder, J.B.; Raines, R.T.; Maravelias, C.T. (2012). Conversion of biomass to sugars via ionic liquid hydrolysis: process synthesis and economic evaluation, *Biofuels, Bioprod. Bioref.* 6: 444–452.
- [58] García, A.C. (2013). Dissolution of Wood of *Pinus Radiata* and *Eucalyptus Globulus* in 1-Alkyl-3-Methyl Imidazolium Cation-based ionic liquid and Regeneration of Cellulose and Lignin, PhD Thesis, Universidad Complutense de Madrid, Spain.
- [59] Khonsari, Y.N.; Mirshokraei, S.A.; Abdolkhani, A. (2013). Dissolution of wood flour and lignin in 1-butyl-3-methyl-1-imidazolium chloride, *Oriental J. Chemistry* 29(3): 889–904.
- [60] Li, D. (2010). Evaluation of Ionic Liquids as Direct Solvents for the Manufacturing of Novel Products from Cellulose, Master Thesis, Chalmers University of Technology, Göteborg, Sweden.
- [61] Ungurean, M.; Fitigau, F.; Paul, C.; Ursoiu, A.; Peter, F. (2011). Ionic liquid pretreatment and enzymatic hydrolysis of wood biomass, *World Academy of Science, Engineering and Technology* 5: 344–348.
- [62] Shamsuri, A.A.; Abdullah, D.K. (2010). Isolation and characterization of lignin from rubber wood in ionic liquid medium, *Modern Applied Science* 4(11): 19–27.
- [63] Paţachia, S.; Croitoru, C.; Rusu, V. (2013). Obtaining of ecological composites from wood waste using ionic liquids, *Bulletin of the Transilvania University of Braşov, Series I: Eng. Sciences* 6(55): 45–50.
- [64] Liebert, T.; Heinze, T. (2008). Interaction of ionic liquids with polysaccharides. 5. Solvents and reaction media for the modification of cellulose, *BioResources* 3(2), 576–601.
- [65] Zhang, H.; Wu, J.; Zhang, J.; He, J. (2005). 1-allyl-3-methylimidazolium chloride room temperature ionic liquid: a new and powerful non-derivatizing solvent for cellulose. *Macro-molecules*, 38(20): 8272–8277.
- [66] Fukaya, Y.; Sugimoto, A.; Ohno, H. (2006). Superior solubility of polysaccharides in low viscosity, polar, and halogen-free 1,3-dialkylimidazolium formates. *Biomacromolecules*, 7(12): 3295–3297.
- [67] Fukaya, Y.; Hayashi, K.; Wada, M.; Ohno, H. (2008). Cellulose dissolution with polar ionic liquids under mild conditions: required factors for anions. *Green Chem.*, 10: 44–46.
- [68] Vitz, J.; Erdmenger, T.; Haensch, C.; Schubert, U.S. (2009). Extended dissolution studies of cellulose in imidazolium based ionic liquids. *Green Chem.*, 11(3), 417–424.

- [69] Xu, A.; Wang, J.; Wang, H. (2010). Effects of anionic structure and lithium salts addition on the dissolution of cellulose in 1-butyl-3-methylimidazolium-based ionic liquid solvent systems. *Green Chem.*, 12(2): 268–275.
- [70] Wang, J.; Zheng, Y.; Zhang, S. (2010). The application of ionic liquids in dissolution and separation of lignocellulose, Chap. 4, pp. 71-84, In: Clean Energy Systems and Experiences, K. Eguchi (ed.), InTech, Rijeka, Croatia.
- [71] Zavrel, M.; Bross, D.; Funke, M.; Buchs, J.; Spiess, A. C. (2009). High-throughput screening for ionic liquids dissolving (ligno-)cellulose. *Bioresource Technology*, 100: 2580–2587.
- [72] Mora-Pale, M.; Meli, L.; Doherty, T.V.; Linhardt, R.J.; Dordick, J.S. (2011). Room temperature ionic liquids as emerging solvents for the pretreatment of lignocellulosic biomass, *Biotechnol. Bioeng.* 108: 1229–1245.
- [73] Myllymäki, V., and Aksela, R. (2005). Dissolution and delignification of lignocellulosic materials with ionic liquid solvent under microwave irradiation, WO Pat. 2005/017001.
- [74] Xie, H.; Shi, T. (2006). Wood liquefaction by ionic liquids, *Holzforschung*, 60: 509–512.
- [75] Hyvärinen, S.; Virtanen, P.; Murzin, D.Y.; Mikkola, J.-P. (2010). Towards ionic liquid fractionation of lignocellulosics for fermentable sugars, *Cellulose Chem. Technol.*, 44 (4–6): 187–195.
- [76] Sun, N.; Rahman, M.; Qin, Y.; Maxim, M.L.; Rodríguez, H.; Rogers, R.D. (2009). Complete dissolution and partial delignification of wood in the ionic liquid 1-ethyl-3-methyl imidazolium acetate. *Green Chemistry*, 11(5): 646–655.
- [77] Kilulya, K.F.; Msagati, T.A.M.; Mamba, B.B.; Ngila, J.C.; Bush, T. (2012). Determination of lipophilic extractives in ionic liquid extracts of eucalyptus pulp by gas chromatography-mass spectrometry, *Tanz. J. Sci.* 38(3): 14–26.
- [78] Lebo Jr., S. E.; Gargulak, J. D.; McNally, T. J. (2001). Lignin. In: Kirk-Othmer Encyclopedia of Chemical Technology. John Wiley & Sons, Hoboken.
- [79] Ralph, J.; Marita, J., Ralph, S.; Hatfield, R., Lu, F.; Ede, R.; Peng, J.; Quideau, S.; Helm, R.; Grabber, J.; Kim, H.; Jimenez-Monteon, G.; Zhang, Y.; Jung, H.; Landucci, L.; Mackay, J.; Sederoff, R.; Chapple, C.; Boudet, A. (2000): Solution-state NMR of Lignins. In: Advances in Lignocellulosic Characterization. D. Argyropoulos and T. Rials (eds.); TAPPI Press, Atlanta, USA.
- [80] Lowoko, M.; Henriksson, G.; Gellerstedt, G. (2003): New method for the quantitative preparation of lignin-carbohydrate complex from unbleached softwood Kraft pulp: Lignin-polysaccharides networks I. *Holzforschung* 57: 69-74.
- [81] Wu, B.; Liu, W.; Zhang, Y.; Wang, H. (2009). Do we understand the recyclability of ionic liquids? *Chem. Eur. J.*, 15: 1804–1810.

- [82] Kuzmina, O. (2012). Research of Dissolution Ability of Ionic Liquids for Polysaccharides such as Cellulose, PhD Thesis, Council of Chemical Geosciences, Faculty of Friedrich-Schiller-University Jena, Germany.
- [83] Egorov, V.M.; Smirnova, S.V.; Formanovsky, A.A.; Pletnev, I.V.; Zolotov, Y.A. (2007). Dissolution of cellulose in ionic liquids as a way to obtain test materials for metal-ion detection, *Anal. Bioanal Chem* 387: 2263–2269.
- [84] Scheibel, J.; Kenneally, C.; Menkhaus, J.; Seddon, K.; Chwala, P. (2007). Methods for modifying cellulosic polymers in ionic liquids, Procter & Gamble Co., US7714124 B2.
- [85] Zhao, H.; Jones, C.L.; Baker, G.A.; Xia, S.; Olubajo, O.; Person, V.N. (2009). Regenerating cellulose from ionic liquids for an accelerated enzymatic hydrolysis, *J. Biotechnology*, 139: 47–54.
- [86] Rogers, R.D.; Daniel, D.; Turner, M.; Spear, S.; Holbrey, J. (2007). Ionic liquid reconstituted cellulose composites as solid support matrices, Needle & Rosenberg, P.C., EP 1907470 A4.
- [87] Sashina, E.S.; Novoselov, N.P. (2009). Influence of structure of ionic liquids on its dissolution ability toward natural polymers, *J. General Chem.*, 79(6): 885–890.
- [88] Espinoza-Acosta, J.L.; Torres-Chávez, P.I.; Carvajal-Millán, E.; Ramírez-Wong, B.; Bello-Pérez, L.A.; Montaña-Leyva, B. (2014). Ionic liquids and organic solvents for recovering lignin from lignocellulosic biomass, *BioResources*, 9(2): 3660–3687
- [89] Moniruzzaman, M.; Ono, T.; Yusup, S.; Chowdhury, S.; Bustam, M.A.; Uemura, Y. (2013). Improved biological delignification of wood biomass via ionic liquids pretreatment: A one step process, *J. Energy Technologies & Policy* 3(11): 144–152.
- [90] Marvast, E.H.; Abdulkhani, A.; Hamzeh, Y.; Karimi, A.N. (2013). Dissolution and regeneration of lignocellulosic materials with ionic liquids [Bmim]Cl and [Bmim][MeSO₄] and determination some of mechanical and physical properties, *Industries Magazine, Wood & Paper Industry*, IV(1): 117–130. (In Persian).
- [91] Maki-Arvela, P.; Anugwom, I.; Virtanen, P.; Sjöholm, R.; Mikkola, J.P. (2010). Dissolution of lignocellulosic materials and its constituents using ionic liquids-A review, *Industrial Crops & Products*, 32: 175–201.
- [92] Abdulkhani, A.; Marvast, E.H.; Ashori, A.; Karimi, A.N. (2013). Effects of dissolution of some lignocellulosic materials with ionic liquids as green solvents on mechanical and physical properties of composite films. *Carbohydrate Polymers*, 95(1): 57–63.
- [93] Pinkert, A.; Goetze, D.F.; Marsh, K.N.; Pang, S. (2011). Extracting wood lignin without dissolving or degrading cellulose: investigations on the use of food additive-derived ionic liquids, *Green Chem.*, 13: 3124–3136.
- [94] da Costa Lopes, A.M.; João, K.G.; Morais, A.R.C.; Bogel-Lukasik, E.; Bogel-Lukasik, R. (2013). Ionic liquids as a tool for lignocellulosic biomass fractionation, *Sustainable*

- Chemical Processes*, 1(3): 1–31. <http://www.sustainablechemicalprocesses.com/content/1/3/3>
- [95] Holm, J.; Lassi, U. (2011). Ionic liquids in the pretreatment of lignocellulosic biomass, Chap. 24, pp. 545–560, In: *Ionic Liquids: Applications and Perspectives*, A. Kokorin (ed.) InTech, Rijeka, Croatia, ISBN 978-953-307-248-7.
- [96] Lee, S.H.; Doherty, T.V.; Linhardt, R.J.; Dordick, J.S. (2009). Ionic liquid-mediated selective extraction of lignin from wood leading to enhanced enzymatic cellulose hydrolysis, *Biotechnol. Bioeng.*, 102(5): 1368–1376.
- [97] Zakzeski, j.; Bruijninx, P.C.A.; Jongerius, A.L.; and Weckhuysen, B.M. (2010). The Catalytic Valorization of Lignin for the Production of Renewable Chemicals, *Chem. Rev.*, 110: 3552–3599.
- [98] Yinghuai, Z.; Yuanting, K.T.; Hosmane, N.S. (2013). Applications of ionic liquids in lignin chemistry, Chap. 13, pp. 315–346, In: *Ionic Liquids-New Aspects for the Future*, J.-I. Kadokawa (ed.), InTech, Rijeka, Croatia, ISBN 978-953-51-0937-2
- [99] Hossain, Md. M.; Aldous, L. (2012). Ionic liquids for lignin processing: dissolution, isolation, and conversion, *Aust. J. Chem.*, 65: 1465–1477.
- [100] Leskinen, T.; King, A.W.T.; Argyropoulos, D.S. (2014). Fractionation of lignocellulosic materials with ionic liquids, Chap. 6, pp. 145–168, In: *Production of Biofuels and Chemicals with Ionic Liquids (Biofuels and Biorefineries 1)*, Z. Fang, R.L. Smith, Jr. and X. Qi (eds.), Springer, USA.
- [101] Argyropoulos, D.S. (2008). Use of lignocellulosics solvated in ionic liquids for production of biofuels. US Patent 2008/0190013 A1
- [102] Muhammad, N.; Man, Z.; Khalil, M.A.B. (2012). Ionic liquid– a future solvent for the enhanced uses of wood biomass, *Eur. J. Wood Prod.*, 70: 125–133.
- [103] Gibril, M.E.; Yue, Z. Xin, L.; Huan, L.; Xuan, Z.; Feng, L.H.; Muhuo, Y. (2012). Current status of applications of ionic liquids for cellulose dissolution and modifications: Review, *Int. J. Eng. Sci. & Technol. (IJEST)*, 4(7): 3556–3571.
- [104] Turgis, R.; Estager, J.; Draye, M.; Bonrath, W.; Lévêque, J.M. (2010). Reusable task-specific ionic liquids for a clean ϵ -caprolactam synthesis under mild conditions. *ChemSusChem*, 3(12): 1403–1408.
- [105] Li, B.; Filpponen, I.; Argyropoulos, D.S. (2010-a). Acidolysis of wood in ionic liquids, *Ind. Eng. Chem. Res.*, 49(7): 3126–3136.
- [106] Zhang, Z.-G.; Chen H.-Z. (2012). Enhancement of the enzymatic hydrolysis of wheat straw by pretreatment with 1-allyl-3-methyl imidazolium chloride [Amim]Cl, *African J. Biotechnology*, 11(31): 8032–8037.
- [107] Li, D.; Sevastyanova, O.; Ek, M. (2012). Pretreatment of softwood dissolving pulp with ionic liquids, *Holzforschung*, 66: 935–943.

- [108] Li, B.; Asikkala, J.; Filpponen, I.; Argyropoulos, D.S. (2010-b). Factors affecting wood dissolution and regeneration of ionic liquids. *Ind. Eng. Chem. Res.*, 49, 2477–2484.
- [109] Tan, S.S.Y.; MacFarlane, D.R.; Upfal, J.; Edye, L.A.; Doherty, W.O.S.; Patti, A.F.; Pringle, J.M.; Scott, J.L. (2009). Extraction of lignin from lignocellulose at atmospheric pressure using alkyl benzene sulfonate ionic liquid. *Green Chem.*, 11: 339–345.
- [110] Tan, H.T.; Lee, K.T.; Mohamed, A.R. (2011). Pretreatment of lignocellulosic palm biomass using a solvent-ionic liquid [Bmim]Cl for glucose recovery: An optimisation study using response surface methodology, *Carbohydrate Polymers* 83: 1862–1868.
- [111] Lateef, H.; Grimes, S.; Kewcharoenwong, P.; Feinberg, B.J. (2009). Separation and recovery of cellulose and lignin using ionic liquids: a process for recovery from paper-based waste, *J. Chem. Technol. Biotechnol.*, 84: 1818–1827.
- [112] Mattinen, M.-L.; Maijala, P.; Nousiainen, P.; Kontro, J.; Asikkala, J.; Smeds, A.; Kontro, J.; Sipilä, J.; Tamminen, T.; Willför, S.; Viikari, L. (2011). *J. Mol. Catal. B: Enzym.*, 72: 122–129.
- [113] Fu, D.; Mazza, G.; Tamaki, Y. (2010). Lignin extraction from straw by ionic liquids and enzymatic hydrolysis of the cellulosic residues. *J. Agric. Food Chem.*, 58: 2915–2922.
- [114] Kim, J.; Shin, E.; Eom, I.; Won, K.; Kim, Y.H.; Choi, D.; Choi I.G.; Choi, J.W. (2011). Structural features of lignin macromolecules extracted with ionic liquid from poplar wood. *Bioresour. Technol.*, 102: 9020–9025.
- [115] Pischinger, S. (coordinator), (2009). Cluster of excellence, tailor-made fuels from biomass, (EXC 236), Yearly Report, www.fuelcenter.rwth-aachen.de
- [116] Leskinen, T.; King, A.W.T.; Kilpeläinen, I.; Argyropoulos, D.S. (2011). Fractionation of lignocellulosic materials with ionic liquids. 1. Effect of mechanical treatment, *Ind. Eng. Chem. Res.*, 50: 12349–12357.
- [117] Qiu, Z. (2012). The Use of Ionic Liquids for the Pretreatment of Energy Cane Bagasse, Master Thesis, Louisiana State University, USA.
- [118] Casas, A.; Oliet, M.; Alonso, M.; Rodriguez, F. (2012). Dissolution of *Pinus radiata* and *Eucalyptus globulus* woods in ionic liquids under microwave radiation: Lignin regeneration and characterization, *Separation & Purification Technology*, 97: 115–122, IL-SEPT2011 Special Issue.
- [119] King, A.W.T.; Zoia, L.; Filpponen, I.; Olszewska, A.; Xie, H.; Kilpeläinen, I.; Argyropoulos, D.S. (2009). In situ determination of lignin phenolics and wood solubility in imidazolium chlorides using ³¹P NMR, *J. Agric. Food Chem.*, 57: 8236–8243.
- [120] Kyllönen, L.; Parviainen, A.; Deb, S.; Lawoko, M.; Gorlov, M.; Kilpeläinen, I.; King, A.W.T. (2013). On the solubility of wood in ionic liquids, *Green Chem.*, 15: 2374–2378.

- [121] Xie, H.; Zhao, Z.K. (2011). Selective breakdown of lignocellulose in ionic liquids, Chap. 4, pp. 61–80, In: *Ionic Liquids: Applications and Perspectives*, A. Kokorin (ed.), InTech, Rijeka, Croatia.
- [122] Orlandi, M.; Luca, Z.; Salanti, A. (2013). Characterization of lignocellulosic materials during the biorefinery process of *Arundo donax* for “fine” chemicals production, COST FP0901: Analytical Techniques for Biorefineries, Turku Seminar, Åbo Akademi University, Finland.
- [123] Ahn, I.-S.; Yang, J.-H.; Kim, J.; Lee, S.; Mhin, B.J. (2013). Search for a new cellulose de-crystallization agent for the pretreatment of lignocellulosic biomasses, Int. Symp. & Annual meeting, IS4-3, p.191, *The Korean Society for Microbiology & Biotechnology*, www.korimb.or.kr
- [124] Wasserscheid, W.; Welton, T. (2008). *Ionic Liquids in Synthesis*, Wiley-VCH Verlag: Weinheim, Germany, ISBN-13 978-1-4020-4087-0 (e-book).
- [125] Abu-Eishah, S.I. (2011). Ionic liquids recycling for reuse. Chap. 11, pp. 239-272, In: *Ionic Liquids – Classes and Properties*. S.T. Handy (ed.), InTech, Rijeka, Croatia.
- [126] Peric, B.; Martí, E.; Sierra, J.; Cruañas, R.; Garau, M. A. (2012), Green chemistry: Eco-toxicity and biodegradability of ionic liquids, Chap. 6, pp. 89–113, In: *Recent Advances in Pharmaceutical Sciences II*, D. Muñoz-Torrero, D. Haro and J. Vallès (eds.), ISBN: 978-81-7895-569-8.

Ionic Liquid as Green Solvent for Ring-Opening Graft Polymerization of ϵ -Caprolactone onto Hemicelluloses

X.Q. Zhang, M.J. Chen, H.H. Wang, X.X. Wen,
C.F. Liu and R.C. Sun

Additional information is available at the end of the chapter

<http://dx.doi.org/10.5772/59679>

1. Introduction

The depletion of fossil fuels has led to rapidly increasing interest in the utilization of environmentally friendly, readily available, biodegradable, and renewable biomass to produce biofuels, biocomposites, biochemicals, and a host of other bioproducts [1-3]. Agricultural crop residues, such as cereal straws and sugarcane bagasse (SCB), are underutilized lignocellulosic biomass and have great potential for the production of biocompatible and biodegradable materials to replace fossil-based products [4,5].

Hemicelluloses, the second most abundant class of renewable and biodegradable polysaccharides found in nature after cellulose, account for on average about 20-35% of most plant materials [6,7]. Compared with cellulose and lignin, the exploiting of hemicelluloses was paid little attention until the last decades due to their inherent low molecular weight and heterogeneous structure. In their natural state, hemicelluloses are generally considered to be non-crystalline, with a DP of 80 to 200. They are heterogeneous polymers of pentose (xylose, arabinose), hexoses (mannose, glucose, and galactose), and sugar acids. Xylans are the most abundant hemicelluloses [8]. In many plant materials, xylans are heteropolysaccharides with homopolymeric backbone chains of 1,4-linked β -D-xylopyranose (Xylp) units [9]. In addition, there can be *O*-acetyl, α -L-arabinofuranosyl, α -1,2-linked glucuronic, or 4-*O*-methylglucuronic acid substituents on the backbone [10].

Chemical modification is an important way to impart biomass with desired properties for specific applications [11-13]. From the chemist point of view, a broad variety of chemical modification reactions both at OH groups and the C atoms are possible [14]. Ring-opening graft polymerization (ROGP) is a multifunctional modification technique for the synthesis of

polymers from cyclic monomers that can endow polymers with controlled molecular weights and molecular weight distributions [15-17]. Due to their excellent biodegradability, biocompatibility, and permeability, considerable attention has been paid to aliphatic polyesters from lactones and lactides, among which poly (ϵ -caprolactone) (PCL) is especially interesting for its applications [1,18,19]. It is a hydrophobic aliphatic polyester with excellent biocompatibility, low immunogenicity, nontoxicity, and good mechanical and thermoplastic properties, making it a potential matrix candidate in biocomposites [1,20,21]. Much consideration had been paid to graft copolymerization between cellulose derivatives and aliphatic polyesters [1,22,23]. In contrast to cellulose, there is a little information about the graft polymerization of biodegradable aliphatic polyesters onto hemicellulose. Moreover, reactions on hemicellulose are not easy, mainly because of the almost impossible proposition of dissolving hemicellulose in a suitable solvent without significant degradation.

In recent years, with the development of green chemistry and the requirement for environment protection, much attention has been focused on the utilization of ionic liquids as novel solvents and reaction media due to their eco-friendliness, negligible vapor pressure, non-flammability, chemical stability, good thermal stability, and high reaction rates [24]. In general, ionic liquids are screened with a range of anions, from small hydrogen-bond acceptors (Cl^-) to large noncoordinating anions, including Br^- , SCN^- , $[\text{PF}_6]^-$, and $[\text{BF}_4]^-$ [25]. They are capable of dissolving complex polymeric materials and macromolecules, such as carbohydrates. The ionic liquids can break the extensive hydrogen-bonding network in the polysaccharides and promote their dissolution [26]. Various polysaccharide derivatives have been prepared in ionic liquids from cellulose [27,28], hemicelluloses [11,26] and starch [29]. These results indicated that there are no derivatization reactions occur during the dissolution of polysaccharides in ionic liquids. They are satisfactorily homogeneous media [30], and can be desirable alternatives to conventional solvents and reaction media in modification.

The aim of the present research was to investigate homogeneous ROGP of ϵ -CL onto hemicelluloses using 1-butyl-3-methylimidazolium chloride ($[\text{C}_4\text{mim}]\text{Cl}$) ionic liquid as a homogeneous reaction medium with 4-dimethylaminopyridine (DMAP) as a catalyst to prepare hemicellulose-g-PCL copolymers. The physico-chemical properties of the graft copolymers were characterized by FT-IR, ^1H -NMR, ^1H - ^1H Correlation Spectroscopy (COSY), ^{13}C -NMR, ^1H - ^{13}C Correlation 2D NMR (HSQC), XRD, SEM and thermal analysis.

2. Experimental

2.1. Materials

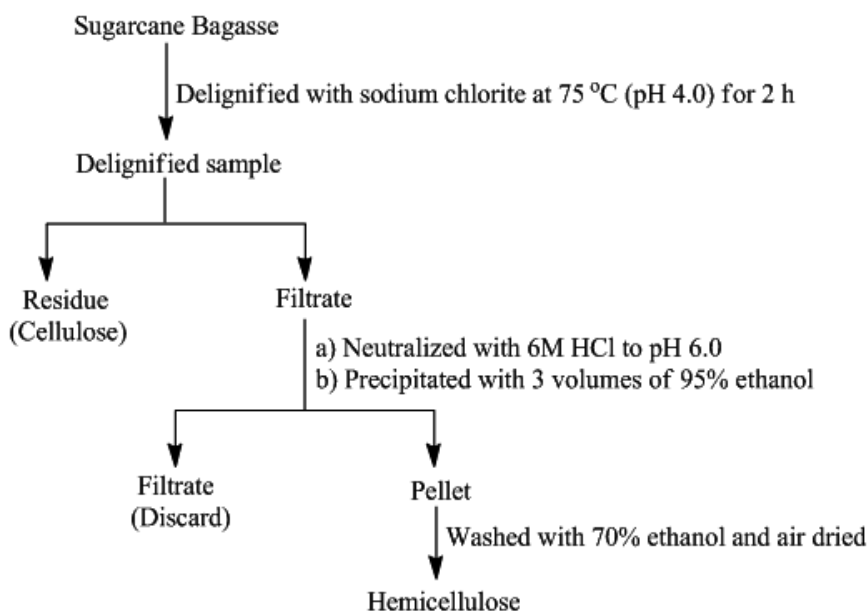
Sugarcane bagasse (SCB) was obtained from a local sugar factory (Guangzhou, China). It was dried in sunlight and then cut into small pieces. The cut SCB was ground to pass a 0.8-mm screen. It was dried in a cabinet oven with air circulation for 20 h at 50°C.

4-Dimethylaminopyridine (DMAP, 99%) and ϵ -caprolactone (ϵ -CL, 99%) were supplied by Aladdin Reagents Co., Ltd. (Shanghai, China). The ionic liquid 1-butyl-3-methylimidazolium

chloride ($[C_4mim]Cl$, 99%) was purchased from Cheng Jie Chemical Co., Ltd. (Shanghai, China), and dried in vacuum for 48 h at 70°C before used. All other chemicals were of analytical reagent grade and directly used without further purification.

2.2. Isolation and characterization of the native hemicellulose from SCB

Sugarcane bagasse was first delignified with sodium chlorite in acidic solution (pH 4.0, adjusted by 10% acetic acid) at 75 °C for 2 h. The hemicelluloses were then extracted from the holocellulose with 10% NaOH for 10 h at 20 °C with a liquor ratio of 1 to 20, followed by the acidification of the supernatant to pH 6.0 with 6M HCl and then the precipitation in 3 volumes of 95% ethanol. After filtration, the pellets of the hemicelluloses were washed with acidified 70% ethanol and then air dried. The main procedure of isolation hemicelluloses is shown in Scheme 1.



Scheme 1 Extraction of hemicelluloses from sugarcane bagasse

2.3. Synthesis of Hemicellulose-g-PCL copolymers in $[C_4mim]Cl$

Dry hemicelluloses (0.33 g, 0.005 mol of hydroxyl group in hemicelluloses) were added to $[C_4mim]Cl$ (7.5 g) in a 50-mL dried three-neck flask. The mixture was stirred at 85°C for 1 h under the protection of nitrogen to achieve a homogenous solution. Then, the required quantities of ϵ -CL and DMAP were added gradually over a period of 2 min into the solution. The ROGP reaction was carried out under the protection of nitrogen with vigorous stirring for 24 h. After the required time, the solution was cooled to room temperature and the resultant

graft copolymer was precipitated in excessive ethanol and dialyzed with a 3000-molecular weight dialysis bag in ultrapure water for 7 days. The final product was freeze-dried for 48 h. Each sample was duplicated under the same conditions to reduce errors and confirm the results.

2.4. Characterization of hemicelluloses and hemicellulose-g-PCL copolymers

FT-IR spectra of unmodified hemicelluloses and hemicelluloses-g-PCL copolymers were recorded on an FT-IR spectrophotometer (Tensor 27, Germany) from a KBr disc containing 1% (w/w) finely ground samples in the range of 4000 to 400 cm^{-1} . Thirty-two scans were taken for each sample, with a resolution of 2 cm^{-1} in the transmittance mode.

The $^1\text{H-NMR}$, $^1\text{H-}^1\text{H COSY}$, $^{13}\text{C-NMR}$, and $^1\text{H-}^{13}\text{C HSQC}$ spectra of unmodified hemicellulose and hemicellulose-g-PCL copolymers were recorded from 40 mg samples in 0.5 mL DMSO-d_6 on a Bruker Avance III 400 M spectrometer (Germany) with a 5 mm multinuclear probe. For the $^1\text{H-NMR}$ analysis, the detailed collecting and processing parameters were listed as follows: number of scans, 64; receiver gain, 456; acquisition time, 1.3631 s; relaxation delay, 3.0 s; pulse width, 3.0 s; spectrometer frequency, 400.13 MHz; and spectral width, 6009.6 Hz. For the $^1\text{H-}^1\text{H COSY}$ analysis, the detailed collecting and processing parameters were listed as follows: number of scans, 8; receiver gain, 447; acquisition time, 0.4588 s; relaxation delay, 2.0 s; pulse width, 9.0 s; spectrometer frequency, 400.13/400.13 MHz; and spectral width, 4000.0/4000.0 Hz. For the $^{13}\text{C-NMR}$ analysis, the detailed collecting and processing parameters were listed as follows: number of scans, 2112; receiver gain, 2048; acquisition time, 0.3296 s; relaxation delay, 5.0 s; pulse width, 9.8 s; spectrometer frequency, 100.61 MHz; and spectral width, 25062.7 Hz. For the $^1\text{H-}^{13}\text{C HSQC}$ analysis, the detailed collecting and processing parameters were listed as follows: number of scans, 28; receiver gain, 2050; acquisition time, 0.0639 s; relaxation delay, 2.0 s; pulse width, 8.5 s; spectrometer frequency, 400.13/100.61 MHz; and spectral width, 8012.8/20161.3 Hz. The detailed structure factors of hemicellulose-g-PCL copolymers, including the degree of polymerization of PLA (DP_{PLA}), the molar substitution of PLA (MS), the degree of substitution of PLA (DS), and the weight content of PLA side chains (W_{PLA}), were determined by $^1\text{H-NMR}$.

The thermal stability of the samples was performed using thermogravimetric analysis (TGA) and derivative thermogravimetry (DTG) on a Q500 thermogravimetric analyzer (TA, USA). Samples weighing between 9 and 11 mg were heated from room temperature to 600°C at a thermal ramp of 10°C/min under nitrogen flow.

The surface morphology was examined by SEM on a field emission microscopy (LEO 1530 VP, LEO, Germany). The samples were prepared by casting few solids onto a mica sheet followed by gold-plating.

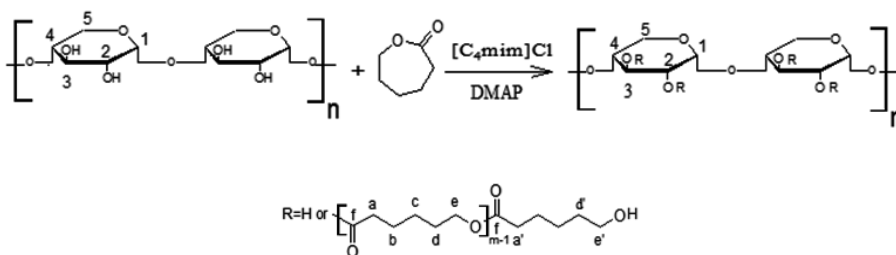
XRD was determined on a D/Max-III X-ray diffractometer (Rigaku, Japan) equipped with the high-intensity monochromatic nickel-filtered $\text{Cu K}_{\alpha 1}$ radiation ($\lambda=0.154$ nm). The operating voltage and current were 40 kV and 40 mA, respectively. Data were collected with diffraction angle 2θ ranging from 5 to 60° with a step size of 0.04° and time per step of 0.2 s at room temperature.

3. Results and discussion

3.1. Synthesis of hemicellulose-g-PCL copolymers in $[C_4mim]Cl$

DMAP and ϵ -CL could be easily dissolved in $[C_4mim]Cl$ within several minutes. Therefore, the homogeneous ROGP reaction of ϵ -CL onto hemicelluloses was performed with DMAP as a catalyst, and a schematic reaction is shown in scheme 2. The effects of reaction conditions, including reaction temperature, the molar ratios of ϵ -CL to anhydroxylose units (AXU) in hemicelluloses, and the dosage of DMAP catalyst on the detailed structure factors, were investigated. Table 1 shows the preparation conditions of hemicellulose-g-PCL copolymers and their detailed structural factors calculated from 1H -NMR.

According to the results in Table 1, an increase in reaction temperature from 110 °C to 120 °C resulted in an increase in DS from 0.03 to 0.09, DP from 1.39 to 1.45, MS from 0.04 to 0.13 and W_{PCL} from 3.33% to 10.09%, which was probably due to the favorable effect of temperature on the molecule motion and collision with the increased temperature. However, further improvement of reaction temperature from 120 °C to 130 °C led to a decrease in DS from 0.09 to 0.06, DP from 1.45 to 1.26, MS from 0.13 to 0.07 and W_{PCL} from 10.09% to 5.71%, probably due to the increased degradation of hemicelluloses in ionic liquid at a higher temperature under the given conditions. The DS, DP, MS and W_{PCL} of the products remarkably increased from 0.09 to 0.22, 1.45 to 1.48, 0.13 to 0.32 and 10.09% to 21.65%, respectively, with an increase in the dosage of DMAP catalyst from 2% to 3%, indicating the good catalytic ability of DMAP for ROGP of ϵ -CL onto hemicelluloses in $[C_4mim]Cl$; while it significantly decreased with a further increase in DMAP dosage to 4%, indicating the detrimental effects of excessive DMAP, which was probably due to the fact that the strong basicity of DMAP inhibited the attachment of PCL onto hemicelluloses. Increasing the molar ratio of ϵ -CL to AXU in hemicelluloses from 1:1 to 3:1 resulted in an improvement of DS from 0.04 to 0.22, DP from 0.93 to 1.48, MS from 0.04 to 0.32 and W_{PCL} from 3.34% to 21.65%, which was probably due to the greater availability of ϵ -CL in the proximity of the reactive hydrogel groups in hemicelluloses at a higher molar ratio of ϵ -CL to AXU. However, a further increase in the molar ratio of ϵ -CL to AXU from 3:1 to 5:1 led to decrease in DS, DP, MS and W_{PCL} , which was probably due to the quick self-polymerization of ϵ -CL.



Scheme 2. The ring opening graft copolymerization of ϵ -CL onto hemicelluloses in $[C_4mim]Cl$ with DMAP as a catalyst

Sample No.	Temp (°C)	Catalyst (wt%)	ϵ -CL/AXU	Time (h)	DP _{PCL} ^a	MS ^b	DS ^c	W ^d _{PCL}
1	110	2%	3:1	24	1.39	0.04	0.03	3.33%
2	120	2%	3:1	24	1.45	0.13	0.09	10.09%
3	130	2%	3:1	24	1.26	0.07	0.06	5.71%
4	120	3%	3:1	24	1.48	0.32	0.22	21.65%
5	120	4%	3:1	24	1.39	0.03	0.02	2.52%
6	120	3%	1:1	24	0.93	0.04	0.04	3.34%
7	120	3%	2:1	24	1.26	0.07	0.06	5.70%
8	120	3%	4:1	24	1.38	0.21	0.13	13.45%
9	120	3%	5:1	24	1.29	0.11	0.08	8.68%

^a The degree of polymerization of PCL, calculated by ¹H-NMR.

^b Molar composition in the graft copolymer, calculated by ¹H-NMR.

^c The degree of substitution of the copolymer, calculated by ¹H-NMR.

^d The PCL content, calculated by ¹H-NMR.

Table 1. Properties of hemicellulose-g-PCL copolymers under various conditions in [C₄mim]Cl.

3.2. FT-IR spectra

The FT-IR spectra of the isolated hemicelluloses and hemicellulose-g-PCL copolymer samples 2 and 4 are shown in Figure 1. The sharp peak at 893 cm⁻¹ is indicative of typical β -anomers, indicating the primary β -glycosidic linkages between the sugar units in the hemicellulosic fractions [26]. The strong absorption band at 1045 cm⁻¹ is largely due to the C-O stretching in the C-O-C linkages [26]. The small band at 1252 cm⁻¹ originates from the C-O antisymmetric stretching in ester. The band at 1382 cm⁻¹ corresponds to the C-H bending, and that at 1638 cm⁻¹ originates from the bending mode of the absorbed water. The peak at 1736 cm⁻¹ is the characteristic absorption of C=O stretching. The characteristic absorbance at 3431 cm⁻¹ is assigned to the hydroxyl group stretching vibrations, and that at 2910 cm⁻¹ is attributed to the C-H stretching vibrations. In the FT-IR spectra of hemicellulose-g-PCL copolymers, the increased intensities of the bands at 2910, 1738, 1252, and 1170 cm⁻¹, from C-H stretching, C=O stretching, C-O antisymmetric stretching, and C-O-C vibration, respectively, were observed compared with those in unmodified hemicelluloses, indicating the successful modification of hemicelluloses in [C₄mim]Cl under the given conditions.

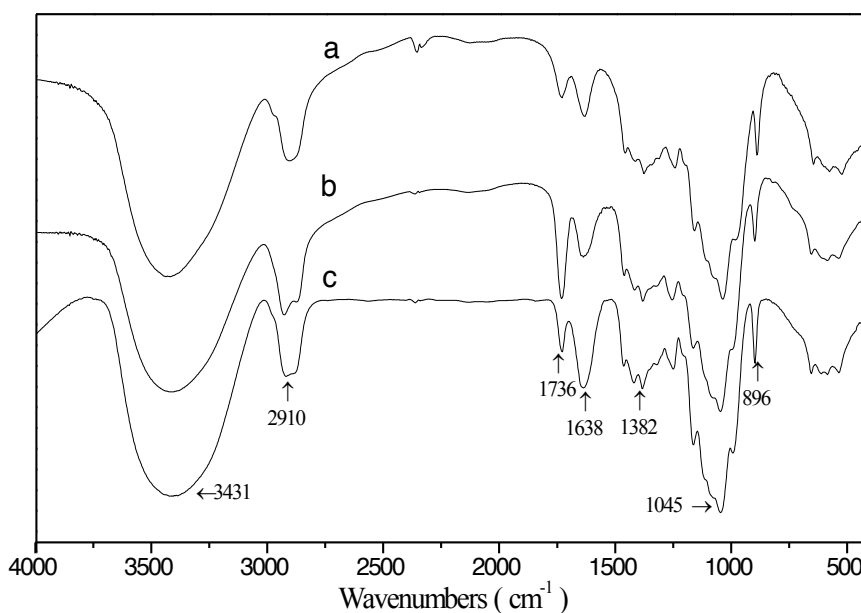


Figure 1. FT-IR spectra of unmodified hemicelluloses (spectrum a) and hemicellulose-g-PCL copolymer samples 2 (spectrum b) and 4 (spectrum c) prepared in $[C_4mim]Cl$

3.3. 1H -NMR, 1H - 1H COSY, ^{13}C -NMR and 1H - ^{13}C HSQC spectra

Figure 2 shows the 1H -NMR spectrum of hemicellulose-g-PCL copolymer sample 2. The resonance peaks derived from the protons of xylan appear at 4.26, 3.03, 3.25, 3.49, 3.17 and 3.78 ppm, assigned to H-1, H-2, H-3, H-4, H-5a and H-5e, respectively[31]. The signals from the methylene proton in PCL appeared at 2.25 ppm (-COCH₂-, a), 1.53 ppm (-CH₂-, b, d), 1.30 ppm (-CH₂-, c), 1.41 ppm (-CH₂-, d'), 3.87 ppm (-CH₂O-, e), 3.38 ppm (-CH₂O-, e') and 4.39 ppm (-CH₂OH-, e', end unit) [17]. These observations confirmed the attachment of PCL onto hemicelluloses in ionic liquid $[C_4mim]Cl$. In addition, the signals at 4.53 and 4.87 ppm are associated with the protons at substituted C-2 and C-3 positions, respectively, confirming the attachment of PCL on C-2 and C-3 positions in AXU. Meanwhile, the detailed structural factors of hemicellulose-g-PCL copolymers, including DS, MS, DP_{PCL} , and W_{PCL} , could be calculated from the peak intensity of corresponding signals based on the following equations:

$$DS = \frac{CL_{Terminal}}{AXU} = \frac{I_e / 2}{I_{H4}} = \frac{(I_a - I_e)}{I_{H4}} \quad (1)$$

$$MS = \frac{CL}{AXU} = \frac{I_a}{2I_{H4}} \quad (2)$$

$$DP = \frac{CL_{Total}}{CL_{Terminal}} = \frac{I_{(e+e')}}{I_{e'}} = \frac{I_a}{I_a - I_e} \quad (3)$$

$$W_{PCL} = \frac{114 MS}{132 + 114 MS} \times 100\% \quad (4)$$

where DS is the degree of substitution of PCL, DP is the degree of polymerization of PCL, MS is the molar substitution of PCL, W_{PCL} is the weight content of PCL side chains, AXU is anhydroxylose unit, $CL_{Terminal}$ is the end unit of PCL, CL_{Total} is the total units of PCL, 2 is two protons in each methylene group, I_e , $I_{e'}$ and I_a are the integral area of the resonances of the corresponding methylene protons at e, e', and a positions of PCL, and I_{H4} is the integral area of the resonance assigned to H_4 of AXU. The 114 g mol⁻¹ and 132 g mol⁻¹ in equation (4) are the molecular weight of ϵ -caprolactone and the molecular weight of xylan unit, respectively.

The DS, MS, DP_{PLA} and W_{PLA} values calculated from ¹H-NMR are listed in Table 1. The results indicated that the xylan derivatives with DS 0.02–0.22, DP 0.93–1.48, MS 0.03–0.32 and W_{PCL} 2.52–21.65% were obtained under the selected conditions, lower than those of cellulose-g-PCL prepared in [Bmim]Cl [18]. Considering the linear macromolecular structure of cellulose with more hydroxyl groups available, which allowed for more side chains attached on the biopolymer, the estimated DS, MS, DP_{PLA} and W_{PLA} values of hemicellulose-g-PCL copolymers in the present study were reasonable and acceptable. In addition, the different calculation equation based on the different assignments of the typical proton signals [18] was also responsible for the differences of DS, MS, DP_{PLA} and W_{PLA} of the copolymers in ionic liquids.

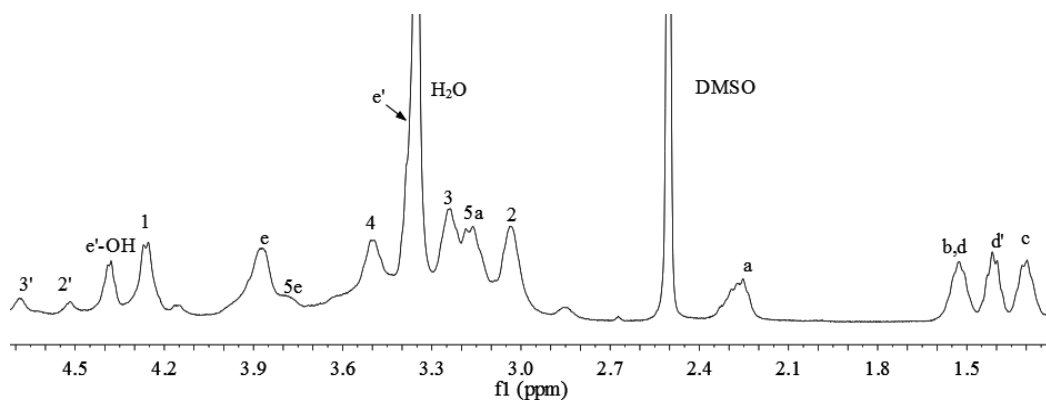


Figure 2. ¹H-NMR spectrum of hemicellulose-g-PCL copolymer sample 2

To confirm the correct assignment of the primary proton signals of the attached PCL side chains, Figure 3 shows the ¹H-¹H COSY spectrum of hemicellulose-g-PCL copolymer sample 2. To clearly show the cross-correlations of the protons on the attached PCL side chains, the

spectrum is illustrated at higher contour level and as a result the primary signals in AXU and their cross-correlations are not shown. The cross-correlations of PCL side chains, a/b, b/c, c/d', d'/e', e'/e'-OH, were clearly observed, indicating the assignment of the proton signals was correct. Moreover, the cross-correlations for repeating unit indicated the DP of xylan-g-PCL copolymers was over 1, which was corresponded to the results in Table 1.

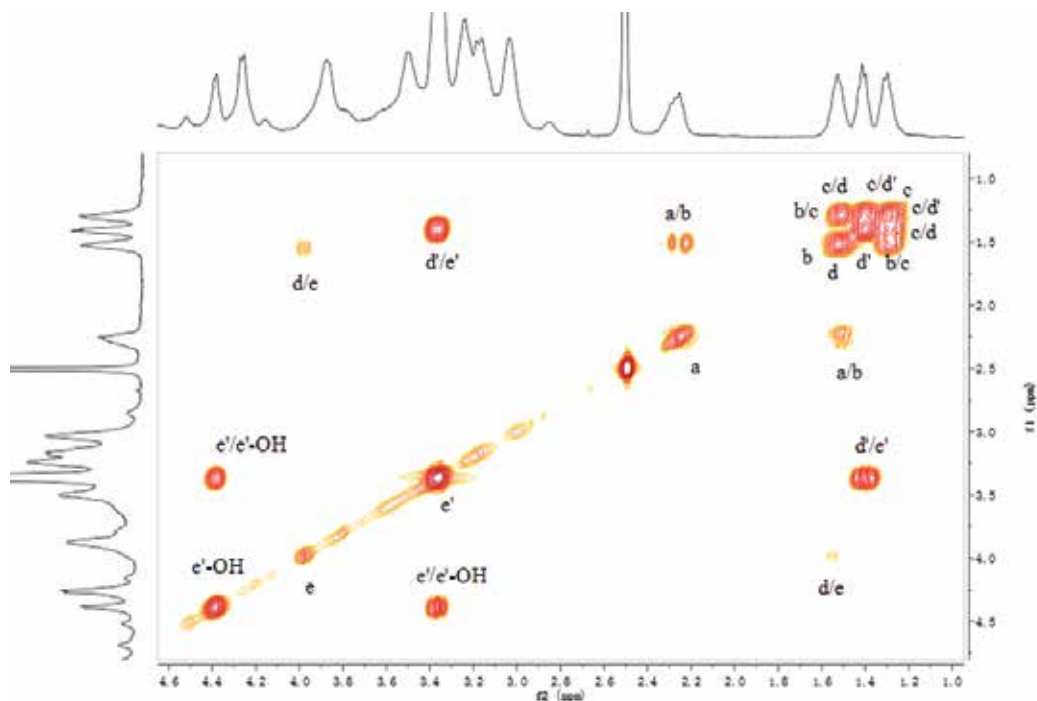


Figure 3. ^1H - ^1H COSY spectrum of hemicellulose-g-PCL copolymer sample 2

Figure 4 illustrates the ^{13}C -NMR spectra of unmodified hemicelluloses (A) and hemicellulose-g-PCL copolymer sample 2 (B). In Figure 4A, the five major signals at 101.8, 75.6, 74.4, 73.4, and 63.5 ppm correspond to C-1, C-4, C-2, C-3, and C-5 of the 1,4-linked β -D-Xylp (xylopyranose) units, respectively [32]. The signals at 97.6, 71.6, 69.9, 82.4, 171.7, and 59.1 ppm can be assigned to C-1, C-3, C-2, C-4, C-6, and the methoxy group of the 4-O-methyl-D-glucuronic acid residue is linked to C-3 of the backbone of the β -D-Xylp units[30]. These results indicated that the native hemicelluloses were composed of 4-O-methyl-D-glucuronic acid-D-xylans. In Figure 4B, the signal at 171.8 ppm is attributed to the carbonyl carbon (in position f) in the PCL segment, and those at 33.5, 24.7, 25.1, 32.1, 32.1, 63.2 and 60.4 ppm correspond to the methylene carbon signals of PCL in the a, b, d, d', e, and e' positions, respectively. The main signals of the β -D-Xylp units are all observed, indicating no significant structural changes in the hemicellulosic backbone. Compared with spectrum A, the relative intensity of the signal of C-3 in the β -D-Xylp units slightly decreased in spectrum B, suggesting that a partial substitution occurred at the C-3 hydroxyl group.

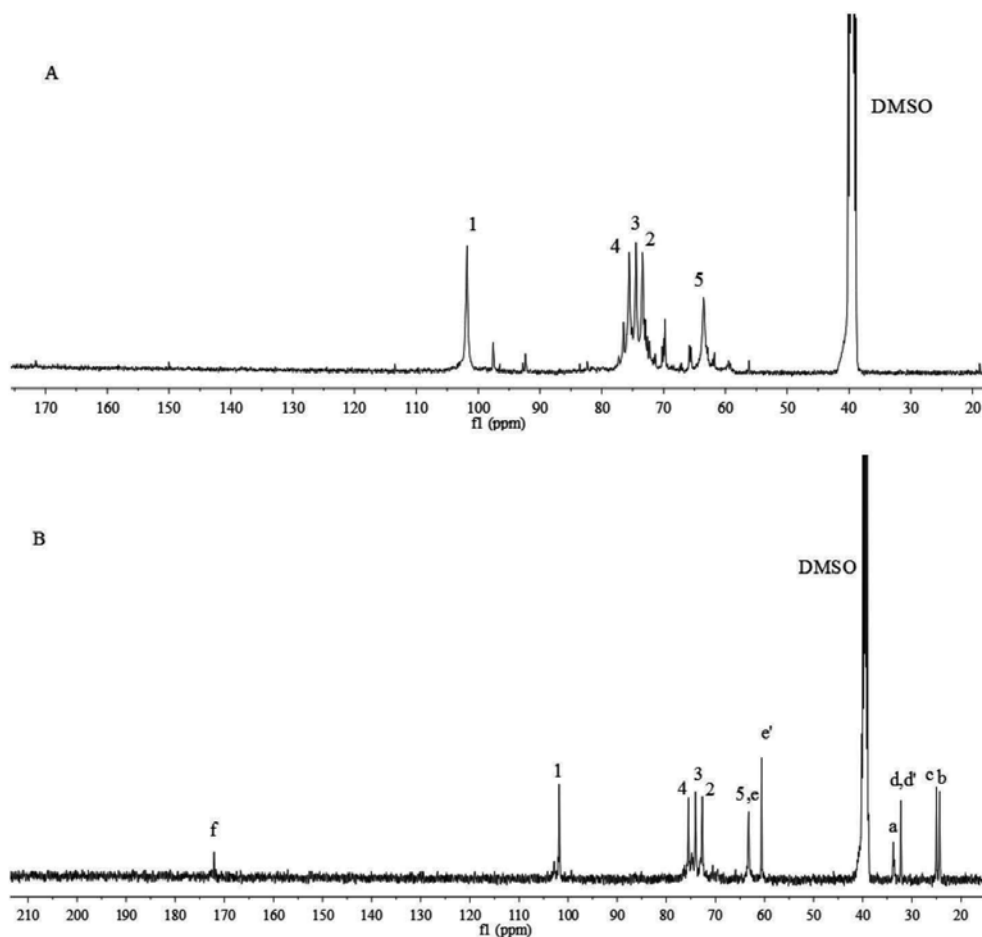


Figure 4. ^{13}C -NMR spectra of unmodified hemicelluloses (A) and hemicellulose-g-PCL copolymer sample 2 (B)

^1H - ^{13}C HSQC provides detailed information of signals overlapped in ^1H - and ^{13}C -NMR spectra, and could be applied for qualitative and quantitative analysis of chemical structure. HSQC spectrum of sample 2 was illustrated in Figure 5. To exhibit the primary correlations both unsubstituted and substituted, the spectrum is illustrated at a relatively low contour level. The strong correlations at $\delta_{\text{C}}/\delta_{\text{H}}$ 33.2/2.26, 24.2/1.52, 24.8/1.30, 31.9/1.38, 32.9/1.52, 60.8/3.39 and 62.7/3.88 ppm are associated with $\text{C}_a\text{-H}_a$, $\text{C}_b\text{-H}_b$, $\text{C}_c\text{-H}_c$, $\text{C}_d\text{-H}_d$, $\text{C}_d\text{-H}_d$, $\text{C}_e\text{-H}_e$ and $\text{C}_e\text{-H}_e$, respectively, indicated that the PCL side chains were successfully attached onto xylan. Clearly, the strong correlations in carbohydrate region at $\delta_{\text{C}}/\delta_{\text{H}}$ 102.4/4.24, 72.9/3.02, 73.8/3.23, 75.7/3.49, 63.6/3.79, and 63.6/3.14 ppm are attributed to $\text{C}_1\text{-H}_1$, $\text{C}_2\text{-H}_2$, $\text{C}_3\text{-H}_3$, $\text{C}_4\text{-H}_4$, $\text{C}_{5e}\text{-H}_{5e}$ and $\text{C}_{5a}\text{-H}_{5a}$ in AXU of xylan, respectively. More importantly, the correlations at $\delta_{\text{C}}/\delta_{\text{H}}$ 72.7/4.51 and 75.1/4.81 for substituted $\text{C}_2\text{-H}_2$ ($2'$) and substituted $\text{C}_3\text{-H}_3$ ($3'$), respectively, provided the possible quantitative estimation of ROGP reaction occurred at C_2 and C_3 positions. Clearly, more PCL side chains were attached to C_3 position than to C_2 position. The integrated resonances for

substituted and unsubstituted C_2/H_2 and C_3/H_3 indicated that 16.34% and 83.66% of PCL side chains were attached to C_2 and C_3 positions of AXU, respectively.

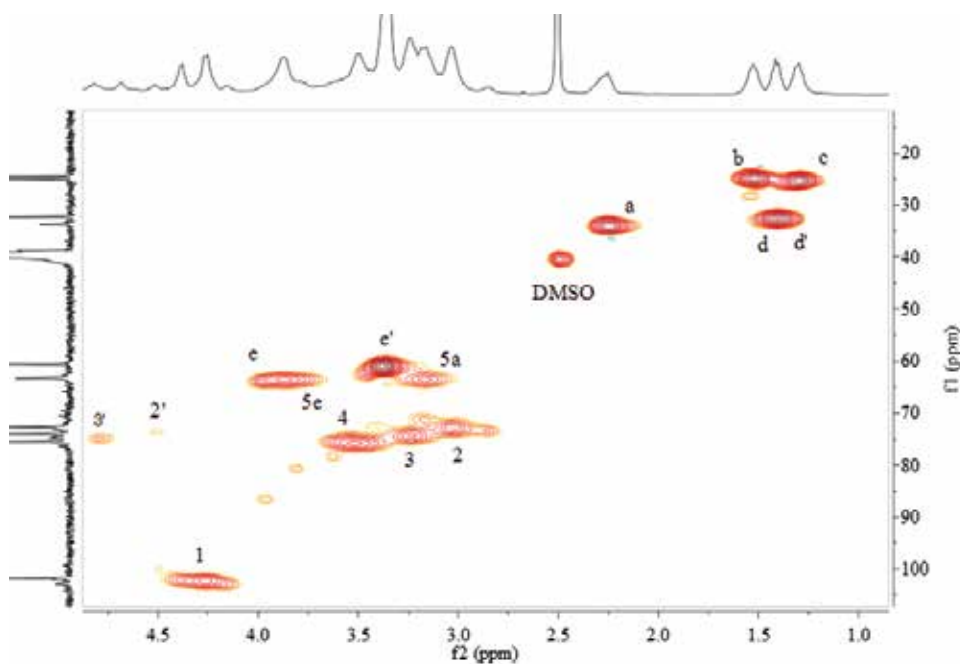


Figure 5. HSQC spectrum of hemicellulose-g-PCL copolymer sample 2

3.4. Thermal analysis

The thermal properties of unmodified hemicelluloses and hemicellulose-g-PCL copolymers were studied using TGA (Figure 6A) in the temperature range from 50°C to 600°C under a nitrogen atmosphere. Clearly, the thermal decomposition can be divided into three distinct stages. In the first stage, the weight loss observed below 100°C was the result of evaporation of moisture. At the second stage, the unmodified hemicelluloses began to decompose at about 215°C, while hemicellulose-g-PCL copolymer samples 2 and 4 started to decompose at about 200°C. The decomposition temperature for a 50% weight loss occurred at 280°C for unmodified hemicelluloses, 275°C for hemicellulose-g-PCL copolymer sample 2, and 270°C for sample 4. In the third stage, the weight marginally decreased after 300°C for unmodified hemicelluloses, after 320°C for sample 2, and after 350°C for sample 4. These results indicated that the thermal stability of hemicellulose-g-PCL copolymers decreased after grafting in ionic liquid compared with that of unmodified hemicelluloses. In addition, complete thermal decomposition of hemicellulose-g-PCL copolymers required either a higher temperature or a longer time.

To further explore the thermal degradation process, derivatives of TGA for the unmodified hemicelluloses and the hemicellulose-g-PCL copolymers were studied, as shown in Figure 6B.

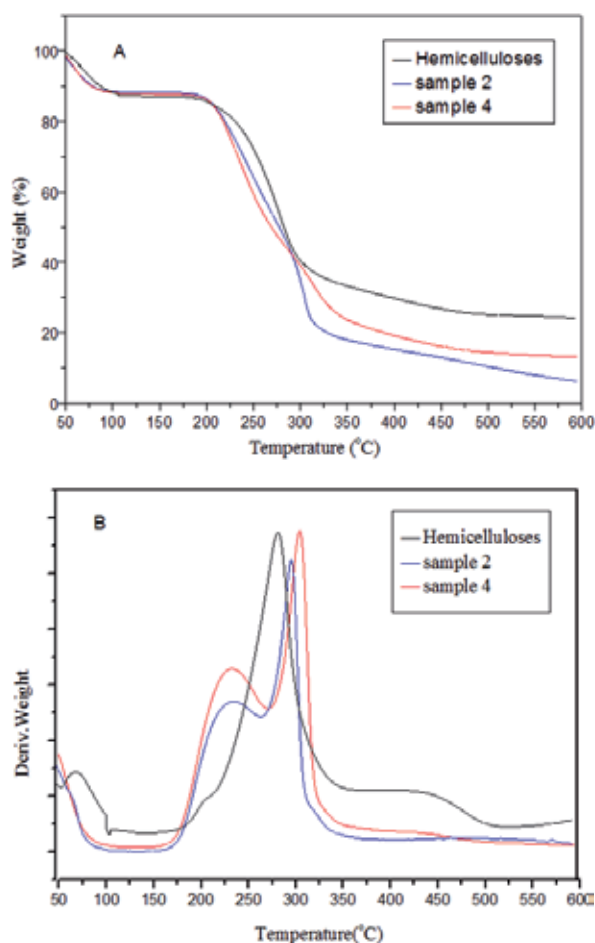


Figure 6. TGA (A) and DTG (B) curves of unmodified hemicelluloses and hemicellulose-g-PCL copolymer samples 2 and 4

DTG_{max} represents the maximum degradation rate and can be used to compare the thermal stability between the samples [33]. Unmodified hemicelluloses showed the maximum degradation rate at about 278°C, while hemicellulose-g-PCL copolymer sample 2 showed two degradation peaks, at 231°C and 293°C. In general, it is impossible to avoid the degradation of biopolymers during dissolution and derivatization in ionic liquids [24,34]. The former DTG_{max} was due to the decomposition of hemicelluloses, providing the evidence of degradation of the hemicellulose substance in ionic liquids. Sample 4 exhibited a similar thermal stability to that of hemicelluloses, with a DTG_{max} at 231 °C, indicating the similar degradation of hemicelluloses in $[C_4mim]Cl$ under the given conditions. These results indicated that the thermal stability of hemicellulose-g-PCL copolymers decreased after grafting in ionic liquid compared with that of unmodified hemicelluloses. The latter DTG_{max} was due to the decomposition of PCL side chains. Compared with sample 2, the second DTG_{max} of sample 4 with

increased attachment of PCL increased to 304°C, indicating improved thermal stability with the enhanced PCL attachment. The higher thermal stability of the attached PCL compared to that of hemicelluloses was confirmed. A similar improved thermal stability of glucuronoxylan from aspen wood was also reported after acetylation [35].

3.5. SEM

To investigate how chemical modification affects the morphology of hemicelluloses, a series of SEM observation of native hemicelluloses and hemicelluloses-g-PCL copolymers are illustrated in Figure 7. The changes of the morphology of the native and modified hemicelluloses were clearly observed with different reaction conditions. The unmodified hemicelluloses showed fluffy block structure, with a smooth and dense surface, and porous structure was clearly observed for the native and modified hemicelluloses. Compared with native hemicelluloses, the all hemicelluloses-g-PCL copolymers displayed more smaller and ruleless lamellar structure when grafting PCL onto it.

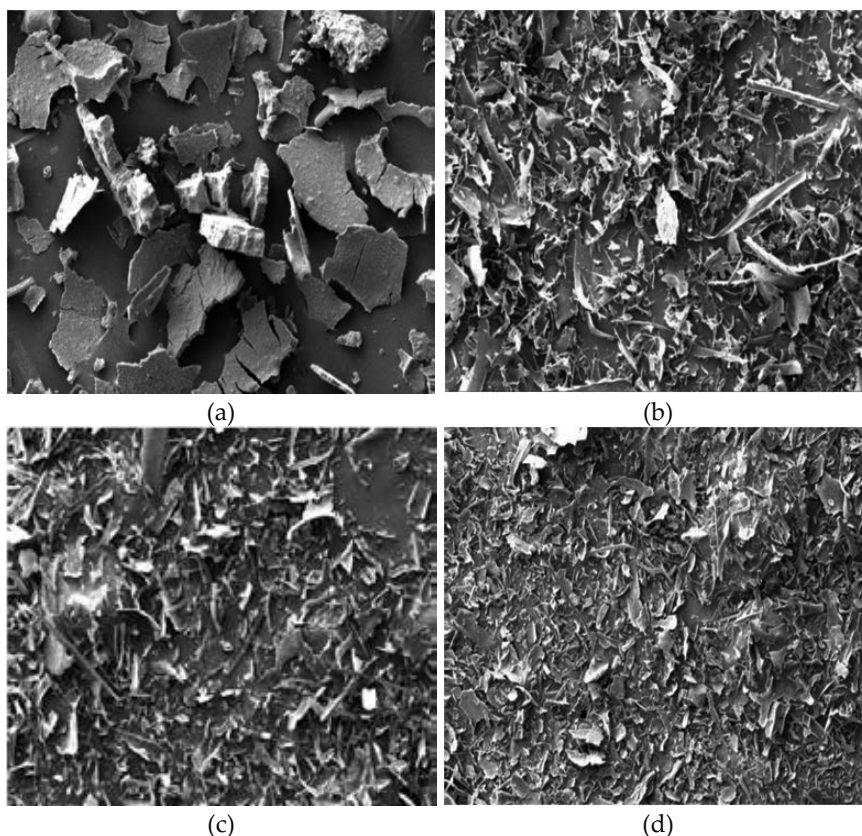


Figure 7. Scanning electron micrographs of the surface of unmodified hemicelluloses (a) and hemicelluloses-g-PCL copolymer samples 2 (b), 4 (c) and 8 (d)

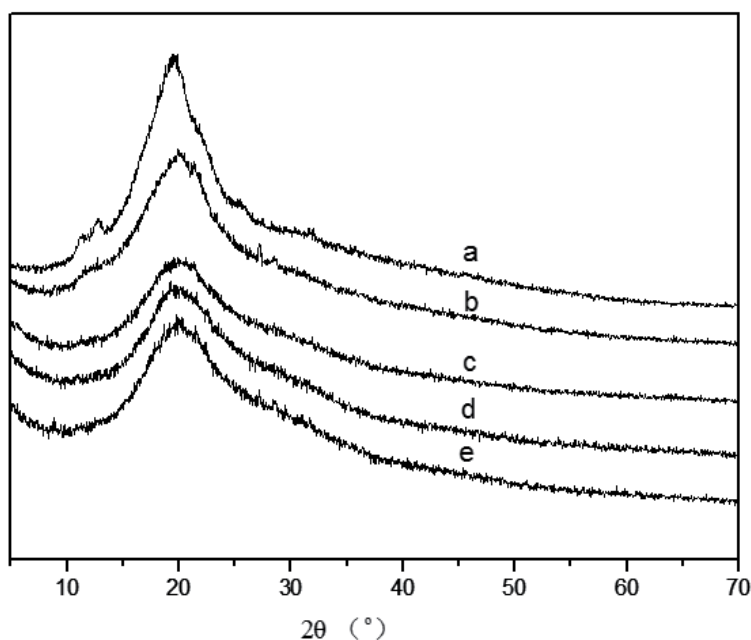


Figure 8. X-ray diffraction patterns of unmodified hemicelluloses (a) and hemicelluloses-g-PCL copolymers samples 2 (b), 4 (c), 8 (d) and 9 (e)

3.6. XRD

The crystal structure of hemicelluloses and hemicelluloses-g-PCL copolymers were studied using X-ray diffraction analysis and the X-ray diffraction patterns are shown in Figure 8. In spectrum a of native hemicelluloses, there are two small significant diffraction peaks at 2θ 11.2° and 12.4° , and a strong peak at 19.1° . The strong diffraction peak are shifted in the spectra of hemicelluloses-g-PCL samples 2, 4, 8, and 9 to 20.2° (b), 20.9° (c), 20.4° (d) and 19.8° (e), respectively, and the intensity of diffraction patterns decreased. The small peaks at 11.2° and 12.4° could not be observed in the diffraction patterns of hemicelluloses-g-PCL copolymers. These changes suggested that the original crystalline structure of hemicelluloses was disrupted by modification under homogeneous conditions in ionic liquid.

4. Conclusions

Homogeneous ring opening graft polymerization (ROGP) of ϵ -caprolactone (ϵ -CL) onto hemicelluloses was achieved using 4-dimethylaminopyridine (DMAP) as a catalyst in 1-butyl-3-methylimidazolium chloride ($[C_4mim]Cl$) ionic liquid. The detailed structural factors determined from 1H -NMR indicated that the optimized synthesis of hemicellulose-g-PCL copolymers with a PCL content of 21.65% was performed at $120^\circ C$ for 24 h with the molar ratio of ϵ -CL to AXU 3:1 and 3% DMAP. The results from FT-IR, 1H -NMR, ^{13}C -NMR, COSY and

HSQC analyses confirmed the attachment of PCL to hemicelluloses. TGA/DTG suggested the decreased thermal stability of hemicelluloses after ROGP in $[\text{C}_4\text{mim}]\text{Cl}$ and confirmed the higher thermal stability of the attached PCL than that of hemicelluloses. Considering the good biodegradability of hemicellulose and PCL, this kind of hemicellulose-g-PCL copolymers could be used as environmentally friendly materials.

Acknowledgements

This work was financially supported by the National Natural Science Foundation of China (31170550), Program for New Century Excellent Talents in University (NCET-11-0154), the Fundamental Research Funds for the Central Universities, and the National Program for Support of Top-notch Young Professionals.

Author details

X.Q. Zhang¹, M.J. Chen¹, H.H. Wang¹, X.X. Wen¹, C.F. Liu^{1*} and R.C. Sun^{1,2}

*Address all correspondence to: chfliu@scut.edu.cn

1 State Key Laboratory of Pulp and Paper Engineering, South China University of Technology, Guangzhou, P. R. China

2 Beijing Key Laboratory of Lignocellulosic Chemistry, Beijing Forestry University, Beijing, P. R. China

References

- [1] Lönnberg H, Zhou Q, Brumer H, Teeri TT, Malmström E, Hult A. Grafting of cellulose fibers with poly(ϵ -caprolactone) and poly(L-lactic acid) via ring-opening polymerization. *Biomacromolecules* 2006;7(7): 2178-2185.
- [2] Roy D, Semsarilar M, Guthrie JT, Perrier S. Cellulose modification by polymer grafting: A review. *Chemical Society Reviews* 2009;38(7): 2046-64.
- [3] Tosh B, Routray CR. Grafting of cellulose based materials: A review. *Chemical Science Review and Letters* 2014;10.
- [4] Söderqvist Lindblad M, Albertsson A-C, Ranucci E, Laus M, Giani E. Biodegradable polymers from renewable sources: Rheological characterization of hemicellulose-based hydrogels. *Biomacromolecules* 2005;6(2): 684-690.

- [5] Yang JY, Zhou XS, Fang J. Synthesis and characterization of temperature sensitive hemicellulose-based hydrogels. *Carbohydrate Polymers* 2011;86(3): 1113-1117.
- [6] Hansen NML, Plackett D. Sustainable films and coatings from hemicelluloses: A review. *Biomacromolecules* 2008;9(6): 1493-1505.
- [7] Puls J, Schröder N, Stein A, Janzon R, Saake B. Xylans from oat spelts and birch kraft pulp. *Macromolecular Symposia* 2005;232(1): 85-92.
- [8] Sarossy Z, Plackett D, Egsgaard H. Carbohydrate analysis of hemicelluloses by gas chromatography-mass spectrometry of acetylated methyl glycosides. *Analytical and Bioanalytical Chemistry* 2012;403(7): 1923-1930.
- [9] Edlund U, Albertsson AC. A microspheric system: Hemicellulose-based hydrogels. *Journal of Bioactive and Compatible Polymers* 2008;23(2): 171-186.
- [10] Saha B. Hemicellulose bioconversion. *Journal of Industrial Microbiology and Biotechnology* 2003;30(5): 279-291.
- [11] Peng XW, Ren JL, Zhong LX, Sun RC. Homogeneous synthesis of hemicellulosic succinates with high degree of substitution in ionic liquid. *Carbohydrate Polymers* 2011;86(4): 1768-1774.
- [12] Chung YL, Olsson JV, Li RJ, Frank CW, Waymouth RM, Billington SL, Sattely ES. A renewable lignin-lactide copolymer and application in biobased composites. *ACS Sustainable Chemistry & Engineering* 2013;1(10): 1231-1238.
- [13] Chen CY, Chen MJ, Zhang XQ, Liu CF, Sun RC. Per-o-acetylation of cellulose in dimethyl sulfoxide with catalyzed transesterification. *Journal of Agricultural and Food Chemistry* 2014;62(15): 3446-3452.
- [14] Barthel S, Heinze T. Acylation and carbanilation of cellulose in ionic liquids. *Green Chemistry* 2006;8(3): 301-306.
- [15] Carlmark A, Larsson E, Malmström E. Grafting of cellulose by ring-opening polymerisation – a review. *European Polymer Journal* 2012;48(10): 1646-1659.
- [16] Endo T, Shibasaki Y, Sanda F. Controlled ring-opening polymerization of cyclic carbonates and lactones by an activated monomer mechanism. *Journal of Polymer Science Part A: Polymer Chemistry* 2002;40(13): 2190-2198.
- [17] Xu Q, Kennedy JF, Liu L. An ionic liquid as reaction media in the ring opening graft polymerization of ϵ -caprolactone onto starch granules. *Carbohydrate Polymers* 2008;72(1): 113-121.
- [18] Guo YZ, Wang XH, Shen ZG, Shu XC, Sun RC. Preparation of cellulose-graft-poly(ϵ -caprolactone) nanomicelles by homogeneous rop in ionic liquid. *Carbohydrate Polymers* 2013;92(1): 77-83.

- [19] Yuan W, Yuan J, Zhang F, Xie X. Syntheses, characterization, and in vitro degradation of ethyl cellulose-graft-poly(ϵ -caprolactone)-block-poly(L-lactide) copolymers by sequential ring-opening polymerization. *Biomacromolecules* 2007;8: 1101-1108.
- [20] Habibi Y, Dufresne A. Highly filled bionanocomposites from functionalized polysaccharide nanocrystals. *Biomacromolecules* 2008;9(7): 1974-1980.
- [21] Kim MS, Hyun H, Seo KS, Cho YH, Won Lee J, Rae Lee C, Khang G, Lee HB. Preparation and characterization of mpeg-pcl diblock copolymers with thermo-responsive sol-gel-sol phase transition. *Journal of Polymer Science Part A: Polymer Chemistry* 2006;44(18): 5413-5423.
- [22] Youssef Habibi ALG, Nancy Schiltz, Emmanuel Duquesne, Philippe Dubois. Bionanocomposites based on poly(3-caprolactone)-grafted cellulose nanocrystals by ring-opening polymerization. *Journal of Materials Chemistry* 2008;18: 9.
- [23] Krouit M, Bras J, Belgacem MN. Cellulose surface grafting with polycaprolactone by heterogeneous click-chemistry. *European Polymer Journal* 2008;44(12): 4074-4081.
- [24] El Seoud OA, Koschella A, Fidale LC, Dorn S, Heinze T. Applications of ionic liquids in carbohydrate chemistry: A window of opportunities. *Biomacromolecules* 2007;8(9): 2629-2647.
- [25] Swatloski RP, Spear SK, Holbrey JD, Rogers RD. Dissolution of cellulose with ionic liquids. *Journal of the American Chemical Society* 2002;124(18): 4974-4975.
- [26] Ayoub A, Venditti RA, Pawlak JJ, Sadeghifar H, Salam A. Development of an acetylation reaction of switchgrass hemicellulose in ionic liquid without catalyst. *Industrial Crops and Products* 2013;44(0): 306-314.
- [27] Li WY, Wu L, Chen D, Liu CF, Sun RC. Dmap-catalyzed phthalylation of cellulose with phthalic anhydride in bmimcl. *BioResources* 2011;6(3): 2375-2385.
- [28] Liu CF, Zhang AP, Li WY, Yue FX, Sun RC. Homogeneous modification of cellulose in ionic liquid with succinic anhydride using n-bromosuccinimide as a catalyst. *Journal of Agricultural and Food Chemistry* 2009;57(5): 1814-1820.
- [29] Biswas A, Shogren RL, Stevenson DG, Willett JL, Bhowmik PK. Ionic liquids as solvents for biopolymers: Acylation of starch and zein protein. *Carbohydrate Polymers* 2006;66(4): 546-550.
- [30] Wang HT, Yuan TQ, Meng LJ, She D, Geng ZC, Sun RC. Structural and thermal characterization of lauroylated hemicelluloses synthesized in an ionic liquid. *Polymer Degradation and Stability* 2012;97(11): 2323-2330.
- [31] Cao XF, Sun SN, Peng XW, Zhong LX, Sun RC. Synthesis and characterization of cyanoethyl hemicelluloses and their hydrated products. *Cellulose* 2013;20(1): 291-301.

- [32] Xu F, Sun JX, Liu CF, Sun RC. Comparative study of alkali-and acidic organic solvent-soluble hemicellulosic polysaccharides from sugarcane bagasse. *Carbohydrate Research* 2006;341(2): 253-261.
- [33] Nadji H, Diouf PN, Benaboura A, Bedard Y, Riedl B, Stevanovic T. Comparative study of lignins isolated from alfa grass (*stipa tenacissima* l.). *Bioresource Technology* 2009;100(14): 3585-3592.
- [34] Ren JL, Sun RC, Liu CF, Lin L, He BH. Synthesis and characterization of novel cationic scb hemicelluloses with a low degree of substitution. *Carbohydrate Polymers* 2007;67(3): 347-357.
- [35] Grondahl M, Teleman A, Gatenholm P. Effect of acetylation on the material properties of glucuronoxylan from aspen wood. *Carbohydrate Polymers* 2003;52(4): 359-366.

Electrochemical Applications

Electrochemical Preparation of Titanium and its Alloy in Ionic Liquid

Cunying Xu and Yixin Hua

Additional information is available at the end of the chapter

<http://dx.doi.org/10.5772/59141>

1. Introduction

Titanium and its alloys are widely used in aerospace, medical and structural applications because of their unique specific strength that is maintained at elevated temperature, high corrosion resistance and excellent biocompatibility. However, the use of them has been highly selective due to high cost resulting from their high energy consumption and complicated procedure. Therefore, researchers around the world attempt to find a cheap and simple process for production of titanium and its alloys. Electrochemical preparation is a promising method for fabrication of titanium and its alloys, because it is simple, manufacturable, inexpensive, and its ability to control crystal structure and morphology of them by adjusting electrochemical parameters. Since the deposition potential of titanium is more negative than that of hydrogen, the deposition of titanium or its alloys from aqueous solution is impossible. As a result, aprotic solvents such as molten salts, in which the evolution of hydrogen is precluded, may be good alternatives to aqueous solution for the electrochemical preparation of titanium and its alloys. The electrochemical preparation of titanium and its alloys has been widely studied in conventional inorganic molten salts, but the results are disappointed because these fused salts have many disadvantages, such as high melting point, high viscosity, and high corrosivity.

In recent three decades, ionic liquids as environmentally benign solvents have drawn much attention and have been found wide applications in the organic synthesis, catalyst, electrochemistry, and extraction separation. For electrochemical application ionic liquids combine the advantages of both aqueous solution and high temperature molten salt: they display wide electrochemical window, excellent electrical conductivity, negligible vapor pressure, low melting point (100°C), wide temperature range for the liquid phase, and free from hydrogen evolution. Thus, Ionic liquids are good solvents for the electrochemical preparation of metals and alloys, especially for active elements. The electrochemical preparation of titanium and its

alloys from ionic liquids has been investigated by several researchers. Based on our previous work and those reported by others, we will show the electrochemical preparation of titanium and its alloys such as Al-Ti, Zn-Ti and Al-Mn-Ti in ionic liquid.

2. Electrochemical preparation of titanium from ionic liquid

2.1. Electrodeposition of titanium from ionic liquid

Titanium is an industrially important metal used in many applications, because of its unique properties such as excellent corrosion resistance and high specific strength. Since the electro-deposition of titanium is impossible from aqueous solution, the high temperature molten salt as a promising electrolyte for the production of titanium has been investigated by many researchers. The electrodeposition of titanium from high temperature molten salt had been developed and scaled up until a pilot plant by Italian Ginatta Titanium Turin and America New-Jersey Company. The obtained titanium had low impurity contents, depending on the purity of the TiCl_4 . However, this process was eventually abandoned due to some technology and economic problems, including uncontrollable back reaction of between TiCl_2 and chlorine to TiCl_4 , difficulties to change the cathodes and high corrosion caused by the hot chlorine gas. Recently, there were some attempts to electrodeposit titanium at room temperature in the air and water-stable ionic liquid using TiCl_4 as a source of titanium [1-4]. Freyland et al. reported for the first time electrodeposition of titanium in 1-methyl-3-butyl-imidazolium bis(trifluoromethylsulfone)imide ([Bmim]BTA) and 1-butyl-3-methylimidazolium bis((trifluoromethyl)sulfonyl)amide ([Bmim]Tf₂N) containing TiCl_4 as a source of titanium at room temperature [1, 2]. The cyclic voltammograms showed that Ti(IV) was reduced to Ti(II) and subsequently reduced to Ti(0) in [Bmim]Tf₂N ionic liquid. In situ scanning tunneling microscopy (STM) measurements showed that titanium may be electrodeposited at the step edge of highly oriented pyrolytic graphite (HOPG) in nanowires [1] and on Au(111) substrate in ultrathin layers [2].

However, Endres et al. reported that their attempts to deposit micrometer thick titanium deposits with the recipe in Ref. [2] failed. Instead of titanium metal, polymeric subvalent titanium halide species are obtained. Moreover, they extensively investigated whether titanium could be electrodeposited from its halides (TiCl_4 , TiF_4 , TiI_4) in different ionic liquids, namely 1-ethyl-3-methylimidazolium bis(trifluoromethylsulfonyl)amide ([Emim]Tf₂N), 1-butyl-1-methyl-pyrrolidinium bis(trifluoromethylsulfonyl)amide ([BMP]Tf₂N), and trihexyltetradecylphosphonium bis(trifluoromethylsulfonyl)amide ([P_{14,6,6,6}]Tf₂N). The cyclic voltammetry and electrochemical quartz crystal microbalance (EQCM) measurements show that, instead of elemental Ti, only non-stoichiometric halides are formed, for example with average stoichiometries of $\text{TiCl}_{0.2}$, $\text{TiCl}_{0.5}$ and $\text{TiCl}_{1.1}$ [3]. Wallace et al. used pyrrole and polypyrrole as a nucleating agent to induce titanium deposition in [Emim]Tf₂N [4]. Titanium containing polypyrrole codeposits have been achieved, but bulk metallic titanium is not observed. The measurement results from in situ EQCM indicate that the viscosity of ionic liquid electrolyte increases significantly in the process of electroreducing TiCl_4 , furthermore

titanium deposition might change with breakdown of Tf_2N [5]. Abbott has explained that the obvious increase in electrolyte viscosity results from the change of double layer interface structure during electrolysis [6]. In addition, we also tried to electrodeposit titanium in the ionic liquids 1-butyl-3-methylimidazolium tetrafluoroborate ($[Bmim]BF_4$) and 1-butyl-3-methylimidazolium hexafluorophosphate ($[Bmim]PF_6$) containing $TiCl_4$. There is again no evidence for the titanium electrodeposited from both ionic liquids except $TiCl_x$ deposited on the surface of cathode. The formation of insoluble titanium chloride complex usually involves the solvent, which was proved by the experimental results obtained from electrochemical and chemical reduction of $TiCl_4$ in ionic liquids. Thermodynamically, the electrodeposition of Ti should be possible in ionic liquids, as its electrode potential is -1.64 V vs. NHE. Aluminum has practically the same electrode potential for reduction (about -1.67 V vs. NHE), which can be electrodeposited quite easily in different ionic liquids. Nevertheless, more effort is required to find a suitable ionic liquid and especially the right titanium precursors for a technically relevant process.

2.2. Direct electrochemical reduction of titanium oxide to titanium

At present, titanium is industrially produced by the Kroll process in which titanium tetrachloride is reduced to titanium sponge by magnesium. This is a complicated and time-consuming batch process, which makes titanium an expensive metal [7]. Although titanium has many very useful properties such as high strength, low density and very good corrosion resistance, its application is restricted by the high processing cost. With this background, much effort has been directed towards the development of alternative low-cost processes to produce titanium. Various new methods have been developed, including FFC [8], OS [9], EMR [10] and PRP [11]. The FFC method is considered as the most promising alternative method for production of titanium, but it is potentially limited by high reaction temperature.

Recently, we reported for the first time that the direct electrochemical reduction of titanium dioxide to metallic titanium at room temperature in in Lewis basic $AlCl_3$ -1-butyl-3-methylimidazolium ($AlCl_3$ -BMIC) ionic liquid [12, 13]. The TiO_2 film obtained by oxidizing titanium foil in a furnace at 823 K in air for 144 h was used as the working electrode and a silver wire as the reference electrode. The typical cyclic voltammograms of oxidized titanium electrode in $AlCl_3$ -BMIC melt at 343 K was shown in Figure 1. The initial sweep toward more negative potentials exhibits two clearly-defined reduction waves A and B at -0.33 and -0.60 V (vs. Ag), which may be owing to reduction of the TiO_2 film. Furthermore, the anodic peak observed in the solid curve at -0.18 V (vs. Ag) is indicative of metal dissolution, which has been formed in the original cathodic sweep. After 5 minute electrolysis, the oxidation peak at the cathode potential of -1.6 V (dash line) becomes greater, which indicates that a substantial amount of fresh titanium metal was available for the oxidation.

For more extensive reduction, the oxidized Ti strip was held at a potential of -1.6V for 8 h. The reduction waves and their corresponding anodic waves were absent, and the appearance of cyclic voltammogram was very similar to that of the bare Ti foil. The result indicates that titanium oxide can be electroreduced to Ti metal.

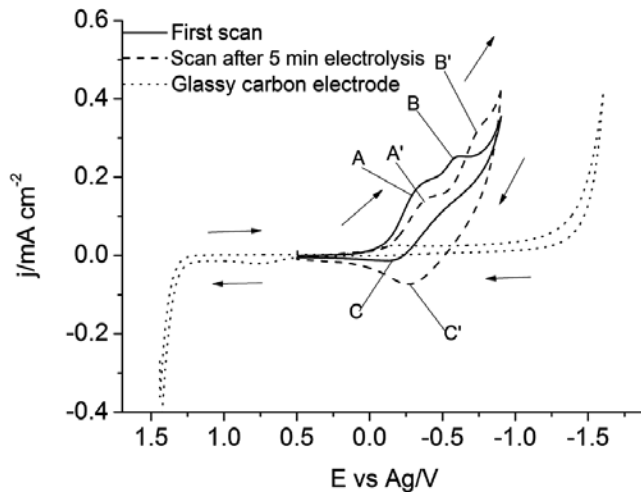


Figure 1. Cyclic voltammograms of oxidized Ti foil and glassy carbon electrode in Lewis basic $\text{AlCl}_3\text{-BMIC}$ obtained at 50 m V s^{-1} and 343 K . [Ref.12]

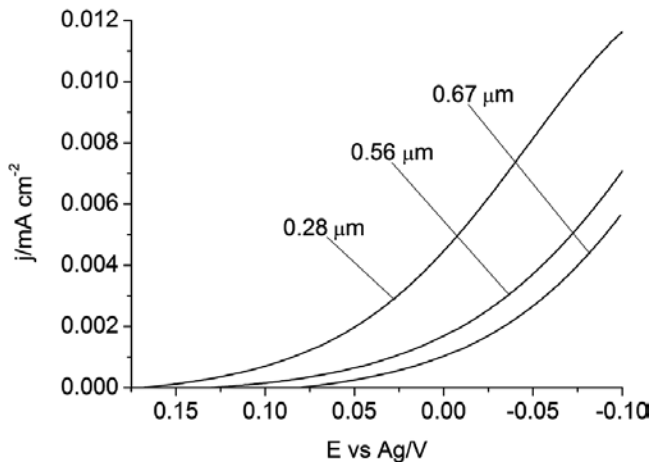


Figure 2. Cathode polarization curves for oxidized Ti foils with different thickness of titanium oxide film in Lewis basic $\text{AlCl}_3\text{-BMIC}$ at 343 K and 5 m V s^{-1} . [Ref.12]

The cyclic voltammetry experiments demonstrated a dependence of the reduction potential on the thickness of TiO_2 film formed on the Ti foil, as shown in Figure 2. The initial reduction potentials shift to more negative potential with increasing the thickness of oxide film. An increase in thickness of oxide film (resistance) might enhance the cathode polarization, which was resulted from the cathode inhibition effect of the oxide film on the reduction process. Thus the direct electrochemical reduction of bulk TiO_2 should need a greater overpotential.

Tafel curves recorded at oxidized Ti foil with different thickness of TiO_2 film indicated that equilibrium potential negatively shifted, and the exchange current density as well as cathode

Tafel slope decreased along with an increasing linear polarization resistance when TiO_2 film became thicker. Obviously, direct electrochemical reduction of bulk TiO_2 should need a greater driving force. This conclusion was in agreement with the cyclic voltammetry measurement.

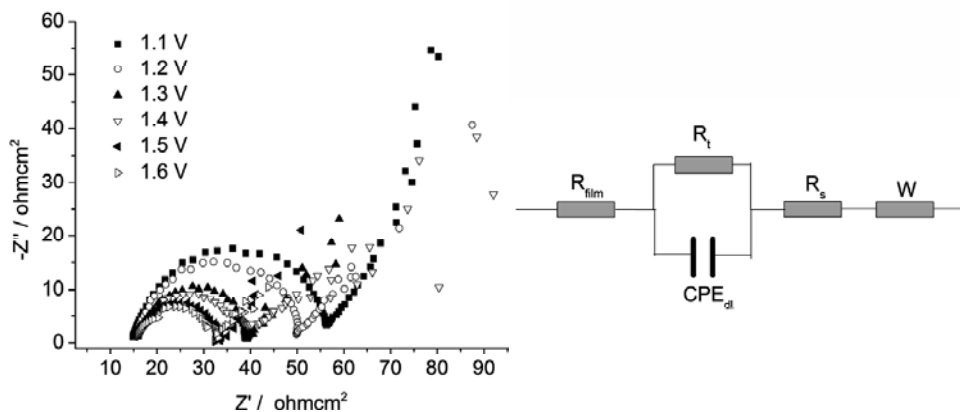


Figure 3. Alternating current impedance spectra of oxidized Ti foil in Lewis basic AlCl_3 -BMIC at 343 K and corresponding equivalent circuit. [Ref.13]

Alternating current impedance spectra of oxidized Ti foil clearly showed that an increase in cathodic overpotential led to a decrease in reduction charge resistance (see Figure 3). One semicircle was observed in the higher frequency region of all Nyquist plots obtained at different cathodic potential, suggesting that the interface charge transfer process between the TiO_2 film and ionic liquid could be the rate-determining step for the reduction of TiO_2 film. On the contrary, a nearly linear increasing of $-Z''$ with Z' at the low frequency region may be attributed to the mass transfer in the ionic liquid. The equivalent circuit has been used to simulate the Ti/ TiO_2 film/IL (ionic liquid) system, which fitted the experimental data best (Figure 3). In this system, R_{film} and CPE_{film} represent the resistance and capacity of oxide film respectively; R_t refers to the charge transfer resistance process occurring on the oxide film surface; CPE_{dl} delegates the double capacity at the interface between the oxide film and tested IL; R_s can be explained to be the resistance of the tested IL; W can describe the diffusion control process at low frequency. Fitted results from Alternating current impedance spectra of oxidized Ti foil with different TiO_2 thickness showed that the R_{film} increased with increasing of thickness of TiO_2 film.

For increasing the reduction rate of this process, the dependence of electrochemical behavior of TiO_2 film on the reaction temperature was investigated. The cathode polarization curves of oxidized titanium foil in AlCl_3 -BMIC at different temperatures showed that cathode overpotential decreased with an increase in reaction temperature. Accordingly, it is concluded that increasing reaction temperature can weaken the cathode inhibition of this reduction process. Alternating current impedance experiments of TiO_2 films at different temperatures showed that the resistance of the electrochemical reduction decreased with the reaction temperature increasing. The parameters fitted from experimental data by the equivalent circuit mentioned

above showed increasing temperature made the charge transfer resistance R_t and tested IL resistance R_s decline.

Metallographic microscopic image showed the reduced TiO_2 film obviously has metallic luster, implying that TiO_2 film was reduced to metal. It was found that a lot of bubbles were generated at the bottom of cathode and less at anode during the electrochemical reduction process of TiO_2 film. It could be predicted that the reduction of TiO_2 film in basic $AlCl_3$ -BMIC was possibly occurred at the edges of the foil, mostly due to the different potential distribution at the edges of the electrode.

From the above results, it is evident that TiO_2 film can be electroreduced in $AlCl_3$ -BMIC ionic liquid. As further proof of this conclusion, the electrochemical reduction of titanium dioxide pellet in ionic liquid was investigated. After electrochemical reduction for 48 h, the TiO_2 pellet visually turned to bright black. The X-ray photoelectron spectroscopy indicated the electroreduced TiO_2 pellet contains a small amount of titanium metal, suggesting that TiO_2 may be reduced to metallic Ti in this experiment, but the reaction rate is very low.

The mechanism for electroreduction of TiO_2 in high temperature molten salt has been extensively studied. It is generally known that oxygen ions are formed at cathode and oxygen evolves at the surface of the anode [7]. However, a lot of bubbles are generated in cathode region during the electrochemical reduction of TiO_2 and only a few of bubbles are observed in anode region, indicating that the reduction process of TiO_2 in ionic liquid is different from that in high temperature molten salt and may be attributed to interfacial electrochemical reaction mechanism. TiO_2 is an n-type semiconductor that has a wide band gap ($E_g \approx 3.2$ eV) [14-16], which makes charge transfer more difficult than other narrow ones. The increase in cathodic polarization may cause the electronic bands bending downward at the interface between TiO_2 and ionic liquid, resulting in a decrease of the space-charge region of TiO_2 with formation of electron-accumulation layer at the surface of TiO_2 , where oxygen ions are formed, and as a consequence, the TiO_2 is reduced [17]. Correspondingly, it is considered that TiO_2 film is reduced in $AlCl_3$ -BMIC melt according to these steps below (Figure 4).

(1) With negative shift of cathode potential, the electronic bands at the interface between TiO_2 and ionic liquid bent downward, where charge transfer occurred. In other words, oxygen ions are generated as a result of TiO_2 molecules reacting with electrons at the interface of TiO_2 /ionic liquid ($TiO_2 + 4e \rightarrow Ti + 2O^{2-}$). (2) The space formed among these reduced Ti would be filled with ionic liquid at once. (3) The oxygen ions dissolved in ionic liquid would diffuse through the porous layer of reduced titanium. (4) Oxygen ions diffused from cathode region to the surface of the anode and anodically discharged to form O_2 ($2O^{2-} \rightarrow O_2 \uparrow + 4e$). (5) When new generated titanium film formed which then served as anode, O_2 was generated at the interface of new generated titanium, TiO_2 and ionic liquid. At this moment, the anode just acted as a conductor.

In short, TiO_2 film on titanium foil can be electroreduced to metallic Ti in $AlCl_3$ -BMIC melt at room temperature. However, reduction of bulk TiO_2 needs greater overpotential, so the electrochemical reduction of TiO_2 to metal is very difficult. More effort is required to find a

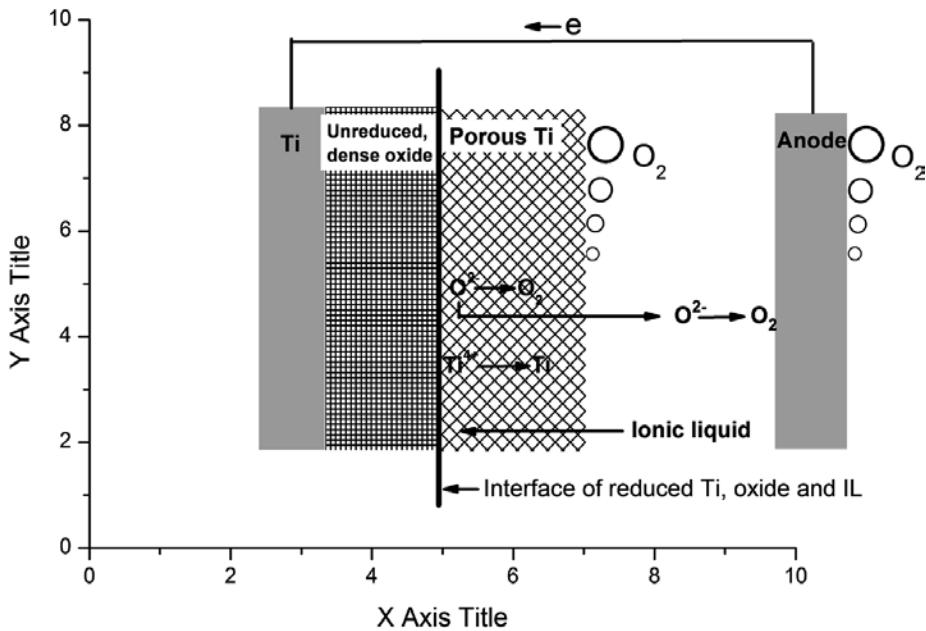


Figure 4. Model for the reduction process of oxides film on titanium foil in Lewis basic AlCl_3 -BMIC ionic liquid. [Ref. 13]

suitable ionic liquid and especially the right methods of making TiO_2 electrode to improve conductivity of TiO_2 with a technically relevant process.

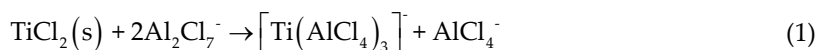
3. Electrodeposition of titanium alloys in ionic liquid

3.1. Electrodeposition of Al-Ti alloy

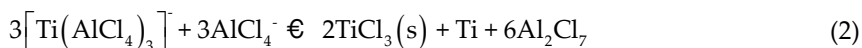
Al-Ti alloys are widely used in aerospace industry because of their excellent corrosion resistance, high temperature oxidation resistance and mechanical properties [18, 19]. As Al and Ti are reactive metal ($E^\circ_{\text{Al(III)/Al}} = -1.67 \text{ V vs. NHE}$, $E^\circ_{\text{Ti(II)/Al}} = -1.64 \text{ V vs. NHE}$), Al-Ti alloy can not be obtained from an aqueous electrolyte. The electrolytes for Al, Ti and Al-Ti alloy electrodeposition must be aprotic, such as high temperature molten salt or ionic liquid. The electrodeposition of Al-Ti alloys from high temperature molten salt has been extensively investigated [20], but many disadvantages such as high melting point, high viscosity, and high corrosivity limit its practical application. In recent years, the development of room-temperature ionic liquid has resulted in another potential approach for Al-Ti alloy electrodeposition. Tsuda et al. firstly investigated the electrochemical preparation of Al-Ti alloys from Lewis acidic AlCl_3 -EMIC (aluminum chloride-1-ethyl-3-methylimidazolium chloride) melts with various concentration of Ti(II) at 353K [21, 22]. The Ti(II) ions used here can be obtained by the addition of TiCl_2 or by chemical reduction of TiCl_3 dissolved into ionic liquid by Al metal. In additions, our investigations conducted in AlCl_3 -BMIC indicate that Ti(II) can also be obtained

in ionic liquid by the direct reduction of TiCl_4 with Al metal. Since TiCl_4 and TiCl_3 , as well as aluminum, are much less expensive than TiCl_2 , the in situ reduction of TiCl_4 or TiCl_3 to Ti(II) by aluminum metal may be a useful method for introducing Ti(II) into chloroaluminate ionic liquid.

It was proposed that TiCl_2 dissolves in the liquid by forming $[\text{Ti}(\text{AlCl}_4)_3]^-$ and its solubility increases with increasing ionic liquid acidity, i.e., with increasing Al_2Cl_7^- concentration.



The liquid acidity is decreased by changing the molar ratio of AlCl_3 to BMIC from 2:1 to 3:2, leading to the disproportionation reaction of the $[\text{Ti}(\text{AlCl}_4)_3]^-$ for the production of TiCl_3 precipitates and metal Ti [21, 22].



Ti(II) species tends to form polymers or aggregates upon increasing the Ti(II) concentration or the liquid acidity. The value of $D_{\text{Ti(II)}}$ decreases with the increase of the Ti(II) concentration, which is attributed to that the formation of a polymeric or aggregated species leads to a diffusing entity with a larger solvodynamic radius. Electrochemical, galvanostatic or potentiostatic, oxidation of Ti metal produces either insoluble passive TiCl_3 film or volatile TiCl_4 which can escape from the liquid. At higher potential, the TiCl_3 passive film breaks down and generates Ti(IV) . The oxidation of metallic titanium to Ti(II) by direct anodization of Ti metal in this liquid has not been studied by Tsuda et al. Our observation indicates that the galvanostatic oxidation of titanium at the current density of 2-20 mA cm^2 produces Ti(IV) . Furthermore, we can not obtain the Ti(II) in AlCl_3 based ionic liquid using either galvanostatic oxidation of titanium. These results suggest that anodic oxidation of metallic titanium is almost impossible for introducing Ti(II) because of the difficulty of controlling the oxidation potential.

From the cyclic voltammograms of stationary and rotating Pt disk electrodes in the acidic AlCl_3 -EMIC melt containing Ti(II) , it can be seen that the reduction potential of Ti(II) to Ti(0) is close to the deposition potential of Al [21, 22]. The potential of the stripping wave shifts positively due to the codeposition of Ti with Al to form Al-Ti alloy, which is more difficult to oxidize than pure Al. Furthermore, the value of negative shifts increases as the concentration of Ti(II) increases. The electrodeposition of bulk Al-Ti alloys is performed under constant current at a current density of 10 mA cm^{-2} in an ionic liquid with saturated Ti(II) [21]. The content of Ti in the Al-Ti alloys deposited in this way becomes higher with a decrease in applied current density, implying that the reduction of Ti(II) to Ti(0) occurs at a more positive potential than the deposition of Al. At low reduction current densities and correspondingly less negative potentials, the partial current density for the electrodeposition of Ti metal would be a larger fraction of the total current density. Increasing the total applied reduction current densities or making the applied potential more negative, the partial current for the electrodeposition of Ti

quickly increases to a mass transport limited value because Al (III) concentration is much more than Ti(II), while the partial current density for Al deposition will keep increasing, which causes an decrease in the Ti content of Al-Ti alloys deposited. The maximum content of titanium in Al-Ti alloys that are electrodeposited from this ionic liquid depends on the saturation concentration of TiCl_2 in the ionic liquid and the minimum current density that can be practically used. It can be seen from scanning electron images of the Al-Ti alloy electrodeposited that the deposits were compact, dense and composed of nodular crystals [21, 22]. The nodular crystals grow up as current density is increased or Ti content is decreased, indicating that the grain refinement is driven by the incorporation of Ti metal into the alloy rather than the deposition overpotential. This nicely demonstrates that the impurities and alloying additions have an impact on morphology of the deposit. The XRD (X-ray powder diffraction) analysis results indicate that electrodeposited Al-Ti alloys with the Ti content of 7.0-18.4 at.% are the disordered face-centered cubic (fcc) structure, as highly similar with the structure of Al. The lattice parameters of the alloys decrease, which is to be expected as the smaller Ti atoms substitute for Al atoms in the fcc lattice [22]. Furthermore, X-ray reflection peaks of the Al-Ti alloys broaden with increasing Ti content, suggesting a decrease in the grain size of the deposit. Recorded for Al-Ti alloys electrodeposited on copper electrodes in deaerated aqueous NaCl solution, the potentiodynamic anodic polarization curves show that the pitting potential of electrodeposited Al-Ti alloys significantly increases as compared to that of pure Al, which is in accord with that is observed for Al-Ti alloys obtained by sputter deposition [21].

Aliet al. examined the electrodeposition of Al-Ti alloys on platinum electrode in $\text{AlCl}_3\text{-BPC-TiCl}_4$ (molar ratio 6.14:3.07:0.09) ionic liquid using controlled-potential and pulse potential method at 298K [23]. Al-Ti alloys containing up to 27 % atomic fraction (a/o) titanium can be electrodeposited from this electrolyte at the deposition potential of -0.06 V vs. Al/Al(III), but the titanium content of these alloys decreases as the reduction current density is increased or the deposition potential is negatively shifted. The Al-Ti alloy deposits obtained either by controlled-potential or by pulse potential method are compact and smooth. The efficiency of the process is about 97%. The X-ray powder diffraction (XRD) patterns of the electrodeposits show that the electrodeposited alloy containing 27 at.% Ti is composed of Al, Ti and Al_3Ti , but a single phase of Al solid solution with Ti are obtained as the Ti content in electrodeposited alloy decreases to 15 at.%.

The electrodeposition of Al-Ti alloys on Au(111) in an acidic aluminum chloride-1-butyl-3-methylimidazolium chloride ($\text{AlCl}_3\text{-BMIC}$) containing 10 mmol TiCl_4 at 298 K was also reported by Freyland et al. [22, 24]. From cyclic voltammograms, it is found that Ti(IV) can be firstly electroreduced to Ti(III) and subsequently reduced to Ti(II), whereby Ti (III) is formed precipitates on the electrode as sparingly soluble TiCl_3 . The reduction of Ti(III) to Ti(II) occurs at a potential where underpotential deposition (UPD) of Al on Au(111) also occurs. Furthermore, the codeposition of Al and Ti is followed by the deposition of bulk Al. A stripping peak is observed at more negative potential relative to the Al stripping during an anodic scan, which is assigned to oxidation of Al-Ti alloy. The electrochemical scanning tunneling microscopy (EC-STM) analysis for the underpotential deposits show that Al preferentially grow up along the step edges of Au substrate resulting in step edge decoration, whereas Al-Ti grow into

smaller clusters homogeneously spread on the Au electrode. Furthermore, the Al-Ti clusters are clearly smaller in size than the Al clusters. The formation of an Al-Ti alloy phase in the electrodeposits is further confirmed by an X-ray photoelectron spectra (XPS) analysis.

Reddy et al. attempted electrochemical production of Al-Ti alloys from AlCl_3 -BMIC- TiCl_4 (molar ratio 2:1:0.019) and AlCl_3 -BMIC (molar ratio 2:1) ionic liquids at temperature between 70-125°C and constant voltage between 1.5-3.0 V [25, 26]. The Al-Ti alloys containing about 15-27 at% Ti are produced with a current efficiency of about 25-38%. Ti content in Al-Ti alloy deposits decreases as the applied cell voltage increases or the temperature increases. Increasing the applied cell voltage probably leads to mass-transport-limited value for Ti deposition, while the total charge passed through the cell still increases, resulting in the Ti content in the alloy deposits decreasing. The scanning electron micrographs show that the deposits are nodular but not so dense or compact. As the applied voltage decreases, average particle size decreases and deposits become uniform and compact. In addition, the deposits particle size increases slightly with the temperature increasing from 70 to 100°C. But increasing temperature beyond 100°C, particles begin to grow quickly, which results in the formation of clusters rather than separated particles. At low voltage or low temperature, lower the migration rate of reducible ions and growth rate of crystal nuclei make the deposits become smoother and fine grained. Finally, the optimum conditions for production of smooth, compact, fine particle size and high Ti content Al-Ti alloys are 1.5-2.0 V voltage and 70-100°C temperature. The X-Ray diffraction (XRD) analysis of electrodeposited alloy confirms the formation of Ti-Al alloy. The cathodic current efficiency in AlCl_3 -BMIC- TiCl_4 electrolyte is very low (25-38%) for all experiments. The lower current efficiency is due to the formation of TiCl_3 passive layer on electrode surfaces, which retards the kinetics of redox reaction, and reduces the cathode current efficiency. This obstacle of low current efficiency can be overcome by using AlCl_3 -BMIC instead of AlCl_3 -BMIC- TiCl_4 . Titanium metal is used as the anode and its dissolution serves the source of Ti ion in the electrolyte. The cathodic current efficiency of the process in AlCl_3 -BMIC as electrolyte is up to 78-87%. The absence of TiCl_4 in the electrolyte reduces the formation of TiCl_3 passive layer on the electrodes because TiCl_4 is easily reduced to TiCl_3 . The energy consumption for the production of Ti-Al alloy using this ionic liquid is about 3.92-9.47 kWh/kg, which is far lower than that for the commercially production of Al-Ti in molten salt.

Although the Al-Ti alloy can be successfully produced using constant voltage in AlCl_3 -BMIC- TiCl_4 (molar ratio 2:1:0.019) and AlCl_3 -BMIC (molar ratio 2:1) electrolytes, the studies on process variables are limited to applied voltage and temperature. Our group investigated the electrodeposition of Al-Ti alloy by using galvanostatic on copper, titanium and stainless steel from an acidic AlCl_3 -BMIC (2:1 molar ratio) ionic liquid containing TiCl_4 [27]. The substrates have great influence on the morphology and composition of the alloy deposits. The Ti content of Al-Ti alloys prepared at a current density of -5 mA cm^{-2} in this ionic liquid containing $0.2 \text{ mol L}^{-1} \text{ TiCl}_4$ on copper, titanium and stainless steel is 4.9 at.%, 6.3 at.% and 9.0 at.%, respectively. The scanning electron micrographs show that the deposits on both copper and stainless steel are nodular, whereas deposits on titanium are sheet-like structures. Furthermore, the particle size on copper is smaller than that on stainless steel. It is observed that the Ti content in Al-Ti alloy deposited on these substrates decreases with increasing current density. Since

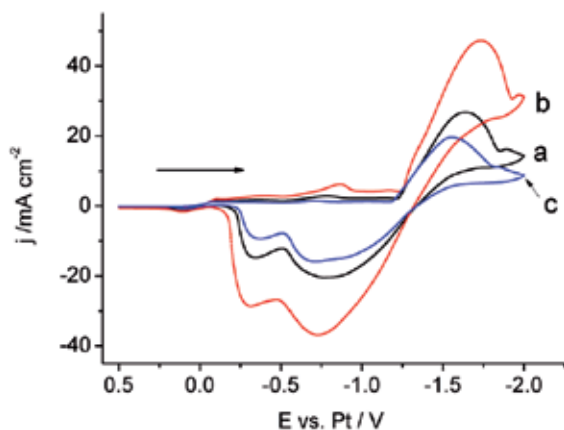


Figure 5. Cyclic voltammograms obtained at glassy carbon electrode at 50 mV s^{-1} in $\text{AlCl}_3\text{-BMIC-TiCl}_4$ (molar ratio 2:1:0.037) (a) and with the following additives: (b) 0.25 mol dm^{-3} toluene and (c) 0.25 mol dm^{-3} NH_4Cl

the reduction current of Ti(II) reaches limiting current condition more quickly than that of Al_2Cl_7^- , the partial current for the Al deposition remains increasing when partial current for the Ti deposition reaches a limiting current density, which results in a decrease in the Ti content of the alloys electrodeposited with an increase in current density [21]. Also, it is found that the content of Ti in Al-Ti alloys increases with increasing Ti(IV) concentration in ionic liquid. Results from SEM examinations reveal that the morphology of the Al-Ti deposits varies with the alloy composition. The deposit particle decreases in size with increasing Ti composition, decreasing current density and increasing Ti(IV) concentration.

The Al-Ti alloys can be successfully electrodeposited on different substrates in ionic liquids, but deposits are not very dense, smooth or bright, limiting its practically plating application. Quite recently we examined the addition of toluene and NH_4Cl additives and their effect upon the composition and morphology of electrodeposited Al-Ti alloys [28]. The cyclic voltammetric responses of $\text{AlCl}_3\text{-BMIC-TiCl}_4$ (molar ratio 2:1:0.037) in the absence and presence of equimolar quantities of the additives toluene and NH_4Cl indicate that the shape of the voltammograms and peak current densities is dependent on the additives used (see Figure 5). From these results it is evident that either the Al-Ti alloys deposition or stripping processes is affected by the addition of the additives. The onset of the Al-Ti alloy deposition potentials shifted anodically in the presence of NH_4Cl , suggesting that the NH_4Cl promotes the reduction of Al-Ti alloy. However, the opposite shifts are observed for the addition of toluene, suggesting that toluene restrains the deposition of Al-Ti alloy. Additionally, it should be noted that the charge passed during Al-Ti alloy reduction is greatly increased in the presence of toluene, but decreased in the presence of NH_4Cl relative to the additive free solution. These results indicate that the presence of the additives affects the Al-Ti deposition processes and various additives have different effect on Al-Ti electrodeposition, leading to change in the composition and morphology of Al-Ti alloy. The EDS analysis indicates that Ti content of Al-Ti alloy deposits increases in the presence of toluene, but decreases in the presence of NH_4Cl . The Al-Ti morphology is further modified upon the introduction of NH_4Cl or toluene to the solution. In contrast to the

deposits in the absence of additive, the deposits particles size obviously decreases and deposits become more smooth, dense, and uniform in the presence of additives.

3.2. Electrodeposition of Zn-Ti alloys

Zn-Ti alloys are used widely as metallic coatings in the corrosion protection of iron and steel due to their excellent corrosion resistance [29]. The electrodeposition is one of most promising techniques to prepare Zn-Ti alloy because it is simple and inexpensive, and is able to tailor the properties of the deposit by adjusting the deposition conditions. However, the electrodeposition of Zn-Ti alloys from aqueous solutions is impossible by the fact that hydrogen evolves before Ti deposition. The electrodeposition of Zn-Ti alloys were investigated by our group in a ZnCl₂-urea (1:3 molar ratios) eutectic-based ionic liquid containing 0.27 mol L⁻¹ TiCl₄ [30]. Cyclic voltammograms recorded at glassy carbon electrode in the ZnCl₂-urea (1:3 molar ratios) eutectic-based ionic liquid are shown in Figure 6. Only a pair of redox peaks appears in the cyclic voltammogram of pure ZnCl₂-urea ionic liquid, which can be attributed to the deposition and stripping of Zn. After the addition of TiCl₄ to ZnCl₂-urea liquid, two additional reduction waves are observed in the voltammetry curve. Voltammetric data show that the first cathodic wave at -0.36 V (vs. Pt) corresponds to the reduction of Ti(IV) to Ti(III). It is noted that the violet passivating film is formed on the electrode surface after this reaction, indicating that Ti(III) is insoluble in ZnCl₂-urea eutectic-based ionic liquid. Thus, the reaction of Ti(IV) to Ti(III) in ZnCl₂-urea liquid involves the following sequence of reactions:



The second wave (B) at the more positive potential than that of Zn electrodeposition is contributed to the reduction of Ti(III) to Ti(II). Furthermore, the wave ascribed to the reduction of Zn(II) shows a small negative shift and the oxidation wave shifts to more positive potentials in the presence of TiCl₄. The positive shift of the stripping wave indicates formation of Zn-Ti alloy that is more stable toward oxidation than pure Zn.

The Zn-Ti alloys are electrodeposited on Cu substrate from ZnCl₂-urea deep eutectic ionic liquid with TiCl₄. The effects of deposition potential and temperature on the surface morphology and composition of electrodeposited Zn-Ti alloys are studied. The obtained alloys are adherent onto Cu substrate, but not very compact or dense. The EDX analysis shows that the deposits are composed of Zn and Ti, which are chloride-free. At the same temperature, the Ti content in Zn-Ti alloy increases with increasing potential from -1.3 to -1.8 V, but the Ti content tends to decrease as potential increased from -1.8 to -2.2 V. Because the initial deposition potential of Zn is more positive than that of Ti, the partial current for the electrodeposition of Ti metal would increase with increasing the deposition potential at lower deposition potential [8]. However, the Ti ion concentration (0.27 mol L⁻¹) is much less than Zn ion concentration

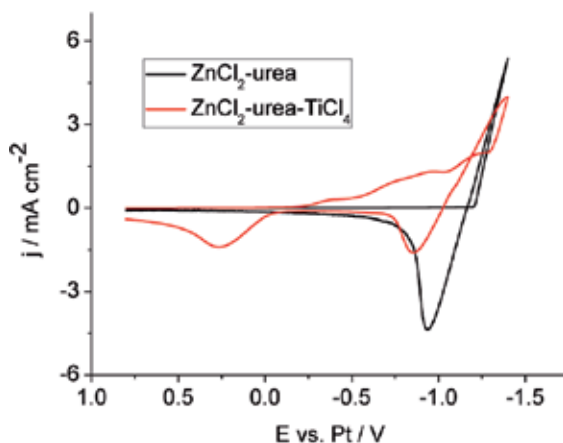


Figure 6. Cyclic voltammograms recorded at a glassy carbon electrode in the ZnCl_2 -urea (1:3 molar ratios) eutectic based ionic liquid with and without TiCl_4 at 353 K. The sweep rate was 0.02 V s^{-1} . [Ref. 30]

(4.79 mol L^{-1}) in the electrolyte. With further increasing of the deposition potential from -1.8 to -2.2 V , the partial current for the reduction of Ti (II) ions probably reaches a limiting value, whereas partial current for the reduction of Zn (II) ions continues to increase, and then Ti content in Zn-Ti alloys decreases. Under the same deposition potential, the Ti content in the deposits increases as the temperature increases. Ti ion concentration is very low in the electrolyte and the reduction of Ti is controlled by mass-transport process [25, 31]. An increase in the temperature would enhance the mass transport rate of Ti(II), and increase the deposition rate of Ti. The XRD patterns for electrodeposits show that the Zn-Ti alloy exhibits a chemically disordered hexagonal close-packed (hcp) structure very similar to that of pure zinc. The largest lattice parameters (a) corresponding lattice expansion ($\Delta a/a$) of 0.67% occur at an alloy with Ti content about 8.4 at.%, suggesting the formation of Zn-Ti alloys. The SEM images shown in Figure 7 demonstrate the particle size increases gradually as the deposition potential becomes more negative or temperature increases. When the deposition potential becomes negative to -2.0 V or temperature is increased up to 363 K, deposited grains grow quickly and the deposits become a little rough. At low deposition potentials or low temperature, the discharge rate of reducible ions on the electrode is lower and nucleation rate is faster than the crystal-growth rate, which results in fine-grained deposit.

In addition, the effect of substrates on the morphology and composition of the deposits was also investigated. The Ti content of Zn-Ti alloys on mild steel is significantly lower than that on copper and particle size on mild steel is obviously smaller than that on copper.

In contrast to DC plating, pulsed electrodeposition (PED) offers unique advantages, such as deposition of uniform and crack free coating with desirable characteristics. Recently, our group investigated that the electrodeposition of Zn-Ti alloys on mild steel in a ZnCl_2 -urea (1:3 molar ratios) eutectic-based ionic liquid [32]. At constant current off-time and pulse current density, the grain size decreases with decreasing current on-time, deposits become more compact and refined grain structure (see Figure 8). In contrast, an increase in the current off-time at constant

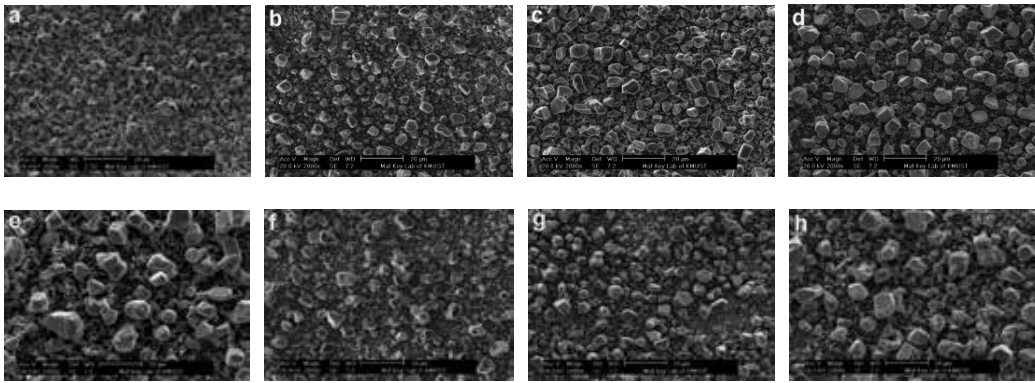


Figure 7. SEM images of the Zn-Ti alloys prepared in ZnCl_2 -urea ionic liquid containing $0.27 \text{ mol L}^{-1} \text{ TiCl}_4$ under different potentials and various temperatures: (a) -1.3 V , 353 K ; (b) -1.5 V , 353 K ; (c) -1.8 V , 353 K ; (d) -2.0 V , 353 K ; (e) -2.2 V , 353 K ; (f) -1.8 V , 333 K ; (g) -1.8 V , 343 K ; (h) -1.8 V , 363 K . [ref. 30]

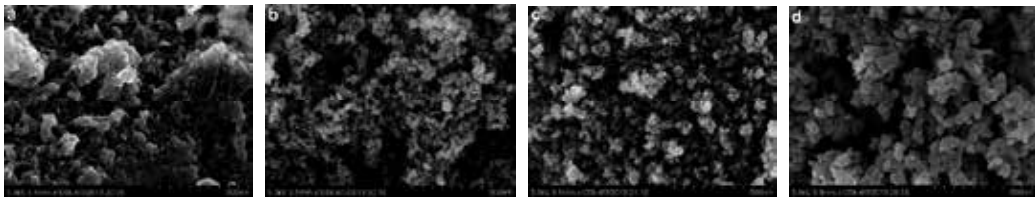


Figure 8. The scanning electron micrographs of Zn-Ti alloy coatings obtained by pulse electrodeposition plating. (a) $j=10 \text{ mA cm}^{-2}$, $t_{\text{on}}=4.0 \text{ ms}$; (b) $j=10 \text{ mA cm}^{-2}$, $t_{\text{on}}=2.0 \text{ ms}$; (c) $j=10 \text{ mA cm}^{-2}$, $t_{\text{on}}=1.0 \text{ ms}$; (d) $j=5 \text{ mA cm}^{-2}$, $t_{\text{on}}=2.0 \text{ ms}$.

current on-time and pulse current density results in the grain growth. The turned-on time is reduced and the turned-off time keeps constant, namely increasing the effective number of cycles ($t_{\text{on}}+t_{\text{off}}$), lead to an increase in the number of nuclei. As a result, the size of grain reduces. When the average current density in pulsed electrodeposition is equal to the current density applied in the continuous process, deposit obtained by pulsed electrodeposition shows a more refined granulation, due to the higher nucleation rate. At constant current on-time and off-time, the grain size of deposits decreases with increasing pulse current density.

Regarding the composition of deposits, higher on-time and current density causes a decrease in the content of titanium in the deposit. Furthermore, the Ti content in deposits obtained by continuous electrodeposition is smaller than that of the pulse deposited. This is important and should be taken into account when preparing deposits of a desired composition. It was also noticed that the proportion of Ti in the coating is higher than its proportion in the bath, indicating its preferential deposition. The reasons for this type of behavior are discussed in several works, without reaching a conclusion [33, 34]. Galvanic corrosion tests show that corrosion resistance of Zn-Ti alloy coatings increased with increasing Ti content.

The Zn-Ti alloys can be successfully electrodeposited from ZnCl_2 -urea eutectic-based ionic liquid, but deposits are not very compact or bright. So we investigated the effect of additives

on the composition and morphology of electrodeposited Zn-Ti alloys [35]. The cyclic voltammograms obtained in ZnCl₂-urea (molar ratio 10:1) containing 0.43 mol L⁻¹ TiCl₄ in the absence and the presence of equimolar quantities of the additives LiCl, NaCl, KCl, NH₄Cl or etramethylammonium chloride (TMAC) demonstrate that the presence of the additive causes changes in the shape and position of the voltammograms. These results indicate that the presence of the additives affects both the Zn-Ti alloys deposition and stripping processes. The current crossovers in the cathodic region are evident in all the systems, indicating that nucleation and growth of Zn-Ti centre occur under the tested conditions. The deposition potential of the Zn-Ti alloy is negatively shifted in the presence of these additives, suggesting that the additives restrain the deposition of Zn-Ti alloy.

The EDX analysis indicates that Ti content of Al-Ti alloy deposits is almost unchanged in the presence of various additives. SEM images of Zn-Ti alloy deposits show that deposits become smooth and grain size decreases in the presence of NaCl or KCl additives (see Figure 9 a, c and d). In addition, the decrease in particle size is not obvious but deposits become more smooth in the presence of LiCl, NH₄Cl and TMAC (see Figure 9 a, b, e and f).

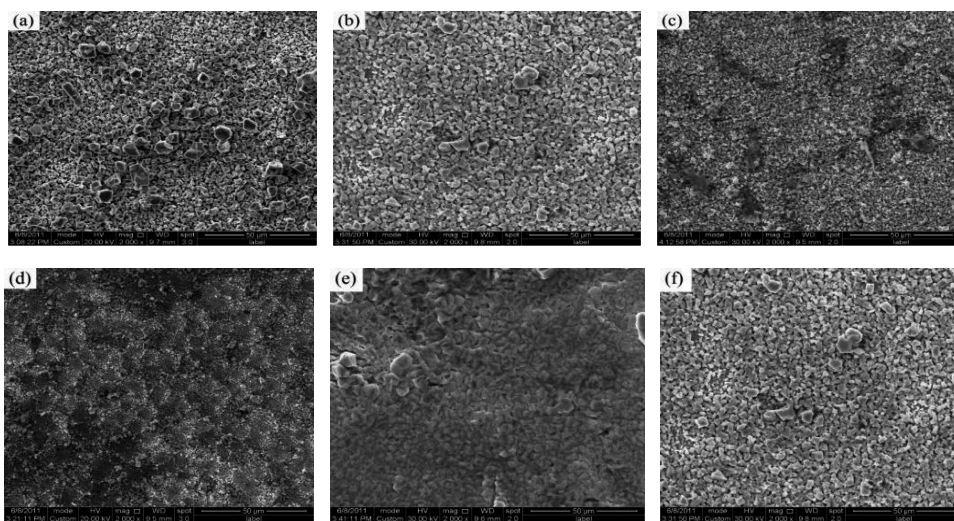


Figure 9. Representative scanning electron micrographs of Zn-Ti alloys electrodeposited on mild steel from ZnCl₂-urea (molar ratio 10:1) containing 0.43 mol L⁻¹ TiCl₄ (a) and with 1.67 mol L⁻¹ following additives: (b) LiCl, (c) NaCl, (d) KCl, (e) NH₄Cl and (f) TMAC.

The electrodeposition of Zn-Ti alloy from ZnCl₂-urea-TiCl₄ in the presence of NaCl was further investigated at different deposition potential and temperature. The Ti content of the electrodeposited alloys increases with increasing current density and temperature under our experimental conditions. As the reduction potential of Zn (II) is more positive than that of Ti (II), the partial current for the deposition of Ti increases quickly with increasing current density. As a result, the Ti content of the electrodeposited alloys increases with increasing current density. It is also noted that the Ti content in Zn-Ti alloys increases with increasing Ti

(IV) concentration in ionic liquid. Results from SEM examinations reveal that the structure of the Al-Ti deposits varies with the alloy composition. The deposit particle decreases in size with increasing Ti composition, resulting from the increase in current density, temperature and Ti (IV) concentration.

3.3. Electrodeposition of Al-Mn-Ti alloy

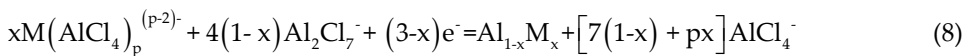
The Ti addition to Al-Mn alloy can effectively improve high temperature oxidation and pitting corrosion resistance. Since both Al-Ti [21] and Al-Mn [36] alloys can be electrodeposited from Lewis acidic AlCl_3 -EMIC (or BMIC) ionic liquid, we investigated the electrodeposition of the Al-Mn-Ti ternary alloys in the AlCl_3 -BMIC (2:1 molar ratios) ionic liquid at the temperature range from 80 to 100°C [37]. Mn(II) and Ti ions were introduced into the ionic liquid by dissolution of MnCl_2 and anodic dissolution of titanium sheet, respectively. Based on the relationship between the charge passed and weight loss of titanium sheet, the number of electrons involved in the reaction was calculated from Faraday's law to be approximately 4, indicating that the anodic oxidation of metal Ti produced Ti(IV) ions in AlCl_3 -BMIC ionic liquid. It was found that Ti(IV) was reduced to Ti(II) in two one-electron steps.



As discussed previously, Al deposition occurs by the electrochemical reduction of the coordinately unsaturated Al_2Cl_7^- ion in Lewis acidic AlCl_3 -BMIC ionic liquid [38]



However, when Mn(II) or Ti(II) is present in the ionic liquid, this reaction becomes



Where $\text{M}(\text{AlCl}_4)_p^{(p-2)-}$ represents Mn(II) or Ti(II) solvated in the chloroaluminate ionic liquid by AlCl_4^- and $\text{Al}_{1-x}\text{M}_x$ denotes the resulting aluminum-transition metal alloy. In the pure melt, a stripping wave for electrodeposited Al begins at ~0 V, but this wave is replaced by waves corresponding to the stripping of the electrodeposited Al-Mn and Al-Ti alloys in the solutions containing Mn(II) or Ti(II), respectively [21, 36].

The cyclic voltammograms recorded at a glassy carbon electrode for the solutions revealed that the presence of Mn(II) in the solution inhibits the nucleation of Al (see Figure 10a and b). The cyclic voltammograms recorded at glassy carbon electrode in the ionic liquid containing

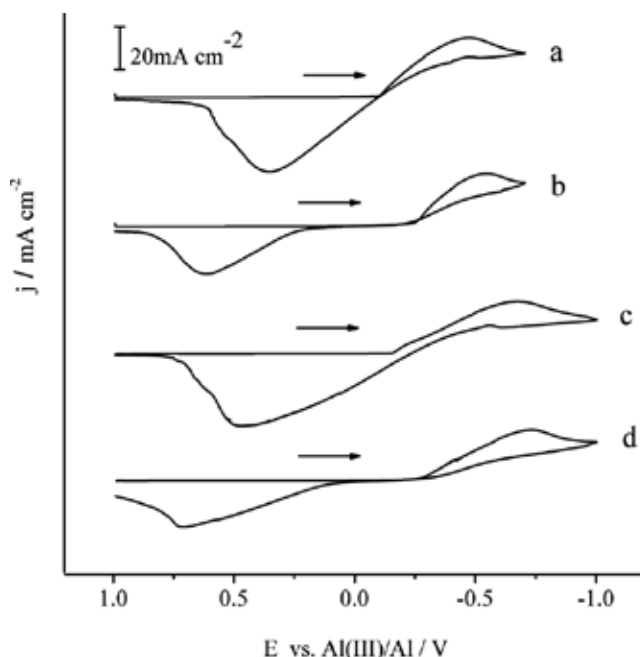


Figure 10. Cyclic staircase voltammograms recorded at a glassy carbon in Lewis acidic $\text{AlCl}_3\text{-BMIC}$ ionic liquid: (a) pure ionic liquid, (b) $25 \text{ mmol L}^{-1} \text{ Mn(II)}$, (c) $25 \text{ mmol L}^{-1} \text{ Ti(IV)}$, (d) $25 \text{ mmol L}^{-1} \text{ Mn(II)} + 25 \text{ mmol L}^{-1} \text{ Ti(IV)}$. The scan rate was 0.05 V s^{-1} , and the temperature was 323 K .

both Mn(II) and Ti(II) is similar in appearance to that recorded in the Mn(II) solution (see Figure 10b and d). This implies that the formation of Al-Mn dominates the ternary Al alloy deposition process. In fact, the Ti content of all of the Al-Mn-Ti alloys produced during this investigation was less than 3.8 at. \% .

Controlled current techniques were employed to prepare Al-Mn , Al-Ti and Al-Mn-Ti alloy samples at a copper substrate. In the case of the binary alloys that were prepared in solutions containing only one of the two transition metal precursors [i.e., either Mn(II) or Ti(II)], the Mn content of the Al-Mn alloys is always greater than the Ti content of the corresponding Al-Ti alloys when the two binary alloys were prepared under identical conditions such as applied current density, concentration of the precursor ions, and temperature. This same result carries over to the ternary alloys, including those prepared with $C_{\text{Mn(II)}} = C_{\text{Ti(II)}}$, because the Ti content of these alloys is always smaller than the Mn content. The j_t signifies the total applied current density, and j_{Ti} , j_{Mn} , and j_{Al} express the partial current densities for Ti , Mn , and Al , respectively. From plots of $-j_{\text{Ti}}$, $-j_{\text{Mn}}$, and $-j_{\text{Al}}$ against $-j_t$ it can be seen that $-j_{\text{Al}}$ depends linearly on $-j_t$, whereas the variations of $-j_{\text{Mn}}$ and $-j_{\text{Ti}}$ with $-j_t$ show more complex behavior. $-j_{\text{Ti}}$ increases at low values of $-j_t$ but reaches a limiting value as $-j_t$ is increased. This behavior explains why the Ti content of the Al-Ti and Al-Mn-Ti alloys decreases as $-j_t$ is increased, because once $-j_{\text{Ti}}$ reaches a limiting value, it becomes a smaller fraction of $-j_t$ whereas $-j_{\text{Al}}$ becomes an increasingly larger fraction of $-j_t$ as the latter is increased. This result was noted during previous studies of the electrodeposition of Al-Ti in a similar ionic liquid, and it is based on the fact that the concen-

tration of Ti(II) in the solvent is much smaller than the concentration of the reducible Al(III) species. On the other hand, $-j_{\text{Mn}}$ increases with $-j_v$, so that the Mn content of the alloys increases with increasing $-j_t$. Furthermore, the $-j_{\text{Ti}}$ derived from the solution containing Mn(II) and Ti(II) is generally smaller than the value observed in the solution containing Ti(II), but no Mn(II), suggesting that the deposition of Ti is inhibited by Mn(II). Overall, the Al-Mn-Ti alloys rich in Ti are obtained at small $-j_v$, whereas the alloys rich in Mn are obtained at large $-j_t$. The inhibition of the deposition of the nobler component, Ti, by the less noble component, Mn, makes the codeposition of Al, Ti, and Mn an anomalous process.

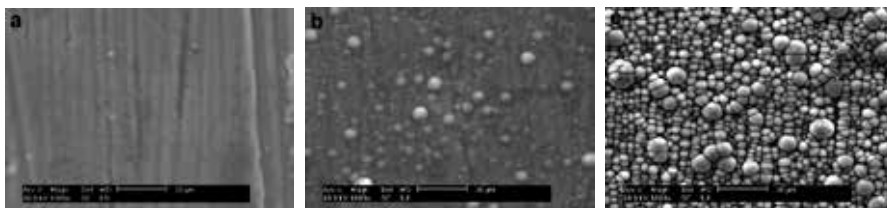


Figure 11. SEM micrographs of electrodeposited Al-Mn-Ti alloy samples at 80°C by different current density. (a) 4mAcm⁻², (b) 6mAcm⁻², (e) 8mAcm⁻²

SEM images of the Al-Mn-Ti alloy deposits reveal that the morphology varies from spherical nodules to a shining surface, depending on the current density and the Mn concentrations (see Figure 11). The EDX analysis of the Al-Mn-Ti alloy deposits indicates that Al, Mn and Ti were distributed uniformly in the deposits. XRD analysis revealed that the Al-Mn-Ti alloy deposits are an amorphous phase similar to Al-Mn deposits [36]. Pitting potential measurements of the electrodeposited Al-Mn-Ti alloys revealed that the addition of relatively modest amounts of Ti and Mn to the alloy resulted in a significant increase in corrosion resistance, compared with pure Al and the comparable binary alloy containing only titanium metal components.

3.4. Electrodeposition of Ni-Ti alloy

Ni-Ti alloys are widely used in industrial and medical devices because of their unique shape memory, excellent corrosion resistance, and good biocompatibility [39]. The electrodeposition is an effective, cheap and ready method to prepare alloy coating. However, the electrodeposition of Ni-Ti alloy is very difficult owing to the larger difference of electrode potential between Ni and Al. Recently, our group preliminarily investigated the codeposition of Ni-Ti alloy from the BMIC-EG (molar ratio 1:2) eutectic based ionic liquid containing TiCl₄ and NiCl₂. The total concentration of TiCl₄ and NiCl₂ in the bath kept 0.15 mol/L while the TiCl₄/NiCl₂ mole ratio was varied. The cyclic voltammograms recorded at a glassy carbon electrode in BMIC-EG, BMIC-EG-NiCl₂ and BMIC-EG-TiCl₄ solution are shown in Figure 12. For the BMIC-EG-NiCl₂ liquid, only one redox couple due to the cathodic deposition and anodic stripping of Ni was observed in the cyclic voltammograms. It is noted that reduction potential of BMIC-EG positively shifted in the presence of Ni(II), suggesting Ni(II) may promote the decomposition of ionic liquids. The addition of TiCl₄ produced an additional reduction wave at a potential more negative than reduction potential of Ni(II). Multiple stripping waves

appeared in the presence of TiCl_4 and relative magnitude of these stripping waves depends on the reversing potential, indicating the codeposition of Ti and Ni. The dense and compact Ni-Ti alloys could be electrodeposited by potentiostatic electrolysis at Cu substrate (see Figure 13). The XPS analysis showed that the deposits contained Ti metal in addition to Ni. The EDS analysis indicated that the Ni and Ti were distributed uniformly in the alloy. It was found that the Ti content of electrodeposited Ni-Ti alloy is increased with an increase in current density (or cathodic overpotential), suggesting that the Ti is deposited at a more negative potential as compared to pure Ni. In addition, the composition of the alloy could also be controlled by the ionic liquid bath composition.

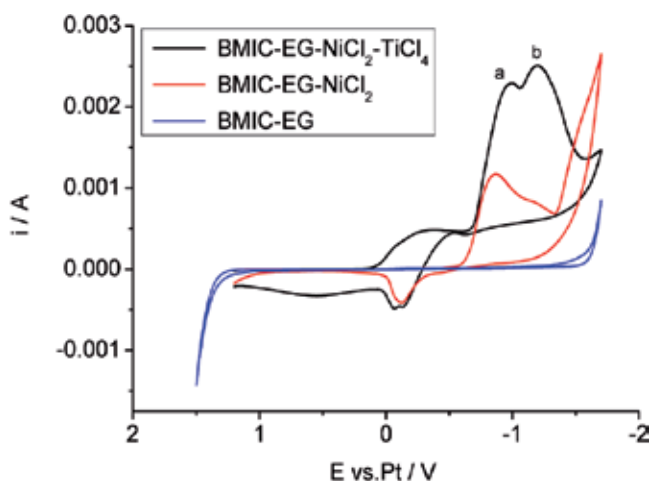


Figure 12. cyclic voltammograms recorded at a glassy carbon electrode in BMIC-EG containing NiCl_2 , TiCl_4 and a mixture of NiCl_2 and TiCl_4 at 353 K. The scan rate is 10 mV s^{-1} .

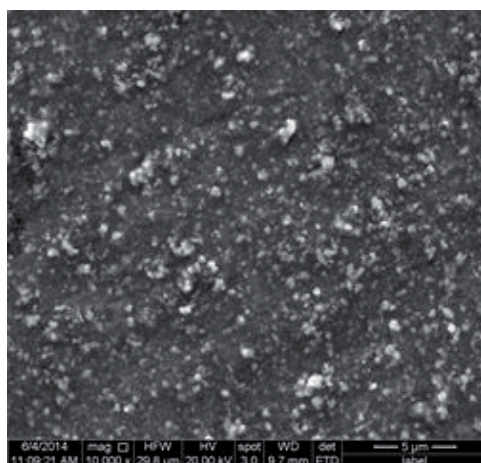


Figure 13. SEM micrograph of the deposits formed potentiostatically on Cu in BMIC-EG containing NiCl_2 and TiCl_4 at a potential of -1.3V (vs. Pt) and 353 K.

4. Conclusion

In this chapter we have summarized the findings from literature and our studies on the electrochemical preparation of titanium and its alloys in ionic liquids. It has been demonstrated that elemental titanium can not be electrodeposited from ionic liquid in the presence of chloride. The successful deposition of titanium in ionic liquids will require the development of tailored titanium precursors. In addition, it is difficult to preparation of titanium by direct electrochemical reduction of titanium dioxide in ionic liquid due to very slow reduction rate. However, it is shown that titanium could be co-deposited in ionic liquid with aluminum and transition metal, such as zinc and nickel. Some titanium alloys like Al-Ti, Zn-Ti, Al-Mn-Ti and Ni-Ti can be successfully electrodeposited from ionic liquid. In this context, ionic liquids are very promising for titanium alloys preparation. Both wide electrochemical window and high thermal stability allow these processes of Ti and its alloy electrodeposition which are impossible in aqueous or organic solvents.

Acknowledgements

The following coworkers in our laboratory should be acknowledged for their cooperation: Dr. Xiao Ying Zhang, Mr. Ya Wei Liu, Mr. Zhen Wang, Mr. Qing Wu, Mr. Cheng Hu Liu, Mr. Pi Qiang Li.

Author details

Cunying Xu* and Yixin Hua

*Address all correspondence to: xucunying@aliyun.com, xucunying@kmust.edu.cn

Department of Metallurgy, Kunming University of Science and Technology, P. R. China

References

- [1] Mukhopadhyay I, Freyland W. Electrodeposition of Ti Nanowires on Highly Oriented Pyrolytic Graphite from an Ionic Liquid at Room Temperature. *Langmuir* 2003; 19 195-1953.
- [2] Mukhopadhyay I, Aravinda CL, Borissov D, Freyland W. Electrodeposition of Ti from TiCl_4 in the Ionic Liquid 1-Methyl-3-butyl-imidazolium Bis(trifluoromethylsulfone)imide at Room Temperature: Study on Phase Formation by In Situ Electrochemical Scanning Tunneling Microscopy. *Electrochimica Acta* 2005; 50 1275-1281.

- [3] Endres F, Abedin SZ El, Saad A, Moustafa EM, Borissenko N, Price WE, Wallace GG, MacFarlane DR, Newmanc PJ, Bund A. On the Electrodeposition of Titanium in Ionic Liquids. *Phys. Chem. Chem. Phys.* 2008; 10 2189-2199.
- [4] Ding J, Wu J, MacFarlane D, Price WE, Wallace G. Induction of Titanium Reduction Using Pyrrole and Polypyrrole in the Ionic Liquid 1-Ethyl-3-methylimidazolium Bis(trifluoromethane- sulphonyl)amide, *Electrochemistry Communications* 2008; 10(2) 217-221.
- [5] Endres F, Abedin SZE, Borissenko N. Probing Lithium and Alumina Impurities in Air and Water Stable Ionic Liquids by Cyclic Voltammetry and In Situ Scanning Tunneling Microscopy. *Phys. Chem.* 2006; 220(10-11) 1377-1394.
- [6] Endres F, Abbott AP, MacFarlane DR. Electrodeposition from Ionic Liquids. In: Schubert T, Zein S, Abedin E, Abbott AP. (ed.) *Electrodeposition of Metals*. Weinheim: Wiley-VCH; 2008. p83-120.
- [7] Wartman FS, Baker DH, Nettle JR, Homme VE. Some Observations on the Kroll Process for Titanium. *J. Electrochem. Soc.* 1954; 101(10) 507-513.
- [8] Chen GZ, Fray DJ, Farthing TW. Direct Electrochemical Reduction of Titanium Dioxide to Titanium in Molten Calcium Chloride. *Nature* 2000; 407 361-363.
- [9] Ono K, Suzuki RO. A New Concept for Producing Ti Sponge: Calciothermic Reduction. *J. Met.* 2002; 54(2) 59-61.
- [10] Abiko T, Park I, Okabe TH. *Proceedings 10th World Conference on Titanium*, July 14-19 2003, Germany. Hamburg; 2003.
- [11] Okabe TH, Oda T, Mitsuda Y. Titanium Powder Production by Preform Reduction Process (PRP). *Journal of Alloys and Compounds* 2004; 364(1-2) 156-163.
- [12] Zhang XY, HuaYX, Xu CY, Zhang QB, Cong XB, Xu N. Direct Electrochemical Reduction of Titanium Dioxide in Lewis Basic AlCl_3 -1-butyl-3-methylimidazolium Ionic Liquid, *Electrochim. Acta* 2011; 56 8530-8533.
- [13] Zhang XY, Hua YX, Xu CY, Xu N, Xue H. The Electrochemical Behavior of Titanium Dioxide Film in Lewis Basic AlCl_3 -1-butyl-3-methylimidazolium Ionic Liquid, *Electrochim. Acta* 2012; 63 197-203
- [14] Xu XH, Hussey CL. The Electrochemistry of Tin in the Aluminum Chloride-1-methyl-3- ethylimidazolium Chloride Molten Salt. *J. Electrochem. Soc.* 1993; 140(3) 618-626
- [15] Schultze JW, Lohrengel MM. Stability, Reactivity and Breakdown of Passive Films. *Problems of Recent and Future Research. Electrochim. Acta* 2000; 45(15-16) 2499-2513.
- [16] Piazza S, Santamaria M, Sunseri C, Quarto DF. Recent Advances in Photocurrent Spectroscopy of Passive Films. *Electrochim. Acta* 2003; 48(9) 1105-1114

- [17] Kong DS, Wu JX. An Electrochemical Study on the Anodic Oxygen Evolution on Oxide Film Covered Titanium. *J. Electrochem. Soc.* 2008; 155(1) C32-C40
- [18] Nagai H, Takahashi T, Oikawa H. Effect of Grain Size on Creep of Ti-53.4Mol%Al Intermetallics at 1100 K. *Journal of Materials Science*, 1990; 25 629-632.
- [19] Frankel GS, Russak MA, Jahnes CV, Mirzamaani M, BrusicVA. Pitting of Sputtered Aluminum Alloy Thin Films. *J. Electrochem. Soc.* 1989; 136 1243-1244.
- [20] Ashraf Imam M, Froes FH, Dring KF. High Temperature Electrolysis of Ti and Its Alloys with a DC-ESR Unit. *Key Engineering Materials* 2010; 436, 85-91.
- [21] Tsuda T, Hussey CL, Stafford GR, Bonevich JE. Electrochemistry of Titanium and the Electrodeposition of Al-Ti Alloys in the Lewis Acidic Aluminum Chloride-1-ethyl-3-methyl- imidazolium Chloride Melt. *J. Electrochem. Soc.* 2003; 150(4) C234-C243.
- [22] Endres F, Abbott AP, MacFarlane DR. Electrodeposition from Ionic Liquids. In: Sun IW, and Chen PY. (ed.) *Electrodeposition of Alloys*. Weinheim: Wiley-VCH; 2008. P125-145.
- [23] Ali MR, Nishikata A, Tsuru T. Electrodeposition of Al-Ti Alloys from Aluminum Chloride-N-(n-Butyl) Pyridinium Chloride Room Temperature Molten Salt. *Indian Journal of Chemical Technology*, 2003; 10 14-20.
- [24] Aravinda CL, Mukhopadhyay I, Freyland W. Electrochemical in situ STM Study of Al and Ti-Al Alloy Electrodeposition on Au(111) from a Room Temperature Molten Salt Electrolyte. *Phys. Chem. Chem. Phys.* 2004; 6 5225-5231
- [25] Pradhan D, Reddy RG, Electrochemical Production of Ti-Al Alloys Using TiCl_4 - AlCl_3 - 1-butyl-3-methylimidazolium Chloride (BmimCl) Electrolytes. *Electrochim. Acta* 2009; 54 1874-1880.
- [26] Pradhan D, Reddy RG, Lahiri A. Low-Temperature Production of Ti-Al Alloys Using Ionic Liquid Electrolytes: Effect of Process Variables on Current Density, Current Efficiency, and Deposit Morphology. *Metallurgical and Materials Transactions* 2009; 40 B114-122
- [27] Liu YW, The electrodeposition of Al-Ti alloy from ionic liquid. M.E. thesis. Kunming University of Science and Technology; 2010.
- [28] Wu Z, The electrodeposition of Ti-Al alloy in ionic liquid. M.E. thesis. Kunming University of Science and Technology; 2012.
- [29] Wilcox GD, Gabe DR. Electrodeposited Zinc Alloy Coatings. *Corrosion Science* 1993; 35(5-8) 1251-1258.
- [30] Xu CY, Wu Q, Hua YX, Li J. The Electrodeposition of Zn-Ti Alloys from ZnCl_2 -urea Deep Eutectic Solvent. *J Solid State Electrochemistry* 2014; 18 2149-2155,

- [31] Brenner A. *Electrodeposition of Alloys: Principles and Practice*. New York: Academic Press; 1963.
- [32] Li PQ, Pulsed electrodeposition of Zn-Ti alloy from ionic liquid. M.E. thesis. Kunming University of Science and Technology; 2013.
- [33] Mathias MF, Chapman TW. The Composition of Electrodeposited Zinc-Nickel Alloy Coatings. *J. Electrochem. Soc.* 1987; 134 (6) 1408-1415.
- [34] Hall DE. Electrodeposited Zinc-Nickel Alloy Coatings-a Review. *Plating Surf. Finishing* 1983; 70 (11) 59-65.
- [35] Liu CH. The electrodeposition of Al-Ti alloy from ionic liquid. M.E. thesis. Kunming University of Science and Technology; 2010.
- [36] Ruan S, Schuh CA. Electrodeposited Al-Mn Alloys with Microcrystalline, Nanocrystalline, Amorphous and Nano-quasicrystalline Structures. *Acta Materialia* 2009; 57(13) 3810-3822.
- [37] Rao S. The electrodeposition of Al-Mn and Al-Mn-Ti alloy from ionic liquid. M.E. thesis. Kunming University of Science and Technology; 2013.
- [38] Karpinski ZJ, Osteryoung RA. Determination of Equilibrium Constants for the Tetrachloro- aluminate Ion Dissociation in Ambient-Temperature Ionic Liquids. *Inorg. Chem.* 1984; 23(10) 1491-1494.
- [39] Dutta RS, Madangopal K, Gadiyar HS, Banerjee S. Biocompatibility of Ni-Ti Shape Memory Alloy. *Corrosion Engineering, Science and Technology* 1993; 28(3) 217-221

High-Performance Supercapacitors Based on Ionic Liquids and a Graphene Nanostructure

Elaheh Kowsari

Additional information is available at the end of the chapter

<http://dx.doi.org/10.5772/59201>

1. Introduction

Climate change and the limited availability of fossil fuels have greatly affected the world's economy and ecology. With a fast-growing market for portable electronic devices and the development of hybrid electric vehicles, there has been an ever increasing and urgent demand for environmentally friendly high-power energy resources [1]. The production of electrochemical energy is under serious consideration as an alternative energy/power source, as long as the consumption of this energy is designed to be more sustainable and more environmentally friendly. Systems for electrochemical energy storage and conversion include batteries, fuel cells and electrochemical capacitors (ECs) [2]. Electrochemical capacitors (ECs) are known by different names such as ultracapacitors, EDLC, or super capacitors. These names were invented by different manufactures of the ECs. The trade name of the first commercial device made by Nippon Electric Company (NEC) was supercapacitors, but Pinnacle Research Institute (PRI) called the ECs ultracapacitors. Whatever the trade name of ECs, they all refer to a capacitor, which stores electrical energy in the interface between an electrolyte and a solid electrode. Because of the low capacitance values of the electrostatic capacitors, they are limited to low power applications or at most short term memory back-up supplies [3-7]. A large capacitance value and a high operating cell voltage are required for a supercapacitor to have good performance [8, 9]. Hence, the development of both novel electrode materials with increased capacitance, such as grapheme-based materials [10–16], and electrolytes with wider potential windows, such as ionic liquid electrolytes or organic electrolytes, is required to optimize the overall performance of the supercapacitor [17]. Carbide-derived carbons have been investigated for use as electrodes in EDLCs. High surface area carbon materials mainly include activated carbon [18,19], porous carbon [20], carbide-derived carbon [21], onion-like carbon, carbon aerogels [22], carbon nanotubes (CNTs) [23, 24], carbon shell [25], graphene

[26], and graphene quantum dots [27]. CNT, especially the single-walled carbon nanotube (SWCNT), has intrinsically excellent properties as an active material, such as high SSA, high conductivity, high flexibility, regular pore structures, and electrochemical stability. Woong et al. fabricated all-solid-state flexible SCs using CNTs, regular office papers, and ionic-liquid-based silica gel electrolyte [28]. Although CNTs possess high electrical conductivity and large SSA, CNT-based supercapacitors still cannot meet an acceptable performance, which is probably due to the observed contact resistance between the electrode and the current collector. Compared with traditional porous carbon materials, graphene has very high electrical conductivity, large surface area, and a profuse interlayer structure. Hence, graphene-based materials are hugely favourable for their application to EDLCs [29, 30]. The advent of new forms of carbon materials such as high quality graphene sheets (single layer to a few layers) with superior electrical properties have allowed for the development of new engineered carbons for energy storage [31-35]. Owing to their large in-plane conductivities, graphene films are expected to play a crucial role in the development of electrodes for a variety of energy applications such as photovoltaics [36-39] and supercapacitors [40]. These materials have recently been used in supercapacitor devices to replace conventional carbon electrodes and have shown very good performance [41-46].

Graphene has been found to exhibit exceptionally high thermal conductivity, electrical conductivity and strength. [47-49]

Another outstanding characteristic of graphene is its exceptionally high specific surface area of up to $2675 \text{ m}^2/\text{g}$. Most significantly, the intrinsic capacitance of graphene was recently found to be $21 \text{ } \mu\text{F}/\text{cm}^2$, [50] which sets the upper limit of EDL capacitance for all carbon-based materials. This study asserts that graphene is the ideal carbon electrode material for EDL supercapacitors because it is capable of storing an EDL capacitance value of up to 550 F/g , provided the entire $2675 \text{ m}^2/\text{g}$ is fully utilized. Another advantage of graphene in a supercapacitor electrode is the notion that both major surfaces of a graphene sheet are exterior surfaces readily accessible by electrolyte [51]. For EDLCs, ionic liquids (ILs) [52], room temperature molten salts composed of organic cation (and anion) are widely considered the electrolyte of the future. Ionic liquids are solventless electrolytes with many properties that make them attractive for electrochemical energy storage: high chemical and thermal stability, negligible vapour pressure, a broad electrochemical stability potential window and an immense parameter space in terms of ion selection and resulting properties. The most popular ionic liquids are based on imidazolium and several salts with the 1-ethyl-3-methyl-imidazolium cation (EMI), which displays a cathodic stability of -1.8 V vs. NHE, and with such anions as BF_4 , PF_6 , $(\text{CF}_3\text{SO}_2)_2\text{N}$, CF_3SO_3 , which in turn divergently affect the limit of the anodic window, the melting point and hence the conductivity of the ionic liquids were developed [53-55]. The compatibility is between graphene sheets and ionic liquids, which are significantly larger than the molecular sizes of aqueous and other organic liquid electrolytes.

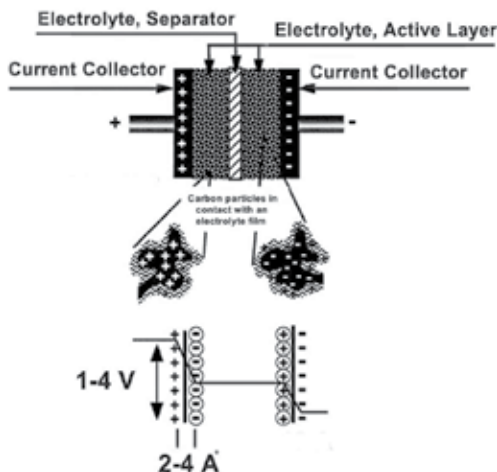
In this chapter, the efficacy of ionic liquids in supercapacitors and the research lines for the design of advanced electrode materials and configurations for graphene and IL-based high-performance supercapacitors are reviewed and discussed.

2. Discussion

2.1. Operating principles of double-layer capacitors

2.1.1. Device configuration

An ES is a charge-storage device similar to batteries in design and manufacturing. As shown in Fig. 1, electrochemical capacitors (supercapacitors) consist of two electrodes separated by an ion permeable membrane (separator), and an electrolyte connecting both electrodes electrically. By applying a voltage to the capacitor, an electric double layer is formed at both electrodes, which has a positive or negative layer of ions deposited in a mirror image on the opposite electrode [56, 57]. The principles of a single-cell double-layer capacitor and an illustration of the potential drop at the electrode/electrolyte interface are shown in figure1.



[Reprinted from [57] Kotz K, Carlen M. Principles and applications of electrochemical capacitors, *Electrochim. Acta*. 2000, 45, 2483-2498, Copyright (2000), with permission from Elsevier].

Figure 1. Principles of a single-cell double-layer capacitor and illustration of the potential drop at the electrode/electrolyte interface.

2.1.2. Capacitance distribution

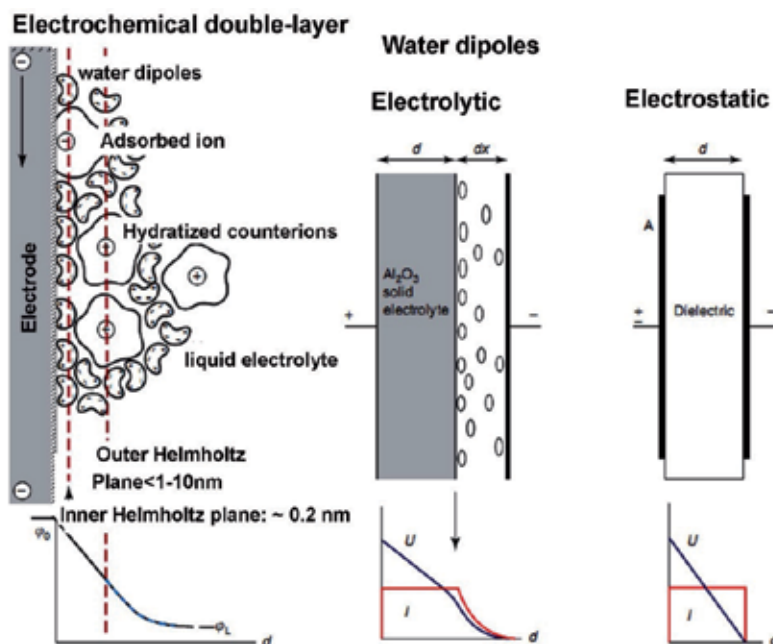
The two electrodes form a series circuit of two individual capacitors C_1 and C_2 . The total capacitance C_{total} is given by equation 1:

$$C_{total} = \frac{C_1.C_2}{C_1 + C_2} \quad (1)$$

Supercapacitors may have either symmetric or asymmetric electrodes. Symmetry implies that both electrodes have the same capacitance value. If $C_1 = C_2$, then $C_{\text{total}} = 0.5 C_1$. For symmetric capacitors the total capacitance value equals half the value of a single electrode. For asymmetric capacitors, one of the electrodes typically has a higher capacitance value than the other. If $C_1 \gg C_2$, then $C_{\text{total}} \approx C_2$. Thus, with asymmetric electrodes the total capacitance may be approximately equal to the smaller electrode [56, 57].

Ultracapacitors based on electrochemical double-layer capacitance (EDLC) are electrical energy storage devices that store and release energy by nanoscopic charge separation at the electrochemical interface between an electrode and an electrolyte. As the energy stored is inversely proportional to the thickness of the double layer, these capacitors have an extremely high energy density compared to conventional dielectric capacitors. This simple Helmholtz EDL model was further modified by Gouy and Chapman [58, 59] with the consideration of a continuous distribution of electrolyte ions (both cations and anions) in the electrolyte solution, driven by thermal motion, which is referred to as the diffuse layer. However, the Gouy–Chapman model leads to an overestimation of the EDL capacitance. The capacitance of two separated arrays of charges increases inversely with their separation distance, hence a very large capacitance value would arise in the case of point charge ions close to the electrode surface. Later, Stern [60] combined the Helmholtz model with the Gouy–Chapman model to explicitly recognize two regions of ion distribution, the inner region called the compact layer or the Stern layer and the diffuse layer [61, 62]. The structure of the electrolytic double layer and absorbed intermediates in electrode processes in aqueous solutions is shown in figure 2.

Research efforts have focused on increasing the energy and power densities of supercapacitors by increasing the surface area of porous electrodes and tailoring their morphology or pore size distribution [63]. Wang et al. presented general mathematical formulations for simulating electric double-layer capacitors (EDLCs) with three-dimensional ordered structures. A general set of boundary conditions was derived in order to account for the Stern layer without simulating it in the computational domain. These boundary conditions were valid for planar, cylindrical, and spherical electrode particles or pores. They conducted the simulations of EDLCs with as complex geometries as possible while rigorously accounting for both the Stern and diffuse layers. The model also simultaneously accounted not only for 3D electrode morphology but also for finite ion size and field-dependent electrolyte dielectric permittivity. It was used to faithfully simulate the complex structure of an EDLC electrode consisting of ordered bimodal mesoporous carbon, featuring both macropores and mesopores. Areal and gravimetric capacitances were predicted based on non-solvated and solvated ion diameters. These two cases set the upper and lower bounds for the predicted capacitances. The capacitances predicted using non-solvated ion diameter were found to be in good agreement with experimental data reported in the literature. All surfaces contributed to the overall capacitance of the EDLCs. The gravimetric capacitance of different bimodal carbons increased linearly with increasing specific surface area corresponding to constant areal capacitance.



[Reprinted from [62] P. Kurzweil Capacitors | Electrochemical Double-Layer Capacitors, Reference Module in Chemistry, Molecular Sciences and Chemical Engineering Encyclopedia of Electrochemical Power Sources, 2009, Pages 607–633, Copyright (2009), with permission from Elsevier].

Figure 2. Structure of the electrolytic double layer and absorbed intermediates in electrode processes in aqueous solutions. Below: potential profile through the rigid Helmholtz layer and the diffuse layer. Right: comparison of electrolytic and electrostatic capacitors.

2.2. State-of-the-art of constituent materials of a symmetrical carbon/carbon supercapacitor

2.2.1. Electrode

Static storage mechanisms in EDLCs efficiently store charges upon the electrodes at high rates. Unlike rechargeable batteries, ES involves no chemical breakdown or redeposition of electrode materials during the operation. This lowers the risk of electrode phase changes during operation and enables long electrode cycle lives. The important requirements for the optimization of electrode materials include: minimal irreversible redox processes, high specific surface area, thermodynamic stability for a large potential window of operation, ability to control morphology, pore size, particle size, and material distribution, surface wettability, and high electrical conductivity.

The most suitable carbon structures used as active material for EDLC electrodes are: activated carbon, carbide derived carbon, onion-like carbons, carbon nanotubes and graphene. Carbon-based electrodes are of great interest as they are light-weight, of moderate cost, abundant, easy to process, possess high electronic conductivity and high specific surface area (high charge storage). A large surface area can be obtained owing to their versatility which enables the

different nanostructures to be produced, providing a wide variety of physical properties, to tailor for different types of applications.

2.2.1.1. Carbon materials for EDLC supercapacitors¹

Activated Carbon (AC)

Activated carbon (AC) was the first material chosen for the EDLC electrodes. It has an electrical conductivity of 1,250 to 3,000 S/m, approximately 0.003% of metallic conductivity, but sufficient for supercapacitors [64,65].

Solid activated carbon, also called consolidated amorphous carbon (CAC), is the most used electrode material for supercapacitors and may be cheaper than other carbon derivatives. It is produced from activated carbon powder pressed into the desired shape, forming a block with a wide distribution of pore sizes. An electrode with a surface area of about 1000 m²/g results in a typical double-layer capacitance of about 10 μF/cm² and a specific capacitance of 100 F/g. Activated carbon electrodes exhibit a predominantly static double-layer capacitance, but also exhibit pseudocapacitance. Pores with diameters <2 nm are accessible only to de-solvated ions and enable faradaic reactions [66].

Carbide-derived Carbon (CDC)

Carbide-derived carbon (CDC), also known as tunable nanoporous carbon, is the common term for carbon materials derived from carbide precursors, such as binary (e.g., SiC, TiC), or ternary carbides, also known as max phases (e.g., Ti₂AlC, Ti₃SiC₂) [67-71]. CDCs have also been derived from polymer-derived ceramics such as Si-O-C or Ti-C, and carbonitrides, such as Si-N-C [72-74]. CDCs can occur in various structures, ranging from amorphous to crystalline carbon, from sp²- to sp³-bonded, and from highly porous to fully dense. Carbide-derived carbons are used as an active material in electrodes for electric double-layer capacitors which have become commonly known as supercapacitors or ultracapacitors. This is because of their good electrical conductivity combined with high surface area [75], large micropore volume [76] and pore size control [77] that enable them to match the porosity metrics of the porous carbon electrode to a certain electrolyte [78].

Onion-like carbons

Onion-like carbons are 0-dimensional carbon nanomaterials yielding a non-porous but highly conductive carbon network. They provide a SSA of up to 600 m² g⁻¹ which is fully accessible for ions. The combination of high conductivity and ion accessibility yield a high specific power. However, due to the small SSA the specific capacitance is limited to approximately 30 F g⁻¹ [79].

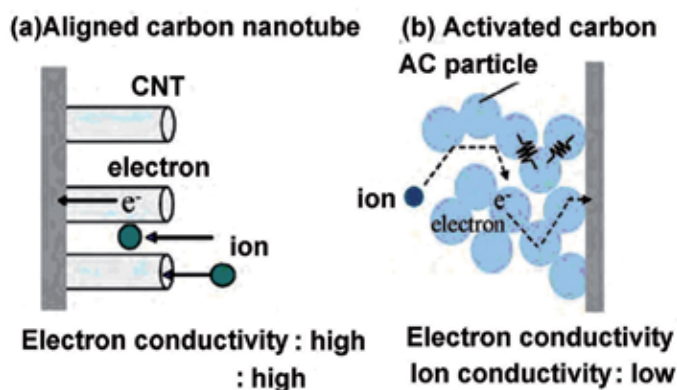
Carbon nanotubes

Carbon nanotubes (CNTs) are expected to also be attractive for capacitor electrode materials. Their important and promising characteristics as capacitor electrode materials include not only on their large area of exposed surface and different storage spaces for electrolyte ions, but also

¹ The content has been taken from Wikipedia and [80]

their high electrical conductivity. Comparison on conducting paths for electron and electrolyte ion is in an aligned carbon nanotubes and granular activated carbon.

Irreversible electrochemical reactions, such as electrolyte decomposition, easily occur at a high potential, which prevent the use of the capacitor at high voltage. On such an ideal surface of CNTs, therefore, a large capacitance of EDL is expected to be accompanied by a wide potential window. However, most of the CNTs are known to be bundled with each other due to the van der Waals force, where only the outermost tubes in a bundle are exposed to the electrolyte and so-called bundle spaces among tubes are difficult to use for the formation of EDL. Consequently, the debundling of most of the CNTs is required in order to make all the surfaces of the tubes available for EDL formation. The inner surface of nanotubes is also useful for the access of electrolyte ions if suitable openings are formed. An interlayer space in the wall of multi-walled nanotubes can be intercalated by an electrolyte ion such as Li^+ . Therefore, the intercalation might be possible also as a faradaic reaction to give a pseudo-capacitance. However, it must be pointed out that excess enlargement of the interlayer spaces by intercalation will cause some degradation of the electrode which shortens the cycle life of the capacitor. In Fig. 3, the conducting paths for electrolyte ions and electrons in the aligned CNTs are schematically compared with activated carbon (AC) [80].



[Reprinted from [80] Inagaki M, Konno H, Tanaike O. Carbon materials for electrochemical capacitors. *Journal of Power Sources*. 2010, 195, 7880–7903, Copyright (2010), with permission from Elsevier].

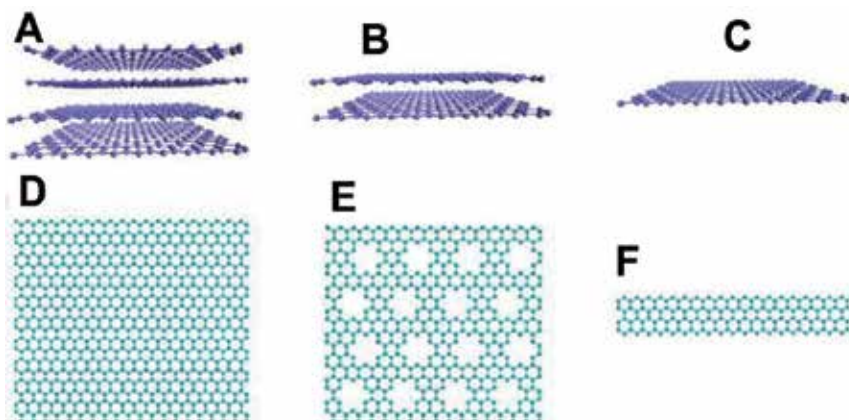
Figure 3. Comparison of conducting paths for electron and electrolyte ion in an aligned carbon nanotubes and granular activated carbon.

Graphene

Overview of the properties of graphene

Graphene is a two-dimensional material consisting of a single layer of carbon atoms arranged in a honeycomb. It has been the subject of considerable research activities owing to its unusual and intriguing mechanical, thermal, electrical and optical properties [81–85]. Generally, a material's electrical and optical properties are closely related to its size and dimensions. This

is particularly reflected in the dimension control of graphene, both vertically and laterally [86] (figure 4).



[Reprinted from [86] Sun, D. K. James, J.M. Tour, Graphene Chemistry: Synthesis and Manipulation, *J. Phys. Chem. Lett.* 2011, 2, 2425–2432., Copyright (2011), with permission from ACS].

Figure 4. Manipulation of the geometry of graphene. Vertical control of graphene from (A) few-layer graphene to (B) bilayer graphene to (C) monolayer graphene. Lateral control of graphene from (D) plane sheet to (E) graphene mesh to (F) graphene ribbons.

With the advent of atomically thin and flat layers of graphene, new designs for thin film energy storage devices with good performance have become possible [87].

2.3. Utilization of graphene for EDLCs

One graphene-based supercapacitor uses curved graphene sheets that do not stack face-to-face, forming mesopores that are accessible to and wettable by environmentally friendly ionic electrolytes at voltages up to 4 V. They have a specific energy density of 85.6 Wh/kg (308 kJ/kg) at room temperature equalling that of a conventional nickel metal hydride battery, but with a power density 100-1000 times greater [88, 89].

The two-dimensional structure of graphene improves its charging and discharging. Charge carriers in vertically oriented sheets can quickly migrate into or out of the deeper structures of the electrode, thus increasing currents. Such capacitors may be suitable for 100/120 Hz filter applications, which are unreachable by supercapacitors using other carbons [90].

2.4. Graphene-based electrodes for EDLCs

The first utilization of graphene as an active material for an EDLC electrode was reported by Vivekchand et al. in early 2008 [91]. In order to develop energy storage devices with high power and energy densities, electrodes should hold well-defined pathways for efficient ionic and electronic transport. Choi et al. [92] demonstrate high-performance supercapacitors by building a three-dimensional (3D) macroporous structure that consists of chemically modified

graphene (CMG). These 3D macroporous electrodes, namely, embossed-CMG (e-CMG) films, were fabricated by using polystyrene colloidal particles as a sacrificial template. Furthermore, for a further capacitance boost, a thin layer of MnO₂ was additionally deposited onto e-CMG. The porous graphene structure with a large surface area facilitates fast ionic transport within the electrode while preserving decent electronic conductivity and thus endows MnO₂/e-CMG composite electrodes with excellent electrochemical properties, such as a specific capacitance of 389 F/g at 1 A/g and 97.7% capacitance retention upon a current increase to 35 A/g. Moreover, when the MnO₂/e-CMG composite electrode was asymmetrically assembled with an e-CMG electrode, the assembled full cell shows remarkable cell performance: an energy density of 44 Wh/kg, a power density of 25 kW/kg and an excellent cycle life.

Yoo et al. [93] reported an “in-plane” fabrication approach for ultrathin supercapacitors based on electrodes comprised of pristine graphene and multilayer reduced graphene oxide. The in-plane design is straightforward to implement and efficiently exploits the surface of each graphene layer for energy storage. The open architecture and the effect of graphene edges enable even the thinnest of devices, made from as-grown 1-2 graphene layers, to reach specific capacities up to 80 μFcm⁻², while much higher (394 μFcm⁻²) specific capacities are observed in multilayer reduced graphene oxide electrodes. The performances of devices with pristine as well as thicker graphene-based structures are examined using a combination of experiments and model calculations. The demonstrated all solid-state supercapacitors provide a prototype for a broad range of thin-film-based energy storage devices. Table 1 shows a performance evaluation and comparison of the G and RMGO 2D “In-plane” supercapacitors.

mater	method	device properties ^a				electrode properties ^b			
		N	T (nm)	capacitance (μF)	mass (μg)	geometrical area (cm ²)	specific capacity		
							F g ^{-1c}	μF cm ^{-2d}	μF cm ^{-2e}
G	CVD	1		3.333		0.1 × 0.835	80	80	
RMGO	LBL	2 ^f	10	35	0.283	0.085 × 2.1	247	394	

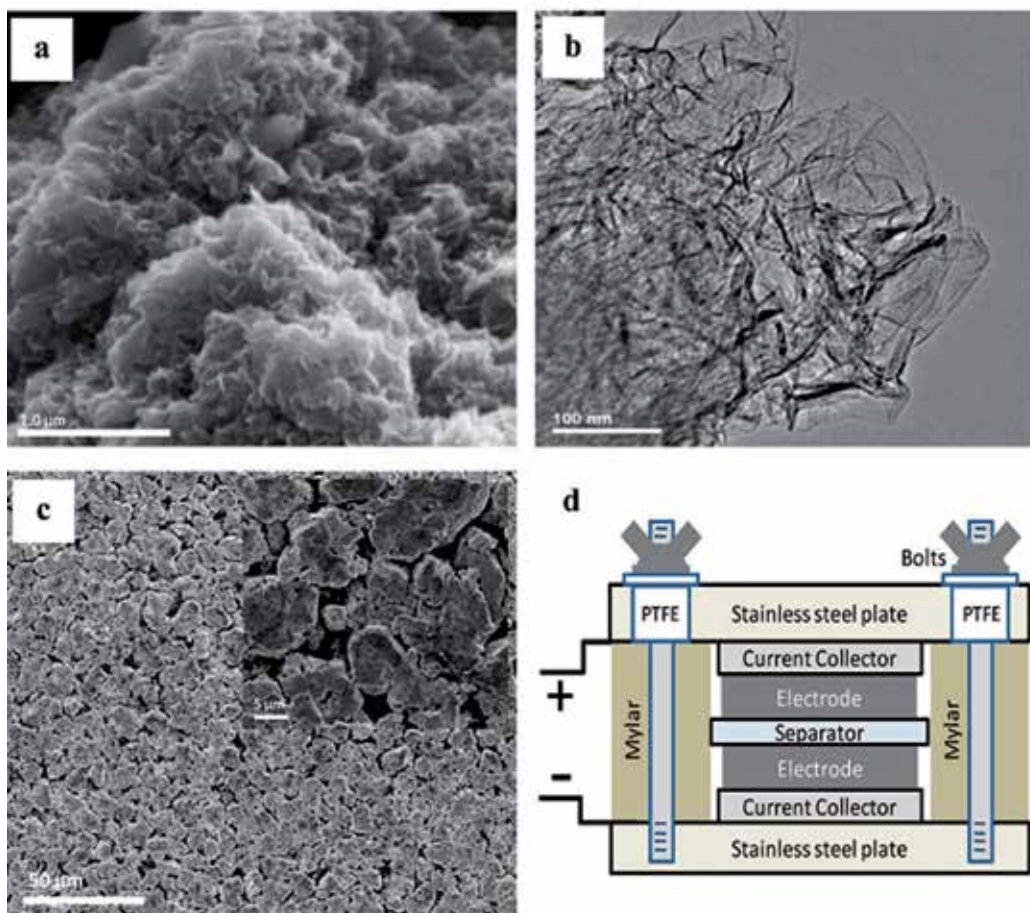
^a N = number of layers; T = thickness of the electrode. The capacitance values are reported for the best performance obtained using the CD curves with current density of 281 n Acm⁻² for RMGO and 630 mAcm⁻² for G. ^b Electrode capacitance converted from the device capacitance assuming asymmetrical capacitor. ^c Normalized by the electrode mass. ^d Normalized by one electrode’s geometrical area. ^e Normalized by one electrode’s interface area. ^f Calculated using the mass, the geometrical area, and the specific area of one side of graphene (1310 m² g⁻¹).

[Reprinted from [93] Yoo J J, Balakrishnan K, Huang J, Meunier V, Sumpter B G, Srivastava A, Conway M, Mohana Reddy AL, Yu J, Vajtai R, Ajayan PM. Ultrathin Planar Graphene Supercapacitors, Nano Lett. 2011, 11, 1423–1427, Copyright (2011), with permission from ACS].

Table 1. Performance Evaluation and Comparison of the G and RMGO 2D “In-Plane” Supercapacitors

Ruoff group [94] has pioneered a new carbon material that we call chemically modified graphene (CMG). CMG materials are made from one-atom thick sheets of carbon, functionalized as needed, and here they demonstrate their performance in an ultracapacitor cell. Specific capacitances of 135 and 99 F/g in aqueous and organic electrolytes, respectively, have been measured. In addition, high electrical conductivity gives these materials consistently good

performance over a wide range of voltage scan rates. These encouraging results illustrate the exciting potential for high performance, electrical energy storage devices based on this new class of carbon material. Figure 4 shows a SEM image of a CMG particle surface, TEM image showing individual graphene sheets extending from the CMG particle surface, low and high (inset) magnification SEM images of CMG particle electrode surfaces, and the schematic of a test cell assembly. Figure 5d also shows a schematic of the two-electrode ultracapacitor test cell and fixture assembly. CMG-based ultracapacitor cells were tested with three different electrolytes commonly used in commercial EDLCs.



[Reprinted from [94] Stoller M D, Park S, Zhu Y, An J, Ruoff R S, Graphene-Based Ultracapacitors. *Nano Lett.*,2008; 8, 3498-3502, Copyright (2008), with permission from ACS]

Figure 5. (a) SEM image of CMG particle surface, (b) TEM image showing individual graphene sheets extending from CMG particle surface, (c) low and high (inset) magnification SEM images of CMG particle electrode surface, and (d) schematic of a test cell assembly.

A supercapacitor with graphene-based electrodes was found to exhibit a specific energy density of 85.6 Wh/kg at room temperature and 136 Wh/kg at 80 °C (all based on the total electrode weight), measured at a current density of 1 A/g by Liu et al. [95]. These energy density values are comparable to those of the Ni metal hydride battery, but the supercapacitor can be charged or discharged in seconds or minutes. The key to success was the ability to make full utilization of the highest intrinsic surface capacitance and the specific surface area of single-layer graphene by preparing curved graphene sheets that will not restack face-to-face. The curved morphology enables the formation of mesopores accessible to and wettable by environmentally benign ionic liquids capable of operating at a voltage >4V. Highly corrugated graphene sheets (HCGS) were prepared by a rapid, low-cost and scalable approach through the thermal reduction of graphite oxide at 900 °C followed by rapid cooling using liquid nitrogen by Yan et al. [96]. The wrinkling of the graphene sheets can significantly prevent them from agglomerating and restacking against one another face to face and thus increase the electrolyte-accessible surface area. The maximum specific capacitance of 349 F g⁻¹ at 2mV s⁻¹ is obtained for the HCGS electrode in a 6 M KOH aqueous solution. Additionally, the electrode shows excellent electrochemical stability along with an approximately 8.0% increase of the initial specific capacitance after 5000 cycle tests. These features make the present HCGS material a quite promising alternative for the next generation of high-performance supercapacitors.

2.5. The electrolytes

The performance of a supercapacitor is not only dependent on the electrode materials, but is also strongly affected by the electrolytes employed. A high cell operating voltage provides both high energy density and power density, but is limited by the stability of the electrolyte in the applied potential. The most recent supercapacitors available in the market use electrolytes based on aprotic solvents, typically acetonitrile or carbonate-based solvents (i.e., propylene carbonate) [97].

2.5.1. Electrolyte solution²

Most of the commercial EDLCs use non-aqueous electrolyte solutions to achieve a high terminal voltage, V , because the capacitor energy, E , and the maximum power, P_{\max} are given by:

$$E = CV^2/2 \text{ and } P_{\max} = V^2/4R$$

where C is the cell capacitance in F and R is the internal resistance in Ω . The EDLCs that use non-aqueous electrolyte solutions dominate the market for capacitors focusing on energy storage, but those that use aqueous electrolyte solutions are also marketed. Aqueous solutions are potentially beneficial to large installations for the storage of surplus power and unsteady

² The content has been taken from [80]

electricity generated by natural energy resources, because of their low cost, high safety, long lifetime and low internal resistance. Representative electrolytes and solvents (with abbreviations) are listed in Table 1, where some of their properties are also indicated [80, 98].

In EDLCs, the sizes of the cation and anion of the electrolyte are important factors in relation to the surface area, effective for the adsorption of the ions, of the electrode carbons. In the case of non-aqueous electrolyte solutions numerous combinations of electrolytes, both organic and inorganic, with solvents are possible. The solvent itself also affects the capacitance [99,100] and one combination is not always optimum for all carbon materials. When the electrolytes containing lithium ions were used in EDLC, it was shown that the intercalation of Li^+ ions occurred together with its adsorption onto the surface of the carbon electrode [101], which is also used in hybrid capacitors, as will be described below [80]. Table 2 shows electrolytes and solvents that are often used.

Electrolytes	Ion size (nm)		Melting point (°C)	Viscosity (Pas ⁻¹)	Dielectric constant, ϵ
	Cation	Anion			
Organic electrolytes					
(C ₂ H ₅) ₄ N-BF ₄ (TEA ⁺ BF ₄ ⁻)	0.686	0.458			
(C ₂ H ₅) ₂ (CH ₃) ₂ N-BF ₄ (TEMA ⁺ BF ₄ ⁻)	0.654	0.458			
(C ₂ H ₅) ₄ P-BF ₄ (TEP ⁺ BF ₄ ⁻)		0.458			
(C ₄ H ₉) ₄ N-BF ₄ (TBA ⁺ BF ₄ ⁻)	0.830	0.458			
(C ₆ H ₁₃) ₄ N-BF ₄ (THA ⁺ BF ₄ ⁻)	0.96	0.458			
(C ₂ H ₅) ₄ N-CF ₃ SO ₃	0.686	0.540			
(C ₂ H ₅) ₄ N-(CF ₃ SO ₂) ₂ N (TEA ⁺ TFSI ⁻)	0.68	0.650			
Inorganic electrolytes					
H ₂ SO ₄		0.533			
KOH	0.26 ^a				
Na ₂ SO ₄	0.36 ^a	0.533			
NaCl	0.36 ^a				
Li-PF ₆	0.152 ^b	0.508			
Li-ClO ₄	0.152 ^b	0.474			
Solvents					
Acetonitrile (AN)	-43.8		0.369	36.64	
γ -Butyrolactone (GBL)	-43.3		1.72	39.0	
Dimethyl ketone (DMK)	-94.8		0.306	21.01	
Propylene carbonate (PC)	-48.8		2.513	66.14	
Water					

^a Stokes diameter of hydrated ions.

^b The diameter in PC, depending strongly on the solvent used.

[Reprinted from [80] Inagaki M, Konno H, Tanaike O. Carbon materials for electrochemical capacitors. Journal of Power Sources. 2010, 195, 7880–7903, Copyright (2010), with permission from Elsevier].

Table 2. Electrolytes and solvents that are often used.

Ionic liquid (IL)-based electrolytes containing molecular solvents were also shown to be attractive for extreme temperature applications in electric double-layer capacitors (EDLCs).

2.5.1.1. Supercapacitors: Ionic liquid electrolytes³

Certain unique properties of these environmentally friendly ionic liquids, including high ionic conductivity (up to 10^{-2} Scm^{-1}), large liquid phase range (-100 – 400 °C), wide electrochemical window (4 – 6V), non-volatility, non-flammability, and non-toxicity, have made them an excellent electrolyte for electrochemical energy. The ionic liquids mainly studied for supercapacitor application are imidazolium, pyrrolidinium and asymmetric aliphatic quaternary ammonium salts of anions such as tetrafluoroborate (BF_4), trifluoromethanesulfonate (Tf), bis(trifluoromethanesulfonyl)imide (TFSI) (bis(fluorosulfonyl)imide (FSI), and hexafluorophosphate (PF_6), and all feature an ESW wider than that of the conventional organic electrolytes at RT. The ESW is defined as the potential range limited by the cathodic and anodic stability potentials evaluated on glassy carbon or platinum smooth electrodes. Figure 6 shows conductivity and ESW data at RT of some ionic liquids based on 1-ethyl-3-methylimidazolium (EMI), 1-butyl-3-methylimidazolium (BMIM), N-diethyl- N-methyl(2-methoxyethyl)ammonium (DEME), N-butyl-N-methyl-pyrrolidinium (PYR_{14}), N-methyl- N-propyl-pyrrolidinium (PYR_{13}), and N-methoxyethyl- N-methylpyrrolidinium cations with different anions [102].

The interface models developed for high-temperature molten salts are not completely appropriate for ionic liquids, mainly because of the weaker cation–anion interactions in ionic liquids than in molten salts. On the contrary, the absence of solvents in ionic liquids implies that the double layer cannot be described by the Helmholtz model developed for conventional concentrated electrolyte solutions, as depicted in Figure 7. In such solutions, the solvent molecules in the inner Helmholtz plane (IHP) separate electrode surface charges and electrolyte counter ions located in the outer Helmholtz plane (OHP) by a distance l , so that the solvent molecular size, rather than ion size, and solvent dielectric constant (ϵ) significantly affect electrode capacitance (C_e), which is given by:

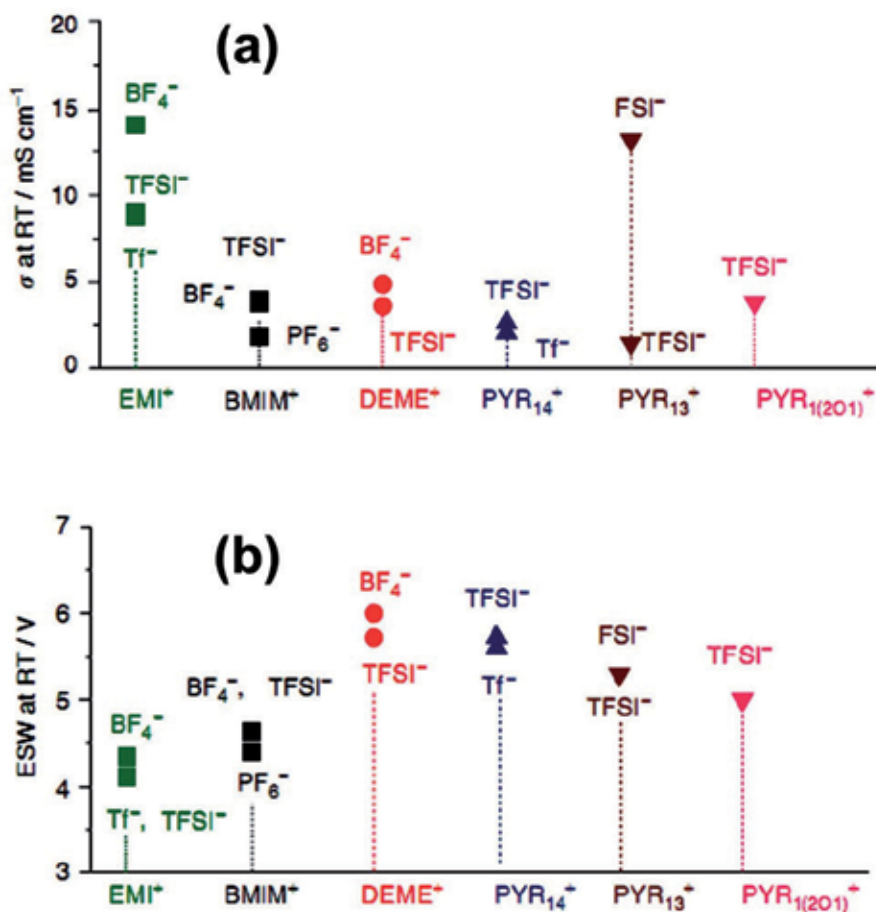
$$C_e = \kappa^0 \epsilon A / l \quad (2)$$

where $\kappa^0 = 8.85 \times 10^{-12} \text{ Fm}^{-1}$ and A is the electrode surface area. In the case of solvent-free ILs, the electrified electrode surface comes up against the ionic liquid counter ions located in the IHP. Thus, the relation between C_e and A depends on the ionic liquid ion chemistry and structure at the electrode–IL interface. The size, orientation under electric field and polarizability of ionic liquids directly affect thickness, the dielectric constant of the double layer, and the capacitive response of the electrodes [102].

2.5.1.2. Ionic liquids as electrolyte for activated carbon, carbon nanotubes and associated composite supercapacitors

Before protic ionic liquid as an electrolyte for high-density electrochemical double-layer capacitors with activated carbon electrode material prior can be implemented for grid-scale applications of the energy storage devices, there remain several key issues to address including

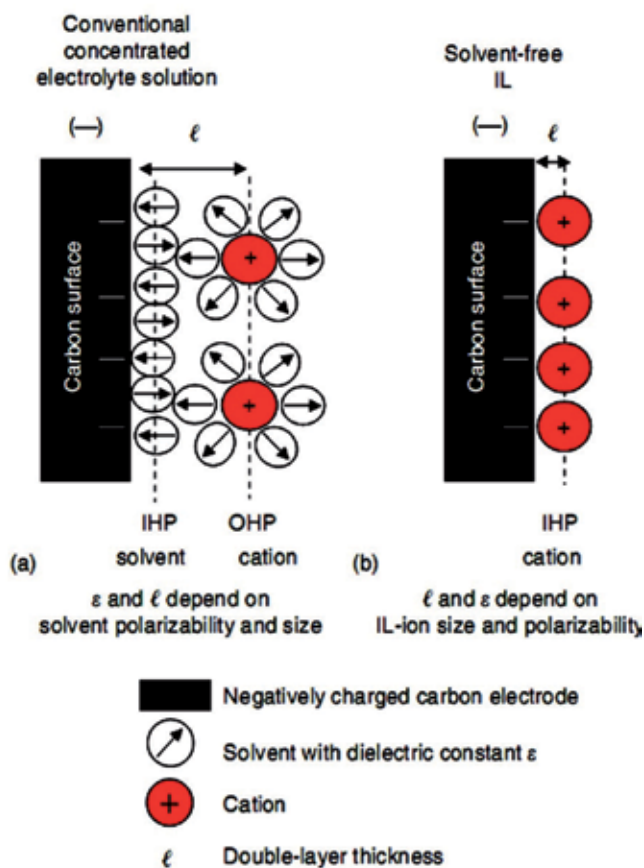
³ The content has been taken from [102]



[Reprinted from [102] Mastragostino M, Soavi F. *Electrochemical Capacitors: Ionic Liquid Electrolytes*, Reference Module in Chemistry, Molecular Sciences and Chemical Engineering, Elsevier, 2009, Pages 649–657, Copyright (2009), with permission from Elsevier].

Figure 6. (a) Conductivity (σ) and (b) electrochemical stability window (ESW) data at room temperature of ILs based on 1-ethyl-3-methylimidazolium (EMI), 1-butyl-3-methylimidazolium (BMIM), N-diethyl-N-methyl(2-methoxyethyl)ammonium (DEME), N-butyl-N-methyl-pyrrolidinium (PYR₁₄), N-methyl-N-propyl-pyrrolidinium (PYR₁₃), and N-methoxyethyl-N-methylpyrrolidinium cations with different anions.

the development of low-cost, high-performance materials and electrolytes which are environmentally friendly and compatible with low-temperature and large-scale processing. Anouti et al. [103] reported the preparation, characterization and comparative application of two protic ionic liquids namely, diisopropylethylammonium methanesulfonate, [DIPEA][MeSO₃], and pyrrolidinium methanesulfonate, [Pyrr][MeSO₃], in a mixture with water as an electrolyte for supercapacitor applications. Different electrochemical measurements like cyclic voltammetry (CV), electrochemical impedance spectroscopy (EIS), and galvanostatic charge–discharge were conducted to study the performance of these aqueous solutions as supercapacitors with an activated carbon electrode.

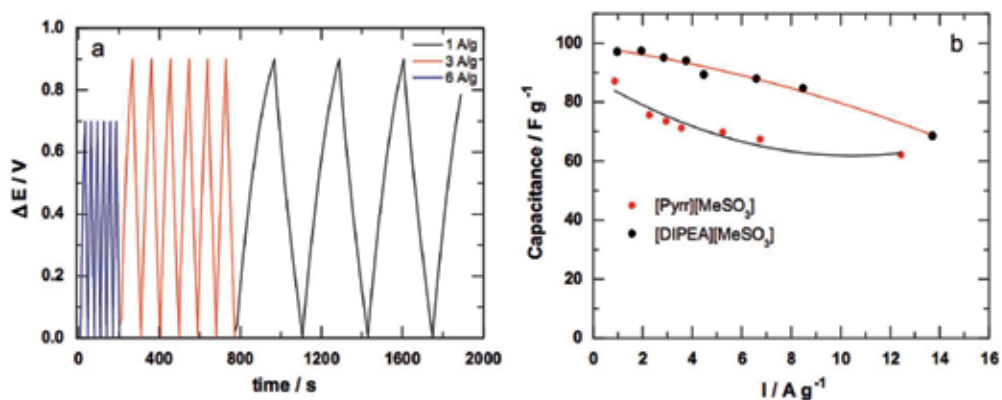


[Reprinted from [102] Mastragostino M, Soavi F. *Electrochemical Capacitors: Ionic Liquid Electrolytes*, Reference Module in Chemistry, Molecular Sciences and Chemical Engineering, Elsevier, 2009, Pages 649–657, Copyright (2009), with permission from Elsevier].

Figure 7. Schematic representation of the double layer at the negatively charged carbon electrode–electrolyte interface in (a) conventional electrolyte solution and (b) solvent-free ionic liquid electrolyte.

From this work, good specific capacitances of up to 102 F g^{-1} have been observed even at high-rate cyclability, as well as an increase of the specific power close to 13.9 kW kg^{-1} at a high current density of 15 A g^{-1} . Fig. 7 shows galvanostatic charge/discharge and capacitance as a function of current density for DIPEA methanesulfonate in water ($w = 0.707$) and pyrrolidinium methanesulfonate in water ($w = 0.557$). Figure 8 shows galvanostatic charge/discharge and capacitance as a function of the current density for DIPEA of methanesulfonate in water and pyrrolidinium methanesulfonate in water.

Balducci et al. [104] present results on the electrochemical and cycling characterizations of a supercapacitor cell using a microporous activated carbon as the active material and N-butyl-N-methylpyrrolidinium bis(trifluoromethanesulfonyl)imide (PYR14TFSI) ionic liquid as the electrolyte. The microporous activated carbon exhibited a specific capacitance of 60 F g^{-1}



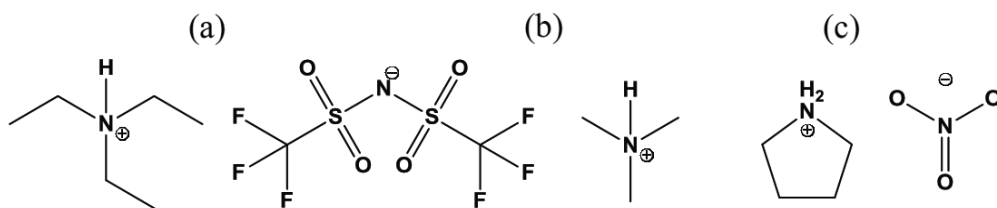
[Reprinted from [103] Anouti M, Couadou E, Timperman L, Galiano H. Protic ionic liquid as electrolyte for high-densities electrochemical double-layer capacitors with activated carbon electrode material. *Electrochimica Acta*. 2012, 64, 110–117, Copyright (2012), with permission from Elsevier].

Figure 8. Galvanostatic charge/discharge (a) and capacitance (b) as a function of current density for DIPEA methanesulfonate in water ($w = 0.707$) and pyrrolidinium methanesulfonate in water ($w = 0.557$).

measured from the three-electrode cyclic voltammetry experiments at a 20mVs^{-1} scan rate, with a maximum operating potential range of 4.5V at $60\text{ }^{\circ}\text{C}$. A coin cell assembled with this microporous activated carbon and $\text{PYR}_{14}\text{TFSI}$ as the electrolyte were cycled for 40,000 cycles without any change in cell resistance (9cm^2), at a voltage up to 3.5V at $60\text{ }^{\circ}\text{C}$, demonstrating a high cycling stability as well as a high stable specific capacitance in this ionic liquid electrolyte. These high performances now make this type of supercapacitor suitable for high temperature applications ($\geq 60\text{ }^{\circ}\text{C}$). Protic ionic liquids (PILs) have been proposed as novel electrolytes for supercapacitors by Brandta et al. [105]. Nevertheless, so far the long term cycling stability of PIL-based supercapacitors has never been investigated in detail. Since high cycling stability is essential for such devices, a study about this aspect therefore appears to be of importance for understanding the advantages and the limits of PIL-based systems. In this work we showed that using protic ionic liquids as electrolytes, it is possible to implement electrochemical double-layer capacitors (EDLCs) with an operative voltage as high as 2.4V , able to feature good cycling stability in a broad range of temperatures. Moreover, we also showed that the pseudo-capacitive behaviour of activated carbon (ACs) in these electrolytes strongly depends on the water content and on the surface groups present on the ACs. When protic ionic liquids with a lower content of water were used in combination with AC containing few surface groups, PIL-based supercapacitors exhibit specific capacitance comparable to classical organic electrolytes without any evident pseudo-capacitive contribution.

Figure 9 shows the chemical structures of the protic ionic liquids (a) triethylammonium bis(tetrafluoromethylsulfonyl)imide (Et_3NHTFSI), (b) trimethylammonium bis(tetrafluoromethylsulfonyl)imide (Me_3NHTFSI) and (c) pyrrolidinium nitrate (PYRNO_3).

Table 3 shows ionic conductivities, electrochemical stability windows (ESWs) and the protic ionic liquids' mole fractions of the used electrolytes containing protic ionic liquids at $20\text{ }^{\circ}\text{C}$.



[Reprinted from [105] Brandt A, Pires J, Anouti M, Balducci A. An investigation about the cycling stability of supercapacitors containing protic ionic liquids as electrolyte components. *Electrochimica Acta* 2013,108, 226– 231, Copyright (2013), with permission from Elsevier].

Figure 9. Chemical structures of the protic ionic liquids (a) triethylammonium bis(tetrafluoromethylsulfonyl)imide (Et₃NHTFSI), (b) trimethylammonium bis(tetrafluoromethylsulfonyl)imide (Me₃NHTFSI) and (c) pyrrolidinium nitrate (PYRNO₃).

Electrolyte	Conductivity (mS cm ⁻¹)	ESW (V)	PIL mole fraction (%)
Et ₃ NHTFSI	4	3.8	100
PC-Me ₃ NHTFSI	13.6	3.9	23
PC-PYRNO ₃	14.0	2.6	42

[Reprinted from [105] Brandt A, Pires J, Anouti M, Balducci A. An investigation about the cycling stability of supercapacitors containing protic ionic liquids as electrolyte components. *Electrochimica Acta* 2013,108, 226– 231, Copyright (2013), with permission from Elsevier].

Table 3. Ionic conductivities, electrochemical stability windows (ESWs) and protic ionic liquids' mole fractions of the used electrolytes containing protic ionic liquids at 20 °C.

Coadou et al. [106] report a comparative study on the performances of two bis[(trifluoromethyl)sulfonyl]imide-based protic (PIL) and aprotic (AIL) ionic liquids, namely, trimethylammonium bis[(trifluoromethyl)sulfonyl]imide ([HN₁₁₁][TFSI], PIL) and trimethyl-sulfonium bis[(trifluoromethyl)sulfonyl]imide ([S₁₁₁][TFSI], aprotic ionic liquids), as mixtures with three molecular solvents: gamma butyrolactone (γ-BL), propylene carbonate (PC) and acetonitrile (ACN) as electrolytes for supercapacitor applications. After an analysis of their transport properties as a function of temperature, cyclic voltammetry (CV), electrochemical impedance spectroscopy (EIS), and galvanostatic charge–discharge, measurements were conducted at 25 and –30 °C to investigate the performance of these mixtures as electrolytes for supercapacitors using activated carbon as the electrode material. Surprisingly, for each solvent investigated, no significant differences were observed between the electrolytes based on the protic ionic liquids and aprotic ionic liquids in their electrochemical performance due to the presence or the absence of the labile proton. Furthermore, good specific capacitances were observed in the case of γ-BL-based electrolytes even at low temperatures. Capacitances of up to 131 and 80 F

g^{-1} are observed for the case of the $[\text{S}_{111}][\text{TFSI}] + \gamma\text{-BL}$ mixture at 25 and $-30\text{ }^\circ\text{C}$, respectively. This latter result is very promising particularly for the formulation of new environmentally friendly electrolytes within energy storage systems even at low temperatures. Lu reported [107] a new class of nanocomposite electrodes for the development of high-performance supercapacitors with environmentally friendly ionic liquid electrolytes. Having high-surface-area activated carbons, carbon nanotubes, and ionic liquids as integrated constituent components, the resultant composites show significantly improved charge storage and delivery capabilities. In an ionic liquid electrolyte, the composites possess a superior capacitance (188 F/g) over a pure carbon nanotube electrode (20 F/g) and a conventional activated carbon electrode (90 F/g). On the basis of these nanocomposite electrodes and an ionic liquid electrolyte, we have further developed prototype supercapacitors with a high cell voltage (4 V), and superior energy and power densities (50 Wh/kg and 22 kW/kg, respectively, in terms of the mass of the active electrode material). The nanocomposite supercapacitors developed in this study clearly outperform the current supercapacitor technology, providing a new approach in fabricating advanced supercapacitors with a high-performance, inherently safe operation and long lifetime. Zhao et al. [108] reported the synthesis of novel nanocomposite electrodes based on MnO_2 nanosheets, Pt, Au, or Pd nanoparticles (NPs), exfoliated carbon nanotubes (CNTs), and Ni foam (NF) substrates. The $\text{MnO}_2\text{-Pd-CNT-NF}$ electrode in 1-butyl-3-methylimidazolium hexafluorophosphate (BMIM-PF_6)/N, N-dimethylformamide (DMF) electrolyte exhibits a high specific capacitance of 559.1 F/g based on MnO_2 with a wide potential window (2.1 V). To the best of our knowledge, this is one of the highest capacitance for MnO_2 in ionic liquid (IL) electrolytes ever reported. The IL hybrid supercapacitors are assembled using $\text{MnO}_2\text{-Pd-CNTs-NF}$ positive electrodes, activated carbon (AC) negative electrodes, and $\text{BMIM-PF}_6/\text{DMF}$ electrolyte displaying a high operating voltage (3 V), high energy density (78.4Wh/kg) and high power density (12.7 kW/kg). The superior performances of the MnO_2 IL hybrid supercapacitors suggest their potential application for the future generation of electrochemical power sources. The ionic liquids (ILs) *N*-butyl-*N*-methyl-pyrrolidinium trifluoromethanesulfonate (PYR_{14}Tf) and *N*-methyl-*N*-propyl-pyrrolidinium bis(fluorosulfonyl)imide ($\text{PYR}_{13}\text{FSI}$) are investigated as electropolymerization media for poly(3-methylthiophene) (pMeT) in view of their use in carbon/IL/pMeT hybrid supercapacitors by Biso et al. [109]. Data on the viscosity, solvent polarity, conductivity and electrochemical stability of PYR_{14}Tf and $\text{PYR}_{13}\text{FSI}$ as well as the effect of their properties on the electropolymerization and electrochemical performance of pMeT, which features $>200\text{ Fg}^{-1}$ at 60°C when prepared and tested in such ionic liquids, are reported and discussed; the results of the electrochemical characterization in *N*-butyl-*N*-methyl-pyrrolidiniumbis(trifluoromethanesulfonyl)imide of the so-obtained pMeT are also given, for comparison.

2.5.1.3. Ionic liquids as electrolyte for graphene, graphene oxide and associated composite supercapacitors

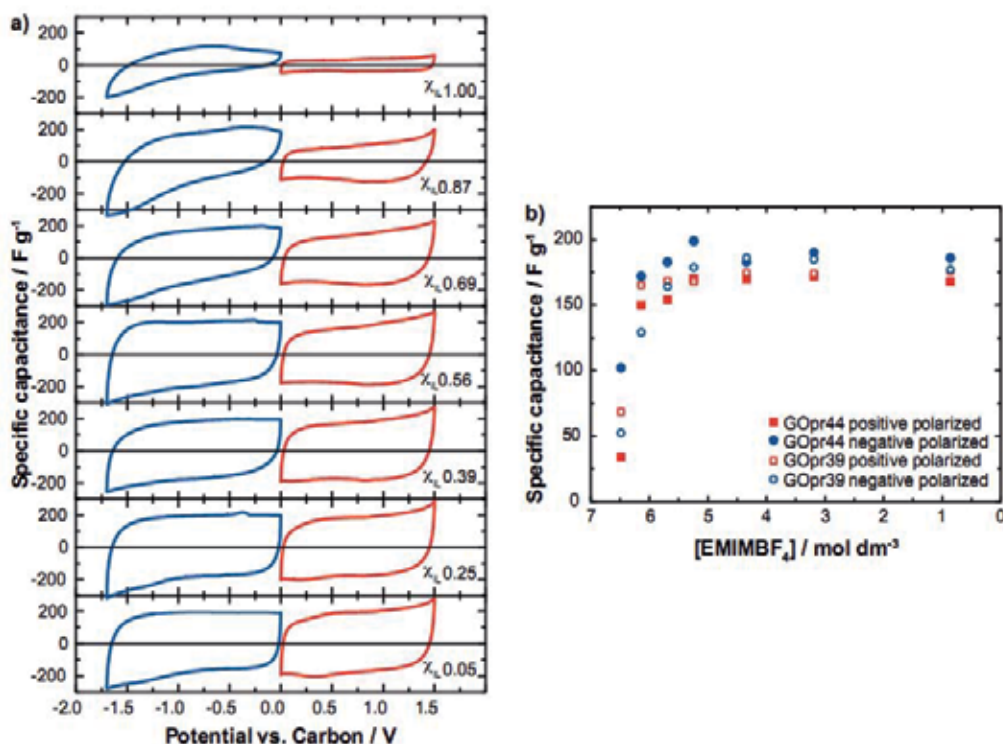
The activation behaviour and achievable specific capacitance of intercalation-like carbon materials, such as partially reduced graphite oxide (GOpr), employing pure and diluted ionic liquids were investigated by Hantel et al. [110]. The electrochemical activation of two different GOprs with interlayer distances of 3.9 and 4.4 \AA and a graphite was studied with the ionic

liquid 1-ethyl-3-methyl-imidazolium tetrafluoroborate (EMIMBF₄). Furthermore, the effect of the organic solvent acetonitrile (AN) on the activation was tested by a stepwise dilution of the ionic liquid. It is shown that a rudimentary electrochemical activation of GO_{pr} is possible with EMIMBF₄. However, the resulting specific capacitance was below 100 F g⁻¹ indicating an incomplete activation reaction. By the stepwise dilution of EMIMBF₄ with AN, the specific capacitance was increased up to approximately 180 F g⁻¹. Therefore, it seems that the electrochemical activation of intercalation-like carbon materials was based on both a reaction with the ions as well as with the employed solvent. Moreover, this experimental study indicates that an increased molarity of organic electrolytes has no influence on the maximum achievable specific capacitance. Figure 8 visualizes the specific capacitances for the different molarities of EMIMBF₄/AN, which are calculated from galvanostatic discharge measurements at 0.1 A g⁻¹. If a decreased molarity and thus a lack of ions results in a decreasing specific capacitance, they double and reach a stable value for molarities smaller than 5.2 M EMIMBF₄/AN. For molarities between 0.9 and 5.2 M EMIMBF₄/AN, the specific capacitances of GO_{pr44} and GO_{pr39} are similar with approximately 180 ± 10 F g⁻¹. Therefore, even an ion concentration of 0.9 M seems to be enough to reach the maximum achievable specific capacitance. A summary of positive (red) and negative (blue) polarization cycles after electrochemical activation for a changing concentration of EMIMBF₄/AN for GO_{pr44} is shown in figure 10.

Tamilarasan et al. [111] reported the fabrication of a mechanically stable, flexible graphene-based all-solid-state supercapacitor with ionic liquid incorporated polyacrylonitrile (PAN/[BMIM][TFSI]) electrolyte for electric vehicles (EVs). The PAN/[BMIM][TFSI] electrolyte shows high ionic conductivity (2.42 mS/cm at 28 °C) with high thermal stability. The solid-like layered phase of ionic liquid is observed on the surface of the pores of the PAN membrane along with a liquid phase which made it possible to hold 400 wt% of the mobile phase. This phase formation is facilitated by the ionic interaction of C≡N moieties with the electrolyte ions. A supercapacitor device, comprised of PAN/[BMIM][TFSI] electrolyte and graphene as the electrode, is fabricated and its performance is demonstrated. Several parameters of the device, such as energy storage and discharge capacity, internal power dissipation, operating temperature, safe operation and mechanical stability, meet the requirements of future EVs. In addition, a good cyclic stability is observed even after a drop of 1000 cycles of potential.

Figure 10 shows the energy density and power density of 30.51 Wh/kg and 15.34 kW/kg, respectively, at the specific current of 10 A/g corresponding to the C_s of 98 F/g, in terms of the mass of the total electrode material. The Ragone plot drops faster with the power due to the fast voltage decay during discharge at high power. The maximum energy storage capacity (E_{max}) and the maximum reduced graphene oxide (RGO) was prepared with HBr as a reducing reagent. RGO-based supercapacitors in two-electrode systems have been fabricated in ionic liquid electrolytes of 1-butyl-3-methylimidazolium hexafluorophosphate (BMIPF₆) and 1-butyl-3-methylimidazolium tetrafluoroborate (BMIBF₄), respectively by Chen et al. [112].

RGO in BMIBF₄ shows a higher capacitance of 74 F g⁻¹ at 10 mV s⁻¹, while RGO in BMIPF₆ merely exhibits 45 F g⁻¹. However, due to the wider potential window of 4 V for BMIPF₆, RGO in BMIPF₆ has higher energy and power densities. The highest power density of 27.8 kWkg⁻¹

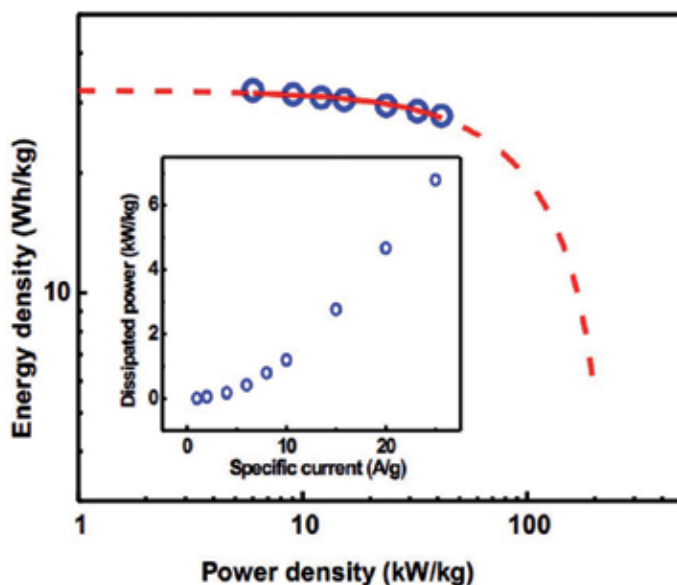


[Reprinted from [110] Birbilis N, Bouzek K, Bultel Y, Cuesta A, Ferapontova E, Hartl F, Hebert K, Jones D J, Komaba S, Kuhn A, Hantel M M, Plátek A, Kaspar T R, Nesper R, Wokaun A, Kötz R. Investigation of diluted ionic liquid 1-ethyl-3-methyl-imidazolium tetrafluoroborate electrolytes for intercalation-like electrodes use supercapacitors. *Electrochimica Acta*.2013; 110, 234–239, Copyright (2013), with permission from Elsevier].

Figure 10. (a) Summary of positive (red) and negative (blue) polarization cycles after electrochemical activation for a changing concentration of EMIMBF₄/AN for GOpr44. The CVs were all taken with a sweep rate of 1 mV s⁻¹. (b) Specific capacitance calculated from the galvanostatic discharge of a positive polarized (red squares) or negative polarized (blue circles) GOpr39 (open symbols) and GOpr44 (filled symbols), respectively at 0.1 Ag⁻¹ as a function of the molarity of EMIMBF₄/AN. (For an interpretation of the references to colour in this figure legend, the reader is referred to the web version of this article.)

is obtained at 14 A g⁻¹ and the maximum energy density of 18.9 Wh kg⁻¹ at 1 Ag⁻¹ for BMIPF₆. The exciting results suggest the potential application of RGO in BMIPF₆. High specific surface area (SSA ~2000 m²/g) porous KOH-activated microwave exfoliated graphite oxide ('a-MEGO') electrodes have been tested in a eutectic mixture of ionic liquids (1:1 by weight or molar ratio N-methyl-N-propylpiperidinium bis(fluorosulfonyl)imide (PIP13-FSI) and N-butyl-N-methylpyrrolidinium bis(fluorosulfonyl)imide (PYR14-FSI)) as an electrolyte for supercapacitor applications by Tsai et al. [113].

By optimizing the carbon/electrolyte system, outstanding capacitive performance has been achieved with high capacitance (up to 180 F/g) and a wide electrochemical window (up to 3.5 V) over a wide temperature range from -50 °C to 80 °C. This is the first demonstration of a

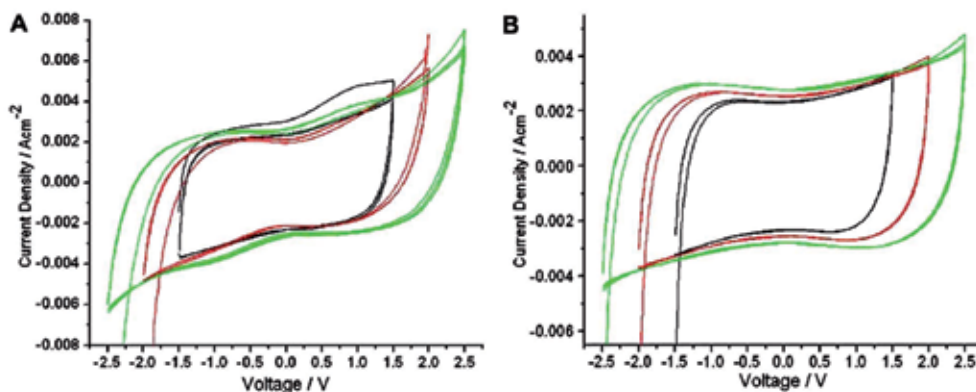


[Reprinted from [111] Tamarasari P, Ramaprabhu S. Graphene-based all-solid-state supercapacitors with ionic liquid incorporated polyacrylonitrile electrolyte, *Energy*.2013; 51, 374-381, Copyright (2013), with permission from Elsevier].

Figure 11. Ragone plot of HEG e PAN/[BMIM][TFSI] supercapacitor. Inset: power dissipated in equivalent series resistance RESR (PESR) as a function of specific current.

carbon–ionic liquid system capable of delivering capacitance in excess of 100 F/g below room temperature. The excellent electrochemical response of the proposed couple shows that optimization of the carbon/electrolyte interface is of great importance for improving capacitive energy storage. Wei et al. studied [114] the application of different types of room temperature ionic liquids (RTILs) into flexible supercapacitors. Typical RTILs including 1-butyl-3-methylimidazolium [BMIM][Cl], trioctylmethylammonium bis(trifluoromethylsulfonyl)imide [OMA][TFSI] and triethylsulfonium bis(trifluoromethylsulfonyl)imide ([SET₃][TFSI]) were studied. [SET₃][TFSI] shows the best result as an electrolyte in electrochemical double-layer (EDLC) supercapacitors, with a very high specific capacitance of 244 F/g at room temperature, overceiling the performance of conventional carbonate electrolytes such as dimethyl carbonate (DMC) with a more stable performance and much larger electrochemical window. Fig. 12 shows the cyclic voltammogram curves of the supercapacitors with electrolytes.

Chatterjee et al. [115] demonstrate the electrochemical stability of nanostructured silicon in corrosive aqueous, organic, and ionic liquid media enabled by conformal few-layered graphene heterogeneous interfaces. They demonstrate direct gas-phase few-layered graphene passivation ($d = 0.35$ nm) at temperatures that preserve the structural integrity of the nanostructured silicon. This passivation technique is transferrable both to silicon nanoparticles (Si-NPs) as well as to electrochemically etched porous silicon (P-Si) materials. For Si-NPs, we find the graphene-passivated silicon to withstand physical corrosion in NaOH aqueous conditions

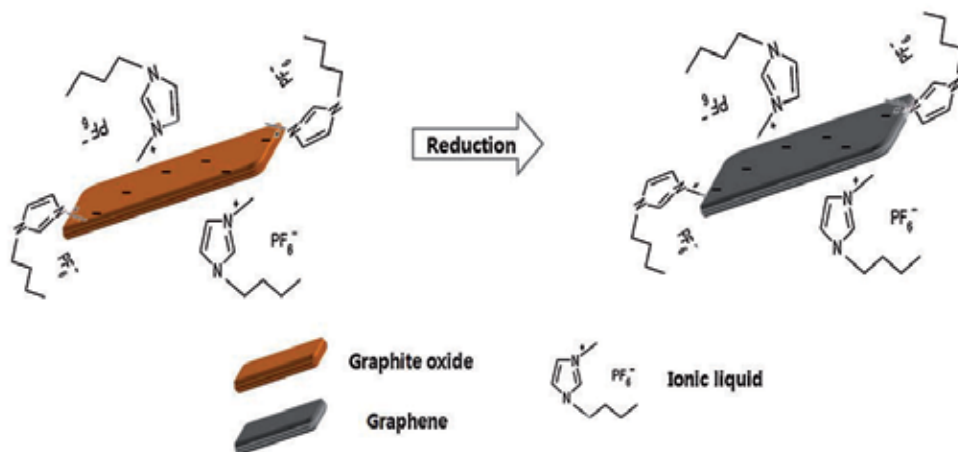


[Reproduced from [114] Wei D, Ng T W. Application of novel room temperature ionic liquids in flexible supercapacitors, *Electrochemistry Communications*.2009; 11, 1996–1999, Copyright (2009), with permission from Elsevier].

Figure 12. The cyclic voltammogram curves of the supercapacitors with electrolytes of (A) 5 wt% LiTFSI in DMC (B) 5 wt% LiTFSI in [SET3][TFSI]. Electrochemical window is in the range of -1.5 to 1.5 V, -2.0 to 2.0 V and -2.5 to 2.5 V with a scan rate of 50 mV/s

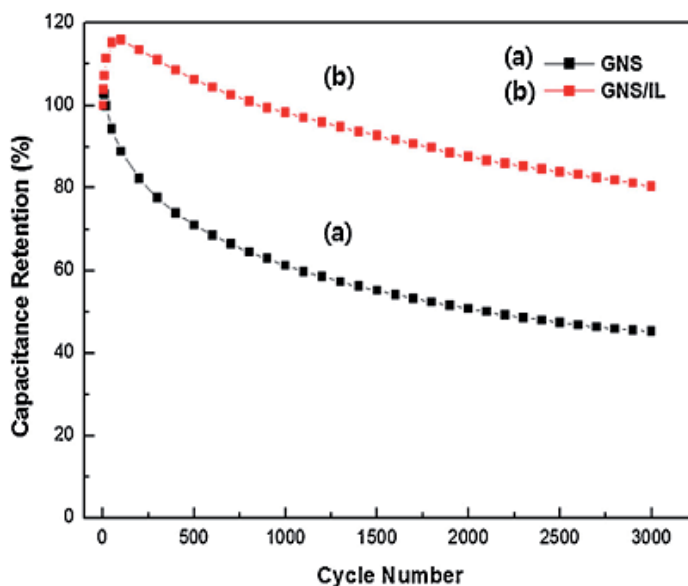
where unpassivated Si-NPs spontaneously dissolve. For P-Si, we demonstrate electrochemical stability with widely different electrolytes, including NaOH, enabling these materials for use in electrochemical supercapacitors. This leads us to develop high-power on-chip porous silicon supercapacitors capable of up to 10 Wh/kg and 65 kW/kg energy and power densities, respectively, and 5 Wh/kg energy density at 35 kW/kg—comparable to many of the best high-power carbon-based supercapacitors. As surface reactivity wholly dictates the utilization of nanoscale silicon in diverse applications across electronics, energy storage, biological systems, energy conversion, and sensing, we strongly suggest the direct formation of few-layered graphene on nanostructured silicon as a means to form heterogeneous on-chip interfaces that can maintain stability in even the most reactive of environments. Graphene nanosheets (GNS) were modified by 1-Butyl-3-methylimidazolium hexafluorophosphate, which is one of the ionic liquids (IL). Owing to the modification of graphene with ionic liquids, graphene can not only be structurally stabilized, but also showed the highest charge transfer that allows it to exhibit an enhanced electrochemical performance. Furthermore, a graphene aggregation by the intersheet van der Waals interaction can be prevented because ionic liquids act as an effective agent for the exfoliation of graphene sheets. The prepared composites showed the enhanced electrochemical performance such as high rate capability and excellent cycle performance [116]. Figure 13 shows a schematic representation of the preparation process of GNS/IL composites.

Figure 14 shows the cycle performance of the pristine GNS and GNS/IL composites. The cycle stability of the prepared composites was evaluated at a potential range between -0.8 V to 0.2 V at a scan rate of 100 mVs⁻¹ for 3000 cycles. The GNS/IL composite electrode exhibits an excellent cycle performance (~80% of initial value for 3000 cycles), which was higher than the 45% retention of the pristine GNS.



[Reproduced from [116] Kim J, Kim S. Preparation and electrochemical property of ionic liquid-attached graphene nanosheets for the application of a supercapacitor electrode. *Electrochimica Acta*. 2014; 119, 11– 15, Copyright (2014), with permission from Elsevier].

Figure 13. Schematic representation of the preparation process of GNS/IL composites.



[Reproduced from [116] Kim J, Kim S. Preparation and electrochemical property of ionic liquid-attached graphene nanosheets for the application of a supercapacitor electrode. *Electrochimica Acta*. 2014; 119, 11– 15, Copyright (2014), with permission from Elsevier].

Figure 14. Cycling performances of pristine GNS and GNS/IL composites.

2.5.1.4. Poly ionic liquid as an electrolyte for graphene supercapacitors

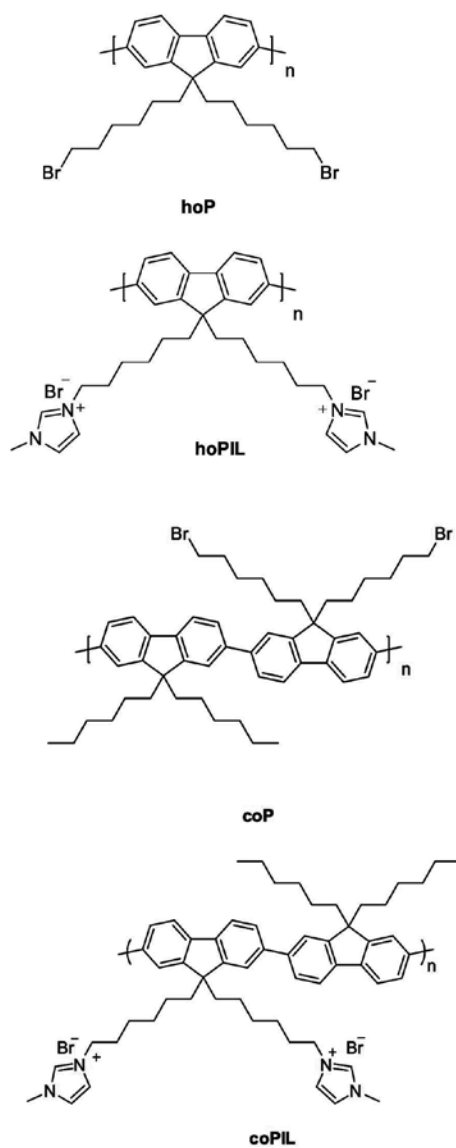
Mao et al. reported [117] a new concept of using conjugated polyfluorene imidazolium ionic liquids (PILs) intercalated reduced graphene oxide for high-performance supercapacitor electrode materials. Two polyfluorene homo-polymers (hoPIL) and co-polymers (co-PIL) carrying hexyl imidazolium bromide side chains were designed and synthesized. Their corresponding intercalated reduced graphene oxide materials, hoPIL-RGO and coPIL-RGO, exhibited good electrochemical performance in aqueous electrolytes as well as in ionic liquid electrolyte 1-butyl-3-methylimidazolium tetrafluoroborate (BMIMBF₄). High specific capacitances of 222 F g⁻¹ at a current density of 0.2 A g⁻¹ and 132 F g⁻¹ at 0.5 A g⁻¹ were obtained for coPIL-RGO in 6 M KOH and BMIMBF₄ accordingly. When assembled into a symmetric two-electrode cell with graphene materials as electrodes and BMIMBF₄/acetonitrile (1:1) as an electrolyte, an energy density of 14.7 Wh kg⁻¹ was obtained for coPIL-RGO at a current density of 0.5 A g⁻¹, and a maximum power density of 347 kW kg⁻¹ was achieved for hoPIL-RGO at a current density of 5 A g⁻¹ with good cycling stability.

Figure 15 shows the chemical structure of conjugated polyfluorenes and their corresponding conjugated polyfluorene imidazolium ionic liquids.

Improving the electrolyte's accessibility to the surface of the carbon nanomaterials is a challenge to be overcome in supercapacitors based on ionic liquid electrolytes. Trigueiro et al. [118] report the preparation of supercapacitors based on reduced graphene oxide (RGO) electrodes and ionic liquid as the electrolyte (specifically, 1-methyl-1-propylpyrrolidinium bis(trifluoromethylsulfonyl)imide or [MPPy][TFSI]).

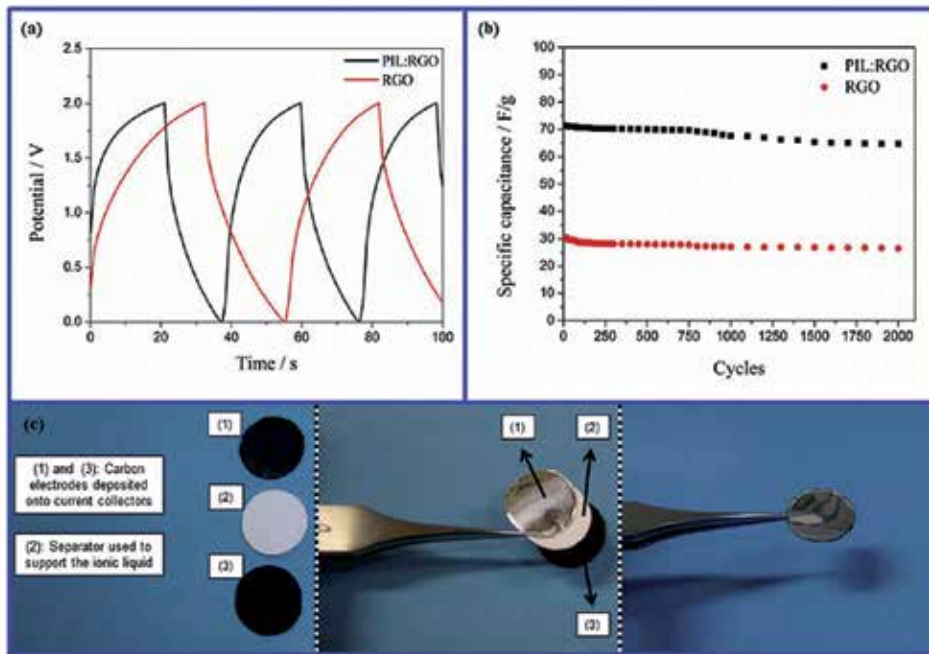
Two types of electrodes were compared: the RGO-based electrode and a poly(ionic liquid)-modified RGO electrode (PIL:RGO). The supercapacitor produced with the PIL:RGO electrode and [MPPy][TFSI] showed an electrochemical stability of 3 V and provided a capacitance of 71.5 F g⁻¹ at room temperature; this capacitance is 130% higher with respect to the RGO-based supercapacitor. The decrease of the specific capacitance after 2000 cycles is only 10% for the PIL:RGO-based device. The results revealed the potential of the PIL:RGO material as an electrode for supercapacitors. This composite electrode increases the compatibility with the ionic liquid electrolyte compared to an RGO electrode, promoting an increase in the effective surface area of the electrode accessible to the electrolyte ions. Galvanostatic charge/discharge curves for RGO and PIL:RGO capacitors at 25 °C (current density: 0.2 A g⁻¹) are shown in figure 16.

Kim et al. [119] reported a high-performance supercapacitor incorporating a poly(ionic liquid)-modified reduced graphene oxide (PIL:RG-O) electrode and an ionic liquid (IL) electrolyte (specifically, 1-ethyl-3-methylimidazolium bis(trifluoromethylsulfonyl)amide or EMIM-NTf₂). PIL:RG-O provides enhanced compatibility with the IL electrolyte, thereby increasing the effective electrode surface area accessible to electrolyte ions. The supercapacitor assembled with PIL:RG-O electrode and EMIM-NTf₂ electrolyte showed a stable electrochemical response of up to a 3.5 V operating voltage and was capable of yielding a maximum energy density of 6.5 W h/kg with a power density of 2.4 kW/kg. These results demonstrate the potential of the PIL:RG-O material as an electrode in high-performance supercapacitors.



[Reprinted from [117] Mao L, Li Y, Chi C, Chan H, Wu J. Conjugated polyfluorene imidazolium ionic liquids intercalated reduced graphene oxide for high-performance supercapacitor electrodes, *Nano Energy* 2014; 6, 119–128, Copyright (2014), with permission from Elsevier].

Figure 15. Chemical structure of conjugated polyfluorenes and their corresponding conjugated polyfluorene imidazolium ionic liquids.



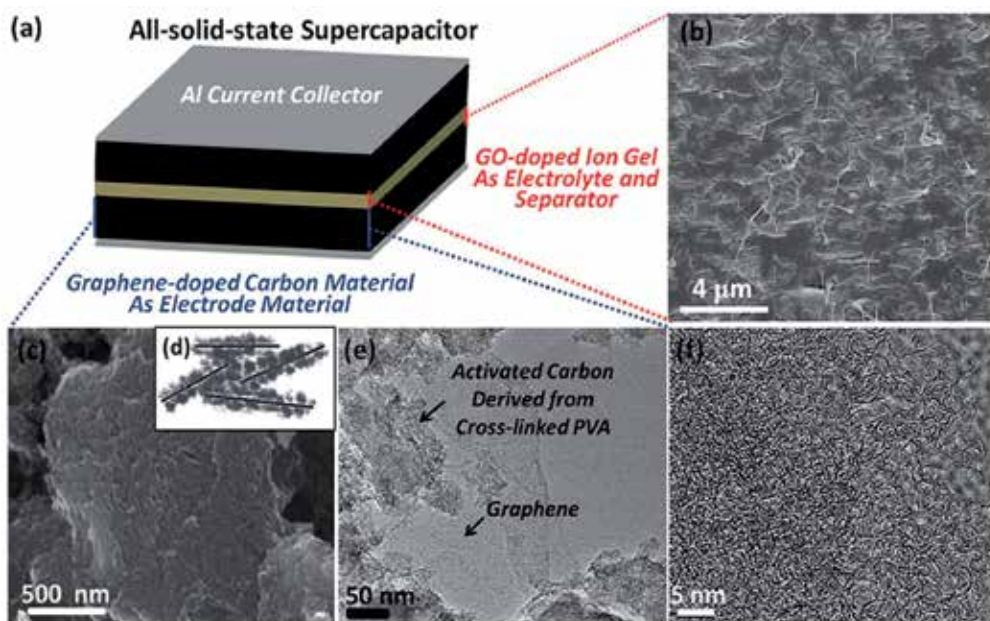
[Reprinted from [118] Trigueiro J P C, Lavall R L, Silva G G. Supercapacitors based on modified graphene electrodes with poly(ionic liquid) *Journal of Power Sources*.2014: 256, 264-273, Copyright (2014), with permission from Elsevier].

Figure 16. Galvanostatic charge/discharge curves for RGO and PIL:RGO capacitors at 25 °C (current density: 0.2 A g⁻¹) (a). The specific capacitance change as a function of the number of charge/discharge cycles (b). Optical images of the prototype supercapacitor developed in this work. From left to right: electrodes of carbon nanomaterials and the separator soaked with ionic liquid, the sequence used for the preparation of the device and the resulting device (c)

2.5.1.5. Miscellaneous application of ionic liquids in supercapacitors based on graphene

Beta-nickel hydroxide nanowires/reduced graphene oxide (RGO) composites are fabricated by a one-step reactable ionic liquid-assisted hydrothermal method, using the versatile 1-butyl-3-methylimidazolium trifluoroacetate as templates, co-solvents and reactants as used by Liu et al. [120]. The results show that β -Ni(OH)₂ nanowires are well dispersed on the surface of the reduced graphene oxide sheets, and the as-prepared β -Ni(OH)₂ nanowires/RGO composite exhibits a huge BET surface area of 216.99 m²g⁻¹ with a pore volume of 0.34 m³g⁻¹. Furthermore, a β -Ni(OH)₂ nanowires/RGO composite as an electrode material for supercapacitors displays high specific capacitance, good cycling stability and coulombic efficiency. An extremely high specific capacitance of ~1875 F g⁻¹ can be obtained at 1 A g⁻¹ in 6M KOH aqueous solution, and retains 98.3% of its original capacity after 1000 charge/discharge cycles at 8 A g⁻¹. The resulting composite is a promising candidate as an electrode material for extensive applications in energy storage systems.

Reduced graphene oxide (rGO)/ionic liquids (IL) composites with different weight ratios of IL to rGO were synthesized by Kim et al. [121] using a simple method. In these composites, IL contributed to the exfoliation of rGO sheets and to the improvement of the electrochemical



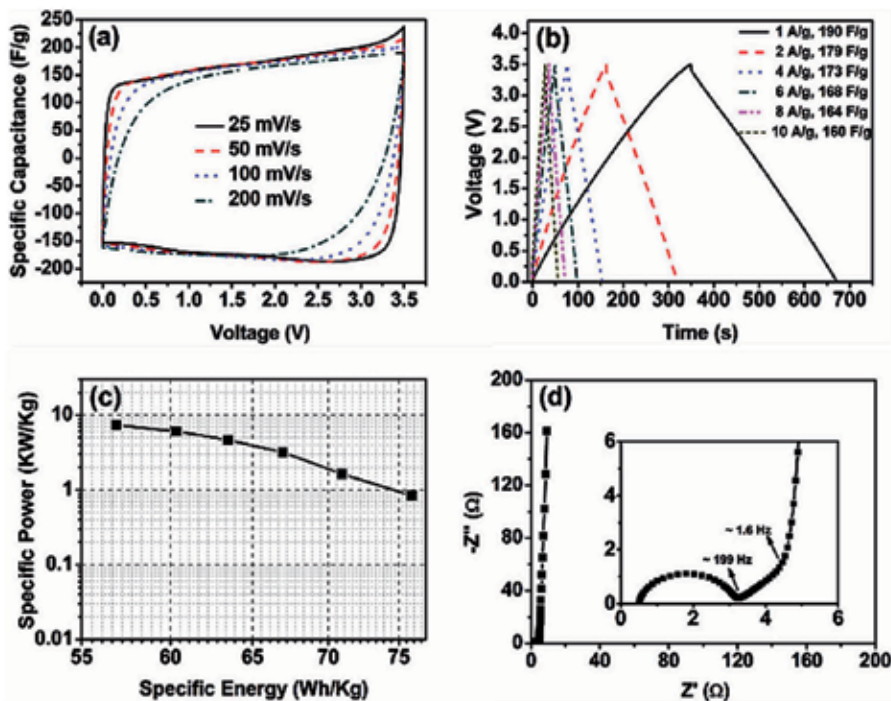
[Reproduced from [122] Yang X, Zhang L, Zhang F, Zhang T, Huang Y, Chen Y. A high-performance all-solid-state supercapacitor with graphene-doped carbon material electrodes and a graphene oxide-doped ion gel electrolyte. *Carbon*.2014; 72, 381 – 386, Copyright (2014), with permission from Elsevier].

Figure 17. (a) Diagram of an all-solid-state supercapacitor. (b) Low-magnification scanning electron microscopy (SEM) image of the morphology of the GO-doped ion gel. (c) SEM image of graphene-doped carbon material. The activated carbon is dispersed and coated on the graphene sheets. (d) Schematic of the structure of the graphene-doped carbon material. (e) Transmission electron microscopy (TEM) image of the graphene-doped carbon material. (f) High-resolution transmission electron microscopy (HR-TEM) image of the activated carbon, coated on the graphene sheets.

properties of the resulting composites by enhancing the ion diffusion and charge transport. The TEM images showed that IL was coated on the surface of rGO in a translucent manner. The electrochemical analysis of the prepared composites was carried out by performing cyclic voltammetry (CV), galvanostatic charge/discharge, and electrochemical impedance spectroscopy (EIS). Among the prepared composites, the one with a weight ratio of rGO to IL of 1:7 showed the highest specific capacitance of 147.5 Fg^{-1} at a scan rate of 10 mVs^{-1} . In addition, the rate capability and cycle performance of the composites were enhanced compared to pristine rGO. These enhanced properties make the composites suitable as electrode materials for better performance supercapacitors.

Yang et al. [122] demonstrated a high-performance all-solid-state supercapacitor with a graphene-doped carbon electrode material and a graphene oxide (GO)-doped ion gel as a gel polymer electrolyte and separator. The configuration of the all-solid-state supercapacitor described here is schematically shown in Figure 17.

Because of the ultrahigh specific surface area ($3193 \text{ m}^2 \text{ g}^{-1}$), suitable pore-size distribution (primarily 1–4 nm), and excellent electrical conductivity (67 Sm^{-1}) of the graphene-doped carbon material, as well as the broad electrochemical window (0–3.5 V) and high ionic



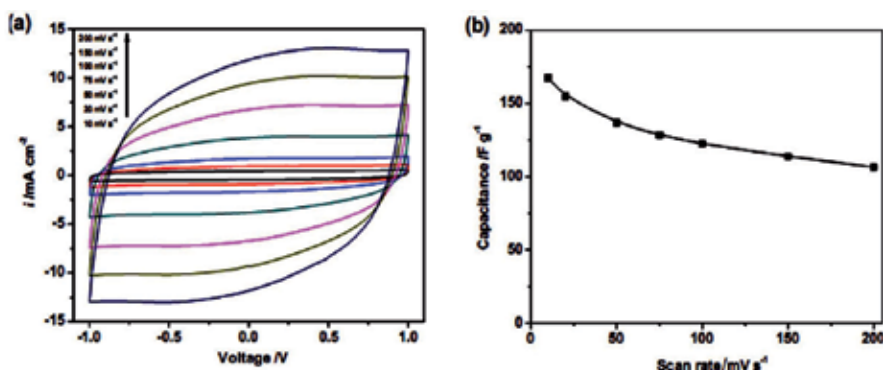
[Reproduced from [122] Yang X, Zhang L, Zhang F, Zhang T, Huang Y, Chen Y. A high-performance all-solid-state supercapacitor with graphene-doped carbon material electrodes and a graphene oxide-doped ion gel electrolyte. *Carbon*.2014; 72, 381 – 386, Copyright (2014), with permission from Elsevier].

Figure 18. Performance characteristics of the all-solid-state supercapacitor. (a) Cyclic voltammetry (CV) curves at various scan rates. (b) Galvanostatic charge/discharge curves under different current densities. (c) Ragone plot. (d) Nyquist impedance plots in the frequency range 10–100 kHz. The inset shows a magnified view of the high frequency region of the impedance spectra.

conductivity of the GO-doped ion gel, the all-solid-state supercapacitor demonstrates outstanding performance with a specific capacitance of 190 F g^{-1} and an energy density of 76 Wh kg^{-1} at 1 A g^{-1} , and a specific capacitance of 160 F g^{-1} and an energy density of 57 Wh kg^{-1} at 10 A g^{-1} . In addition, the all-solid-state supercapacitor exhibits similar and excellent performance as does the compared conventional liquid supercapacitor with respect to specific capacitance, capacitance retention, internal resistance, and frequency response. The performance characteristics of the all-solid-state supercapacitors are shown in figure 18. Tamilarasan et al. [123] reported the fabrication of a mechanically stable, flexible grapheme-based all-solid-state supercapacitor with ionic liquid incorporated polyacrylonitrile (PAN/[BMIM][TFSI]) electrolyte for electric vehicles (EVs). The PAN/[BMIM][TFSI] electrolyte shows high ionic conductivity (2.42 mS/cm at $28 \text{ }^\circ\text{C}$) with high thermal stability. The solid-like layered phase of ionic liquid is observed on the surface of the pores of the PAN membrane along with the liquid phase which made it possible to hold 400 wt% of the mobile phase. This phase formation is facilitated by the ionic interaction of C[^]N moieties with the electrolyte ions. A supercapacitor device, comprised of PAN/[BMIM][TFSI] electrolyte and graphene as an electrode, is fabri-

cated and the performance is demonstrated. Several parameters of the device, such as, energy storage and discharge capacity, internal power dissipation, operating temperature, safe operation and mechanical stability, meet the requirements of future EVs. In addition, a good cyclic stability is observed even after 1000 cycles.

All-solid-state thin supercapacitors were fabricated by Pandey et al. [124] using current pulse polymerized poly(3,4-ethylenedioxythiophene) (PEDOT) over carbon fibre paper and ionic liquid-based gel polymer electrolyte. The performance characteristics of the supercapacitor cells were evaluated by ac impedance spectroscopy, cyclic voltammetry and galvanostatic charge/discharge techniques. The PEDOT electrode shows the specific capacitance of 154.5 F g^{-1} , which corresponds to the cell area-normalized capacitance of 85 mF cm^{-2} . The maximum specific energy and specific power of the solid-state supercapacitor cell, calculated from charge/discharge characteristics, are 6.5 Wh kg^{-1} and 11.3 kW kg^{-1} , respectively. The solid-state supercapacitor shows good cycle durability and time stability. The thin, lightweight, gel electrolyte-based supercapacitor shows considerable potential for low-cost, high-performance energy storage applications. Cyclic voltammetry (CV) curves of the supercapacitor cell at different scan rates are shown in figure 19.



[Reproduced from [124] Pandey G P, Rastogi A C, Westgate C R. All-solid-state supercapacitors with poly(3,4-ethylenedioxythiophene)-coated carbon fiber paper electrodes and ionic liquid gel polymer electrolyte. *Journal of Power Sources*.2014; 245, 857-865, Copyright (2014), with permission from Elsevier].

Figure 19. (a) Cyclic voltammetry (CV) curves of supercapacitor cells at different scan rates. (b) Variation in the capacitance of the PEDOT electrode, calculated from CV curves, as a function of the scan rates.

3. Conclusions

Graphene-based materials have great potential for application in supercapacitors and other green energy devices. There has been much interest in graphene-based electronic devices because graphene provides excellent electrical, optical and mechanical properties. While the supercapacitors available today perform well, it is generally agreed that there is considerable scope for improvement (e.g., improved performance at higher frequencies). Thus, it is likely

that graphene will continue to play a principal role in supercapacitor technology, mainly through the further optimization of porosity, surface treatments to promote wettability, and reduced inter-particle contact resistance. The use of ILs as solvent-free electrolytes in supercapacitors permits a high cell voltage and is the most powerful strategy for increasing specific energy. An effective application in supercapacitors requires that ILs be designed to match wide ESWs to high conductivity and wide duty temperature. The design and synthesis of new nanostructures and architectures based on graphene and modern ionic liquids will be an important task in the future.

Author details

Elaheh Kowsari*

Address all correspondence to: kowsarie@aut.ac.ir

Department of Chemistry, Amirkabir University of Technology, Tehran, Iran

References

- [1] Zhang L L, and Zhao X S. Carbon-based materials as supercapacitor electrodes. *Chem Soc Rev.* 2009; 38, 2520–2531.
- [2] Winter M, Brodd R J, What Are Batteries, Fuel Cells, and Supercapacitors. *Chem Rev.* 2004; 104, 4245–4269.
- [3] Conway B E. *Electrochemical Supercapacitors: Scientific Fundamentals and Technological Applications.* New York, Kluwer-Plenum 2009.
- [4] Burke A. Ultracapacitors: why, how, and where is the technology. *Journal of Power Sources.* 2000; 91(1): 37-50.
- [5] Kotz R, Carlen M. Principles and applications of electrochemical capacitors. *Electrochimica Acta* 2000; 45, 2483-2498.
- [6] Aricò A S, Bruce P, Scrosati B, Tarascon J M, Schalkwijk W V. Nanostructured materials for advanced energy conversion and storage devices. *Nature Materials.* 2005; 4, 366-377.
- [7] Sharma P, Bhatti T S. A review on electrochemical double-layer capacitors. *Energy Conversion and Management* 2010; 51, 2901–2912.
- [8] Stoller M D, Ruoff R S. Best practice methods for determining an electrode material's performance for ultracapacitors *Energy Environ Sci.* 2010; 3, 1294–1301.

- [9] Peng C, Zhang S, Zhou X, Chen G Z. Unequalisation of electrode capacitances for enhanced energy capacity in asymmetrical supercapacitors. *Energy Environ. Sci.* 2010; 3, 1499–1502.
- [10] Liu C, Li F, Ma L P, Cheng H M. *Advanced Materials for Energy Storage*. *Adv. Mater.* 2010; 22, E28–E62.
- [11] Frackowiak E. Carbon materials for supercapacitor application. *Phys. Chem. Chem. Phys.* 2007; 9, 1774–1785.
- [12] Hall P J, Mirzaeian M, Fletcher S I, Sillars F B, Rennie A J R, Shitta-Bey G O, Wilson G, Cruden A, Carter R. Energy storage in electrochemical capacitors: designing functional materials to improve performance. *Energy Environ. Sci.* 2010; 3, 1238–1251.
- [13] Pumera M. Graphene-based nanomaterials for energy storage. *Energy Environ. Sci.* 2011; 4, 668–674.
- [14] Sun Y, Wu Q, Shi G. Graphene based new energy materials. *Energy Environ. Sci.* 2011; 4, 1113–1132.
- [15] Huang X, Zeng Z, Fan Z, Liu J, Zhang H. Graphene-Based Electrodes, *Adv. Mater.* 2012; 24, 6004–5979..
- [16] Li Z, Luppi G, Geiger A, Josel H P, Cola L D. Bioconjugated Fluorescent Zeolite L Nanocrystals as Labels in Protein Microarrays, *Small* 2011; 7, 3193–3201.
- [17] Zhang L L, Zhao X S. Carbon-based materials as supercapacitor electrodes. *Chem Soc Rev.* 2009, 38, 2520–2531.
- [18] Wei L, Nitta N, Yushin G. Lithographically patterned thin activated carbon films as a new technology platform for on-chip devices, *ACS Nano* 2013,7, 6498-6506.
- [19] Wang G, Wang H, Lu X, Ling Y, Yu M, Zhai T, Tong Y, Li Y. Solid-state supercapacitor based on activated carbon cloths exhibits excellent rate capability. *Adv. Mater.* 2014, 26, 2676-2682.
- [20] Wang D W, Li F, Liu M, Lu G Q, Cheng H M. 3D Aperiodic Hierarchical Porous Graphitic Carbon Material for High-Rate Electrochemical Capacitive Energy Storage, *Angew. Chem. Int. Ed.* 2008, 47, 373-376.
- [21] Chmiola J, Yushin G, Gogotsi Y, Portet C, Simon P, Taberna P L. Anomalous Increase in Carbon Capacitance at Pore Sizes Less Than 1 Nanometer, *Science.* 2006; 313, 1760-1763.
- [22] Wu X L, Wen T, Guo H L, Yang S, Wang X, Xu A W. Biomass-derived sponge-like carbonaceous hydrogels and aerogels for supercapacitors., *ACS Nano* 2013;7, 3589-3597.

- [23] Portet C, Yushin G, Gogotsi Y. Electrochemical performance of carbon onions, nano-diamonds, carbon black and multiwalled nanotubes in electrical double layer capacitors. *Carbon*. 2007; 45, 2511-2518.
- [24] Cheng Z, Jinping L. Carbon nanotube network film directly grown on carbon cloth for high-performance solid-state flexible supercapacitors. *Nanotechnology*. 2014; 25, 035402.
- [25] Zheng H, Zhai T, Yu M, Xie S, Liang C, Zhao W, Wang SCI, Zhang Z, Lu X. TiO₂@C core-shell nanowires for high-performance and flexible solid-state supercapacitors. *J Mater Chem C* 1 2013; 225-229.
- [26] Swu Z S, Sun Y, Tan Y Z, Yang S, Feng X, Müllen K. Three-dimensional graphene-based macro- and mesoporous frameworks for high-performance electrochemical capacitive energy storage. *J Am Chem Soc* 2012; 134 19532-19535.
- [27] Liu W W, Feng Y Q, Yan B X, Chen J T, Xue Q J. Superior Micro-Supercapacitors Based on Graphene Quantum Dots. *Adv Funct Mater*. 2013; 23, 4111-4122.
- [28] Jin K Y, Haegeun C, Chi-Hwan H, Woong K. All-solid-state flexible supercapacitors based on papers coated with carbon nanotubes and ionic-liquid-based gel electrolytes, *Nanotechnology*. 2012; 23, 065401.
- [29] Yoon S, Lee J W, Hyeon T, Oh SM. Electric Double-Layer Capacitor Performance of a New Mesoporous Carbon, *J Electrochem Soc* 2000; 147, 2507-2512.
- [30] Chmiola J, Yushin G, Gogotsi Y, Portet C, Simon P, Taberna P L. Anomalous increase in carbon capacitance at pore sizes less than 1 nanometer. *Science*. 2006; 313,1760-1763.
- [31] Geim A K, Novoselov K S. The rise of graphene, *Nat. Mater*. 2007; 6, 183-191.
- [32] Li X, Cai W, An J, Kim S, Nah J, Yang D, Piner R, Velamakanni A, Jung I, Tutuc E, Banerjee S K, Colombo L, Ruoff R S. Large-Area Synthesis of High-Quality and Uniform Graphene Films on Copper Foils. *Science* 2009; 324, 1312-1314.
- [33] Soldano C, Mahmood A, Dujardin E. Production, properties and potential of graphene. *Carbon*. 2010; 48, 2127-2150.
- [34] Srivastava A, Galande C, Ci L, Song L, Rai C, Jariwala D, Kelly K F, Ajayan P M. Novel Liquid Precursor-Based Facile Synthesis of Large-Area Continuous, Single, and Few-Layer Graphene Films. *Chem Mater* 2010; 22, 3457-3461.
- [35] Biswas S, Drzal L T. Multilayered Nano-Architecture of Variable Sized Graphene Nanosheets for Enhanced Supercapacitor Electrode Performance. *ACS Appl Mater Interfaces* 2010; 2, 2293-2300.
- [36] Kim K S, Zhao Y, Jang H, Lee S Y, Kim J M, Kim K S, Ahn J H, Kim P, Choi J Y, Hong B H. Large-scale pattern growth of graphene films for stretchable transparent electrodes, *Nature* 2009, 457, 706-710.

- [37] Wu J, Becerril H A, Bao Z, Liu Z, Chen Y, Peumans P. Organic solar cells with solution-processed graphene transparent electrodes, *Appl Phys Lett*. 2008; 92, 263302-263303.
- [38] Becerril H A, Mao J, Liu Z, Stoltenberg R M, Bao Z, Chen Y. Evaluation of solution-processed reduced graphene oxide films as transparent conductors, *ACS Nano* 2008; 2, 463–470.
- [39] [39] Eda G, Fanchini G, Chhowalla M. Large-area ultrathin films of reduced graphene oxide as a transparent and flexible electronic material, *Nat. Nanotechnol.* 2008; 3, 270–274.
- [40] Kinoshita K. *Carbon: Electrochemical and Physiochemical Properties*. Wiley-Interscience: New York. 1988.
- [41] Vivekchand S R C, Rout C S, Subrahmanyam K S, Govindaraj A, Rao C N R. Graphene-based electrochemical supercapacitors, *J Chem Sci*. 2008, 120,9–13.
- [42] Stoller M D, Park S, Zhu Y, An J, Ruoff R S. Graphene-Based Ultracapacitors. *Nano Lett*. 2008, 8, 3498–3502.
- [43] Wang Y, Shi Z, Huang Y, Ma Y, Wang C, Chen M, Chen Y. Supercapacitor Devices Based on Graphene Materials, *J. Phys. Chem. C* 2009, 113, 13103–13107.
- [44] Wang D W, Li F, Wu Z S, Ren W, Cheng H-M. Electrochemical interfacial capacitance in multilayer graphene sheets: Dependence on number of stacking layers. *Electrochem. Commun.* 2009; 11, 1729–1732.
- [45] Liu C, Yu Z, Neff D, Zhamu A, Jang B Z. Graphene-based supercapacitor with an ultrahigh energy density. *Nano Lett*. 2010; 10, 4863–4868.
- [46] Pumera M. Graphene-based nanomaterials for energy storage, *Energy Environ. Sci.* 2011; 4, 668-674.
- [47] Balandin A, Ghosh S, Bao W, Calizo I, Teweldebrhan D, Miao F, Lau C N. Superior Thermal Conductivity of Single-Layer Graphene, *Nano Lett*. 2008; 8, 902–907.
- [48] Lee C, Wei X, Kysar J W, Hone J. Measurement of the Elastic Properties and Intrinsic Strength of Monolayer Graphene *Science* 2008; 321, 385–388.
- [49] Jang B Z, Aruna Z. Processing of nanographene platelets (NGPs) and NGP nanocomposites: a review *J. Mater. Sci.* 2008, 43, 5092–5101.
- [50] Xia J, Chen F, Li J, Tao N. Measurement of the quantum capacitance of graphene. *Nat. Nanotechnol.* 2009; 4, 505–509.
- [51] Liu C, Yu Z, Neff D, Zhamu A, Jang B Z. Graphene-Based Supercapacitor with an Ultrahigh Energy Density. *Nano Lett*. 2010, 10, 4863–4868.
- [52] Armand M, Endres F, MacFarlane D R, Ohno H, Scrosati B. Ionic-liquid materials for the electrochemical challenges of the future, *Nat Mater* 2009; ;8, 621-629.

- [53] Nanjundiah C, McDevitt S F, Koch V R. Differential Capacitance Measurements in Solvent-Free Ionic Liquids at Hg and C Interfaces, *J. Electrochem. Soc.* 1997; 144, 3392-3397.
- [54] McEwen A B, Ngo H L, Compte K L, Goldman J L. Electrochemical Properties of Imidazolium Salt Electrolytes for Electrochemical Capacitor Applications *J. Electrochem. Soc.* 1999; 146, 1687-1695.
- [55] Balducci A, Bardi U, Caporali S, Mastragostino M, Soavi F. Ionic liquids for hybrid supercapacitors, *Electrochemistry Communications* 2004;6, 566–570
- [56] Supercapacitor, <http://en.wikipedia.org/wiki/Supercapacitor>, (accessed 10 August 2014)
- [57] Kotz K, Carlen M. Principles and applications of electrochemical capacitors, *Electrochim Acta.* 2000, 45, 2483-2498.
- [58] Gouy G. The surface charge of a cell lipid membrane, *J Phys*, 1910; 4, 457-468.
- [59] Chapman D L. A contribution to the theory of electrocapillarity. *Philos. Mag.* 1913; 6, 475-481.
- [60] Stern O Z. Schematic of double layer in a liquid at contact with a negatively-charged solid. *Electrochem.* 1924; 30, 508-516.
- [61] Zhang L, Zhao X S. Carbon-based materials as supercapacitor electrodes. *Chem Soc Rev*, 2009; 38, 2520–2531.
- [62] Kurzweil P. Capacitors | Electrochemical Double-Layer Capacitors, Reference Module in Chemistry, Molecular Sciences and Chemical Engineering Encyclopedia of Electrochemical Power Sources, 2009; 607–633.
- [63] Wang H, Pilon L. Mesoscale modeling of electric double layer capacitors with three-dimensional ordered structures. *Journal of Power Sources*, 2013; 221,252-260.
- [64] Halper M S, Ellenbogen J C. Supercapacitors: A Brief Overview (Technical report, March2006)). MITRE Nanosystems Group. Retrieved 2014-01-20.
- [65] Namisnyk A M. A survey of electrochemical supercapacitor technology (Technical report). Retrieved 2013-04-02.
- [66] (a) Frackowiak E, Beguin F. Carbon materials for the electrochemical storage of energy in Capacitors. *Carbon.* 2001, 39 937–950.(b) http://en.wikipedia.org/wiki/Activated_carbon
- [67] Carbide-derived-carbon. <http://en.wikipedia.org/wiki>.
- [68] Presser V, Heon M, Gogotsi Y. Carbide-Derived Carbons – From Porous Networks to Nanotubes and Graphene. *Advanced Functional Materials* 2011;21 (5): 810–833.

- [69] Kyotani T, Chmiola J, Gogotsi Y. Carbon Materials for Electrochemical Energy Storage Systems. CRC Press/Taylor and Francis. 2009; 77–113.
- [70] Yushin G, Nikitin A, Gogotsi Y. Carbon Nanomaterials, Y. Gogotsi (ed.) CRC Taylor & Francis. 2006; 211–254.
- [71] Nikitin A, Gogotsi Y. Encyclopedia of Nanoscience and Nanotechnology H.S. Nalwa(ed.), American Scientific Publishers 2004 :7 553–574.
- [72] Rose M, Korenblit Y, Kockrick E, Borchardt L, Oschatz M, Kaskel S, Yushin G. Hierarchical Micro-and Mesoporous Carbide-Derived Carbon as a High-Performance Electrode Material in Supercapacitors. *Small*. 2011;7 (8): 1108–1117.
- [73] Yeon S H, Reddington P, Gogotsi Y, Fischer J E, Vakifahmetoglu C, Colombo P. Carbide-derived-carbons with hierarchical porosity from a preceramic polymer. *Carbon* 2010; 48: 201–210.
- [74] Presser V, Zhang L, Niu J J, McDonough J, Perez C, Fong H, Gogotsi Y. Flexible Nano-Felts of Carbide-Derived Carbon with Ultra-High Power Handling Capability. *Advanced Energy Materials*. 2011;1 (3): 423–430.
- [75] Pandolfo A G, Hollenkamp A F. Carbon properties and their role in supercapacitors. *Journal of Power Sources*. 2006 157: 11–27.
- [76] Arulepp M, Leis J, Lätt M, Miller F K, Rumma K, Lust E, Burke A F. The advanced carbide-derived carbon based supercapacitor. *Journal of Power Sources* 2006;162 (2): 1460–1466.
- [77] Simon P, Gogotsi Y. Materials for electrochemical capacitors. *Nature Materials* 2008; 7 (11): 845–854.
- [78] (a) Chmiola J, Yushin G, Gogotsi Y, Portet C, Simon P, Taberna PL. Anomalous Increase in Carbon Capacitance at Pore Sizes of Less Than 1 Nanometer. *Science* 2006,313 (5794): 1760–1763. (b) http://en.wikipedia.org/wiki/Carbide-derived_carbon
- [79] McDonough G, Gogotsi Y. Carbon Onions: Synthesis and Electrochemical Applications, *Interface*. Fall. 2013; 61-66.
- [80] Inagaki M, Konno H, Tanaike O. Carbon materials for electrochemical capacitors. *Journal of Power Sources*. 2010; 195, 7880–7903
- [81] Geim A K, Novoselov K S. The rise of graphene, *Nat. Mater*. 2007; 6, 183–191.
- [82] Li D, Kaner R B. Graphene-based materials. *Science* 2008; 320, 1170–1171.
- [83] Westervelt R M, Graphene nanoelectronics, *Science*. 2008; 320; 324–325.
- [84] Wu Z S, Ren W C, Xu L, Li F, Cheng H M. Doped graphene sheets as anode materials with superhigh rate and large capacity for lithium ion batteries, *ACS Nano* 2011;5, 5463–5471.

- [85] Li Y, Chen Q, Xu K, Kaneko T, Hatakeyama R. Synthesis of graphene nanosheets from petroleum asphalt by pulsed arc discharge in water. *Chemical Engineering Journal* 2013; 215-216, 45–49.
- [86] Sun D K, James J M. Tour, Graphene Chemistry: Synthesis and Manipulation, I J. *Phys. Chem. Lett.* 2011, 2, 2425–2432.
- [87] Yoo J J, Balakrishnan K, Huang J, Meunier V, Sumpter B G, Srivastava A, Conway M, Reddy A L M, Jin Y, Vajtai R, Ajayan P M. Ultrathin Planar Graphene Supercapacitors, *Nano Lett.* 2011; 11, 1423–1427.
- [88] Graphene supercapacitor breaks storage record, physicsworld.com.
- [89] Liu C, Yu Z, Jang B Z, Aruna Z, Jang B Z. Graphene-Based Supercapacitor with an Ultrahigh Energy Density. *Nano Letters.* 2010,10 (12): 4863–4868.
- [90] (a) Miller J R, Outlaw R A, Holloway B C. Graphene Double-Layer Capacitor with ac Line-Filtering Performance, *Science* 2010, 329 : 1637-1639.(b) <http://en.wikipedia.org/wiki/Graphene>
- [91] Vivekchand S R C, Rout C S, Subrahmanyam K S, Govindaraj A, Rao C N R. Graphene-based electrochemical supercapacitors. *J Chem Sci.* 2008;120 : 9-13.
- [92] Choi B G, Yang M H, Hong W H, Choi, J W, Huh Y S. 3D Macroporous Graphene Frameworks for Supercapacitors with High Energy and Power Densities. *ACS Nano.* 2012; 6, 4020-4028.
- [93] Yoo J, Balakrishnan K, Huang J, Meunier V, Sumpter B G, Srivastava A, Conway M, Reddy A L M, Yu J, Vajtai R, Ajayan P M. Ultrathin Planar Graphene Supercapacitors. *Nano Lett.* 2011; 11, 1423–1427.
- [94] Stoller M D, Park S, Zhu Y, An J, Ruoff R S. Graphene-Based Ultracapacitors. *Nano Letters,* 2008; 8(10) 3498-3502
- [95] Liu C, Yu Z, Neff D, Zhamu A, Jang B Z. Graphene-Based Supercapacitor with an Ultrahigh Energy Density *Nano Lett.* 2010; 10, 4863–4868.
- [96] Yan J, Liu J, Fan Z, Wei T, Zhang L. High-performance supercapacitor electrodes based on highly corrugated graphene sheets. *Carbon.* 2012; 50, 2179 – 2188.
- [97] Zhang L L, Zhao X S. Carbon-based materials as supercapacitor electrodes, *Chem.Soc.Rev.* 2009, 38, 2520–2531.
- [98] Ue M. Mobility and ionic association of lithium and quaternary ammonium salts in propylene carbonate and γ -Butyrolactone. *J Electrochem Soc.* 1994;141(12): 3336-3342.
- [99] Arulepp M, Permann L, Leis J, Perkson A, Rumma K, Jaenes A, Lust E. Influence of the solvent properties on the characteristics of a double layer capacitor *J. Power Sources.* 2004; 133: 320-328.

- [100] Morita M, Kaigaishi T, Yoshimoto N, Egashira M, Aida T. Effects of the Electrolyte Composition on the Electric Double-Layer Capacitance at Carbon Electrodes. *Electrochem. Solid State Lett.* 2006; 9(8): A386-A389
- [101] Lust E, Nurk G, Jaenes A, Arulepp M, Nigu P, Moeller P, Kallip S, Sammelselg V. Electrochemical properties of nanoporous carbon electrodes in various nonaqueous electrolytes. *J Solid State Electrochem.* 2003; 7 :91-105.
- [102] Mastragostino M, Soavi F. Electrochemical Capacitors: Ionic Liquid Electrolytes, Reference Module in Chemistry. *Molecular Sciences and Chemical Engineering.* 2009; 649–657.
- [103] Anouti M, Couadou E, Timperman L, Galiano H. Protic ionic liquid as electrolyte for high-densities electrochemical double layer capacitors with activated carbon electrode material. *Electrochimica Acta.* 2012; 64, 110–117.
- [104] Balducci A, Dugas R, Taberna P L, Simon P, Plee D, Mastragostino M, Passerini S. High temperature carbon–carbon supercapacitor using ionic liquid as electrolyte. *Journal of Power Sources.* 2007; 165 (2):922-927.
- [105] Brandt A, Pires J, Anouti M, Balducci A. An investigation about the cycling stability of supercapacitors containing protic ionic liquids as electrolyte components. *Electrochimica Acta.* 2013,108, 226– 231.
- [106] Coadou E, Timperman L, Jacquemin J, Galiano H, Hardacre C, Anouti M. Comparative Study on Performances of Trimethyl-Sulfonium and Trimethyl-Ammonium Based Ionic Liquids in Molecular Solvents as Electrolyte for Electrochemical Double Layer Capacitors. *Phys. Chem. C,* 2013, 117 (20): 10315–10325.
- [107] Lu W, Hartman R. Nanocomposite Electrodes for High-Performance Supercapacitors. *J.Phys.Chem.Lett.* 2011, 2, 655–660
- [108] Zhao D, Zhao Y, Zhang X, Xu C, Peng Y, Li H, Yang Z. Application of high-performance MnO₂ nanocomposite electrodes in ionic liquid hybrid supercapacitors. *Materials Letters.* 2013, 107: 115–118
- [109] Biso M, Mastragostino M, Montaninob M, Passerinib S, Soavi F. Electropolymerization of poly(3-methylthiophene) in pyrrolidinium-based ionic liquids for hybrid supercapacitors. *Electrochimica Acta.* 2008; 53, 7967–7971.
- [110] Birbilis N, Bouzek K, Bultel Y, Cuesta A, Ferapontova E, Hartl F, Hebert K, Jones DJ, Komaba S, Kuhn A, Hantel M M, Płatek A, Kaspar T R, Nesper R, Wokaun A, Kötz R. Investigation of diluted ionic liquid 1-ethyl-3-methyl-imidazolium tetrafluoroborate electrolytes for intercalation-like electrodes use supercapacitors *Electrochimica Acta* 2013;110, 234–239.
- [111] Tamilarasan P, Ramaprabhu S. Graphene based all-solid-state supercapacitors with ionic liquid incorporated polyacrylonitrile electrolyte, *Energy.* 2013; 51, 374-381.

- [112] Chen Y, Zhang X, Zhang D, Ma Y. High power density of graphene-based supercapacitors in ionic liquid electrolytes. *Materials Letters*. 2012; 68, 475–477.
- [113] Tsai W Y, Lin R, Murali S, Zhang L L, McDonough J K, Ruoff R S, Taberna P L, Gogotsid Y, Simon P. Outstanding performance of activated graphene based supercapacitors in ionic liquid electrolyte from -50 to 80 °C, *Nano Energy*. 2013; 2, 403–411.
- [114] Wei D, Ng T W. Application of novel room temperature ionic liquids in flexible supercapacitors, *Electrochemistry Communications*. 2009; 11, 1996–1999.
- [115] Chatterjee S, Rachel Carter R, Oakes L, Erwin W R, Bardhan R, Pint C L. Electrochemical and Corrosion Stability of Nanostructured Silicon by Graphene Coatings: Toward High Power Porous Silicon Supercapacitors. *J. Phys. Chem. C*, 2014, 118 (20), pp 10893–10902.
- [116] Kim J, Kim S. Preparation and electrochemical property of ionic liquid-attached graphene nanosheets for an application of supercapacitor electrode. *Electrochimica Acta*. 2014; 119, 11–15.
- [117] Maa L, Li Y, Chi C, Chan H, Wu J. Conjugated polyfluorene imidazolium ionic liquids intercalated reduced graphene oxide for high performance supercapacitor electrodes. *Nano Energy*. 2014; 6, 119–128.
- [118] Trigueiro J P C, Lavall R L, Silva G G. Supercapacitors based on modified graphene electrodes with poly(ionic liquid). *Journal of Power Sources*. 2014; 256, 264–273.
- [119] Kim T Y, Lee H W, Stoller M, Dreyer D R, Bielawski C W, Ruoff R S, Suh K S. High-performance supercapacitors based on poly(ionic liquid)-modified graphene electrodes. *ACS Nano*, 2011; 5 (1): 436–442.
- [120] Liu W, Ju C, Jiang D, Xu L, Mao H, Wang K. Ionic liquid-assisted grown of beta-nickel hydroxide nanowires on reduced graphene oxide for high-performance supercapacitors. *Electrochimica Acta*. 2014, 143:135–142.
- [121] Kim J, Kim S. Surface-modified reduced graphene oxide electrodes for capacitors by ionic liquids and their electrochemical properties. *Applied Surface Science*. 2014; 295, 31–37.
- [122] Yang X, Zhang L, Zhang F, Zhang T, Huang Y, Chen Y. A high-performance all-solid-state supercapacitor with graphene-doped carbon material electrodes and a graphene oxide-doped ion gel electrolyte. *Carbon*. 2014; 72, 381 – 386.
- [123] Tamilarasan P, Ramaprabhu S. Graphene based all-solid-state supercapacitors with ionic liquid incorporated polyacrylonitrile electrolyte. *Energy* 2013; 51, 374–381.
- [124] Pandey G P, Rastogi A C, Westgate C R. All-solid-state supercapacitors with poly(3,4-ethylenedioxythiophene)-coated carbon fiber paper electrodes and ionic liquid gel polymer electrolyte. *Journal of Power Sources*. 2014; 245, 857–865

Applications

Vibrational Spectroscopic Study on Lubrication and Corrosive Wear Mechanisms of Imidazolium Based Ionic Liquids

Seiya Watanabe, Miki Nakano, Koji Miyake,
Chiharu Tadokoro and Shinya Sasaki

Additional information is available at the end of the chapter

<http://dx.doi.org/10.5772/59132>

1. Introduction

Ionic liquids are liquid (molten) salts, distinguished by having melting points below room temperature [1]. The favorable properties of ionic liquids such as high thermal stability, low volatility, non-flammability, low melting point, and broad liquid range make them suitable for use in superior lubricants and additives. Moreover, the physical and chemical properties of ionic liquids can be tailored by changing the structure and type of the cation or anion. However, there are difficulties hindering the practical use of ionic liquids as lubricants. One of the most critical problems is that almost ionic liquids undergo a complex tribochemical reaction with metal surfaces [2-4]. In addition, the ionic liquid forms a characteristic structure at solid-liquid interface; the effect of this interfacial structure on the tribological properties has not been assessed because of the difficulties associated with the analysis [5-8]. Hence, for the molecular design of ionic liquids that can be used as lubricants, the mechanisms of corrosive wear and lubrication should be clarified. In this respect, developing an in situ technique that enables direct observation of the ionic liquid molecule under lubricating conditions is an important step toward understanding the complex molecular behavior of ionic liquids.

In this paper, we explain our recent research at attempting to clarify the mechanisms of corrosive wear and lubrication of ionic liquids. Specifically, we examined the corrosive wear induced by a tribochemical reaction via Fourier transform infrared (FT-IR) spectroscopy and the lubrication mechanism via sum frequency generation (SFG) spectroscopy.

2. Effect of water in ionic liquid on corrosive wear – Analysis by FT-IR spectroscopy [3,9]

2.1. Experimental

In general, the corrosive wear caused by an ionic liquid is attributed to the reaction between the halogen species in the anion part and water which is a common contaminant in ionic liquids. We used the hygroscopic 1-butyl-3-methylimidazolium trifluoromethanesulfonate ([BMIM] OTf) as a model ionic liquid and investigated the effect of water on corrosive wear against AISI 52100, which is a typical friction material. We used an FT-IR instrument equipped with a pin-on-disk tribometer for the analysis, with a calcium fluoride disk and an AISI 52100 pin with a diameter of 8 mm. The weight of the pin was 36 mN. This apparatus helped us obtain molecular information of the ionic liquid film sandwiched between the pin and the disk. To investigate the molecular behavior of water contained in the ionic liquid, the IR spectrum in the static state (without disk rotation) was mainly examined.

2.2. Results and discussion

Figure 1(a) shows time variations in the IR spectrum of the ionic liquid under static conditions (humidity: 4.6–6.9 g/m³, relative humidity: 20–30%). The test duration was 72 h. Figure 1(b) shows the surface image of the pin after the test. The IR spectra recorded over the test period showed that the ionic liquid absorbed water from the air. At the same time, it is important to note that two mixture phase of water were observed. The O-H stretching mode at ~3506 cm⁻¹ and ~3582 cm⁻¹ increased from the start of the test until 4–5 h had elapsed. However, after 5–7 h, a new peak at 3400 cm⁻¹ was observed, and the intensity of this peak started to increase.

IR analysis focusing on water in the ionic liquid was previously carried out by Cammarata et al. Figure 2 shows the IR spectrum of water mixed with different hydrophilic ionic liquids, from that study. The peaks for the O-H stretching mode at ~3506 cm⁻¹ and ~3582 cm⁻¹ were found to be attributed to “free water,” and this state corresponded to water molecules showing weak interactions with the anion [10]. The peak of the O-H stretching mode at 3400 cm⁻¹ was attributed to the three-coordinate integrated water state, that is, “liquid-like water,” and this state corresponded to water molecules interacting with one another to form a network structure [11].

From the above results, it was inferred that water is initially absorbed into the ionic liquid as free water, and after the elapse of 5–7 h, the amount of liquid-like water increases. Figure 1(b) shows the optical image of the pin surface after the test, indicating severe corrosion. On the other hand, when the test was stopped before the observed increase in the amount of liquid-like water (Figure 3), corrosion did not occur at the pin surface. From these results, it is evident that there is some relationship between the amount of liquid-like water and corrosion.

Subsequently, to clarify the relationship between sliding, corrosion, and the generation of liquid-like water, we attempted to investigate the water behavior in the rotating state. Tests were conducted at 10 rpm of disk rotation from the test start. The test duration was 8 h, and

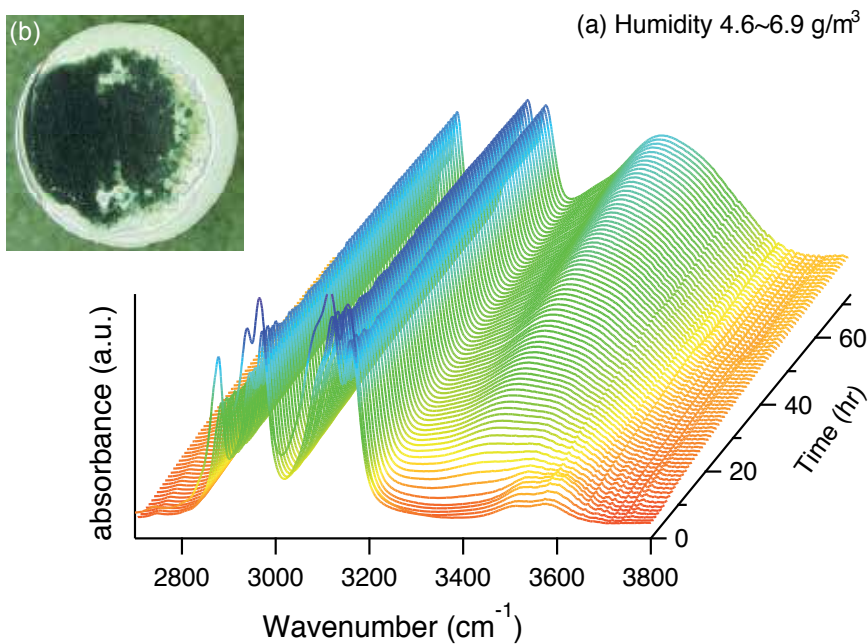


Figure 1. Static condition test for 72 hours at 4.6 ~ 6.9 g/m³ (a) Time dependent change of FT-IR spectra of [BMIM]OTf, (b) Pin surface image after the test [9]

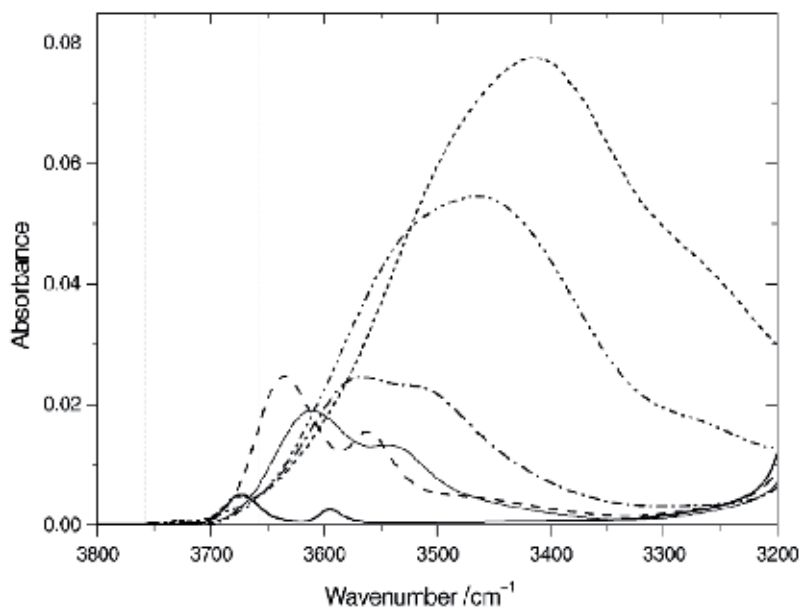


Figure 2. ATR-IR spectra of water in six ionic liquids [10]

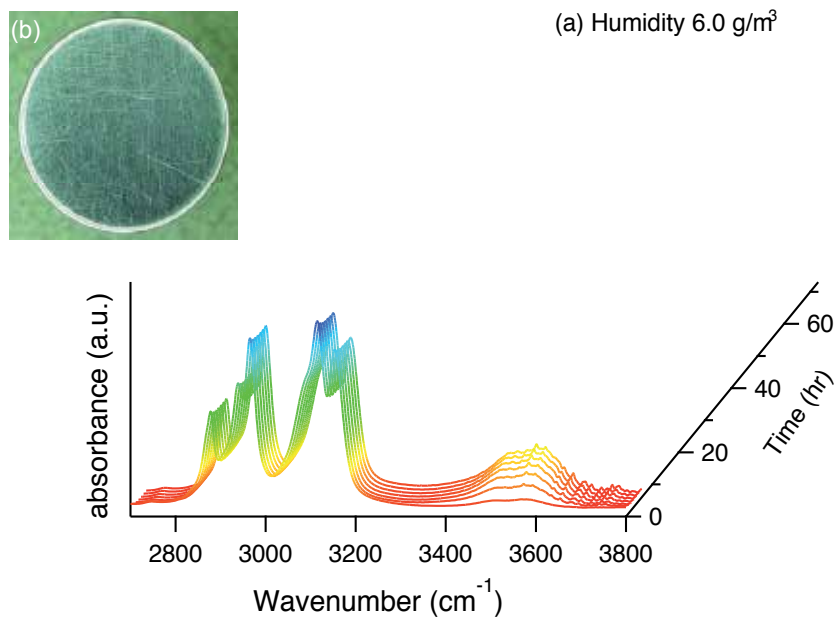


Figure 3. Static condition test for 5 hours at 6.0 g/m³ (a) Time dependent change of FT-IR spectra of [BMIM]OTf, (b) pin surface image after the test [9]

the humidity was 3.8 g/m³ (relative humidity: 20%). Time variations in the IR spectrum are shown in Figure 4(a). During the test period, the O-H stretching mode corresponding to liquid-like water was not observed, indicating that water is absorbed into the ionic liquid as free water. Corrosion was observed from the surface image after the test (Figure 4(b)), even though liquid-like water was not observed. The reason for this result is because scratch scars induced by sliding were created at the pin surface. The scars gave rise to a topical potential difference, consequently resulting in a galvanic corrosion environment. The absence of liquid-like water under rotating conditions was rationalized as follows: even if liquid-like water was produced near the frictional surface, it was instantly emitted from the shear field and went undetected by FT-IR. On the other hand, under static conditions, liquid-like water produced on the surface remained at the site of generation and increased in amount with time.

To confirm this consideration, we performed the test in the following sequence: the rotating state was maintained from the start of the test until 0.5 h had elapsed; subsequently, the disk was stopped and kept in a static state for 8 h. The test duration was set to 8 h for comparison with the rotation test. The humidity was 4.0 g/m³ (relative humidity: 22%). Figure 5(a) shows the variation in the IR spectrum over time. The intensity of the O-H peak corresponding to liquid-like water increased immediately after stopping the disk rotation. The corrosion proceeded in the rotation and static test (Figure 5(b)) than in the rotation test (Figure 4(b)). This result agrees with the results observed under static conditions; that is, the increase in the amount of liquid-like water relates to the corrosion.

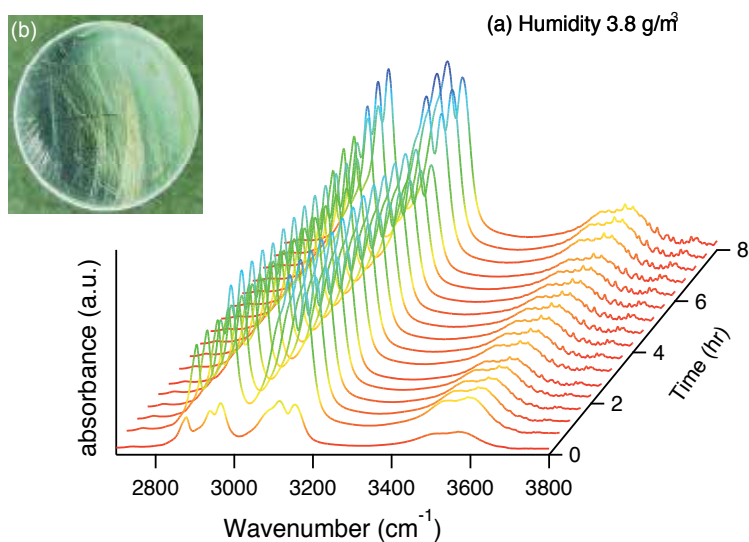


Figure 4. Rotation condition test for 8 hours at 3.8 g/m^3 (a) Time dependent change of FT-IR spectra of [BMIM]OTf, (b) pin surface image after the test [9]

In summary, there are two states of water in [BMIM] OTf: free water and liquid-like water. In addition, it is indicated that liquid-like water significantly affects the corrosion of ferrous materials.

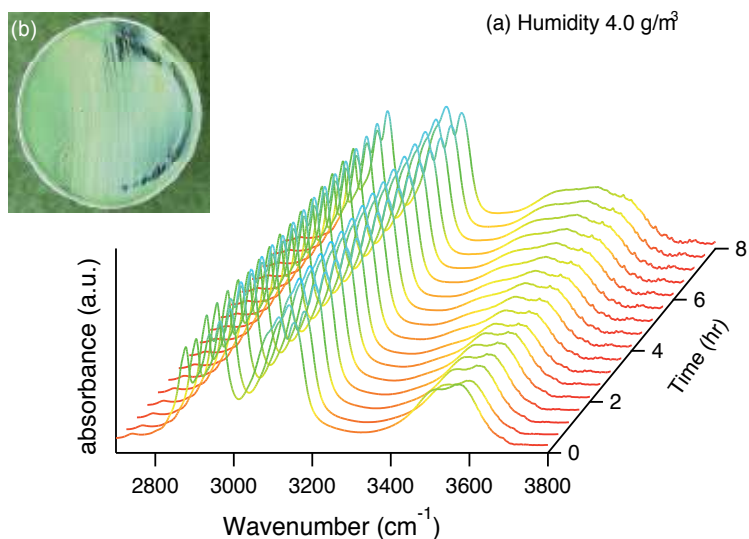


Figure 5. Rotation and static condition test for 8 hours at 4.0 g/m^3 (a) Time dependent change of FT-IR spectra of [BMIM]OTf, (b) pin surface image after the test

3. Effect of the solid-liquid interface of ionic liquid on frictional property – Analysis by SFG spectroscopy [12]

3.1. Experimental

For the effective design of ionic liquids to be used as lubricants in practical applications, it is important to clarify the relationship between molecular structure and frictional properties. Because an ionic liquid forms a characteristic interfacial structure that differs from the liquid bulk, we investigated the relationship between the frictional properties and the layer structure of ionic liquid formed at the interface. As mentioned in section 2, ionic liquids are understood to undergo complex chemical reactions with the surface of ferrous materials. Therefore, to minimize the influence of such reactions, we used a self-assembly monolayer (SAM) formed on a gold substrate as a model surface. In this study, we analyze the interfacial structure of an ionic liquid at SAM surfaces using SFG spectroscopy and discuss the effect of the interfacial structure of imidazolium-based ionic liquids on the frictional properties. Three 1-butyl-3-methylimidazolium [BMIM]-based ionic liquids were used: [BMIM]OTf, which is miscible with water; hexafluorophosphate ([BMIM]PF₆), which is water-insoluble; and tricyanomethide ([BMIM]TCC), which is water-insoluble and halogen-free. Mercaptohexadecanoic acid (MHDA), which forms a hydrophilic surface, was selected. The basics of SFG are as follows. Two pulsed laser beams, one of mode-locked visible frequency (ω_{vis}) and the other of variable-wavelength IR frequency (ω_{IR}) are overlapped at a surface, and the nonlinear optical effect of SFG results in the emission of light at $\omega_{\text{SFG}} = \omega_{\text{vis}} + \omega_{\text{IR}}$; this SFG light is detected. The intensity of the SFG light (I_{SFG}) is proportional to $|\chi^{(2)}|^2$, where $\chi^{(2)}$ is the second-order nonlinear susceptibility. Because $\chi^{(2)}$ is zero in centrosymmetric environments, SFG spectroscopy can be used to selectively probe the surface and interface [13, 14]. SFG measurements were conducted over the 2800–3200 cm⁻¹ wavenumber range, which includes the C-H stretching mode peaks and polarization of ppp (SFG, visible, infrared). In addition, the molecular orientation can be determined from the SFG intensity. In this study, the orientation angle of the imidazolium ring was analyzed. The obtained SFG spectra were fitted using the following function [15,16]:

$$I^{\text{SFG}}(\omega_2) \propto \left| \chi_{\text{NR}}^{(2)} + \sum_q \frac{A_q}{\omega_2 - \omega_q + i\Gamma_q} \right|^2 \quad (1)$$

$\chi_{\text{NR}}^{(2)}$ represents the nonresonant term and ω_2 represents the frequency of the IR light. A_q , ω_q , and Γ_q correspond to the amplitude, vibration frequency, and damping factor of the qth vibrational mode, respectively. We calculated the peak intensity from the relationship between A and Γ , which is obtained from the fitting result.

$$I_v = \left(\frac{A_v}{\Gamma_v} \right)^2 \quad (2)$$

The molecular orientation angle of the imidazolium ring was analyzed by the relation between the theoretical value and the experimental result of the peak intensity ratio of $\nu_{SS}HC_{(4)}-C_{(5)}H$ to $\nu_{AS}HC_{(4)}-C_{(5)}H$. We assumed the stretching vibration of methylene but omitted the detailed molecular orientation analysis [17, 18]. Figure 6 shows the definition of the orientation angle (θ , φ , χ) of the imidazolium ring. A tilt angle θ of 0° is defined as the surface normal and that of 90° as parallel to the surface plane. A twist angle φ of 0° is defined as parallel to the surface and that of 90° as perpendicular to the surface. The azimuthal angle χ is within the plane of the surface. In this calculation, the average of the Euler angles can be calculated for the rotationally isotropic system in the interface plane, i.e., with no azimuthal angle χ dependence. Baldelli et al. noted that the twist angle φ of an imidazolium ring ranges from 0° to 30° because of molecular steric hindrance [17]. Therefore, we calculated the value of φ in this range.

In addition, we performed friction tests to investigate the effect of the interfacial structure of the ionic liquid at the MHDA surface on the frictional properties using a pin-on-plate reciprocating friction tester. We used MHDA, which forms a hydrophilic surface on a gold substrate, as the plate specimen and borosilicate glass, with a tip diameter of 3 mm, as the pin. We conducted a sliding test at a reciprocating frequency of 0.1 Hz, amplitude of 10 mm, sliding speed of 1 mm/s, and load of 10 mN. The test duration was 180 min, and the friction test was performed four times for each ionic liquid.

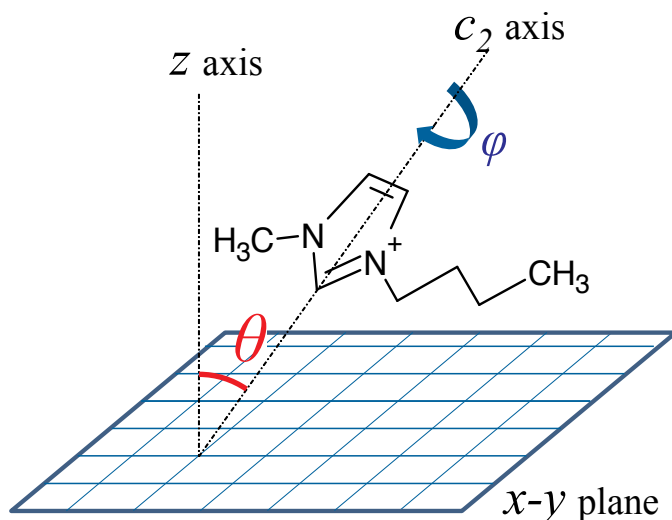


Figure 6. Definition of imidazolium orientation angle in the laboratory coordination

3.2. Results and discussion

Figure 7 shows the SFG spectrum of each ionic liquid spin-coated on the MHDA surface, in the range of 3200–3050 cm^{-1} . Three dip peaks were observed, which were attributed to the C-H stretching mode derived from the imidazolium ring: $\sim 3127 \text{ cm}^{-1}$ ($\nu_{\text{C}_2\text{H}}$), $\sim 3153 \text{ cm}^{-1}$ ($\nu_{\text{AS}}\text{HC}_{(4)}\text{-C}_{(5)}\text{H}$), and $\sim 3174 \text{ cm}^{-1}$ ($\nu_{\text{SS}}\text{HC}_{(4)}\text{-C}_{(5)}\text{H}$) [18,19].

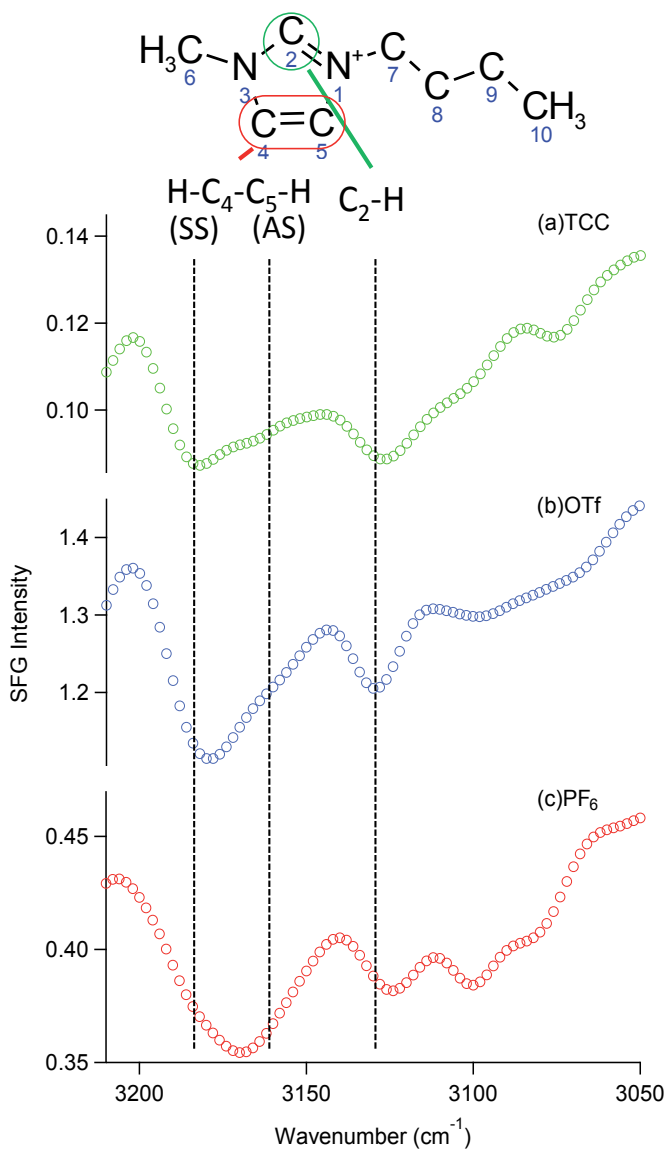


Figure 7. SFG spectrum in the range of 3200 – 3050 cm^{-1} which includes C-H stretching mode peaks derived from cation of (a) TCC, (b) OTf and (c)PF₆.

Figure 8 shows the relationship between the SFG intensity ratio and the molecular orientation angle of the imidazolium ring, which is theoretically calculated. In addition, the figure includes the intensity ratios obtained from the fitting result of the SFG spectra in Figure 7. From the result of the molecular orientation analysis of the imidazolium ring, the imidazolium tilt angle θ is determined to be 30–33° for [BMIM]TCC, 40–45° for [BMIM]OTf, and 61–65° for [BMIM]PF₆. This difference between the tilt angles for the three ionic liquids could be attributed to the respective anion sizes. The anion radii follow the order PF₆ (1.57 Å) < OTf (1.94 Å) < TCC (2.57 Å); that is, PF₆ had the smallest size. Thus, there is a clear relationship between the anion size and the tilt angle of the imidazolium ring; that is, a smaller anion results in a larger tilt angle.

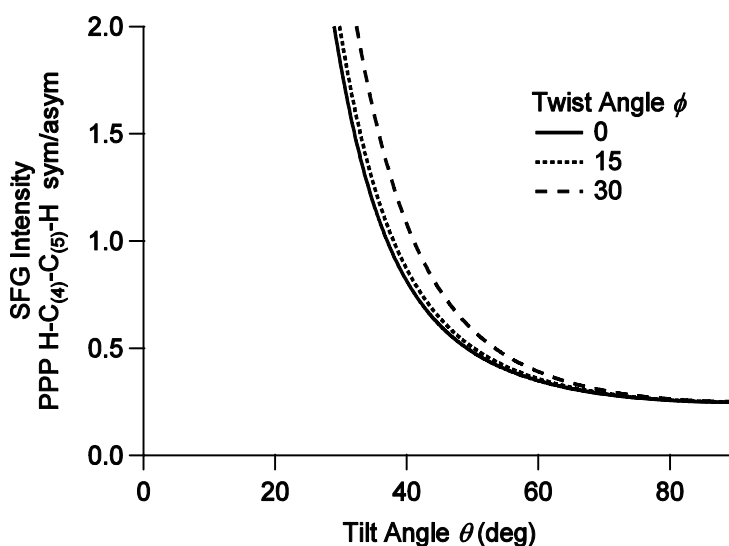


Figure 8. The relation between SFG intensity ratio of $\nu_{SS}HC(4)-C(5)H$ to $\nu_{AS}HC(4)-C(5)H$ and molecular orientation angle of imidazolium ring.

Figure 9 shows the relationship between the tilt angle of the imidazolium ring and the mean value of the friction coefficient. [BMIM]PF₆ exhibited the lowest friction coefficient, followed by [BMIM]OTf and [BMIM]TCC. In addition, the results indicated a clear trend: the larger the imidazolium ring tilt angle, the smaller was the corresponding friction coefficient.

We now discuss how the tilt angle of the imidazolium ring affects the frictional properties under a shear field. We propose two possible explanations for the tilt-angle dependence on the frictional properties: the film formation ability and the energy loss by molecular motion.

- Film formation ability

A small anion forms a dense film because in this case, the distance between the anion and the cation is short. This dense film is capable of supporting a load and preventing serious breakdown, consequently leading to friction reduction.

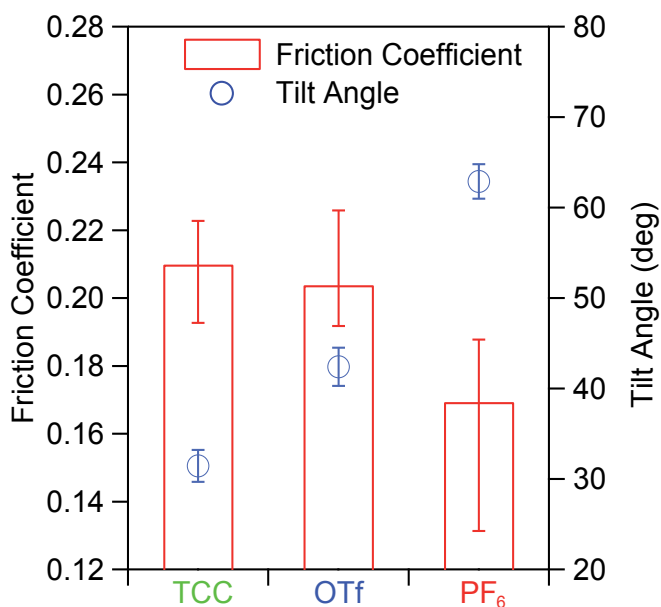


Figure 9. The relation between tilt angle of imidazolium and friction coefficient

- Energy loss by molecular motion

The molecular motion hypothesis is based on the supposition that the entire surface layer of the ionic liquid has sufficient ability to support a load and prevent serious breakdown. The diagonal length of the imidazolium ring is approximately 1.12 Å, which is comparable to the radius of the PF₆ anion (1.57 Å); consequently, a smoother and better-defined shear plane is formed [20]. This smooth surface limits energy loss by the rotation of the imidazolium ring, and the shear-induced increase in the lattice spacing of the surface layer of the ionic liquid. As a result, friction would be reduced. On the other hand, the difference in size between the imidazolium ring and the OTf or TCC anion might make the surface rough. Under a shear field, energy is needed for the rotation of the imidazolium ring and extension of the lattice spacing of the surface layer of the ionic liquid, so that the rough surface is smoothed.

4. Conclusion

We investigated the mechanisms of corrosive wear and lubrication of ionic liquids from the viewpoint of molecular behavior. FT-IR results indicated the presence of two types of water phases within [BMIM]OTf, viz., free water and liquid-like water; the liquid-like water has a more pronounced effect on corrosion. In addition, comparison of the results of molecular orientation analysis by SFG spectroscopy and the results of friction tests revealed that the tilt angle of the imidazolium ring affects the frictional properties of the ionic liquid.

Thus, a combination of friction tests with FT-IR or SFG spectroscopy enables us to evaluate tribochemical reactions or the relationship between the interfacial molecular arrangement and the frictional properties. These methods serve to advance the understanding of interfacial phenomena in the field of tribology.

Author details

Seiya Watanabe¹, Miki Nakano², Koji Miyake², Chiharu Tadokoro¹ and Shinya Sasaki^{1*}

*Address all correspondence to: s.sasaki@rs.tus.ac.jp

1 Tokyo University of Science, Niijuku, Katsushika-ku, Tokyo, Japan

2 National Institute of Advanced Industrial Science and Technology, Namiki, Tsukuba, Ibaraki, Japan

References

- [1] Wilkes JS, Zaworotko M J. Air and water stable 1-ethyl-3-methylimidazolium based ionic liquids. *J. Chem. Soc., Chem. Commun.* 1992;13 965-967.
- [2] Swatloski RP, Holbrey JD, Rogers RD. Ionic liquids are not always green: Hydrolysis of 1-butyl-3-methylimidazolium hexafluorophosphate. *Green Chem.* 2003;5 361-363.
- [3] Watanabe S, Nakano M, Miyake K, Tsuboi R, Sasaki S. Effect of Water on Tribocorrosion of Imidazolium Based Ionic Liquid. *Transactions of the Japan Society of Mechanical Engineers Series C* 2013;79 3272-3284. [in Japanese]
- [4] Watanabe S, Takiwatari K, Nakano M., Miyake K, Tsuboi R, Sasaki S. Molecular Behavior of Room-temperature Ionic Liquids under Lubricating Condition. *Tribol. Lett.* 2013;51 227-234.
- [5] Mezger M., Schröder H, Reichert H, Schramm S, Okasinski JS, Schöder S, Honkimäki V, Deutsch M, Ocko BM, Ralston J, Rohwerder M, Stratmann M, Dosch H. Molecular Layering of fluorinated ionic liquids at a charged sapphire (0001) surface. *Science* 2008;322424-428.
- [6] Sweeney J, Hausen F, Hayes R, Webber GB, Endres F, Rutland MW, Bennowitz R, Atkin R. Control of nanoscale friction on gold in an ionic liquid by a potential-dependent ionic lubricant layer. *Phys. Rev. Lett.* 2012;109 155502.
- [7] Baldelli S. Surface structure at the ionic liquid-electrified metal interface. *Acc. Chem. Res.* 2008;41(3) 421-431.

- [8] Iwahashi T, Miyamae T, Kanai K, Seki K, Kim D, Ouchi Y. Anion configuration at the air/liquid interface of ionic liquid [bmim]OTf studied by sum-frequency generation spectroscopy. *J. Phys. Chem. B* 2008;112 (38) 11936-11941.
- [9] Watanabe S, Nakano M, Miyake K, Tsuboi R, Sasaki S. Spectroscopic Study on Lubrication and Tribo-Corrosion Mechanisms of Ionic Liquid. *J. Surf. Sci. Soc. Jpn.* 2014;35 (8) 443-448. [in Japanese].
- [10] Cammarata L, Kazarian SG, Salter PA, Welton T. Molecular states of water in room temperature ionic liquids. *Phys. Chem. Chem. Phys.* 2001;3 5192-5200
- [11] Noguchi H, Okada T, Uozaki K. SFG study on potential-dependent structure of water at Pt electrode/electrolyte solution interface. *Electrochimica Acta* 2008;53 6841-6844.
- [12] Watanabe S, Nakano M, Miyake K, Tsuboi R, Sasaki S. Effect of Molecular Orientation Angle of Imidazolium Ring on Frictional Properties of Imidazolium-based Ionic Liquid. *Langmuir* 2014;30 8078-8084.
- [13] Zhu XD, Suhr H, Shen YR. Surface vibrational spectroscopy by infrared-visible sum frequency generation. *Phys. Rev. B* 1987;35 (6) 3047-3050.
- [14] Hirose C, Akamatsu N, Domen K. Formulas for the analysis of surface sum-frequency generation spectrum by CH stretching modes of methyl and methylene groups. *J. Chem. Phys.* 1992;96 (2) 997-1004.
- [15] Zhuang X, Miranda PB, Kim D, Shen YR. Mapping molecular orientation and conformation at interfaces by surface nonlinear optics. *Phys. Rev. B* 1999;59 (14) 12632-12640.
- [16] Wei X, Hong S, Zhuang X, Goto T, Shen YR. Nonlinear optical studies of liquid crystal alignment on a rubbed polyvinyl alcohol surface. *Phys. Rev. E* 2000;62 (4) 5160-5172..
- [17] Romero C, Moore HJ, Lee T R, Baldelli S. Orientation of 1-butyl-3-methylimidazolium based ionic liquids at a hydrophobic quartz interface using sum frequency generation spectroscopy. *J. Phys. Chem. C* 2007; 111 (1), 240-247.
- [18] Romero C, Baldelli S. Sum frequency generation study of the room-temperature ionic liquids/quartz interface, *J. Phys. Chem. B* 2006;110(12) 6213-6223.
- [19] Heimer NE, Del Sesto RE, Meng Z, Wilkes JS, Carper WR. Vibrational spectra of imidazolium tetrafluoroborate ionic liquids. *J. Mol. Liq.* 2006;124 84-95.
- [20] Li H, Rutland WM, Atkin R. Ionic liquid lubrication: Influence of ion structure, surface potential and sliding velocity. *Phys. Chem. Chem. Phys.* 2013;15 14616-14623.

Ionic Liquids Applied to Improve the Dispersion of Solids in Elastomers

Magdalena Maciejewska and Marian Zaborski

Additional information is available at the end of the chapter

<http://dx.doi.org/10.5772/58980>

1. Introduction

Rubber compounds consist of an elastomer matrix and solid additives. The most important role of these additives is to act as fillers and vulcanization activators in the case of sulfur crosslinked elastomers. Elastomers are filled with small and hard particles to improve their mechanical properties, such as resistance to abrasion, elastic modulus, and hardness [1]. Reinforcing fillers added to an elastomer can provide a rubber product with a very high tensile strength or tear resistance [2]. The basic requirement to achieve the optimum reinforcement is a fine and homogeneous dispersion of filler particles in the elastomer matrix, which results in effective interactions and good adhesion at the elastomer/filler interface. Due to their unique physical and chemical properties, over the past few years polymer composites with nanofillers such as nanosilica, carbon black, layered silicates, and carbon nanotubes have been widely discussed [3, 4]. It has been proven that the degree of dispersion of nanofiller particles is crucial to achieve the ultimate required properties of nanocomposites [5]. Unfortunately, nanofillers exhibit a high tendency to agglomerate in the elastomer matrix because of their high surface energy [6, 7]. Therefore, it is technologically challenging to obtain a homogeneous dispersion of filler nanoparticles in elastomers.

Recently, ionic liquids (ILs) have been widely used to improve the degree of dispersion of nanoparticles in polymers, particularly in elastomers [8-10]. ILs are typically organic salts with the melting points below 100 °C [11]. Due to their unique properties such as thermal, chemical, and electrochemical stability, low vapor pressure, and high ionic conductivity, ILs have attracted much attention for applications in polymer science [11-13], particularly toward developing conducting polymer composites. ILs have excellent ionic conductivity up to their decomposition temperature, which enables them to play an important role in electrolyte matrices. For example, N-ethylmethylimidazolium bis(trifluoromethanesulfonyl)imide

(EMITFSI) was used for the preparation of flexible solid polymer electrolytes based on acrylonitrile-butadiene elastomers and poly(ethylene oxide) [14]. The formation of either cationic and anionic interpenetrating or semi-interpenetrating polymer networks caused a considerable increase in the tensile strength and elasticity of the polymer electrolyte. When swollen in EMITFSI, the composites exhibited good mechanical properties and elongation at break, and an ionic conductivity higher than 10^{-4} S cm⁻¹ at room temperature. Similar results were obtained for interpenetrating polymer networks containing alkylpyrrolidinium bis(trifluoromethanesulfonyl)imides [15]. Conductive NBR composites with an ionic conductivity of 2.54×10^{-4} S cm⁻¹ have also been prepared using 1-butyl-3-methylimidazolium bis(trifluoromethylsulfonyl)imide [16]. This ionic liquid was also used to produce conductive composites from poly(methyl methacrylate) containing in situ formed silica [17]. When increasing the IL content, the conductivity of the obtained hybrid ionogels increased, and a decrease in the Young's modulus was observed as a result of the plasticizing effect of ILs. Similar results were reported for N-ethylimidazolium bis(trifluoromethylsulfonyl)imide (EITFSI). Composites consisting of NBR and ionic liquid were prepared as elastic and thermally stable polymer electrolytes, and EITFSI showed good miscibility with NBR. The presence of lithium salts in NBR/EITFSI composites enhanced the ionic conductivity approximately 100 times to reach 1.0×10^{-4} S cm⁻¹ at 30 °C [18].

Moreover, some ILs have been suggested to be used for solubilizing metal oxides [19]. This property could be useful in the improvement of dispersion degree of metal oxide particles in elastomers. 1-allyl-3-methylimidazolium chloride (AMICl) was applied to improve the dispersion of particles in carbon black-filled elastomers. Attractive interactions between the carbon black surface and AMICl, which result from the interaction of π -electrons of graphitic structures at the carbon black surface with the cations of ionic liquid, have been demonstrated. AMICl acted as plasticizer at the carbon black surface and accelerated the formation of the carbon black network in the elastomer matrix, supporting the depletion of polymer chains from the space between carbon black aggregates. Moreover, an increase in the conductivity of elastomer composites was observed [10]. ILs have also been reported to improve the dispersion of silica and clays [20, 21]. For example, 1-methylimidazolium sorbate was used as modifier for silica to increase the interfacial interactions between the filler and styrene-butadiene rubber (SBR). As a result, the mechanical performance of SBR/silica composites were effectively improved, and similar results were also achieved for 1-methylimidazolium methacrylate (MimMa). The ionic liquid was reactive toward SBR through the graft copolymerization onto elastomer chains during vulcanization. Hydrogen bonding between silica particles and the ionic unit of MimMa was shown to be present. As a result, the interactions between silica particles were weakened, and the filler networking of silica in SBR was effectively restrained. An improvement in the dispersion of silica and the mechanical properties of vulcanizates, particularly damping behavior and abrasion resistance, was observed [8]. Imidazolium salts have been demonstrated as excellent cationic treatments for layered silicates (clays). The best activity was achieved when one of the imidazolium alkyl groups of the IL was a C16 aliphatic chain [22]. This IL exhibited excellent compatibility with polymers, and due to its high thermal stability, it enabled high-temperature curing and melt processing. Trihexyltetradecylphosphonium tetrafluoroborate was used for cationic exchange on the surfaces of natural and

synthetic nanoclays [21]. Significant enhancements in the thermal stability of nanoclays were achieved, up to 150 °C, compared with conventional quaternary ammonium-modified silicates. These IL-modified nanoclays have been melt blended with poly(ethylene terephthalate) (PET), and optically transparent nanocomposites with high levels of exfoliation have been produced, in which nanoclay platelets were uniformly dispersed in the PET matrix.

Polymer composites filled with carbon nanotubes (CNTs) are of particular interest for the development of conductive polymer nanocomposites or nanoelectronic devices [23, 24]. A major problem in this field is to ensure the homogeneous dispersion of carbon nanotubes in the polymer matrix due to the high ability of these tubes to agglomerate. One of the techniques to improve the dispersion of CNTs in polymers is their chemical modification through covalent or noncovalent attachments of CNT functional groups with the matrix [25]. To enhance the CNT/polymer interactions, ILs have been commonly used. For example, conducting polychloroprene rubber composites were developed using 1-butyl-3-methylimidazolium bis(trifluoromethylsulfonyl)imide and multi-walled carbon nanotubes (MWCNTs). The cation- π -interactions between the ionic liquid and tubes resulted in improved dispersion and the formation of a percolating MWCNT network that significantly increased the conductivity of the rubber composite. It was believed that the bundles of MWCNTs were uniformly distributed due to the strengthening of filler-rubber interactions, as well as the reduction in the inter-tubular interactions between the tubes. This was confirmed by the Payne effect in the composite, which is associated with the network formation of exfoliated carbon nanotubes in the rubber matrix. This secondary aggregate network of filler is broken down with the increase in the strain amplitude, and as a consequence, a decrease in the storage module was observed in the dynamic mechanical analysis. Moreover, the ILs acted as a plasticizer, affecting the storage module of the composite [9, 26].

ILs have also been applied to ensure better compatibility and enhance the dispersibility of MWCNTs in a blend of solution-SBR and polybutadiene rubber [27]. The best activity was found for the ionic liquid with a double bond in the cation (AMICl). In this case, the best reinforcing effect of the MWCNTs toward the rubber blend was achieved. It was suggested that the double bond in the AMICl molecules was chemically linked with the diene rubber double bonds by sulfur bridges. Additionally, in the presence of AMICl, the nanotubes strongly adhered to the rubber phase and formed a special type of bound rubber aggregation. No agglomeration of the MWCNTs was observed, leading to a continuous percolation network that increased the electrical and mechanical performance of the composites. Moreover, dynamic behavior in the vicinity of the CNT surface was detected by observing an extra relaxation peak at a temperature of approximately 80 °C. It was hypothesized that AMICl, having a reactive double bond towards sulfur vulcanization, reacted with the other reactive sites of the diene rubber. In this way, relaxation of the bound rubber that was very close to the surface of the CNTs took place at higher temperatures. In general, the use of imidazolium ILs gives rise to new possibilities to develop CNT composites with commodity polymers such as polystyrene (PS). For example, 1-cetyl-2, 3-dimethylimidazolium tetrafluoroborate was reported as an excellent compatibilizer for MWCNTs toward polystyrene [28]. This PS composite contained highly dispersed individual carbon nanotubes. However, the mixture of

the MWCNTs and ionic liquid needed pretreatment at 185°C before it was added to the polymer; otherwise, the MWCNTs were hardly dispersed in the PS and formed large agglomerates. Evidence for π interactions between the nanotubes and the imidazolium cation of the ILs was also reported. Moreover, the 20 °C improvement in the thermal stability of the PS composites was also demonstrated, which was explained by the enhanced degree of dispersion of the carbon nanotubes in the polymer matrix and better interfacial bonding between them.

Regarding elastomer compounds, one of the most important solid additives is vulcanization activator. Zinc oxide is widely used as an activator of the vulcanization of unsaturated elastomers by sulfur. It increases the amount of bound sulfur and as a result improves the efficiency of the crosslinking system. Additionally, zinc oxide reduces the vulcanization time of rubber compounds and improves the processing and physical properties of vulcanizates. Despite the important role of zinc oxide in sulfur vulcanization, its concentration in rubber compounds must be restricted to at least below 2.5% because zinc oxide is classified as being toxic to aquatic life. The release of zinc from rubber products occurs during their manufacturing, use, and recycling or disposal in landfills. Therefore, over the past several years, human activity has caused a significant increase in the amount of zinc in the environment. Designed EU legislation regarding environmental protection requires a reduction in the use of zinc oxide and zinc-containing compounds in technology. For elastomer technology, the most important of these is the European Commission Directive 2003/105/EC, which dictates that rubber products containing more than 2.5% of zinc compounds are considered to be highly toxic to aquatic ecosystems. Thus, methods to reduce the amount of zinc oxide in elastomers have been widely studied. The possibilities of reducing the ZnO content by incorporating zinc with a higher chemical activity in the form of reactive zinc complexes has been reported [29]. The availability of zinc ions in a complex molecule is believed to be higher than that in ZnO crystals. It has been shown that the zinc oxide content in natural rubber or ethylene-propylene-diene elastomer compounds can be reduced to 2 phr without affecting their vulcanizate properties [30]. Further reduction requires the use of anti-reversion agents. Another demonstrated approach to reduce the amount of Zn²⁺ ions in rubber compounds is the deposition of zinc ions on the surface of layered aluminosilicate, which also could serve as a filler [31]. However, the crosslink density of vulcanizates was significantly lower due to the low content of zinc ions in the crosslinking system and their limited availability for interaction. According to Nieuwenhuizen [32], the ZnO surface acts as a catalytic reaction template by activating and joining reactants. Accelerator particles, sulfur, and fatty acids diffuse through the elastomer matrix and are adsorbed onto the ZnO surface, forming intermediate reactive complexes. Therefore, the contact between the ZnO particles and accelerators in the elastomer matrix should be maximized to enhance the efficiency of zinc oxide during vulcanization. This contact depends on the ZnO particle shape, size, and specific surface area. Therefore, to reduce the amount of ZnO in rubber compounds, we intend to apply nanosized zinc oxide. A reduction in the particle size results in an increase in the zinc oxide specific surface area, providing better contact between the zinc oxide, accelerators, and sulfur particles. However, the dispersion of zinc oxide particles in an elastomer is also very important for the activation of sulfur vulcanization. Unfortunately, zinc oxide exhibits a high tendency to agglomerate in the elastomer matrix because of its high surface energy [6, 33]. From a technological point of view, it is difficult to

obtain a homogeneous dispersion of ZnO nanoparticles in elastomers. Because zinc oxide and vulcanization accelerators are insoluble in rubber, it is assumed that the crosslinking reactions occur in a two-phase system and are catalyzed by conventional phase transfer catalysts. ILs are thought to catalyze the interfacial reactions; therefore, they can be assumed to play the same role in the crosslinking process [11]. Traditionally, stearic acid is used to improve the dispersion of zinc oxide in the elastomer. A complex of zinc, an accelerator, and fatty acid is formed during the vulcanization and consists of a central zinc cation, two stearyl anions, and accelerator residues. This complex is strongly polar and also exhibits a tendency to agglomerate in the elastomer. The crosslinking efficiency depends on the mobility of zinc ions in the complex molecule and on the diffusion rate of the remaining components in the crosslinking system. Therefore, the application of ligands with higher degrees of solvation towards zinc cations than towards stearyl anions should improve the dispersion of the components of the crosslinking system in the elastomer matrix, which is a role that ILs could play [33].

Designing ILs with special and functional structures is of crucial importance in exploring novel dispersing agents for nanosized zinc oxide and silica in elastomer composites. ILs can be fabricated with a high efficiency, and their structure can be easily tailored using various commercially available and cheap raw materials. Our preliminary studies have shown that an improvement in the dispersion of ZnO nanoparticles due to the ILs reduced the zinc ion content in vulcanizates, according to European Commission Directive 2003/105/EC. ILs also reduced the vulcanization time of the rubber compounds significantly and increased the crosslink density of the vulcanizates. Applying alkyylimidazolium chlorides and tetraalkylammonium bromides allowed for the production of vulcanizates with the amount of zinc oxide, sulfur, and MBT reduced to 1.3 phr. These vulcanizates exhibit tensile strengths comparable to those without a dispersing agent [33].

Therefore, in this work, we intended to apply long-chain alkyylimidazolium salts of chlorides, bromides, tetrafluoroborates, and hexafluorophosphates to improve the dispersion degree of zinc oxide nanoparticles in the butadiene-styrene (SBR) and ethylene-propylene-diene elastomers (EPDM) and, as a result, increase its activity during crosslinking. Moreover, because of the catalytic activity of ILs during interfacial reactions, an increase in the crosslinking efficiency is expected. In these studies, ILs such as alkyylimidazolium salts with decyl-, didecyl-, dodecyl-, octadecyl-, and hexadecyl-chains in the cation, together with nanosized zinc oxide, were used to develop elastomer composites with a reduced amount of vulcanization activator. Vulcanizates were filled with nanosized silica in order to improve their mechanical performance.

2. Experimental section

2.1. Materials

The butadiene-styrene elastomer (KER 1500) containing 22-25 wt % styrene was obtained from Synthos Dwory, Oswiecim (Poland). Its Mooney viscosity was (ML1+4 (100°C):46-54). It was vulcanized with sulfur (Siarkopol Tarnobrzeg, Poland) with microsized zinc oxide as the

standard activator (ZnO, Aldrich, Germany). 2-mercaptobenzothiazole (MBT, Aldrich, Germany) and N-cyclohexyl-2-benzothiazolesulfenamamide (CBS, Aldrich, Germany) were applied as accelerators.

Ionic Liquid	Symbol
1-Decyl-3-methylimidazolium chloride	DMICI
1-Decyl-3-methylimidazolium tetrafluoroborate	DMIBF ₄
1, 3-Didecyl-2-methylimidazolium chloride	DIDMICI
1-Dodecyl-3-methylimidazolium chloride	DODMICI
1-Dodecyl-3-methylimidazolium bromide	DODMIBr
1-Dodecyl-3-methylimidazolium tetrafluoroborate	DODMIBF ₄
1-Dodecyl-3-methylimidazolium hexafluorophosphate	DODMIPF ₆
1-Hexadecyl-3-methylimidazolium chloride	HDMICI
1-Hexadecyl-3-methylimidazolium tetrafluoroborate	HDMIBF ₄
1-Hexadecyl-3-methylimidazolium hexafluorophosphate	HDMIPF ₆
1-Methyl-3-octadecylimidazolium chloride	MODICI
1-Methyl-3-octadecylimidazolium hexafluorophosphate	MODIPF ₆

Table 1. Ionic liquids used in this study

The ethylene-propylene-diene elastomer (Buna 5450) containing 48-56 wt % ethylene and 3.7-4.9 wt % ethylidene norbornene was obtained from Lanxess (Germany). Its Mooney viscosity was (ML1+4 (125°C):41-51). It was vulcanized with sulfur (Siarkopol Tarnobrzeg, Poland) with micro-sized zinc oxide as the standard activator (ZnO, Aldrich, Germany). 2-mercaptobenzothiazole (MBT, Aldrich, Germany), tetramethylthiuram monosulfide (TMTM, Akrochem Corporation, USA) and zinc dibutyldithiocarbamate (ZDBC, Performance Additives, Malaysia) were applied as accelerators.

To reduce the amount of zinc ions in the rubber compounds, nanosized zinc oxide (nZnO, Nanostructured & Amorphous Materials, Inc., USA) was used as an alternative to micro-sized ZnO. Silica with a specific surface area of 380 m²/g (Aerosil 380, Evonic Industries, Germany) was used as a filler. The ionic liquids given in Table 1 were obtained from IoLiTec (Germany).

2.2. Preparation and characterization of rubber compounds

Rubber compounds with the formulations given in Table 2 were prepared using a laboratory two-roll mill. The samples were cured at 160 °C until they developed a 90% increase in torque, as measured by a rotational rotorless rheometer. The kinetics of rubber compound vulcanization was studied using a DSC1 (Mettler Toledo) analyzer by decreasing the temperature from 25 to 100 °C at a rate of 10 °C/min and then heating to 250 °C with the same heating rate.

The crosslink densities (ν_T) of the vulcanizates were determined by their equilibrium swelling in toluene, based on the Flory-Rehner equation [34]. The Huggins parameter of the SBR-solvent interaction (χ) was calculated from the equation 1

$$\chi = 0.370 + 0.560V_r \tag{1}$$

where V_r is the volume fraction of elastomer in the swollen gel and for the EPDM-solvent interaction.

$$\chi = 0.425 + 0.340V_r \tag{2}$$

The tensile properties of the vulcanizates were measured according to the ISO-37 standard procedures using a ZWICK 1435 universal machine.

SBR (phr)		EPDM(phr)	
Elastomer	100	Elastomer	100
Sulfur	2	Sulfur	2.5
*ZnO	5	*ZnO	5
MBT	1	MBT	1
CBS	1	TMTM	1
Silica	30	ZDBC	1.5
Ionic liquid	1.5	Silica	30
-		Ionic liquid	1.5

Table 2. Composition of the SBR and EPDM-based rubber compounds (*2 phr of nanosized zinc oxide was used as an alternative to 5 phr of standard activator)

2.3. Dynamic-mechanical analysis

Dynamic-mechanical measurements were carried out in tension mode using a DMA/SDTA861^e analyzer (Mettler Toledo). Measurements of the dynamic moduli were performed over the temperature range of -80-100°C with a heating rate of 2°C/min, a frequency of 1 Hz, and a strain amplitude of 4 μm. The temperature of the elastomer glass transition was determined from the maximum of $\tan \delta=f(T)$, where $\tan \delta$ is the loss factor and T is the measurement temperature.

2.4. Scanning Electron Microscopy (SEM)

The degree of dispersion of crosslinking agents and filler nanoparticles in the elastomer matrix was estimated using scanning electron microscopy with a LEO 1530 SEM. The vulcanizates were broken down in liquid nitrogen and the surfaces of the vulcanizate fractures were examined. Prior to the measurements, the samples were coated with carbon.

2.5. Thermogravimetric analysis

The thermal stability of the vulcanizates was studied using a TGA/DSC1 (Mettler Toledo) analyzer. Samples were heated from 25 °C to 700 °C in an argon atmosphere (60 ml/min) with

a heating rate of 10 °C/min. Decomposition temperatures at a weight loss of 2% (T_{02}), 5% (T_{05}), 50% (T_{50}), and the total weight loss during decomposition of the vulcanizates were determined.

2.6. Thermo-oxidative and UV aging

The thermo-oxidative degradation of the vulcanizates was performed at a temperature of 100 °C for 240 h. The UV degradation of the vulcanizates was carried out for 120 h using a UV 2000 (Atlas) machine in two alternating segments: a day segment (irradiation 0.7 W/m², temperature 60 °C, time 8 h) and a night segment (without UV radiation, temperature 50 °C, time 4 h).

To estimate the resistance of the samples to aging, their mechanical properties and crosslink densities after aging were determined and compared with the values obtained for the vulcanizates before the aging process. The aging factor (S) was calculated as the numerical change in the mechanical properties of the samples upon aging (Equation 3) [35], where TS is the tensile strength of the vulcanizates and EB is the elongation at break:

$$S = \frac{(TS \cdot EB)_{\text{after aging}}}{(TS \cdot EB)_{\text{before aging}}} \quad (3)$$

3. Results and discussion

3.1. SBR composites containing ILs

Dispersion degree of activator and filler nanoparticles in the SBR

The degree of dispersion of zinc oxide nanoparticles in the elastomer matrix is very important to the activation of sulfur vulcanization. Homogeneous dispersion of ZnO nanoparticles provides better contact between the activator and other components of the crosslinking system and, as a consequence, enhances the efficiency of zinc oxide during vulcanization. SEM images were taken to estimate the dispersion degree of zinc oxide particles in the elastomer in the presence of ILs (Figures 1-6).

The zinc oxide nanoparticles (Figure 1) are not homogeneously distributed in the SBR. They create microsized agglomerates with different shapes, consisting of nanosized primary particles. The high tendency of ZnO particles to agglomerate results from their high surface energy and ability for specific interactions [6]. The agglomeration of zinc oxide particles causes their surface area to decrease, followed by a decrease in the interface between the ZnO, accelerator, and sulfur particles. As a result, the efficiency of elastomer crosslinking decreases. In general, the ILs improved the dispersibility of ZnO and silica nanoparticles in the SBR, but to different degrees. Homogeneous dispersion of the nanoparticles was achieved for DMICl, DDMIBF₄, and MODIPF₆. These ILs seemed to be the best dispersing agents, which effectively prevented ZnO and filler nanoparticles from agglomeration. In the case of HDMICl- and MODICl-containing vulcanizates, some agglomerates of nanoparticles can be seen; however, they are of smaller size and better elastomer wettability than those observed for the vulcani-

zates without IL. The different effect of ILs on the dispersibility of nanoparticles in the elastomer matrices could result from their different miscibilities with the elastomers during the preparation of rubber compounds. For example, HDMICI and MODICI exhibited poorer miscibility with SBR than other ILs and caused elastomer crumbling during the preparation of rubber compounds.

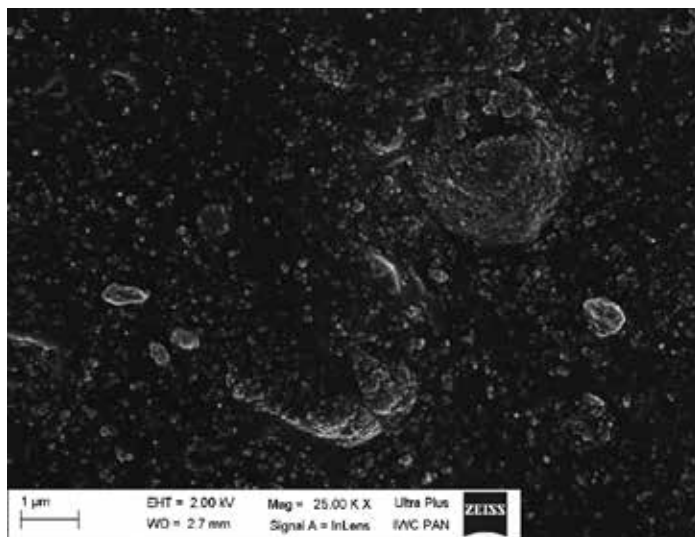


Figure 1. SEM image of SBR vulcanizates containing NZnO without IL

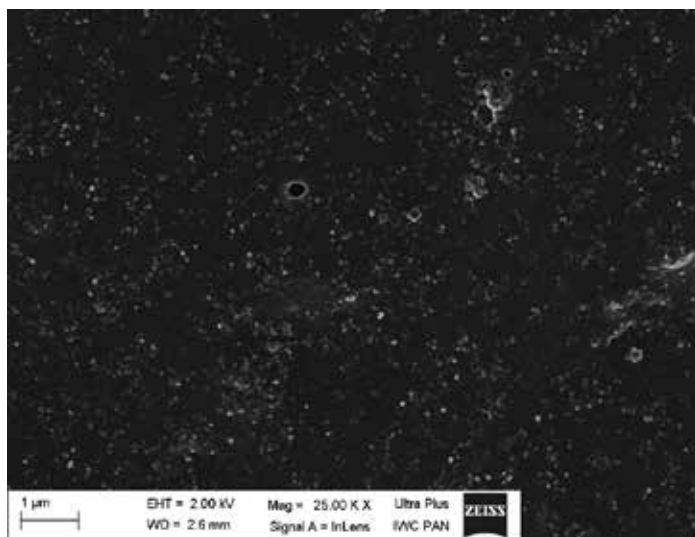


Figure 2. SEM image of SBR vulcanizates containing NZnO and DMICI

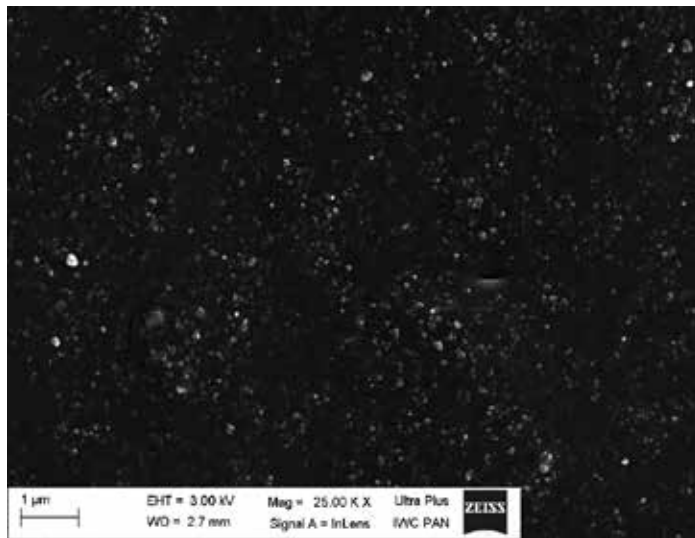


Figure 3. SEM image of SBR vulcanizates containing NZnO and DODMIBF₄

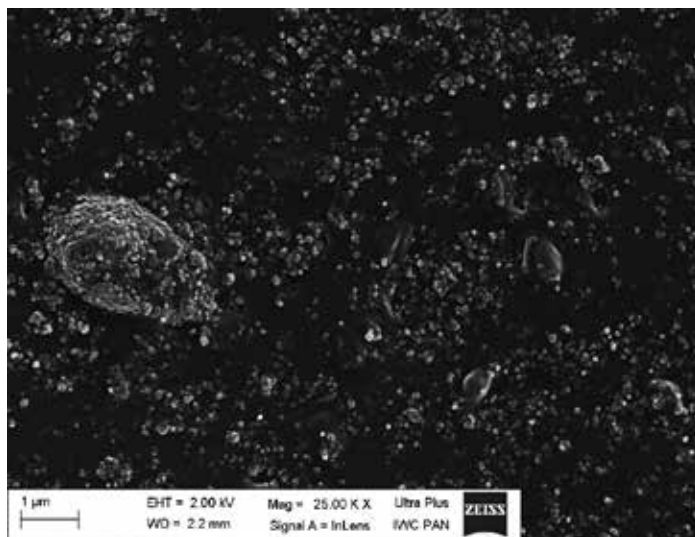


Figure 4. SEM image of SBR vulcanizates containing NZnO and HDMICI

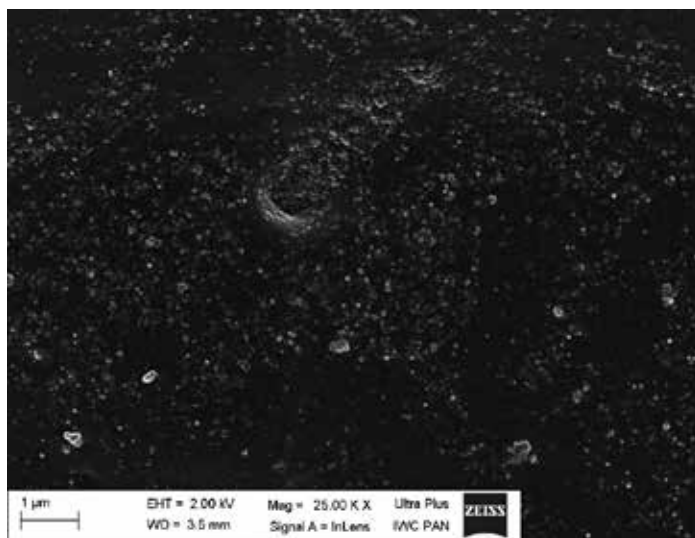


Figure 5. SEM image of SBR vulcanizates containing NZnO and MODICI

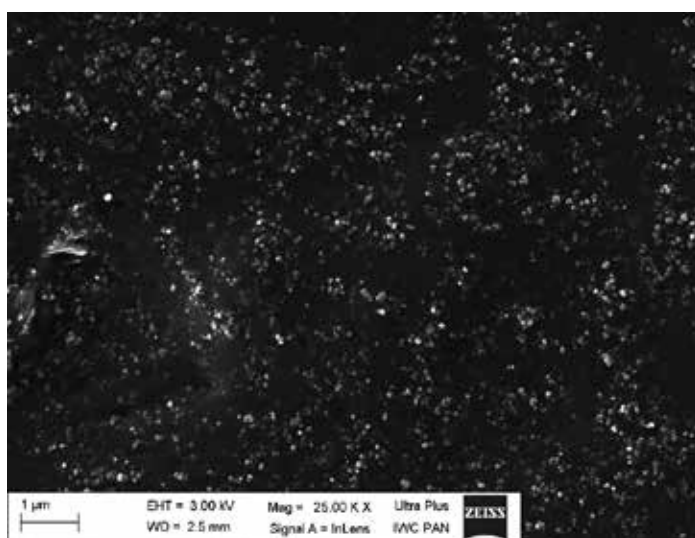


Figure 6. SEM image of SBR vulcanizates containing NZnO and MODIPF₆

Curing characteristics and the crosslink density of SBR vulcanizates

Because the ILs improved the degree of dispersion of the activator nanoparticles and are considered to catalyze the interface reactions, they should affect the vulcanization efficiency of SBR compounds. The influence of the ILs on the vulcanization process was estimated based

on rheometer measurements. The cure characteristics of SBR compounds and crosslink densities of vulcanizates are given in Table 3.

The nanosized zinc oxide used alternatively to microsized activator increased the crosslink density of the vulcanizates and, as a result, the torque increment during the vulcanization of the rubber compounds. It also decreased the vulcanization time of the SBR compounds by 10 minutes and reduced the scorch time by a factor of two. Applying ILs resulted in a considerably shorter vulcanization time compared with micro- or nano-ZnO systems. This confirms that ILs act as catalysts of interface crosslinking reactions. The influence of the anion present in the ILs on the vulcanization time was also observed: the shortest cure times were exhibited by rubber compounds containing alkylimidazolium tetrafluoroborates, whereas the longest t_{90} values were observed for rubber compounds with alkylimidazolium bromide and chlorides. The length of the alkyl chains in the ILs did not significantly affect the torque increment of the rubber compounds during vulcanization. There was also no correlation between the length of the IL alkyl chains and the vulcanization time. However, the length of the alkyl chains in the imidazolium cation seemed to have an impact on the crosslink density. The highest crosslink densities were exhibited by the elastomer compounds with 1-hexadecyl-3-methylimidazolium salts.

ILs	ΔG (dNm)	t_{90} (min)	t_p (min)	$v_T * 10^4$ (mol/cm ³)
ZnO	18.8	60	0.7	15.4
NZnO	20.8	50	0.3	16.5
DMICI	21.5	36	0.5	17.9
DMIBF ₄	20.6	29	0.5	17.7
DIDMICI	20.6	27	0.5	17.3
DODMICI	22.2	33	0.5	16.9
DODMIBr	22.4	40	0.5	17.4
DODMIBF ₄	19.8	24	0.5	17.4
DODMIPF ₆	19.4	27	0.5	17.1
HDMICI	19.5	30	0.5	18.4
HDMIBF ₄	20.2	25	0.5	20.0
HDMIPF ₆	19.8	29	0.4	18.1
MODICI	18.9	36	0.5	17.8
MODIPF ₆	20.6	32	0.6	18.2

Table 3. Curing characteristics and crosslink densities of SBR vulcanizates (ΔG -increment of torque in the rubber compound during vulcanization; t_{90} -optimal vulcanization time; t_p -scorch time, v_T - crosslink density of vulcanizates)

Having studied the effect of nanosized zinc oxide and ILs on the curing characteristics of SBR compounds, we then examined their influence on the temperature and energetic effects of vulcanization using DSC analysis. The results for SBR compounds are given in Table 4.

The vulcanization of SBR is an exothermic process that takes place in a temperature range of 179-232 °C, with an energetic effect of 10 J/g. Nanosized zinc oxide had no significant influence on the temperature and heat of vulcanization compared with those of the SBR compounds containing microsized ZnO. However, it is worth noting that ILs decreased the vulcanization onset temperature by 30°C compared with rubber compounds with micro- or nanosized activator. This is important for technological reasons because application of these ILs allows the SBR elastomer to be cured at lower temperatures than the commonly used 160°C. The highest onset vulcanization temperatures were achieved for hexafluorophosphates, whereas the lowest were observed for alkylimidazolium chlorides. ILs decreased the energetic effect of vulcanization, particularly hexafluorophosphates. The influence of the cations was also observed: the energetic effect of vulcanization was the lowest for rubber compounds containing ILs with 1-hexadecyl-3-methylimidazolium and 1-methyl-3-octadecylimidazolium cations.

ILs	Vulcanization temperature range	Energetic effect of vulcanization
	(°C)	(J/g)
ZnO	179-232	10.0
NZnO	181-226	9.1
DMICI	148-239	8.4
DMIBF ₄	149-234	7.6
DIDMICI	148-239	9.0
DODMICI	148-241	9.9
DODMIBr	149-239	7.7
DODMIBF ₄	148-235	6.5
DODMIPF ₆	154-233	6.7
HDMICI	150-223	6.4
HDMIBF ₄	150-233	6.4
HDMIPF ₆	154-230	5.3
MODICI	145-236	5.6
MODIPF ₆	157-233	4.7

Table 4. Temperature and energetic effects of SBR vulcanization measured by DSC

Mechanical properties of SBR vulcanizates

The aim of applying the ILs was to achieve a homogeneous dispersion of the zinc oxide and silica nanoparticles in the elastomer and thereby improve the mechanical properties of the vulcanizates, such as the tensile strength. Agglomerates of zinc oxide particles may be responsible for local increases in the crosslink density of vulcanizates and the formation of densely crosslinked domains with low elasticity, which may initiate breaking of the sample under external stress. Filler nanoparticle agglomerates can also concentrate stress and contribute to a deterioration of the strength parameters of the vulcanizates.

The mechanical properties of the SBR vulcanizates were studied under static and dynamic conditions. The results of the tensile tests are presented in Table 5.

ILs	TS (MPa)	EB (%)
ZnO	18.3	777
NZnO	22.4	781
DMICI	29.1	964
DMIBF ₄	28.5	982
DIDMICI	26.1	962
DODMICI	24.2	889
DODMIBr	29.8	954
DODMIBF ₄	27.2	985
DODMIPF ₆	22.1	973
HDMICI	20.7	972
HDMIBF ₄	22.5	915
HDMIPF ₆	26.5	987
MODICI	21.5	946
MODIPF ₆	24.8	989

Table 5. Tensile strengths (TS) and elongation at breaks (EB) of the SBR vulcanizates

SBR crosslinked with micro-sized zinc oxide used as a vulcanization activator exhibited a tensile strength of 18.3 MPa and an elongation at break of approximately 777%. Nanosized zinc oxide increased the tensile strength of vulcanizate by 4 MPa, whereas the elongation at break did not change. ILs caused a further increase in the tensile strengths of the vulcanizates. This effect was most significant for vulcanizates containing ILs with decyl-, didecyl-, and dodecyl-chains in the cation. It should be noted that these ILs allowed for a homogeneous dispersion of ZnO and filler nanoparticles in the SBR elastomer. The lowest tensile strengths were exhibited for vulcanizates with HDMICI and MODICI due to the poor dispersion of nanoparticles in the elastomer matrix.

In addition to the mechanical properties under static conditions, the dynamic mechanical properties are also important for the technological application of rubber products. The influence of ILs on the loss factor ($\tan \delta$) was determined with DMA. The loss factor is a measure of the material ability to dampen vibration. A plot of $\tan \delta$ as a function of temperature for the vulcanizates containing ILs is presented in Figure 7, and the data are also shown in Table 6. The presence of the glass transition of the SBR elastomer can be observed, with a maximum that represents the glass transition temperature T_g .

ILs	T_g (°C)	$\tan \delta$ at T_g (-)	$\tan \delta$ at 25 °C (-)	$\tan \delta$ at 100 °C (-)
ZnO	-40.9	0.58	0.13	0.09
NZnO	-40.1	0.63	0.13	0.09
DMICI	-37.3	0.70	0.11	0.08
DMIBF ₄	-35.1	0.86	0.09	0.07
DODMIBr	-36.4	0.74	0.13	0.10
DODMIBF ₄	-38.0	0.76	0.09	0.06
HDMIPF ₆	-36.9	0.68	0.12	0.10
MODIPF ₆	-35.1	0.73	0.13	0.10

Table 6. Glass transition temperature (T_g) and loss factor ($\tan \delta$) of SBR vulcanizates

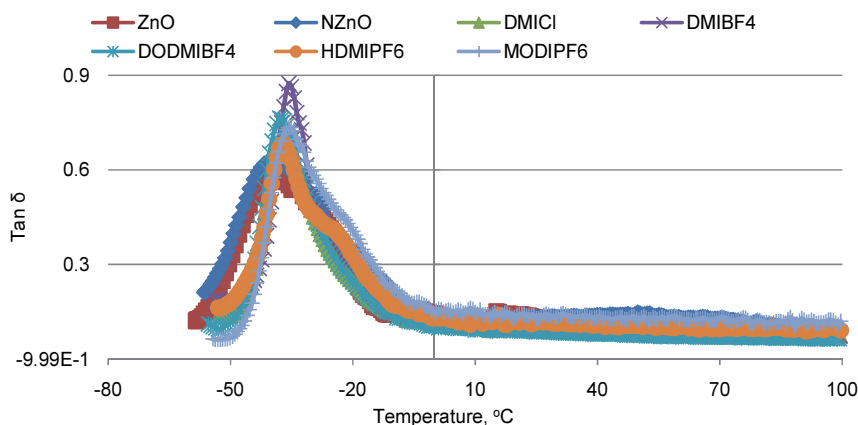


Figure 7. Loss factor ($\tan \delta$) versus temperature for SBR vulcanizates

Applying nanosized ZnO had no influence on the glass transition temperature of SBR and the values of the loss factor. However, an increase in the T_g of the vulcanizates was observed when using ILs, which was the result of the crosslink density increase. The densely crosslinked elastomer network that was formed during vulcanization restricted the mobility of the SBR chains. Regarding the loss factor, tetrafluoroborates increased the value of $\tan \delta$ at T_g but

decreased the loss factor at room temperature and elevated temperatures. Other ILs slightly increased the values of the loss factor at the glass transition temperature but had no significant effect on $\tan \delta$ at 25 °C and 100 °C. Considering the magnitude of the change in the value of loss factor, it can be concluded that the use of ILs had no significant effect on the ability of vulcanizates toward vibration damping. In addition, vulcanizates exhibited stable dynamic properties at the temperatures studied.

Thermal stability and aging resistance of SBR vulcanizates

Thermal stability is very important for the technological application of rubber products. Therefore, ILs used to improve the degree of dispersion of zinc oxide and silica in the elastomer should not deteriorate this property. The thermal stabilities of the vulcanizates were examined based on their decomposition temperature and the total weight loss of the sample determined by TGA analysis. The results are presented in Table 7.

The thermal decomposition of SBR containing microsized zinc oxide began at 288 °C. Replacing the standard activator with nanosized zinc oxide improved the thermal stability of SBR. The decomposition of the vulcanizate began at a temperature that was 15 °C higher than that of the reference vulcanizate. The use of ILs caused a further increase in the thermal stability of SBR, likely due to the homogeneous dispersion of the nanoparticles in the elastomer matrix. The highest T_{02} temperature was achieved for vulcanizates with DMICl and DMIBF₄, where filler and activator nanoparticles were the most uniformly distributed in the SBR. The network created by the filler nanoparticles may be a barrier for the transport of gases and volatile pyrolysis products, thus increasing the thermal stability of the composite. Additionally, ILs did not affect the temperatures at 5% and 50% weight loss. A 5% weight loss was achieved in the temperature range of 357-361 °C, and a 50% weight loss occurred at 441-442 °C. The total weight loss during decomposition was similar for all vulcanizates and was in the range of 74-77%.

ILs	T_{02} (°C)	T_{05} (°C)	T_{50} (°C)	Total weight loss (%)
ZnO	288	362	442	74.2
NZnO	303	360	442	76.9
DMICl	320	362	442	75.6
DMIBF ₄	314	360	444	75.5
DODMIBr	318	361	441	76.0
DODMIBF ₄	314	361	444	75.3
HDMIPF ₆	306	357	442	75.0
MODIPF ₆	306	357	441	75.3

Table 7. Decomposition temperatures at a weight loss of 2% (T_{02}), 5% (T_{05}), 50% (T_{50}), and total weight loss during the decomposition of SBR vulcanizates

One of the most important properties of rubber products is their aging resistance. Therefore, the effect of nanosized zinc oxide and ILs on vulcanizate resistance to UV and thermo-oxidative aging was examined through the change in their mechanical properties and crosslink density.

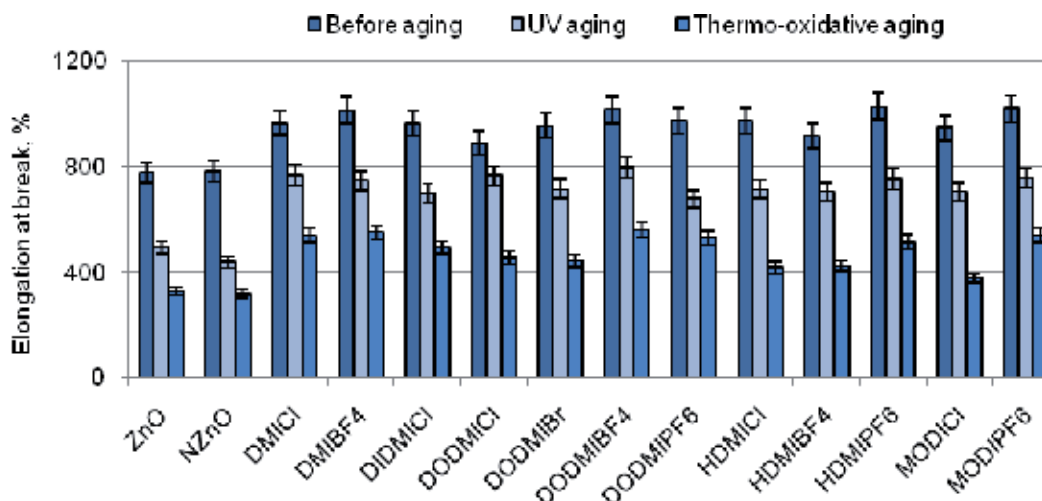


Figure 8. Elongation at breaks of SBR vulcanizates after aging

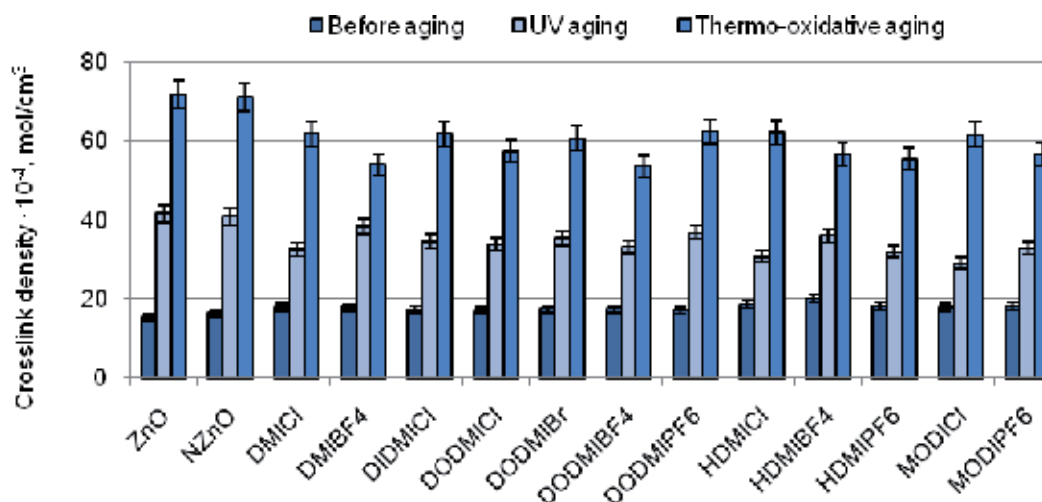


Figure 9. Crosslink densities of SBR vulcanizates after aging

In Figure 8, the change in elongation at break upon aging is given for SBR vulcanizates. The aging process had a considerable impact on the elongation at break of vulcanizates, causing it

to decrease by approximately 200% for UV aging and 300-400% for thermo-oxidative aging. These changes reflect the large increase in the crosslink density of the vulcanizates. Under the influence of aging factors such as UV radiation and elevated temperature, further crosslinking of the elastomer took place. In the case of vulcanizates containing ILs, the extent of further crosslinking of the elastomer was greatly reduced (Figure 9). UV radiation caused a twofold increase in the crosslink density of the vulcanizates, while in the case of the thermo-oxidative aging, a threefold increase in the crosslink density was observed. Due to the considerable changes in the crosslink density of SBR vulcanizates, the aging process deteriorated their tensile strength. The smallest change in the tensile strength was achieved for the vulcanizate containing DODMIPF₆ and MODICI (Figure 10).

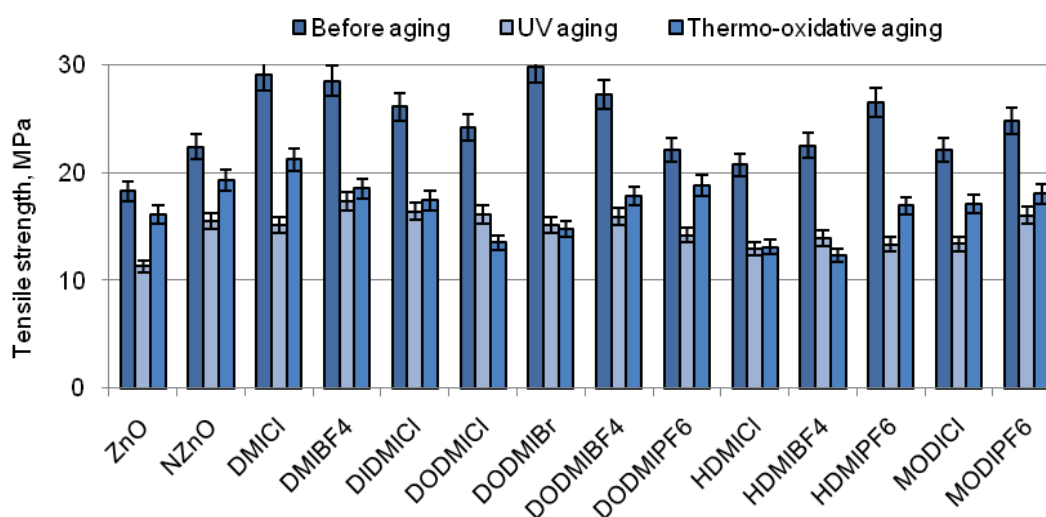


Figure 10. Tensile strengths of SBR vulcanizates after aging

To quantitatively estimate the change in the mechanical properties of vulcanizates due to aging, the aging factor S was calculated (Table 8). This factor is a measurement of the changes in the sample deformation energy caused by the aging process. Values of the S -factor that are closer to 1 indicate smaller changes in the mechanical properties of the vulcanizates from the aging process.

The aging factor (S) for vulcanizates without ILs is 0.39 (UV aging) and 0.35 (thermo-oxidative aging). Therefore, it can be concluded that the SBR vulcanizates are characterized by a susceptibility to degradation under prolonged exposure to elevated temperature or UV radiation. The application of ILs did not significantly improve the resistance of SBR to UV aging. The highest values of S_{UV} were observed for the vulcanizates containing DODMICI and HDMICI, which were 0.57 and 0.51, respectively. These ILs provided the best protection for SBR against UV aging. No improvement in the SBR resistance to thermo-oxidative aging was observed.

ILs	S _{UV} (-)	S _T (-)
ZnO	0.39	0.35
NZnO	0.39	0.35
DMICI	0.41	0.41
DMIBF ₄	0.45	0.35
DIDMICI	0.46	0.34
DODMICI	0.57	0.28
DODMIBr	0.38	0.23
DODMIBF ₄	0.46	0.36
DODMIPF ₆	0.45	0.39
HDMICI	0.51	0.30
HDMIBF ₄	0.47	0.25
HDMIPF ₆	0.37	0.32
MODICI	0.45	0.32
MODIPF ₆	0.48	0.38

Table 8. UV and thermo-oxidative aging factors for SBR vulcanizates

3.2. EPDM composites containing ILs

Dispersion degree of activator and filler nanoparticles in the EPDM

Having established the effects of nanosized zinc oxide and ILs on the SBR properties, we then examined the EPDM vulcanizates. EPDM is widely applied to manufacture rubber products for the automotive industry (tires and damping elements) and the building industry (sealing profiles) due to its useful properties such as resistance to ozone and elevated temperature and elasticity at low temperatures. Therefore, it is reasonable to search for new substances to improve the degree of dispersion of zinc oxide and silica nanoparticles in EPDM elastomer.

As expected, zinc oxide and filler nanoparticles were not homogeneously distributed in the EPDM elastomer matrix, and poor dispersion was observed. They created microsized agglomerates with complex structures, as shown in Figure 11. The size of the agglomerates was several micrometers, whereas the primary particles were below 300 nm in size. Moreover, the agglomerates displayed poor adhesion to the elastomer. We found that ILs prevented the nanoparticles from agglomeration, with the most effective being alkylimidazolium chlorides and bromides, which allowed for a homogeneous distribution of nanoparticles in the EPDM elastomer (Figures 12, 13, 15). In the case of tetrafluoroborates, some agglomerates are observed in the SEM images. However, they are smaller in size and exhibit better adhesion to the elastomer than for the vulcanizate without ILs (Figures 14, 16). Therefore, it can be concluded that the efficiency of ILs as dispersing agents in EPDM depends mainly on the anion type and not the length of alkyl chains in the imidazolium cation.

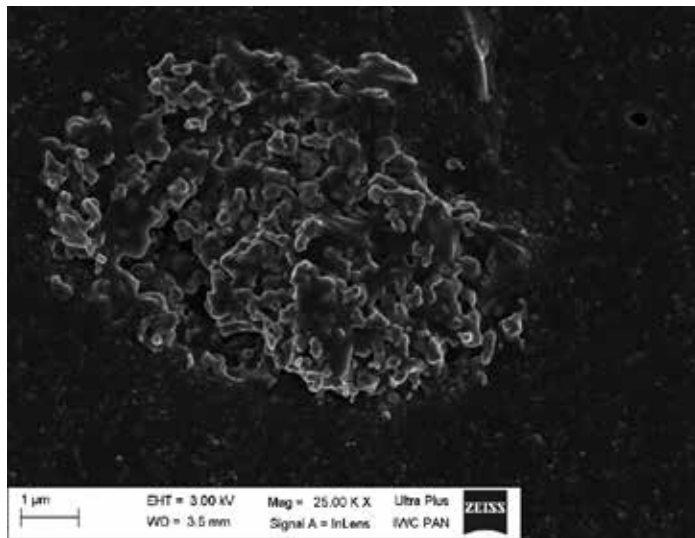


Figure 11. SEM images of SBR vulcanizates containing NZnO without IL

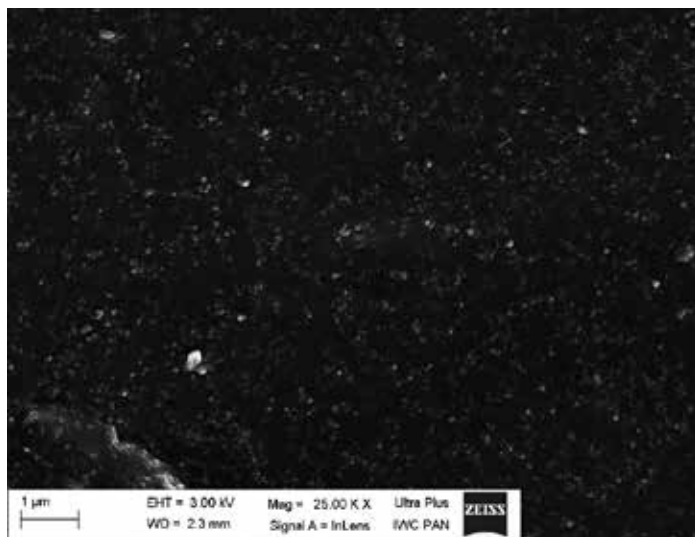


Figure 12. SEM images of SBR vulcanizates containing NZnO and DODMIBr

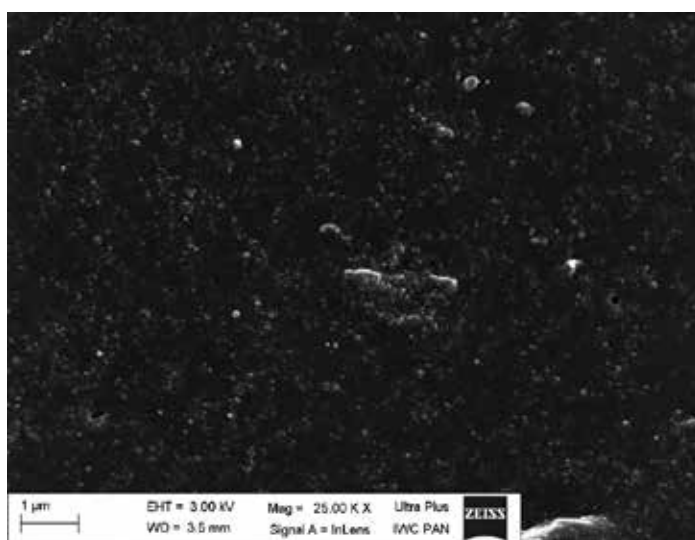


Figure 13. SEM images of SBR vulcanizates containing NZnO and DMICI

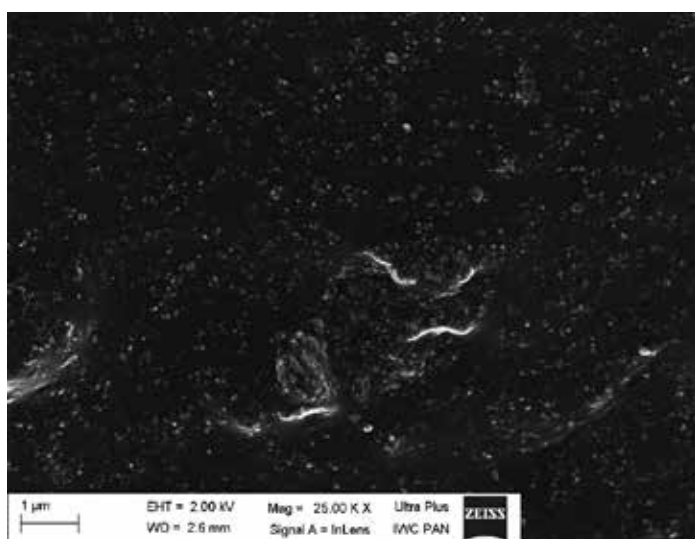


Figure 14. SEM images of SBR vulcanizates containing NZnO and DMIBF₄

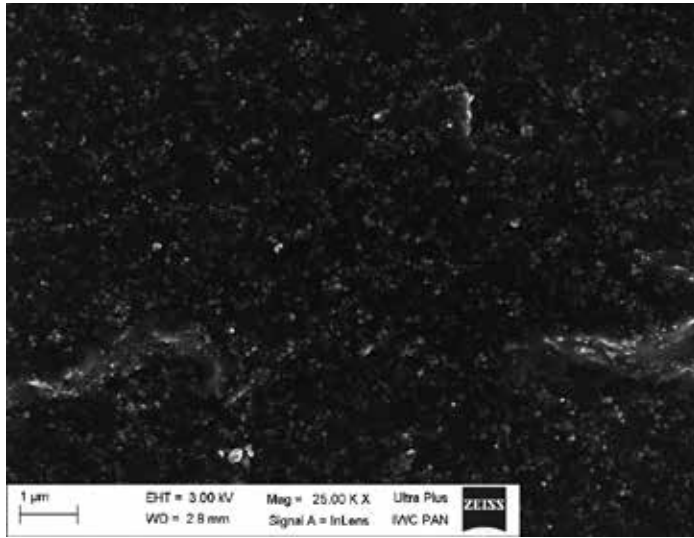


Figure 15. SEM images of SBR vulcanizates containing NZnO and HDMICI

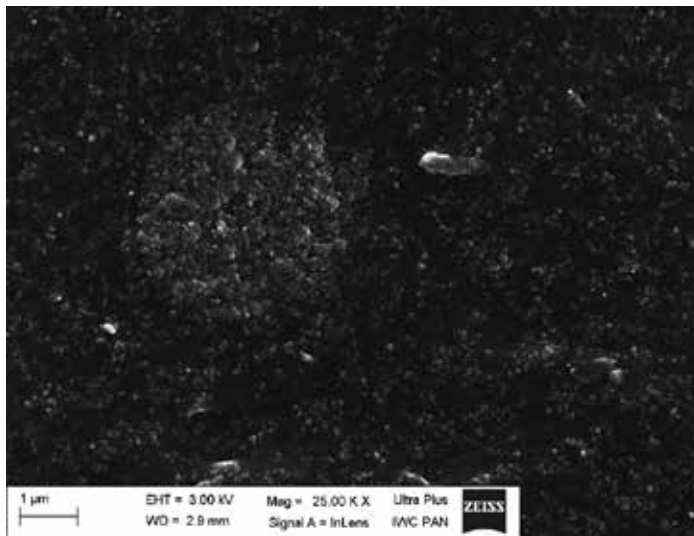


Figure 16. SEM images of SBR vulcanizates containing NZnO and HDMIBF₄

Curing characteristics and the crosslink density of EPDM vulcanizates

Rheometric measurements were performed to study the effect of nanosized zinc oxide and ILs on the torque increment during vulcanization, which corresponds to the crosslinking degree of the elastomer. The vulcanization times and scorch times were also determined (Table 9).

Replacing 5 phr of microsized zinc oxide with 2 phr of zinc oxide nanoparticles increased the torque increment during vulcanization and therefore the crosslink density of vulcanizates, despite the reduction in the amount of zinc oxide in the rubber compound. As discussed, this reduction is important for ecological reasons. There was no considerable effect on the vulcanization time or scorch time observed. ILs caused a further increase in the crosslink densities of the vulcanizate and, as a consequence, the torque increment during vulcanization. It should be noticed that the highest crosslink densities were achieved for vulcanizates containing alkylimidazolium bromide and chlorides, which provided a homogeneous dispersion of zinc oxide nanoparticles in the elastomer. As a result, the interface between the activator particles and other components of the crosslinking system increased, improving the efficiency of the vulcanization process. Regarding the cation type of IL, the lowest crosslink densities were observed for vulcanizates containing 1-methyl-3-octadecylimidazolium cation. ILs, especially those with decyl-, didecyl-, and dodecyl-chains, reduced the vulcanization time of rubber compounds. A small reduction in the scorch times was also observed, but it was not of technological significance.

ILs	ΔG (dNm)	t_{90} (min)	t_p (s)	$v_T * 10^5$ (mol/cm ³)
ZnO	16.5	40	50	9.3
NZnO	18.0	38	45	10.6
DMICI	20.4	25	36	14.0
DMIBF ₄	21.0	28	32	12.2
DIDMICI	20.8	28	35	13.5
DODMICI	23.1	25	39	14.6
DODMIBr	22.0	30	35	14.0
DODMIBF ₄	20.0	30	33	12.0
DODMIPF ₆	21.4	36	38	14.1
HDMICI	22.7	33	42	14.7
HDMIBF ₄	18.5	33	38	12.1
HDMIPF ₆	21.2	35	40	12.2
MODICI	18.9	30	42	12.1
MODIPF ₆	20.4	32	42	11.3

Table 9. Curing characteristics and crosslink densities of EPDM vulcanizates (ΔG -increment of torque in the rubber compound during vulcanization; t_{90} -optimal vulcanization time; t_p -scorch time, v_T – crosslink density of vulcanizates)

Using DSC, we determined the vulcanization temperature range and the energetic effect of vulcanization for the rubber compounds (Table 10).

IL	Vulcanization temperature range (°C)	Energetic effect of vulcanization (J/g)
ZnO	133-193	10.3
NZnO	139-199	9.8
DMICI	112-229	7.4
DMIBF ₄	114-228	6.8
DIDMICI	110-225	7.4
DODMICI	112-229	8.5
DODMIBr	114-239	7.2
DODMIBF ₄	120-234	8.3
DODMIPF ₆	112-223	8.4
HDMICI	120-226	6.5
HDMIBF ₄	121-232	6.4
HDMIPF ₆	120-224	7.4
MODICI	142-227	4.4
MODIPF ₆	139-223	4.7

Table 10. Temperature and energetic effects of EPDM vulcanization measured by DSC

The vulcanization of EPDM is an exothermic process that takes place in the temperature range of 133-193°C, with an energetic effect of 10.3 J/g for microsized ZnO. Nanosized activator had no significant influence on the temperature and heat of vulcanization compared with the microsized ZnO. The catalytic effect of ILs on the interface crosslinking reactions is also apparent in the case of EPDM. ILs decreased the vulcanization onset temperature by 20-30°C and the energetic effect of vulcanization compared with rubber compounds without alkyliimidazolium salts. Exeptions are ILs with 1-methyl-3-octadecylimidazolium cation, which did not influence the vulcanization temperature. However, they considerably decreased the energetic effect of vulcanization and therefore the vulcanization efficiency. It should be mentioned that in the case of these ILs, the smallest crosslink densities of EPDM vulcanizates were also achieved.

Mechanical properties of EPDM vulcanizates

Having established the effect of alkyliimidazolium salts on the degree of dispersion of zinc oxide and silica nanoparticles in the elastomer and on the crosslink density of vulcanizates, we then examined the mechanical properties of EPDM vulcanizates (Table 11).

Applying nanosized zinc oxide alternatively to the corresponding microsized activator decreased the tensile strength of the vulcanizate. This was likely due to the agglomeration of nanoparticles in the EPDM. Agglomerates with poor wettability with the elastomer can

concentrate stress during deformation, resulting in the destruction of the sample. The increase in the tensile strength of vulcanizates containing ILs is closely related to the improvement of the degree of dispersion of the nanoparticles in the EPDM and to the increase in the crosslink density of the vulcanizates. The more uniform the dispersion of nanoparticles is in the elastomer, which results in a higher the crosslink density of the vulcanizates, the higher their tensile strength. In general, ILs increased the elongation at break of vulcanizates due to the increase in their elasticity.

ILs	TS (MPa)	EB (%)
ZnO	13.4	529
NZnO	10.7	569
DMICI	20.7	690
DMIBF ₄	13.4	566
DIDMICI	19.5	667
DODMICI	25.1	735
DODMIBr	22.1	715
DODMIBF ₄	13.2	528
DODMIPF ₆	18.6	643
HDMICI	19.5	765
HDMIBF ₄	12.5	581
HDMIPF ₆	16.6	690
MODICI	19.6	778
MODIPF ₆	18.3	702

Table 11. Tensile strengths (TS) and elongation at breaks (EB) of EPDM vulcanizates

The influence of ILs on the dynamic mechanical properties was determined with DMA. The loss factor as a function of temperature for the EPDM vulcanizates containing ILs is presented in Table 12. Measurements were performed for vulcanizates containing alkyimidazolium chlorides.

The determined glass transition temperatures for the vulcanizates with microsized and nanosized ZnO were approximately -45.4°C and -44.0°C, respectively, whereas the T_g value was slightly higher for the vulcanizates with ILs. This was likely due to the higher crosslink densities of the vulcanizates containing ILs. Nanosized zinc oxide and ILs did not considerably affect the values of the loss factor ($\tan \delta$). Therefore, it can be concluded that vulcanizates with ILs exhibit damping properties comparable to the reference sample containing microsized ZnO.

ILs	T_g (°C)	$\tan \delta$ at T_g (-)	$\tan \delta$ at 25 °C (-)	$\tan \delta$ at 100 °C (-)
ZnO	-45.4	0.56	0.08	0.09
NZnO	-44.0	0.60	0.10	0.09
DMICI	-42.1	0.52	0.11	0.09
DIDMICI	-41.8	0.55	0.10	0.10
DODMICI	-43.5	0.58	0.09	0.09
HDMICI	-43.3	0.66	0.10	0.08
MODICI	-39.3	0.49	0.08	0.09

Table 12. Glass transition temperatures (T_g) and loss factors ($\tan \delta$) of EPDM vulcanizates

Thermal stability and aging resistance of EPDM vulcanizates

TGA analysis was performed to determine the effect of nanosized zinc oxide and alkylimidazolium salts on the thermal stability of EPDM vulcanizates. The results are given in Table 13.

The onset decomposition temperatures (T_{02}) for EPDM vulcanizates crosslinked with micro-sized activator was 354 °C. Applying nanosized zinc oxide alternatively to the standard activator increased the values of T_{02} and T_{05} by 9 °C and 4 °C, respectively, but had no influence on the T_{50} temperature. The use of ILs considerably increased the onset decomposition temperature of the vulcanizates and increased the T_{05} and T_{50} values by 14-17°C and 6-10°C, respectively. The increase in the thermal stability of vulcanizates resulted from the gas barrier effect of the filler network in the elastomer matrix, similar to the results obtained for the SBR elastomer. The total weight loss was approximately 75% for all examined vulcanizates.

ILs	T_{02} (°C)	T_{05} (°C)	T_{50} (°C)	Total weight loss (%)
ZnO	354	418	468	72.8
NZnO	363	422	467	75.3
DMICI	419	436	474	75.4
DIDMICI	418	436	474	75.0
DODMICI	421	437	475	75.6
HDMICI	416	437	476	75.4
MODICI	421	439	478	75.9

Table 13. Decomposition temperatures at a weight loss of 2% (T_{02}), 5% (T_{05}), 50% (T_{50}), and total weight loss during the decomposition of EPDM vulcanizates

EPDM, as previously mentioned, is widely applied in the manufacturing of rubber products for the automotive and building industries. Such rubber products are exposed to external factors such as increased temperature and UV radiation. Therefore, ILs applied as dispersing

agents should not deteriorate these properties. The resistance of EPDM vulcanizates to thermo-oxidative and UV aging was studied based on the changes in the tensile parameters and crosslink densities of the vulcanizates.

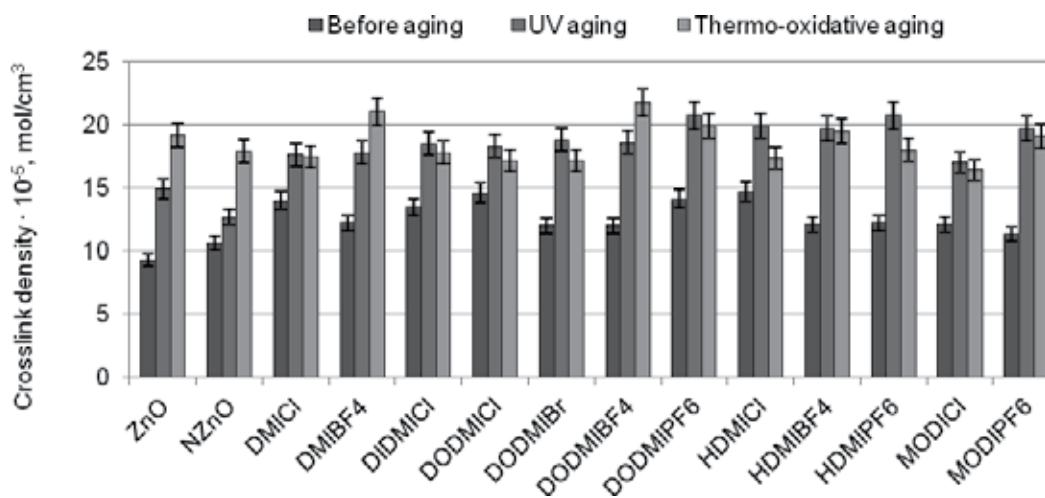


Figure 17. Crosslink density of EPDM vulcanizates after aging

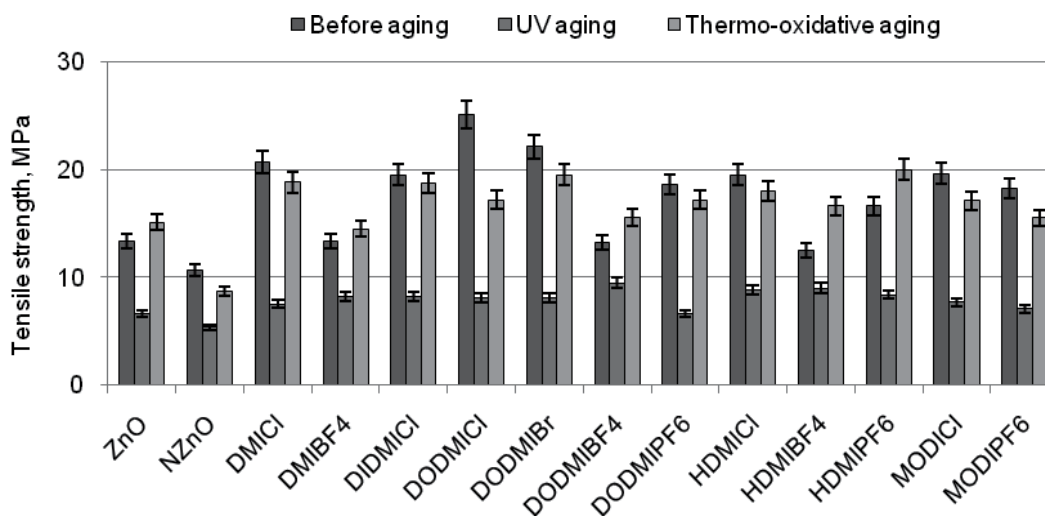


Figure 18. Tensile strength of EPDM vulcanizates after aging

Thermo-oxidative and UV aging caused the crosslink densities of the vulcanizates to increase considerably (Figure 17). It is shown that prolonged exposure to elevated temperatures and UV radiation resulted in the further crosslinking of the EPDM, similar to the case of SBR. However, the increase in the crosslink density was smaller in the case of the vulcanizates

containing nanosized ZnO with DMICI, DODMICI, HDMICI, and MODICI. UV aging deteriorated the tensile strength of the vulcanizates with ILs, as the vulcanizates with nanosized ZnO (Figure 18). The highest decrease in TS was achieved for vulcanizates containing alkylimidazolium chlorides, whereas the smallest changes in TS were observed for tetrafluoroborates. Thermo-oxidative aging had less impact on the tensile strength of EPDM vulcanizates in comparison with UV radiation, and only small changes in the TS values were observed.

The aging factor was calculated to quantitatively estimate the change in the mechanical properties of the vulcanizates (Table 14). EPDM vulcanizates are highly susceptible to UV degradation. The S_{UV} values are very low (approximately 0.11). Small improvements in the S_{UV} values were achieved for vulcanizates containing alkylimidazolium tetrafluoroborates. EPDM vulcanizates exhibited higher resistance to thermo-oxidative aging, for which ILs increased the S_T values. The most active in preventing the degradation of vulcanizates upon thermo-oxidative aging were also alkylimidazolium tetrafluoroborates.

ILs	S_{UV} (-)	S_T (-)
ZnO	0.11	0.45
NZnO	0.11	0.38
DMICI	0.11	0.62
DMIBF ₄	0.25	0.76
DIDMICI	0.12	0.67
DODMICI	0.10	0.52
DODMIBr	0.10	0.60
DODMIBF ₄	0.32	0.79
DODMIPF ₆	0.10	0.56
HDMICI	0.11	0.56
HDMIBF ₄	0.25	0.90
HDMIPF ₆	0.15	0.83
MODICI	0.10	0.53
MODIPF ₆	0.10	0.47

Table 14. Thermo-oxidative and UV aging factors for EPDM vulcanizates

4. Conclusions

Alkylimidazolium salts considerably improved the degree of dispersion of zinc oxide and filler (silica) nanoparticles in SBR and EPDM, of which the most active seemed to be alkylimidazolium chlorides and bromide. In the IL-containing vulcanizates, nanoparticles of zinc oxide and

silica were homogeneously distributed in the elastomer matrix. It can be concluded that ILs decreased the intermolecular interactions between nanoparticles and reduced their tendency for agglomeration in the elastomer.

Applying nanosized zinc oxide allowed for a reduction in the amount of ZnO by 60% in the comparison with commonly used microsized ZnO. Nanosized zinc oxide used with ILs resulted in the shortening of the optimal vulcanization time and decreased the onset vulcanization temperature by 20-30°C, which is very important from a technological and economical point of view. An increase in the crosslink density of vulcanizates was also achieved. Despite the reduced amount of zinc oxide, SBR and EPDM composites containing ILs exhibited tensile strengths higher or comparable to the standard vulcanizates crosslinked with the microsized activator. The positive effect of ILs on the vulcanization kinetics and crosslink densities of the vulcanizates results from the improvement in the degree of dispersion of ZnO nanoparticles in the elastomer. This leads to better contact between the vulcanization activator particles and other components of the crosslinking system. Of equal importance is the catalytic action of ILs in the interfacial crosslinking reactions.

Alkylimidazolium salts considerably increased the thermal stability of the vulcanizates, while ILs did not significantly increase the resistance of SBR and EPDM to UV aging. Regarding the resistance of the vulcanizates to thermo-oxidative aging, some improvement was achieved for EPDM, especially for vulcanizates containing alkylimidazolium tetrafluoroborates.

Acknowledgements

The authors wish to acknowledge the National Centre for Research and Development (Poland) for supporting this research.

Author details

Magdalena Maciejewska* and Marian Zaborski

*Address all correspondence to: magdalena.maciejewska@p.lodz.pl

Technical University of Lodz, Poland

References

- [1] Sabu T, Ranimol S., editors. Rubber Nanocomposites. Preparation, Properties and Applications. Singapore: John Wiley & Sons; 2010.
- [2] Wypych G., editor. Handbook of Fillers. Toronto: ChemTec Publishing; 2010.

- [3] Gong H, Liu J, Baskaran S, Voise RD, Young JS. Surfactant-Assisted Processing of Carbon Nanotube/Polymer Composites. *Chemistry of Materials* 2000;12(4): 1049-52. <http://pubs.acs.org/doi/full/10.1021/cm9906396> (accessed 17 March 2000).
- [4] Dondero WE, Gorga RE. Morphological and Mechanical Properties of Carbon Nanotube/Polymer Composites via Melt Compounding. *Journal of Polymer Science Part B Polymer Physics* 2006;44(5): 864-78. <http://onlinelibrary.wiley.com/doi/10.1002/polb.20743/pdf> (accessed 25 January 2006)
- [5] Ikeda Y, Poompradub S, Morita Y, Kohjiya S. Preparation of High Performance Nanocomposite Elastomer: Effect of Reaction Conditions on In Situ Silica Generation of High Content in Natural Rubber. *Journal of Sol-Gel Science and Technology* 2008;45(3): 299-306. <http://link.springer.com/article/10.1007%2Fs10971-008-1682-7> (accessed 6 February 2008).
- [6] Przybyszewska M, Krzywania A, Zaborski M, Szyrkowska MI. Surface Properties of Zinc Oxide Nanoparticles Studied by Inverse Gas Chromatography. *Journal of Chromatography A* 2009;1216(27): 5284-91. <http://www.sciencedirect.com/science/article/pii/S0021967309006827> (accessed 6 May 2009).
- [7] Maciejewska M, Krzywania-Kaliszewska A, Zaborski M. Surface Properties of Calcium and Magnesium Oxide Nanopowders Grafted with Unsaturated Carboxylic Acids Studied with Inverse Gas Chromatography. *Journal of Chromatography A* 2012;1257(1): 141-8. <http://www.sciencedirect.com/science/article/pii/S0021967312011995> (accessed 8 August 2008).
- [8] Lei YD, Tang ZH, Guo BC, Zhu LX, Jia DM. Synthesis of Novel Functional Liquid and its Application as a Modifier in SBR/Silica Composites. *eXPRESS Polymer Letters* 2010;4(11): 692-703. http://www.expresspolymlett.com/articles/EPL-0001670_article.pdf (accessed November 2010).
- [9] Subramaniam K, Das A, Heinrich G. Development of Conducting Polychloroprene Rubber Using Imidazolium Based Ionic Liquid Modified Multi-Walled Carbon Nanotubes. *Composite Science and Technology* 2011;71(11): 1441-9. <http://www.sciencedirect.com/science/article/pii/S0266353811001928> (accessed 2 June 2011).
- [10] Kreyenschulte H, Richter S, Götze T, Fischer D, Steinhauser D, Klüppel M, Heinrich G. Interaction of 1-Allyl-3-Methylimidazolium Chloride and Carbon Black and Its Influence on Carbon Black Filled Rubbers. *Carbon* 2012;50(10): 3649-58. <http://www.sciencedirect.com/science/article/pii/S0008622312002850> (accessed 24 March 2012).
- [11] Lu J, Yan F, Texter J. Advanced Applications of Ionic Liquids in Polymer Science. *Progress in Polymer Science* 2009; 34(5): 431-48. <http://www.sciencedirect.com/science/article/pii/S0079670008001226> (accessed 13 January 2009).

- [12] Rogers RD, Seddon KR. Ionic Liquids-Solvents of the Future? *Science* 2003;302(5646): 792-3. <http://www.sciencemag.org/content/302/5646/792.full.pdf> (accessed 31 October 2003).
- [13] Wasserscheid P, Welton T., editor. *Ionic Liquids in Synthesis*. New York: Wiley-VCH; 2008.
- [14] Goujon LJ, Khaldi A, Maziz A, Plesse C, Nguyen GTM, Aubert P-H, Vidal F, Chevrot C, Teyssié D. Flexible Solid Polymer Electrolytes Based on Nitrile Butadiene Rubber/Poly(ethylene oxide) Interpenetrating Polymer Networks Containing Either LiTFSI or EMITFSI. *Macromolecules* 2011;44(24): 9683-91. <http://pubs.acs.org/doi/abs/10.1021/ma201662h> (accessed 21 November 2011).
- [15] Shaplov AS, Ponkratov DO, Vlasov PS, Lozinskaya EI, Malyshkina IA, Vidal F, Aubert P-H, Armand M, Vygodskii YS. Solid-State Electrolytes Based on Ionic Network Polymers. *Polymer Science, Series B* 2014;56(2): 164-77. <http://link.springer.com/article/10.1134%2FS1560090414020134> (accessed 30 April 2014)
- [16] Cho M, Seo H, Na J, Choi H, Koo J, Lee Y. High Ionic Conductivity and Mechanical Strength of Solid Polymer Electrolytes Based on NBR/Ionic Liquid and Its Application to an Electrochemical Actuator. *Sensors and Actuators B* 2007;128(1):70-4. <http://212.51.210.219/han/ss/vls2.icm.edu.pl/pdflinks/14070321375705959.pdf> (accessed 31 May 2007).
- [17] Gayet F, Viau L, Leroux F, Mabilie F, Monge S, Robin J-J, Voix A. Unique Combination of Mechanical Strength, Thermal Stability and High Ion Conduction of PMMA-Silica Nanocomposites Containing High Loadings of Ionic Liquid, *Chemistry of Materials Communication* 2009;21(23): 5575-7. <http://pubs.acs.org/doi/abs/10.1021/cm9027918> (accessed 12 November 2009).
- [18] Marwanta E, Mizumo T, Nakamura N, Ohno H. Improved Ionic Conductivity of Nitrile Rubber/Ionic Liquid Composites. *Polymer* 2005;46(11): 3795-800. <http://212.51.210.219/han/ss/vls2.icm.edu.pl/pdflinks/14070321101005219.pdf> (accessed 7 April 2005).
- [19] Nockemann P, Thijs B, Pittois S, Thoen J, Glorieux C, van Hecke K, van Meervelt L, Kirchner B, Binnemans K. Task-Specific Ionic Liquid for Solubilizing Metal Oxides. *Journal of Physical Chemistry B* 2006;110(42): 20978-92. <http://pubs.acs.org/doi/full/10.1021/jp0642995> (accessed 21 September 2006).
- [20] Guo BC, Chen F, Lei YD, Liu XL, Wan JJ, Jia DM. Styrene-Butadiene Rubber/Halloysite Nanotubes Nanocomposites Modified by Sorbic Acid. *Applied Surface Science* 2009;255(16): 7329-36. <http://www.sciencedirect.com/science/article/pii/S0169433209003663> (accessed 8 August 2008).
- [21] Byrne C, McNally T. Ionic Liquid Modification of Layered Silicates for Enhanced Thermal Stability. *Macromolecular Rapid Communications* 2007;28(6): 780-4. <http://onlinelibrary.wiley.com/doi/10.1002/marc.200600754/full> (accessed 21 March 2007).

- [22] Gilman JW, Awad WH, Davis RD, Shields J, Harris RH, Davis C, Morgan AB, Sutto TE, Callahan J, Trulove H, De Long H. Polymer/Layered Silicate Nanocomposites from Thermally Stable Trialkylimidazolium-Treated Montmorillonite. *Chemistry of Materials* 2002;14(9): 3776-85. <http://pubs.acs.org/doi/full/10.1021/cm011532x> (accessed 16 August 2002).
- [23] Rotkin SV, Zharov I. Nanotube Light-Controlled Electronic Switch. *International Journal of Nanoscience* 2002;1(3&4): 347-55. <http://www.worldscientific.com/doi/pdf/10.1142/S0219581X02000280> (accessed June 2002).
- [24] Bachtold A, Hadley P, Nakanishi T, Dekker C. Logic Circuits with Carbon Nanotubes Transistors. *Science* 2001;294(5545): 1313-7. <http://www.sciencemag.org/content/294/5545/1317> (accessed 4 October 2001).
- [25] Du F, Fischer JE, Winey KI. Coagulation Method for Preparing Single-Walled Carbon Nanotube/Poly(methyl methacrylate) Composites and Their Modulus, Electrical Conductivity, and Thermal Stability. *Journal of Polymer Science Part B Polymer Physics* 2003;41(24): 3333-8. <http://onlinelibrary.wiley.com/doi/10.1002/polb.10701/full> (accessed 4 November 2003).
- [26] Steinhauser D, Subramanian K, Das A, Heinrich G, Klüppel M. Influence of Ionic Liquids on the Dielectric Relaxation Behavior of CNT Based Elastomer Nanocomposites. *eXPRESS Polymer Letters* 2012;6(11): 927-36. <http://www.expresspolymlett.com/> (accessed November 2012).
- [27] Das A, Stöckelhuber KW, Jurk R, Fritzsche J, Klüppel M, Heinrich G. Coupling Activity of Ionic Liquids Between Diene Elastomers and Multi-Walled Carbon Nanotubes. *Carbon* 2009;47(14): 3313-21. <http://www.sciencedirect.com/science/article/pii/S0008622309004898> (accessed 3 August 2009).
- [28] Bellayer S, Gilman JW, Eidelman N, Bourbigot S, Flambard X, Fox DM, De Long HC, Trulove PC. Preparation of Homogeneously Dispersed Multiwalled Carbon Nanotube/Polystyrene Nanocomposites via Melt Extrusion Using Trialkyl Imidazolium Compatibilizer. *Advanced Functional Materials* 2005;15(6): 910-6. <http://onlinelibrary.wiley.com/doi/10.1002/adfm.200400441/pdf> (accessed 27 May 2005).
- [29] Heideman G, Noordermeer JWM, Datta RN. Effect of Zinc Complexes as Activator for Sulfur Vulcanization in Various Rubbers. *Rubber Chemistry and Technology* 2005;78(2): 245-57. <http://rubberchemtechnol.org/doi/abs/10.5254/1.3547881> (accessed May 2005).
- [30] Chapman A, Johnson T. The Role of Zinc in the Vulcanization of Styrene-Butadiene Rubbers. *Kautschuk und Gummi Kunststoffe* 2005;58(7-8): 358-361.
- [31] Heideman G, Noordermeer JWM, Datta RN, van Baarle B. Zinc Loaded Clay as Activator in Sulfur Vulcanization: A New Route for Zinc Oxide Reduction in Rubber Compounds. *Rubber Chemistry and Technology* 2004;77(2): 336-55. <http://www.rubberchemtechnol.org/doi/pdf/10.5254/1.3547827> (accessed May 2004).

- [32] Nieuwenhuizen PJ. Zinc accelerator complexes.: Versatile homogeneous catalysts in sulfur vulcanization. *Applied Catalysis A: General* 2001;207(1-2): 55-68. <http://www.sciencedirect.com/science/article/pii/S0926860X0000613X> (accessed 8 May 2000).
- [33] Przybyszewska M, Zaborski M. Effect of Ionic Liquids and Surfactants on Zinc Oxide Nanoparticle Activity in Crosslinking of Acrylonitrile Butadiene Elastomer. *Journal of Applied Polymer Science*, 2010;116(1): 155-64. <http://onlinelibrary.wiley.com/doi/10.1002/app.31519/pdf> (accessed 23 November 2009).
- [34] Flory PJ, Rehner J. Statistical Mechanics of Cross-Linked Polymer Networks. II. Swelling. *Journal of Chemical Physics* 1943;11(11): 521-6. <http://scitation.aip.org/content/aip/journal/jcp/11/11/10.1063/1.1723792> (accessed 22 December 2004).
- [35] Masek A, Zaborski M, Kosmalka A. Derivatives of Flavonoides as Anti-Ageing Substances in Elastomers. *Comptes Rendus Chimie* 2011;14(5): 483-8. <http://www.sciencedirect.com/science/article/pii/S1631074811000026> (accessed 15 February 2011).

Ionic Liquids in the Vulcanization of Elastomers

Magdalena Maciejewska and Filip Walkiewicz

Additional information is available at the end of the chapter

<http://dx.doi.org/10.5772/59064>

1. Introduction

Vulcanization is the basic process used in elastomer technology. The first patent for the sulfur vulcanization of natural rubber was issued to Charles Goodyear in 1839. The most important disadvantage of sulfur vulcanization at its creation was the long process time of several hours. In 1906, Oenslager discovered the accelerating effect of aniline on sulfur vulcanization [1]. This discovery was followed by the introduction of guanidines. Other organic vulcanization accelerators, such as thiazole and sulfenamide, were developed in 1930 [2]. In later years, thiurames and dithiocarbamates were applied. Although vulcanization is one of the oldest and best known processes, thiazoles, sulfenamides and dithiocarbamates were the last significant accelerator classes to be introduced in industry. Soon afterward, it was discovered that zinc oxide could activate the sulfur vulcanization process. Zinc oxide reacts with accelerators to form zinc complexes, which are more reactive than free accelerators. Sulfur is then incorporated into these complexes, and active sulfating agents are formed that react with the allylic hydrogen atoms of unsaturated elastomers to form crosslink precursors. These precursors then react with other rubber chains to generate crosslinks that contain large amounts of sulfur atoms in their bridges. In the next step of the vulcanization process, crosslink shortening, usually accompanied by side reactions, produces the final elastomer network [3].

It is commonly postulated that acceleration of sulfur vulcanization results from homogeneous catalysis by zinc complexes or zinc salts [3]. Traditionally, stearic acid is used together with zinc oxide to activate sulfur vulcanization. In this way, a complex composed of zinc, an accelerator, and stearic acid is formed during vulcanization and includes a central zinc cation, two stearyl anions, and accelerator residues. This complex and other components of the crosslinking system are strongly polar and also reveal a tendency for agglomeration in the elastomer, resulting in the reduction of vulcanization efficiency [4]. Therefore, the application

of novel ionic liquids (ILs)-the derivatives of 2-mercaptobenzothiazole-as accelerators for the vulcanization process seems to be reasonable. Because of their catalytic activity [5], ILs increase the rates of interfacial crosslinking reactions. Moreover, because of their ionic character, ILs should be able to form salts or complexes with zinc ions, similarly to standard accelerators; however, these complexes are more reactive than zinc-accelerator complexes. Additionally, the application of ligands with higher solvation power towards zinc cations than stearyl anions should improve the dispersion degree of the active sulfurating agent as well as of the crosslinking system components in the elastomer. As a result, the crosslinking rate and efficiency should increase considerably.

Recently, IL research has been one of the most rapidly growing fields in chemistry and industry, mainly due to the many unique properties of ionic liquids, such as chemical, electrochemical and thermal stability, low vapor pressure and high ionic conductivity [6]. ILs are generally defined as salts with melting temperatures lower than 100 °C and commonly consist of an asymmetric, organic cation and a rather weakly coordinating organic or inorganic anion [6,7]. Most ILs have good miscibility with organic solvents or monomers, are able to solvate a large variety of organic polar and nonpolar compounds, and show potentially “environmentally-friendly” characteristics due to their negligible vapor pressure and flammability [8]. ILs are nonvolatile compounds; thus, the chance for fugitive emissions during their use in technology is limited. Due to their ionic character, ILs are highly polar but non-coordinating, so they may affect the course of ionic reactions [9]. Therefore, ILs can be used as solvents for electrochemical processes [6,10], and their chemical and physical properties can be tailored by varying the cations and anions for a wide range of potential applications. In recent years, ILs have been widely used in polymer science, mainly as solvents in different types of polymerizations (e.g., free radical polymerization [11], atom transfer radical polymerization [12] or ionic polymerization [13]). Wang et al. used room-temperature ILs such as triethylamine hydrochloride-aluminum chloride ($\text{Et}_3\text{NHCl-AlCl}_3$) as an initiator for the cationic copolymerization of 1,3-pentadiene with styrene [14]. The best results were obtained for AlCl_3 content of 60 wt%. The reaction produced a high-molecular-weight copolymer with a smaller molecular weight distribution than that produced when using an organic solvent. Increasing the concentration of IL led to an increase of copolymerization yield. Moreover, as the concentration of ionic liquid increased, more crosslinked products were achieved as a result of the higher concentration of macromolecular chains in the reaction medium, which favored the intermolecular reaction of carbocations with the copolymer. The cationic ring-opening polymerization of 3,3-bis(chloromethyl)oxacyclobutane was carried out in 1-butyl-3-methylimidazolium tetrafluoroborate and hexafluorophosphate [15]. The polymerization process proceeded to high conversions, although polymer molecular weights were limited, similar to polymerization in organic solvents. ILs were able to be separated from other reagents and reused. The moisture-stable ionic liquid composed of choline chloride and zinc chloride was applied to the radiation-induced copolymerization of vinyl monomers – styrene and methyl methacrylate. The mechanism of copolymerization was the same as in conventional organic solvents at room temperature, and the copolymer was produced with

high efficiency [16]. The IL 1-butyl-3-methylimidazolium hexafluorophosphate was also used as a solvent in the radical polymerization of methyl methacrylate [17]. A considerable increase in the rate constant of propagation was observed that was related to increasing polarity of the polymerization medium that favored a transition state involving charge transfer or complex formation between IL and either monomer or radical. The rate of polymerization was approximately 10 times higher than in traditionally used benzene. The molecular weights of polymers were also considerably higher, indicating a decrease in the rate of termination. This ionic liquid can be successfully used for synthesis of styrene and methyl methacrylate block copolymers [18]. The IL 1-butylpyridinium tetrafluoroborate was used in the radical polymerization of 2-hydroxyethyl methacrylate [19]. Transparent and highly conductive polymer electrolytes were obtained and characterized with high mechanical strength. ILs can serve as solvents for the organotellurium-mediated living radical polymerization (TERP) of methyl methacrylate (MMA), methyl acrylate (MA), and styrene [20]. The reaction rate of MMA and MA polymerization significantly increased, and the controllability of the polydispersity index (PDI) was also improved. The TERP of MMA yielded poly(methyl methacrylates) with PDI less than 1.1. The improved control of polymerization was ascribed to a faster degenerative chain transfer reaction that is a key parameter in the control of PDI for TERP. Moreover, facile separation of polymers from ILs and the possibility of IL recycling were described.

ILs can also be polymerized to form ionic gels [21-23]; 1-(8-(acryloyloxy)octyl)-3-methylimidazolium chloride was reported to photopolymerize and form a hydrogel through self-assembly [24]. This hydrogel was physically crosslinked and possessed an ordered lamellar structure that enabled reversible swelling in water up to 200 times its original volume.

ILs can be used to dissolve polymers such as cellulose [25], starch [26], or silk fibroin [27] and have shown great potential as effective wood preservatives. Hydrophobic ammonium-based ILs, which are air- and moisture-stable, possess anti-bacterial and anti-fungal activity [28]. The ability to dissolve cellulose was described for 1-butyl-3-methylimidazolium chloride, acetate and formate [29]. Pernak et al. reported the possibility of dissolving cellulose using ILs with 4-benzyl-4-methylmorpholinium and alkyl(cyclohexyl)dimethylammonium cations [30,31]. Alkylimidazolium 1,2,4-triazolates and benzotriazolates were tested for fungistatic activity against strains of *Aspergillus* and *Penicillium* molds. The highest antifungal activity was demonstrated by 1-dodecyl-methylimidazolium 1,2,4-triazolate, which effectively protected paper against molds [32].

ILs are used for filler modification to increase the interactions between a filler and an elastomer matrix and to improve the dispersion of filler particles in the elastomer, especially in the case of silica, clays, carbon black and carbon nanotubes [33-35]. ILs such as 1-butyl-3-methylimidazolium chloride, tetrafluoroborate and hexafluorophosphate were used to improve the dispersion degree of magnetic fillers in an ethylene-octene copolymer [36]. ILs increased the magnetorheological effect of composites due to the homogeneous distribution of magnetic filler nanoparticles in the polymer. A significant improvement of the mechanical properties of composites, such as tensile strength, was achieved.

Due to very high ionic conductivity below their decomposition temperature, ILs can have an important role in electrolyte matrices. The application of ILs provides the polymer electrolyte with high tensile strength and elasticity by giving conductivity to elastomers. Conductive butadiene-acrylonitrile elastomer (NBR) composites with an ionic conductivity of $2.54 \times 10^{-4} \text{ S cm}^{-1}$ have previously been prepared using 1-butyl-3-methylimidazolium bis(trifluoromethylsulfonyl)imide [37]. The use of ILs resulted in the development of conductive polychloroprene rubber containing a low concentration of multi-walled carbon nanotubes [38]. Stable polymer electrolytes with an ionic conductivity of over $10^{-4} \text{ S cm}^{-1}$ were obtained from polymerizable ionic liquids with an imidazolium cation [39].

Despite the wide applications of ionic liquids in polymer and elastomer science, their use as accelerators for the sulfur vulcanization of unsaturated elastomers has not yet been reported, with the exception of our previous publications [40,41]. Thus, this chapter represents an innovative and original solution.

For our studies, we believe that the application of ILs will result in the development of new eco-friendly accelerators for elastomer sulfur vulcanization. The most popular accelerator (MBT) is an allergenic agent. Like guanidines, sulfenamides are amine derivatives with different amine moiety contents. Therefore, their application in technology should be limited because of toxicity. The proposed ILs are derived from conventional accelerators, but due to their greater activity, the amount of crosslinking system components (sulfur, zinc oxide, accelerator) in rubber products can be reduced. Moreover, because of the application of ILs, conductive elastomer composites should be possible. Preliminary studies have confirmed that mercaptobenzothiazolate or dithiocarbamate anions could be successfully incorporated into IL structures [40]. The proposed solution could make an original contribution to both the synthesis of novel ionic liquids and their application as well as provide for the development of new, environmentally friendly accelerators for elastomer vulcanization. Traditional accelerators have been applied in the rubber industry for years. However, severe European Union directives regarding environmental protection require the reduction of sulfur and zinc oxide contents in rubber products and modification of recipes for producing elastomer composites. Novel vulcanization accelerators based on ILs may allow the requirements of EU legislation to be met and improve the properties of the obtained rubber products.

Because of their catalytic activity, ILs can accelerate the process of elastomer crosslinking and increase the efficiency of sulfur consumption. As a result, reduction in the sulfur content of rubber products should be achieved for ecological reasons. Moreover, ILs may act as dispersants, improving the dispersion of crosslinking system components (sulfur or activator) in elastomers. The dispersion degree of zinc oxide, sulfur, and accelerator is very important for the activation of sulfur vulcanization. Our preliminary studies confirmed the high activity of synthesized ILs with 2-mercaptobenzothiazolate in the vulcanization of elastomers [40,41]. This result was most likely due to the more homogeneous dispersion of crosslinking agents in the elastomer. SEM images showed that, in the case of a standard NBR vulcanizate with 2-mercaptobenzothiazole (MBT), zinc oxide particles were not homogeneously distributed in the elastomer matrix. The agglomeration of zinc oxide particles caused the particle surface area

to decrease, which was followed by a reduction in the interfacial area between crosslinking system components. As a result, the efficiency of elastomer crosslinking decreased. In the case of vulcanizates produced with the prepared ILs, more homogeneously dispersed crosslinking agent particles were observed. The application of ILs increased the crosslink density of the vulcanizates. Therefore, the application of appropriately structured ILs as vulcanization accelerators seems to be reasonable.

In these studies, ILs such as alkylimidazolium and alkylammonium salts of 2-mercaptobenzothiazole as well as nanosized zinc oxide were used to successfully form pro-ecological elastomer composites with reduced amounts of vulcanization accelerators and activators. Several aspects were analyzed, including crosslink density, static and dynamic mechanical properties of the vulcanizates, as well as their thermal stability and resistance to UV and thermo-oxidative aging.

Pro-ecological composites based on NBR and SBR elastomers containing ILs as vulcanization accelerators were manufactured and studied. Elastomers were vulcanized with sulfur and nanosized zinc oxide in the presence of ILs as accelerators, alternatively to standard 2-mercaptobenzothiazole (MBT) and N-cyclohexyl-2-benzothiazolesulfenamide (CBS). As accelerators, the salts of 2-mercaptobenzothiazole with the following cations were used: dioctyldimethylammonium (C8DM), didecyldimethylammonium (C10DM), dodecyltrimethylammonium (C12TMA), 1-butyl-3-methylimidazolium (C4mim), 1-methyl-3-octylimidazolium (C8mim), and 1-dodecyl-3-methylimidazolium (C12mim).

2. Experimental section

2.1. Materials

The acrylonitrile-butadiene elastomer (EUROPREN N3960) containing 39 wt % acrylonitrile was obtained from Polimeri Europa (Rome, Italy). The Mooney viscosity was (ML1+4 (100°C): 60). This elastomer was vulcanized with sulfur (Siarkopol, Poland) with microsized zinc oxide as the activator (ZnO, Aldrich, Germany).

The butadiene-styrene elastomer (KER 1500) containing 22-25 wt % styrene was obtained from Synthos Dwory, Oswiecim (Poland). The Mooney viscosity was (ML1+4 (100°C):46-54). This elastomer was vulcanized with sulfur (Siarkopol Tarnobrzeg, Poland) with microsized zinc oxide as the standard activator (ZnO, Aldrich, Germany). Accelerators included 2-mercaptobenzothiazole (MBT, Aldrich, Germany) and N-cyclohexyl-2-benzothiazolesulfenamide (CBS, Aldrich, Germany).

To reduce the number of zinc ions in rubber compounds, nanosized zinc oxide (nZnO, Nanostructured & Amorphous Materials, Inc., USA) was used as an alternative to microsized ZnO. Silica with a specific surface area of 380 m²/g (Aerosil 380, Evonic Industries, Germany) was used as a filler. The ionic liquids listed in Table 1 were synthesized at the Poznan University of Technology, according to a procedure described elsewhere [40,41].

Ionic Liquid	Symbol
Diocetyltrimethylammonium 2-mercaptobenzothiazolate	C8DMA
Didecyltrimethylammonium 2-mercaptobenzothiazolate	C10DMA
Dodecyltrimethylammonium 2-mercaptobenzothiazolate	C12TMA
1-Butyl-3-methylimidazolium 2-mercaptobenzothiazolate	C4mim
1-Methyl-3-octylimidazolium 2-mercaptobenzothiazolate	C8mim
1-Dodecyl-3-methylimidazolium 2-mercaptobenzothiazolate	C12mim

Table 1. Ionic liquids used in this study

2.2. Preparation and characterization of rubber compounds

Rubber compounds with the formulations given in Table 2 were prepared using a laboratory two-roll mill. The samples were cured at 160 °C until they developed a 90% increase in torque, as measured by an oscillating disc rheometer (Monsanto).

	SBR (phr)		NBR (phr)	
	Without IL (reference sample)	With IL	Without IL (reference sample)	With IL
Elastomer	100	100	Elastomer	100
Sulfur	2	2	Sulfur	2
*ZnO	5	2	*ZnO	2
MBT	1	-	MBT	2
CBS	1	-	Silica	30
Silica	30	30		
Ionic liquid	-	3	Ionic liquid	2.5

Table 2. Composition of SBR-and NBR-based rubber compounds (*2 phr of nanosized zinc oxide was used alternatively with 5 phr of standard activator)

The kinetics of rubber compound vulcanization was studied using a DSC1 (Mettler Toledo) analyzer by decreasing the temperature from 25 to-100 °C at a rate of 10 °C/min and then heating to 250 °C with the same heating rate.

The crosslink densities (v_1) of the vulcanizates were determined by their equilibrium swelling in toluene, based on the Flory-Rehner equation [42]. The Huggins parameter of the SBR-solvent

interaction (χ) was calculated from the equation $\chi=0.3700+0.5600V_r$ (Equation 1), where V_r is the volume fraction of elastomer in the swollen gel, and $\chi=0.3809+0.6707V_r$ for NBR-solvent interaction (Equation 2).

The tensile properties of the vulcanizates were measured according to ISO-37 standard procedures using a ZWICK 1435 universal machine.

2.3. Dynamic-mechanical analysis

Dynamic-mechanical measurements were carried out in tension mode using a DMA/SDTA861^e analyzer (Mettler Toledo). Measurements of the dynamic moduli were performed between -80 and 100°C with a heating rate of 2°C/min, a frequency of 1 Hz and a strain amplitude of 4 μm . The temperature of the elastomer glass transition was determined from the maximum of $\tan \delta=f(T)$, where $\tan \delta$ is the loss factor and T is the measurement temperature.

2.4. Scanning Electron Microscopy (SEM)

The dispersion degree of zinc oxide and filler nanoparticles in the elastomer matrix was estimated using scanning electron microscopy with an LEO 1530 SEM. The vulcanizates were broken down in liquid nitrogen, and the surfaces of the vulcanizate fractures were examined. Prior to measurements, the samples were coated with carbon.

2.5. Thermogravimetry analysis

The thermal stability of the vulcanizates was studied using a TGA/DSC1 (Mettler Toledo) analyzer. Samples were heated from 25 °C to 700 °C in an argon atmosphere (60 ml/min) with a heating rate of 10 °C/min. Decomposition temperatures at weight losses of 2% (T_{02}), 5% (T_{05}), 50% (T_{50}) and total weight loss during decomposition of vulcanizates were determined.

2.6. Thermo-oxidative and UV aging

The thermo-oxidative degradation of the vulcanizates was performed at a temperature of 100 °C for 240 h. The UV degradation of the vulcanizates was carried out for 120 h using a UV 2000 (Atlas) machine in two alternating segments: a day segment (irradiation 0.7 W/m², temperature 60 °C, time 8 h) and a night segment (without UV radiation, temperature 50 °C, time 4 h).

To estimate the resistance of the samples to aging, their mechanical properties and crosslink densities after aging were determined and compared with the values obtained for vulcanizates before the aging process. The aging factor (S) was calculated as the numerical change in the mechanical properties of the samples upon aging (Equation 3) [43], where TS is the tensile strength of the vulcanizate, and EB is the elongation at break:

$$S = (TS \cdot EB)_{\text{after aging}} / (TS \cdot EB)_{\text{before aging}} \quad (1)$$

3. Results and discussion

3.1. SBR composites containing ILs

3.1.1. Curing characteristics and crosslink densities of SBR vulcanizates

The activity of novel ILs as accelerators in the sulfur vulcanization of SBR was estimated based on rheometry measurements. The curing characteristics of the SBR compounds and the crosslink densities of the vulcanizates are given in Table 3. To reduce the amount of vulcanization activator, nanosized zinc oxide was applied (2 phr) alternatively with the normally used microsized ZnO (5 phr).

SBR	ΔG (dNm)	t_{90} (min)	t_p (min)	$v_T \cdot 10^4$ (mol/cm ³)
ZnO	53.3	60	3.7	15.4
nZnO	59.3	50	3.3	16.5
C8DMA	72.3	30	2.1	19.9
C10DMA	64.1	30	2.5	18.3
C12TMA	60.5	30	2.0	17.5
C4mim	72.9	35	2.6	20.8
C8mim	69.2	35	2.8	18.3
C12mim	67.8	35	2.5	17.3

Table 3. Curing characteristics and crosslink densities of SBR vulcanizates (ΔG -increment of torque in the rubber compound during vulcanization; t_{90} -optimal vulcanization time; t_p -scorch time, v_T – crosslink density of vulcanizates).

Nanosized zinc oxide seems to be very active in SBR vulcanization. Despite the reduced amount of vulcanization activator, an increase in the crosslink density of vulcanizates is observed, and, as a consequence, the torque increment during vulcanization is comparable to that of the reference rubber compound with microsized ZnO. Moreover, a reduction of vulcanization time by 10 min was achieved. The nanosized zinc oxide does not influence the scorch time of rubber compounds. Applying ILs as vulcanization accelerators results in a further increase in torque increment during the vulcanization process because of the increase in vulcanizate crosslink densities. Alkylammonium and alkylimidazolium salts of MBT seem to catalyze the interface crosslinking reactions, which is evident from the considerable reduction of vulcanization time (approximately 25-30 min) and scorch time (approximately 1.5 min) compared to conventionally crosslinked SBR compounds. Alkylammonium and alkylimidazolium ILs have comparable activity in the vulcanization of SBR. However, the crosslink density of vulcanizates decreases slightly with the increase of alkyl chain length in the ammonium or imidazolium cation of ILs.

The most important parameters of the vulcanization process are temperature and energetic effect. The influence of nanosized zinc oxide and novel ILs on these parameters is given in Table 4.

SBR	Vulcanization temperature range (°C)	Energetic effect of vulcanization (J/g)
ZnO	175-231	10.0
nZnO	173-226	9.1
C8DMA	156-236	4.9
C10DMA	152-234	4.4
C12TMA	150-237	8.8
C4mim	147-235	9.8
C8mim	148-237	8.6
C12mim	149-236	8.0

Table 4. Temperatures and energetic effects of SBR vulcanization measured by DSC

Nanosized zinc oxide has no significant influence on the temperature and heat of vulcanization in comparison with SBR compounds containing a microsized activator. Vulcanization is an exothermic process that occurs in a temperature range of 173-226 °C, with an energetic effect of 9 J/g. 2-Mercaptobenzothiazolate ILs, especially alkylimidazolium salts, decrease considerably the onset temperature of vulcanization. The vulcanization process begins in the temperature range of 150-156 °C for SBR compounds containing alkylammonium ILs and 147-149 °C in the case of alkylimidazolium salts. This result confirms the catalytic effect of ILs on interfacial crosslinking reactions. The energetic effect of vulcanization ranges from 8.0 J/g to 9.8 J/g and decreases with alkyl chain length for rubber compounds with alkylimidazolium salts. A considerable reduction in the heat of vulcanization is achieved for alkyldimethylammonium ILs, indicating a decrease in the efficiency of the vulcanization process and confirming that the structure of the accelerator (ILs) affects vulcanization efficiency.

3.1.2. Dispersion degree of crosslinking system particles in SBR

Having concluded that the novel ILs catalyze interfacial crosslinking reactions and influence the efficiency of vulcanization, we then examined their effect on the dispersion degree of crosslinking system components in the SBR elastomer. The homogeneous distribution of ZnO, sulfur and accelerator particles is very important for the activation of sulfur vulcanization. Sulfur and accelerator diffuse inside the elastomer matrix and are adsorbed on the zinc oxide surface during vulcanization.

For the vulcanizate with MBT, crosslinking system particles are not homogeneously distributed in the elastomer matrix (Figure 1). Microsized agglomerates (several micrometers in size) are created. The agglomeration of particles causes their surface area to decrease, followed by

a reduction of the interface between zinc oxide, sulfur, and the accelerator. As a result, the efficiency of elastomer crosslinking decreases.

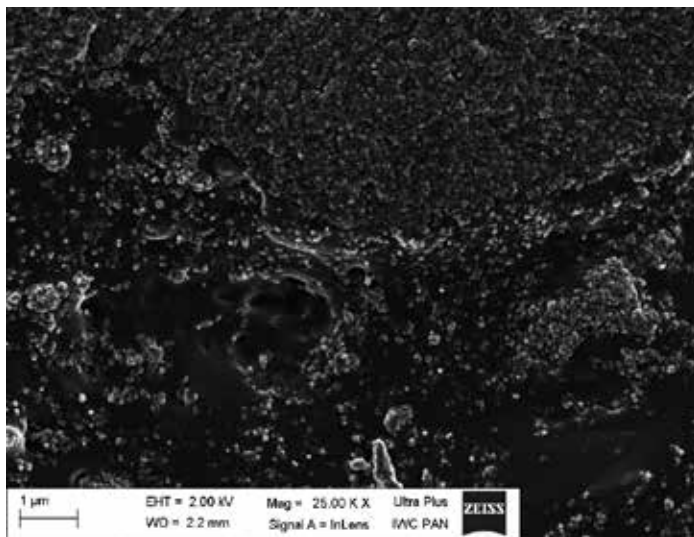


Figure 1. SEM images of SBR vulcanizates containing nZnO without IL

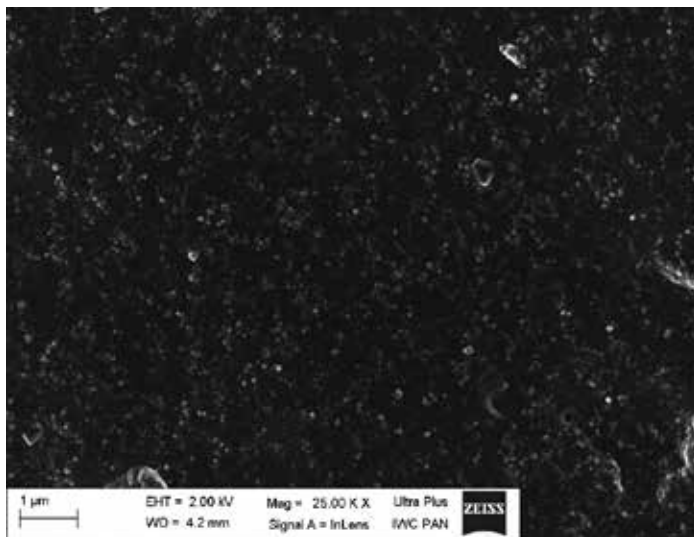


Figure 2. SEM images of SBR vulcanizates containing nZnO with C8DMA

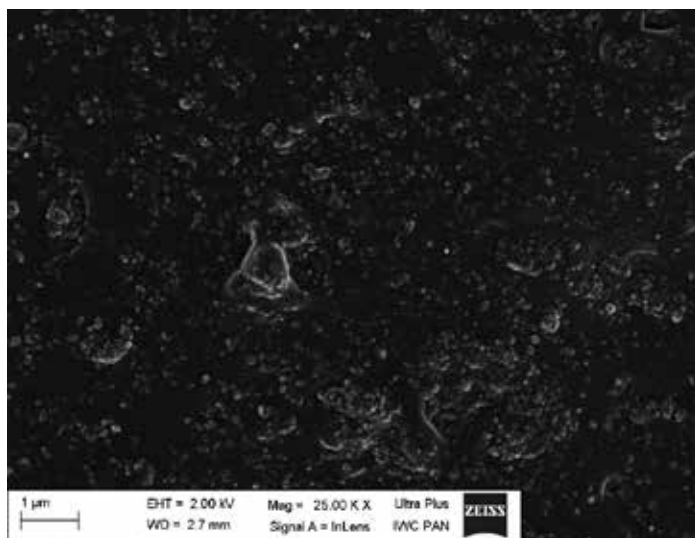


Figure 3. SEM images of SBR vulcanizates containing nZnO with C10DMA

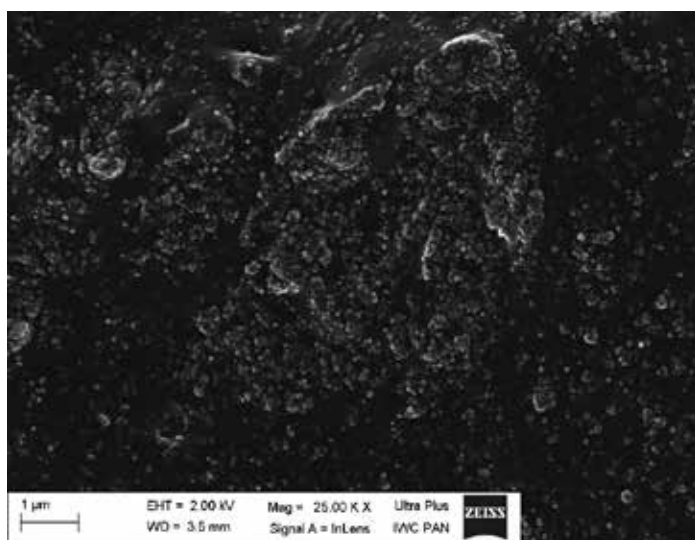


Figure 4. SEM images of SBR vulcanizates containing nZnO with C12TMA

In the case of vulcanizates with novel ILs, a more homogeneous distribution of crosslinking agent particles in SBR is observed (Figures 2-6). The dispersion degree depends on the IL structure and improves with the decrease in the ammonium or imidazolium cation alkyl chain length. In the case of ILs with C8 chains in the cation, particles of the crosslinking system are homogeneously distributed in the elastomer, and no agglomeration is observed. For ILs with C12 chains, some agglomerates can be observed in the SEM images but with a smaller size

than conventionally crosslinked SBR vulcanizates. Therefore, it can be concluded that, apart from accelerating action, ILs act as dispersing agents that prevent crosslinking system particles from agglomeration. The homogeneous dispersion of particles provides better contact between the activator and other components of the crosslinking system, resulting in higher vulcanization efficiency.

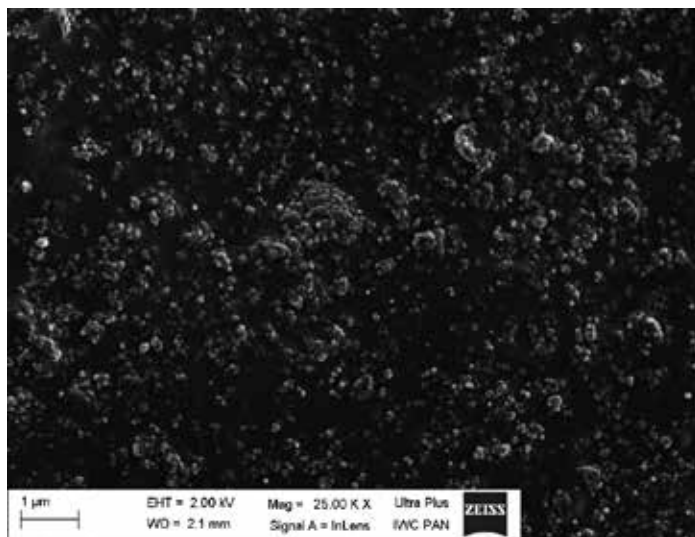


Figure 5. SEM images of SBR vulcanizates containing nZnO with C8mim

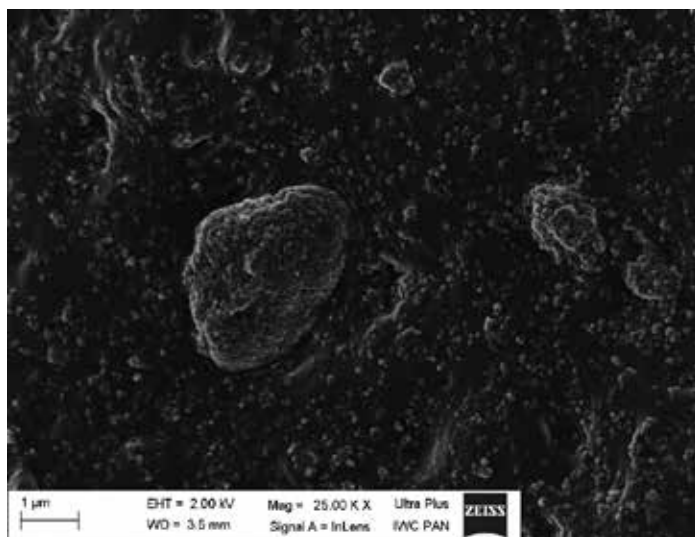


Figure 6. SEM images of SBR vulcanizates containing nZnO with C12mim

3.1.3. Mechanical properties of SBR vulcanizates

Having established the influence of ILs on the vulcanization process and on the crosslink density of vulcanizates, we then examined their mechanical properties. The results are given in Table 5.

SBR	TS (MPa)	EB (%)
ZnO	18.3	777
nZnO	22.4	781
C8DMA	32.0	634
C10DMA	25.5	635
C12TMA	24.2	580
C4mim	28.2	607
C8mim	27.2	651
C12mim	26.0	665

Table 5. Tensile strength (TS) and elongation at break (EB) of SBR vulcanizates

Despite the reduced amount of zinc oxide, vulcanizates containing nanosized ZnO exhibit approximately 4 MPa higher tensile strength than the reference sample. The elongation at break is similar in both vulcanizates. Applying ILs increases the tensile strength of SBR by 10 MPa in the case of C8DMA as a result of the improved dispersion degree of crosslinking system and filler particles in the SBR. The tensile strength decreases with the increase in IL alkyl chain length, as the dispersion degree of crosslinking system particles deteriorates. The elongation at break is reduced by 100–150% due to the increase in the crosslink density of the vulcanizates.

For technological applications of SBR, dynamic mechanical properties are very important. Rubber products must meet requirements of rigidity and strength so that their stability during use is sufficient. Even more important is their ability to dampen vibrations. Using DMA, the influence of ILs on the loss factor ($\tan \delta$) was determined. The loss factor, $\tan \delta$, as a function of temperature for the vulcanizates containing ILs is presented in Figure 7 and Table 6.

The existence of one transition can be observed (Figure 7), the glass transition of SBR, with a maximum that represents T_g . Applying nanosized zinc oxide alternatively with microsized activator does not influence the glass transition temperature of SBR, which is approximately 41.0 °C. Vulcanizates containing ILs exhibit higher glass transition temperatures than the reference samples because of their higher crosslink density. A greater number of crosslinks in the elastomer network results in greater restriction of mobility of the elastomer chains and, as a consequence, higher T_g . As expected, the highest T_g values occur for vulcanizates with the highest crosslink densities.

Nanosized zinc oxide or ILs have no significant effect on the $\tan \delta$ values of SBR vulcanizates (Table 6). Only a slight increase in the $\tan \delta$ at glass transition temperature is observed for IL-

containing vulcanizates. The loss factor is practically unchanged in the temperature range of 25-100 °C. Therefore, it could be concluded that SBR vulcanizates exhibit stable dynamic mechanical properties at application temperatures. It is worth noting that ILs applied as novel vulcanization activators alternatively to standard MBT and CBS do not deteriorate the dynamic mechanical properties of SBR and its ability for vibration damping, which is very important for technological reasons.

SBR	T_g (°C)	$\tan \delta$ at T_g (-)	$\tan \delta$ at 25 °C (-)	$\tan \delta$ at 100 °C (-)
ZnO	-40.9	0.58	0.13	0.09
nZnO	-40.1	0.63	0.13	0.09
C8DMA	-33.4	0.71	0.09	0.07
C10DMA	-36.1	0.73	0.12	0.11
C12TMA	-38.0	0.69	0.12	0.11
C4mim	-36.8	0.68	0.12	0.09
C8mim	-38.8	0.71	0.13	0.12
C12mim	-38.9	0.68	0.11	0.09

Table 6. Glass transition temperature (T_g) and loss factor ($\tan \delta$) of SBR vulcanizates

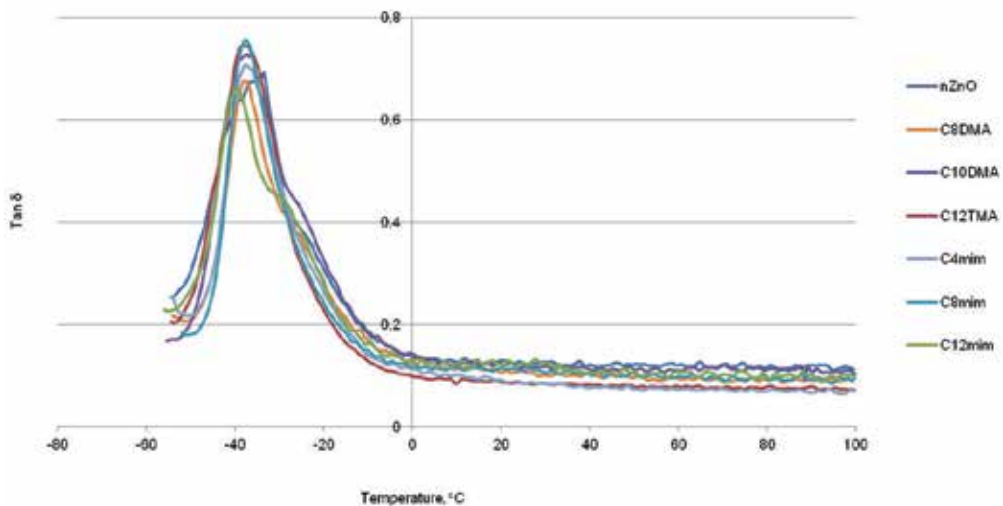


Figure 7. Loss factor ($\tan \delta$) versus temperature for SBR vulcanizates

3.1.4. Thermal stability and aging resistance of SBR vulcanizates

Rubber products often work at elevated temperatures. Therefore, novel vulcanization accelerators must not reduce the thermal stability of vulcanizates. Using TGA analysis, the effect of ILs on the thermal stability of SBR vulcanizates was determined (Table 7).

Nanosized zinc oxide increases the onset decomposition temperature of SBR (T_{02}) by 15 °C. Most likely, the network created by the zinc oxide and filler nanoparticles is a barrier for the transport of gases and volatile pyrolysis products during the decomposition process, thus increasing the thermal stability of the elastomer. ILs result in a further increase in the onset decomposition temperature of SBR, likely due to the improved dispersion degree of the nanoparticles in the elastomer matrix. The T_{02} for IL-containing vulcanizates is in the range of 363-365 °C. No influence of nanosized ZnO and ILs is achieved for T_{05} and T_{50} temperatures as well as for the total weight loss during decomposition (approximately 76%).

SBR	T_{02} (°C)	T_{05} (°C)	T_{50} (°C)	Total weight loss (%)
ZnO	288	362	442	74.2
nZnO	303	360	442	76.9
C8DMA	325	364	445	75.9
C10DMA	324	365	445	76.3
C12TMA	322	363	445	75.8
C4mim	326	365	444	76.3
C8mim	324	364	444	75.9
C12mim	325	364	444	76.4

Table 7. Decomposition temperatures at weight losses of 2% (T_{02}), 5% (T_{05}), 50% (T_{50}) and total weight loss during the decomposition of SBR vulcanizates

Having established the effects of nanosized zinc oxide and ILs on thermal stability, we then examined SBR resistance to thermo-oxidative and UV aging. The influence of ILs on aging resistance was studied through changes in mechanical properties and the crosslink density of the vulcanizates (Figures 8-10).

Thermo-oxidative and UV aging significantly increase the crosslink densities of SBR vulcanizates (Figure 8). This change is most evident in the case of thermo-oxidative degradation, where an almost threefold increase in the number of crosslinks is determined. Prolonged exposure to elevated temperatures results in further crosslinking of SBR. However, the increase in crosslink density is slightly smaller in the case of vulcanizates containing ILs. The elongation at break is reduced by 300-400% in comparison with vulcanizates before the aging process. This change is due to the large increase in the crosslink density of vulcanizates (Figure 9). In most cases, thermo-oxidative and especially UV aging deteriorate the tensile strength of vulcanizates with ILs, as in the case of vulcanizates with standard accelerators (Figure 10).

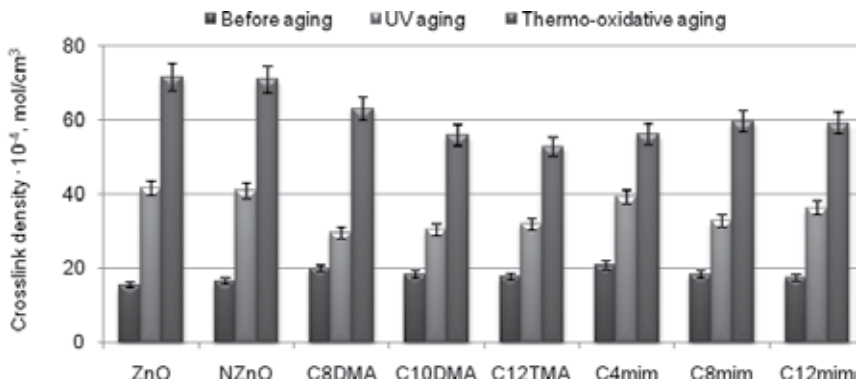


Figure 8. Crosslink density of SBR vulcanizates after aging

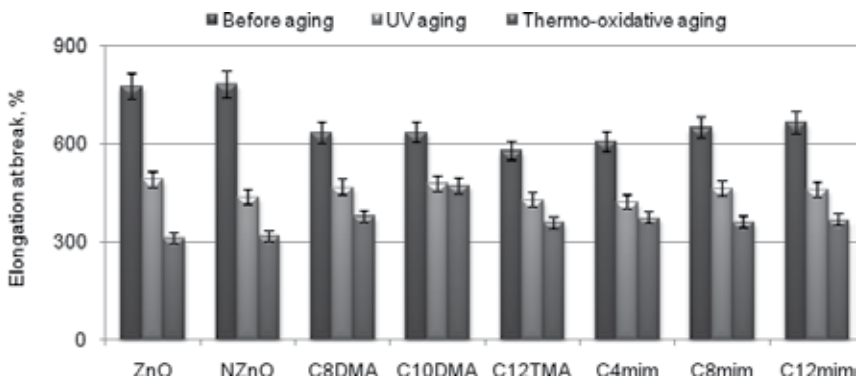


Figure 9. Elongation at break of SBR vulcanizates after aging

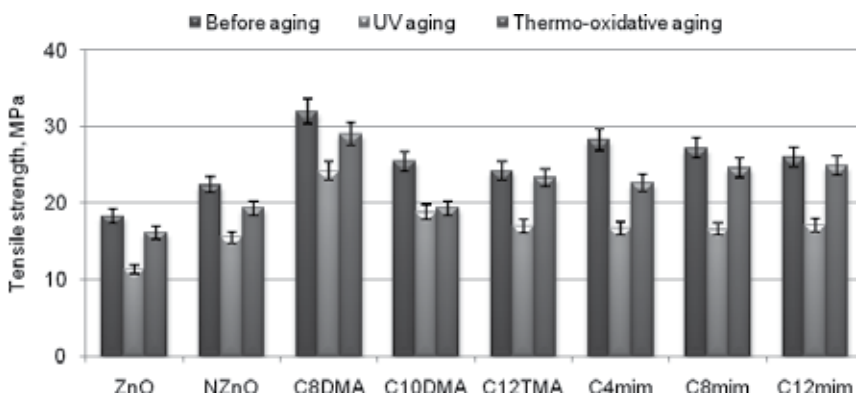


Figure 10. Tensile strength of SBR vulcanizates after aging

The aging factor S was calculated to quantitatively estimate the change in mechanical properties of vulcanizates. This factor is the change in the sample deformation energy under the aging process (Table 8).

Nanosized zinc oxide used as an alternative to the micro-sized ZnO does not influence the resistance of vulcanizates to aging. ILs, mainly alkylammonium salts, improve the resistance of SBR vulcanizates to thermo-oxidative and UV aging, most likely due to the limitation of the increase in vulcanizate crosslink density. An increase in the S_T and S_{UV} values of 0.2 is achieved for alkylammonium salts.

SBR	S_{UV} (-)	S_T (-)
ZnO	0.39	0.35
NZnO	0.39	0.35
C8DMA	0.54	0.56
C10DMA	0.56	0.55
C12TMA	0.59	0.52
C4mim	0.49	0.41
C8mim	0.50	0.43
C12mim	0.53	0.45

Table 8. Thermo-oxidative and UV aging factors for SBR vulcanizates

3.2. NBR composites containing ILs

Acrylonitrile-butadiene elastomer (NBR) is characterized by high resistance to oil, petrol and aliphatic hydrocarbons. As a result, NBR is widely applied to the manufacture of seals, inner tubes, hoses for liquid fuels and oils as well as elements used for damping vibration. Therefore, the use of novel ILs as accelerators for sulfur vulcanization of NBR was studied. To reduce the amount of zinc oxide in NBR compounds, nanosized ZnO was applied (2 phr) alternatively with traditionally used micro-sized activator (5 phr).

3.2.1. Curing characteristics and crosslink densities of NBR vulcanizates

Based on rheometric measurements, the effect of nanosized zinc oxide and ILs on the curing characteristics of NBR compounds was examined. Results are given in Table 9.

Nanosized zinc oxide increases the torque increment during vulcanization by approximately 20 dNm compared with the reference NBR compound containing micro-sized ZnO due to the increase in crosslink density of the vulcanizate. The amount of nanosized ZnO is 60% lower than for the micro-sized activator. Therefore, nanosized zinc oxide effectively activates the sulfur vulcanization of NBR. Zinc oxide particle size does not appear to affect vulcanization time or scorch time. Applying ILs causes a threefold increase in the torque increment during vulcanization compared to the rubber compound with micro-sized ZnO and a twofold increase

in ΔG in comparison with nanosized ZnO-containing NBR. These results occur because of the considerable increase in the crosslink density of vulcanizates. Moreover, ILs reduce the vulcanization time of NBR compounds by 10-20 min, whereas no influence is observed for scorch time. Higher activity in the vulcanization process is observed for alkylimidazolium salts of MBT. The length of alkyl chains in the imidazolium or ammonium cations of ILs does not seem to affect their activity in vulcanization.

NBR	ΔG (dNm)	t_{90} (min)	t_p (s)	$v_r \cdot 10^5$ (mol/cm ³)
ZnO	44.5	50	2.2	19.8
nZnO	67.8	50	2.9	20.4
C8DMA	113.1	40	2.9	25.4
C10DMA	122.2	40	3.0	24.8
C12TMA	122.9	35	2.8	24.5
C4mim	127.6	30	2.6	26.3
C8mim	127.0	35	2.5	26.0
C12mim	127.2	35	2.4	25.1

Table 9. Curing characteristics and crosslink densities of NBR vulcanizates (ΔG -increment of torque in the rubber compound during vulcanization; t_{90} -optimal vulcanization time; t_p -scorch time, v_r – crosslink density of vulcanizates)

Having established the effect of nanosized zinc oxide and ILs on the vulcanization time and crosslink density of vulcanizates, we then examined their influence on vulcanization temperature and energetic effect (Table 10).

NBR	Vulcanization temperature range (°C)	Energetic effect of vulcanization (J/g)
ZnO	163-240	10.1
nZnO	165-231	14.6
C8DMA	144-232	6.1
C10DMA	148-231	5.5
C12TMA	143-220	13.5
C4mim	141-220	12.8
C8mim	142-220	9.7
C12mim	143-220	10.4

Table 10. Temperatures and energetic effects of NBR vulcanization measured by DSC

Despite the reduced amount of ZnO, nanosized zinc oxide has no significant influence on vulcanization temperature. Moreover, the heat of vulcanization is higher in comparison with

the NBR compound containing microsized ZnO, so the vulcanization is most likely more effective. Vulcanization is an exothermic process that occurs in a temperature range of 165-231 °C, with an energetic effect of 14.6 J/g. Therefore, nanosized ZnO can be applied as an activator for NBR without detrimental effects on vulcanization characteristics. ILs decrease the vulcanization temperature by 17-24 °C. Alkylammonium ILs, especially dioctyl- and didecyldimethylammonium salts decrease the energetic effect of vulcanization. Alkylimidazolium salts also reduce the amount of heat generated during vulcanization but to a smaller degree than in the case of alkylammonium ILs.

The reduction of vulcanization time and temperature as well as the increase in the crosslink densities of vulcanizates could be due to the catalytic action of ILs during NBR crosslinking, similar to the SBR vulcanization process. However, the dispersion degree of crosslinking system components in the elastomer should be taken into account.

3.2.2. Dispersion degree of crosslinking system particles in NBR

Assuming that particles of accelerators, sulfur, and fatty acids diffuse through the polymer matrix and are adsorbed on the surface of zinc oxide to form intermediate complexes, the dispersion of zinc oxide nanoparticles in the elastomer matrix has great importance to the activation of sulfur vulcanization. SEM images of the vulcanizate surfaces were collected to estimate the dispersion degree of activator particles and other components of crosslinking system in the NBR elastomer (Figures 11-16).

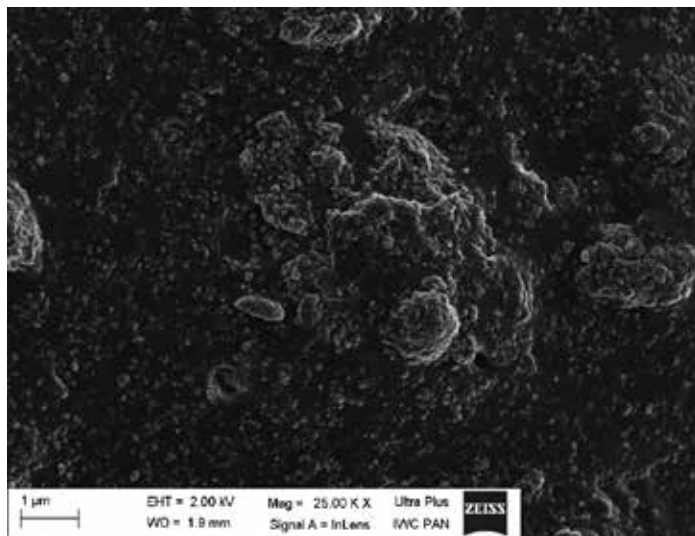


Figure 11. SEM images of NBR vulcanizates containing nZnO without IL

ZnO nanoparticles are poorly dispersed in the elastomer matrix (Figure 11), creating micro-sized clusters of particles with complex structures. The agglomeration of zinc oxide nanoparticles decreases the efficiency of vulcanization. However, in IL-containing vulcanizates,

particles are homogeneously distributed in the elastomer (Figures 12-16). The estimated size of crosslinking system particles seems to be in the nanometer range, which makes their surfaces available for interactions. Thus, the interactions of these particles with sulfur and accelerators are more efficient. Furthermore, filler nanoparticles are also homogeneously distributed in the elastomer.

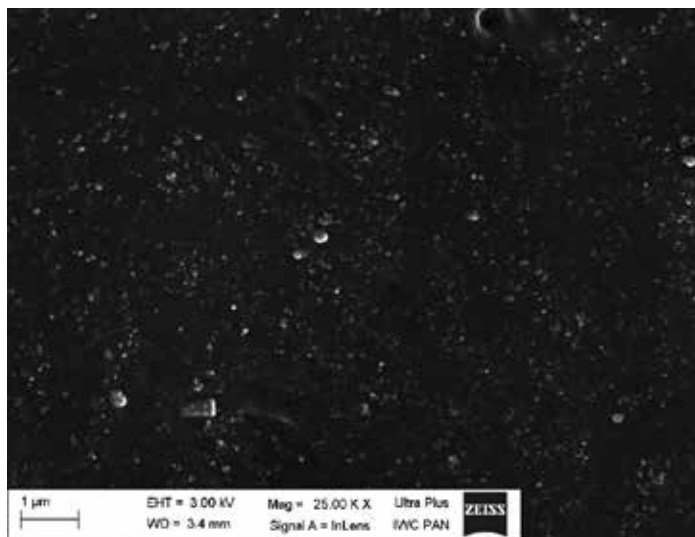


Figure 12. SEM images of NBR vulcanizates containing nZnO with C8DMA

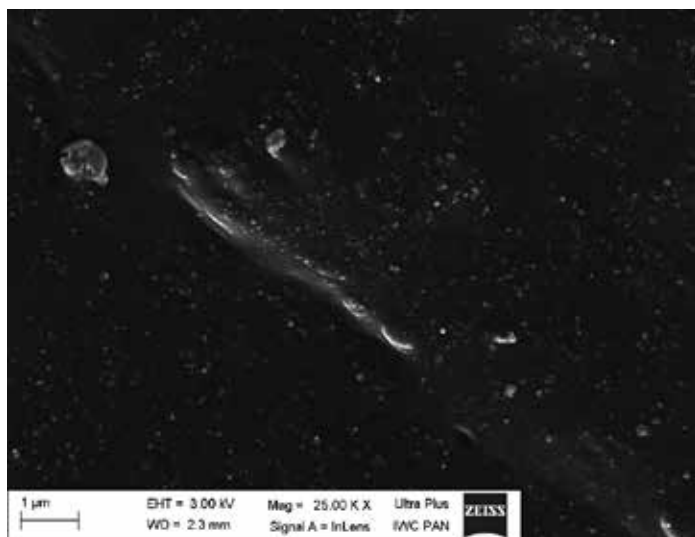


Figure 13. SEM images of NBR vulcanizates containing nZnO with C10DMA

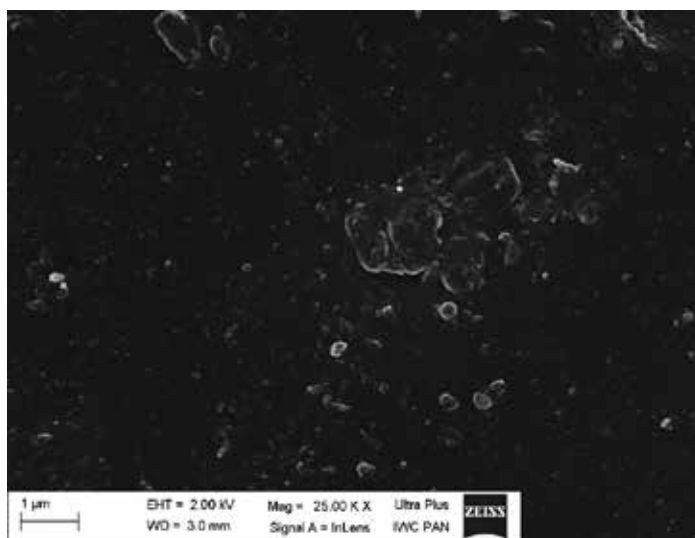


Figure 14. SEM images of NBR vulcanizates containing nZnO with C12TMA

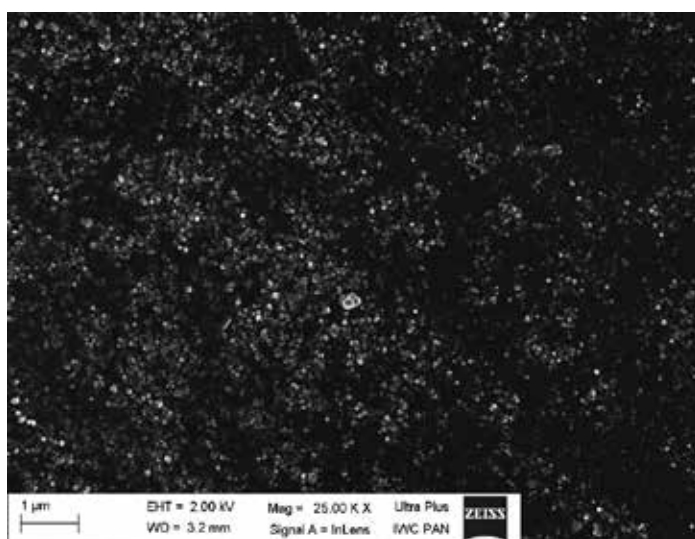


Figure 15. SEM images of NBR vulcanizates containing nZnO with C8mim

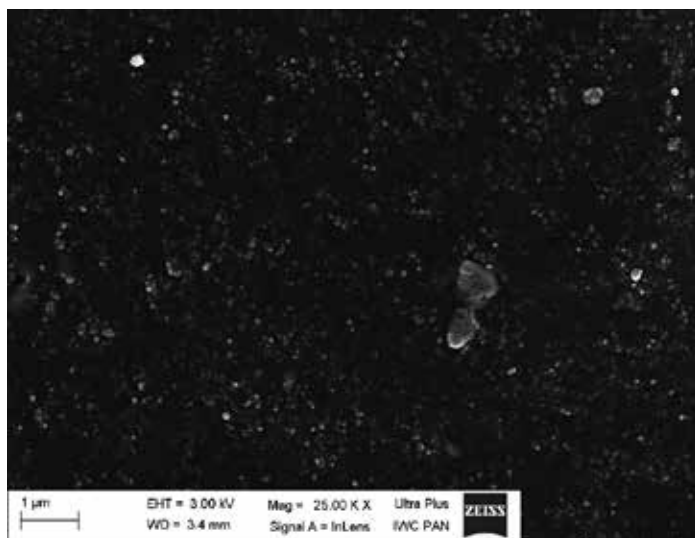


Figure 16. SEM images of NBR vulcanizates containing nZnO with C12mim

3.2.3. Mechanical properties of NBR vulcanizates

Due to the industrial applications of novel ILs as accelerators for the sulfur vulcanization of NBR, their effect on the mechanical properties of vulcanizates should be studied.

NBR	TS (MPa)	EB (%)
ZnO	20.4	531
nZnO	22.6	526
C8DMA	33.4	418
C10DMA	32.1	433
C12TMA	26.5	398
C4mim	29.4	411
C8mim	30.7	415
C12mim	28.3	420

Table 11. Tensile strength (TS) and elongation at break (EB) of NBR vulcanizates

From the data compiled in Table 11, the application of nanosized zinc oxide increases by 2 MPa the tensile strength of vulcanizate compared to the use of conventional ZnO. Therefore, it is possible to reduce the amount of ZnO by 60% without a detrimental effect on the tensile parameters. In addition, ILs used as an alternative to standard accelerators considerably increase the tensile strength of NBR vulcanizates, which is very important technologically. The highest

tensile strength is exhibited by vulcanizates with dioctyl- and didecyldimethylammonium salts (approximately 33 MPa). The lowest TS value of the C12TMA-containing vulcanizate is the result of an inhomogeneous distribution of nanoparticles in the elastomer matrix. In the case of alkylimidazolium ILs, the tensile strength of vulcanizates is between 28 MPa (C12mim) and 31 MPa (C8mim). Vulcanizates containing ILs exhibit approximately 100% lower elongation at break compared to reference vulcanizates, which results from their higher crosslink densities.

The effect of nanosized zinc oxide and ILs on the dynamic mechanical properties was examined using DMA and is presented in Table 12 and Figure 17.

NBR	T_g (°C)	$\tan \delta$ at T_g (-)	$\tan \delta$ at 25 °C (-)	$\tan \delta$ at 100 °C (-)
ZnO	-7.3	0.58	0.11	0.06
nZnO	-6.1	0.79	0.15	0.08
C8DMA	-5.9	0.86	0.19	0.10
C10DMA	-5.3	0.84	0.14	0.08
C12TMA	-6.5	0.85	0.14	0.07
C4mim	-4.4	0.88	0.20	0.09
C8mim	-5.5	0.82	0.21	0.10
C12mim	-6.6	0.86	0.17	0.09

Table 12. Glass transition temperatures (T_g) and loss factors ($\tan \delta$) of NBR vulcanizates

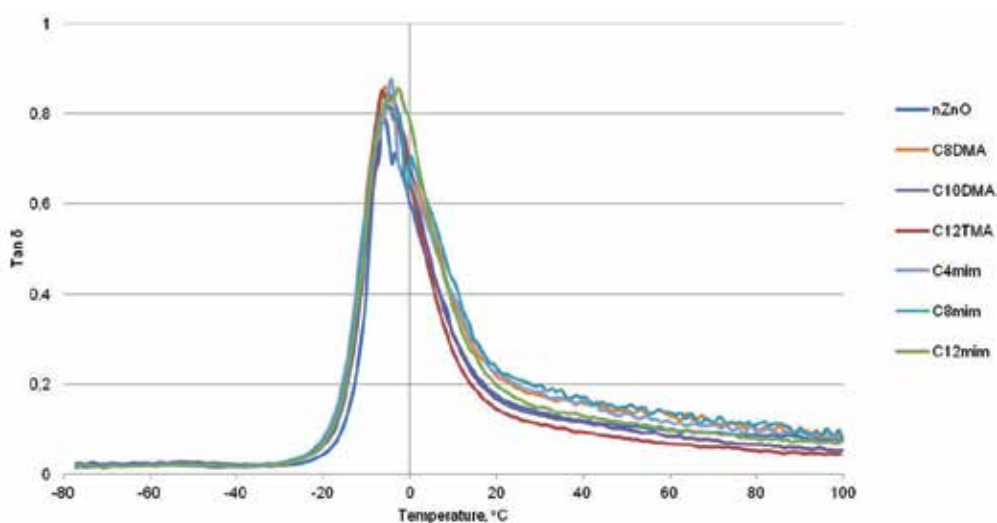


Figure 17. Loss factor ($\tan \delta$) versus temperature for NBR vulcanizates

The glass transition temperature for conventionally crosslinked NBR vulcanizates is -7.3 °C. Nanosized zinc oxide slightly increases the T_g of NBR. An increase is observed for loss factor values at T_g and temperatures of 25 °C and 100 °C. ILs cause a further increase in glass transition temperature due to the higher crosslink density of vulcanizates, which reduces the mobility of elastomer chains. An increase in the loss factor is also achieved, so vulcanizates containing ILs should exhibit a higher ability for vibration damping compared with the reference sample. These properties are important for the industrial application of rubber products based on NBR elastomers.

3.2.4. Thermal stability and aging resistance of NBR vulcanizates

In Table 13, the effect of nanosized zinc oxide and ILs on decomposition temperature and weight loss for NBR vulcanizates is given.

NBR	T_{02} (°C)	T_{05} (°C)	T_{50} (°C)	Total weight loss (%)
ZnO	300	368	446	68.5
nZnO	320	367	448	72.6
C8DMA	323	364	447	76.1
C10DMA	324	367	447	77.3
C12TMA	324	369	448	77.3
C4mim	323	371	446	77.8
C8mim	324	370	446	76.1
C12mim	329	374	446	76.6

Table 13. Decomposition temperatures at weight losses of 2% (T_{02}), 5% (T_{05}), 50% (T_{50}) and total weight loss during the decomposition of NBR vulcanizates

Replacing microsized zinc oxide with a nanosized activator increases the onset decomposition temperature of NBR by 20 °C. Applying ILs as vulcanization accelerators does not considerably influence the thermal stability compared with a vulcanizate containing nanosized ZnO. The thermal decomposition of vulcanizates begins at a temperature range of 323 – 329 °C. A weight loss of 5% is achieved in the temperature range of 364 – 374 °C, whereas 50% weight loss occurs at 446 – 448 °C. ILs increase the total weight loss during NBR decomposition, which is approximately 77%. The positive effect of nanosized ZnO and ILs on the thermal stability of NBR is, as in the case of SBR, caused by the network formed by nanoparticles in the elastomer, which restrains the diffusion of gases and volatile decomposition products in the elastomer matrix.

NBR rubber products often work at elevated temperatures and are exposed to factors that cause aging (e.g., temperature and UV radiation). If ILs are industrially used as accelerators instead of MBT, they should not deteriorate the aging resistance of vulcanizates.

Prolonged exposure to UV radiation and especially elevated temperatures results in further crosslinking of NBR. The increase in crosslink density is comparable for all NBR vulcanizates (Figure 18). Thermo-oxidative aging, despite the increase in crosslink density, has no considerable influence on the tensile strength of vulcanizates (Figure 19). UV degradation deteriorates the tensile strength of vulcanizates with ILs, as it does to vulcanizates with standard accelerator and nanosized zinc oxide. There is no influence of IL structure on the change in crosslink density or tensile strength of vulcanizates. In the case of vulcanizates without ILs, the aging process causes a reduction in elongation at break of approximately 100% for UV radiation and approximately 300% for elevated temperatures (Figure 20). These results arise from the increase in crosslink density of vulcanizates as well as their stiffness and fragility. ILs decrease the changes in elongation at break, especially under thermo-oxidative aging. This result is most evident for vulcanizates containing alkylimidazolium salts. It is possible that these ILs limit the loss of vulcanizate elasticity during aging. Vulcanizates containing these ILs are less rigid, which could confirm this assumption.

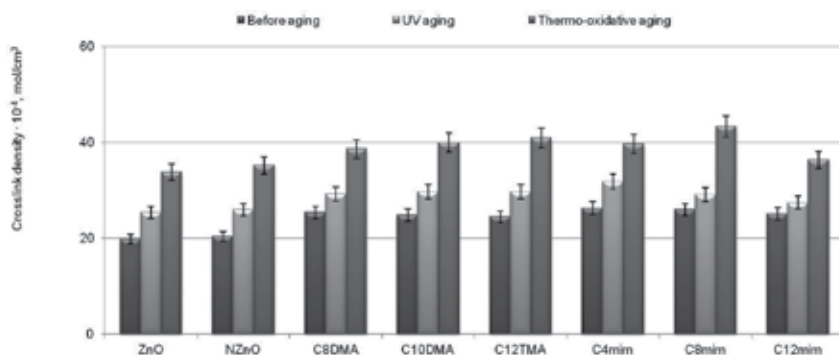


Figure 18. Crosslink density of NBR vulcanizates after aging

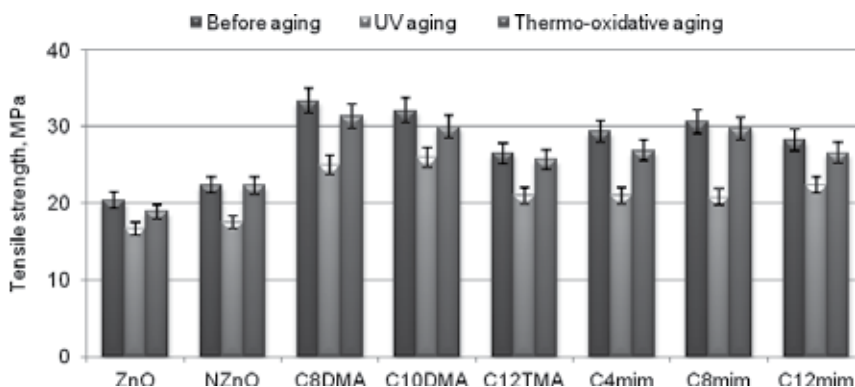


Figure 19. Tensile strength of NBR vulcanizates after aging

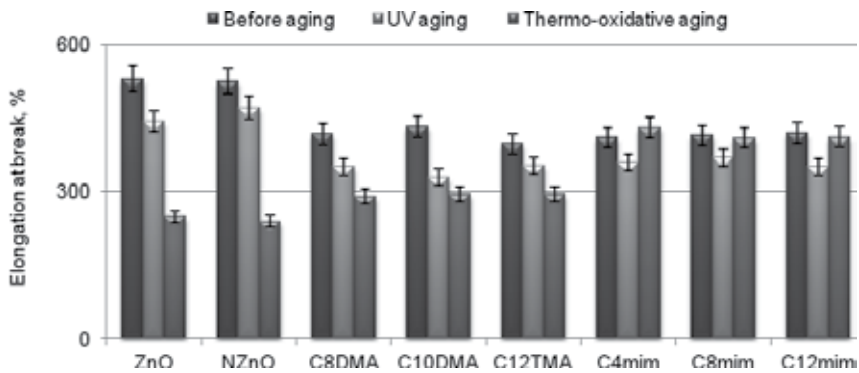


Figure 20. Elongation at break of NBR vulcanizates after aging

Based on the above results, it is difficult to estimate the resistance of NBR vulcanizates to the aging process considering the changes in tensile strength and elongation at break separately. Therefore, UV and thermo-oxidative aging factors were calculated to quantitatively estimate changes in mechanical properties of NBR vulcanizates (Table 14).

NBR	S_{UV} (-)	S_T (-)
ZnO	0.68	0.43
nZnO	0.70	0.45
C8DMA	0.63	0.65
C10DMA	0.62	0.64
C12TMA	0.70	0.72
C4mim	0.63	0.96
C8mim	0.60	0.96
C12mim	0.66	0.92

Table 14. UV and thermo-oxidative aging factors for NBR vulcanizates

In terms of S_{UV} factor, nanosized zinc oxide and ILs do not affect the resistance of NBR to UV degradation. However, ILs increase the resistance of vulcanizates to thermo-oxidative aging. In the case of vulcanizates containing alkylammonium ILs, an increase in S_T values from approximately 0.45 to 0.72 is achieved. A considerable improvement of resistance to thermo-oxidative degradation is observed for NBR containing alkyimidazolium salts. The values of S_T are close to 1, so the mechanical properties of vulcanizates with alkyimidazolium ILs do not change under the influence of thermo-oxidative aging.

4. Conclusions

Applying ILs allowed for the replacement of standard accelerators in sulfur vulcanization of SBR and NBR elastomers, resulted in the shortening of the optimal vulcanization time and

decreased the temperature of vulcanization by approximately 20 °C. These results are very important for technological and economical reasons. NBR and SBR composites containing ILs exhibited tensile strengths and crosslink densities higher than those of standard vulcanizates crosslinked with MBT and CBS. These results were due to the considerable improvement of crosslinking system nanoparticle distribution in the elastomer. ILs restrained the tendency of nanoparticles to agglomerate in the elastomer; as a result, the surface of contact between nanosized zinc oxide and other components of crosslinking system was maximized and the efficiency of vulcanization increased. Moreover, ILs could catalyze the interface crosslinking reaction that improves the efficiency of vulcanization.

Nanosized zinc oxide and ILs increased the thermal stability of elastomers. The onset decomposition temperature increased by approximately 20 °C. Most likely, the network created by zinc oxide and filler nanoparticles homogeneously distributed in the elastomer may be a barrier for the transport of gases and volatile pyrolysis products during the decomposition process, thus increasing the thermal stability of the elastomer.

NBR and SBR composites containing ILs exhibited stable dynamic properties at the temperature of use. Moreover, NBR vulcanizates could be expected to demonstrate better damping properties than conventionally crosslinked samples. ILs, especially alkylimidazolium salts, increased the resistance of NBR vulcanizates to thermo-oxidative aging. In the case of SBR, improved resistance to UV and thermo-oxidative degradation was achieved, mainly for alkylammonium ILs. Further crosslinking of elastomers during aging was greatly reduced in comparison with vulcanizates containing standard accelerators.

Most important, applying nanosized zinc oxide and ILs allowed for the reduction of zinc oxide amount by 60% as well as the elimination of CBS from SBR composites and, in the case of NBR, reduction in the amount of MBT, an allergic agent, by 30-50% in comparison with conventional rubber compounds (Table 15). This result is very important ecologically.

Accelerator	Accelerator content in NBR compound (g)	MBT content in accelerator (mmol/g)	MBT content in NBR compound (mmol/100 g of NBR)
NBR			
MBT	2.0	5.98	11.96
C8DM	2.5	1.39	3.48
C10DM	2.5	2.69	6.27
C12TMA	2.5	2.52	6.30
C4mim	2.5	3.25	8.12
C8mim	2.5	2.75	6.88
C12mim	2.5	2.38	5.95

Table 15. MBT content in accelerators applied in NBR compounds

Acknowledgements

The authors wish to acknowledge the National Centre for Research and Development (Poland) for supporting this research.

Author details

Magdalena Maciejewska^{1*} and Filip Walkiewicz²

*Address all correspondence to: magdalena.maciejewska@p.lodz.pl

1 Technical University of Lodz; Institute of Polymer and Dye Technology, Lodz, Poland

2 Poznan Technical University; Institute of Technology and Chemical Engineering, Poznan, Poland

References

- [1] Oenslager G. Organic Accelerators. *Industrial & Engineering Chemistry* 1933;25(2): 232-7.
- [2] Harman M.W., U.S. Patent 2,100,692 (1937).
- [3] Nieuwenhuizen PJ. Zinc Accelerator Complexes. Versatile Homogeneous Catalysts in Sulfur Vulcanization. *Applied Catalysis A: General* 2001;207(1): 55-68. <http://www.sciencedirect.com/science/article/pii/S0926860X0000613X> (accessed 8 May 2000).
- [4] Heideman G, Noordermeer JWM, Datta RN. Effect of Zinc Complexes as Activator for Sulfur Vulcanization in Various Rubbers. *Rubber Chemistry and Technology* 2005;78(2): 245-57. <http://rubberchemtechnol.org/doi/abs/10.5254/1.3547881> (accessed May 2005).
- [5] Lu J, Yan F, Texter J. Advanced Applications of Ionic Liquids in Polymer Science. *Progress in Polymer Science* 2009; 34(5): 431-48. <http://www.sciencedirect.com/science/article/pii/S0079670008001226> (accessed 13 January 2009).
- [6] Rogers RD, Seddon KR. Ionic Liquids-Solvents of the Future? *Science* 2003;302(5646): 792-3. <http://www.sciencemag.org/content/302/5646/792.full.pdf> (accessed 31 October 2003).
- [7] Wasserscheid P, Welton T., editor. *Ionic Liquids in Synthesis*. New York: Wiley-VCH; 2008.

- [8] Kubisa P. Application of Ionic Liquids as Solvents for Polymerization Processes. *Progress in Polymer Science* 2004;29(1): 3-12. <http://www.sciencedirect.com/science/article/pii/S0079670003001199> (accessed January 2004).
- [9] Freemantle M. New Horizons for Ionic Liquids. *Chemical & Engineering News* 2001;79(1): 21-5. <http://pubs.acs.org/doi/pdf/10.1021/cen-v079n001.p021> (accessed 01 January 2001).
- [10] Lu W, Fadeev AG, Qi B, Mattes BR. Fabricating Conducting Polymer Electrochromic Devices Using Ionic Liquids. *Journal of The Electrochemical Society* 2004;151(2): 33-9. <http://jes.ecsdl.org/content/151/2/H33> (accessed 8 January 2004).
- [11] Zhang H, Hong K, Mays JW. Synthesis of Block Copolymers of Styrene and Methyl Methacrylate by Conventional Free Radical Polymerization in Room Temperature Ionic Liquids. *Macromolecules* 2002; 35(15): 5738 – 41. <http://pubs.acs.org/doi/full/10.1021/ma025518x> (accessed 17 June 2002).
- [12] Shen Y, Ding S. Catalyst Separation in Atom Transfer Radical Polymerization. *Progress in Polymer Science* 2004;29(10): 1053-78. <http://www.sciencedirect.com/science/article/pii/S0079670004000814> (accessed October 2004).
- [13] Vijayaraghavan R, MacFarlane DR. Living Cationic Polymerization of Styrene in an Ionic Liquid. *Chemical Communications* 2004; 6: 700-1. <http://pubs.rsc.org/en/content/articlehtml/2004/cc/b315100j?page=search> (accessed 13 February 2003).
- [14] Wang YY, Jiang D, Wang R, Dai LY. Application of Et₃NHCl-AlCl₃ Ionic Liquid as Initiator in Cationic Copolymerization of 1,3-Pentadiene with Styrene, Reaction Kinetics and Catalysis *Letters* 2007;90(1): 69-76. <http://link.springer.com/article/10.1007%2Fs11144-007-4999-2> (accessed 01 February 2007).
- [15] Wang YY, Li W, Dai LY. Cationic Ring-Opening Polymerization of 3,3-Bis(Chloromethyl)oxacyclobutane in Ionic Liquids. *Chinese Chemical Letters* 2007;18(10): 1187–90. <http://vls2.icm.edu.pl/cgi-bin/sciserv.pl?collection=elsevier&journal=10018417&issue=v18i0010> (accessed October 2007).
- [16] Liu Y, Wu G. On the Mechanism of Radiation-Induced Polymerization of Vinyl Monomers in Ionic Liquid. *Radiation Physics and Chemistry* 2005;73(3): 159-62. <http://www.sciencedirect.com/science/article/pii/S0969806X04004633> (accessed 14 October 2004).
- [17] Harrison S, MacKenzie SR, Haddleton DM. Unprecedented Solvent-Induced Acceleration of Free-Radical Propagation of Methyl Methacrylate in Ionic Liquid. *Chemical Communications* 2002;2850-1. <http://pubs.rsc.org/en/content/articlehtml/2002/cc/b209479g?page=search> (accessed 28 October 2002).
- [18] Zhang H, Hong K, Mays JW. Synthesis of Block Copolymers of Styrene and Methyl Methacrylate by Conventional Free Radical Polymerization in Room Temperature

- Ionic Liquids. *Macromolecules* 2002;35(15): 5738-41. <http://pubs.acs.org/doi/full/10.1021/ma025518x> (accessed 17 June 2002).
- [19] Noda A, Watanabe M. Highly Conductive Polymer Electrolytes Prepared by In Situ Polymerization of Vinyl Monomers in Room Temperature Molten Salts. *Electrochimica Acta* 2000;45(8-9): 1265-70. <http://www.sciencedirect.com/science/journal/00134686/45/8-9> (accessed 3 January 2000).
- [20] Feng S, Xu W, Nakanishi K, Yamago S. Highly Controlled Organotellurium-Mediated Living Radical Polymerization (TERP) in Ionic Liquids (ILs). The New Role of ILs in Radical Reactions. *ACS Macro Letters* 2012;1(1): 146-9. <http://pubs.acs.org/doi/full/10.1021/mz200133d> (accessed 8 December 2011).
- [21] Lu J, Yan F, Texter J. Advanced Applications of Ionic Liquids in Polymer Science. *Progress in Polymer Science* 2009; 34(5): 431-48. <http://www.sciencedirect.com/science/article/pii/S0079670008001226> (accessed 13 January 2009).
- [22] Yoshizawa M, Ogihara W, Ohno H. Novel Polymer Electrolytes Prepared by Copolymerization of Ionic Liquid Monomers. *Polymers for Advanced Technology* 2002;13(8): 589-94. <http://onlinelibrary.wiley.com/doi/10.1002/pat.261/pdf> (accessed 15 August 2002).
- [23] Ohno H. Design of Ion Conductive Polymers Based on Ionic liquids. *Macromolecular Symposia* 2007;249(1): 551-6. <http://onlinelibrary.wiley.com/doi/10.1002/masy.200750435/pdf> (accessed 28 March 2007).
- [24] Batra D, Hay DNT, Firestone MA. Formation of Biomimetic Liquid-Crystalline Hydrogel by Self-Assembly and Polymerization of an Ionic Liquid. *Chemistry of Materials* 2007;19(18): 4423-31. <http://pubs.acs.org/doi/full/10.1021/cm062992z> (accessed 7 August 2007).
- [25] Sun N, Rahman M, Qin Y, Maxim ML, Rodriguez H, Rogers RD. Complete Dissolution and Partial Delignification of Wood in the Ionic Liquid 1-Ethyl-3-Methylimidazolium Acetate. *Green Chemistry* 2009;11(5): 646-55. <http://pubs.rsc.org/en/content/articlehtml/2009/gc/b822702k?page=search> (accessed 13 March 2009).
- [26] Biswas A, Shogren RL, Stevenson DG, Willett JL, Bhowmik PK. Ionic Liquids as Solvents for Biopolymers: Acylation of Starch and Zein Protein. *Carbohydrate Polymers* 2006;66(4): 546-50. <http://www.sciencedirect.com/science/article/pii/S0144861706001834> (accessed November 2006).
- [27] Phillips DM, Drummy LF, Conrady DG, Fox DM, Naik RR, Stone MO, Trulove PC, De Long HC, Mantz RA. Dissolution and Regeneration of Bombyx mori Silk Fibroin Using Ionic Liquids. *Journal of American Chemical Society* 2004; 126(44): 14350-1. <http://pubs.acs.org/doi/full/10.1021/ja046079f> (accessed 19 October 2004).
- [28] Pernak J, Smiglak M, Griffin ST, Hough WL, Wilson TB, Pernak A, Zabielska-Matejuk J, Fojutowski J, Kita K, Rogers RD. Long Alkyl Chain Quaternary Ammonium-Based Ionic Liquids and Potential Applications. *Green Chemistry* 2006;8(9): 798-806. <http://pubs.rsc.org/en/content/articlehtml/2006/gc/b612702k> (accessed 13 March 2009).

- pubs.rsc.org/en/content/articlehtml/2006/gc/b604353d?page=search (accessed 13 July 2006).
- [29] Swatlowski R, Spear SK, Holbrey JD, Rogers RD. Dissolution of Cellulose with Ionic Liquids. *Journal of American Chemical Society* 2002;124(18): 4974-75. <http://pubs.acs.org/doi/full/10.1021/ja025790m> (accessed 17 April 2002).
- [30] Pernak J, Borucka N, Walkiewicz F, Markiewicz B, Fochtman P, Stolte S, Steudte S, Stepnowski P. Synthesis, Toxicity, Biodegradability and Physicochemical Properties of 4-Benzyl-4-Methylmorpholinium-Based Ionic Liquids. *Green Chemistry* 2011;13(10): 2901-10. <http://pubs.rsc.org/en/content/articlehtml/2011/gc/c1gc15468k?page=search> (accessed 2 August 2011).
- [31] Pernak J, Kordala R, Markiewicz B, Walkiewicz F, Poplawski A, Fabianska S, Janowski S, Lozynski M, Synthesis and Properties of Ammonium Ionic Liquids with Cyclohexyl Substituent and Dissolution of Cellulose. *RSC Advances* 2012; 2(22): 8429-38. <http://pubs.rsc.org/en/content/articlehtml/2012/ra/c2ra21502k?page=search> (accessed 24 July 2012).
- [32] Kozirog A, Wysocka-Robak A, Przybysz K, Michalczyk A, Walkiewicz F. Imidazolium Azolates. Antifungal Activity and the Stability to Use in Papermaking. *Chemical Review* 2013;92(9): 1618-1620.
- [33] Kreyenschulte H, Richter S, Götze T, Fischer D, Steinhäuser D, Klüppel M, Heinrich G. Interaction of 1-Allyl-3-Methylimidazolium Chloride and Carbon Black and its Influence on Carbon Black Filled Rubbers. *Carbon* 2012;50(10): 3649-58 <http://www.sciencedirect.com/science/article/pii/S0008622312002850> (accessed 24 March 2012).
- [34] Lei YD, Tang ZH, Guo BC, Zhu LX, Jia DM. Synthesis of Novel Functional Liquid and its Application as a Modifier in SBR/Silica Composites. *eXPRESS Polymer Letters* 2010;4(11): 692-703. http://www.expresspolymlett.com/articles/EPL-0001670_article.pdf (accessed November 2010).
- [35] Guo BC, Chen F, Lei YD, Liu XL, Wan JJ, Jia DM. Styrene-Butadiene Rubber/Halloysite Nanotubes Nanocomposites Modified by Sorbic Acid. *Applied Surface Science* 2009;255(16): 7329-36. <http://www.sciencedirect.com/science/article/pii/S0169433209003663> (accessed 8 August 2008).
- [36] Maslowski M, Zaborski M. Magnetorheological Elastomers Containing Ionic Liquids. In: Handy S. (ed.) *Applications of Ionic Liquids in Science and Technology*. Rijeka: InTech; 2011. p213-32. Available from <http://cdn.intechopen.com/pdfs-wm/20212.pdf> (accessed 22 September 2011).
- [37] Marwanta E, Mizumo T, Nakamura N, Ohno H. Improved Ionic Conductivity of Nitrile Rubber/Ionic Liquid Composites. *Polymer* 2005;46(11): 3795-800. <http://www.sciencedirect.com/science/article/pii/S0032386105003393> (accessed 7 April 2005).

- [38] Subramaniam K, Das A, Heinrich G. Development of Conducting Polychloroprene Rubber Using Imidazolium Based Ionic Liquid Modified Multi-Walled Carbon Nanotubes. *Composites Science and Technology* 2011; 71(11): 1441-9. <http://www.sciencedirect.com/science/article/pii/S0266353811001928> (accessed 2 June 2011).
- [39] Yoshizawa M, Ogihara W, Ohno H. Novel Polymer Electrolytes Prepared by Copolymerization of Ionic Liquid Monomers. *Polymers Advanced Technologies* 2002;13(8): 589-94. <http://onlinelibrary.wiley.com/doi/10.1002/pat.261/pdf> (accessed 15 August 2012).
- [40] Pernak J, Walkiewicz F, Maciejewska M, Zaborski M. Ionic Liquids as Vulcanization Accelerators. *Industrial Engineering & Chemical Research* 2010; 49(10): 5012-17. <http://pubs.acs.org/doi/full/10.1021/ie100151n> (accessed 23 April 2012).
- [41] Maciejewska M, Walkiewicz F, Zaborski M. Novel Ionic Liquids as Accelerators for the Sulfur Vulcanization of Butadiene–Styrene Elastomer Composites. *Industrial Engineering & Chemical Research*, 2013, 52(25): 8410–15. <http://pubs.acs.org/doi/full/10.1021/ie303167z> (accessed 17 May 2013).
- [42] Flory PJ, Rehner J. Statistical Mechanics of Cross-Linked Polymer Networks. II. Swelling. *Journal of Chemical Physics* 1943;11(11): 521-6. <http://scitation.aip.org/content/aip/journal/jcp/11/11/10.1063/1.1723792> (accessed 22 December 2004).
- [43] Masek A, Zaborski M, Kosmalka A. Derivatives of Flavonoides as Anti-Ageing Substances in Elastomers. *Comptes Rendus Chimie* 2011;14(5): 483-8. <http://www.sciencedirect.com/science/article/pii/S1631074811000026> (accessed 15 February 2011).

Ionic Liquids Facilitate the Development of Absorption Refrigeration

Shiqiang Liang, Wei Chen, Yongxian Guo and
Dawei Tang

Additional information is available at the end of the chapter

<http://dx.doi.org/10.5772/58982>

1. Introduction

The rapid progress in the development of ionic liquids has generated enthusiasm for their application in many traditional fields and renewed interest in absorption refrigeration. New absorption refrigeration working pairs containing ionic liquids have gained widespread attention in the past decade. In a chapter entitled “The Latent Application of Ionic Liquids in Absorption Refrigeration” [1] that we have published 3 years ago with InTech in the book entitled “Applications of Ionic Liquids in Science and Technology” achieved impressive readership results and has so far been accessed more than 4000 times. Over the past 3 years, progress in this field has been outstanding, and a few commercially competitive new working pairs were discovered. In this chapter, we describe the latest progress in the development of a few mentionable new working pairs containing ionic liquids for absorption refrigeration and a type of completely new conceptual absorption refrigeration working pair that was proposed by us and is expected to lead to a major breakthrough in the development of absorption refrigeration.

2. Recent progress in absorption refrigeration working pairs containing ionic liquids

In the past 3 years, enthusiasm for studies on absorption refrigeration working pairs containing ionic liquids seems to have waned. The once preferred ionic liquid working pairs, such as Freon-IL, CO₂-IL, and NH₃-IL, do not receive attention from researchers any longer. However, some impressive progress is still being made for working pairs composed of a refrigerant and [RR'Im]DMP (1-R,3-R'-imidazolium dimethylphosphate).

2.1. [mmIm]DMP-CH₃OH

Zhao Jie et al. [2] measured the saturation vapor pressure of [mmIm]DMP-CH₃OH at $T = 303.15\text{--}363.15$ K and over a low methanol mole fraction range for x including 0.529, 0.558, 0.582 and 0.605. Zhao Jin et al. [3] measured the saturation vapor pressure of [mmIm]DMP-CH₃OH at $T = 280\text{--}370$ K and over the high methanol mole fraction range for x including 0.8222, 0.9123, 0.9418 and 0.9652. These experimental results were confirmed by Chen et al. [4] using the UNIFAC model and the Wilson model to predict the vapor pressure and the excess enthalpy, respectively. Figs. 1 and 2 show the predicted vapor pressure and excess enthalpy, respectively, at $T = 280\text{--}380$ K and $x = 0\text{--}1$.

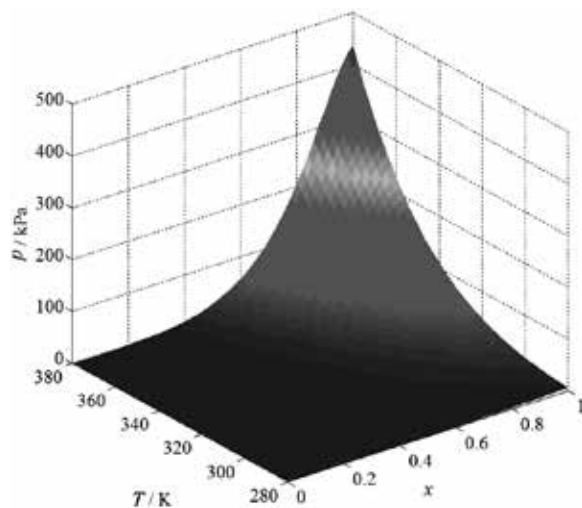


Figure 1. The predicted vapor pressure of [mmIm]DMP-CH₃OH.

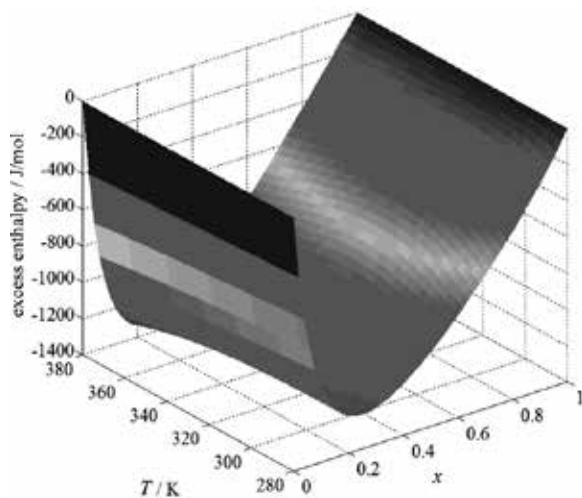


Figure 2. The predicted excess enthalpy of [mmIm]DMP-CH₃OH.

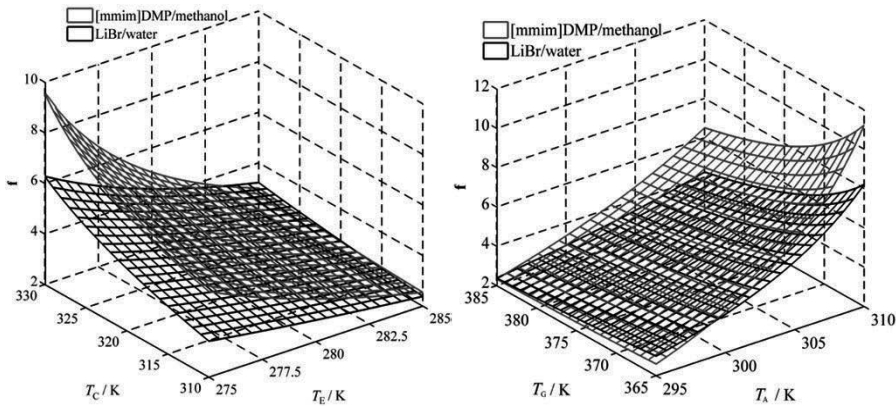


Figure 3. Effects of operating temperatures on the f of the [mmIm]DMP-CH₃OH system.

The thermodynamic performances of single effect [mmIm]DMP-CH₃OH absorption refrigeration have been simulated and analyzed. Fig. 3 shows the effects of the operating temperatures [condensing temperature (T_C), evaporating temperature (T_E), generating temperature (T_G), and absorption temperature (T_A)] on the circulation ratio, f , of the single system. From Fig. 3, the f of [mmIm]DMP-CH₃OH is higher than that of LiBr/H₂O but still acceptable for operation, and the coefficient of performance (COP) of the [mmIm]DMP-CH₃OH absorption refrigeration will remain good, if the heat transfer areas of the regenerator are designed appropriately.

Fig. 4 shows the effects of the operating temperatures on the COP of the single system. From Fig. 4, the COP of the [mmIm]DMP-CH₃OH absorption refrigeration is lower than that of LiBr/H₂O absorption refrigeration under the same temperature conditions, but higher than that of H₂O/NH₃ absorption refrigeration under most temperature conditions. When the heat source temperature is greater than 400 K, [mmIm]DMP-CH₃OH absorption is still possible with a high COP close to that of LiBr/H₂O absorption refrigeration. In general, [mmim]DMP/methanol has excellent potential for application as the working pair in absorption refrigeration.

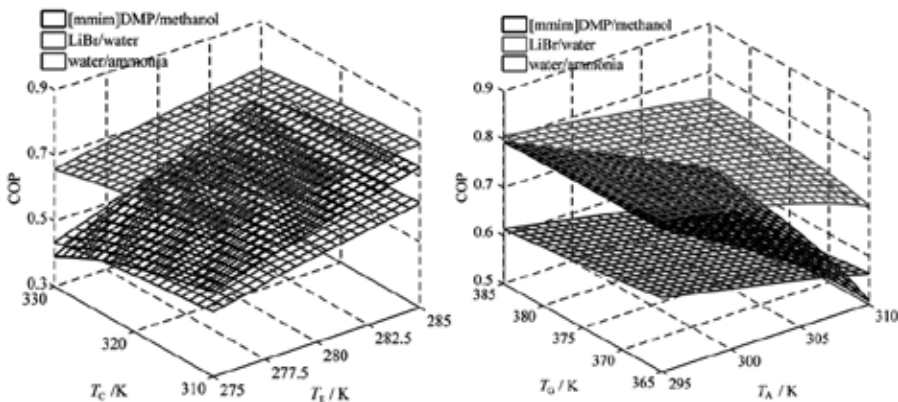


Figure 4. Effects of operating temperatures on the COP of the [mmIm]DMP-CH₃OH system.

2.2. [dmIm]DMP-H₂O

Dong et al. [5] studied the thermophysical properties of the [dmIm]DMP-H₂O system. The vapor pressures of the [dmIm]DMP-H₂O system at mass fractions of ionic liquids, ω , in the range of 0.10 to 0.90 were measured and correlated using a non-random two-liquid (NRTL) model. The experimental data and the model predictions are presented in Fig. 5.

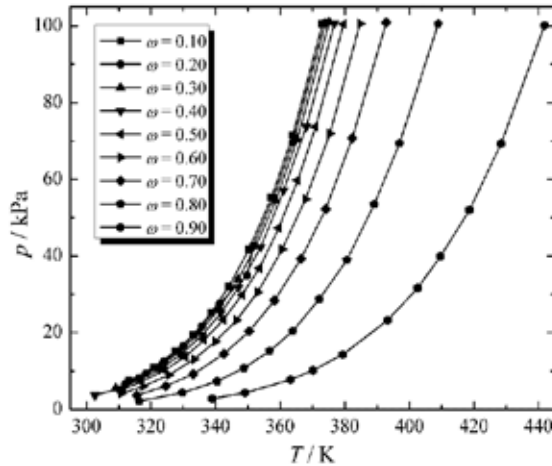


Figure 5. Vapor pressures of [dmIm]DMP-H₂O.

The heat capacities of [dmIm]DMP-H₂O at a ω in the range of 0.10 to 0.90 and a temperature range of 303.15–353.15 K were determined by a BT2.15 Calvet microcalorimeter. Fig. 6 presents the experimental data and the corresponding correlation results.

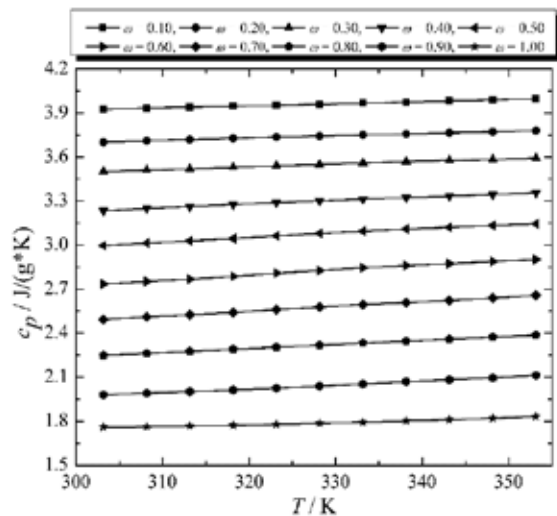


Figure 6. Heat capacities of [dmIm]DMP-H₂O.

The performance characteristics of [dmIm]DMP-H₂O and LiBr-H₂O single effect absorption refrigeration at $t_E = 10\text{ }^\circ\text{C}$, $t_C = 40\text{ }^\circ\text{C}$, $t_A = 30\text{ }^\circ\text{C}$, and $t_G = 80\text{ }^\circ\text{C}$ were calculated and are listed in Table 1. It can be seen that the COP of the [dmIm]DMP-H₂O system is slightly lower than but close to that of the traditional working pair LiBr-H₂O.

Working pair	ω_2	ω_1	f	COP
[dmIm]DMP-H ₂ O	0.867	0.768	8.77	0.829
LiBr-H ₂ O	0.537	0.486	6.59	0.835

Table 1. Comparison of performance characteristics between the [dmIm]DMP-H₂O and LiBr-H₂O systems

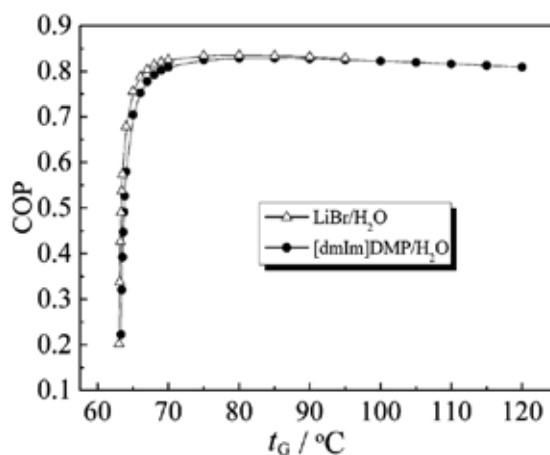


Figure 7. Effects of t_G on the COPs of the [dmIm]DMP-H₂O and LiBr-H₂O systems.

Fig. 7 shows the effects of changes in the t_G on the COP for the [dmIm]DMP-H₂O and LiBr-H₂O systems with $t_E = 10\text{ }^\circ\text{C}$, $t_C = 40\text{ }^\circ\text{C}$, and $t_A = 30\text{ }^\circ\text{C}$. It can be seen that as the t_G is increased, the COPs of the [dmIm]DMP-H₂O and LiBr-H₂O systems stabilize after a sharp rise, and there is an optimum t_G , at which the COP reaches the highest value. When reaching the stable stage, the COP of the [dmIm]DMP-H₂O system is very close to that of the LiBr-H₂O system. Moreover, the operating temperature range has been extended and operational safety has been achieved for the [dmIm]DMP-H₂O working pair, because it has no limitation of crystallization. These findings indicate that [dmIm]DMP-H₂O has the potential to be novel working pair for absorption refrigeration.

2.3. [emIm]DMP-H₂O

Ren et al. [6] measured the vapor pressure of the [emIm]DMP-H₂O binary system at different IL mole fractions, x , ranging from 0.1 to 0.5, and the experimental data were fitted using the NRTL model (Fig. 8).

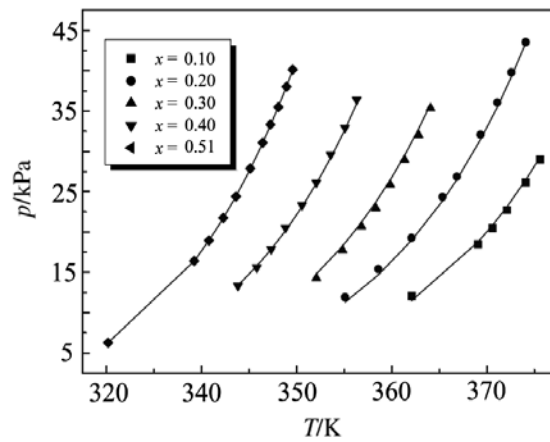


Figure 8. Vapor pressure of [emIm]DMP-H₂O with different mole fractions of IL and at different temperatures.

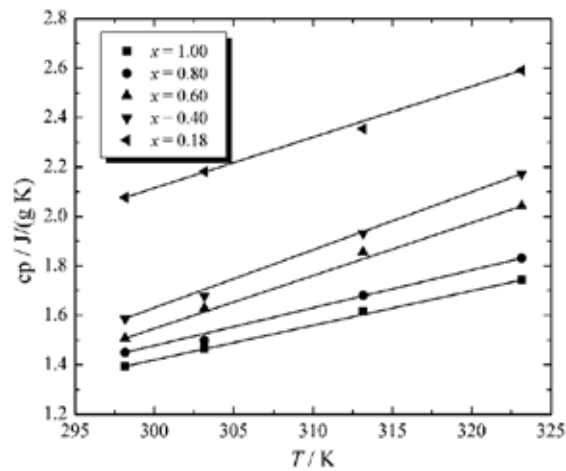


Figure 9. Specific heat capacities of [emIm]DMP-H₂O with different mole fractions of IL and at different temperatures.

The specific heat capacities of the [emIm]DMP-H₂O binary system were also measured at $T = 298.15\text{--}323.15\text{ K}$ and with different IL mole fractions, x , ranging from 0.18 to 1. Fig. 9 presents the experimental data and the model predictions.

Based on the above thermophysical properties, Zhang et al. [7] investigated the thermodynamic performance of an absorption chiller employing the [emIm]DMP-H₂O working pair. Fig. 10 shows the effect of t_E on the COP of the system at $t_C = 80\text{ }^\circ\text{C}$, $t_C = 40\text{ }^\circ\text{C}$, and $t_A = 35\text{ }^\circ\text{C}$. The results indicated that, at the same t_C and t_A , the COP of the [emIm]DMP-H₂O system is less than that of an aqueous solution of LiBr-H₂O but still greater than 0.7, whereas the t_C is less than that of the LiBr-H₂O system. Thus, [emIm]DMP-H₂O has the potential to be a new working pair for use in an absorption chiller driven by low-grade waste heat or hot water generated by a common solar collector.

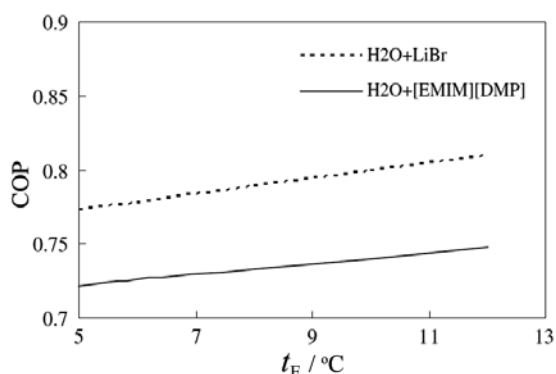


Figure 10. Effects of t_E on the COP of the [emIm]DMP-H₂O system.

2.4. Summary

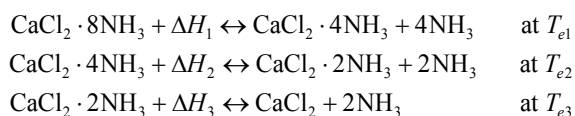
All three of the working pairs described above possess good theoretical cycle characteristics that are better than those of H₂O-NH₃, but still slightly lower than those of LiBr-H₂O. Due to the advantages of the negligible vapor pressure of the absorbent, no corrosion, and no crystallization, these three working pairs can be applied in a wider range of operating conditions than H₂O-NH₃ or LiBr-H₂O. Therefore, it is expected that these three working pairs have enormous potential in industrial applications and strong possibilities for commercial development.

3. A new conceptual chemical absorption refrigeration working pair consisting of ammonia and a metal chloride-containing ionic liquid

3.1. The proposal

Adsorption refrigeration is a type of environmentally friendly refrigeration that has been studied for many years. The most commonly used working pairs in adsorption refrigeration systems are ammonia-activated carbon, methanol-activated carbon, water-zeolite, ammonia-calcium chloride, and methanol-calcium chloride. The first three are physical adsorption working pairs, and the last two are chemical adsorption working pairs. The following review begins with the NH₃-CaCl₂ system.

Calcium chloride reacts with ammonia to form coordination compounds:



where $\Delta H_1 \sim \Delta H_3$ are the enthalpies of the reaction, and $T_{e1} \sim T_{e3}$ are the equilibrium temperatures. Benefiting from the reaction, the most impressive advantage of the $\text{NH}_3\text{-CaCl}_2$ system lies in its higher adsorption capacity compared to the others, while the main disadvantages are the low performances of heat and mass transfer and the phenomena of swelling and agglomeration in the process of adsorption [8]. Much effort has been spent attempting to overcome these defects. For example, Kai Wang et al. [9] proposed a new type of compound adsorbent composed of CaCl_2 and an expanded graphite adsorbent, which could mitigate the deterioration of the adsorption capacity that occurs in the long-term adsorption/desorption process. Using the compound adsorbent, Liwei Wang et al. [10] designed a multi-effect heat pipe-type adsorption refrigeration system, and a COP for their system of 0.39 was reported at a low t_E of $-20\text{ }^\circ\text{C}$. Obviously, these improvements have little effect, and many other similar efforts [11] proved futile. The essence of all these failures can be attributed to the fact that the adsorbent is a solid. Except for CaCl_2 , typical metal chlorides used as an ammonia adsorbent include SrCl_2 , LiCl_2 , and ZnCl_2 , among others. If only the solid metal chlorides could be dissolved in ionic liquids, there would be no problem that could not be solved in the absorption or adsorption systems. Fortunately, a few ionic liquids containing metal chlorides have been synthesized, including $[\text{bmim}]\text{Zn}_2\text{Cl}_5$ [12], that offer high hydrothermal stability and negligible vapor pressure to perfectly meet the absorbent criteria for absorption refrigeration. Compared with a solid adsorbent or other ionic liquids, the advantage of the ionic liquid $[\text{bmim}]\text{Zn}_2\text{Cl}_5$ is self-evident. The chemical reaction between NH_3 and Zn^{2+} will largely enhance the solubility of NH_3 in the absorbent and reduce the pressure of vapor phase as well as in the $\text{NH}_3\text{-CaCl}_2$ system, and no defects in heat and mass transfer, swelling, or agglomeration are a problem. Some other metal cations such as Ni^{2+} [13], Cu^{2+} [14], and Fe^{3+} [15] were also found to dissolve in ionic liquids, and thus, a family of new conceptual chemical absorption refrigeration working pairs consisting of ammonia and metal chloride-containing ionic liquids seems ready to be developed.

3.2. VLE behavior of the binary system of $\text{NH}_3\text{-}[\text{bmim}]\text{Zn}_2\text{Cl}_5$

In order to reveal the promising latent application of $\text{NH}_3\text{-}[\text{bmim}]\text{Zn}_2\text{Cl}_5$ as a working pair in absorption refrigeration, the vapor pressure data of the binary system of $[\text{bmim}]\text{Zn}_2\text{Cl}_5/\text{NH}_3$ are urgently needed. In our previous work [16], VLE data for the binary system of $\text{NH}_3\text{-}[\text{bmim}]\text{Zn}_2\text{Cl}_5$ were measured and fitted using the modified UNIFAC (Dortmund) model.

3.2.1. Experimental data [16]

$100x_2$	$p^{\text{exp}}/\text{kPa}$	$p^{\text{cal}}/\text{kPa}$	$100x_2$	$p^{\text{exp}}/\text{kPa}$	$p^{\text{cal}}/\text{kPa}$	$100x_2$	$p^{\text{exp}}/\text{kPa}$	$p^{\text{cal}}/\text{kPa}$
$T = 323.15\text{ K}$			$T = 383.15\text{ K}$			$T = 483.15\text{ K}$		
85.78±0.04	67.4	65.6	91.34±0.05	699.6	704.5	86.04±0.04	1148.2	1148.5
86.84±0.04	77.4	77.0	92.39±0.05	829.7	828.8	87.34±0.05	1287.2	1188.0
87.76±0.05	87.7	88.6	93.67±0.06	1040.8	1029.9	89.05±0.05	1516.9	1517.5
88.92±0.05	103.5	106.7	$T = 403.15\text{ K}$			$T = 483.15\text{ K}$		
90.42±0.06	134.9	137.2	84.79±0.03	488.6	489.8	90.58±0.06	1787.3	1787.5
						83.62±0.02	1081.2	1080.8

$100x_2$	p^{exp}/kPa	p^{cal}/kPa	$100x_2$	p^{exp}/kPa	p^{cal}/kPa	$100x_2$	p^{exp}/kPa	p^{cal}/kPa
91.76±0.06	170.8	174.2	85.90±0.04	544.9	546.5	84.83±0.03	1183.8	1182.7
92.77±0.07	210.6	210.8	86.86±0.05	602.3	603.5	85.88±0.04	1283.9	1284.4
93.99±0.08	285.6	269.6	88.08±0.05	687.5	689.4	87.21±0.05	1434.2	1435.1
$T = 343.15\text{ K}$			89.68±0.06	829.9	832.7	88.94±0.05	1682.0	1682.2
85.65±0.03	119.6	117.8	91.11±0.06	1000.0	1003.1	90.49±0.06	1970.7	1972.3
86.72±0.04	137.4	136.5	92.19±0.07	1170.8	1170.1	$T = 503.15\text{ K}$		
87.63±0.05	155.8	155.6	93.51±0.07	1452.6	1439.7	83.48±0.02	1187.0	1185.3
88.80±0.05	183.4	184.8	$T = 423.15\text{ K}$			84.71±0.03	1294.9	1293.3
90.31±0.06	230.9	234.5	84.39±0.03	668.4	669.3	85.77±0.04	1400.7	1400.5
91.66±0.06	286.5	294.5	85.53±0.04	740.5	741.4	87.11±0.05	1558.8	1559.2
92.68±0.07	347.7	353.5	86.51±0.05	813.4	813.5	88.87±0.05	1816.5	1818.8
93.91±0.08	461.2	448.4	87.76±0.05	921.9	921.9	$T = 523.15\text{ K}$		
$T = 363.15\text{ K}$			89.41±0.06	1100.9	1101.8	83.32±0.02	1300.6	1300.4
85.45±0.03	202.5	202.2	90.88±0.06	1313.0	1314.9	84.57±0.03	1414.3	1413.5
86.52±0.04	230.7	230.7	91.99±0.07	1523.0	1523.6	85.65±0.04	1525.2	1525.2
87.45±0.05	259.6	259.8	93.35±0.07	1859.8	1861.3	87.01±0.05	1688.7	1690.1
88.62±0.05	303.0	304.1	$T = 443.15\text{ K}$			88.80±0.05	1955.7	1957.8
90.15±0.06	375.1	378.9	84.08±0.03	821.5	821.4	$T = 543.15\text{ K}$		
91.52±0.06	463.8	468.7	85.24±0.04	905.7	905.1	83.11±0.02	1443.5	1443.6
92.55±0.07	555.1	557.1	86.25±0.05	989.4	988.8	84.38±0.03	1563.9	1563.5
93.81±0.08	711.8	699.5	87.53±0.05	1114.1	1114.0	85.48±0.04	1681.1	1681.5
$T = 383.15\text{ K}$			89.21±0.06	1320.9	1320.6	86.87±0.04	1853.9	1854.1
85.15±0.03	327.4	325.3	90.71±0.06	1564.7	1564.5	$T = 563.15\text{ K}$		
86.25±0.04	368.5	366.5	91.85±0.07	1805.7	1802.7	83.02±0.02	1535.6	1535.8
87.19±0.05	410.7	408.2	$T = 463.15\text{ K}$			84.30±0.03	1661.9	1661.4
88.38±0.05	473.6	471.4	83.82±0.02	961.2	960.8	85.41±0.04	1784.8	1784.6
89.94±0.06	577.1	577.5	85.01±0.03	1055.2	1054.8	86.82±0.04	1964.6	1964.5

Table 2. The P - T - x data of binary solutions [bmim] Zn_2Cl_5 (1) + NH_3 (2)

The pressure-temperature-composition (p - T - x) data of the binary solutions [bmim] Zn_2Cl_5 (1) + NH_3 (2) with NH_3 mole fractions of $x_2 = 0.83$ – 0.94 at $T = 323.15, 343.15, 363.15, 383.15, 403.15, 423.15, 443.15, 463.15, 483.15, 503.15, 523.15, 543.15,$ and 563.15 K are summarized in Table 2. The uncertainties in the NH_3 mole fraction in the binary solution, which can be due to the random and systematic errors in the experimental method and the calculation accuracy of the ammonia equation of state (EOS), are also presented in the table.

3.2.2. The modified UNIFAC (Dortmund) model [16]

Because of the non-volatilization of the ionic liquid [bmim]Zn₂Cl₅, the vapor phase of the binary system [bmim]Zn₂Cl₅ (1) + NH₃ (2) consists only of NH₃, and the total pressure p of the binary solution can be given by [17],

$$p = x_2 \gamma_2 P_2^{S'} \exp\left(\frac{(V_2^L - B_2)(p - P_2^{S'})}{RT}\right) \quad (1)$$

where x_2 is the mole fraction of NH₃ in the binary solution, γ_2 is the activity coefficient of NH₃, V_2^L is the liquid mole volume of NH₃, B_2 is the second virial coefficient in the ammonia EOS, and $P_2^{S'}$ is the vapor pressure of pure NH₃. When the temperature T is below the T_C , $P_2^{S'}$ is equal to the saturation vapor pressure, P^S , which can be calculated by [18],

$$\ln P_2^{S'} = \frac{1}{T_r - 0.101947} \left(-4.2522 T_r^2 + 7.929445 T_r^3 + 0.3807783 T_r^7 - 4.039557 \right) \quad (2)$$

where T_r is the ratio of the solution temperature T and T_C . When the temperature T is higher than the T_C , the $P_2^{S'}$ is defined as the pure NH₃ pressure at T and the critical mole fraction V_C which can be calculated by the RK type EOS as follows [19]:

$$P_2^{S'} = \frac{RT}{V_C - b} - \frac{a(T)}{V_C(V_C + b)} \quad (3)$$

$$a(T) = 0.42748 \alpha(T) R^2 T_C^2 / P_C \quad (4)$$

$$b = 0.08664 RT_C / P_C \quad (5)$$

where the temperature dependent term $\alpha(T)$ can be written by:

$$\alpha(T) = \sum_{k=0}^2 \beta_k (1/T_r - T_r)^k \quad (6)$$

The EOS constants for NH₃, β_k and the critical parameters T_C , V_C , and P_C are given in Table 3.

β_0	β_1	β_2	T_C / K	P_C / kPa	$V_C / \text{m}^3 \text{mol}^{-1}$
1.00027	0.45689	-0.05772	406.15	11424	0.00427

Table 3. EOS constants and critical parameters for NH₃

In the UNIFAC model, the excess Gibbs free energy is composed of two contributing parts, the combinatorial part and the residual part, and the activity coefficient γ_i can be given as follows:

$$\ln \gamma_i = \ln \gamma_i^C + \ln \gamma_i^R \quad (7)$$

where γ_i^C is the combinatorial activity coefficient and γ_i^R is the residual activity coefficient.

The combinatorial activity coefficient γ_i^C describes the repulsive interaction attributed to the molecular size and shape, which can be calculated by:

$$\ln \gamma_i^C = \ln \frac{\varphi_i}{x_i} + \frac{Z}{2} q_i \ln \frac{\theta_i}{\varphi_i} + l_i - \frac{\varphi_i}{x_i} \sum_j x_j l_j \quad (8)$$

$$l_i = \frac{Z}{2} (r_i - q_i) - (r_i - 1) \quad (9)$$

$$\theta_i = q_i x_i / \sum_j q_j x_j \quad (10)$$

$$\varphi_i = r_i x_i / \sum_j r_j x_j \quad (11)$$

$$q_i = \sum v_k^{(i)} Q_k \quad (12)$$

$$r_i = \sum v_k^{(i)} R_k \quad (13)$$

where Z is normally set to 10, $v_k^{(i)}$ is the number of group k in component i , and R_k and Q_k are the volume and surface parameters of the group k , respectively. The values of R_k and Q_k for the group used in our experiment are listed in Table 4.

	[bmim] ⁺	Zn ²⁺	Cl ⁻	NH ₃
R_k	6.0334 [20]	3.0 [21]	0.6560 [20]	0.8239 [22]
Q_k	4.7910 [20]	3.0 [21]	0.6730 [20]	0.7780 [22]

Table 4. Volume parameters R_k and surface parameters Q_k

The residual activity coefficient γ_i^R accounts for the intermolecular forces resulting from the corresponding group interaction, which is described as the summation of the group activity coefficient Γ for group k of component i ,

$$\ln \gamma_i^R = \sum_k^N v_k^{(i)} (\ln \Gamma_k - \ln \Gamma_k^{(i)}) \quad (14)$$

where Γ_k and $\Gamma_k^{(i)}$ are the activity coefficients for group k in binary solution and in the component i , respectively, and can be described as:

$$\ln \Gamma_k = Q_k \left[1 - \ln \left(\sum_{m=1}^N \theta_m \phi_{mk} \right) - \sum_{m=1}^N \left(\frac{\theta_m \phi_{km}}{\sum_{n=1}^N \theta_n \phi_{nm}} \right) \right] \quad (15)$$

$$\theta_m = Q_m X_m / \sum_{n=1}^N Q_n X_n \quad (16)$$

$$X_m = \sum_{j=1}^M v_m^{(j)} x_j / \sum_{j=1}^M \sum_{n=1}^N v_n^{(j)} x_j \quad (17)$$

Eqs. 15–17 can also be used to calculate $\ln \Gamma_k^{(i)}$, except that the group composition variable X_m is now the group fraction of group k in component i . For the modified UNIFAC (Dortmund) model, the group interaction parameters between groups n and m , $\phi_{n,m}$, is described as:

$$\phi_{n,m} = \exp \left(- \frac{a_{nm} T^2 + b_{nm} T + c_{nm}}{T} \right) \quad (18)$$

where a_{nm} (K^{-1}), b_{nm} and c_{nm} (K) are the adjustable interaction parameters for correlating the experimental vapor pressure data. The corresponding correlation results are listed in Table 5.

n	m	a_{nm}/K^{-1}	b_{nm}	c_{nm}/K
NH ₃	[bmim] ⁺	0.00617	-1.9768	-378.1920
NH ₃	Zn ²⁺	-0.02754	2.7884	1119.6973
NH ₃	Cl ⁻	0.03904	-39.2835	11459.2768
[bmim] ⁺	NH ₃	-0.00915	-2.7566	2059.6872
[bmim] ⁺	Zn ²⁺	-0.01720	-12.6476	5508.8668
[bmim] ⁺	Cl ⁻	22.62142	-82.6723	-5307.7598
Zn ²⁺	NH ₃	-0.00911	-3.0401	2070.4982
Zn ²⁺	[bmim] ⁺	-0.02991	-6.8487	12385.2753
Zn ²⁺	Cl ⁻	16.45937	66.7508	-2708.8868
Cl ⁻	NH ₃	-0.00281	-1.6807	-548.2453
Cl ⁻	[bmim] ⁺	0.09208	313.3495	-86.4292
Cl ⁻	Zn ²⁺	0.19296	59.8376	-5434.4813

Table 5. Adjustable interaction parameters for UNIFAC model

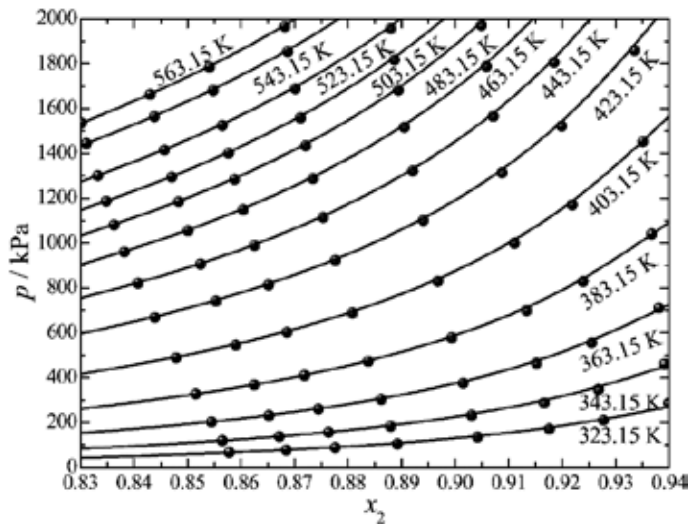


Figure 11. P - T - x phase diagrams (Lines: calculated with the UNIFAC model. Symbols: experimental data) [16].

The P - T - x phase diagrams with symbols for experimental data and lines for the UNIFAC model calculations are shown in Fig. 11. It can be seen from the figure that with an increase in the NH_3 mole fraction, the vapor pressure also increases, and the rising trend becomes increasingly more obvious. With an increase in the binary solution temperature, the vapor pressure increases rapidly. When the temperature is below the T_C the rate of increase becomes more rapid, but when the temperature is higher than the T_C of NH_3 , the rate of increase tends to slow and the vapor pressure even declines slightly.

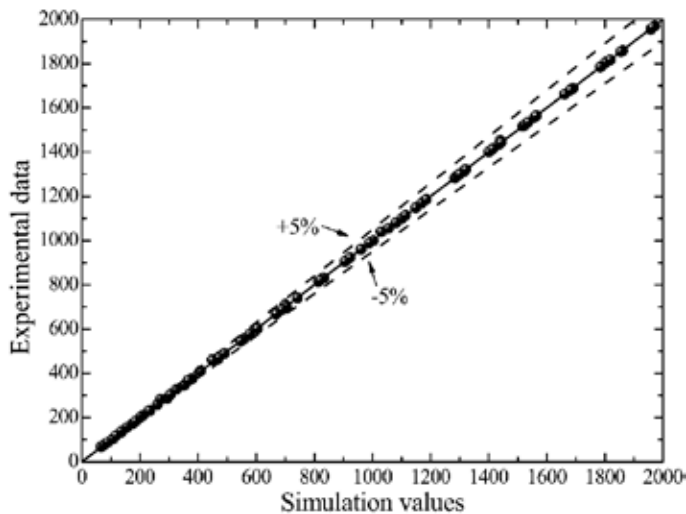


Figure 12. Comparison of experimental data and the UNIFAC model calculations [16].

A comparison of the experimental data and the UNIFAC model calculations is shown in Fig. 12. All deviations are below 5.0% and are mainly produced by the uncertainties in the volumes of the high pressure vessel (0.7%) and liquid phase of binary system (1.1%), the weights of [bmim]Zn₂Cl₅ (0.01%) and NH₃ (0.05%), the temperature distribution in the high pressure vessel (0.7%), EOS calculation accuracy (1.2%), and the fitting uncertainty (1.6%). Based on the above uncertainties, the total uncertainty of the measurements is estimated to be within 4.3%.

3.2.3. Comparison with normal ionic liquids and ZnCl₂

Fig. 13 compares the vapor pressures of [bmim]Zn₂Cl₅/NH₃ solutions with $x_2 = 0.9507$ and 0.9231 to those of ZnCl₂·6NH₃ [23] at $T = 330$ – 420 K. When $x_2 = 0.9507$, the NH₃ mass fraction of the binary solution is equal to the NH₃ mass fraction in ZnCl₂·6NH₃, and when $x_2 = 0.9231$, the mole ratio of NH₃ and Zn²⁺ is 6, which is equal to that in ZnCl₂·6NH₃. From Fig. 13, the vapor pressures of NH₃ in [bmim]Zn₂Cl₅ with $x_2 = 0.9507$ and 0.9231 are 2–3 times higher than that of ZnCl₂·6NH₃, which can be attributed to the effects of the ionic liquid [bmim]Cl on the complexation reaction production of NH₃ and Zn²⁺ ions.

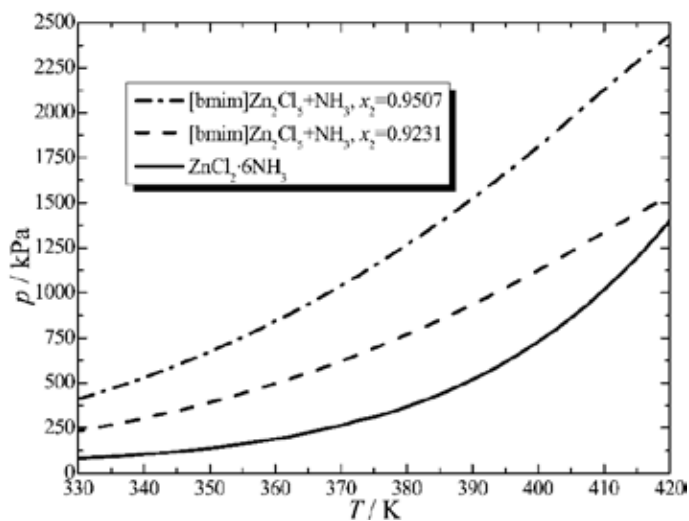


Figure 13. Comparison of vapor pressures of NH₃-[bmim]Zn₂Cl₅ solution and ZnCl₂·6NH₃ [16].

Fig. 14 compares the vapor pressure of the NH₃-[bmim]Zn₂Cl₅ solution and ammonia solutions containing ionic liquids [19] [emim][Ac], [emim][SCN], [emim][EtOSO₃], and [DMEA][Ac] at $T = 348$ K and $x_2 = 0$ – 1 . From Fig. 14, the vapor pressure of NH₃ in [bmim]Zn₂Cl₅ is one order of magnitude smaller than that in normal ionic liquids at $x_2 = 0$ – 0.95 , which means that the complexation reaction of NH₃ and Zn²⁺ ions can largely reduce the vapor pressure of NH₃ in the ionic liquid and largely enhance the solubility of NH₃ in the ionic liquid.

Based on the results in Figs. 13 and 14, the absorption characteristics of [bmim]Zn₂Cl₅ are much better than those of normal ionic liquids but slightly lower than those of ZnCl₂. Additionally,

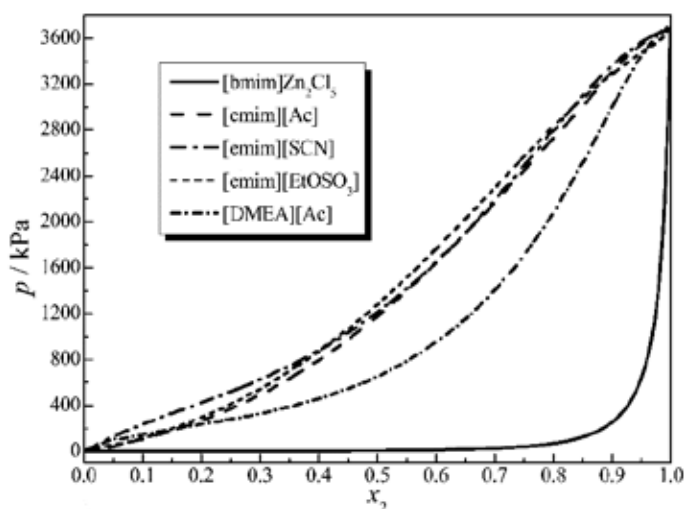


Figure 14. Comparison of vapor pressures of $[\text{bmim}]\text{Zn}_2\text{Cl}_5/\text{NH}_3$ solution and ammonia solutions containing the ionic liquids $[\text{emim}][\text{Ac}]$, $[\text{emim}][\text{SCN}]$, $[\text{emim}][\text{EtOSO}_3]$ and $[\text{DMEA}][\text{Ac}]$ [16].

the liquid form of $[\text{bmim}]\text{Zn}_2\text{Cl}_5$ offers a major advantage over ZnCl_2 , which will completely resolve the abovementioned limitations to improve the cycle performance for $\text{ZnCl}_2/\text{NH}_3$ adsorption refrigeration. Therefore, working pairs of NH_3 - $[\text{bmim}]\text{Zn}_2\text{Cl}_5$ have good latent application potential in absorption refrigerator and heat pump operation.

3.3. Heat capacities and excess enthalpies of the NH_3 - $[\text{bmim}]\text{Zn}_2\text{Cl}_5$ system

In order to investigate the cycle characteristics of $[\text{bmim}]\text{Zn}_2\text{Cl}_5/\text{NH}_3$ absorption refrigeration, data for the heat capacities of $[\text{bmim}]\text{Zn}_2\text{Cl}_5$ and excess enthalpies of $[\text{bmim}]\text{Zn}_2\text{Cl}_5/\text{NH}_3$ are urgently needed. In our previous work, the heat capacities of $[\text{bmim}]\text{Zn}_2\text{Cl}_5$ for $T = 210.15$ – 383.15 K were obtained by differential scanning calorimetry (DSC), and the excess enthalpies of $[\text{bmim}]\text{Zn}_2\text{Cl}_5/\text{NH}_3$ at various ammonia mole fractions for $T = 288.15$ – 333.15 K were measured experimentally. The data for excess enthalpies were fit by a five-parameter NRTL model. Based on the heat capacity of $[\text{bmim}]\text{Zn}_2\text{Cl}_5$ and the excess enthalpy of $[\text{bmim}]\text{Zn}_2\text{Cl}_5/\text{NH}_3$, the enthalpies of $[\text{bmim}]\text{Zn}_2\text{Cl}_5/\text{NH}_3$ solution at $x_1 = 0$ – 1 for $T = 273.15$ – 343.15 K were calculated.

3.3.1. Heat capacities of $[\text{bmim}]\text{Zn}_2\text{Cl}_5$

Fig. 15 shows the result of TG scanning for $[\text{bmim}]\text{Zn}_2\text{Cl}_5$, which was determined using a TGA/SDT instrument. Onset of a 2.5% weight loss in a nitrogen atmosphere occurs at 676.15 K, and approximately 40% of the mass is gone by 774.15 K, which is a typical volatilization temperature for imidazolium salts. Continued heating of $[\text{bmim}]\text{Zn}_2\text{Cl}_5$ eventually results in a constant weight near 1043.15 K, with a residual weight of 36.4%. These results indicate that $[\text{bmim}]\text{Zn}_2\text{Cl}_5$ possesses high thermal stability at $T < 673.15$ K.

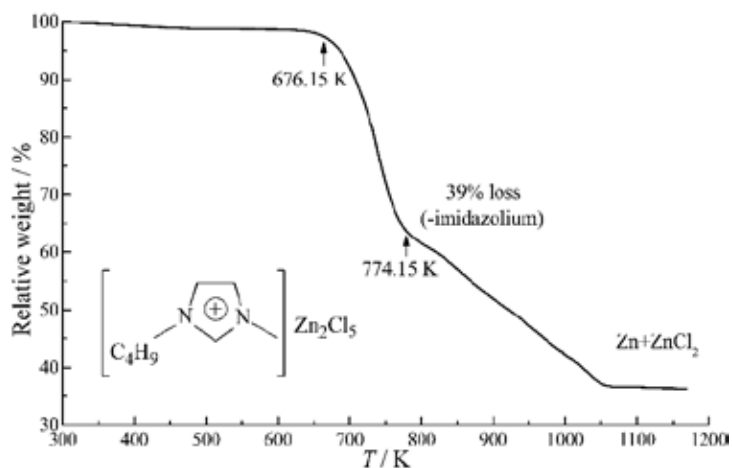


Figure 15. Thermogravimetric (TG) scan results for [bmim]Zn₂Cl₅.

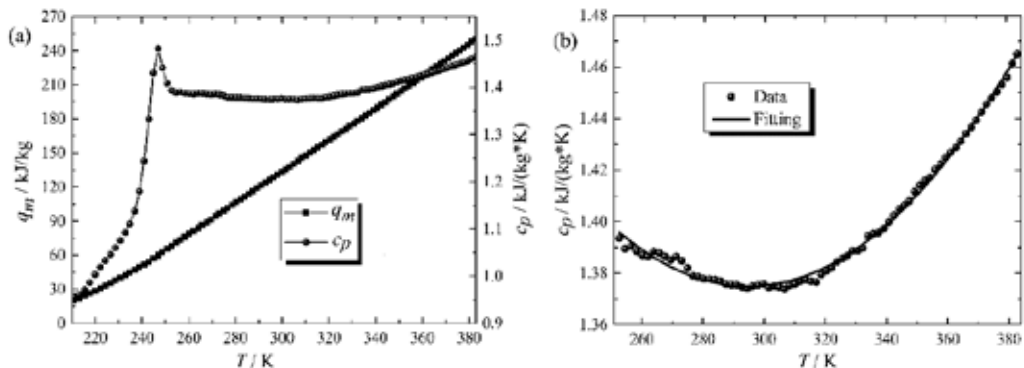


Figure 16. DSC scanning results for [bmim]Zn₂Cl₅. (a) variations in heat flow, q_m and specific heat capacity, c_p along with the temperature of [bmim]Zn₂Cl₅; (b) c_p - T diagram of [bmim]Zn₂Cl₅ for $T = 243.15$ – 383.15 K.

Fig. 16(a) shows the variation in the specific heat flow, q_m , and the specific heat capacity, c_p , along with temperature variations for [bmim]Zn₂Cl₅. The specific heat flow increases with an increase in temperature. The rate of increase of the specific heat flow rises at $T < 243.15$ K, and the variation in the rate of increase of the specific heat flow is minor for $T > 243.15$ K. The specific heat capacity increases with an increase in the [bmim]Zn₂Cl₅ temperature at $T < 243.15$ K, and the rate of increase also increases. The specific heat capacity presents an increasing trend after a decline for $T > 251.15$ K. These results indicate that the melting temperature of [bmim]Zn₂Cl₅ is near 243.15 K. By careful observation, it is found that variations in the specific heat capacity with $T > 251.15$ K can be well fitted by the following quadratic equation:

$$c_p = 2.39327 - 0.00691T + 0.000011767T^2 \quad (19)$$

Fig. 16(b) shows the c_p - T diagram for $T = 243.15$ – 383.15 K. The symbols represent the experimental data, and the lines represent the calculated conic curve. It can be seen that variation in the specific heat capacity with temperature is accurately described by the quadratic curve.

3.3.2. Experimental data for excess enthalpy of NH_3 -[bmim] Zn_2Cl_5

Temperature-component-molar excess enthalpy (T - x - H^E) data for the binary systems [bmim] Zn_2Cl_5 (2) + NH_3 (1) at ammonia mole fractions of $x_1 = 0.60$ – 0.95 and $T = 288.15, 303.15, 318.15,$ and 333.15 K are summarized in Table 6. Uncertainties in the temperature, ammonia mole fraction, and molar excess enthalpy are also presented in the table. The uncertainties are due to random errors as well as systematic errors for the experimental apparatus and the calculation accuracy of the UNIFAC model for the VLE of NH_3 /[bmim] Zn_2Cl_5 . With an increase in the ammonia mole fraction, x_1 , the molar excess enthalpy presents an increasing trend after an initial decline.

T/K	x_2	$H^E/\text{J/mol}$	T/K	x_2	$H^E/\text{J/mol}$
288.15	0.617	-6052	318.15	0.631	-6237
288.15	0.709	-6446	318.15	0.725	-6795
288.15	0.819	-6385	318.15	0.796	-6825
288.15	0.873	-6007	318.15	0.877	-6301
288.15	0.935	-4778	318.15	0.929	-5282
303.15	0.614	-6102	333.15	0.622	-6233
303.15	0.718	-6657	333.15	0.698	-6851
303.15	0.782	-6665	333.15	0.773	-6870
303.15	0.866	-6242	333.15	0.854	-6638
303.15	0.947	-4393	333.15	0.931	-5412

Table 6. Mole excess enthalpy of binary systems [bmim] Zn_2Cl_5 (1) + NH_3 (2).

3.3.3. NRTL model

Based on the local composition representation of the excess Gibbs energy, G^E , Renon and Prausnitz [24] proposed the NRTL model. The G^E for the NRTL model can be described by:

$$\frac{G^E}{RT} = x_1 x_2 \left(\frac{\tau_{21} G_{21}}{x_1 + x_2 G_{21}} + \frac{\tau_{12} G_{12}}{x_2 + x_1 G_{12}} \right) \quad (20)$$

$$\tau_{12} = \frac{g_{12} - g_{22}}{RT}, \tau_{21} = \frac{g_{21} - g_{11}}{RT} \quad (21)$$

$$G_{12} = \exp(-\alpha\tau_{12}), G_{21} = \exp(-\alpha\tau_{21}) \quad (22)$$

where g_{ij} and g_{ji} are the interaction energy between ij and jj component pairs, respectively, and α is the non-random parameter. The relationship between G^E and the activity coefficient is given by:

$$G^E = RT \sum_i \ln \gamma_i + \sum_{k \neq i} \left(\frac{\partial G^E}{\partial x_i} \right)_{T,P,x_{j \neq ik}} \quad (23)$$

Therefore, the activity coefficients of components 1 and 2 in a binary mixture can be written as:

$$\ln \gamma_1 = x_2^2 \left[\tau_{21} \left(\frac{G_{21}}{x_1 + x_2 G_{21}} \right)^2 + \left(\frac{\tau_{12} G_{12}}{(x_2 + x_1 G_{12})^2} \right) \right] \quad (24)$$

$$\ln \gamma_2 = x_1^2 \left[\tau_{12} \left(\frac{G_{12}}{x_2 + x_1 G_{12}} \right)^2 + \left(\frac{\tau_{21} G_{21}}{(x_1 + x_2 G_{21})^2} \right) \right] \quad (25)$$

The definition of the activity coefficient for ammonia, γ_{1v} , is presented in our previous work [16]. For the NRTL model, the interaction energy between the ij and jj component pairs are defined as:

$$g_{12} - g_{22} = A_1 + B_1 T \quad (26)$$

$$g_{21} - g_{11} = A_2 + B_2 T \quad (27)$$

The Gibbs-Helmholtz equation for excess enthalpy is:

$$-\frac{H^E}{T^2} = \left[\frac{\partial(G^E/T)}{\partial T} \right]_{P,x} \quad (28)$$

For the five-parameter NRTL model, the excess enthalpy can be calculated by:

$$H^E = -x_1 x_2 \left\{ \frac{A_2 G_{21} [x_1 \tau_{21} (\alpha \tau_{21} - 1) - x_2 G_{21}]}{(x_1 + x_2 G_{21})^2} + \frac{A_1 G_{12} [x_2 \tau_{12} (\alpha \tau_{12} - 1) - x_1 G_{12}]}{(x_2 + x_1 G_{12})^2} \right\} \quad (29)$$

The correlation results are shown in Table 7.

α	A_1/Jmol^{-1}	$B_1/\text{Jmol}^{-1}\text{K}^{-1}$	A_2/Jmol^{-1}	$B_2/\text{Jmol}^{-1}\text{K}^{-1}$
0.1043	14062.6306	419.6197	-164.3040	-256.9565

Table 7. Binary parameters and non-random parameters for NRTL model

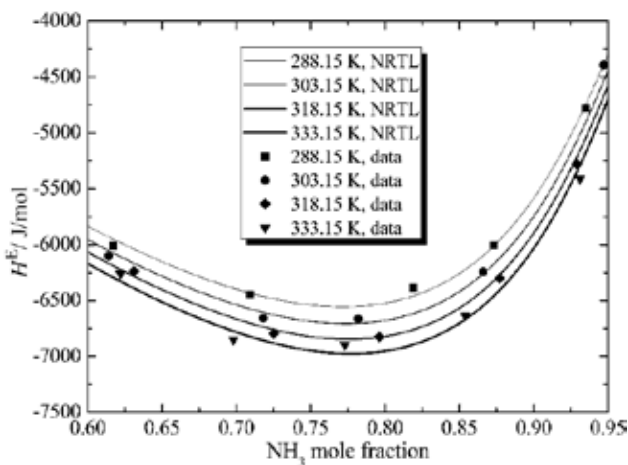


Figure 17. T - x - H^E diagram of $[\text{bmim}]\text{Zn}_2\text{Cl}_5/\text{NH}_3$ for $T = 288.15\text{--}333.15$ K.

Fig. 17 shows the T - x - H^E diagram for the binary system of $[\text{bmim}]\text{Zn}_2\text{Cl}_5/\text{NH}_3$ at $T = 288.15\text{--}333.15$ K. The symbols represent the experimental data, and the lines represent the calculations from the NRTL model. From Fig. 17, with an increase in the NH_3 mole fraction, the excess enthalpy shows an increasing trend after a decline. There are minimum excess enthalpies for each temperature: -6555.7 , -6707.1 , -6846.3 , and -6974.7 J/mol appear at $x_1 = 0.772$, 0.774 , 0.776 , and 0.777 for $T = 288.15$, 303.15 , 318.15 , and 333.15 K, respectively.

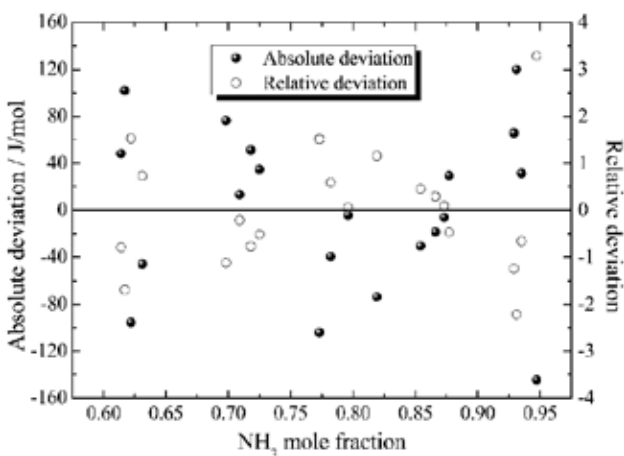


Figure 18. Absolute deviations and relative deviations with the NRTL model.

Fig. 18 shows the absolute deviations and relative deviations between the experimental data and the values predicted by the NRTL model for excess enthalpy data. The results indicate that all deviations for excess enthalpy data are less than 3.9%. The measurement deviations are mainly produced by the uncertainties in volumes of the high pressure vessels (0.5%), the little tank (0.5%) and the liquid phase of binary system (0.2%); the weights of [bmim]Zn₂Cl₅ (0.01%), NH₃ (0.05%) and water (0.01%); temperature distributions in the water bath (1.4%) and the bath container (1.2%); and the UNIFAC calculation accuracies (0.9%). Based on the above uncertainties, the total uncertainty of measurement is estimated to be less than 4.8 %.

3.3.4. Enthalpy of [bmim]Zn₂Cl₅/NH₃ solution

The enthalpy of a solution of [bmim]Zn₂Cl₅/NH₃ at T and a given NH₃ mass fraction ω_1 can be calculated by:

$$h = (1 - \omega_1)h_1 + \omega_1 h_2 + h^E \quad (30)$$

The enthalpy of [bmim]Zn₂Cl₅, h_1 , can be calculated by:

$$h_1 = \int_{T_0}^T c_p dT \quad (31)$$

where c_p is the specific heat capacity of [bmim]Zn₂Cl₅, which can be calculated using Eq. (1), and T_0 is defined as 273.15 K. The enthalpy of NH₃ can be calculated by [19]:

$$h_2 = \sum_{i=0}^6 a_i (T - 273.15)^i \quad (32)$$

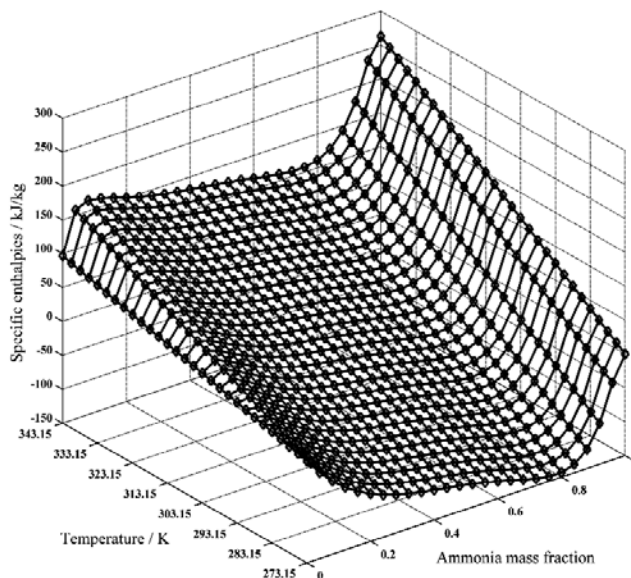


Figure 19. Calculations for enthalpies of [bmim]Zn₂Cl₅/NH₃ solution at $x_1 = 0-1$ for $T = 273.15-343.15$ K.

Fig. 19 shows the calculated enthalpies for [bmim]Zn₂Cl₅/NH₃ solution at $\omega_1 = 0-1$ and $T = 273.15-343.15$ K. Based on the VLE properties and the enthalpies of [bmim]Zn₂Cl₅/NH₃ solutions, the thermodynamic performances of the [bmim]Zn₂Cl₅/NH₃ absorption system can be investigated.

3.4. Thermodynamic analysis of an absorption system using NH₃-[bmim]Zn₂Cl₅ as the working pair [25]

In our previous work, the modified UNIFAC model was used to describe the VLE properties of [bmim]Zn₂Cl₅/NH₃ [16] and the NRTL model was used to predict the excess enthalpic properties of [bmim]Zn₂Cl₅/NH₃. Based on a single-effect absorption refrigeration model, the thermodynamic performance of the [bmim]Zn₂Cl₅/NH₃ absorption system was simulated and compared with that of the NaSCN/NH₃ adsorption system. The coefficients of performance for cooling (COP) and heating (COP^h) and circulation ratios under the condition of a subzero evaporating temperature were calculated and analyzed.

3.4.1. System description and simulation

Fig. 20 shows a schematic diagram of the single effect absorption system. The main system is composed of the generator (G), the absorber (A), the condenser (C), the evaporator (E), the regenerator (R), the valves (V), and the solution pump (P). In Fig. 20, the status point numbers are given, and the fluids at each point are marked: *i* denotes the [bmim]Zn₂Cl₅/NH₃ solution from the absorber with a high NH₃ mass fraction, *ii* denotes the [bmim]Zn₂Cl₅/NH₃ solution from the generator with a low NH₃ mass fraction, and *iii* denotes the refrigerant NH₃. The symbols q_E , q_C , q_A , and q_G represent the heat flow of the evaporator, the condenser, the absorber, and the generator, respectively.

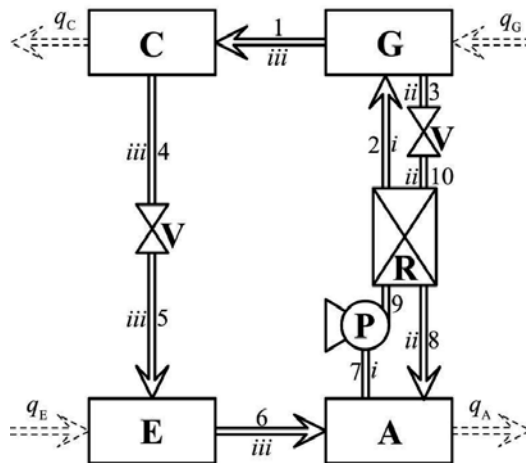


Figure 20. Schematic diagram of the single effect absorption system [25].

In order to simulate the thermodynamic performance of an absorption system using [bmim]Zn₂Cl₅/NH₃ as a working pair, several assumptions were made as follows [25]:

1. The simulation is conducted under steady state;
2. The vapor pressure losses are neglected, the pressure of the evaporator is equal to that of the absorber, and the pressure of the condenser is equal to that of the generator;
3. The refrigerant flowing out of the condenser is in a saturated liquid state, and the refrigerant flowing out of the evaporator is in a saturated gas state;
4. The heat recovery rate of the regenerator is set to 0.80 [26]; and
5. The thermal losses and pumping work are negligible.

The mass and energy conservation equations for the evaporator are given by:

$$m_5 = m_6 \quad (33)$$

$$q_E = m_6 h_6 - m_5 h_5 \quad (34)$$

The mass and energy conservation equations for the condenser are given by:

$$m_1 = m_4 \quad (35)$$

$$q_C = m_1 h_1 - m_4 h_4 \quad (36)$$

For the absorber, the mass conservation equation of the solution, the mass conservation equation of IL, and the energy conservation equation are given by:

$$m_7 = m_6 + m_8 \quad (37)$$

$$m_7(1 - \omega_7) = m_6 + m_8(1 - \omega_8) \quad (38)$$

$$q_A = m_6 h_6 + m_8 h_8 - m_7 h_7 \quad (39)$$

For the generator, the mass conservation equation of the solution, the mass conservation equation of IL, and the energy conservation equation are given by:

$$m_2 = m_1 + m_3 \quad (40)$$

$$m_2(1 - \omega_2) = m_1 + m_3(1 - \omega_3) \quad (41)$$

$$q_G = m_1h_1 + m_3h_3 - m_2h_2 \quad (42)$$

For the regenerator, the energy conservation equation is given by:

$$m_2(h_2 - h_9) = m_3(h_{10} - h_8) \quad (43)$$

Based on the above assumptions and the conservation equations for mass and energy conservation, the heat flow values of q_G , q_C , q_E , and q_A ; mass flow values of m_2 and m_3 ; and mass fractions of ω_2 and ω_3 , can be calculated. The circulation ratio (f) is calculated by:

$$f = \frac{m_3}{m_1} = \frac{1 - \omega_3}{\omega_2 - \omega_3} \quad (44)$$

The COP for cooling is defined by:

$$COP = \frac{q_E}{q_G} \quad (45)$$

The exergy efficiency (η_{ex}) for cooling is given by:

$$\eta_{ex} = \frac{q_E \left(\frac{T_0}{T_E} - 1 \right)}{q_G \left(1 - \frac{T_0}{T_G} \right)} \quad (46)$$

The COP* for heating is defined as:

$$COP^* = \frac{q_A + q_C}{q_G} = 1 + \frac{q_E}{q_G} \quad (47)$$

The exergy efficiency for cooling (η_{ex}^*) is given by:

$$\eta_{ex}^* = \frac{q_C \left(1 - \frac{T_0}{T_C} \right) + q_A \left(1 - \frac{T_0}{T_A} \right)}{q_G \left(1 - \frac{T_0}{T_G} \right)} \quad (48)$$

3.4.2. Results and discussion

Fig. 22 shows variations in the COP and η_{ex} of [bmim]Zn₂Cl₅/NH₃ absorption refrigeration with variations in t_A and t_C at a $t_C = 90$ °C and $t_E = -10$ °C. These results show that both the COP and η_{ex} decline with increases in t_A and t_C . This is because increases in t_A and t_C lead to a decrease in the mass fraction of solution from the absorber (ω_2) and an increase in the mass fraction of solution from the generator (ω_3). These changes in both ω_2 and ω_3 result in a decrease of q_E . The slopes of both the COP and η_{ex} curves are less steep when t_A and t_C are lower, and as t_A and t_C continue to increase, the slopes become increasingly steep. This can be explained by the fact that, with the continuous increases in t_A and t_C , the difference between ω_2 and ω_3 continues to become smaller. By comparison, the thermal performance of the [bmim]Zn₂Cl₅/NH₃ system is better than that of the NaSCN/NH₃ system when t_A and t_C are low. However, when t_A and t_C are high, the thermal performance of the NaSCN/NH₃ system is better than that of the [bmim]Zn₂Cl₅/NH₃ system, and the upper operating limit of t_A and t_C for NaSCN/NH₃ is higher than that for the [bmim]Zn₂Cl₅/NH₃ system. This can also be explained by the properties of NH₃ solubility in [bmim]Zn₂Cl₅ and NaSCN. The higher solubility of NH₃ in [bmim]Zn₂Cl₅ ensures that the [bmim]Zn₂Cl₅/NH₃ system possesses better thermal performance than the NaSCN/NH₃ system with operating conditions of low t_A and t_C . The stronger combination of NH₃ and [bmim]Zn₂Cl₅ demonstrates that the upper operating limit of t_A and t_C for the [bmim]Zn₂Cl₅/NH₃ system are lower than those of the NaSCN/NH₃ system.

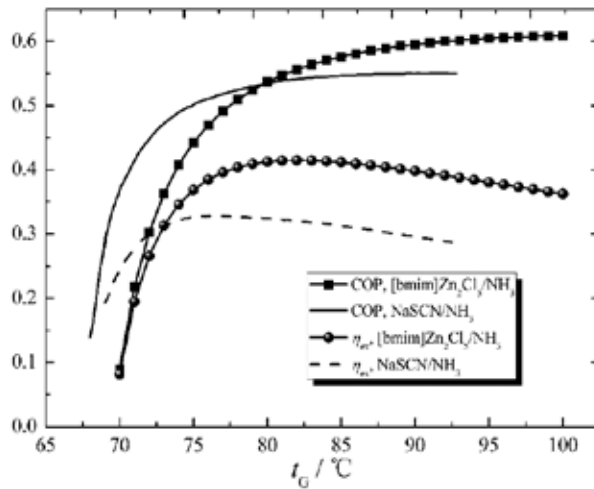


Figure 21. Variations in the COP and η_{ex} of [bmim]Zn₂Cl₅/NH₃ absorption refrigeration with changes in T_C for $t_A = t_C = 25$ °C and $t_E = -10$ °C [25].

Fig. 23 shows the effects of t_C on the COP for $t_C = 110$ – 230 °C with $t_A = t_C = 35$ °C and $t_E = -10$ °C, -20 °C, -30 °C, or -40 °C. With an increase in t_C the COP presents a trend of first increasing and the decreasing. The reason for this trend is that the increase in t_C has both positive and negative effects on the COP. The positive and negative effects are the same as indicated by the analysis of the trend in COP shown in Fig. 2. When t_C is lower, the positive effect is predominant, and

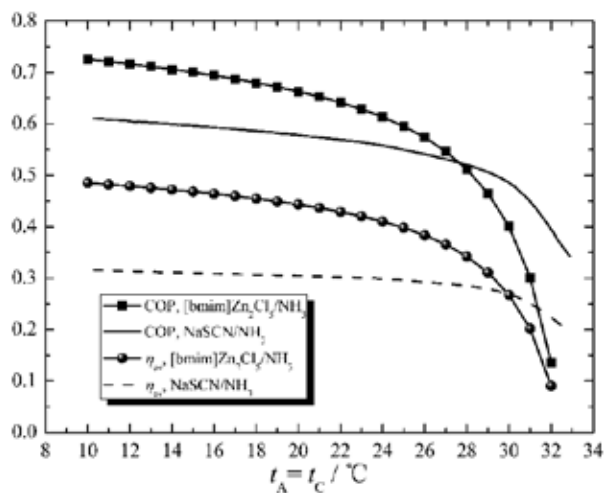


Figure 22. Variations in the COP and η_{ex} of [bmim] Zn_2Cl_5/NH_3 absorption refrigeration with varying t_A and t_C for $t_C = 90\text{ }^\circ\text{C}$ and $t_E = -10\text{ }^\circ\text{C}$ [25].

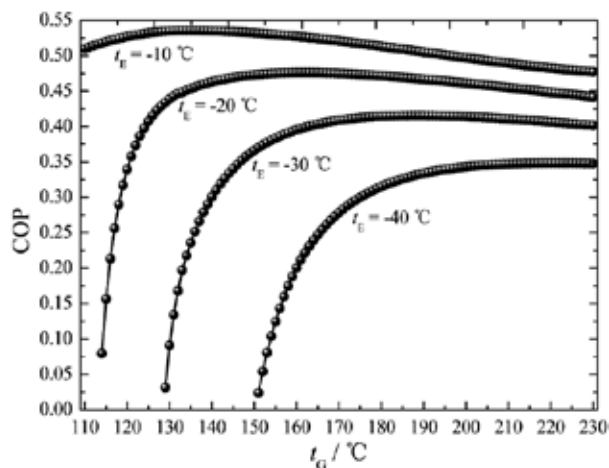


Figure 23. Effects of T_C on the COP for $t_C = 110\text{--}230\text{ }^\circ\text{C}$, $t_A = t_C = 35\text{ }^\circ\text{C}$ and $t_E = -10\text{ }^\circ\text{C}$, $-20\text{ }^\circ\text{C}$, $-30\text{ }^\circ\text{C}$, or $-40\text{ }^\circ\text{C}$ [25].

the COP increases with an increase in t_C . With a further increase in t_C , the negative effect is gradually enhanced, and the rate at which the COP increases is continually reduced until it finally becomes negative. When t_C is higher, the negative effect is predominant, and the COP decreases with an increase in t_C . For $t_E = -10\text{ }^\circ\text{C}$, $-20\text{ }^\circ\text{C}$, $-30\text{ }^\circ\text{C}$, and $-40\text{ }^\circ\text{C}$, the maximum COPs for the [bmim] Zn_2Cl_5/NH_3 system of 0.54, 0.48, 0.42, and 0.35 appear at $t_C = 133\text{ }^\circ\text{C}$, $161\text{ }^\circ\text{C}$, $188\text{ }^\circ\text{C}$, and $225\text{ }^\circ\text{C}$, respectively. When $t_E = -10\text{ }^\circ\text{C}$ and $-20\text{ }^\circ\text{C}$, the maximum COPs for the NaSCN/ NH_3 system occurs at $t_C = 81\text{ }^\circ\text{C}$ and $98\text{ }^\circ\text{C}$, respectively [27]. These results indicate that the required temperature of the heat source for the [bmim] Zn_2Cl_5/NH_3 system is higher than that of the NaSCN/ NH_3 system.

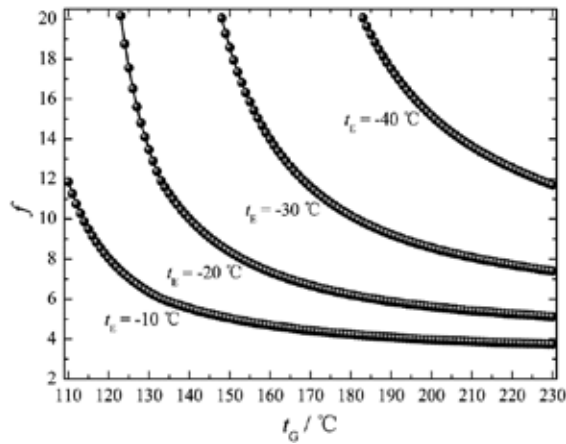


Figure 24. Effects of t_G on f for $t_G = 110\text{--}230\text{ }^\circ\text{C}$, $t_A = t_C = 35\text{ }^\circ\text{C}$ and $t_E = -10\text{ }^\circ\text{C}$, $-20\text{ }^\circ\text{C}$, $-30\text{ }^\circ\text{C}$, or $-40\text{ }^\circ\text{C}$ [25].

Fig. 24 shows effects of t_G on the f for $t_G = 110\text{--}230\text{ }^\circ\text{C}$ with $t_A = t_C = 35\text{ }^\circ\text{C}$ and $t_E = -10\text{ }^\circ\text{C}$, $-20\text{ }^\circ\text{C}$, $-30\text{ }^\circ\text{C}$, or $-40\text{ }^\circ\text{C}$. With an increase in t_G , the f declines, because the increase in t_G is conducive to desorption of NH_3 in the generator. With an increase in t_E , the f grows, because the increase in t_E will decrease the absorption pressure of the absorber. Thus, the absorption ability of the absorber will be decreased. The f is an important parameter for absorption refrigeration. An increase in the f will lead to an increase in the amount of energy used to heat the solution from t_A to t_C . If the f is greater than 10, the COP decreases, even when the efficiency of the regenerator is greater than 0.9. For $t_E = -10\text{ }^\circ\text{C}$, $-20\text{ }^\circ\text{C}$, and $-30\text{ }^\circ\text{C}$, the circulation ratios are less than 10 when t_G is greater than $115\text{ }^\circ\text{C}$, $139\text{ }^\circ\text{C}$, or $187\text{ }^\circ\text{C}$, respectively. Based on the results shown in Figs. 23 and 24, the $[\text{bmim}]\text{Zn}_2\text{Cl}_5/\text{NH}_3$ system can be used when $t_E = -10$ to $-30\text{ }^\circ\text{C}$.

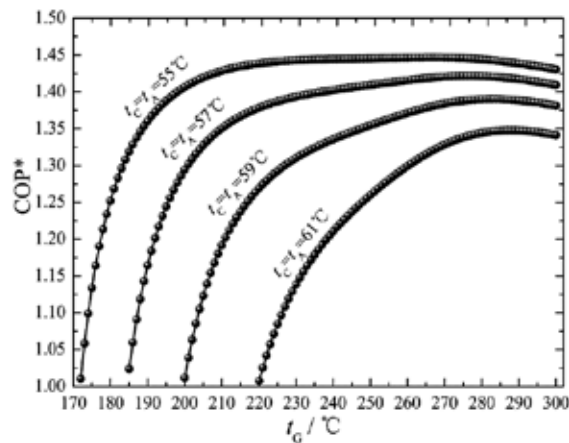


Figure 25. Effects of t_G on the COP^* for $t_G = 170\text{--}300\text{ }^\circ\text{C}$ with $t_A = t_C = 55\text{ }^\circ\text{C}$, $57\text{ }^\circ\text{C}$, $59\text{ }^\circ\text{C}$, or $61\text{ }^\circ\text{C}$ and $t_E = -10\text{ }^\circ\text{C}$ [25].

Fig. 25 shows the effects of t_G on the COP^* for $t_G = 170\text{--}300\text{ }^\circ\text{C}$ with $t_A = t_C = 55\text{ }^\circ\text{C}$, $57\text{ }^\circ\text{C}$, $59\text{ }^\circ\text{C}$, or $61\text{ }^\circ\text{C}$ and $t_E = -10\text{ }^\circ\text{C}$. The COP^* presents a trend of declining after increasing with an increase

in t_C . For $t_A = t_C = 55\text{ }^\circ\text{C}$, $57\text{ }^\circ\text{C}$, $59\text{ }^\circ\text{C}$, and $61\text{ }^\circ\text{C}$, the maximum COP* values of 1.447, 1.422, 1.390, and 1.348 appear at $t_C = 266\text{ }^\circ\text{C}$, $276\text{ }^\circ\text{C}$, $283\text{ }^\circ\text{C}$, and $289\text{ }^\circ\text{C}$, respectively. The COP* decreases with increases in t_A and t_C , because the increase in t_A is not conducive to absorption of NH_3 in the absorber. In addition, the increase in t_C is not conducive to desorption of NH_3 in the generator.

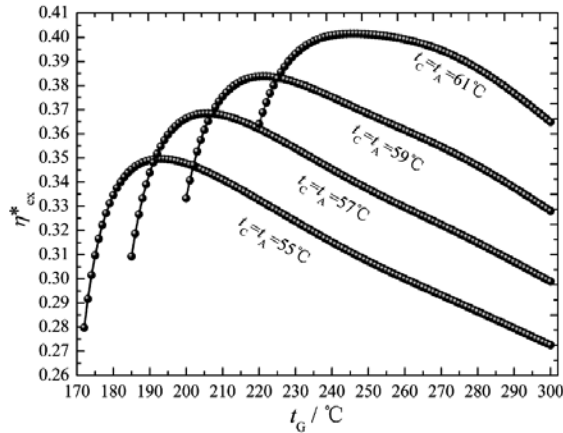


Figure 26. Effects of t_C on η_{ex}^* for $t_G = 170\text{--}300\text{ }^\circ\text{C}$ with $t_A = t_C = 55\text{ }^\circ\text{C}$, $57\text{ }^\circ\text{C}$, $59\text{ }^\circ\text{C}$, or $61\text{ }^\circ\text{C}$ and $t_E = -10\text{ }^\circ\text{C}$ [25].

Fig. 26 shows the effects of t_G on η_{ex}^* for $t_G = 170\text{--}300\text{ }^\circ\text{C}$ with $t_A = t_C = 55\text{ }^\circ\text{C}$, $57\text{ }^\circ\text{C}$, $59\text{ }^\circ\text{C}$, or $61\text{ }^\circ\text{C}$ and $t_E = -10\text{ }^\circ\text{C}$. With an increase in t_C , the η_{ex}^* presents a trend of decreasing after initially increasing. For $t_A = t_C = 55\text{ }^\circ\text{C}$, $57\text{ }^\circ\text{C}$, $59\text{ }^\circ\text{C}$, and $61\text{ }^\circ\text{C}$, the maximum values of η_{ex}^* of 0.341, 0.368, 0.384, and 0.402 appear at $t_G = 193\text{ }^\circ\text{C}$, $206\text{ }^\circ\text{C}$, $221\text{ }^\circ\text{C}$, and $246\text{ }^\circ\text{C}$, respectively. It can be seen that the optimal η_{ex}^* occurs at a lower t_G than did the optimal COP*. This is because the increase in t_C leads to an increase in the exergy proportion in q_E , which induces a decreasing trend in η_{ex}^* but has no effect on the COP*.

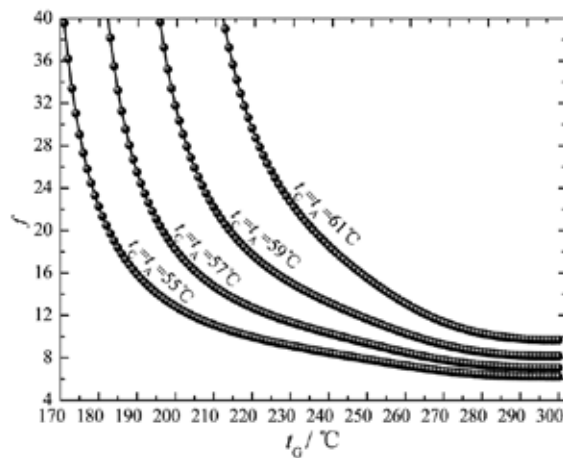


Figure 27. Effects of t_C on the f for $t_G = 170\text{--}300\text{ }^\circ\text{C}$ with $t_A = t_C = 55\text{ }^\circ\text{C}$, $57\text{ }^\circ\text{C}$, $59\text{ }^\circ\text{C}$, or $61\text{ }^\circ\text{C}$ and $t_E = -10\text{ }^\circ\text{C}$ [25].

Fig. 27 shows the effects of t_G on the f for $t_G = 170\text{--}300\text{ }^\circ\text{C}$ with $t_A = t_C = 55\text{ }^\circ\text{C}$, $57\text{ }^\circ\text{C}$, $59\text{ }^\circ\text{C}$, or $61\text{ }^\circ\text{C}$ and $t_E = -10\text{ }^\circ\text{C}$. The variation in the f is the same as that for the COP for cooling in Fig. 6. For $t_A = t_C = 55\text{ }^\circ\text{C}$, $57\text{ }^\circ\text{C}$, $59\text{ }^\circ\text{C}$, and $61\text{ }^\circ\text{C}$, the f values are less than 10 when t_G is greater than $220\text{ }^\circ\text{C}$, $244\text{ }^\circ\text{C}$, $263\text{ }^\circ\text{C}$, and $285\text{ }^\circ\text{C}$, respectively. Overall, the results in Figs. 21–27 indicate that the $[\text{bmim}]\text{Zn}_2\text{Cl}_5/\text{NH}_3$ absorption system is suitable for use in heating applications.

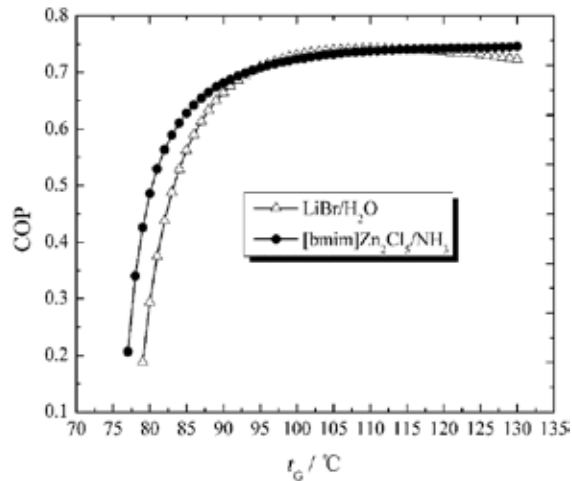


Figure 28. Effects of t_G on the COP for $t_G = 75\text{--}130\text{ }^\circ\text{C}$ with $t_A = 35\text{ }^\circ\text{C}$, $t_C = 40\text{ }^\circ\text{C}$, and $t_E = 5\text{ }^\circ\text{C}$.

The theoretical cycle characteristic of the $[\text{bmim}]\text{Zn}_2\text{Cl}_5/\text{NH}_3$ absorption system is also compared with that of the $\text{LiBr}/\text{H}_2\text{O}$ system. Fig. 28 shows the effects of t_G on the COP for $t_G = 75\text{--}130\text{ }^\circ\text{C}$ with $t_A = 35\text{ }^\circ\text{C}$, $t_C = 40\text{ }^\circ\text{C}$, and $t_E = 5\text{ }^\circ\text{C}$ and a heat recovery rate of the regenerator of 0.75. For both systems, the COP initially exhibits a significant increase as the t_G increases. As t_G continues to increase though, the slope of the COP curve for the $[\text{bmim}]\text{Zn}_2\text{Cl}_5/\text{NH}_3$ system becomes less steep, whereas the COP curve for the $\text{LiBr}/\text{H}_2\text{O}$ system presents a trend of a slight decrease after the increase. When $t_G < 95\text{ }^\circ\text{C}$, the COP of the $[\text{bmim}]\text{Zn}_2\text{Cl}_5/\text{NH}_3$ system is slightly higher than that of the $\text{LiBr}/\text{H}_2\text{O}$ system. When $95 < t_G < 115\text{ }^\circ\text{C}$, the COP of the $[\text{bmim}]\text{Zn}_2\text{Cl}_5/\text{NH}_3$ system is slightly less than that of the $\text{LiBr}/\text{H}_2\text{O}$ system. When $t_G > 115\text{ }^\circ\text{C}$, the COP of the $[\text{bmim}]\text{Zn}_2\text{Cl}_5/\text{NH}_3$ system is higher than that of the $\text{LiBr}/\text{H}_2\text{O}$ system. As t_G continues to increase, the COP curve for the $[\text{bmim}]\text{Zn}_2\text{Cl}_5/\text{NH}_3$ system still maintains the upward trend with a small slope, but the COP curve of the $\text{LiBr}/\text{H}_2\text{O}$ system shows a downward trend with a small slope. Although the COP of the $[\text{bmim}]\text{Zn}_2\text{Cl}_5/\text{NH}_3$ system is less than the COP of the $\text{LiBr}/\text{H}_2\text{O}$ system at some specific temperatures, the overall theoretical cycle characteristic of the $[\text{bmim}]\text{Zn}_2\text{Cl}_5/\text{NH}_3$ system is slightly better than that of the $\text{LiBr}/\text{H}_2\text{O}$ system, especially at higher t_G values.

3.5. Summary

The vapor pressures of the binary solution of $[\text{bmim}]\text{Zn}_2\text{Cl}_5/\text{NH}_3$ with NH_3 mole fraction $x_2 = 0.83\text{--}0.94$ at $T = 323.15\text{--}563.15\text{ K}$ were measured via a static method with a total uncertainty of measurement below 4.3% [16]. The experimental data were fit using the modified UNIFAC

model, and new group interaction parameters between any two of the four tested groups were obtained with a maximum deviation less than 5% [16]. Vapor pressures were compared between $\text{ZnCl}_2 \cdot 6\text{NH}_3$, ammonia solutions containing normal ionic liquids ([emim][Ac], [emim][SCN], [emim][EtOSO₃] and [DMEA][Ac]), and [bmim] $\text{Zn}_2\text{Cl}_5/\text{NH}_3$. The results indicate that the absorption characteristics of [bmim] Zn_2Cl_5 are much better than those of normal ionic liquids but slightly lower than those of ZnCl_2 . However, the liquid form of [bmim] Zn_2Cl_5 offers a major advantage over ZnCl_2 . Therefore, working pairs of [bmim] $\text{Zn}_2\text{Cl}_5/\text{NH}_3$ have good latent application in absorption refrigerator and heat pump operation.

TG scanning of [bmim] Zn_2Cl_5 was carried out using a TGA/SDT instrument over the range of $T = 323.15\text{--}1173.15$ K. The results indicate that [bmim] Zn_2Cl_5 possesses high thermal stability for $T < 637.15$ K. Heat capacity data at $T = 210.15\text{--}383.15$ K were obtained by using a DSC 910S operated with a rate of temperature increase of 5 Kmin^{-1} and a nitrogen volume flow of $40 \text{ cm}^3\text{min}^{-1}$. Molar excess enthalpy data for [bmim] $\text{Zn}_2\text{Cl}_5/\text{NH}_3$ at $x_1 = 0.60\text{--}0.95$ for $T = 288.15, 303.15, 318.15,$ and 333.15 K were measured. The excess enthalpy data were fit using the NRTL model. Measurement uncertainties and the maximum deviation of correlations for the excess enthalpy data were lower than 4.8% and 3.9%, respectively. With an increase in the NH_3 mole fraction, excess enthalpy showed a trend of increasing after declining. Minimum excess enthalpies of $-6555.7, -6707.1, -6846.3,$ and -6974.7 J/mol appeared at $x_1 = 0.772, 0.774, 0.776,$ and 0.777 for $T = 288.15, 303.15, 318.15,$ and 333.15 K, respectively. Based on the heat capacity of [bmim] Zn_2Cl_5 and the excess enthalpy of [bmim] $\text{Zn}_2\text{Cl}_5/\text{NH}_3$, the enthalpies of [bmim] $\text{Zn}_2\text{Cl}_5/\text{NH}_3$ solutions can be calculated, which makes it feasible to investigate the thermodynamic performances of the [bmim] $\text{Zn}_2\text{Cl}_5/\text{NH}_3$ absorption system.

Based on the modified UNIFAC model and the NRTL model, the thermodynamic performance of a single effect absorption system using [bmim] $\text{Zn}_2\text{Cl}_5/\text{NH}_3$ as the working pair was simulated and compared with those of the NaSCN/NH_3 adsorption system [25] and the $\text{H}_2\text{O}\text{-LiBr}$ absorption system. The thermal performance of the [bmim] $\text{Zn}_2\text{Cl}_5/\text{NH}_3$ system is better than that of the NaSCN/NH_3 system when the t_C is high and t_A and t_C are low and also better than that of the $\text{H}_2\text{O}\text{-LiBr}$ absorption system in some cases. With an increase in t_C , the COP and COP^* present trends of declining after increasing, and the circulation ratios show a decreasing trend. When $t_E = -30 \text{ }^\circ\text{C}$ and $t_A = t_C = 35 \text{ }^\circ\text{C}$, the maximum COP of the [bmim] $\text{Zn}_2\text{Cl}_5/\text{NH}_3$ system is still greater than 0.42. When $t_E = -10 \text{ }^\circ\text{C}$ and $t_A = t_C = 60 \text{ }^\circ\text{C}$, the maximum COP^* is still greater than 1.40. Under these two operating conditions, the circulation ratios remain acceptable. Although the COP of the [bmim] $\text{Zn}_2\text{Cl}_5/\text{NH}_3$ system is less than that of the $\text{LiBr}/\text{H}_2\text{O}$ system in some specific temperature ranges, the overall theoretical cycle characteristic of the [bmim] $\text{Zn}_2\text{Cl}_5/\text{NH}_3$ system is slightly better than that of the $\text{LiBr}/\text{H}_2\text{O}$ system, especially when t_C is high. Overall, these results indicate that the [bmim] $\text{Zn}_2\text{Cl}_5/\text{NH}_3$ absorption system offers good thermal performance for use in both cooling and heating applications.

4. Conclusions and outlook

Ten years have passed since ionic liquids were introduced in the field of absorption refrigeration, and unfortunately, the research progress pertaining to absorption refrigeration working pairs containing ionic liquids has been disappointing to us. Most of the working pairs proposed

by researchers from all over the world are gradually fading from view due to a lack of practical applications. Particular attention was paid to ionic liquid working pairs containing [RR'Im]DMP (1-R,3-R'-imidazolium dimethylphosphate). When applied in absorption refrigeration, the cycle characteristics of the three representative working pairs of [dmIm]DMP-H₂O, [emIm]DMP-H₂O and [mmIm]DMP-CH₃OH are better than that of H₂O-NH₃, but still slightly lower than those of LiBr-H₂O. So far, the new conceptual chemical absorption refrigeration working pairs containing an ionic liquid, with [bmim]Zn₂Cl₅/NH₃ as the representative, are the most ideal ionic liquid-type working pairs for absorption refrigeration. The thermodynamic performances of absorption refrigeration using the proposed chemical working pairs are comparable to those achieved with the LiBr-H₂O system. Additionally, the ranges of operating conditions for the chemical working pairs are wider than those of the conventional working pairs. At present, promoting the industrial application of [bmim]Zn₂Cl₅/NH₃ is our next priority. The discovery of chemical absorption refrigeration working pairs containing an ionic liquid is a milestone in the development of absorption refrigeration technology. It is foreseeable that the application of ionic liquids in absorption refrigeration will achieve a major breakthrough in the development of this technology, with the continued discovery of similar ionic liquid working pairs based on the chemical reaction.

Acknowledgements

This work was supported by the National Basic Research Program of China (973 Program) under Grant No. 2015CB251503 and the National Natural Science Foundation of China under Grant No. 51276180.

Author details

Shiqiang Liang^{1*}, Wei Chen², Yongxian Guo¹ and Dawei Tang¹

*Address all correspondence to: liangsq@mail.etp.ac.cn

1 Institute of Engineering Thermophysics, Chinese Academy of Sciences, Beijing, P.R. China

2 College of Electromechanical Engineering, Qingdao University of Science and Technology, Qingdao, P.R. China

References

- [1] S Q Liang, W Chen, K Y Cheng et al. The latent application of ionic liquids in absorption refrigeration. In: Application of ionic liquid in science and technology. InTechOpen, Croatia 2011:467-494.

- [2] J Zhao, S Q Liang, J Chen, et al. VLE for the High Concentration [MMIm]DMP-Methanol Solutions. *Chemical Engineering*, 38 (2010) 52-56
- [3] J Zhao, X C Jiang, C X Li. Vapor Pressure Measurement for Binary and Ternary Systems Containing a Phosphoric Ionic Liquid. *Fluid Phase Equilibria*, 247 (2006) 190-198.
- [4] W Chen, S Q Liang, Y X Guo et al. Thermodynamic performances of [mmim]DMP/methanol absorption refrigeration. *Journal of Thermal Science*, 21 (2012) 557-563.
- [5] L Dong, D X Zheng, N Nie et al. Performance prediction of absorption refrigeration cycle based on themeasurements of vapor pressure and heat capacity of H₂O + [DMIM]DMP system. *Applied Energy*, 98 (2012) 326-332.
- [6] J Ren, Z C Zhao, X D Zhang. Vapor pressures, excess enthalpies, and specific heat capacities of the binary working pairs containing the ionic liquid 1-ethyl-3-methylimidazolium dimethylphosphate, *Journal of Chemical Thermodynamics*, 43(2011) 576-583.
- [7] X D Zhang, D P Hu. Performance simulation of the absorption chiller using water and ionic liquid 1-ethyl-3-methylimidazolium dimethylphosphate as the working pair. *Applied Thermal Engineering*, 31 (2010) 3316-3321.
- [8] R Z Wang, L W Wang. Adsorption refrigeration- green cooling driven by low grade thermal energy. *Chinese Science Bulletin*, 50 (2005) 193-204.
- [9] K Wang. Performance and application of CaCl₂/expanded graphite adsorbent for double heat pipes type refrigeration. Ph. D dissertation of Shanghai Jiao Tong University, Shanghai, 2007.
- [10] L W Wang, R Z Wang, J Y Wu. Design of heat pipe type adsorption ice-making for fishing boats. *Journal of Chemical Engineering*, 13 (2005) 403-410.
- [11] T X Li, R Z Wang, R G Oliveira. Performance analysis of an innovative multimode, multisalt and multieffect chemisorption refrigeration system. *Journal of American Institute of Chemical Engineers*, (2007) 3222-3230.
- [12] Y Wei, Q G Zhang. Properties of ionic liquid based on zinc chloride BMIZn₂Cl₅. *Acta Chemica Sinica*, 66 (2008) 1879-1883.
- [13] M B Meredith, C H McMillen, J T. Goodman. Ambient temperature imidazolium-based ionic liquids with tetrachloronickelate(II) anions. *Polyhedron*, 28(2009) 2355-2358.
- [14] I Lin, C S Vasam. Metal-containing ionic liquids and ionic liquid crystals based on imidazolium moiety. *Journal of Organometallic Chemistry* 690 (2005) 3498-3512.
- [15] W Guan, L Li, H Wang et al. Studies on thermochemical properties of ionic liquids based on transition metal. *Journal of Thermal Analysis and Calorimetry*, 94 (2008)507-510.

- [16] W Chen, S Q Liang, Y X Guo et al. Investigation on vapor-liquid equilibria for binary systems of metal ion-containing ionic liquid [bmim] Zn_2Cl_5/NH_3 by experiment and modified UNIFAC model. *Fluid Phase Equilibria*, 360 (2013) 1-6.
- [17] A W Islam, M H Rahman. A review of Barker's activity coefficient method and VLE data reduction. *Journal of Chemical Thermodynamics*, 44 (2012) 31-37.
- [18] S Li, Z L Cheng, Y Q Ma et al. The new concise equation of state for ammonia. *Journal of Engineering Thermophysics*, 21 (2000) 17-19.
- [19] A Yokozeki, M B Shiflett. Vapor-liquid equilibria of ammonia + ionic liquid mixtures. *Applied Energy*, 84 (2007) 1258-1273.
- [20] R S Santiago, G R Santos, M Aznar. Liquid-liquid equilibrium in ternary ionic liquid systems by UNIFAC: new volume, surface area and interaction parameters. *Fluid Phase Equilibria*, 295 (2010) 93-97.
- [21] L Lemos, P Patrício, G Rodrigues et al. Liquid-liquid equilibrium of aqueous two-phase systems composed of poly(ethylene oxide) 1500 and different electrolytes ((NH_4) $_2SO_4$, $ZnSO_4$ and K_2HPO_4): Experimental and correlation. *Fluid Phase Equilibria*, 305 (2011) 19-24.
- [22] J A Gonzalez, I G Fuente, J C Cobos. Thermodynamics of mixtures with strongly negative deviations from Raoult's Law Part 4. Application of the DISQUAC model to mixtures of 1-alkanols with primary or secondary linear amines. Comparison with Dortmund UNIFAC and ERAS results. *Fluid Phase Equilibria*, 168 (2000) 31-58.
- [23] L Chen, S H Yu, Y K Tan. An experimental study on the adsorption refrigeration characteristics of ammonia. *Journal of Refrigeration*, 4 (2000) 18-22.
- [24] H Renon, J M Prausnitz. Local compositions in thermodynamic excess functions for liquid mixtures. *Journal of American Institute of Chemical Engineers*, 14 (1968) 135-144.
- [25] W Chen, S Liang, Y Guo, D Tang. Thermodynamic analysis of an absorption system using [bmim] Zn_2Cl_5/NH_3 as the working pair. *Energy Conversion and Management*, 85 (2014) 13-19.
- [26] L H Zhu, J J Gu. Second law-based thermodynamic analysis of ammonia/sodium thiocyanate absorption system. *Renewable Energy*, 35 (2010) 1940-1946.
- [27] L G Farshi, C A I Ferreira, S M S Mahmoudi et al. First and second law analysis of ammonia/salt absorption refrigeration systems. *Journal of Refrigeration*, 40 (2014) 111-121.

New Class of Ionic Liquids for Dye-Sensitized Solar Cells

Chun-Ting Li, Ling-Yu Chang, Miao-Syuan Fan,
Pei-Yu Chen, Jiang-Jen Lin, Kuo-Chuan Ho and
Chuan-Pei Lee

Additional information is available at the end of the chapter

<http://dx.doi.org/10.5772/59057>

1. Introduction

1.1. Dye-Sensitized Solar Cells (DSSCs)

Nowadays, the raising consumption of fossil fuel illustrates the urgent needs for alternative energy resources. Considering the variable environmental issues, renewable clean energy resources is the most reliable replacement for the sustainable usage in the future due to their unlimited energy input onto the earth. Among various kinds of renewable clean energy, solar energy is the only external energy source derived from outer space. Solar energy is nominated for its clean, non-hazardous, sufficient, and infinite power supply, and it is remarkable that a mere 10 min of solar irradiation onto the earth's surface is equal to the total yearly human energy consumption [1]. Thereby, solar energy can be considered as the most promising renewable power supplement without limitation in the next generation. Solar energy conversion can be divided into three parts: solar-to-electricity conversion, solar-to-chemical conversion, and solar-to-thermal conversion. For the case of solar-to-electricity conversion, plenty of solar cells have been widely explored for decades; the most common solar cell is the inorganic solid-state junction devices, including GaAs or CdTe tandem cells, crystalline or amorphous silicon solar cells, and CIGS or CZTS solar cells. However, the expensive, energy-intensive, high-temperature, and high-vacuum processes is needed for the fabrication of inorganic solid-state junction devices, thereby the extremely high cost of those solar cells limits their usages and applications. Therefore, the third generation solar cells are designed to cost down and are based on the cheap, simple, and easy fabrication process.

In recent years, dye-sensitized solar cells (DSSCs) have been extensively investigated and wildly developed due to its outstanding advantages, *i.e.*, low-cost production, large-scale fabrication, and good conversion efficiency. In 1991, Professor M. Grätzel introduced the

nanoporous films as the dye-derived wide-band semiconductor and made the breakthrough in the solar-to-chemical conversion efficiency of DSSCs [2]. In 2014, by incorporating the novel porphyrin dye (SM315), the DSSC containing the cobalt complex redox electrolyte reached the highest efficiency record of 13.00% [3], which encouraged lots of explorations of new organic materials for higher efficiency. As shown in Figure 1, a DSSC device is in a sandwich-like construction, which is composed of three adjacent thin layers [4]: (1) working electrode contains a high band-gap nanocrystalline semiconductor-based mesoporous film adsorbed with dye molecules; (2) the electrolyte contains a redox mediator and several additives; (3) counter electrode contains a electrocatalytic film. Generally, for a working electrode, the titanium dioxide (TiO_2) semiconductor is used for the mesoporous film, and the ruthenium bipyridyl derivatives (N3, N719, Z907 or black dye, *etc.*) are employed for the dye sensitizers. For the counter electrode, the platinum thin film is usually applied for collecting electrons and triggering the redox reaction of the electrolyte. The electrolyte mostly contains iodide/triiodide (I^-/I_3^-) redox couple, which is obtained by the mixing of iodine (I_2) and inorganic or organic salts with iodide anion in suitable non-aqueous solvents.

The solar-to-electricity conversion mechanism of the DSSCs [4-5] is motivated from the solar illumination as shown in Figure 2. Upon absorption of light, a photo-induced electron is injected from a metal-to-ligand charge transfer excited state of the dye into the conduction band of the TiO_2 film. The rate of this electron injection reaction is ultrafast, typically occurring on the order of hundreds of femtoseconds to tens of picoseconds. The injected electron transports through the TiO_2 film via a "hopping" mechanism, which is driven by a chemical diffusion gradient (rather than an electric field), and is collected at a transparent conductive substrate of fluorine doped tin oxide glass. After passing through an external circuit, the electron is reintroduced into the solar cell at the platinum counter electrode, where triiodide ion is reduced to iodide ion. The iodide then regenerates the oxidized dye, thereby completing the circuit without net chemical change. Among a DSSC, the electrolyte is a key part to determine the cell performance, because it provides the necessary ionic conductivity in the bulk of the electrolyte solution and sets the proper potential barrier for the energy conversion. In addition, it offers a reduction reaction at the counter electrode and helps for the dye regeneration by the charge-transfer reaction with the dye molecules. However, the DSSCs encounter two virtual problems induced by using the conventional liquid electrolytes: (i) limited conversion efficiency and (ii) poor long term stability. The limited conversion efficiency is mainly caused by some unfavorable reactions, including the recombination between the photo-induced electrons and I_3^- ions, and the delayed dye regeneration due to the low diffusivity and ionic conductivity of the electrolyte, *etc.* The poor long term stability is attributed to the evaporation and leakage of organic solvent in the liquid electrolyte; also, the permeation of oxygen and water and their corresponding side reactions with the electrolyte can damage the stability. To solve these two problems, ionic liquids (ILs) can be considered to be most attractive for replacing the conventional electrolytes due to their low melting points (below 100°C), good chemical and electrochemical stability, high thermal stability, non-toxic, non-flammability, negligible vapor pressure, and high ionic conductivity [6-8].

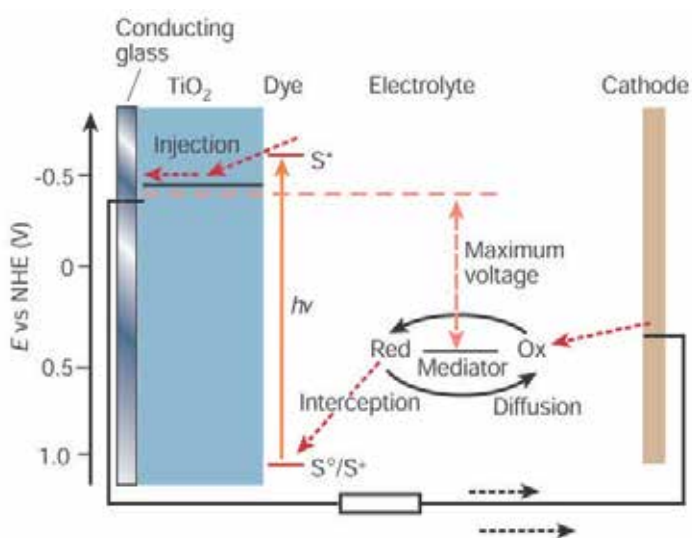


Figure 1. The construction of dye-sensitized solar cells (DSSCs) [4].

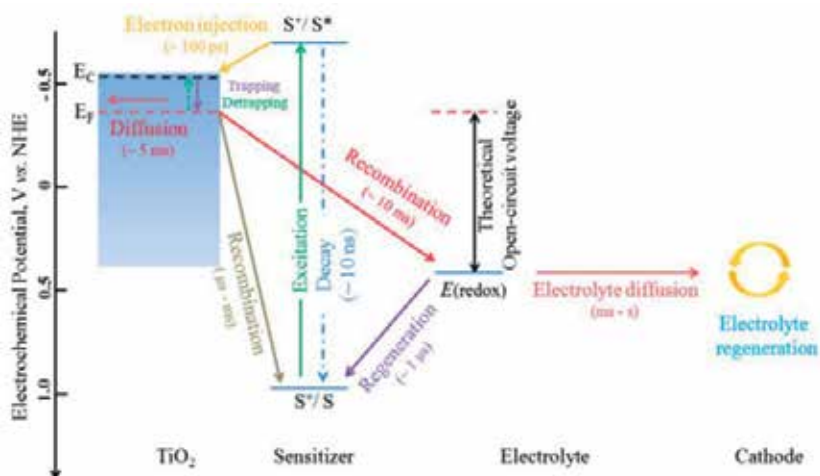


Figure 2. The energy diagram of the kinetics of DSSC function [5].

1.2. Ionic liquids as the mediator for DSSCs

Traditional ILs are composed by only ions and are characterized by the weak interactions between the large cations and a charge-delocalized anions. Therefore, the ILs are in a low tendency to crystallize due to the flexibility caused by the anions and the dissymmetry caused by the cations. ILs are basically composed of organic cations and anions [6-8]; the cations include imidazolium, N-substituted imidazolium, benzimidazolium, pyridinium, pyrrolidi-

nium, alkylammonium, alkylphosphonium, guanidinium, alkylpyrrolidinium, and alkylsulfonium groups, *etc.*, and the anions include chloride (Cl⁻), iodide (I⁻), bromide (Br⁻), tetrafluoroborate, hexafluorophosphate, trifluoromethanesulfonate, bis(trifluoromethylsulfonyl)imide, bis(fluorosulphonyl)imide groups, *etc.* The versatility of ILs, in terms of molecular structure, conductivity, hydrophobicity, melting point, viscosity, solubility, *etc.*, can be varied by altering the substitutive group on the cation part, or the combined anion type. Various kinds of salts can be used to design the ILs with the desired properties for the specific applications.

For the use as the “mediator” in the DSSCs, a specific group of ILs containing the redox species (Cl⁻, I⁻, Br⁻, S²⁻, CN⁻, *etc.*) as the anions has been highlighted. Lee *et al.* [9] employed two iodide-based ILs, 1-ethyl-3-methylimidazolium iodide (EMII) and 1-methyl-3-propyl imidazolium iodide (PMII), as the redox mediator. The binary IL electrolyte rendered a cell efficiency of 3.49% to its all-solid-state DSSC. Chen *et al.* [10] applied two kinds of IL mediators, 1-butyl-3-methylimidazolium iodide (BMII) and 1-butyl-3-methylimidazolium thiocyanate (BMISCN) for the electrolyte of DSSCs. In the binary electrolyte, the BMISCN was used to lower the viscosity, enhance the ionic conductivity, and reduce the interfacial charge transfer resistance of the electrolyte. The pertinent cell efficiency of 5.55% was obtained by using the binary IL electrolyte containing BMII, BMISCN, and lithium bis(trifluoromethanesulfonyl)imide (LiTFSI). Chi *et al.* [11] synthesized two solid-state iodide-based ILs, 1-[(4-ethenylphenyl)methyl]-3-butyl-imidazolium iodide (EBII) with a single aliphatic C=C bond and 1-[(4-ethenylphenyl)methyl]-3-vinyl-imidazolium iodide (EVII) with two aliphatic C=C bonds. The EBII exhibited weaker π - π stacking interactions, longer d-spacing, and a lower melting temperature. Therefore, the solid-state EBII-based DSSC reached higher efficiency of 4.7% than that of the EVII-based DSSC (3.8%) due to its facile charge transport and lower electron recombination. Hsu *et al.* [12] synthesized four kinds of iodide-based ILs, 1-allyl-3-ethylimidazolium iodide (AEII), 1-allyl-3-propylimidazolium iodide (APII), 1,3-diallylimidazolium iodide (DAII), and 1-methyl-3-propylimidazolium iodide (MPII), as the mediators in the novel agarose gel electrolytes. The agarose gel electrolyte containing AEII exhibited the highest I₃⁻ diffusion coefficient of $7.7 \times 10^{-6} \text{ cm}^2 \text{ s}^{-1}$ and thereby gave the best DSSC efficiency of 5.89%. Liu *et al.* [13] synthesized two kinds of sulfide-based ILs, tetra-methylammonium sulfide (TMAS) and 1-propyl-2,3-dimethylimidazolium sulfide (DMPIS), as the sulfide/polysulfide mediators. In their research, several iodide-based ILs (EMII, 1,3-dimethylimidazolium iodide (DMII) or PMII) were applied as another kind of the mediators. The electrolyte containing TMAS, EMI and DMII as the IL mediators can provide its DSSC a cell efficiency of 6.40%, while the electrolyte containing DMPIS and PMII as the IL mediators can provide its DSSC a cell efficiency of 6.20% under 100 mW cm⁻² illumination and a higher cell efficiency of 6.60% under 10 mW cm⁻² illumination. Furthermore, by controlling the concentration of TMAS, the electrolyte containing TMAS and 1,2-dimethyl-3-propylimidazolium iodide (DMPII) as the IL mediators can provide its DSSC a cell efficiency of 9.10% [14].

Except for the anions, the cations of IL mediators also play important roles in determining the conversion efficiency of the DSSCs. For example, the imidazolium cations were reported as the efficient functional group to retard the charge recombination at the working electrode/electrolyte interface [15]. And the alkyl chain-substituted imidazolium cations were de-

signed for prolonging the electron lifetime within a DSSC[16]. Therefore, different functional group-substituted cations of the IL mediators can be designed for compensating the defaults of the DSSCs with traditional electrolyte. Recently, the development of new classes of functional group-substituted IL mediators has been demonstrated as a promising strategy to further enhance the efficiency and the long-term stability of DSSCs. This chapter mainly reviewed the recent researches on the topic of new classes of ILs used as the electrolyte in DSSCs. Here the new classes of ILs employed in the electrolytes of DSSCs can be divided into two sections: (i) the applications in liquid electrolytes in DSSCs and (ii) the applications in quasi/all-solid-state electrolytes in DSSCs.

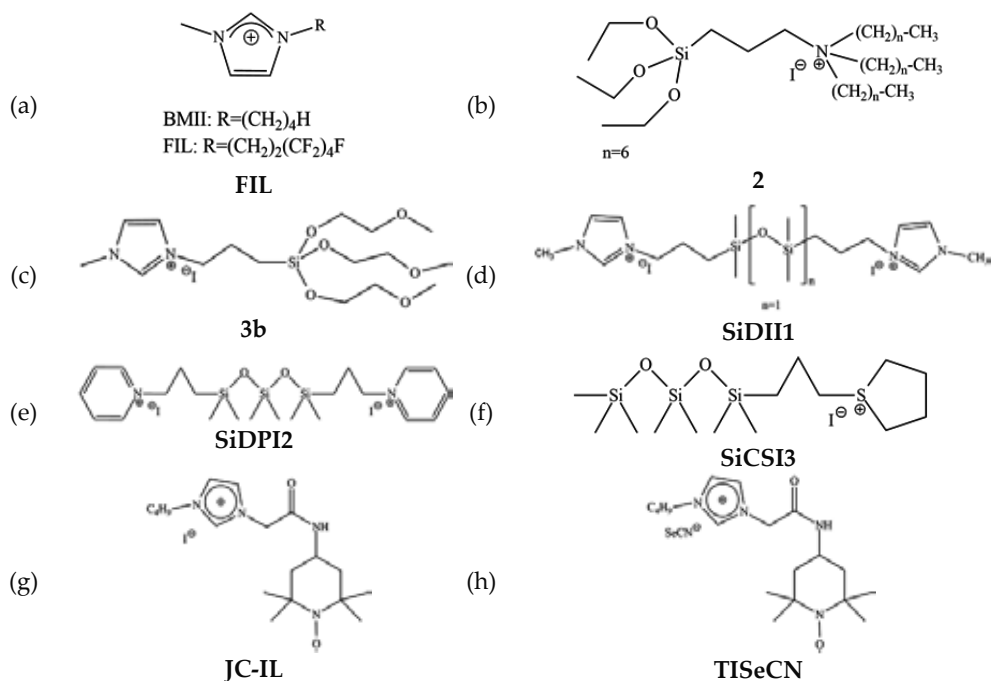


Figure 3. A partial literature review of the molecular structure of novel functional IL mediators for the application for the liquid electrolytes in DSSCs.

2. New class of ionic liquids

2.1. Applications in liquid electrolytes in DSSCs

To improve the conversion efficiency of the IL-based DSSCs, novel functional IL mediators were investigated by incorporating versatile organic functional groups into the traditional IL mediators. Those organic functional groups on the newly synthesized ILs were designed for enhancing the ionic conductivity, lowering viscosity, or speeding up the redox reaction of the

pristine ILs. Abate *et al.* [17] synthesized a polyfluorinated IL, 1-methyl-3-(3,3,4,4,5,5,6,6,6-nonafluorohexyl)imidazolium iodide (FIL, Figure 3a). The high electronegative 3,3,4,4,5,5,6,6,6-nonafluorohexyl functional group is designed for making FIL to improve the dye regeneration and facilitate the charge transport by providing a microphase separation (fluorophobic effect) between the long alkyl chains of the amphiphilic dye and the fluorine environment in the electrolyte. Therefore, a cell efficiency (η) of 5.10% was obtained with an open-circuit voltage (V_{OC}) of 610 mV, short-circuit current (J_{SC}) of 11.50 mA cm⁻², and fill factor (FF) of 0.73. Cerneaux *et al.* [18] synthesized three new triethoxysilanes bearing quaternary ammonium alkyl iodides ILs, N,N,N-triethyl-3-(triethoxysilyl)propan-1-aminium iodide (1), N,N,N-triethyl-3-(triethoxysilyl)propan-1-aminium iodide (2), and N,N,N-tridodecyl-3-(triethoxysilyl)propan-1-aminium iodide (3). The alkylsilane functional groups were introduced due to their benefits to the solubility and electron transfer of the electrolytes. By adjusting the compositions of IL-based liquid electrolyte containing 2 (Figure 3b), the pertinent DSSC showed the best efficiency of 5.00% under 100 mW cm⁻² and provided a very high efficiency of 8.1% under 10 mW cm⁻². Zalas *et al.* [19] synthesized three Si-tripodand-functionalized ILs by using the polyoxaethylene chains with different lengths to attach to the central silicon atom, namely 1-methyl-3-(3-(trimethoxysilyl)propyl)imidazolium iodide (3a), 1-methyl-3-(3-(tris(2-methoxyethoxy)silyl)propyl)imidazolium iodide (3b), and 1-methyl-3-(3-(tris(2-(2-methoxyethoxy)ethoxy)silyl)propyl)imidazolium iodide (3c). Those Si-tripodand-functionalized ILs are thermally stable (decomposition temperatures, $T_d \approx 270$ °C) and electrochemically stable. The 3b (Figure 3c) exhibited specific conductivity adequate for DSSCs, and thereby the pertinent electrolyte possessed a very high conductivity approaching 10⁻² S cm⁻¹ at ambient temperature. And the DSSC containing 3b showed a η of 5.10% with V_{OC} of 688 mV, J_{SC} of 14.30 mA cm⁻², and FF of 0.52. In 2013, Lee *et al.* introduced three novel classes of siloxane-functionalized ILs, including (i) siloxane diimidazolium iodides [20], (ii) siloxane pyridinium iodides [21], and (iii) siloxane cyclic sulfonium iodides [22], as the liquid electrolytes for DSSCs. Siloxane chains possessed highly thermal stability (up to 350 °C), relatively low permittivity, excellent flexibility and good amphiphilicity. Additionally, oxygens of siloxane were expected to have a complex with TiO₂ and capturing effect of cation, which could enhance the stability of the electrolytes and possibly be advantageous to the transportation of anionic species in the cell. The three types of the siloxane-functionalized ILs are depicted as follows:

- i. For the case of siloxane diimidazolium iodides (SiDII) ILs [20], three siloxane moieties with different chain lengths were separately incorporated between two imidazolium cations to form three different SiDII ILs (SiDII1, SiDII2, and SiDII3). The synthesized SiDII were viscous liquids with different colors and with good thermal stability (decomposition temperatures, $T_d \approx 380$ °C). With an increase in the siloxane chain lengths, the flexibilities and diffusion coefficients of the SiDII ILs increased, but the viscosities and conductivities decreased; the unusual decrease in their viscosities was attributed to that the amphiphilic siloxane chains could make SiDII ILs reduce the surface tension of both water and organic solvents. Among the SiDII-based DSSCs, the cell containing SiDII1 (Figure 3d) in the electrolyte showed a maximum conver-

sion efficiency (η) of 6.20% with an open-circuit voltage (V_{OC}) of 721 mV, short-circuit current (J_{SC}) of 12.90 mA cm⁻², and fill factor (FF) of 0.67. In addition, SiDII1-based DSSC showed better long-term stability than the DSSC with other conventional liquid type electrolytes.

- ii. For the case of siloxane pyridinium iodides (SiDPI) ILs [21], three siloxane moieties with different chain lengths were separately incorporated between two pyridinium cations to form three different SiDPI ILs (SiDPI1, SiDPI2, and SiDPI3). All SiDPI ILs showed good thermal stability ($T_d \approx 300$ °C). The solid-state SiDPI1 with short chain length was brown. The gel-state SiDPI2 and SiDPI3 with long chain length were shown as the highly viscous ILs. The DSSC containing SiDPI2 (Figure 3e) in the electrolyte achieved the highest η of 6.80% with V_{OC} of 703 mV, J_{SC} of 15.85 mA cm⁻², and FF of 0.61, which could be attributed to the reason that SiDPI2 had the relative low viscosity and the largest diffusion coefficient.
- iii. For the case of siloxane cyclic sulfonium iodides (SiCSI) ILs [22], two siloxane moieties with different chain length were separately incorporated between two cyclic sulfonium cations to form SiCSI1 and SiCSI2 ILs, and the SiCSI3 IL is constructed by a siloxane chain sited as the terminal group of one cyclic sulfonium cation. The thermooxidative stabilities of SiCSI ILs were lower than those of SiDII ILs because the bond strength of S⁺-C in sulfonium was lower than that of N⁺-C in imidazolium. The bis-sulfonium electrolytes (SiCSI1 and SiCSI2) were solid due to their high molecular weight and large size of sulfur element even though they had siloxane group; meanwhile, they were with relative low thermal stability ($T_d \approx 260$ °C). The mono-sulfonium (SiCSI3) electrolyte maintains gel state owing to its low molecular weight and free siloxane functional group; thereby SiCSI3 (Figure 3f) possesses the best thermal stability ($T_d \approx 300$ °C), highest ionic conductivity, and the largest diffusion coefficient than those values of SiCSI1 and SiCSI2 ILs. The SiCSI3-based liquid electrolyte renders its DSSC the highest η of 7.30% with V_{OC} of 689 mV, J_{SC} of 18.03 mA cm⁻², and FF of 0.59.

Among all the functional IL mediators for the liquid electrolyte in DSSCs, a novel class of free radical-substituted IL mediators brings the brand new level and broadens the horizons of the ILs applications recently. A free radical-substituted IL mediator can provide double redox channels: one is the free radical-substituted cation, and the other is the anion. The free radical-substituted IL mediator was designed to largely improve the redox potential, ionic conductivity, diffusion coefficient, and the intrinsic redox reaction of the liquid electrolytes for DSSCs. In 2014, our group (Chu *et al.* [23]) synthesized a new IL mediator, 1-butyl-3-(2-oxo-2-((2,2,6,6-tetramethyl-piperidin-1-oxyl-4-yl)amino)ethyl)-1H-imidazol-3-ium iodide (JC-IL, Figure 3g). The synthetic pathway to JC-IL was depicted in Figure 4a. The 2,2,6,6-tetra-methylpiperidin-N-oxyl (TEMPO) functional group could provide a nitroxide free radical (N-O.), which was notable for its simple one-electron redox reaction, extremely fast charge transfer ability, high redox potential, and large diffusion coefficient. Therefore, the JC-IL possessed dual redox channels, the TEMPO-substituted imidazolium cation and the iodide anion, which made the

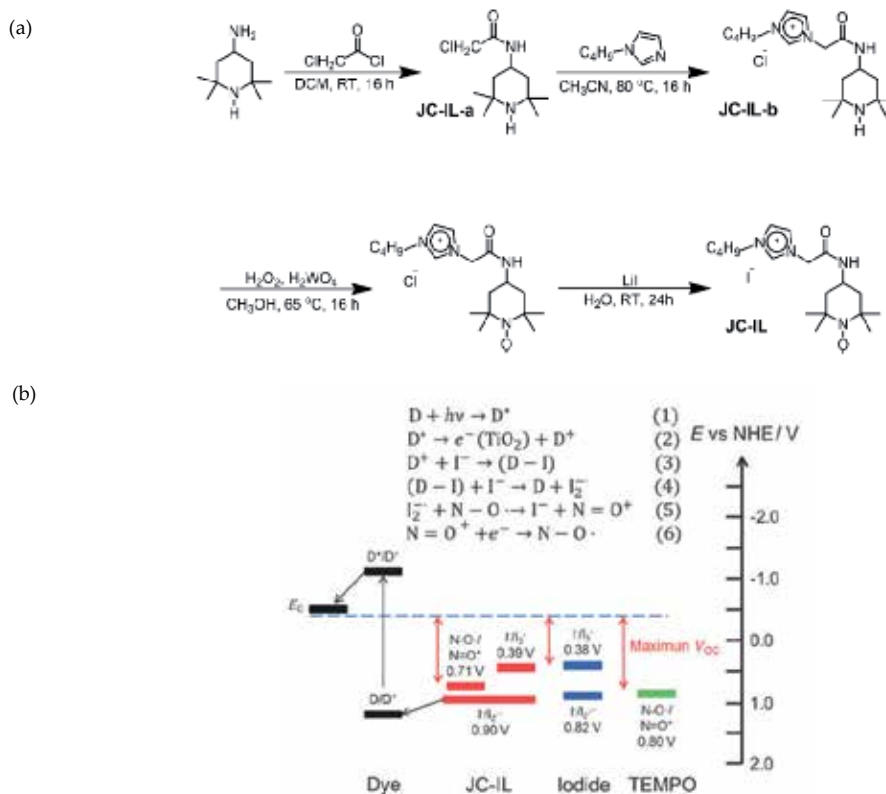


Figure 4. (a) The synthetic pathway to JC-IL. (b) Mechanism for the function of JC-IL, iodide, and TEMPO in DSSCs; energy levels of these charge mediators and those of the dye at ground and excited states are also shown [23].

JC-IL to exhibit three electron transfer redox reaction, high distinct redox potential (Figure 4b), large diffusion coefficient, and rapid intrinsic heterogeneous electron-transfer rate. The DSSC with JC-IL electrolyte showed a good cell efficiency of 8.12% with remarkably high V_{oc} of 858 mV, J_{sc} of 13.70 mA cm⁻², and FF of 0.69. The high open-circuit voltage of DSSCs with JC-IL was over 850 mV, which was approximately 150 mV higher than that of the DSSCs with a standard iodide-based liquid electrolyte. Currently, we further exchanged the iodide (I⁻) to another redox anion, selenocyanate (SeCN⁻), to synthesize a novel iodide-free IL mediator, 1-butyl-3-(2-oxo-2-((2,2,6,6-tetramethyl-piperidin-1-oxyl-4-yl)amino)ethyl)-1H-imidazol-3-ium selenocyanate (TISECN, Figure 3h). Since the selenocyanate was beneficial for faster kinetic electron transfer for redox reaction accompanying with a high redox potential, the TISECN electrolyte could facilitate the charge transportation within the electrolyte and thus greatly reduced the energy loss in the cell. Thus, a DSSC with TISECN-based liquid electrolyte showed a good cell efficiency of 8.38% with a high V_{oc} value of 854.3 mV, J_{sc} of 14.70 mA cm⁻², and FF of 0.67 [24].

Table 1 is a partial list of the DSSCs' performance containing above novel functional IL mediators in the liquid electrolytes.

ILs	Liquid electrolytes	Dye	η (%)	V_{oc} (mV)	J_{sc} (mA cm ⁻²)	FF	Ref.
FIL	0.6 M FIL, 0.03 M I ₂ , 0.1 M GuSCN, 0.5 M TBP in ACN/VN (v/v = 85/15)	Z907	5.10	610	11.50	0.73	[17]
2	1.5 M 2, 0.08 M I ₂ , 0.1 M GuSCN, 0.5 M TBP in ACN	Z907	4.40	769	13.50	0.42	[18]
3b	0.6 M 3b, 0.03 M I ₂ , 0.1 M GuSCN, 0.5 M TBP in ACN	N3	5.10	688	14.30	0.52	[19]
SiDIII	0.5M SiDIII, 0.05M I ₂ , 0.1 M GuSCN, 0.5 M TBP in MPN	N719	6.20	721	12.90	0.67	[20]
SiDPI2	0.6 M SiDPI2, 0.05M I ₂ , 0.1 M GuSCN, 0.5 M TBP in MPN	N719	6.80	703	15.85	0.61	[21]
SiCSI3	0.6 M SiCSI3, 0.05M I ₂ , 0.1 M GuSCN, 0.5 M TBP in MPN	N719	7.30	689	18.03	0.59	[22]
JC-IL	0.4 M JC-IL, 0.04 M NOBF ₄ in ACN	CR147	8.12	858	13.70	0.69	[23]
TlSeCN	0.2 M TlSeCN and 0.05 M (SeCN) ₂ in ACN.	CR147	8.38	854	14.70	0.67	[24]

Note: Guanidinium thiocyanate (GuSCN), tert-butylpyridine (TBP), acetonitrile (ACN), valeronitrile (VN), 3-methoxypropionitrile (MPN), nitrosyl tetrafluoroborate (NOBF₄)

Table 1. A partial literature review of the DSSCs' performance containing the novel functional IL mediators in the liquid electrolytes.

2.2. Applications in quasi/all-solid-state electrolytes in DSSCs

To further enhance the long-term stability of the IL-based DSSCs, several classes of functional IL mediators are designed in the quasi-solid-state or all-solid-state to prevent the leakage and volatilization of the electrolyte. Various organic functional groups were designed for enhancing the ionic conductivity, charge transfer ability, and mechanical stability of the newly synthesized ILs.

First, conductive IL mediators were introduced to enhance the conductivity of electrolyte and thereby improved the electron/hole transfer ability within a quasi/all-solid-state DSSC. Midya *et al.* [25] synthesized three solid-state conductive IL mediators, namely SD1 (Figure 5a), SD2 (Figure 5b), and SD3, which all contained carbazole-substituted imidazolium cations. Considering the iodide species as the redox couple, two carbazole-imidazolium iodide (CBZ-IMDZ-I) ILs, SD2 and SD3, were composed of an iodide (I⁻) anion and a carbazole-substituted imidazolium cation, which were the 1-carbazole-3-methyl-imidazolium and 1-carbazole-3-hexyl-imidazolium, respectively. In the presence of iodine (I₂), the LUMO-state dye was regenerated by oxidizing an I into the triiodide (I₃⁻) ion, and the I₃⁻ ion was subsequently reduced to I⁻ by the cation of CBZ-IMDZ-I because it could transport the holes to the counter electrode via a hole hopping mechanism (Figure 6a). Moreover, the hole hopping mechanism in the CBZ-IMDZ-I might assist the traditional Grotthuss-type exchange mechanism or work in parallel, leading to a fast I₃⁻ diffusion in the electrolyte. In a CBZ-IMDZ-I IL conductor, the carbazole functional group worked as the hole conductor to facilitate the dye regeneration via a hole hopping mechanism (Figure 6a) and to transport the iodine radical to the counter electrode via a Grotthuss-type mechanism (Figure 6b). Therefore, the solid-state electrolyte

containing SD2 can provide dual channels for hole/iodide transportation, and thereby could render its solid-state DSSC a cell efficiency of 2.85% with V_{OC} of 718 mV, J_{SC} of 6.23 mA cm⁻², and FF of 0.64. Furthermore, the SD1 contained a 1-carbazole-3-hexyl-imidazolium cation with a thiocyanate (SCN⁻) anion, and thereby the pertinent solid-state DSSC reached a cell efficiency of 1.43% with V_{OC} of 726 mV, J_{SC} of 3.10 mA cm⁻², and FF of 0.64. Wang *et al.* [26] synthesized two conductive IL mediators, namely propargyl-substituted imidazolium iodide (PMIm) and propargyl-functionalized piperidinium (PMPi). The pendent propargyl group possessed a lamellar structure, which was favorable for charge transfer and was expected to yield high conductivity. As compared to the alkyl-substituted imidazolium iodide, the introduction of unsaturated propargyl group to the imidazolium ring enhanced the conductivity by more than 4 orders. The newly synthesized propargyl-functionalized IL were in the solid state below 80 °C and had good thermal stability ($T_d \approx 330$ °C); they were also with good solubility in common organic solvents such as methanol and ethanol, which was advantageous to solution processing for pore-filling of the solid-state electrolyte in the DSSCs. Moreover, the PMIm and PMPi could be used directly as the single-component solid-state electrolyte for the DSSCs, which could perform efficiently without any additives in the electrolyte and any post-treatments on the dye-loaded TiO₂ films. By coupling an organic sensitizer (MK2), the DSSC with solely PMIm (Figure 5c) as the solid-state electrolyte achieved cell efficiency of 6.30% with V_{OC} of 710 mV, J_{SC} of 12.65 mA cm⁻², and FF of 0.70, and exhibited good long-term stability under continuous 1 sun illumination for 1,500 h. Besides, they also synthesized five kinds of ester-substituted IL mediators [27], 1-(2-methoxy-2-oxylethyl)-3-alkyl imidazolium iodide, containing different alkyl chain (methyl, ethyl, propyl, hexyl, dodecyl). The ester functional group possessed advantages over inorganic and organic hole conductors. First, the ester-substituted IL can form a three-dimensional (3D) ionic channel of iodides, which was advantageous for fast movement of iodides and charge transfer along the polyiodide chain. Secondly, the coordination interactions between esters and Li⁺ ions (typically used cations in the electrolyte of DSSCs) could form dimers of conductor molecules, and thus the distance of adjacent polyiodides was reduced, resulting in faster charge transfer and higher conductivity. In addition, the molecular size of the ester-substituted IL permitted a deep penetration of the electrolytes into the porous TiO₂ films, which facilitated the reduction of the oxidized dye molecules and favored high photocurrent generation. Among their five ester-substituted IL mediators, the 1-(2-methoxy-2-oxylethyl)-3-methyl imidazolium iodide (1, Figure 5d) showed the best conductivity of 5.76 mS cm⁻¹ because of the formation of ionic channels and the interaction of Li⁺ with the oxygen in the ester group, which resulted in fast charge transfer along the polyiodide chain. Thus, the pertinent DSSC exhibited a cell conversion efficiency as high as 6.63% with V_{OC} of 660 mV, J_{SC} of 13.77 mA cm⁻², and FF of 0.73, and exhibited excellent long-term stability remained at 100% of the initial value after continuous light soaking for 1,000 h. Li *et al.* [28] synthesized a novel solid-state conductive IL mediator, hydroxyethyl and ester co-substituted imidazolium iodide (HEII, Figure 5e). The ester functional group could significantly enhance the ionic conductivity of the IL electrolyte and thus to remarkably improve DSSC performance. The oxygen and hydrogen atoms within the hydroxyethyl functional group were designed to participate in hydrogen bonding, which was favorable to form a closely packed structure towards high conductivity. The solid-state HEII started to decompose at 150 °C and had a melting point of 79 °C. By coupling an organic sensitizer (MK2), the DSSC with HEII in the solid-state electrolyte achieved cell efficiency of 7.45% with a V_{OC}

of 733 mV, J_{SC} of 14.66 mA cm⁻², and FF of 0.69. Under continuous 1 sun illumination for 1,000 h, the cell efficiency maintained 96% and exhibited good long-term stability. Additionally, they synthesized a double-ester-substituted imidazolium iodide, 1,3-di(2-methoxy-2-oxoethyl)imidazolium iodide (DEII, Figure 5f) to act as the electron donor [29]. The donor (DEII) was deposited in the photoanode for efficient dye regeneration preceded by electron injection from the excited dye to the conduction band of TiO₂, while the acceptor (mixture of DEII and iodine) was deposited on the counter electrode surface for efficient electron relay for circuit completion. The counter electrode was placed on top of the photoanode to form a close contact between the donor and acceptor, which was then sealed into a solid device. As compared to the redox mixture electrolyte based device A (Figure 7), separating the electron donor and acceptor of a redox couple in device B (Figure 7) could significantly retard charge recombination because of the absence of I₃⁻ in the photoanode. Device A produced a cell efficiency of 2.41% (with a V_{OC} of 562 mV, J_{SC} of 7.02 mA cm⁻², and FF of 0.61), while device B produced a cell efficiency of 6.50% (with a V_{OC} of 633 mV, J_{SC} of 16.29 mA cm⁻², and FF of 0.63). Briefly, with the new device structure, the DSSC performance could be further improved by increasing the ionic conductivity of IL mediator through molecular design. Upon separation of the donor and acceptor of the IL mediator, the new device structure opened up a new way for optimization of the solar cell performance. Miao *et al.* [30] synthesized a novel solid-state conductive IL mediator, namely ILMC (Figure 5g), which was composed of the carboxyl-substituted imidazolium-europium (Eu) complex as the cation and the bromide as the anion. ILMC was synthesized through a green route by simply adding europium oxide into the carboxyl-substituted imidazolium IL, and the component, Eu, was selected as the metal center due to its excellent photophysical properties of the corresponding complexes. Thus, ILMC possessed the advantages of an easy and green preparation process, simple composition, light color, high conductivity, superior stability as well as the most important property of high efficiency. The solid-state DSSC with ILMC in the solid-state electrolyte achieved cell efficiency of 6.99% with a V_{OC} of 640 mV, J_{SC} of 15.28 mA cm⁻², and FF of 0.72. Xu *et al.* [31] synthesized a pyridylheptyl-substituted IL, N-butyl-N-(4-pyridylheptyl)imidazolium bromide ([BuPyIm]Br, Figure 5h). The pyridylheptyl functional group gave [BuPyIm]Br the good thermal stability ($T_d \approx 360$ °C) and a good solubility in aqueous solution. The DSSC containing [BuPyIm]Br in the electrolyte exhibited higher V_{OC} than the cell without [BuPyIm]Br. The enhanced V_{OC} of cell could be assigned from the suppression of the charge recombination at the TiO₂/electrolyte interface, and it was attributed to that the nitrogen-containing pyridylheptyl functional group anchored on the free areas of the dye-coated TiO₂ surface. Besides, the iodine could form anion complexes with some anions such as I₂Br⁻, and the imidazolium rings could interact strongly with I₂Br⁻ because the bigger anions had a lower charge density. Therefore, these anion complexes could also reduce the recombination between the photo-induced electrons and I₃⁻, thus enhanced the V_{OC} of the DSSC. However, the electrolyte containing [BuPyIm]Br provided the smaller values of both ionic conductivity and diffusion coefficient than those of the electrolyte without [BuPyIm]Br. Under the optimized condition with the addition of 0.1 M [BuPyIm]Br in the electrolyte, the highest conversion efficiency is 5.67 % under 100 mW cm⁻² and 6.69% under 15 mW cm⁻². The pertinent [BuPyIm]Br-based DSSC maintained almost 95% of its initial efficiency after 60 days long-term test under 80 °C, and thereby the [BuPyIm]Br IL could render a promising stability to its DSSC.

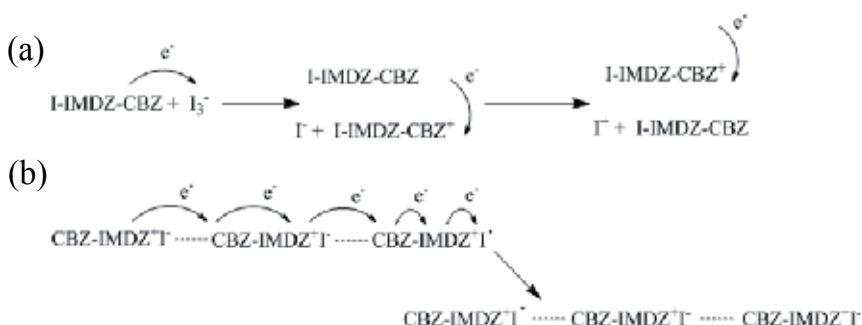


Figure 6. Schematic illustration of charge transfer phenomenon of the CBZ-IMDZ solid state IL conductor via (a) hole hopping mechanism and (b) Grotthuss-type mechanism [25].

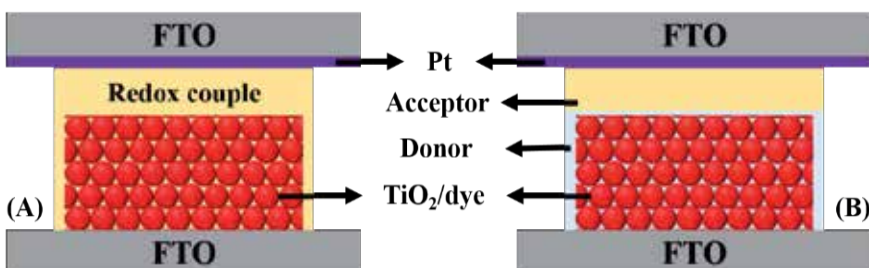


Figure 7. The device structures for device A and device B. A redox-couple mixture is used as the solid-state electrolyte in device A while the electron donor and acceptor of the redox-couple are separated in device B: the donor is in the photoanode layer but the acceptor (the mixture of donor and acceptor) is on top of the photoanode in contact with the counter electrode [29].

Second, quasi/all-solid-state alkylsilane-substituted IL mediators were also studied for their benefits of electron transfer within the electrolytes. Wu *et al.* [32] synthesized a room temperature (RT) IL, 1-methyl-3-(trimethylsilyl)methyl-imidazolium iodide (MSII, Figure 5i). The trimethylsilyl functional group was designed to reduce the viscosity and to enhance the conductivity of the IL. The DSSCs with a MSII-based quasi-solid-state IL electrolyte showed the largely decreased electron transfer resistance (R_{ct}) and increased electron lifetime (τ_e); thereby a cell efficiency (η) of 3.23% is provided with an open-circuit voltage (V_{OC}) of 600 mV, short-circuit current (J_{SC}) of 8.97 mA cm⁻², and fill factor (FF) of 0.61. Lee *et al.* [33] synthesized a novel quasi-solid-state alkylsilane-substituted IL, 3-(iodohexyl)-1-(3-(triethoxysilyl)propyl-carbamoyl)-1H-benzo[d]imidazol-3-ium iodide (SSBI, Figure 5j) by using the 1,6-diiodohexane and the silane-substituted benzimidazole (SSB), N-[3-(triethoxy-4-silyl)propyl]-1H-benzimidazole-1-carboxamide, as the reagents. The quasi-solid-state SSBI was prepared through the in-situ gelation, which was induced by the reaction of 1,6-diiodohexane and SSB in a DSSC cell heated at 60 °C for 30 min. The SSBI presumably formed a three-dimensional network due to the formation of hydrogen bonds among the amide groups of the silane-substituted benzimidazolium and the van der Waals force between the two iodoethyl moieties. Therefore,

the SSBI was able to immobilize the cations and facilitate the anionic transport in the quasi-solid-state DSSC, which showed a cell efficiency of 5.0 % with a V_{OC} of 710 mV, J_{SC} of 11.20 mA cm^{-2} , and FF of 0.63. The DSSC with quasi-solid-state SSBI-based electrolyte decreased to 52% of its initial value, while the cell with liquid electrolyte decreased to 79% of its initial value. Fontaine *et al.* [34] synthesized a novel alkylsilane-substituted IL, 1,3-(3-propyltriethoxysilane, 3-propyltrimethoxysilane)-4,5-dihydroimidazolium iodide (Si-IL, Figure 5k), which was used to form a hybrid ionogel containing silica-based matrix and imidazolium iodide redox mediator as shown in Figure 8. In the ionogel with 3-D architecture, ILs were immobilized through covalent bonds with silane groups. The Si-IL ionogel constructed multiple ion channels to facilitate the transport of iodide ions; thus the charge transfer at the electrode/electrolyte interfaces would be enhanced and then the reaction with the hole and the iodide would be facilitated, avoiding electron/hole recombination. The DSSC coupled with solely Si-IL as the ionogel electrolyte showed an efficiency of 1.25% with a V_{OC} of 680 mV, J_{SC} of 2.80 mA cm^{-2} , and FF of 0.65. The presence of covalent bonds between silica and ILs might avoid leakage or volatilization of ILs and prevent electrolyte from leaking. These conditions were more favorable for long-term performances and the flexible applications.

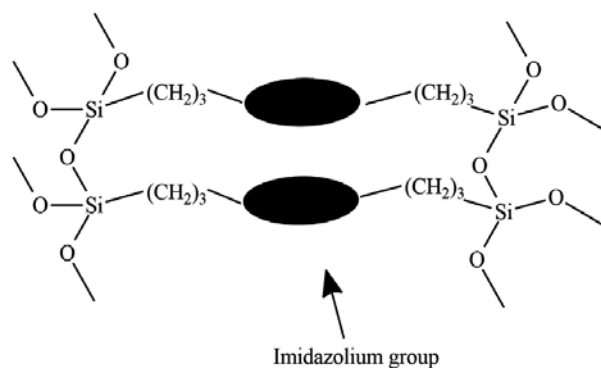


Figure 8. Schematic of the organization of the imidazolium groups into the silica network [34].

Third, polymeric IL mediators were designed by incorporating the polymer chain into the ILs as the gelator for the solidification of ILs-based electrolytes. Wang *et al.* [35-37] synthesized a group of solid-state IL polymers, poly(1-alkyl-3-(acryloyloxy)hexylimidazolium iodide) (PAAII) with four different alkyl side chains (methyl, ethyl, propyl, and butyl). The PAAII was synthesized by a thermal bulk polymerization of IL monomers, 1-alkyl-3-(acryloyloxy)hexylimidazolium iodide; thereby, multiple comb-like imidazolium iodide ILs were fixed onto the main chain of PAAII containing three ethylene units. The PAAII was a flexible solid with good ionic conductivity and good thermal stability ($T_d \approx 380$ °C) due to its specific functions, including charge transport of target ions, specific polar environment, and mechanical strength. Among all the PAAII ILs, the one with an ethyl side chain, namely poly(1-ethyl-3-(acryloyloxy)hexylimidazolium iodide) (PEAII, Figure 5l), showed the highest ionic conductivity (3.63×10^{-4} S cm^{-1}) and good charge transport ability. Due to the conjugation effect of imidazolium ring and the steric hindrance of polymer backbone, the attraction between the cation and the

iodide anion was weak, resulting in easy diffusion of iodide anions in PEAIL. A π -stacked imidazolium chain in PEAIL can provide the favorable channel for holes transport from the photoanode to the counter electrode. The electron was fast transported from the counter electrode to the dye by diffusion of I⁻. Therefore, without the presence of iodine (I₂), the DSSC assembled with solid-state PEAIL electrolyte reached the good cell efficiency of 5.29% with a V_{OC} of 838 mV, J_{SC} of 9.75 mA cm⁻², and FF of 0.65. Under long-term stability test for 1,000 h, the DSSC assembled with PEAIL electrolyte maintained about 85% of their initial efficiency after 1,000 h without sealing. Fang *et al.* [38] synthesized an acidic IL polymer, P[(3-(4-vinylpyridine) propanesulfonic acid) iodide]-co-(acrylonitrile)] (P-HI, Figure 5m), which was composed of a co-polymer chain (polyethylene and polyacrylonitrile) and a sulfonic acid group. The sulfonic acid group possessed strong electronegativity, which was beneficial to form the homogeneous and continuous framework of ILs polymer for enhancing transportation of redox couples in the electrolyte. Without the addition of I₂, the DSSC containing P-HI in the solid-state electrolyte achieved the cell efficiency of 6.95% with a V_{OC} of 643 mV, J_{SC} of 15.10 mA cm⁻², and FF of 0.72. Chi *et al.* [39] designed and synthesized a polymerized IL, poly((1-(4-ethenylphenyl)methyl)-3-butyl-imidazolium iodide) (PEBII, Figure 5n). An (4-ethenylphenyl)methyl functional group was anchored on 1-butylimidazolium iodide IL and served as the self-polymerization site and rendered high conductivity (2.0×10^{-4} S cm⁻¹ at 25 °C) to the PEBII due to the strong π - π stacking interaction between the benzene groups. For the application of iodine-free solid-state electrolyte in DSSCs, the solid-state PEBII was able to deeply penetrate into mesoporous TiO₂ film, perfectly fill the nanopores between the TiO₂ nanoparticles, and prevent the formation of cavities during solvent evaporation. Therefore, the charge transfer at the electrode/electrolyte interface and the electron lifetime within the pertinent cell were significantly improved, and the conversion efficiency of the solid-state DSSC with PEBII electrolyte reached 5.93%, measured at 100 mW cm⁻². Furthermore, by coupling a photoanode containing double layer mesoporous TiO₂ beads, the PEBII electrolyte rendered its DSSC an enhanced cell efficiency up to 6.70% with a V_{OC} of 760 mV, J_{SC} of 16.60 mA cm⁻², and FF of 0.53 [40]. Chang *et al.* [41] synthesized a novel polymeric IL, poly(1-(2-acryloyloxyethyl)-3-methyl-imidazol-1-ium iodide) (poly(AMImI), Figure 5o), by using an atom transfer radical polymerization (ATRP) method. The monomeric IL, 1-(2-acryloyloxyethyl)-3-methyl-imidazol-1-ium iodide (AMImI), possessed a 2-acryloyloxyethyl functional group anchoring on 1-methylimidazolium iodide IL. The 2-acryloyloxyethyl functional group served as the self-polymerization site. The solid-state DSSC with poly(AMImI)-based electrolyte reached the 1.16%. By adding multi-wall carbon nanotubes (MWCNTs) into the poly(AMImI)-based electrolyte, the pertinent DSSC achieved 3.55% with a V_{OC} of 646 mV, J_{SC} of 8.51 mA cm⁻², and FF of 0.64.

Recently, our group (Chang *et al.* [42]) synthesized a novel polymeric IL, poly(oxyethylene)-imide imidazolium iodide (POEI-II, Figure 5p). The synthetic pathway to POEI-II was depicted in Figure 9. A poly(oxyethylene)-segmented oligo(imide) (POEI) functional group incorporated with two 1-butylimidazolium iodide ILs at both ends of POEI. The POEI possessed aromatic imides and hydrophilic POE segments with multiple dipole-dipole interaction sites, which rendered POEI-II a high solubility in aqueous solutions as well as in organic solvents. The POE segment in the POEI-II could chelate lithium cations (Li⁺) within

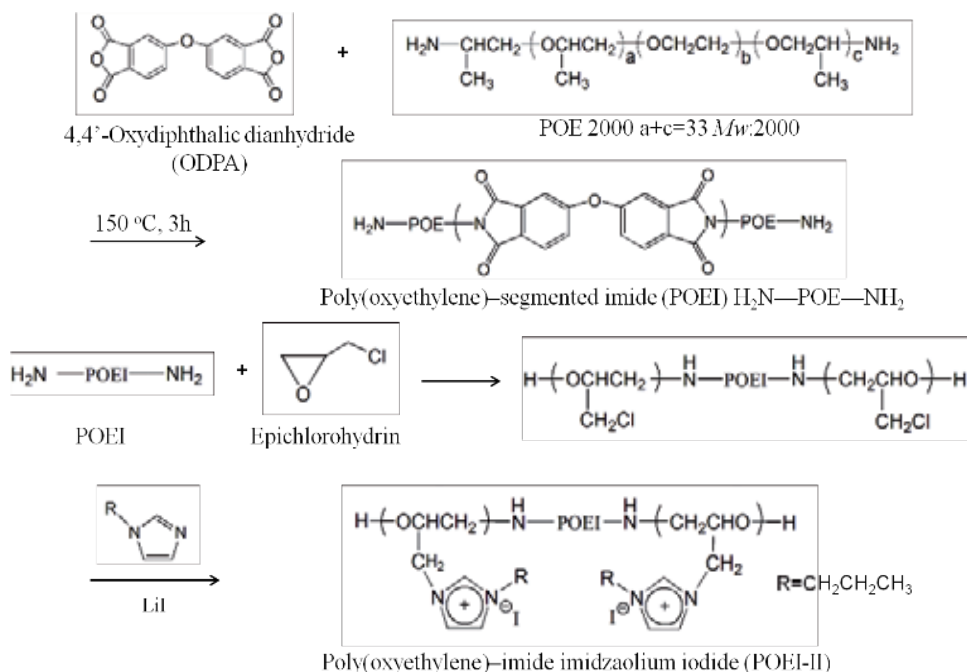


Figure 9. Synthetic pathway to poly(oxyethylene)-imide imidazolium iodide (POEI-II) [42].

the electrolyte to improve the V_{OC} value of a DSSC and enable the strong inner π - π and long-pair- π electron interactions to enhance the ionic conductivity and the diffusivity of POEI-II. Consequently, the quasi-solid-state DSSC with POEI-II gel electrolyte reached a high cell efficiency of 7.19%. In addition, MWCNTs were incorporated into POEI-II gel electrolyte (Figure 10) as the extended electron transfer material (EETM) to facilitate charge transfer from counter electrode to redox mediator, which benefited the dye regeneration more efficiently. Meanwhile, the POE segments on POEI-II could prevent the MWCNTs from aggregation, which made the well dispersed MWCNTs to largely expose to I^-/I_3^- redox mediators and thereby gave more charge transfer active sites. The highest cell efficiency of 7.65% was achieved by using the MWCNTs/POEI-II gel electrolyte and showed an unflinching durability of greater than 1,000 h under $50\text{ }^{\circ}\text{C}$ as shown in Figure 11.

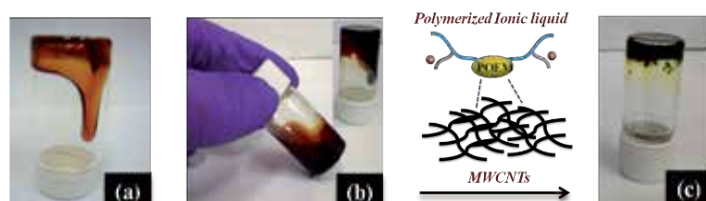


Figure 10. Photographs of the (a) pristine POEI-II, (b) POEI-II gel electrolyte, and (c) POEI-II/MWCNTs gel electrolyte [42].

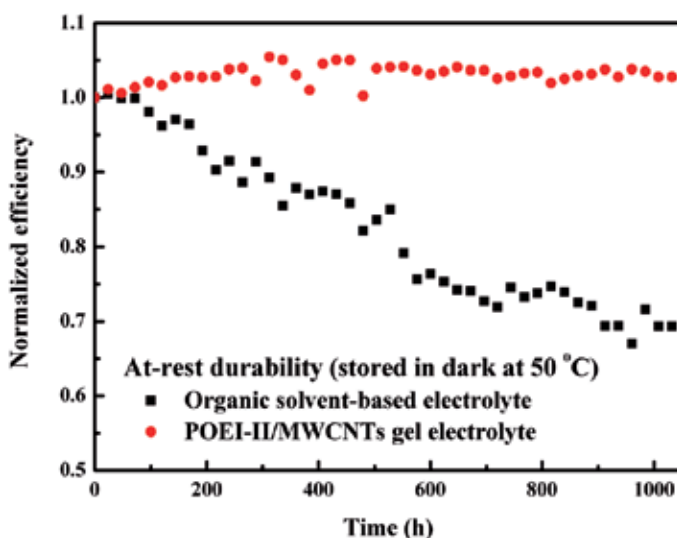


Figure 11. At-rest durability data of the DSSCs (stored in dark at 50 °C) with POEI-II/MWCNTs gel electrolyte and with an organic solvent electrolyte [42].

Table 2 is a partial list of the DSSCs’ performance containing above novel functional IL mediators in the quasi/all-solid-state electrolytes.

ILs	Quasi/All-solid-state Electrolytes	Dye	η (%)	V_{oc} (mV)	J_{sc} (mA cm ⁻²)	FF	Durability (% to the initial η)	Ref.
SD1	0.12 M SD1, 0.03 M I ₂ , 0.1 M TBP, 0.12 M LiTFSI, 0.012 M EMIB(CN) ₄	N719	1.43	726	3.10	0.64	N.A.	[25]
SD2	0.12 M SD2, 0.03 M I ₂ , 0.1 M TBP, 0.12 M LiTFSI, 0.012 M EMIB(CN) ₄	N719	2.85	718	6.23	0.64	84% (after 1 month)	[25]
PMIm	PMIm	MK2	6.30	710	12.65	0.70	100% (after 1500 h)	[26]
1	1/I ₂ /LiI/EMIBF ₄ = 5/1/1.25/0.25	MK2	6.63	660	13.77	0.73	100% (after 1000 h)	[27]
HEII	HEII/I ₂ /LiI/NMBI/MPII = 12:1:3:10:0.5	MK2	7.45	733	14.66	0.69	96% (after 1500 h)[28]	
DEII	For WE: DEII; For CE: DEII/I ₂ = 6:1	FNE29	6.50	633	16.29	0.63	N.A.	[29]
ILMC	0.1 M I ₂ , 0.1 M LiI in PMII/ILMC (v/v = 3/1)	N719	6.99	640	15.28	0.72	100% (after 1000 h)	[30]

ILs	Quasi/All-solid-state Electrolytes	Dye	η (%)	V_{oc} (mV)	J_{sc} (mA cm ⁻²)	FF	Durability (% to the initial η)	Ref.
[BuPyIm]Br	0.1 M [BuPyIm]Br, 0.2 M I ₂ , 0.14 M GuSCN in PMII/EMISCN (v/v = 13/7)	Z907	5.67	640	13.60	0.66	96% (after 60 days)	[31]
MSII	MSII/I ₂ /BI/GuSCN (24/2/2/0.4)	DPP-I	3.23	600	8.97	0.61	N.A.	[32]
SSBI	0.05 M I ₂ , 0.1 M LiI, 0.5 M TBP, 0.053 M SSB, 0.22 M diiodoalkane in MPN	N719	5.00	710	11.20	0.63	52% (after 1000 h)[33]	
Si-IL	Si-IL	D5	1.25	680	2.80	0.65	N.A.	[34]
PEAII	PEAII	N3	5.29	838	9.75	0.65	85% (after 1000 h)[35-37]	
P-HI	20 wt% of P-HI in HMII/AMII/NMBI/GuSCN (8/8/1.2/1.2)	N3	6.95	643	15.10	0.72	N.A.	[38]
PEBII	PEBII	N719	6.70	760	16.60	0.53	N.A.	[39-40]
poly (AMImI)	0.5 wt% MWCNT/AMBIml, 0.05 M I ₂ , 0.17 M NMBI, 0.013 M GuSCN, and 1 g poly(AMImI) in ACN	N3	3.55	646	8.51	0.64	N.A.	[41]
POEI-II	5 wt% MWCNTs, 0.1 M LiI, 0.05 M I ₂ , 0.5 M TBP, and 0.3 M POEI-II in N719 ACN/MPN (v/v = 1/1).	N719	7.65	784	14.50	0.67	100% (after 1000 h)	[42]

Note: 1-ethyl-3-methylimidazolium tetracyanoborate (EMIB(CN)₄), ethanol (EtOH), 1-methyl-3-ethyl-imidazolium tetrafluoroborate (EMIBF₄), 1-methylbenzimidazole (NMBI), 1-Ethyl-3-methyl-imidazolium thiocyanate (EMISCN), benzimidazole (BI), 1-hexyl-3-methylimidazolium iodide (HMII), 1-allyl-3-methylimidazoliumiodide (AMII), 1-(2-acryloyloxy-ethyl)-3-methyl-benzimidazol-1-ium iodide (AMBIml)

Table 2. A partial literature review of the DSSCs' performance containing the novel functional IL mediators in the quasi/all-solid-state electrolytes.

3. Summary and future prospects

Traditional ILs are organic salts basically composed of variable cation-anion unions that exhibit low volatility accompanying with high thermal stability, excellent electrochemical stability, and high ionic conductivity. These characteristics of ILs create the possibility of designing ideal electrolytes for DSSCs. Recently, the development of new classes of functional group-substituted ILs, *i.e.* conductive ILs, dual redox mediators-based ILs, and polymeric ILs, etc., has been demonstrated as a promising strategy to further enhance the efficiency and the long-term stability of ILs electrolyte-based DSSCs. In this chapter, we mainly review the recent researches on the topic of new classes of ILs used as the electrolyte in DSSCs, and our last relevant works

are also introduced for comparison. The new classes of ILs employed in the electrolytes of DSSCs are divided into two sections: (i) the applications in liquid electrolytes in DSSCs and (ii) the applications in quasi/all-solid-state electrolytes in DSSCs.

Among section (i), our group synthesized a novel IL with TEMPO-imidazole complex coupling with I, namely JC-IL, for preparing the liquid electrolyte for DSSCs. Due to its dual redox mediators of nitroxide radical (N-O \cdot) and I \cdot , this kind of electrolyte exhibited not only faster regeneration rate toward oxidized dye but also the more positive redox potential in DSSCs than the traditional electrolyte containing only I redox mediator. As a result, the DSSC with JC-IL-based liquid electrolyte showed a good cell efficiency of 8.12% with remarkably high V_{OC} of 858 mV. Based on the structure of JC-IL, we further exchanged I to SeCN \cdot for synthesizing an iodide-free IL mediator coded as TISECN. The combination of the dual charge transfer mediators, *i.e.* N-O \cdot and SeCN \cdot , in the TISECN-based liquid electrolyte could facilitate the charge transportation within the electrolyte and greatly reduced the energy loss in the cell, such as charge recombination, usually occurring in a DSSC with I/I $_3$ redox couple. An impressive cell efficiency of 8.38% with a high V_{OC} of 854 mV, J_{SC} of 14.70 mA cm $^{-2}$, and FF of 0.67 was achieved for the iodide-free DSSC by using the TISECN-based liquid electrolyte.

In section (ii), an polymeric IL, POEI-imidazole complex coupling with I (coded as POEIII), was synthesized for preparing the gel electrolyte for quasi-solid-state DSSCs. Herein, POEIII, which acted simultaneously as a redox mediator for dye regeneration and a gelator for the solidification of organic solvent-based electrolyte, was used to improve cell durability. The presence of the POE segment in the POEIII could chelate lithium cations (Li $^+$) within the electrolyte to improve the V_{OC} of a DSSC and enable the strong inner π - π and long-pair- π electron interactions to enhance the ionic conductivity and the diffusivity of redox couple within the gel electrolyte. Consequently, the quasi-solid-state DSSC with POEIII gel electrolyte reached a high cell efficiency of 7.19%. In addition, appropriate amount of MWCNTs were incorporated into POEIII gel electrolyte as the extended electron transfer materials to facilitate charge transfer from counter electrode to redox mediator, which benefited the dye regeneration more efficiently. Meanwhile, the POE segments in POEIII could prevent the MWCNTs from aggregation, which made the well dispersed MWCNTs to largely exposed to I/I $_3$ redox mediators. The highest cell efficiency of 7.65% was achieved by using the MWCNTs/POEIII gel electrolyte and showed a unfailling durability of greater than 1,000 h under 50 $^{\circ}$ C.

Up to now, most quasi/all-solid state DSSCs with IL electrolyte achieved relatively low cell efficiency as compared to the traditional DSSCs with liquid electrolyte. Despite the former system which showed superior durability than that of the latter, the cell efficiency indeed needs to be further improved because both stability and solar-to-electricity efficiency are the two essential criteria for a good DSSC. Besides, iodine-free electrolyte is desirable for developing flexible DSSCs where a metal substrate is prone to corrosion by iodine. Accordingly, in the future, we can synthesize a novel IL with TEMPO-Imidazole-POEI complex coupling with SeCN \cdot for preparing an iodine-free and quasi-solid state electrolyte for DSSCs. This kind of multi-functional ILs could potentially provide dual channels for charge transportation within the DSSCs, and simultaneously acts as a gelator for the solidification of organic solvent-based electrolyte. This idea would be a key issue for future study.

Acknowledgements

This work was supported by National Taiwan University.

Author details

Chun-Ting Li¹, Ling-Yu Chang², Miao-Syuan Fan¹, Pei-Yu Chen¹, Jiang-Jen Lin², Kuo-Chuan Ho¹ and Chuan-Pei Lee^{3*}

*Address all correspondence to: 1983725leecp@gmail.com

1 Department of Chemical Engineering, Institute of Polymer Science and Engineering, Taiwan

2 Institute of Polymer Science and Engineering, Taiwan

3 Institute of Photonics and Optoelectronics and Department of Electrical Engineering, National Taiwan University, Taipei, Taiwan

References

- [1] J. H. Yum, E. Baranoff, S. Wenger, M. K. Nazeeruddin, M. Grätzel. Panchromatic engineering for dye-sensitized solar cells. *Energ. Environ. Sci.*, 2011, 4, 842-857.
- [2] B. O'Regan, M. Grätzel. A low-cost, high-efficiency solar cell based on dye-sensitized colloidal TiO₂ films. *Nature*, 1991, 253, 737-740.
- [3] S. Mathew, A. Yella, P. Gao, R. Humphry-Baker, B. F. Curchod, N. Ashari-Astani, I. Tavernelli, U. Rothlisberger, M. K. Nazeeruddin, M. Grätzel. Dye-sensitized solar cells with 13% efficiency achieved through the molecular engineering of porphyrin sensitizers. *Nat. Chem.*, 2014, 6, 242-247.
- [4] M. Grätzel. Photoelectrochemical cells. *Nature*, 2001, 414, 338-344.
- [5] F. Hao, H. Lin. Recent molecular engineering of room temperature ionic liquid electrolytes for mesoscopic dye-sensitized solar cells. *RSC Adv.*, 2013, 3, 23521-23532.
- [6] H. Niedermeyer, C. Ashworth, A. Brandt, T. Welton, P. A. Hunt. A step towards the a priori design of ionic liquids. *Phys. Chem. Chem. Phys.*, 2013, 15, 11566-11578.
- [7] B. Qiu, B. Lin, F. Yan. Ionic liquid/poly(ionic liquid)-based electrolytes for energy devices. *Polym. Int.*, 2013, 62, 335-337.
- [8] J. M. Pringle. Recent progress in the development and use of organic ionic plastic crystal electrolytes. *Phys. Chem. Chem. Phys.*, 2013, 15, 1339-1351.

- [9] C. P. Lee, L. Y. Lin, P. Y. Chen, R. Vittal, K. C. Ho. All-solid-state dye-sensitized solar cells incorporating SWCNTs and crystal growth inhibitor. *J. Mater. Chem.*, 2010, 20, 3619-3625.
- [10] J. Chen, T. Peng, W. Shi, R. Li, J. Xia. An efficient binary ionic liquid based quasi solid-state electrolyte for dye-sensitized solar cells. *Electrochim. Acta*, 2013, 107, 231-237.
- [11] W. S. Chi, H. Jeon, S. J. Kim, D. J. Kim, J. H. Kim. Ionic liquid crystals: synthesis, structure and applications to I₂-free solid-state dye-sensitized solar cells. *Macromol. Res.*, 2013, 21, 315-320.
- [12] H. L. Hsu, C. F. Tien, Y. T. Yang, J. Leu. Dye-sensitized solar cells based on agarose gel electrolytes using allylimidazolium iodides and environmentally benign solvents. *Electrochim. Acta*, 2013, 91, 208-213.
- [13] J. Liu, X. Yang, J. Cong, L. Kloo, L. Sun. Solvent-free ionic liquid electrolytes without elemental iodine for dye-sensitized solar cells. *Phys. Chem. Chem. Phys.*, 2012, 14, 11592-11595.
- [14] J. Cong, X. Yang, Y. Hao, L. Kloo, L. Sun. A highly efficient colourless sulfur/iodide-based hybrid electrolyte for dye-sensitized solar cells. *RSC Adv.*, 2012, 2, 3625-3629.
- [15] S. Kambe, S. Nakade, T. Kitamura, Y. Wada, S. Yanagida. Influence of the electrolytes on electron transport in mesoporous TiO₂-electrolyte systems. *J. Phys. Chem. B*, 2002, 106, 2967-2972.
- [16] W. Kubo, K. Murakoshi, T. Kitamura, S. Yoshida, M. Haruki, K. Hanabusa, H. Shirai, Y. Wada, S. Yanagida. Quasi-solid-state dye-sensitized TiO₂ solar cells: effective charge transport in mesoporous space filled with gel electrolytes containing iodide and iodine. *J. Phys. Chem. B*, 2001, 105, 12809-12815.
- [17] A. Abate, A. Petrozza, V. Rofani, S. Guarnera, H. Snaith, F. Matteucci, G. Lanzani, P. Metrangola, G. Resnati. A polyfluoroalkyl imidazolium ionic liquid as iodide ion source in dye sensitized solar cells. *Org. Electronics*, 2012, 13, 2474-2478.
- [18] S. A. Cerneaux, S. M. Zakeeruddin, M. Grätzel, Y. B. Cheng, L. Spiccia. New functional triethoxysilanes as iodide sources for dye-sensitized solar cells. *J. Photochem. Photobiol. A*, 2008, 198, 186-191.
- [19] M. Zalas, M. Walkowiak, B. Gierczyk, M. Osińska-Broniarz, P. Pótrolniczak, G. Schroeder. Novel Si-tripodand functionalized ionic liquids as iodide sources for dye-sensitized solar cells. *Electrochim. Acta*, 2013, 108, 736-740.
- [20] S. Lee, Y. Jeon, Y. Lim, M. A. Hossain, S. Lee, Y. Cho, H. Ju, W. Kim. A new siloxane containing imidazolium iodide as electrolyte for dye-sensitized solar cell. *Electrochim. Acta*, 2013, 107, 675-680.

- [21] S. Lee, Y. Jeon, Y. Lim, Y. Cho, S. Lee, W. Kim. Novel pyridinium iodide containing siloxane high performance electrolyte for dye-sensitized solar cell. *B. Kor. Chem. Soc.*, 2013, 34, 2583-2588.
- [22] S. H. Lee, Y. D. Lim, D. W. Seo, M. A. Hossain, H. H. Jang, H. C. Lee, W. G. Kim. Novel cyclic sulfonium iodide containing siloxane high performance electrolyte for dye-sensitized solar cell. *J. Ind. and Eng. Chem.*, 2013, 19, 322-326.
- [23] T. C. Chu, R. Y. Lin, C. P. Lee, C. Y. Hsu, P. C. Shih, R. Lin, S. R. Li, S. S. Sun, J. T. Lin, R. Vittal, K. C. Ho. Ionic liquid with a dual-redox couple for efficient dye-sensitized solar cells. *ChemSusChem*, 2014, 7, 146-153.
- [24] C. T. Li, C. P. Lee, C. T. Lee, S. R. Li, S. S. Sun, K. C. Ho. Dye-sensitized solar cells with high V_{OC} using a novel iodide-free ionic liquid mediator containing TEMPO radicals and selenocyanate. *Adv. Energ. Mater.*, 2014, (under review).
- [25] A. Midya, Z. Xie, J. X. Yang, Z. K. Chen, D. J. Blackwood, J. Wang, S. Adams, K. P. Loh. A new class of solid state ionic conductors for application in all solid state dye-sensitized solar cells. *Chem. Commun.*, 2010, 46, 2091-2093.
- [26] H. Wang, J. Li, F. Gong, G. Zhou, Z. S. Wang. Ionic conductor with high conductivity as single-component electrolyte for efficient solid-state dye-sensitized solar cells. *J. Am. Chem. Soc.*, 2013, 135, 12627-12633.
- [27] H. Wang, X. Zhang, F. Gong, G. Zhou, Z. S. Wang. Novel ester-functionalized solid-state electrolyte for highly efficient all-solid-state dye-sensitized solar cells. *Adv. Mater.*, 2012, 24, 121-124.
- [28] J. Li, H. Wang, G. Zhou, Z. S. Wang. Hydroxyethyl and ester co-functionalized imidazolium iodide for highly efficient solid-state dye-sensitized solar cells. *Chem. Commun.*, 2013, 49, 9446-9448.
- [29] J. Li, W. Zhang, L. Zhang, Z. S. Wang. Separating the redox couple for highly efficient solid-state dye-sensitized solar cells. *Phys. Chem. Chem. Phys.*, 2014, 16, 7334-7338.
- [30] Q. Miao, S. Zhang, H. Xu, P. Zhang, H. Li. A novel ionic liquid-metal complex electrolyte for a remarkable increase in the efficiency of dye-sensitized solar cells. *Chem. Commun.*, 2013, 49, 6980-6982.
- [31] D. Xu, X. Chen, L. Wang, L. Qiu, H. Zhang, F. Yan. Performance enhancement for high performance dye-sensitized solar cells via using pyridinyl-functionalized ionic liquid type additive. *Electrochim. Acta*, 2013, 106, 181-186.
- [32] W. Wu, X. Zhang, Y. Hu, B. Jin, J. Hua. A Silicon-based imidazolium ionic liquid iodide source for dye-sensitized solar cells. *Chin. J. Chem.*, 2013, 31, 388-392.

- [33] J. P. Lee, B. Yoo, T. Suresh, M. S. Kang, R. Vital, K. J. Kim. Novel silane-substituted benzimidazolium iodide as gel electrolyte for dye-sensitized solar cells. *Electrochi. Acta*, 2009, 54, 4365-4370.
- [34] O. Fontaine, A. Touidjine, M. Maréchal, C. Bonhomme, F. Ribot, B. Geffroy, B. Jous-selme, C. Sanchez, C. Laberty-Robert. A one-pot route to prepare class II hybrid iono-gel electrolytes. *New J. Chem.*, 2014, 38, 2008-2015.
- [35] G. Wang, L. Wang, S. Zhuo, S. Fang, Y. Lin. An iodine-free electrolyte based on ionic liquid polymers for all-solid-state dye-sensitized solar cells. *Chem. Commun.*, 2011, 47, 2700-2702.
- [36] G. Wang, S. Zhuo, L. Wang, S. Fang, Y. Lin. Mono-ion transport electrolyte based on ionic liquid polymer for all-solid-state dye-sensitized solar cells. *Solar Energy*, 2012, 86, 1546-1551.
- [37] G. Wang, S. Zhuo, Y. Lin. An ionic liquid-based polymer with π -stacked structure as all-solid-state electrolyte for efficient dye-sensitized solar cells. *J. Appl. Polym. Sci.*, 2013, 127, 2574-2580.
- [38] Y. Fang, W. Xiang, X. Zhou, Y. Lin, S. Fang. High-performance novel acidic ionic li- quid polymer/ionic liquid composite polymer electrolyte for dye-sensitized solar cells. *Electrochem. Commun.*, 2011, 13, 60-63.
- [39] W. S. Chi, J. K. Koh, S. H. Ahn, J.-S. Shin, H. Ahn, D. Y. Ryu, J. H. Kim. Highly effi- cient I_2 -free solid-state dye-sensitized solar cells fabricated with polymerized ionic liquid and graft copolymer-directed mesoporous film. *Electrochem. Commun.*, 2011, 13, 1349-1352.
- [40] D. K. Roh, J. A. Seo, W. S. Chi, J. K. Koh, J. H. Kim. Facile synthesis of size-tunable mesoporous anatase TiO_2 beads using a graft copolymer for quasi-solid and all-solid dye-sensitized solar cells. *J. Mater. Chem.*, 2012, 22, 11079-11085.
- [41] Y. H. Chang, P. Y. Lin, S. R. Huang, K. Y. Liu, K. F. Lin. Enhancing photovoltaic per- formance of all-solid-state dye-sensitized solar cells by incorporating ionic liquid- physisorbed MWCNT. *J. Mater. Chem.*, 2012, 22, 15592-15598.
- [42] L. Y. Chang, C. P. Lee, C. T. Li, M. H. Yeh, K. C. Ho, J. J. Lin. Synthesis of a novel amphiphilic polymeric ionic liquid and its application in quasi-solid-state dye-sensi- tized solar cells. *J. Mater. Chem. A*, 2014, (under revise).

Edited by Scott Handy

Ionic liquids continue to attract a great deal of research attention in an even increasing number of areas, including more traditional areas such as synthesis (organic and materials) and physical properties studies and predictions, as well as less obvious areas such as lubrication and enzymatic transformations. In this volume, recent advances in a number of these different areas are reported and reviewed, thus granting some appreciation for the future that ionic liquids research holds, and affording inspiration for those who have not previously considered the application of ionic liquids in their area of interest.

Photo by Alik MuLikov / DollarPhotoClub

IntechOpen

